



STISWB 2018

Proceedings of

**the 10th International Conference on Science,
Technology and Innovation for Sustainable Well-Being 2018**



"Moving Towards Smart and Sustainable Technologies"

11th – 13th July, 2018

Don Chan Palace Hotel & Convention

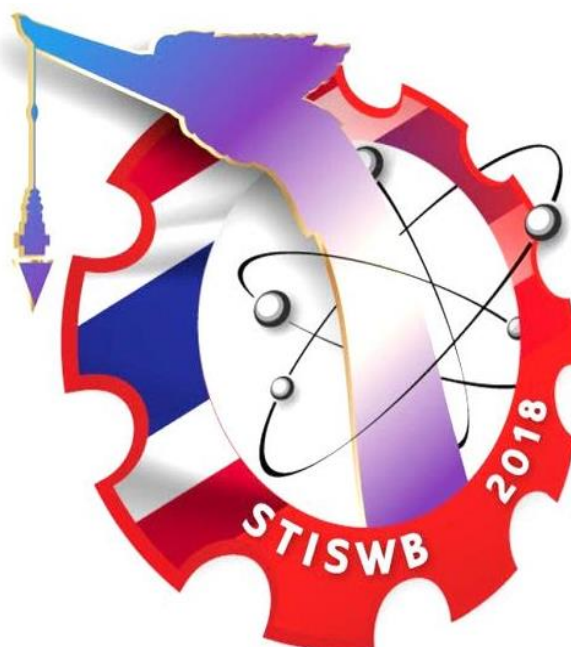
Vientiane, Lao PDR.

Organized by:

**The Faculty of Engineering,
Rajamangala University of Technology Phra Nakhon**



The 10th International Conference on Science, Technology and Innovation for Sustainable Well-Being 2018



THE 10th STISWB 2018
Moving Towards Smart and Sustainable Technologies



Proceedings of the 10th International Conference on Science, Technology and Innovation for Sustainable Well-Being 2018 (STISWB 2018)

11th – 13th July, 2018

Don Chan Palace Hotel & Convention
Vientiane, Lao PDR

First Edition: July 2018

Ownership/Copyright Owner: Faculty of Engineering,
Rajamangala University of Technology Phra Nakhon
1381 Pracharat 1 Road, Bangsue, Bangkok 10800, Thailand

ISBN 978-974-625-805-0

Publisher : ODEON STORE CO., LTD.
1/35-39 BOROMMARATCHONNANI RD.,
BANGKOKNOI, BANGKOK. 10700
TEL. 0-2884-6871-2



Proceedings of The 10th International Conference on Science, Technology and Innovation for Sustainable Well-Being 2018



THE 10th STISWB 2018 Moving Towards Smart and Sustainable Technologies



KMUTNB



11th – 13th July, 2018
Don Chan Palace Hotel & Convention
Vientiane, Lao PDR.



The 10th International Conference on Science, Technology and Innovation for Sustainable Well-Being 2018

THE 10th STISWB 2018

Host-Organized by:



The Faculty of Engineering,

Rajamangala University of Technology Phra Nakhon, Thailand

“MOVING TOWARDS SMART AND SUSTAINABLE TECHNOLOGIES”

Co - Organized Network:

1. Faculty of Engineering, Chiang Mai University, Thailand
2. Graduated School, Mahasarakham University, Thailand
3. Faculty of Engineering, Mahasarakham University, Thailand
4. Faculty of Environment and Resource Studies, Mahasarakham University, Thailand
5. Faculty of Industrial Technology and Management,
King Mongkut's University of Technology North Bangkok, Prachinburi Campus, Thailand
6. Faculty of Engineering and Industrial Technology, Sanam Chandra Palace Campus,
Silpakorn University, Nakhon Pathom, Thailand
7. Faculty of Engineering and Agro-Industry, Maejo University, Thailand
8. Faculty of Engineering, Rajamangala University of Technology Lanna, Thailand
9. Faculty of Engineering, Rajamangala University of Technology Isan,
Khonkean Campus, Thailand
10. Rambhai Bami Rajabhat University, Thailand
11. Faculty of Industrial Technology, Rajabhat Rajanagarindra University, Thailand



**Message from the President
of
Rajamangala University of Technology Phra Nakhon**



Welcome to the 10th International Conference on Science, Technology and Innovation for Sustainable Well-Being 2018 or STISWB 2018 held at Don Chan Palace Hotel & Convention, Laos, during 11th -13th July 2018. The conference is hosted by Rajamangala University of Technology Phra Nakhon in cooperation with 12 networks from 10 institutions.

This international conference aimed to establish networking and academic partners in all levels with both private and public sectors. It is also aimed to provide an opportunity for graduate students and interested persons to exchange and share research studies to promote the excellence in research corresponded to RMUTP Vision that is a university that inspires, develops systematic thinking skills, and creates technological excellence to serve the country and the community.

In 2018, the Thai government has announced Thailand 4.0 policy aimed at improving all industries by moving forward with the innovation and technology. Research is the key driver of innovation. With this reason, RMUTP visualizes the importance of research development. We inspire, support and promote our academic personnel and students to create new knowledge that can be applied into the community development at both national and international levels.

Again, Rajamangala University of Technology Phra Nakhon welcomes you to the 10th International Conference on Science, Technology and Innovation for Sustainable Well-Being 2018. I sincerely hope that this conference bring you all the benefits you are looking for, an opportunity to share and exchange your research ideas together, to utilize the knowledge, research, and innovation to make our countries and communities the better place for us in the future.

Assoc. Prof. Supatra Kosaiyakanont

President

Rajamangala University of Technology Phra Nakhon





Message from the Dean
The Faculty of Engineering
Rajamangala University of Technology Phra Nakhon



The Northern Bangkok Engineering School is considered as a school in a field of Industrial Technology and was established in B.E. 2501 (1958). Later, it was promoted to be “The Northern Bangkok Technical Institute”. In B.E. 2531(1988), the Institute was known as Rajamangala Institute of Technology North Bangkok Campus. It was elevated to university status in B.E. 2548 (2005) until now to the Faculty of Engineering, Rajamangala University of Technology Phra Nakhon (RMUTP), totally over 60 years. Today, the Faculty of Engineering organizes the instruction in various academic fields, which including, Pre-Engineering or Vocational Certificate, Bachelor’s Degree level, Master’s Degree level, and Doctoral Degree level.

On the occasion of the faculty of engineering which will reach 60 years from the Northern Bangkok Engineering School to the Faculty of Engineering, RMUTP on 14th July, 2018. And for celebrating such occasion, the Faculty of Engineering gets an honor from the STISWB network’s committee, to be responsible as a host for organizing the STISWB conference and presenting the international researches entitled the 10th International Conference on Science Technology and Innovation for Sustainable Well-Being 2018 (STISWB 2018) under the concept of “Moving Towards Smart and Sustainable Technologies”. The conference will be held at the Don Chan Palace Hotel & Convention, Vientiane, Lao PDR, between 11th – 13th July, 2018 which will be beneficial for the instructions and researches development toward students, lecturers, educators, researcher, and interested persons. Furthermore, it will promote and publicize the research contributions to achieve the international level by presenting in the form of Oral Presentation. In addition, this will be a good opportunity for all lecturers, researchers, educators, and interested persons from various organizations to mutually discuss and have good interactions. The participants of this academic conference consist of students, researchers, lecturers, personnel from both government and private sectors, including general people both domestic and foreign countries.

On this occasion, I would like to thank you to all participants, researchers and authors from all organizations which submit papers and attend to the 10th STISWB 2018. Furthermore, I feel thankful for the research paper reviewers and all committees who have sacrificed the precious time to consider articles from every field which helps increase the quality of researches to be more valuable on the academic fields. The Faculty of Engineering will create and develop academic contributions and research works to be a part of crucial mechanisms to drive our national growth further and lead to the leading organization to construct values to the society according to the vision determined, which is,
“Faculty of Engineering, the First Leadership to Produce Engineers as Professional Practitioners”

Wirote Ritthong

(Asst. Prof. Dr. Wirote Ritthong)
Dean of the Faculty of Engineering
Rajamangala University of Technology Phra Nakhon





The 10th International Conference on Science, Technology and Innovation for Sustainable Well-Being 2018

ABOUT THE 10th STISWB 2018

The International Conference on Science, Technology and Innovation for Sustainable Well-Being (STISWB) is one of major international conferences organized by Thai University Network. The conference brings together researchers and engineers who work in the related engineering fields.

The conference aims at providing a virtual international forum for presentation and discussion of the state-of-the-art research and development as well as to give opportunities for cooperation among participants in various sub-disciplines of engineering, science and technology, education and other related fields. The conference also aims to bring together the knowledge of different fields so as to put forward the existing science, technology and innovation into practice in order to ultimately create sustainable well-being to humankind.

On the occasion of the faculty of engineering, Rajamangala University of Technology Phra Nakhon which will reach 60 years from the Northern Bangkok Engineering School, since B.E. 2501 (1958) to the Faculty of Engineering, RMUTP on 14th July, 2018. And for celebrating such occasion, the Faculty of Engineering gets an honor from the STISWB network's committee, to be responsible as a host for organizing the STISWB conference and presenting the international researches entitled the 10th International Conference on Science Technology and Innovation for Sustainable Well-Being 2018 (STISWB 2018) under the concept of **"Moving Towards Smart and Sustainable Technologies"**.

The Faculty of Engineering, Rajamangala University of Technology Phra Nakhon, is pleased to host the 10th STISWB 2018. The conference will be held at the Don Chan Palace Hotel and Convention, Vientiane, Lao PDR, between 11th – 13th July, 2018.

THE 10th STISWB 2018
Moving Towards Smart
and Sustainable Technologies



The 10th International Conference on Science, Technology and Innovation for Sustainable Well-Being 2018

STISWB 2018 TOPICS CONSIDERED

1. Education

- Engineering Business & Management
- Engineering Education
- Industrial and Technical Education
- Sports and Exercise Science
- Education Science
- Related Topics

2. Engineering

- Agricultural, Biological and Food Engineering
- Alternative Energy and Combustion
- Agricultural Farm Machinery
- Applied Mechanics and Materials
- Biomechanics, Robotics and Controls
- Civil and Environmental Engineering
- Computational and Simulation Techniques
- Computer Engineering
- Electrical Engineering
- Electronics and Telecommunication Engineering
- Mechanical Engineering
- Mapping, GIS and Remote Sensing
- Railway and Transport Engineering
- Disaster Engineering
- Industrial Engineering
- Logistics Engineering & Management
- Related Topics

3. Sciences and Technology

- Environmental Management
- Energy Technology and Management
- Manufacturing and Process Management
- Food Science and Biotechnology
- Advanced Materials and Nanotechnology
- Related Topics.



The 10th International Conference on Science, Technology and Innovation for Sustainable Well-Being 2018

The History of STISWB Conferences

STISWB	Date	Venue	Organizers
STISWB I	July 23 - 24, 2009	Pullman Raja Orchid Hotel, Khon Kaen, Thailand	MSU, Thailand KKU, Thailand UBU, Thailand SUT, Thailand
STISWB II	August 12 - 15, 2010	Quang Binh University, Vietnam	MSU, Thailand QBU, Vietnam
STISWB III	August 12 -15, 2011	The University of Danang, Vietnam	SU, Thailand UD, Vietnam
STISWB IV	August 10-12, 2012	The Zign Hotel, Pattaya, Thailand	KMUTNB, Thailand
STISWB V	September 4-6, 2013	The grand Luang Prabang Hotel&Resort, Luangprabang, Laos	MSU, Thailand NUOL, Laos Souphanouvong University, Laos
STISWB VI	August 28-30, 2014	Apsara Ankor Resort & Conference, Siem Reap, Kingdom of Cambodia	RMUTI, Khonkean Campus, Thailand
STISWB VII	July 30 – Aug 2, 2015	Nakhon Pathom, Thailand	SU, Thailand
STISWB VIII	June 15-17, 2016	Yangon, Myanmar	SU, Thailand
STISWB IX	June 26 – 28, 2017	Kunming University of Science and Technology, Kunming, China	RMUTL, Thailand
STISWB X	July 11 – 13, 2018	The Don Chan Palace Hotel & Convention, Vientiane, Lao PDR.	RMUTP, Thailand



STISWB2018 Committees

International Organizing Committee

1. Prof. Kambiz Vafai
Faculty of Engineering, University of California at Riverside, CA, USA
2. Prof. Helen Lu
Faculty of Biomedical Engineering, Columbia University, NY, USA.
3. Prof. Lisa Konofagou
Faculty of Biomedical Engineering, Columbia University, NY, USA.
4. Prof. Van C. Mow
Faculty of Biomedical Engineering, Columbia University, NY, USA.
5. Prof. Dr. Aliakbar Akbarzadeh
School of Aerospace, Mechanical and Manufacturing Engineering, RMIT University, Australia
6. Prof. Dr. R. B. Dobson
Department of Mechanical Engineering, University of Stellenbosch, South Africa
7. Prof. Dr. Masahide Murakami
Institute of Engineering Mechanics and Systems, University of Tsukuba, Japan
8. Prof. Dr. Heiko Gerhauser
Energy Research Centre of the Netherlands (ECN), Netherlands
9. Prof. Dr. Le Kim Hung
Danang University of Technology, Viet Nam
10. Assoc. Prof. Dr. Nguyen Huynh
Phan Quang Binh University, Viet Nam
11. Prof. Dr. Le Thi Hoai Thu
Quang Binh University, Viet Nam
12. Dr. Bui Khac Son
Quang Binh University, Viet Nam
13. Assoc. Prof. Dr. John Morris
University of Auckland, New Zealand
14. Prof. Dr. Yulong Ding
School of Chemical Engineering, University of Birmingham, UK



STISWB2018 Committees

15. Prof. Dr. Yun-Hwa P Hsieh
Florida State University, USA
16. Prof. Dr. Hideaki Imura
Kumamoto University, Japan
17. Prof. Dr. Joon Hong Boo
Hankuk Aviation University, Korea
18. Assoc. Prof. Dr. Buddhi Lamsal
Iowa state university, USA.
19. Prof. Dr. Pradit Terdtoon
Mahasarakham University, Thailand
20. Prof. Dr. Wu Xing
Kunming University of Science and Technology, China
21. Prof. Dr. Sang Yong Lee
Korea Advanced Institute of Science and Technology, Korea
22. Assoc. Prof. Dr. Nguyen Truong Thinh
Ho Chi Minh city University of Technology and Education, Viet Nam
23. Prof. Dr. Akihiro Nakanou
National Institute of Advanced Industrial Science and Technology, Japan
24. Prof. Dr. Nobuhiro Kimura
Cryogenics Science Center, High Energy Accelerator Research Organization, Japan
25. Prof. Dr. Hirotaka Nakai
Accelerator Laboratory, High Energy Accelerator Research Organization, Japan
26. Assoc. Prof. Dr. Chao, Chun-Tang
Southern Taiwan University of Science and Technology, Taiwan
27. Asst. Prof. Dr. See Aaron Raymond Ang
Southern Taiwan University of Science and Technology, Taiwan
28. Dr. Noel Kristian
Singapore Polytechnic, Singapore



STISWB2018 Committees

Local Co-Organizing Committee

1. **Asst. Prof. Dr. Wirote Ritthong**
Rajamangala University of Technology Phra Nakhon, Thailand
2. **Assoc. Prof. Dr. Anongrit Kangrang**
Mahasarakham University, Thailand
3. **Asst. Prof. Dr. Nitipong Saponpongpiat**
Silpakorn University, Thailand
4. **Asst. Prof. Dr. Krisadakorn Buddachan**
King Mongkut's University of Technology North Bangkok, Thailand
5. **Assoc. Prof. Dr. Phrut Sakulchangsattajai**
Chiang Mai University, Thailand
6. **Dr. Narong Srihajong**
Rajamangala University of Technology Isan, Thailand
7. **Dr. Narin Koolnapadol**
Rajabhat Rajanagarindra University, Thailand
8. **Asst. Prof. Dr. Numpon Panyoyai**
Maejo University, Thailand
9. **Asst. Prof. Dr. Wirote Ritthong**
Rajamangala University of Technology Phra Nakhon, Thailand
10. **Asst. Prof. Dr. Yanyong Inmuong**
Mahasarakham University, Thailand
11. **Asst. Prof. Dr. Pracha Yeunyongkul**
Rajamangala University of Technology Lanna, Thailand



STISWB2018 Committees

Host Organizing Committee

Steering Committee

1. Asst. Prof. Dr. Wirote Ritthong (Host Organizing Chair)
2. Dr. Natworapol Rachsirivatcharabul
3. Mr. Korn Puangnak
4. Asst. Prof. Pichaya Daraphong
5. Asst. Prof. Kullayot Suwataroj
6. Mr. Pichet Jiraprasertwong
7. Mr. Nilamit Nilas
8. Mr. Suttipong Jumroonrut
9. Ms. Aphichata Thongrak

Finance Chair

Mr. Korn Puangnak

Sponsor Chair

Dr. Natworapol Rachsirivatcharabul

General Chair

Plt. Off. Dr. Ponlakit Jariyatantiwait

Technical Program Chair

1. Plt. Off. Dr. Ponlakit Jariyatantiwait (Engineering)
2. Asst. Prof. Kullayot Suwataroj (Education)
3. Dr. Supachai Lakkam (Science and Technology)

Registration Chair

Mr. Korn Puangnak

Publication Chair

Plt. Off. Dr. Ponlakit Jariyatantiwait

Secretariat

Miss. Supaporn Latum



The 10th International Conference
on Science, Technology and Innovation
for Sustainable Well-Being 2018

STISWB 2018

Moving Towards

Smart & Sustainable Technologies



The 10th International Conference on Science, Technology and Innovation for Sustainable Well-Being 2018

11th - 13th July, 2018

@ **Vientiane, Lao PDR.**

Don Chan Palace Hotel

& Convention



CALL FOR PAPERS

Participants Receive 12 PDU.

of the Continuing Professional Development (CPD.)
for engineer, certified by the Council of Engineers, Thailand



IMPORTANT DATES

- ✦ Full Paper Submission Deadline 4th May, 2018
- ✦ Full Paper Accepted Notification 25th May, 2018
- ✦ Revised Full Paper Deadline 15th June, 2018
- ✦ Payment Registration Deadline 22nd June, 2018
- ✦ Final Program Announcement 29th June, 2018
- ✦ Conference Dates 11th - 13th July, 2018



Prof. Dr. Kosin Chamnongthai

King Mongkut's University
of Technology Thonburi

**KEYNOTE
SPEAKERS**



Assoc. Prof. Dr. Yodchanan Wongsawat

Mahidol University, Thailand



Prof. Dr. Prayoot Akkaraekthalin

King Mongkut's University
of Technology North Bangkok



STISWB2018 TOPICS CONSIDERED



1. Engineering

- Agricultural, Biological and Food Engineering
- Alternative Energy and Combustion
- Agricultural Farm Machinery
- Applied Mechanics and Materials
- Biomechanics, Robotics and Controls
- Civil and Environmental Engineering
- Computational and Simulation Techniques
- Computer Engineering
- Disaster Engineering

- Electrical Engineering
- Electronics and Telecommunication Engineering
- Industrial Engineering
- Logistics Engineering & Management
- Mechanical Engineering
- Mapping, GIS and Remote Sensing
- Railway and Transport Engineering
- Related Topics



2. Education

- Engineering Education
- Engineering Business & Management
- Education Science
- Industrial and Technical Education
- Sports and Exercise Science
- Related Topics



3. Science and Technology

- Advanced Materials and Nanotechnology
- Environmental Management
- Energy Technology and Management
- Food Science and Biotechnology
- Manufacturing and Process Management
- Related Topics.

WWW.STISWB2018.ORG

Contact Organizer:

*Faculty of Engineering,
Rajamangala University of Technology Phra Nakhon*

Tel. (+66) 2836-3000 Ext. 4118 1381 Pracharat1 Road, Bangsue,
E-mail : STISWB2018@gmail.com Bangkok 10800, Thailand



www.stiswb2018.org

REGISTRATION FEES (1 USD. For 34 THB.)

Regular Registration	Types	THB.	USD.
General	Speaker	10,400	310
	Non - Speaker	7,200	210
Staff / Student	Speaker	6,500	190
	Non - Speaker	5,100	150



REVIEWERS LIST

EDUCATION

1. Assoc. Prof. Dr. Krischonme Bhumkittipich Rajamangala University of Technology Thanyaburi
2. Assoc. Prof. Dr. Nattachote Rugthaicharoencheep Rajamangala University of Technology Phra Nakhon
3. Asst. Prof. Dr. Supavich Pengnate North Dakota State University
4. Asst. Prof. Dr. Khanista Namee King Mongkut's University of Technology North Bangkok
5. Asst. Prof. Dr. Rungaroon porncharoen Rajamangala University of Technology Phra Nakhon
6. Asst. Prof. Dr. Thanya Parametthanuwat King Mongkut's University of Technology North Bangkok
7. Asst. Prof. Dr. Vallop Phupa Ramangala University of Technology Phra Nakhon
8. Asst. Prof. Dr. Wiharn Deepanya Rajamangala University of Technology Phra Nakhon
9. Asst. Prof. Dr. Kullkanit Thongngao Rajamangala University of Technology Thungyai
10. Asst. Prof. Dr. Nattapong Phanthuna Rajamangala University of Technology Phra Nakhon
11. Dr. Watthana Suksiripakonchai Srinakharinwirot University
12. Dr. Pornpat Sirithumgul Rajamangala University of Technology Phra Nakhon
13. Dr. Ponlakit Jariyatantiwait Rajamangala University of Technology Phra Nakhon
14. Dr. Pitsanu Tongkhaw Rajamangala University of Technology Phra Nakhon
15. Dr. Pakamas Choosit Rajamangala University of Technology Phra Nakhon
16. Asst. Prof. kullayot suwantaraj Rajamangala University of Technology Phra Nakhon
17. Asst. Prof. Somkieat Thongkeaw Rajamangala University of Technology Phra Nakhon
18. Asst. Prof. Aroon Charangsut Rajamangala University of Technology Phra Nakhon
19. Asst. Prof. Supawud Nedphokaew Rajamangala University of Technology Phra Nakhon
20. Asst. Prof. Udomdeja Polyium Rajamangala University of Technology Phra Nakhon



REVIEWERS LIST

ENGINEERING

1. Prof. Dr. Sutthisak Phongthanapanich King Mongkut's University of Technology North Bangkok
2. Assoc. Prof. Dr. Sarawuth iEMAT
3. Assoc. Prof. Dr. Nattachote Rugthaicharoencheep Rajamangala University of Technology Phra Nakhon
4. Assoc. Prof. Dr. Krischonme Bhumkittipich Rajamangala University of Technology Thanyaburi
5. Assoc. Prof. Dr. I Dewa Made Cipta Santosa Bali State Polytechnic
6. Assoc. Prof. Dr. Narin Watanakul Thammasat university
7. Assoc. Prof. Ping Jack Soh Universiti Malaysia Perlis
8. Asst. Prof. Dr. Chonlatee Photong Mahasarakham University
9. Asst. Prof. Dr. Jukkrit Kluabwang Rajamangala University of Technology Lanna Tak
10. Asst. Prof. Dr. Khanista Namee King Mongkut's University of Technology North Bangkok
11. Asst. Prof. Dr. Sutheera Puntheeranurak King Mongkut's Institute of Technology Ladkrabang
12. Asst. Prof. Dr. Krawee Treeamnuk Suranaree University of Technology
13. Asst. Prof. Dr. Nattapong Phanthuna Rajamangala University of Technology Phra Nakhon
14. Asst. Prof. Dr. Prasert Wirotcheewan Rajamangala University of Technology Phra Nakhon
15. Asst. Prof. Dr. Rungaroon porncharoen Rajamangala University of Technology Phra Nakhon
16. Asst. Prof. Dr. Sakhon Woothipatanapan Rajamangala University of Technology Phra Nakhon
17. Asst. Prof. Dr. Sanya Khunkhao Rajamangala University of Technology Phra Nakhon
18. Asst. Prof. Dr. Suriya Kaewarsa Rajamangala University of Technology Isan
19. Asst. Prof. Dr. Thanya Parametthanuwat King Mongkut's University of Technology North Bangkok
20. Asst. Prof. Dr. Vallop Phupa Ramangala University of Technology Phra Nakhon
21. Asst. Prof. Dr. Wiharn Deepanya Rajamangala University of Technology Phra Nakhon
22. Asst. Prof. Dr. Wuttiwat Kongrattanaprasert Rajamangala University of Technology Krungthep
23. Asst. Prof. Dr. Pracha Yeunyongkul Rajamangala University of Technology Lanna
24. Dr. Att Phayomhom Metropolitan Electricity Authority (MEA)
25. Dr. Chaoyong Soemphol Mahasarakham University



REVIEWERS LIST

26. Dr. Chatkaew Jariyatantiwait	Rajamangala University of Technology Phra Nakhon
27. Dr. Winyou Silabut	Rajamangala University of Technology Isan
28. Dr. Varinthorn Boonyaroj	Rajamangala University of Technology Phra Nakhon
29. Dr. Weeranut Intagun	Silpakorn University
30. Dr. Surachai Karnjanakom	Rajamangala University of Technology Phra Nakhon
31. Dr. Sovan Mukherjee	Memorial Sloan Kettering Cancer Center
32. Dr. Supachai Lakkam	Rajamangala University of Technology Phra Nakhon
33. Dr. Pornpat Sirithumgul	Rajamangala University of Technology Phra Nakhon
34. Dr. Pitsanu Tongkhow	Rajamangala University of Technology Phra Nakhon
35. Dr. Ponlakit Jariyatantiwait	Rajamangala University of Technology Phra Nakhon
36. Dr. Pakamas Choosit	Rajamangala University of Technology Phra Nakhon
37. Dr. Krisada Lekdee	Ramangala University of Technology Phra Nakhon
38. Dr. Jittimon Wongsabangkok	King Mongkut's University of Technology North
39. Dr. Kiattisin Kanjanawanishkul	Maharakham University
40. Asst. Prof. Aroon Charangsut	Rajamangala University of Technology Phra Nakhon
41. Assoc. Prof. Dr. Azremi Abdullah Al-Hadi	Universiti Malaysia Perlis
42. Asst. Prof. kullayot suwantaroj	Rajamangala University of Technology Phra Nakhon
43. Asst. Prof. Somkieat Thongkeaw	Rajamangala University of Technology Phra Nakhon
44. Asst. Prof. I Made Rajendra	Bali State Polytechnic - Indonesia
45. Asst. Prof. Padipan Tinprabath	Ramangala University of Technology Phra Nakhon
46. Asst. Prof. Songwut Mongkonlerdmanee	Rajamangala University of Technology Phra Nakhon
47. Asst. Prof. Sopa Cansee	Maharakham University
48. Asst. Prof. Supawud Nedphokaew	Rajamangala University of Technology Phra Nakhon



REVIEWERS LIST

SCIENCES AND TECHNOLOGY

1. Assoc. Prof. Dr. Krischonme Bhumkittipich Rajamangala University of Technology
Thanyaburi
2. Assoc. Prof. Dr. Nattachote Rugthaicharoencheep Rajamangala University of Technology Phra
Nakhon
3. Asst. Prof. Dr. Chonlatee Photong Mahasarakham University
4. Asst. Prof. Dr. Khobkul Nongnutch Rajamangala University of Technology Isan
5. Asst. Prof. Dr. Suriya Kaewarsa Rajamangala University of Technology Isan
6. Asst. Prof. Dr. Thanya Parametthanuwat King Mongkut's University of Technology North
Bangkok
7. Asst. Prof. Dr. Vallop Phupa Ramangala University of Technology Phra Nakhon
8. Asst. Prof. Dr. Pracha Yeunyongkul Rajamangala University of Technology Lanna
9. Dr. Varinthorn Boonyaroj Rajamangala University of Technology Phra Nakhon
10. Dr. Weeranut Intagun Silpakorn University
11. Dr. Pitsanu Tongkhow Rajamangala University of Technology Phra Nakhon
12. Dr. Ponlakit Jariyatantiwait Rajamangala University of Technology Phra Nakhon
13. Dr. Surachai Karnjanakom Rajamangala University of Technology Phra Nakhon
14. Dr. Pakamas Choosit Rajamangala University of Technology Phra Nakhon
15. Dr. Jittimon Wongsu King Mongkut's University of Technology North
Bangkok
16. Asst. Prof. Aroon Charangsut Rajamangala University of Technology Phra Nakhon
17. Asst. Prof. Supawud Nedphokaew Rajamangala University of Technology Phra Nakhon
18. Asst. Prof. kullayot suwantaraj Rajamangala University of Technology Phra Nakhon
19. Asst. Prof. Sopa Cansee Mahasarakham University
20. Asst. Prof. Woravith Chansuvarn Rajamangala University of Technology Phra Nakhon
21. Asst. Prof. Udomdeja Polyium Rajamangala University of Technology Phra Nakhon



List of Participating Organizations

No.	Organizations	Number of Papers
1	Chiang Mai University	4
2	Chiangmai Technical College Chiangmai, Thailand	1
3	King Mongkut's University of Technology North Bangkok	5
4	King Mongkut's Institute of Technology Ladkrabang	1
5	King Mongkut's University of Technology North Bangkok Prachinburi Campus	1
6	Maejo university	17
7	Maharakham University	8
8	Naresuan University	1
9	Rajamangala University of Technology Isan	2
10	Rajamangala University of Technology Isan Khon Kaen Campus	10
11	Rajamangala University of Technology Lanna	3
12	Rajamangala University of Technology Lanna Tak	4
13	Rajamangala University of Technology Lanna, Chiang Mai	1
14	Rajamangala University of Technology Phra Nakhon	22
15	Rajamangala University of Technology Thanyaburi	1
16	Rennes 1 University	1
17	Silpakorn University	25
18	South-East Asia University	1
19	Suranaree University of Technology	1
20	Uttaradit Technical College Uttaradit, Thailand	1
Total		110 papers



List of Participating Research Topics

Total number of research papers	110
--	------------

1. EDUCATION

- Engineering Business & Management	4
- Engineering Education	4
- Industrial and Technical Education	2
- Related Topics.	1

2. ENGINEERING

- Agricultural, Biological and Food Engineering	5
- Alternative Energy and Combustion	9
- Applied Mechanics and Materials	2
- Civil and Environmental Engineering	1
- Computational and Simulation Techniques	4
- Electrical Engineering	7
- Mechanical Engineering	2
- Industrial Engineering	5
- Computer Engineering	9
- Related Topics.	1

3. SCIENCES and TECHNOLOGY

- Environmental Management	4
- Energy Technology and Management	1
- Food Science and Biotechnology	3
- Related Topics.	7

Total	110
--------------	------------



CONTINUING PROFESSIONAL DEVELOPMENT (CPD)



The Continuing Professional Development (CPD) Certified by the Council of Engineers, Thailand (COE)

There are many ways to increase quality of engineers. One of the acceptances and used in many countries is the Continuing Professional Development (CPD) activities. The Council of Engineers (COE), Thailand has provided ongoing professional development of engineers already, like in the APEC and ASEAN Engineering group, which holds as an engineering agreement.

For engineers who have graduated and are working in the field of engineering, need to develop their knowledge and skills continuously. The Continuing Professional Development is one of the ways to help engineers improve their skills, professional knowledge, quality, creation, and safety. The Council of Engineers has issued regulations governing the Continuing Professional Development in B.E. 2551(2008). The differences of unit weights are identified by activities. The conceptual for getting points is counting the Professional Development Unit (PDU) units of practical hours and participated on 8 items of CPD's activities.

The COE has determined the activities which engineers can take for their CPD. Those activities are counted as the PDU and are divided into 8 items as follows:

1. Formal learning
2. Informal learning
3. Seminar, conference and meeting
4. Participation in professional activities
5. Service activities
6. Industry involvement
7. Contribution to knowledge
8. Patents



The Faculty of Engineering, Rajamangala University of Technology Phra Nakhon is accredited as a continuing professional development organization. The code of organization is number 3023, certified by the Council of Engineers (COE) on September 11th, 2017. The organizer authorizes to offer the Professional Development Unit (PDU) for participants of the 10th International Conference on Science, Technology and Innovation for Sustainable Well-Being 2018(STISWB 2018). The members of the Council of Engineers, Thailand who are participated the 10th STISWB 2018 will receive 12 PDU. **The Activity Code is: 303-00-3023-00 / 6107-001**



CONTINUING PROFESSIONAL DEVELOPMENT (CPD)



The details of CPD's activity on the 10th STISWB 2018. The Faculty of Engineering, Rajamangala University of Technology Phra Nakhon offers 12 PDU for participants, certified by the Council of Engineers (COE), Thailand.

รายละเอียดกิจกรรม			
รหัสกิจกรรม:	303-00-3023-00/6107-001		
ประเภทกิจกรรม:	ประเภทที่ 3 การเข้าร่วมสัมมนาและการประชุมทางวิชาการ หรือวิชาชีพ (seminar, conference and meeting)		
กิจกรรม:	303. การเข้าฟังการสัมมนาและการประชุมทางวิชาการหรือวิชาชีพ ระหว่างประเทศ		
ชื่อหัวข้อกิจกรรม:	The 10th International Conference on Science, Technology and Innovation for Sustainable Well-Being 2018 (STISWB2018)		
น้ำหนัก:	1.5		
รายละเอียดการจัดกิจกรรม:	The International Conference on Science, Technology and Innovation.		
สาขา:			
ประเภทกิจกรรม:	กิจกรรมทางเทคนิค		
Keyword:	อื่น ๆ		
ลักษณะงาน:	Conference		
Website:	www.stiswb2018.org		
จำนวนวิทยากร:	3		
ลำดับที่	ชื่อวิทยากร	รหัส	จำนวนชั่วโมง
1	ยศชนัน วงศ์สวัสดิ์	ไม่เป็นสมาชิก	.5
2	ประยุทธ์ อัจฉรณานัน	30561	.5
3	โกสินทร์ จ่านอง	ไม่เป็นสมาชิก	.5
วันเวลา/ค่าเข้าร่วมกิจกรรม			
จำนวนชั่วโมง:	8		
ค่า PDU:	12		
วันที่เริ่มรับสมัคร:	01 ธ.ค. 2560		
วันหมดเขตรับสมัคร:	22 มี.ย. 2561		
วันเริ่มจัดกิจกรรม:	11 ก.ค. 2561 เวลา 09.00		
วันสิ้นสุดกิจกรรม:	13 ก.ค. 2561 เวลา 17.00		
สถานที่จัดกิจกรรม:	Vientiane, Lao PDR.		
ค่าเข้าร่วมกิจกรรม:	Member	6500 บาท	
	Government	10400 บาท	
	State Enterprise	10400 บาท	
	Non Member	10400 บาท	
	Student	6500 บาท	
เอกสารประกอบ:	ไม่มีเอกสารประกอบ		
รายละเอียดผู้ติดต่อ			
ชื่อ:	Miss Pompit Sirima		
โทรศัพท์:	028363000 ext. 4181 โทรสาร: 028363000 ext. 4118		
Email:	pompit.s@mutp.ac.th		

Reference: <http://www.coe.or.th/CPD3/modules.php?name=OrgActivity1&mode=preview&id=5149>

The Activity Code: 303-00-3023-00 / 6107-001

Conference Schedule 11-13 July, 2018
The 10th International Conference on Science, Technology and Innovation for Sustainable Well-Being 2018
Hosted by Faculty of Engineering, Rajamangala University of Technology Phra Nakhon

Wednesday, July 11 th - Pre-conference meeting								
12.00 - 16.00	Registration							
13.00 - 16.00	Knowledge Management (KM) Program							
14.00 - 16.00	STISWB Network Meeting (CEO and Representatives)							
18.00 - 20.00	Welcome party							
Thursday, July 12 th - The conference day								
08.00 - 09.00	Registration							
09.00 - 09.30	Welcome speech							
09.30 - 11.00	Opening ceremony - President of Rajamangala University of Technology Phra Nakhon							
	Keynote Speakers							
	1. Prof. Dr. Kosin Chamnongthai - King Mongkut's University of Technology Thonburi, Thailand							
	2. Prof. Dr. Prayoot Akkarakethalin - King Mongkut's University of Technology North Bangkok, Thailand							
	3. Assoc.Prof. Dr.Yodchanan Wongsawat - Faculty of Engineering, Mahidol University, Thailand							
Coffee Break								
Parallel Sessions	Room 01	Room 02	Room 03	Room 04	Room 05	Room 06	Room 07	
Chairperson	Asst.Prof.Dr.Pracha Yeunpongkul	Dr.Chantima Rewlay-ngoen	Assoc.Prof.Dr.Uthen Karmnam	Dr.Supachai Lakkam	Dr.Sunya Khunkhao	Dr.Jirasak Tharajak	Dr.Chantana Papattha	
Co-chairperson	Dr.Patiwat Khomwachirakul	Dr.Surachai Karnjanakorn	Dr.Chatkaew Jariyatanitwait	Mr.Siripol Tongom	Dr.Anchalee Manosueb	Dr.Kanawut Inkaew	Mr.Kreadisak Lappanitchayakul	
11.00 - 12.00	ENG 01 - ENG 03	ENG 17 - ENG 19	ENG 31 - ENG 33	ENG 47 - ENG 49	ENG 65 - ENG 68	SCI 01 - SCI 03	EDU 01 - EDU 02	
12.00 - 13.00	Lunch							
13.00 - 14.45	ENG 04 - ENG 08	ENG 20 - ENG 23	ENG 34 - ENG 37	ENG 50 - ENG 55	ENG 69 - ENG 74	SCI 04 - SCI 08	EDU 03 - EDU 05	
14.45 - 15.00	Coffee Break							
Chairperson	Asst.Prof.Dr.Padiphan Tinprabath	Asst.Prof.Dr.Thibordin Sangsawang	Asst.Prof.Dr.Poramatr Aronmee	Dr.Krisada Lekdee	Dr.Paisan Kanthang	Dr.Jirasak Tharajak	Dr.Chantana Papattha	
Co-chairperson	Dr.Chatkaew Jariyatanitwait	Ms.Vichuda Mettanant	Dr.Ponlakit Jariyatanitwait	Dr.Therdpong Daengsi	Dr.Chanwit Prabpayak	Dr.Kanawut Inkaew	Mr.Kreadisak Lappanitchayakul	
15.00 - 17.45	ENG 09 - ENG 16	ENG 24 - ENG 30	ENG 38 - ENG 46	ENG 56 - ENG 64	SCI 17 - SCI 25	SCI 09 - SCI 16	EDU 06 - EDU 11	
18.30 - 21.30	Banquet							
Welcome speech by the conference host								
Cultural shows								
STISWB Talk - Prof.Dr.Pradit Terdtoon, Dean of Graduate School, Mahasarakham University, Thailand								
Flag transfer ceremony for the next STISWB 11 th								
Friday, July 13 th - On-Site Visiting								
08.30 - 10.00	National University of Laos							
10.00 - 12.00	Lao National Museum							
12.00 - 13.00	Lunch							
13.00	Traveling to Airport							



Table of Contents

Paper No.	Title	page
Topic : Education		
1. Engineering Business & Management		
EDU01	Knowledge and Behavioral Factors Influencing the Gas-fuel Car Owner in Making Decision to Use LPG and NGV: Case Study in Muang District, Samutprakarn Province <i>D. Ratsanasart and C. Sangvorniyotin</i>	1
EDU02	Study of Safety Behavior for Manufacturing Employees: A Case Study of Paper Pulp Factory Cluster <i>Chongrug Pariwatnanont and Chantana Sangvorniyotin</i>	4
EDU03	Factors Influencing Decision to Purchase the Design Engineering Software in Companies in Navanakorn Industrial Estate, Pathumthani Province <i>C. Sangvorniyotin D. Ratsanasart and C. Pariwatnanont</i>	8
EDU04	Performance Measurement Faculty of Engineering RMUTP for Digital University <i>Chalakorn Udomraksasakul Singkaew Pokterng Kompan Chomsamutr and Watchara Songserm</i>	12
2. Engineering Education		
EDU05	The Construction and Efficiency Finding of Instructional Package on the Topic of ASK in Digital Modulation for Applciation to Vocational Education <i>Natthawut Panitjaroen and Anchalee Panitjaroen</i>	17
EDU06	The Construction and Efficiency Finding of Instructional Package on the Module of Video and Audio Analog Optical Fiber Link <i>Anchalee Panitjaroen Hansa Khetbunphot and Natthawut Panitjaroen</i>	21
EDU07	Motives to study Bachelor of Technology Program in Engineering Business, Silpakorn University <i>Supachai Wasananon Teerachai Surachotivet and Jarut Kunanoppadol</i>	26
EDU08	Lecture and test in Moodle Platform: the Teaching Innovation on Thermo-fluid Coursework <i>Nitipong Soponpongpiat and Ittipol Thinnoiwong</i>	29
3. Industrial and Technical Education		
EDU09	Benchmark of Desired Attributes of Technology Graduates in Thailand: Basis for Improving <i>Hansa Khetbunphot Anchalee Panitjaroen and Natthawut Panitjaroen</i>	34
EDU10	The Development of the Interactive e-book on the 38 Steps Towards Enlightened Living <i>Nitigan Nakjuatong and Beesuda Daoruang</i>	38
4. Related Topics		
EDU11	Analyzing Graduate Production Costs of Faculty of Industrial and Technology Management, King Mongkut's University of Technology North Bangkok Prachinburi <i>Jumreans Srikamta and Nantiya Jantralux</i>	42



Paper No.	Title	page
Topic : Engineering		
1. Agricultural, Biological and Food Engineering		
ENG01	Effect of various conditions on ultrasonic-assisted extraction of allicin from garlic(<i>Allium Sativum</i> Linn.) <i>Suphitchaya Kalantakasuwan Yardfon Tanongkankit Jaturapatr Varith and Kanjana Narkprasom</i>	47
ENG02	Solar Drying House for Drying Herbs <i>Sakultala Wannapakhe and Khidsadakhon Booddachan</i>	51
ENG03	Temperature Distribution Inside Biochar Kiln for Biochar Production <i>Numpon Panyoyai Thanasit Wongsiriamnuay and Tipapon Khamdaeng</i>	56
ENG04	Disassembled Solar Greenhouse Dryer for Agricultural Products <i>Nattapol Poomsa-ad and Lamul Wiset</i>	61
ENG05	Effects of Drying Temperatures and Pretreatment conditions on the Drying Kinetic and Color Quality of Japanese Pumpkin Powder obtained from Hot Air Drying <i>Surwit Paengkanya Pathomphong Jumnonphan and Rarisara Impaprasert</i>	65
2. Alternative Energy and Combustion		
ENG06	Thermal Efficiency Behavior of Hot Air Production from Fluidized Bed Kiln by Waste Biomass <i>Phairoach Chunkaew</i>	70
ENG07	Investigation of Fuel Delivery of Common Rail Injector using a Volumetric Injection Meter <i>Narin Srithikarn Nimit Ratsamee Ronnachart Munsin Nawee Nuntapap Tarapong Karnjanaparichat Wasin Wongkum and Nattaporn Chaiyat</i>	74
ENG08	Improvement of physical properties of heterogeneous biomass pellets using fermented cassava rhizome and kratin-wood residue: effect of fermentation time <i>Kedsara Rattawan Weeranut Intagun and Wirojne Kanoksilapatham</i>	80
ENG09	Tank-to –Wheel Analysis of Environmental and Economic Evaluation from Passenger Cars Transportation <i>Chantima Rewlay-ngoen Siripol Tongorn and Seksan Papong</i>	85
ENG10	Effects of air staging on emission characteristics and combustion efficiency in a twin-cyclonic swirling fluidized-bed combustor firing rubberwood sawdust <i>Tananon Srisamran and Kasama Sirisomboon</i>	90
ENG11	The improvement of biomass properties by torrefaction rotary kiln <i>Nattarat Chutwiboonkun and Nattawut Tharawadee</i>	96
ENG12	Ultrasound-Assisted Acetylation of Glycerol for Triacetin Production over Green Catalyst <i>Surachai Karnjanakom Chantip Samart Guoqing Guan and Panya Maneechakr</i>	102
ENG13	An alternate numerical algorithm for minimization of unconstrained non-linear functions for Solving Combustion Equations <i>Paramust Juntarakod</i>	106
ENG14	Production of Briquette from Agricultural Residue <i>Numpon Panyoyai Samerkhwan Tantikul Tipapon Khamdaeng and Thanasit Wongsiriamnuay</i>	113



Paper No.	Title	page
3. Applied Mechanics and Materials		
ENG15	Effect of Temperature on Change of Microstructure of Hadfield Steel <i>Jirutthitikalpongsri Hirunyagird Prin Nachaisit and Yuttana Srilamai</i>	116
ENG16	Surface Improvement of SCM 440 by the Ballburnishing Technique <i>Montri Kawsuk and Sirichai Torsakul</i>	120
4. Civil and Environmental Engineering		
ENG17	Using Unmanned Aerial Vehicle Photogrammetry for Surveying a Landslide <i>Thitibhorn Phantachang and Pradit Jiagulprasert</i>	125
ENG18	A Review on Difference of Contracting for Works of Regulations on Procurement, B.E. 2535 (1992) between Government Agency and Local Government, Thailand <i>Boonruk Vanborsel and Kumpon Subsomboon</i>	130
ENG19	Efficiency of alkaline fuel cell for produce hydrogen gas, in conjunction with electric production by using PEM membrane fuel cell <i>Janjira Yatom and Natthanicha Sukasem</i>	135
ENG20	Feasibility on the Development of Power Generation using the Stainless Steel and Aluminium as Electrodes in PEM Fuel Cell Technology <i>Jirawat Leaksantad Pattarachai Noppakun and Natthanicha Sukasem</i>	141
ENG21	Optimal Rule Curves of Small Reservoir using Wind Driven Optimization and Flower Pollination Algorithm <i>Rapeepat Techarungruengsakul and Anongrit Kangrang</i>	146
ENG22	Application of Genetic Programming and Flower Pollination Algorithm for Searching Optimal Rule Curves of small reservoir <i>Ratsuda Ngamsert and Anongrit Kangrang</i>	152
ENG23	The Embodied Energy & Greenhouse Gas Emission of Residential Building in Silpakorn University, Nakhon Pathom, Thailand <i>Teerachai Surachotivet and Thibordin Sangsawang</i>	158
ENG24	Application of Optimization Techniques for Searching Optimal Reservoir Rule Curves for Medium Reservoir <i>Teerawat thongwan and Anongrit Kangrang</i>	163
ENG25	Mechanical Properties of Pavement Concrete Containing Reclaim Asphalt Aggregate <i>Somporn Leekongbub Prinya Chindaprasirtat and Patcharapol Posi</i>	169
ENG26	Consolidation Behavior of Cement and High Calcium Fly ash Stabilized Loess soil <i>Apichit Kampala Luan Suerpadgorn and Anukun Arngbunta</i>	173
5. Computational and Simulation Techniques		
ENG27	Wildfire Detect and Monitoring System using Wireless Sensor Network and Mobile Application <i>Nimit Srikamta</i>	178
ENG28	Adaptive Discrete Kirchhoff Quadrilateral Element for Thermal Bending Analysis of Thin Plate <i>Chatthanon Bhothikhun and Poramet Arromdee</i>	182
ENG29	Risk Assessment for Drought in Thailand Using Hidden Markov Models <i>Pitsanu Tongkhow and Rachadasak Supengcum</i>	188



Paper No.	Title	page
ENG30	Wurtzite-to-Rocksalt like Phase Transformations in Case of LiGaO ₂ from First principles <i>Wutthigrai Sailuam and Kanoknan Parcheruk</i>	192
6. Electrical Engineering		
ENG31	Performance Testing of Transformers used in Distribution Systems <i>S. Siriporananon B. Suechoey and N. Pringsakul</i>	196
ENG32	Implementation of Load Cycle Simulation for Studies of Loss Energy and Lifetime of Oil-Immersed Transformers <i>B. Suechoey A.Thongrak S. Siriporananon and N. Pringsakul</i>	202
ENG33	Low Cost Submarine for Under Water <i>Nattapong Phanthuna and Somkieat Thongkeaw</i>	208
ENG34	Smart Home Control Unit via Mobile Ringtone <i>Vitawat Sittakul and Nattapong Phanthuna</i>	212
ENG35	Comparison of Performance of Regenerative Power for Electric Vehicles between Single and Dual DC Motor Drive Systems <i>Suriyun Srisongkham Saharat Phuaklek Phurich Ngamkong Wilaiporn Ngermbath and Chonlatee Photong</i>	216
ENG36	Analysis of High Performance Savonius Wind Turbines for Low Speed Wind Applications <i>Kwanjai Nachaiyaphum and Chonlatee Photong</i>	220
ENG37	Design and Construction of a Simple Dual DC Motor Drive System for Three Wheel Electric Vehicles <i>Kritsada Thiangphadung Kmonchanok Adkalan Wilaiporn Ngermbath Phurich Ngamkong and Chonlatee Photong</i>	225
7. Mechanical Engineering		
ENG38	Application of Heat Pipes to cool down high power Light-Emitting Diode <i>Benjamin Gérard and Thanad Katpradit</i>	230
ENG39	Simulation of Straight Line Trajectory Planning for a Manipulator based on Modified RMRC Method <i>Supachock Tuntivivat Sarun Chattunyakit Witcha Upaphai Adisorn Jarunvorakunvong and Amnat Chenjitsiri</i>	233
ENG40	A Study of the Injury Mitigation of Pedestrians based on Head Injury Criterion Using the Lifted-up Hood Technique <i>Supachai Lakkam and Kullayot Suwantaraj</i>	237
ENG41	Simulation on Porosity of Twisted Fiber Bundle Wick <i>Jetsadaporn Simsiriwong Niti Kammuang-lue Phrut Sakulchangsattajai and Pradit Terdtoon</i>	241
ENG42	Effect of flattening of heat pipe with double heat sources on thermal resistance of grooved - fibre heat pipes <i>Wisoot Sanhan Phrut Sakulchangsattajai Niti Kammuang-lue and Pradit Terdtoon</i>	247
ENG43	Development of Remote Monitoring System of Locomotive Engine via Cloud Network for the State Railway of Thailand <i>Kullayot Suwantaraj Supachai Lakkam and Anan Tempiem</i>	251
ENG44	Mathematical Model of the Optimal Closed-loop Pulsating Heat Pipe Used in an Evacuated Glass Tube Solar Water Heater <i>Methida Siritan Phrut Sakulchangsattajai Niti Kammuang-lue and Pradit Terdtoon</i>	255



Paper No.	Title	page
ENG45	Effects of using a solid desiccant dehumidifier with an air conditioner on energy consumption <i>Phornrak Wangnamjai and Thosapon Katejanekarn</i>	260
ENG46	Thermal Comfort of People in Textile Factories <i>Suthimon Kuirat and Thosapon Katejanekarn</i>	268
ENG47	Effect of drying temperature on colour and anthocyanin contents in purple corn kernel <i>Dhetsuwan Khum-oh Suparerk Charmongkolpradit Bhuchiss Tanwanichkul and Wichien Sang-aroon</i>	276
ENG48	Performance Limit of Closed-Loop Pulsating Heat Pipe Filled with Water-Ethanol Blended Working Fluid <i>Adisak Janthothai Niti Kammuang-lue Phrut Sakulchangsattajai and Pradit Terdtoon</i>	281
ENG49	A Study of Geo-polymer Concrete by Using Waste Powder Coating <i>Pawin Kantawong Parkpoom Jarupoom Pracha Yeunyongkul Pasinee Siriprapa and Watcharee Funfuenha</i>	286
ENG50	Simulation of molasses cooling using carbon steel thermosyphon heat pipe heat exchanger <i>Thanasit Wongsiriamnuay Tipapon Khamdaeng Pisuthi klinkajorn Nyanakorn Sutassanamarlee Numpon Panyoyai Passawat atcharadumrongsak and Taweesuk Taweewitayakarn</i>	290
ENG51	Review on Heat Transfer and Pressure Drop in Circular Tube with Twisted Tape <i>Kittisak Khuwaranyu and Pongsiri Jaruyanon</i>	294
ENG52	Experimental Determination of Discharge Coefficient of Through Rectangle Trapezoid Shape and Triangle Weir <i>Nasru Tuenga Rotjapun Nirunsin Churat Thararux and Tanate Chaichana</i>	303
ENG53	Effect of blade radius to characteristics of undershot water wheel <i>Muhammadkhori Hayibaka Rotjapun Nirunsin Churat Tararuk and Tanate Chaichana</i>	308
ENG54	Computational Simulation on Hydrodynamics Behaviour of Air-Sand Bed in Twin Cyclonic Fluidized-bed Combustor <i>Poramet Arromdee Kasama Sirisomboon and Chatthanon Bhothikhun</i>	312
ENG55	Energy Consumption Evaluated of Compact Solar Drying Chamber <i>Sivapong Phetsong Vichuda Mettanant and Nantawatana Weerayuth</i>	317
ENG56	Study of Cooling of Compressors in Underground Wells <i>Boonrueang Ponil Taweesak Taweewithyakarn Pracha Yeunyongkul and Ronnachart Munsin</i>	322
ENG57	Numerical Study of High-Moisture Parboiled Paddy Drying in an Impinging Stream Dryer <i>Patiwat Khomwachirakul and Wirote Ritthong</i>	328
ENG58	Braking Performance Comparison between Hole Profiles on Brake Rotors under Various Operating Temperatures <i>Siripol Tongom Songwut Mongkonlerdmanee and Chaiyot Damrongkijkosol</i>	334
ENG59	A Study Performance of Split Type Air-Condition System using 5 Plus Technology <i>Wirote Ritthong Watcharin Pachittyen Patiwat Khomwachirakul and Nutthawut Singthuean</i>	338



Paper No.	Title	page
8. Industrial Engineering		
ENG60	A Study on the mechanical properties of polypropylene at different mixing ratios by molding test pieces according to ASTM D638-10 and D256-10 <i>Thawachchai Chattamnan Prasong Kankaew Prasit Phangphet and Jack Chum-in</i>	342
ENG61	GEE and LMM with Spatial Effects for Cassava and Rubber Yields in Thailand <i>Krisada Lekdee and Pornpit Sirima</i>	346
ENG62	Comparative Eco-efficiency of Ferrous and Non-Ferrous Parts Manufacturer : a Case Study of Part Manufacturing Industry in Thailand <i>Suwat Paengteerasukkamai and Natworapol Rachsirivatcharabul</i>	350
ENG63	An Ergonomic Risk Improvement in a Hard Disk Drive Production Process <i>Thanapon Jilao Wanchai Leelakaweewong Kedsarin Phoosup Phuwisa Phetchuay and Nutthipong Vilaiyawong</i>	354
ENG64	Designing Fixture to Reduce Loss During Stopper Ring Assembly: A Case Study of Automotive Parts Factory <i>Sukanya Cherdchoongam and Kullanan Lakul</i>	359
9. Computer, Electronics and Telecommunication Engineering		
ENG65	postal alert and security system via line application <i>Sunthorn Wiriya and Chayakorn Sripichetkul</i>	364
ENG66	A Talking Device of Weight and Height for the Visually Impaired Students <i>Upady Hatthasin</i>	368
ENG67	The Realization of Four-mode First-order Allpass Filter Based-on CCCCTAs <i>Thitiporn Janda Wichcha Onsa-ard and Adirek Jantakun</i>	372
ENG68	Electrochromic properties of WO ₃ thin film <i>Sanya Khunkhao Aphichata Thongrak and Korn Puangnak</i>	377
ENG69	Load Sharing and Fault Tolerant Systems over Multiple Inter-Domain Paths <i>Khanista Namee and Jirawat Paiboon</i>	383
ENG70	Voltage Controlled Sinusoidal Oscillator Based-on Commercially Available VDGA's <i>Songyos Rungsa Adirek Jantakun and Thitiporn Janda</i>	389
ENG71	Electrical Power Consumption Monitoring and Control of Appliances with IoT <i>Wanapun Waiyawut</i>	395
ENG72	A Circularly Polarized Loop Antenna with Reflector for RFID Handheld Reader <i>Kittima Lertsakwimarn and Chuwong Phongcharoenpanich</i>	399
ENG73	MISO Current-mode Universal Biquadratic Filter Using VDCC <i>Pukanit Thuibuengchim and Saweth Hongprasit</i>	403



Paper No.	Title	page
10. Related Topics		
ENG74	Development of School Bus Passenger Notification System Using RFID and Arduino Module <i>Therdpong Daengsi Praveen Maiget and Pongpisit Wuttidittachotti</i>	407
Topic : Sciences and Technology		
1. Environmental Management		
SCI01	Study of Greenhouse Gases Emission and Storage of Suranaree University of Technology, Thailand <i>Wichayanee Puttipiriyangkul and Sudjit Karuchit</i>	412
SCI02	Investigating the Role of Factors Determining Drainage System Performance for Water-Efficient Toilet <i>Anurak Kusolchoo and Wichitra Singhirunnusorn</i>	417
SCI03	Health risks due to radon in groundwater at Amphoe Muang Maha Sarakham <i>Vitsanusat Atyotha and Junthara Somtua</i>	423
SCI04	Estimation of attenuation coefficient of solar radiation in the atmosphere of Thailand <i>Sayan Phokate</i>	427
2. Energy Technology and Management		
SCI05	Feasibility on the Utilization of Agricultural Unused Banana Trees as the Feedstock for the Ethanol Fermentation <i>Natthanicha Sukasem and Pawinee Phetnok</i>	430
SCI06	Enhancement of Hydrogen Production under Alkaline Condition using Various Electrode Materials and Shape Types <i>Pattarachai Noppakun Jirawat Leaksantad and Natthanicha Sukasem</i>	436
SCI07	Evaluation of Acid and Alkaline Pretreatments, to Enhance Enzymatic Hydrolysis and Fermentation Ethanol by Agricultural Corn Cob. <i>Pawinee Phetnok and Natthanicha Sukasem</i>	440
SCI08	Simple PV-Slat Window Control Method for Net-Zero Buildings <i>Vichuda Mettanant and Sivapong Phetsong</i>	446
SCI09	The Study of Knowledge, Understanding, and Behavior on Electric Power in Household in Muang District, Nakhon Pathom Province <i>Kittisak Khuwaranyu and Duangkamol Ruen-ngam</i>	449
SCI10	Fuzzy Logic Concepts for Investment Decision Making: A review <i>P. Samartkit P. Tongard and S. Pullteap</i>	455
SCI11	Development of a Capital Investment Decision Function via a Spreadsheet Program: A Case Study of LED T8 Production in Thailand Industry <i>T. Tanongtanachai G. Smithisup and S. Pullteap</i>	461
SCI12	Biogas Production from Wastewater of Yeast Fermentation with Microorganism under Mesophilic Condition <i>Thanatcha Santhadkha Teerasak Hudakorn and Noppong Srirakul</i>	465
SCI13	Using closed loop oscillating heat pipe for cooling battery in charging process <i>Poomin Krisangsri Teerasak Hudakorn and Noppong Srirakul</i>	470



Paper No.	Title	page
SCI14	Biogas Production from Water Hyacinth Leaf and Petiole co-digestion with Microorganism under Mesophilic Condition <i>Chessadabhorn Kitjettanee and Teerasak Hudakorn</i>	475
SCI15	A review of thermochemical heat storage <i>Aumarit Panthai Teerasak Hudakorn and Pongsiri Jaruyan</i>	480
3. Food Science and Biotechnology		
SCI16	Microbial production of syrup from broken organic jasmine rice grain <i>Kanokwan Tandee Chananya Ramanan Pattayamon Mekyapisit and Junjira Wunchana</i>	486
SCI17	Production of Yanang Leaves (<i>Tiliacora triandra</i>) Powder by Drying Techniques <i>Jittimon Wongsas and Suchada Sadang</i>	492
SCI18	Development of local Thai traditional cough drop <i>Kanokwan Sathonghon Kewalin Poonoppakhun and Wiwat Wangcharoen</i>	496
4. Related Topics		
SCI19	Surface Modification of Perlite by Using Silane for the Enhancement of Heat Aging Resistance of Natural Rubber Vulcanisates <i>Tithinun Rattanaplome and Napat Chantaramee</i>	500
SCI20	Green Natural Rubber Foam filled with Spent Coffee Grounds <i>Worawan Pechurai Sitthinan Saengdian and Wanichaya Chairuen</i>	505
SCI21	A Spacecraft Trajectory Optimization and Modified Local Search Algorithm <i>Jukkrit Kluabwang Sawat Yukalang Amorn Onkrong and Santipab Kotthale</i>	511
SCI22	Natural rubber latex foam for seedling <i>Philaiwan Pornprasit and Aroonsri Aiemrum</i>	515
SCI23	A Solution of Tsunami Wave by Using the Modified Adomian Decomposition Method <i>Jeerawan Saelao and Nopporn Patcharaprakiti</i>	520
SCI24	Dynamic Capability Assessment <i>Jarut Kunanoppadol and Supachai Wasananon</i>	524
SCI25	Building a Crack Processing Toolkit <i>Wangwon Khorchaiyphurn John Morris Krit Chaimoon Sahalaph Homwuttiwong and Preetham Kumar Konda</i>	529



EDUCATION

- Engineering Business & Management
- Engineering Education
- Industrial and Technical Education
- Sports and Exercise Science
- Education Science
- Related Topics





Knowledge and Behavioral Factors Influencing the Gas-fuel Car Owner in Making Decision to Use LPG and NGV: Case Study in Muang District, Samutprakarn Province

D. Ratsanasart*, C. Sangvornyotin
Department of Mechanical Engineering, Silpakorn University
Nakhon Prathom, Thailand
*E-mail: dechaphanbkk@gmail.com

Abstract—This research was aimed at exploring knowledge and behavioral factors for the gas car owner in making decision to use LPG and NGV. Referring to Yamane sample calculation and type of sample organizations, the research was conducted to 400 car owner in Muang district. The data was collected by questionnaire and analyzed by mean, SD, Chi-Square, t-Test, One-way ANOVA and Scheffe post hoc analysis at 0.05 level of significance.

The research findings indicated that most respondents had knowledge and understanding on gas-fuel setting car at medium level while the Chi-Square showed that the knowledge and understanding level was depended on three major elements type of car, type of fuel, and maximum capacity of gas per gallon. Referring to the comparison analysis between behavior and attitude level, it was found the major difference in type of fuel. Eventually, the result of comparison between knowledge and attitude level revealed that there were difference in two factors convenience and satisfaction at .05 significance level of statistical difference.

Keywords— Behavior, Decision Making, LPG and NGV

I. INTRODUCTION

Currently, in Thailand, there have been two types of renewable energy which have increasingly been replaced as fuel oil -- Liquefied Petroleum Gas (LPG) and Compressed Natural Gas (CNG). Both energy have also been called as Natural Gas for Vehicle or NGV. One of the major reasons for their becoming popular is the fluctuated and unanticipated global crude oil price which really affects fuel oil price in Thailand. According to oil price compared between 2005 and 2015 by PTT Public Company, it can be seen that the price of Gasoline 95 rises from 20.09 THB/liter in 2005 to 31.76 THB/liter in 2015 whereas that of Diesel rises from 14.59 THB liter to 23.69 THB/ liter Energy Policy and Planning Office Ministry of Energy [1]

II. METHODOLOGY

Research Objective to identify the knowledge and behavioral factors in gas-fuel car owner in making decision to use LPG or NGV. Research Benefits to understand on the knowledge and behavioral factors in gas-fuel car owner in making decision to use LPG or NGV. Research Hypothesis the difference in knowledge and behavioral factors in gas-fuel car owner significantly affect the different opinion in making decision to use gas fuel. This study was quantitative research which the data was collected from the people who lives in Muang district, Samutprakarn province. The population was 113,545 Department of Provincial Registration, Department of Government, Ministry of Interior [2] and according to Yamane's sample calculation, the researcher finalized the sample group to the 400 gas-fuel car owner in Muang district, Samutprakarn province at 95% level of confidence and $\pm 5\%$ margin of error In this research, the researcher designed the questionnaire by research objective and research framework. This consists of five main parts – personal information; customer behavior in using gas-fuel car; knowledge and understanding on gas-fuel car, attitude towards decision making to use car-fuel car; and open-ended suggestion. Data Analysis the descriptive statistics was analyzed in terms of frequency, mean, and SD while the inference statistics was used as Parametric Inference which consists of Chi Square, t-Test, Analysis of Variance: ANOVA, and Scheffe post hoc analysis.

III. LITERATURE REVIEW

Engel [3] defined customer behavior as any action to acquire the consumption and purchasing the product or service as well as decision making before and after the action. Siriwan Serirat [4] also proposed that customer's purchasing behavior as the action of purchasing in the end customer for himself/ herself or for their household. Prin Laksitanont [5] stated that the customer behavior is the action by someone directly related to providing and utilizing products which includes the decision making process before the action and relatively leads to the



action. Simon [6] indicated that the decision making is the process which consists of three main elements – detecting opportunity to make decision, designing possible solutions, and finding out the most suitable solution. Sciffman and Kanuk [7] defined the decision making process as choosing products from more than two options based on emotions (cognitive) and physical appearance. [8] proposed that decision making is to demonstrate behavior to respond any problems on making decision for further action. Siriwan Serirat and Amornsak Boonrueng [9] also defined marketing mix as business strategy which influences to customer behavior in terms of product, price, place, promotion. Seri Wongmontha [10] indicated that marketing mix is the ability to provide product to serve the targeted group of customer in reasonable and cost-efficient price so that eventually customer is willing to purchase. Leung [11] investigated the renewable energy vehicles and LPG vehicles in China and Hong Kong and found that more than 80% of vehicles in Guangzhou had changed fuel to LPG due to clean energy, less pollution emission, and reasonable price. Bischoff [12] also monitored the situation in using LPG in Ghana and concluded that LPG could serve the user needs in terms of reasonable price and cost saving.

IV. RESULTS AND DISCUSSION

Referring to research findings, it could be seen as follows:

For Chi-Square, it was indicated that the knowledge and understanding on gas-fuel setting car depends on behavior in using gas-fuel setting car as shown in Table 1.

TABLE I. CHI-SQUARE FOR RELATIONSHIP BETWEEN BEHAVIOR IN USING GAS-FUEL SETTING CAR AND KNOWLEDGE AND UNDERSTANDING ON GAS-FUEL CAR

Behavior in Using Gas-fuel Setting Car	Pearson Chi-Square
Car brand	0.36
Car type	0.00*
Fuel type	0.00*
Year of service since registration	0.20*
Gas maximum capacity	0.00*

*At 0.05 statistical level of significance

From the Chi-Square in table 1, it was seen that there was relationship between knowledge and understanding on gas-fuel setting car and behavior in using gas-fuel setting car in terms of car type, fuel type, and gas maximum capacity while there was no relationship with other factors at 0.05 level of significance.

In addition, it was found the difference between behavior and attitude in using gas-fuel setting car as table 2.

TABLE II. THE RESULT OF DATA COMPARISON ON FACTORS INFLUENCING THE DECISION TO PURCHASE DESIGN ENGINEERING SOFTWARE BY SCHEFFÉ'S METHOD

THE REGISTERED CAPITAL	\bar{x}	< 50 MBHT.	50 - 200 MBHT.	> 200 MBHT.
		2.94	3.32	3.89
< 50 MBHT.	2.94	-	-0.39	-0.96*
50 - 200 MBHT.	3.32		-	-0.57
> 200 MBHT.	3.89			-

*At 0.05 statistical level of significance

TABLE III. COMPARISON BETWEEN MEAN OF BEHAVIORAL FACTORS WHICH INFLUENCE USING LPG AND NGV IN CAR

Behavior in Using Gas-fuel Setting Car	F-Value (t-Value)	P-Value
Car brand	2.47	0.08
Car type	1.03	0.53
Fuel type	8.88	0.01*
Year of service since registration	4.63	0.13
Gas maximum capacity	(1.15)	0.57

*At 0.05 statistical level of significance

As illustrated in table 2, it indicated that the behavior in using gas-fuel setting car was different in terms of fuel type whereas there was no difference in other factors at 0.05 level of significance.

V. CONCLUSION

The difference in behavioral factors significantly affected the different attitude towards decision making in using gas-fuel setting car. Furthermore, the different knowledge factors in using gas-fuel significantly affected the different attitude in making decision in using gas-fuel in car at 0.05 level of significance. It was found that the research findings was both aligned and not aligned to the related studies as follows:

Key point 1: Referring to the analysis on knowledge and understanding on gas-fuel setting in car, it was found that most respondents had knowledge and understanding at medium and high level, followed by those who had knowledge and understanding at low level, and high level respectively. This findings was in line with the research by Jarinya Mas-Aroon [15] and Wirat Kaewchaisa [13] but not in line with that of Chananun Ritnapadul [14] which proposed that most respondents had knowledge and understanding at high level, followed by medium, and low respectively.



Key point 2: As for the data analysis on attitude in using gas-fuel setting in car, it was seen that by overall most respondents had attitude towards expense and convenience at high level, followed by engine and safety at medium level, and satisfaction at low level. This findings was aligned to the research by Wirat Kaewchaisa [13].

Key point 3: It indicated that behavioral factors in using gas-fuel car significantly affected decision making to set LPG and NGV in car. All factors including car brand, fuel type, years of service since registration, and gas maximum capacity significantly, except car type, affected the decision making to set gas-fuel in car. This findings was in line with the research by Chananun Ritnapadul [14] It is suggested that the gas-fuel setting business should focus on setting service fee, maintenance fee, and reasonable price of LPG and NGV conversion kit. In addition, the car owner who plans to set up LPG and NGV kit, it is necessary to study the cost efficiency and estimated cost as well as select the vendor who provides the reasonable fee and standardized conversion kit. The researcher recommended that the further study should be conducted for the targeted group and area outside Samutprakarn province in order to see whether the findings and result might differ due to various context.

ACKNOWLEDGMENT

The authors would like to thank the Department of Mechanical Engineering Faculty of Engineering and Industrial Technology, Silpakorn University for their valuable support.

REFERENCES

- [1] EPPO (Energy Policy and Planning Office Ministry of Energy), The Ministry of Energy, "Oil price today and the price.NGV LPG 2005-2016.
- [2] The Registration Admintration Bureau, Department of Provincial Administration Population in Muang Samutprakarn, 2015.
- [3] F. James, Engel, Blackwell, D. Roger Miniard and W. Paul, "Consumer behavior (7th ed.)", Fort Worth, The Dryden Press, 1993.
- [4] Siriwan Sareera, Prin Laksitanon, Supaorn Serirat and Ong-Art Padavanija , "Marketing management (revised edition)," Bangkok, Thammasan Printing, 2003.
- [5] Prin Laksitanon, "Consumer behavior analysis (2nd ed.)," Bangkok, Love&Love Publishing, 1993.
- [6] A. Herbert and Simon, "Administrative behavior," New York, The McMillen Company, 1960.
- [7] L.G. Schiffman and L.L. Kanuk, "Consumer behavior (5th ed.), Englewood Cliffs, N.J. Prentice-Hall, 1994.
- [8] A. Tversky, "Dicision making: Selected readings," Combs, Phillip, Penguin Books, 1967.
- [9] Siriwan Sareerat and Amornsak Boonruang, "Marketing management," Bangkok, Diamond in Business World, 2003.
- [10] Seri Wongmonta, "Marketing Strategy Marketing Plan," Bangkok, DK Today, 2011.
- [11] V. Leung, "Slow diffusin of LPG vehicles in China-Lessons from Shanghai, Guangzhou and Hong Kong, vol. 39, Energy Policy, 2011.
- [12] R. Biscoff, M. Akple, R. Turkson and W. Klomegah, "Wcenario of the emerging shift from gasoline to LPG fuelled cards in Ghana: A case study in Ho Municipality, Volta Region," vol. 44, 2012, pp. 354-361.
- [13] Wirat Kawechaisa, "Behaviors and opinions LPG users for personal car in Bangkok and Greater Bangkok Area," Master of Business Administration, Kasetsart University, 2007.
- [14] Chananan Ritnapadul, "Factors related to the opinions of motorists in using Natural Gas (NGV): A case study of Passenger Cars (Taxi) in Bangkok," Master of Public Administration, Burapa University, 2005.
- [15] Jarinya Masarun, "Marketing responses to LPG GAS according to automobile consumers opinions," Master of Business Administration, Dhurakij Pundit University, 2009.



Study of Safety Behavior for Manufacturing Employees: A Case Study of Paper Pulp Factory Cluster

Chongrug Pariwatnanont

Department of Mechanical Engineering
Faculty of Engineering and Industrial Technology,
Silpakorn University, Nakorn Pathom, Thailand
chongrug.pariwatnanont@hotmail.com

Chantana Sangvorniyotin

Department of Mechanical Engineering
Faculty of Engineering and Industrial Technology,
Silpakorn University, Nakorn Pathom, Thailand
Chantana-30@hotmail.com

Abstract

This research aimed to investigate the effect of individual factor on safety behavior in manufacturing workers and level of safety support from company. The data was collected from 300 employees by using a questionnaire and sample size was calculated from Taro Yamane at 95% confidence level and 5% error. The data analyzed by mean, standard deviation (SD), t-test, F-test (One-way ANOVA) and Scheffe's post hoc analysis at 0.05 level of significance.

The results of statistical analysis of the difference between individual factors and safety behavior in manufacturing workers showed that the difference was in all aspects, except for income and the difference between individual factor and level of safety support from company was found in three aspects: gender, status and education at .05 significance level of statistical difference.

Keywords— Behavior, Safety, Manufacturing worker, Paper and factory

I. INTRODUCTION

In amidst of currently dynamic and challenging economic and social circumstance in Thailand, the entrepreneurs across industries necessarily adjust and enhance their performance. With high caliber in product exported worldwide and high competitiveness, Thai manufacturers improve potential and develop their technology and operational excellence to ensure efficiency, effectiveness, and productivity. To achieve this mission, the infrastructure and people are critical as foundation for future growth. In addition, the safety awareness is as highlighted to ensure the smooth operation with zero accident and occupational hygiene. If there are any injuries or illness, these definitely impede the operation and business continuity at the end.

Any accident or problem in employee really impacts to all concerned parties organization, the management, supervisors, and employee in terms of manpower, expense, cost, retraining to new employee, productivity, etc. Suphot Denduang (1998) [1]. Consequently, the occupational safety is so essential that both organization and employee needs to have strong awareness. It was also found that most problems were from machine, engine, and equipment, followed by chemicals used

in maintenance and manufacturing works. Furthermore, it was indicated that Thailand was ranked as higher accident country to other countries and safety behavior in Thai workers tends to risk to accidents e.g. not taking personal protective equipment (PPE), not following safety regulations. It really implies that "safety culture" was not well established.

II. METHODOLOGY

Research Objective: to study difference between individual factor and safety behavior in manufacturing workers and level of safety support from company, a case study of paper pulp factory cluster. **Research Hypothesis:** the different individual factor significantly affects the different occupational safety behavior and different level of organizational support towards occupational safety. **Research Benefits:** to understand the difference between individual factor and safety behavior in manufacturing workers and level of safety support from company, a case study of paper pulp factory cluster. The researcher calculated the optimum number of sample by Yamane's sample calculation method (1987) [2] and finalized at 1,168 workers from paper pulp factory No. 1, No. 2, and No. 3, at 95% of confidence and $\pm 5\%$ of margin error. After that, the 5-rated Likert-scale questionnaire was distributed (Rensis A. Likert, 1961) [3] and the mean was interpreted as the main criteria (Chatchawan Ruengprapan, 2000) [4]. The descriptive statistics was analyzed in terms of frequency, ratio, mean, and SD while the inference statistics was used as Parametric Inference which consists of t-Test, Analysis of Variance: ANOVA, and Scheffe post-hoc Analysis.

III. LITERATURE REVIEW

Occupational Safety

Occupational safety refers to action or activity from someone to something under the safe condition without the near-miss incident or accident which causes to injury, disability, or death to human, assets, or environment. Somtawin Muangpra (1994) [5] stated that according to behavioral science, the safety behavior can occur by many interrelated factors which can be divided into three characteristics. The first



one is related to knowledge, understanding, belief, attitude, and value of individual towards hygienic behavior from personal learning and experience. Secondly, the factor from opportunity to use equipment and service i.e. clinic, food service area, or PPE. The last one is other factors from the first two e.g. individual action both directly and indirectly to operation work from family, relatives, friends, employer, other staffs, and also the people outside family or workplace. This group of people has influence to cultivating or changing hygienic behavior through teaching, training, motivating, persuading, role modeling, monitoring, and encouraging to the new habits which lead to the appropriate occupational behavior. It can be concluded that safety behavior can take place due to three factors – persuading, supporting, and motivating. Without any one factor, the accident can actually break out.

Related Research

Saowanee Paomuang (2011) [6] studied occupational safety behavior of operation workers in CTS Electronics Corporation (Thailand) Limited and found that the difference in sex, age, education background, position, and year of service significantly affected the different occupational safety behavior whereas safety factors had the relationship to occupational safety behavior.

Brian H.W. Guo and others (2015) [7] conducted the research on the forecasted safety behavior in construction industry: the development and testing integrated model and found that safety management significant affected social support and pressure were important factors to safety while knowledge and motives had significantly effect to the safety. Moreover, the knowledge and motives on safety was significantly positive to safety.

Sharon Clarke (2004) [8] investigated the weather safety in automotive manufacturer: impact to working environment, communication, and safety attitude towards accident and unsafe behavior. The findings was in line with the previous research in the United Kingdom that the all-weather safety did not affect the accident in the factory whereas the worker's response to safety and working environment awareness were significant indicators on accidents and unsafe behaviors.

IV. RESULTS

Referring to research findings, it was found that the difference in individual factor which consists of sex, age, marital status, education background, and year of service affected the different occupational safety behavior at 0.05 level of statistical significance. Additionally, when analyzing the education factors by item, in the level of occupational safety at survey statement "While operating, you do only as assigned by your supervisor" at 0.05 level of statistical significance, it was found that those who graduated in vocational certificate/ high vocational certificate had higher level of occupational safety behavior than those who graduated in Bachelor's Degree. As table I-II:

TABLE I. THE RESULT OF DATA COMPARISON ON SAFETY BEHAVIOR IN MANUFACTURING EMPLOYEES CLASSIFIED BY EDUCATION

Factor; While operating, you do only as assigned by your supervisor	Df	SS	MS	F-Value	P-Value
With in Group	297	168.57	0.568		
				3.504	0.031*
Between Group	2	3.978	1.989		
Total	299	172.55			

*At 0.05 statistical level of significance

TABLE II. THE RESULT OF DATA COMPARISON ON SAFETY BEHAVIOR IN MANUFACTURING EMPLOYEES BY SCHEFFÉ'S METHOD

EDUCATION	\bar{X}	vocational certificate/ high vocational certificate	Bachelor's Degree	higher Bachelor's Degree
		4.40	4.05	4.50
vocational certificate/ high vocational certificate	4.40	-	0.343*	0.105
Bachelor's Degree	4.05		-	0.447
higher Bachelor's Degree	4.50			-

*At 0.05 statistical level of significance

Next, when analyzing the age factor by item, regarding to occupational safety at survey statement "In case of accident or fire accident, you always report to your supervisor" at 0.05 level of statistical significance, it could be seen that those who had 4-6 years of service had higher level of occupational safety behavior than those who had more than 9 years of service. As table III-IV:

TABLE III. THE RESULT OF DATA COMPARISON ON SAFETY BEHAVIOR IN MANUFACTURING EMPLOYEES CLASSIFIED BY AGE FACTORY

Factor; In case of accident or fire accident, you always report to your supervisor	Df	SS	MS	F-Value	P-Value
With in Group	296	89.635	0.303		
				3.425	0.018*
Between Group	3	3.111	1.037		
Total	299	92.747			

*At 0.05 statistical level of significance



TABLE IV. THE RESULT OF DATA COMPARISON ON SAFETY BEHAVIOR IN MANUFACTURING EMPLOYEES BY SCHEFFÉ'S METHOD

AGE FACTORY	\bar{X}	1-3 years	4-6 years	7-9 years	> 9 years
		4.91	4.55	4.71	4.79
1-3 years	4.91	-	0.366	0.203	0.125
4-6 years	4.55		-	0.163	0.240*
7-9 years	4.71			-	0.078
> 9 years	4.79				-

*At 0.05 statistical level of significance

However, it was found that the different personal income did not affect the occupational safety behavior. In addition, it was found that the difference in individual factor which consists of sex, age, marital status, education background, and year of service affected the different attitude towards organization's support to occupational safety at 0.05 level of statistical significance. When analyzing the marital status by item, regarding to organization's support to occupational safety at survey statement "Company promotes to use PPE" at 0.05 level of statistical significance, it was found that those who are married agree to the organization's support to occupational safety at higher level than those who are divorce/widowed. Also, at survey statement "Company shows the safety signs in the appropriate spot", it was found that those who are single and those who are married agree to the organization's support to occupational safety at higher level than those who are divorce/widowed. In terms of educational background, regarding to organization's support to occupational safety at survey statement "Company provides enough PPE for employees", it could be seen that those who graduated in vocational certificate/ high vocational certificate had higher level of organization's support to occupational safety behavior than those who graduated in Bachelor's Degree. However, it was found that the different age, year of service, and personal income did not affect attitude towards organization's support to occupational safety.

V. DISCUSSION

It was found that the research findings was both aligned and not aligned to the related studies as follows:

Sex: The findings revealed that the different sex significantly affected the different occupational safety behavior, which was in line with the result from research by Saowanee Paomuang (2011) [6] and Kasem Kitwassana (2010) [9].

Age: Referring to research findings, it was seen that the different age significantly affected the different occupational safety behavior, which was aligned to the findings from research by Saowanee Paomuang (2011) [6] and Jeerawat

Srithep (2010) [10]. Also, it was seen that the different age did not affected the organization's support to occupational safety, which was aligned to the findings from research by Chonticha Rid-ngarn (2001) [11].

Marital status: The research findings showed that the different marital status significantly affected the different occupational safety behavior, which was in line with the research by Kasem Kitwassana (2010) [9]. In addition, the different marital status significantly affected the different level of organization's support to occupational safety, which was in line with the research by Rassalee Jor-prayoon (2008) [12] and Wanchalerm Phon-In (2006) [13].

Education Background: According to research findings, it was seen that the different educational background significantly affected the different occupational safety behavior, which was in line with the research by Saowanee Paomuang (2011) [6], Kasem Kitwassana (2010) [9], Wanchalerm Phon-In (2006) [13], and Kaewruethai Kaewchaithiam (2005) [14]. Furthermore, it was found that the different educational background significantly affected the different level of organization's support to occupational safety, which was in line with the research by Wanchalerm Phon-In (2006) [13].

Year of Service: Research findings indicated that the different year of service significantly affected the different occupational safety behavior, which was in line with the research by Saowanee Paomuang (2011) [6], Kasem Kitwassana (2010) [9] and Kaewruethai Kaewchaithiam (2005) [14].

VI. CONCLUSION

According to the statistical analysis, it was found that the factors on sex, age, marital status, and year of service significantly affected the different occupational safety whereas the difference in sex, marital status, and educational background significantly affected the different organization's support to occupational safety.

ACKNOWLEDGMENT

It is highly recommended that the scope of next studies should cover the other industries and other safety-related topics e.g. factors to accident in workplace, worker's awareness on safety management, occupational safety awareness, etc.

REFERENCES

- [1] Suphot Denduang, "Security culture, review of knowledge, situations and related factors under the project of Thai culture to longevity health," Nonthaburi: Department of Medical Technology Development, Ministry of Public Health, 1998.
- [2] Yamane Taro, "Statistics: An Introductory Analysis," Second edition, New York: Harper and Row, 1987.
- [3] Likert, Rensis A, "New Patterns of Management," New York: McGraw-Hill Book Company Inc, 1961.
- [4] Chatchawan Ruengprapan, "Basic statistics," Khon Kaen: Klang Nana Witaya Printing, 2000.
- [5] Sontawin Muangpra, "A study of the health behavior of workers at the operational level, Occupational accident prevention: Case study of metal products industry, machinery and equipment in Bangpakong district



- Chachoengsao,” Master of Social, Labor and Welfare Development, Thammasat University, 1994.
- [6] Saowanee Paomuang, “The safety behaviors for manufacturing employees, CTS electronics corporation company (Thailand),” Master of Business Administration, Rajamangala University of Technology Thanyaburi, 2011.
- [7] Brian H.W. Guo and others, “Predicting safety behavior in the construction industry: Development and test of an integrative model,” *Safety Science* Vol. 84, pp. 1–11, Department of Civil and Environmental Engineering, The University of Auckland, 1142 Auckland, New Zealand, 2015.
- [8] Sharon Clarke, “Safety climate in an automobile manufacturing plant: The effects of work environment, job communication and safety attitudes on accidents and unsafe behavior,” *Emerald Insight* Vol. 35, pp. 413–430, Manchester Business School, University of Manchester, Manchester, UK, 2004.
- [9] Kasem Kitwassana, “Perception of safety management and employee safety behavior of Thai Industrial Gases public company limited,” The Graduate School, Kasetsart University, 2010.
- [10] Jeerawat Srithep, “Perception of policy and behavior in workplace of employees of S. Maha-umnaj company limited,” Master of Business Administration (General Management), Rajabhat Thonburi University, 2010.
- [11] Chonticha Rid-ngarm, “Employee participation in enhancing work safety: A case study of Khon Kaen Fishnet factory in Khon Kaen,” Master Thesis of Liberal Arts, Khon Kaen University, 2001.
- [12] Rassalee Jor-prayoon, “The factors related to employee safety, Carton Optics (Siam) company limited,” Master of Business Administration (General Management), Rajabhat Pra Nakorn Si Ayutthaaya University, 2008.
- [13] Wanchalerm Phon-In, “Supporting for the safety and health of the organization, safety behavior and quality of life of employees of Siam Cement Thungsong company limited,” Master of Arts, King Mongkut's Institute of Technology North Bangkok, 2006.
- [14] Kaewruethai Kaewchaithiam, “Perception of safety management and safety behaviors of the operational staff,” Master of Arts (Industrial and Organizational Science Department of Humanities), King Mongkut's Institute of Technology North Bangkok, 2005.



Factors Influencing Decision to Purchase the Design Engineering Software in Companies in Navanakorn Industrial Estate, Pathumthani Province

C. Sangvornyotin*, D. Ratsanasart and C. Pariwatnanont

Department of Mechanical Engineering, Silpakorn University
Nakhon Prathom, Thailand

*E-mail: chantana-30@hotmail.com

Abstract—The objectives of this research were to study behavior in making decision to purchase the design engineering software and to compare the marketing mix which affects the customer in making decision to purchase the design engineering software. Referring to Yamane sample calculation and type of sample organizations, the research was conducted to 66 companies in Navanakorn Industrial Estate. The data was collected by questionnaire and analyzed by mean, SD, t-Test, F-Test (One-way ANOVA) and Scheffe's post hoc analysis at 0.05 level of significance.

According to research findings from comparison analysis on type of organizations and factors influencing decision to purchase design engineering software, it was found as follows: Product – capability and usability; Price – vendor, cash discount for long-term payment, and reasonable price; Place – on-line channel availability, on-site product demonstration by staff; Promotion – advertisement in various channels e.g. magazine, internet, etc.; Process – online-helpdesk; and People – skilled staffs, at .05 significance level of statistical difference.

Keywords—Decision Making, Design Engineering Software, Industrial Real Estate

I. INTRODUCTION

Software Industry Promotion Agency (SIPA) [1] collected the data regarding to software industry since this becomes interesting and more important as high thrust in Thailand's business expansion. In this industry, it is not only reasonable investment but also less manpower required into running and sustaining the business. As for production value and consumption value in 2015, it was indicated that the importing software for consumption acquired 33 % (32,944 million THB); the production value for domestic acquired 49% (49,231 million THB); the exportation value for organization acquired 3% (3,330 million THB); and software development value acquired 15% (14,903 million THB) respectively. For Thailand, the software production value for exportation was less than the importing one at 30% of the total amount of software production and consumption value. From this data, it significantly implied that the Thai software developer companies really need to boost up potential and therefore need

to understand the user needs in order to efficiently level up the software from Thailand to meet the international standard. From this reason, the researcher determined to explore factors which influence the decision to purchase design engineering software in companies in Navanakorn Industrial Estate, Pathumthani province. The key criteria to focus on this area was that this industrial zone was established for 45 years and was the center of a wide variety of industrial clusters e.g. electronics, food, automotive parts, medical instrument, and packaging, etc. which definitely requires engineering software to multipurpose usages such as product design, equipment production for both being used in factories and being produced as final product to end customers.

II. METHODOLOGY

Research Objectives. To study customer behavior in making decision to purchase the design engineering software in companies in Navanakorn Industrial Estate in Pathumthani province. To compare levels of factors which influence the decision to purchase the design engineering software in companies in Navanakorn Industrial Estate in Pathumthani province categorized by types of organization. Research Benefits. To understand customer behavior and level of factors which influence the decision to purchase the design engineering software in companies in Navanakorn Industrial Estate in Pathumthani province categorized by types of organization. Research Hypothesis. Companies which hold the different characteristics would have different factors which influence the decision to purchase the design engineering software. The population of this research was the group of 192 companies located in Navanakorn Industrial Estate in Pathumthani province. The researcher applied Yamane's sample [2] calculation at 90% level of confidence and $\pm 10\%$ margin of error to come up with the number of 66 companies in Navanakorn Industrial Estate in Pathumthani province. The questionnaire was applied in this study of which score can be divided into 5 Likert scale [17]. The data was calculated in mean and was interpreted as standard criteria [18]. The descriptive statistics was analyzed in terms of frequency, mean, and SD while the inference statistics was used as Parametric Inference which consists of t-Test, Analysis of Variance: ANOVA, and Scheffe post hoc analysis.



III. LITERATURE REVIEW

Customer behavior refers to any action to acquire the consumption and purchasing the product or service as well as decision making before and after the action [3]. Additionally, it can be defined as the action of someone to acquire and use good and service including the decision making before which lead to that action [4]. Customer behavior analysis can refers to identifying customer's purchasing behavior in order to understand customer's needs. In doing that, the marketing expert applies question and answer (Q&A) technique so as to gain input and insights more solid enough to eventually develop marketing strategy [5]. The 6Ws and 1H which consists of Who-What-Why-Who-When-Where-How are the key set of questions used to explore the answer of 7Os which is composed of Occupants-Objects-Objectives-Organizations-Occasions-Outlets-Operations[6] whereas in the service business sector, the Marketing Mix or 7Ps is relatively applied [7].

Studied the research on customer satisfaction in selecting the accounting software in order to explore factors in using accounting software and satisfaction towards accounting software [14] and found that the capability factors were regarded as the most important; 24-hour operating, compatibility to the operating system (OS) used in company, and quick response at excellent level. [15]Conducted the research on using CAD/ CAM software for small enterprises and proposed that the main criteria in choosing CAD/CAM were capability and efficiency while the supportive factors were flow analysis and specific characteristics in each type of industry.[16] Investigated the impact from CAD in designing engineering processes in order to understand the relationship between CAD technology and effectiveness in product development and validate whether CAD was the key factor for organizational success. Referring to research findings, it was found that CAD had influence to efficiency of product design and organizational success whereas training to staffs in using CAD and the training assessment significantly affected using CAD.

IV. RESULTS AND DISCUSSION

Referring to the result of data comparison on factors influencing the decision to purchase design engineering software at 0.05 statistical level of significance, it could be seen that when classified by registered capital, as for Price marketing mix - the reasonable price of design engineering software, the different amount of registered capital significantly affected the decision to purchase software at different level. In addition, it was seen that when classified by registered capital, as for Price marketing mix - the cash discount for long-term payment, the different the different amount of register capital significantly affected the decision to purchase software at different level.

At 0.05 statistical level of significance, when classified by year of operation, as for Place marketing mix - the online channel availability, the different year of operation significantly affected the decision to purchase software at different level. When classified by number of employees, as for

Price marketing mix – cash discount for long-term payment, the different number of employees significantly affected the decision to purchase software at different level as follows table 1-4

TABLE I. THE RESULT OF DATA COMPARISON ON FACTORS INFLUENCING THE DECISION TO PURCHASE DESIGN ENGINEERING SOFTWARE CLASSIFIED BY ORGANIZATIONAL CHARACTERISTICS OF THE REGISTERED CAPITAL

Factor; Cash discount for long-term payment	<i>Df</i>	<i>SS</i>	<i>MS</i>	<i>F-Value</i>	<i>P-Value</i>
With in Group	63	57.5	0.91		
				4.52	0.02*
Between Group	2	8.26	4.13		
Total	65	65.76			

*At 0.05 statistical level of significance

TABLE II. THE RESULT OF DATA COMPARISON ON FACTORS INFLUENCING THE DECISION TO PURCHASE DESIGN ENGINEERING SOFTWARE BY SCHEFFE'S METHOD

THE REGISTERED CAPITAL	\bar{X}	< 50 MBHT.	50 - 200 MBHT.	> 200 MBHT.
		2.94	3.32	3.89
< 50 MBHT.	2.94	-	-0.39	-0.96*
50 - 200 MBHT.	3.32		-	-0.57
> 200 MBHT.	3.89			-

*At 0.05 statistical level of significance

TABLE III. THE RESULT OF DATA COMPARISON ON FACTORS INFLUENCING THE DECISION TO PURCHASE DESIGN ENGINEERING SOFTWARE CLASSIFIED BY ORGANIZATIONAL CHARACTERISTICS, THE NUMBER OF EMPLOYEES IN THE ORGANIZATION

Factor; Cash discount for long-term payment	<i>Df</i>	<i>SS</i>	<i>MS</i>	<i>F-Value</i>	<i>P-Value</i>
With in Group	63	58.74	0.93		
				3.76	0.03*
Between Group	2	7.02	3.51		
Total	65	65.76			

*At 0.05 statistical level of significance



TABLE IV. THE RESULT OF DATA COMPARISON ON FACTORS INFLUENCING THE DECISION TO PURCHASE DESIGN ENGINEERING SOFTWARE BY SCHEFFÉ'S METHOD

EMPLOYEES IN THE ORGANIZATION	\bar{x}	1-50.	51 - 200	> 200
		3.44	2.80	3.60
1 - 50	3.44	-	0.64	-0.15
51 - 200	2.80		-	-0.80*
> 200	3.60			-

*At 0.05 statistical level of significance

It was found that the research findings was both aligned and not aligned to the related studies as follows:

Product: The findings indicated that by overall the respondents considered product marketing mix at excellent level. The capability of design engineering software and usability were ranked as the most important factors, which was aligned to the research by [13-14].

Price: Referring to research findings, by overall the respondents recognized price marketing mix at excellent level. The reasonable price was ranked as the most influential factor, which was aligned to the study by [8] but was contrast to research by [9] which proposed that price marketing mix was regarded at medium level since the design engineering software was ubiquitous and had no price competition.

Place: The findings showed that by overall the respondents regarded place marketing mix at excellent level. The service center being located nearby and on-site product demonstration by staff were also ranked at the most indispensable factors, which was in line with research by [9].

Promotion: Referring to research findings, by overall the respondents considered promotion marketing mix at excellent level. The product trial offer and advertisement in various channels e.g. magazine, online, etc., and campaigns such as price discount, redemption, any promotions, etc. were ranked as the most vital factors, which was similar to research findings by [10-12].

Environment: The research findings indicated that by overall the respondents recognized environment marketing mix at excellent level. The software availability at service center and PC for demonstration and enough space for customer service were ranked as the most critical factors, which was in line with the research by [11].

Process: Referring to research findings, it could be found that by overall the respondents regarded process marketing mix at the most excellent level. The prompt troubleshooting, help-desk call, and on-site service were the most crucial factors, which was aligned to the research by [9-11]

People: The findings indicated that the respondents considered people marketing mix at excellent level. The skilled staff was ranked as the most significant factor, which was in line with [9-11]

V. CONCLUSION

Referring to the result of data analysis in comparing all major factors influencing the decision to purchase design engineering software, it was seen that the difference in type of industry, amount of registered capital, year of operation, and number of employees significantly affected the different decision to purchase design engineering software. It is recommended that the further research be conducted in other industrial estate where the design engineering software is purchased for more holistic and comprehensive decision making

ACKNOWLEDGMENT

The authors would like to thank the Department of Mechanical Engineering Faculty of Engineering and Industrial Technology, Silpakorn University for their valuable support.

REFERENCES

- [1] SIPA (Software Industry Promotion Agency) Public Organization, "Software Industry in the Digital Economy," 2016.
- [2] Yamane Taro, "Statistics: An Introductory Analysis," Third edition, Harper and Row Publication, Newyork, 1973.
- [3] F. Jame Engle, D. Roger Blackwell and W. Paul Miniard, "Consumer behavior," Orlando, Dryden Press, 1990.
- [4] Thongchai Santiwong, "Consumer behavior," Bangkok, Thai Wattana Panich, 1992.
- [5] P. Kotler, "Marketing management: analysis, planning implementation and control," New Jersey, Asimmon&Schuster, 1997.
- [6] Siriwan Sareerat and others, "Organization and Management (Complete Edition)," Bangkok, Thammasan, 2003.
- [7] Siriwan Sareerat and others, "New Market Service," Bangkok, Theera Firm & Scitex, 1998.
- [8] Anothai Muangthip, "Factors influencing the decision to buy accounting software packages of small and medium enterprises, Case study of wholesale business in Bangkok," Master of Business Administration, Rajamangala University of Technology Rattanakosin, 2008.
- [9] Kattima Sompongmitr, "Marketing mix factors affecting to decision in purchase accounting software packages case study Accounting Service Office, Phuket Province," Master of Business Administration, Phuket Rajabhat University, 2006.
- [10] Naraphon Sakhakorn, "Infulencing factor of hardware and software computer buyers through internet among students in Public University (Concentration in Bangkok)," Master Science in Industrial Education (Computer and Information Technology), King Mongkuts University of Technology Thonburi, 2002.
- [11] Kittipong Boonmesiritipong, "Factors affecting the purchase of computer program of business in urban area, Nakhon Ratchasima province," Master of Business Administration, Mahasarakham University, 2004.
- [12] Narongkorn Pradip Na Thalang, "Marketing factors influencing the decision to buy software for Pastic and Textile factories in Bangkok Metropolitan Area," Master of Business Administration, Kasetsart University, 2010.
- [13] Uraivan Hongchai, "Factors influencing the selection of accounting software program, Enterprise Resource Planning (ERP) systems in



- Amata Nakorn Industrial Estate, Chonburi province,” Master of Accountancy, Burapa University, 2011.
- [14] S.H.I. Ivancevich, M. Daniel and Fara Elikai, “Accounting systems; User behavior” Attitue surveys, Technology adoption, 2010, pp. 66-72.
- [15] B. Mercer Timothy, “CAD/CAM selection for samll manufacturing companies.” Master of Science in Management Technology, The Graduate School University of Wisconsin, 2000.
- [16] Alfredo Herrera, “CAD-a lean engineering tool-impacting human efficiency in the design engineering process.” Doctor of business administration, Nova Southeastern University, H. Wayne Huizenga School of Business and Engerpreneurship, 2003.
- [17] A. Likert Rensis, “New pattern of management”, New York, McGraw-Hill, 1961.
- [18] Chatchawan Ruangpraphan, “Basic statistics.” Khon Kaen, Klung Nana Wittaya Printing.



Performance Measurement Faculty of Engineering RMUTP for Digital University

Chalakorn Udomraksasakul*, Singkaew Pokterng, Kompan Chomsamutr and Watchara Songserm

Department of Mechatronics Engineering, Faculty of Engineering,
Rajamangala University of Technology Phra Nakhon
Bangkok 10800, Thailand
*chalakorn.u@rmutp.ac.th

Abstract— The objective of this research work was to arrange a performance measurement for finding factors which will have influence on the capacity of Faculty of Engineering, Rajamangala University of Technology Phra Nakhon, leading it to become a digital university. The results of making a survey on the data from the personnel of the Faculty of Engineering showed that: the factor that had the most influence on the capacity of the Faculty of Engineering, Rajamangala University of Technology Phra Nakhon was the factor of knowledge and attitudes (the mean was 3.61, which stood at the level of comments "high"); regarding the level of comments, this was followed by the factor that had influence on the capacity of the Faculty of Engineering in terms of the environment in the organization (the overall mean was 3.49, which stood at the level of comments "moderate"); the factor that had influence on the capacity of the Faculty of Engineering in terms of participation came in the last place (the mean was 3.41, which stood at the level of comments "moderate"). The basics results obtained from this research work will be partly used as an approach to help improve the processes of the Faculty of Engineering. This will support stepping into becoming a digital university in the future.

Keywords— *Performance Measurement; Digital University*

I. INTRODUCTION

From the economic, social and technological change of Thailand that is entering the age of Industry 4.0 which is complicated and rapidly changes, a number of universities realize the necessity to develop organization's strategy in both approach and defensive way to be ready in handling with the changing circumstances. Rajamangala University of Technology Phra Nakhon (RMUTP), under the leadership of the rector, announces a policy to develop the university to achieve the goal of being "the leading university to produce professional graduates" within 5 years. It will expand educational spaces to become larger to support future educational services and step forward to be the digital university. With such policy, every faculty in the university needs to adapt themselves in terms of educational curriculum, research, lecturers or even supportive personnel.

Rajamangala University of Technology Phra Nakhon holds the principle to produce graduates who are practical, seeking knowledge, persevere, technologically skillful and moral with the instructions in 9 faculties. Faculty of Engineering is a part to drive Faculty of Engineering. Currently, Faculty of Engineering needs to respond the university's policy by developing it to reach the goal of being "the leading university to produce professional graduates". However, to accomplish the university's policy, different factors need to be considered such as lecturer factor, supportive personnel factor, knowledge and attitude factor, in-house environment factor, instructional instrument factor and educational curriculum etc. As a result, the fact that Faculty of Engineering at Rajamangala University of Technology Phra Nakhon will turn it to become the digital university interests the researcher to know what factors affect Faculty of Engineering. Data are surveyed from personnel in Faculty of Engineering and performance measurement is conducted. The result from this research will comes with factors and fundamental opinions affecting the performance of Faculty of Engineering at Rajamangala University of Technology Phra Nakhon to become the digital university. It will be a guideline of improvement and planning for further development of Faculty of Engineering.

II. THEORY AND RELATED STUDIES

A. Industry 4.0

Industry 4.0 [1] or the 4th industrial revolution age is the change in production system and method from traditional system to the new one. It is an integration of internet network connection with every unit in the production system (Internet of Things: IOT) starting from raw materials, machines, equipment and automatic mechanics to be installed in the network system enabling users to communicate, manage and exchange information independently. It also enhances production capacity for more flexible production system that can be adjusted to conform to production conditions making it more convenient in production system. Additionally, users can evaluate overall effectiveness of machines and plan the production that they can anticipate the outcomes and inspect it



by installing machine inspection program so that the machines are effective and available with longer useful life.

B. Digital University

Currently, world situations are considerably changing and information technology or IT is implemented to utilize the information more conveniently, rapidly and effectively. It can be used in almost every area at any time for compatible devices. Therefore, the government drives a policy of Digital Economy to develop digital infrastructure (Convergence) in 3 terms including information technology (IT), telecommunication and broadcasting. It comes with innovation as a foundation of extension for national development economically and socially. Every sector will become advance to follow world trends and become competitive in terms of production, digital product trading and digital using to support services in business, financial or other sectors. As a result, Rajamangala University of technology Phra Nakhon [2] is driving the strategy of digital university by announcing a policy of university development to achieve the goal of being "Rajamangala University of Technology Phra Nakhon, the leading university to produce professional graduates" within 5 years (academic year 2014-2018). This is to support future services and become the digital university to perform main tasks of higher-education institution with integration of knowledge for national development. it is defined as a sector support modern information technology services for education, research and university administration. It is applied from strategy of (3P) including practicality- the leader to produce graduates meeting need of labor market, profitability- the prosperity creator for the organization from earning income in different forms and people connectivity- the benefit giver to society, stakeholders for sustainability of the nation.

C. Performance Measurement

The meaning of performance [3][4] is defined variously; for example, performance refers to knowledge, ability, attributes and skills in practices for accomplishment. Therefore, performance measurement is applied with each organization or divided by purposes. Currently, the concept about performance has been implemented in both government and private organizations in Thailand in evaluating performance. Speaking of organization's performance, Sink [5] mentioned that main work system of each organization is designed to have monitoring system, assessment, control and management of the system. To evaluate system capability requires performance measurement.

Wireman [6] explained that performance measurement requires collection of performance indicator by category so that the performance measurement covers the organization's objectives and goals. Following 4 items need to be considered for development of the performance indicator.

- 1) Emphasis on clear organization's objectives
- 2) Objectives in relation to other parts of the organization
- 3) Focus on factors of critical success
- 4) Identification of possible and realistic solutions

Working in organization consist of different objectives and goals. As a result, it is necessary to manage the system to have indicators of each sector differently to match its objectives and goals. This reflects working condition of that sector clearly.

III. METHODOLOGY

A. Identification of populations and samples

This study is a qualitative research with survey research that can be divided in to following topics

- Populations

Populations in scope of this study are personnel in faculty of Engineering, Rajamangala University of Technology Phra Nakhon including 168 academic personnel and supportive personnel and 2,430 high-vocation, undergraduate and graduate students. Total populations are 2,598 persons (reference from academic year 2/2016)

- Samples

This study calculates sample size with method of Taro Yamane 1973 [7] and in this work, the deviation is 5%

$$n = \frac{N}{1+Ne^2} \quad (1)$$

where n = number of samples

N = total populations

e = level of deviation

$$n = \frac{2,598}{1+[2,598 \times (0.05^2)]} = 347$$

In this research, the researcher increases the sample size for 355 persons.

B. Research instrument

As mentioned above, this study is the qualitative research with survey method. A questionnaire is an instrument for data collection divided in to following topics

- Studying concepts, theories and related studies and determining factors in consistence with the study objectives. The questionnaire in this research is developed from Supacha which is the work finding factors with effects on participation of personnel in public sector management quality award (PMQA) of Department of Irrigation.
- The questionnaire is created with division into two parts
Part 1: demographic information of the respondents
Part 2: The questionnaire regarding factors affecting the study of performance measurement of Faculty of Engineering at Rajamangala University of Technology Phra Nakhon to become the digital university. This part contains open-ended questions including factors of knowledge and environmental attitude in the organization and participation. In this work, the researcher determines



score of the opinions by Likert Scale [8] i.e. the highest score equal to 5 and the lowest score equal to 1.

C. Data collection

To collect data, the researcher begins from sampling and collecting data by determined number of the samples. After that, data are verified and recorded for further analysis and conclusion.

D. Data analysis

To analyze data, after questionnaire verification, data are analyzed with descriptive statistics including frequency, percentage and mean before conclusion.

IV. RESULT

The result of finding factors affecting performance of Faculty of Engineering at Rajamangala University of Technology Phra Nakhon reveals that it has potential to respond the government policy with expectation for Thailand to have better economic, social and technological conditions with following details.

Part 1: The result of analysis of respondents' demographic information

TABLE I. DATA OF STATUS OF RESPONDENT

Respondents' demographic information	Frequency	Percentage
1. In-house personnel		
1.1 Academic personnel	17	53.13
1.2 Supportive personnel	15	46.88
2. vocational students		
2.1 1 st year	7	24.14
2.2 2 nd year	5	17.24
2.3 3 rd year	17	58.62
3. Undergraduate students		
3.1 1 st year	82	29.39
3.2 2 nd year	82	29.39
3.3 3 rd year	86	30.82
3.4 4 th year	29	10.39
4. Graduate students		
4.1 1 st year	7	46.67
4.2 2 nd year	8	53.33
Total	355	100

Part 2: The result of analysis of factors affecting performance measurement of Faculty of Engineering, Rajamangala University of Technology Phra Nakhon to become Digital University

According to table II, the respondents has opinions on factors affecting the study of performance measurement to become the digital university in terms of knowledge and attitude with mean score of 3.61 at high level. when considered mean score of knowledge, it was 3.61 at high level. In overall, the personnel and students have opinions that development as the digital university is beneficial to organizational development. The means score of attitude aspect is 3.62 at high level of opinion. The personnel and

students perceive that the current world is moving fast with self-development to support that change.

TABLE II. ANSWERS IN QUESTIONNAIRE REGARDING NUMBERS OF FACTORS IN TERMS OF KNOWLEDGE AND ATTITUDE.

Factor studied	Mean	Opinion level
Knowledge and attitude		
Knowledge		
1. You are transmitted knowledge about development as the Digital University	3.64	High
2. You have knowledge and understanding regarding criteria of development to become the Digital University	3.43	Moderate
3. You have knowledge and understanding in process of development to be the Digital University	3.47	Moderate
4. In general, you perceive that development to be the Digital University is beneficial	3.76	High
5. If you have adequate knowledge and understanding about development to be the Digital University, you want to take part in the development	3.75	High
Knowledge average score	3.61	High
6. You perceive that current world is changing rapidly and you develop yourself to support such changes	3.92	High
7. You have benefit from the development to be The Digital University	3.89	High
8. You are ready to participate in development as the digital university to achieve the goal	3.85	High
9. You think that development as the digital university increases work burden.	3.34	Moderate
10. In your opinion, Faculty of Engineering at RMUTP has no need to be developed to be the Digital University	3.09	Moderate
Attitude average score	3.62	High
Knowledge and attitude average score	3.61	High

TABLE III. ANSWERS IN QUESTIONNAIRE REGARDING FACTORS OF IN-HOUSE ENVIRONMENT

Factor studied	Mean	Opinion level
In-house environment		
Organization management		
11. Faculty of Engineering at RMUTP designs and provides good system to support participatory development as the digital university	3.47	Moderate
12. Faculty of Engineering at RMUTP has proper resources for developing personnel to operate the development as the Digital University efficiently	3.47	Moderate
13. Atmosphere in Faculty of Engineering at RMUTP is appropriate to stimulating personnel to participate in the development as the Digital University	3.39	Moderate
Average score of organization management	3.44	Moderate
Organizational culture		
14. In your opinion, the organizational culture is suitable to develop as the Digital University	3.48	Moderate



TABLE III. ANSWERS IN QUESTIONNAIRE REGARDING FACTORS OF
IN-HOUSE ENVIRONMENT (CONTINUE)

Factor studied	Mean	Opinion level
15. You think that personnel adept to suit organizational culture to achieve the target of development as the Digital University	3.48	Moderate
16. You think that Faculty of Engineering at RMUTP should improve organizational culture.	3.72	High
Average score of organizational culture	3.56	High
Communication		
17. You can give opinions or suggestions of the development as the Digital University	3.50	High
18. When you encounter a problem of development as the Digital University, you discuss with relevant persons conveniently leading to the solution.	3.50	High
19. In case of conflicts related to the development as the Digital University, such conflicts are resolved immediately.	3.37	Moderate
Average score of communication	3.46	Moderate
Average score of in-house environment	3.49	Moderate

According to table III the respondents had opinions on factors affecting the study of performance measurement to become the Digital University in term of in-house environment with total mean score of 3.49 at moderate level. When considered each aspect of the organization management, mean score is 3.44 at moderate level. The respondents agree that Faculty of Engineering at RMUTP designs and provides good system to support the participatory development as the Digital University. It also has sufficient resources for developing the personnel so that they can continue development as the Digital University efficiently. When considering mean score of organizational culture, the researcher found that mean score is 3.56 at high level of opinion. The respondents agree that Faculty of Engineering at RMUTP should improve organizational cultures while mean score of communication is 3.46 at moderate level. The respondents had opinions that they could express their opinions or suggestions in development as the Digital University. When the personnel have problems about the development as the Digital University that they could discuss with relevant persons conveniently leading to the solutions.

TABLE IV . ANSWERS OF QUESTIONNAIRE ABOUT FACTORS OF PARTICIPATION

Factor studied	Mean	Opinion level
Participation		
Participation in decision making		
20. You jointly think and make a decision on defining a guideline of development as the Digital University	3.38	Moderate
21. You participate in decision making to select a project or activity for development to achieve the goal	3.32	Moderate
Average score of participation in decision making	3.35	Moderate
Participation in operation		
22. You participate in development as the Digital University to be effective and efficient	3.38	Moderate

TABLE IV . ANSWERS OF QUESTIONNAIRE ABOUT FACTORS OF PARTICIPATION
(CONTINUE)

Factor studied	Mean	Opinion level
23. You participate in determining policy, action plan, project or activity at Faculty of Engineering at RMUTP to achieve the goal of development as the Digital University	3.39	Moderate
Average score of participation in operation	3.38	Moderate
24. You participate in evaluating, giving suggestions and guidelines of solution for improvement of the development as the Digital University.	3.51	High
25. You participate in reporting the result of development and improvement of the development as the Digital University.	3.46	Moderate
Average score of participation in evaluation	3.49	Moderate
Total average score of participation	3.41	Moderate

According to table IV, the respondents had opinions on factors affecting the study of performance measurement to become the digital university in participation term with mean score of 3.41 at moderate level. When specifically considered participation in decision making, the mean score is 3.35 at moderate level of opinion. The respondents agree that they can jointly think and make a decision in determining a guideline of development as the Digital University. When considering participation in operation, the researcher finds that mean score is 3.38 at moderate level. the respondents had opinions that they could participate in compliance with policies, action plans, projects or activities to achieve the goal of development as the Digital Development. Mean score of participation in evaluation is 3.49 at moderate level of opinion provided that the respondents had opinions that they could participate in evaluating, giving suggestions and guidelines of improvement of development as the Digital University

V. CONCLUSION

From current world situations, information technology or IT is implemented in routine life as users can access and utilize information conveniently, rapidly and effectively. The government thus promulgates the policy of digital economy to support the implementation of information technology to apply with economic and social activities in national development leading to digitality. The goals cover every area with sufficient size, stability and reasonable price. From such policy, the University provides a guideline to respond the government by driving strategies of the Digital University. It announces the policy of university development to achieve the target of success of being "Rajamangala University of Technology Phra Nakhon to produce professional graduates" within 5 years to perceive the guideline of development.

The researcher studies samples from Faculty of Engineering with objectives to provide performance measurement for findings factors affecting performance of Faculty of Engineering, Rajamangala University of Technology Phra Nakhon to become the Digital University. The result from surveying data with 355 personnel in Faculty of Engineering could be summarized with factors divided into 3 terms including



1) knowledge and attitude with mean score of 3.61 at high level, 2) organization's environment with mean score of 3.49 at moderate level and 3) participation with mean score of 3.41 at moderate level, respectively.

A. Recommendation

From results from data survey with personnel in Faculty of Engineering from the questionnaires the respondents completed, following are recommendations toward the study of performance measurement as the digital university as follows

- Instruments and equipment including instructional media and supporting utensils should be updated to match with current technology.
- Speed of internet system and connection, system stability and signal distribution system should be improved to cover all areas of Faculty of Engineering.
- Personnel and students should be well and correctly trained and educated about information of the digital university.

ACKNOWLEDGMENT

Thank you Rajamangala University of Technology Phra Nakhon and Institute of Research and Development for supporting this research.

REFERENCES

- [1] Wilaiphan S. "Industry 4.0". Article Design Prapas Talk Solidwork. 2017.
- [2] Lakhana , C. "RMUTP Digital University" MAG RMUTP. December issue 01, 2015.
- [3] Kennerley, M. and Neely, A. , "A Framework of the factors affecting the evolution of performance measurement systems", International Journal of Operations & Production Management, Vol. 22, No. 11, 2002, pp.1222-45.
- [4] Hamid Kazemkhanlou, "Study of Performance Measurement Practices in Supply Chain Management." Proceedings of the 2014 International Conference on Industrial Engineering and Operations Management Bali, Indonesia, January 7 – 9, 2014, pp. 273-285.
- [5] Sink, D.S., "Productivity Management: Planning, Measurement and Evaluation." Control and Improvement, Wiley, New York, 1985.
- [6] Wireman, T., "Developing Performance Indicators for Managing Maintenance." Industrial Press, Inc, New York, 1998.
- [7] Yamane, Taro. "Statistics: an introductory analysis." New York : Harper & Row, 1973.
- [8] Likert, Rensis. "A Technique for the Measurement of Attitudes." Archives of Psychology 140 ,1932, pp.1-55.



The Construction and Efficiency Finding of Instructional Package on the Topic of ASK in Digital Modulation for Application to Vocational Education

Natthawut Panitjaroen

Department of Electrical Engineering
Rajamangala University of Technology Lanna Tak
Tak, Thailand
e-mail: nattrit@gmail.com

Anchalee Panitjaroen

Department of Electrical Engineering
Rajamangala University of Technology Lanna Tak
Tak, Thailand
e-mail: anchalee.tak@gmail.com

Abstract—The objective of this study were construction and efficiency finding of Teaching Package on the Topic of ASK in Digital Modulation for Application to Vocational Education on diploma student. In addition, it is to compare the learning achievement of the students between both before and after teaching and learning the teaching set. This study is the Experimental Research with one group pre-test post-test design. There were 25 students in sampling group. They were the last year student in semester 2, academic year 2017, who were studying in Diploma Program in Electronics and had studied Telecommunication system, Rajamangala University of Technology Lanna Tak. The efficiency of teaching set could be found from the value analysis of E1/E2 and compared with the learning achievement of the students both before and after teaching and learning by the teaching set. There was analyzed by test t-test Value. According to the research result, it showed that teaching set constructed by the researcher reach the efficiency of 84.48/81.60, higher than the standard criteria. When comparing the difference between the values of the scores on before and after teaching and learning by the statistic of t-test, it showed statistically significant level. As a result, the new teaching set constructed by researcher had the efficiency level which increased at the statistical significance level 0.05.

Keywords— teaching package; digitalmodulation; ASK.

I. INTRODUCTION

Digital Modulation provides more information capacity, high data security, quicker system availability with great quality communication. Hence, digital modulation techniques have a greater demand, for their capacity to convey larger amounts of data than analog modulation techniques.

There are many types of digital modulation techniques and also their combinations, depending upon the need. Of them all, we will discuss the prominent ones; (1) ASK – Amplitude Shift Keying. The amplitude of the resultant output depends upon the input data whether it should be a zero level or a variation of positive and negative, depending upon the carrier frequency, (2) FSK – Frequency Shift Keying. The frequency of the output signal will be either high or low, depending upon the input data applied. (3) PSK – Phase Shift Keying. The phase of the output signal gets shifted depending upon the input. These are mainly of two types, namely Binary Phase Shift Keying (BPSK) and Quadrature Phase Shift Keying (QPSK), according to the number of phase shifts. The other one is Differential Phase Shift Keying (DPSK) which changes the phase according to the previous value.

Amplitude Shift Keying (ASK) is a type of Amplitude Modulation which represents the binary data in the form of variations in the amplitude of a signal. Any modulated signal has a high frequency carrier. The binary signal when ASK modulated, gives a zero value for Low input while it gives the carrier output for High input. The following figure represents ASK modulated waveform along with its input.

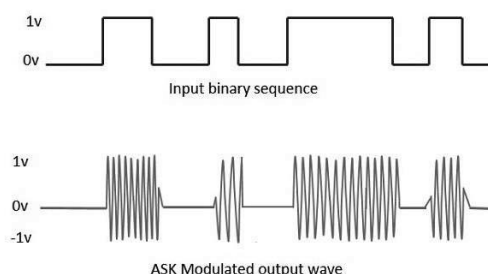


Fig.1. ASK modulated waveform.



A. ASK Modulator

The ASK modulator block diagram comprises of the carrier signal generator, the binary sequence from the message signal and the band-limited filter. Following is the block diagram of the ASK Modulator.

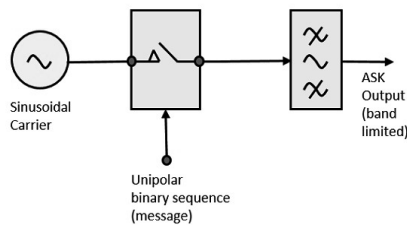


Fig.2 The block diagram of the ASK Modulator.

The carrier generator, sends a continuous high-frequency carrier. The binary sequence from the message signal makes the unipolar input to be either High or Low. The high signal closes the switch, allowing a carrier wave. Hence, the output will be the carrier signal at high input. When there is low input, the switch opens, allowing no voltage to appear. Hence, the output will be low. The band-limiting filter, shapes the pulse depending upon the amplitude and phase characteristics of the band-limiting filter or the pulse-shaping filter.

B. ASK Demodulator

There are two types of ASK Demodulation techniques. They are

- Asynchronous ASK Demodulation/detection
- Synchronous ASK Demodulation/detection

The Asynchronous ASK detector consists of a half-wave rectifier, a low pass filter, and a comparator. Following is the block diagram for the same. The modulated ASK signal is given to the half-wave rectifier, which delivers a positive half output. The low pass filter suppresses the higher frequencies and gives an envelope detected output from which the comparator delivers a digital output.

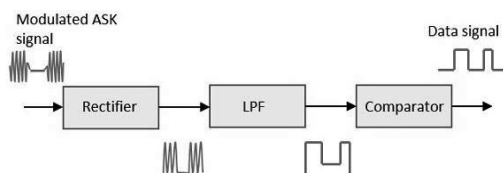


Fig.3 The Asynchronous ASK detector.

Synchronous ASK detector consists of a Square law detector, low pass filter, a comparator, and a voltage limiter. Following is the block diagram for the same.

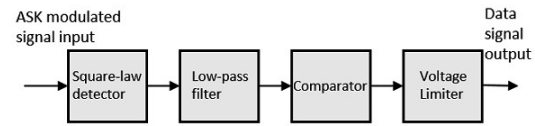


Fig.4. The Synchronous ASK detector.

The ASK modulated input signal is given to the Square law detector. A square law detector is one whose output voltage is proportional to the square of the amplitude modulated input voltage. The low pass filter minimizes the higher frequencies. The comparator and the voltage limiter help to get a clean digital output.

II. RESEARCH METHODOLOGY

A. Research Objectives

construction and efficiency finding of Teaching Package on the Topic of ASK in Digital Modulation for Application to Vocational Education on diploma student.

B. Research hypothesis

The teaching package was designed to be used effectively in the 80/80 standard.

C. Scope of Research

The instruction set was used for the practical study on the topic of ASK in Digital Modulation.

D. Initial agreement

- This research did not consider gender, age, economic, social, emotional, and study time of the sample.
- In this test, the students in this course have the same qualifications. They passed the entrance examination for the same course.
- The opinions of the experts are considered at the discretion of the sincerity, which express the true feelings of the group of experts.

E. Definitions used in research.

- The instruction set is a set of teaching materials on telecommunication in the topic of ASK in Digital Modulation. The researcher composed of Teaching Guide, The instructional materials include instructional plans, behavioral objectives, leaflets, test papers, and instructional media.
- Performance of the instructional package refers to the quality of the instruction set as measured by the average score of all student tests.
- The 80/80 means the average score of the test; The first 80 marks the average score obtained from all student test papers as a percentage, The second 80 means the mean score obtained from the post test of all students, calculated as a percentage



- The test is a set of tests that students do during class to evaluate progress.
- A test suite mean tests used to measure student achievement after completing all the course topics.
- Qualified persons are those who have experience teaching in the field of information communication or who teach subjects with similar content or educational qualifications not lower than the master's degree or experienced. The design of the collision media for at least 5 years.

F. Research Methodology

This research is experimental. To construction and efficiency finding of Teaching Package on the Topic of ASK in Digital Modulation for Application to Vocational Education on diploma student at RMUTL TAK. The researcher performs the following steps;

- Determine population and sample,
Diploma student who registered Telecommunication System Course at RMUTL TAK,
The samples used in this study were the second year students in the 2nd semester of the academic year 2017 of the curriculum using the Purposive Sampling from the population.
- Research tools;
Construction Teaching Package;
Analyze the subject by means of a framework of documents, courses, documents and related texts, and Define the behavioral objectives of all topic, and Analyze content Subjects are included in the curriculum analysis table, and Prepare the teaching materials and then practice the experts to assess. Improve quality and develop integrity. The design of digital modulation circuits was used as a tool for this research, and data collection.
- To create the test is divided into 2 parts.
First, the test is a test to measure the progress of students during the teaching of the subject is multiple choice questions based on four options behavioral objectives for each topic.
Second, the test is a set of test items to measure test achievement as 4 multiple choice options, which are based on behavioral objectives.
- Evaluation of research tools;
First, The test was administered to 5 experts who assessed the consistency of the test for achievement with the behavioral objective by finding IOC consistency and, Expert assessments of the IOC will be equal to or greater than 0.5 will be considered valid. If lower, need to improve.
- To evaluate the satisfaction of the teaching set by using the test to evaluate the opinions.
- Data collection.
- One short case study and one trial case. The experiment was conducted to test the results.

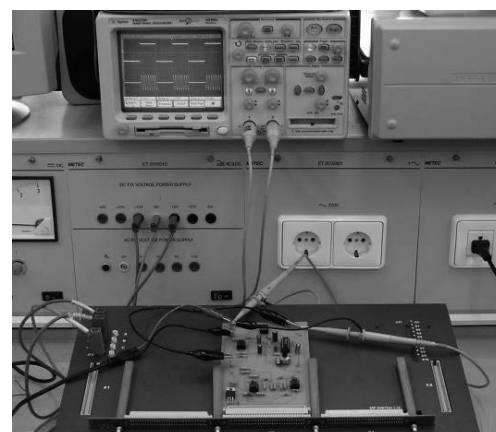


Fig.5. The module was constructed into the instruction package.

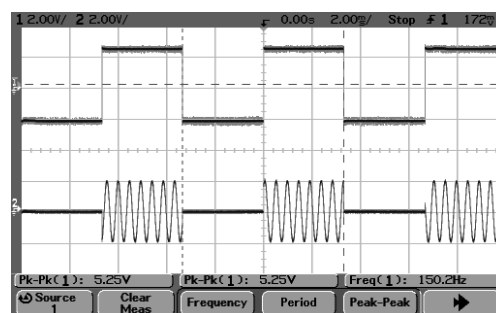


Fig.6. The signal test results of ASK.

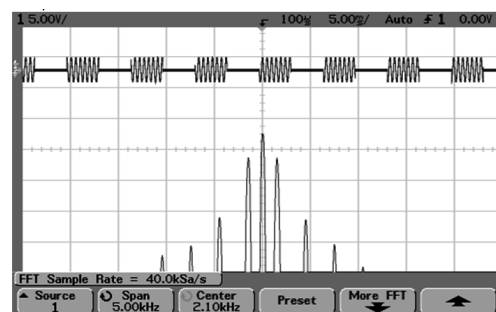


Fig.7. The frequency spectrum of ASK.

III. THE RESULTS OF THE STUDY

A. Analyze the effectiveness of the instruction set.

Analyze the effectiveness of the instructional package from the sample. The results are shown in Table 1.



TABLE I. RESULTS OF INSTRUCTIONAL PACKAGE PERFORMANCE.

Test suite	N	score	sum	mean	%
<i>pre-test</i>	25	30	222	8.88	29.60
Quiz 1	25	5	104	4.16	83.20
Quiz 2	25	5	108	4.32	86.40
Quiz 3	25	5	107	4.28	85.60
Quiz 4	25	5	104	4.16	83.20
Quiz 5	25	5	105	4.20	84.00
<i>summary</i>	25	25	528	4.22	84.48
<i>post-test</i>	25	30	612	24.48	81.60

The sample were made to measure the progress of the course average was 84.48% and tested for achievement average was 81.60%. To measure the effectiveness of the instructional package is 84.48 / 81.60.

TABLE II. RESULTS OF INSTRUCTIONAL PACKAGE PERFORMANCE.

Score	N	mean	ΣD	ΣD^2	t
pre-test	25	8.88	390	6170	41.21*
post-test	25	24.48			

*The statistical significance level 0.05

The results show that 25 samples tested the achievement before and after the study when testing the difference between pre-test and t-test scores, the t-value calculated more than the t-value from the table indicates that the average of the pre-test and post-test scores there were statistically significant differences at the 0.05 level. That is, learning with this instructional package. The learners have higher knowledge and learners have higher average scores than before.

IV. CONCLUSIONS

- A. The instruction package was constructed with efficiency of 84.48 / 81.60. The instructional package is 80/80 effective based on the research hypothesis.
- B. The student's achievement was higher after testing the difference between the pre-test and the post-test scores using the t-test. The t-values that were calculated more than the t-values from the table showed that after learning with the set The teaching that the researcher created. The students had higher academic achievement at the statistical significance level of 0.05.

V. DISCUSSIONS

The instruction package was constructed and effectiveness of the ASK instruction package the discussion is as follows;

- A. The effectiveness of the instruction package. The effectiveness of the instructional package was higher than the criterion of 84.48/81.60 and the content is tested individually. This allows students to memorize formulas and form the equations well. In addition, the instructional package is planned as a step-by-step process. Planning the teaching methods, using media, broadcasting content. The teaching is tight, the time is right. And the students get more details of the content.
- B. The scores of the pre-test and post-test measures were 29.60 and 81.60 percent, respectively. When tested by means of the statistic, the mean scores from the post-test were higher than those from the pre-test at the 0.05 level, according to the assumptions set. Because after learning through teaching the teaching set. The students have a better understanding of the content. The students used the knowledge to apply in the test achievement. As a result, students have higher academic achievement.

VI. ACKNOWLEDGMENTS

The research team would like to thank Rajamangala University of Technology Lanna Tak who supporting this research and Mr. Warakorn Panitjaroen for proofreading.

VII. REFERENCES

- [1] Andrew Leven, "Telecommunication Circuits and Technology", Academic Press 2000.
- [2] G M. Miller and J S. Beasley, "Modern Electronic Communication", 8/E Prentice Hall, 2005.
- [3] K. Hess. "Communication Circuits, Analysis and Design", Addison Wesley 1994.
- [4] P. Dondon, J. M. Micouleau, P. Kadionik, "Improving learning efficiency for digital modulation courses" in WSEAS Engineering education, Greece., 2005.
- [5] R. W. Lucky, J. Salz, E. J. Weldon, Principles of Data Communication, New York:McGraw-Hill Book Company, 1968.
- [6] Smith Jack, "Modern Communication Circuits", New York, McGraw-Hill 1998.
- [7] Syed. Karimulla, P.S. Niranjana Kumar, Gulam Amer, "Enhancement of power transmission system performance", *Emerging Trends in Electrical and Computer Technology (ICETECT) 2011 International Conference on*, pp. 50-56, 2011.
- [8] W. R. Bennett, J. R. Davey, Data Transmission, McGraw-Hill Book Company, 1965.
- [9] W. Song, J. Zhang, Q. Yao, "Design and Implementation of BPSK Modulator and Demodulator on Modern DSP Technology", *3rd IEEE International Symposium on Microwave Antenna Propagation and EMC Technologies for Wireless Communications*, pp. 1135-1137, 2009.



The Construction and Efficiency Finding of Instructional Package on the Module of Video and Audio Analog Optical Fiber Link

Anchalee Panitjaroen

Department of Electrical Engineering
Rajamangala University of Technology Lanna Tak
Tak, Thailand
e-mail: anchalee.tak@gmail.com

Hansa Khetbunphot

Department of General Education
Uttaradit Technical College
Uttaradit, Thailand
e-mail: hansa_khet@hotmail.com

Natthawut Panitjaroen

Department of Electrical Engineering
Rajamangala University of Technology Lanna Tak
Tak, Thailand
e-mail: nattrit@gmail.com

Abstract—The objective of this study were construction and efficiency finding of Teaching Package on the Topic of the modular instructional package of video and audio analog optical fiber link. Circuit designed to test signal performance to come out as expected. This is to introduce the knowledge gained from the creation and the efficiency of the modulation circuit. The instructional package was created to convey to the sample students are high school diploma. Enrollment in the second semester of academic year 2560, at RMUTL TAK: Rajamangala University of Technology Lanna Tak. Then take the test to measure the achievement. Then the scores were calculated for the instructional package. The results of this research show that the instruction package developed by the researcher was 80.30/80.15 and the students' satisfaction was at the high level (mean 4.48) Performance based on research hypothesis.

Keywords— teaching package; optical communication; optical fiber link.

I. INTRODUCTION

A. Fiber Optics

An optical fiber can be understood as a dielectric waveguide, which operates at optical frequencies. The device or a tube, if bent or if terminated to radiate energy, is called a waveguide, in general. Following image depicts a bunch of fiber optic cables. The electromagnetic energy travels through it in the form of light. The light propagation, along a

waveguide can be described in terms of a set of guided electromagnetic waves, called as modes of the waveguide.

B. Working Principle

A fundamental optical parameter one should have an idea about, while studying fiber optics is Refractive index.

By definition, "The ratio of the speed of light in a vacuum to that in matter is the index of refraction n of the material." It is represented as

$$n = \frac{c}{v} \quad (1)$$

Where

c = the speed of light in free space = 3×10^8 m/s

v = the speed of light in dielectric

Generally, for a travelling light ray, reflection takes place when $n_2 < n_1$. The bent of light ray at the interface is the result of difference in the speed of light in two materials that have different refractive indices. The relationship between these angles at the interface can be termed as Snell's law. It is represented as

$$n_1 \sin \phi_1 = n_2 \sin \phi_2 \quad (2)$$

Where, ϕ_1 is the angle of incidence

ϕ_2 is the refracted angle

n_1 and n_2 are the refractive indices of two materials



For an optically dense material, if the reflection takes place within the same material, then such a phenomenon is called as internal reflection. The incident angle and refracted angle are shown in the following figure. If the angle of incidence ϕ_1 is much larger, then the refracted angle ϕ_2 at a point becomes $\Pi/2$. Further refraction is not possible beyond this point. Hence, such a point is called as Critical angle ϕ_c . When the incident angle ϕ_1 is greater than the critical angle, the condition for total internal reflection is satisfied. The following figure shows these terms clearly.

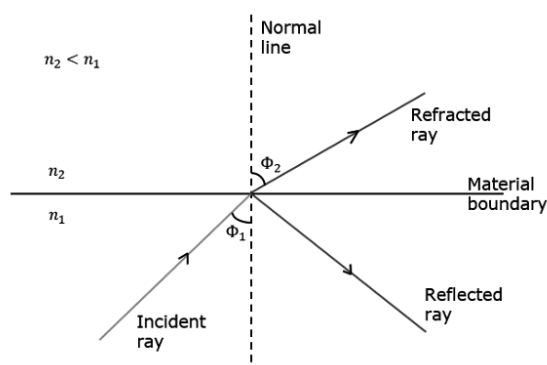


Fig.1. Internal reflection

A light ray, if passed into a glass, at such condition, it is totally reflected back into the glass with no light escaping from the surface of the glass.

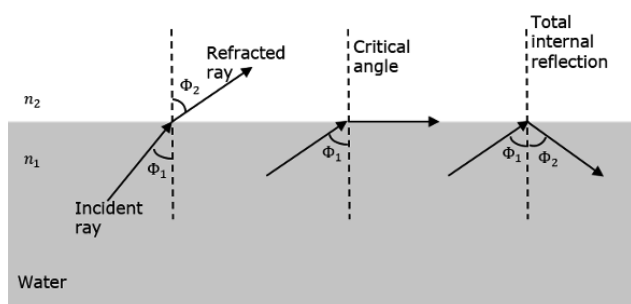


Fig.2. Total internal reflection

C. Parts of a Fiber

The most commonly used optical fiber is single solid dielectric cylinder of radius and index of refraction n_1 . The following figure explains the parts of an optical fiber.

This cylinder is known as the Core of the fiber. A solid dielectric material surrounds the core, which is called

as Cladding. Cladding has a refractive index n_2 which is less than n_1 .

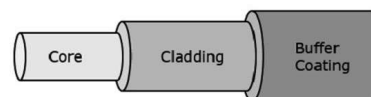


Fig.3. Parts of a fiber

D. Types of Optical Fibers

Depending upon the material composition of the core, there are two types of fibers used commonly. They are

- Step-index fiber- The refractive index of the core is uniform throughout and undergoes an abrupt change (or step) at the cladding boundary.
- Graded-index fiber- The core refractive index is made to vary as a function of the radial distance from the center of the fiber.

Both of these are further divided into

- Single-mode fiber- These are excited with laser.
- Multi-mode fiber- These are excited with LED.

E. Optical Fiber Communications

The communication system of fiber optics is well understood by studying the parts and sections of it. The major elements of an optical fiber communication system are shown in the following figure.

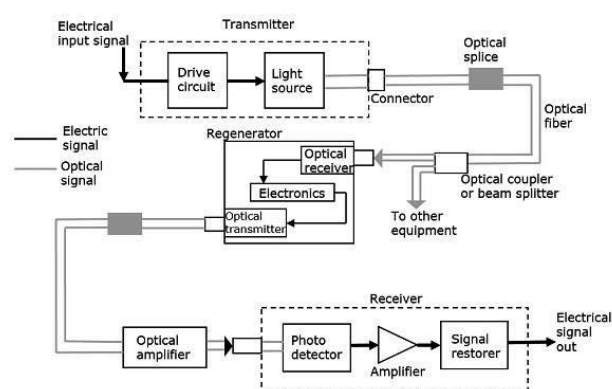


Fig.4. Optical fiber communication system

The basic components are light signal transmitter, the optical fiber, and the photo detecting receiver. The additional elements such as fiber and cable splicers and connectors, regenerators, beam splitters, and optical amplifiers are



employed to improve the performance of the communication system.

F. Applications of Fiber Optics

The optical fibers have many applications. Some of them are as follows

- Used in telephone systems
- Used in sub-marine cable networks
- Used in data link for computer networks, CATV Systems
- Used in CCTV surveillance cameras
- Used for connecting fire, police, and other emergency services.
- Used in hospitals, schools, and traffic management systems.
- They have many industrial uses and also used for in heavy duty constructions.

II. RESEARCH METHODOLOGY

A. Research Objectives

Construction and efficiency finding of teaching package on the topic of the modular instructional package of video and audio analog optical fiber link.

B. Research hypothesis

The teaching package was designed to be used effectively in the 80/80 standard and the opinions of students are satisfied at a high level.

C. Scope of Research

The instruction set was used for the practical study on the topic of video and audio optical fiber link.

D. Initial agreement

- This research did not consider gender, age, economic, social, emotional, and study time of the sample.
- In this test, the students in this course have the same qualifications. They passed the entrance examination for the same course.
- The opinions of the experts are considered at the discretion of the sincerity, which express the true feelings of the group of experts.

E. Definitions used in research.

- The instruction set is a set of teaching materials on telecommunication in the topic of video and audio optical fiber link. The researcher composed of teaching guide, The instructional materials include instructional plans, behavioral objectives, leaflets, test papers, and instructional media.

- Performance of the instructional package refers to the quality of the instruction set as measured by the average score of all student tests.
- The 80/80 means the average score of the test; The first 80 marks the average score obtained from all student test papers as a percentage, The second 80 means the mean score obtained from the post test of all students, calculated as a percentage
- The test is a set of tests that students do during class to evaluate progress.
- A test suite mean tests used to measure student achievement after completing all the course topics.
- Qualified persons are those who have experience teaching in the field of information communication or who teach subjects with similar content or educational qualifications not lower than the master's degree or experienced. The design of the collision media for at least 5 years.

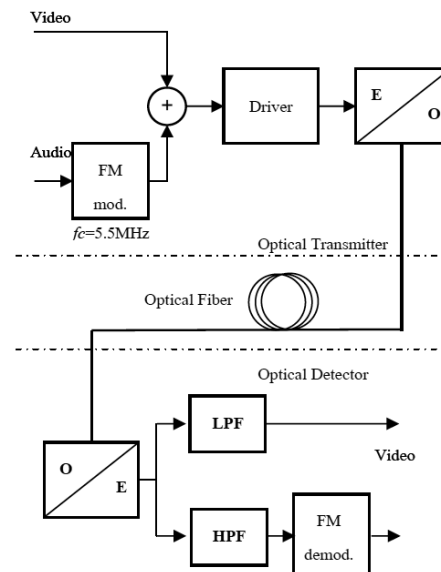


Fig.5. The module was constructed into the instruction package.



Fig.6. The fiber optic multimode type in the instruction package.

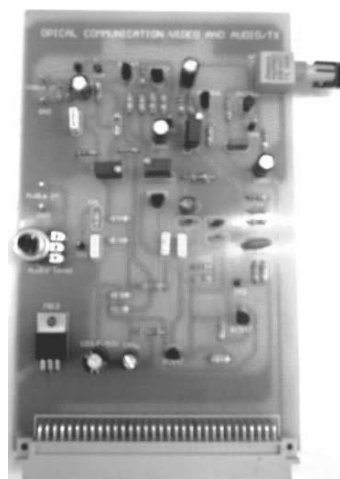


Fig.7. The modules for sending.

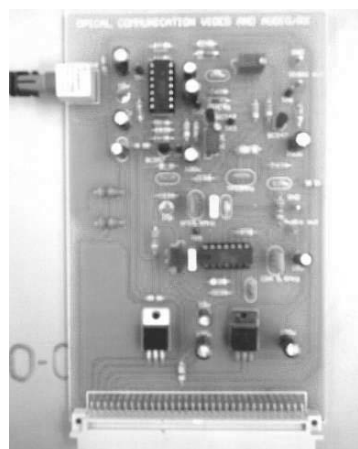


Fig.8. The receiving module



Fig.9. The composition of the entire system for education.

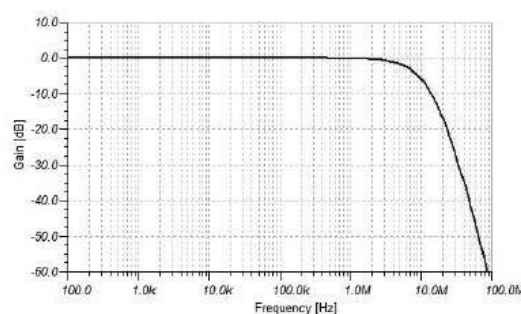


Fig.10. The frequency response of the video signal

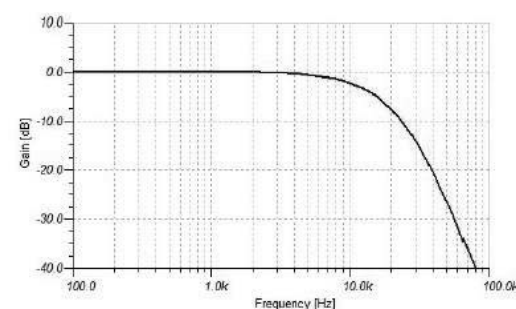


Fig.11. The frequency response of the audio signal

F. Research Methodology

This research is experimental. To construction and efficiency finding of Teaching Package on the Topic of video and audio optical fiber link on diploma student at RMUTL TAK. The researcher performs the following steps;

- Determine population and sample,
Diploma student who registered Telecommunication System Course at RMUTL TAK, The samples used in this study were the second year students in the 2nd semester of the academic year 2017 of the curriculum using the Purposive Sampling from the population.
- Research tools;
Construction Teaching Package;
Analyze the subject by means of a framework of documents, courses, documents and related texts, and Define the behavioral objectives of all topic, and Analyze content Subjects are included in the curriculum analysis table, and prepare the teaching materials and then practice the experts to assess. Improve quality and develop integrity. The design of digital modulation circuits was used as a tool for this research, and data collection.
- To create the test is divided into 2 parts.
First, the test is a test to measure the progress of students during the teaching of the subject is multiple choice questions based on four options behavioral objectives for each topic. Second, the test is a set of



test items to measure test achievement as 4 multiple choices options, which are based on behavioral objectives.

- Evaluation of research tools;
First, The test was administered to 5 experts who assessed the consistency of the test for achievement with the behavioral objective by finding IOC consistency and, Expert assessments of the IOC will be equal to or greater than 0.5 will be considered valid. If lower, need to improve.
- To evaluate the satisfaction of the teaching set by using the test to evaluate the opinions.
- Data collection.

III. THE RESULTS OF THE STUDY

A. Analyze the effectiveness of the instruction set.

Analyze the effectiveness of the instructional package from the sample. The results are shown in Table 1.

TABLE I. Results of Instructional Package Performance.

Test suite	N	sum	mean	%
exercise	33	1325	40.15	80.30
test	33	529	16.03	80.15

The sample were made to measure the progress of the course average was 80.30% and tested for achievement average was 80.15%. To measure the effectiveness of the instructional package is 80.30 / 80.15.

TABLE II. THE OPINIONS OF STUDENTS

Description	mean	SD
1. Ease of use in education	4.40	0.45
2. Suitability to education level	4.50	0.89
3. Create skills and knowledge	4.60	0.96
4. Easy maintenance Easy maintenance	4.40	0.55
5. Safety	4.48	0.82
Total	4.48	0.73

The opinions of students are satisfied at a high level. (mean=4.48, SD=0.73)

IV. CONCLUSIONS

- The instruction package was constructed with efficiency of 80.30 / 80.15. The instructional package is 80/80 effective based on the research hypothesis.
- The opinions of students are satisfied at a high level. (mean=4.48, SD=0.73)

V. DISCUSSIONS

The effectiveness of the instruction package. The effectiveness of the instructional package was higher than the criterion of 80.30/80.15 and the content is tested individually. This allows students to memorize formulas and form the equations well. In addition, the instructional package is planned as a step-by-step process. Planning the teaching methods, using media, broadcasting content. The teaching is tight, the time is right and the students get more details of the content. The opinions of students are satisfied at a high level. (mean=4.48) Performance based on research hypothesis.

VI. ACKNOWLEDGMENTS

The research team would like to thank Rajamangala University of Technology Lanna Tak and Uttharadit technical college who supporting this research.

VII. REFERENCES

- [1] Andrew Leven, "Telecommunication Circuits and Technology", Academic Press 2000.
- [2] G M. Miller and J S. Beasley, "Modern Electronic Communication", 8/E Prentice Hall, 2005.
- [3] Jiwook Youn, Bupjoong Kim, Wooyoung Choi, Hyunjae Lee, Hongju Kim, Jaehoon Yu, "Demonstration of packet-optic integrated transport system", *Optical Internet (COIN) 2010 9th International Conference on*, pp. 1-3, 2010.
- [4] K. Hess. "Communication Circuits, Analysis and Design", Addison Wesley 1994.
- [5] R. Olshansky, "RF multiplexing techniques applied to video distribution in local networks", *Proc. 13th Euro. Conf. Optical Commun.*, vol. II, pp. 122, 1987-Sept.-13-17.
- [6] Smith Jack, "Modern Communication Circuits", New York, McGraw-Hill 1998.
- [7] W. E. Stephens, T. R. Josephs, "A 1.3- μ m microwave fiber optic link using a direct-modulated laser transmitter", *J. Lightwave Technol.*, vol. LT-3, pp. 308-315, 1985.
- [8] Wei Wei, Junqiang Hu, Dayou Qian, Philip N. Ji, Ting Wang, Xin Liu, Chunming Qiao, "PONIARD: A Programmable Optical Networking Infrastructure for Advanced Research and Development of Future Internet", *Lightwave Technology Journal of*, vol. 27, pp. 233-242, 200



Motives to study Bachelor of Technology Program in Engineering Business, Silpakorn University

Supachai Wasananon, Teerachai Surachotivet, Jarut Kunanoppadol

Department of Mechanical Engineering
Faculty of Engineering and Industrial Technology,
Silpakorn University
Nakhon Pathom, Thailand
e-mail address: wasananon@gmail.com

Abstract— The purpose of this research was to find motives for studying a Bachelor of Technology Program in Engineering Business at the Faculty of Engineering and Industrial Technology at Silpakorn University. The population in this survey research was 639 students of the program who were asked to complete the self-administered questionnaires. The collected data were then analyzed by using statistic methods including; percentage, mean, S.D. and F-test. The results revealed that motives behind most students' enrollments in this program were the reputation and recognition of Silpakorn University while a suggestion by others was partially affect their decision. Evidently, the experiment on the hypothesis of different background of students influenced their motives to study the program was at 0.05 statistical significance.

Keywords— Motives; B.Tech. (Engineering Business)

chance or having facilities. However, motives are divided into two types [3, 4] which are; 1) intrinsic motives that come from an individual's attitude, interest, value, or needs, which can permanently affect their behaviors, [5] and 2) extrinsic motives which are the surroundings of an individual that influence particular behaviors. This type of motives can be in forms of compliment or praise; therefore, they are temporary affect an individual's behavior. [6, 7] Changes on number of students enrolling in the program each year may be because of different motives; either intrinsic or extrinsic motives, or even internal factors of the university. It is suggested that the findings of this research on students' motives to study in the program can be useful for teaching developments, which can ensure the production of well-qualified graduates. In addition, the results of this study will be useful for future advertisements and the guidance for further study.

I. INTRODUCTION

Business and industrial developments in Thailand are growing widely and rapidly. This means more graduates with knowledge of business administration and engineering are required to meet the demands. The faculty of engineering and industrial technology at Silpakorn University recognized the importance of this development; therefore, launched a Bachelor of Technology Program in Engineering Business, which was the first institute in Thailand to offer this program. Knowledge of business and general engineering were integrated to generate this interdisciplinary program which consists of 4 major sciences; engineering, accounting, management and administration, and English. The program was officially launched in 2009. Graduates of this program have several career opportunities such as engineering entrepreneurs, construction contractors, machine installation services, engineering material suppliers, finance and accounting officers, purchasing and inventory officers, procurement assistants to an engineer, or overseas sales coordinators. [1]

Motives to study depend on several factors. Rogers Carl R [2] suggested that there are 4 different motives to study including; 1) vocation motives, 2) self-development motives, 3) social motives, and 4) other motives such as getting second

II. METHODOLOGY

A. The population

The population in this survey research was 639 students in the academic year 2016 of the Bachelor of Technology Program in Engineering Business. The period that the population involved in this research was between May 2016 and February 2017.

B. The instrument used to collect data

The instrument used to collect data was the self-administered questionnaires with topics on motives to study the Bachelor of Technology Program in Engineering Business at Silpakorn University. After doing some relevant research, authors created the questionnaires and submit them to the five experts to check the content suitability, proof read, and find the Index of Item-Objective Congruence (IOC) which was equal to or more than 0.5; therefore, the questionnaires were good for use. Then the questionnaires were tried out with the experimental group of 50 and tested for reliability. In total, the reliability of the questionnaires was equal to 0.95. The questionnaires were in checklist format and included open-ended questions to collect data in which 90.91% completed this section.



C. Data analysis

Data analysis was completed by using mean, standard deviation, F value in the ANOVA test using Exploratory Factor Analysis.

D. Research process

Research process was summarized in Fig.1

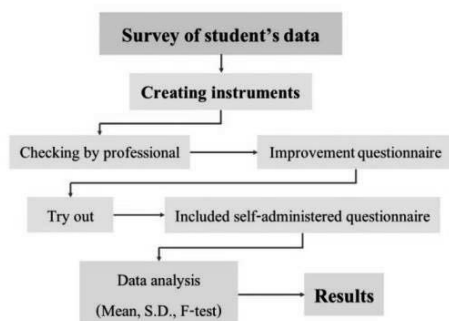


Fig.1. Research process

III. FINDINGS

A. Information of Students of B.Tech (Engineering Business)

Information of Students of B.Tech (Engineering Business): 639 students of the Bachelor of Technology Program in Engineering Business of academic year 2016 consisted of; female students (76%) which was the majority, hometown in central Thailand (68.67%), high school graduated from Science-Math program (53.33%), achievement scores ≥ 3.25 (38.33%), parents' salary range THB15,000 - THB30,000 (46.00%), parents' education level lower than senior-high school (28%), and parents' common occupation (29.67%).

B. Motives to study B.Tech (Engineering Business) was summarized in TABLE I

TABLE I. Mean and S.D. of motives to study B.Tech (Engineering Business)

Motives to study B.Tech (Engineering Business)	Level of Motives		
	Mean	S.D.	Results
1. Vocation			
1.1 Ability to be a freelance	3.907	0.730	High
1.2 High remuneration	3.590	0.719	High
1.3 Employment guarantee	3.633	0.784	High
2. Self-Development			
2.1 Personal interest	3.467	0.831	High
2.2 Increase knowledge engineering business	3.577	0.757	High
2.3 Pathway for higher study	3.597	0.793	High
3. Social			
3.1 Accepted in the society	3.743	0.868	High
3.2 Recognition in the society	4.013	0.749	High
4. The Program			
4.1 Meets the demand in Thailand	3.553	0.732	High
4.2 Interesting	3.627	0.741	High
4.3 Modern and applicable	3.683	0.752	High

Motives to study B.Tech (Engineering Business)	Level of Motives		
	Mean	S.D.	Results
5. Institute			
5.1 Silpakorn University's reputation and recognition	4.317	0.701	Highest
5.2 Suitable environment in Silpakorn University	4.263	0.746	Highest
5.3 Academic experts	4.097	0.723	High
6. Economy			
6.1 Acceptable tuition fee	3.513	0.848	High
6.2 Acceptable special fee	3.187	0.888	Medium
7. Suggestion from others			
7.1 Family members	3.123	1.051	Medium
7.2 Friends	3.007	1.025	Medium
7.3 Senior students	2.520	1.061	Low
7.4 Teachers from previous educational institute	2.927	1.137	Medium

From TABLE I, the main motive to study B.Tech (Engineering Business) was the reputation and recognition of Silpakorn University (Mean = 4.317, S.D. = 0.701), while suggestions from others were barely the motive to study the program (Mean = 2.520, S.D. = 1.061).

C. Relationship between students' information and their motives to study B.Tech (Engineering Business) was summarized in TABLE II

TABLE II. F-test of motivation to study B.Tech. (Engineering Business)

Motivation to study B.Tech. (Engineering Business)	F value in the ANOVA test						
	Gender	Hometown	Program	Achievement score	Parents' education	Parents' salary	Parents' occupation
1. Vocation	0.077	0.710	3.329*	1.568	0.923	1.388	0.985
2. Self-Development	0.714	0.420	0.598	1.860	0.911	3.182*	0.415
3. Social	3.947*	0.336	1.410	2.295	1.210	0.234	1.066
4. The Program	0.872	0.374	2.946*	1.039	0.782	2.507	1.980*
5. Institute	3.603	0.604	1.729	0.610	1.064	0.548	0.431
6. Economy	2.035	0.891	0.650	0.965	2.245*	2.502	1.258
7. Suggestion from others	0.280	0.675	0.299	0.844	0.559	1.759	1.058

*statistical significance was 0.05

From TABLE II, gender, social, vocation, the program, parents' education level, economy, parents' salary, parents' occupation all affected students' motives to study at the statistical significance of 0.05.

IV. DISCUSSION AND CONCLUSIONS

The main motive for students to study the program was the reputation and recognition of Silpakorn University. This finding matched the research on "Motivation to study in graduate programs of graduate students at Ubon Ratchathani Rajabhat University by Sopa, Chareon [8]", which showed that students motives to study Master degree at Ubon Ratchathani



Rajabhat University was because of its reputation while suggestions from others were barely affect their motives. The result of this study also was in line with the research on “Motivation to study Master degree program in the faculty of GEO-information science, Burapa University” by Petchdee, Kittiya [9], which found that suggestions from senior students were barely the motives to study in the program (8.3%). Moreover, students’ gender influenced their motives to study B.Tech (Engineering Business), which also matched the study on “Motivation in selecting the commercial program of the vocational education students at Siam Institute of Technology” by Pookjampha, Boobpha [10] which found that different gender had different motives to study commercial program with statistical significance of 0.01. The experiment on the hypothesis revealed that different background information of students had different motives to study the Bachelor of Technology Program in Engineering Business at Silpakorn University with statistical significance of 0.05. This results also conformed with the study on “Factors affecting a first year student’s motivation for pursuing a teaching professional education program of Nakhon Pathom Rajabhat University” by Saengloetuthai, Jittirat [11] which found that factors influencing motives to study education program were relevant at the statistical significance of 0.01, which was high and positive.

V. PROPOSED

From the research on Motives to study Bachelor of Technology Program in Engineering Business at Silpakorn University, the authors proposed the following suggestions:

- 1) *More advertisement channels should be available to provide more opportunities to wider audience in the country.*
- 2) *Opportunities for teachers and students to showcase their academic works domestically and internationally which can be another channel for advertising the program and create reliability in labour market and entrepreneurs.*
- 3) *Improve the enrolment process to meet students’ demands to study.*

ACKNOWLEDGEMENT

The authors gratefully acknowledge the Department of Mechanical Engineering, Faculty of Engineering and Industrial Technology, Silpakorn University for all supports.

REFERENCES

- [1] Department of Mechanical Engineering. (2017). Thai Qualifications Framework for Higher Education of Bachelor of Technology Program in Engineering Business. Nakhon Pathom, Thailand: Faculty of Engineering and Industrial Technology at Silpakorn University.
- [2] Rogers, C.R. (1969). Freedom to Learn. Columbus, Ohio: Charles E. Merrill.
- [3] Vilnai-Yavetz, I. and Levina, O. (2018). “Motivating social sharing of e-business content: Intrinsic motivation, extrinsic motivation, or crowding-out effect?”. Computers in Human Behavior 79(February): 181-191.
- [4] Kuvaas, B., Buch, R., Weibel, A., Dysvik, A. and Nerstad, C.G.L. “Do intrinsic and extrinsic motivation relate differently to employee outcomes?” Journal of Economic Psychology 61(August): 244-258.
- [5] Rawolle, M., Wallis, M.S.v., Badham, R. and Kehr, H. M. (2016). “No fit, no fun: The effect of motive incongruence on job burnout and the mediating role of intrinsic motivation”. Personality and Individual Differences 89(January): 65-68.
- [6] Rothes, A., Lemos, M.S. and Gonçalves, T. (2014). “Motives and Beliefs of Learners Enrolled in Adult Education”. Procedia - Social and Behavioral Sciences 112(February): 939-948.
- [7] Finkelstien, M. A. (2009). “Intrinsic vs. extrinsic motivational orientations and the volunteer process”. Personality and Individual Differences 46, 5–6(April): 653-658.
- [8] Sopa, Chareon. (2008) “Motivation to study in graduate programs of graduate students at Ubon Ratchathani Rajabhat University”. Thesis of M.B.A (General Management) at Ubon Ratchathani Rajabhat University.
- [9] Petchdee, Kittiya. (2016). “Motivation to study master degree program in the faculty of GEO-information science, Burapa University”. Thesis of M.B.A (Business Administration for Executives) at Burapa University.
- [10] Pookjampha, Boobpha. (2010). “Motivation in selecting the commercial program of the vocational education students at Siam Institute of Technology”. Thesis of M.Ed. (Business Education) at Srinakharinwirot University.
- [11] Saengloetuthai, Jittirat. (2014). “Factors affecting a first year student’s motivation for pursuing a teaching professional education program of Nakhon Pathom Rajabhat University”. Graduate Studies Journal 11, 52(Jan.-Mar.): 139-147.



Lecture and test in Moodle Platform: the Teaching Innovation on Thermo-fluid Coursework

Nitipong Soponpongpiat, Ittipol Thinnoiwong

Department of Mechanical Engineering
Faculty of Engineering and Industrial Technology, Silpakorn University, Nakhon Pathom, Thailand
Nitipongsopon@gmail.com

Abstract—The learning platform called Moodle was applied to develop the calculation skill of thermos-fluid students. The teaching videos were added in Moodle platform to facilitate the student to access the thermos-fluid coursework at anywhere and anytime. Ten problems from exercises database were randomly selected to establish the weekly test and retest. Moodle was used to score the digital answer sheet of each student and report their score after the test was over. More than 60% of total test score was required before approving the students to access the lesson and test in next week. If students cannot meet this requirement, they were assigned to review the lecture content in video format contained in Moodle platform before retest. The weekly score of classroom was recorded and analyzed. The number of F grade point obtained student was compared between 2 sections which were applied a different coursework management. The observation found that using the Moodle platform to manage the weekly test and announce the score in real-time induced the student's stress. However, this teaching technique resulted in the increase of percentage of class average testing score and student's learning ability. In addition, the number of F grade point obtained student was significantly lower than the conventional coursework management.

Keywords—Moodle; Thermo-fluid; Coursework; Learning platform; teaching innovation

I. INTRODUCTION

Nowadays, Information and Communication Technologies (ICTs) is widely used as learning and teaching tools for higher education. The advantage of these tools is ability to response the student requirements both class meeting time and place. Students can access the learning materials at anywhere and anytime. The well-known learning platform named Moodle was widely applied as learning management system by many universities [1-7]. Moodle provided 7 activities to support the teaching and learning process including Creation, Organization, Delivery, Communications, Collaboration, Assessment, and Reusability [1]. Many works indicated the usefulness of Moodle in professional training such as teacher [2], accountant [3], and businesspeople [6]. Although ICTs lead to an increase of student learning ability, there is a question on a suitability when Moodle platform is used for training of engineering business student especially in design and calculation skill. Recently problem on training of engineering business students is they spend insufficient time for practice in calculation. Many students spend a lot of time to

read and try to remember the text which is useless. In fact, engineering business students are expected to have ability to calculate and design the system. Thus, the students will loss the opportunity to get a job if they do not have enough skill to fulfill the above expectation. In the past, writing and explanation of the calculation example in front of the classroom was the most popular teaching technique. By using this technique, students were expected to do more practice after the class meeting. Homework was used as a tool to increase the calculation skill and experience. However, checking their homework was time-consuming resulting in loss of opportunity to encourage student to correct their mistake. To defeat this limitation, the new teaching innovation, i.e. lecture and test in Moodle learning format was developed. The ability of Moodle to announce the testing score in real time and ability to define the right to access the given lesson and test for each student were used to encourage engineering business students to improve their calculation skill. However, this technique is a new idea and has no evidence to confirm its achievement. In this work, lecture and test in Moodle learning format on thermos-fluid coursework was conducted. The effectiveness of this teaching technique was evaluated. In addition, student's stress resulting from this teaching technique was also investigated.

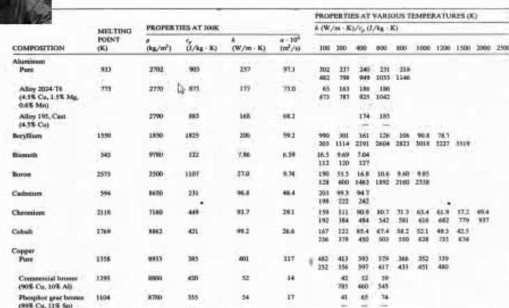
II. METHODOLOGY

A. Thermo-fluid content in video clip format

Lecture content was divided into 9 chapters including introduction, properties of pure substance, work heat and first law of thermodynamics, power and refrigeration cycle, fluids at rest, control volume analysis, dimensionless and similarity, internal and external flow, introduction to heat transfer. The lecture video was produced by Camtasia Studio 8 and SWITF Sound Editor program. The talking head and screen capture technique were applied to produce all lecture videos (Fig.1). It was necessary to control a video playback time to avoid loss in concentration from hour-long hearing. Each chapter composed of many video clips to control the playback time in range of 30-40 minutes (Table 1). All videos were installed into the Lessons Module of Moodle and compatibility checking was also conducted. To record all activities done by each student, the registration will be done before enter the lecture content

B. Lecture and test in Moodle learning format

Chapter	Chapter name	Number of video clip	Playback time (minutes)
1	Introduction	3	28.40/26.06/19.06
2	Properties of pure substance	8	38.38/15.33/16.51/22.04/40.26/22.11/16.59/10.30
3	work heat and first law of thermodynamics	8	23.37/34.21/27.55/11.48/35.50/36.38/40.11/31.59
4	Power and refrigeration cycle	9	23.53/40.07/40.34/40.56/16.47/27.25/33.37/23.15/22.53
5	Fluids at rest	4	31.40/16.40/29.26/13.51
6	Control volume analysis	3	18.40/20.32/15.12
7	Dimensionless and similarity	2	13.06/21.58
8	Internal and external flow	3	24.09/29.35/22.12
9	Introduction to heat transfer	11	12.56/8.43/19.35/24.35/11.16/18.42/18.34/31.26/22.12/32.18/5.57



มหาวิทยาลัยเทคโนโลยีราชมงคลธัญบุรี

Home > General Information > Information System (InfoSys)

Course categories: [เลือกหมวดหมู่วิชา] ▼

Course	
สาขาวิชา THERMODYNAMICS 1	
สาขาวิชา MECHANICAL	
สาขาวิชา Engineering (Automotive & Learning)	
611232-55 THERMOFLUIDS LABORATORY	● ●
614193 BASIC ELECTRICAL ENGINEERING LABORATORY	● ● ●
680108 INFORMATION TECHNOLOGY (Theory and Experiment for MS)	
611281 เทคโนโลยีสารสนเทศศาสตร์ (ELECTRIC & ELECTRONIC) Electrical Engineering for Mechanical Engineers	
611213 สารสนเทศศาสตร์ (Mechanics of Mechanics)	
612311 Control system (Thermal - Fluid)	
611 231 ระบบควบคุมอัตโนมัติ (Basic Thermodynamics)	
611393 ELECTRICAL ENGINEERING LABORATORY FOR MECHANICAL ENGINEERS	●
611113 ENGINEERING MECHANICS (CONCRETE)	●
611372 MECHANICAL ENGINEERING LABORATORY II	●
611351 Safety Equipment (Safety Design)	●
611381-1 Introduction to Safety Engineering	●
611362 Automotive Technology Laboratory	●
611361 Automotive Technology	●
611284-4 Circuit Theory and Electrical Device Laboratory	●
611112 Engineering Mechanics	●
611370 Mechanical Engineering Laboratory	●

[No content shown via Add & new course]

ชื่อ username หรือ password คือ

ชื่อรหัส 0057014

The password must have at least 8 characters, at least 1 digit(s), at least 1 lower case letter(s), at least 1 upper case letter(s), at least 1 non-alphanumeric character(s)

อีเมล Mail@0057014 @ yahoo.co.th

กรุณาระบุข้อมูลส่วนตัว

ชื่อ * ชื่อ@gmail.com

นามสกุล * Mail@gmail.com

เลข 0057014-XXXXX

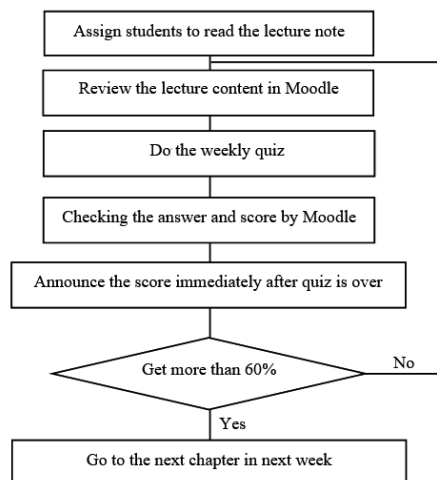
วันเกิด * วันเกิด

ชื่อเล่น * นามสกุล

อาชีพ * Type ▼


สมัคร account ใหม่ | ติดต่อ

The new teaching technique called lecture and test in Moodle learning format can be described as follows. The content of each chapter was provided in form of lecture note and video clip in Moodle platform. Students will be assigned to read the lecture note before class meeting. In class room, students have to create their account by sign up the platform. All activities done by students will be recorded into system. After sign in the system, students will be assigned to review a lecture content in Moodle system. The playback time of each video clip opened by each student was recorded and monitored by lecturer at main server system. When students finish the lecture review, the weekly test has begun. The answer of each student will be checked and testing score will be recorded into system in real-time. After the weekly test is over, testing score of all students will be announced. Students are required to get more than 60 percentage of total score, if not, they will be assigned to review the lecture again and retest will be allowed after finish reviewing. The lecture and retest is done in cycle until the student get more than 60 percentage of weekly test. The student who cannot meet this criteria will be prohibited to enter the next chapter. This procedure is hold for all chapter. The diagram of lecture and test in Moodle platform was shown in Fig.3. It should be noted that the test for each week composed of ten problems which were randomly selected from exercise database. The random process was also done for all retest. The example of test item in Moodle platform was shown in Fig 4.



Current Category Default for ~~English~~ THERMODYNAMICS 1 (235) ☒ Use This Category

Save in Category Default for ~~English~~ THERMODYNAMICS 1 (235)

Question text 

A refrigerator has a steady flow of R-22 as saturated vapor at -20°C into the adiabatic compressor that brings it to $1,000\text{ kPa}$. After the compressor, the temperature is measured to be 60°C . Find the actual compressor work and the actual cycle coefficient of performance.

kJ/kg

28/6/2561 15:36:58



Fig.5 shows the test score of each student after the test was over. Lecturer can monitor the score of each problem in the weekly test. This feature is useful for evaluating the learning ability of each student.

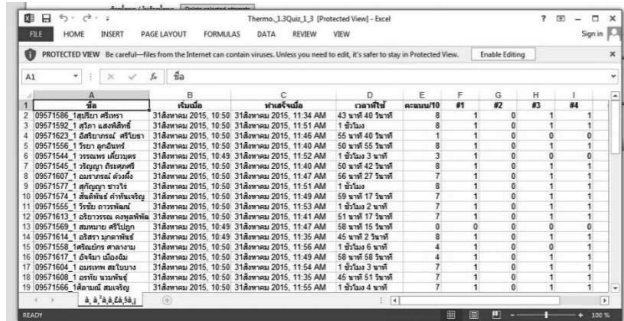


Fig.5 Test score monitoring report exported from Moodle platform to Excel

C. Evaluation of Teaching effectiveness

To evaluate the effectiveness of lecture and test in Moodle platform, the testing scores and grade point data of students from 2 sections were collected. The new technique was applied to 126 students of the first section (denoted Section A) and conventional technique, talking head in front of classroom, was applied to 195 students of the second section (denoted Section B). Students in section B were allowed to enter the lesson and test in next week without any condition on testing score. The evaluation of teaching effectiveness was done by investigating the percentage of class average testing score (PCATS) of each week which can be calculated by following equation.

$$PCATS = \frac{\sum_{i=1}^n (QS)_i}{(n \cdot TS)} \times 100 \quad (1)$$

where QS represents the testing score of each student, n means number of student in each section and TS equals to the total testing score.

The number of F grade point obtained student was also used to evaluate the teaching effectiveness. Finally, the stress of students was also investigated by questionnaire. The data were gathered by teaching assistance who support and service the students when the technical problems occurs. Description of questionnaire, its objective and interpretation score were shown in TABLE II. The weekly stress index (WSI) was defined as following equation.

$$WSI = \frac{\sum_{j=1}^4 \sum_{i=1}^3 (n_i \cdot AIS_i)_j}{(5 \cdot 4 \cdot n)} \quad (2)$$

where n_i represents the number of student who selected answer choice. It is noted that there are three answer choice in each question. Subscript j denotes the number of question and there are 4 questions in questionnaire. The high WSI indicates the increase of student's stress resulting from the coursework management.

TABLE II. DESCRIPTION OF QUESTIONNAIRE

Item	Description	Objective	Answer Interpretation score (AIS)		
			Yes	No idea	No
1	How about the test? Is it hard?	To evaluate the stress resulting from student ability	5	3	1
2	How do you feel after the test?	To evaluate the stress resulting from the test	Good 1	No idea 3	Tired 5
3	Are you boring when you cannot meet the test requirement?	To evaluate the stress resulting from student expectation	Yes 5	No idea 3	No 1
4	Do you like this course management?	To evaluate the attitude of student	Yes 1	No idea 3	No 5

III. RESULTS AND DISSCUSSION

A. Weekly class testing score

Fig. 6 shows percentage of class average testing score (PCATS) of each week. For Section A, the slightly increase of PCATS was found from week 1 to week 3. The PCATS increased from 15.0% to 28.5%. The dramatically increase of PCATS was found from week 3 to week 4. Since week 4, the PCATS of Section A slightly changed in range of 67.0% to 76.6%. When consideration was done on Section B, the maximum PCATS was 51.86% at week 5. From week 5 to week 9, the PCATS tend to decrease from 51.86% to 25.68%. From week 9 to week 11, the PCATS increased again from 25.68% to 40.42%. After week 11, the PCATS decreased from 40.42% to 30.99%. It can be seen that, from week 1 to week 3, there was no difference between Section A and B. This was because basic knowledge and calculation skill of students from both sections were similar. From week 1 to week 3, lecture content focused on the relationship between SI units and others units, basic algebra, and law of ideal gas. Students had studied these contents since they were first-year student. The new teaching technique, thus, had no effect on learning ability in this period. Significantly difference of PCATS between Section A and B was found after week 3. The PCATS of Section A was higher than that of Section B. After week 3, lecture content was specific and more calculation skill was needed. By using the new teaching technique, Section A students were forced to practice the calculation skill through retest mechanism before enter a new lesson and test. In fact, Section A students were in retest situation more than 4 times for each week. This resulted in the increase of their calculation skill and long-term memory. For Section B students, they had only one chance to practice themselves through a weekly test. Their skill may be increased by doing homework but it was difficult to control the students to do homework by themselves. This result indicated that immediately announcing the testing score, after students had finished the test, can be used to identify learning ability and calculation skill of each student. Moreover, the requirement before enter the next lesson and test encouraged students to pay more attention on practice their skill. In conclusion, teaching by means of lecture and test in Moodle platform resulted in the increase of calculation skill and learning ability of students. However, the advantage of this technique did not clearly be seen in starting period of coursework.

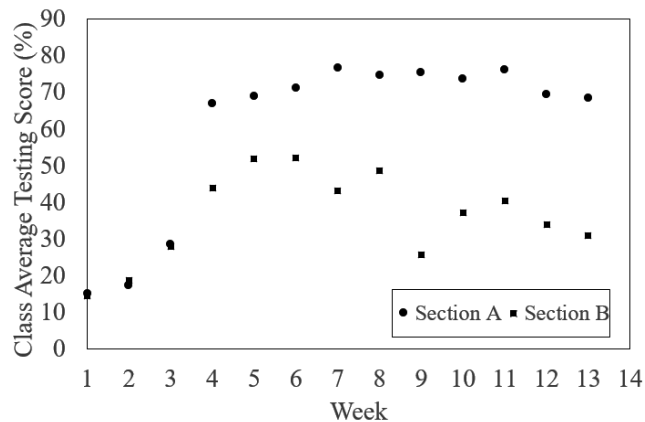


Fig.6 Class average testing score of Section A and Section B students

B. Number of F grade point obtained student

Fig. 7 shows the grade point distribution of students. The percentage of students at each grade point were as follows. For section A, the 26.98%, 8.73%, 19.04%, 16.67%, 4.76%, 8.73%, 6.35%, and 8.74% were found at grade point of A, B+, B, C+, C, D+, D, and F, respectively. For section B, the 21.54%, 5.13%, 12.31%, 6.67%, 7.69%, 11.79%, 11.28%, and 23.59% were found. The average grade point was 2.66 for Section A and 2.02 for Section B. The percentage of F grade point obtained student of Section B was higher than that of Section A for 2.7 times. This result indicated that Section B students spent insufficient time to practice calculation skill after class meeting. In other words, the students abandon the weekly homework. Insufficient calculation skill was barrier to understand the content in next week. Accumulation of this problem during semester resulted in the higher percentage of F grade point obtained student of Section B comparing with that of Section A. For Section A, some student spent 3 or 4 days per week to attend many times of retest. Thus, retest mechanism was equivalent to weekly homework. It can be concluded that the new teaching technique can be used to relieve the abandon homework problem.

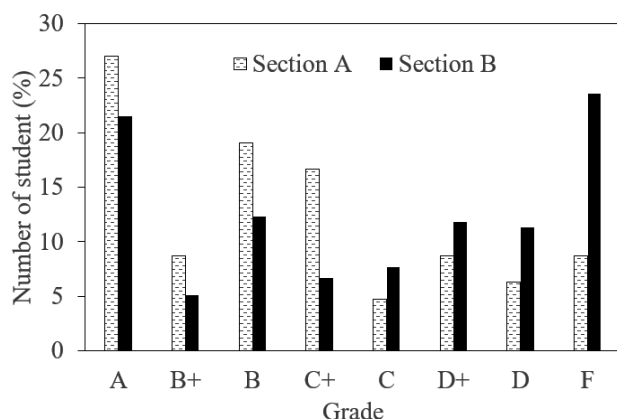


Fig.7 Student's grade point distribution

C. Student's stress resulting from class management

Although the new teaching technique contributed the increase of calculation skill and the decrease of insufficient practice time problem, this teaching technique resulted in the increase of student's stress. As seen in Fig.8, Weekly Stress Index (WSI) of both sections was similar during week 1 to week 7. During this period, the WSI increased from 0.078 to 0.211 and the WSI linearly increased with number of week. This result agreed with work of Fimian et al. [8]. Dramatically increasing of WSI for Section A students after Week 8 resulted from the beginning of midterm examination and tiredness from retest activity. During Week 8 to Week 13, many Sections A students answered the weekly questionnaire that they did not like course management by means of lecture and test in Moodle learning platform and they feel bored with the test and its requirement before enter the next lesson and test. After midterm examination, there were many things to do for other subjects and retest in thermos-fluids course was time consuming activity. However, they decided to attend retest activity to avoid obtaining F grade point. It was noted that the WSI of Section A students increased continuously with high rate. If semester time was longer than fourteen weeks, the decrease in PCATS may be found. Further study on the optimum WSI for this new teaching technique should be conducted. It was clearly seen that the new teaching technique caused in the dramatically increase of student's stress. Although the increase of WSI did not affect to the PCATS in this report, the dramatically increase of student's stress should be concerned when lecture and test in Moodle platform was used for a long time.

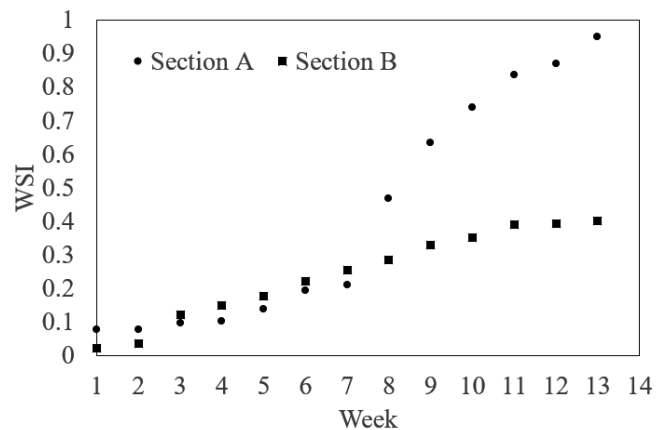


Fig.8 Weekly stress index of Section A and Section B students

IV. CONCLUSIONS

This work introduced the new teaching innovation called lecture and test in Moodle platform. Thermo-fluids coursework was selected to be case study for evaluating the effectiveness of this technique. It was found that teaching by means of lecture and test in Moodle platform resulted in the increase of calculation skill and learning ability of students. However, the advantage of this technique did not clearly be seen in starting period of coursework. The new teaching technique can be used to relieve the abandon homework problem. Finally, this



teaching innovation caused in the dramatically increase of student's stress. Although the increase of WSI did not affect to the MCQS in this report, the dramatically increase of student's stress should be concerned when lecture and test in Moodle platform was used for a long time.

ACKNOWLEDGMENT

The authors would like to thank Department of Mechanical Engineering, Faculty of Engineering and Industrial Technology, Silpakorn University, Thailand for supporting research fund.

REFERENCES

- [1] C. Costa, H. Alvelos, and L. Teixeira, "The use of Moodle e-learning platform: a study in a Portuguese University", *Procedia Technology*, 5, pp. 334 – 343, 2012.
- [2] F. Paragina, S. Paragina, A. Jipa, T. Savu, A. Dumitrescu, "The benefits of using MOODLE in teacher training in Romania", *Procedia Social and Behavioral Sciences*, 15, pp. 1135 – 1139, 2011.
- [3] P. Merello-Gimenez, A. Zorio-Grima, "Moderating role of gender in the performance of Moodle questionnaires in an introductory Accounting course", *Procedia Social and Behavioral Sciences*, 228, pp. 407 – 412, 2016.
- [4] KC. Deepak, "Evaluation of Moodle features at Kajaani University of Applied Sciences – Case Study", *Procedia Computer Science*, 116, pp. 121-128, 2017.
- [5] A. Muñoz, R. Delgado, E. Rubio, C. Grilo, V. Basto-Fernandes, "Forum participation plugin for Moodle: Development and Discussion", *Procedia Computer Science*, 121, pp. 982-989, 2017.
- [6] "Business undergraduates' perceived use outcomes of Moodle in a blended learning environment: The roles of usability factors and external support", *Telematics and Informatics*, 35, pp. 93 – 102, 2018.
- [7] "Fostering students questioning through Moodle: does it work?", *Procedia Social and Behavioral Sciences*, 116, pp. 2537 – 2542, 2014.
- [8] M. J. Fimian, P. A. Fastenau, J. H. Tashner, A. H. Cross, "The measure of classroom stress and burnout among gifted and talented students", *Psychology in the Schools*, 26-2, pp. 139 – 153, 1989.



Benchmark of Desired Attributes of Technology Graduates in Thailand: Basis for Improving

Hansa Khetbunphot^{1st}, Anchalee Panitjaroen*, Natthawut Panitjaroen*

^{1st}Department of General Education

Uttaradit Technical College Uttaradit, Thailand

*Department of Electrical Engineering

Rajamangala University of Technology Lanna Tak Tak, Thailand

e-mail: hansa_khet@hotmail.com, anchalee.tak@gmail.com, nattrit@gmail.com

Abstract— This study used descriptive method to create a benchmark of desired attributes of Technology graduates in Thailand which can be used as basis for improving attributes of Electronic Technology graduates. The study utilized a survey questionnaire which has been validated and pilot-tested with a Cronbach alpha value of 0.92 and conducted using two sectors in Thailand; the industry sector and the school sector. The selection of respondents utilized a purposive sampling. Graduate attributes are highly manifested as perceived by the two groups of respondents. The School is able to produce graduates who have the cognitive skills, knowledge, communication skills, leadership skills, ethical and moral skills, technical and job-related competencies in the field of electronics technology. Although there are some significant differences in the three domains, namely knowledge, communication and leadership skills, in most of the domains, there is no significant difference. This therefore is on indication that the School is able to produce graduates who are fit for the jobs available in the industry, who can be competitive and who can be assets in their respective organizations. The School needs to focus in those three areas where the university scored higher than their industry counterpart. The university can focus more on these three domains knowledge, communication and leadership skills. The curriculum can be re-designed in order to address these concerns. Deeper understanding of theories in industrial technology and how this is integrated to other related fields must be enhanced. Language deficiency can be addressed by integrating more practical activities to improve their communication skills, whether verbal, written or technical. Leadership skill can be developed by offering more curricular and co-curricular activities for the students. Having determined the desired attributes of technology graduates in Thailand, this study finds it relevant to use this benchmark as basis for recommendations for improving attributes of graduates of Electronic Technology.

Keywords— graduates attributes; f; benchmark of desired; technology graduates in thailand.

I. INTRODUCTION

In Thailand, Education is the main purpose of the Thai government development [5] as they realize that human Resources can be improved depending on education. The education system will be reformed one more time from kindergarten till graduate level. Actually, for all Thai citizens between the ages of six and fifteen, education is free and compulsory; children between three and five also have the option of attending nursery and preschool. There are two types of education, namely, formal and informal education [6]. Formal education is the education that children receive in schools whether public or private schools. Informal education, however, is provided outside the school. The children may study in libraries, museums, authentic places; rice field, animal farms, fruit farms, or through educational TV programmes and university broadcast and etc. However, most students have access to a formal education system.[7]

Formal education in Thailand is divided into early years education, basic education, vocational education and higher education. The bachelor's degree in Thailand is typically studied for 4 years after completing their secondary level (Matthayom 6). Another way is to study in vocational education (Office of Vocational Education Commission, 2006). Starting after Matthayom 3, it takes 3 years for Certificates Level, and 2 more years for Diploma Level and another 2 years for the bachelor's degree. Thus, graduate profession in Thailand is divided into two groups, namely Academic Graduate (Engineering program) and Practical Graduate (Technology program). The designed learning or curriculum design in higher education or bachelor's degree is different depending on the education background of the individual and the culture of learning at the foundation of education. However, The Office of the Higher Education Commission has determined that the outcomes of graduates



will have at least 5 domain attributes. The outcome of graduate attributes consists of 5 domains: ethical and moral, knowledge, cognitive skill and responsibility and analytical communication skill.

Therefore, the researcher realized the importance of producing graduates, particularly in the field of electronics, telecommunications and information technology professionals. Engineering and Industrial Technology graduates are capable of operating in the same industry. The curriculum design is important to achieve the objectives of producing graduates and it is the purpose of the researcher to conduct this research to conduct this research through this research topic.

This study intended to determine, compare and analyze the attributes of Industrial technology graduates based on the needs of the industry and Thai Qualifications Framework for Higher Education. Specifically, it sought answers to the following questions:

1) What is the current level of manifestation of the graduate attributes in the industrial technology and engineering program in terms of the following domains:

- 1.1 cognitive skills;
- 1.2 knowledge;
- 1.3 responsibility and leadership skills;
- 1.4 community skills;
- 1.5 technical and job-related competencies; and
- 1.6 ethical and moral?

2) Is there a significant difference in the level of manifestation of desired graduate attributes between industry and vocational education school expectations?

3) What skills training program would significantly enhance the attainment of the desired level of graduate attributes?

This study is important because the findings of the study may provide rich material in developing a curriculum for Industrial Technology. Specifically, the study hopes to benefit the respondents who reveal their expectations through the questionnaire, the school and industry expectations. The findings may serve the needs of those organization in terms of deciding employment of the graduates who achieve the expected graduate outcome through the Technology Curriculum. The needs of those organization should be clearly directed through the result of the questionnaire gathering. Therefore, the graduates attributes should be;

1) Able to apply conceptual and procedural knowledge, and solve the related problem or emergency situations logically;

2) Able to infer the theory in Industrial technology, follow academic and technology discipline, and also integrate the target knowledge to other related field;

3) Able to communicate in both languages, Thai and English, in writing and speaking skill through reports;

4) Able to apply social concerns, interpersonal and social etiquette, participate and collaborate in teamwork appropriately either in leadership and followership;

5) Able to demonstrate, practice, observe and show their responsibility, work discipline, punctuality, technical and

professional ethics, and value for the dignity of the human person; and

6) Able to demonstrate competencies in Electronics Technology.

The conduct of this study necessitated certain delimitations, as follows;

The study focused on the graduate attributes. It involved mainly the graduates who might gain undoubtedly in at least five domains which were structural objectives of the Thailand Office of the Higher Education Commission. The domains in this study consisted of:

- 1.1 Cognitive Skills
- 1.2 Knowledge
- 1.3 Responsibility and Leadership Skills
- 1.4 Community Skills
- 1.5 Ethical and Moral
- 1.6 Technical and job-related competencies

The study was delimited to the needs of Industry Technology groups who were the respondents. Their needs were expected to appear distinctly as the questionnaires were analyzed by using computer program.

II. RESEARCH METHODOLOGY

A. Methodology

The purpose of this study was to create a benchmark of desired attributes of Industrial Technology graduates in Thailand to achieve a basis for curriculum enhancement in Electronic Communications and Information Technology. This chapter focuses on the research instruments, the population and sample of study, data collection procedures and data analysis.

B. Research Design

The descriptive study was a benchmark of desired attributes of Industrial Technology graduates in Thailand in order to find a basis for enhancing the curriculum in Electronic Communications and Information Technology such that graduates would be suitable for the employment world.

C. Research Locale

The study was conducted in the industry section and school section in Thailand. The data were collected from January, 2018 to March, 2018.

D. Population and Sampling

The population of this study consisted of (1) the industry sector: Telephone Organization of Thailand group, Mobile Operator group, Telecommunication service group, and (2) University Teachers. The researcher used purposive sampling technique by using 90 respondents from the industry sector, and 30 respondents from among University teachers.



E. Research Instruments

The research instruments were questionnaires used to collect data for the research. The questionnaire included two parts:

Part 1. It consists of the profile of respondents and their position in the workplace, experience, and business/organization.

Part 2. It consists of questions asking the opinion of the respondents about the attributes of Industrial Technology graduates.

The scale used to represent the level of preference in industrial sector and university is as follows:

- 4=highly manifested
- 3=moderately manifested
- 2=slightly manifested
- 1=not manifested at all

F. Instrument Quality Check and Validation

- To determine face and content validity of instrument, the questionnaire was validated by a panel of experts.
- Pilot testing of the questionnaire to 30 respondents who were not part of the study but with the same characteristics as the target population was done to determine the reliability of the instrument used. The reliability test yields acceptability if the Cronbach alpha is at least 0.70.
- Revise the questionnaire if there was a need.

Actual data gathering to all respondents was throughout Thailand.

G. Data Gathering Procedures

- The researcher sent questionnaires to the target respondents personally or through the mail.
- When the questionnaires were not returned after a week, the researcher conducted a follow-up the following week.

H. Data Analysis Procedures

Actual data were analyzed in two parts:

Part 1. The general information about the respondents were analyzed using frequency tabulation and percentage computation. Data were presented in tables with captions.

Part 2. The options of the respondents about the attributes of Industrial Technology graduates were determined by using mean and standard deviation. Data were presented in tables with captions.

The following interpretation were used:

- 3.51 to 4.00 - Most strongly evident
- 2.51 to 3.50 - Strongly evident
- 1.51 to 2.50 - Less evident
- 1.00 to 1.50 - Not evident at all

- Descriptive statistics was used for describing the general characteristics of the samples' opinions about the attributes of Industrial Technology graduates. The statistical treatments were frequency, percentage, the average and standard deviation.

- Data were statistically treated using t-test in the case of two respondent groups at 0.05 level of significance. To facilitate computation, SPSS version 22 was utilized.

III. THE RESULTS OF THE STUDY

This topic presents the findings of the study conducted, the analysis and interpretation of data gathered from the questionnaire floated and documents pertinent to the study. Findings are hereby presented according to the sequence of problems stated. Current Level of Manifestation of Graduate Attributes in Industrial Technology

TABLE I. CURRENT LEVEL OF MANIFESTATION OF THE GRADUATE ATTRIBUTES IN INDUSTRIAL TECHNOLOGY IN TERMS OF COGNITIVE SKILLS

Domain	Mean	s.d.	Interpretation
Domain 1: Cognitive skill	3.83	0.22	Highly manifested
Domain 2: Knowledge	3.64	0.40	Highly manifested
Domain 3: Communication skill	3.69	0.40	Highly manifested
Domain 4: Responsibility and Leadership Skills	3.83	0.21	Highly manifested
Domain 5: Ethical and Moral	3.77	0.23	Highly manifested
Domain 6: Technical and job-related competencies	3.52	0.24	Highly manifested

N=120; 1.00 to 1.50 - Not evident at all; 1.51 to 2.50 - Less evident; 2.51 to 3.50 - Strongly evident; 3.51 to 4.00 - Most strongly evident.

The following table shows the results of the t-test conducted on the ratings made by the University and the industry sector as to the levels of manifestation of desired graduate attributes.

TABLE 2 T-TEST RESULTS OF THE LEVEL OF MANIFESTATION OF DESIRED GRADUATE ATTRIBUTES BETWEEN INDUSTRY AND VOCATIONAL EDUCATION SCHOOL EXPECTATIONS

Domain	Stake holders	Mean	s.d.	t	Sig.	interpretation
cognitive	Industry	3.79	0.21	-2.274	0.024	Significant
	School	3.88	0.22			
Knowledge	Industry	3.63	0.40	-0.004	0.997	Not significant
	School	3.64	0.38			
communication	Industry	3.68	0.33	-0.112	0.911	Not significant
	School	3.68	0.33			
responsibility	Industry	3.81	0.21	-0.874	0.384	Not significant
	School	3.85	0.20			
Ethical/moral	Industry	3.73	0.25	-2.764	0.006	Significant
	School	3.84	0.15			
technical	Industry	3.47	0.24	-0.275	0.007	Significant
	School	3.58	0.21			
Attributes	Industry	3.69	0.14	-2.322	0.021	Significant
	School	3.74	0.12			

When tested for any significant difference in the perception between the school and the industry on the level of manifestation of desired graduate attributes between industry and vocational education school expectation, the respondents showed no significant difference in three domains, knowledge, communication and responsibility.



IV. CONCLUSIONS

Based on the above findings of the study, the following conclusions were drawn. Many of the graduate attributes are highly manifested as perceived by the two groups of respondents. The school is able to produce graduates who have the necessary cognitive skills, knowledge, communication skills, and leadership skills, ethical and skills. However, in terms of the technical and job-related competencies in electronics technology, there is much left to be desired, thus, requiring enhancement of the syllabi and efficiency of delivery of instruction in the subjects that cover these competencies.

It appears that the University perceives more highly the demonstration of desired attributes by its graduates than what is seen by the industry sector in the said graduates, specifically in the attributes related to cognitive skills, ethical/moral, and technical, and in the overall expected attributes. Hence, the University has to exert more effort in improving its program to satisfy better the expectations of the industry sector among the graduates.

Although there are some significant differences in three domains, that is knowledge, communication and leadership skills, in most of the domains, there attributes in most of the competencies is an indication that, on the whole, the University is able to produce who are somewhat fit for the jobs available in the industry, who can be competitive and who can be assets in their respective organization.

V. DISCUSSIONS

Basis for enhancing the curriculum in Industrial Technology for Electronics, Communication and Information Technology can be modeled by KSA to include the following:

A. Knowledge

Courses that develop the cognitive knowledge of the students with emphasis on the conceptual and procedural knowledge as well as the pedagogies that would develop their critical thinking skills in order to fill the gap between the industry's expectation and those begin delivered by the university. Developing the critical thinking of graduates would prepare them in practical solutions to problems.

B. Skills

In terms of professional courses, emphasis should be given to foundation engineering courses like mathematics, design, systems and logic circuits. The university needs to focus more on the following courses because these serve as the strong theoretical foundation in the curriculum of their program.

C. Attitude

The fact that the industry sector does not perceive the manifestation of these attributes as highly as does the school indicates that the University must enhance the training of the students along this area. The school should put priority in molding the students' moral and ethical values. In the current situation, where students are more engrossed and engaged in gadgets, and considering other social factors, it is imperative that they be given more awareness of the moral and ethical issues that they may be confronted with not only in their everyday life but more importantly, in the workplace. Discipline, sense of responsibility, and diligence are necessary components in building the character of an individual. And these must be developed while they are still young. In summary, the curriculum should be designed focusing on the holistic development of the individual. This is the new direction in teaching and learning, a learner centered curriculum focused on both technical, theoretical content as well as pedagogies.

VI. ACKNOWLEDGMENTS

The research team would like to thank Institute of Vocational Education Northern Region 3 who supporting this research, The director of uttaradit technical college and Mr. Kittu Kuttanan head of electronics technology department from uttaradit technical college.

VII. REFERENCES

- [1] A. Atrons, R. W. Truss, A. Dahle, G. B. Schaffer, D. H. ST John & C. CAA Ceres, et al.(2004). *Graduate Attributes in Relation to Curriculum Design and Delivery in a Bachelor of Materials Engineering Programme*. Int. J. Engng Ed. Vol. 20, No. 5, (pp. 834-848)
- [2] Bank of Thailand. (2007). *Thailand at a Glance*. Retrieved January, 5, 2013. From http://www.bot.or.th/bothomepage/databank/Econcond/index_eng_i.asp.
- [3] Ministry of Education. (2006). *National Qualifications Framework for Higher Education in Thailand*. Bangkok: Author.
- [4] Ministry of Education. (2010). *The Education System in Thailand*. Bangkok: Author.
- [5] Ministry of Information and Communication Technology. (2009). *The Second Thailand Information and Communication Technology (ICT) Master Plan 2009-2013*. Bangkok: Author.
- [6] Pornnaree Sophabutr. (2012). *An Approach to Developing Competencies of Associate Industrial Engineers for the Preparedness of ASEAN Economic Community* (master's thesis), NIDA, Thailand.
- [7] Tanaboon Sasipanudach, Yutthachai Sillapawicharn, Rattapon Jinawong, kritsada Thongsomboon, Songtham Deewanichsakul, & Rawat Somsuk, et al. (2009). *The graduates attributes of the Bachelor of Science in Technical Education. Needs of workplace*. Bangkok, Thailand: Rajamangala University of Technology Thanyaburee.
- [8] Weerayute Sudsomboon, & Anusit Anmanatarku. (2007). *Competency-based Curriculum Development on Automotive Technology Subjects for Mechanical Technology Education Program*. The 5th International Conference on Developing Real-Life Learning Experiences :Education Reform through educational Standards. ERS2007 : Thailand (pp. 35-44)



The Development of the Interactive e-book on the 38 Steps Towards Enlightened Living

Nitigan Nakjuatong^{1st}, Beesuda Daoruang

Department of Information Technology

Faculty of Industrial Technology and Management

King Mongkut's University of Technology North Bangkok Prachinburi Campus, Prachinburi, Thailand

nitigan.n@fitm.kmutnb.ac.th, beesuda.p@fitm.kmutnb.ac.th

Abstract—This research was conducted to; (1) study results of an interactive electronic book (e-book) used for teaching of the 38 Steps Towards Enlightened Living (2) study performance of the said interactive electronic book. Research samples were 30 of the bachelor degree students at the Department of Information Technology, Faculty of Industrial Technology and Management, King Mongkut's University of Technology North Bangkok (Prachinburi Campus) who were selected by Purposive Sampling method. Research tools including interactive electronic book on the 38 Steps Towards Enlightened Living, pretest-posttest of each lesson, overall test after completion of the entire studies. Hypothesis of the research was based on post-study results which were anticipated that, after using the said interactive electronic book, the posttest scores were higher than that of the pretest ones at statistical significance level with performance value of 80/80. Data was assessed by using averaged value, percentage, standard deviation and t-test. According to the results, the above mentioned interactive electronic book; (1) raised student's posttest scores higher than that of the pretest ones at statistical significance level of .05 (2) resulted in performance values of 89.50/84.60, against the expected values of 80/80.

Keywords—Interactive electronic book; Steps Towards Enlightened Living; Study results; Media performance

I. INTRODUCTION

In response to deity's question of which moral principle may construe a successful life, the Lord Buddha replied that auspiciousness or thirty-eight practical blessings is the source of happiness and life advancement. The above statement was extracted from Mangala Sutta which illustrates the thirty-eight practical blessings of enlightening life. The conducted a research on problems related to Buddhism teaching for found that problems were originated from 6 aspects, teachers, students, curriculum, studying activities, assessments, and studying media [1]. The results revealed that learning media used in teaching of Buddhism at Department of General Education-registered high schools was the main issue which teachers and schools' administrators mutually agreed that learning media needs further developments.

The venerable suggested that traditional book fails to motivate students to continuously focus on their lessons' contents [2]. Teachers responsible for Dharma discipline

lessons often resorted to conventional verbal lecturing without using any teaching material which poorly attracted students' interests. Therefore, it is suggested that teachers should utilize teaching media during their teaching instead of relying solely on the verbal lecturing. The suggested that Buddhism teaching should incorporate variety of techniques for certain topics and arrange appropriate contents that would attract students' interests [3].

Electronic book is capable of attracting and motivating learners as contents are presented via multimedia format that learners are able to interact with and enjoy the learning experiences [4]. The concluded in his research regarding electronic book on science subject for Prathom1 students that the electronic book which was developed for iPad motivated students to read and attempted to do more research. Traditional books are printed with changeless pictures whilst electronic book employs hypermedia that enhances skills development as the electronic book engages students with their lessons which helps them to develop thoughts and other learning skills.

A research to compare learning results and knowledge retention of Prathom 6 students who used the electronic book to study [5] cardiovascular system and found that the students' posttest scores were higher than that of the pretest one at statistical significance level of .05. Furthermore, students were able to retain knowledge acquired from the use of electronic book better than what they could have retained from studying via printed books. The venerable conducted a research on the use of electronic book for the teaching of Karava 6 (6 Reverences) which forms a part of sociology [6], religious, and cultural subject cluster and found that electronic book resulted in learning efficacy index which was higher than that of the learning objectives. Electronic book provides learners with opportunities to study at their own pace with no time constraint, the environment which helps to reduce differences of learning capacity between learners. Moreover, students are able to review their lessons as required as well as having interactions with the learning content, thus, helps them to understand the contents better.

As electronic book raises learners' interests of the subject, it is anticipated that learning results would also be heightened. According who studied the use of electronic book for teaching of atmospheric studies [7], a part of scientific subject cluster,





Mattayom 1 students achieved higher posttest score than that of the pretest ones at the statistical significance level of .01. The higher results were due to an interesting and enticing teaching media which comprised of voice messages, and colorful images. Furthermore, learning through this media allows students who are not competent at reading to learn as effective as their classmates and the lessons can be repeated as per students' needs.

The developed a computer network-based electronic book to teach Pañcasila and Pañcadhamma (Five Precepts and Five Dharma) for Pratom 6 students [8]. A research on the use of this electronic media revealed that students achieved higher posttest results than that of the pretest ones at the statistical significance level of .05. Students were highly satisfied with the use of electronic book because it incorporated different types of media, offered beautiful images, can be used easily, presented easily legible texts, and offered images that represented relevant meanings.

An electronic book on the 38 Steps Towards Enlightened Living developed was launched and a satisfaction survey was subsequently [9] conducted which found that overall satisfaction about the electronic book was highly satisfied (at average score of 4.36) , content and design was highly satisfied (4.45), benefit of the book was also highly satisfied (4.36). As per the understanding of lessons' contents, before the use of the electronic book, students' understanding was at moderate level (3.05) whereas after the use of the media, the understanding was increased to high level (4.13)

II. PURPOSES

To study learning results of the interactive electronic book on the 38 Steps Towards Enlightened Living.

To assess performance of the said electronic book against the predetermined performance of 80/80.

To assess learner's the differences in pretest scores and posttest scores.

III. RESEARCH METHODOLOGY

1.Materials were interactive electronic book on the 38 Steps Towards Enlightened Living which made up of 10 lessons, 4-choice pretest and posttest for each of the lesson and an overall test after completing the entire studies.

2.Methods, Thirty research participants from the first year students who enrolled in the 4-year bachelor degree course at Department of Information Technology, Faculty of Industrial Technology and Management, King Mongkut's University of Technology North Bangkok (Prachinburi Campus) were recruited by using Purposive Sampling method. Subsequently, the experiment was conducted as per the One Group Pretest-Posttest Design.

Participants were required to take the pretest, study the lesson's contents and then attempt the posttest of each lesson. Participants were required to repeat the same steps which took

approximately 10 minutes for each lesson, until all of the lessons were completed. After completing the entire studies, participants were required to take the overall exam which covered the contents of all lessons.

This research was conducted based on the One Group Pretest-Posttest Design whilst the results of the pretest and the posttest were assessed by Matched-paired t-test for dependent samples. The assessments were completed by using SPSS.

Analysis of lessons' performance was made by assessing test results at the end of each lesson for E1 value whereas the overall test results were used to calculate E2 value. The following formula were used for the said analysis;

$$E_1 = \frac{\left(\frac{\sum X_a}{N}\right) \times 100}{A} \quad (1)$$

$$E_2 = \frac{\left(\frac{\sum X_b}{N}\right) \times 100}{B} \quad (2)$$

E₁ : Represents performance while the studies were being conducted, calculated as percentage of average scores of all the posttest results.

E₂ : Represents performance after the entire learning was completed, calculated as percentage of average scores of the overall test results.

$\sum X_a$: Represents learner's combined scores of all the posttest results

$\sum X_b$:Represents learner's combined scores of the overall test

A: Represents total full scores of the posttest

B: Represents total full scores of the overall test

N: Represents number of participants

IV. RESULTS

Developmental results of the interactive electronic book on the 38 Steps Towards Enlightened Living



Fig. 1. First page of the interactive electronic book on the 38 Steps Towards Enlightened Living.

Learning results assessment According to the learning results assessments, 30 participants took the pretests and the



posttest (80 questions for each test) for the results were consequently assessed by using SPSS and Dependent Samples t-test. The assessments are illustrated in table I, II, and III as following;

TABLE I. PAIRED SAMPLES STATISTICS

Order	Mean	Number	Std. Deviation	Std. Error Mean
Pre-Test	48.9667	30	6.57311	1.20008
Post-Test	71.6000	30	4.14063	.75597

According to table I, an average value of the pretest is 48.9667, the standard deviation is 6.57311, and the standard error mean is 1.20008. On the other hand, an average value of the posttest is 71.6000, the standard deviation is 4.14063, and the standard error mean is 0.75597.

TABLE II. PAIRED SAMPLES CORRELATIONS WHICH WAS USED TO TEST RELATION OF THE VARIABLES

Pair	Number (N)	Correlation	Sig.
1 Pretest and Posttest	30	.843	.000

As per table II, Pearson Correlation value (r_{xy}) between the pretest and the posttest scores is 0.843 whereas the probability values used in hypothesis testing, under the statistical hypothesis were

H_0 : Refers to the pretest and the posttest scores that are unrelated

H_1 : Refers to the pretest and the posttest scores that are related

As per the data analysis, Sig. value that the program calculated was .000 which was less than the predetermined significance level ($\alpha = .05$). As the results reject hypothesis H_0 , this can be concluded that pretest score results are related to that of the posttest ones at statistical significant level of .05.

TABLE III. PAIRED SAMPLES TEST

Pair 1	Paired Differences					t	df.	Sig. (2-tailed)
	mean	Std. Deviation	Std. Error Mean	95% Confidence Interval of the Difference				
				Lower	Upper			
Pretest-Posttest	22.6333	3.80094	.69395	21.21404	24.05263	32.615	29	.000

Table III reveals differences between the pretests and the posttest average scores which is 22.6333, standard deviation is

3.80094, standard error mean is 0.69395, the Interval of the Difference Lower is 21.21404 whereas the Interval of the Difference Upper is 24.05263, hence, $21.21404 < \mu_d < 24.05263$. Statistical value of the test $H_0 : \mu_{After} - \mu_{Before} = 0$ where t is equal to 32.615, degree of Freedom : df of the t-test =29 and significance of the t-test is .000 which is lower than the predetermined significance level of .05.

According to the research's hypothesis;

$$H_0 : \mu_{After} - \mu_{Before} = 0$$

$$H_1 : \mu_{After} - \mu_{Before} > 0$$

When μ_{After} represents average scores of the posttest

μ_{Before} represents average scores of the pretest

This research, the predetermined statistical significance level is .05 with Sig. (2-Tailed) value of the t-test that was programmed for the calculation is .000 which is less than the value of alpha that was set at .05. Therefore, the main hypothesis of $H_0 : \mu_{After} - \mu_{Before} = 0$ is rejected and the hypothesis of $H_1 : \mu_{After} - \mu_{Before} > 0$ is accepted.

As the interactive electronic book resulted in the higher posttest scores than that of the pretest one at the statistical significance level of .05, it can be concluded that the electronic book helped learners to increase their knowledge level.

A. Assessment of the electronic book's performance

The results of each lesson's posttest scores and the overall test scores were used to assess performance of the lesson (E1/E2). The anticipated performance must follow the predetermined performance of 80/80. The research revealed that the average test scores obtained while the studies was being conducted was 89.50 whilst the overall scores after the studies were completed was 84.60 which are higher than the predetermined values of 80/80.

V. CONCLUSION AND DISCUSSION

As per the research, the posttest scores were higher than that of the pretest ones which due to the use of the electronic book in learning. The electronic book is multimedia-based which presents contents via images, message, background music; animated information which accompanied by characters' voices, narration and music. Learners can select the type of media that best suit their interests, thus, helps them to enthusiastically follow the contents via these interactive images, the features that traditional books cannot present. Furthermore, electronic book can be presented as cartoon that features explanatory texts and music which, upon clicking on the cartoon image, an animation appears with voice information. The animation can entice students to search for more information, and follow through the story until the end of the lesson. This argument is supported by a 2009 which stated that electronic book which illustrates cartoon and music



conveys an enthusiastic learning environment which results in enjoyable learning, and higher learning outcomes [10] .

According to the book's performance, the values of 89.50/84.60 were achieved in line with the predetermined values of 80/80. The interactive electronic book has been developed by using animations, characters' voices, narration and music instead of still images and recorded dialogues. Hence, the electronic book allows learners to study lessons as per their individual preferences. Therefore, the interactive electronic book on the 38 Steps Towards Enlightened Living is enjoyable, allows learners to memorize its contents via images, can be learnt irrespective of time constraint, no consecutive order of the story that must be followed. A research on electronic book for sociology, religious, and cultural studies which was developed for Mattayom1 students that the media is presented as Polymedia Books that express learning contents via still images, motion images, voices, and menu windows that facilitate the learning process [11]. Learners are well motivated and are more enthusiastic about their learning.

As per the above mentioned arguments, the interactive electronic book can be effectively used in the teaching of the 38 Steps Towards Enlightened Living.

VI. ACKNOWLEDGMENTS

This research was completed with kind cooperation of the 1st year students and the assistance from the Department of Information Technology, Faculty of Industrial Technology and Management, King Mongkut's University of Technology North Bangkok (Prachinburi Campus).

REFERENCES

- [1] Athapol Anunthavorasakul. (1996). State and problem of Buddhism Subject Instruction in Secondary Schools under the Jurisdiction of the Department of General Education. Master of Education. Department of Secondary Education Graduate School. Chulalongkorn University, Bangkok.
- [2] Supot Tapasilo (Ketnakorn). (2001). Conditions and Problems of Instruction of Dhammavinaya at The Upper Secondary Level in The General Education Program of Ecclesiastical Schools in Educational Region Ten. Master of Education (Curriculum and Instruction). Sukhothai Thammathirat Open University, Nonthaburi.
- [3] Ploynuan Atcharawan. (2007). The interest toward learning and teaching buddhism of secondary School Student at Schools in Phanomsarakham district under the office of Chachoengsao educational service area 2. Master of Education. Burapha University. Chonburi.
- [4] Jaturong Eusukchaikul. (2012). Development of Electronic Book on Science for Phathomsuksa 1. (Special Problem) Information Technology. King Mongkut's University of Technology North Bangkok, Bangkok.
- [5] Lunnaluck Sujira. (2009). Comparison of Learning Achievement and Retention of Prathomsuksa 6 Students Using Electronic Book on Blood Circulation System. Master of Education (Educational Technology). Department of Educational Technology. Kasetsart University, Bangkok.
- [6] Sommai Rotpetch. (2009). Development an Electronics Book no Garava 6 in Social, Religino and Culture Subject. for Prathomsueksa 6 Studens. Master Thesis, M.Ed. (Educational Technology and Communications). Bangkok : Graduate School, Chandrakasem Rajabhat University, Bangkok.
- [7] Watcharee Kraikan. (2010). Learning Activity Management via Electronic Books for Science Strand entitle:The Atmosphere, for Grade 7 Students. Master of Education (Curriculum and Instruction). Rajabhat Maha Sarakham University. Mahasarakham.
- [8] Suwaree Rinros. (2008). Development of electronic book via computer network on the five precepts and the five ennobling virtues for Prathomsuksa 6 students. Master of Education (Educational Technology). Educational Technology, Department of Educational Technology. Kasetsart University, Bangkok.
- [9] Beesuda Daoruang, Rattaphong Putpim and Thitinun Onrwiarn. (2016). The Study of Users'Satisfaction with the Interactive e-book for 38 Blessing of Life. NCIT2016 : The 8th National Conference on Information Technology (254-258). Walailak University, Nakornsrihammarach.
- [10] Kulissara Baosuk. (2009). The Effects of Using and Electronic Book Entitled Picture Decoration on Learning Achievement and Attitudes toward Learning in the Career and Pongkonsao School in Saraburi Province. The Degree of Master of Education in Curriculum and Instruction School of Educational Studies. Sukhothai Thammathirat Open University, Nonthaburi.
- [11] Thongsuk Khamkaew. (2010) Development of Electronic Book (E-book) of Social Science, Religion and Culture for Matayom Suksa I Student M.Ed. (Educational Technology) Burapha University, Chonburi.



Analyzing Graduate Production Costs of Faculty of Industrial and Technology Management, King Mongkut's University of Technology North Bangkok Prachinburi

Jumrean Srikamta and Nantiya Juntralux
Faculty of Industrial Technology and Management
King Mongkut's University of Technology North Bangkok
Prachinburi, Thailand
Jumrean.s@fitm.kmutnb.ac.th, Nantiya.s@fitm.kmutnb.ac.th

Abstract— Abstract—This study analyzed and calculation of graduate production cost in higher education, case study of Faculty of Industrial and Technology Management (FITM) King Mongkut's University of Technology North Bangkok (KMUTNB) by using data in the academic year 2013-2016. Analyze data using descriptive statistics method such as frequency, percentage, and mean to explain the information available and ration the indirect cost by using full-time equivalent student (FTES).

The analyzing graduate production costs result of FITM found that unit cost of a 4-year program is 247,787.44 Baht and from a 2-year continuing program is 114,198.20 Baht. But after included the number of dropouts and average study time the value is changed to 416,972.95 and 216,845.93 Baht respectively. That is the real graduate production costs highly relate to a number of students, number of dropouts and average study time.

Keywords— graduate production costs, unit cost, higher education

I. INTRODUCTION

A. Background

Calculation of production costs is one of the standard financial management of the government authority to prepare for entering into the budget-oriented strategy. Budget control and performance evaluation of government sector is one element of the metric to evaluate the completion of a contract to the public service agreement. (PSA) and it also used as a benchmark to compare with or between another government sector. The purpose is to analysis and improvement of operational efficiency to the organization. Calculation of production costs is very important in both private organizations and government organizations because every organization must have a cost of production. Production cost is regarded as a very important tool for management services for public benefit organization such as a hospital, educational

institution, government public service sector, and other non-profit organization. The purpose and mission of high education institution are to supply qualified graduate to the society, to encourage research and academic work, to support public academic services, and to maintain national arts and culture. To do this mission sustainable we need to carry out costing services especially graduate production cost which is a main mission of the university. [1] Because graduate production costs is a main of key performance indicators to evaluate the high education institutions to make a decision for management improvement.[2]

Faculty of Industrial and Technology Management King Mongkut's University of Technology North Bangkok Prachinburi campus has a main mission is to supply qualified graduate to the society and the country. The operation cost of our university are form national budget and a university revenue so we have to show the efficiency and the worthiness to the society and the country. This research proposal is to study and analyzing graduate production costs to use as data to faculty administrator, department administrator and other interested people to understand all cost behavior in the organization.

B. Objective

To Analyzing Graduate Production Costs of Faculty of Industrial and Technology Management, King Mongkut's University of Technology North Bangkok Prachinburi in both faculty and department level.

C. Research scope

This research did not include expenses from department of tourism and hotel Management in both direct and indirect expenses. Calculate only cost which supports from the government, not classified by student's years level which hypothesis that each student's year level used the same cost.



The conceptual framework to analyzing graduate production costs is calculated from all direct cost and indirect cost which also consider to the number of fallen students and the number of years of study until graduate.

II. RESEARCH METHODOLOGY

This research used data of students from Faculty of Industrial and Technology Management (FITM) KingMongkut's University of Technology North Bangkok (KMUTNB) who enroll in the academic year 2013-2016. The data in this research is a secondary data which collect from the database system of KMUTNB's academic services division, TQF7 report from every programme, KMIT-38 form, the record of expenditure items for national budgets form in the year 2013-2016. Analyze data using descriptive statistics method such as frequency, percentage, and mean to explain the information available and ration the indirect cost by using full-time equivalent student (FTES) value.

III. RESULT

A. Results analysis of the number of students

TABLE I. NUMBER OF STUDENT IN 2013-2016

Program	Year	Number of Student Year			
		2013	2014	2015	2016
4 year Program	Year 1	219	283	293	250
	Year 2	224	204	272	272
	Year 3	211	209	189	239
	Year 4	232	194	198	187
	Total	886	890	952	948
Continuing Program	Year 1	211	212	169	131
	Year 2	225	194	197	154
	Total	436	406	356	285
Total		1,322	1,296	1,318	1,233

The number of FITM's student from the year 2013 is shown in table.1. The total number of student is 1,322, from a 4-year program is 886 and from a continuing program is 436, in 2014 the total number of student is 1,296, from a 4-year program is 890 and from a continuing program is 406,

in 2015 the total number of student is 1,318 from a 4-year program is 952 and from a continuing program is 356, and in 2016 the total number of student is 1,233 which from a 4-year program is 948 and from a continuing program is 285. The number of FITM's enrollments and dropout students from the year 2013-2016 is shown in table 2.

From table 2.the largest amount enrolled students are in 2014 and the least is in 2016 and the largest number of dropout is in 2014 and the least is in 2013.

Average study time for 4-year program student is 4.2036 years and for continuing program is 2.3531 years, details by a department is shown in table 3.

TABLE III. AVERAGE STUDY TIME

Department	4 year Program	Continuing Program
IT	4.2195	2.5258
IM	4.1215	2.2605
AEI	4.3362	2.3899
CDM	4.1014	-
FITM	4.2036	2.3531

From table 3.show that time for 4-year program, student from Department of Product Design Technology and Construction Industrial Management used the shortest time (4.1014 years) and the longest are from Department of Design and Production Technology of Agricultural Industry (4.3362 years).

For 2-year continuing program, student from Department of Industrial Management used the shortest time (2.2605 years) and the longest are from Department of Information Technology(2.5258 years).

Graduate production costs have both direct and indirect cost. The indirect cost cannot clearly be identified what the cost is from any department. The central expenses, in this case, are calculated from FTES (Full Time Equivalent Student).

TABLE II. NUMBER OF ENROLLMENTS AND DROPOUT STUDENT IN 2013 – 2016

year	Status (Number)								
	4 year Program			Continuing Program			Total		
	Enrollments	Dropout	%	Enrollments	Dropout	%	Enrollments	Dropout	%
2013	219	37	16.89	211	36	17.06	430	73	16.98
2014	283	105	37.10	212	58	27.36	495	163	32.93
2015	293	72	24.57	169	40	23.67	462	112	24.24
2016	250	32	12.80	131	37	28.24	381	69	18.11
Total	1,045	246	23.54	723	171	23.65	1,768	417	23.59

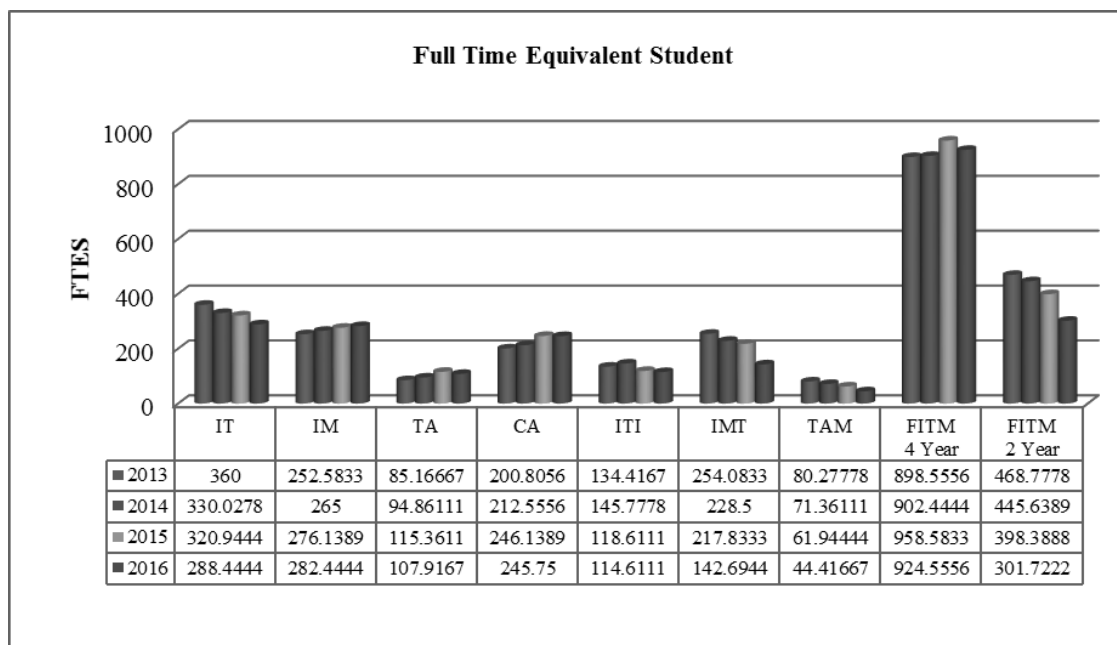


Fig. 1. Chart 1 : Full Time Equivalent Student

From fig 1. show that from a 4-year program, the largest FTES is from IT in all four years. The largest number of IT's FTES was 360 in 2013, IM was 282.44 in 2016, TA was

115.36 in 2015 and CA was 246.13 in 2015. For a 2-year continuing program, ITI was 145.77 in 2014, IMT was 254.08 in 2013 and TAM was 80.27.

B. Analyzing Graduate Production Costs Result

From table 4. explore that the total Graduate Production Costs of FITM in 2013-2016 were 325,838,261.35 Baht which are from national budget 244,224,500.03 Baht and from university revenue 81,613,761.31 Baht. The largest

cost are from staff statements (143,909,520.47 Baht) the other are operating statements (98,914,181.21 Baht), depreciation and amortization (80,058,196.62), and the lowest is subsidy (2,956,363.04 Baht).

TABLE IV. GRADUATE PRODUCTION COSTS OF FITM

Expenses	Year				Total
	2013	2014	2015	2016	
National budget					
Staff statements	25,134,442.49	31,439,930.49	36,016,561.62	36,469,845.50	129,060,780.10
Operating statements	8,571,875.89	8,826,321.88	9,562,278.96	21,684,158.66	48,644,635.39
Subsidy	54,472.65	37,033.10	-	286,528.15	378,033.90
Depreciation	16,012,520.80	15,882,557.71	15,297,339.29	18,948,632.83	66,141,050.64
Total	49,773,311.83	56,185,843.18	60,876,179.88	77,389,165.14	244,224,500.03
University revenue					
Staff statements	2,944,501.19	3,475,580.82	4,294,291.70	4,134,366.67	14,848,740.37
Operating statements	11,829,468.33	10,836,873.75	12,950,528.73	14,652,675.01	50,269,545.81
Subsidy	1,138,930.96	288,281.11	792,056.87	359,060.20	2,578,329.14
Depreciation	2,911,677.82	2,817,346.23	3,921,652.99	4,266,468.94	13,917,145.98
Total	18,824,578.30	17,418,081.91	21,958,530.28	23,412,570.82	81,613,761.31
Total	68,597,890.13	73,603,925.09	82,834,710.16	100,801,735.96	325,838,261.35



TABLE V. UNIT COST OF FITM STUDENT IN 2013-2016

Program	Direct cost	Indirect cost	Total cost	No. Student	Unit cost	%
4 year Program						
2013	23,163,854.00	21,837,340.99	45,001,194.99	886	50,791.42	20.49
2014	26,435,524.04	22,777,000.13	49,212,524.16	890	55,294.97	22.32
2015	32,618,047.51	25,769,165.59	58,387,213.11	952	61,331.11	24.75
2016	36,029,454.35	40,161,253.70	76,190,708.05	948	80,369.95	32.44
Total	118,246,879.90	110,544,760.41	228,791,640.31	3,676	247,787.44	100.00
Continuing Program						
2013	12,204,121.67	11,392,573.47	23,596,695.14	436	54,120.86	47.39
2014	13,143,819.88	11,247,581.05	24,391,400.93	406	60,077.34	52.61
Total	25,347,941.56	22,640,154.52	47,988,096.07	842	114,198.20	100.00

From actual expenses in table 4., we can break the total cost into the direct cost and indirect cost and ration by FTES(Full Time Equivalent Student), the result is shown in table 5.

Table 5. shows the calculated unit cost of FITM's student in the academic year 2013-2016. The calculation did not include the number of dropouts and average study time. We found that the unit cost of a 4-year program is 247,787.44 Baht and from a 2-year continuing program is 114,198.20 Baht. But if we calculate with dropouts and average study time the true result is shown in table 6.

TABLE VI. GRADUATE PRODUCTION COSTS RESULT OF FITM

Item	4 year Program	Continuing Program
Average unit cost /year	61,946.86	57,099.10
Average study time	4.3362	2.3899
Unit cost	268,613.97	136,461.14
Percent of graduate	64.42	62.93
real graduate production costs	416,972.95	216,845.93

Table 6. show the analyzing graduate production costs result of FITM found that real unit cost of a 4-year program is 416,972.95 Baht and from a 2-year continuing program is 216,845.93 Baht. If we break down the cost for each department, it will show in fig 2 and fig 3.

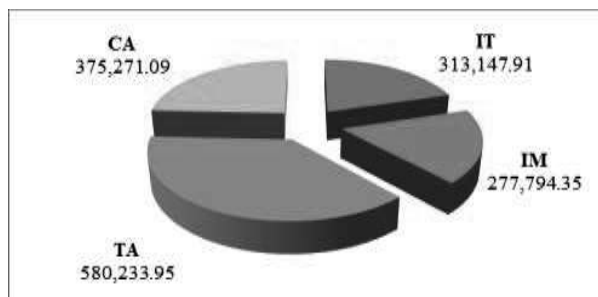


Fig. 2. Cost of the graduate produce: 4 year Program

From Fig 2. explore that from a 4-year program. The largest cost are from TA with 580,233.95 Baht and the lowest cost are from IM with 277,794.35 Baht.

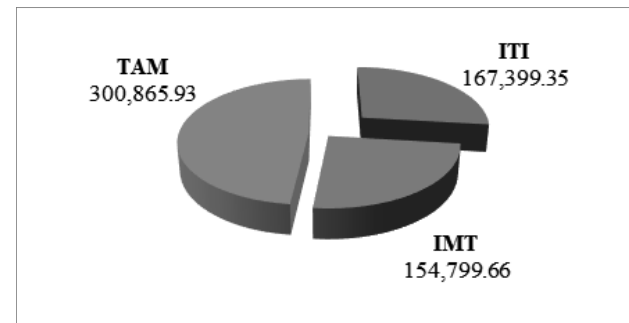


Fig. 3. Cost of the graduate produce: Continuing Program

From Fig 3. explore that from a 2-year continuing program. The largest cost are from TAM with 300,865.93 Baht and the lowest cost are from IMT with 154,799.66 Baht.

IV. CONCLUSION AND DISCUSSIONS

The analyzing graduate production costs result of FITM found that unit cost of a 4-year program is 247,787.44 Baht and from a 2-year continuing program is 114,198.20Baht. But it is not a real cost because it is not included the number of dropouts and average study time, so after we add this parameter, the calculation is changed to 416,972.95 and 216,845.93 Baht respectively. The study shows that the real graduate production costs relate to a number of students, number of dropouts and average study time. This is consistent with the results of the study of JutamasWeerasak [3] which found that the unit cost of faculty of engineering, Prince of Songkla University is depend on number of dropouts and average study time and it also consistent with the results of the study of VanchaiLaemlaksakul[4].

We can see that the real graduate production costs highly relate to a number of students, number of dropouts and average study time. So the way to cut graduate production costs has both direct and indirect method. The direct method is to cut the cost. And the indirect method to cut off the cost is to enhance



the efficiency of education management to allow students to complete their studies on time and reduce the number of dropouts.

ACKNOWLEDGMENT

Faculty of Industrial Technology and Management, King Mongkut's University of Technology North Bangkok.

REFERENCES

- [1] Nikorn Noiprom and Narong Kamondhit, "A Cost funtion for undergraduate students in Loei Rajabhat University," Journal of Research and Development Journal Loei Rajabhat University Vol. 10 No 32 April-June 2015 pp. 47-56.
- [2] Charassri Jutajindakhet. 2015. Expenses and Graduate Production Costs of Faculty of Education Khon Kean University 2014. Research of Faculty of Education, Khon Kean University.
- [3] Jutamas Weerasak. 2007. The Cost accounting study on the graduate produce of Faculty of Engineering, Prince of Songkly University, Hatyai Campus. Research of Prince of Songkly university, Songkla.
- [4] Vanchai Laemlaksakul. 2002. Cost analysis of undergraduate student in Industrial Technology Program College of Industrial Techmoly, King Mongkut's Institute of Technology North Bangkok. Research of , King Mongkut's Institute of Technology North Bangkok.



ENGINEERING

- Agricultural, Biological and Food Engineering
- Alternative Energy and Combustion
- Agricultural Farm Machinery
- Applied Mechanics and Materials
- Biomechanics, Robotics and Controls
- Civil and Environmental Engineering
- Computational and Simulation Techniques
- Computer Engineering
- Electrical Engineering
- Electronics and Telecommunication Engineering
- Mechanical Engineering
- Mapping, GIS and Remote Sensing
- Railway and Transport Engineering
- Disaster Engineering
- Industrial Engineering
- Logistics Engineering & Management
- Related Topics





Effect of various conditions on ultrasonic-assisted extraction of allicin from garlic(*Allium Sativum* Linn.)

Suphitchaya Kalantakuwan, Yardfon Tanongkankit, Jaturapatr Varith and Kanjana Narkprasom

Department of Food Engineering
Faculty of Engineering and Agro-Industry, Maejo University
Chiang Mai, Thailand

Medicinal properties of garlic (*Allium Sativum* Linn.) have been studied extensively, even though it has been used as a traditional remedy. This study examined the effects of various ultrasonic frequency (28, 45 and 100 kHz), extraction temperatures (20, 30 and 40°C) and extraction time (20, 40 and 60 min) on the extraction yield of allicin content from garlic. Extraction was most efficient at 45 kHz, while the extraction temperature of 30°C and time of 40 min. Under the optimal conditions, the allicin content was 6.282 ± 0.010 mg/ml. This study is important due to its ability to improve extraction of allicin content using ultrasonic-assisted extraction method.

Keywords—ultrasonic-assisted extraction; garlic; allicin

I. INTRODUCTION

In the recent years there has been an increase of interest for use of natural compound in the prevention and treatment of various diseases such as cancer, arthritis, diabetes, etc. [1, 2, 3, 4, 5, 6] Furthermore the utilization of natural compounds from various sources has been increased in the food industry. This is in an accordance with demand to replace synthetic and toxic additives with natural and safe one in food industry. Many previous studies have shown that various spices are used in food recipe not only for taste but also for food preservation since they possess antimicrobial compounds [7, 8, 9].

Garlic (*Allium Sativum* Linn.) which is one of spices can be consumed as fresh or utilized as a raw material in many dishes. It has been claimed to contain bioactive compounds having potential inhibitor for food poisoning and spoilage and increase shelf life in processed foods [10]. The health benefits of garlic have been attributed to its thiosulfates content.

Allicin (diallylthiosulfate) is the best know active compound of garlic and it represents approximately 70% of the overall thiosulfates. Allicin is not found in fresh garlic. The chemistry of garlic is extremely complex. Fresh garlic contains non-protein amino acid alliin abundant in garlic cloves and the enzyme alliinase (alliin lyase, EC 4.4.1.4), which are contained in different parts of the garlic plant. This unique structure is designed as a defense mechanism against microbial pathogens of the soil. When fungi or other soil

pathogens attack the cloves, the membrane of those compartments is destroyed, alliin is converted into a new compound called allicin. Can explain that allicin present or formed upon crushing the cloves. It is produced by the interaction of alliin with the enzyme alliinase.

Allicin is known to possess a vast variety of biological effect. Its pharmacological actions of anti-oxidant, anti-fungal, anti-hypertensive, anti-inflammatory, and inhibition of tumor [9, 11, 12]. Therefore, the extraction of this compound from plant cell is attractive.

Various extraction methods of bioactive compounds from plant matrices have been reported. Ultrasonic-assisted extraction (UAE) has been recommended by various reports as a one of the most efficient, inexpensive and simplest existing extraction systems which can be suitably operated for large-scale preparations [13, 14]. During the process, the collapse of cavitation bubbles leads to better cell disruption through the formation of micro jets due to asymmetrical bubble collapse near a solid surface. The occurring cavitation effect consequently facilitates the release of extractable compound by disrupting the plant cell walls, allowing greater penetration of solvent into the sample matrix, increasing the contact surface area between the solid and liquid phase. Using ultrasonic, extractions can be completed in short time with high reproducibility, reducing the consumption of solvent, simplifying manipulation and work-up, extraction at lower temperatures, giving higher purity of the final product, faster extraction rates and greater yields of product [15,16]. However, applied extraction process can substantially affect the quality and concentration of targeted compounds in extract production.

Therefore, the aim of the present study was to investigate the effect of ultrasonic-assisted extraction variables on allicin content. Effects of different extraction parameters such as ultrasonic frequency, extraction temperature and extraction time were investigated to best ultrasonic-assisted extraction condition with the highest allicin content.



II. MATERIALS AND METHODS

A. Preparation of the plant material

Fresh garlic (*Allium Sativum* Linn.) was obtained at local farm (Chiang Mai, Thailand). Garlic clove was cleaned and peeled outer skin off, then blend with water: 100 ml per 10 g. (0.1 g/ml) of garlic [17].

B. Ultrasonic-assisted extraction (UAE)

The garlic blended of 10 ml was extracted in an ultrasonic-assisted extraction sonication bath (W113 series, Japan). The suspension obtained was centrifuged at 4000 rpm for 20 minute. The single factor experiment was performed in a designed ultrasonic frequency ranged from 28 to 100 kHz, temperature ranged from 20 to 40°C and ultrasonic time ranged from 20 to 60 min. One factor was changed, while the other factors kept constant, and each single factor experiment was repeated thrice [18].

C. Conventional extraction

The conventional extraction process was carried out at the optimal condition obtained during UAE of garlic. The extraction was carried out incubated at 30°C for 30 min. After extraction, the extract was centrifuged at 4000 rpm for 20 min then filtrated and stored for further analysis [19].

D. Analytical methodology

The concentration of allicin in each extracts was determined spectrophotometrically by reaction with the thiol 4-mercaptopyridine [16]. Briefly, varying quantities of garlic extract were incubated with 4-mercaptopyridine (10^{-4} M) in 50 mM phosphate buffer 2 mM EDTA pH 7.2 which results in the formation of a mixed disulphide 4-allylmercaptopyridine, and the consequent shift in absorbance at 324 nm (λ_{max}) was monitored. ϵ_M 39,600 $M^{-1}cm^{-1}$ at 324 nm was used for the calculation of allicin concentration [20].

III. RESULTS AND DISCUSSION

A. Effect of ultrasonic frequency on allicin content.

In order to obtain the maximum allicin content form garlic, ultrasonic frequency were performed at three extraction frequency (28, 45 and 100 kHz). The effect of different ultrasonic frequency on allicin content shown in Fig. 1. It was reported that high frequency favors the more allicin content than low frequency. Likewise, at 45 and 100 kHz, increasing the ultrasonic frequency significantly increased the allicin content. But further in term of energy, 45 kHz was chosen as the ultrasonic frequency in succeeding experiments [13, 14, 15].

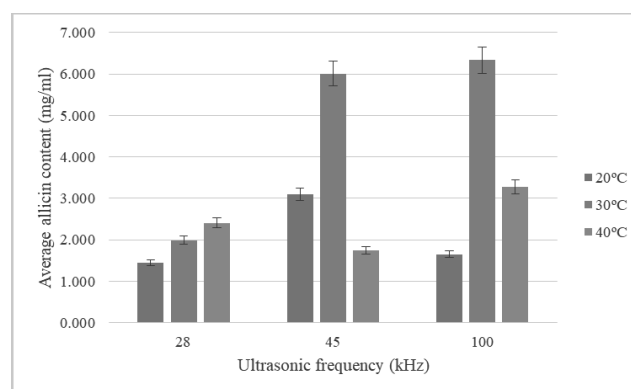


Fig. 1 Effect of ultrasonic frequency on allicin content while different extraction temperature.

B. Effect of temperature on allicin content

In this work, extraction temperature were carried out at 20, 30 and 40°C. As shown in Fig. 2, the allicin content was initially increased when the temperature increased from 20°C to 30°C and then decreased. Therefore, the extraction temperature at 30°C was chosen for further optimization studies [9, 11, 14].

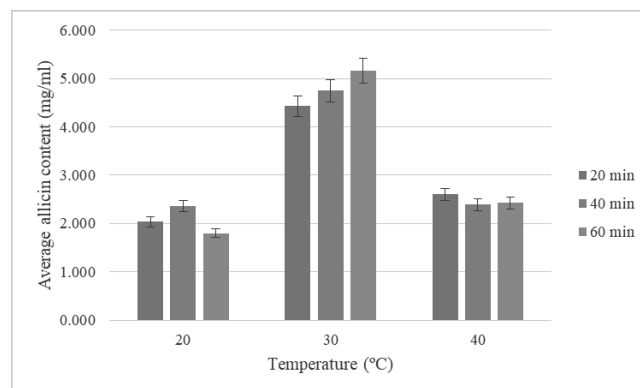


Fig. 2 Effect of extraction temperatures on allicin content while different extraction time.

C. Effect of extraction time on allicin content

The allicin content from garlic increased as the extraction time between 20 to 60 min, (Fig. 3) which significant not differences existed among 20, 40 and 60 min. However, at 60 min, the allicin content decrease. Thus, in practice, an extraction time of 40 min would be suitable due to the observed combined effects of good allicin content.

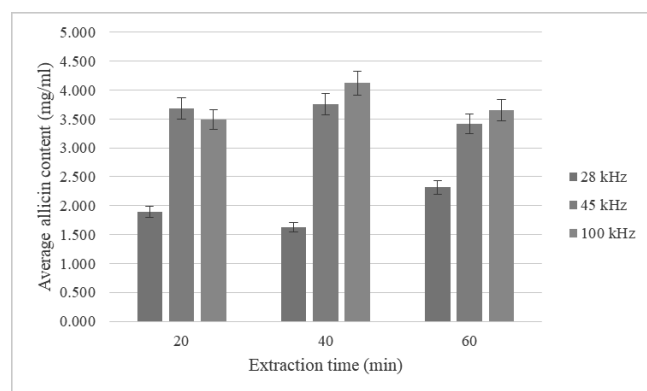


Fig. 3 Effect of extraction time on alliin content while different ultrasonic frequency.

IV. CONCLUSIONS

In the present study, various frequency and temperature significantly influenced the alliin content from garlic. Therefore, 45 kHz is a suitable extraction frequency. At 30°C exhibited the most efficient extraction while the ultrasonic frequency is 45 kHz could be used in terms of the combined effects of the alliin content. Furthermore, the ultrasonic frequency at 100 kHz and extraction time from 20 to 60 min exhibited a relatively high alliin content. As the extraction efficiency of alliin content depend largely on the combined effects of frequency, temperature and time, further investigation and optimization would be required. Since this present study focuses on ultrasonic assisted extraction of garlic (*Allium Sativum* Linn.); three influencing factors in the aqueous extraction which frequency, temperature and time were investigated.

ACKNOWLEDGMENT

The authors are grateful to Faculty of Engineering and Agro-Industry Maejo University, Chiang Mai, Thailand for providing insight and expertise that greatly assisted the research.

REFERENCES

- [1] Casella, S., Leonardi, M., Melai, B., Fratini, F., & Pistelli, L. 2013. The role of diallyl sulfides and dipropyl sulfides in the in vitro antimicrobial activity of the essential oil of garlic, *Allium sativum* L., and leek, *Allium porrum* L. **Phytotherapy Research**, 27(3), 380-383.
- [2] El-Hamidi, M., & El-Shami, S. M. 2015. Scavenging activity of different garlic extracts and garlic powder and their antioxidant effect on heated sunflower oil. **American Journal of Food Technology**, 10(4), 135-146.
- [3] Kopec, A., Piatkowska, E., Leszczynska, T., & Sikora, E. 2013. Healthy properties of garlic. **Current Nutrition & Food Science**, 9(1), 59-64.
- [4] Martins, N., Petropoulos, S., & Ferreira, I. C. 2016. Chemical composition and bioactive compounds of garlic (*Allium sativum* L.) as

affected by pre-and post-harvest conditions: A review. **Food chemistry**, 211, 41-50.

- [5] Zeng, Y., Li, Y., Yang, J., Pu, X., Du, J., Yang, X., & Yang, S. 2017. Therapeutic role of functional components in Alliums for preventive chronic disease in human being. **Evidence-Based Complementary and Alternative Medicine**, 2017.
- [6] Lanzotti, V., Barile, E., Antignani, V., Bonanomi, G., & Scala, F. 2012. Antifungal saponins from bulbs of garlic, *Allium sativum* L. var. **Voghiera. Phytochemistry**, 78, 126-134.
- [7] Lanzotti, V., Bonanomi, G., & Scala, F. 2013. What makes Allium species effective against pathogenic microbes?. **Phytochemistry reviews**, 12(4), 751-772.
- [8] Marchese, A., Barbieri, R., Sanches-Silva, A., Daglia, M., Nabavi, S. F., Jafari, N. J., Nabavi, S. M. 2016. Antifungal and antibacterial activities of alliin: A review. **Trends in Food Science and Technology**, 52, 49-56.
- [9] Baghalian, K., Ziai, S. A., Naghavi, M. R., Badi, H. N. & Khalighi, A. 2005. Evaluation of alliin content and botanical traits in Iranian garlic (*Allium sativum* L.) ecotypes. **Scientia Horticulturae**, 103(2), 155-166.
- [10] Eric Block. 2010. **Garlic and Other Alliums: The Lore and the Science**. RSC Publishing.
- [11] Daljit S. Arora & Jasleen Kaur. 1999. Antimicrobial activity of spices. **International Journal of Antimicrobial Agents**, 12(3), 257-262.
- [12] Serge Ankri & David Mirelman. 1999. Antimicrobial properties of alliin from garlic. **Microbes and Infection**, 1(2), 125-129.
- [13] Deng, J., Xu, Z., Xiang, C., Liu, J., Zhou, L., Li, T., Yang, Z. & Ding, C. 2017. Comparative evaluation of maceration and ultrasonic-assisted extraction of phenolic compounds from fresh olives. **Ultrasonics Sonochemistry**, 3, 328-334.
- [14] Kimbaris, A. C., Siatis, N. G., Daferera, D. J., Tarantilis, P. A., Pappas, C. S. & Polissiou, M. G. 2006. Comparison of distillation and ultrasound-assisted extraction methods for the isolation of sensitive aroma compounds from garlic (*Allium sativum*). **Ultrasonics sonochemistry**, 13(1), 54-60.
- [15] Chemat, F. & Khan, M. K. 2011. Applications of ultrasound in food technology: processing, preservation and extraction. **Ultrasonics sonochemistry**, 18(4), 813-835.
- [16] Picó, Y. 2012. **Chemical analysis of food: Techniques and applications**. Academic Press.
- [17] Lawson, L. D. & Gardner, C. D. 2005. Composition, stability, and bioavailability of garlic products used in a clinical trial. **Journal of agricultural and food chemistry**, 53(16), 6254-6261.
- [18] Wang, L. & Weller, C. L. 2006. Recent advances in extraction of nutraceuticals from plants. **Trends in Food Science & Technology**, 17(6), 300-312.
- [19] Olech, Z., & Zaborska, W. 2012. A spectrophotometric assay for total garlic thiosulfonates content. Kinetic aspects of reaction with chromogenic thiols. **Polish Journal of Food and Nutrition Sciences**, 62(1), 23-29
- [20] Miron, T., Shin, I., Feigenblat, G., Weiner, L., Mirelman, D., Wilchek, M. & Rabinkov, A. 2002. A spectrophotometric assay for alliin, alliinase (alliin lyase) with a chromogenic thiol: reaction of



Proceedings of the 10th International Conference on Sciences, Technology and Innovation for Sustainable Well-Being (STISWB 2018)
Vientiane, Lao PDR. July 11th -13th, 2018



4-mercaptopyridine with thiosulfates. **Analytical biochemistry**, 307(1), 76-83.

- [21] Wang, H., Li, X., Liu, X., Shen, D., Qiu, Y., Zhang, X. & Song, J. 2015. Influence of pH, concentration and light on stability of allicin in garlic (*Allium sativum* L.) aqueous extract as measured by UPLC. **Journal of the Science of Food and Agriculture**, 95(9), 1838-1844.



Solar Drying House for Drying Herbs

Sakultala Wannapakhe^{1st} and Khidsadakhon Booddachan

Department of Agricultural Engineering for Industry,
Faculty of Industrial Technology and Management, KMUTNB,
129 Moo 21, Tumbol Noen-Hom, Amphur Muang,
Prachinburi Province, 25230, Thailand
Sakultala.W@fitm.kmutnb.ac.th, Khidsadakhon.B@fitm.kmutnb.ac.th

Abstract— This research was to investigate and designed of solar drying house for drying herbs. The solar drying house in this research was double layers, the outside layer was made from clear polycarbonate and the inner layer was made from galvanized sheet. The one side of galvanized sheet was painted by black color for absorption of solar radiation. The 2 of roof ventilators were set at the top of solar drying house. Moreover, the ten of radiator fans motors 12V DC 90 W were set at galvanized wall. The herbs for experimental were Curcuma sliced and Beijing grass from Baan Dong Bung herb group, Prachin Buri Province, Thailand. The 100 g of Curcuma (*Curcuma longa* Linn.) sliced and Beijing grass (*Murdannia loriformis*) were set up distribution in drying racks at inner drying house. The temperatures at three points of front, center and back zones and the weight of herbs were measured every one hour until the average of herbs moisture content were decreased to the standard of Baan Dong Bung herb group. It was found that the temperature of inner solar drying house by turn on fans was nearly the temperature of inner solar drying house by turn off fans (the maximum of temperature difference in case of turn on fans as 2°C). The maximum of the efficiency of solar drying house was 16.05%. The drying time by using solar drying house at turn on fans was lower than drying time of by using solar drying house at turn off fans.

Keywords— *Curcuma*; *Beijing Grass*; *Drying House*; *Solar Energy*

I. INTRODUCTION (HEADING 1)

Nowadays, there are many alternative energy sources such as wind, water, geothermal, biomass and solar energies. Especially solar energy in Thailand, solar radiation is enough to applications. Because of the latitude of Thailand is 7 °N-20 °N (near equatorial). The annual average of total daily solar radiation in Thailand is 5.06 kWh/m²-day [1]. The solar drying in Thailand was reviewed by Somchart Soponronnarit in 1995 [2]. The review write about research and development work in solar drying in Thailand during the 1987 – 1995. Technical and economic results indicate that solar drying for some crops such as paddy, multiple crops and fruit is feasible. In addition, Thailand is suitable solar energy for usage, Thailand is agricultural country. Thailand has many herbs. Thai herbal plants are popular both inside and outside the country. One of kind of Thai herbal popular is Curcuma. In Prachin Buri Province, Thailand has Baan Dong Bung herb group, the location of Baan Dong Bung herb group is Moo 6, Tambon

Dong Khi Lek, Amphur Muang, Prachin Buri Province, Thailand. The Baan Dong Bung herb group produces dried herbs to Chao Phya Abhaibhubejhr hospital. The drying process of Baan Dong Bung herb group had two steps as 1. drying by using drying house as shown in figure 1 until the herbs moisture content were decreased to the standard of Baan Dong Bung herb group and 2. the herbs from step 1 were dried by oven gas. In Thailand, Chao Phya Abhaibhubejhr hospital focuses on herbal therapy and has developed medicinal products. From past to present, many researchers study about drying and application of solar energy. Example in 2002, Pangavhane and others studied for design, development and performance testing of a new natural convection solar dryer. The grape fruits were used for testing. The temperature in solar dryer was 50 - 55°C, the drying time was 4 days, it can reduce the drying time of the original (7 days) [3]. Bala and others (2003) studied to solar drying of pineapple using solar tunnel dried [4]. Dilip Jain and Tiwari (2004) studied to the effect of greenhouse on crop drying under natural and forced convection, thermal modeling and experimental validation [5]. Ashraf and others (2005) studied to experimental and neural network prediction of the performance of a solar tunnel drier for drying jackfruit bulbs and leather. The solar tunnel drier was made from transparent plastic sheet. The solar tunnel drier chamber has solar cells for direct electric transmission to two fans. The solar tunnel drier can be dried fruits about 120 – 150 kg [6]. Prasad J. and others (2006) studied on performance evaluation of hybrid drier for turmeric (*Curcuma Longa* L.) drying at village scale. The dryer was consisted of 2 parts of solar drier and combustion from biomass. The turmeric can be dried in 2 days; the temperature for drying was 50°C - 60°C. If drying by sun, the drying time was 15 days. The quality of dried turmeric by using solar drier was better than drying by sun. Alonge, A. F., and O. A. Adeboye (2012) studied about drying rates of some fruits and vegetables with passive solar dryers. They found that the drying rate with the direct passive solar dryer was found to be higher than that with indirect passive solar dryer [7]. A.A. El-Sebaai and S.M. Shalaby review of solar drying of agricultural products, they found that drying can be divided into several types as 1. direct solar dryers and 2. indirect solar dryers 3. solar dryers with heat storage media and 4. mixed-type solar dryers [8]. There were also several other researchers who are studying about solar drying [9-14].



Fig. 1. The old drying house at the Baan Dong Bang group

As a result, the solar drying house for agricultural products drying avoids expose to sunlight because of the sunlight can make the color difference from original products or fresh herbs. Moreover, the high drying temperature can make loss of some substances. Therefore, in this research, the solar drying house was designed to double layers. The outside layer was made from clear polycarbonate and the inner layer was made from galvanized sheet. The inner layer was opaque material therefore it can protect direct sunlight to product. The heat was storage between clear polycarbonate and galvanized sheet. The hot air in cavity was suck for drying.

II. EXPERIMENTAL SETUP AND PROCEDURE

A. The solar drying house for drying herbs design

For the first step of designing the solar drying house was studied the area for building. The area for building must not have the shadows of tree or house in this area. The solar drying house can get the sun all day. The size of land area in this research was 6 x 12 m as shows in figure 2.



Fig. 2. The land area for building solar drying house

From the area in figure 2 and from the result of distance of tree and house shadows, the area for building solar drying house was limited as only 4 x 10 m. In this research the solar drying house was double layers, the outside layer was made from clear polycarbonate and the inner layer was made from galvanized sheet. The one side of galvanized sheet was painted by black color for absorption of solar radiation. The edge of clear polycarbonate cover was set distance from the ground as 10 cm and the edge of galvanized sheet cover was set distance from the ground as 20 cm. The 2 of roof

ventilators were set at the top of solar drying house. The hot air is transfer by principle of hot air mass dynamic. Moreover, the ten of radiator fans motor 12 V DC 90 W were set at galvanized wall as shows in figure 3 for the air circulating in the house and sucking hot air from cavity of clear polycarbonate and galvanized sheets. The figure 4 shows schematic diagram of air flow inside the solar drying house. The solar drying house was showed in figure 5. Rack for putting herbs was designed and build by using same dimension of Baan Dong Bung herb group (width of 0.5 m, length of 2 m). The rack can be used for drying of the 6 kg of Curcuma sliced and 4.5 kg of Beijing grass per one layer. The rack for using in this research was three layers; the distance of layers was 50 cm. the 8 of rack was set in solar drying house as shown in figure 6 and 7.

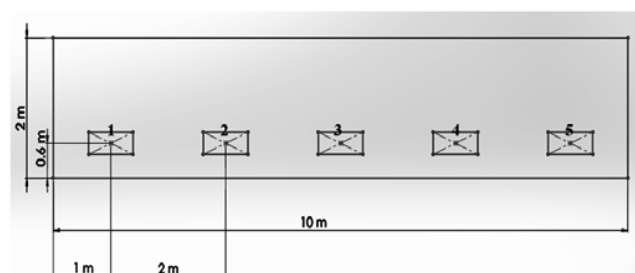


Fig. 3. The position setting of radiator fans motor 12V DC at one side (right side), the number 1-6 were the position setting radiator fan motor

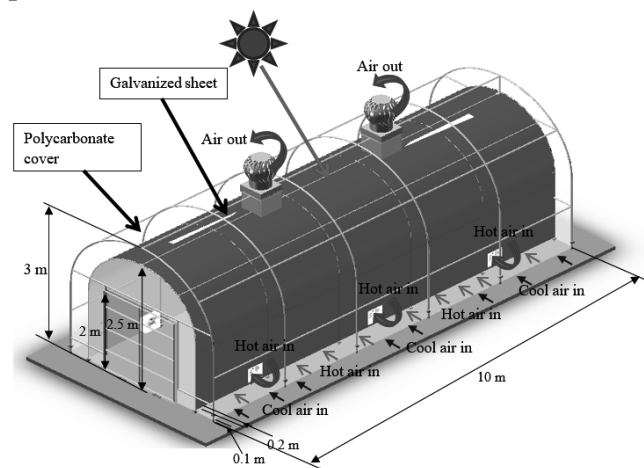


Fig. 4. Schematic diagram of air flow inside the solar drying house



Fig. 5. The solar drying house

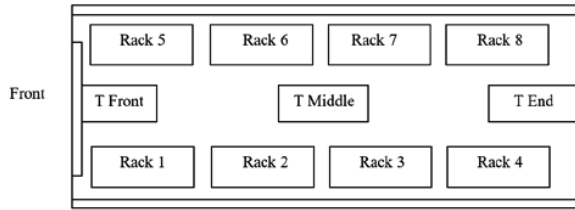


Fig. 6. The positions setting of rack and the temperature sensors



Fig. 7. Inside the solar drying house

B. Experimental setup and procedure

The herbs for experimental were two types of Curcuma sliced and Beijing grass from Baan Dong Bung herb group, Moo 6, Tambon Dong Khi Lek, Amphur Muang, Prachin Buri Province, Thailand as shown in figure 8. The 100 g of Curcuma sliced and Beijing grass were set up distribution in drying racks at inner drying house (the total of herb weight for experimental was 1,800 g). The time for drying in each day was 8.00 a.m. – 6.00 p.m. The data experimental was collected during November to December. The temperatures at three points of front, center and back zones and the weight of herbs were measured every one hour until the average of herbs moisture content were decreased to standard of Baan Dong Bung herb group. The moisture content for stopping drying in solar drying house of Curcuma sliced and Beijing grass were not over 50 and 600 %db, respectively. After that the herbs were dried by using hot air oven until the moisture content to 10 %db. The moisture content (% dry basis) of herbs was calculated by using equation 1. The mass of dry herb (d) was used oven for drying at 103 °C, 72 hours [15]. The Curcuma and Beijing grass dries were measured color by color meter (Hunter Lab, Miniscan EZ). The a^* and b^* were provided for measuring of Beijing grass and Curcuma dried.

$$M_d = \frac{w - d}{d} \times 100\% \quad (1)$$

where M_d is moisture content (% dry basis)
w is the mass of the wet herbs at any level and at any time (kg)
d is the mass of the dry herb (kg)

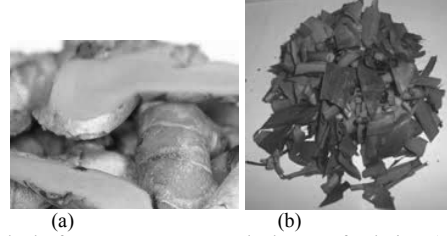


Fig. 8. The herbs from Baan Dong Bung herb group for drying: (a) Curcuma sliced, (b) Beijing grass

The efficiency of solar drying house can be calculated by equation 2. The equation 2 is used to predict the temperature of the drying house. The Global solar radiation in Thailand was 570 W/m², the value was get from solar radiation map of Thailand [1] (Prachinburi province, solar day as 8 hrs, experiment in November). The absorber area is only one side area of galvanized sheet as 35.7 m². The average of ambient temperature is 30 °C. The mass flow rate of air with setting ten fans and without setting fan are 0.1 kg/s and 0.06 kg/s, respectively.

$$\eta = \frac{\dot{m} \times c_p \times (T_o - T_i)}{G_T \times A_c} \times 100\% \quad (2)$$

- η = The efficiency of solar drying house (%)
- \dot{m} = mass flow rate (kg/s)
- C_p = Specific heat capacity (J/kg.°C)
- T_o = Outlet temperature of fluid (°C)
- T_i = Inlet temperature of fluid (°C)
- G_T = Global solar radiation (W/m²)
- A_c = Absorber area (m²)

III. RESULTS AND DISCUSSIONS

A. The result of air temperature in solar drying house

In figure 9 shows the temperature in solar drying house in case of experimental without setting ten fans, the maximum of temperature was 45 °C. The maximum of efficiency of solar drying house was 12.04%. In figure 10 shows the temperature in solar drying house in case of experimental with setting ten fans, the maximum of temperature was 42 °C. The maximum of efficiency of solar drying house was 16.05%. The temperature in solar drying house at turn off and turn on fans were over 40 °C in 11.00 a.m. – 15.00 p.m., it was suitable for drying herbs. The temperature in solar drying house was over 40 °C because of the solar radiation in afternoon was more than morning time, it was affected to the air between the galvanized and polycarbonate sheets therefore the air inside solar drying house was high temperature in afternoon.

B. The result of moisture content with drying time

In figure 11 - 14 show the results of the moisture content with drying time of Curcuma sliced and Beijing grass. In this research case, the moisture content considered a minimum



moisture content of Baan Dong Bung herb group, the end moisture content of Curcuma sliced and Beijing grass were not over 50 %db and 600 %db, respectively. The drying time by using the old drying house of Baan Dong Bung herb group was 72 hours. The old drying house of Baan Dong Bung herb group was no ventilator as figure 1. The old drying has only door for conveying herbs. The outside of the old drying house is covered with trees. The drying times of Curcuma sliced and Beijing grass by using solar drying house without fans (at turn off fan) were 17 and 18 hours, respectively. When the ten fans were set into the solar drying house, the drying times of Curcuma sliced and Beijing grass were 11 and 10 hours, respectively. When the fans were set into solar drying house, the drying time was decreased because of the air mass is moving better as a result of the moisture content of herbs were taken out better.

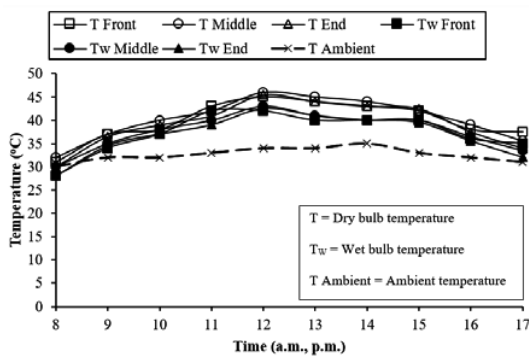


Fig. 9. The air temperature inside the solar drying house without setting ten

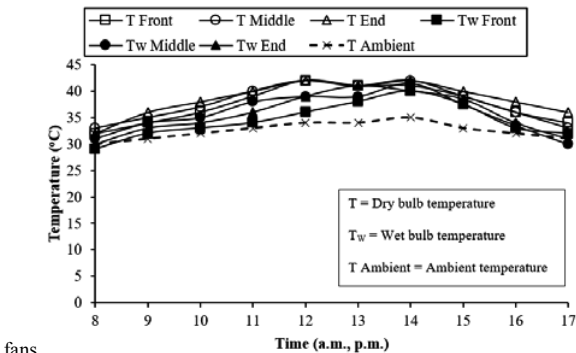


Fig. 10. The air temperature inside the solar drying house with setting ten

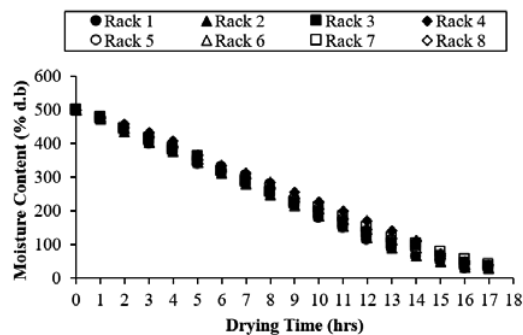


Fig. 11. The moisture content with drying time of Curcuma sliced by using solar drying house without setting fan

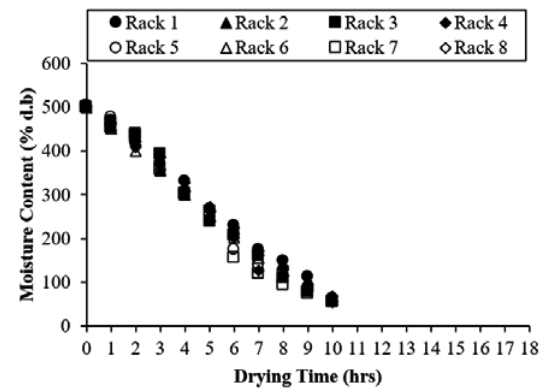


Fig. 12. The moisture content with drying time of Curcuma sliced by using solar drying house with setting ten fans

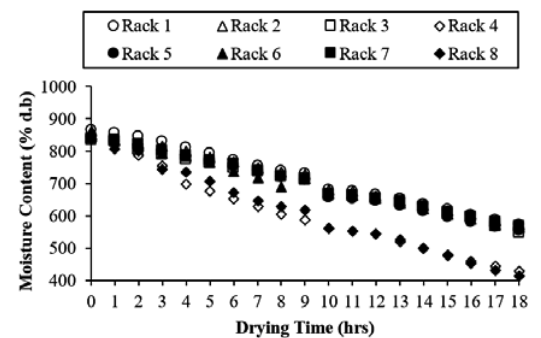


Fig. 13. The moisture content with drying time of Beijing grass by using solar drying house without setting fan

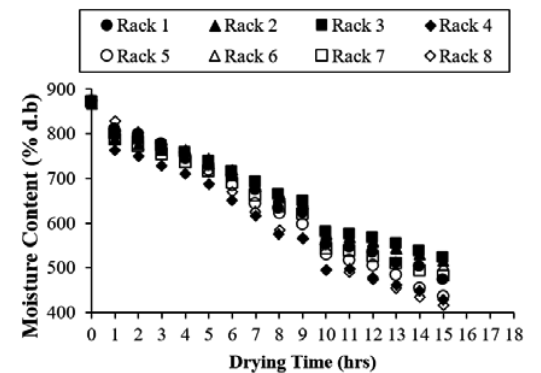


Fig. 14. The moisture content with drying time of Beijing grass by using solar drying house with setting ten fans

C. The result of color values of drying herbs

The color analyses of dried herbs in this case, the a^* and b^* values were used as a basis for comparison. In table 1 shows the color values of dried herbs, it was found that the color value of Curcuma sliced and Beijing grass by using solar drying house (both cases of setting fans and not setting fan) were nearly color analysis of fresh herbs because of the herbs were not direct sunlight and the temperature in solar drying



house were not over for drying herbs. The results of color analysis were accorded with Prasad J. and others (2006) [9].

Table I The color values of dried herbs

Type of herb	Drying method	Color values		
		L*	a*	b*
Curcuma Sliced	Sun	27.46±2.52	12.50±4.05	13.98±1.56
	The old drying house of Baan Dong Bung herb group	25.64±2.06	7.94±0.96	19.19±1.73
	The solar drying house without setting fans	28.59±2.65	11.21±1.39	14.63±1.30
	The solar drying house with setting fans	31.74±4.03	14.50±3.56	16.69±2.43
	Fresh Curcuma	47.53±2.08	35.98±1.66	28.03±1.46
	Sun (Outdoor solar drying)	24.23±4.86	-3.91±2.09	28.63±1.44
Beijing grass	The old drying house of Baan Dong Bung herb group	6.63±3.67	7.93±1.34	11.05±6.53
	The solar drying house without setting fans	29.31±2.7	-4.93±1.08	24.69±3.19
	The solar drying house with setting fans	27.99±2.7	-4.58±1.07	27.42±1.23
	Fresh Beijing grass	27.07±1.90	-11.99±2.98	28.94±6.16

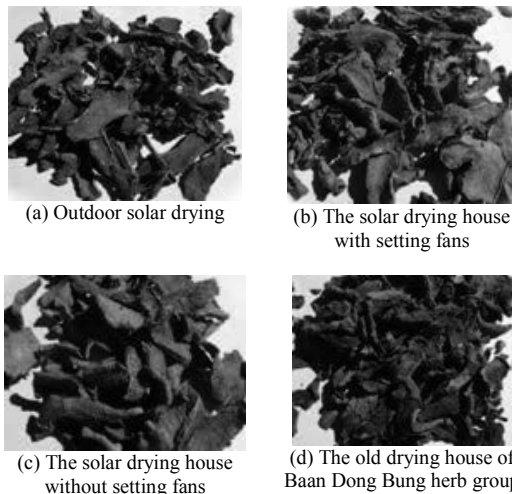


Fig. 15. The sample of Curcuma sliced after drying in difference drying methods

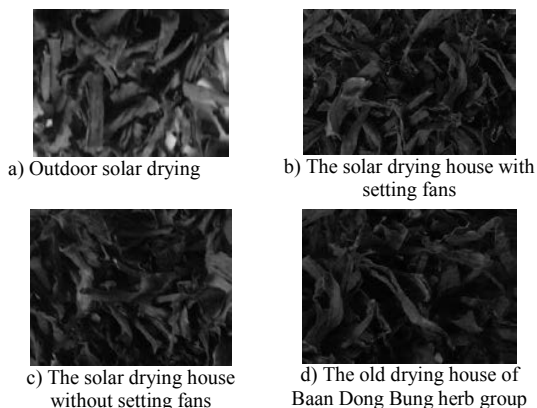


Fig. 16. The sample of Beijing grass after drying in difference drying methods

IV. CONCLUSIONS

This research studied about designing and building the solar drying house for drying herbs. The herbs for this testing were Curcuma sliced and Beijing grass. The temperature of drying house in both of set of ten fans and not set ten fans were over 40 °C in 1100 a.m. – 15.00 p.m., it was suitable for drying herbs. The maximum of efficiency of solar drying house was 16.05%. In case of comparison of drying time of dried herbs, it was found that the drying time of herbs drying by using solar drying house were less than drying by using original drying house. Moreover, the color analyses of herbs drying by using solar drying house were nearly color analysis of fresh herbs.

REFERENCES

- [1] The Department of Alternative Energy Development and Efficiency (DEDE): <http://www.dede.go.th>.
- [2] S. Soponronnarit. "Solar drying in Thailand," Energy for Sustainable Development. 2:19-25, 1995.
- [3] D. R. Pangavhane and others. "Design, Development and Performance Testing of a New Natural Convection Solar Dryer," Energy. 27: 579–590, 2002.
- [4] B.K. Bala and others. "Solar Drying of Pineapple Using Solar Tunnel Dried," Renewable Energy. 28: 183–190, 2003.
- [5] D. Jain and G.N. Tiwari. "Effect of Greenhouse on Crop Drying Under Natural and Forced Convection II. Thermal Modeling and Experimental Validation," Energy Conversion and Management. 45: 2777–2793, 2004.
- [6] B.K. ASHraf and others. "Experimental and Neural Network Prediction of the Performance of a Solar Tunnel Drier for Drying Jackfruit Bulbs and Leather," Journal of Food Engineering. Vol. 28 : 552–566, 2005.
- [7] A. F. Alonge and O. A. Adeboye. "Drying rates of some fruits and vegetables with passive solar dryers," International Journal of Agricultural and Biological Engineering 5(4) : 83-90, 2012.
- [8] A.A. El-Sebaai and S.M. Shalaby. "Solar drying of agricultural products: A review," Renewable and Sustainable Energy Reviews 16 : 37–43, 2012.
- [9] J. Prasad and others. "Study on Performance Evaluation of Hybrid Drier for Turmeric (Curcuma Longa L.) Drying at Village Scale," Journal of Food Engineering. 75: 497-502, 2006.
- [10] U. Tawan and others. "Experimental Performance of a Solar Tunnel Dryer for Drying Silkworm Pupae," Biosystems Engineering. 101: 209-216, 2008.
- [11] A. Yano and others. "Electrical Energy Generated by Photovoltaic Modules Mounted Inside the Roof of a North- South Oriented Greenhouse," Biosystems Engineering. 103: 228–238, 2009.
- [12] R.D. Singh and G.N. Tiwari. "Energy Conservation in the Greenhouse System a Steady State Analysis," Energy. 35: 1-7, 2010.
- [13] P.J. Sonneveld and others. "Performance Results of a Solar Greenhouse Combining Electrical and Thermal Energy Production," Biosystems Engineering. 106: 48-57, 2010.
- [14] S. Janjai. "A greenhouse type solar dryer for small-scale dried food industries: Development and dissemination," International Journal of Energy and Environment. 3(3) : 383-398, 2012.
- [15] S. Soponronnarit. "Drying Grains and Some Types of Foods", 7th edition, KMITT, Bangkok, 338p. (in Thai), 1997.



Temperature Distribution Inside Biochar Kiln for Biochar Production

Numpon Panyoyai, Thanasit Wongsiriamnuay and Tipapon Khamdaeng*

Faculty of Engineering and Agro-Industry

Maejo University

San Sai, Chiang Mai, Thailand 50290

*Corresponding author: tipapon@mju.ac.th

Abstract—Biochar is a carbon-rich solid product of thermal pyrolysis of organic matter used for soil fertility improvement. The quantity and quality of biochar are mainly influenced by the pyrolysis temperature. To achieve the maximum yield and high quality of biochar, the biochar kiln was therefore designed with the optimized process parameter. The kiln with a dimension of 467 mm × 384 mm (height × diameter) was developed consisting of the core with diameter of 114.3 mm located at the kiln center. The different core puncture diameters (3.18 mm, 4.76 mm, and 6.35 mm) were investigated. The computer simulation was applied on this study aimed at determining the effect of the core puncture diameter on the temperature distribution. To validate the model, the simulation results were compared with the experimental results. From the simulation, all core puncture diameters showed the same temperature distribution, i.e., the highest temperature was respectively found at the middle, top, and base of the kiln. The temperature averagely over the radial positions at the middle part of the kiln was found to be equal to 574.0 ± 164.6 °C, 487.3 ± 126.7 °C, and 463.7 ± 114.2 °C for the core puncture diameter of 3.18 mm, 4.76 mm, and 6.35 mm, respectively. Based on this simulation results, it can reveal the characteristic of the temperature distribution, affecting to the yield and quality of biochar.

Keywords—agricultural residues; biochar kiln; slow pyrolysis; temperature distribution; thermal simulation

I. INTRODUCTION

Biochar has been used as a soil amendment and applied to agricultural land for the better crop production as well as the environmental management. It is a stable carbon-rich product obtained from the thermal pyrolysis of biomass. The biomass is heated to temperature varying between 400 to 1,250 °C under the absence of oxygen or low oxygen concentrations with time span varying between 1 s to 3 h, depending on the types of pyrolysis process used [1]. For the slow pyrolysis, the biomass is heated under the low to moderate temperature ranging from 400 to 500 °C for a long time span varying between 30 min to 3 h. The fast pyrolysis depends on the moderate to high temperature heating approximately 850 to 1,250 °C for a short time span varying between 1 to 10 s with high heating rate. The intermediate pyrolysis has the process conditions in between the slow and fast pyrolysis, operating with the temperature of 500 to 650 °C and time span varying between 300 to 1,000 s.

The product yields of biomass pyrolysis depend on these types of pyrolysis process. For the biochar production, the slow pyrolysis is focused to efficiently achieve the maximum yield of biochar. It produced relatively high biochar yield compared to the fast pyrolysis (i.e., 35-50 wt. % for the slow pyrolysis and 12-25 wt. % for the fast pyrolysis) [2, 3]. Furthermore, the process parameters, such as pyrolysis temperature, heating time, heat rate, particle size, and gas flow rate, have been reported to influence the yield and properties of biochar [4-8].

The alkalinity and surface area of biochar have been reported to be mainly affected by the pyrolysis temperature [8-10]. The alkalinity of biochar is utilized for the acidic sandy soil which is neutralized the soil pH and improved the nitrification [11]. The high surface area contributed by the pores can increase the water holding capacity of soil and maintain the soil nutrients, which is preferable to microorganism habitation and activity [12]. The other biochar properties, such as total organic carbon, fixed carbon, and mineral elements of biochar, were found to be most affected by the feedstock properties [9].

There are many different types of the small or farmer scale biochar kilns [7, 13]. The kiln design and biochar production process depend on the purpose of local users. The techniques of small scale biochar production are not widely available as they have been provided for the industrial biochar production. The design information and discussion of the effect of process parameters on the productivity and quality of biochar have been investigated in a few numbers of studies. In this study, the biochar kiln was designed in detail. The computer simulation was applied to evaluate the temperature distribution inside the kiln with different core puncture diameters (i.e., 3.18 mm, 4.76 mm, and 6.35 mm). The effect of the core puncture diameters on the temperature distribution along with the yield and properties of biochar was also investigated.

II. MATERIALS AND METHODS

A. Biochar Kiln Construction

Biochar kiln was made of carbon steel with the height of 467 mm, outer diameter of 384 mm, and thickness of 1.5 mm. The lid and bottom of the kiln was punctured with the diameter of 111.1 mm. The composition of the biochar kiln, including flue and sieve platform, is shown in Fig. 1. The flue and sieve



platform help to improve the oxygen circulation during the combustion of fuel. The carbon steel cylinder pipe with the height of 467 mm, inner diameter of 110.7 mm, and thickness of 3.6 mm was placed at the kiln center as inner chamber (Fig. 2(a)). The inner chamber or core of the kiln was opened to the air while the outer chamber was tightly closed. The core dimension is shown in Fig. 2(b). The core was punctured in circumferential locations at the height of 50 mm, 200 mm, and 340 mm. The different core puncture diameters were investigated in this study, i.e., 3.18 mm, 4.76 mm, and 6.35 mm. The distance between each core puncture at the same height was equal to 3 mm.

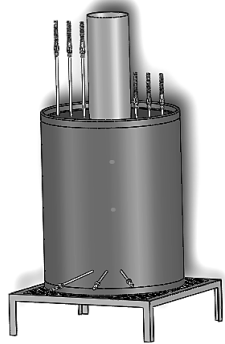


Fig. 1. Biochar kiln including flue and sieve platform

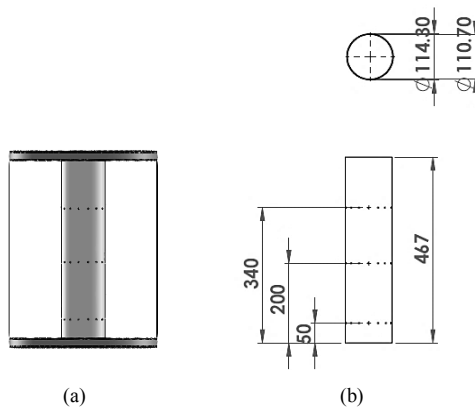


Fig. 2. (a) Double chamber of biochar kiln with core at its center and (b) core dimension in millimeter

B. Data Acquisition

To acquire the temperature distribution inside the biochar kiln, nine K-type thermocouples were set at the different axial and radial locations of the kiln, as shown in Fig. 3, where h_1 , h_2 , and h_3 respectively indicate the axial locations at the height of 50 mm, 200 mm, and 340 mm from the bottom of the kiln (Fig. 3(a)) and r_1 , r_2 , and r_3 respectively indicate the radial locations at 52 mm, 124 mm, and 190 mm from the center of the kiln (Fig. 3(b)). The real-time temperatures acquired from the thermocouples were stored using data logger (Wisco Online Datalogger OD04). The steady-state temperatures obtained

from experiment with the nine locations of thermocouples were selected and were furthermore compared with those obtained from the simulation.

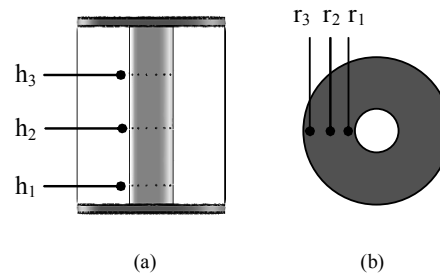


Fig. 3. Positions of thermocouple attachment at (a) axial locations ($h_1 = 50$ mm, $h_2 = 200$ mm, and $h_3 = 340$ mm) and (b) radial locations ($r_1 = 52$ mm, $r_2 = 124$ mm, and $r_3 = 190$ mm) inside biochar kiln

C. Experimental Procedure

Seven kilograms of corncobs with moisture content of 10% wet basis (wb) were used to produce biochar in each condition. The corncobs were loaded into the outer chamber of the kiln, surrounding the core of the kiln. The nine thermocouples were set inside the kiln following the locations as aforementioned. The lid was then tightly closed. The biochar kiln was placed on the sieve platform before fuel loaded. The briquettes from rubber sawdust were used as fuel. Three kilograms of fuel briquettes were continuously loaded with the identical quantities into the core of the kiln during the experiments. The fuel briquette was ignited from the top of the kiln. The combustion then continued downwards to the bottom of the kiln using approximately 3 hours of heating time until the fuel briquettes were empty. The pyrolysis temperatures inside the kiln were acquired and stored during the experiment. The steady-state temperatures at the nine locations of thermocouples were selected and were plotted along the radial directions at the different heights of the kiln. After the kiln cooled down, the solid yields of the process were completely obtained. The solid yields were categorized into 3 groups, i.e., biochar, non-biochar, and fuel ash. The non-biochar was corncobs with incomplete thermochemical decomposition, varying inversely with the yield of biochar. The biochar, obtained from each experiment with different core puncture diameters, was weighed to calculate the percent of biochar yield and was compared with the others.

Furthermore, the effect of core puncture diameter on the biochar quality was investigated by evaluating the physico-chemical properties of the biochar. The pH of the biochar was measured using pH meter. The content of potassium (K_2O) and phosphorous (P_2O_5) and carbon to nitrogen ratio (C/N ratio) were obtained using in-house method based on AOAC.

III. SIMULATION ANALYSIS

The temperature distributions inside the biochar kiln were simulated in this study. The governing equations, initial and boundary conditions under consideration were numerically solved using computer simulation software. The temperature



distribution in biochar kiln was modeled in three dimensions. To simplify the problem, the axisymmetric heat transfer was considered. Thus, the temperature distribution in biochar kiln can be illustrated in two dimensions. The further assumptions were detailed as follows.

- 1) The model was considered in steady-state heat transfer.
- 2) The transfer of heat from inner core surface to outer core surface was conduction.
- 3) The transfers of heat from outer core surface to outer chamber (containing corncobs) were conduction, convection, and radiation.
- 4) The transfer of heat from outer kiln wall to surroundings was free convection.

Since the temperature distribution was significantly affected the quantity and quality of product yields, the effect of core puncture diameter on the temperature distribution was investigated in order to reveal the heat transfer characteristics inside biochar kiln with different core puncture diameters. To assure the model fits, the simulation results for each core puncture diameter were compared with the experimental results.

IV. RESULTS AND DISCUSSION

A. The Comparison of Temperature Distribution Between Simulation and Experimental Results

The simulation results were validated with the experimental results in order to verify the accuracy of the model. The comparisons between simulation and experimental results of the temperature versus radial distance of biochar kiln at the height of 50 mm, 200 mm, and 340 mm from the bottom of the kiln with different core puncture diameters were illustrated in Figs. 4-6.

The good agreement between the simulation results and the experimental results is noted for each core puncture diameter. From the simulation, at the core puncture diameter of 3.18 mm, the minimum and maximum errors of temperature averagely over three radial locations were respectively found to be equal to $3.1 \pm 3.7\%$ at the height of 200 mm (middle) and $31.1 \pm 35.6\%$ at the height of 50 mm (base) of the kiln. At the core puncture diameter of 4.76 mm, the minimum and maximum errors of temperature averagely over three radial locations were respectively found to be equal to $4.8 \pm 4.9\%$ at the height of 200 mm (middle) and $13.1 \pm 10.0\%$ at the height of 50 mm (base) of the kiln. At the core puncture diameter of 6.35 mm, the minimum and maximum errors of temperature averagely over three radial locations were respectively found to be equal to $2.7 \pm 1.1\%$ at the height of 50 mm (base) and $5.8 \pm 6.4\%$ at the height of 200 mm (middle) of the kiln. The temperature distribution can be, however, most accurately predicted at the height of 200 mm (middle) of the kiln for all core puncture diameters. The error between results was caused by the model assumptions and numerical scheme used.

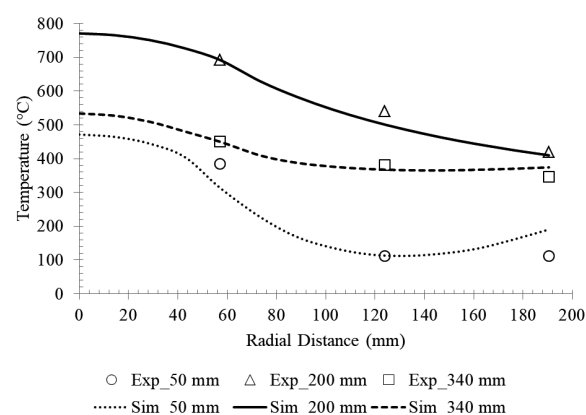


Fig. 4. Comparison between simulation and experimental results of the temperature versus radial distance of biochar kiln at the height of 50 mm, 200 mm, and 340 mm from the bottom of the kiln with core puncture diameter of 3.18 mm

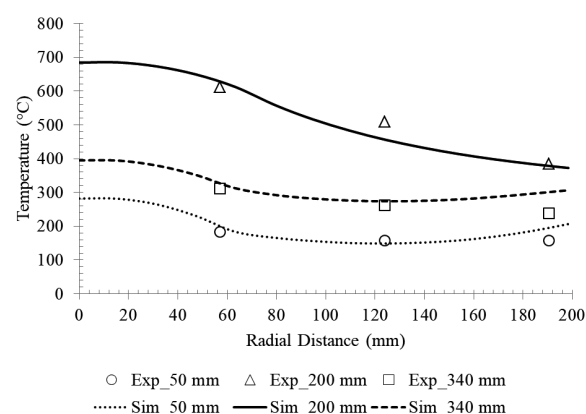


Fig. 5. Comparison between simulation and experimental results of the temperature versus radial distance of biochar kiln at the height of 50 mm, 200 mm, and 340 mm from the bottom of the kiln with core puncture diameter of 4.76 mm

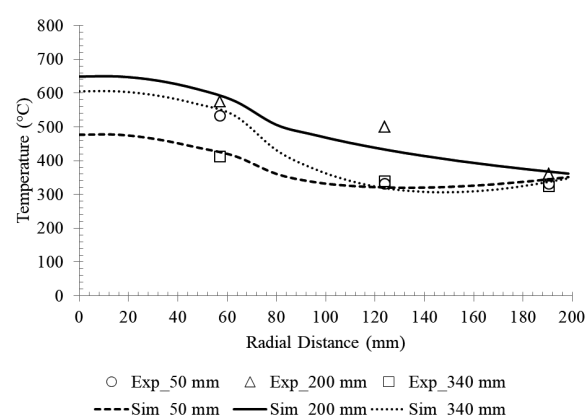


Fig. 6. Comparison between simulation and experimental results of the temperature versus radial distance of biochar kiln at the height of 50 mm, 200 mm, and 340 mm from the bottom of the kiln with core puncture diameter of 6.35 mm



Both simulation and experimental results show that the same temperature distribution was observed in all core puncture diameters. The highest temperature in axial location was found at the height of 200 mm (middle), 340 mm (top), and 50 mm (base) of the kiln, respectively, and the temperature decreased outwards the kiln center. Furthermore, the kiln with the core puncture diameter of 3.18 mm was found to be higher in the temperature range than that with the core puncture diameter of 4.76 mm and 6.35 mm, respectively.

B. Effect of Core Puncture Diameter on Temperature Distribution

Figs. 7-9 show the temperature distribution inside biochar kiln with the different core puncture diameters. The temperature distributions were simulated corresponding to the variations of temperature and radial distance of the biochar kiln as shown in Figs. 4-6.

The heat transfer through the wall of core was conduction and continued inside the kiln by conduction, convection, and radiation. The kiln with the core puncture diameter of 6.35 mm was more uniform in temperature distribution than that with the core puncture diameter of 4.76 mm and 3.18 mm, respectively. The larger heat transfer surface area of the core puncture diameter of 3.18 mm caused the higher temperature around the core as shown in Fig. 7. The lower uniform temperature distribution occurred in the kiln with the smaller core puncture diameter (3.18 mm) which it might be due to the non-continuous circulation of released gas, resulting in the decrease in the heat convection inside the kiln. On the other hand, the continuous circulation of released gas increased with increasing the core puncture diameter (6.35 mm). The higher uniform temperature distribution, as shown in Fig. 9, was caused by the increase in the heat convection inside the kiln. The moderate uniform temperature distribution was shown in Fig. 8.

The temperature distributions were captured when the pyrolysis temperatures reached the steady-state. The high temperatures were observed at the middle core of the kiln as a result of the appearance of the combustion of fuel briquettes. At the middle part of the kiln, all core puncture diameters provided the temperature range of the slow pyrolysis, i.e., 574.0 ± 164.6 °C, 487.3 ± 126.7 °C, and 463.7 ± 114.2 °C for the core puncture diameter of 3.18 mm, 4.76 mm, and 6.35 mm, respectively. The process parameters have been reported to significantly affect the yield of biochar and its quality. The heating rate, heating time, and pyrolysis temperature were not necessarily the variable parameters in this study. However, the standard deviation of temperature range higher than 20% would influence the biochar properties [13]. The capabilities of heat convection inside the kiln and gas release for each core puncture diameter as aforementioned were supposed to affect the temperature distribution as well as the yield and quality of biochar.

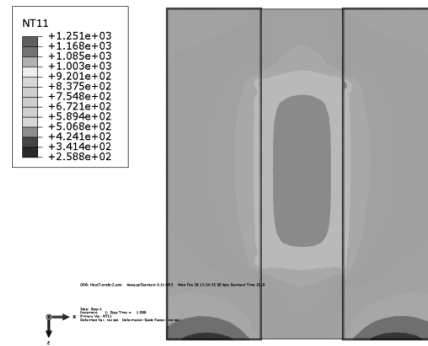


Fig. 7. Temperature distribution in biochar kiln with core puncture diameter of 3.18 mm (unit: K)

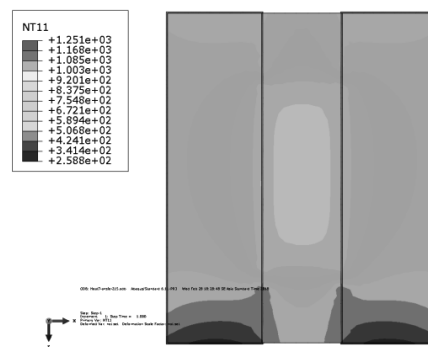


Fig. 8. Temperature distribution in biochar kiln with core puncture diameter of 4.76 mm (unit: K)

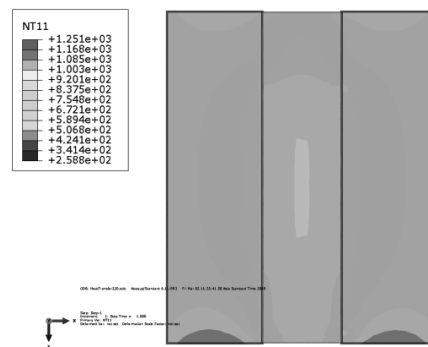


Fig. 9. Temperature distribution in biochar kiln with core puncture diameter of 6.35 mm (unit: K)

C. Quantity and Quality of Biochar

The yield and physiochemical properties of biochar for each core puncture diameter were shown in Table 1. The biochar was mostly found at the middle part of the biochar kiln at which the corncobs chemically decomposed in the temperature range of slow pyrolysis. The biochar yield was calculated from the percentage of the ratio of weight of biochar to weight of total solid yields. The highest yield of biochar was found to be equal to 24.12 wt. % at the core puncture diameter of 4.76 mm. The maximum biochar yield



was relatively small in this study [6, 13] due to the fuel applied restriction and process limitation. The temperature distribution inside biochar kiln with the core puncture diameter of 4.76 mm provided the proper condition for decomposition, i.e., the heat generation and circulation were optimized to ignite the corncobs. The core puncture diameter of 3.18 mm and 6.35 mm were approximately 2 times smaller in biochar yield than the core puncture diameter of 4.67 mm. Both lower and higher capabilities of heated gas circulation caused the decrease in the biochar yield. For the smaller core puncture diameter (3.18 mm), the heated gas could not properly circulate and could not start to ignite some of the corncobs under pyrolysis. The greater core puncture diameter (6.35 mm), on the contrary, provided the continuous circulation of heated gas which might rapidly drive out the thermal volatiles, resulting in the increase in the produced gas and consequent decrease in the biochar yield.

The proper temperature distribution of the kiln with the core puncture diameter of 4.67 mm was, furthermore, found to provide the carbon to nitrogen ratio (C/N ratio), phosphorus content (P) and potassium content (K) in the biochar higher than the other ones. This C/N ratio was utilized for microbial activity and considerably small compared to the previous reports [6, 14]. The pH of the biochar obtained after the pyrolysis was found to increase with the core puncture diameter. This alkaline of the biochar can improve the soil quality by neutralizing acidic soils.

TABLE I. YIELD AND PHYSIOCHEMICAL PROPERTIES OF BIOCHAR AT DIFFERENT CORE PUNCTURE DIAMETERS

Core Puncture Diameter (mm)	Yield (wt.%)	pH (-)	C/N Ratio (-)	P (wt.%)	K (wt.%)
3.18	10.62	7.76	21 : 1	0.99	1.81
4.76	24.12	8.15	31 : 1	3.16	2.13
6.35	12.24	9.40	18 : 1	1.80	1.80

The yield and physiochemical properties of biochar depended on the temperature distribution. The optimal core puncture diameter could limit the inlet air meanwhile the heat could be sufficiently generated for the pyrolysis under the proper condition of the heated gas circulation. The amount of the total fuel briquettes and types of feedstock applied will be further investigated to achieve the maximum yield and high quality of biochar efficiently.

V. CONCLUSIONS

The temperature distributions inside the biochar kiln with the different core puncture diameters were investigated in this study. The domains of the biochar kiln were modeled using the simplified equations of heat transfer. The simulation results were found to be in good agreement with the experimental results. The continuous circulation of the heated gas inside the biochar kiln could be inferred from the uniform temperature

distribution. For the biochar production, the core puncture diameter of 4.76 mm was optimal to provide the proper temperature distribution, resulting in the increase in the yield and quality of biochar.

ACKNOWLEDGMENT

This study was supported by the Faculty of Engineering and Agro-Industry, Maejo University, Chiang Mai, Thailand. The authors wish to thank Potjaman Promngam for conducting the experiments and for her assistance.

REFERENCES

- [1] M. Tripathi, J.N. Sahu, P. Ganesan, Effect of process parameters on production of biochar from biomass waste through pyrolysis: A review, *Renewable and Sustainable Energy Reviews*, vol. 55, pp. 467-481, March 2016.
- [2] S.P. Sohi, E. Krull, E. Lopez-Capel, R. Bol, A review of biochar and its use and function in soil, in: D.L. Sparks (Ed.) *Advances in Agronomy*, Burlington: Academic Press, 2010, pp. 47-82.
- [3] Q. Yan, H. Toghiani, F. Yu, Z. Cai, J. Zhang, Effects of pyrolysis conditions on yield of bio-chars from pine chips, *Forest Products Journal*, vol. 61, pp. 367-371, 2011.
- [4] D. Chen, X. Yu, C. Song, X. Pang, J. Huang, Y. Li, Effect of pyrolysis temperature on the chemical oxidation stability of bamboo biochar, *Bioresource Technology*, vol. 218, pp. 1303-1306, October 2016.
- [5] A. Demirbas, Effects of temperature and particle size on bio-char yield from pyrolysis of agricultural residues, *Journal of Analytical and Applied Pyrolysis*, vol. 72, pp. 243-248, November 2004.
- [6] X. Liu, Y. Zhang, Z. Li, R. Feng, Y. Zhang, Characterization of corncob-derived biochar and pyrolysis kinetics in comparison with corn stalk and sawdust, *Bioresource Technology*, vol. 170, pp. 76-82, October 2014.
- [7] S. Mia, N. Uddin, S. Abdullah, A.M. Hossain, R. Amin, F.Z. Mete, T. Hiemstra, Production of biochar for soil application: A comparative study of three kiln models, *Pedosphere*, vol. 25, pp. 696-702, October 2015.
- [8] A. Shaaban, S.M. Se, M.F. Dimin, J.M. Juoi, M.H.M. Husin, N.M.M. Mitran, Influence of heating temperature and holding time on biochars derived from rubber wood sawdust via slow pyrolysis, *Journal of Analytical and Applied Pyrolysis*, vol. 107, pp. 31-39, May 2014.
- [9] L. Zhao, X. Cao, O. Masek, A. Zimmerman, Heterogeneity of biochar properties as a function of feedstock sources and production temperatures, *Journal of Hazardous Materials*, vol. 256-257, pp. 1-9, July 2013.
- [10] J. Zhang, J. Liu, R. Liu, Effects of pyrolysis temperature and heating time on biochar obtained from the pyrolysis of straw and lignosulfonate, *Bioresource Technology*, vol. 176, pp. 288-291, January 2015.
- [11] J.H. Yuan, R.K. Xu, H. Zhang, The forms of alkalis in the biochar produced from crop residues at different temperatures, *Bioresource Technology*, vol. 102, pp. 3488-3497, February 2011.
- [12] S. Gul, J.K. Whalen, B.W. Thomas, V. Sachdeva, Physico-chemical properties and microbial responses in biochar-amended soils: Mechanisms and future directions, *Agriculture, Ecosystems and Environment*, vol. 206, pp. 46-59, August 2015.
- [13] D.K. Boris Merlain, S.E. Allaire, A.D. Munson, Quality of biochars made from eucalyptus tree bark and corncob using a pilot-scale retort kiln, *Waste Biomass Valorization*, vol. 9, pp. 899-909, June 2018.
- [14] H. Zhang, R.P. Voroney, G.W. Price, Effects of temperature and processing conditions on biochar chemical properties and their influence on soil C and N transformations, *Soil Biology & Biochemistry*, vol. 83, pp. 19-28, April 2015.



Disassembled Solar Greenhouse Dryer for Agricultural Products

Nattapol Poomsa-ad

Drying Technology for Agricultural Products Research Unit
Faculty of Engineering, Mahasarakham University
Maha Sarakham, Thailand
nattapol.p@msu.ac.th

Lamul Wiset

Postharvest Technology and Agricultural Machinery
Research Laboratory, Faculty of Engineering,
Mahasarakham University
Maha Sarakham, Thailand
lamulwiset@hotmail.com

Abstract— The purpose of this research is to design, construct and testing a solar greenhouse for agricultural products drying. The housing can be easily assembled and disassembled using polyvinyl chloride (PVC) pipe and fitting as a main structure. In this study, the two cable slings were used to support the pipe for more rigid structure. The housing has a shape of a 45 degree triangular prism with a base of 7.3 m x 4 m and a height of 4.4 m. The 0.5 mm thick of transparent polyethylene sheet was used to cover and the 0.5 mm thick of dark polyethylene sheet was used as the solar absorber. The drying area was 18.24 m². Results found that the 120 kg soybean can be dried from the initial moisture content of 53.9% wet basis down to 10% wet basis within 3 days for safe storage. In addition, the average thermal efficiency of this greenhouse was 6.5%.

Keywords—drying efficiency; greenhouse; solar energy; soybean

I. INTRODUCTION

Drying is a process for prolonging shelf-life of agricultural products. However, dryer needs to consume heat and electricity for operating. This is a limitation of a rural area which has no electricity supply. Solar dryer is an alternative way applied for drying. Solar greenhouse dryer is widely used due to convenience and high amount of product can be dried.[1][2] There are natural circulation [3] and forced circulation worked with solar cell.[4][5]

Some agricultural produce is only harvested once a year. With this reason, the solar greenhouse dryer is used for a short term during only working period. Then, the dryer is left and exposed to the sunlight until next season. This situation leads to the reduction of the solar greenhouse dryer lifetime and this leads to high maintenance cost. Therefore, the objective of this research is to design and construct as well as test the performance of an easily disassembled solar dryer. The materials used for the dryer are available in the market. We used the polyvinyl chloride pipe as a structural dryer.

II. EXPERIMENTATION PROCEDURE

A. Experimental period

In this study, the experiments were carried out at Faculty of Engineering, Mahasarakham University, Kantarawichai, Maha Sarakham Province in the northeastern of Thailand (latitude, 16.24°N; longitude, 103.253556°E) during May 2-10, 2018. During this period, the climate data based on 30 years found that the days are considered as partly cloudy and the sunshine duration was about 13 h per day. However, The sunshine hour with the potential solar intensity is only 10 h per day (9.00 am-5.00 pm)

B. Solar Greenhouse Dryer

A solar greenhouse dryer in this study is shown in Fig. 1. This solar greenhouse dryer was designed and constructed at Faculty of Engineering, Mahasarakham University. The housing can be easily assembled and disassembled using polyvinyl chloride (PVC) pipes and fitting as a main structure as shown in Fig 2. The two cable slings were used to support the pipe for more rigid structure. The housing has a shape of a 45 degree triangular prism with a base of 7.3 m x 4 m and a height of 4.4 m. The 0.5 mm thick of transparent polyethylene sheet was used as cover and the 0.5 mm thick of dark polyethylene sheet was used as a solar absorber. The drying area was 18.24 m² with two layer racks.

C. Experimental Setup

Dried soybean was purchased from a local market in Kalasin province, north eastern region of Thailand. Then, the dried soybean was rewetted until the moisture content reached approximately 50% wet basis. Before drying, soybean was sampling to determine the moisture content. There were 3 experiments in this research. The samples with different capacities of 75, 100 and 120 kg were placed in the greenhouse dryer. Each day sample was weighted at 9.00 am and 6.00 pm to calculate the evaporated water. The sample was dried until the final moisture content lower than 10% wet basis. Average temperature inside greenhouse dryer was recorded every 1 hr.



Fig. 1 Photography of solar greenhouse dryer

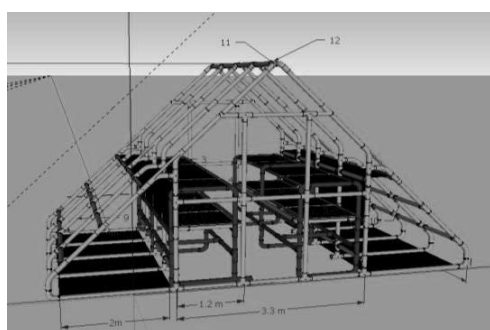


Fig. 2 PVC Structure of Solar Greenhouse Dryer

D. Dryer Performance Evaluation

Drying rate and the dryer efficiency is the mainly parameter for evaluation the dryer permanence. In this study, the overall performance and daily performance were calculated. Firstly, the weigh changed during drying were determined. The drying rate can be express as Eq. (1)

$$DR = (m_i - m_f) / t \quad (1)$$

Where DR is drying rate (kg/h)
M_i is initial mass of sample (kg)
M_f is final mass of sample (kg)

t is drying time (h)

The dryer efficiency is the ratio of the energy required to evaporate moisture from the product to the heat supplied by solar intensity to the dryer. Both parameters can be express by Eq. (2-4)

$$Q_e = (m_i - m_f) h_{fg} \quad (2)$$

$$E_s = 3600 G_t A t \quad (3)$$

$$\eta = (Q_e / E_s) 100 \quad (4)$$

where h_{fg} is the latent heat of evaporation (kJ/kg)
Q_e is the required to evaporate moisture (kJ)
G_t is the solar intensity (kW/m²)
A is the dryer area (m²)
E_s is the heat supplied by solar intensity (kJ)
η is the dryer efficiency (%)

III. RESULT AND DISCUSSION

The performance of the solar greenhouse dryer by different capacities of 75, 100 and 120 kg are expressed in Table 1, 2 and 3, respectively. You can see that in the first day of each batch, the moisture can be easily removed from the product to the environment due to the excess water of product especially the surface moisture content. This led to a high drying rate in the first day, resulting in high efficiency. The drying rate and efficiency decreased in the following day. This due to the soybean surface was dried and this step the moisture diffusion plays the role on moisture transfer from inside to the surface. The diffusion is decreased with the average moisture content of product.

The comparison of sample capacities is shown in Table 4. All capacities can reduce the moisture content lower than 10% within 3 days which is safe level for storage. The final moisture content was 4-6% wet basis which is similarly. The drying rate increased with the capacity which resulted in the high efficiency. The efficiency is in the range of 4.32-6.62%. This finding agree with the previous study of Aritesty and Wulandani [6] and Nayak and Tiwari [7]

TABLE I. THE PERFANANCE TESTING RESULT FOR CAPACITY OF 75 KG

Day dd/mm/yy	Initial mass (kg)	Initial moisture content (%wb.)	Final mass (kg)	Final moisture content (%wb.)	temperature inside dryer (°C)	Drying time (h)	Solar intensity (W/m ²)	Drying rate (kg/h)	Dryer Efficiency (%)
02/05/18	75.00	53.90	56.26	38.55	41.38	11	523.12	1.70	6.08
03/05/18	56.80	37.14	45.91	27.84	41.72	11	386.86	0.99	4.78
04/05/18	45.10	28.38	37.16	6.97	38.76	11	577.12	0.72	3.31



TABLE II. THE PERANANCE TESTING RESULT FOR CAPACITY OF 100 KG

Day dd/mm/yy	Initial mass (kg)	Initial moisture content (%wb.)	Final mass (kg)	Final moisture content (%wb.)	temperature inside dryer (°C)	Drying time (h)	Solar intensity (W/m ²)	Drying rate (kg/h)	Dryer Efficiency (%)
05/05/18	101.14	53.9	81.23	42.61	41.92	11	313.23	1.81	7.27
06/05/18	75.44	43.28	62.68	25.62	42.09	11	470.12	1.16	4.34
07/05/18	59.89	22.16	49.03	6.06	46.20	11	699.13	0.95	3.14

TABLE III. THE PERANANCE TESTING RESULT FOR CAPACITY OF 120 KG

Day dd/mm/yy	Initial mass (kg)	Initial moisture content (%wb.)	Final mass (kg)	Final moisture content (%wb.)	temperature inside dryer (°C)	Drying time (h)	Solar intensity (W/m ²)	Drying rate (kg/h)	Dryer Efficiency (%)
09/05/18	123.21	53.90	101.91	44.26	44.35	11	366.42	1.93	9.02
10/05/18	95.80	40.71	72.06	21.13	49.11	11	596.11	1.97	4.78
11/05/18	70.69	19.65	59.24	4.12	41.13	11	677.23	1.06	3.31

TABLE IV. THE OVERALL DRYING RATE AND OVERALL DRYER EFFICIENCY WITH DIFFERENT CAPACITY

Drying Period dd-dd/mm/yy	Initial mass (kg)	Initial moisture content (%wb.)	Final moisture content (%wb.)	Overall Drying time (h)	Overall Drying rate (kg/h)	Overall Dryer Efficiency (%)
02-05/05/18	75.00	53.9	6.97	33	1.15	4.32
06-08/05/18	101.14	53.9	6.06	33	1.57	5.96
09-11/05/18	123.21	53.9	4.12	33	1.93	6.62

The average temperature inside the dryer with capacities of 75, 100 and 125 kg is presented in Fig. 3, 4 and 5, respectively. The temperature is different each day depended on the weather of that day. Normally, the temperature inside dryer in the afternoon is high because the accumulated heat since in the morning. However, it was cloudy some days, resulted in low temperature as shown in Fig. 5

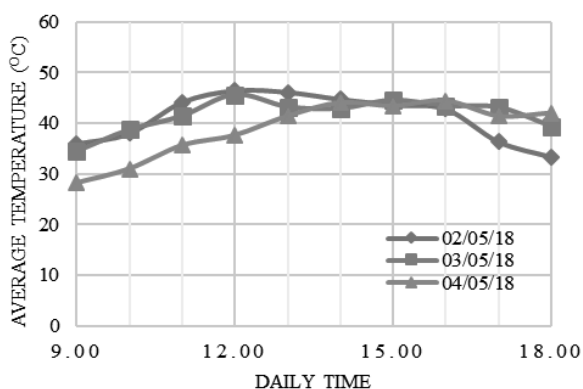


Fig. 3 The average temperature inside the solar greenhouse dryer with capacity of 75 kg

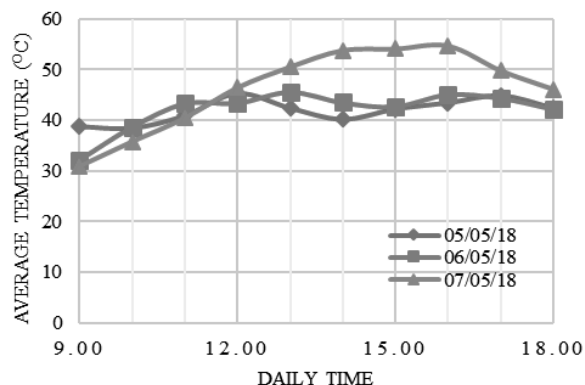


Fig. 4 The average temperature inside the solar greenhouse dryer with capacity of 100 kg

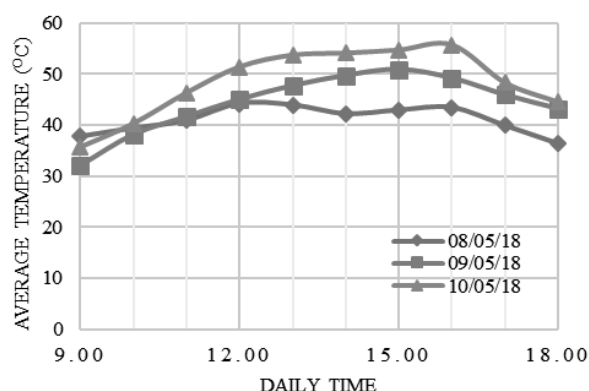


Fig 5. The average temperature inside the solar greenhouse dryer with capacity of 100 kg

IV. CONCLUSION

Experiments were conducted in a natural circulation solar greenhouse dryer in order to study the drying rate and dryer efficiency. It can be concluded that

- Soybean can be dried from the initial moisture content of 53.9% wet basis down to 10% wet basis within 3 days for safe storage.
- The maximum drying rate was 1.93 kg/h
- The average overall dryer efficiency of this greenhouse was 4.3-5.5%.

ACKNOWLEDGMENT

The authors would like to express their sincere thanks to Faculty of Engineering, Mahasarakham University for financial support and fund for conference participation. The authors would like to thank Mr. Siriwanon Laon and Mr. Rungwitaya Mankong for their hard working on collecting the experimental data.

REFERENCES

- [1] Kumar, A. and Shrivastava, V., 2017. Historical Trends and Recent Developments in Solar Greenhouse Dryer Operated Under Active Mode: A Review. *Indian Journal of Science and Technology*, 10(33). Pp.1-16
- [2] Prakash, O. and Kumar, A., 2014. Solar greenhouse drying: A review. *Renewable and Sustainable Energy Reviews*, 29, pp.905-910.
- [3] Rathore, N. S., and Panwar, N. L. 2010. Experimental studies on hemi cylindrical walk-in type solar tunnel dryer for grape drying. *Applied Energy*, 87(8), pp. 2764-2767.
- [4] Barnwal, P. and Tiwari, G.N., 2008. Grape drying by using hybrid photovoltaic-thermal (PV/T) greenhouse dryer: an experimental study. *Solar Energy*, 82(12), pp.1131-1144.
- [5] Tiwari, S., Tiwari, G.N. and Al-Helal, I.M., 2016. Performance analysis of photovoltaic-thermal (PVT) mixed mode greenhouse solar dryer. *Solar Energy*, 133, pp.421-428.
- [6] Aritesty, E. and Wulandani, D., 2014. Performance of the rack type-Greenhouse effect solar dryer for wild ginger (*Curcuma Xanthorrhiza* Roxb.) drying. *Energy Procedia*, 47, pp.94-100..
- [7] Nayak, S. and Tiwari, G.N., 2008. Energy and exergy analysis of photovoltaic/thermal integrated with a solar greenhouse. *Energy and Buildings*, 40(11), pp.2015-2021.



Effects of Drying Temperatures and Pretreatment Conditions on the Drying Kinetic and Color Quality of Japanese Pumpkin Powder obtained from Hot Air Drying

Suwit Paengkanya, Pathomphong Jumnongphan
Department of Sustainable Industrial Management
Engineering, Faculty of Engineering,
Rajamangala University of Technology Phra Nakhon,
Bangkok, Thailand
suwit.p@rmutp.ac.th, jumnongphan.j@rmutp.ac.th

Rarisara Impaprasert
Department of Microbiology, Faculty of Science,
King Mongkut's University of Technology Thonburi,
Bangkok, Thailand
rarisara.imp@kmutt.ac.th

Abstract—The product color is one of an important factor for consumer acceptance. It can be improved by blanching or steaming before drying process. Therefore, the objective of this research is to study the effects of drying temperature and pretreatment conditions on the drying kinetic and color quality of Japanese pumpkin powder obtained from hot air (HA) drying. The Japanese pumpkin slices were blanched or steamed for 30 and 60 seconds and then the sample dried by HA drying (60-90 °C). The drying kinetics and color quality of Japanese dried pumpkin were considered. The results showed that the moisture ratio of dried Japanese pumpkin slices obtained from HA90 drying was more changed than other cases and as a result in shorter drying time. However, the results showed that drying at 70 °C resulted in the best color qualities of the Japanese pumpkin powder. The lightness (L) and yellowness (+b) value were higher and the redness (+a) value was lower than those of other drying conditions. When considering the effect of pretreatment conditions on color quality of dried Japanese pumpkin, blanching process for 60 seconds shows the most effective condition for preserving the color quality of Japanese pumpkin powder. The sample had higher lightness and yellowness values but lower redness than the other pretreatment conditions. In conclusion, the most effective condition for producing Japanese pumpkin powder is a blanching the sample with hot water at a temperature of 90 °C for 60 seconds and dried by HA70 condition.

Keywords— color; japanese pumpkin powder; drying kinetic; pretreatment

I. INTRODUCTION

Japanese pumpkin is a nutritious plant food that has a range of fantastic health benefits. It is a good source of fiber, active proteins, essential amino acids, and minerals, such as phosphorus, calcium, and iron [1]. Moreover, it contains a large amount of beta-carotene which can improve some

functions of the immune system with regard to cancer prevention. Its seeds also help to prevent the prostate enlargement and gallstones. For this reason, Japanese pumpkin is desired for health food business and as a resulted to enlarge its production. However, the fresh-cut pumpkin process causes a lot of waste as well which increases the cost of disposal. Therefore, the utilization of pumpkin waste to produce pumpkin powder is an interesting choice. This product can be used more versatile, such as mixing with other flours for making bakery, pasta, snacks, soups and baby food products. However, the improper drying process results in low quality pumpkin powder, such as dark color. This is due to unsuitable drying conditions such as a high temperature or long drying time which greatly affects the qualities of dried Japanese pumpkin. Moreover, most of fruits and vegetables easily occur browning reaction which is the process of food turning brown due to the chemical reactions that take place within. Enzymatic browning is one of the most important reactions that takes place in most fruits and vegetables as well as in seafood [2]. However, the browning can be slowed down by preventing the enzyme from working properly. Blanching or steaming sample before drying can help to retard browning reaction and improve the product color. From a report of Raikham et al. [3] found that blanching can improve the product color. The color of puffed banana had golden yellow after pretreatment by blanching process. Therefore, the objective of this research is to investigate the effect of hot air temperatures and pretreatment conditions on kinetics of drying and color quality of Japanese pumpkin powder. In order to obtain the optimum condition for producing Japanese pumpkin powder using hot air drying. The drying kinetic and color quality of Japanese pumpkin powder were considered.



II. MATERIAL AND METHOD

A. Sample Preparation

Japanese pumpkin used in this research obtained from Royal Project Monngo, Chiang Mai province. The samples were peeled and removed seeds. Then they were cut into 1 millimeter thickness. The sliced samples were treated in four different methods: blanching at 90 °C for 30 and 60 seconds and steaming for 30 and 60 seconds. After which the treated samples were placed on the sieve to drain excess water. As a result of this process, the starch in the pumpkin becomes gelatinized [3]. The treated samples were placed on a drying tray with an initial weight of about 150 ± 1 g. Then, they were dried at temperature of 60, 70, 80 and 90 °C until the final moisture content of sample was less than 4% (d.b.). Finally, dried Japanese pumpkin is packed in an aluminum foil bag for further experiment. The initial and final moisture contents of the sliced samples can be determined by AOAC [4].

The moisture ratio (*MR*) of sliced Japanese pumpkin can calculate as followed by:

$$MR = \frac{M_t - M_e}{M_i - M_e} \quad (1)$$

When M_t is the moisture content of sample at any time, kg/kg (%d.b.); M_e is the equilibrium moisture content of sample, kg/kg (%d.b.) and M_i is the initial moisture content of sample, kg/kg (%d.b.).

B. Drying Experiment

The dryer used in this experiment is a hot air oven (MEMMERT, memmert-UNE / UFE, Germany) as shown in Fig. 1. It has a capacity of 53 liters with 4 trays. A hot air temperature was set in the range of 40-250 °C with accuracy of ± 0.5 °C. An air ventilation in the drying chamber and control is LED (Digital Display).



Fig. 1. Hot air oven.

C. Experimental Method

Drying of Japanese pumpkin begins with the warming up the dryer until reached the desired temperature. Then the Japanese pumpkin slices were placed on the tray and dried at temperatures of 60, 70, 80 and 90 °C until the final moisture content of samples were less than 4.0% (d.b.). During drying, samples were weighed every 30 minutes with digital weighing scales (Sartorius, model CP3202S, Germany) with accuracy of ± 0.01 grams. Each experiment was repeated three times.

D. Color Measurement

The dried Japanese pumpkin slices were ground and sifted to a sieve size of 60 mesh before a color measurement. After that they were measured a color using a colorimeter (HunterLab, ColorFlex, UK) with CIE measurement system (L, a, and b). The L value is the lightness of the object (0 is black, 100 is white) a value is red/green (+red, -green) and b value is yellow/blue (+yellow, -blue). Before each measurement, the colorimeter was calibrated with standard color black and white plates. The measurement was repeated three times in each experimental condition.

E. Statistical Analysis

The data obtained from the color quality of Japanese pumpkin powder was analyzed statistically with Analysis of variance (ANOVA) and compared to mean difference using Duncan's New Multiple Range test using SPSS program. Experiments were conducted to find the mean difference for 95% confidence intervals.

III. RESULT AND DISCUSSION

A. Drying Kinetic of Japanese Pumpkin Slices

Japanese pumpkin slices with a thickness of 1 mm and an initial moisture content of 427.8-571.6% were dried by a hot air (HA) drying until the final moisture content of sample was lower than 4% dry basis (d.b.). Drying kinetic of Japanese pumpkin slices using HA drying at various drying conditions are shown in Fig. 2.

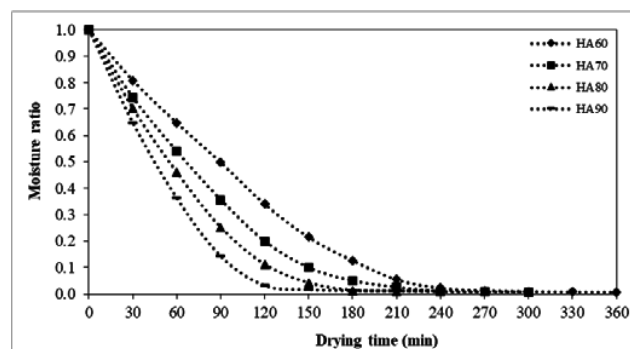


Fig. 2. Changes in moisture ratio of Japanese pumpkin slices during drying at different drying temperatures in case of untreated sample [HA is a hot air drying and 60 is a drying temperature].



It was found that all cases of Japanese pumpkin dried by HA at a temperature of 90 °C provided changing the moisture ratio higher than that of other conditions. As a result, the shortest drying time was 210 minutes due to the highest drying temperature. Drying at high temperature results in rapid diffusion of moisture into the surface. Thus, the drying time was shorter than the drying of Japanese pumpkin slices at lower temperatures [5, 6]. When considering the effect of pretreatment conditions on the samples prior to drying, it was found that all cases of pretreatment conditions did not affect to the drying kinetics and drying time of the samples.

B. Color of Dried Japanese Pumpkin

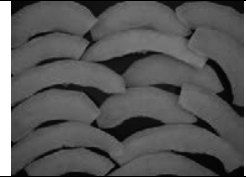


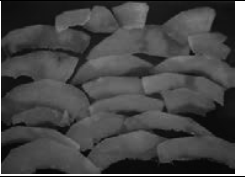
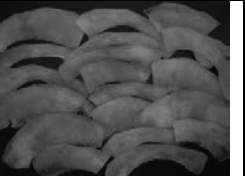
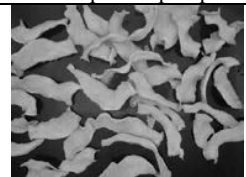
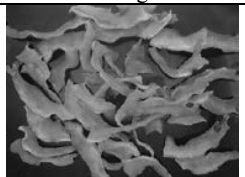
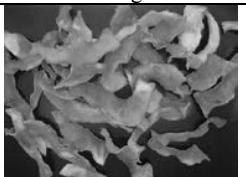
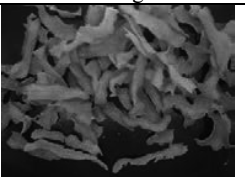
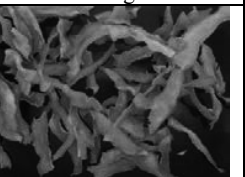

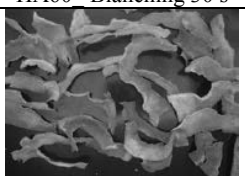
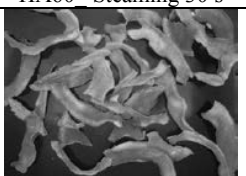
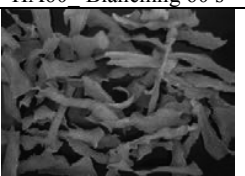
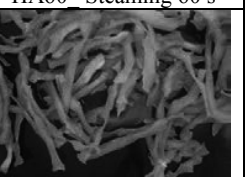
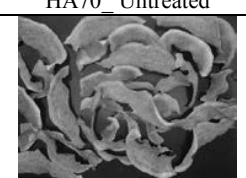
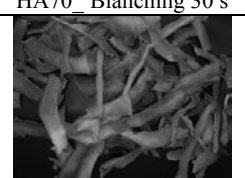
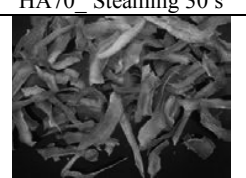
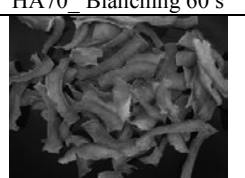
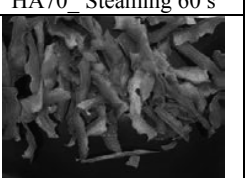
The characteristics of dried Japanese pumpkin slices at various pretreatment conditions and drying temperatures are shown in Table 1. Whereas the color values of dried Japanese pumpkin powder at various drying conditions are shown in Fig. 3. It was found that all cases of untreated Japanese pumpkin provided higher values of the lightness (L) and yellowness (+b), but lower in the redness (+a) value than that of pretreated sample. The higher lightness value is due to the starch powder coating on the surface of the dried pumpkin slices. Thus, the blanched sample had decreased in lightness and increased in yellowness value due to gelatinization of starch [3]. All cases of dried Japanese pumpkin obtained from blanching with hot water for 60 seconds gave higher value of lightness and

yellowness, but redness value was lower than that other treated cases. This is because the enzyme browning reaction can be inhibited by heat. Therefore, blanching for 60 seconds is more effective than blanching at 30 seconds. While compared to the steaming method, it was found that the color of blanched Japanese pumpkin powder had higher lightness and yellowness values, but lower redness value than steamed sample.

However, the result indicated that blanching is more effective for inhibiting of browning reaction than steaming at the same period of time. Since the lower heat transfer coefficient in blanching process, the brown reaction was occurred slower than in steaming process at the same period of time.

When considering the effect of drying temperature on the color quality of Japanese pumpkin powder, it was found that all cases of a treated sample dried by HA drying at a temperature of 70 °C, had higher lightness and yellowness values, but the redness value was lower than that of other cases, which was subjected to hot air drying at different experimental conditions. Due to HA drying at temperatures higher than 70 °C, the material was exposed to higher drying temperatures, thereby accelerating the non-browning reaction [7]. At drying temperature of 60 °C drying material exposed to drying temperature for a long time (360 minutes), resulted in an increase in non-enzymatic browning reaction. As a result, products are dark color.

Table 1. Characteristics of fresh and dried Japanese pumpkin slices at different pretreatment and drying conditions

				
Fresh Japanese pumpkin	Blanching 30 s	Steaming 30 s	Blanching 60 s	Steaming 60 s
				
HA60 Untreated	HA60 Blanching 30 s	HA60 Steaming 30 s	HA60 Blanching 60 s	HA60 Steaming 60 s
				
HA70 Untreated	HA70 Blanching 30 s	HA70 Steaming 30 s	HA70 Blanching 60 s	HA70 Steaming 60 s
				
HA80 Untreated	HA80 Blanching 30 s	HA80 Steaming 30 s	HA80 Blanching 60 s	HA80 Steaming 60 s

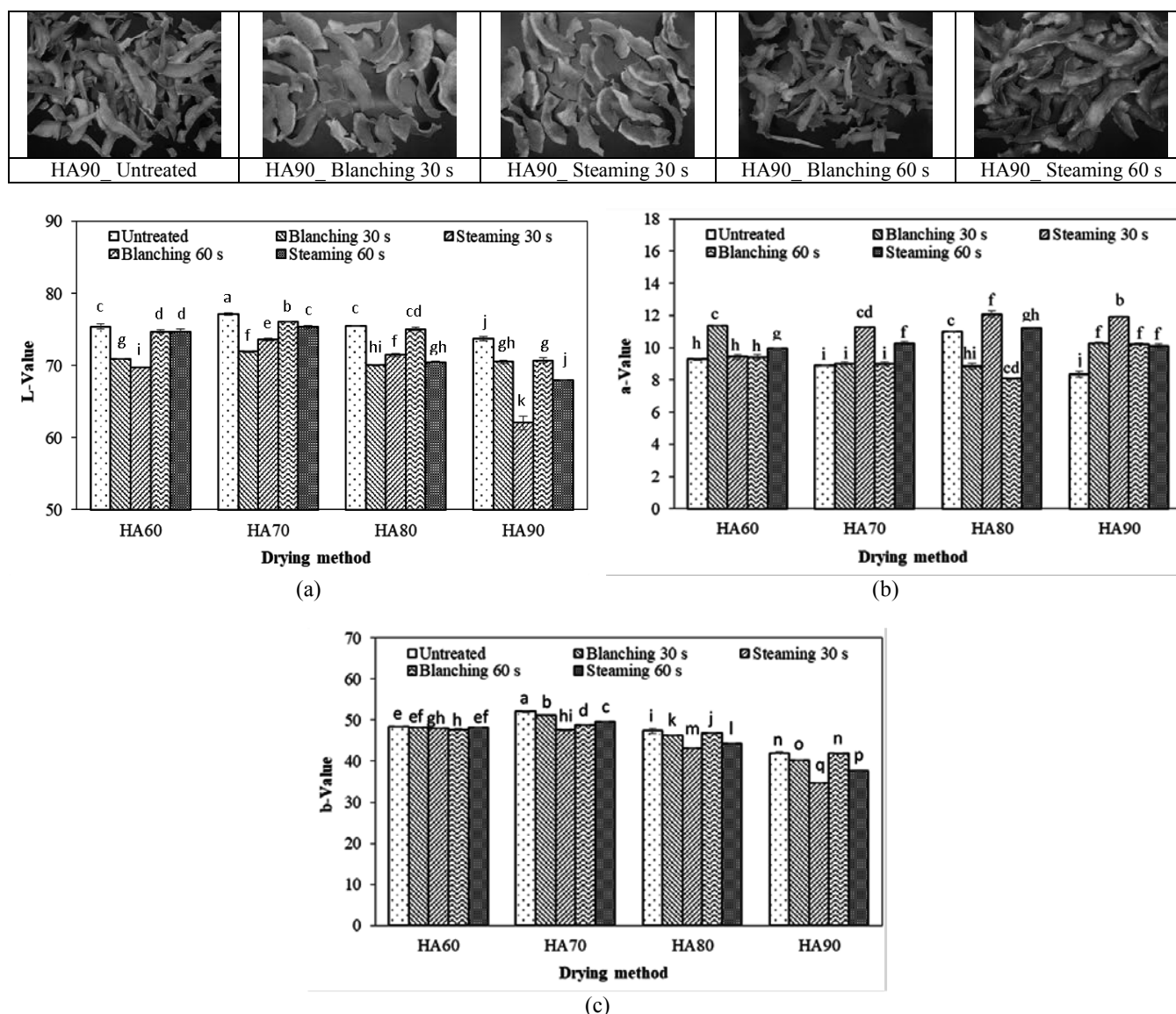


Fig. 3. Color values of Japanese pumpkin powder at different drying and pretreatment conditions; (a) L-value, (b) a-value and (c) b-value.

CONCLUSION

The effects of drying temperature and pretreatment conditions on the drying kinetic and color quality of Japanese dried pumpkin powder obtained from hot air (HA) drying were evaluated. It was found that all cases of Japanese pumpkin drying using HA drying at a temperature of 90 °C provided changing in higher moisture ratio than other drying conditions resulting to a shortest drying time. However, the pretreatment of sample before drying was not different in the drying kinetic. While all cases of treated sample dried by HA at a temperature of 70 °C provided higher values of lightness and yellowness, the redness value is lower than other conditions. The sample was treated by blanching process for 60 s gave higher lightness

and yellowness values, but redness value is lower than the other pretreatment conditions. Therefore, the recommended condition for producing Japanese pumpkin powder is a blanching for 60 s and dried by HA at a temperature of 70 °C.

ACKNOWLEDGMENT

The authors would like to acknowledge the Innovation Hub-Agriculture & Food Research Fund for the creation of a country's economic innovation base 4.0, Contract No. 083/2560 for financial support and Rajamangala University of Technology Phra Nakhon and King Mongkut's University of Technology Thonburi for the research facilities.



REFERENCES

- [1] A. B. EI-Kalek, EI-Aziz Abd and H.H. Abd. Antimicrobial proteins and oil seeds from pumpkin (*Cucurbita moschata*). Nature and Science, Retrieved from <http://www.sciencepub.net>, pp. 1-15, 2011.
- [2] D. Holderbaum, "Enzymatic Browning, Polyphenol Oxidase Activity, and Polyphenols in Four Apple Cultivars: Dynamics during Fruit Development" Hortscience, Vol. 45(8), pp.1150–1154, 2010.
- [3] C. Raikham, S. Prachayawarakorn, S. Soponronnarit, and A. Nathakarakule, "Influences of pretreatments and drying process including fluidized bed puffing on quality attributes and microstructural changes of banana slices", *Drying Technology*, Vol. 33, pp.915-925, 2015.
- [4] Association of Official Analytical Chemists Official Methods of *Analysis of the AOAC International*, 16th ed., Gaithersburg, MD., 1995.
- [5] S. Tabtiang, S. Prachayawarakorn and S. Soponronnarit, "Effects of osmotic treatment and superheated steam puffing temperature on drying characteristics and texture properties of banana slices", *Drying Technology*, Vol. 104, pp. 114-122, 2012.
- [6] R. Thuwapanichayanan, S. Prachayawarakorn, J. Kunwisawa, and S. Soponronnarit, "Determination of effective moisture diffusivity and assessment of quality attributes of banana slices during drying", *LWT-Food Science and Technology*, Vol. 44, pp. 1502-1510, 2011.
- [7] S. Paengkanya, S. Soponronnarit, and A. Nathakarakule, "Application of microwave for drying of durian chips", *Food and Bioproducts Processing*, Vol. 96, pp.1-11, 2015.



Thermal Efficiency Behavior of Hot Air Production from Fluidized Bed Kiln by Waste Biomass

Phairoach Chunkaew

Department of Mechanical Engineering
Rajamangala University of Technology LannaTak
Tak, Thailand
phairoac9@gmail.com

Abstract—The aim of this study is to investigate thermal efficiency behavior of hot air production from fluidized bed kiln by waste biomass. A hot air production had the main parts of a fluidized bed kiln, an air chamber, a biomass fuel feeder set, a blower motor of fluidized bed kiln, an air blower, fire burn pocket, cyclone and a control box. Hot air temperature control was to design by control waste biomass feeding and air flow of fluidized bed kiln. Experiments were performed by waste biomass types of rice husk, sawdust and minor leaf. They were test under conditions 170 °C of air temperature with flow rate of 0.0715 kg s⁻¹ during 180 minutes. It was found that average thermal efficiencies of rice husk, sawdust and minor leaf were 25.82±11.70, 25.8±11.70 and 28.03 ±13.98 %, respectively.

Keywords—waste biomass; hot air production; rice husk; sawdust; minor leaf

I. INTRODUCTION

Fluidized beds are widely used for drying particulate or granular solids in agricultural and food industries. They promote excellent mixing and have high effective heat and mass transfer coefficients. The fluidized bed technique is used in many applications in chemical process, drying and combustion. Technology fluidized kiln is applied in combustion process by using small biomass fuel. It can burn the biomass fuel which is high moisture content. Hot air production for drying process from fuel wood can reduce the expenses of energy because the fuel wood has no payment about raw material by wood at countryside. The high temperature of hot air needs to use for more applications in drying process and the technology fluidized kiln can apply to generate heat.

Waste biomass in Thailand has more from many productions of agriculture such as rice husk, sawdust and leaf. All waste biomass type can apply to fuel wood for fluidized kiln. In drying process, the main source which is used the most energy comes from the air temperature heating rate. Chunkaew *et al.* (2017)[1] modified hot air dryer using waste heat from a 200 liter kiln by using wood with drying bananas. This research, the fuel wood is big size and must use fixed bed kiln. Next, Chunkaew *et al.* (2017) [2] developed a hot air dryer using waste heat from a 200 liter kiln for drying bananas, and to investigate its drying performance. The dryer was developed by designing a drying chamber on the top of a 200 liter kiln to reduce heat lost in the structure and an exhaust

gas heat exchanger was developed using groups of copper tubes for increasing then heat transferred to the air. The new concept of this research, the all waste biomass types of small size can burn in a fluidized bed kiln. The heat in fluidized bed kiln is transferred to outside of kiln wall and an air around outside of kiln wall is increased. The fluidized bed kiln can control waste biomass feeder to be appropriate with using hot air temperature.

The objective of this research is to modify a fluidized bed kiln in order to use waste biomass types of rice husk, sawdust and minor leaf for the hot air production. Thermal efficiency is to calculate and to present in this paper.

II. MATERIALS AND METHODS

A. Hot air production from fluidized bed kiln with waste biomass

1. Fluidized bed kiln with waste biomass

Figure 1 shows details of fluidized bed kiln. A feeder set has a container with dimensions of 0.3 m x 0.295 m x 0.55 m. It has spiral gear with 90 Watt AC motor for feeding the waste biomass from the container to the fluidized bed kiln. The feeder set consists of temperature controller, inverter with control program and AC motor. The inverter receives commands from temperature controller. Motor operates at high speed with high frequency and at low speed with low frequency. This behavior of this shows the feeding rate which various following the speed of the motor. Parameters at inverter must key to appropriate with each types of waste biomass. Blower of fluidized bed kiln is driven by AC motor with 0.5 horsepower which is controlled speed by inverter related to fluidized velocity of each types of waste biomass. The inverter receives command from the temperature controller. For fluidized bed kiln is a vertical kiln which has 0.23 m in diameter and 2 m of height. The fluidized bed kiln make from steel. The bottom of fluidized bed kiln installs a distributor and joins with tube set and blower.

2. Air chamber is designed in a shape as same as fluidized bed kiln and it has 0.334 m in outlet diameter. The heat from burning biomass of rice husk in fluidized bed kiln is transferred from inside to outside of the kiln. Then, the air in chamber will be increased temperature and flows up from the



hot air chamber. The outside of air chamber does not install insulation. Air flow system, at the top of hot air chamber is installed blower and the bottom of hot air chamber is installed a hot air tube for other load of application.

3. Cyclone, at the top of fluidized bed kiln is connected with exhaust tube and cyclone. Ash occurs while burning the waste biomass in fluidized bed kiln. It has small weight and flows up into the cyclone. Then, the ash is separated at the cyclone and the smoke will be flowed out to the surrounding.

4. Control box consists of two inverters, temperature controller, kWh meter and safety switch.

B. Materials

Rice husk, sawdust and minor leaf are waste biomass and are used to test thermal efficiency behavior of hot air production from fluidized bed kiln. The rice husk is a fuel wood which is an agricultural waste from head rice yield production at Tak Province, Thailand. Sawdust is the by-product of wood. The sawdust is waste biomass from sawmill. Leafs of Indian almond are waste biomass in the area of Rajamangala University of Technology Lanna Tak (Thailand). They are milled from big size to small size before to test and are defined name of minor leaf. High heating values of rice husk, sawdust and minor leaf were 13.79, 18.83 and 15.9 MJ kg⁻¹, respectively.

They were tested by bomb calorimeter in laboratory at a department of mechanical engineering, Rajamangala University of Technology LannaTak Tak, Thailand.

Muhammad et al. (2013) [3] found that the rice husk has heating value of 16.10 MJ kg⁻¹. The heat value of wood with 20% moisture is about 15 MJ/kg because some heat is consumed as heat of evaporation and heat of wetting during the combustion process.

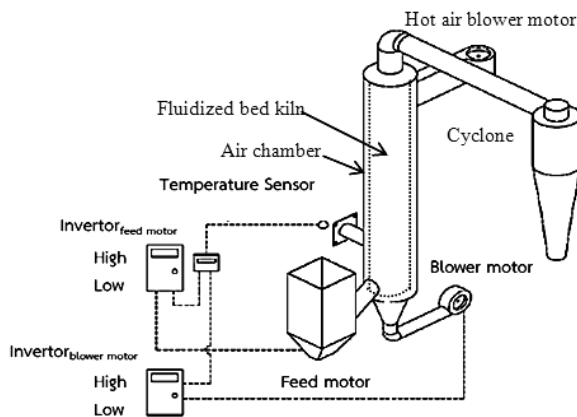


Fig.1 Apparatus of hot air production from fluidized bed kiln with waste biomass

C. Experiment set up

Experimental procedure is performed under waste biomass types of rice husk, sawdust and minor leaf. It is tested the hot air production from fluidized bed kiln at a constant

temperature of 170 °C [4] with mass flow rate of air 0.0715 kg s⁻¹ in time period of 180 minutes.

The mass flow rate is calculated by product of (cross section area) (an air velocity) (density of air). Inlet air temperature is between 27-29 °C. All experiments are tested in three times. Three meters are used to record energy consumptions of fluidized bed kiln blower, feed motor and air blower. The weight of rice husk is recorded by used capacity and used to calculate energy consumption. A temperature recorder (BTM-4208SD) is used to measure several temperatures in the hot air production from fluidized bed kiln with biomass of rice husk such as kiln outside surface temperature and kiln temperature. An ambient temperature and relative humidity of ambient are recorded in order to determine humidity ratio. All data are recorded every 30 minutes.

C. Analysis methods

Thermal efficiency of hot air production from fluidized bed kiln (η_{th}) can be calculated as shown below:

$$\eta_{th} = \frac{\dot{Q}_{out}}{\dot{Q}_{in}} \quad (1)$$

when

\dot{Q}_{out} = heat transfer to the air (kW)

\dot{Q}_{in} = total power input (kW)

$$\dot{Q}_{in} = \left[\frac{m_{biomass} HHV}{t} \right] + 2.6(P_{feed\ motor} + P_{blower\ motor} + P_{hot\ air\ blower\ motor}) \quad (2)$$

$m_{biomass}$ = mass of biomass (kg)

t = used time (s)

HHV = high heating value of waste biomass

2.6 = factor for changing to primary energy [5]

$P_{feed\ motor}$ = power of feed motor (kW)

$P_{blower\ motor}$ = power of blower motor (kW)

$P_{hot\ air\ blower\ motor}$ = power of hot air blower motor (kW).

The dry air and vapor are fluid flow at the air chamber. The heating rate can be calculated as shown below:

$$\dot{Q}_{out} = \dot{m}_a [(C_{a2} T_2 + W C_v T_2) - (C_{a1} T_1 + W C_v T_1)] \quad (3)$$

when

\dot{Q}_{out} = heat transfer to the air (kW)

\dot{m}_a = mass flow rate of dry air (kg s⁻¹)

C_{a1} = specific heat capacity of dry air of inlet heat exchanger (kJ kg⁻¹ °C⁻¹)

C_{a2} = specific heat capacity of dry air of outlet heat exchanger (kJ kg⁻¹ °C⁻¹)



W = humidity ratio ($\text{kg}_{\text{water}} \text{kg}_{\text{dry air}}^{-1}$)

C_v = specific heat capacity of vapor ($1.88 \text{ kJ kg}^{-1} \text{ } ^\circ\text{C}^{-1}$ [6])

T_1 = temperature of inlet of dry air at heat exchanger ($^\circ\text{C}$)

T_2 = temperature of outlet of dry air at heat exchanger ($^\circ\text{C}$).

III. RESULTS AND DISCUSSIONS

A. Behaviors of kiln outside surface temperature, kiln temperature and amount of waste biomass

1. Rice husk

At condition of 170°C with air flow rate of 0.0715 kg/s from 0 to 180 minutes shows that after 30 minutes has passed, an average kiln outside surface temperature is $277.23 \pm 8.33^\circ\text{C}$, an average kiln temperature is $551.27 \pm 31.45^\circ\text{C}$ and a biomass amount is $25 \pm 11.85 \text{ kg}$ as shown in Table 1. Figure 2, at the period of 30 minutes has more rice husk because fluidized bed kiln is being to burn and some heat is absorbed by structure of the fluidized bed kiln. After time of 30 minutes has passed, the rice husk is decreased because the system of the fluidized bed kiln is beginning to stabilize.

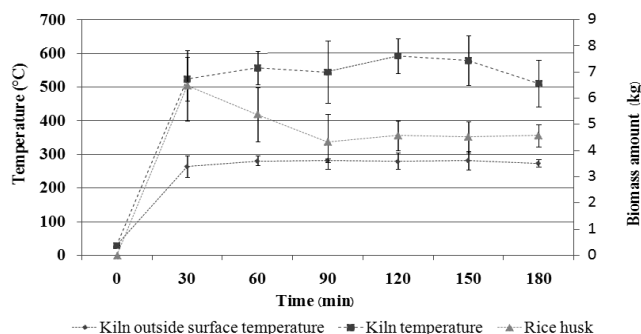


Fig.2. Behaviors of kiln outside surface temperature, kiln temperature and amount of rice husk

2. Sawdust

At condition of 170°C with air flow rate of 0.0715 kg/s from 0 to 180 minutes shows that after time of 30 minutes has passed, an average kiln outside surface temperature is $259.94 \pm 8.16^\circ\text{C}$, an average kiln temperature is $498.11 \pm 53.23^\circ\text{C}$ and a biomass amount is $26 \pm 11.7 \text{ kg}$ as shown in Table 1. Figure 3, at the period of 30 minutes has more sawdust same the rice husk because fluidized bed kiln is being to burn and some heat is absorbed by structure of the fluidized bed kiln. After time of 30 minutes has passed, the sawdust is decreased because the system of the fluidized bed kiln is beginning to stabilize. This behavior result of sawdust is same with behavior result of rice husk.

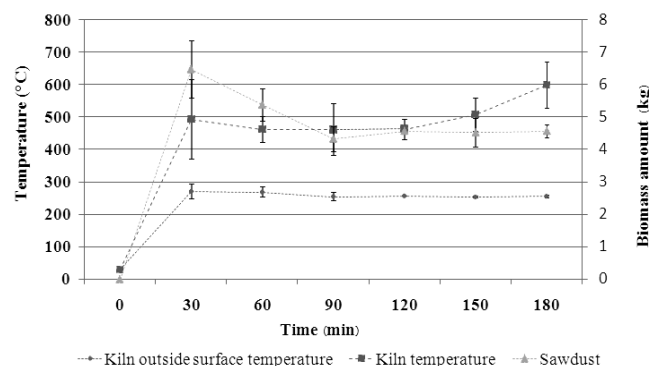


Fig.3. Behaviors of kiln outside surface temperature, kiln temperature and amount of sawdust

3. Minor leaf

At condition of 170°C with air flow rate of 0.0715 kg/s from 0 to 180 minutes shows that after time of 30 minutes has passed, an average kiln outside surface temperature is $270.33 \pm 8.22^\circ\text{C}$, an average kiln temperature is $686.95 \pm 65.56^\circ\text{C}$ and a biomass amount is $28 \pm 13.98 \text{ kg}$ as shown in Table 1. Figure 4, at the period of 30 minutes has more minor leaf same the rice husk and sawdust because fluidized bed kiln is being to burn and some heat is absorbed by structure of the fluidized bed kiln. After time of 30 minutes has passed, the sawdust is decreased because the system of the fluidized bed kiln is beginning to stabilize. This behavior result of minor leaf is same with behavior results of rice husk and sawdust.

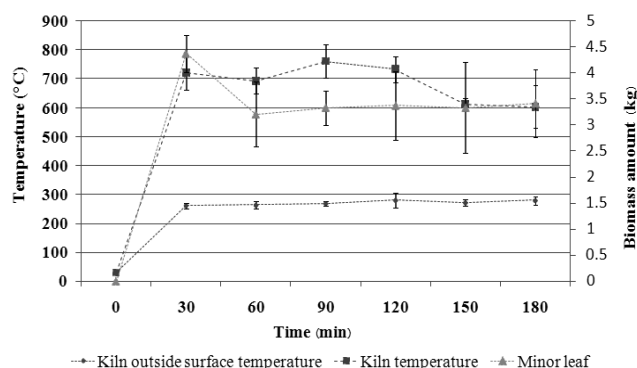


Fig.4. Behaviors of kiln outside surface temperature, kiln temperature and amount of minor leaf

A. Behavior of thermal efficiency

From equation 2, a power input consists of a power of feed motor, a power of blower motor, power of hot air blower motor and heat rate from the rice husk. It was found that behavior of power input of rice husk, sawdust and minor leaf had same behavior of feeding rice husk. The behavior of thermal efficiency is increased during the period of time from 0 to 90 minutes after that the thermal efficiency will be stable as shown in figure 5. The average thermal efficiencies of rice



husk, sawdust and minor leaf were 25.82 ± 11.70 , 25.8 ± 11.70 and 28.03 ± 13.98 %, respectively as shown in Table 1.

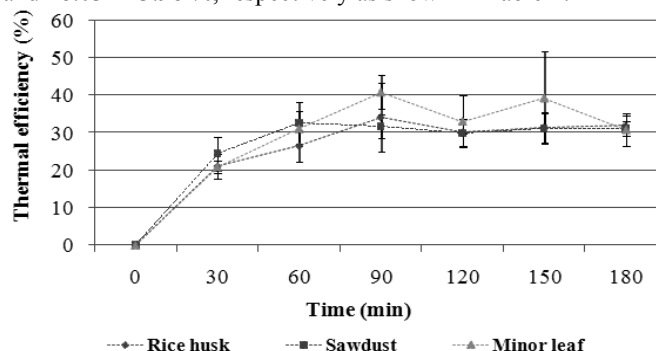


Fig.5. Behavior of thermal efficiency of three types of waste biomass versus time at temperature of 170 °C with mass flow rate of air 0.0715 kg s⁻¹

Table I shows the calculation values of experimental results for hot air production at 170°C with air flow rate of 0.0715 kg s⁻¹ from 0-180 minutes. Amount of waste biomass and ash, rice husk was used more than minor leaf and the minor leaf was used more than sawdust because the rice husk, minor leaf and sawdust had high heating values of 13.79, 15.9 and 18.83 MJ kg⁻¹, respectively. Thermal efficiency of minor leaf had the maximum in this study because heat of burning minor leaf in the fluidized bed kiln could transfer to the air chamber more than sawdust and rice husk. This result was conformed to the result of exhaust temperature. The exhaust temperature of minor leaf was lower than sawdust and rice husk. This behavior, burning the minor leaf had drift in fluidized bed kiln to long time.

Table I The calculation values of experimental results for hot air production at 170°C with air flow rate of 0.0715 kg s⁻¹ from 0-180 minutes.

Description	Rice husk	Sawdust	Minor leaf
Waste biomass (kg)	25±11.85	26±11.7	28±13.98
Ash (kg)	5.83±1.39	0.72±0.03	0.733±0.028
Ambient temperature (°C)	28.12±0.93	28.24±0.29	28.56±0.28
Relative humidity of ambient (%)	94.26±11.24	77.67±10.65	93.3±2.26
Hot air temperature (°C)	171.01±3.09	173.81±1.66	172.12±0.91
Kiln outside surface temperature (°C)	277.23±8.33	259.94±8.16	270.33±8.22
Kiln temperature (°C)	551.27±31.45	498.11±53.23	686.95±65.56
Exhaust temperature (°C)	412.36±42.97	438.82±33.88	379.88±33.61
Heat transfer to the air (kW)	10.8±0.32	10.96±0.19	10.85±0.18
Total input heating rate (kW)	38.51±6.312	37.12±4.52	35.44±8.82
Thermal efficiency (%)	25.03±11.70	25.82±11.7	28.03±13.98

IV. CONCLUSIONS

The hot air production from fluidized bed kiln with biomass of rice husk introduce a new concept of heat in the fluidized bed kiln which transfer from inside kiln to outside kiln. The air in chamber beside an outside kiln is flowed up. Then, the air blower produces the air flow which has

temperature at the set point. The temperature controller is used to control the burning of waste biomass types of rice husk, sawdust and minor leaf in the fluidized bed kiln by using two inverters to control the feeder motor and blower motor of fluidized bed kiln. Experiments were performed by three waste biomass types and were test under conditions 170 °C of air temperature with flow rate of 0.0715 kg s⁻¹ during 180 minutes. It was found that thermal efficiencies of rice husk, sawdust and minor leaf were 25.82 ± 11.70 , 25.8 ± 11.70 and 28.03 ± 13.98 %, respectively. The minor leaf had the maximum efficiency in this study.

ACKNOWLEDGMENT

The authors express their sincere appreciation to Rajamangala University of Technology Lanna (Thailand) for financially supporting this study.

REFERENCES

- [1] P. Chunkaew, A. Khadwilard and Ch.Thawonngamyingsakul, "Drying bananas with a modified hot air dryer using waste heat from a 200 liter kiln," RMUTI journal, vol.10, no.3, 2017, pp. 1-12.
- [2] P. Chunkaew, A. Tavata, A. Khadwilard and Y. Sriudom, "Bananas dryer performance with a developed hot air dryer using waste heat from charcoal production process," The 9th International Conference on Sciences, Technology and Innovation for Sustainable Well-Being (STISWB 2017), Kunming University of Sciences and Technology, China, 26-28 June 2017, pp. 18-21.
- [3] S. Muhammad, A. Bakar and J.O. Titiloye, "Catalytic pyrolysis of rice husk for biooil production," J. Anal. Appl. Pyrol. 103, 2013, pp. 362–368.
- [4] P. Chunkaew, A. Achariyaviriya, S. Achariyaviriya, C. M. James and S. Sriwattana, "Operating parameters effects on drying kinetics and salted sunflower seed quality utilizing a fluidized bed," International Journal of Advanced Research in Engineering & Technology (IJARET), 4 (6), 2013, pp. 256-268.
- [5] A. Achariyaviriya, "Simulation and optimization of the drying strategy for longan drying," Doctor of Engineering Energy Technology Program School of Energy and Materials. King Mongkut's University of Technology Thonburi, 2001.
- [6] B.K. Bala, "Drying and storage of cereal grains," Science Publisher. Inc. New Hampshire, 1997.



Investigation of Fuel Delivery of Common Rail Injector using a Volumetric Injection Meter

Narin Srithikarn and Nimit Ratsamee

Department of Automotive
Chiangmai Technical College
Chiangmai, Thailand
narin.stg@gmail.com

Wasin Wongkum
Maker Asia Co., Ltd.
Chiangmai, Thailand

Ronnachart Munsin, Nawee Nuntapap and

Tarapong Karnjanaparichat
Rajamangala University of Technology Lanna
Chiangmai, Thailand

Nattaporn Chaiyat
School of Renewable Energy
Maejo University
Chiang Mai, Thailand

Abstract—This work investigates fuel delivery of common rail injector with different injection strategies. Injection delivery was investigated by an in-house fuel injection measurement system, which was calibrated by comparing with the commercial device. For single and double injection strategy, the experiments were operated by injection pressure and duration in the range of 250-1400 bar and 250-1400 microseconds, respectively, with different the first injection duration, second injection duration and dwell times. The typical diesel selling in Thailand's market was used for experiments. The results indicate that increasing injection pressure and injection duration increase fuel injection and return quantities for single injection strategy. At injection duration shorter than 800 microseconds, Fuel injection and returning quantities are dominated by injection duration related to the needle opening. For double injection, the first injection duration and second injection duration show the similar trend of the injected quantity and return as single injection at given conditions. Short dwell time gives higher injected fuel quantity due to incompletely closing nozzle holes.

Keywords—fuel delivery, common rail; volumetric injection meter; injector

I. INTRODUCTION

Compression ignition engines or diesel engines have played an important role in developing both social and economic. However, the operating diesel engines have the environmental impact of particulate matter and emissions, leading to serious concerns and the tightening legislation launched to limit the pollutant emission.

The deposit of fuel injector are an important factor of low power, low fuel economy performance and pollutant emissions [1, 2]. Typically, diesel injectors can precisely deliver fuel injection quantity and spray quality, which is enhanced by some technics, e.g. multiple injections, laser drilling, flash

boiling and ultrahigh pressure injection, resulting better fuel atomization, mixing and combustion. Nevertheless, deposits can be occurred around the nozzle tip due to extremely surrounding condition in the combustion chamber, i.e. high temperature and pressure [3]. The deposits result in fuel flow rate and deterioration of spray, including spray angle and penetration [4-7]. Lindgren et.al. [8] and Wang et. al. [9] showed that the spray penetration length could be increased by injector deposits. The piston and cylinder walls could be impinged by more fuel that is the main source of emissions. The relationship between injector deposits, diffusion flame and particulate emissions was shown by Kazour et al [10] and Berndorfer et al [11]. They concluded that diffusion flame occurs due to the remained fuel on the injector deposits, resulting to increasing particulate matter. This is the difficulty of reduction of pollutant emission to meet the stringent regulation. Although these effects can be fixed by compensation of fuel flow, the overall spray deterioration is difficult to remedy.

Nowadays, there are many ways to diagnose injection flow including injection quantity, injection rate and injection delay, e.g. Zeuch's method [12], Bosch measuring method [13] and deformation method [14]. For Zeuch's method, the test fuel will be injected into a constant volume chamber filled with test fuel at a certain pressure. Then injection flow rate can be calculated from conservation of mass with the increased chamber pressure. Bosch measuring method has the different concept. It finds an injection rate by measuring the pressure waves that is generated by the injector. Test fuel is injected into a tube contained the same test fuel. Then injection rate can be obtained by pressure-velocity equation and continuity equation. For the deformation method, it is expressed by the deformation of membrane occurring due to the collision of the pressure wave against the membrane. It is based on the calculation of



the fuel velocity by the pressure-velocity equation and continuity equation, but this method have separated the membrane for each hole of the nozzle. All the measuring methods give accurate results of the injection rate in single-hole and multi-hole nozzles. However, in practical uses, these methods are still sensitive, complicated and high cost.

Another way to check fuel delivery with the simple and low cost operation is the volume measurement by injecting fuel into a volume metering devices. This measurement is typically used for commercial purpose, but systematic testing data and analysis are available. In addition, the results including fuel injection and return quantity in case of both single and multiple injections are also limited. Therefore, this work aims to investigate fuel delivery of common rail injector with different injection strategies using the volume measurement by injecting fuel into a volume metering devices.

II. METHODOLOGY

The various test points cover leak test, full load test, pre-injection test, part load test (or emission test) and idle test. Measurement points of the common rail injector depend on the injector type and age of the injector. Each test could be used to confirm the injector ability in different operation [15] as shown in Table I. These tests cover wide range conditions of injection pressure and injection durations of 250-1800 bar and 150-1800 μ s.

TABLE I. INJECTION TESTING

Test Points	To confirm
Leak	<ul style="list-style-type: none"> the nozzle spring can keep the nozzle closed the needle is not stuck in the open position no debris is trapped between the nozzle needle and nozzle seat there are no external leaks there are no cracks in the injector body the injector nozzle does not leak internal leakage is not excessive
Full load	<ul style="list-style-type: none"> Maximum fuel delivery of the injector <ul style="list-style-type: none"> Low Power Over fueling Excessive return quantity <ul style="list-style-type: none"> Low rail pressure Hard start
Pre-injection	<ul style="list-style-type: none"> Components are able to react to the minimum actuation time <ul style="list-style-type: none"> White smoke Misfire Engine noise Aftertreatment issues
Part load	<ul style="list-style-type: none"> Specific points of the performance map as agreed upon by the OEM. <ul style="list-style-type: none"> Mid-range performance Misfires Smoke
Idle	<ul style="list-style-type: none"> Specific points of the performance map as agreed upon by the OEM <ul style="list-style-type: none"> Mid-range performance Misfires Smoke

III. EXPERIMENT

A. Experiment Setup

This work have set all new apparatus by using the OEM parts. A schematic diagram of the in-house fuel injection measurement system is shown in Fig. 1. It consists of a common rail, high pressure pump, motor, controller, oscilloscope and measuring pipettes. High pressure pump is driven by motor to build up fuel pressure and deliver to common rail. Then controller energizes injector with the setting conditions, e.g. injection pressure, injection duration and dwell time. Injection and return fuel quantity can be measured by using measuring pipettes. Range of injection and return quantities is between 1-100 cm³. Rail pressure is adjustable in range of 200 – 1400 bar. Double injection can be operated with independently setting of dwell time, the first and second injection duration. Injection duration is selectable in the range of 200-4000 μ s. Oscilloscope can monitor the injection signal from controller. The injection parameters could be adjusted manually through control panel as shown in Fig. 2. Two different types of injector were used for testing. Their specifications are shown in Table II.

B. Experiment Conditions

Before the injection parameters are studied, the calibration of the in-house fuel injection measurement system was done by comparison of the fuel injection quantity with the commercial measurement system. The single injection strategy was selected for calibration. The injection pressure and duration were tested in the range of 250-1400 bar and 250-1400 μ s, respectively. The typical diesel selling in the market was used for experiments.

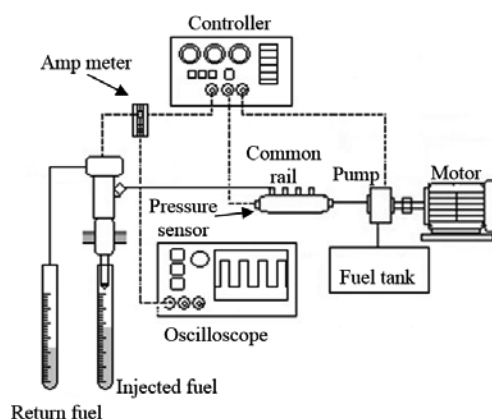


Fig. 1. Schematic diagram of fuel injection system.

TABLE II. INJECTOR SPECIFICATION

Injector	Nozzle No.	Nozzle Diameter	Angle
No.1	6	0.145 mm	145
No. 2	6	0.15 mm	145



To study the injection parameter of common rail injection system for both single and double injection strategy, the test conditions as shown in Table III are set. For double injection strategy, the injection pressures were tested at different point of 600 and 800 bar. The first and second injection durations were operated between 300-1400 μ s. Dwell time is varied in the range of 300-1500 μ s. The injector is operated at a fixed rail pressure and the injection duration is increased from 100 μ s to the maximum injection duration in 50 μ s increments. The injection signal of single injection and double injection are shown in Fig. 3.

TABLE III. TEST MATRIX

Injection strategy	Parameters	Value
Single	Injection pressure	250-1400 bar
	Injection duration	250-1400 μ s
Double	Injection pressure	600 and 800 bar
	1 st injection duration	300-1400 μ s
	2 nd injection duration	300-1400 μ s
	Dwell time	300-1500 μ s

For each test, fuel was injected with 1000 strokes to measure the injection and return quantities. The surrounding condition was kept constant at air ambient pressure and temperature of 0.1 MPa and 25 °C, respectively, and was used consistently for all experiments. The results of injection were averaged from 10 tests to check repeatability. Then the injection and return quantities for each test will be compared and analyzed.

IV. RESULTS AND DISCUSSION

A. Fuel Delivery Calibration and Injector Mapping

Fig. 4 shows the comparison of fuel injection quantity measured from the commercial injection measurement system and in-house injection measurement system, testing at injection pressure of 250-1400 bar and injection duration of 250-850 μ s. The results show that the fuel injection quantities of both injector measuring by in-house injection measurement system give the similar value and have the same trends as those of the commercial injection measurement system. The maximum difference is less than 15% at some points. From these maps, the test points are determined as the injectors can be operated at a wide range of pressure and injection duration.

Fig. 5 shows the map of injector no.1 tested at injection pressure of 250-1200 bar and injection duration of 250-1700 μ s. Fuel injection and return quantity are measured as shown in Fig. 5 (a) and (b), respectively. Increasing injection pressure and duration increase injection quantity for all tests. The injection quantity increases steeply at injection duration less than 800 μ s for all injection pressure, because shorter injection duration is a transitional zone of needle opening giving the smaller nozzle flow area. At this point, fuel return quantity also increases, because most supplied fuel could not go through the nozzle hole due to the smaller flow area, resulting a higher return amount. It can be postulated that fuel injection amount and return are dominated by the combined effect of injection duration and needle opening, relating flow area, at injection duration shorter than 800 μ s. However, at injection duration higher than 800 μ s for all injection pressure, fuel injection quantity increases slowly with increase of injection duration, while fuel return quantity is lower than that of the shorter injection duration. It could be explained that at long injection duration, the stabilized zone of injection is reached that gives the maximum flow area and a constant fuel flow rate as shown in Munsin et al [16]. With a maximum flow area at a given

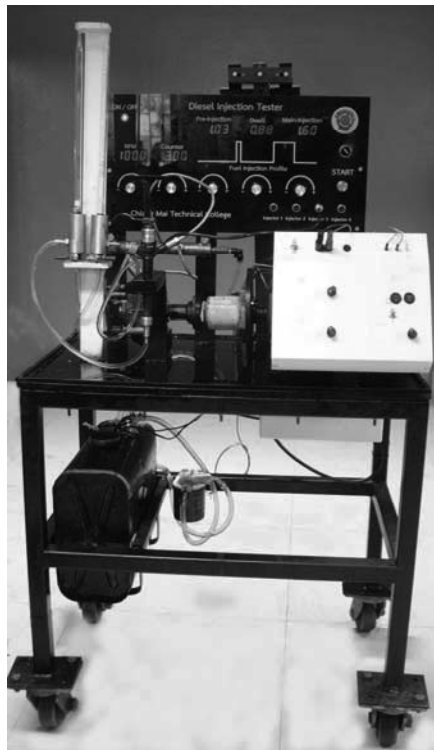


Fig. 2. In-house fuel injection measurement system.

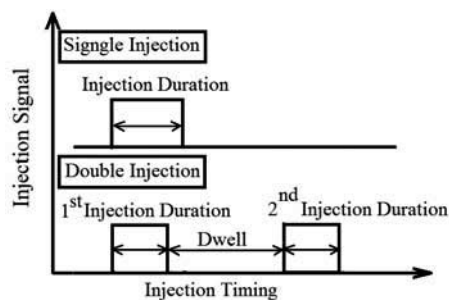


Fig. 3. Injection signal of single and double injections.

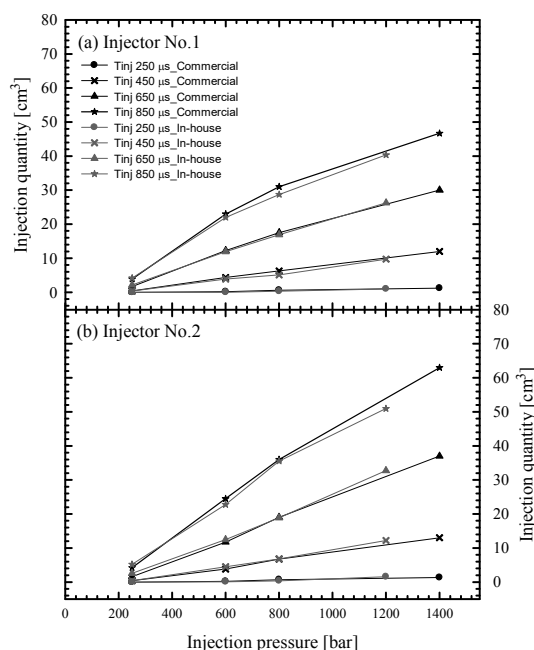


Fig. 4. Comparison of fuel injection quantity measured from the commercial injection measurement system and in-house injection measurement system, testing at injection pressure of 250-1400 bar and injection duration of 250-850 μ s.

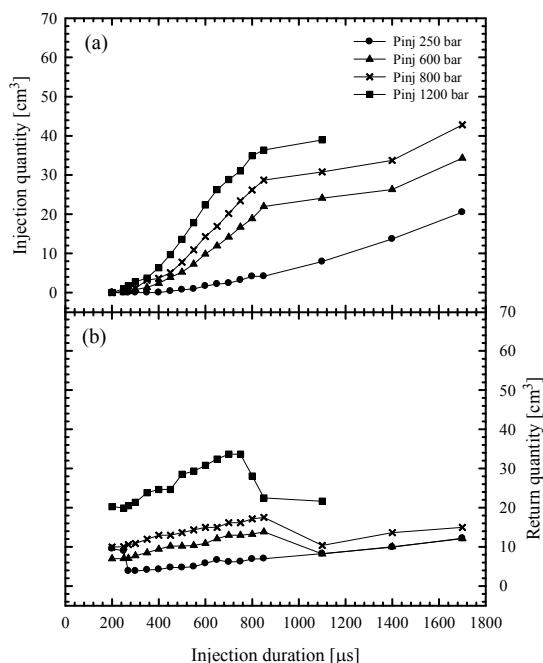


Fig. 5. Map of injector no.1 tested at injection pressure of 250-1200 bar and injection duration of 250-1700 μ s; (a) fuel injection quantity and (b) fuel return quantity.

injection pressure, the increase of fuel injection amount relies only injection duration, resulting to the slow increase of injection amount. The reason for dropped fuel return quantity is explained that most supplied fuel from common rail was pushed through the nozzle hole because of the maximum flow area, and less fuel could return to the fuel tank.

Fig. 6 shows the map of injector no.2 tested at injection pressure of 250-1200 bar and injection duration of 250-1700 μ s. Injection quantity and return are measured as injector no.1. From the experiments, the injector no.2 shows the similar trends of fuel injection and return quantities with those of the injector no.1. Nevertheless, fuel injection and return quantities are higher for the injector no.2 because of the bigger nozzle hole giving the larger flow area.

B. Fuel Delivery of Double Injection

Fig. 7. and Fig. 8. show effect of the first injection duration or the second injection duration on fuel delivery of both common rail injectors, respectively, with double injection strategy. Both injectors show the similar results at given conditions. Increasing the first injection duration and the second injection duration increase injected quantities as single injection strategy, while the return quantities are slightly increased.

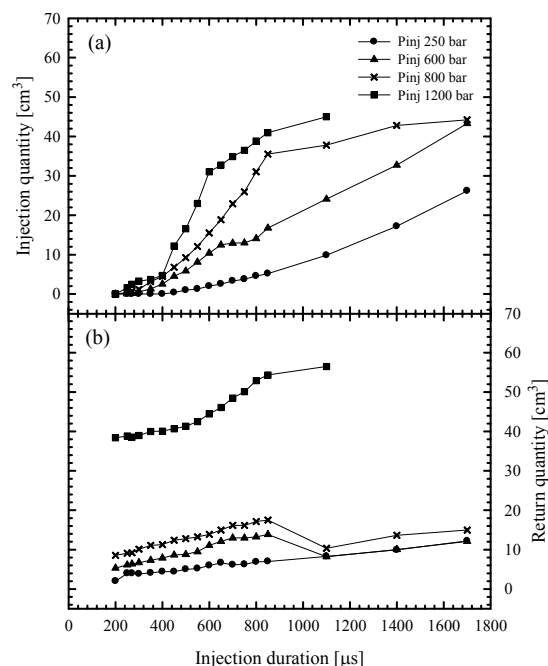


Fig. 6. Map of injector no.2 tested at injection pressure of 250-1200 bar and injection duration of 250-1700 μ s; (a) fuel injection quantity and (b) fuel return quantity.

Fig. 9. shows effect of dwell time on fuel delivery of both injectors using double injection strategy. From the results, it can be observed that increase of dwell time insignificantly changes injected fuel and return quantities for dwell time of

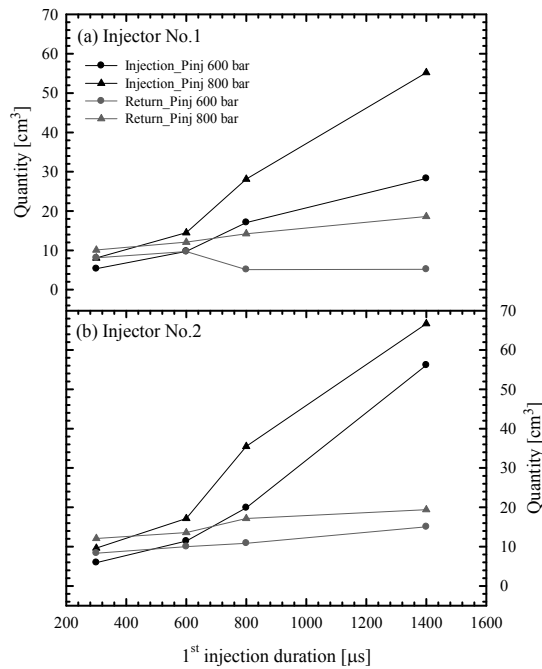


Fig. 7. Map of injector no.1 (a) and no.2 (b) tested with double injection strategy. The first injection duration was varied between 250-1400 μs, and dwell time and the second injection duration were kept constant at 500 μs and 600 μs, respectively.

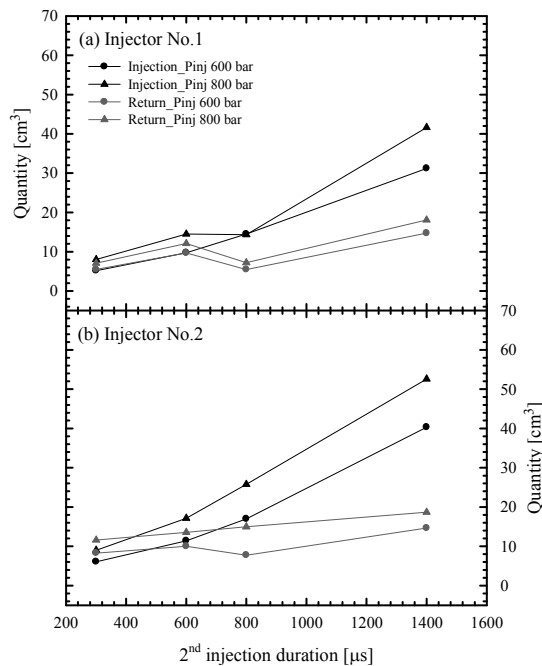


Fig. 8. Map of injector no.1 (a) and no.2 (b) tested with double injection strategy. The second injection duration was varied between 250-1400 μs, and dwell time and the first injection duration were kept constant at 500 μs and 600 μs, respectively.

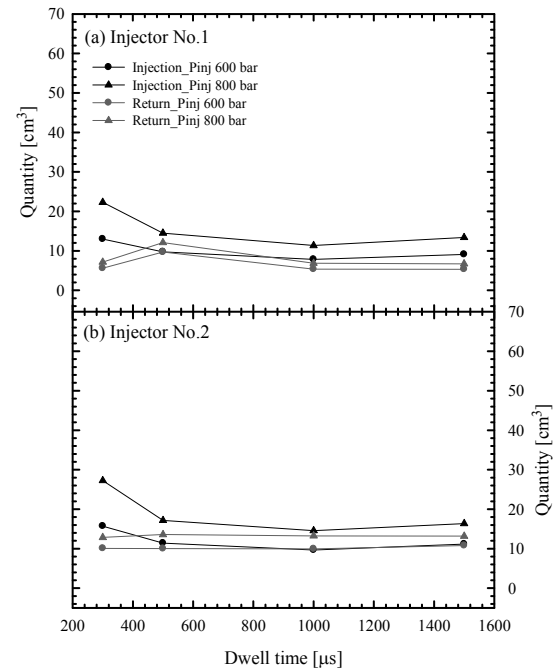


Fig. 9. Map of injector no.1 (a) and no.2 (b) tested with double injection strategy. Dwell time was varied between 300-1500 μs, and the first and the second injection duration were kept constant at 600 μs and 600 μs, respectively.

500-1500 μs. This means the transition zone of needle closing is complete. However, at dwell time of 300 μs, the injected fuel quantity of both injectors are higher than that of the others. It is possible that dwell time of 300 μs is too short for closing nozzle holes by the needle, which allow fuel flowing through the nozzle. In other word, fuel still delivered during short dwell time, caused by mechanical delay and resistance by fuel viscosity in the transition zone of needle closing.

V. CONCLUSION

The fuel delivery of common rail injector with different injection strategies using the volumetric injection measurement meter was investigated. The main conclusions are that:

- For single injection strategy, increasing injection pressure and injection duration increase fuel injection and return quantities for all tests. Fuel injection and return quantities are dominated by injection duration and needle opening at injection duration shorter than 800 μs.
- For double injection strategy, the change of first injection duration and the second injection duration in the range of 300-1400 μs gives the similar trends of injected fuel quantity and return at given injection conditions.
- Increase of dwell time insignificantly changes injected fuel and return quantities for dwell time above 500 μs. However, at dwell time of 300 μs, the injected fuel quantity are higher due to incompletely closing nozzle holes, which allow fuel delivery.



ACKNOWLEDGMENT

The financial support of Narin Srithikarn from Institute of Vocational Education: Northern Region 1 is gratefully acknowledged. The authors also acknowledge Prasert Diesel Co., Ltd. (Chiangmai) for help during the experimental work.

REFERENCES

- [1] J. Zhou, Y. Pei, Z. Peng, Y. Zhang, J. Qin, L. Wang, C. Liu and X. Zhang, "Characteristics of Near-Nozzle Spray Development from a Fouled GDI Injector," *Fuel*, vol. 219, pp. 17-29, May 2018.
- [2] C. Behrendt, and A. Smith, "A Study of Diesel Fuel Injector Deposit Effects on Power and Fuel Economy Performance," SAE Technical Paper 2017-01-0803, 2017.
- [3] M. Kinoshita, A. Saito, S. Matsushita, H. Shibata, Y. Niwa, "A Method for Suppressing Formation of Deposits on Fuel Injector for Direct Injection Gasoline Engine," SAE Technical Paper 1999-01-3656, 1999.
- [4] P. China and J.P. Rivere, "Development of a Direct Injection Spark Ignition Engine Test for Injector Fouling," SAE Technical Paper 2003-01-2006, 2006.
- [5] P.S. Von Bacho, J.K. Sofianek, J.M. Galante-Fox and C.J. McMahon, "Engine Test for Accelerated Fuel Deposit Formation on Injectors used in Gasoline Direct Injection Engines," SAE Technical Paper 2009-01-1495, 2009.
- [6] R. Lindgren, M. Skogsberg, H. Sandquist and I. Denbratt, "The Influence of Injector Deposits on Mixture Formation in a DISC SI Engine," SAE Technical Paper 2003-01-1771, 2003.
- [7] A.A. Aradi, B. Imoehl, N.L. Avery, P.P. Wells and R.W. Grosser, "The Effect of Fuel Composition and Engine Operating Parameters on Injector Deposits in a High-Pressure Direct Injection Gasoline (DIG) Research Engine," SAE Technical Paper 1999-01-3690, 1999.
- [8] R. Lindgren, M. Skogsberg, H. Sandquist and I. Denbratt, "The Influence of Injector Deposits on Mixture Formation in a DISC SI Engine," SAE Technical Paper 2003-01-1771, 2003.
- [9] B. Wang, T. Badawy, Y. Jiang, H. Xu, A. Ghafourian and X. Zhang, "Investigation of Deposit Effect on Multi-Hole Injector Spray Characteristics and Air/Fuel Mixing Process," *Fuel*, vol. 191, pp. 10-24, 2017.
- [10] J. Kazour, B. Befrui, H. Husted, M. Raney and D. Varble, "Innovative Sprays and Particulate Reduction with GDI Injectors," SAE Technical Paper 2014-01-1441, 2014.
- [11] A. Berndorfer, S. Breuer, W. Piock and P. Von Bacho, "Diffusion Combustion Phenomena in GDI Engines caused by Injection Process," SAE Technical Paper 2013-01-0261, 2013.
- [12] W. Zeuch, "Neue Verfahren zur Messung des Einspritzgesetzes und Einspritz-Regelmässigkeit von Diesel-Einspritzpumpen," *MTZ, Jahr. 22, Heft 9*, pp. 415-420, 1961.
- [13] W. Bosch, "The Fuel Rate Indicator: A New Measuring Instrument for Display of the Characteristics of Individual Injection," SAE Paper 660749, 1966.
- [14] M. Marcic, "Measuring method for diesel multihole injection nozzles," *Sensors and Actuators A*, vol 107, pp. 152-158, 2003.
- [15] DSD SL 15-23 Common Rail Injector Test Points EPS205 / EPS815 with CRI_CRIN, Diesel Service. (2018, March 28). Retrieved from https://gldiesel.com/wp-content/uploads/2016/08/Common_Rail_Test_Results_205_Legend.pdf.
- [16] R. Munsin, Y. Laoonual, S. Jugjai, M. Matsuki, H. Kosaka, "Effect of Glycerol Ethoxylate as an Ignition Improver on Injection and Combustion Characteristics of Hydrous Ethanol under CI Engine Condition," *Energy Conversion and Management*, vol 98, pp. 282-289, 2015.



Improvement of Physical Properties of Heterogeneous Biomass Pellets using Fermented Cassava rhizome and Kratin-wood residue: Effect of Fermentation Time

Kedsara Rattawan, Weeranut Intagun* and Wirojne Kanoksilapatham
Department of Mechanical Engineering, Faculty of Engineering and Industrial Technology,
Silpakorn University, Nakhon-Pathom, 73000, Thailand
*corresponding author; e-mail: weeranut_n@hotmail.com

Abstract—The objective is to study effect of fermentation time on binding property of fermented cassava rhizome and physical properties of a heterogeneous biomass pellet product. Rhizome of cassava (*Manihot esculenta*) and a wood residue from kratin tree (*Leucaena leucocephala*) were collected from local agricultural areas in Ratchaburi and Phetchaburi provinces, respectively. Cassava rhizome and fermented cassava rhizome were employed as mixers for pelletizing of kratin-wood residues. Fermentation of cassava rhizomes were conducted at room temperature, allowing growth of natural microorganisms for one and three days, respectively. The fermented cassavas obtained were termed “FC1” and “FC3”, respectively. The FC1 and FC3 were mixed with kratin-wood residue (ratio 1:1) prior to be molded using a flat-die pellet mill machine. Moisture content (30% of raw material) and initial die temperature (75 °C) were controlled. Heterogeneous of mixture of kratin-wood and cassava (LNFC0) and homogeneous cassava pellets (L100) were employed as control and reference, respectively. Biomass pellet products were determined for bulk density and durability following the standard methods set by Pellet Fuels Institute Standard. Bulk density and durability of the homogeneous L100 pellet values of $655 \pm 2.09 \text{ kg/m}^3$ and $94.25 \pm 0.31\%$ were determined, respectively. Comparing to the L100, both bulk densities and durability of the heterogeneous pellets were increased corresponding to the increased fermentation period: $682.13 \pm 1.13 \text{ kg/m}^3$ and $97.03 \pm 1.86\%$, $686.74 \pm 3.04 \text{ kg/m}^3$ and $98.76 \pm 0.47\%$, and $691.89 \pm 3.94 \text{ kg/m}^3$ and $98.87 \pm 0.97\%$ for the LNFC0, LFC1, and LFC3, respectively. The results suggest that cassava rhizome and fermented cassava are able to improve the physical properties of heterogeneous pellets such that they meet the standard requirement of the Pellet Fuels Institute (PFI) Program Standards.

Keywords—Biomass pellet fuel; Pelletizing; Fermentation time

I. INTRODUCTION

Plants and agricultural residues contain large amount of lingo-cellulosic fibers that can be burned for heat production. Pelletizing is a process of molding biomass fuels to improve the quality of raw materials. Generally, direct utilization of agricultural residues as biomass fuel has several limitations including high moisture content, low bulk density and asymmetrical forms [1]. One of the solutions to reduce the

limitations is compressing the raw material into the shape of a pellet.

Nowadays, biomass has been considered as attractive renewable energy sources due to agricultural residues provide a clean, renewable, and sustainable source of energy [2]. As an agricultural country, Thailand has many population engaged in farming and also left behind large amount of agriculture residues that can be applied as heat energy such as rice straw, sugarcane bagasse and wood and wood chips [3]-[5]. Kratin tree (*Leucaena leucocephala*) is a fast growing plant. Generally, it can be found widely in Thailand. Young leaf can be used as food and leaf can be used as animal feed. The remaining twigs are usually leaved as waste or can be burned for heat production. Because of its high heating value, it has high potential to be applied as a biomass fuel to reduce utilization of coal for generation of electricity [6]. The heating value of kratin-wood was estimated previously about 16-20 MJ/kg. However, molding of kratin-wood raw material is usually difficult due to its poor quality of pellets and requiring several manufacturing loops. Consequently, increase cost of pellet production [7]-[8]. *Manihot esculenta* (cassava) is considered one of the most important economic crops in Thailand [9]. Rhizome residues remained after tuberous roots have been cut off for commercial and food, the leaves and aerial rhizome can be sun-dried to prepared animal feed. Because of its starchy property, rhizome can be applied as an adhesive binder for biomass fuel pelletizing process, and also as a cheap supply of fermentable carbohydrates for cultivation of microorganisms, particularly amylolytic and cellulolytic bacteria [10]-[16].

Soil microorganisms play essential role in bio-transformation and modification of biomass and agricultural products. By using their lingo-cellulosic enzymes and other unknown intrinsic factors, polymeric structures, reducing powers and other chemically active groups of the fibers can be modified during the partially fermentation [17]-[20]. The objective of this study is to improve physical properties of a biomass pellet product produced using mixture of fermented cassava rhizome and kratin-wood residues. Different fermented rhizomes prepared by naturally inhabited microbes were investigated as a mixer in pelletizing of kratin-wood residue.



II. MATERIAL AND METHOD

A. Raw Materials

Two biomass raw materials were used in this study: krathin-wood and cassava rhizome residues. Kratin-wood and cassava rhizome residues were purchased from local areas in Cha-am district, Phetchaburi province, and Damnoen Saduak district, Ratchaburi province, respectively. They were harvested during January 2018. The materials were cleaned by praying with water and sun dried. They were grinded to small particles (approx. size of 5 mm) using a hammer mill screen size machine. Initial moisture of kratin-wood (9-10%) and cassava particles (12-15%) were determined at 105 °C in an oven following standard method. Images of the grinded particles are shown in Figure 1.

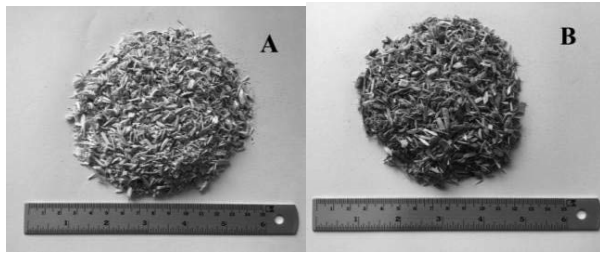


Fig. 1 Raw material A) Particles from krathin (*Leucaena leucocephala*), B) Particles from rhizome of cassava (*Manihot esculenta*).

B. Pellet Fuel Producing Processes

Preparation of fermented rhizome particles was performed by addition of 1.5 kg of water to 3 kg of rhizome particle. The wet rhizomes were incubated at room temperature for zero, one and three days. The rhizomes (called in this study as “NFC0”, “FC1” and “FC3”) were mixed with kratin-wood particle with a ratio of 1:1 prior to be molded using a flat-die pellet mill machine. Moisture content (30% of raw material) and initial die temperature (75 °C) were controlled. Nonfermented cassava rhizome as a mixer (LNFC0) and kratin-wood residue without a mixer (L100) were employed as control and reference, respectively.

C. Pellet Fuel Qualities Testing

The physical properties (bulk density and durability and fine) of pellets were determined following the standard method of the Pellet Fuel Institute (PFI) Standard Specification. The bulk density of pellets was determined according to method described in the ASTM E-873-82 [21]. The pellet bulk density was calculated using the following equation (1).

$$\rho_{bulk} = \frac{W_b}{V_b} \quad (1)$$

When, ρ_{bulk} is pellets bulk density (kg/m³), W_b is total weight of the pellets (kg) and V_b is volume of the measuring standard box (m³)

Durability was determined using tumbling method following the standard method according to the BS EN 15210-1 [22]. Briefly, 500 g of pellet sample was filled into a standard chamber (305x140x305 mm³). The filled chamber was rotated at 500 rpm for 10 minutes. Then the samples were sieved through a 1/8-inch screen to remove fine particles. The procedure was repeated with another 500 g of the pellet sample. Course particles were weighted and pooled. Percentage of whole pellets was calculated using the following equation (2).

$$PDI = \frac{(WPW)}{IW} \times 100 \quad (2)$$

When, PDI is Pellet durability index (%), WPW is Weight of pellets after tumbling (kg) and IW is Weight of pellets before tumbling (kg)

The percentage of fine particle was calculated using the following equation 3.

$$\%Fines = \frac{[(W_p + W_f)] - W_p}{W_i} \times 100 \quad (3)$$

When, $\%Fines$ is Fines product or pellet fines content (%), W_p is Weight of base pan (g), W_f is Weight of fines (g) and W_i is Initial weight (g)

D. Energy cost

Energy cost of pellets product was estimated on energy consumption, final product mass and energy charge using the following equation (4).

$$EC = \frac{E_{consum}}{F_m} \times E_{charge} \quad (4)$$

When, EC is energy cost (baht/kg), E_{consum} is energy consumption (kWh), F_m is final mass (kg) and E_{charge} is electricity charge (bath/kWh)



III. RESULTS AND DISCUSSION

A. Effects of fermentation time on physical characteristics

Pellet products are shown in Fig. 2. In Figure 2, products from rhizome supplementing pellets (heterogeneous pellets) appeared more smooth and shiny than the homogeneous pellets (L100).

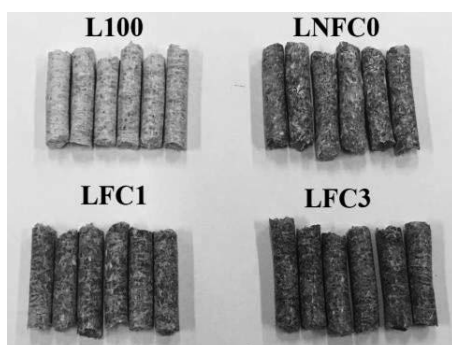


Fig. 2 Images of pellet products. Symbols: L100, LNFC0, LFC1 and LFC3 represent final pellet products molded using 100% kratin-wood particles, 50% kratin-wood mixed with nonfermented cassava (day zero), 50% kratin-wood mixed with one day fermented cassava and 50% kratin-wood mixed with three day fermented cassava, respectively.

B. Effects of fermentation time on bulk density

Bulk density values of pellets are shown in Fig.3. The results of the pellet bulk density of kratin-wood residue (L100), kratin-wood residue with day zero fermented cassava (LNFC0), kratin-wood residue with day one fermented cassava (LFC1) and kratin-wood residue with day three fermented cassava (LFC3) are listed as follows: 655.81 ± 2.09 , 682.13 ± 1.13 , 686.74 ± 3.04 and 691.89 ± 3.94 kg/m^3 , respectively. The results revealed an increasing trend from day zero- to day three-fermentation comparing to the reference (L100). These values are in the acceptable range required by the PFI (608-768 kg/m^3).

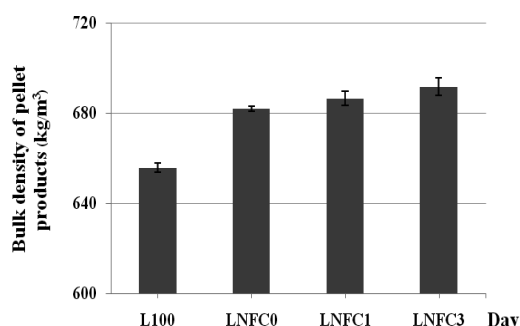


Fig. 3 Bulk density of pellet products. Symbols: L100, LNFC0, LFC1 and LFC3 represent final pellet products molded using 100% kratin-wood particles, 50% kratin-wood

mixed with nonfermented cassava (day zero), 50% kratin-wood mixed with one day fermented cassava and 50% kratin-wood mixed with three day fermented cassava, respectively.

C. Effects of fermentation time on durability and fines content

The results of the pellet durability of the L100, LNFC0, LFC1 and LFC3 are listed as follows: 94.25 ± 0.31 , 97.03 ± 1.86 , 98.76 ± 0.47 and $98.87 \pm 0.97\%$, respectively. It was found that durability of the L100 was the lowest value and it is below the minimal requirement of the PFI. In addition, an increasing of 2.92, 4.56 and 4.67%, trend was estimated on the LNFC0, LFC1 and LFC3, respectively. The results confirmed that cassava rhizome as a mixer is able to improve durability of kartin-wood pellet to meet the standard values ($\geq 95.0\%$). In addition, three day fermented cassava was observed the highest.

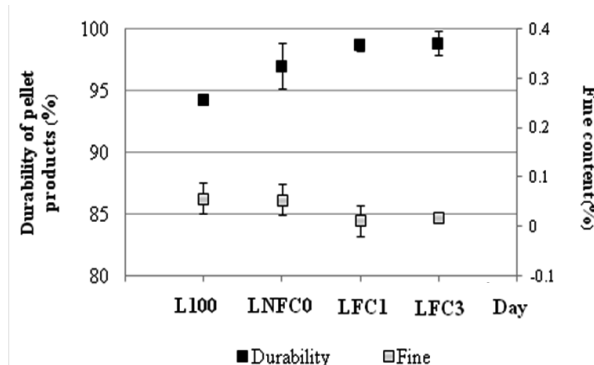


Fig. 4 Effect of the binder on durability and fine content. Symbols: L100, LNFC0, LFC1 and LFC3 represent final pellet products molded using 100% kratin-wood particles, 50% kratin-wood mixed with nonfermented cassava (day zero), 50% kratin-wood mixed with one day fermented cassava and 50% kratin-wood mixed with three day fermented cassava, respectively.

D. Effects of fermentation time on energy cost

Energy cost of pellets product was estimated based on energy consumption, final product mass and energy charge as described above in materials and methods. For small business, electricity charge in Thailand of 3.9086 baht per unit was employed. Estimated of the L100 (2.55 baht/kg), LNFC0 (2.48 baht/kg), LFC1 (1.96 baht/kg) and LFC3 (1.58 baht/kg), were summarized in Fig. 5. The lower energy costs were resulted from better yields of the mixed biomass pellets.

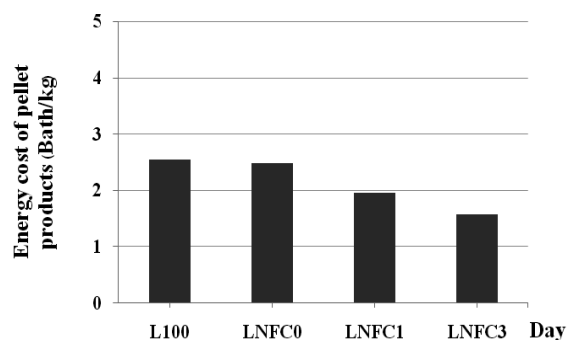


Fig. 5 Effect of the binder on energy cost

IV. CONCLUSION

It can be concluded from this research that physical properties of all pellets meet the requirements of the Pellet Fuels Institute Standard Specification for Residential/Commercial Densified. Comparing to reference (L100; $655.81 \pm 2.09 \text{ kg/m}^3$ for bulk density and $94.25 \pm 0.31\%$ for durability), both bulk densities and durability of pellets mixed with cassava rhizome (NFC0; $682.13 \pm 1.13 \text{ kg/m}^3$ and $97.03 \pm 1.86\%$), with one day (LFC1; $686.74 \pm 3.04 \text{ kg/m}^3$ and $98.76 \pm 0.47\%$) and three day (LFC3; $691.89 \pm 3.94 \text{ kg/m}^3$ and $98.87 \pm 0.97\%$) fermented cassava, were increased corresponding to time of fermentation, respectively. The highest values were observed on the heterogeneous pellets using three day fermented cassava. Whether or not heterogeneous pellet products supplemented with prolong incubation period of fermented cassava (>3 days) have better quality remained to be investigated.

Plants and agricultural residues contain water insoluble, strong integrity lingo-cellulosic fibers in their cell walls (as physical protective structure). Pelletizing is a process of compressing biomass fuels to improve the quality of raw materials. Generally, biomass raw materials were grinded to asymmetrical form prior to be re-enforced by heat induced bonding mechanism to form tightly pellets. Soil microorganisms play essential role in bio-transformation and modification of biomass and agricultural products. By using their lingo-cellulosic enzymes and other unknown intrinsic factors, crystalline polymeric structures of the substrates can be nicked to open up the cell wall polymers, and exposed chemically active reducing ends and phenolic ends of the partially fermented fiber substrates [17]-[19]. In this study, pellet's quality was improved by fermented cassava that underwent complicate biochemical transformation. It is likely that a mechanism involves heat induced adhesive property of cassava rhizome, as well as increased formation of inter fiber bonding presumably by the exposed phenolic groups of lignin.

ACKNOWLEDGMENT

The authors gratefully acknowledge the Department of Mechanical Engineering, Faculty of Engineering and Industrial Technology, Silpakorn University for all supports.

REFERENCES

- [1] S. Mani, L. Tabilb, and S. Sokhansanj, "Effects of compressive force, particle size, and moisture content on mechanical properties of biomass pellets from grasses," *Biomass and Bioenergy*, vol. 30, pp.648–654, July 2006.
- [2] M. F. Demirbas, M. Balat, and H. Balat, "Potential contribution of biomass to the sustainable energy development," *Energy Conversion and Management*, vol. 50, pp. 1746–1760, March 2009.
- [3] M. Hoogwijk, A. Faaij, B. Eickhout, B. de Vries, and W. Turkenburg, "Potential of biomass energy out to 2100, for four IPCC SRES land-use scenarios," *Biomass and Bioenergy*, vol. 29, pp. 225–257, October 2005.
- [4] Sy. Yokoyama, T. Ogi and A. Nalampoon, "Biomass energy potential in Thailand," *Biomass and Bioenergy*, vol. 18, pp. 405–410, May 2000.
- [5] S. Prasertsan, and B. Sajjakulnukit, "Biomass and Biogas Energy in Thailand: Potential Opportunity and Barriers," *Renewable Energy*, vol. 31, pp. 599–610, April 2006.
- [6] S. Chotchutima, K. Kangvansaichol, S. Tudsri, and P. Sripichitt, "Effect of spacing on growth, biomass yield and quality of *Leucaena leucocephala* (Lam.) de Wit.) for renewable energy in Thailand," *Journal of Sustainable Bioenergy Systems*, vol. 3, pp. 48–56, March 2013.
- [7] S. Noha, M. Mahmoud, D. Abdel, G. Angela, and Z. Montserrat, "Influence of densification parameters on quality properties of rice straw pellets," *Fuel Processing Technology*, vol. 138, pp. 56–64, October 2015.
- [8] P. Jetsada, S. Amrit, S. Wanphut, and S. Panmanas, "Rapid non-destructive evaluation of moisture content and higher heating value of *Leucaena leucocephala* pellets using near infrared spectroscopy," *Energy*, vol. 107: 464–472, July 2016.
- [9] C. Ratanawaraha, N. Senanarong, and P. Suriyapan, "Status of cassava in Thailand: Implications for future research and development," *International fund for Agricultural Development (BFAD)*, vol. 3, p. 103–153, 2001.
- [10] C. Martin, M. G. Wei, S. J. Xiong, and L. J. Jönsson, "Enhancing saccharification of cassava stems by starch hydrolysis prior to pretreatment," *Industrial Crops and Products*, vol. 97, pp. 21–31, March 2017.
- [11] B. Zhu, A. Lestander, H. Örberg, G. Wei, B. Hedman, J.W. Ren, G. H. Xie, and S. J. Xiong, "Cassava stems: a new resource to increase food and fuel production," *Global Change Biology Bioenergy*, vol. 7(1), pp. 72–83, July 2015.
- [12] A. D. Uchekukwu-Agua, O. J. Caleb, and U. L. Opara, "Postharvest handling and storage of fresh cassava root and products: a review," *Food Bioprocess Technology*, vol. 8, pp. 729–748, January 2015.
- [13] S. H. M. Azhar, R. Abdulla, S. A. Jambo, H. Marbawi, J. A. Gansau, A. A. M. Faik, and K. F. Rodrigues, "Yeasts in sustainable bioethanol production: A review," *Biochemistry and Biophysics Reports*, vol. 10, pp. 52–61, July 2017.
- [14] M. G. Wei, W. B. Zhu, G. H. Xie, T. A. Lestander, and S. J. Xiong, "Cassava stem wastes as potential feedstock for fuel ethanol production: a basic parameter study," *Renewable Energy*, vol. 83, pp. 970–978, November 2015.
- [15] N. Sarkar, S. K. Ghosh, S. Bannerjee, and K. Aikat, "Bioethanol production from agricultural wastes: An overview," *Renewable Energy*, vol. 37, pp. 19–27, January 2012.
- [16] M. Vihinen, and P. Mantsiila, "Microbial amylolytic enzyme," *Critical Reviews in Biochemistry and Molecular Biology*, vol. 24, pp. 329–418, 1989.



- [17] L. Chen, F. Hong, X. Yang, and S. Han, "Biotransformation of wheat straw to bacterial cellulose and its mechanism," *Bioresource Technology*, vol. 135, pp. 464–468, May 2013.
- [18] T. D. H. Bugg, M. Ahmad, E. M. Hardiman, and R. Singh, "The emerging role for bacteria in lignin degradation and bio-product formation," *Current Opinion in Biotechnology*, vol. 22, pp. 394–400, June 2011.
- [19] S. H. Lee, T. V. Doherty, R. J. Linhardt, and J. S. Dordick, "Ionic liquid-mediated selective extraction of lignin from wood leading to enhanced enzymatic cellulose hydrolysis," *Biotechnology and Bioengineering*, vol. 102, pp. 1368–1376, April 2009.
- [20] D. L. Crawford and R. L. Crawford, "Microbial degradation of lignocellulose: the lignin component," *Applied and Environmental Microbiology*, vol. 31, pp. 714–717, May 1976.
- [21] ASTM International, "E 873-82: Standard test method for bulk density of densified particulate biomass fuels," *Annual book of ASTM Standards*, 11.06: 112–113, 2013.
- [22] BS standard: EN 15210-1., *Solid biofuels, determination of mechanical durability of pellets and briquettes, Part 1, Pellets*, 2009.



Tank-to –Wheel Analysis of Environmental and Economic Evaluation from Passenger Cars Transportation

Chantima Rewlay-ngoen* and Siripol Tongorn

Department of Mechanical Engineering, Faculty of Engineering, Rajamangala University of Technology Phra Nakhon, Bangkok, 10300, Thailand

*Corresponding author: chantima.r@rmutp.ac.th

Seksan Papong

National Metal and Materials Technology Center (MTEC), National Science and Technology Development Agency (NSTDA), Thailand Science Park, Pathum Thani, 12120, Thailand

Abstract—Electric vehicles are considered as technology which can significantly reduce the problems related to transportation such as increasing greenhouse gas emissions, hazardous air pollution and energy import dependency. The main objective of this paper is to analyze the current environmental impact perspective on present global warming potential and economic characterization of different types of electric vehicles and fuels are compared (petro, diesel, Hybrid Electric Vehicles (HEVs), Battery Electric Vehicles (BEVs)) on their level of global warming potential impact and economic value per one hundred kilometer. Resulting indicate that in term of vehicle use (Tank-to-Wheel perspective) the electric vehicle shows a lower environmental impact and economic value. Futuremore, Emissions during fuel production should be addressed and also impacts with the production of vehicle. Moreover, the different pollutants result in different environmental damages.

Keywords—Tank-to-Wheel, electric vehicles, economic, emissions,

including gas, coal, oil, biomass, wind and solar-reducing oil dependency and uniqueness of energy security. EVs are soundless and have zero emissions while driving at least on the Tank-to-Wheel (TTW) [3] basis. However, EVs are still not a mature technology. The term EV covers a range of vehicles types, e.g. hybrid EVs and battery EVs. Hybrid has an electric and a combustion engine. This research distinguishes the following two different types of electric vehicle:

-Conventional International Combustion Engine (ICE): it is using gasoline, gasohol or diesel

-Batter Electric Vehicle (BEV): these vehicles have only an electric engine

-Hybrid Electric Vehicle (HEV: it is an ICE vehicle by an electric engine (battery is charged by regenerated energy during breaking)

The main objective of this paper is to analyze the current environmental impact perspective on present global warming potential and economic characterization of different types of electric vehicles and fuels are compares (petro, diesel, HEV, and BEV).

I. INTRODUCTION

Bangkok, Thailand is the top ten cities with the worst traffic has been arising serious environmental concerns over the increase of greenhouse gas emissions, hazardous air pollution and dependence on reduce fossil fuel reserves. Nowadays, the oil price concerns over the volatility of oil prices and security of fuel supply from politically unstable countries has further spurred the quest for increased energy efficiency and low emission alternatives to conventional fossil fuel-based powertrains [1]. Several national and international policies have been put more stringent limits on fuel consumption and/or CO₂ emissions of vehicles. A first approach for decreasing vehicle emissions is by increasing the efficiency of the Internal Combustion Engine (ICE). One of strategies is engine downsizing [2], using alternative fuels (LPG, CNG, biofuels) or Electric Vehicles (EVs) (hybrid, battery electric, plug-in hybrid), are entering the market. EVs can be fuelled by a wide variety of primary energy source-

II. LIFE CYCLE ASSESSMENT

Life Cycle Assessment (LCA) is a tool used in assessing the environmental impact of a product throughout its life cycle. It considers impacts from raw materials procurement, manufacturing process, transportation, use, and disposal, all the stages of a product's life from-cradle-to-grave. LCA is covered by ISO 14040 [4]. Standard Series which includes 4 steps.

1. Goal and scope definition
2. Life Cycle Inventory (LCI)
3. Life Cycle Impact Assessment (LCIA)
4. Interpretation

In the first step of LCA, the goal and scope of the study should be defined. This includes an extract formulation of what is to be investigated, and how the investigation is to be carried out. The functional unit (FU) and system boundary are chosen



and respected. The next step, LCI, gathers data on all inputs and outputs of industrial processes that occur during the life cycle of a product. The third phase, LCIA, according to ISO 14042/14044 standard, aims to convert the inventory data into potential environmental impact [5,6,7].

A. Goal and scope definition

This study focuses on the tank-to-wheel cycle and analyzes the global warming of passenger cars. The TTW of vehicle used estimates is based on Messagie, *et al.* [8] that presented vehicle consumption in Belgium. The functional unit that set is 209,470 km.

B. Life Cycle Inventory

The second step of LCA involves data collection on the inputs and outputs of passenger cars, based on the LCI. These inventory data were gathered from Messagie, *et al.* Figure 1 shows an overview of the different vehicles that are selected for the analysis. Three car segments are investigated: the small city cars, the medium sized cars and luxurious premium cars. All these cars compared for different vehicle technologies: petrol, diesel, hybrid and battery electric [8].

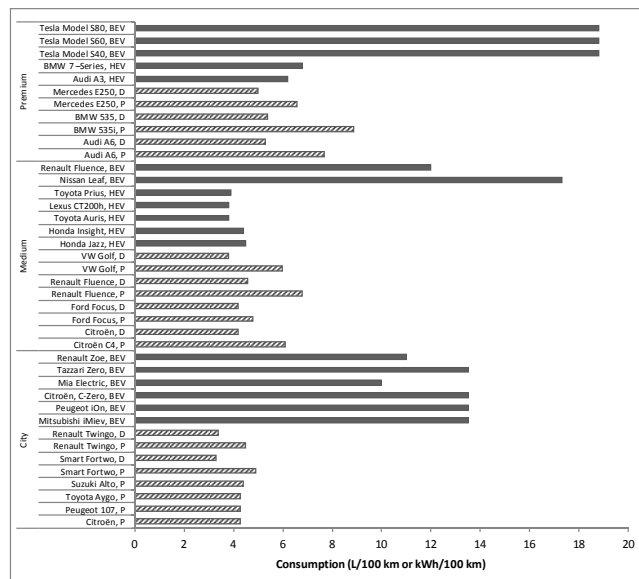


Fig. 1. Fuel consumption of passenger car [8]

Note: P = petrol, D = diesel, BEV = battery electric vehicle.

■ Fuel consumption unit L/100 km
▨ Fuel consumption unit kWh/100 km

C. Life Cycle Impact Assessment

The international standard for LCIA, ISO 14042, considered selected impacted categories, classification, characterization to be mandatory elements of LCIA. Normalization, grouping, and weighting are an optional element to be included depending on the goal and scope of the

study. This research included mandatory and weighting is on optional element. The environmental impact is calculated based on LIME method [9,10] only considering global warming impact for this study. However for mandatory element used emission factor from TGO [11] but weighting used factor based on LIME method. For the resulting of LIME method can be expressed as monetary amount as shown in equation (1)

$$I = \sum_e \sum_s (Inv_s \times Damage Factor_{s,e} \times WF_e) \quad (1)$$

Where

- I: a result of weighting (Baht)
 Inv_s: LCI of CO₂ emission (kg)
 WF_e: weighting factor for one unit of damage to a safeguard subject (Baht/unit damage)

LIME method, global warming impact links the emission to consequences on human damage and social assets. For emission factor, damage factor and weighting factor are presented in Table 1.

Table I. Emission factor, damage factor and weighting factor for global warming with calculation

Emission Factor [11]	Unit	Amount
Electricity	kg CO ₂ eq./kWh	0.6093
Diesel	kg CO ₂ eq./liter	2.7446
Gasohol	kg CO ₂ eq./liter	2.1896
Damage Factor [10]	Unit	Amount
CO ₂ on human health	DALY/substance	1.63 x 10 ⁻⁷
CO ₂ on social assets	Baht/substance ¹	0.3860
Weighting Factor [9]	Unit	Amount
Human health	Baht/DALY ¹	3.98 x 10 ⁶
Social assets	Baht/Baht ¹	0.1205

Note: Conversion value is 0.1205 based on GDP(PPP) in Thailand at 15,681.80 Baht, and Japan at 38,239.80 Baht and based on 2017 and exchange rate 29.3957 Baht/100 yen [12].

However, the main objective of this research is to analyze the environmental and economic characteristics of difference types of vehicle, following three difference types of vehicle [3] are ICE, BEV and HEV.

The common architectures of those vehicles are shown in Table 2



Table II. Classification of various types of vehicle [3]

Architectures of vehicle	Type of vehicle
	ICE is taken as reference. It using diesel and gasoline for fuel consumption.
	HEV are propelled by ICE and an electric motor/generator in series or parallel configuration. The ICE allows the vehicles an extended driving range, while the electric motor increases efficiency by regenerating energy during braking and storing excess energy from the ICE during costing.
	BEV uses chemical energy stored in rechargeable battery packs. BEV uses electric motors and motor controllers instead of internal combustion engines for propulsion.
Symbols: ICE Tank Battery Generator Electro motor Power converter Fuel cell H2-Tank Transmission	

III. RESULTS

Figure 2 shows the global warming potential from 100 km of passenger car, when considering the tank-to-wheel. The results indicate that HEV had the lowest impact and following BEV. When comparing petro with diesel, it was found that petro produced greater global warming potential.

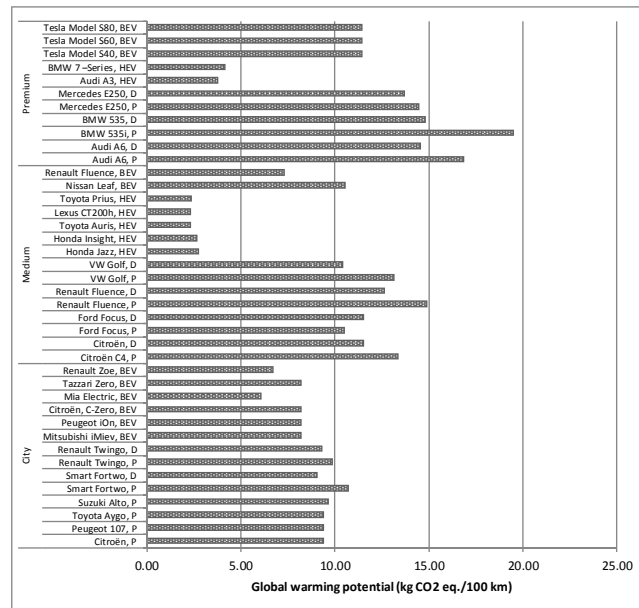


Fig. 2. Global warming potential of passenger car

Figure 3 shows the economic value from environmental cost and production cost. The environmental cost calculated from equation (1) and production cost based on fuel consumption and converted into economic value by using average electricity sale is 3.821 Baht/kWh [14] and average oil sale price for petro (gasohol) is 26.33 Baht/liter and diesel 27.52 Baht/liter were based on 2017 [15].

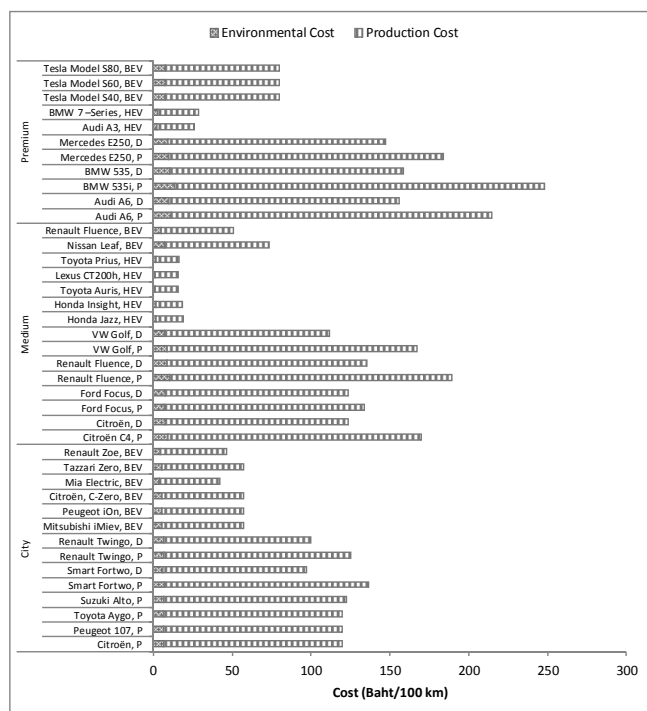


Fig. 3. Economic value of passenger cars

In the comparison with economic value, the highest economic was from BMW535i and lowest economic was from Toyota Auris and Lexus CT220h that total economic are 14.52 Baht/100 km.

The balance between the environmental LCA results (only considered GWP) and economic value (based on LIME in unit Baht) is presented in Figure 4. On the X-axis, the economic value is shown, whereas the Y-axis presented the LCA. The matrix shows four quadrants. The quadrants are determined by two reference lines that adjust to the average of the x coordinates and the y coordinates.

The first quadrant, the lower left is characterized by car with a low environmental (LCA < 9.68 kg CO₂ eq./100 km) and a high cost efficiency (<100.68 Baht/100 km). These cars are mainly represented by city cars (orange) and medium cars (red) and some premium cars (green).

The second quadrant (upper left) contains cars which are not environmentally friendly, but which are cost efficiency. Those car are Nissan Leaf and Teala Model cars.

Most of cars are mainly situated in the third quadrant (upper right). Cars in this quadrant includes medium cars, premium cars and only Smart Fortwo (P) this is city car include in this quadrant.

Finally quadrant is lower right includes the expansive cars, which are environmental friendly.

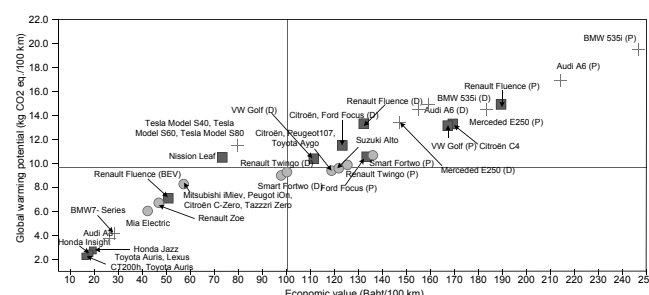


Fig. 4. Balancing the cost efficiency and environmental friendliness of vehicles

IV. CONCLUSION AND RECOMMENDATION

Comparing the environmental impact of vehicles with alternative systems is challenging. Only considered tail-pipe emissions, that also mean only CO₂ emissions. Furthermore, Emissions during fuel production should be addressed and also impacts with the production of vehicle. Moreover, the different pollutants result in different environmental damages. This paper concludes that electric vehicles are more environmental friendly when compared to the conventional petrol and diesel of passenger cars.

For economic value found that for conventional fuels, the high cost when compared with electric vehicle due to consider only fuel production this is limitation of this study.

The environmental impacts with economic results. Cars from the first quadrant (low environmental impact and high cost effectiveness) are mainly presented electric city cars and medium cars only Audi A3 and BMW7-Series from premium cars. The second quadrant cars that shown the results by a higher environmental impact but which still are cost efficient are Nissan Leaf and Teala Model cars. In quadrant 3 and 4, which are cost-inefficient and which have a respectively high and low environmental impacts. Most of cars have environmentally friendliness and cost-inefficient.

ACKNOWLEDGMENT

We would like to express our profound gratitude to National Science and Technology Development Agency (NSTDA) for the financial support.

REFERENCES

- [1] J., Martins, F.P., Btito, D., Pedrosa, V., Monteiro, and L., Afonso, (2013). "Real-life comparison between diesel and electric car energy consumption," Development of the Over-Expansion Cycle-POCI-EME/59186/2004.
- [2] C., Silva, M., Ross, and T., Farias, (2009). "Analysis and simulation of "low-cost" strategies to reduce fuel consumption and emissions in conventional gasoline



- light-duty vehicles,” Energy Conversion and Management, 215-222.
- [3] A., Ajsnovic, (2013). “Recent developments in electric vehicles for passenger car transport. World Academy of Science, Engineering and Technology,” International Journal of Transport and Vehicle Engineering 7 (3), 136 – 140.
- [4] ISO, (2006a). “Environmental management–life cycle assessment–life cycle impact assessment,” International Standard ISO14042.
- [5] S., Ryding, (1999). “ISO 14042 Environmental management • Life cycle assessment • Life cycle impact assessment,” Int. J. LCA 4(6), 307.
- [6] ISO, (2006b). “ISO 14044: Environmental management–life cycle assessment– requirements and guidelines.”
- [7] M., Margni and M.A., Curran, (2012). “Chapter 4: Life Cycle Impact Assessment,” Life Cycle Assessment Handbook MA Curran (ed) Scrivener-Wiley Publishing, Salem, Massachusetts.
- [8] M., Messagie, K., Lebeay, T., Coosemans, C., Macharis, and J., van Mierlo, (2013). “Environmental and Financial Evaluation of Passenger Vehicle Technologies in Belgium,” Sustainability (5), 5020-5033; doi:10.3390/su5125020.
- [9] N., Itsubo, M., Sakagami, T., Washida, K., Kokubu, and A., Inaba, (2004). “Weighting across safeguard subjects for LCIA through the application of conjoint analysis,” Int J LCA 9(3): 196 – 205.
- [10] C., Rewlay-ngoen, (2013). “Development of life cycle environmental impact assessment model by endpoint analysis” Chiang Mai University.
- [11] TGO (Thailand Greenhouse gas management Organization (TGO) (Public Organization)), (2018). “Emission Factor,” Online [http://thaicarbonlabel.tgo.or.th/products_emission/products_emission.pnc].
- [12] Bank of Thailand, (2018). “Rates of exchange of commercial banks,” Online: [https://www.bot.or.th/thai/_layouts/application/exchange_rate/exchangerate.aspx].
- [13] A., Ajanovic, (2013). “Recent developments in electric vehicles for passenger car transportation,” World Academy of Science, Engineering and Technology, International Journal of Transport and Vehicle Engineering 7 (3), 136 – 140.
- [14] Metropolitan Electricity Authority, (2018). “Rate of electricity,” Online: [http://www.mea.or.th/upload/download/file_4432fed72763bdc538c0a8ef0208df35.pdf]
- [15] Energy Policy and Planning Office, Ministry of Energy, (2018). “Energy and Electricity Situation of Thailand on January 2018,” Online: [http://www.eppo.go.th/index.php/th/information/services/situation-energy].



Effects of Air Staging on Emission Characteristics and Combustion Efficiency in a Twin-cyclonic Swirling Fluidized-bed Combustor Firing Rubberwood Sawdust

Tananon Srisamran and Kasama Sirisomboon,

Laboratory of Advance Combustion Technology and Energy Systems (LACTES),
Department of Mechanical Engineering, Faculty of Engineering and Industrial Technology,
Silpakorn University, Nakhon Pathom 73000, Thailand

*Corresponding Author: tananon_229@hotmail.com, (+6634) 259 025 Fax: (+6634) 219 367

Abstract— The experimental tests were conducted in a twin-cyclonic swirling fluidized-bed combustor (TFBC) firing with rubberwood sawdust with different operating parameters, constant fuel feed rate of 20 kg/h, secondary air ratio (S/T) at 0–0.5 for excess air 20–80%. Silica sand of particle size range 450–550 μm was used as the bed material at static bed height 30 cm above the annular spiral air distributor. The temperature and gas concentrations of O_2 , CO, and NO were measured along the axial directions of the combustor. CO and NO emissions was experimentally investigated at the stack for all tests prior using CO emission for calculating heat loss owing to incomplete combustion. Fly ash was sampling from ash collector with the aim to calculate the heat loss due to unburned carbon. The combustion efficiency was then calculated by indirect heat losses method. As revealed from the experimental results, CO emission decrease with rising of excess air but increase when secondary air ratio rising, while NO emission present inverse trends with CO. For firing rubberwood sawdust in TSFBC at EA 60–80% and S/T 0–0.1, as leading to high (~97%) combustion efficiency (η_c) and acceptable levels CO and NO emission with Thailand emission standard.

Keywords— Fluidized bed; Silica sand; Excess air; Emission; Combustion, Efficiency

I. INTRODUCTION

Biomass is considered to be a promising renewable energy. It is carbon neutral and contains low levels of sulfur. In Thailand, biomass is one potential source of renewable energy. The rubberwood sawdust derived from sawn timber process of wooden furniture. A number of rubberwood sawdust from local furniture factories approximate about 85×10^5 tons/year [1,2] and it has a relatively high calorific value (of about 16 MJ/kg) [3].

Fluidized bed combustor (FBC) is most favor for firing solid fuel like coal and biomass. FBC is a clean combustion technology because it can be operated at high efficiency under the low temperature (750–950°C), therefore thermal NO_x can

be reduced [4]. In the swirling FBC, Chakritthakul et al., [3] conducted the experimental tests for co-firing of eucalyptus bark and rubberwood sawdust. In the tests, fuel feed rate was maintained at about 60 kg/h. Excess air was supplied from 20–80 % while secondary air was injected into splash zone at constant flowrate at 0.021 Nm^3/s . From the experimental results, the increasing proportion of the bark reduced NO emission compare to firing sawdust on its own do to high-moisture eucalyptus bark at 47.5 wt%. This trend also resemble with Kuprianov et al., [5]

The effects of air-staging combustion in FBC have been studied by many researchers. Kuprianov et al., [6] also investigated staged air combustion on emission performance and combustion efficiency. This experimental studied on firing 80 kg/h of rice husk while secondary to primary air ratio was ranged 0.26–0.75, and excess air was fixed at 40%. The results showed that, CO emission significantly increased from about 360 to 450 ppm (on 6% O_2 dry gas basis) at secondary to primary air ratio from 0.26 to 0.75, while the NO emission reduced from 150 to 140 ppm. However, C_xH_y emissions increased from 120 to 1400 ppm. Sirisomboon et al., [7] studied emission characteristics on air staging with sunflower shells in a conical fluidized-bed combustor. The fuel was fed 45 kg/h, while the secondary air to total ratio was tangential injected to the combustor at 0–0.4 for excess air of 20–80 %. The experimental results showed the significant effect of secondary on emissions, NO emission decreased with the increasing of secondary air (SA) while CO and C_xH_y significantly decreased. The NO concentration decreased up to 27% (from 166 to 121 ppm) when combustor was operated at EA=40% and SA=0.3

In the vortexing FBC (VFBC), Chyang et al., [4] studied combustion characteristics of corncob in three combustion modes; included direct combustion, staged combustion and flue gas recirculation (FGR). From the tests, the NO emission could be reduced 15% by staging combustion while 30% in



FGR mode. Duan et al., [8] conducted the experimental tests for firing peanut shell in the same combustor as Chyang [4] and found that, CO emission decreased with the excess air, and secondary air while NO emission showed an inverse trend. Combustion efficiency significantly increased for increasing of secondary air. Duan et al., [9], performed the tests to study the formation of the major gaseous pollutants (CO and NO) in the VFBC when firing rice husk with flue gas recirculation. The experiment tests were conducted at fixed primary gas flow rate of 3 Nm³/min and fixed secondary gas flow rate of 2 Nm³/min. The excess oxygen ratio was ranged from 40–70%, and the in-bed stoichiometric oxygen ratio was ranged from 70–100%. The results showed that, CO emission increased with in-bed stoichiometric oxygen ratio, and NO emission showed inverse trend. The maximum temperature was observed at bed surface due to high volatile content of rice husk.

Madhiyanon et al., [11] studied emission characteristics of rice-husk in a short-combustion-chamber fluidized-bed combustor. In this investigation, primary airflow velocity was in the range of 1–2 m/s, while secondary and tertiary air were in the range of 7.8–8, and 13.6–15 m/s, respectively. The result showed that combustion zone occurred in the lower combustor. The bed temperature decreased with the increasing of primary air velocity due to insufficient resident time.

In this study, the experimental work was aimed to observe the effects of operating condition on combustion characteristics and emission performance with firing rubberwood sawdust in a the twin-cyclonic swirling fluidized-bed combustor. The temperature and emissions concentration were gathered along the combustor as well as the stack. Moreover, the combustion efficiency was also discussed.

II. MATERIALS AND METHODS

A. Materials

Rubberwood sawdust particles of average size 0.599 mm with bulk density 135.36 kg/m³ were fired as the biomass fuel in the experiments. Silica sand of 450–550 µm particle size was used as the inert bed materials at 30 cm static bed height. Table I presented the proximate and ultimate analysis as well as the lower heating value, of rubberwood sawdust used in the tests.

B. Combustor test facility

Fig 1 shows the components of this experimental set-up included the twin-cyclonic swirling fluidized-bed combustor (TSFBC) equipped with an annular spiral air distributor, a start-up burner, a cyclone, a fuel screw feeder, and blowers. The combustor consisted of 7-mm-thick, and it was completely insulated to avoid the convection and radiation heat losses with a 100-mm-thick refractory cement. The annular spiral air distributor made from eleven blades at an

angle of 14° to the horizontal (swirl number 2.76) was installed at bottom the combustor.

The lower combustor and upper combustor was connected with connecting pipe (diameter 200 cm). The primary air (PA) was supplied by a 10-hp blower while secondary air (SA) was controlled by a 7.5-hp blower. The secondary air was tangentially injected into the combustor. The lower secondary air was injected at (Z = 0.5 m) and upper secondary air was injected at (Z = 1.6 m) with 10-cm pipe diameter above annular spiral air distributor. At each layer had two pipe in opposite side for inject second air. The lower and upper side.

The temperatures were measured with the seven stationary Chromel-Alumel thermocouples (of type K) along the combustor height at 0.23, 0.46, 0.95, 1.47, 1.85, 2.08 and 2.57 m above the air distributor. The gas concentrations were analysed along axial direction of combustor, including emission gas on a stack. A “Testo-350XL” gas analyzer (Testo, Germany) was used to measure the temperature and gasconcentrations, with the measurement accuracies were ±0.5% for the temperature, ±5% for CO and C_xH_y ranged from 100 to 2000 ppm, ±10% for CO and C_xH_y higher than 2000 ppm, ±5% for NO, and ±0.2 vol.% for O₂.

C. Experimental planning

The experimental tests were conducted to examine the major emissions and efficiency performance of the combustor including studied concentration profiles for emission (CO, and NO), temperature and O₂ profiles along the combustor height. The rubberwood sawdust was burned at the fixed feed rate (FR), 20 kg/h, and excess air (EA) was controlled at about 20–80 %. To avoid the defluidization of bed material due to the low primary air supply, the maximum secondary to total air ratio (S/T) was controlled at 0.5

To determine excess air for each trials, the O₂ and CO concentrations were measured in the flue gas at the stack outlet, and EA was calculated by the following equation:

$$\alpha = \frac{21}{21 - (O_2 - 0.5CO)} \quad (1)$$

In this study, the combustion efficiency η_c was calculated using heat-loss method. This method had two parts of major loss, heat loss due to incomplete combustion of CO (%), and heat loss due to incomplete combustion of carbon. Therefore, η_c was calculated by following equation :

$$CombustionEfficiency = 100 - (q_{uc} + q_{ic}) \quad (2)$$

Where :

- q_{uc} heat loss of non-combustible carbon (%)
- q_{ic} heat loss of incomplete combustion (%)



Table I Proximate and ultimate analyses of rubberwood sawdust

Biomass Fuel	Ultimate analysis basis (wt. %, as-received basis)					Proximate analysis basis (wt. %, as-received basis)				Heating value (MJ/kg)	
	C	H	O	N	S	W	A	VM	FC	HHV	LHV
Sawdust	43.24	6.61	48.20	0.17	0.00	9.36	1.78	74.71	14.15	16.74	15.36

Heat loss of non-combustible carbon (q_{uc}) was incomplete combustion of carbon in fly ash. It was quantified by following equation:

$$q_{uc} = \frac{32,866}{LHV} \left(\frac{C_{fa}}{100 - C_{fa}} \right) A \quad (3)$$

Where:

LHV low heating value (kJ/kg)

C_{fa} unburn carbon on cottom ash (wt. %)

A ash on proximate analysis basis (wt %)

Heat loss of incomplete combustion (q_{ic}) was quantified as the percentage of LHV based on the CO from the combustor (both in ppm, on a dry gas basis and at 6% O₂) by the following equation:

$$q_{ic} = (126.4CO)_{@6\%O_2} 10^{-4} V_{dg@6\%O_2} \left(\frac{100 - q_{uc}}{LHV} \right) \quad (4)$$

Where:

$CO_{@6\%O_2}$ cabon monoxide from major emission dry g

$V_{dg@6\%O_2}$ volume of dry fule gas at 6% O₂

III. RESULT AND DISCUSSION

A. Temperature and oxygen concentration profile

Fig.2 shows the axial temperature and O₂ concentration profiles in TSFBC for firing rubberwood sawdust at excess air about 40% and secondary air 0–0.5. In this study, rubberwood sawdust was fed between upper secondary air injector and lower secondary air injector at 0.95 m above air distributor. The secondary air injection showed the slightly effect on the temperature profiles. As can be seen, the temperature was highest at in splashing zone (feed point) due to 1) high volatile matter of fuel particles and 2) vigorously firing of elevated lightweight particles. Similary to the research work conducted by Duan et al., [9] the maximum temperature also found in this area. The O₂ concentration profiles gradually decreased along the combustor height, however, the secondary air injection had the effect to increase the O₂ concentration for all tests at the free board region. On the other hand, effects of secondary air injection on the O₂ concentration seems to be insignificant in the splashing zone.

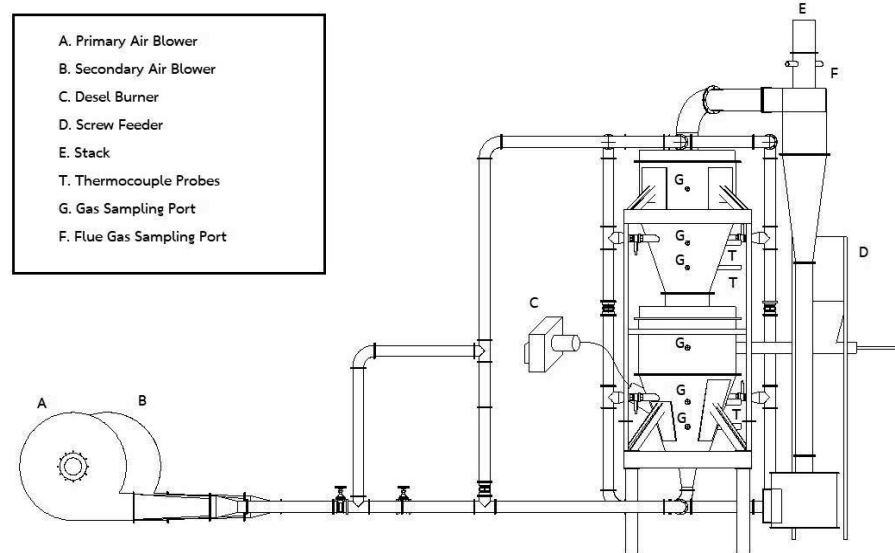


Fig. 1. Schematic diagram of twin-cyclonic swirling fluidized-bed combustor (TSFBC)

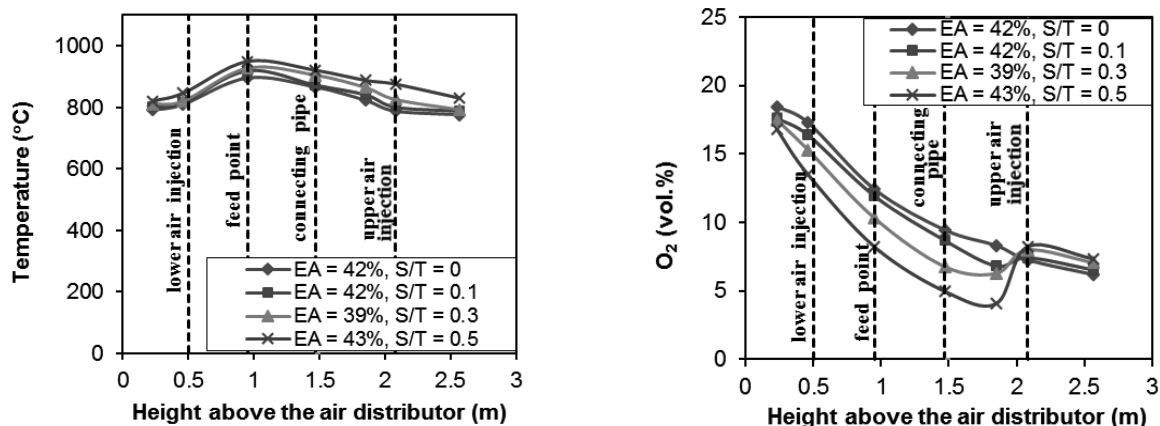


Fig. 2. Effects of the secondary to total air ratio on the axial temperature (a) and O₂ concentration (b) profiles in a twin-cyclonic swirling fluidized-bed combustor.

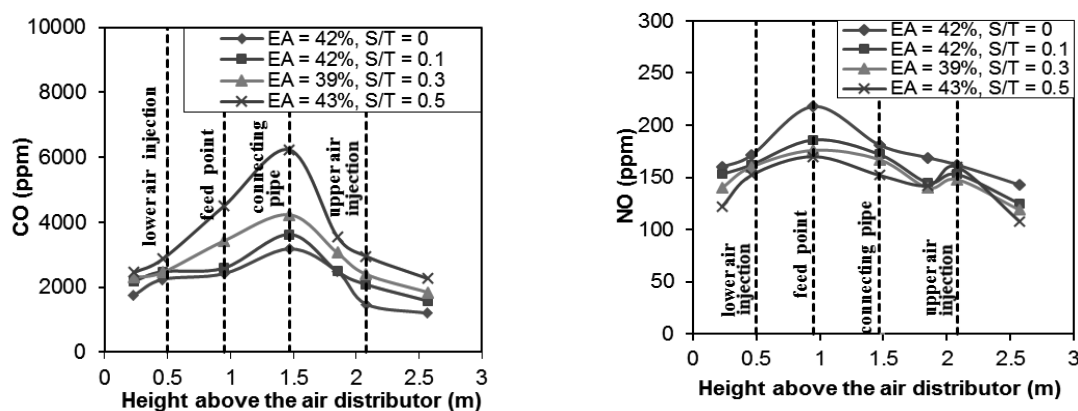


Fig. 3. Effects of the secondary to total air ratio on the CO (a) and NO (b) concentration profile in a twin-cyclonic swirling fluidized-bed combustor.

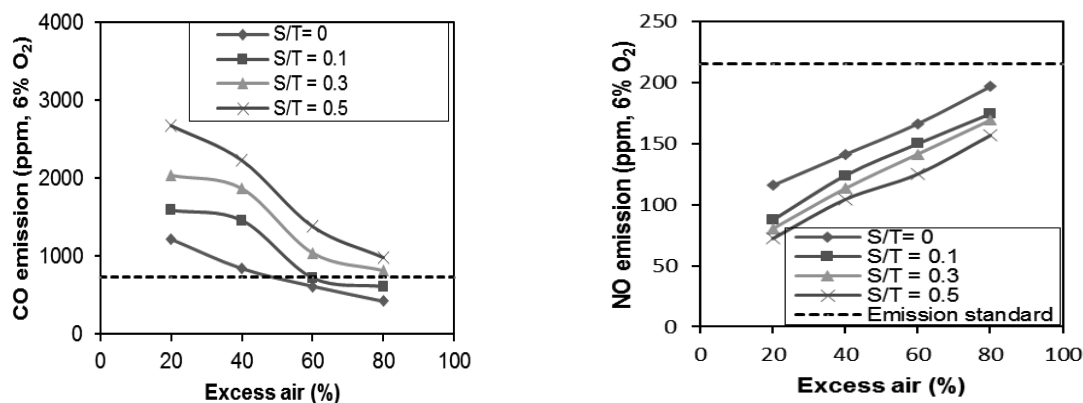


Fig. 4. Effects of the secondary to total air ratio on the major emission of CO (a) and NO (b) concentration from twin-cyclonic swirling fluidized-bed combustor with rubberwood sawdust.



B. Emission characteristics of air-staging combustion

Fig. 3 shows the axial CO and NO concentration profiles in the TSFBC at the same operating conditions as Fig. 2. As can be seen, the axial CO concentration profiles were found to have the maximum values at in the connecting pipe between lower and upper reactors (at $Z = 1.47$ m) for all of operating conditions. It can be explained that the fuel devolatilization normally occurred near fuel feeding level (at $Z = 0.95$ m), however, the combustion processes (formation and reduction) still continually occurred in the upper combustor. With increasing of S/T, the CO concentration was found to be increased at any location along the height of the combustor. To increase S/T at the same EA, primary air decreased, while secondary air increased to fixed total air at the same flow rate. Therefore, the reduction of CO oxidation rate can be described by the lower primary air, and too-short resident time for complete burning of combustible matter.

Fig. 4. Effects of the secondary to total air ratio on the major emission of CO (a) and NO (b) concentration from twin-cyclonic swirling fluidized-bed combustor with rubberwood sawdust. The axial NO concentration profiles were also found to have the maximum concentration at connecting pipe region ($Z = 1.47$ m) as CO for all of operating conditions. For all experimental tests, the axial NO concentration was found to be decreased along the height of the lower reactor, and increased again in the upper reactor after secondary air injection. As seen from the experimental results, with an increasing of S/T NO concentration at each level of the combustor can be controlled by the decomposed reactions with CO.

C. Major emission combustion efficiency

Fig. 4 shows effects of excess air and secondary to total air ratio on the CO and NO emissions from the conical TSFBC firing rubberwood sawdust at fuel feed rate 20 kg/h. Like the other studies on biomass combustion in fluidized-bed combustion systems, the excess air and secondary air seems to be the important parameter to control CO and NO emissions.

The results showed that with rising S/T at fixed EA, the CO emission was found to be increased, vice versa with NO emission that was found to be decreased. Meanwhile, for the rising S/T at fixed EA, the CO emission was found to be increased, however, NO emission has inverse trend. As reveal from the experimental results for all tests, to satisfy Thai emission standard for firing rubberwood sawdust in this combustor, excess air should be limited in the range of 60–80% and S/T should not exceed 0–0.1.

Table II shows combustion efficiency and major emissions at the stack outlet. Combustion efficiency was calculated by indirect heat loss method, with respect to heat losses due to unburned carbon and incomplete combustion. The combustion efficiency depended on excess air and secondary air ratio. Unburned carbon (q_{uc}) from these experimental tests was small in the range 0.04–0.25%, while incomplete combustion (q_{ic}) has more significant impact at 0.58–2.51%. It can be seen in Table 2 that with an increasing of secondary ratio, combustion efficiency was found to be decreased. Conversely with excess air. In this study of firing rubberwood sawdust in the TSFBC, the combustion efficiency was found to be in the range of 97.29–99.38%

Table II Emission and combustion efficiency of twin-cyclonic swirling fluidized-bed combustor for variable operating condition.

FR (kg/h)	S/T	EA (%)	O ₂ (%)	Emission (ppm)		C _{fa} (%)	q _{uc} (%)	q _{ic} (%)	Combustion efficiency (%)
				CO	NO				
20	0	22	3.79	1219	116	1.05	0.04	1.14	98.82
		42	6.21	843	141	2.84	0.11	0.92	98.97
		59	7.79	617	166	0.75	0.03	0.76	99.22
		78	9.20	424	197	0.94	0.04	0.58	99.38
20	0.1	20	3.50	1591	87	6.07	0.25	1.47	98.29
		42	6.21	1461	124	1.41	0.05	1.60	98.35
		61	7.96	725	150	1.28	0.05	0.90	99.05
		80	9.33	612	174	1.10	0.04	0.85	99.11
20	0.3	21	3.64	2038	80	1.52	0.06	1.90	98.04
		39	5.89	1868	113	1.15	0.04	2.00	97.96
		58	7.71	1043	141	0.65	0.02	1.27	98.70
		80	9.33	817	169	0.85	0.03	1.13	98.83
20	0.5	22	3.79	2675	72	5.09	0.20	2.51	97.29
		43	6.31	2229	104	1.96	0.08	2.46	97.47
		56	7.54	1383	125	1.68	0.07	1.66	98.27
		79	9.27	984	157	2.81	0.11	1.36	98.53



IV. CONCLUSIONS

From the experimental results, emission characteristics was indicated by axial temperature, O₂, CO, and NO concentration profiles. The CO emissions was increased with increasing secondary to total air ratio but CO emission decreased with increasing Excess air. And NO emission was showed the opposite trend. Considering the optimum operating for firing rubberwood sawdust seem to be in the range of excess air 60–80% and at S/T range 0–0.5. The emissions are emitted under Thailand emission standard and the combustion efficiency was found to be high at 97.29–99.38%.

ACKNOWLEDGMENTS

The authors wish to acknowledge financial supports from Department of Mechanical Engineering, Faculty of Engineering and Industrial Technology, Silpakorn University.

REFERENCES

- [1] V.I. Kuprianov., P. Arromdee., S. Chakritthakul., R. Kaewklum., and K. Sirisomboon. (2011). "Combustion of some Thai agricultural and wood residues in a pilot swirling fluidized-bed combustor," World Renewable Energy Congress-Sweden.
- [2] L.H. Zhang., C.S. Chyang., F. Duan., and P.S. Li., "Comparison of the thermal behaviors and pollutant emissions of pelletized bamboo combustion in a fluidized bed combustor at different secondary gas injection modes," *Energy*, Vol.116, pp. 306-316, 2016.
- [3] S. Chakritthakul., and V.I. Kuprianov., "Co-firing of eucalyptus bark and rubberwood sawdust in a swirling fluidized-bed combustor using an axial flow swirler," *Bioresour Technol*, Vol.102, pp. 8268-8278, 2011.
- [4] C.S. Chyang., F. Duan., S.M. Lin., and J. Tso., "A study on fluidized bed combustion characteristics of corncob in three different combustion modes," *Bioresour Technol*, Vol.116, pp. 184-189, 2012.
- [5] V.I. Kuprianov., and W. Permchart., "Emissions from a conical FBC fired with a biomass fuel," *Applied Energy*, Vol.74, pp. 383-392, 2003.
- [6] V.I. Kuprianov., R. Kaewklum., and S. Chakritthakul., "Effects of operating conditions and fuel properties on emission performance and combustion efficiency of a swirling fluidized-bed combustor fired with a biomass fuel," *Energy*, Vol.36, pp.2038-2048, 2011.
- [7] K. Sirisomboon., and P. Charemporn., "Effects of air staging on emission characteristics in a conical fluidized-bed combustor firing with sunflower shells," *Journal of the Energy Institute*, Vol.90, pp. 316-323, 2017.
- [8] F. Duan., C.S. Chyang., Y.J. Wang., and J. Tso., "Effect of secondary gas injection on the peanut shell combustion and its pollutant emissions in a vortexing fluidized bed combustor," *Bioresour Technology*, Vol.154, pp. 201-208, 2014.
- [9] F. Duan., C.S. Chyang., S.M. Lin., and J. Tso., "Experimental study on rice husk combustion in a vortexing fluidized-bed with flue gas recirculation (FGR)," *Bioresour Technol*, Vol.134, pp. 204-211, 2013.
- [10] F. Duan., C.S. Chyang., Y. Chin., and J. Tso., "Pollutant emission characteristics of rice husk combustion in a vortexing fluidized bed incinerator," *Journal of Environmental Sciences*, Vol.25, pp. 335-339, 2013.
- [11] T. Madhiyanon., P. Sathitruangsak, and S. Soponronnarit, "Combustion characteristics of rice-husk in a short-combustion-chamber fluidized-bed combustor (SFBC)," *Applied Thermal Engineering*, Vol.30, pp. 347-353, 2010.
- [12] S. Hussachu., and P. Arromdee., "Effects of Secondary Air on Combustion Efficiency and Emission Performance of a Twin-cyclonic Swirling Fluidized-bed Firing with Shredded Peanut Shells," *The 9th International Conference on Sciences, Technology and Innovation for Sustainable Well-Being (STISWB 2017)*.



The Improvement of Biomass Properties by Torrefaction Rotary Kiln

Nattarat Chutwiboonkun, Nattawut Tharawadee*

Department of Mechanical Engineering, Faculty of Engineering and Industrial Technology, Silpakorn University
Sanamchandra Campus, Rachamanka Rd., Muang district, Nakhonpathom 73000

*aeygamer@hotmail.com

Abstract— This research studies the effect of torrefaction process by using rotary kiln on torrefied biomass properties. Corncob was used in this research. In this research the effect of torrefaction temperature and rotation speed of the rotary kiln on biomass properties were investigated. The torrefaction rotary kiln (6 meters length and 0.3 meters diameter) was used in this research. Liquid petroleum gas was selected as heat source. The temperature of torrefaction process were set at 230, 250 and 270 degrees Celsius. The rotation speed was at 1, 2 and 3 rpm. The temperature distribution, temperature profile, characteristic of torrefied biomass, moisture content, particle distribution, mass yield and energy yield reported. It was concluded that, the rotary kiln can be used for torrefaction process. The biomass after torrefaction with torrefaction rotary kiln was uniform product. The moisture content of torrefied product was sharply decrease. The particle size after torrefaction was smaller than raw biomass. The large particle size was sharply decrease (>3.35 mm) and the smaller particle was slightly increase (1.7-3.35 mm). The mass yield and energy yield were decrease when the torrefaction was increase. On the other hand, the mass yield and energy yield were increase when rotation speed was increase. It was concluded that, the optimum condition of torrefied corncob in this research was 230 °C with 3 rpm.

Keywords—torrefaction process; rotary kiln; mass yield; energy yield

I. INTRODUCTION

At the present, energy is the main factor to response the demand for human. The trend of energy consumption has been increasing steadily. Therefore, renewable energy was focused for people around the world. Biomass energy is the one of renewable energy widely used. Biomass is a storage of natural energy in the form of organic matter. It can convert to energy and fuel in many form [1]. However, biomass has some weakness such as high moisture content, low energy density, inhomogeneous, low heating value and difficult to storage. The torrefaction process has been developed to solved this problem. Torrefaction process was a mild thermal pretreatment in temperature range 200 to 300 degree Celsius (oxygen-free atmosphere) [2-4]. So, the disadvantage of biomass was solved by torrefaction process [5-6]. However, it has many parameters to effect on torrefaction process such as raw material, residence time, temperature and torrefaction time. Many researches were studied about the temperature of torrefaction process on biomass properties. Md. Ahiduzzaman

et al. [7] was investigated the effect of temperature on the torrefied biomass properties. They were found the temperature have some effects on biomass properties. When the temperature was increase, moisture content, ash, higher heating value (HHV), mass yield and energy yield have been changed. Rice husk was used in this experimental. When the temperature was increase, the mass yield and moisture content of torrefied biomass was decrease. Ash was increase too. Baptiste Colin et al, [8] the effect of operating parameter (temperature, residence time, solid-hold up) on properties of torrefied biomass. Beech wood was used in this experimental. The mass yield and volatile matter of torrefied product was decrease when the temperature increase.

The torrefaction reactor was used for torrefaction process. It has some many kind of reactor for torrefaction process [9]. The fixed bed torrefaction reactor is the simplest reactor. The biomass was filled inside the reactor and was heated up from the heat source outside surface of reactor. The water molecules inside biomass was vibrated by electromagnetic wave. Then, the temperature of biomass was increase. Fluidized bed torrefaction reactor is the one type of torrefaction reactor. The raw biomass was placed on the grate. The hot gas was flown from the bottom through the raw biomass bed. The raw biomass floated and behaved like a fluid. However, the torrefied biomass form torrefaction reactor as mentioned before was non-uniform product.

Rotary kiln was widely used in industrial because rotary kiln can distribute the heat thoroughly to the biomass. The heat transfer in the material was conduction and radiation [10]. The pilot rotary kiln was established and studied for torrefaction process. The torrefied product form rotary kiln was uniform product.

In this research, the effect of temperature and rotation speed on biomass properties was studied by using rotary kiln. The temperature distribution, characteristic of torrefied biomass, moisture content, particle distribution, mass yield and energy yield have been investigated in this experiment.



II. MATERIAL AND METHOD

A. Raw material preparation

The corncob was used in this research. Before torrefaction process, raw material was mince to 5 mm to reduce its size. Initial moisture content of raw material was 12 ± 0.6 % wet basis. An initial condition of biomass was shown in table I.

Table I. Raw material preparation

Parameters	condition
Biomass	corncobs
Initial moisture content	12 ± 0.6 %
Particle size	≤ 5 mm.
Higher Heating Value (HHV)	16.47 MJ/kg (raw material)
Inclination angle	2 degrees form horizontal
Controlled temperature	230 250 and 270 °C
Rotation speed	1 2 and 3 rpm

B. Torrefaction experiment

Torrefaction rotary kiln was used for the torrefaction as shown in Figure.1. The pilot torrefied rotary kiln consists of the rotating cylinder. The cylinder is 6 meters length and 0.3 meters diameter. The L-shape lifters were attached inside the cylinder. The cylinder was used to convey a biomass and cover with 0.5 m diameter cylinder. The hopper was used in a feeding system (feed rate 4 kg/hours). Liquid petroleum gas was used for heat source. The rotation speed was varied at 1, 2 and 3 rpm. The slope of rotary kiln was set at 2 degrees from horizontal. The temperature profile inside the rotary kiln was monitored by data logger (midi logger GL 820 accuracy $\pm 0.05\%$) and thermocouple type K (accuracy ± 1 °C). The reactor was setup at the end of rotary kiln. The reactor was heated up to torrefaction temperature. After the temperature of reactor was steady, the raw material was fed into the rotary kiln (4 kg/hours). The biomass and hot air was counter-current flow and not direct contact (to prevent an oxidation). Metal container was used to collect a torrefied biomass. The container is hermitically closed to avoid the oxidation of product during cooling.

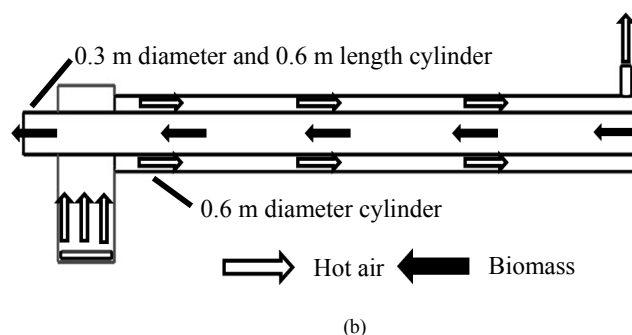
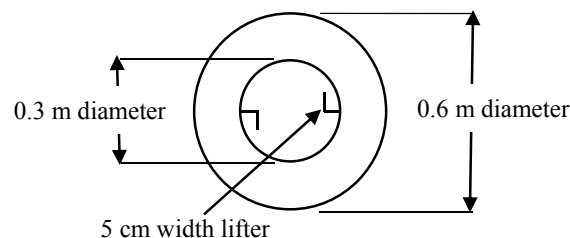
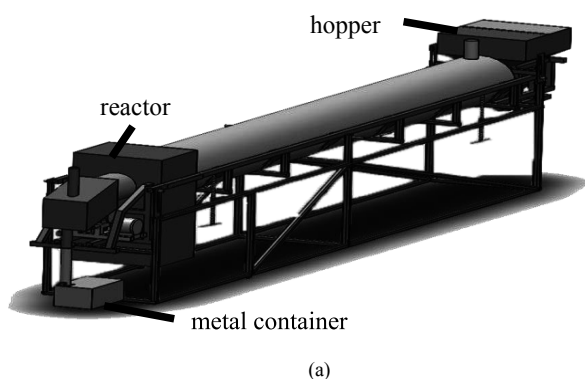


Fig.1. (a) torrefaction rotary kiln; (b) torrefaction rotary kiln in section view

C. Methodology

- Particle size distribution

Particle size distribution was determined by using ASTM D422 standard. Particle size was tested by 6 layers sieve analysis (sieve size 3.35 to 0.425 mm.). Particle size distribution can be calculated in equation 1.

$$\text{SIEVE (\%)} = (S/W) \times 100\% \quad (1)$$

Where, S is weight of sieve(g)

W is total weight (g)

- Moisture content

Moisture content was determined by using ASTM D2216-10 standard. Moisture content was collected by heating oven (Redline By Binder 230 volt, accuracy ± 0.3 °C). The biomass was drying at 105 °C for 24 hours. Moisture content can be calculated as follow:

$$M = ((W_0 - W_f) / W_0) \times 100\% \quad (2)$$

Where W_0 is initial weight (g)

W_f is final weight (g)

M is moisture content (%)



- Mass and Energy yield

The mass yield and energy yield can be calculated using the following equation:

$$Y_m = (M_t/M_r) \times 100\% \quad (3)$$

Where Y_m is mass yield (%)

M_t is mass of torrefied biomass (g)

M_r is mass of raw material (g)

$$Y_e = (HHV_t/HHV_r) \times Y_m \quad (4)$$

Where Y_e is energy yield (%)

HHV_t is higher heating value of torrefied biomass (MJ/kg),

HHV_r is higher heating value of raw material (MJ/kg)

III. RESULT AND DISCUSSIONS

A. Characteristics of raw biomass and torrefied biomass

Raw biomass and torrefied biomass was shown in Figure 2. The torrefied biomass from rotary kiln was uniform product. It was found that, the biomass after torrefaction was darker, smaller and brittle than raw biomass. The similar result has also been observed by other researcher [11]. moisture content of raw biomass and torrefied biomass was shown in Figure 3. the moisture content of torrefied biomass was less than raw biomass. the moisture content of raw biomass was 11.93%. The moisture content of torrefied biomass was 3.83 %. The moisture of torrefied biomass was less than raw biomass 67.89%. After torrefaction the moisture content was removed. The similar result has also been observed by other [6]. The moisture content of torrefied biomass was less than raw biomass.



(a)



(b)

Fig. 2. (a) raw biomass (b) torrefied biomass

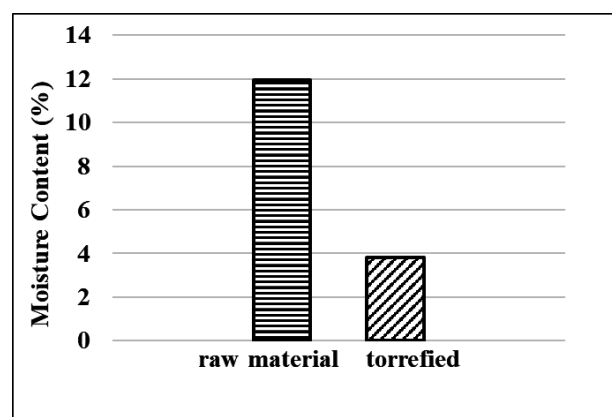


Fig. 3. Moisture content

B. Temperature distribution in rotary kiln

The temperature distribution in rotary kiln for torrefaction process was shown in Figure 4. The temperature distribution was collected in a steady state. It was found that, the temperature distribution in rotary kiln was divided into 3 zones. The first zone was heating zone. The heating zone temperature was around 100 – 200 °C. the moisture content in biomass was evaporated. After that, the biomass was flown into torrefaction zone. The torrefaction zone temperature was around 200 – 300 °C. The average torrefaction temperature at the reference point were 231.63, 250.01 and 270.42 °C respectively. Meanwhile, dehydration, dihydroxylation, and decarboxylation reaction were generated. Finally, the biomass was flown through the third zone. The third zone was cooling zone (metal container). The temperature inside ware decrease along the distance between the reactor and hopper. Thus, the torrefaction process was normally operated by the pilot torrefaction rotary kiln. The container is hermitically closed to avoid the oxidation of product during cooling.

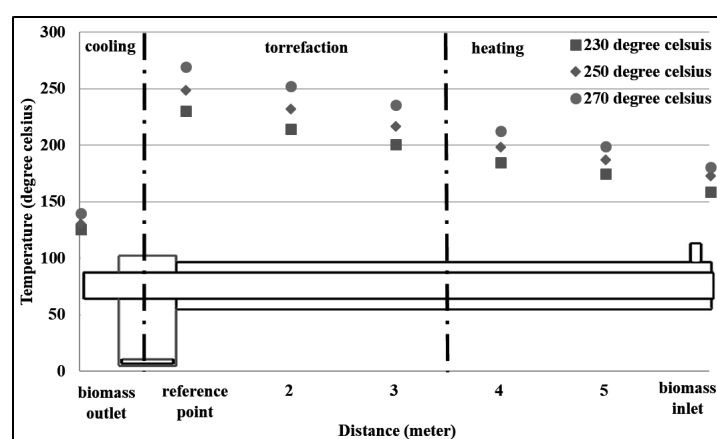
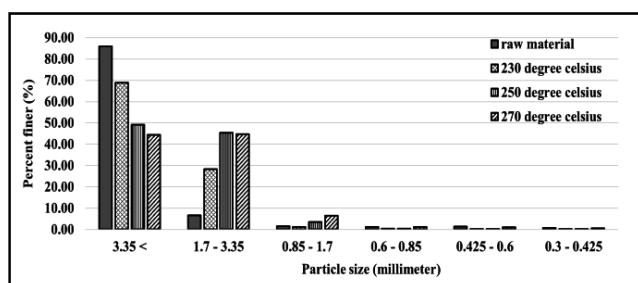


Fig. 4. Temperature distribution in rotary kiln

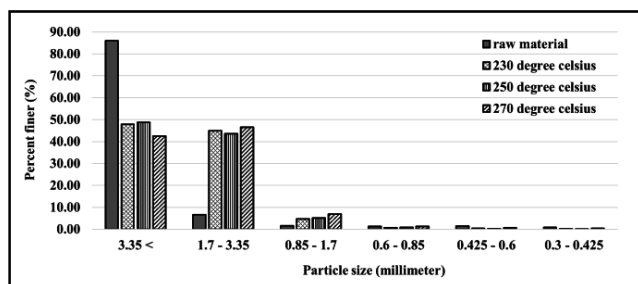


C. Particle size distribution

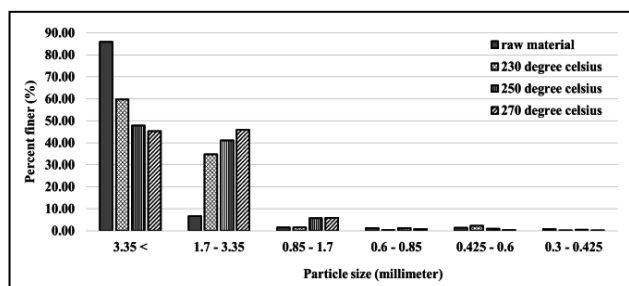
The particle size distribution of raw material and torrefied biomass were investigated. Figure 5(a), 5(b) and 5(c) were shown particle distribution at 1, 2 and 3 rpm respectively. The highest amount of particle size in raw material was observe at >3.35 mm. After torrefaction process, the particle size of torrefied biomass was smaller than raw biomass. The percentage of large particle decrease when the torrefaction temperature increase. The degradation of biomass was occurred between torrefaction process. The degradation was a decomposition reaction of cellulose, hemicellulose and lignin in biomass [12]. At 1 rpm, the large particle was sharply decrease (>3.35 mm.) and the smaller particle was slightly increase (1.7 – 3.35 mm.). At the 2 and 3 rpm have the same trend with 1 rpm. It was concluded that, particle size of biomass after torrefaction process was smaller than raw biomass. The similar result has also been observed by others [13-15]. Figure 5(d), 5(e) and 5(f) was shown particle size distribution at 230, 250 and 270 °C respectively. The residence time of process increase when the rotation speed of rotary kiln decrease. At the low rotation speed, the biomass in rotary kiln was heat longer than high rotation speed. As a result, the degradation was increased depend on residence time. The smaller particle size was increase when the rotation speed decrease. At 230 °C, the large particle was sharply decrease (>3.35 mm.) and the smaller particle was slightly increase (1.7 – 3.35 mm.). At the 250 and 270 °C have the same trend with 1 rpm. It was concluded that, the torrefaction temperature and rotation speed have effect on particle distribution. At the high temperature and low rotation speed, the large particle was decrease and the small particle was increase.



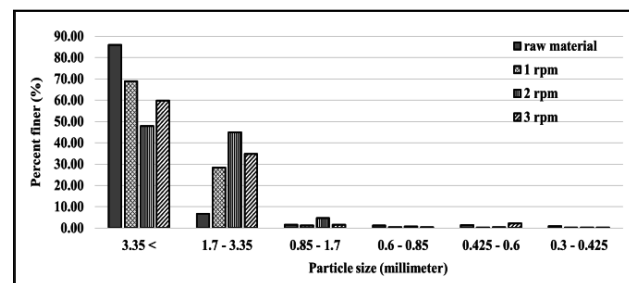
(a) particle size distribution at 1 rpm



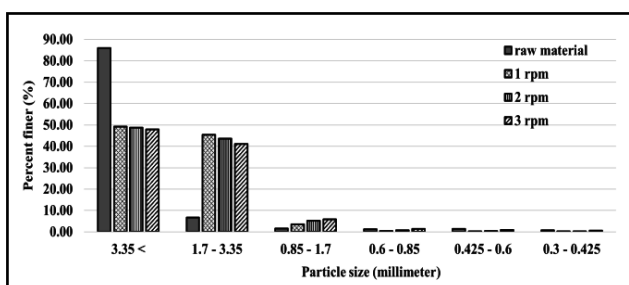
(b) particle size distribution at 2 rpm



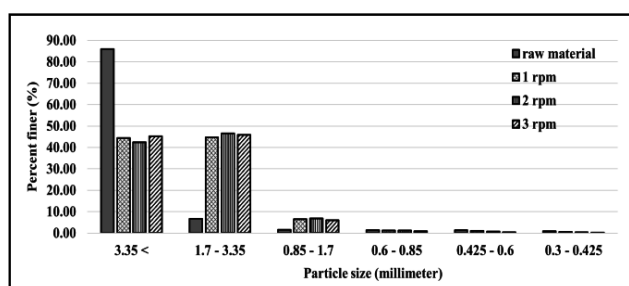
(c) particle size distribution at 3 rpm



(d) particle size distribution at 230 °C



(e) particle size distribution at 250 °C



(f) particle size distribution at 270 °C

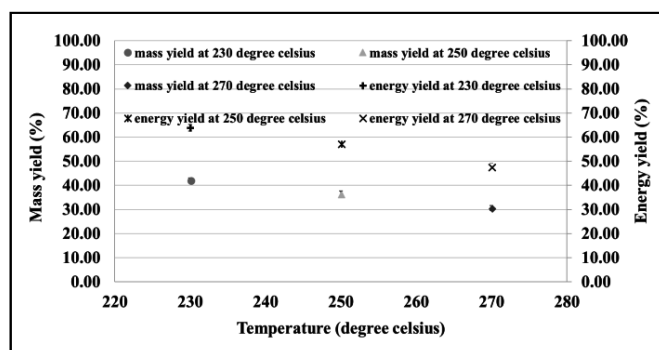
Fig. 5. particle size distribution

D. Mass yield and energy yield

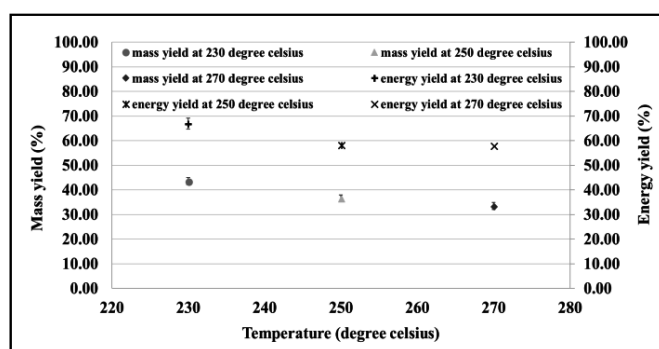
The effect of torrefaction temperature on mass yield and energy yield at 1,2 and 3 rpm was shown in Figure 6(a), 6(b) and 6(c) respectively. The torrefaction temperature had more impact on mass yield. The mass yield of torrefied product was decrease when the torrefaction temperature was increase.



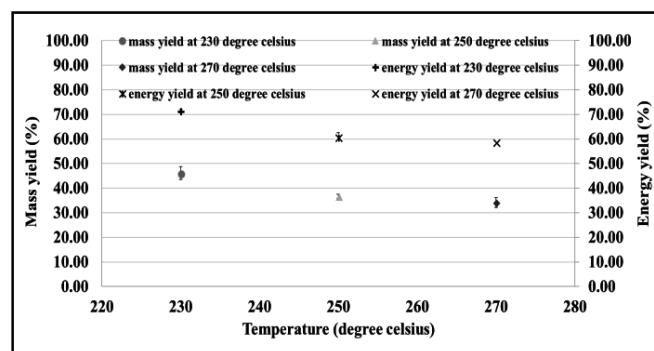
Moisture content and volatile matter were removed during torrefaction process. The degradation was a decomposition reaction of cellulose, hemicellulose and lignin in biomass. At 1 rpm, mass yield was found to be 42.20%, 36.48% and 30.60% for 230, 250 and 270 °C respectively. At 2 rpm, mass yield was found to be 43.63%, 36.67% and 33.50% for 230, 250 and 270 °C respectively. At 3 rpm, mass yield was found to be 46.08%, 36.69% and 34.14% for 230, 250 and 270 °C respectively. The highest mass yield was found at 3 rpm with 230 °C. the mass yield was decrease with increasing torrefaction temperature. Similar results were report for other type of biomass such as torrefied rice husk [16-18]. The energy yield was indicated the improvement of torrefied biomass. After torrefaction process, heating value of torrefied biomass was increase. The energy yield was shown a trend similar to the mass yield. The energy yield of torrefied biomass was decrease when torrefaction temperature increase. At 1 rpm, energy yield was found to be 63.90%, 57.37% and 47.76% for 230, 250 and 270 °C respectively. At 2 rpm, energy yield was found to be 66.91%, 58.34% and 57.98% for 230, 250 and 270 °C respectively. At 3 rpm, energy yield was found to be 71.27%, 60.75% and 58.75% for 230, 250 and 270 °C respectively. The highest energy yield was found at 3 rpm with 230 °C. The similar result has also been observed by others [19-20]. It was concluded that, the optimum condition was 3 rpm with 230 °C.



(a) Mass yield and energy yield at 1 rpm



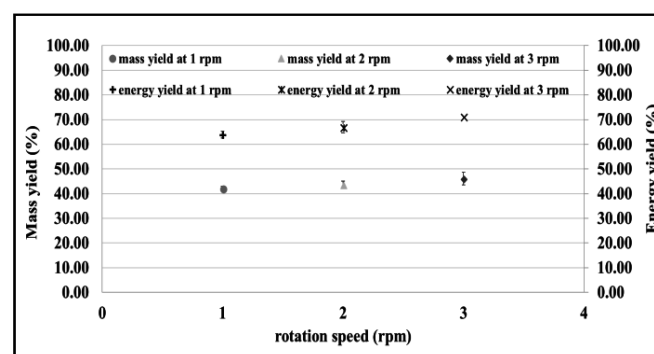
(b) Mass yield and energy yield at 2 rpm



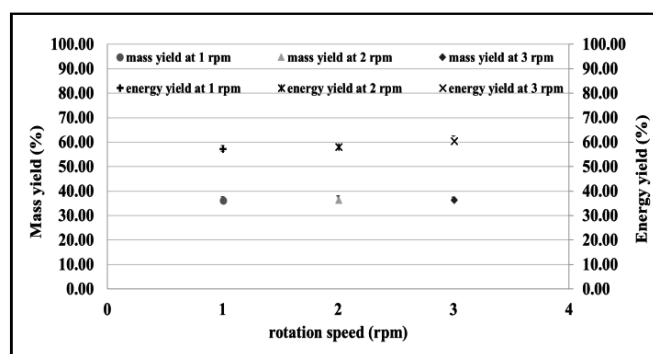
(c) Mass yield and energy yield at 3 rpm

Fig.6. Mass yield and Energy yield at 1, 2 and 3 rpm

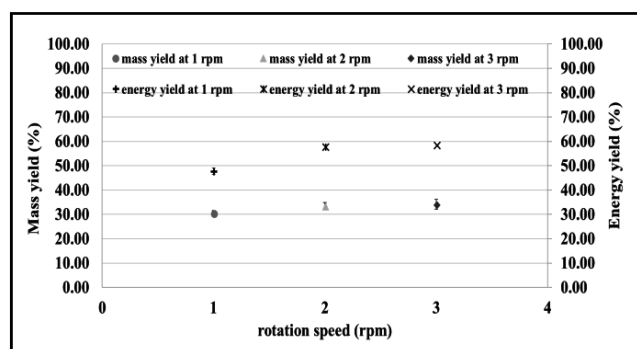
The effect of rotation speed on mass and energy yield was shown in Figure 7(a), 7(b) and 7(c) respectively. The mass yield of torrefied biomass was increase with increasing rotation speed. At the high rotation speed, the residence time of biomass in rotary kiln was less than low rotation speed. At low rotation speed, moisture content and volatile matter was removed more than high rotation speed. At 230 °C, mass yield was found to be 42.40%, 43.63% and 46.08% for 1, 2 and 3 rpm respectively. At 250 °C, mass yield was found to be 36.48%, 36.67% and 36.69% for 1, 2 and 3 rpm respectively. At 270 °C, mass yield was found to be 30.60%, 33.50% and 34.18% for 1, 2 and 3 rpm respectively. The energy yield was shown a trend similar to the mass yield. The energy yield of torrefied biomass was increase when the rotation speed increase. At 230 °C, energy yield was found to be 63.90%, 66.91% and 71.27% for 1, 2 and 3 rpm respectively. At 250 °C, energy yield was found to be 57.37%, 58.34% and 60.75% for 1, 2 and 3 rpm respectively. At 270 °C, energy yield was found to be 47.76%, 57.98% and 58.75% for 1, 2 and 3 rpm respectively. It was concluded that, the optimum condition was 230 °C with 3 rpm.



(a) Mass yield and Energy yield at 230 °C



(b) Mass yield and Energy yield at 250 °C



(c) Mass yield and Energy yield at 270 °C

Fig.7. Mass yield and Energy yield at 230, 250 and 270 °C

IV. CONCLUSION

The pilot scale rotary kiln for torrefaction process was established. The torrefaction process was normally operated by using the torrefaction rotary. The temperature distribution, characteristic of torrefied biomass, moisture content, particle distribution, mass yield and energy yield were studied in this research. It was concluded that, the rotary kiln can be used for torrefaction process. The biomass product after torrefied process has uniform quality. The moisture content of torrefied product was sharply decrease. The particle size after torrefaction was smaller than raw biomass. The large particle size was sharply decrease (>3.35 mm) and the smaller particle size was slightly increase (1.7-3.35 mm). The mass yield and energy yield were decrease when the torrefaction was increase. On the other hand, the mass yield and energy yield were increase when rotation speed was increase. It was concluded that, the optimum condition of torrefied corncob in this research was 230 °C with 3 rpm.

ACKNOWLEDGMENT

The authors wish to acknowledge the financial support from Department of Mechanical Engineering, Faculty of Engineering and Industrial Technology and Silpakorn University Fund for Research and Creative work.

REFERENCES

- [1] A. Zheng, Z. Zhao, S. Chang, Z. Huang, F. He, H. Li, Effect of torrefaction temperature on product distribution from two-staged pyrolysis of biomass, *Energy and Fuels*. 26 (2012) 2968–2974.
- [2] S.W. Park, C.H. Jang, K.R. Baek, J.K. Yang, Torrefaction and low-temperature carbonization of woody biomass: Evaluation of fuel characteristics of the products, *Energy*. 45 (2012) 676–685.
- [3] W.H. Chen, P.C. Kuo, Torrefaction and co-torrefaction characterization of hemicellulose, cellulose and lignin as well as torrefaction of some basic constituents in biomass, *Energy*. (2011)
- [4] N. Soponpongpiat, D. Sittikul, P. Comsawang, Prediction model of higher heating value of torrefied biomass based on the kinetics of biomass decomposition, *J. Energy Inst.* 89 (2016) 425–435.
- [5] V. V. Kosov, V.A. Sinelshchikov, G.A. Sytchev, V.M. Zaichenko, Effect of torrefaction on properties of solid granulated fuel of different biomass types, *High Temp.* 52 (2014) 907–912.
- [6] J. Kihedu, Torrefaction and Combustion of Ligno-Cellulosic Biomass, *Energy Procedia*. 75 (2015) 162–167.
- [7] M. Ahiduzzaman, A.K.M. Sadrul Islam, Energy yield of torrefied rice husk at atmospheric condition, *Procedia Eng.* 105 (2015) 719–724.
- [8] B. Colin, J.L. Dirion, P. Arlabosse, S. Salvador, Experimental study of wood chips torrefaction in a pilot scale rotary kiln, *Chem. Eng. Trans.* 37 (2014) 505–510.
- [9] W. Junsatien, N. Soponpongpiat, S. Phetsong, Torrefaction reactors, *J. Sci. Technol. MSU*. 32 (2013).
- [10] A.A. Boateng, Rotary kilns transport phenomena and transport process.
- [11] W.H. Chen, H.C. Hsu, K.M. Lu, W.J. Lee, T.C. Lin, Thermal pretreatment of wood (Lauan) block by torrefaction and its influence on the properties of the biomass, *Energy*. 36 (2011) 3012–3021.
- [12] Y. Mei, R. Liu, Q. Yang, H. Yang, J. Shao, C. Draper, S. Zhang, H. Chen, Torrefaction of cedarwood in a pilot scale rotary kiln and the influence of industrial flue gas, *Bioresour. Technol.* 177 (2015) 355–360.
- [13] N. Tharawadee, N. Thuchayapong, Effects of Torrefaction Process on Physical Properties and Operating Cost of Biomass Powder, *Journal of research and Application in Mechanical engineering(JRAME)*, 3 (2015) 83-88
- [14] S. Zhang, T. Chen, Y. Xiong, Q. Dong, Effects of wet torrefaction on the physicochemical properties and pyrolysis product properties of rice husk, *Energy Convers. Manag.* 141 (2017) 403–409.
- [15] M. Phanphanich, S. Mani, Impact of torrefaction on the grindability and fuel characteristics of forest biomass, *Bioresour. Technol.* 102 (2011) 1246–1253.
- [16] M.J. Wang, Y.F. Huang, P.T. Chiueh, W.H. Kuan, S.L. Lo, Microwave-induced torrefaction of rice husk and sugarcane residues, *Energy*. 37 (2012) 177–184.
- [17] D. Chen, J. Zhou, Q. Zhang, X. Zhu, Q. Lu, Upgrading of rice husk by torrefaction and its influence on the fuel properties, *BioResources*. 9 (2014) 5893–5905.
- [18] D. Chen, J. Zhou, Q. Zhang, X. Zhu, Q. Lu, Torrefaction of rice husk using TG-FTIR and its effect on the fuel characteristics, carbon, and energy yields, *BioResources*. 9 (2014) 6241–6253.
- [19] S.X. Li, C.Z. Chen, M.F. Li, X. Xiao, Torrefaction of corncob to produce charcoal under nitrogen and carbon dioxide atmospheres, *Bioresour. Technol.* 249 (2018) 348–353.
- [20] J.J. Lu, W.H. Chen, Product yields and characteristics of corncob waste under various torrefaction atmospheres, *Energies*. 7 (2014) 13–27



Ultrasound-Assisted Acetylation of Glycerol for Triacetin Production over Green Catalyst

Surachai Karnjanakom

Department of Sustainable Industrial Management
Engineering (SIME), Faculty of Engineering,
Rajamangala University of Technology Phra Nakhon,
Bangkok 10300, Thailand
surachai.k@rmutp.ac.th

Guoqing Guan

Energy Conversion Engineering Group, Institute of
Regional Innovation (IRI), Hirosaki University,
2-1-3, Matsubara, Aomori 030-0813, Japan
guan@hirosaki-u.ac.jp

Chanatip Samart

Department of Chemistry, Faculty of Science and
Technology,
Thammasat University,
Pathumthani 12120, Thailand
chanatip@tu.ac.th

Panya Maneechakr

Department of Chemistry, Faculty of Science,
Rangsit University,
Pathumthani 12000, Thailand
panya.m@rsu.ac.th

Abstract—Upgrading of crude glycerol to high value-added chemical products is an attractive process in biomass conversion and biorefinery industry. In this work, production of triacetin from direct conversion of glycerol with acetic anhydride over SO₃H-glycerol-carbon catalyst assisted with ultrasound was investigated for the first time. The catalyst was also prepared from glycerol via *in-situ* carbonization and sulfonation. The triacetin selectivity (100%) was successfully achieved in mild conditions via acetylation reaction. The obtained results indicated that the contribution of catalyst acidity with ultrasonic power was responsible for determining triacetin selectivity.

Keywords—Triacetin; Glycerol; Carbon-based solid brønsted acid catalyst; Acetylation; Ultrasonic

I. INTRODUCTION

The demand of biodiesel production via transesterification of vegetable oils with methanol in the presence of alkali catalysts has attracted significant attention in recent years. Unavoidably, a large amount of crude glycerol was also produced as a by-product with an approximate portion equivalent to 10 wt.% of the total biodiesel produced [1]. However, the direct application of excess glycerol in industry might be not suitable due to its impurities including soap, methanol and water, leading to increasing of waste product in environment. Moreover, high cost for purification of glycerol is required in order to meet industrial grade (98% purity) [2]. Therefore, it is necessary to find new ways for effective utilization of glycerol. Recently, the chemical conversion of glycerol into high value-added chemical products via different reaction routes such as esterification, acetylation, dehydration and hydrogenolysis [3]. Among them, acetylation of glycerol with acetic acid into glycerol-esters (monoacetin (MAG), diacetin (DAG), and triacetin (TAG)) is more attractive. Preferably, TAG has been reported as the most attractive acetin due to its wide applications as building blocks of polyester and cryogenics, cosmetic and bio-fuel additives [4]. Many

researchers have tried to investigate this topic. In general, the glycerol acetylation can be easily catalyzed by homogeneously acidic catalysts such as H₂SO₄, H₃PO₄, HCl and/or acidic ionic liquids [5]. It is reported that the acidity of the catalyst is the key toward the selective formation of the favored DAG and TAG products. However, in an industrial process, the high corrosion to equipment, high toxicity to environmental and recycling difficulty of these homogeneously acidic catalysts always exist. From this point of view, the heterogeneous acid catalysts can be preferentially considered and applied since their environmental friendly. Many heterogeneous acid catalysts such as zeolites, Amberlyst-15, sulfated zirconia and sulfonic mesostructured silica have been found to exhibit good activity for catalyzing glycerol acetylation, however, low selectivity and stability for TAG production as well as high production cost hinder their applications [6]. As such, novel heterogeneous catalysts with high activity as well as high selectivity and stability should be developed and process enhancement should be considered.

In this study, glycerol acetylation with ultrasound assistance was investigated. The application of ultrasound may offer advantages, since the cavitation effect by it can create intense turbulence and liquid circulation at micro scale which could decrease the mass transfer resistance in the presence of heterogeneous catalysts, resulting in faster reaction rate and higher product yield. Moreover, herein, glycerol was also applied as a feedstock for preparing SO₃H-glycerol-carbon catalyst via *in-situ* carbonization and sulfonation processes. To the best of our knowledge, there is no information available concerning on this topic, especially for improving the selectivity of TAG in our system. The optimization for glycerol acetylation was systematically investigated with various parameters such as reaction time, reaction temperature, catalyst loading amount and ultrasonic power. We expected to provide a facile way for selective production of TAG and preparation of green catalyst from glycerol.



II. EXPERIMENTAL

A. Catalyst Synthesis

In-situ hydrothermal carbonization and sulfonation were applied for synthesis of SO₃H-glycerol-carbon catalyst. In brief, a certain mixture of glycerol with conc. H₂SO₄ was added into autoclave and heated at 150 °C for 24 h. Here, the mass ratio of H₂SO₄ to glycerol (2 to 1) was fixed in this work. Thereafter, the SO₃H-glycerol-carbon catalyst (black precipitate) was filtered, washed for several times with distilled water and ethanol to remove excess sulfate ions and finally dried in vacuum oven at 110 °C for 12 h. The physical and chemical properties of catalyst were investigated by N₂ sorption, thermogravimetry (TG), Fourier transform infrared spectroscopy (FT-IR), scanning electron microscopy (SEM) and titration analyses.

B. Catalytic Activity Test

The catalytic conversion of glycerol into acetylated products (MAG, DAG and TAG) was performed in a three-neck round bottom flask equipped with a reflux condenser and an ultrasonic horn as well as a thermocouple. In each batch, the stirring speed and the frequency of the ultrasonic probe were fixed at 650 rpm and 40 kHz, respectively. 5 g of glycerol, 0.25 g of catalyst and a certain amount of acetic acid (a molar ratio of acetic acid to glycerol = 8 to 1) were loaded into reactor. Then, reaction was conducted at different temperatures (60-120 °C), times (30-210 min) and ultrasonic powers (40-100 W) in an oil bath. After finishing reaction, the mixture product was cooled in an ice-bath. The spent catalyst was separated from liquid product by centrifugation, washed for several times with ethanol to remove the adsorbed by-products prior to reuse in the next run, and then dried at 110 °C for 12 h. The liquid product was analyzed by gas chromatography (GC, Agilent 7820A) equipped with a flame ionization detector (FID) and a capillary column (ZB5-HT, 30 m × 0.25 mm × 0.25 μm). The glycerol conversion and the product selectivity were quantified using external standard method and calculated using the following equations (1) and (2):

$$\text{Glycerol conversion (\%)} = \frac{\text{Mole percentage of glycerol reacted}}{\text{Mole percentage of initial glycerol}} \quad (1)$$

$$\text{Product selectivity (\%)} = \frac{\text{Mole percentage of product produced}}{\text{Mole percentage of glycerol reacted}} \quad (2)$$

III. RESULTS AND DISCUSSION

A. Characterization of As-Synthesized Catalyst

Textural properties and acidity of catalyst are shown in Table 1. As expected, the SO₃H-glycerol-carbon catalyst exhibited lower surface area, pore volume and pore size than glycerol-carbon, suggesting a well dispersion of sulfonic group functionalized on glycerol-carbon structure. The total acid amount on catalyst based on titration method was 3.68 mmol/g. As shown in Fig. 1, the existence of sulfonic group with its well distribution on glycerol-carbon structure was clearly observed in SEM-EDS image. The TG curve of catalyst is shown in Fig. 2. Here, the initial weight loss before temperature of 150 °C was due to the water desorption

from catalyst surface. As significantly observed, the weight loss at temperature range of ~250-450 °C was found, attributing to the main decomposition of sulfonic group on catalyst [7]. This indicates that the SO₃H-glycerol-carbon catalyst had thermal stability at a temperature close to 250 °C under oxygen free conditions. The FT-IR result is shown in Fig. 3. The strong bands at 1030 cm⁻¹ and 1175 cm⁻¹ could be identified as the stretching modes of sulfonic groups. Another band at 1701 cm⁻¹ could be attributed to the stretching mode of carboxylic group [8].

TABLE I. PHYSICO-CHEMICAL PROPERTIES OF CATALYST

Catalyst	Surface area (m ² /g)	Pore size (nm)	Total acidity (mmol/g)
Glycerol-carbon	57.1	9.7	0.34
SO ₃ H-glycerol-carbon	32.5	6.3	3.68

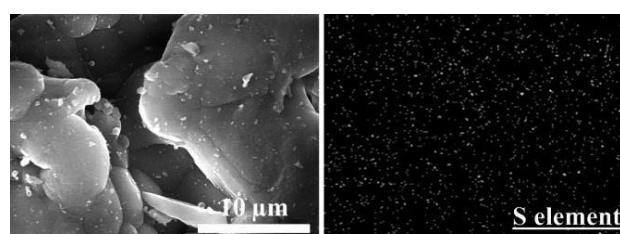


Fig. 1. SEM-EDS image of SO₃H-glycerol-carbon catalyst.

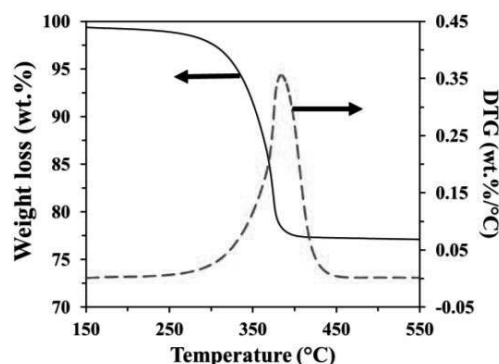


Fig. 2. TG curve of SO₃H-glycerol-carbon catalyst.

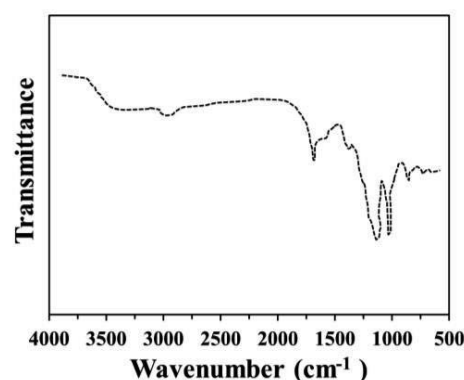


Fig. 3. FT-IR spectrum of SO₃H-glycerol-carbon catalyst.



B. Catalytic Acetylation of Glycerol

Fig. 4 shows the effect of reaction temperature on glycerol conversion into acetylated products. It should be noted that in this study, a molar ratio of acetic acid to glycerol used was 8 to 1, which was an excess amount (based on a consecutive three step stoichiometric reaction as 3 mol acetic acid to 1 mol glycerol, shifting the equilibrium forward to the TAG product. As observed, at a low temperature, the main product is MAG. Increasing the reaction temperature from 60 to 90 °C resulted in a substantial increase in glycerol conversion and DAG and TAG selectivity, suggesting that higher temperature enhanced the endothermic process and promoted further deprotonation of glycerol. The glycerol was completely converted with a best TAG selectivity (68%) was obtained at the optimum reaction temperature of 100 °C. The effect of reaction time and comparison of the obtained results using ultrasound assistance technique and conventional system are shown in Fig. 5. The conversion of glycerol and the selectivity of TAG increased to some extent with the increase in reaction time for both systems. Interestingly, much higher conversion of glycerol obtained due to the use of ultrasonic system could be attributed to the physical effects of the cavitation phenomena. It should be noted that the physical effects in terms of intense turbulence and microstreaming generated during the cavitation could play a dominating role in glycerol acetylation with acetic acid, resulting in faster reaction and higher TAG product when compared with the conventional system.

Based on the above results, the reaction conditions of 100 °C for 150 min were selected as the optimum conditions based on highest TAG selectivity for further study on the effect of ultrasonic power. Here, the ultrasonic power is considered to improve TAG selectivity by influencing the degree of glycerol acetylation processing. Fig. 6 shows the effect of ultrasonic power on glycerol conversion into acetylated products. With an increase in ultrasonic power from 40 W to 80 W, a steady increase in the TAG selectivity from 75.6% to 100% was found, indicating that the higher ultrasonic power enhanced the TAG yield due to the protonation of the remaining hydroxyl groups of glycerol molecule by interaction with the active sites on the catalyst surface.

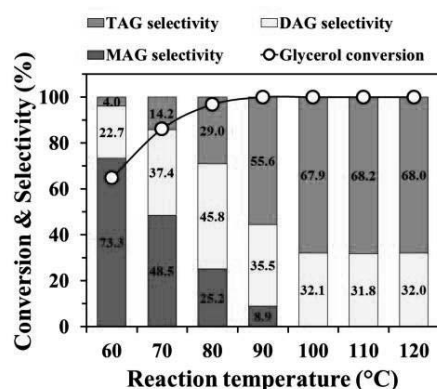


Fig. 4. Effect of reaction temperature on TAG production from catalytic conversion of glycerol over SO₃H-glycerol-carbon in ultrasonic system. Reaction conditions: catalyst = 5 wt.% of glycerol, molar ratio of acetic acid to glycerol = 8 to 1, reaction time = 90 min and ultrasonic power = 50 W.

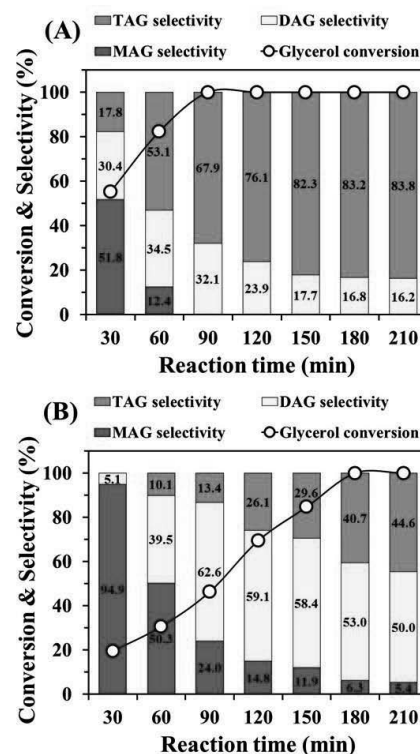


Fig. 5. Effect of reaction time on TAG production from catalytic conversion of glycerol over SO₃H-glycerol-carbon in (A) ultrasonic system and (B) reflux system. Reaction conditions: catalyst = 5 wt.% of glycerol, molar ratio of acetic acid to glycerol = 8 to 1, reaction temperature = 100 °C and ultrasonic power = 50 W.

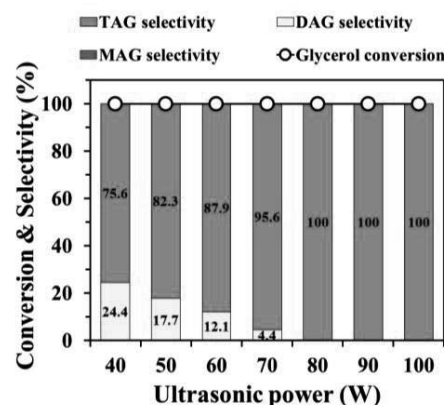


Fig. 6. Effect of ultrasonic power on TAG production from catalytic conversion of glycerol over SO₃H-glycerol-carbon in ultrasonic system. Reaction conditions: catalyst = 5 wt.% of glycerol, molar ratio of acetic acid to glycerol = 8 to 1, reaction temperature = 100 °C and reaction time = 150 min.

It is also possible that increasing of ultrasonic power may be related with the number of cavitation bubbles formed in the medium, and thus, improving the TAG formation. Moreover, the energy generated due to cavitation is transferred to the reaction system, which could improve the process of interfacial area or mass transfer on the substrate towards a fast reaction rate. For a further increase in the power to 100 W, the TAG



selectivity remained almost the constant. Therefore, ultrasonic power (80W) was defined as the optimum power dissipation here.

The possible reaction mechanism for glycerol acetylation with acetic acid over acid catalyst was reported in previous literature [9]. Firstly, the proton from acid catalyst will be interacted with carbonyl group of acetic acid to form an acylium ion. Then, the activated carbonyl group of acetic acid (positive charge) is attacked by glycerol molecule (nucleophilic attack) to generate MAG with releasing of water molecule. Furthermore, MAG molecule is further reacted with the activated carbonyl group to form DAG and TAG molecules. From our obtained results, high activity of SO₃H-glycerol-carbon catalyst for selective conversion of glycerol into TAG may be due to its high acidity and large pore size, resulting in facile formation of electrophilic intermediate and well diffusion of big molecule, leading to high glycerol conversion. The increasing of reaction time, reaction temperature and ultrasonic power are the key for enhancing the interaction between substrate and catalyst, resulting in increasing of TAG formation rate.

C. Catalyst Reusability

In this study, the catalyst was reused for 7 cycles on glycerol conversion at 100 °C for 150 min with an ultrasonic power of 80 W. As shown in Fig. 6, no obvious reduction in catalytic performance based on glycerol conversion (100%) was found from the first to the third reaction cycles. However, the dramatic decreasing in glycerol conversion and TAG selectivity was observed while DAG selectivity increased to some extent after the third reaction cycle. This phenomenon should be attributed to the deactivation of catalyst, occurring from leaching of sulfonic group on catalyst and partial blocking of the catalyst pores and surfaces by adsorbed reactants, which restricted the entry of glycerol molecules into the active sites [10]. From these results, the regeneration process of spent catalyst was required in the future study. It is expected to provide a green way for the selective production of TAG from acetylation of crude glycerol at mild reaction conditions.

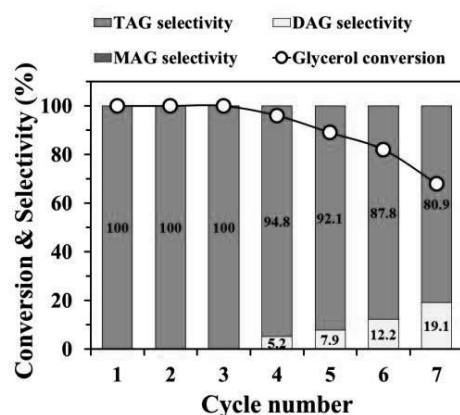


Fig. 7. Reusability of SO₃H-glycerol-carbon on TAG production from catalytic conversion of glycerol in ultrasonic system. Reaction conditions: catalyst = 5 wt.% of glycerol, molar ratio of acetic acid to glycerol = 8 to 1, reaction temperature = 100 °C, reaction time = 150 min and ultrasonic power = 80 W.

IV. CONCLUSIONS

In summary, the glycerol conversion into acetylated products (MAG, DAG and TAG) catalyzed by SO₃H-glycerol-carbon was studied using an ultrasonic system. The SO₃H-glycerol-carbon exhibited high acid site concentration, surface area and pore size for the glycerol acetylation. The increasing of ultrasonic power significantly resulted in the TAG selectivity enhancement. The optimum conditions including catalyst amount (5 wt.% of glycerol), molar ratio of acetic acid to glycerol (8 to 1), reaction temperature (100 °C), reaction time (150 min) and ultrasonic power (80 W) were obtained, providing a maximum TAG selectivity of 100%. The SO₃H-glycerol-carbon exhibited good stability in its catalytic activity when reused at least three consecutive batch cycles.

ACKNOWLEDGMENT

The authors wish to acknowledge Department of Sustainable Industrial Management Engineering (SIME), Faculty of Engineering, Rajamangala University of Technology Phra Nakhon and all University participated for supporting this research.

REFERENCES

- [1] M. Goncalves, C.S. Castro, L.C.A. Oliveira and W.A. Carvalho, "Green acid catalyst obtained from industrial wastes for glycerol etherification," *Fuel Process. Technol.*, vol. 138, pp. 695-703, October 2015.
- [2] L. Zhou, T.H. Nguyen and A.A. Adesina, "The acetylation of glycerol over amberlyst-15: Kinetic and product distribution," *Fuel Process. Technol.*, vol. 104, pp. 310-318, December 2012.
- [3] J.A. Sánchez, D.L. Hernández, J.A. Moreno, F. Mondragón and J.J. Fernández, "Alternative carbon based acid catalyst for selective esterification of glycerol to acetylglycerols," *Appl. Catal., A*, vol. 405, pp. 55-60, October 2011.
- [4] L.J. Konwar, P.M. Arvela, P. Begum, N. Kumar, A.J. Thakur, J.P. Mikkola, R.C. Deka and D. Deka, "Shape selectivity and acidity effects in glycerol acetylation with acetic anhydride: Selective synthesis of triacetin over Y-zeolite and sulfonated in glycerol acetylation with acetic anhydride: Selective synthesis of triacetin over Y-zeolite and sulfonated mesoporous carbons," *J. Catal.*, vol. 329, pp. 237-247, September 2015.
- [5] J. Gui, X. Cong, D. Liu, X. Zhang, Z. Hu and Z. Sun, "Novel Brønsted acidic ionic liquid as efficient and reusable catalyst system for esterification," *Catal. Commun.*, vol. 5, pp. 473-477, September 2004.
- [6] I. Kim, J. Kim and D. Lee, "A comparative study on catalytic properties of solid acid catalysts for glycerol acetylation at low temperatures," *Appl. Catal., B*, vol. 148-149, pp. 295-303, April 2014.
- [7] Y. Zhao, H. Chen, Y. Huang, Y. Zhao, Y. Fu and J. Shen, "Sulfonated carbon materials with hydrophilic and lipophilic properties," *J Energy Chem.*, vol. 2, pp. 156-163, March 2014.
- [8] M. Gonçalves, R. Rodrigues, T.S. Galhardo and W.A. Carvalho, "Highly selective acetalization of glycerol with acetone to solketal over acidic carbon-based catalysts from biodiesel waste," *Fuel*, vol. 181, pp. 46-54, October 2016.
- [9] J. Sun, X. Tong, L. Yu and J. Wan, "An efficient and sustainable production of triacetin from the acetylation of glycerol using magnetic solid acid catalysts under mild conditions," *Catal. Today*, vol. 264, pp. 115-122, April 2016.
- [10] B.O.D. Costa, H.P. Decolatti, M.S. Legnoverde and C.A. Querini, "Influence of acidic properties of different solid acid catalysts for glycerol acetylation," *Catal. Today*, vol. 289, pp. 222-230, July 2011.



An Alternate Numerical Algorithm for Minimization of Unconstrained Non-linear Functions for Solving Combustion Equations

Paramust Juntarakod

Department of Mechatronic Engineering, Faculty of Engineering
Rajamangala University of Technology Isan, Khonkaen Campus.
150 Srichan Road, NaiMuang, Muang, Khonkaen 40000
paramust_kmitnb@hotmail.com

Abstract— For a specific fuel combustion problem involving calculations of several species at the equilibrium state, it was simpler to write a general computer program and calculate the combustion concentration. Original work describes, an adaptation of Newton-Raphson method was used for solving the highly nonlinear system of equations describing the formation of equilibrium products in reacting of fuel-additive-air mixtures. This study also showed how possible of the results. It presented the efficient numerical algorithms for solving the combustion problem. Nonlinear equations based on a few alternate numerical algorithms for minimization of unconstrained non-linear functions by using the modified Adomian decomposition method, and the modified Householder's iteration method with the Taylor series to spread the equation that the new method was able to compete by Karthikeyan [17, 18]. These results illustrations were given to show the efficiency of algorithms. According to comparisons of results by the general solving method of original Newton-Raphson Method. Nitromethane-Air be used example of this case, that the result data indicated that the new Matlab routines were reliable, and typical deviations from general results were less than 1%.

Keywords— Non-linear equation, Newton-Raphson Method, fuel and Combustion products, Minimization, Adomian decomposition method, Householder's iteration method.

I. INTRODUCTION

When considering a general chemical equilibrium, there are several disadvantages in the equilibrium constant method such as the system of chemical equilibrium are nonlinear equations which has more data and recoding. Including are numerical difficulties with the use of components and more difficulties in solving. On the other hand, the equilibrium constant method is simpler to adopt and formulate for a simple situation. It was also found that for most combustion problems, it gave satisfactory results without elaborate and complicated computer programs McBride [1].

Mohamed [2] and Caton [3] developed procedures that algebraically combined the equilibrium equations, eliminated some unknowns, and scaled the simplified equations to obtain a set of simultaneous nonlinear equations which were solved with linear algebra. Their procedures combined the Gauss-Seidel and Newton methods. They claimed that the Gauss-Seidel was unreliable and the Newton-Raphson method was

slow. In this way, there is a possibility that it can be done in other mathematical ways by iteration techniques of nonlinear equations [4-8].

Buttworth [9], an effort was made by developing a combustion mathematical model to simulate exhaust emissions in fuels. Based on Equilibrium Constants Method (ECM), a computer program using MATLAB had been developed for the fuels to calculate the mole fractions of the emission gases. ECM was based on thermodynamic measurements and empirical calculations. Thermodynamic data for elements, combustion products and many pollutants were available in a compilation published by the National Bureau of Standards, called the JANAF (Joint Army-Navy-Air Force) tables. The equilibrium constant data from JANAF [16] tables using polynomial curve fitted had been used in calculating the combustion products.

Lewis [10] and Ferguson [11] were a solution for the properties of equilibrium combustion products based on an equilibrium constant method (ECM) with the gas phase products of combustion of hydrocarbon fuels. The use of equilibrium constants was based on minimization of the Gibbs free energy of the gas. The equilibrium constant method was simpler than the Lagrange multiplier approach when considering restricted species lists. However, the equilibrium constant method required the equilibrium reactions, such as the water-gas reaction.

Scientists and engineers have adapted the application of iterative methods in nonlinear algebraic equations such as Newton-Raphson method and High-order iteration method lately. It is because these methods simplify complex problems into simple solutions [4-8]. Newton-Raphson method is the most popular and powerful method for solving non-linear combustion equations. For example, Rakopoulos [12] was also used this method to solve equations of chemical equilibrium combustion model in 11 species diesel alone combustion products, Masood [13] used this method to solve equations of low-temperature combustion model with only 10 products species, Rashidi [14] combined Newton-Raphson with successive substitution methods to solve combustion problem of hydrocarbon fuel with 18 products species and concluded





that the combined method gave fast and reliable convergence during iteration process.

The present study suggests and analyzes the new iterative methods for solving nonlinear equations. That is the new two-step method, it was applied to construct the numerical algorithms by the iterative method to compute nonlinear equations from some numerical experiments illustrate that the new method could be competed with Basto method Feng[15]. And, it was applied to get the results by developing a combustion mathematical model to simulate exhaust emissions in hydrocarbon fuel. Based on Equilibrium Constants Method (ECM), a computer program using MATLAB had been developed for the fuels to calculate the mole fractions of the emission gases.

II. METHODS

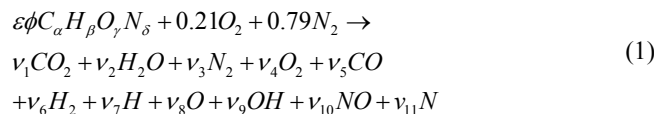
A. Problem formation

This problem involves the computing and comparing the Original work of Newton-Raphson method [NRM], Householder's iteration method (HoIM), Adomian Decomposition method (ADM) and Modified Adomian Decomposition method (MADM), Modified Householder's iteration method (MHoIM). These method are compute the mole fraction of each of the exhaust species when the hydrocarbon fuel is burnt along with air and the results are presented. The proportion of hydrocarbon in the hydrocarbon-air blend affecting the mole fraction of the exhaust species is also calculated.

The fuel is to be specified in terms of the C, H, O and N atoms in the fuel. For the blend of fuel-air considered. The other parameters that need to be specified are equivalence ratio, pressure and temperature. For the calculation of equilibrium constant, the data for constants is considered from JANAF [16] tables. The molar-air fuel ratio is calculated from the number of carbon, hydrogen, nitrogen and oxygen atoms present in the fuel.

B. Logic of the Numerical Calculation

The basis of the equilibrium combustion products with Multi-fuel-air mixture model is a solution to the atom balance equations from the chemical reaction equation of fuel and air forming. This mixture equation is given in Eq-(1) for the condition of equivalence ratio ($\phi < 3$). This process based on conservation of mass that was modified form Ferguson [11], where the following equation represents the chemical reaction with the relevant species involved which was added gasoline supplied as given below,



$$\text{Where, } \varepsilon = \frac{0.210}{\alpha + 0.25\beta - 0.5\gamma}$$

Nitromethane (CH₃NO₂) be used by this example. There is the conservation of 4 atoms and from mixture equation, so atom balancing can be written,

$$C \quad \varepsilon\phi\alpha = y_1 + y_5 \quad (2)$$

$$H \quad \varepsilon\phi\beta = 2y_2 + 2y_6 + y_7 + y_9 \quad (3)$$

$$O \quad \varepsilon\phi\gamma + 0.42 = 2y_1 + y_2 + 2y_4 + y_5 + y_8 + y_9 + y_{10} \quad (4)$$

$$N \quad \varepsilon\phi\delta + 1.58 = 2y_3 + y_{10} + y_{11} \quad (5)$$

Also, the constraint that the mole fractions add up to unity must be satisfied,

$$y_1 + y_2 + y_3 + y_4 + y_5 + y_6 + \quad (6)$$

$$y_7 + y_8 + y_9 + y_{10} + y_{11} - 1 = 0$$

The expression for atom balance of each equation can be eliminated by dividing Eq-(2) by Eq-(3). The equation can be written as next equation.

$$2y_2 + 2y_6 + y_7 + y_9 - d_1(y_1 + y_5) = 0 \quad (7)$$

Likewise, the Eq-(3) and Eq-(4), the equation can be written as

$$2y_1 + y_2 + 2y_4 + y_5 + y_8 + y_9 + y_{10} - [d_2(y_1 - y_5)] = 0 \quad (8)$$

$$2y_2 + y_{10} + y_{11} - [d_3(y_1 + y_5)] = 0 \quad (9)$$

Equations of constant value for a simple studied can be defined as,

$$d_1 = \frac{\beta}{\alpha} \quad d_2 = \frac{\gamma}{\alpha} + \frac{0.42}{\varepsilon\phi\alpha} \quad d_3 = \frac{\delta}{\alpha} + \frac{1.58}{\varepsilon\phi\alpha}$$

The above 4 equations (Eq-(6) through Eq-(9)) have 10 unknowns (y_1, y_2, \dots, y_{11}), therefore in order to solve for these 10 unknowns other 6 more equations are needed which may be derived from the consideration of equilibrium among products. The equilibrium constant can be related to the partial pressure of the reactants and products.

$$CO_2 \leftrightarrow CO + \frac{1}{2}O_2 \quad K_1 = \frac{y_5 y_4^{1/2} P^{1/2}}{y_1} \quad (10)$$

$$H_2 + \frac{1}{2}O_2 \leftrightarrow H_2O \quad K_2 = \frac{y_2}{y_4^{1/2} y_6 P^{1/2}} \quad (11)$$

$$\frac{1}{2}H_2 + \frac{1}{2}O_2 \leftrightarrow OH \quad K_3 = \frac{y_9}{y_4^{1/2} y_6^{1/2}} \quad (12)$$

$$\frac{1}{2}H_2 \leftrightarrow H \quad K_4 = \frac{y_7 P^{1/2}}{y_6^{1/2}} \quad (13)$$

$$\frac{1}{2}O_2 \leftrightarrow O \quad K_5 = \frac{y_8 P^{1/2}}{y_4^{1/2}} \quad (14)$$

$$\frac{1}{2}N_2 \leftrightarrow N \quad K_6 = \frac{y_{11} P^{1/2}}{y_3^{1/2}} \quad (15)$$

$$\frac{1}{2}O_2 + \frac{1}{2}N_2 \leftrightarrow NO \quad K_7 = \frac{y_{10}}{y_4^{1/2} y_3^{1/2}} \quad (16)$$



And, the partial pressure of a component is defined relative to the total pressure and the mole fraction, thus the equilibrium constant can be rewritten as,

$$y_1 = c_1 y_5 y_4^{1/2} \quad \text{where } c_1 = P^{1/2} / K_1 \quad (17)$$

$$y_2 = c_2 y_4^{1/2} y_6 \quad \text{where } c_2 = K_2 P^{1/2} \quad (18)$$

$$y_9 = c_3 y_4^{1/2} y_6^{1/2} \quad \text{where } c_3 = K_3 \quad (19)$$

$$y_7 = c_4 y_6^{1/2} \quad \text{where } c_4 = K_4 / P^{1/2} \quad (20)$$

$$y_8 = c_5 y_4^{1/2} \quad \text{where } c_5 = K_5 / P^{1/2} \quad (21)$$

$$y_{11} = c_6 y_3^{1/2} \quad \text{where } c_6 = K_6 / P^{1/2} \quad (22)$$

$$y_{10} = c_7 y_4^{1/2} y_3^{1/2} \quad \text{where } c_7 = K_7 \quad (23)$$

The equilibrium constants are treated as a function of gas temperature (T, Kelvin). It is the highest possible temperature that can be achieved during combustion. For computation of temperature, it is assumed that no heat will be transferred through combustion chamber walls, that is heat must be zero and all energy transferred to engine work and exhaust product. Values for K have been tabulated for several reactions at various temperatures. These values come from the above relations, which are determined by statistically thermodynamics. Equilibrium constant in Eq-(17) to Eq-(23) are curve fitted to the Thermo chemical Table, Ferguson [11] and their expressions are,

$$K_p = \exp \left(\frac{\Delta a_1 (\ln T - 1) + \frac{\Delta a_2 T}{2} + \frac{\Delta a_3 T^2}{6} + \frac{\Delta a_4 T^3}{12} + \frac{\Delta a_5 T^4}{20} - \frac{\Delta a_6}{T} + \Delta a_7 \right) \quad (24)$$

Where T is temperature (Kelvin). For the range of $3500 \leq T \leq 5000K$, coefficients for calculating the equilibrium constant K, Substitution of the equilibrium constants from Eq-(24) and the curve-fit coefficient constants into Eq-10 through Eq-(16) and rearranging to express mole fractions of all species in terms of y_3, y_4, y_5 and y_6 , the mole fractions of CO, H₂, O₂ and N₂ respectively. The expressions resulted are four nonlinear equations in four unknowns are as follows,

$$f_j(y_3, y_4, y_5, y_6) = 0 \quad j = 1, 2, 3, 4 \quad (25)$$

where

$$f_1(y_3, y_4, y_5, y_6) = c_1 y_5 y_4^{1/2} + c_2 y_4^{1/2} y_6 + y_3 + y_4 + y_5 + y_6 + c_4 y_6^{1/2} + c_5 y_4^{1/2} + c_3 y_4^{1/2} y_6^{1/2} + c_7 y_4^{1/2} y_3^{1/2} + c_6 y_3^{1/2} - 1 \quad (26)$$

$$f_2(y_3, y_4, y_5, y_6) = 2(c_2 y_4^{1/2} y_6) + 2y_6 + c_4 y_6^{1/2} + c_3 y_4^{1/2} y_6^{1/2} - d_1(c_1 y_5 y_4^{1/2} + y_5) \quad (27)$$

$$f_3(y_3, y_4, y_5, y_6) = 2(c_1 y_5 y_4^{1/2}) + c_2 y_4^{1/2} y_6 + 2y_4 + y_5 + c_5 y_4^{1/2} + c_3 y_4^{1/2} y_6^{1/2} + c_7 y_4^{1/2} y_3^{1/2} - d_2(c_1 y_5 y_4^{1/2} - y_5) \quad (28)$$

$$f_4(y_3, y_4, y_5, y_6) = 2(c_2 y_4^{1/2} y_6) + c_7 y_4^{1/2} y_3^{1/2} + c_6 y_3^{1/2} - d_3(c_1 y_5 y_4^{1/2} + y_5) \quad (29)$$

C. The Original work of Newton–Raphson Method

The given equations can be solved by using the Newton Raphson method. The general form of Taylor series for nonlinear equation systems is

$$Y_{k+1} = Y_k - \frac{f(x_k)}{f'(x_k)} \quad (30)$$

k is iterations. Each of these may be expanded in Taylor expansion of $f(x)$ to a higher order for Newton Raphson method,

$$f_j + \frac{\partial f_j}{\partial y_3} \Delta y_3 + \frac{\partial f_j}{\partial y_4} \Delta y_4 + \frac{\partial f_j}{\partial y_5} \Delta y_5 + \frac{\partial f_j}{\partial y_6} \Delta y_6 \approx 0, j = 1, 2, 3, 4 \quad (31)$$

Functions (f) are evaluated from the solution of interested functions (Eq-(26) through Eq-(29)). $f_j = f_{(1,2,3,4)}$ The independent set of derivatives is obtained by solution of matrix equation that results from differentiating with respect to mole fraction. The above can be arranged as set of linear equations in the matrix form, $[A][Z] - [B] = 0$, Where

$$[A] = \left[\frac{\partial f}{\partial y} \right], [B] = [f_j], [Z] = [\Delta y] \quad (32)$$

Where $[A]$ see the appendix below.

D. The modified Householder's Iteration Method

The given equations can be solved by using Householder's iteration method. The general form of equation is

$$(f(x_k) + f^2(x_k)f''(x_k)f'^{-2}(x_k)) + f'(x_k)(Y_{k+1} - Y_k) = 0 \quad (33)$$

Each of these may be expanded in Taylor expansion of $f(x)$ to a higher order for Householder's iteration method, see Eq-33. That is,

$$f_j = f(x_k) + f^2(x_k)f''(x_k)f'^{-2}(x_k) \quad (35)$$

From the alternate iterative numerical algorithms for minimization of unconstrained nonlinear function was presented by Karthikeyan [17, 18], It is the aim of this research, the few alternate numerical algorithms are the modified Householder's Iteration method.

$$f_{k+1} = f_k - \frac{f'(x_k)}{f''(x_k)} - \frac{f^2(x_k)f''(x_k)}{2f'^3(x_k)} \quad (36)$$

k is iterations. Functions (f) are evaluated from the solution of interested functions (Eq-(26) through Eq-(29)). The independent set of derivatives is obtained by solution of matrix equation that results from differentiating with respect to mole fraction. The above can be arranged as set of linear equations in the matrix form, $[A][Z] - [B] = 0$, where

$$[A] = \left[\frac{\partial f}{\partial y} \right], [B] = f_k - \frac{f'(x_k)}{f''(x_k)} - \frac{f^2(x_k)f''(x_k)}{2f'^3(x_k)} \quad (37)$$

$[Z] = [\Delta y]$

Where see the Appendix below.

E. The modified Adomian Decomposition Method

The given equations can be solved by using Adomian Decomposition method. The general form is



$$\left(\frac{f(x_k) + f^2(x_k)f'(x_k)f'^{-2}(x_k)}{2} + \frac{f^3(x_k)f'^2(x_k)f'^{-4}(x_k)}{2} \right) + f'(x_k)(Y_{K+1} - Y_K) = 0 \quad (38)$$

Each of these may be expanded in Taylor expansion of $f(x)$ to a higher order for Adomian Decomposition method, that is

$$f_j = f(x_k) + f^2(x_k)f'(x_k)f'^{-2}(x_k) + \frac{f^3(x_k)f'^2(x_k)f'^{-4}(x_k)}{2} \quad (39)$$

From the alternate iterative numerical algorithms for minimization of unconstrained nonlinear function was presented by Karthikeyan [17, 18], It is the aim of this research, the few alternate numerical algorithms are the modified Adomian decomposition method.

$$f_{k+1} = f_k - \frac{f'(x_k)}{f''(x_k)} - \frac{f'^2(x_k)f''(x_k)}{2f'^3(x_k)} - \frac{f'^3(x_k)f''^2(x_k)}{2f'^5(x_k)} \quad (40)$$

k is iterations. Functions (f) are evaluated from the solution of interested functions (Eq-(26) through Eq-(29)) see Eq-(35). The independent set of derivatives is obtained by solution of matrix equation that results from differentiating with respect to mole fraction. The above can be arranged as set of linear equations in the matrix form, $[A][Z] - [B] = 0$, where

$$[A] = \left[\frac{\partial f}{\partial y} \right], [Z] = [\Delta y] \quad (41)$$

$$[B] = \frac{f'(x_k)}{f''(x_k)} - \frac{f'^2(x_k)f''(x_k)}{2f'^3(x_k)} - \frac{f'^3(x_k)f''^2(x_k)}{2f'^5(x_k)}$$

Where $[A]$ see the appendix below.

F. MATLAB inputs

In this study, MATLAB program code for the combustion simulation has been developed. The input parameters that need to be provided into the MATLAB program were percentage of Nitromethane-air ($\text{CH}_3\text{NO}_2 + 0.21\text{O}_2 + 0.79\text{N}_2$) substitution in term of equivalence ratio such as 0.5 to 2.0. Assumed the adiabatic temperatures were 2000 to 3000 K with constant pressure was 10 atm and the difference convergence was 1.0×10^{-10} .

III. RESULTS AND DISCUSSION

This section presents summarized Eq-(26) through Eq-29 to illustrate the efficiency of the iterative method proposed in this paper. We compared the method [denoted by Iteration method] with Newton-Raphson method (NRM), Householder's iteration method (HoIM), Adomian Decomposition method (ADM) and The modified Householder's Iteration Method (MHoIM) and The modified Adomian Decomposition Method (MADM). The results compared the number of iteration in each method obtained solution or mole fraction of combustions and difference value of combustion products from all CO_2 , H_2O , N_2 , O_2 , CO , H , H , O , OH , NO and N respectively. Numerical computations had been carried out by using the software Matlab 2010. And the results were presented in Tables I to II compared with the original working by Newton-Raphson

method of combustion products mole fractions and the graph of equivalence ratio 0.8 to 1.2 with the graph temperature of 2000 to 3000 K.

At low adiabatic temperature of 2000 K, the number of iterations of High order (HoIM and ADM)'s are less than the old method of Newton Raphson in Table. However, the solutions computed by the new method are more accurate with similar values.

At high adiabatic temperature of 3000 K, the number of iterations of High order (MHoIM and MADM)'s is more than the old method of Newton Raphson method in Table 1, 2 and Table 3, but the solutions computed by the new method are more accurate with similar values.

The results illustrating composition shifts with temperature and equivalence ratio are given in Figure 1 and 2 for the combustion of C_7H_{17} at $P=50$ bar. Composition as a function of temperature is shown in Figure 1. The largest mole fractions are N_2 , H_2O and CO_2 . At this pressure, the composition predicted by using Newton Raphson method is a good approximation for all temperature 2000-3000 K, compared with [9, 11]. At low pressure, dissociation is even greater than at atmospheric pressure. Newton-Raphson method is a low order iteration method which is valid for all temperature. The satisfying result was an experiential rise in product species such as CO , NO , OH , O_2 , O , H_2 and H .

For lean $\phi < 2$ condition, the O_2 fraction is relatively insensitive to temperature. For rich condition, the H_2 mole fraction first decreases, then increases with increasing temperature.

TABLE I. OBTAINED SOLUTION OF $\phi = 0.8$, TEMP = 2500 K

Species	NRM	HoIM	ADM	MHoIM	MADM
H_2	0.149692	0.000129	0.00022	0.000358	0.000129
CO	0.224539	0.01072	0.016464	0.023991	0.01072
N_2	0.599734	0.502362	0.50266	0.503295	0.502362
O_2	0.027926	0.115954	0.111226	0.106329	0.115954
H_2O	1.00E-25	0.126037	0.126269	0.126551	0.126037
CO_2	1.00E-25	0.124036	0.117424	0.109821	0.124036
H	7.11E-16	0.000792	0.001219	0.001799	0.000792
O	0.000205	0.000418	0.000683	0.001074	0.000418
OH	4.77E-14	0.108192	0.110471	0.111303	0.108192
NO	0.006091	0.01136	0.013364	0.01548	0.01136
N	1.22E-08	1.12E-08	2.93E-08	7.15E-08	1.12E-08
H_2	0.149692	0.000129	0.00022	0.000358	0.000129
Iteration	254	298	298	301	301

TABLE II. OBTAINED SOLUTION OF $\phi = 1.2$, TEMP = 2500

Species	NRM	HoIM	ADM	MHoIM	MADM
H_2	4.45E-05	8.42E-05	0.00015	0.000256	0.000415
CO	0.004715	0.008121	0.013195	0.020288	0.029595
N_2	0.437736	0.437671	0.437878	0.438436	0.439393
O_2	0.114049	0.109317	0.104395	0.099239	0.093841
H_2O	0.154699	0.1549	0.155191	0.155585	0.156077
CO_2	0.173109	0.167472	0.160904	0.153185	0.144203
H	0.000331	0.00056	0.000902	0.001392	0.002062
O	0.000129	0.000232	0.000396	0.000646	0.001009
OH	0.108251	0.113207	0.116924	0.119184	0.119818
NO	0.006935	0.008437	0.010063	0.01179	0.013588
N	1.17E-09	3.66E-09	1.04E-08	2.74E-08	6.68E-08
H_2	4.45E-05	8.42E-05	0.00015	0.000256	0.000415
Iteration	300	308	308	320	320

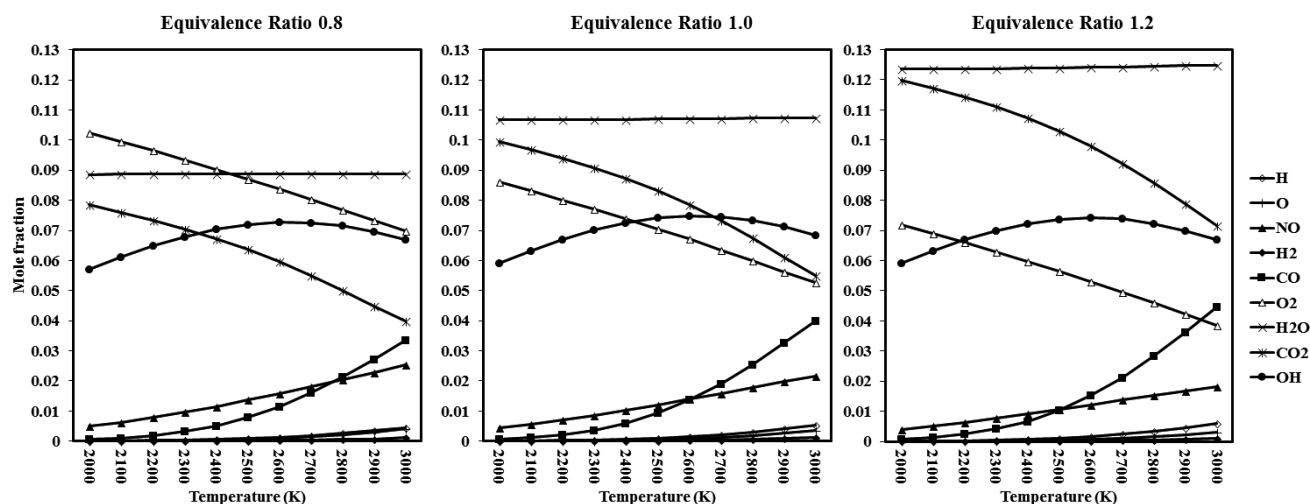


Fig. 1. The combustion products H, O, NO, H₂, CO, O₂, H₂O, CO₂, OH of CH₃NO₂ at T = 2000 to 3000 K equivalence ratio 0.8,1.0,1.2 and P = 30 atm by the modified Adomian Decomposition Method (MADM)

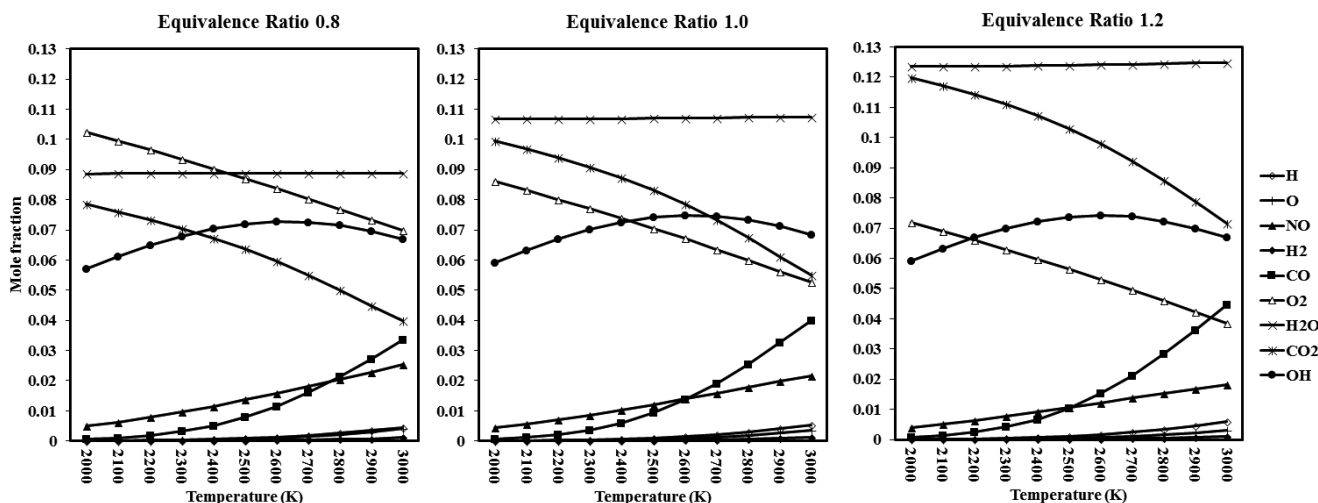


Fig. 2. The combustion products H, O, NO, H₂, CO, O₂, H₂O, CO₂, OH of CH₃NO₂ at T = 2000 to 3000 K equivalence ratio 0.8,1.0,1.2 and P = 30 atm by the modified Householder's Iteration Method (MHoIM).

IV. CONCLUSIONS

The accuracy of the MATLAB program equilibrium combustion products of benzene routine was established through comparison with a comparable MATLAB program routine. Maximum differences in molar concentrations less than 1% were typical apparent over the range of conditions calculated by the four routines NRM, HoIM, ADM and MHoIM, MADM. Adiabatic flame temperature calculations (2000 to 3000 K) also confirmed that differences between the new Matlab routines and established results were typically less than the round-off errors in the established results around 1% but the new method is the iteration number more than the original working of Newton Raphson Method.

Comparison of the example engine calculation using the new high order iteration method to Matlab routines and the original results obtained by Buttsworth [9] and Ferguson [11] demonstrates that routines produce accurate results. According to the combustion products calculated by the four methods, the differences are less than around 1%.

We suggest and analyze high order iterative methods for solving nonlinear equations. The new iterative method has quadratic convergence. Some numerical experiments illustrate the performance of the new method better than Newton-Raphson method which has low number of iterations convergence.



ACKNOWLEDGMENT

Department of Mechatronic Engineering, Faculty of Engineering, Rajamangala University of Technology Isan, Khonkaen Campus, 150 Srichan Road, NaiMuang, Muang, Khonkaen, 40000, Thailand.

REFERENCES

- [1] B. J. McBride, M. J. Zehe, S. Gordon, Coefficients for Calculating Thermodynamic Properties of Individual Species, NASA/TP-2002-211556, 2002.
- [2] M. Mohamed, E. Awad, Determining the Thermodynamic Properties of Fuel Blends for Use with Air-Fuel Models of IC Engines. in: International Conference on Trends in Industrial and Mechanical Engineering, Dubai, UAE, (ICTIME'2012) March 24-25, 2012.
- [3] J.A. Caton, The thermodynamic characteristics of high efficiency, Internal Combustion Engines, Energy Conversion and Management 58 (2012). P 3-30.
- [4] G. Adomian, Nonlinear Stochastic Systems, Theory and Applications to Physics, Kluwer Academic Publishers, Dordrecht, 1989.
- [5] E. Babolian, J. Biazar, Solution of nonlinear equations by modified Adomian decomposition method, Applied Mathematics and Computation 132 (2002), 167-172.
- [6] P. Sebah, X. Gourdon, Newton's method and high order iterations, numbers, [online]
- [7] S. Abbasbandy, Improving Newton-Raphson method for nonlinear equations by modified Adomian decomposition method, Applied Mathematics and Computation 145 (2003), 887-893.
- [8] A.S. Householder, The Numerical Treatment of a Single Nonlinear Equation, McGraw-Hill, New York, USA 1970.
- [9] D. R. Buttsworth, Spark Ignition Internal Combustion Engine Modeling using Matlab, Faculty of Engineering & Surveying Technical Reports, University of Southern Queensland
- [10] G. N. Lewis, M. Randall, Thermodynamics, McGraw-Hill, New York, USA, 1961.
- [11] C. R. Ferguson, Internal Combustion Engines, Applied Thermo sciences, John Wiley and Sons, New York, USA, 1986.
- [12] C. D. Rakopoulos, D. T. Hountalas, E. I. Tzanos, G. N. Taklis, A fast algorithm for calculating the composition of diesel combustion products using 11 species chemical equilibrium scheme, Advances in Engineering Software 19 (1994) 109-119.
- [13] M. Masood, M.M. Ishrat, Computer simulation of hydrogen-diesel dual fuel exhaust gas emissions with experimental verification, Fuel 87 (2008) 1372-1378.
- [14] M. Rashidi, Calculation of equilibrium composition in combustion products, Chem. Eng. Technol 20 (1997) 571-575.

- [15] J. Feng, A New Two-step Method for Solving Nonlinear Equations, International Journal of Nonlinear Science Vol.8)2009(No.1, pp.40-44.
- [16] JANAF, Thermo chemical Tables, U.S National Bureau of Standards Publications, NSRDS-NBS 37, 1971.
- [17] K. Karthikeyan Alternate Iterative Numerical Algorithms for Minimization of Unconstrained Nonlinear Functions, International Journal of Pure and Applied Mathematics, Volume 106 No. 1 2016.
- [18] K. Karthikeyan, Comparative study of certain numerical algorithms for solving non-linear equations. Advances in Applied Science Research, 2011, 2 (3): 232-238.

APPENDIX

A. The element of the Jacobian metric

$$D_{ij} = \partial y_i / \partial y_j, i=1,2,7,8,9,10,11 \text{ and } j=3,4,5,6$$

$$D_{76} = \frac{\partial y_7}{\partial y_6} = \frac{1}{2} \frac{c_4}{y_6^{1/2}} \quad D_{103} = \frac{\partial y_{10}}{\partial y_3} = \frac{1}{2} \frac{c_7 y_4^{1/2}}{y_3^{1/2}}$$

$$D_{84} = \frac{\partial y_8}{\partial y_4} = \frac{1}{2} \frac{c_5}{y_4^{1/2}} \quad D_{26} = \frac{\partial y_2}{\partial y_6} = c_2 y_4^{1/2}$$

$$D_{94} = \frac{\partial y_9}{\partial y_4} = \frac{1}{2} \frac{c_3 y_6^{1/2}}{y_4^{1/2}} \quad D_{24} = \frac{\partial y_2}{\partial y_4} = \frac{1}{2} \frac{c_2 y_6}{y_4^{1/2}}$$

$$D_{96} = \frac{\partial y_9}{\partial y_6} = \frac{1}{2} \frac{c_3 y_4^{1/2}}{y_6^{1/2}} \quad D_{14} = \frac{\partial y_1}{\partial y_4} = \frac{1}{2} \frac{c_1 y_5}{y_4^{1/2}}$$

$$D_{104} = \frac{\partial y_{10}}{\partial y_4} = \frac{1}{2} \frac{c_7 y_3^{1/2}}{y_4^{1/2}} \quad D_{15} = \frac{\partial y_1}{\partial y_5} = c_1 y_4^{1/2}$$

B. The matrix elements $[A] = [\partial y_i / \partial y_j]$

$$A_{11} = \frac{\partial f_1}{\partial y_3} = 1 + D_{103} + D_{113}$$

$$A_{12} = \frac{\partial f_1}{\partial y_4} = D_{14} + D_{24} + 1 + D_{84} + D_{104} + D_{94}$$

$$A_{13} = \frac{\partial f_1}{\partial y_5} = D_{15} + 1$$

$$A_{14} = \frac{\partial f_1}{\partial y_6} = D_{26} + 1 + D_{76} + D_{96}$$



$$A_{21} = \frac{\partial f_2}{\partial y_3} = 0$$

$$A_{22} = \frac{\partial f_2}{\partial y_4} = 2D_{24} + D_{94} - d_1 D_{14}$$

$$A_{23} = \frac{\partial f_2}{\partial y_5} = -d_1 D_{15} - d_1$$

$$A_{24} = \frac{\partial f_2}{\partial y_6} = 2D_{26} + 2 + D_{76} + D_{96}$$

$$A_{31} = \frac{\partial f_3}{\partial y_3} = D_{103}$$

$$A_{32} = \frac{\partial f_3}{\partial y_4} = 2D_{14} + D_{24} + 2 + D_{84} + D_{94} + D_{104} - d_2 D_{14}$$

$$A_{33} = \frac{\partial f_3}{\partial y_5} = 2D_{15} + 1 - d_2 D_{15} - d_2$$

$$A_{34} = \frac{\partial f_3}{\partial y_6} = D_{26} - D_{96}$$

$$A_{41} = \frac{\partial f_4}{\partial y_3} = 2 + D_{103} + D_{113}$$

$$A_{42} = \frac{\partial f_4}{\partial y_4} = D_{104} - d_3 D_{14}$$

$$A_{43} = \frac{\partial f_4}{\partial y_5} = d_3 D_{15} - d_3$$

$$A_{44} = \frac{\partial f_4}{\partial y_6} = 0$$



Production of Briquette from Agricultural Residue

Numpon Panyoyai, Samerkhwan Tantikul, Tipapon Khamdaeng and Thanasit Wongsiriamnuay*
Faculty of Engineering and Agro-Industry
Maejo University
Chiang mai, Thailand
t.wongsiriamnuay@gmail.com

Abstract—This study aimed to study biomass fuel from rice husk, maize cob, and rubberwood. Additionally, manufacturing, processes and proportions content in properties of moisture, density, durability, heat value, and compressive strength were investigated. The materials were prepared using a grinder and a sieve with a diameter of 5 mm. After screw extruder compressed that material at a die temperature of 300, 330 and 360 °C. The results in this study show rice husk had the highest durability at the temperature of 300°C (95%). Rice husk mixed with rubberwood had the lowest moisture content at the temperature of 360 °C (6.1%). Rice husk had the highest density at the temperature of 300 °C (520 kg/m³). Finally, Rice husk mixed with rubberwood had the highest heating value at the temperature of 360 °C (16.98 MJ/g).

Keywords—*agricultural residue; biomass; densification; alternative fuel; green energy;*

I. INTRODUCTION

The agricultural residue is potentially an attractive feedstock as a significant part of biomass resource for renewable energy. The five most considerable contributors to the output of agricultural waste in Thailand were rice, rubber, sugar cane, maize and palm [1]. Direct combustion of biomass waste is the primary utilization of biomass energy, mainly burning in the planting area, which causes many problems including emission and lower air quality index. Many conversion technologies encourage economic, environment, social and energy. Densification is a modern and straightforward technology that improve the physical properties and others property for storage, transportation and use as fuel. This study investigated the agricultural residue briquette from rice husk, corn cob and rubber wood for densification as a briquette.

II. MATERIAL AND METHOD

A. Sample preparation

The tested material was an agricultural residue of three kinds of rice husk, corn cob, and rubberwood. This residue was collected and leave in the open air for drying. After that these were ground with screen size (5mm) by using hammer mill.

B. Moisture

The sample was determined the moisture content before and after densification. The samples were dried out within 24 hours at 105°C in the oven and using the following equation

$$w = \frac{m_w - m_d}{m_d} \times 100\% \quad (1)$$

Where m_w = mass of wet material (g)
 m_d = mass of dry material (g)

C. Bulk Density

The density of agricultural residue and briquette were measure following the standard. The bulk density was calculated from the mass of feedstock and briquette that occupied the container and using the following equation

$$Density = \frac{m}{V} \quad (2)$$

Where m = mass of material (kg)
 V = volume of container (m³)

D. Heating value

The calorific value of briquette was determined by using an adiabatic oxygen bomb calorimeter by ASTM D2015-96, the standard method for gross calorific of grinding sample.

E. Densification

There are three zones in a screw extruder: feed, transport, and extrusion. Grinding material was transport from feeding zone to compaction zone via a die. To forming a shape of substantial, heating at a die increase temperature of content then the friction between die wall and material formed a required shape.

F. Durability

$$DU = \frac{m_2}{m_1} \times 100\% \quad (1)$$

m_2 = mass of sieved briquettes after the drum

The briquette was crush to determine compressive strength according to the CEN/TS 3114 standard.

The physical properties of briquettes were examined in this study were limited to moisture, density, heating value, durability, and compressibility.

The moisture content of agricultural residue and briquette were shown in fig. 1 and 2. It is indicated that the moisture content of the residue was around 6-8%. After densification, the moisture content decreased to 3-5%. Increased in die temperature result in lower moisture content of mixed briquette.

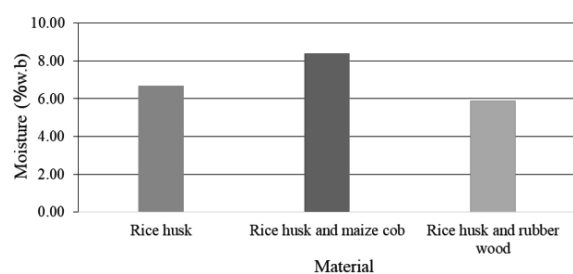


Fig.1. Moisture content of agricultural residue

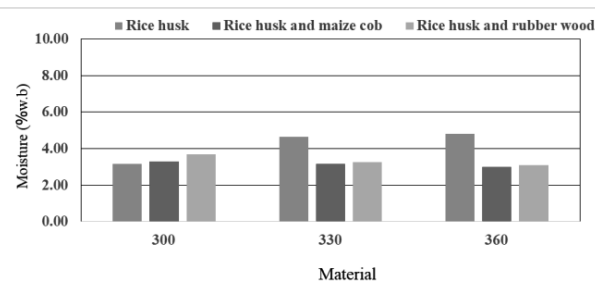


Fig.2. Moisture content of briquette

The bulk density of agricultural residue and briquette were shown in fig. 3 and 4. It is indicated that the density of the residue was around 150-220 kg/m³. After densification, the density increased to 400-550 kg/m³. Increased in die temperature from 300-360C° not effect on briquette density but Demirbaş and Şahin [2] was found that compaction of wheat straw increasing temperature from 80-160°C resulted in increased density from 400-650 °C at 800 MPa. Bulk density increased with pressure and moisture content but decrease with hammer mill screen size[3].

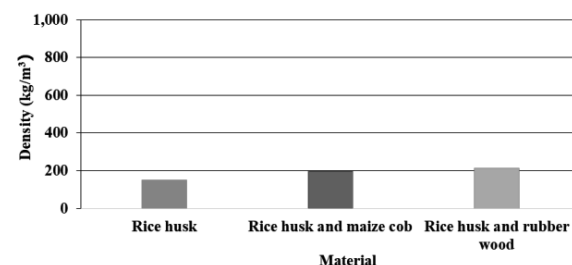


Fig.3. Bulk density of agricultural residue

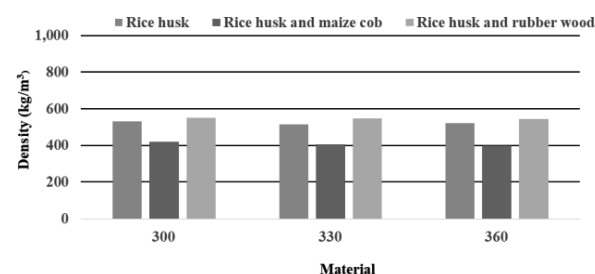


Fig.4. Bulk density of briquette

The heating value of the briquette in this study is

Combine rice husk with cob and rubber wood that increased heating value of briquette around 0.3 and 1 MJ/kg, respectively. Increased in die temperature not effect on the heating value of mixed briquette.



TABLE I. HEATING VALUE OF BRIQUETTE

AGRICULTURAL RESIDUE	DIE TEMPERATURE (°C)	HEATING VALUE (MJ/Kg)
rice husk	300	15.67
	330	15.80
	360	15.95
rice husk and corn cob	300	15.99
	330	16.18
	360	16.28
rice husk and rubberwood	300	16.90
	330	16.83
	360	16.98

D. Durability

The results values showed the high-level mechanical durability of briquette made from mixed agricultural residue was around 90%. That value achieved a briquette quality and improved different agricultural waste to produce under same manufacturing conditions.

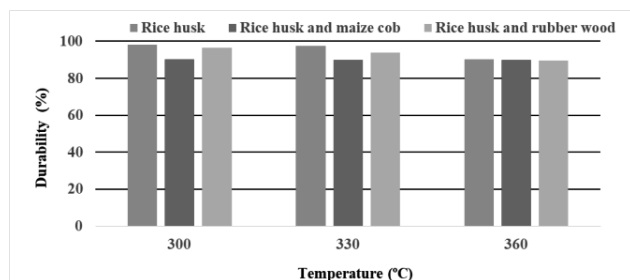


Fig.5. Mechanical durability of briquette

E. Compression

The compression briquette was shown in fig. 6. It is indicated that the compressive strength of the briquettes from rice husk was higher than mixed with others. Increased in die temperature result in lower strength of briquette.

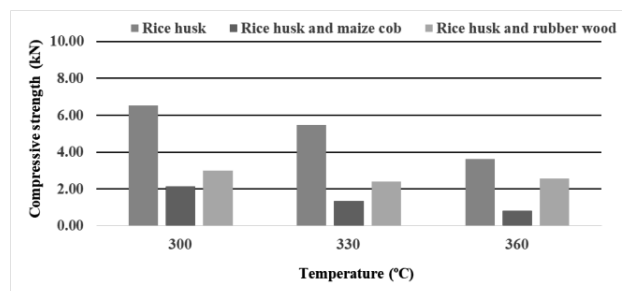


Fig.6. Compression of briquette

IV. CONCLUSION

Briquette is lower moisture content than agricultural waste. Densification improves the density increase two times. Blending residue increased briquette heating value. Different agricultural residue can be produced with same operation condition with mixed residue to achieved DU of 90%. Increased temperature effect on the lower compressive force of briquettes.

ACKNOWLEDGMENT

This research was financially supported by the Thailand Research Fund and Maejo University

REFERENCES

- [1] Economics. [cited 2018 31 May].
- [2] Demirbaş and Şahin. Evaluation of biomass residue: 1. Briquetting waste paper and wheat straw mixtures, *Fuel Processing Technology*. 55(2): pp. 175-183, 1998.
- [3] Guo, Wang, Tabil, and Wang. Compression and relaxation properties of selected biomass for briquetting, *Biosystems Engineering*. 148: pp. 101-110, 2016.



Effect of Temperature on Change of Microstructure of Hadfield Steel

Jirutthitikalpongsri Hirunyagird^{1st}, Yuttana Srilamai^{3rd}
Dept. Metallurgical Engineering, Faculty of Engineering
Rajamangala University of Technology Isan, Khon Kaen,
Thailand
e-mail: tonau_metal@hotmail.com, Sryuttana@gmail.com

Prin Nachaisit^{2nd}
Dept. Industrial Engineering, Faculty of Engineering,
Rajamangala University of Technology Isan, Khon Kaen,
Thailand
e-mail: nsuchart2001@yahoo.com

Abstract—This research objective is to study effect of temperature on change of microstructure in heat treatment process of high manganese steel (Hadfield steel). Samples were heat at temperature range 1050 °C for 2 hours, then samples were immerse into water. Samples were heat for reduce residual stress by tempering process, tempering temperature at 350, 450, 550 and 650 °C for 2 hours and cool in air. Finally, Samples were examined the microstructure by OM and SEM. Hardness was measured by hardness tester and crystal structure was determined by XRD technique.

From microstructure results, it was found that after Solutionizing step at temperature range 1050 °C for 2 hours, then samples were immerse into water. Microstructure shown only austenite phase. The residual stress was measured. It was found that the residual stress increased from as-cast condition. Tempering temperature at 350, 450, 550 and 650 °C for 2 hours, microstructure results, it was found that tempering at 350 °C without manganese carbide, tempering at 450 °C occur manganese carbide at grain boundary, tempering at 550 °C and tempering at 650 °C occur manganese carbide with increasing along grain boundary.

Keywords—Heat treatment; Austenitic manganese steel; Hadfield

I. INTRODUCTION

Steel industry is considered as the primary industry of various industries such as mining, power, construction and machinery, ect. These industries need to use materials that are suitable for use. Both metallic and non-metallic materials, the mechanical properties were considered to be used. Therefore, mechanical properties have been improved through various techniques to improve the materials to suit the application [1].

High-manganese steel, commonly known as hadfield steel, is a special steel that is more wear and shock resistant than steel. This is due to the influence of manganese in iron. When this materials was hit with impact force. The austenite structure was semi-equilibrium structure (Meta stable phase)

changes into a martensite structure with a higher hardness than the austenite. It has good wear resistance. The microstructure under the surface is not affected by the impact, which remains the same structure as austenite phase. This makes the metal parts tough, not cracking, resulting in more durable. Hadfield steel can also improve mechanical properties such as: 1. by adding alloying element 2. by heat treatment processes. If these steel was heat at an unsuitable temperature and time in treatment process, the manganese carbide on the grain edge will result in a grain edge crack that will not be suitable for use [2-4].

II. EXPERIMENTAL PROCEDURE

Cutting step; as-cast sample was cut with wire-cut machine, diameter 25 mm, length 20 mm.

Solutionizing step: the samples were heated at 1050 °C and held at this temperature for 2 hours to allow the segregated carbides dissolve completely in austenite phase (soaking time 25mm/1h)

Quenching step: then the samples were quenched quickly in a 100 L agitated water tank to prevent carbide occurred and allowed to cool room temperature. Samples after quenching (as-quenching) was measured the residual stress by X-Ray residual stress measurement.

Tempering step: After quenching step, the samples (as-tempering) were reheated to relieve the stress at 350, 450, 550 and 650 °C for 2 hours and cool in air. To find the temperature that makes carbide appeared.

Chemical composition was monitored by arc spectrometer and Energy Dispersive X-ray Spectrometer as shown table I.

As-cast and as-heat treatment microstructure analysis, samples were cut and ground using SiC paper down to 4000 grit with water and then samples were also polished with alumina particle down to 0.03 µm for investigating microstructure by optical microscope and scanning electron microscope.



Crystal structure was determined by X-Ray Diffractometer.

Hardness was measured by hardness tester with Brinell Scale following ASTM E10-17.

Table I. Chemical composition result of as-cast from arc spectrometer.

Elemental composition (%)					
C	Si	Mn	Cr	S	P
1.3	0.7	12.5	2.0	0.05	0.05

III. RESULTS AND DISCUSSIONS

A. Microstructure results

Figure 1, Microstructure of as-cast consists of austenite phase as matrix and a manganese carbide ((Fe, Mn)₃C) at grain boundary.



Fig.1 The optical micrograph(100x) of as-cast showing significant heterogeneously dispersed manganese carbide at grain boundary

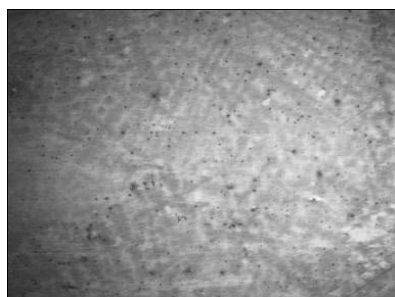


Fig.2 The optical micrograph(100x) of sample after solutionizing at 1050 °C for 2 hours and quenching in water at room temperature showing highly homogenous structure.

From Figure 2, microstructure of sample after solutionizing and quenching (solutionizing at 1050 °C for 2 hours and then samples were immersed in water at room temperature) then immediately dipped with water to prevent manganese from being combined with carbon to manganese carbide at grain boundary. It was found that the microstructure show austenite phase only.

From Figure 3-6, microstructure of after tempering step at 350-650 °C. Tempering at 350 °C for 2 h, the microstructure is a single phase as austenite phase. When comparing with the microstructure of sample after solutionizing and quenching (see Figure 2), there was no difference in microstructure. Tempering at 450 °C for 2 h, manganese carbide appears to show up at 450 °C for 2 h as the temperature at which manganese can coalesce with carbon has resulted in manganese carbide. In other words, at this temperature carbide is formed and is likely to occur along the grain boundary. Tempering at 550 °C for 2 h, microstructure of manganese carbide increased. At 650 °C for 2 h, the microstructure showed that manganese carbide was increased with increasing tempering temperature and carbide occurred at the grain boundary. As a result, the toughness and wear of high manganese steel is reduced [5].

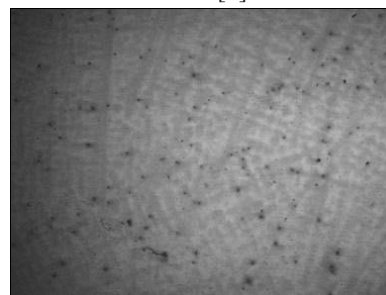


Fig.3 The optical micrograph(100x) of sample after tempering at 350 °C for 2 h. Nital 2% etchant.

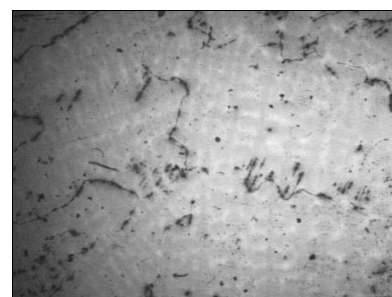


Fig.4 The optical micrograph(100x) of sample after tempering at 450 °C for 2 h. Nital 2% etchant.

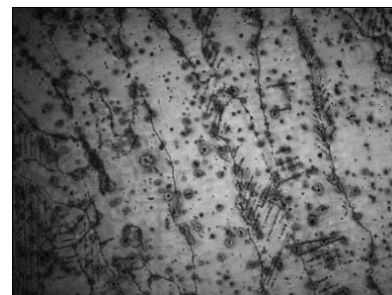


Fig.5 The optical micrograph(100x) of sample after tempering at 550 °C for 2 h. Nital 2% etchant.

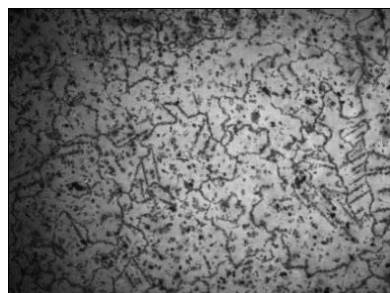


Fig.6 The optical micrograph(100x) of sample after tempering at 650 °C for 2 h. Nital 2% etchant.

The SEM micrograph with the corresponding EDS of the as-cast is shown in Figure 7 and Table II. It was observed from the micrograph that the second phase as manganese carbide particle is dispersed with the austenitic matrix.

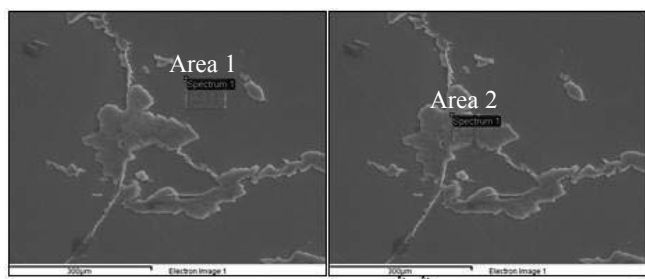


Fig.7 The SEM micrograph of As-cast

Table II. Chemical composition result of As-cast by EDS technique.

Element (wt.%)	Area 1	Area 2
C	11.25	26.21
Si	1.28	-
Cr	1.55	1.66
Mn	9.55	12.48
Fe	76.37	59.65
Total	100	100

The SEM micrograph with the corresponding EDS of the heat treated manganese steel in as-tempering at 450 °C for 2 h is shown in Figure 8 and Table III. It was observed from the micrograph that the second phase as manganese carbide particle is dispersed with the austenitic matrix.

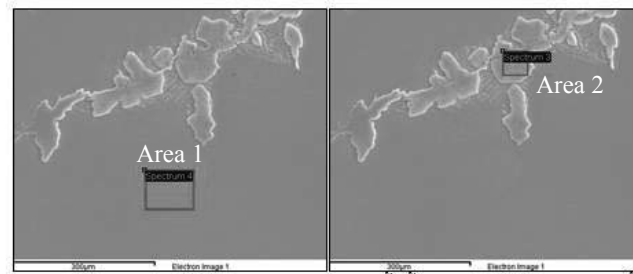


Fig.8 The SEM micrograph of sample after tempering at 450 °C for 2 h.

Table III. Chemical composition result of sample after tempering at 450 °C by EDS technique.

Element (wt.%)	Area 1	Area 2
C	11.61	23.34
Si	-	-
Cr	2.17	1.97
Mn	13.26	11.93
Fe	72.96	62.71
Total	100	100

As shown in Figure 9, a comparison of the As-Cast and sample after tempering at 450 °C for 2 h, crystalline structure showed that the XRD peak contained the austenite and manganese carbide (Fe, Mn)₃C. The angles of these compounds are similar. The intensity of as-cast sample is higher than tempering samples that of all peaks. It can be concluded that tempering at 450 °C for 2 h is the temperature at which manganese carbide starts.

The results of XRD and EDS are consistent. The particles that appear along the grain boundary are expected to be carbide, if the carbide is continuous or network at grain boundary induces intergranular crack [6].

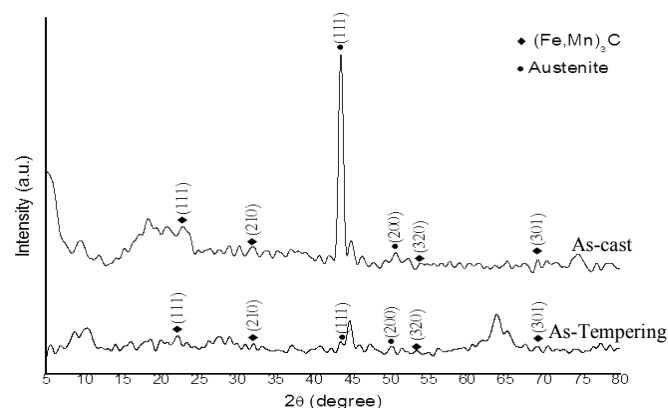


Fig9. XRD profile of as-cast and sample after tempering at 450 °C.



B. Residual stress results

Residual stress values were measured by residual stress techniques as shown in Figure 8 and table IV.

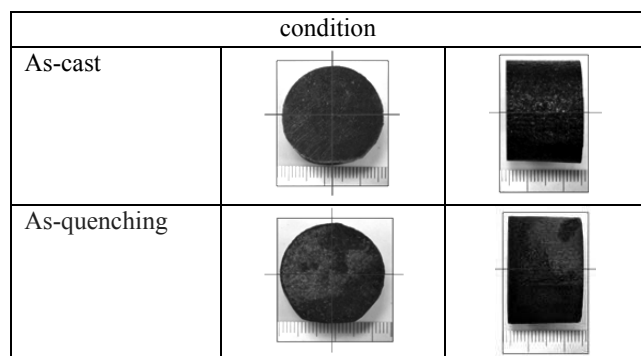


Fig.10 show point for residual stress measurement.

By measuring the residual stress values of as-cast sample, it was found that the stresses of point 1-6 as shown in table IV. In comparison, it can be seen that the residual stress of as-quenching sample is higher than as-cast sample due to rapid dipping of the samples into the water. The high heat transfer rate results in more stress than as-cast condition (cooled in sand mold). It is necessary to bring as-quenching sample to reduce the internal stress by tempering step.

Table IV. Results of Residual stress measurement

condition	Residual stress values (MPa), point					
	1	2	3	4	5	6
As-cast	-261.99	-295.67	N.A.	-329.09	N.A.	N.A.
As-quenching	-187.35	-197.83	-367.60	-172.74	-164.84	N.A.

C. Hardness result

The result of the hardness test is presented in Table V. The solution heat treatment process increased the hardness of the sample. The increase in hardness might be due to fairly uniform distribution of the carbide phase in the austenite phase [5].

Table. V Results of hardness measurement

Description	Hardness, (HB)
As-cast	212
As-quenching	223
As-tempering at 350 °C	212
As-tempering at 450 °C	223
As-tempering at 550 °C	229
As-tempering at 650 °C	240

IV. CONCLUSION

1. The as-cast microstructure of Hadfield steel consist of austenitic matrix and carbide $(Fe,Mn)_3C$ present at grain boundary.
2. The solution treatment temperature at 1050 °C for 2 h, lead to the formation of a purely austenitic structure.
3. The hardness values of as-cast about 212 HB and increasing the tempering temperature to 650 °C for 2 h raises the hardness values to 240 HB.
4. The tempering step at different temperatures but the same time is 2 hours and cooled in the air. Increasing the tempering temperature to 450 °C, manganese carbide was formed and at 550-650 °C, manganese carbide was increased and aggregates on the grain boundary, which is clearly observe.

ACKNOWLEDGMENT

The authors gratefully acknowledge the support from Faculty of Engineering, rajamangala University of technology Isan, Khon Kaen Campus for The financial supported.

The authors would like to thank NHK SPRING (THAILAND) CO., LTD., for instrument as X-Ray Residuals stress and Scanning Electron Microscope.

REFERENCES

- [1] A.H. Mokken, "The use of stainless steels in the mining industry"; In: Proceedings Symposium on Stainlesssteels, Johannesburg, 1969, pp.83-102.
- [2] S.A. Balogun, D.E.Esezobor, J.O. Agunsoye, "Effect of melting temperature on the wear characteristics of austenitic manganese steel", Journal of Minerals and Materials Characterization and Engineering, Vol. 7, No. 3, 2008, pp. 277-289.
- [3] W. Yan, L. Fang, K.Sun, Xu, Y, "Effect of surface work hardening on wear behavior of Hadfield steel", Journal of Materials Science and Engineering: A, Vol. 460-461, 2007, pp. 542-549, doi: 10.1016/j.msea.2007.02.094.]
- [4] S. Aribio, , K.K. Alaneme, , D.O. Folorunso, , Aramide, F.O., "Effect of precipitation hardening on hardness and microstructure of austenitic manganese steel", Journal of Minerals and Materials Characterization and Engineering, Vol. 9, No. 2, 2010, pp.157-164.
- [5] J.O. Agunsoye, S.I. Talabi, , O. Bello, "Wear characteristics of heat-treated Hadfield austenitic manganese steel for engineering application", Journal of Advances in Production Engineering & Management, Vol. 7, 2015, pp. 97-107.
- [6] M. G.Fontana, "Corrosion Engineering", third ed., McGraw-Hill, Inc., Singapore.



Surface Improvement of SCM 440 by the Ball-burnishing Technique

Montri Kawsuk*

Department of Industrial Engineering,
Faculty of Engineering, Rajamangala University of
Technology Thanyaburi
Patumtani, Thailand
e-mail montri.k@mail.rmutt.ac.th

Sirichai Torsakul

Department of Industrial Engineering,
Faculty of Engineering, Rajamangala University of
Technology Thanyaburi
Patumtani, Thailand
e-mail sirichai.to@en.rmutt.ac.th

Abstract—The objective of this research was to develop a new ball-burnishing tool integrated with a CNC milling, to improve the surface roughness, hardness, and residual stress of the material used in the present study, the Low-alloy steel SCM 440. The surface burnishing parameters for the ball-burnishing tool were determined after conducting the experimental methods. Based on the experimental results, the adequate combination of the process parameters was as follows, the burnishing pressure constantly from 200 to 600 bars, when machining using a low depth of cut 0.5 and 0.6 mm/rev, the velocity of 2 m/min, fluid as lubricant hydraulic oil (HLP 68). The quality of the surface roughness was studied. The final quality was similar to grinding, even reaching 0.349 μm Ra on average by using the adequate burnishing parameters. Corresponding to a before surface and to the same surface after being burnished with two different burnishing depth, roughness parameters improved about 75% when burnishing was applied. The burnishing surface hardness was increased to HV 586 on average.

Keywords; ball-burnishing; surface roughness; surface hardness; SCM440

I. INTRODUCTION

Mechanical surface treatments have been widely used to improve the physical-mechanical properties of metallic components [1–3]. As a consequence of plastic deformations, compressive residual stress states, work hardening, micro-structural alterations and a favorable roughness are produced; improving the fatigue strength and wear resistance [4,5]. Ball burnishing and Roller (also known as surface plastic deformation processes) are methods for improving metal surface finishing, surface hardness and dimensional accuracy [6–9]. Ball-burnishing is a rapid, simple and cost-effective mechanical surface treatment. In the process, the deformation element is the hard ball. As ball acts as a tool in deformation the surface layer, for the given normal force it gives high specific pressure, more fatigue strength, micro hardness & depth of work hardening layer as compared to ball burnishing. The materials used for the ball are alumina carbide-ceramic, cemented carbide, silicon nitride ceramic, silicon carbide ceramic and bearing steel. Burnishing tools are also now widely applied in nonautomotive applications for a variety of benefits; to produce better and longer lasting seal surfaces; to improve

wear life; to reduce friction and noise levels in running parts; and to enhance cosmetic appearance. Examples include valves, pistons of hydraulic or pneumatic cylinders, lawn and garden equipment components, shafts for pumps, shafts running in bushings, bearing bores, components of plastic molds, cold mold, hot work and general auto parts [10].

Parameters that have an influence on the ball burnishing process are; the normal burnishing force (measured at the hydraulic installation by the fluid pressure), the burnishing feed, prior hard turning feed, burnishing speed, prior hard turning insert nose radius and lubrication. Original roughness is also expected to exert an important effect. Other interesting data are; surface hardness, microhardness underneath the burnished surface and microstructure photographs.

II. THE BASIS OF HYDROSTATIC BALL-BURNISHING

The principle of the ball-burnishing tool is shown in Fig. 1. It is based on the hydrostatic principle [11]. The pressure is supplied by a hydraulic pump, which feeds on its own coolant tank and is capable of pumping at a pressure of 600 bar. The hydraulic pump is placed next to the machine where is mounted the burnishing equipment. The key element is a ceramic ball pressed against the surface of the workpiece so that crushes the surface roughness peaks. This material exhibits silicon nitride (Si_3N_4) ceramic with a diameter of 6mm. The ceramic ball is entirely supported by the fluid, freely rotating on the workpiece surface.

In the hydrostatic technology, the normal force depends only on the pump pressure.

This setup has several advantages, as follows [12]:

- the normal force is constant, proportional to the fluid pressure; the process is then consistent and easy to reproduce;
- the ball can rotate freely in any direction; this prevents any sliding contact with the workpiece;
- the tool can be installed on a regular or CNC milling, as shown in Fig. 2; burnishing can be thus carried out with the workpiece in the same clamped position as the previous operation;
- the tool has a long life and it is easy to maintain.



The burnishing technique can be used on cylindrical surfaces, flat surfaces, profiled surfaces, conical surfaces, zones of sharp section changes, etc.

III. EXPERIMENTAL DESIGN

The material used in the present study was the Low-alloy steel SCM 440, the chemical composition of which was given in Table 1. The material was heat-treated steel, with hardness 42-57 HRC.[13] The alloy steel contained moderate amounts of carbon (0.40%). It also contained chrome / molybdenum. SCM440 was used in thermal-refining or induction-hardening treatment for the automotive industry.

Table 1. Chemical composition of SCM 440 steel (mass%).

C	Si	Mn	Cr	Mo	Ni
0.41	0.30	0.07	1.10	0.20	1.5

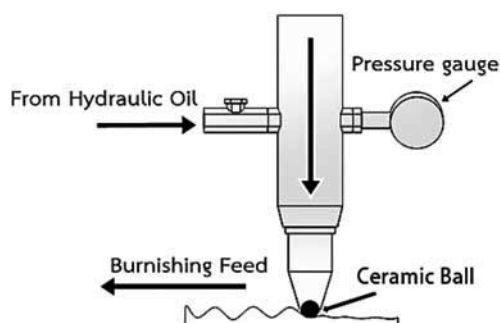


Fig 1. Principle schema of ball burnishing

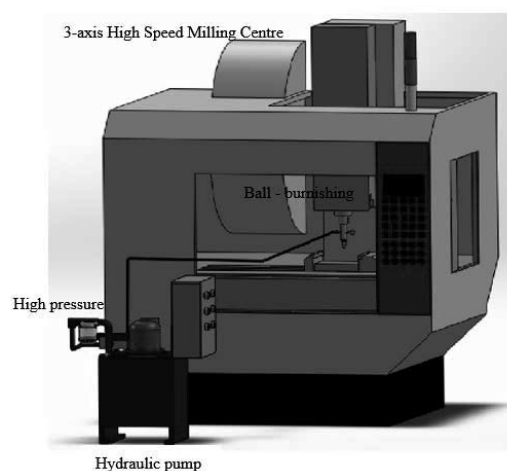


Fig. 2. Ball burnishing placed on the milling machine

To prepare the specimens, a face milling process had to be carried out. In this work, a CNC milling insert was used. All the burnishing tests Hydraulic oil HLP 68 were high-performance hydraulic oil with optimal anti-wear properties (AW-Additives) and high load capacity of the lubrication film. The process

variables for ball-burnishing were the burnishing pressure (P_b) and the burnishing depth (a_c).

The studies determined the burnishing parameters influencing on surface roughness and residual stress. Each specimen was initially size turned on a length of 60 mm width 40 mm and a thickness of 10 mm and then divided into several regions, each of them with different burnishing parameters. Some region was left without burnishing for initial surface roughness measurement.

- Surface roughness was measured using the 3D Optical Profiler from BRUKER.
- Surface hardness was measured using a Vickers hardness test method. The Vickers hardness test method also referred to as a micro hardness test method mostly used for small parts, thin sections, or case depth work.
- The plastic deformation produced on the part surface during ball burnishing causes a significant alteration of the residual stress state. X-ray diffraction (XRD) techniques were used for the residual stress measurement. XRD allows to measure the stress field on the surface or close to the surface.

The studies examined the surface improvement which was obtained from burnishing parameters. Three test parts were analyzed; surface hardness, surface roughness and residual stresses were measured. In Table 2, the parameters used for each test part were shown.

Table 2. Experimental of the burnishing tests

Input parameter	Test 1	Test 2	Test 3
Burnishing pressure (bar)	200	400	600
Burnishing depth (mm)	0.5, 0.6	0.5, 0.6	0.5, 0.6

IV. ANALYSIS OF THE SUPFACE QUALITY

The goal of the research is to give the manufacturer a set of options in term of burnishing parameters and original hardness in order to obtain a target hardness of 412 HV (42 HRC) after burnishing.

A. Surface hardness

The direct effect of burnishing parameters on surface hardness, the initial surface hardness of the test specimen is about HV 312.5 on average. After finishing the experiments with SCM440, Fig. 3 illustrates the surface hardness on the nine areas have been measured and averaged by the Vickers micro-hardness test instrument, Model MXT-70. The burnishing pressure variation in hardness reveals that the surface hardness increases with the increased burnishing pressure constantly from 200 to 600 bars. Further increase of burnishing depth results in the decrease of surface hardness. The surface hardness is increased to HV 58 6 on average, possibly, due to the squeezing of the grain boundary.

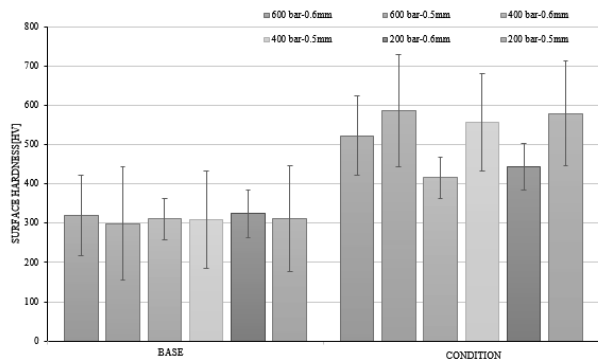


Fig. 3. Measured surface hardness on the burnished surface

B. Surface roughness

Measuring roughness surface topography using coherence scanning interferometry (CSI), CSI is a non-contacting measurement technique. It uses a broadband light source and combines vertical (z-axis) scanning techniques with optical interferometry techniques, to achieve a three-dimensional (3D) surface measurement. The core S parameters expanded from the roughness (2D) parameter are identified in Table 3. As previously explained for the profile parameters, the range of the real parameters available to the user will be dependent on the CSI instrument manufacturer. S parameters have also been developed as analogies to the range of material ratio parameters defined in ISO 4287

Table 3. 3D parameter expanded from the roughness (2D) parameter

3D Parameter	2D Roughness	Description	Typical Units
S_a	R_a	Arithmetical mean height	μm
S_q	R_q	Root mean square length of the scale limited surface	μm
S_p	R_p	Maximum peak height	μm
S_v	R_v	Maximum pit depth	μm
S_z	R_z	Maximum height of the scale limited surface	μm
S_{sk}	R_{sk}	Skewness of the scale limited surface	
S_{ku}	R_{ku}	Kurtosis of the scale limited surface	

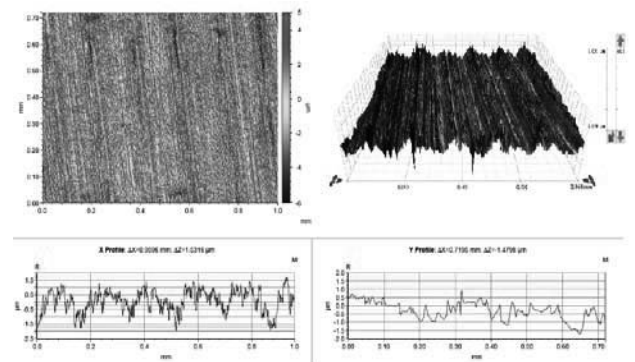
A set of tests was carried out in order to check the relation between roughness and the burnishing pressure (P_b) and burnishing depth (a_c). Table 4, the values of roughness for several external pressures are gathered, for different depths of burnishing of the CNC milling. Burnishing was always performed at feed 2m/min.

At the view of results, the first conclusion is that the higher the pressure, the lower the mean roughness, but there is little difference between case 400 and 600 bars. As a conclusion, at 400 bar the final roughness results are better, can be obtained when machining using a high depth of cut (0.6 mm) than when using a low depth of cut (0.5 mm).

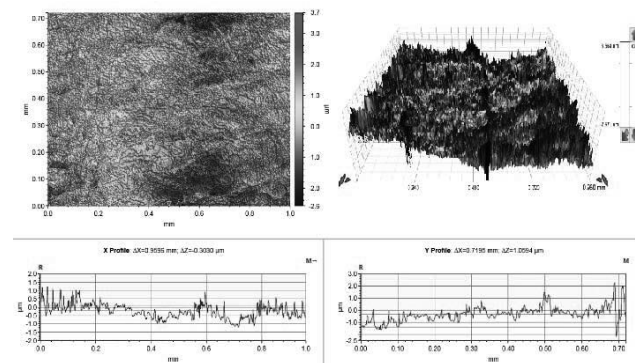
Table 4. Main pump pressure, roughness parameter, burnishing depth

Burnishing parameter	Burnishing depth (mm)	Roughness parameter						
		R_a (μm)	R_q (μm)	R_p (μm)	R_v (μm)	R_z (μm)	R_{sk}	R_{ku}
Before		1.395	1.674	5.513	-6.464	11.977	0.120	2.702
200 bar	0.6	0.588	0.735	3.316	-2.711	6.027	0.498	2.782
	0.5	0.638	0.860	4.000	-9.689	13.689	-2.532	51.697
400 bar	0.6	0.592	0.767	4.398	-4.064	8.462	-0.135	4.730
	0.5	0.349	0.454	3.707	-1.493	5.200	1.100	5.570
600 bar	0.6	0.874	1.049	4.057	-4.384	8.441	-0.031	2.630
	0.5	0.833	0.962	4.617	-4.827	9.444	-0.134	3.576

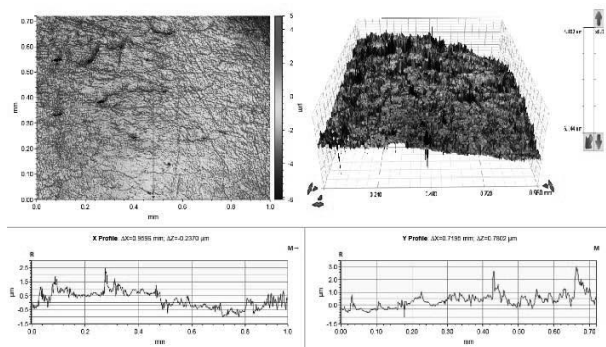
The quality of the surface roughness was studied. The surface topography before and after burnishing is presented, a complete analysis of the surface characteristics is addressed. After burnishing, the roughness reduction is more than an order of magnitude. The final quality is similar to grinding, even reaching $0.349 \mu\text{m}$ R_a . Topographies are shown in Fig. 4(a), Fig. 4(b) and Fig. 4(c); corresponding to a before surface and to the same surface after being burnished with two different burnishing depth. Roughness parameters improved about 75% when burnishing is applied.



a) Before burnishing



b) $P_b=400\text{bar}$, $a_c=0.5 \text{ mm}$



c) $P_b=400$ bar, $a_e = 0.6$ mm

Fig. 4. 2D and 3D Topographies and roughness profiles (a) before burnishing (b) after burnishing operation ($P_b=400$ bar, $a_e=0.5$ mm) (c) after burnishing operation ($P_b=400$ bar, $a_e = 0.6$ mm).

C. Compressive residual stresses

The plastic deformation produced on the part surface during ball burnishing causes a significant alteration of the residual stress state. It is well known that the generation of residual stress depends upon the interplay of many factors such as inhomogeneous plastic deformation induced by mechanical and thermal events associated with the process[10]. X-ray diffraction (XRD) techniques are used for the residual stress measurement. XRD allows measuring the stress field on burnishing surface. The variation of the compressive residual stress on the burnished surface has been measured by an X-ray diffractometer is shown in table 5. The horizontal compressive residual stress on the burnished surface was increased up to 369 MPa, possibly, due to the modification of the microstructure. The residual stresses have a significant dependence on the burnishing direction.[14]

To achieve a good surface hardness and the compressive residual stresses, are the keys for a remarkable improvement of the fatigue life and wear resistance of the burnishing components, the optimum condition could be $P_b=600$ bar; $a_e=0.5$ mm, as shown in Fig. 5.

Table 5. Residual stress value

Sample	Point	X	Y
200 bar-0.5 mm	Base	-206.3±15.2	141.3±9.0
	Surface	-366.7±15.3	-992.0±19.1
200 bar-0.6 mm	Base	7.2±10.8	39.8±9.4
	Surface	-350.1±6.2	-729±13.2
400 bar-0.5 mm	Base	109.4±18.0	362.1±15.6
	Surface	-342.3±12	-815.1±19.8
400 bar-0.6 mm	Base	296.4±16.1	451.1±16.9
	Surface	-340.4±5.6	-693.1±9.9
600 bar-0.5 mm	Base	-335.4±22.1	22±21.1
	Surface	-369.4±15.7	-787.4±17.1
600 bar-0.6 mm	Base	162.3±12.4	234.9±9.3
	Surface	-343.8±7.1	-711.2±8.2

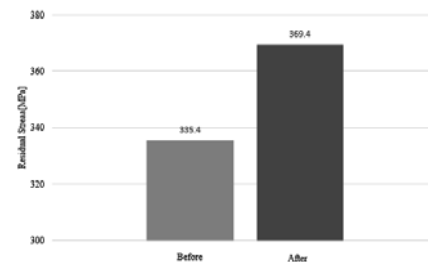


Fig. 5. Variation of the compressive residual stress on the burnished surface.

V. CONCLUSIONS

A ball burnishing tool integrated with a CNC milling was developed to improve the surface roughness, hardness, and residual stress of the material used in the present study, the Low-alloy steel SCM 440. The surface burnishing parameters for the ball-burnishing tool were determined after conducting the experimental methods. The burnishing pressure constantly from 200 to 600 bars, when machining using a burnishing depth 0.5 and 0.6 mm., the velocity of 2 m/min., the fluid as lubricant hydraulic oil (HLP 68) were used. The quality of the surface roughness was studied. The final quality was similar to grinding, even reaching $0.349 \mu\text{m}$ Ra on average, using the adequate burnishing parameters, corresponding to a before surface and to the same surface after being burnished with two different burnishing depth, roughness parameters improved about 75 % when burnishing was applied. The burnishing surface hardness was increased to HV 586 on average, possibly due to the squeezing of the grain boundary. X-ray diffraction (XRD) techniques were used for the residual stress measurement. The horizontal compressive residual stress on the burnished surface was increased up to 369 MPa.

References

- [1] W. Zhuang, and B. Wicks, "Mechanical Surface Treatment Technologies for Gas Turbine Engine Components," ASME J. Eng. Gas Turbines Power 125, 2003, pp.1021-1025.
- [2] V. Schulze. "Modern Mechanical Surface Treatment," Wiley-VCH, Weinheim, 2006.
- [3] E. Maawad, H.-G. Brokmeier, L. Wagner, Y. Sano, Ch. Genzel. "Investigation on the surface and near-surface characteristics of Ti-2.5Cu after various mechanical surface treatments," Surf. Coat. Technol. 205, 2011, pp.3644-3650.
- [4] M. Korzynski, A. Pacana, J. Cwanek. "Fatigue strength of chromium coated elements and possibility of its improvement with slide diamond burnishing," Surf. Coat. Technol. 203, 2009, pp.1670-1675.
- [5] M. Korzynski, A. Dzierwa, A. Pacana, J. Cwanek. "Fatigue strength of chromium coated elements and possibility of its improvement with slide diamond burnishing," Surf. Coat. Technol. 204, 2009, pp.1670-1676.
- [6] Yung-Chang Yen. "Modelling of metal cutting and ball burnishing prediction of tool wear and surface properties," PhD Thesis, the Ohio State University, 2004.
- [7] F. Klocke, and J. Liermann. "Roller burnishing of hard turned surfaces," J. of Machine Tools and Manufacture 38, 1996, pp.419-423.
- [8] M.H. El-Axir, and M.M. El-Khabeery. "Influence of orthogonal burnishing parameters on surface characteristics for various materials," Journal of Materials Processing Technology., 132 (1-3), 2003, pp.82-89.



- [9] A. Mahmood Hassan. "The effects of ball- and roller-burnishing on the surface roughness and hardness of some non-ferrous metals," *Journal of Materials Processing Technology*, 72 (3), 1997, pp.385–391.
- [10] Deepak Mahajan, and Ravindra Tajane. "A Review on Ball Burnishing Process," *International Journal of Scientific and Research Publications*, Volume 3, Issue 4, April 2013, pp. 1-8.
- [11] L.N. López de Lacalle, A. Lamikiz, J. Muñoa, J.A. Sánchez. "Quality improvement of ball-end milled sculptured surfaces by ball burnishing" *Int. J. Mach. Tool Manu.* 45, 2005, pp.1659-1668.
- [12] Liviu Luca, Sorin Neagu-Ventzel, and Ioan Marinescu. "Effects of working parameters on surface finish in ball-burnishing of hardened steels," *Precision Engineering*, 29, 2005, pp.253–256.
- [13] SCM440 www.tandemmetal.com [online]
- [14] Peirong Zhang, and Zhanqiang Liu. "Effect of sequential turning and burnishing on the surface integrity of Cr–Ni-based stainless steel formed by laser cladding process," *Surface & Coatings Technology*, 276, 2015, pp. 327–335.



Using Unmanned Aerial Vehicle Photogrammetry for Surveying a Landslide

Thitibhorn Phantachang 1st, Pradit Jiagulprasert
Department of Civil Engineering Faculty of Engineering
Rajamangala University of Technology Lanna
Chiang Mai, Thailand
Thitibhorn@rmult.ac.th, Pardit@rmult.ac.th

Abstract— Unmanned Aerial Vehicle (UAV) technology has recently been promoted for many Civil Engineering applications such as terrain survey, quarry mining survey and landslide hazard mapping. UAV photogrammetry combines classical manned aerial photogrammetry and ground survey techniques. This paper aims to use a UAV for landslide survey because it is well known that a UAV can provide accurate data at low-cost and less time consuming than ground survey methods. The landslide site is located 28 km northeast of Lampang Province, Thailand. A photogrammetric project was carried out with images taken from a Phantom 3 ADVANCED with a 12.76 Megapixels camera. We used photogrammetry software DJI Go 4, Pix4D Capture and Agisoft PhotoScan applications to process the data. The flight was designed to cover the whole survey area. This study has successfully shown that the UAV has capability to produce a three dimensional model and imaging fissures, illustrating ground displacement on the landslide surface.

Keywords— *landslides; slope instability; unmanned aerial vehicle; UAV; surveying*

I. INTRODUCTION

Aerial survey by Unmanned Aerial Vehicle (UAV) has been developed over few decades and much research has been carried out using UAV systems [1-2]. Two types of UAV are available, fixed wing and rotary. The fixed wing design is based on manned aircraft, the rotary design is based on helicopters with single or multi rotors [3]. The advantages of the UAV are widely used for multi purposes in recent years.

Most of Civil Engineering works require accurate terrain survey for structure building therefore UAV can play an important role in applications such as terrain survey, quarry mining survey [4], quarry surveys [5], construction sites, volumetric measurements reports, site mapping for safety and landslide hazard mapping [6-8]. UAV is also becoming increasing useful for landslide studies [9-10].

Slope stability analysis is required to assess the safe design of man-made or natural slopes and the equilibrium conditions. To performing stability analysis of landslides can be with limit equilibrium and numerical methods. The former is based on the static method and equilibrium of force and/or moment e.g. Simplified Bishop, Simplified Janbu, Spence and Morgenstern-Prices methods. The latter is based on the static and slope deformations. It can be point that two approaches require soil

basic and engineering properties and accurate in-situ slope geometry. Therefore, ground surveying is a traditional core service for slope geometry survey but requires surveying accessories such as theodolite or total station and GPS and, especially man-power. Furthermore, ground survey cannot perform in inaccessible landslide areas. Therefore the UAV technique has advantages over traditional methods with high resolution, high accuracy, low cost, less time-consuming and coverage of inaccessible areas.

This study aims to use UAV technology for terrain survey and applying it to evaluate the geometry of landslide and soil borehole positions. In this paper also attention is given to the landslide occurred in Mae Moh village, Lampang Province, to describe the geological investigated, soil basic properties test results and interpret the mass movements.

II. METHODOLOGY

The study was carried out at the landslide located on Mae Moh village Lampang Province, North Thailand. The landslide is 127 m long, the elevation difference between crown and toe was 6.5 m. In 20th October 2017 a UAV flight was carried out in the landside area (500 x 700 m) or around 219 Rai. The flight plan was designed to cover the potential landslide area.


The UAV used in this study was a Phantom 3 ADVANCED model by DJI with a 12.76 Megapixel camera, FPV 94 degree and built-in GPS record. The UAV specification is shown in Table I.

The automatic control of UAV at 70 m height provides a ground resolution of approximately 0.05 m per pixel Using DJI Go [11] compatible software with UAV. The longitudinal and transversal overlaps were 70% and 80% respectively along the landslide area. The flight used velocity of 2.5 m/s. Fig. 1(a) shows Pix4D application [12] runs on OIS mobile application for flight plan and Fig. 1(b) illustrates the setup flight area and flight plan.

Before flight mission, a skilled operator carried out UAV operation during takeoff, flight mission and landing to avoid any damages on UAV. This flight mission took 14 minutes. DTM generation was carried out using the photogrammetric process software, Agisoft photoscan professional v.1.4.2 [13]. Fig. 2 shows mosaic of the project photo and position of shooting points (164 photos).



TABLE I UAV PHANTOM 3 ADVANCED SPECIFICATIONS [14]

	UAV type	Dimension	Max ascent speed	Max speed	Max Tilt Angle	Max. take-off weight
	Phantom 3 ADVANCED	52x52x19.3 cm.	5 m/s	16 m/s	35°	1280 g
	Camera and sensor type	Lens	Sensor size (mm)	Image size (Pixel)	Pixel size (mm)	Focus length (mm)
	Sony EXMOR	FOV 94°	1/2.3"CMOS	4000×3000	12.76 M	2.8

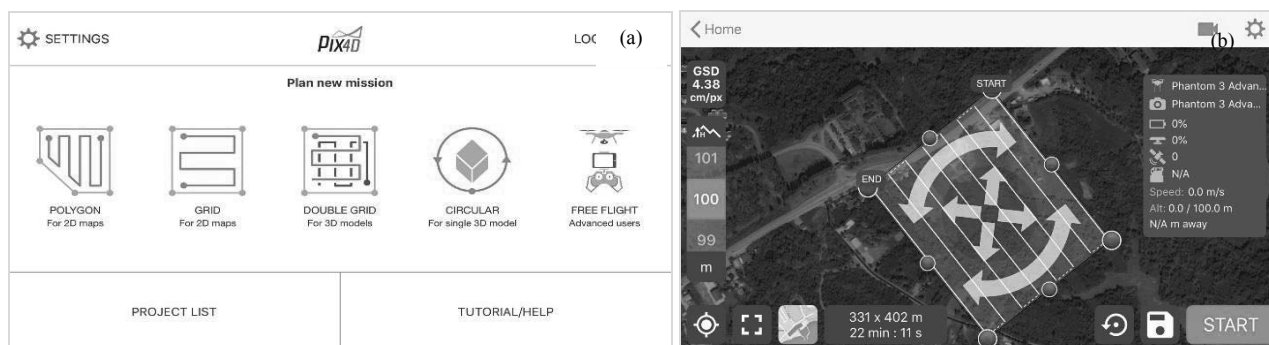


Fig. 1 (a) Pix4D Capture (OIS application) (b) Pix4D Capture map view [12]

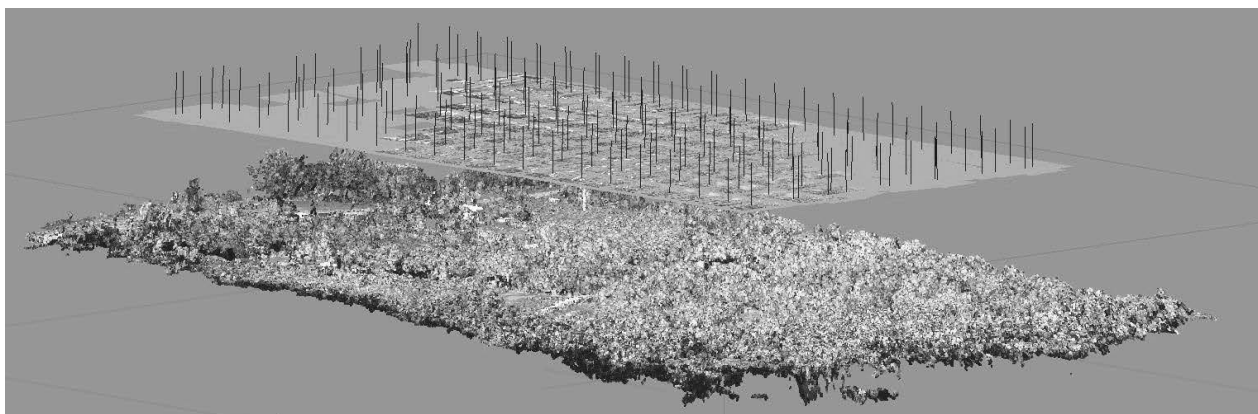


Fig. 2 Mosaic with point cloud of the project photos and shooting point positions

During image processing, we found that some images had quality problems due to high winds and clouds which caused blurred images and color balancing errors therefore another flight was carried out.

Fig. 3 shows the digital ortho image and soil borehole positions.

Fig. 4(a) shows the landslide at Mae Moh village. Fig. 4(b) shows the microdrone UAV, remote control and operator. Auger boring for soil investigation at the center line of landslide is shown in Fig. 4(c).

III. GEOTECHNICAL INVESTIGATION

We investigated this landslide with radio controlled unmanned aerial vehicles. The landslide occurred on October 17th 2017, Mae Moh village, about 28 km northeast of Lampang city, Thailand. Mae Moh village is located in Mae Moh district, this region has the average elevation of 335 meters above sea level. The regional geology of Mae Moh village is Tertiary sedimentary and subdivided into several rock units. Tandicul et al. [15] described the geological log of Mae Moh from bottom to the top as Lower Claystone, Lignite Q Seam, Interburden Claystone, Lignite K Seam unit overburden Claystone and the Red Bed or weathered Claystone unit. Slope



failure frequently occurred in weathered Claystone and overburden Claystone layers.

On October 20th 2017 the landslide was observed along a 127 m long, the direction of the landslide is NW to SE with mean slope angle is approximately 6°. The UAV photogrammetry and geological survey were carried out at the landslide site.

The Mae Moh landslide occurred on gentle slope or flat terrain and involved multiple of soil failure blocks movement (Fig. 4(a) and Fig. 5). This landslide can be classified by area in plan as the small landslide (in case area in plan 200-2,000 sq-m) [16]. The overburden soil was a low plasticity clay in saturated condition, loose, and cohesion-less. The occurrence mode of movement is lateral extension accompanied by shear or tensile fractures. The slope failure is triggered by water flow through the overburden sediments.

Three boreholes were drilled at the landslide area (as shown in Fig. 4(c)) on Oct 20th, 2017. A 3 in diameter hand auger was used to investigate all boreholes. A summary of the soil basic properties is presented in Table II.

Borehole BH01 was drilled at the crown of the landslide to a total depth of 2.0 m. Average water content was 25.92%, $G_s = 2.71$, $W_{LL} = 30.90-38.08\%$, $W_{PL} = 20.86-22.48\%$. The uppermost soil clay content can be classified in the Unified Soil Classification System (USCS) as low plasticity clay (CL); water was encountered at a depth of 1.5 m. below the ground.

Borehole BH02 was drilled at the middle of the embankment load to a depth of 1.35 m. Natural water content was 25.00%, $G_s = 2.79$, $W_{LL} = 32.0\%$, $W_{PL} = 20.21\%$. According to the USCS system the soil can be classified as CL.

Borehole BH03 was drilled at the toe of the landslide to a depth of 1.10 m. At depth of 0.00-0.50 and 0.50-0.80 m can be classified as CL. Natural water content was 21.87%, $G_s = 2.65$, $W_{LL} = 39.0\%$, $W_{PL} = 23.49\%$, can be classified as silt clay (CL-ML)

and at depth 0.80-1.10 m. Natural water content of 28.51%, G_s of 2.67, $W_{LL} = 50.0\%$, $W_{PL} = 30.66\%$ that could be classified as silt (ML); water was encountered at a depth of 1.0 m. below the ground.

Fig. 5 shows a three dimensional view of landslide area. The photos show the landslide slope from UAV images. Contour lines also be generated at the slope area and at the flat area. Therefore, UAV images were capable of providing high quality data for GIS use.

The soil profile can be plotted according to soil boreholes with ground surface along the slope failure and existing slope were illustrated in Fig.6.



Fig. 3 Digital Ortho-rectified image and borehole positions

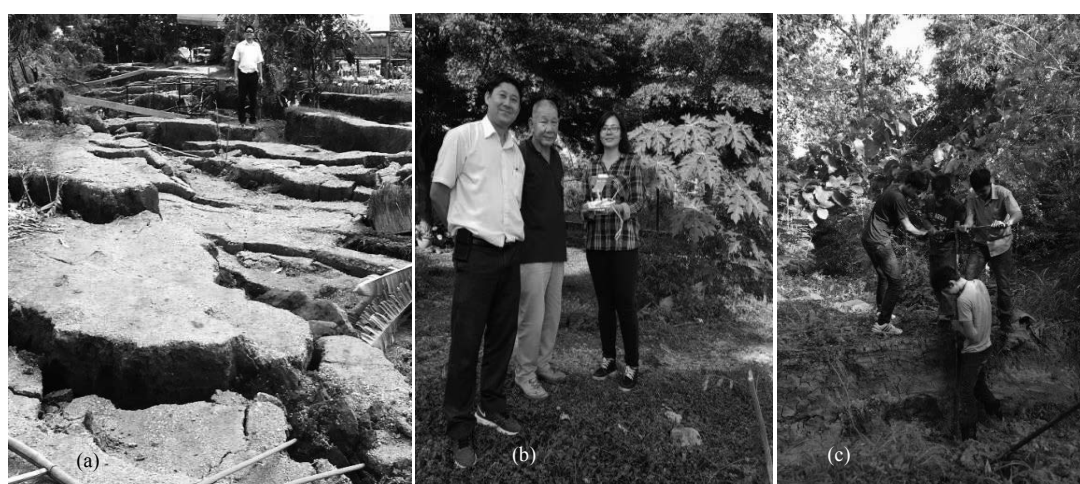


Fig.4 (a) Photos of landslide (b) UAV control (c) Hand auger soil boring



TABLE II SUMMARY OF SOIL TESTING RESULTS (BASIC PROPERTIES)

Boring No.	Depth (m)		Water content, w%	Unit weight T/m ³	Specific gravity	Percent passing	Atterberg Limit Tests, %			USCS
	From	To					W _{LL}	W _{PL}	PI	
BH01-01	0.00	0.90	20.57	1.80	2.74	84.90	30.90	20.86	10.04	CL
BH01-02	0.90	1.60	31.76	1.81	2.70	69.00	38.08	23.13	14.95	CL
BH01-03	1.60	2.00	25.44	1.85	2.67	79.26	34.66	22.48	12.18	CL
BH02-01	0.00	1.35	25.00	1.75	2.79	87.61	32.10	21.21	10.89	CL
BH03-01	0.00	0.50	21.87	1.89	2.65	94.00	39.00	23.49	15.51	CL
BH03-02	0.50	0.80	23.94	1.85	2.68	70.40	28.50	21.64	6.86	CL - ML
BH03-03	0.80	1.10	28.51	1.85	2.67	79.60	50.00	30.66	19.34	ML



Fig. 5 (a) Photos of 3D model of the overall landslide area (b) Zoom view

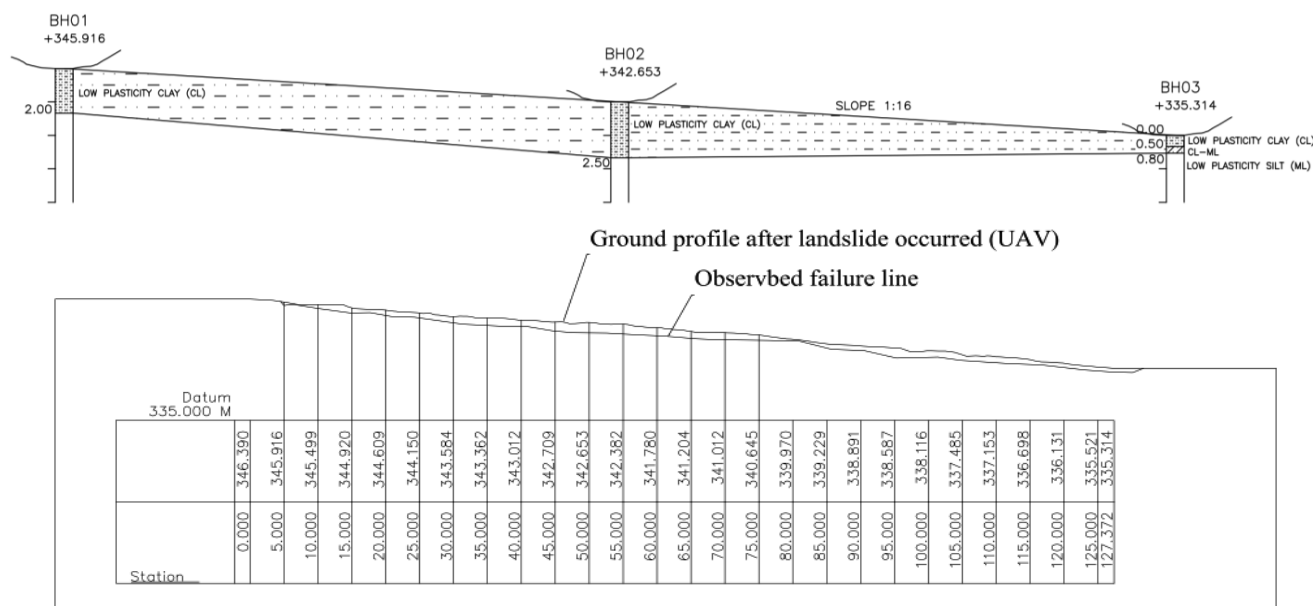


Fig. 6 Soil profile and Slope geometry



In this study, two primary result sets are produced, firstly, digital elevation and digital ortho images which then allow contour and position on the ground to be evaluated. Secondly, the soil in-situ investigation and soil basic properties were evaluated, allowing slope geometry and soil profile to be presented.

IV. CONCLUSIONS

This paper presents the results of a photogrammetric survey using UAV images to investigate a landslide. The digital ortho-image and three dimensional model of the landslide are presented. The borehole position and slope geometer of the landslide establish the usefulness of UAV photography. The results show that UAV images were able to present an accurate three dimensional model of the landslide. In future work, the results of DEM and ortho-images can be used for landslide stability and slope movement monitoring.

ACKNOWLEDGMENT

The authors sincerely thank Mr. Ekachai Kitivarakun, photogrammetry expert and senior lecturer in Civil Engineering Department RMUTL Chiang Mai who gave advice and assistance for this study. The authors are also grateful to the land owner who provided information on the study area. Thanks also go to RMUTL students for their help and support. We thank Soil Mechanics Laboratory, RMUTL Chiang Mai for providing institutional and laboratory facilities. Finally, the authors would like to thank Prof. David Higgs for constructive criticism of the manuscript.

REFERENCES

- [1] U. Niethammer, M. R. James, S. Rothmund, J. Travelletti and M. Joswig, "UAV-based remote sensing of the Super-Sauze landslide : evaluation and results," *Engineering Geology*, vol. 128 (1), pp. 2-11, 2012.
- [2] F. Carvajal, F. Agüera and M. Pérez, " Surveying a landslide in a road embankment using unmanned aerial vehicle photogrammetry," *International Conference on Unmanned Aerial Vehicle in Geomatics (UAV-g)*, Zurich. *International Archives of the Photogrammetry, Remote Sensing and Spatial Information Sciences XXXVIII-1/C22*, pp. 201-206. September 2011.
- [3] KN. Tahar, "A new approach on production of slope map using autonomous Unmanned aerial vehicle," *Int. J. of Recent Research and Applied Studies*, vol. 13, pp. 780-785, 2012.
- [4] F. Nex and F. Remondino, "UAV for 3D mapping applications: a review," *Applied geomatics*, vol. 6 (1), pp. 1-15, 2014.
- [5] W. Stempfhuber and M. Buchholz, "A precise, low-cost RTK GNSS system for UAV applications," *International Archives of Photogrammetry, Remote Sensing and Spatial Information Science*, vol. 38, pp. 1-C22, 2011.
- [6] A. Lucieer, S.M.D. Jong, and D. Turner, "Mapping landslide displacements using Structure from Motion (SfM) and image correlation of multi-temporal UAV photography," *Progress in Physical Geography*, vol. 38 (1), pp. 97-116, 2014.
- [7] J.Y. Rau, J.P. Jhan, C.F. Lo, and Y.S. Lin, "Landslide mapping using imagery acquired by a fixed-wing UAV," *Int. Arch. Photogramm. Remote Sens. Spat. Inf. Sci.*, vol. 38, pp. 1-C22, 2011.
- [8] S. M. Adams and C. J. Friedland, "A Survey of Unmanned Aerial Vehicle (uav) Usage for Imagery Collection in Disaster Research and Management." 2011.
- [9] Niethammer, U., S. Rothmund, U. Schwaderer, J. Zeman, and M. Joswig, "Open source image-processing tools for low-cost UAV-based landslide investigations." *International Archives of the Photogrammetry, Remote Sensing and Spatial Information Sciences*, vol. 38 (1), pp. 1736-1757, 2011.
- [10] Lindner, Gerald, Klaus Schraml, Reinfried Mansberger, and Johannes Hübl, "UAV monitoring and documentation of a large landslide." *Applied Geomatics*, vol. 8 (1), pp. 1-11, 2016.
- [11] DJI, Phantom 3 ADVANCED user manual V.1.0, 2015, Accessed on: April. 1, 2018. [Online]. Available: <https://archaeology.sites.unc.edu/files/2017/01/DJI-Phantom-3-Advanced-User-Manual.pdf>.
- [12] DJI Go app. DJI, Shenzhen, China, 2018; software available at <https://www.dji.com/goapp>.
- [13] Pix4D Capture app. Pix4D, Inc., Lausanne, Switzerland, 2018; software available at <https://pix4d.com/product/pix4dcapture/>.
- [14] Agisoft Photoscan Profesional (Demo) 1.4.2. Agisoft LLC, St. Petersburg, Russia, 2018; software available at <http://www.agisoft.com/downloads/installer/>.
- [15] W. Tandicul, N. Muangnoicharoen and N. Gumperayarnont, "The slope stability problem at Mae Moh Lignite Mine, Lampang Province., Northern Thailand," *GEOSEA V Proceedings*, Geol. Soc. Malaysia, vol. 1, pp. 613-625, April 1986.
- [16] Cornforth, D., *Landslides in practice: investigation, analysis, and remedial/preventative options in soils*, Wiley, 2005.



A Review on Difference of Contracting for Works of Regulations on Procurement, B.E. 2535 (1992) between Government Agency and Local Government, Thailand

Boonruk Vanborsel and Kumpon Subsomboon

Civil Engineering Department

Engineering Faculty NU

Phitsanulok, Thailand

boonruk_vanborsel@yahoo.com, kumpons@gmail.com

Abstract— Operational framework and different standards resulted in problems and barriers to purchasing and contracting for works of Thai Government. This research aims to compare the differences of the Regulation on the Office of the Prime Minister's procurement B.E. 2535 (OPM Regulation 1992) and Regulation on the Ministry of Interior on the procurement of Local Administration Organization B.E. 2535 (MOI Regulation 1992). The findings revealed that the differences of the regulations on procurement, B.E. 2535 (1992) were 1) the person having in charge of these regulations 2) application 3) committee in charge of procurement (CCP) 4) plan for procurement 5) pre-qualification for purchasing and contracting for works 6) procedure on purchasing and contracting for works and 7) penalty for person excluded from procurement programs.

Keywords—regulation; procurement; government agency; local government

I. INTRODUCTION

For the last decades, procurement of Thai Government act under Regulation on the Office of the Prime Minister's procurement B.E. 2535 (OPM Regulation 1992) [1], applicable to government agency "government agency" means a Ministry, Sub-Ministry, Department, Office or other government units in the central administration and provincial administration or in abroad, excluding state enterprise, government body established under the law on local administration, other units set up by law with the status of a local administration and Regulation on the Ministry of Interior on the procurement of Local Administration Organization B.E. 2535 (MOI Regulation 1992) [2], applicable to government body established under the law on local administration "government body established under the law on local administration" means Provincial Administrative Organization, Municipality, and Subdistrict Administrative Organization. There are many problems that affect the efficiency and effectiveness of the administration of the parcel. The government loses its budget and damages the overall picture of the country. The problems were frequent and intensified continuing to the present, for example, corruption in

procurement by virtue of legal space and legal discretion in fraud, disqualification of participants and the auction unfair qualification or conditions for bidding, locking specification price negotiation between entrepreneurs, inspection, and acceptance of work is not realistic, corruption in the process of disbursement, the use of regulatory authority to seek benefits.

Corruption is caused by unclear regulations and practices, a gap of regulation, standard price, or the official estimated pricing inappropriate, a disbursement system that lacks balance between authorized payer and payer, the monitoring mechanism is not comprehensive. The most problems mentioned above arise from provisions of law and the compliance of the relevant authorities [3]-[6].

Y. Phanboot et al. [4] and K. Puang-ngam [5] studied only in the MOI Regulation 1992, whereas V. Yensab [6] studied in the OPM Regulation 1992. However, these research that compare the differences of both Regulations. Therefore this research is interested in studying this issues by reviewing and comparing Regulation on the Office of the Prime Minister's procurement B.E. 2535 and Regulation on the Ministry of Interior on the procurement of Local Administration Organization B.E. 2535, in order to compare the differences in regulations showing the barriers of contracting for works. Hopefully, the content has been analyzed. It is useful to those interested, to use as a guideline for future research, by a study conduct in conjunction with Government Procurement and Supplies Management Act, BE 2560 (2017).

II. METHODOLOGY

The educational process is as follows:

A. Studying and Analysis of the Regulations

Content analysis was used in this research, it is to study and analyze the Regulation on the Office of the Prime Minister's procurement B.E. 2535 and Regulation of the Ministry of Interior on the procurement of the local administration organization B.E. 2535.



B. Summary the Issues

After the studying and analysis, it is to summarize the issues by compared the differences the issues of contracting for works of Regulations on Procurement, B.E. 2535 (1992).

III. RESULTS AND DISCUSSION

From table 1 shows the comparison of the differences of the Regulations on Procurement B.E. 2535 (1992) between Government Agency and Local Government. The results are as follows.

A. The person having in charge of these regulations

The Permanent Secretary of Ministry of Finance shall take charge of Regulation on the Office of the Prime Minister's procurement B.E. 2535 while the Permanent Secretary of Ministry of Interior shall take charge of Regulation on the Ministry of Interior on the procurement of Local Administration Organization B.E. 2535.

B. Application

Regulation on the Office of the Prime Minister's procurement B.E. 2535 shall apply to government agencies that carry out the procurement by utilizing government budget, loan and grant aid while Regulation on the Ministry of Interior on the procurement of Local Administration Organization B.E. 2535 shall apply to government body established under the law on local administration that carry out the procurement by utilizing government budget, loan, grant aid, the off-budgetary and borrowing from accumulated retirement.

C. Committee in Charge of Procurement (CCP)

Only Regulation on the Office of the Prime Minister's procurement B.E. 2535 specified this issue. It stated that there shall be a Committee in Charge of Procurement called in abbreviation as "CCP", to be composed of Permanent Secretary of Ministry of Finance. The CCP has the following authorities:

- to interpret and make recommendation pertaining to the enforcement of these Regulations.
- to grant a reprieve or exemption in the event that the government agency concerned cannot comply with these Regulations.
- to consider the complaint in case that the government agency does not comply with these Regulations, Penalty Components of CCP.
- to propose the Cabinet for the alternation or improvement of these Regulations.
- to set up the form of sample including adding, alter or set the guideline to be in line with these Regulations.
- to recommend the person authorized to act under these regulations in considering and circulating the persons excluded from procurement programs and placing order to withdraw from the department list of government agency,

government body established under the law on local administration, other units set up by law with the status of a local administration and state enterprise.

- to set the percentage of price .
- to set the classification or type of materials which are necessary to be purchased from abroad.
- to invite government officers and government employees or staffs and employees of state enterprise or the persons involved for inquiry or statement, as well as to request for the submission of document from the relating government agency, government body under the law on local administration, other units set up by law with a status of a local administration or state enterprise.
- to appoint sub-committee to perform any duty assigned by the committee.
- to carry out any work assigned by the cabinet.
- to consider the report on contracting for works.
- to set up consultant's remuneration.
- to set up criteria for fixing penalty rate.
- to set up criteria, guidelines and procedures as in these Regulations.

D. Plan for procurement

Only Regulation on the Office of the Prime Minister's procurement B.E. 2535 specified this issue. It stated that after knowing the money limit for procurement, the government agency has to carry out the procurement plan and follow step by step in accordance with these regulations, depending on the case, in order to be ready for the prompt contracting after receiving the financial approval.

E. Pre-qualification for Purchasing and Contracting for Works

Any government agency or Government body established under the law on local administration who requires making a pre-qualification for purchasing and contracting for works can be performed only in the case which necessitate limiting for the qualified bidders. The notice with the specification on criteria and selection method will be put up at a conspicuous place. But only Regulation on the Office of the Prime Minister's procurement B.E. 2535 shall be also submitted to the CCP.

F. Procedure on Purchasing and Contracting for Works

The purchasing or contracting for works according to Regulation on the Office of the Prime Minister's procurement B.E. 2535 may be carried out in any of the following 6 methods:

- Price agreeing (negotiating) method.
- Price inquiry (selective tendering) method.
- Competitive bidding (open tendering) method
- Special (limited tendering) method.
- Special case method.
- E-auction method.



TABLE I. COMPARISON OF DIFFERENCES OF CONTRACTING FOR WORKS OF REGULATIONS ON PROCUREMENT, B.E. 2535 (1992)

Issues	Regulation on the Office of the Prime Minister's procurement B.E. 2535	Regulations on the Ministry of Interior on the procurement of Local Administration Organization B.E. 2535
The person having in charge of these regulations	The Permanent Secretary of Ministry of Finance.	The Permanent Secretary of Ministry of Interior
Application	Government agencies	Government body established under the law on local administration
Committee in charge of procurement (CCP)	There shall be a Committee in charge of procurement called in abbreviation as "CCP", to be composed of Permanent Secretary of Ministry of Finance, The CCP has the 15 authorities:	Not specify
Plan for procurement	After knowing the money limit for procurement, the government agency has to carry out the procurement plan and follow step by step in accordance with these regulations, in order to be ready for the prompt contracting after receiving the financial approval. For the procurement by price inquiry method and competitive bidding method, government agency shall make a plan for procurement and has to procure as planned.	Not specify
Pre-qualification for purchasing and contracting for works	Any government agency who requires making a pre-qualification for purchasing and contracting for works can be performed only in the case which necessitate limiting for the qualified bidders. The notice with the specification on criteria and selection method will be put up at a conspicuous place and shall be also submitted to the CCP.	Any government agency who requires making a pre-qualification for purchasing and contracting for works can be performed only in the case which necessitate limiting for the qualified bidders. The notice with the specification on criteria and selection method will be put up at a conspicuous place.
Procedure on purchasing and contracting for Works	The purchasing or contracting for works may be carried out in any of the following 6 methods: 1) Price agreeing (negotiating) method shall apply in the case of a single contract of not more than Baht 100,000. 2) Price inquiry (selective tendering) method shall apply in the case of a single contract of more than Baht 100,000 but not more than Baht 2,000,000. 3) Competitive bidding (open tendering) method shall apply in the case of a single contract of more than Baht 2,000,000. 4) Special (limited tendering) method is that of more than Baht 100,000 each. 5) Special case method is that of more than Baht 100,000 each. 6) E-Auction method shall apply in the case of a single contract of more than Baht 2,000,000.	The purchasing or contracting for works may be carried out in any of the following 5 methods: 1) Price agreeing (negotiating) method shall apply in the case of a single contract of not more than Baht 100,000. 2) Price inquiry (selective tendering) method shall apply in the case of a single contract of more than Baht 100,000 but not more than Baht 2,000,000. 3) Competitive bidding (open tendering) method shall apply in the case of a single contract of more than Baht 2,000,000. 4) Special (limited tendering) method is that of more than Baht 100,000 each 5) Special case method is that of more than Baht 100,000 each.
Penalty for person excluded from procurement programs	The head of government agency shall propose the report together with his comments to Permanent Secretary promptly in order to approve the selected bidder, seller, contractor or sub-contractor who get permission from government to subcontract as a person excluded from procurement programs, depending on the case. When the Permanent Secretary considers that such person should be a person excluded from procurement programs, Permanent Secretary shall submit the name of that person to the person having in charge of these Regulations for approving as person excluded from procurement programs recently. In the case that it is a big project along with the criteria and within money limit specified by CCP, if Permanent Secretary considers that such person should be person excluded from procurement programs, person having charge of these Regulations shall place an order him as person excluded from procurement programs by naming in a debarment list and circulate his name to all government agencies for information. The person who abandons the work shall be informed by registered mail as well.	The head of the local administration organization shall propose the report together with his comments to Governor promptly in order to approve the selected bidder, seller, contractor or sub-contractor who get permission from government to subcontract as a person excluded from procurement programs, depending on the case. When the Governor considers that such person should be a person excluded from procurement programs, Governor shall place an order him as person excluded from procurement programs and send the name list to the Permanent Secretary of Ministry of Interior in order to submit the name of that person to the Permanent Secretary of Ministry of Finance for approving and circulate his name to all government agencies for information. The person who abandons the work shall be informed by registered mail as well. After that the Permanent Secretary of Ministry of Interior shall circulate debarment list to all Government body established under the law on local administration.



The purchasing or contracting for works according to Regulation on the Ministry of Interior on the procurement of Local Administration Organization B.E. 2535 may be carried out in any of the following 5 methods:

- Price agreeing (negotiating) method.
- Price inquiry (selective tendering) method.
- Competitive bidding (open tendering) method
- Special (limited tendering) method.
- Special case method.

G. Penalty for Person Excluded from Procurement Programs

The government agency and government body established under the law on local administration are not permitted to do any juristic relation with any person in the debarment list, except the person having in charge of these Regulations will withdraw his name from the list.

Prohibition government agency to do any juristic relation with any person in the debarment list.

Person or juristic person, pending a consideration to be person excluded from procurement programs according to the specification in this chapter, has a right to quote the price or submit work proposal to government agency. But if there is a consideration later that the person having in charge of these Regulations places an order to person or juristic person to be person excluded from procurement programs, Permanent Secretary shall exclude his name from the list of selected bidder or cancel the price inquiry envelope-opening, competitive bidding or the signing in the contract of purchasing or engaging which has been proceeded before person having in charge of these Regulations places an order. Except in the case that Permanent Secretary considers it will be beneficial to government agency, such person's name may not be excluded from the list. Or the price inquiry envelop-opening, competitive bidding may not be canceled or the signing in the contract of purchasing or engaging which has been proceeded before person having in charge of these Regulations places an order may not be cancelled.

Cause of debarment, when the following situations happen:

- 1) The selected bidder does not sign the contract or agreement with the government agency within the time limit.
- 2) The contractor or sub-contractor who gets permission from government to sub-contract breaks the contract or agreement.
- 3) Materials to be purchased or contracted are defected within the period specified in the contract or agreement and are not restored by seller, contractor or materials to be purchased or contracted do not get standard or used materials do not get standard or are not delivered in the amount specified in the contract or agreement which cause seriously damaged to work.
- 4) In the case of infrastructure construction, materials or equipment to be purchased or contracted or used by subcontractor, who gets permission from government agency to subcontract, deteriorate or do not get standard or are not in the amount of according to (3).

The head of the local administration organization shall propose the report together with his comments to Governor promptly in order to approve the selected bidder, seller, contractor or sub-contractor who get permission from government to subcontract as a person excluded from procurement programs, depending on the case. When the Governor considers that action according to 1), 2), 3) or 4) is undertaken without appropriate reason and such person should be a person excluded from procurement programs, Governor shall place an order him as person excluded from procurement programs and send the name list to the Permanent Secretary of Ministry of Interior in order to submit the name of that person to the Permanent Secretary of Ministry of Finance for approving and circulate his name to all government agencies for information. The person who abandons the work shall be informed by registered mail as well. After that the Permanent Secretary of Ministry of Interior shall circulate debarment list to all Government body established under the law on local administration.

While Regulation on the Office of the Prime Minister's procurement B.E. 2535, the head of government agency shall propose the report together with his comments to Permanent Secretary promptly in order to approve the selected bidder, seller, contractor or sub-contractor who get permission from government to subcontract as a person excluded from procurement programs, depending on the case.

When the Permanent Secretary considers that action according to 1), 2), 3) or 4) is undertaken without appropriate reason and such person should be a person excluded from procurement programs, Permanent Secretary shall submit the name of that person to the person having in charge of these Regulations for approving as person excluded from procurement programs recently.

In the case that it is a big project along with the criteria and within money limit specified by CCP, if Permanent Secretary considers that that person should not be person excluded from procurement programs, Permanent Secretary shall report to CCP for information. When person having charge of these Regulation, after receiving the comments of CCP, considers that such person should be person excluded from procurement programs, person having charge of these Regulations shall place an order him as person excluded from procurement programs by naming in a debarment list and circulate his name to all government agencies for information. The person who abandons the work shall be informed by registered mail as well.

IV. CONCLUSIONS

The findings revealed that the differences of the Regulation on the Office of the Prime Minister's procurement B.E. 2535 (OPM Regulation 1992) and Regulation on the Ministry of Interior on the procurement of Local Administration Organization B.E. 2535 (MOI Regulation 1992) were 1) For OPM Regulation 1992, the Permanent Secretary of Ministry of Finance will take charge. However the Permanent Secretary of Ministry of Interior shall take charge for MOI Regulation 1992. 2) OPM Regulation 1992 is applied to government agencies



except government body established under the law on local administration that MOI Regulation 1992 is applied. 3 and 4) For committee in charge of procurement (CCP) and plan for procurement, only OPM Regulation 1992 is specified this issues. 5) For pre-qualification for purchasing and contracting for works, OPM Regulation 1992 should submitted to the CCP. 6) For procedure on purchasing and contracting for works, MOI Regulation 1992 has 5 methods whereas OPM Regulation 1992 add the E-auction as additional method. 7) For penalty for person excluded from procurement programs, MOI Regulation 1992 1 more step needed involving Governor that may take a long time.

REFERENCES

- [1] The Comptroller General's Department, (2017, Dec. 19). Regulations of the Office of the Prime Minister on Procurement B.E. 2535 (1992). [Online]. Available: http://kmcenter.rid.go.th/kcsupply/index.php?option=com_content&view=article&id=18:-2535-&catid=8:2013-08-28-14-48-27&Itemid=4.
- [2] Local Administration Organization, (2017, Dec. 19). Ministerial Regulations _Government Division of Department of Local Administration of Ministry of the Interior (issue 2) B.E. 2559 (2016). [Online]. Available: http://www.dla.go.th/division_dla.jsp.
- [3] N. Thawornluk, Study of environmental factors effecting construction contractor business, M.Eng. project study King Mongkut's Univ. of Technology, Thonburi, Bangkok, 2015.
- [4] Y. Phanboot, T. Jitmahuema and P. Jitmahuema, "Problems on procurement by electronic auction of Local Government Organisation," SSRU Graduate Studies Journal, vol. 1, no. 2, pp. 50-61, 2014.
- [5] K. Puang-ngam, (2017, Nov. 06). The Problem of Corruption in the Local Administration Organization (LAO). [Online]. Available: <http://www.anticorruption.in.th/2016/th/>.
- [6] V. Yensab, Governmental Procurement by Electronic Method, M.Eng. thesis Chulalongkorn Univ., Bangkok, 2008.



Efficiency of alkaline fuel cell for produce hydrogen gas, in conjunction with electric production by using PEM membrane fuel cell

Janjira Yatom¹:

¹School of Renewable Energy, Maejo University,
Chiang Mai, 50290, Thailand
e-mail; janjira_yatom@hotmail.com

Natthanicha Sukasem²:

¹School of Renewable Energy, Maejo University,
Chiang Mai, 50290, Thailand
e-mail; jewy.ja@gmail.com

Abstract— Hydrogen gas is an alternative energy that produces by the alkaline fuel cell. Hydrogen gas uses in electric production via electrochemical reaction in alkaline hydrogen fuel cell. The efficiency of hydrogen coupled with the electricity production was improved by using various types of electrodes; smooth, hole, and net stainless steel, and electrolyte chemical reagents; NaOH, Ca(OH)₂, and KOH at 0.5-2M. The voltages at 1-9V were input in hydrogen production for 30 min at ambient temperature. The 0.5 M of NaOH solution showed the best electrolyte in hydrogen production. Moreover, the stainless steel 604-hole structure generated hydrogen concentration at 329 ppm and produced hydrogen volume at 75 cm³. This generated hydrogen was injected into hydrogen fuel for electricity production. The electric production system showed the high voltage at 2.828 mV, 4.64 A/m², and 2.59 W/m² add an amp and power density. The efficiency of hydrogen production conjugated with the electricity generation was 0.225% theoretical yield.

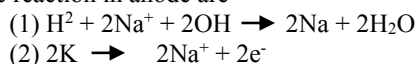
Keywords—component; Hydrogen gas; Alkaline fuel cell; PEM fuel cell; electrolyte chemical; Electricity production.

I. INTRODUCTION

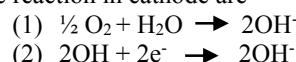
Nowadays around the world, the people realize on the usages of fossil fuels which effects on global warming such as carbon dioxide (CO₂), carbon monoxide (CO), toxic gas day]. Therefore, the looking for renewable energy production technology to produce energies are most important. These renewable energies will be used instead of fossil oil, finally, in the future [1].

Hydrogen is the one kind of the alternative energy which does not release toxic gases and environmental pollutants. Because the hydrogen has the high potential energy, this led hydrogen is used in various application such as car, power plant, and Submarine The electrolysis of water produces hydrogen and other chemical components at cathode and anode in the alkaline fuel cell. The alkaline electrolytes such as electrolyte are electrolyte are NaOH electrolyte are;

The reaction in anode are



The reaction in cathode are



So stainless steel 604 had property, low-alloy steel, electric conductivity is moderate. Stainless steel 604 was reaction between of stainless steel and electrolyte. When input voltage be gated split of the water (Blue color in the figure 1), get hydrogen gas and oxygen gas, so hydrogen gas split in the cathode and oxygen gas split in the anode of electrode shoe in the figure 1

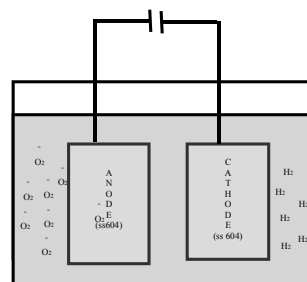
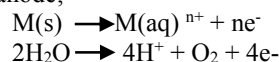
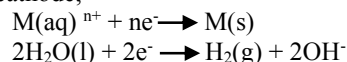


Figure 1 Alkaline fuel cell

Alkaline fuel cell had the reaction of electrode in the process are the anode;



Alkaline fuel cell had the reaction of electrode in the process are the cathode;



M is the material for used electrode, n is the number of electrons. Electro coagulation processes of metal hydroxides, polyhedroids and/or polyhydroxy metallic. Which, compound of electrode was been generate. Materials of electrode contain strong relate to dispersed particle and counter ions.



II. METHODOLOGY

A. Designation and installation system of an alkaline fuel cell connect to PEM fuel cell.

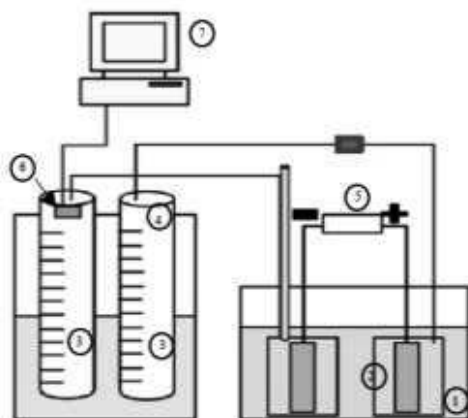


Figure 2 The alkaline hydrogen fuel cell system (1). Electrolyte, (2). Box cover electrode, (3) cylinder, (4) Silicone tube connect with cylinder, (5) power supply, (6) MQ8 sensor, (7) Computer for show data voltage.

The alkaline fuel cell system was shown in figure 2. The 800 ml of the box was used for storage the alkaline electrolyte solution (1). In this box, there were 2-cylinder bottles (200 ml) which covered the stainless 604 electrodes (2), anode and cathode, in each bottle (3). In an electrolysis system, at the cathode, the hydrogen was produced in the cylinder tube and kept in the storage tube (4). At the cathode, the produced oxygen gas was kept in its storage tube. The DC power supply (5) connected to both anode and cathode. The concentration of hydrogen in storage tube was measured by the MQ8 sensor (6) and its data values shown on the computer (7).

B. Install alkaline fuel cell conjunction with PEM fuel cell

The experimental produce hydrogen gas was operating electric by using PEM fuel cell, so processes produce electric was used AFC working with PEMFC. So AFC produce hydrogen gas and oxygen gas get to PEMFC show in the figure 3. The PEM fuel cell consisted of hydrogen storage tank, oxygen storage tank, both stainless steel net 604 electrodes; (anode and cathode (A)), PEM membrane (B) and external loading 1 k Ω external resistance which linked between anode and cathode. (1C) Hydrogen gas send to hydrogen box pass silicone tube same with oxygen gas (2C). Multimeter connect with electric wire of PEM fuel cell (3C). The systems were operated for an hour under ambient temperature. whereas the hydrogen concentrations, hydrogen volume, system temperature, the voltages, were collected during the experiments the electricity was measured by digital whereas the hydrogen concentrations, hydrogen volume, system temperature, the voltages, were collected during the experiments

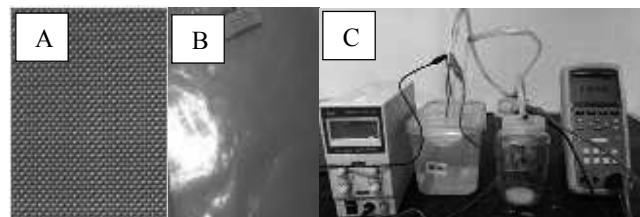


Figure 3. Alkaline fuel cell conjunction with PEM membrane fuel cell (A. stainless steel 604 net, B. Nafion No.117, C. Alkaline fuel cell working with MFC fuel cell (1. Transport line for send gas, 2. Multimeter for measure hydrogen gas, 3. Electric wire connect with PEM fuel cell.))

C. Analysis of the alkaline hydrogen fuel cell and PEM fuel cell.

1. Study on the proper of electrode and volume at various voltage loading into the alkaline fuel cell system.

The experiment of an alkaline fuel cell was operated by used using the 3 types of stainless steel 604 as electrodes, using the NaOH 1M as the electrolyte solution, and inputting the voltage loading at 1-9V into the system. The MQ8 sensor measured the concentration of hydrogen gas.

2. Study on the proper of various the electrolyte solution in the alkaline fuel cell system.

The electrolyte reagents at different types and concentration were tested to optimize conditions of the alkaline hydrogen fuel cell system. Thus, the NaOH, KOH, and Ca(OH)₂ reagents were applied as the electrolytes of the system.

3. Study on the efficiency of the electricity production by using PEM fuel cell working with an alkaline hydrogen fuel cell.

The efficiency of the electricity generation was determined after the couple systems of alkaline hydrogen production and hydrogen PEM fuel cell completely finished. The hydrogen concentration and its volume were also determined same as the amount of generated voltages, electric current density and power density. The equations were bellowed.

Electric current density;

$$I_{\text{density}} = \text{electric current (A)} / \text{area of anode (m}^2\text{)} [2]$$

Electric power density;

$$P_{\text{density}} = \text{electric power (W)} / \text{area of anode (m}^2\text{)} [2]$$

III. RESULT S AND DISCUSSIONS

A. Effects of different electrodes in the hydrogen production on the electricity generation.

The 3 structures of the electrode stainless steel 604; the smooth, hole and net, were used in the alkaline fuel cell



(Figure 4). The electrode area was 20 cm². The hydrogen production was operated by using 1 M of alkaline electrolyte solutions for 30 min. They were at 1M of NaOH, 1M of KOH and 1M of Ca(OH)₂. The MQ8 sensor used for collecting data of the hydrogen concentration in every 3s. After the experiment, the physically surface of electrodes were observed and showed in the figure 3. So, after the experimental, The electrode and electrolyte solution reacted together as the corrosion reaction that made the color of electrode changed. Moreover, the color of stainless steel was not shiny. In addition, there were some rust spots on the electrode.

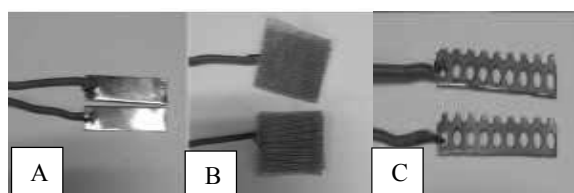


Figure 4 Stainless steel of 3 types for electrodes
(A) Stainless steel 604 smooth, (B) Stainless steel 604 net,
and (C) Stainless steel 604 holes.

Figure 5A showed the concentration of hydrogen gas in the system inputting the voltage at 1.1-9.0 V, the electric current 0.39-1.72, and operating for 30 min. Result show in the table 1 and figure 5.

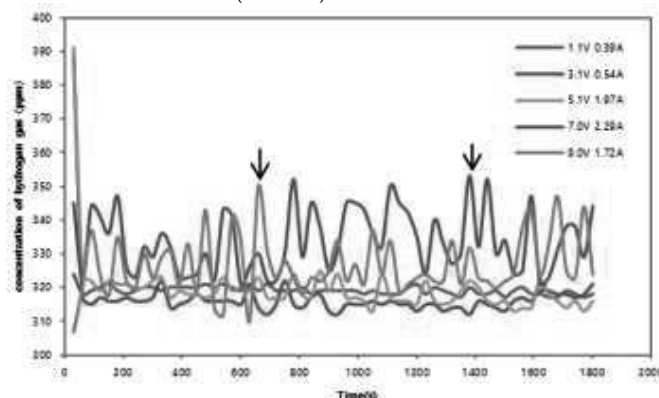
Table 1. Result of alkaline fuel consist electric current and concentration of hydrogen gas.

Type of stainless steel 604	Voltage(V)	Electric current(A)	Concentration of hydrogen gas(ppm)
Smooth	1	0.39	319.100
	3	0.54	317.117
	5	1.97	319.633
	7	2.29	320.983
	9	1.72	326.583
Hole	1	0.35	326.583
	3	0.54	328.583
	5	1.14	327.283
	7	1.68	332.700
	9	2.28	339.083
Net	1	0.35	331.350
	3	0.67	330.483
	5	0.81	330.433
	7	2.11	331.417
	9	2.67	332.383

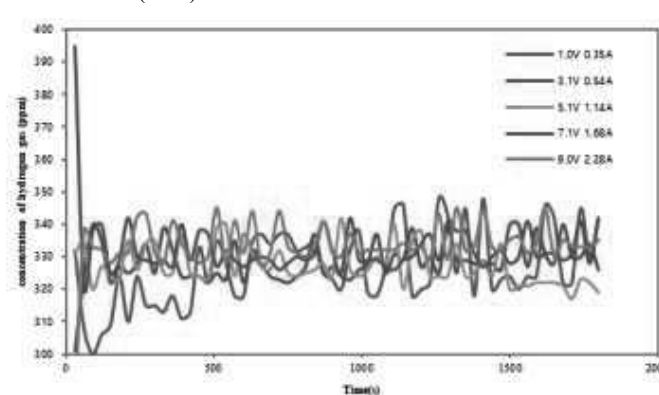
At 7V/1.68A of the system, the stainless steel 604 type with the hole exhibited the maximum concentration of hydrogen gas at 332.700 ppm (Figure 5B) while the electrode in smooth and net structure showed the closely concentration the hole structure because the electrodes were the same material [3] (figure 5, graph 5A). However, the hydrogen concentration of the stainless steel 604 type of smooth at 7V/2.29A and stainless steel 604 type of net at 7V/2.21A were similar concentrations which were 320.983 ppm and 331.417 ppm, respectively (Graph 5C). The results confirmed that which, at voltage and electric current of stainless steel 604 type of net and smooth get to more electric current then

stainless-steel hole, because different of input voltage and different of size of electrode influent to internal resistance when using more voltage into small size of electrode. [4] So, stainless steel of hole at 7V/1.68 was appropriate in the alkaline fuel cell system.

A. Relationship of concentration and time of stainless steel (smooth)



B. Relationship of concentration and time of stainless steel (hole)



C. Relationship of concentration and time of stainless steel (net)

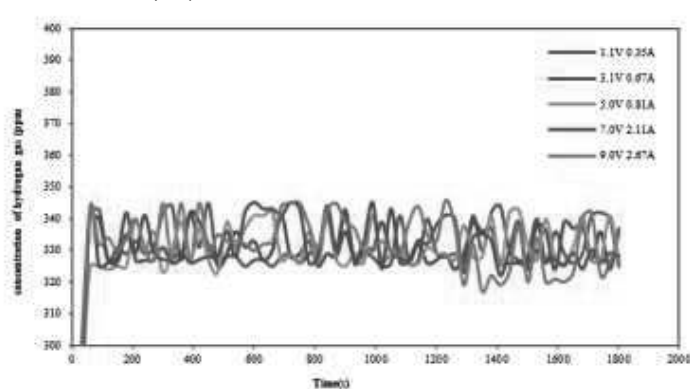


Figure 5 Relationship between of concentration with time of hydrogen gas



Regarding to vary the voltages loading from 1 to 9 V into the hydrogen production system (figure 6), the relationship between the voltage and the hydrogen volume showed the improvement of system performance when the voltage loading increased. [5]

From the above, stainless of 3 types had equally of concentration of hydrogen gas. However, volume of hydrogen gas had a differential so, volume of hydrogen gas show in the figure 6. Stainless steel 604 smooth, hole, and net had maximum of volume hydrogen 76 ml, 102 ml, and 100 ml at voltage 9V, 5V, and 9V respectively. Result of experimental alkaline fuel cell indicates that electrode was used stainless steel type of hole get to more concentration and volume of hydrogen gas than stainless steel type of smooth and net. Which, different of volume depend on volume of the input voltage in the system. Voltage variations affect all transport phenomena and electrochemical kinetics inside the fuel cell. [6] This is increasing trend line of the fuel cell at different operate voltage showed important performance with increasing voltage. From result of difference of voltage, this affects performance fuel cell. Therefore, the voltage is a important factor to working affect the performance of fuel cell. [7]

So, well reaction of stainless steel type of hole in 1M NaOH solution. Different of structure stainless steel duo to reaction in the system because structure that hole can more spread of electricity than the net and smooth. Stainless steel net was found in several layers, So stainless steel net lower spread than stainless-steel hole [8]

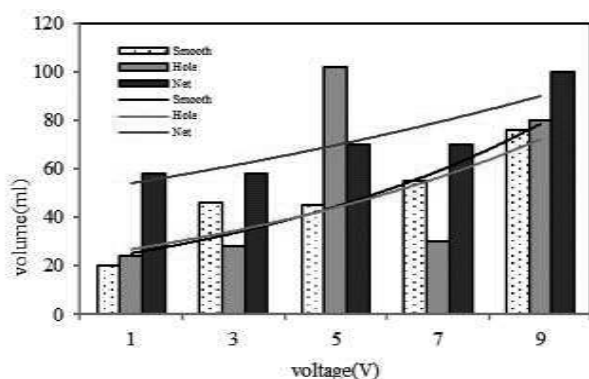


Figure 6 Relationship between of volume and voltage of alkaline fuel cell

A. Effect of electrolytes that influent to electrode for alkaline fuel cell.

The effects of alkaline electrolytes on the performance of fuel cell were observed (figure 7). They were at NaOH 0.5M, NaOH 1M, NaOH 2M, NaOH 3M, Ca(OH)₂ 1M, KOH 1M, and KOH 2M. The experiment at NaOH 1M, the system generated the highest concentration of hydrogen at 330.250 ppm with their volume at 78 ml. However, when the

concentration of electrolyte increased from 0.5 to 3M NaOH, the hydrogen volume did not increase. This is the because of increment of alkaline electrolyte concentration do not affects the fuel cell performance as much as the electrode and electrolyte types. However, while the concentrations of NaOH solution were increasing, the concentration of hydrogen also increased in the same relation. [9] SO, at 0.5 M of NaOH as an alkaline electrolyte was the appropriated condition for the hydrogen production which generated the hydrogen concentration at 330.250 ppm and 86 ml of gas volume (Table 2) .

Table 2 Volume of hydrogen gas bused alkaline electrolyte.

Electrolyte	NaOH 0.5M	NaOH 1M	NaOH 2M	NaOH 3M	Ca(OH) ₂ 1M	KOH 1M	KOH 2M
Volume (ml)	86	78	70	80	70	48	60

From figure 7 NaOH 0.5M, 1M, 2M, and 3M had been like concentration of hydrogen gas because reaction produce hydrogen gas depend on material of electrode and electrolyte. Which, different concentration of NaOH but high concentration depends on to voltage, if height concentration of hydrogen electrolyte renders to height reaction in the system, get to height concentration of hydrogen gas. [10]

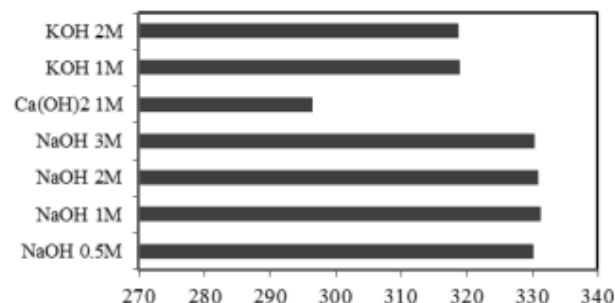


Figure 7 Relationship between concentrations of hydrogen gas with electrolytes.

Ca(OH)₂ was used as the electrolyte but it provided a few concentration of hydrogen gas because Ca(OH)₂ had ability to accept fewer electrons than NaOH and KOH. Since, NaOH is strong bass which has a high ability to accept the electrons [11]. So, the reaction of an electrolyte and electrode were occurred faster. Moreover, the lower NaOH concentration activated the reaction occurred faster than the high NaOH concentration [12]. After the consideration on the chemical reagent which showed high the strong base, the NaOH, KOH, and Ca(OH)₂ solution were the strong bass but they had the different ability to accept the electrons, So, the NaOH had highest the electron acceptability following with KOH and Ca(OH)₂, respectively.

Since the water electrolysis reaction at 0.5 M of NaOH solution was faster than the other electrolyte chemicals, it's electrolyte volume got more higher reduction after the



experiment completed. While that reaction between of electrode and electrolyte had decrees of efficiency due to erosion of electrode. The adsorption of bonded hydrogen to the electrode surface is inhibited by the specific adsorption of halogen ions [13]. Thus, decrease reaction in the system when operate the system few moments. Stainless steel of hole was oxidized with electrolyte influent to low performance of electrode [14].

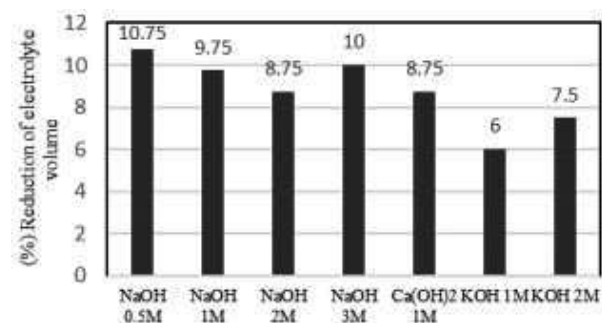


Figure 8 Relationship between of alkaline with percent decreases of volume

B. Effect of H₂ and O₂ connect to PEM fuel cell.

The suitable system at high performance on hydrogen production was settled after the analysis of their critical parameters. The optimization system was performed using stainless steel 604 at hole type and operating in 0.5 M of NaOH solution as the electrolyte at 0.5 voltage loading. Then, the alkaline hydrogen production system connected to PEM fuel cell using the stainless-steel net 3.62 mm² as electrodes and Nafion117 as PEM membrane. The system operated at 7V of loading voltage for an hour.

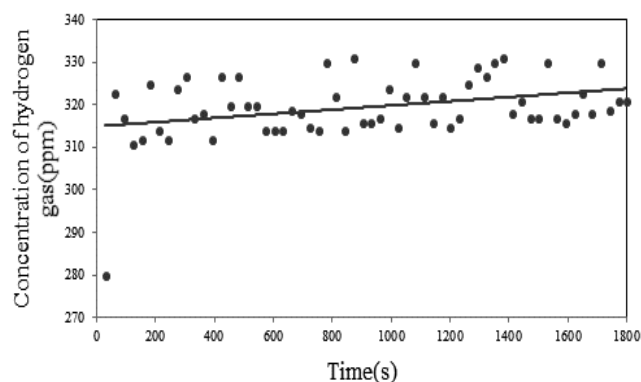


Figure 9 Relationship between of concentrations of hydrogen gas with time.

On the electricity production, the generated hydrogen gas at average at 330.250 ppm injected into the hydrogen PEM fuel. Concentration of hydrogen gas was had mean 330.250 ppm, show in figure 9 during on operate PEM fuel cell for 30 mins time, the both systems generated the voltage, electric

current density, and power density was at 2.475 mV, 4.64 A/W², and 2.59 W/w² respectively (figure 10)

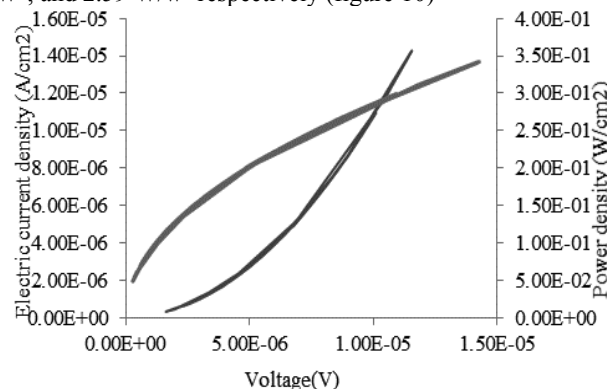


Figure 10 Relationship between of voltage, electric current density and power density.

In this phase, reverse electric current. Rang time of experimental 40-60 mins was ranged of decrees volume that into cathode tank of PEM fuel cell, until no hydrogen gas in the cathode tank, duo to reverse of electric current. [15] Operate of the system changing of temperature duo to increases of temperature was 6 °C and decreases volume of electrolyze was 9 ml. Show in table 3

During the electricity production couple with the alkaline hydrogen production, the water electrolysis to be hydrogen gas and the reaction between the electrode and electrolyte made the hydrogen generation temperature increased let to decrease the volume of electrolyte. The reactions also effected on the corrosion occurred on the electrode surfaces and the copper wires. The worsts were that the efficiency of electron acceptability decreased, the electron transportation also reduced and finally the efficiency of electricity production also decreased. If the corrosion on all materials widely appeared, the electricity could not generate in finally.

Table 3 Result of alkaline fuel conjunction with PEM membrane fuel cell.

	NaOH 0.5M	unit
Volume of H ₂	86	ml
Temperature (start)	24	°C
Temperature (final)	30	°C
Volume final of electrolyte	791	ml
Voltage input to system	7.0	V
Electric current input to system	1.32	A
pH	12.8	
Concentration	330.250	ppm

Electric wire was the copper material which the corrosion occurred faster on material after operating the system in just few moments. These corrosions usually effect



the efficiency of electrons transfer rapidly decreased and they also reduce the reaction rate between the electron and electrolyte until there were no the reaction in the system.

IV. CONCLUSION

An alkaline hydrogen fuel cell was operated by using the stainless steel 604 as the electrodes which soaked in NaOH, Ca(OH)₂, and KOH solutions as the electrolyte in the system. The system produced the maximum concentration of hydrogen gas at mean at 329 ppm. When the electricity generated couple with the hydrogen production, the PEM fuel cell produced the electricity at 2.89 mV, the electric current density at mean at 4.64 $\mu\text{A}/\text{m}^2$, the power density at mean at 2.59 $\mu\text{W}/\text{m}^2$, and the efficiency at 0.225% of theoretical yield.

In the hydrogen production couple with the electricity production technology, the types and shapes of electrode, the voltage loading, types and concentration of the electrolyte reagent, temperature and pH should be the priority considered to prevent the system efficiency loss.

ACKNOWLEDGMENT

I would like to express my sincere thanks to my School of Renewable Energy, Maejo University, and my research advisor; Dr. Natthanicha Sukasem. I am the most grateful for her teaches, advice, and suggestion. She does not only advise me on this research but also suggests me how other methodologies in life should be. I would not have achieved this far and this thesis would not have been completed without all the support that I have always received from her. I am the most grateful for her teaches, advice, and suggestion. She does not only advise me on this research but also suggests me how other methodologies in life should be. I would not have achieved this far and this thesis would not have been completed without all the support that I have always received from her.

Finally, I most gratefully acknowledge my parents and my friends for all their support throughout the period of this research.

REFERENCES

- [1] Appleby, A. J., and F. R. Foulkes, Fuel Cell Handbook, New York, NY: Van Nostrand Reinhold, 1989.
- [2] Asimov, Isaac, Understanding Physics, Vol. I: Motion, Sound and Heat, New York, NY: Bar-nes and Noble Books, 1966.
- [3] Ballard Power Systems, The Ballard Fuel Cell: An Overview, Burnaby, BC, n.d., Doc. No. 710.740.003.
- [4] Brady, James E., and Gerard E. Humiston, General Chemistry: Principles and Structure, 2 ed., New York, NY: John Wiley and Sons, 1978.
- [5] Canadian Hydrogen Association and National Hydrogen Association, The Sourcebook for Hydrogen Applications, for the Department of Natural Resources Canada and the U.S. De-partment of Energy, Montreal, QC: TISEC Inc., 1998.
- [6] Cognizant Media Production, Hydrogen: A Matter of Safety Video and Companion Guide, Studio City, CA: Hydrogen 2000, Inc., n.d.
- [7] College of the Desert, Medium & Heavy Duty Gaseous Fuel Engines & Fuel Systems, Palm Desert, CA: College of the Desert, 2001.
- [8] CylTek Labs Inc., Natural Gas Vehicle Cylinder Care and Maintenance Handbook, for the Gas Research Institute, Natural Gas Vehicle Coalition, Chicago, IL, 1997, Doc. No. GRI-97/0250.
- [9] EDO Canada Limited, EDO Literider NGV Cylinder, All Composite Natural Gas Cylinder Video, 1993.
- [10] Ford Motor Company, Direct-Hydrogen-Fueled Proton-Exchange-Membrane Fuel Cell System For Transportation Applications: Hydrogen Vehicle Safety Report, for the U.S. Department of Energy, Office of Transportation Technologies, Dearborn, MI, 1997, Doc. No. DOE/CE/50389-502.
- [11] Haile, Sossina M. et al., Solid Acids as Fuel Cell Electrolytes, Materials Science, California Institute of Technology, Pasadena, CA, Nature Vol. 410 pp. 910-913, April 19, 2001.
- [12] Hansel, James G., Safety Considerations for Handling Hydrogen: A Seminar for Presenta-tion to Ford Motor Company, Allentown, PA, June 12, 1998
- [13] Winter, M; Brodd, R. J. (2004). "What are batteries, fuel cells, and supercapacitors?". Chemical Reviews. 104 (10): 4245-4269.
- [14] Adams, L. A.; Varcoe, J. R. (2008). Chem Sus Chem. 1: 79-81.
- [15] Shen, P. K.; Xu, C. (2005). Adv. Fuel Cells: 149-179.



Feasibility on the Development of Power Generation using the Stainless Steel and Aluminium as Electrodes in PEM Fuel Cell Technology

Jirawat Leaksantad¹, Pattarachai Noppakun² and Natthanicha Sukasem³
^{1,2,3} School of Renewable Energy, Maejo University, Chiang Mai, 50290, Thailand
E-mail; ¹Oksantad@gmail.com, ²nonnopkun@outlook.co.th
Corresponding author: E-mail; ³jewy.ja@gmail.com

Abstract— The fuel cell type proton exchange membrane (PEMFC) technology represents a method for the electricity generation using the hydrogen from the reaction of water electrolysis. In this study, the two chamber fuel cell with the reassembly of membrane was operated by varying the electrodes materials; stainless steel and aluminium, and shapes; whole sheet, and whole sheet with 0.6 and 0.2 mm of hole diameter. Results indicated that the aluminium in whole sheet type is an appropriate material for anode and cathode. The hydrogen concentration in range of 200 – 300 ppm was injected into the PEMFC which operated using the 2 kΩ of suitable external resistance loading at ambient temperature. The result shows the efficiency of electricity generation at 35.29 mV of voltage output, 17.65 μA of system currents and 50.84 μA/cm² of power density. These results demonstrate that the hydrogen can be used for the power production by PEM fuel cell technology. The development of power generation system should be the first priority done in the future.

Keywords—Stainless steel; aluminium; hydrogen gas; PEM fuel cell; power generation

I. INTRODUCTION

In the present, the electricity is the priority energy which the people in the global world necessary require to use in everyday life for making their living mostly convenience. The demands on the utilization of the electricity energy rapidly increase due to the growth of economy, the development of technology, and also the population growth [1]. However, regarding to the electricity production process, the electricity is normally produced from different the feedstock in various industries such as the electric waste factory [2], the nuclear power plant [3], and coal power plant [4]. Nevertheless, during the electricity production, some toxic may release into the environment and these pollutants may accumulate themselves in our atmospheres and the environment [5]. Since, the coals are the mainly feedstock for the electricity, they are the rapidly decrease. [4]

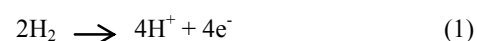
The electricity production by using the various kinds of the fuel cell technology. The proton exchange membrane fuel cell (PEMFC) in the one of fuel cell technology for the electricity

production [6]. This technology changes the chemical energy in hydrogen gas to be the electricity without the combustion process. The hydrogen fuel cell technology generally has the higher the efficiency of energy production than the combustion engine at least 1 to 3 folds [7]. The PEMFC fuel normally generates the electricity by the chemical reaction such as oxidation/reduction. However, due to the comparison of the PEMFC fuel cell and battery, the PEMFC application requires the continuously feeding of the hydrogen and oxygen into system [8] but the battery produces the electricity from chemical reaction [9]

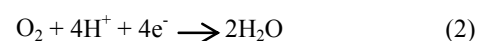
Regard to the principle of PEMFC technology, the inlet hydrogen gas get into the anode chamber and then, release their electrons to the electrode. The electrons move along on the electric wire to the cathode chamber. Moreover, the anode chamber and cathode chamber connect together with the external loading resistance. While, at the same time, the proton from gas pass through the PEM membrane to the cathode chamber. Therefore, after the inlet oxygen at the cathode chamber combine with the hydrogen to be the water molecule in the finally. This principle confirms that the system does not generate the toxic pollutants into the environment. Thus, only the clean energy produces [7].

The equations bellow show the chemical reaction at the both anode and cathode [10], they are

The reaction at anode



The reaction at cathode



The overall reaction is





Normally, the electrodes in PEMFC application mostly are expensive materials. These are nano-graphite with or without Teflon and platinum. In this study, the aluminium and stainless steel have a high conductivity and also resistance to corrosion. Thus, both aluminium and stainless steel were compromised electrode materials in PEMFC. In finally, the goal of this research attempt to improve the PEMFC efficiency by varying the critical factors; the electrode types and shapes and the external loading resistance. The optimizations of conditions were the advantage applications for the next futures such as the electricity production during the waste water pretreatment, others electricity production using fuel cell technology and even in the hydrogen gas production.

II. MATERIALS AND METHODS

A. Designation of hydrogen fuel cell

The two chamber of Proton exchange membrane fuel cell (PEMFC) used for the electricity generation. (Fig 2) The fuel cell consisted of (1) cathode chamber, (2) anode chamber, (3) Nafion117 as PEM membrane, (4) both of anode and cathode at area size of 4x4 cm², and (5) external loading resistance at 2 k Ω . For the construction, the electrode positions of anode and cathode were closely together to protect electric lost inside the fuel cell. The external resistance was connected between the both two electrodes.

B. Activation of electrodes and PEM membrane

Before the system operation, due to increase the conductivity of electrodes, the both electrodes treated with the mixture volume ratio of 65% (v/v) of H₂SO₄ to 65% (v/v) of HNO₃ at 1:3 at ambient temperature for 24 hr. The activation of PEM required for removing the substances or other small particles attached to the membrane and also refresh the membrane activity to ready for the experiment. Therefore, the PEM was also activated by heating in 3% (v/v) of hydrogen peroxide (H₂O₂) for 1 hr and then, continuing with heating up to 80 °C in 15% (v/v) of H₂SO₄ for 1 hr [11].

C. Operation of the hydrogen fuel cell

During the experiment, the inlet hydrogen and oxygen gas were from alkaline hydrogen production. The 200 to 300 ppm (Data didn't show) of hydrogen gas fed into anode chamber whereas the oxygen gas fed into cathode chamber. The digital multimeter (WENS 510) connected between the both anodes to observe the generated voltage of system. The hydrogen fuel cell was operated until the system voltage was stable.

D. Studied on the effects of different electrode types and shapes

The types and structures of anode and cathodes were various to identify the suitable electrodes for the high efficiency of electric production. The 2 types of electrode materials were used. There were stainless steel 304 with activation and aluminium without the activation. Moreover, both electrode materials were in shapes of whole sheet, and

whole sheet with the hole in diameter at 6 mm and 2 mm (Figure 1). The experiment designs shown in table 1.

TABLE I. The experiment design for varying the electrode types and shapes

Material	Test no.	Shapes in	
		Anode	Cathode
Stainless steel 304	1	Whole sheet (S304)	Whole sheet (S304)
	2	Whole sheet with the hole at dia. 6 mm (6S304)	Whole sheet with the hole at dia. 6 mm (6S304)
	3	Whole sheet with the hole at dia. 2 mm (2S304)	Whole sheet with the hole at dia. 2 mm (2S304)
Stainless steel 604	4	Whole sheet with the hole at dia. 5 mm (5S604)	Whole sheet with the hole at dia. 5 mm (5S604)
	5	Stainless steel 604 Net (NS604)	Stainless steel 604 Net (NS604)
Aluminium	6	Whole sheet (AL)	Whole sheet (AL)
	7	whole sheet with the hole at dia. 6 mm (6AL)	whole sheet with the hole at dia. 6 mm (6AL)
	8	whole sheet with the hole at dia. 2 mm (2AL)	whole sheet with the hole at dia. 2 mm (2AL)

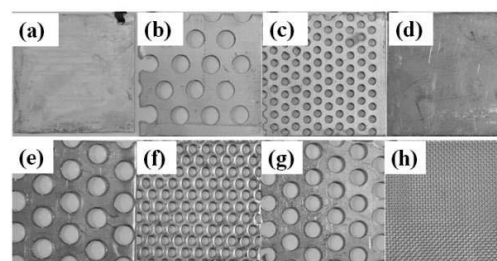


Fig 1. The electrode material types and shapes. The details referred as their code number (a) AL, (b) 6AL, (c) 2AL, (d) S304, (e) 6S304, (f) 2S304, (g) 5S604, (h) NS604

E. Studied on the effects of various external loading resistance

After the previous experiments shown the suitable the electrode types and shapes, the suitable the external loading resistance was also identified. There were 220 Ω , 510 Ω , 1k Ω , 2k Ω , and 3k Ω . The systems were operated under room temperature at least 2 hr or until the system voltages stabled.

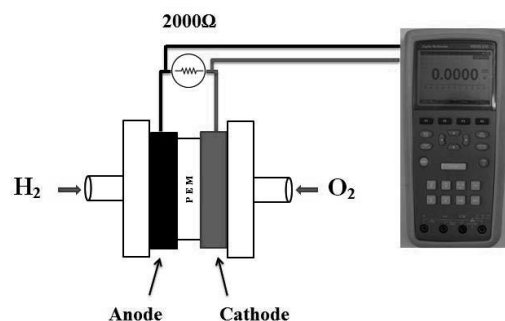


Fig 2. Fuel cell system.

F. Analytical methods

The system currents and other data were calculated by using Ohm's Law that shown in equation 1 to 5

$$I = V/R \quad (1)$$

$$\text{Current density} = I/A \quad (2)$$

$$P = IV \quad (3)$$

$$\text{Power density} = P/A \quad (4)$$

$$R_{in} = P_{Max}/I_{PMax}^2 \quad (5)$$

When I (A) is the current.

V (V) is the cell voltage.

R (Ω) is the resistance value.

A (cm²) is the area of electrode.

P (W) is the power.

P_{max} (W) is the maximum power.

I_{Pmax} (A) is the current at the maximum power.

III. RESULTS AND DISCUSSION

3.1 Effects of different the electrode types and shapes on the electricity production.

To identify the suitable electrode materials and shapes to produce the high electricity by the PEM fuel cell technology, the stainless steels and aluminiums in various types were analyzed. The estimated 300 ppm of hydrogen gas injected into fuel cell chamber, the system voltages for all conditions were shown in figure 3 for the aluminium electrode materials and figure 4 for the stainless steels.

Regard to the electric resistance, the stainless steel has own resistance at $6.90 \times 10^{-7} \Omega \cdot m$ whereas the aluminium has quite low the resistance at $2.65 \times 10^{-8} \Omega \cdot m$. Because of the electric resistance of stainless steel is higher than aluminium estimate about 26 folds, therefore, this property lead to the voltage output of system using aluminium as electrodes are also higher than the stainless steel [12]. The previous research also confirmed that the aluminium could be used as the electrode generating the high electricity power at 897 kW.

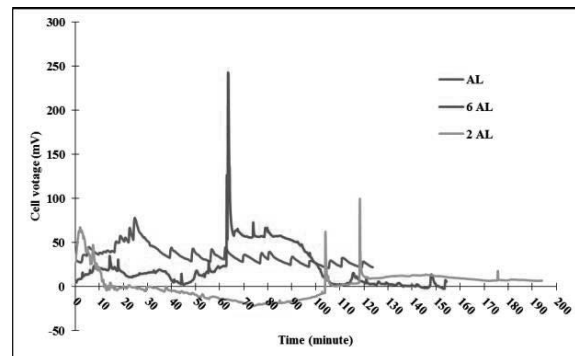


Fig 3. The voltage output of electricity system using the aluminium as electrode materials in various types.

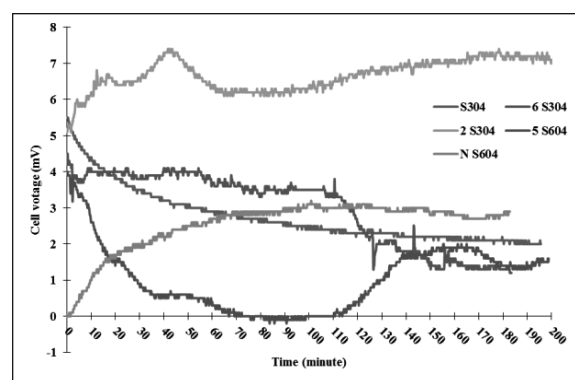


Fig 4. The voltage output of electricity system using the stainless steel as electrode materials in various types.

Moreover, the whole sheet of aluminium electrodes are suitable electrode types which shows the highest of voltage output at 53.29 mV, at 17.65 μA and power density at 50.84 μW/cm² in PEM fuel cell (fig 5). The electrode in whole sheet type shows the higher efficiency than other types because the aluminium electrode in whole sheet type has the surface areas more than other types. Therefore, the whole sheet electrodes possible accept more the electrons than others and lead to increase the electricity in PEM fuel cell [13]

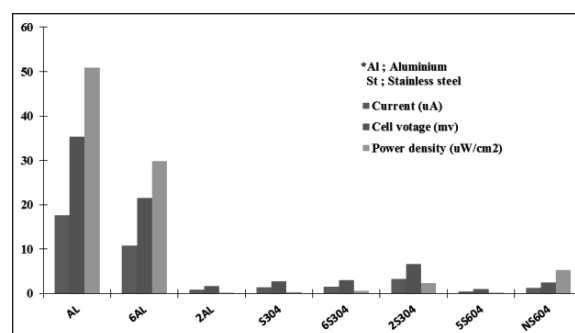


Fig 5. The performance of PEM fuel cell in the electricity generation by using the stainless steel and aluminium in different shape types.



TABLE II. The performance of PEM fuel cell using the stainless steel and aluminium as the electrodes.

Types of electrodes	Current (μA)	Cell voltage (mV)	Power density (μW/cm ²)
Whole sheet aluminium	17.65	35.29	50.84
Stainless steel 304 sheet with the hole at dia.2 mm	3.34	6.68	2.32

TABLE III. Performance of PEM fuel cell at different external resistance loading.

	Cell voltage (mV)	Current (μA)	Current density (μA/cm ²)	Power Density (μW/cm ²)
510Ω	3.35	6.57	0.54	1.80
1000Ω	13.52	13.52	1.10	14.92
2000Ω	35.29	17.65	1.44	50.84
3000Ω	35.58	11.86	0.97	34.45

3.2 Effects of different the external resistance loadings on the electricity production

To improve the efficiency of the electric production, the effects of different resistance external loading systems against on the PEM fuel cell performance were analyzed by using the whole sheet of aluminium electrodes as shown in figure 6.

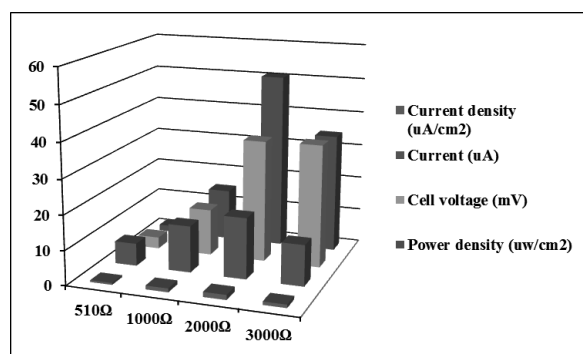


Fig 6. The performance of PEM fuel cell at various external resistance systems.

The figure 6 illustrates that the increment of external resistance loading from 510 Ω to 2 kΩ consequence to accelerate the system voltage outputs. Moreover, it is not only the voltage output increase, the currents and power densities which calculating by equation 1 and 2, respectively, are also increase (TABLE III). Nevertheless, when the external loading is too high value especially at 3 kΩ even the system shows the highest voltage output at 35.58 mV but the current and power density which are 11.86 μA and 34.45 μW/cm² respectively, are lower than at 2 kΩ of external loading that the system performance exhibits the current at 17.65 μA, the current density at 1.44 μA/cm² and power density at 50.84 μW/cm². To select the appropriate external loading condition, at 2 kΩ shows the highest peak of the relationship of current versus the resistance. In addition, at this peak, the external loading is nearly equal to the internal resistance of the PEM fuel cell which is the best system operation [14]. Thus, to confirm that at 2 kΩ of external loading is the right loading; the internal resistance is calculated by using the equation 5 and also compared to the selected system loading. The internal resistance by calculation is approximately at 2,000.76 Ω. This resistance is very closer to the 2 kΩ of selected loading.

The approximate condition for the electric generation by PEM fuel cell was operated again. The relationships of voltage output, the current, and power density versus the operation time were shown in the figure 7.

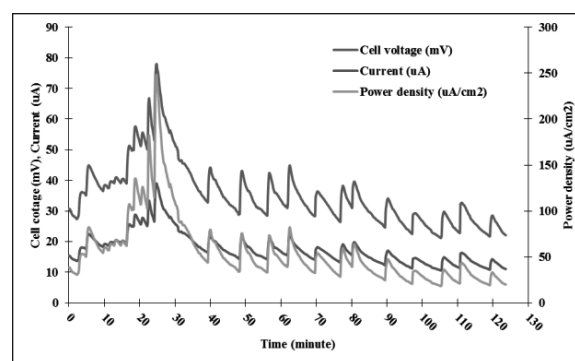


Fig 7. The efficiency of the electric generation by PEM fuel cell technology at appropriate condition.

IV. CONCLUSION

During the electricity generation by using the PEM fuel cell, the electrode material should be the first priority consider as the critical factor affect to the efficiency. The electrode material which has high conductivity and low resistance should be applied. In this research, the aluminium shows the best advantage to be the electrode in the generation of electricity. Moreover, the whole sheet type is optimized shapes that the oxidation reaction of electron donors and acceptors in the PEM fuel cell can be occurred and passes the electron along through the anode to cathode. Thus, the optimized condition of PEM fuel cell is at 2 kΩ of external loading and aluminium in whole sheet type operating at ambient temperature for 3 hr. However, in the further work, the development of electrode properties should be done couple with the reduction of system resistance.

ACKNOWLEDGMENT

Thank you for the School of Renewable Energy, Maejo University to support all facilities in this research. Moreover, I would like to thank my advisor; Dr.Natthanicha Sukasem who gives me the opportunity to participate in this research and also advise me on this research.



REFERENCES

- [1] F.J. Malcolm, G.D. Matthew and G.G. Roger, "A demographic projection of the contribution of assisted reproductive technologies to world population growth," *Reproductive biomedicine online*, vol. 36, January 2018, pp. 455-458.
- [2] K. Zeba, S.M. Alib, B. Khanb, C.A. Mehmoodb, N. Tareenb, W. Dina, U. Faridb and A. Haidera, "A survey on waste heat recovery: Electric power generation and potential prospects within Pakistan," *Renewable and Sustainable Energy Reviews*, vol.75, August 2017, pp. 1142-1155.
- [3] Z. Xiaosong, Z. Rui, Z. Shumeng, W. You and H. Zhen, "Incorporation TACOM and SPAR-H into the operating procedure of nuclear power plants," *Annals of Nuclear Energy*, vol. 114, April 2018, pp. 451-457.
- [4] W. Delu, W. Kaidi and S. Xuefeng, "Quota allocation of coal overcapacity reduction among provinces in China," *Energy Policy*, vol. 116, May 2018, pp. 170-181.
- [5] L. Fangyi, X. Xilin, X. Wu, M. Dawei, S. Zhuo and L. Kunpeng, "Estimating air pollution transfer by interprovincial electricity transmissions," *Journal of Cleaner Production*, vol. 183, May 2018 pp. 56-66.
- [6] W.F. Cheng and P.C. Hsun, "The development of an exchangeable PEMFC power module for electric vehicles," *International Journal of Hydrogen Energy*, vol. 39, March 2014, pp. 3855-3867.
- [7] S.J. Antonio, I. Alfredo, R. Felipe, T. Elvira, L. Eduardo and I. Fernando, "Optimization of a PEM fuel cell operating conditions: Obtaining the maximum performance polarization curve," *International Journal of Hydrogen Energy*, vol. 41, November 2016, pp. 19713-19723.
- [8] K. Nikiforowa, P. Koskib, H. Karimäkib, J. Ihonenb and V. Alopacusa, "Designing a hydrogen gas ejector for 5 kW stationary PEMFC system – CFD-modeling and experimental validation," *International Journal of Hydrogen Energy*, vol. 41, September 2016 pp. 14952-14970.
- [9] W. Lu, V.P. Erik, A. Karian, W. Xuehang, S.A. Mari and B.F. Vullium, "High capacity Mg batteries based on surface-controlled electrochemical reactions," *Nano Energy*, vol. 48, June 2018, pp. 227-237.
- [10] S. Panudda and P. Boonyang, "Study and analysis of 1.2 kW proton exchange membraned fuelcell (PEMFC) electrification," 2554.
- [11] A.A Adedeji, "Effect of basicity on amination of activated carbon pellets modified for CO₂ adsorption," *Journal of Purity, Utility Reaction and Environment Vol. 3*, February 2014, pp. 1-17.
- [12] C.S. Eric, S.R. Brandon, P.L. Michell, I. Fahmida, G.J. Micah and D.A. Michael, "Ignition sensitivity and electrical conductivity of an aluminum fluoropolymer reactive material with carbon nanofillers," *Combustion and Flame*, vol. 162, April 2015, pp. 1417-1421.
- [13] H.R. Alexander, P.G. Antonio and Gordon G. Wallacea, "Effective Area and Charge Density of Iridium Oxide Neural Electrodes," *Electrochimica Acta*, vol. 230, March 2017, pp. 285-292.
- [14] C. Clara and P. Jaume, "Improving domestic wastewater treatment efficiency with constructed wetland microbial fuel cells: Influence of anode material and external resistance," *Science of The Total Environment*, vol. 631-632, August 2018, pp. 1406-1414.



Optimal Rule Curves of Small Reservoir using Wind Driven Optimization and Flower Pollination Algorithm

Rapeepat Techarungruengsakul^{1st} and Anongrit Kangrang

Faculty of Engineering, Mahasarakham University, Kantharawichai District,
Maha Sarakham, Thailand.

rapeepat.tec@msu.ac.th, anongrit.k@msu.ac.th

Abstract— Reservoir operation requires optimal rule curves, for controlling amount of store water and release to downstream. This research proposes the application of the Wind Driven Optimization (WDO) and Flower Pollination Algorithm (FPA) techniques with reservoir simulation model for finding the optimal rule curves. The objective functions of search process were the minimum average water shortage and the minimum average excess spill water. This study considered information of the Huay Sabag reservoir in Yasothorn province as the case study. The historic monthly inflow data from 1996 to 2017, water demand from reservoir, hydrological data and the physical data of the reservoir were considered for the study. In addition 1,000 samples of synthetic inflow were used to evaluate the efficiency of the obtained rule curves that present in term of water shortage and excess release water. The results found that the patterns of new rule curve were different from the current rule curves. The results also present that the new rule curves from WDO can alleviate flood situations more than the current rule curves but less than rule curves from FPA both using historic inflow and synthetic inflow cases. Whereas, the situations of water shortage of the new obtained rule curve were slightly less than the current rule curves.

Keywords—reservoir rule curves; optimization techniques; Wind Driven Optimization; Flower Pollination Algorithm; reservoir operation

I. INTRODUCTION

Water is an important resource for sustaining human life in many aspects especially, to the consumption and water supply. Also, water is important for both industrial and agricultural aspects, especially in Thailand where is the country with most agricultural production 1 in 20 of the world [1]. However, due to the impact of circumstances of the current impacts of climate change and land use changes cause problems of water resource which this issue will affect the life and corrupt all life and property [2-3]. To solve the water

problems, weir, dam and reservoir have been constructed in many areas.

Reservoir management, it is the management of the water available in the reservoir to meet the water demand. It also takes into account the flooding and water shortage which release water on demand, called water allocation. Water allocation is to water storage in the basin to take advantage that sufficient for the needs and does not cause water problems in the future. An important tool for making a decision to allocate water is reservoir rule curves. Reservoir rule curves consist of upper rule curves and lower rule curves which indicative the upper and lower bounds for controlling among of water release and storage. The reservoir management by using rule curves in reservoir operation is a long-term management. When use for 4-5 years, it is necessary to improve the efficiency by finding optimal rule curves again [4].

Currently, there are many applications of optimization techniques to find the answer optimal rule curves such as dynamic programming [5] and the other techniques derived from evolutionary theory. They are effective techniques to find solutions such as genetic algorithm [6] simulated annealing technique [7] and tabu search [8], where researchers have applied these techniques in their searches for searching optimal reservoir rule curve.

Nowadays, one of alternative optimization technique can be adapted to find appropriate value is a Wind Driven Optimization (WDO) technique. WDO is an evolutionary adaptive of the air parcel in the atmosphere, finding the best pressure to balance the atmosphere [9]. Another one is the Flower Pollination Algorithm (FPA) which evolved from the pollen, the pollen grains of the flower. Each flower has a way to lure the bird or insect pollinated in different ways coming, to ensure pollination for reproduction and survival [10]. Both techniques are highly effective technique. There are suitable for use in searching optimal reservoir rule curves.

Therefore, this research aimed to finding appropriate reservoir rule curves using WDO and FPA techniques. There were two objective functions that considered for applying to search process including the minimum average water shortage



and the minimum average excess spill water. The Huay Sabag reservoir where located in the northeast region of Thailand was considered for this case study.

II. MATERIALS AND METHODS

A. Study area

The study area, Huay Sabag reservoir, Yasothorn province is the branch of a Moon river basin point in the Northeast of Thailand (Fig. 1). An area of approximately 52 km², total cumulative annual average runoff of about 22.4 MCM. (Fig. 2). The normal storage capacity is 30.03 MCM. The multi-purpose objectives of the Huay Sabag reservoir are consume, irrigation flood control, domestic water supply and environmental conservation. The flow schematic diagram of the Huay Sabag reservoir is presented in Fig. 3.

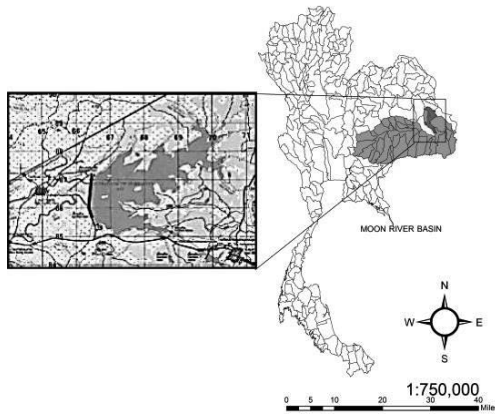


Fig. 1. Location of the Huay Sabag reservoir

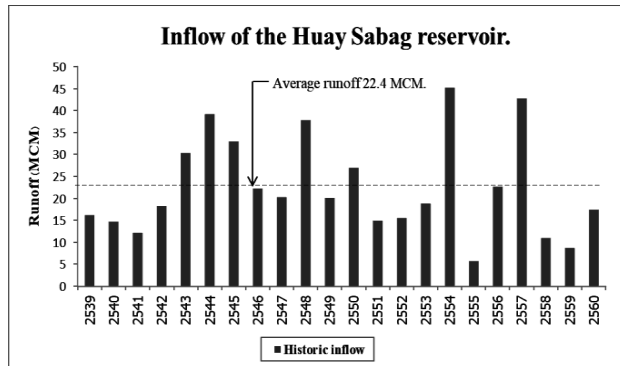


Fig. 2. Inflow record during 1996 to 2017

B. Reservoir operation model

The reservoir operation system consists of the available water that is calculated from the water balance concept and water demands from downstream site. The monthly release water is estimated by considering the monthly available water with release criteria, operating policies and reservoir rule curves.

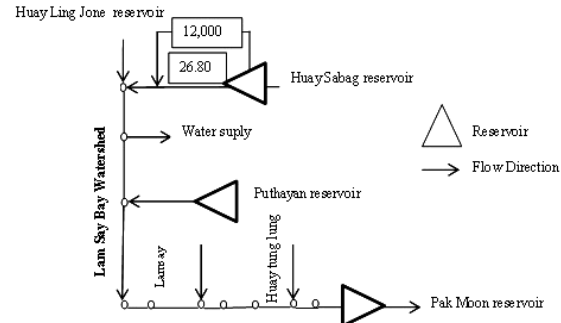


Fig. 3. The flow schematic diagram of the Huay Sabag reservoir

For this study, the reservoir operation model was created following the concept of the water balance. The reservoir operation model is operated under the standard operating policy as expressed in Fig. 4 and equation (1).

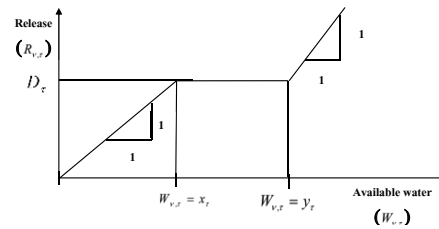


Fig. 4. Standard operating rule [4]

$$R_{v,\tau} = \begin{cases} D_{\tau} + W_{v,\tau} - y_{\tau}, & \text{for } W_{v,\tau} \geq y_{\tau} + D_{\tau} \\ D_{\tau}, & \text{for } x_{\tau} \leq W_{v,\tau} < y_{\tau} + D_{\tau} \\ D_{\tau} + W_{v,\tau} - x_{\tau}, & \text{for } x_{\tau} - D_{\tau} \leq W_{v,\tau} < x_{\tau} \\ 0, & \text{otherwise} \end{cases} \quad (1)$$

Where $R_{v,\tau}$ is the release of water during year v and month τ ($\tau = 1$ to 12 representing January to December), D_{τ} is the net water demand during month τ ; x_{τ} is the lower rule curve of month τ ; y_{τ} is the upper rule curve of month τ and $W_{v,\tau}$ is the available water by calculating the water balance concept during year v and month τ , as described in equation (2):

$$W_{v,\tau} = S_{v,\tau} + Q_{v,\tau} - R_{v,\tau} - E_{\tau} - DS \quad (2)$$

Where $S_{v,\tau}$ is the stored water at the end of month τ ; $Q_{v,\tau}$ is the monthly inflow to the reservoir, E_{τ} is the average value of the evaporation loss and DS is the minimum reservoir storage capacity (dead storage capacity). The operating policy usually reserves the available water ($W_{v,\tau}$) for mitigating the risk of water shortage in the future, when $0 \leq W_{v,\tau} < x_{\tau} - D_{\tau}$ under long term operation. released water from the reservoir was used to calculate the water shortage and excess water release situations, which can be expressed as the frequency of failures in a year and the number of excess water release, as well as the average annual shortage (the first objective function for searching the optimal rule curves) and the average excess spill water per year (the second objective function for searching the optimal rule curves).



C. Application of WDO with the reservoir simulation model for searching optimal rule curves

The WDO connecting with the reservoir simulation model is present as follows: the WDO starts with a set initial population $\{X_1, X_2, \dots, X_n\}$ that is created randomly within the feasible space. The feasible space is the value between the dead storage capacity and the normal high water level of the considered reservoir. There are 24 decision variables. For this study, each decision variable represents the monthly rule curves in the reservoirs, which are denoted as the upper bound and the lower bound (rule curve variables for both upper and lower) for one reservoir. The feasible solution of the iteration is represented as $X_i = [xi_1, xi_2, \dots, xi_{24}]$. The application of WDO and reservoir simulation model for searching the rule curves is described in Fig. 5.

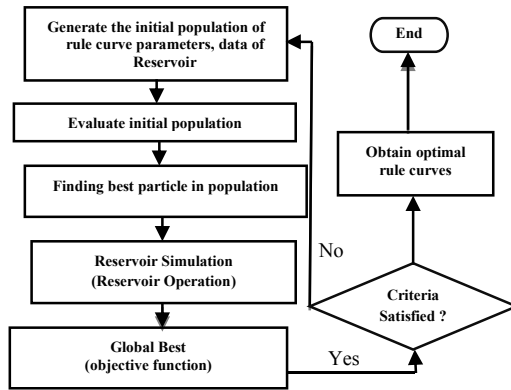


Fig. 5. Application of WDO and reservoir simulation model for searching optimal rule curves

D. Application of FPA with the reservoir simulation model for searching optimal rule curves

The connecting of the FPA and reservoir simulation model starts with input data and all initial necessary data such as upper and lower bound data of reservoir and objective function. The FPA procedure consists of flowers and pollination process. For this study, each decision variable represents the monthly rule curves of the reservoirs, which are defined as the upper rule curves and the lower rule curves. After the first set of flowers in the initial population have been calculated (24 decision variables that consist of 12 values from the upper rule curves and 12 values from lower rule curves), the monthly release water will be re-calculated by the reservoir simulation model considering those rule curves. Next, the released water is used to determine the objective functions that were described in the previous section. After that, the reproduction process will create new rule curve values in the next generation. This procedure is repeated until the 24 values of the rule curves are appropriate. The FPA and reservoir simulation model for searching the rule curves is described in Fig. 6.

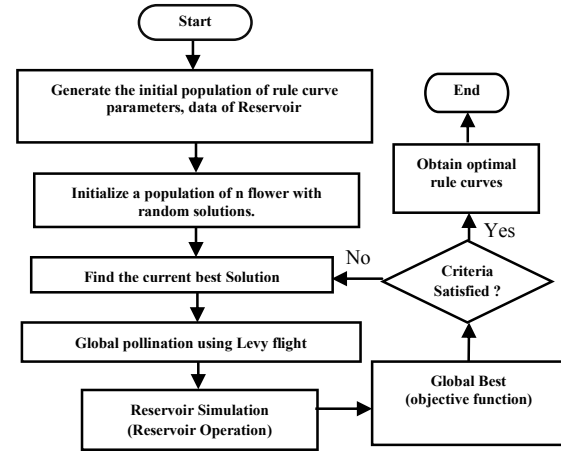


Fig. 6. Application of FPA and reservoir simulation model for searching optimal rule curves

In this study, the first objective function for searching optimal reservoir rule curves is the minimum average water shortage per year $\text{Min } Z_{(avr)}$ as described in the following:

$$\text{Min } Z_{(avr)} = \left(\frac{1}{n} \sum_{v=1}^n Sh_v \right) \quad (3)$$

$$\text{if } R_\tau < D_\tau; \text{Then } Sh_v = \sum_{\tau=1}^{12} (D_\tau - R_\tau) \quad (4)$$

Where n is the total number of considered years, Sh_v is the water shortage during year v (year in which releases do not meet 100% of the target demand). Then, the searching process is continued until the termination criterion is satisfied as described in Fig. 5. This termination criterion is the maximum iteration run.

The second objective function is the minimum average excess spill water per year $\text{Min } U_{(avr)}$ as described in the following:

$$\text{Min } U_{(avr)} = \left(\frac{1}{n} \sum_{v=1}^n Sp_v \right) \quad (5)$$

$$\text{if } R_\tau > D_\tau; \text{Then } Sp_v = \sum_{\tau=1}^{12} (R_\tau - D_\tau) \quad (6)$$

$$\text{Else } Sp_v = 0$$

Where n is the total number of considered years, Sp_v is the excess spill water during year v (year in which releases are higher than the target demand).

III. RESULTS AND DISCUSSION

A. Historic rule curves with objective function

The 22 years (1996-2017) of monthly historic inflow data, monthly data of evaporation, rainfall, irrigation, domestic and industrial water requirements and monthly environmental conservation were imported for processing in the WDO and FPA connected to the simulation model, and the optimal rule curves of each technique were obtained. These obtained rule curves using the minimum average water shortage as the



objective function are plotted in order to compare them with the current rule curves as shown in Fig. 7. They indicated the optimal upper and lower rule curves for the WDO (RC3-WDO) were compared with the current rule curves (RC1-Current) and the rule curves obtained using FPA (RC2-FPA). They indicated that the rule curve patterns of all cases were similar to the current rule curves because of the seasonal inflow effect.

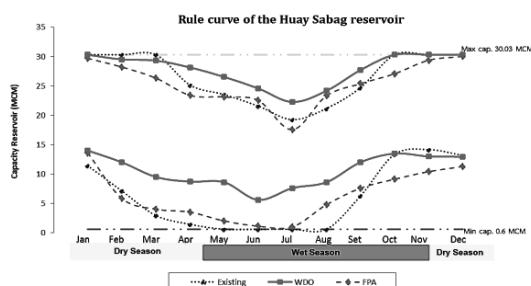


Fig. 7. Optimal rule curves of the Huay Sabag reservoir (using objective function: the minimum average water shortage)

Fig. 8 shows the patterns from the current rule curves (RC1-Current) and the new obtained rule curves obtained from the WDO (RC3-WDO) and the FPA (RC2-FPA) when using the minimum average excess spill water as the objective function. Their patterns are similar. They indicated that the lower rule curves of WDO (RC3-WDO) and FPA (RC2-FPA) are higher than the current rule curves, these can reduce the water release for saving store water. In addition, during the middle rainy season (August–October), the upper rule curves of WDO (RC3-WDO) are higher than the other rule curves; these can increase water storage for next dry season.

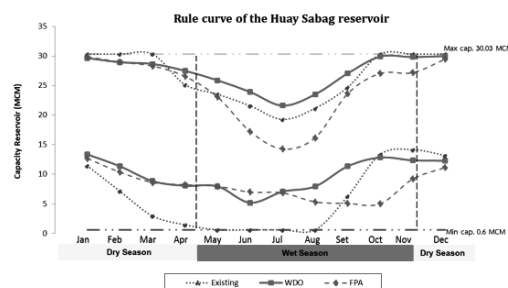


Fig. 8. Optimal rule curves of the Huay Sabag reservoir (using objective function: the minimum average excess spill water)

B. Efficiency of rule curves under using historical data

The efficiency of the obtained rule curves from all cases of searching will be evaluated by using in reservoir simulation model considering the historic inflow data of 22 years (1996–2017). Together with monthly historic inflow data, monthly data of evaporation, rainfall, irrigation, domestic and industrial water requirements and monthly environmental conservation were used in the simulated system. The optimal rule curves from WDO, FPA and the current rule curves were used to evaluate. The results of using all rule curves from using minimal average water shortage and minimal average excess release water were described in Table I and Table II respectively.

For the both tables, they indicated that the situations of excess release water of using rule curves from FPA technique are the least. Whereas the situations of water shortage are the same of zero due to the historic inflow data are enough for downstream water requirement.

TABLE I. The situations of water shortage and excess water considering historic inflow 22 years of search procedure (Objective function: the minimum average water shortage)

Situations	Rule curves	Frequency (times/year)	Volume (Million cubic meters)		Time period (year)	
			Average	Maximum	Average	Maximum
Shortage	RC1-Current	0.000	0.000	0.000	0.000	0.000
	RC2-FPA	0.000	0.000	0.000	0.000	0.000
	RC3-WDO	0.000	0.000	0.000	0.000	0.000
Excess-water	RC1-Current	1.000	3.991	3.991	22.000	22.000
	RC2-FPA	1.000	3.159	3.159	22.000	22.000
	RC3-WDO	1.000	3.973	3.991	22.000	22.000

TABLE II. The situations of water shortage and excess water considering historic inflow 22 years of search procedure (Objective function: the minimum average excess spill water)

Situations	Rule curves	Frequency (times/year)	Volume (Million cubic meters)		Time period (year)	
			Average	Maximum	Average	Maximum
Shortage	RC1-Current	0.000	0.000	0.000	0.000	0.000
	RC2-FPA	0.000	0.000	0.000	0.000	0.000
	RC3-WDO	0.000	0.000	0.000	0.000	0.000
Excess-water	RC1-Current	1.000	3.991	3.991	22.000	22.000
	RC2-FPA	1.000	3.159	3.159	22.000	22.000
	RC3-WDO	1.000	3.991	3.991	22.000	22.000

C. Efficiency of rule curves under synthetic inflow conditions.

For deep evaluation the efficiency of the obtained rule curves from all cases, all rule curves (from WDO, FPA and the current rule curves) were used in reservoir simulation model which considering the 1,000 samples of synthetic

inflow. These data, monthly data of evaporation, rainfall, irrigation, domestic and industrial water requirements and monthly environmental conservation were used in the simulated system too. The results of using all rule curves from using minimal average water shortage and minimal average



excess release water were described in Table III and Table IV respectively. These situations were present in term of frequency, magnitude and duration with the mean (μ) and standard deviation (σ).

For the both tables, they still indicated that the situations of excess release water of using rule curves from

FPA technique are the least (3.159 ± 0.000 MCM./year) as compared with the other rule curves. Whereas the situations of water shortage are still the same of empty due to the inflow data are enough for the water demand in downstream site.

TABLE III. The situations of water shortage and excess water considering synthetic inflow 1,000 events (Objective function: the minimum average water shortage)

Situations	Rule curves		Frequency (times/year)	Volume (Million cubic meters)		Time period (year)	
				Average	Maximum	Average	Maximum
Shortage	RC1-Current	μ	0.000	0.000	0.000	0.000	0.000
		σ	0.000	0.000	0.000	0.000	0.000
	RC2-FPA	μ	0.000	0.000	0.000	0.000	0.000
		σ	0.000	0.000	0.000	0.000	0.000
	RC3-WDO	μ	0.000	0.000	0.000	0.000	0.000
		σ	0.000	0.000	0.000	0.000	0.000
Excess-water	RC1-Current	μ	1.000	3.990	3.991	22.000	22.000
		σ	0.000	0.006	0.000	0.000	0.000
	RC2-FPA	μ	1.000	3.159	3.159	22.000	22.000
		σ	0.000	0.000	0.000	0.000	0.000
	RC3-WDO	μ	1.000	3.973	3.991	22.000	22.000
		σ	0.000	0.011	0.000	0.000	0.000

Note: μ = average, σ = standard deviation

TABLE IV. The situations of water shortage and excess water considering synthetic inflow 1,000 events (Objective function: the minimum average excess spill water)

Situations	Rule curves		Frequency (times/year)	Volume (Million cubic meters)		Time period (year)	
				Average	Maximum	Average	Maximum
Shortage	RC1-Current	μ	0.000	0.000	0.000	0.000	0.000
		σ	0.000	0.000	0.000	0.000	0.000
	RC2-FPA	μ	0.000	0.000	0.000	0.000	0.000
		σ	0.000	0.000	0.000	0.000	0.000
	RC3-WDO	μ	0.000	0.000	0.000	0.000	0.000
		σ	0.000	0.000	0.000	0.000	0.000
Excess-water	RC1-Current	μ	1.000	3.990	3.991	22.000	22.000
		σ	0.000	0.006	0.000	0.000	0.000
	RC2-FPA	μ	1.000	3.159	3.159	22.000	22.000
		σ	0.000	0.001	0.000	0.000	0.000
	RC3-WDO	μ	1.000	3.990	3.991	22.000	22.000
		σ	0.000	0.008	0.000	0.000	0.000

Note: μ = average, σ = standard deviation

D. Efficiency of rule curves under increasing 30 % water demand

Because the previous tests did not show the situation of water shortage in both considering historic inflow and synthetic inflow, the water demand in downstream site were increased 30%. All rule curves were used to test again with the same conditions that described in previous sections (section B and section C). The results were present in tables V and VI

respectively. However, the situations of excess spill water when using the rule curves of WDO and FPA are still less than using current rule curves corresponding to the previous tests (did not increase water demand). Because the situations of excess water when using rule curves of FPA are less than using the other rule curves, hence FPA technique is more effective in mitigating the excess water situation, followed by WDO technique.

TABLE V. The situations of water shortage and excess water considering historic inflow 22 years with increase 30% of water demand (Objective function: the minimum average excess spill water)

Situations	Rule curves	Frequency (times/year)	Volume (Million cubic meters)		Time period (year)	
			Average	Maximum	Average	Maximum
Shortage	RC1-Current	0.955	1.909	2.000	21.000	21.000
	RC2-FPA	0.955	2.864	3.000	21.000	21.000
	RC3-WDO	1.000	1.955	2.000	22.000	22.000
Excess- water	RC1-Current	1.000	3.338	3.338	22.000	22.000
	RC2-FPA	1.000	2.634	2.638	22.000	22.000
	RC3-WDO	1.000	3.329	3.338	22.000	22.000



TABLE VI. The situations of water shortage and excess water considering synthetic inflow 1,000 events with increase 30% of water demand (Objective function: the minimum average excess spill water)

Situations	Rule curves		Frequency (times/year)	Volume (Million cubic meters)		Time period (year)	
				Average	Maximum	Average	Maximum
Shortage	RC1-Current	μ	0.950	1.898	2.000	20.858	20.883
		σ	0.017	0.033	0.000	0.713	0.381
	RC2-FPA	μ	0.953	2.857	3.000	20.959	20.959
		σ	0.012	0.033	0.000	0.263	0.263
	RC3-WDO	μ	0.998	1.954	2.000	21.527	21.913
		σ	0.010	0.024	0.000	2.291	0.426
Excess-water	RC1-Current	μ	1.000	3.337	3.338	22.000	22.000
		σ	0.000	0.006	0.000	0.000	0.000
	RC2-FPA	μ	1.000	2.635	2.638	22.000	22.000
		σ	0.000	0.003	0.000	0.000	0.000
	RC3-WDO	μ	1.000	3.331	3.338	22.000	22.000
		σ	0.000	0.008	0.000	0.000	0.000

Note: μ = average, σ = standard deviation

IV. CONCLUSION

This study applied two alternative optimization techniques connecting with reservoir simulation model for searching optimal reservoir rule curves. These optimization techniques are Wind Driven optimization (WDO) and Flowers Pollination Algorithm (FPA). There were two alternative objective functions that considered for applying to search process such as the minimum average water shortage and the minimum average excess spill water. The Huay Sabag reservoir where located in the northeast region of Thailand was considered for this study. The historic monthly inflow data of 22 years were considered for each searching case. The synthetic inflow data of 1,000 samples were used to simulate the reservoir system for evaluating the performance of the obtained rule curves.

The results found that the proposed model with two objective functions provided the new rule curves. The patterns of these rule curves are similar due to seasonal inflow effect and the same searching conditions. However, there are different points, such as the lower line of new rule curves is higher than the current rule curves. These positions can reduce water release in order to store water for next season. In addition, the upper line of FPA rule curves is lower than the current rule curves and WDO rule curves. These conditions enhance to spill more water from reservoir in order to have reserve volume for preventing food situation.

Then, these obtained rule curves were used to evaluate and compare with the current rule curves. The results present that the rule curves of using average water shortage as an objective function in searching process were not have water shortage situation. This corresponds to the actual situation of the reservoir information that the total inflow data are larger than the downstream water requirement.

For the obtained rule curves from using minimum average excess spill water as the objective function in searching process, the results present that the rule curves from the FPA technique are most effective in mitigating the excess water situation, followed by WDO rule curves and current rule curves respectively. Further, the obtained rule curves of the proposed model using average water shortage and minimum

average excess spill water as the objective functions were used to evaluate with synthetic inflow of 1,000 samples by increasing 30% of water demand. The results also showed that the FPA rule curves can alleviate situations of flood more than the WDO rule curves as well as current rule curves.

ACKNOWLEDGMENT

The authors would like to acknowledge the Royal Irrigation Department and the Huay Sabag reservoir project in Yasothorn province for supporting data in this study.

REFERENCES

- [1] International Monetary Fund "IMF" and CIA World Factbook., (2015). Largest countries by agricultural output according.
- [2] Kumara N., Tischbein B., Kushech J., Lauxd P., Bege M and Bogardi J. (2017). Impact of climate change on water resources of upper Kharun catchment in Chhattisgarh, India. *Journal of Hydrology*, (13) 189-207
- [3] Gashaw T., Tulu T., Argaw M and Worqlul A. W. (2018). Modeling the hydrological impacts of land use/land cover changes in the Andassa watershed, Blue Nile Basin, Ethiopia, *Science of the Total Environment*, 619-620.
- [4] Kangrang A., Pakoktom W., Nualnukul W., and Chaleeraktrakoon C., "Adaptive Reservoir Rule Curves by Optimization and Simulation", *Proceedings of the Institution of Civil Engineers - Water Management*, vol. 170, no. WM5, pp. 219-230, 2017.
- [5] Chaleeraktrakoon C. and Kangrang A. (2005). A Dynamic Programming for Searching Rule Curves. *The proceeding of International Conference on World Water and EnvironmentalResource Congress*, 15-19 May, Anchorage, Alaska, USA.
- [6] Prasanchum H., and Kangrang A., "Optimal reservoir rule curves under climatic and land use changes for Lampao Dam using genetic algorithm", *KSCE Journal of Civil Engineering*, 14 pages, 2017.
- [7] Kangrang A., Compliew S. and Hormwichian R. (2011). Optimal Reservoir Rule Curves Using Simulated Annealing. *Proceedings of the Institution of Civil Engineers - Water Management*, 164(WM1), 27-34.
- [8] Kangrang A., Prasanchum H., Hormwichian R., "Development of Future Rule Curves for Multipurpose Reservoir Operation Using Conditional Genetic and Tabu Search Algorithms", *Advances in Civil Engineering*, Volume 2018, Article ID 6474870, 10 pages.
- [9] Pandey A and Parhi D. R. (2017). Optimum path planning of mobile robot in unknown static and dynamic environments using Fuzzy-Wind Driven Optimization algorithm. *Defence Technology*, (13), 47-58.
- [10] Sharawi M., Emary E., Saroit I.A. and El-Mahdy H. (2014). Flower pollination optimization algorithm for wireless sensor network lifetime global optimization, *International Journal of Soft Computing and Engineering*, 4 pp. 54-59.



Application of Genetic Programming and Flower Pollination Algorithm for Searching Optimal Rule Curves of small reservoir

Ratsuda Ngamsert^{1st} and Anongrit Kangrang

Faculty of Engineering, Mahasarakham University, Kantharawichai Distret,
Mahasarakham, Thailand

ratsuda.nga@msu.ac.th, anongrit.k@msu.ac.th

Abstract— Rule curves of small reservoir are important information for reservoir operation system. This Study presents the Genetic Programming (GP) and Flower Pollination Algorithm (FPA) techniques for searching optimal rule curves of small reservoir. The propose techniques were connected with the reservoir simulation model to search optimal rule curves of reservoir. The objective functions of search procedure were the minimal average water shortage and the minimal excess release water. Monthly rule curves and historic inflow record from 1994 to 2017 of the Huay Ling Jone reservoir, located in Yasothorn province were considered for this study. The 1,000 samples of generated inflow data were used to evaluate the performance of the new obtained rule curves. The results presented situations of water shortage and excess release in terms of frequency, duration, amount of average and maximum. The results found that the patterns of these new rule curves were similar to the existing rule curves because of seasonal inflow effect and the same searching conditions. The results also present that the new obtained rule curves of GP can reduce situations of water shortage and excess release more than the existing rule curves and the FPA rule curves. Then, the obtained rule curves of the proposed models were used to evaluate with synthetic inflow of 1,000 samples. The results also found that the new rule curves from GP can alleviate the situations of water shortage and flood more than the existing rule curves and slightly than rule curve from FPA.

Keywords— *reservoir rule curves, reservoir operation, genetic programming, flower pollination algorithm*

I. INTRODUCTION

It is well known that "water" is an important and limited natural resource. It is a major factor in the livelihoods of humans and ecosystems. At present, the climate changes rapidly direct effect on ecological life, one of the effects of climate change is cycle of water when the water cycle is not

balanced cause the floods, drought and conflicts caused by water users in society [1]. Water resources management is therefore important for the management of water and related resources. In the present water resources management focuses on water management, economic efficiency social justice and environmental sustainability. To get high efficiency in water management have to perform both supply management and demand management, as well as to focus on non-construction management in order to save budget and minimizing other impacts [2]. By this way, the improvement of reservoir operation is an appropriate solution.

Reservoir management must be managed on the basis of natural instability and water demand. The basic and essential tool for water balance analysis in reservoir management is rule curves that an essential tool for improvement of reservoir operation performance [3]. They consist of two graphs; the upper curves and lower rule curves. The reservoir operation performs by using standard operating rule and rule curves, which controls available water within the upper and lower levels in order to reserve water volume for using in dry season and to protect flooding. The management in long term operation may need to improve the rule curves for increasing reservoir operation efficiency.

There are many optimization techniques applied to search the optimal rule curve of reservoir, such as dynamic programming, genetic algorithm, differential evolution algorithm [4-6], etc., that are still available today. However, these techniques are subject to limitations in their work and only appropriate for the specific area of their use. Nowadays, if available optimization technique to be easy to use and suitable for the area, it is worth study.

Recently, Genetic Programming (GP) and Flower Pollination Algorithm (FPA) are the alternative techniques for application of a variety of engineering [7]. The numerical problem solving used GP for resizing structure in order to find the optimal cross section and the connection of the joints to achieve the minimum weight [8]. However, it is not commonly use to find the optimal rule curves. Hence, it an



interesting technique that introduce to apply with reservoir simulation model for solving rule curves problem.

This research presents the application of Genetic Programming and Flower Pollination Algorithm techniques for searching optimal reservoir rule curves of small reservoir. The Huay Ling Jone reservoir, Yasothorn province in the northeast area of Thailand was selected as this case study.

II. MATERIALS AND METHODS

A. Study area

The Huay Ling Jone reservoir is located in Yasothorn province, Thailand (Fig.1). This project has the irrigation area of 19.8768 Km², full storage capacity of reservoir 21.06 MCM., dead storage capacity of 0.4 MCM. The historic inflow record of the Huay Ling Jone reservoir from 1996 to 2017, which has the average of 24.720 MCM./year. The objectives of reservoir are consume, irrigation, flood control, domestic water supply and environ-mental conversation. Fig.2 shows the flow diagram of the Huay Ling Jone reservoir.

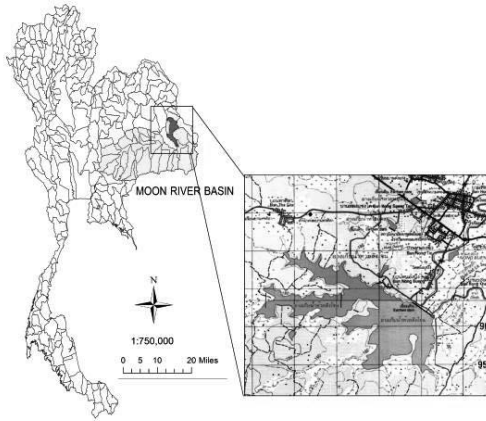


Fig. 1. Location of the Huay Ling Jone reservoir

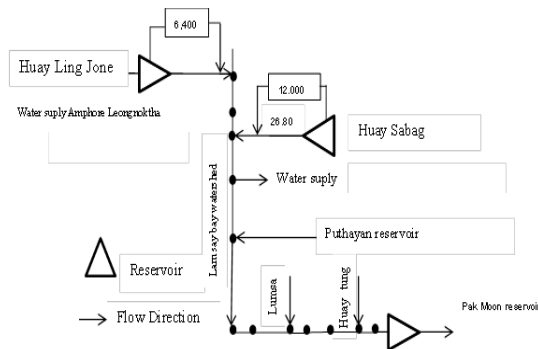


Fig. 2. Flow diagram of the Huay Ling Jone reservoir

B. Reservoir operation model

The reservoir operation system consists of the available water that is calculated from the water balance concept and water demands in downstream site. The monthly release water is estimated by considering the monthly available water with release criteria, operating policies and reservoir rule curves. For this study, the reservoir operation model was created following the concept of the water balance [9]. The reservoir operation model is operated under the standard operating policy as expressed in Fig. 3 and equation (1).

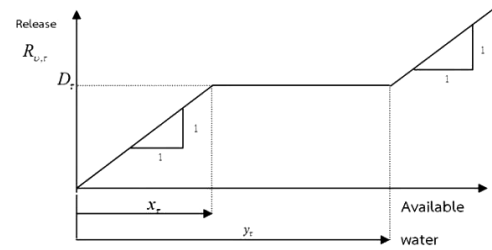


Fig. 3. Standard operating rule.

$$R_{v,\tau} = \begin{cases} D_{\tau} + W_{v,\tau} - y_{\tau}, & \text{for } W_{v,\tau} \geq y_{\tau} + D_{\tau} \\ D_{\tau}, & \text{for } x_{\tau} \leq W_{v,\tau} < y_{\tau} + D_{\tau} \\ D_{\tau} + W_{v,\tau} - x_{\tau}, & \text{for } x_{\tau} - D_{\tau} \leq W_{v,\tau} < x_{\tau} \\ 0, & \text{otherwise} \end{cases} \quad (1)$$

where $R_{v,\tau}$ is the release of water during year v and month τ ($\tau = 1$ to 12 representing January to December), D_{τ} is the net water demand during month τ ; x_{τ} is the lower rule curve of month τ ; y_{τ} is the upper rule curve of month τ and $W_{v,\tau}$ is the available water by calculating the water balance concept during year v and month τ , as described in equation (2):

$$W_{v,\tau} = S_{v,\tau} + Q_{v,\tau} - R_{v,\tau} - E_{\tau} - DS \quad (2)$$

where $S_{v,\tau}$ is the stored water at the end of month τ ; $Q_{v,\tau}$ is the monthly inflow to the reservoir, E_{τ} is the average value of the evaporation loss and DS is the minimum reservoir storage capacity (dead storage capacity). The operating policy usually reserves the available water ($W_{v,\tau}$) for mitigating the risk of water shortage in the future, when $0 \leq W_{v,\tau} < x_{\tau} - D_{\tau}$ under long term operation.

released water from the reservoir was used to calculate the water shortage and excess water release situations, which can be expressed as the frequency of failures in a year and the number of excess water release, as well as the average annual shortage per year (as the first objective function for searching the optimal rule curves in this study.) as shown in equation (3).

$$Min_{(avr)} = \left(\frac{1}{n} \sum_{v=1}^n Sh_v \right) \quad (3)$$



$$\text{if } R_{\tau} < D_{\tau}; \text{Then } Sh_{\tau} = \sum_{\tau=1}^{12} (D_{\tau} - R_{\tau}) \quad (4)$$

Secondly, the minimum average excess spill water per year (U) is set as another objective function of the searching procedure subject to the constraints on the simulation model as in the following:

$$\text{Min } U(X_i) = \left(\frac{1}{n} \sum_{v=1}^n Sp_v \right) \quad (5)$$

$$\text{if } R_{\tau} > D_{\tau}; \text{Then } Sp_v = \sum_{\tau=1}^{12} (R_{\tau} - D_{\tau}) \quad (6)$$

where n is the total number of considered years, Sp_v is the excess spill water during year v (year in which releases are higher than the target demand) and i is the iteration number.

C. Application of GP and reservoir simulation model for searching optimal rule curves

The process of GP starts with a random initial population of computer program. An individual program presents in the population refers to a parse tree, which is generated by the combination of its functions (nodes) and terminals (leaves) that are defined in a function set and terminal set, appropriate to the problem, respectively. A function set may consist of basic arithmetic operators, mathematical functions, conditional operators, Boolean operators, iterative functions and any user defined functions or operators, while a terminal set contains the arguments for the functions. Once the initial population has been created, the next step is repeatedly replacing the current population with a new population (or new generation) by means of applying genetic operators (reproduction, crossover and mutation) probabilistically until the best fitness of the population has reached the desired level, or the maximum number of generations has been reached. The genetic operators applied in a GP are the basic GA operators. The reproduction is the process of copying the selected individual program to the new population. The crossover operation creates a new offspring program for the new population.

In this study, the searching process starts from creating the initial random rule curves (24 values for 1 reservoir). Then, the random rule curves were used in reservoir simulation model for operating along the historic inflow record data. Next, the monthly water release from reservoir simulation will be used to calculate the objective function (fitness function) and evaluate respectively. Then, the criteria of searching will be done for evaluating the stop process. If the condition is out of the criteria, these random rule curves will be performed in reproduction process again. Then, the searching process is continued until the termination criterion is satisfied as

described in Fig. 4. This termination criterion is the maximum iteration. For another objective function (the minimum average excess spill water per year) is performed similar the first objective function.

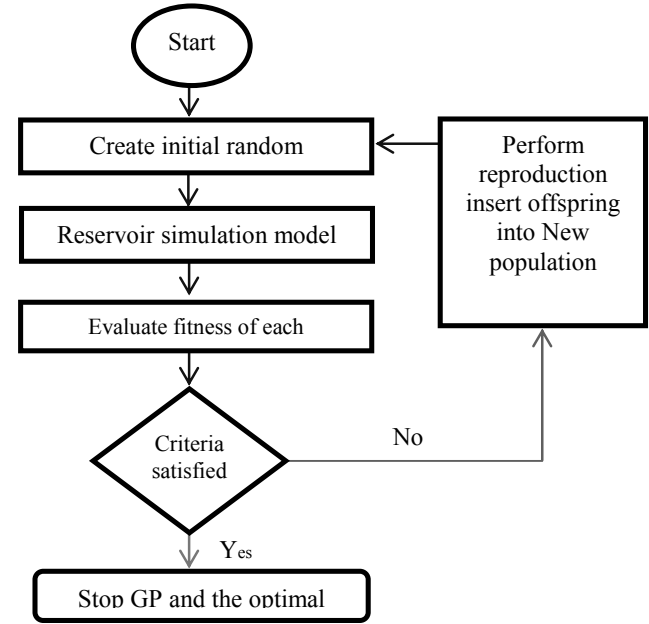


Fig. 4. Application of GP and reservoir simulation model for searching optimal rule curves

For each searching run, the historic inflow data record of 24 years from 1994 – 2017 were used in the reservoir simulation model. Whereas 1,000 sample of synthetic inflow data will be used in evaluating process that run with the same reservoir simulation model. The efficiency of each obtained rule curve will be present and compare with other rule curves.

III. RESULTS AND DISCUSSION

D. Historic rule curves with objective functions

The 24 years (1994-2017) of monthly historic inflow data, monthly data of evaporation, rainfall, irrigation, domestic and industrial water requirements and monthly environmental conservation were imported for processing in the GP and FPA connected to the reservoir simulation model, and the optimal rule curves of each technique were obtained. The optimal rule curves of the Huay Ling Jone reservoir when using the minimization average water shortage as the objective function were plotted in Fig.5. Whereas, Fig.6. shows the optimal rule curves of the Huay Ling Jone reservoir when using the minimization excess release water as the objective function. They indicated that the rule curves patterns of all cases were similar because of the seasonal inflow effect and the same searching conditions.

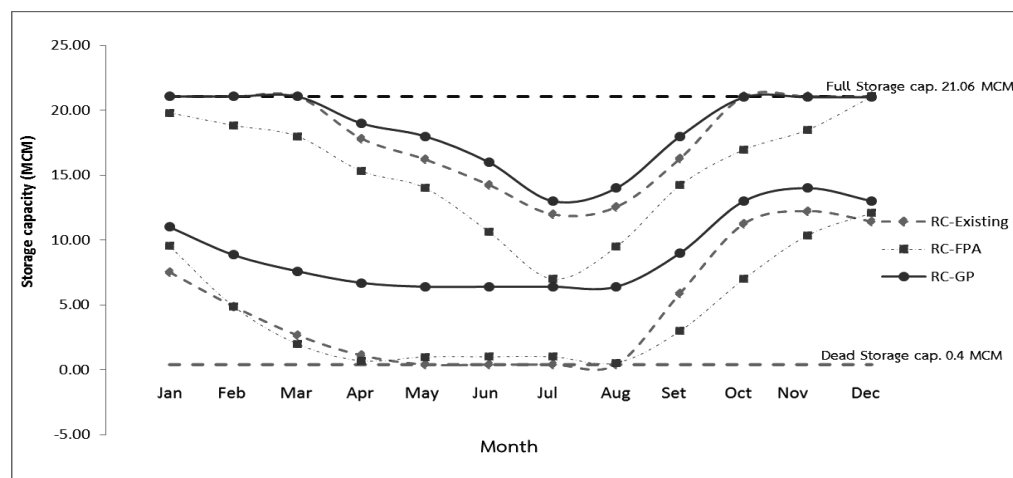


Fig. 5. Optimal rule curves of the Huay Ling Jone reservoir (objective function: minimization water shortage)

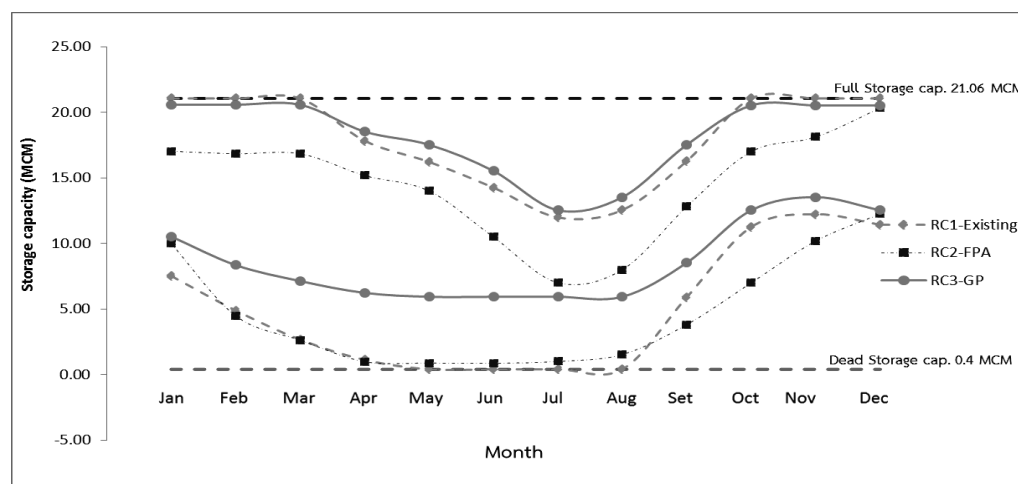


Fig. 6. Optimal rule curves of the Huay Ling Jone reservoir (objective function: minimization excess release water)

The results also show that the lower rule curves of GP (RC-GP) and FPA (RC-FPA) are taller than the existing rule curves; these conditions will control to reduce amount release water. Further, in the middle of wet season (August–October), the upper rule curves of GP (RC-GP) are higher than their rule curves of current (RC-Existing) and FPA (RC-FPA); these can save more water during the beginning of rainy season.

E. Efficiency of rule curves using minimal average water shortage as the objective function

Table I shows the situations of the water shortage and excess release water when using minimization average water shortage as the objective function in the historic scenario. These situations were present in term of frequency, magnitude and duration. The results indicated that the situation of water shortage and excess release water using the GP rule curves are

the least as compared with the other rule curves. In addition, the results also showed that the average water shortage of using GP rule curves is the least of 2.125 MCM./year which corresponding to the objective function of searching.

Table II presents the situations of the water shortage and excess release water when using minimization average water shortage as the objective function in the 1,000 events of synthetic inflow scenario. These situations were present in term of frequency, magnitude and duration with the mean (μ) and standard deviation (σ). The results indicated that the situation of water shortage and excess release water using the GP rule curves are the least as compared with the other rule curves. The results also showed that the average water shortage of using GP rule curves is the least of 2.125 ± 0.000 MCM./year which corresponding to the objective function of searching too.



TABLE I. The situations of water shortage and excess water considering historic inflow 24 years (objective function: minimization water shortage)

Situations	Rule curves	Frequency (times/year)	Volume (MCM.)		Time period (year)	
			Average	Maximum	Average	Maximum
Shortage	RC-Existing	0.792	4.917	12.000	3.800	8.000
	RC-FPA	0.833	5.125	12.000	5.000	14.000
	RC-GP	0.500	2.125	9.000	2.400	3.000
Excess water	RC-Existing	0.958	9.190	15.868	11.500	22.000
	RC-FPA	1.000	9.396	15.868	24.000	24.000
	RC-GP	0.875	6.434	13.705	5.250	12.000

TABLE II. The situations of water shortage and excess water considering considering synthetic inflow 1,000 events (objective function: minimization water shortage)

Situations	Rule curves		Frequency (times/year)	Volume (MCM.)		Time period (year)	
				Average	Maximum	Average	Maximum
Shortage	RC-Existing	μ	0.717	4.601	10.818	5.385	9.432
		σ	0.137	1.042	2.506	3.417	4.063
	RC-FPA	μ	0.718	4.877	11.950	5.471	9.477
		σ	0.137	1.172	1.881	3.410	4.053
	RC-GP	μ	0.500	2.125	9.000	2.400	3.000
		σ	0.000	0.000	0.000	0.000	0.000
Excess water	RC-Existing	μ	0.958	9.623	15.736	15.906	19.108
		σ	0.046	1.526	0.508	7.156	4.987
	RC-FPA	μ	0.983	9.958	15.716	19.916	21.672
		σ	0.028	1.404	0.539	6.146	3.928
	RC-GP	μ	0.875	6.434	13.705	5.250	12.000
		σ	0.000	0.000	0.000	0.000	0.000

Note: μ = average, σ = standard deviation

F. Efficiency of rule curves using minimal excess release water as the objective function

Table III shows the situations of the water shortage and excess release water when using minimization excess release water as the objective function in the historic scenario (24 years). These situations were present in term of frequency, magnitude and duration. The results indicated that the situation of water shortage and excess release water using the GP rule curves are the least as compared with the other rule curves. The least situations are covering all terms such as frequency, magnitude and duration. However, these results are slightly different from the results of using the first objective function (Table I) because of the rule curves of GP technique

with different objective function closed together.

Table IV presents the situations of the water shortage and excess release water when using minimization excess release water as the objective function in the 1,000 events of synthetic inflow scenario. These situations were present in term of frequency, magnitude and duration with the mean (μ) and standard deviation (σ). The results indicated that the situation of water shortage and excess release water using the GP rule curves are the least as compared with the other rule curves. The least situations are covering all terms such as frequency, magnitude and duration. These can conclude that the GP technique connecting with reservoir simulation model can provide the optimal rule curves that have more efficiency to reduce the situation of water shortage and flooding.

TABLE III. The situations of water shortage and excess water considering historic inflow 24 years (objective function: minimization excess release)

Situations	Rule curves	Frequency (times/year)	Volume (MCM.)		Time period (year)	
			Average	Maximum	Average	Maximum
Shortage	RC1-Existing	0.792	4.917	12.000	3.800	8.000
	RC2-FPA	0.833	5.333	13.000	5.000	14.000
	RC3-GP	0.500	2.125	9.000	2.400	3.000
Excess water	RC1-Existing	0.958	9.190	15.868	11.500	22.000
	RC2-FPA	1.000	9.551	15.868	24.000	24.000
	RC3-GP	0.875	6.458	13.705	5.250	12.000



TABLE IV. The situations of water shortage and excess water considering synthetic inflow 1,000 events (objective function: minimization excess release)

Situations	Rule curves		Frequency (times/year)	Volume (MCM.)		Time period (year)	
				Average	Maximum	Average	Maximum
Shortage	RC1-Existing	μ	0.717	4.601	10.818	5.385	9.432
		σ	0.137	1.042	2.506	3.417	4.063
	RC2-FPA	μ	0.731	5.146	11.973	5.855	9.956
		σ	0.291	2.410	3.358	7.486	8.537
	RC3-GP	μ	0.500	2.125	9.000	2.400	3.000
		σ	0.000	0.000	0.000	0.000	0.000
Excess water	RC1-Existing	μ	0.958	9.623	15.736	15.906	19.108
		σ	0.046	1.526	0.508	7.156	4.987
	RC2-FPA	μ	0.988	10.209	15.732	21.040	22.353
		σ	0.041	2.632	0.755	10.089	5.679
	RC3-GP	μ	0.875	6.434	13.705	5.250	12.000
		σ	0.000	0.000	0.000	0.000	0.000

Note: μ = average, σ = standard deviation

IV. CONCLUSION

This research present the application of Genetic Programming and Flower Pollination Algorithm connecting with the reservoir simulation model for searching optimal rule curves of small reservoir in Thailand. The historic monthly inflow data were applied to use with the 2 objective functions of searching process including the minimal average water shortage and the minimal excess release water. The Huay Ling Jone reservoir located in Yasothorn province, Thailand was considered as the case study. The physical information of reservoir, water demand from reservoir, historic inflow to reservoir, as well as related data were used in the connecting model of reservoir simulation and optimization techniques. The 24 years of historic inflow were generated for 1,000 samples in order to evaluate the performance of using new obtained rule curves. The performance was presented in term of situations of water shortage and excess release water. These situations consist of frequency, duration, amount of average and maximum.

The results present that the patterns of these new obtained rule curves and the existing rule curves were similar because of the same seasonal inflow effect. However, the obtained lower rule curves of GP were higher than the FPA and existing curves during dry season (January-May) that can save among of water for next season by reducing water release this dry season. Hence, there were many water scarcities in short term considering but enough water in long term operating. In addition, the GP rule curves were higher than FPA and existing rule curves during the beginning of rainy season that can save high water volume than other curves. These obtained rule curves were used to evaluate and compare with the existing rule curves. The results present that the new obtained from GP can reduce situations of water shortage and excess release water more than the existing rule curves and the FPA rule curves both using historic inflow and synthetic inflow. In conclude the GP is one of optimization technique

that can apply with reservoir simulation model for searching optimal rule curves of small reservoir effectively.

ACKNOWLEDGMENT

This research the authors would like to acknowledge by Royal Irrigation Department of The Huay Ling Jone reservoir and Land Development Department in Yasothorn province for supporting data. The authors would like to acknowledge Faculty of Engineering, Mahasarakham University for supporting research resources.

REFERENCES

- [1] Zhua, Y., Linb, Z., Wanga, J., Zhao, Y. and Hea, F. 2016. Impacts of climate changes on water resources in Yellow River Basin, China. *Procedia Engineering*, 154, 687-695.
- [2] Zhao, G., Gao, H., Naz.B.S., Kao, S. and Voisin, N. 2016. Integrating a reservoir regulation scheme into a spatially distributed hydrological model. *Advances in Water Resources*, 98, 16-31
- [3] Mensika, P. and Martona, D. 2016. Hybrid optimization method for strategic control of water withdrawal from water reservoir with using support vector machines. *Procedia Engineering*, 186, 491-498.
- [5] Chalceraktrakoon C. and Kangrang A. (2005). A Dynamic Programming for Searching Rule Curves. In : The proceeding of International Conference on World Water and Environmental Resource Congress, ASCE 2005, 15-19 May 2005, Anchorage, Alaska, USA, n.p. : pp.234-237.
- [6] Hormwichian, R., Kangrang, A. and LAMOM, A. 2009. A conditional Algorithm Model for Searching Optimal Reservoir Rule Curves, *J. Applied Sci.* 9(19), 3575-3580, 27- 34.
- [7] Salgotra, R. and Singh, U. 2017. Application of mutation operators to flower pollination algorithm, *Expert Systems with Applications*, 79, 112-129.
- [8] Assimi, H., Jamali, A. and Nariman, N. 2017. Sizing and topology optimization of truss structures using genetic programming, *Swarm and Evolutionary Computation*, 37, 90-103.
- [9] Kangrang, A., Compliew, S., & Hormwichian R. 2011. Optimal Reservoir Rule Curves Using Simulated Annealing. *Proceedings of the Institution of Civil Engineers – Water Management*, 164(WM1)



The Embodied Energy & Greenhouse Gas Emission of Residential Building in Silpakorn University, Nakhon Pathom, Thailand

Teerachai Surachotivet, Thibordin Sangsawang

Laboratory of Advance Combustion Technology and Energy System (LACTES),
Department of Mechanical Engineering
Faculty of Engineering and Industrial Technology, Silpakorn University, Nakorn Pathom, Thailand
e-mail address: Teerachai_su@hotmail.com ,Sangsawang_t@su.ac.th

Abstract

The purpose of this study is to analyze the embodied energy and greenhouse gas emission from building materials in terms of MJ and kgCO₂e by Life Cycle Energy. A case study in this research is the 10-storey residential building located in Silpakorn University, Nakhon Pathom, Thailand. The utility space is 17,000 m². This study found that the embodied energy is 121,771,441.61 MJ. The embodied energy is mainly consumed by material fabrication processes. Total embodied energy in building is utilized by steel for 74.26% and concrete for 17.06% respectively and 8.68% for others materials: bricks, PVC, etc. The total greenhouse gas emission is 10,079,258.91 kgCO₂e with 75.22% from steel and concrete for 19.57%.

Keywords—Life cycle analysis (LCA), Life cycle energy (LCE), Building, Energy, Greenhouse gas, Building material

I. INTRODUCTION

Today's buildings are complex and have a variety of building materials. The building materials need more energy for production and called "embodied energy". [1] This word means the energy usage during the production which causes the reduction in the natural resources in the form of electricity generation and effects to the environment as global warming.

Life cycle analysis (LCA) is quantitative analysis. This method analyzes resource usage and emissions released in material processing, manufacture, utilization and disposal. LCA analysis is used to compare environmental impact of products manufacture and to find process to reduce environmental impact.

LCA is a tool used to analyze the energy and greenhouse effect which affects the environment from the original of materials manufacture to demolition. Gerilla et al. [2] studied the environmental impact of wood and reinforced concrete used in house construction. Gustavsson and Sathre [3] compared the energy and carbon dioxide of wood and concrete. Heravi et al. [4] analyzed the energy of materials production and process in building construction. These studies [2-4] found

that steel and concrete had more greenhouse effect to the environment than that of wood due to high energy consumption in production and demolition.

Nässén et al. [6] compared wood and concrete and showed that wood had lower energy content than the concrete. Bonamente et al. [7] improved the structure to increase the brightness of the building. It reduced energy consumption by 30%. Adalberth [8] found that the insulation added to home would reduce the energy consumption in buildings. Thormark [9] found the using of recycled materials, the building's embodied energy decreased from 45% to 30-40%, Moncaster and Symons [10] introduced the TC350 standard to calculate carbon and energy impact of building.

The greenhouse gas emissions were also studied. Blengini and Carlo [11] used LCA to calculate energy saving in house. The low energy house can save the Life cycle energy from the standard house for 50%. Suzuki and Oka [12] studied of LCE and CO₂ emission of office building. They found that the embodied energy of buildings was from building utilization for 80%. Yan et al. [13] studied greenhouse gas emission of building construction. They used One Peking building in Hong Kong as a case study. They found that greenhouse gas emission of concrete and reinforced steel account for 95 % of all building material. Moussavi and Akbarnezhad [14] analyzed Life cycle carbon footprint of building structure. They found that the materials in building structure affected the carbon footprint.

From previous study, this paper is aimed to calculate the life cycle energy of the residential building in Silpakorn University, Sanamchandra Palace campus, in order to estimate the energy and environmental impact of building materials. This 10-floors building in this study is located in the middle region of Thailand, Nakhon Pathom Province, 60 km northwest from Bangkok.



II. METHODOLOGY

Life cycle assessment (LCA) is used to analyze environmental impact. LCA starts from the acquisition of raw materials, transport to the manufacturing plant for production, transported to the end user, operation and end of life or disposal. There are 5 steps of LCA for building. First step is raw material processing. Second step is building material production. Third step is building construction. Forth step is building utilization. Final step is demolition of building materials. The LCA framework starts with goal definition and scope which defines and limits the objectives of the study. The second stage is inventory analysis. Third stage is impact assessment and the final stage is interpretation. In life cycle energy analysis (LCE), energy is the only parameter which are investigated. The details framework of the energy attributable to building is calculated as presented in Fig 1.

However, the framework of this study focuses on the raw material processing and the move to the manufacturing plant for production, transport to the construction area. The embodied energy of building materials are collected and calculated in MJ and greenhouse gas calculation is in kgCO₂e

The quantities of all building materials are converted to be the embodied energy by the equation 1.

$$EE_i = QM * ENF \quad (1)$$

Where EE_i is embodied energy in building material (MJ). QM is quantity of material (kg). ENF is energy factor of material (MJ/kg). The lists of ENF are available from Geoffrey Hammond et al. [1]

$$GHG_i = QM * EMF \quad (2)$$

Where GHG_i is summation of greenhouse gas in building material (kgCO₂e). QM is quantity of material (kg). EMF is emission factor of materials (kgCO₂e/ kg) which are presented in IPCC. [5]

III. CASE STUDY

This research uses a residential building in Silpakorn University, Nakhon Pathom, Thailand. There are 10 floors and area of 17,000 m². The time for construction is 20 months. This building shows in the figure 2. There are 3 floors of parking area and residential for 7 floors.



Fig.2 Residential Building

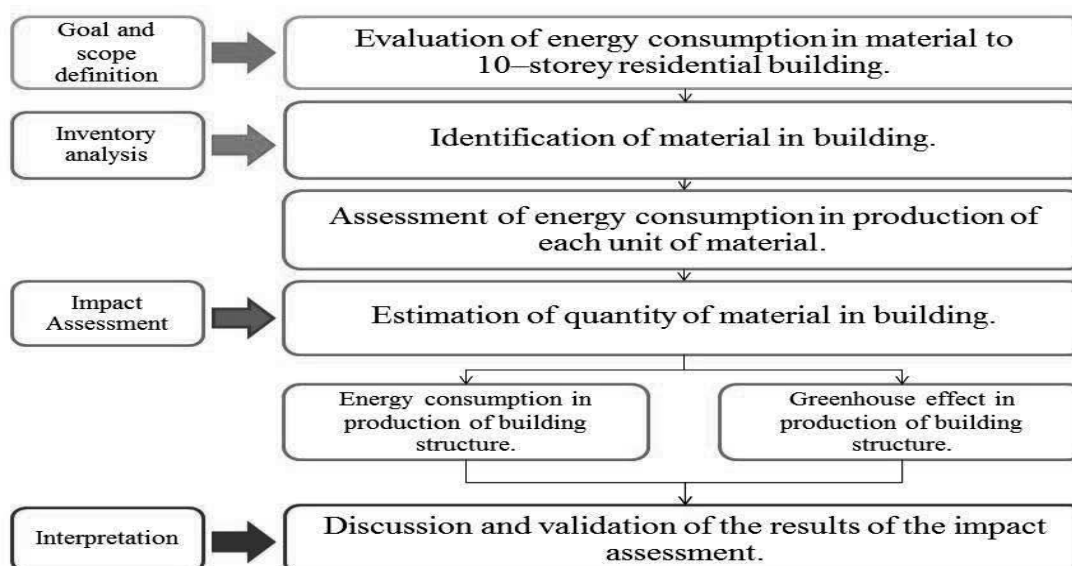


Fig.1 The methodology framework.

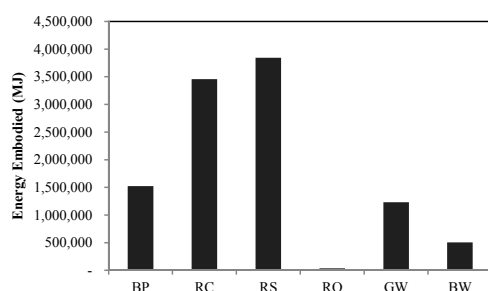


TABLE I. WEIGHT, ENERGY FACTOR, EMISSION FACTOR, EMBODIED ENERGY AND GREENHOUSE GAS

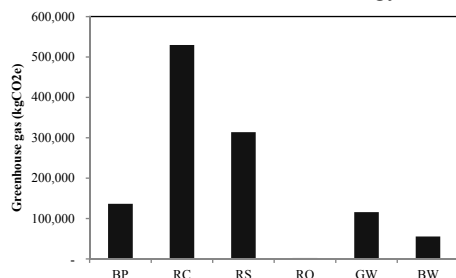
Material	Weight (kg)	Energy Factor (MJ/kg)	Emission Factor (kgCO ₂ e/kg)
Steel	2,623,388.10	35.4	2.89
Concrete	32,333,065.45	0.68	0.061
Timber	40,872.10	7.11	0.59
PVC	10,807.40	67.5	3.23
Bricks	1,882,916.80	3.00	0.24
Sand	268,150.00	0.081	0.0051
Stone	1,210.25	11.00	0.70
Gypsum	32,204.91	6.75	0.39
Total	37,192,615.00		

The table 1 shows the quantities of building materials. The total mass of this building is 37,192,615.00 kg. There are 32,333,065.45 kg (86.93%) of concrete, steel of 2,623,268.10 kg (7.05%) and the brick of 1,882,916.80 kg (5.06%). In addition, embodied energy and emission factors are also presented in table 1. [1, 5]

IV. RESULTS AND DISCUSSION



a. Embodied energy



b. Greenhouse gas

Fig. 3 Embodied energy and Greenhouse gas of foundation.

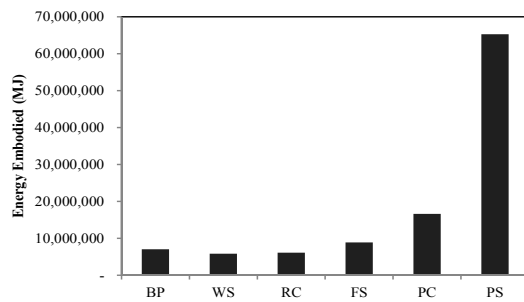
Fig. 3 shows the embodied energy and greenhouse gas of foundation. In this building foundation consists of bearing pile (BP), reinforcement – concrete (RC), reinforcement – steel (RS), reinforcement – other (RO), retaining wall (GW) and base of wall (BW).

There are 3,843,838.20 MJ (36.28%) of Reinforcement - steel (RS) and Reinforcement - concrete (RC) of 3,456,240 MJ (32.62%). There are bearing pile (BP), Ground column and wall (GW), base of wall (BW), reinforcement - other (RO) of 1,522,851.84 (14.37%), 1,231,536.64 (11.62%), 505,159.77 (10.03%), 35,047.87 (0.22%) MJ respectively. (see Fig.3a) Reinforce - steel of 108 tons and 3,216 tons of reinforce - concrete. However, because of the higher energy factor properties, the embodied energy values are higher than that of concrete.

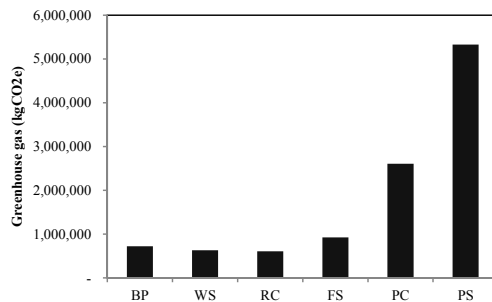
Fig 3b presents the greenhouse gas emission of building foundation. There are 529,752 kgCO₂e (27.20%), 313,804.87 kgCO₂e (45.91%), 136,608.77 kgCO₂e (11.84%), 115,761 kgCO₂e (10.03%), 55,364.90 kgCO₂e (4.80%) and 2,506.20 kgCO₂e (0.22%) of reinforcement - steel (RS), reinforcement - concrete (RC), bearing pile (BP), Ground column and wall (GW), base of wall (BW), reinforcement - other (RO) respectively. Greenhouse gas concrete is larger in mass than steel, thus making it more environmental impact due to the amount of concrete is greater than the amount of steel. However, the steel has more emission factor than concrete as shown in table 1. Then, greenhouse gas content of concrete is higher than that of steel.

Fig. 4 show embodied energy and greenhouse gas of building structure. In this building, structure includes bearing pile (BP), wall and stairs (WS), reinforcement (RC), flat slab (FS), post-tension – concrete (PC) and post-tension – steel (PS)

There are 65,263,404.60 MJ (59.48%), 16,639,344 MJ (15.16%), 8,875,835.42 MJ (8.09%), 7,025,159.77 MJ (6.40%), 6,099,756.50 MJ (5.56%) and 5,825,414.88 MJ (5.31%) of PS, PC, FS, BP, RC, WS respectively. (Fig. 4a) There are 5,328,001.11 kgCO₂e (49.22%), 2,608,329.60 kgCO₂e (24.10%), 926,181.99 kgCO₂e (8.56%), 732,297.55 kgCO₂e (6.68%), 631,811.37 kgCO₂e (5.84%), 606,319.04 kgCO₂e (5.60%) of PS, PC, SB, BP, WS, RC respectively, are illustrated in Fig. 4b. Fig. 4a and Fig.4b show that the embodied energy of PS is the highest since PS consists mainly of steel. And the steel consumes a lot of energy during production, resulting in high energy factor and emission factor.

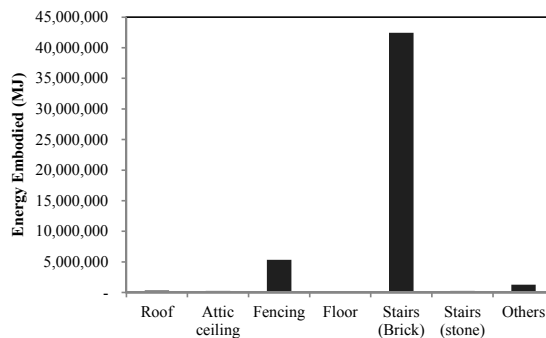


a. Embodied energy

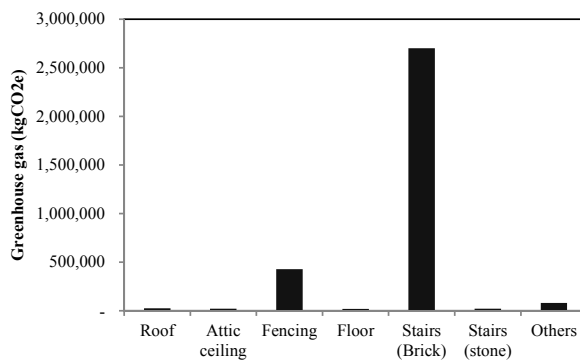


b. Greenhouse gas

Fig. 4. Embodied energy and Greenhouse gas of structure.



a. Embodied energy



b. Greenhouse gas

Fig. 5. Embodied energy and Greenhouse gas of architecture.

Fig. 5 show embodied energy and greenhouse gas of architecture works. In this building, the architecture works are roof, attic ceiling, fencing, floor, stairs - brick (SB), stairs - stone (SS) and other.

There are 42,455,491.82 MJ (84.74%), 5,332,567.56 MJ (10.64%), 326,163.99 MJ (0.65%), 265,928.40 MJ (0.53%), 263,356.14 MJ (0.53%), 183,488.20 MJ (0.37%) and 1,276,837.32 MJ (2.55%) of stairs - brick, fencing, roof, stairs - stone, attic ceiling, floor and others respectively, are illustrated in Fig. 5a There are 2,701,713.12 kgCO₂e (81.85%), 428,171.25 kgCO₂e (12.97%), 26,627.51 kgCO₂e (0.81%), 22,498.99 kgCO₂e (0.68%), 21,274.27 kgCO₂e (0.64%), 19,346.07 kgCO₂e (0.59%) and 81,253.28 kgCO₂e (2.46%) of stairs - brick, fencing, roof, attic ceiling, stairs - stone, floor and others respectively. (Fig. 5b) Fig. 5a and Fig. 5b show that the embodied energy of stairs - brick is the highest because the mass of bricks is greater than the other materials, since the main component of the stairs is bricks for 99%. As a result, the embodied energy and greenhouse gases of bricks are much higher than other materials as presented in the fig.4a and fig. 4b.

TABLE II EMBODIED ENERGY VALIDATION.

	Area (m ²)	Embodied energy (MJ/m ²)
Nassen et al.[6]	192	2,810.00
Bonamente et al. [7]	1,000	14,040.00
Adalberth [8]	347	5,280.00
Thormark [9]	-	4,100.00
Moncaster and Symons [10]	-	15,100.00
This study*	17,000	7,163.28

Table II shows the embodied energy comparison of the building per square meter from various references [6-10]. This investigation shows that the embodied energy of this building is 7,163.28 MJ/m². It is high in-line the energy intensity of the resident buildings with reinforced concrete structure in previous study [6-10]. From the propose method the results of this study is reasonable.

TABLE III GREENHOUSE GAS EMISSION VALIDATION.

	Area (m ²)	Greenhouse gas emission (kgCO ₂ e/m ²)
Nassen et al[6]	192	72.00
Blengni and Carlo[11]	250	770.00
Suzuki and Oka[12]	1857	650.00
Yan et al [13]	43,210	525.00
Zahra et al[14]	3375	233.70
This study*	17000	592.92



Table III shows the greenhouse gas emission intensity comparison of residential building [6, 11-14]. This case found that the greenhouse gas emission of this building is 593.93 kgCO₂e /m². The result is shown in-line of range from 72-770 kgCO₂e /m² and would be acceptable.

V. CONCLUSION

This study conducts to identify the sources of embodied energy and greenhouse gas emission in building materials by LCE method. The case study of this research is a brand new residential building in Silpakorn University, Nakhon Pathom, Thailand. Gate to gate model is applied. This building uses concrete and steel as main materials. The maximum embodied energy and greenhouse gas is from steel for 92,863,690.57 MJ and 7,581,244,379 kgCO₂e, respectively. The embodied energy is 1,972,316.99 kgCO₂e, because steel has more energy to production and environment impact than concrete. This building is built in the conventional method, thus the amount of embodied energy and greenhouse gases come from the material. The data from this research can be used to select building materials as well as building design to reduce the energy consumption and environmental impact. The further study should be preceded on construction, utilization and disposal to complete LCA.

ACKNOWLEDGMENT

The authors would like to thank the Department of Mechanical Engineering Faculty of Engineering and Industrial Technology, Silpakorn University and ISO ENGINEERING CO., LTD. for their valuable support.

REFERENCES

- [1] G. Hammond, C. Jones, E. Lowrie, P. Tse, A BSRIA Guide: Embodied Carbon the Inventory of Carbon, BSRIA, Bracknell (2011).
- [2] G.P. Gerilla, K. Teknomob, K. Hokao, An environmental assessment of wood and steel reinforced concrete housing construction, *Building and Environment* 42 (2007) 2778–2784.
- [3] L. Gustavsson, R. Sathre, Variability in energy and carbon dioxide balances of wood and concrete building materials, *Building and Environment* 41 (2006) 940–951.
- [4] G. Heravi, T. Nafisi, R. Mousavi, Evaluation of energy consumption during production and construction of concrete and steel frames of residential buildings, *Energy and Buildings* 130 (2016) 244–252.
- [5] IPCC (Intergovernmental Panel on Climate Change), Summary for policy-makers, in: *Climate Change 2013: The Physical Science Basis. Contribution of Working Group I to the Fifth Assessment Report of the Intergovernmental Panel on Climate Change*, (2013).
- [6] J. Nässén, F. Hedenus, S. Karlsson, J. Holmberg, Concrete vs. wood in buildings: An energy system approach, *Building and Environment* 51 (2012) 361–369.
- [7] E. Bonamentea, M.C. Mericoa, S. Rinaldia, G. Pignattaa, A.L. Piselloa, F. Cotanaa, A. Nicolini, Environmental impact of industrial prefabricated buildings: Carbon and Energy Footprint analysis based on an LCA approach., *Energy Procedia* 61 (2014) 2841–2844.
- [8] K. Adalberth, Energy use during the Life Cycle of Single-Unit Dwellings: Examples, *Building and Environment*, Vol. 32, No. 4, (1997), 321–329.
- [9] C. Thormark, A low energy building in a life cycle—its embodied energy, energy need for operation and recycling potential, *Building and Environment* 37 (2002) 429 – 435.
- [10] A.M. Moncaster, K.E. Symons, A method and tool for ‘cradle to grave’ embodied carbon and energy impacts of UK buildings in compliance with the new TC350 standards, *Energy and Buildings* 66 (2013) 514–523.
- [11] G.A. Blengini, T.D. Carlo, Energy-saving policies and low-energy residential buildings: an LCA case study to support decision makers in Piedmont (Italy). *Int.J. Life Cycle Assess.* 15(2010), 652–665.
- [12] M. Suzuki, T. Oka, Estimation of life cycle energy consumption and CO₂ emission of office buildings in Japan. *Energy Build.* 28(1998), 33–41.
- [13] H. Yan, Q. Shen, L.C.H. Fan, Y. Wang, L. Zhang, Greenhouse gas emissions in building construction: A case study of One Peking in Hong Kong, *Building and Environment* 45 (2010) 949–955.
- [14] Z.S. Moussavi Nadoushani, A. Akbarnezhad, Effects of structural system on the life cycle carbon footprint of buildings, *Energy and Buildings* 102 (2015) 337–346.



Application of Optimization Techniques for Searching Optimal Reservoir Rule Curves for Medium Reservoir

Teerawat thongwan^{1st}, Anongrit Kangrang

Faculty of Engineering, Mahasarakham University, Kantharawichai District, MahaSarakhm 44150, Thailand
teerawat.th@msu.ac.th, anongrit.k@msu.ac.th

Abstract— Many small and medium reservoirs located in Thailand. Optimal reservoir rule curves are required for operating reservoir system. This study applied the Tabu Search Algorithm (TSA) and Flower pollination algorithm (FPA) connecting with the reservoir simulation model to search the optimal reservoir rule curves. This study considered the Huay Ling Jone and Huay Sabag reservoirs located in Yasothorn Province, Thailand for the case study. Historic inflow data of both reservoirs were used in this study. The 1,000 samples of synthetic inflow of reservoirs were used to simulate the reservoir operation system for evaluating the obtained rule curves as present in term of water situation. The situations of water shortage and excess water were shown in terms of frequency magnitude and duration. The results showed that TSA and FPA connecting with the reservoir simulation model can provide the optima rule curves. The obtained rule curves from TSA and FPA can mitigate drought and flood situations more than the current rule curves.

Keywords—reservoir rule curves; optimization techniques; Tabu Search Algorithm; Flower pollination algorithm; Reservoir Operation

I. INTRODUCTION

Flood and drought situations are increasing in many regions because of high population growth, economic expansion, land use change and climate change, etc. An improvement in water resource management is needed to prevent the mentioned situations. The demand management and supply management sites of water resource management are considered to solve these serious problems. Often a non-construction method is required first to save time and budget, for example, to increase irrigation efficiency, to involve public participation and to improve reservoir operation.

Reservoir rule curves are necessary guidelines for the release and storage of water over long term operation. Generally, the storage and release of water are performed monthly under the conditions of the inflow to the reservoir and downstream demand criteria. A reservoir operating system is a large and complex system [1-2].

Many optimization techniques have been applied to find the optimal rule curves, for example, dynamic programming (DP), simulated annealing algorithm (SA), particle swam optimization (PSO) and cuckoo search (CS), etc. [3-6]. The obtained rule curves are effectively applied with searching conditions, such as historic inflow data, water demand downstream, standard operating, smoothing function rule as well as objective functions of searching procedure. However, there many new effective optimization techniques that have not been applied to find optimal rule curves. Tabu search algorithm (TSA) and flower pollination algorithm (FSA) are effective alternative optimization techniques [7-8].

This study thus proposed the Tabu Search Algorithm (TSA) and the Flower pollination algorithm (FPA) connecting with the reservoir simulation model to search the optimal reservoir rule curves. The Huay Ling Jone and Huay Sabag reservoirs located in Yasothorn Province, Thailand were considered for the case study. The minimum average water shortage per year was used as the objective function of searching process.

II. MATERIALS AND METHODS

A. Study area

The study area is irrigation project in Yasothorn province where located in the northeast region of Thailand. There are two reservoirs were selected for the study; the Haui ling jone reservoir and the Haui Sabag reservoir. These are the branch of a Moon river basin. The study area is shown in Fig. 1. Total area of the Huay Sabag is approximately 52 km², total cumulative annual average runoff of about 22.4 MCM. During 1996 to 2017 (see Fig. 2). The normal storage capacity is 30.03 MCM.

The Huay Ling Jone reservoir has the irrigation area of 19.8768 Km², full storage capacity of reservoir 21.06 MCM., dead storage capacity of 0.4 MCM. The historic inflow data records of the Huay Ling Jone reservoir from 1994 to 2017 were present in Fig.2. The water requirements in downstream site are consume, irrigation, flood control, domestic water supply and environ-mental conservation. The schematic diagram of the reservoirs is presented in Fig. 3.

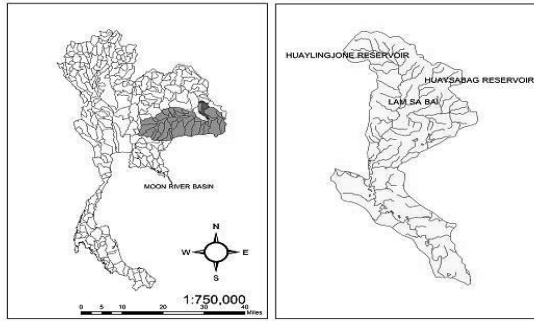


Fig. 1. location of the Huay Ling Jone reservoir and the Huay Sabag reservoir

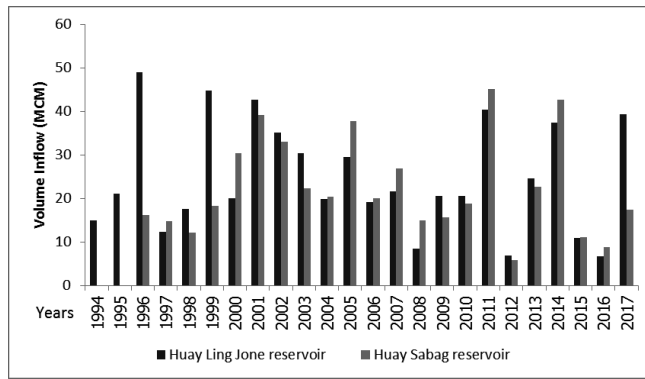


Fig. 2. Historic inflow to the Huay Ling Jone and the Huay Sabag reservoirs

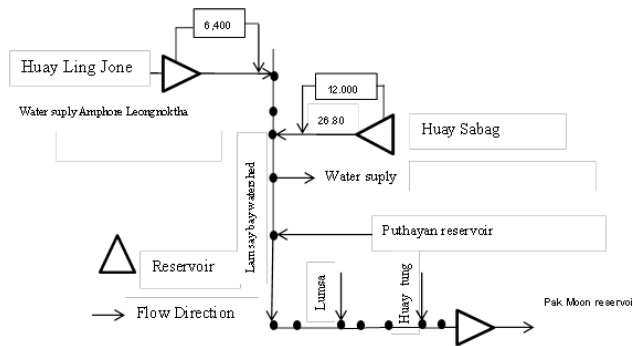


Fig. 3. Schematic diagram of the Huay Ling Jone and the Huay Sabag reservoirs

B. Reservoir operation model

The reservoir operation system consists of the available water that is calculated from the water balance concept.

The monthly release water is estimated by considering the monthly available water with release criteria, operating policies and reservoir rule curves.

For this study, the reservoir simulation model was created following the water balance concept. The reservoir operation model is operated under the standard operating policy as expressed in Fig. 4 and equation (1).

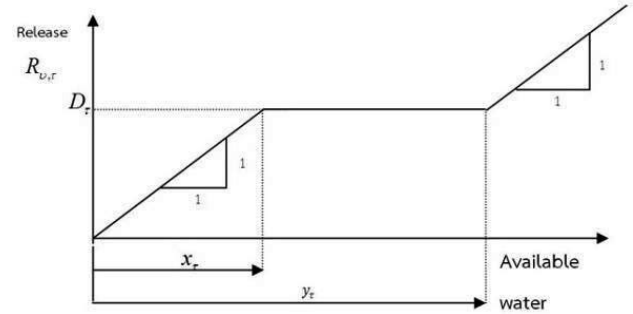


Fig. 4. Standard operating rule

$$R_{v,\tau} = \begin{cases} D_{\tau} + W_{v,\tau} - y_{\tau}, & \text{for } W_{v,\tau} \geq y_{\tau} + D_{\tau} \\ D_{\tau}, & \text{for } x_{\tau} \leq W_{v,\tau} < y_{\tau} + D_{\tau} \\ D_{\tau} + W_{v,\tau} - x_{\tau}, & \text{for } x_{\tau} - D_{\tau} \leq W_{v,\tau} < x_{\tau} \\ 0, & \text{otherwise} \end{cases} \quad (1)$$

where $R_{v,\tau}$ is the release of water during year v and month τ ($\tau = 1$ to 12 representing January to December), D_{τ} is the net water demand during month τ , x_{τ} is the lower rule curve of month τ , y_{τ} is the upper rule curve of month τ and $W_{v,\tau}$ is the available water by calculating the water balance concept during year v and month τ , as described in equation (2):

$$W_{v,\tau} = S_{v,\tau} + Q_{v,\tau} - R_{v,\tau} - E_{\tau} - DS \quad (2)$$

where $S_{v,\tau}$ is the stored water at the end of month τ , $Q_{v,\tau}$ is the monthly inflow to the reservoir, E_{τ} is the average value of the evaporation loss and DS is the minimum reservoir storage capacity (dead storage capacity). The operating policy usually reserves the available water ($W_{v,\tau}$) for mitigating the risk of water shortage in the future, when $0 \leq W_{v,\tau} < x_{\tau} - D_{\tau}$ under long term operation.

Released water from the reservoir simulation model was used to calculate the water shortage and excess water release situations. These situations were used to calculate the objective function of searching process (average annual shortage per year).



C. Applying TSA and FPA for searching optimal rule curves

The TSA connecting with the reservoir simulation model is present as follows: the TSA starts with a set initial population (X_1, X_2, \dots, X_{24}) that is created randomly within the feasible space. The feasible space is the value between the dead storage capacity and the normal high water level of the considered reservoir. There are 24 decision variables (rule curve variables for both upper and lower) for one reservoir. Then, a set of rule curves will be used in the reservoir simulation for computing the procedure. Monthly release water is calculated from the simulation model by considering the set of rule curves. Next, the release water is used to calculate the objective function as mentioned in the previous section. Firstly, the minimum average water shortage per year (Z) is set as the objective function of the searching procedure subject to the constraints on the simulation model as in the following:

$$\text{Min } Z = \left(\frac{1}{n} \sum_{v=1}^n Sh_v \right) \quad (3)$$

$$\begin{aligned} \text{if } R_\tau < D_\tau; \text{ Then } Sh_v &= \sum_{\tau=1}^{12} (D_\tau - R_\tau) \\ \text{Else } Sh_v &= 0 \end{aligned} \quad (4)$$

where n is the total number of considered years, Sh_v is the water shortage during year v (year in which releases do not meet 100% of the target demand). Then, the searching process is continued until the termination criterion is satisfied as described in Fig. 5.

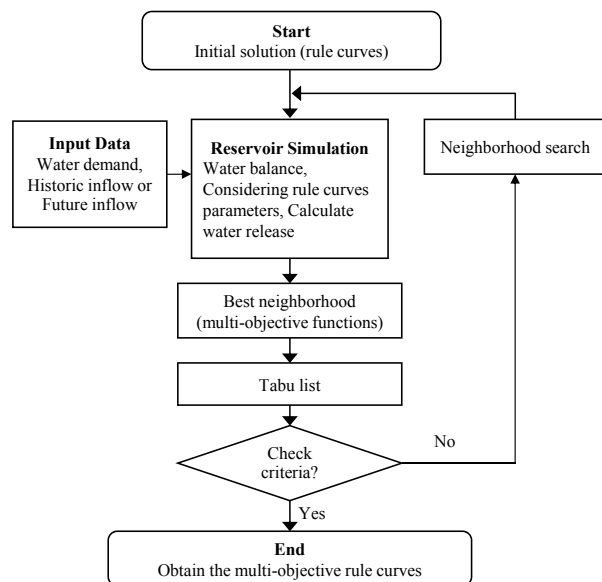


Fig. 5. Tabu search algorithm connecting reservoir simulation for searching rule curves

The connecting of the FPA and reservoir simulation model starts with input data and all initial necessary data such as upper and lower bound data of reservoir and objective function. Each decision variable represents the monthly rule curves of the reservoirs, which are defined as the upper rule curves and the lower rule curves. After the first set of flowers in the initial population were used to calculate the monthly release water in the reservoir simulation model. Next, the released water is used to determine the objective function that was described in the previous section. After that, the reproduction process will create new rule curve values in the next iteration. This procedure is repeated until the termination criterion is satisfied as described in Fig. 6.

This study used TSA and FPA in connection with a reservoir operation model to find optimal rule curves through the MATLAB toolbox.

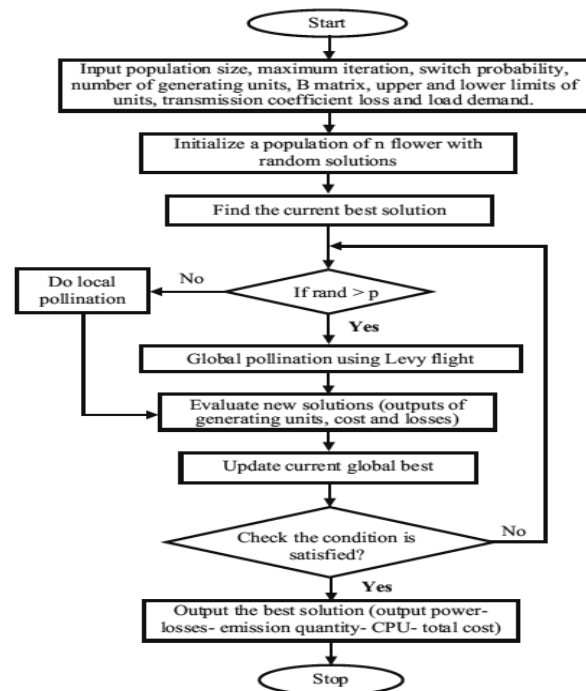


Fig. 6. Flower pollination algorithm connecting reservoir simulation for searching rule curves

III. RESULTS AND DISCUSSION

A. Optimal rule curves

The 24 years (1994-2017) of monthly historic inflow data, monthly data of evaporation, rainfall, irrigation, domestic and industrial water requirements and monthly environmental conservation of the Huay Ling Jone were imported for processing in the TSA and FPA techniques connecting with reservoir simulation model, after run and the optimal rule curves were obtained. For data of the Huay Sabag reservoir were imported to the proposed models and run the same as the Huay Ling Jone reservoir. The optimal rule curves of the Huay



Ling Jone reservoir and the Huay Sabag reservoir were present in Fig.7 and Fig.8 respectively. They indicated that the patterns of all rule curves are similar due to the inflow effect and the same searching conditions. However, the lower rule curves of TSA for the Huay Ling Jone reservoir are higher than the curves of FPA and existing rule curves especially during May to July. Whereas, the obtained lower rule curves of the TSA and FPA for the Huay Sabag reservoir are higher than the existing rule curves. These rule curves were used to evaluate the efficiency with the reservoir simulation in both using historic inflow and using synthetic inflow scenarios. In addition, the increasing 15% of water demand for the Huay Sabag reservoir was additional evaluated both historic inflow and synthetic inflow cases.

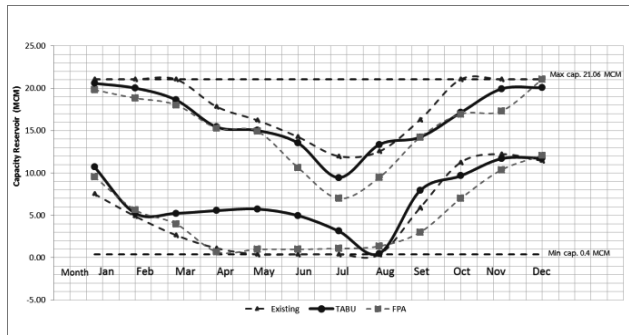


Fig. 7. Optimal rule curves of the Huay Ling Jone reservoir

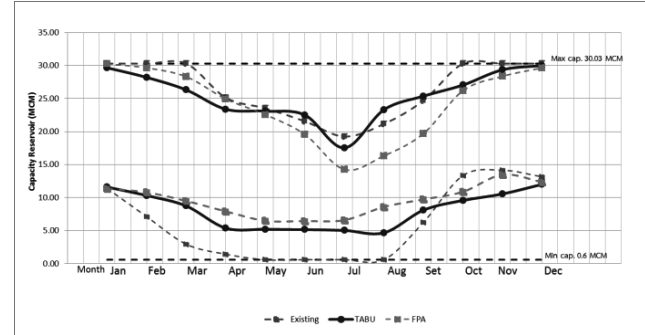


Fig. 8. Optimal rule curves of the Huay Sabag reservoir

B. Efficiency of the obtained rule curves

Tables 1 and 2 show the situations of water shortage and excess release of the Huay Ling Jone reservoir using historic inflow of 24 years and using the synthetic inflow of 1,000 samples respectively. They indicated that the average water shortage and the frequency of water shortage of using TSA rule curves are the lowest (2.750 MCM./year and 2.850 ± 0.999 MCM./year) as compared with the other rule curves both considering historic inflow and synthetic inflow cases. These are corresponded to the objective function of searching use. Moreover, the rule curves of TSA can mitigate excess water better than the other rule curves both two scenarios (7.022 MCM./year and 7.864 ± 1.708 MCM./year).

TABLE I. Situations of water shortage and excess release of the Huay Ling Jone reservoir using historic inflow of 24 years

Situations	Rule curves	Frequency (times/year)	Volume (Million cubic meters)		Time period (year)	
			Average	Maximum	Average	Maximum
Shortage	RC1-Existing	0.792	4.917	12	3.8	8
	RC2-FPA	0.875	4.125	9	7	14
	RC3-TSA	0.708	2.750	11	2.833	6
Excess water	RC1-Existing	0.958	9.191	15.857	11.5	22
	RC2-FPA	0.917	8.512	14.861	7.333	14
	RC3-TSA	0.917	7.022	14.365	7.333	14

TABLE II. Situations of water shortage and excess release of the Huay Ling Jone reservoir using synthetic inflow of 1,000 events

Situations	Rule curves		Frequency (times/year)	Volume		Time period (year)	
				Average	Maximum	Average	Maximum
Shortage	RC1-Existing	μ	0.717	4.599	10.819	5.388	9.433
		σ	0.137	1.041	2.506	3.422	4.074
	RC2-FPA	μ	0.748	3.866	10.588	6.262	10.580
		σ	0.136	1.021	2.208	3.943	4.507
	RC3-TSA	μ	0.585	2.850	10.745	4.401	7.462
		σ	0.147	0.999	2.679	2.362	3.360
Excess water	RC1-Existing	μ	0.958	9.621	15.725	15.902	19.105
		σ	0.046	1.526	0.509	7.160	4.987
	RC2-FPA	μ	0.950	9.059	15.644	14.425	18.143
		σ	0.047	1.555	0.696	7.104	5.118
	RC3-TSA	μ	0.866	7.864	15.577	7.851	12.869
		σ	0.076	1.708	0.865	4.853	4.908

Note: μ = average, σ = standard deviation



Tables 3 and 4 present the situations of water shortage and excess release of the Huay Sabag reservoir using historic inflow of 22 years and using the synthetic inflow of 1,000 samples respectively. They indicated that the average water shortages of all rule curves are zero both considering historic inflow and synthetic inflow cases. These situations

due to the total inflow are too much bigger than the total water demand. The results also present that the situation of excess water of using rule curves form TSA and FPA techniques are lower than their using current rule curves both considering historic inflow and synthetic inflow scenarios.

TABLE III. Situations of water shortage and excess release of the Huay Sabag reservoir using historic inflow of 22 years

Situations	Rule curves	Frequency (times/year)	Volume (Million cubic meters)		Time period (year)	
			Average	Maximum	Average	Maximum
Shortage	RC1-Existing	0	0	0	0	0
	RC2-FPA	0	0	0	0	0
	RC3-TSA	0	0	0	0	0
Excess water	RC1-Existing	1	3.991	3.991	22	22
	RC2-FPA	1	3.159	3.159	22	22
	RC3-TSA	1	3.159	3.159	22	22

TABLE IV. Situations of water shortage and excess release of the Huay Sabag reservoir using synthetic inflow of 1,000 events

Situations	Rule curves		Frequency (times/year)	Volume		Time period (year)	
				Average	Maximum	Average	Maximum
Shortage	RC1-Existing	μ	0	0	0	0	0
		σ	0	0	0	0	0
	RC2-FPA	μ	0	0	0	0	0
		σ	0	0	0	0	0
	RC3-TSA	μ	0	0	0	0	0
		σ	0	0	0	0	0
Excess water	RC1-Existing	μ	1	3.990	3.991	22	22
		σ	0	0	0	0	0
	RC2-FPA	μ	1	3.159	3.159	22	22
		σ	0	0	0	0	0
	RC3-TSA	μ	1	3.159	3.159	22	22
		σ	0	0	0	0	0

Note: μ = average, σ = standard deviation

C. Efficiency of the obtained rule curves of the Huay Sabag reservoir under increasing 15% of water demand

The efficiency of the obtained rule curves from the Hual Sabag reservoir was evaluated again by increasing 15% of water demand in downstream site. The same conditions of reservoir simulation model were used to simulate the reservoir system. These evaluations were performed both historic inflow scenario and synthetic inflow scenario. The results were present in tables V and VI.

The results show that the situations of water shortage of the Huay Sabag using the existing rule curves were less than their using the obtained rule curves of TSA and FPA in all cases. These situations due to the total inflow larger more than the total demand. Whereas, the situation of excess water of using rule curves form TSA and FPA techniques are still lower than their using current rule curves both considering historic inflow and synthetic inflow scenarios. Hence, the TSA and FPA techniques can apply effectively to find the optimal rule curves for the reservoir having excess water.

TABLE V. Situations of water shortage and excess release of the Huay Sabag reservoir using historic inflow of 22 years (increasing 15% of water demand)

Situations	Rule curves	Frequency (times/year)	Volume (Million cubic meters)		Time period (year)	
			Average	Maximum	Average	Maximum
Shortage	RC1-Existing	0.955	1.909	2	21	21
	RC2-FPA	0.955	2.864	3	21	21
	RC3-TSA	1	3	3	22	22
Excess water	RC1-Existing	1	3.338	3.338	22	22
	RC2-FPA	1	2.638	2.638	22	22
	RC3-TSA	1	2.638	2.638	22	22



TABLE VI. Situations of water shortage and excess release of the Huay Sabag reservoir using synthetic inflow of 1,000 events (increasing 15% of water demand)

Situations	Rule curves		Frequency (times/year)	Volume (Million cubic meters)		Time period (year)	
				Average	Maximum	Average	Maximum
Shortage	RC1-Existing	μ	0.950	1.898	2.000	20.858	20.883
		σ	0.017	0.033	0.000	0.713	0.381
	RC2-FPA	μ	0.952	2.856	3.000	20.944	20.944
		σ	0.013	0.038	0.000	0.288	0.288
	RC3-TSA	μ	1.000	2.999	3.000	21.920	21.985
		σ	0.004	0.013	0.000	0.959	0.181
Excess water	RC1-Existing	μ	1.000	3.337	3.338	22.000	22.000
		σ	0.000	0.006	0.000	0.000	0.000
	RC2-FPA	μ	1.000	2.638	2.638	22.000	22.000
		σ	0.000	0.002	0.000	0.000	0.000
	RC3-TSA	μ	1.000	2.638	2.638	22.000	22.000
		σ	0.000	0.000	0.000	0.000	0.000

Note: μ = average, σ = standard deviation

IV. CONCLUSION

This study proposed the optimization techniques connecting with the reservoir simulation model for the searching optimal rule curves of medium reservoir in Thailand. These optimization techniques were Tabu Search Algorithm (TSA) and Flowers Pollination Algorithm (FPA). The results found that the patterns of these rule curves are similar due to seasonal inflow effect and the same searching conditions. However, there are many different points, such as the lower rule curves during dry season (January-April), the upper rule curves during beginning of rainy season (June-August). These situations can control amount of store water and release water for each month effectively. All rule curves were used in reservoir simulation model for evaluate the efficiency in both historic inflow scenario and synthetic inflow scenario.

The results present that the obtained rule curves from TSA and FPA techniques of the Huay Ling Jone reservoir can mitigate situation of water shortage and excess water better than the existing rule curves in both scenarios. These can conclude that the proposed models suitable for searching optimal rule curves of the Huay Ling Jone reservoir where the total inflow and the total demand are closed together.

Whereas, the obtained rule curves of the Huay Sabag from the proposed techniques can mitigate only excess water better than the existing rule curves in historic inflow scenario and synthetic inflow scenario as well as increasing 15% of water demand. The situations of water shortage of the Huay Sabag using the existing rule curves were less than their using the obtained rule curves in all cases. These situations due to the total inflow larger more than the total demand. Hence, the TSA and FPA techniques can apply to

find the optimal rule curves of the reservoir that mitigate flood situation effectively.

ACKNOWLEDGMENT

The authors would like to acknowledge the Royal Irrigation Department for supporting data in this study.

REFERENCES

- [1] G. Eason, B. Noble, and I.N. Sneddon, "On certain integrals of Lipschitz-Hankel type involving products of Bessel functions," Phil. Trans. Roy. Soc. London, vol. A247, pp. 529-551, April 1955. (references)
- [2] Kumara N., Tischbein B., Kushech J., Lauxd P., Bege M and Bogardi J. (2017). Impact of climate change on water resources of upper Kharun catchment in Chhattisgarh, India. Journal of Hydrology: Regional Studies, (13) 189-207
- [3] Gashaw T., Tulu T., Argaw M and Worqlul A. W. (2018). Modeling the hydrological impacts of land use/land cover changes in the Andassa watershed, Blue Nile Basin, Ethiopia, Science of the Total Environment, 619-620.
- [4] A. Kangrang, W. Pakoktom, W. Nualnukul, and C. Chaleeraktragoon, "Adaptive Reservoir Rule Curves by Optimization and Simulation", Proceedings of the Institution of Civil Engineers - Water Management, vol. 170, no. WM5, pp. 219-230, 2017.
- [5] Chaleeraktragoon C. & Kangrang A. (2005). A Dynamic Programming for Searching Rule Curves. The proceeding of International Conference on World Water and EnvironmentalResource Congress, 15-19 May, Anchorage, Alaska, USA.
- [6] Kangrang A., Compliew S. & Hormwichian R. (2011). Optimal Reservoir Rule Curves Using Simulated Annealing. Proceedings of the Institution of Civil Engineers – Water Management, 164(WM1), 27-34.
- [7] M.D.C. Cunha, and L. Ribeiro, (2004). "Tabu search algorithms for water network optimization", European Journal of Operational Research, vol. 157, pp. 746-758.
- [8] Yang, X.S., M. Karamanoglu, and X. S. He. (2013). "Multi-Objective Flower Algorithm for Optimization." Procrdia Computer Science, Vol 18, pp. 861-868.



Mechanical Properties of Pavement Concrete Containing Reclaim Asphalt Aggregate

Somporn Leekongbub¹ Dept. of Civil Engineering,
Faculty of Engineering, Rajamangala University of
Technology Isan KhonKaen Campus, KhonKaen, 40000,
Thailand. E-mail address: skyamerica@windowlive.com

Prinya Chindaprasirtat² Sustainable Infrastructure
Research and Development Center, Department of Civil
Engineering, Faculty of Engineering, KhonKaen University,
KhonKaen 40002, Thailand.
E-mail address: prinya@kku.ac.th

Patcharapol Posi³ Dept. of Civil Engineering, Faculty of
Engineering, Rajamangala University of Technology Isan
KhonKaen Campus, KhonKaen, 40000, Thailand. E-mail
address: Mister_wing@hotmail.com

Abstract— This paper presents a study of properties of pavement concrete containing reclaim asphalt aggregate (RAC). The RAC was sieved and classified as fine aggregate (FA), medium aggregate (MA), and coarse aggregate (CA) with particle sizes ranging between 0.001-12.5 mm. The RAC were used to replace nature aggregate at 10, 20, and 30 %. The compressive strength, modulus of elasticity, flexure strength, volume of water absorption, and porosity of concrete were tested. The results showed that the pavement concretes with 28-day compressive strengths of 27-32 MPa, modulus of elasticity of 37-54 GPa, flexure strength of 4.4-5.3 MPa, and volumes of water absorption and porosity of 1.8-4.5% and 4.2-10.5 % were obtained. The results indicated that the strength of pavement concrete decreased with increasing amount of RAC. However, with the increasing amount of RAC, the water absorption and porosity decreased because asphalt coat reduced the water absorption and enhanced the corrosion resistant of concrete.

Keywords— *Mechanical properties; Pavement concrete; Reclaim asphalt aggregate; Modulus of elasticity*

I. INTRODUCTION

The economic development and urban growth have led to the use of energy and natural resources in industrial, agricultural and transport sectors. It is divided into the energy use in industrial sector (36%) transportation sector (35%), or about 700,000 million baht per year, which contributes to air pollution and environmental problems. The road transport accounted for the highest proportion of 87.5% of total transport. Since road transport has a network and facilities, including there is large quantity and comprehensive.

The highway in Thailand has a distance over 71,470 kilometers per two lanes, of which 92.3% is the macadamized road, or 65,972 kilometers per 2 lanes, the concrete road is 7.5% or more than 5,351 kilometers per 2 lanes, the non-

asphalt road is 0.2 % or over 147 kilometres per 2 lanes. These roads require the maintenance in good conditions for convenience, fast and safe transportation. In the reconstruction of asphalt pavement, there is a method to reclaim asphalt pavement (RAP) and the original pavement to be recycled to use by mixing with cement to restore. Then, make the base and pave the new pavement to replace the original surface. However, the use of large amount of RAP materials in the mixture also increases the amount of cement to achieve standard features. The costs also increase, there is also a number of RAP materials that must be scraped off, and in some cases must scrape off the original pavement that was swollen as a groove or expired. These RAP materials are usually deposited as pavement waste.

Therefore, this study investigated the RAP material for making coarse aggregates in concrete mixtures by sizing the Reclaim Asphalt Aggregate (RAC) and used to replace natural aggregates for the production of pavement concrete containing RAC and adding value to the materials used. Furthermore, it is the development of technology to produce concrete for the sustainable construction industry.

II. RESEARCH METHODOLOGY

A. Materials

Materials used in this research consisted of Type I ordinary Portland cement (OPC), river sand, crush limestone aggregate and reclaim asphalt Aggregate (RAC). The RAC was the waste from the highways transportation of Khon Kaen Highway District, Khon Kaen, Thailand, is shown in Fig 1. The physical properties of materials are shown in Table 1.



B. Details of Mixing

For mixing, OPC and river sand were firstly mixed together until the mixture was homogenous. Next, crushed limestone aggregate and RAC were added and mixed for approximately 3 minutes. Finally, the water was then added and the mixing was done for another 3 minutes.

The fresh concrete was placed in the cylindrical mold size 150x300 mm, beam mold size 150x150x500 mm and cube mold size 100x100x100 mm. The specimens were demolded at 1 day and stored under water.

The studies the effect of the volume of RAC replaced with crushed limestone aggregate to the properties of pavement concrete containing reclaim asphalt aggregate consisted of compressive strength, water absorption, porosity, modulus of elasticity and flexure strength.



Fig. 1. Reclaim Asphalt Aggregate (RAC)

TABLE I. PHYSICAL PROPERTIES OF MATERIALS

Materials	OPC	RAC
Specific gravity	3.16	2.39
Median particle size (μm)	14.6	-
Particle size (mm)	-	4.75-19.1
Fineness modulus	-	-
Unit weight (kg/m ³)	1440	1266
Water absorption (%)	-	0.36

C. Details of Test

Compressive strength

The specimens cylinder size 150x300 mm were tested to determine the compressive strength in accordance with ASTM C39/C39M-16b [1]. The reported compressive strengths and unit weight were the average of three samples.

Water absorption and Porosity

The 100x100x100 mm. cube specimens were tested for water absorption and porosity at the age of 28 days in accordance with ASTM C 642 [2]. The reported porosity was the average of three samples.

Modulus of elasticity

The 150 x 300 mm cylinder specimens were tested for the modulus of elasticity at the age of 28 days in accordance with ASTM C469 [3]. The reported results were the average of three samples.

Flexure strength

The 150x150x500 mm beam were tested for the flexure strength at the age of 28 days in accordance with ASTM C1609/1609M-12 [4]. The reported results were the average of three samples.

III. RESULTS AND DISCUSSIONS

A. Compressive strength and unit weight

The results of compressive strength of pavement concrete containing reclaim asphalt aggregate with various the volume of RAC at 28 days are shown in Fig. 2. The compressive strength decreased with the increasing volume of RAC. For example, the 28-day compressive strengths with the volume of RAC of 0, 10, 20, and 30% by mass were 29.3, 31.9, 29.7, and 26.8 MPa, respectively. The use of RAC with surface area partially covered with asphalt resulted in the reduce bonding of matrix and aggregate and led to a decrease in strength [5, 6].

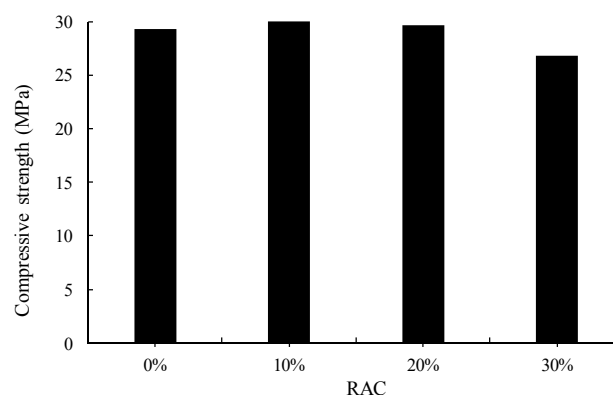


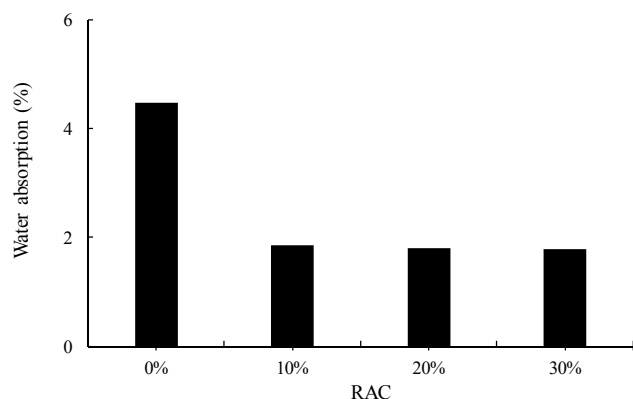
Fig. 2. Compressive strength of pavement concrete

B. Water absorption and Porosity

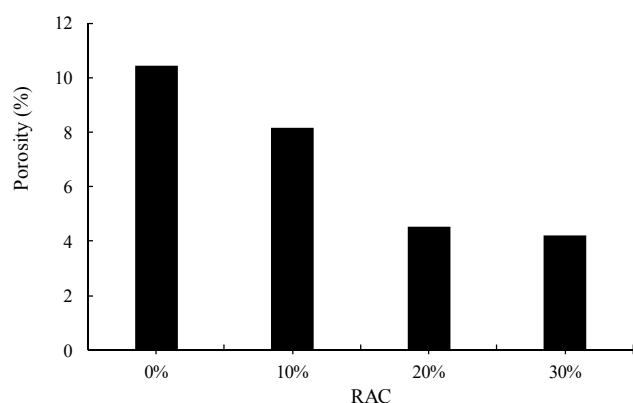
The results of water absorption are shown in Fig. 3a. The water absorption at the age of 28 days decreased with the increasing of the volume of RAC. For example, the water absorption at 28 days with the volume of RAC of 0, 10, 20, and 30 % by mass were 4.48, 1.86, 1.81, and 1.79 %, respectively. The results of porosity of pavement concrete at the age of 28 days are shown in Fig. 3b. The porosity also



decreased with the increasing volume of RAC. The porosity at 28 days with 0, 10, 20, and 30 % by mass were 10.46, 8.17, 4.52, and 4.21 %, respectively. This was due to the RAC was partially coated with asphalt and thus reduced the water absorption.



a. Water absorption



b. Porosity

Fig. 3. Water absorption porosity and of pavement concrete

C. Modulus of elasticity

The results of modulus of elasticity of pavement concrete containing RAC with various the volume of RAC are shown in Fig. 4. The modulus of elasticity of pavement concrete tended to reduce with increasing RAC similar to those of compressive strength [7]. In addition, properties of aggregate, water to binder ratio and compressive strength also affected to the modulus of elasticity of concrete [8]. For example, the modulus of elasticity at 28 days with the volume of RAC of 0, 10, 20, and 30 % by mass were 37.2, 53.10, 48.20, and 44.80 GPa, respectively.

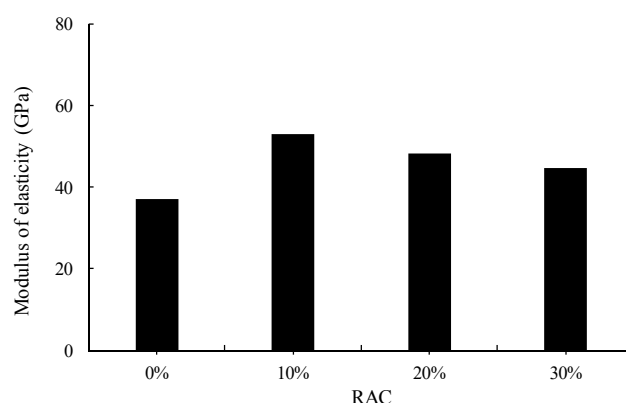


Fig. 4. Modulus of elasticity of lightweight concrete

D. flexure strength

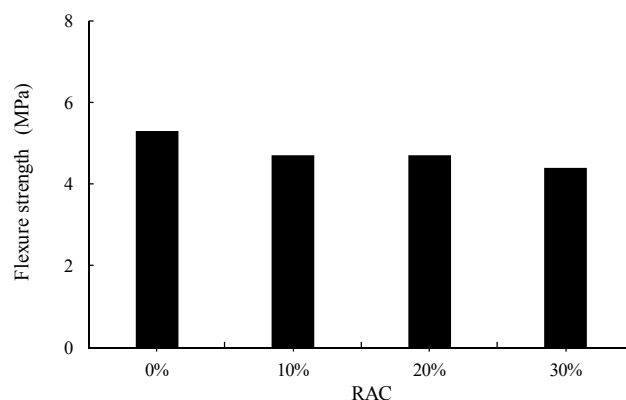


Fig. 5. Flexure strength of lightweight concrete

Fig. 5 shown the flexural strength of pavement concrete containing RAC. The flexural strength of all RAC mixes ranged from 4.40 to 5.30 MPa. The flexural strength of pavement concrete containing RAC lower than the conventional concrete and decreased with increasing RAC. The low bonding with the presence of asphalt at the surface of RAC made the flexural strength of pavement concrete decreased.

IV. CONCLUSION

Based on the obtained data, the following conclusions can be drawn.

1) The increase in the volume of RAC decreased the compressive strength, modulus of elasticity, porosity and water absorption.



2) The increasing amount of RAC resulted in decreased water absorption and porosity because asphalt coating improved the water absorption of concrete.

3) The results showed that the pavement concrete containing RAC with 28-days compressive strengths of 27-32 MPa, modulus of elasticity of 37-54 GPa, flexure strength of 4.4-5.3 MPa, and volumes of water absorption and porosity were 1.7-10.5 %, could be made.

ACKNOWLEDGMENT

The Faculty of Engineering, Rajamangala University of Technology Isan Khon Kaen Campus, and the Thailand Research Fund (TRF) under the TRF Distinguished Research Professor Grant No. DPG6180002 financially supported this work.

REFERENCES

- [1] ASTM C39/C39M-18. Standard test method for compressive strength of cylindrical concrete specimens. Annual Book of ASTM Standard. 2016;Vol 04.02.
- [2] ASTM C642-13. Standard Test Method for Density, Absorption, and Voids in Hardened Concrete. Annual Book of ASTM Standard. 2013;Vol.04.02.
- [3] ASTM C 496. Standard Test Method for Splitting Tensile Strength of Cylindrical Concrete Speciment. Annual Book of ASTM Standard. 2011;Vol.04.01.
- [4] ASTM C1609/C1609 M-12. Standard test method for flexural performance of fiberreinforced concrete (using beam with third-point loading), . Annual Book of ASTM Standard. 2012; Vol.04.01.
- [5] Tajdini M, Mahinroosta R, Taherkhani H. An investigation on the mechanical properties of granular materials in interface with asphaltic concrete. *Construction and Building Materials*. 2014;62:85-95.
- [6] Hassan KE, Brooks JJ, Erdman M. The use of reclaimed asphalt pavement (RAP) aggregates in concrete. In: Woolley GR, Goumans JJM, Wainwright PJ, editors. *Waste Management Series*: Elsevier; 2000. p. 121-8.
- [7] Dilli ME, Atahan HN, Şengül C. A comparison of strength and elastic properties between conventional and lightweight structural concretes designed with expanded clay aggregates. *Construction and Building Materials*. 2015;101, Part 1:260-7.
- [8] Chi JM, Huang R, Yang CC, Chang JJ. Effect of aggregate properties on the strength and stiffness of lightweight concrete. *Cement and Concrete Composites*. 2003;25(2):197-205.



Consolidation Behavior of Cement and High Calcium Fly ash Stabilized Loess soil

Apichit Kampala^{1st}, Luan Suerpadgorn and Anukun Arngbunta

Department of Civil Engineering, Faculty of Engineering,
Rajamangala University of Technology Isan, Khon Kaen Campus, Thailand
E-mail; apichit.ku@outlook.com, MCE_LS@hotmail.com and minanukul@gmail.com

Abstract— Several areas in Northeastern Thailand used Loess as landfill. Loess soil will have a bearing capacity of over than 1000 kPa in the drought and compacted conditions. The coefficient of permeability is about 1×10^{-5} to 1×10^{-7} centimeters per second, and a shrinkage of about 1%; however in wet state or changing of moisture content increased only 5%-8%, the loess soil will have a bearing capacity of under than 50 kPa and the shrinkage rate increased by 8% -10%. Based on the above characteristics, the loess soil is not suitable for civil engineering. This research studied the consolidation behavior of loess modified with cement and fly ash to be used in the landfill and other civil engineering works. The study varies the weight of cement 1, 3 and 5% of dry soil weight and replacing cement with fly ash at the ratio of 0, 10, 20 and 30% of cement weight under standard compaction. Base on test results found that the cement and fly ash stabilized loess soil can be classified the normally consolidated soil and not the pre-consolidation 0) with void ratio (e), and compression index (cc) swelling index (cs) and coefficient of compressibility (mv) decreased with increase of the amount of cement content and curing time. However, the replacement of cement by fly ash did not change the behavior consolidation of soil samples.

Keywords— *Loess soil, Compressibility, Permeability, Soil cement, Landfill*

I. INTRODUCTION

Loess soil is widely distribution. The loess soil is about 10 percent of the earth [1] was found in many countries such as China, Russia, USA, France, Germany, New Zealand, Argentina and Thailand [2-5]. In Thailand, loess soil was found abundantly in the Northeast. Loess soil causes soil engineering problems due to the erosion and change after being disturbed by wind, load, and moisture content [6-7].

Loess soil is normally fine-grained or silty sand (SM) with the low clay content that cannot hold together. Although, Soil grain is held together tightly in the natural condition, the water can penetrate quickly. In dry conditions and compacted soil, loess soil load in the weight more than 1000 kPa, with the coefficient of volume change of about 1×10^{-5} to 1×10^{-7} cm/second, with a shrinkage of about 1% in wet conditions or with a change in soil moisture only 5% -8%. These Loess soil load the capacity less than 8% - 10% kPa and increase a shrinkage value up to 50 in dry conditions [8]. Due to the loess

soil problem collapse easily, there is the problem in civil engineering.

However, in the constructions such as embankment-subgrade, railroad structure (view in Fig.2), pavement, landfill or even the foundations of the building cannot avoid this type of soil. The most popular technique soil improvement is the mixture of soil with cement, lime and fly ash [9-10].

This research studies about the collapse of natural loess soil, loess soil with cement and loess soil with fly ash as a substitution for cement. The results of this study reveal the collapse of engineering parameters including compression index, swelling index, and coefficient of compressibility (mv). The advantages of this research provide the understanding collapse of loess soil, design of applying engineering parameters, estimation of collapsed foundation, land reclamation, or road works, etc., appropriately and accurately in accordance with engineering principles.

II. MATERIALS AND METHODS

A. Materials

The loess soil sample was collected from borrow pit in KhonKaen. It had the proportion of sand to clayey silt as 70.78% to 29.22%. This loess soil sample was classified as Silty Sand (SM). The specific gravity of this sample was equal to 2.63, i.e. it was non-plasticity. The photograph of loess soil and distribution diagram of loess soil particles are shown in Figure 1 and Figure 2 respectively. The chemical composition of the loess soil is shown in Table 1.

The cement used in this study was Portland Cement Type 1 with the specific gravity of 3.15. The fly ash used in this study was Class C with high CaO content of about 33%, and content of SiO_2 , Al_2O_3 and Fe_2O_3 in total was approximately 55% (more than 50%), so it could be used as pozzolanic materials. Such fly ash had the specific gravity of 2.02. The photograph of cement and fly ash are shown in Figure 3. The particle size of the cement and fly ash are shown in Figure 4. The chemical compositions of cement and fly ash are shown in Table 1.

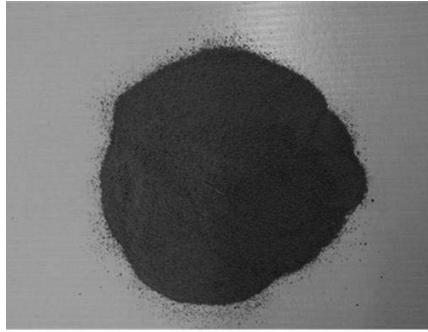


Fig. 1 Loess soil

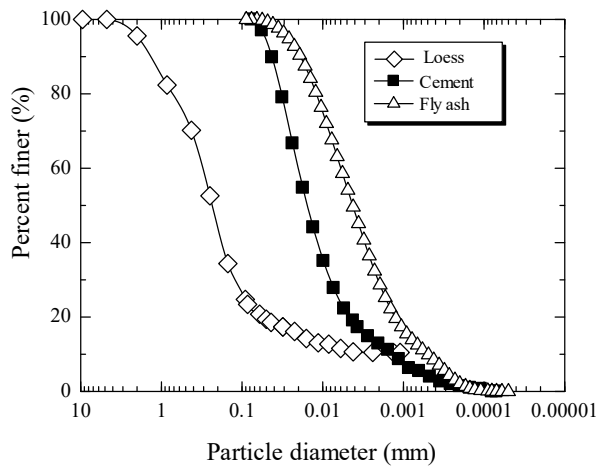
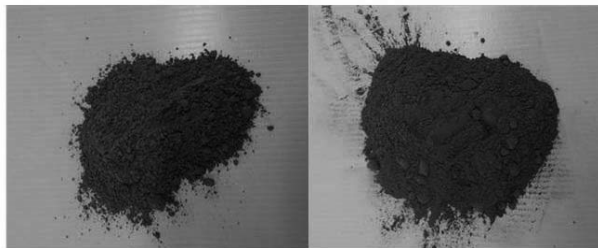


Fig. 2 Distribution of particle size of loess soil, cement and fly ash



(a) Cement

(b) Fly ash

Fig. 3 Cement and fly ash

Table I. Chemical composition of loess soil, cement and fly ash

Chemical Composition	Cement (%)	Fly Ash (%)	Loess (%)
SiO ₂	20.90	26.10	80.42
Al ₂ O ₃	4.76	18.26	13.04
CaO	65.41	33.0	0.21
MgO	1.25	5.54	0.35
Fe ₂ O ₃	3.35	10.84	3.66

B. Basic properties test

The followings are the list of experiments which address 1) physical properties 2) mechanical properties and 3) micro structural observations of cement-saline soil mixtures in this study.

Physical properties;

- Specific gravity tests in accordance with ASTM D 854.
- Soil particle size distribution by wet sieving tests; tests in accordance with ASTM D 422.
- Soil particle size distribution by hydrometer tests in accordance with ASTM D 422-63.
- Liquid limit tests and Plastic limit tests in accordance with ASTM D 4318.
- Standard proctor tests in accordance with ASTM D 698.

C. Engineering Properties Test

Consolidation test was carried out in accordance in ASTM D 2435 with sample compacted by standard compaction of optimum water content (OWC). The diameter of sample is 2 cm, 6.3 cm high. It was cured for 7, 14 and 28 days and pressed consolidation with pressing weight of 10, 20, 40, 80, 160, 320, 640 and 1280 kPa, then rebounded weight to 100 kPa. During the experiment, the sample soil subsidence was read and recorded at each load at 0.25, 0.30, 1, 2, 4, 8, 15, 30, 60, 120, 240, 480, 960, and 1440 minutes.

III. TEST RESULTS AND DISCUSSIONS

Figure 4 shows compaction of loess soil with cement at 0, 1, 3 and 5 percent of dry soil weight. The variable dry weight of the sample with the cement content has similar. The optimum water content is about 8.30, 8.75, 8.50 and 8.50 percent respectively. The highest dry content is 19.76, 19.85, 19.94 and 19.99 kN/m³ respectively. The water saturation level of maximum dry weight is approximately 70 percent.

Figure 5 (a) and (b) shows the consolidation curve of loess soil with cement at 0, 1, 3 and 5 percent which was tested at 7 days and 28 days respectively. The figure shows that for all curing time, the void ratio of loess soil (without cement) is the highest and decreases with the increase in cement content. All samples, the consolidation curve is linear, similar to maximum past pressure or pre-consolidation in short term condition at curing time of 7 days (vive figure. 5 (a)) with 1, 3 and 5



percent cement soil tended to be the same curve, while in the long-term condition at curing time of 28 days (viwe figure. 5 (a)), the consolidation curve of loess soil with cement decreases with the increase in cement content. Figure 6 (a) and (b) show the consolidation curve of loess soil with 3% cement which replaced by fly ash in doses of 10, 20 and 30 percent weight of cement at the all curing time of 7 days and 28 days, respectively the results showed that the void ratio of loess soil with cement was the highest, while the void ratio of the loess soil with cement which was substituted with fly ash of 30% weight of cement was also the highest, followed by 20% and 10% respectively. In all samples, the consolidation curve is linear and similar to the maximum past pressure or pre-consolidation.

Figure 7 shows the relationship between the compression index and fly ash content. The figure shows that the compress index (cc) of loess soil with cement (without fly ash) has the highest value at 0.025 and the compression index of loess soil with cement substituted with fly ash decrease as fly ash content increases at the amount of 0%, 10%, 20% and 30% respectively. The compression index between 0.016 and 0.025, which is less than 0.05 could be concluded that it is the soil of low compression [11].

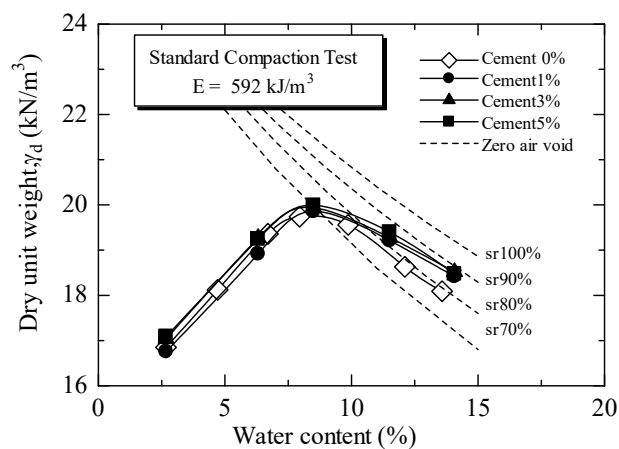


Fig. 4 compaction of loess soil with cement with various quantities.

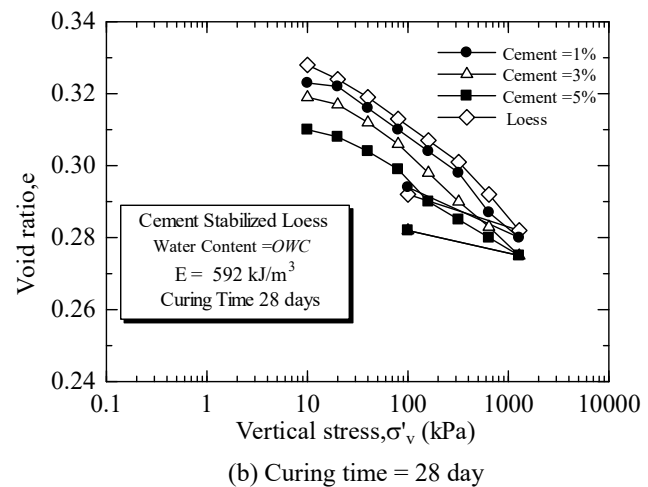
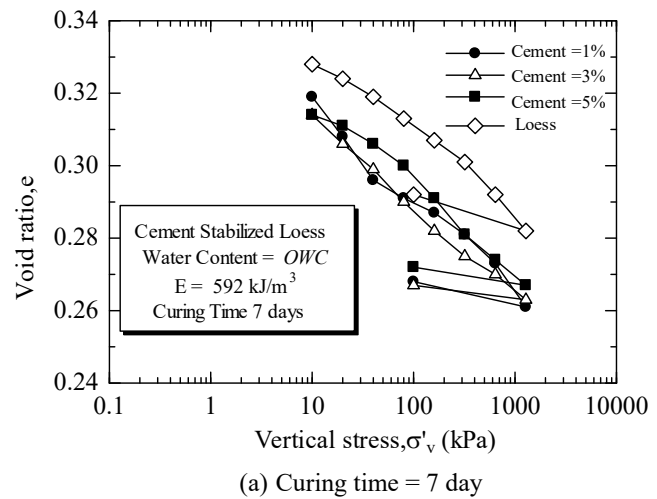


Fig. 5 the consolidation curve of loess soil with cement at 0, 1, 3 and 5 percent

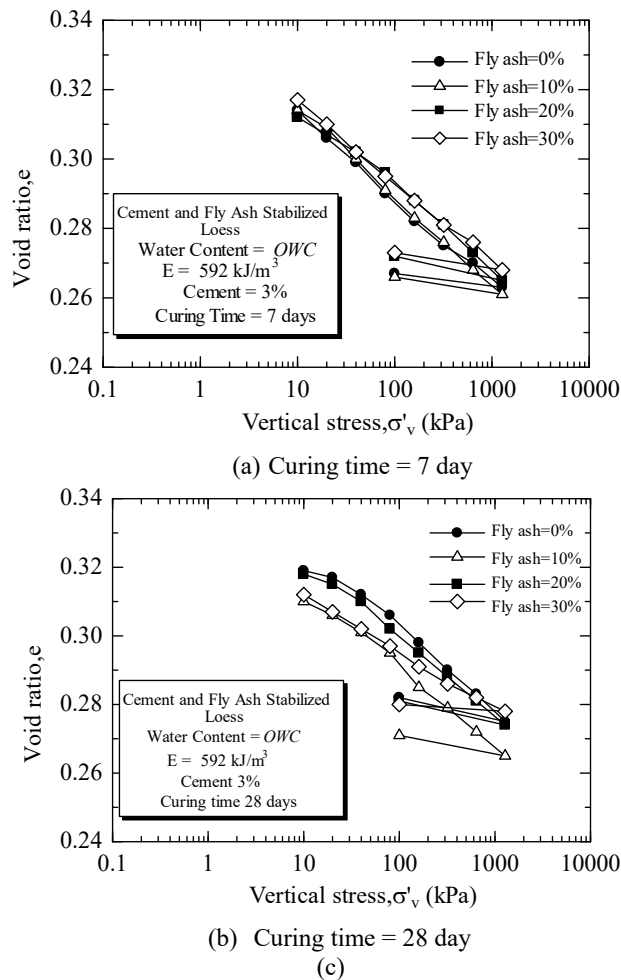


Fig. 6 the Consolidation Curve of loess soil with cement and fly ash in different quantities

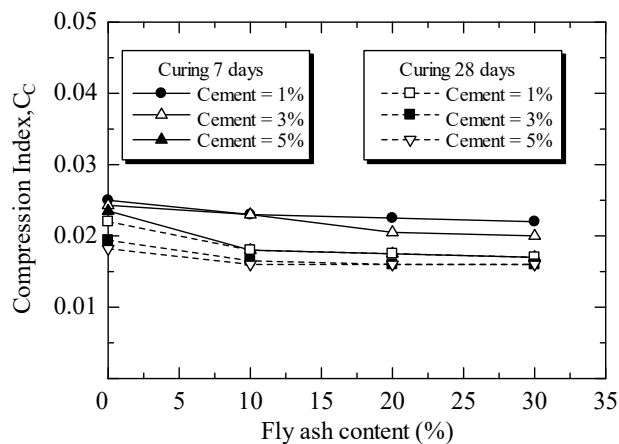


Fig. 7 the relationship between compression index and fly ash content.

Figure 8 shows the relationship between swelling index and fly ash content. It was found that the swelling index of loess soil with cement and fly ash is constant, i.e. It does not depend on fly ash content. The value of swelling index is between 0.005 and 0.007.

Figure 9 shows the relationship between the coefficient of compressibility (m_v) and vertical stress of loess soil with 3% cement which is substituted with fly ash of 10%, 20% and 30% weight of cement and curing time of 7 days. It was found that the coefficient compressibility of cemented soil (without fly ash) was the lowest at 0.5 m^2/MN (10-50 kN/m^2), and decreased with increase of fly ash content (approximately 0.3-0.4 m^2/MN).

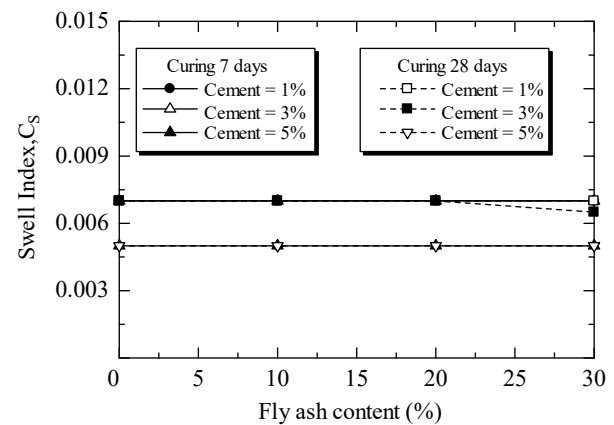


Fig. 8 the relationship between Swelling index and Fly ash content.

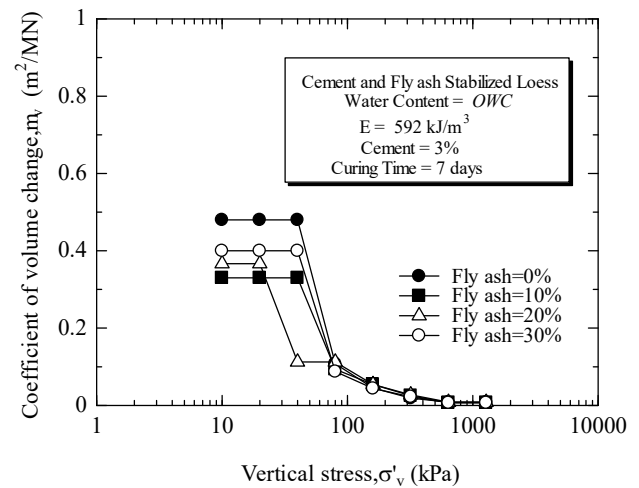


Fig. 9 the relationship between the coefficient of volume change and vertical stress.



IV. CONCLUSIONS

This research studies about the consolidation of the loess soil and cement, where cement is replaced with fly ash. The results can be summarized as the follows:

1. The void ratio of loess soil with cement decreased when the cement content increased. At the same cement content, void ratio of loess soil with cement and cement substitution of fly ash decreased as the fly ash content increased.
2. The consolidation curve of loess soil with cement and cement substitution of fly ash of all cement and fly ash content shows the behavior of normal pressed soil or remolded soil, and past pressure is not found.
3. The compression index (cc) and swelling index loess soil with cement and cement substitution of fly ash decreased as the fly ash content increased, have value of approximately 0.016 - 0.025 and 0.005-0.007 respectively.
4. The coefficient of compressibility (mv) of loess soil with cement and cement substitution of fly ash decreased as the fly ash content increased, have value of approximately 0.3-0.4 m²/MN.

ACKNOWLEDGMENT

This work was supported by Rajamangala University of Technology Isan, Khon Kaen Campus.

REFERENCES

- [1] Jefferson, I., Tye, C. and Northmore, K.J., " Behavior of silt: the engineering characteristics of loess in the UK , " Proc. of the symposium of Problematic Soils, Nottingham, England 2001
- [2] Al-Rawas AA, " State-of-the-art review of collapsible soils, " Science and Technology Review, Special Review, Pages 115-135, 2000
- [3] Gaaver KE, "Geotechnical properties of Egyptian collapsible soils," Alexandria Engineering Journal, Volume 51, Issue 3, Pages 205-210, September 2012
- [4] Nouaouria MS, Guenfoud M, Lafifi B, " Engineering properties of loess in Algeria, " Engineering Geology, Volume 99, Issues 1–2, Pages 85-90, June 2008
- [5] Ryashchenko TG, Akulova VV, Erbaeva MA, " Loessial soils of Priangaria, Transbaikalia, Mongolia, and northwestern China," Quaternary International, Volume 179, Issue 1, Pages 90-95, March 2008
- [6] Zhang F, Wang G, Kamai T, et al, "Undrained shear behavior of loess saturated with different concentrations of sodium chloride solution. " Engineering Geology, Volume 155, Pages 69-79, March 2013
- [7] Li P, Qian H, Wu J , "Environment: Accelerate research on land creation. " Nature, 5:510(7503):29-31, Jun 2014
- [8] Phien-wej, N. Pientong, T. & Balasubramaniam, A.S, "Collapse and strength characteristics of loess in Thailand." Engineering Geology ,Volume 32, Issues 1–2, Pages 59-72, February 1992
- [9] Huawen Xiao, Wei Wang, Siang Huat Goh, "Effectiveness study for fly ash cement improved marine clay." Construction and Building Materials, Volume 157, Pages 1053-1064, December 2017
- [10] Zhang CL, Jiang GL, Su LJ, et al. (2017) "Effect of cement on the stabilization of loess. " Journal of Mountain Science, Volume 14, Issue 11, pp 2325–2336, November 2017
- [11] Nagaraj, T. S., and Srinivasa Murthy, B. R, " A Critical reappraisal of compression index." Geotechnique, 36(1), 27-32, January 1986



Wildfire Detect and Monitoring System using Wireless Sensor Network and Mobile Application

Nimit Srikamta

Faculty of Industrial Technology and Management,
King Mongkut's University of Technology North Bangkok Prachinburi Campus,
Prachinburi, 25230 Thailand
e-mail: nimit.s@fitm.kmutnb.ac.th

Abstract—Wildfire or forest fire problem is frequency encounter in Thailand. Effective firefighting, the firefighter must go to fire point as quickly as possible to stop the fire at the beginning. However, it is difficult to know the fire point and travel route. This paper introduces the system to alert the firefighter to locate the source of fire more quickly and more accuracy via mobile phone. The method to collect a fire data from the forest in this paper is using wireless sensor network because we can spread sensors to cover all area as needed. The data from wireless sensor network will send to the server to process the data if the forest fire is occurring the server will send a fire point and travel route to the firefighter immediately. The system works well using a test condition in KMUTNB Prachinburi campus and has been demonstrated to the officer from Prachinburi forest fire control division and get a good satisfaction.

Keywords—Wildfire Detection, Wireless Sensor Network

I. INTRODUCTION

Forest fire or Wildfire and is a common problem in Thailand. Each year, the country loses a lot of forest land by fire. According to the statistics of the forest fire control division [1], Thailand loses the forest more than one thousand rai each year. In addition, fire does not only destroy the biotic community in the forest. It is also the main cause of dust problem in a big city such as Chiangmai and Bangkok as well. Firefighter have to work hard to protect the forest from fire. But the big problem is that firefighter cannot find the fire as quickly while the fire was just started that make it easier to control the fire. The main purpose of this research is to resolve this problem.

Currently, there are many ways to detect a forest fire but the most 3 methods are a. Using satellite imagery, this method is very popular because no need to use any hardware just only uses an image from satellite but this method is not sensitive to a forest fire in the small area. There are many mobile applications related to wildfire alerts using satellite imagery [2]. b. Using a camera, this method is good but it cannot work in some bad weather condition [3]. c. Using Wireless Sensor Network, we use this method in this research. This method is good for detect fire in a small area, the use of wireless sensor is

works more effectiveness because we can spread many sensors to cover all area as we need [4].

This research has developed a system to alert the firefighter to locate the source of fire more quickly and more accuracy via mobile phone. Because most firefighter in Thailand are already has a smartphone or can get it very easy.

II. MATERIALS AND METHODS

A. Overview of the system

The system in this research consists of three-part, a wireless sensor network, a server, and a mobile application. Wireless sensor function is to get the temperature, humidity, smoke volume or other needed parameters from forest environment and send them to the server on the internet. The server function is to collect all data from wireless sensor network used them with other previous data from the database and calculate the result to send a necessary information to the firefighter mobile phone via its application.

B. Wireless sensor network

The hardware for this research consists of two main parts. 1. A sensor node which function is to collect parameter values from the forest that is temperature, humidity, and smoke volume and send them to the coordinator node. 2. A coordinator node is used to collect data from the sensor node and it also works as a bridge to send a collected data to the server via the internet. The protocol of this wireless sensor network is IEEE 802.15.4 or ZigBee. We have set this network as mesh networking that means all node can communicate to each other automatically to sending information to the coordinator.

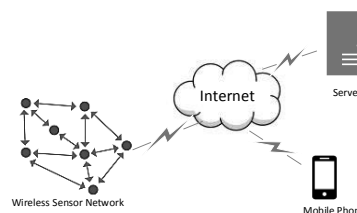


Fig. 1. Structure of a system

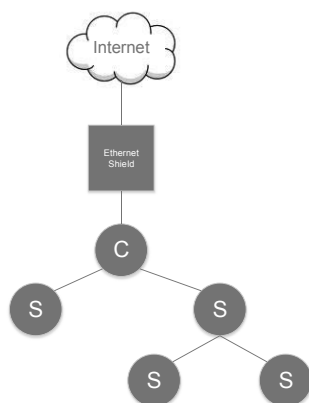


Fig. 2. Wireless sensor network where C is a Coordinator Node and S is a sensor node.

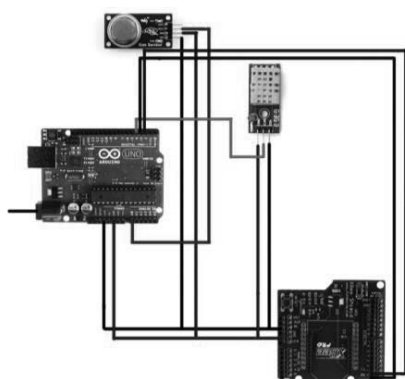


Fig. 3. Sensor node's component

C. A sensor node

Hardware part in this node consists of.

1. Arduino Uno is a controller to get data from sensor and to control XBee module.
2. MQ135 is a sensor to detect the air quality parameter such as HN3, NOx, Benzene, and Smoke.
3. DHT11 is a sensor to detect the temperature and humidity.
4. XBee pro with Arduino shield is used as a transceiver to send and receive data to each other module
5. Power supply module

A sensor node's component picture is shown in fig 3.

D. A coordinator node

Hardware in this node consist of.

1. Arduino Uno is a controller to control XBee and ethernet module.

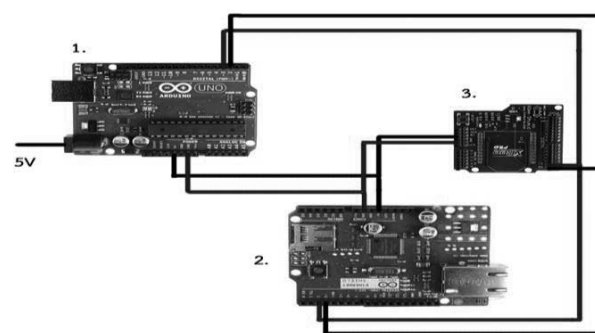


Fig. 4. A coordinator node's component

2. Ethernet Shield is used for connecting the Arduino to the internet.

3. XBee pro with arduino shield is used as a transceiver to send and receive to each other module.

E. Fire Detection Method

The fire detection device in this research we choose a temperature sensor integrated with a smoke sensor to detect both heat and smoke. To detect fire by heat detector we choose both Rate-of-Rise (ROR) method and fixed-temperature method. The advantage of ROR is, it can detect heat faster with less thermal response time index (RTI) than other methods [5]. To detect smoke we choose MQ315 as a smoke detector. In the experiment, we found that the best value setting is 180 ppm for a fire from dried hay and dried leaves in the open space. Steps to detect a fire is according to BRITISH STANDARD BS 54-5:2017 [6] which shown in Fig.5 and Fig.6.

Fig.5 shows the interrupt service routine of a sensor node which will occurs every 10 seconds. The first step is to acquire temperature and smoke volume to the variable TempN and SmkN respectively. After that, we check the condition of fire by five steps. The first checking step is to check the temperature if TempN is 54 or greater will consider that fire. The value 54 is from the BS 54-5 for the fixed-temperature method. The second checking step is to check the smoke volume if SmkN is 180 ppm or greater will consider that fire. The last three checking step is to check the fire by using a ROR method which using a guideline from BS 54-5. The condition that determines fire are, a. If the current temperature is rising up more than 1.5 °C within 40 seconds. b. If the current temperature is rising up more than 3 °C within 3 minutes. c. If the current temperature is rising up more than 5 °C within 5 minutes. If one of the conditions of fire occurs the program will change the static variable Status form normal (Nm) to Ht, Sm, R1, R3 or R5. If there is no sign of fire, variable TempN will save to the first blank position of TEMP array but if the array is full the program will save to the last position and kick out the oldest data (index=0) and rearrange data in the array.

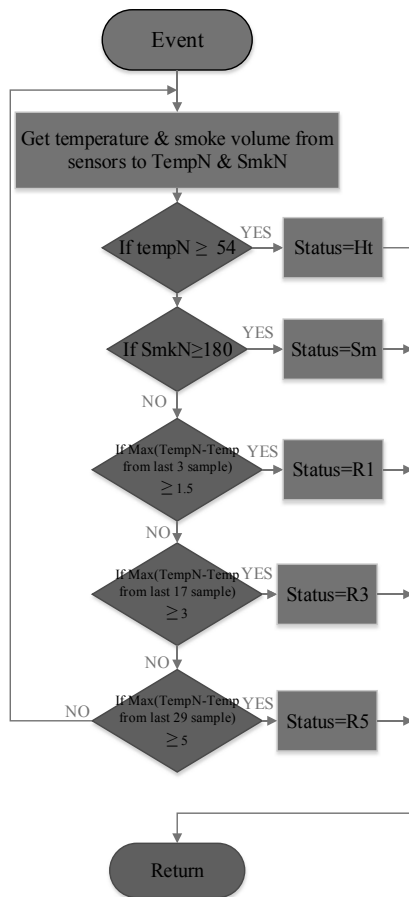


Fig. 5. Part of the program to detect fire.

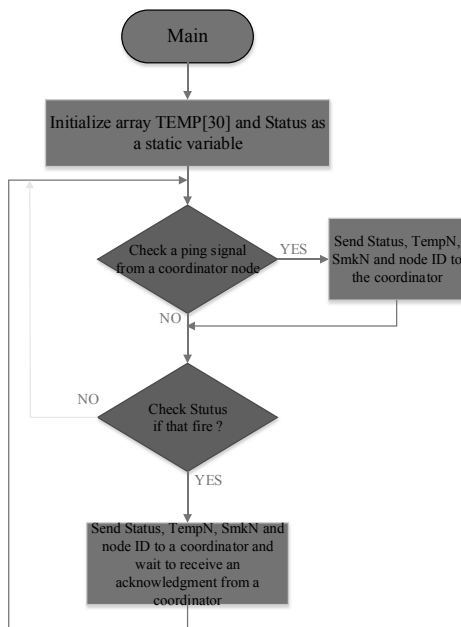


Fig. 6. Main program of the sensor node.

Fig. 6. Shows the main program of a sensor node. The program started with initialize array TEMP[30] and Status as a static variable. After that, the program will check an incoming ping signal from the coordinator node which used to check the existence of a sensor node. The sensor node will send a Status, TempN, SmkN, and node ID back to the coordinator. And then, check the Status, if that fire. The program will send Status, TempN, SmkN, and node ID to the coordinator and wait to receive an acknowledgment.

The function of the coordinator node is to check the existence of a sensor node. It sends a ping signal to all of the sensor nodes every 10 minutes. If some node miss, it will send a report to the server. And the main duty of the coordinator is waiting to receive a fire signal from sensor nodes and send that signal to the server.

F. Software Work

The server used for this research is a PC with AppServ which integrated Apache, PHP, MYSQL altogether.

In normal operation, the coordinator node send a ping signal to every node in the network every 10 minutes and the sensor node will send back the status, temperature, smoke volume, and node ID. And then the coordinator will send that data to keep in the server. If a user wants to see the status of all sensor they can use a mobile application to get them from the server.

In case of fire, the sensor node sends a status and all detecting data to the server immediately via the coordinator node. After that, the server will send the notification to the registration officer via the mobile app.

III. RESULT

Mobile application for this research was developed using Android Studio. User type in this system is divided into two groups, General user, and Officer. General users cannot drop or change data. They can view data only. But the Officer can manage all data in the system.

After opening this app. We will see the user type selection screen as shown in fig. 7.

if we log in to the system in the name of Officer. We will find the screen which able to manage all system data, can add remove or change data of sensor node

if we log in to the system in the name of General user. We will find the screen as shown in fig.8.

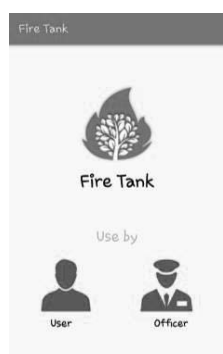


Fig. 7. user type selection screen

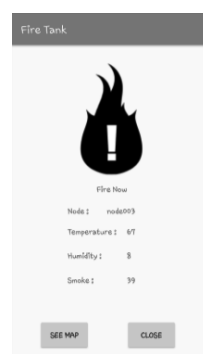


Fig. 9. Notification Screen

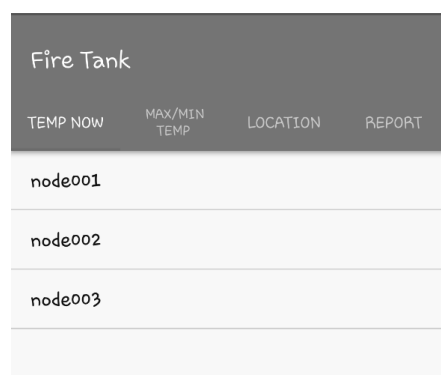


Fig. 8. User screen menu

In the case of fire occurs, the server will send a notification to a mobile phone and then the mobile phone will alert with sound and show the name of the fired node with its status as shown in fig 9. If we tab "SEE MAP" it will display the route map from the current location to the point of fire as shown in fig 10.

This research has been tested many times to adjust the parameter of sensors by burning dried hay and dried leaves in the open space of KMUTNB Prachinburi campus. It works well under a test condition but the range of the wireless sensors network is about 100 meters so it is not good enough in a real situation. And the battery life does not test.

IV. CONCLUSIONS

This paper presented the development the system to alert the fireman to the location of the fire accurately and quickly. Based on the trial from the officer from Prachinburi forest fire control division. The system work quite good. The mobile application is simple but can be used. The number and range of detection are quite small but can improve. Satisfaction is good. The feedback is a guideline to develop in the future.



Fig. 10. Fire point and travel route screen

ACKNOWLEDGMENT

This research was supported by Faculty of Industrial Technology and Management, King Mongkut's University of Technology North Bangkok Prachinburi Campus.

REFERENCES

- [1] Junpen and S. Garivait, "Estimating emissions from forest fires in Thailand using MODIS active fire product and country specific data", *Asia-Pacific Journal of Atmospheric Sciences*, vol.49, pp 389-400, May 2013.
- [2] P. Coppo, "Simulation of fire detection by infrared imagers from geostationary satellites", *Remote Sensing of Environment*, vol.162, pp 84-98, June 2015.
- [3] A. Szajewska, "Development of the Thermal Imaging Camera (TIC) Technology", *Procedia Engineering*, vol.172, pp 1067-1072, 2017.
- [4] A. Bayo, D. Antolin, N. Medrano, B. Calvo and S. Celma, "Early Detection and Monitoring of Forest Fire with a Wireless Sensor Network System", *Procedia Engineering*, pp 248-251, September 2017.
- [5] S. Nam, "Predicting response times of fixed-temperature, rate-of-rise, and rate-compensated heat detectors by utilizing thermal response time index", *Fire Safety Journal*, vol.41, pp 616-627, September 2006.
- [6] The British Standards Institution, "BS EN 54-5:2017 Fire detection and fire alarm systems Part 5: Heat detectors - Point heat detectors", BSI Standards Limited, 2017.



Adaptive Discrete Kirchhoff Quadrilateral Element for Thermal Bending Analysis of Thin Plate

Chatthanon Bhothikhun* and Poramet Arromdee

Department of Mechanical Engineering
Faculty of Engineering and Industrial Technology, Silpakorn University
Nakhon Pathom, Thailand

*Corresponding author's e-mail: chatthanon@outlook.com

Abstract— An adaptive meshing technique is combined with the Discrete Kirchhoff Quadrilateral (DKQ) element to analyze plate bending due to temperature gradient through the thickness of plates. The DKQ plate bending finite element formulation with detailed finite element matrices for thermal plate bending analysis were presented herein. The adaptive meshing technique was also applied to improve the efficiency of the DKQ element. The technique is to generate small elements in the regions of high stress gradient while larger elements are generated in the other regions to reduce the problem unknowns and thus the computational time. The performance of the DKQ element and the combined method were evaluated by some thermal bending of thin plate problems of which the exact or analytical solutions are known. Results demonstrates that solutions obtained from DKQ element perform very well for analyzing thermal bending of thin plate problems, and the combined method can improve the solution accuracy and reduce the computational effort.

Keywords— finite element; adaptive mesh; plate bending; DKQ element

I. INTRODUCTION

The finite element method has been widely used to analyze plate bending problems. To improve the efficiency and solution accuracy, several types of plate bending elements have been developed during the past decades [1-4]. One of the element types which provide high solution accuracy is the Discrete Kirchhoff Quadrilateral element (DKQ) [5]. The four-node quadrilateral DKQ element is based on the discrete Kirchhoff theory with 12 degrees of freedom. Each node of the element has the unknowns of the transverse deflections and the rotations. The capability of the four-node DKQ element will be improved in this paper by including the effect of the temperature gradient through the thickness of plate, so that the element can be used to analyze thermal bending of thin plate problems. Detailed formulation and the corresponding finite element matrices of the DKQ finite element for thermal bending analysis of thin plate will be derived herein. The performance of the DKQ element alone will be evaluated by a problem that has exact solution and compared with the solutions obtained from using the standard four-node rectangular (REC) element [6]. This rectangular element is derived by assuming the displacement in the z direction in the form of incomplete fourth-order polynomial expression which

is simply to understand and derive; however, some discontinuity of normal slope will occur and can be used only in the case of the element is rectangle.

To improve the efficiency of the DKQ element in plate bending analysis, the adaptive meshing technique which has been used to obtain much higher solution accuracy in the structural analysis [7] is then applied in this study. The technique generates small clustered elements in the regions of high stress gradients to provide higher solution accuracy. At the same time, larger elements are generated in the other regions to reduce the total number of unknowns and the computational time.

In this paper, the governing differential equations for predicting the structural response of the plate due to thermal load will be presented first. Then, the corresponding finite element equations and the associated element matrices will be described. The concept of the adaptive meshing technique and the selection of the meshing parameters used for construction of new meshes will be explained. Finally, the performance of the DKQ element and the adaptive meshing technique will be evaluated by several examples.

II. GOVERNING EQUATIONS

The equation for the transverse deflection, w , in the z -direction normal to the x - y plane of a thin plate, is given by the equilibrium equation [8] as,

$$D \left(\frac{\partial^4 w}{\partial x^4} + \frac{\partial^4 w}{\partial x^2 \partial y^2} + \frac{\partial^4 w}{\partial y^4} \right) = p(x, y) - \frac{1}{1-\nu} \left(\frac{\partial^2 M_T}{\partial x^2} + \frac{\partial^2 M_T}{\partial y^2} \right) \quad (1)$$

where $p(x, y)$ is the applied lateral load normal to the plate, D is the bending rigidity and M_T is the thermal moment. The bending rigidity is defined by,

$$D = \frac{Et^3}{12(1-\nu^2)} \quad (2)$$

where E is the modulus of elasticity, t is the thickness of the plate and ν is the Poisson's ratio. The thermal moment M_T in (2) is defined by,



$$M_T = E\alpha \int_{-t/2}^{t/2} T(z) z dz \quad (3)$$

where α is thermal expansion coefficient and $T(z)$ is the temperature distribution along the plate thickness.

III. FINITE ELEMENT EQUATIONS

The four-node DKQ element assumes a cubic distribution of the transverse deflection over the element based on discrete Kirchhoff assumptions [5]. The element equations can be derived by applying the method of weighted residuals to the plate bending governing equation, (1), which leads to the finite element equations in the form of,

$$[K]\{\delta\} = \{F_P\} + \{F_T\} \quad (4)$$

The vector of the element nodal unknowns $\{\delta\}$ consists of the transverse deflections and the rotations. Each node of the DKQ element has a transverse deflection in the element local z -coordinate direction and two rotations about the element local x - y coordinate directions. Thus, there are twelve degrees of freedom per element as follows,

$$\{\delta\}^T = [w_1 \ \theta_{x1} \ \theta_{y1} \ w_2 \ \theta_{x2} \ \theta_{y2} \ w_3 \ \theta_{x3} \ \theta_{y3} \ w_4 \ \theta_{x4} \ \theta_{y4}] \quad (5)$$

The element stiffness matrix, $[K]$, in (4) can be defined by,

$$[K] = \int_A [B]^T [D] [B] dxdy \quad (6)$$

which can be transformed to natural coordinate as,

$$[K] = \int_{-1}^1 \int_{-1}^1 [B(\xi, \eta)]^T [D] [B(\xi, \eta)] |J| d\xi d\eta \quad (7)$$

The strain-displacement interpolation matrix, $[B]$, in (7) is in the form of,

$$[B] = \begin{bmatrix} j_{11}^* \left[\frac{\partial H_x}{\partial \xi} \right] + j_{12}^* \left[\frac{\partial H_x}{\partial \eta} \right] \\ j_{21}^* \left[\frac{\partial H_y}{\partial \xi} \right] + j_{22}^* \left[\frac{\partial H_y}{\partial \eta} \right] \\ \left(j_{21}^* \left[\frac{\partial H_x}{\partial \xi} \right] + j_{22}^* \left[\frac{\partial H_x}{\partial \eta} \right] \right) + \left(j_{11}^* \left[\frac{\partial H_y}{\partial \xi} \right] + j_{12}^* \left[\frac{\partial H_y}{\partial \eta} \right] \right) \end{bmatrix} \quad (8)$$

where the functions H_{xi} and H_{yi} for $i = 1, 2, 3$ is given by,

$$\begin{aligned} H_{x1} &= \frac{3}{2} [a_5 N_5 - a_8 N_8] & H_{y1} &= \frac{3}{2} [d_5 N_5 - d_8 N_8] \\ H_{x2} &= b_5 N_5 + b_8 N_8 & H_{y2} &= -N_1 + e_5 N_5 + e_8 N_8 \\ H_{x3} &= N_1 - c_5 N_5 - c_8 N_8 & H_{y3} &= -b_5 N_5 - b_8 N_8 \end{aligned} \quad (9)$$

For other functions of H_{xi} and H_{yi} , the functions H_{x4} , H_{x5} , H_{x6} and H_{y4} , H_{y5} , H_{y6} are obtained from the above expressions by replacing N_1 by N_2 and indices 8 and 5 by indices 5 and 6, respectively. The functions H_{x7} , H_{x8} , H_{x9} and H_{y7} , H_{y8} , H_{y9} are obtained from the above expressions by replacing N_1 by N_3 and indices 8 and 5 by indices 6 and 7, respectively. Similarly, the functions H_{x10} , H_{x11} , H_{x12} and H_{y10} , H_{y11} , H_{y12} are obtained from

the above expressions by replacing N_1 by N_4 and indices 8 and 5 by indices 7 and 8, respectively. The shape functions N_i (for $i = 1$ to 8) are those of the 8-node Serendipity element [8]. The coefficients a_k , b_k , c_k , d_k and e_k (for $k = 5, 6, 7, 8$ and $ij = 12, 23, 34, 41$) that appear in the functions H_x and H_y depend on the element shape and are given by,

$$\begin{aligned} a_k &= -(x_{ij} / l_{ij}^2) & b_k &= \frac{3}{4} (x_{ij} y_{ij}) / l_{ij}^2 \\ c_k &= \left(\frac{1}{4} x_{ij}^2 - \frac{1}{2} y_{ij}^2 \right) / l_{ij}^2 & d_k &= -(y_{ij} / l_{ij}^2) \\ e_k &= \left(-\frac{1}{2} x_{ij}^2 + \frac{1}{4} y_{ij}^2 \right) / l_{ij}^2 \end{aligned} \quad (10)$$

where the coefficients x_{ij} and y_{ij} (for $ij = 1, 2, 3, 4$) are defined in terms of element nodal coordinates by,

$$x_{ij} = x_i - x_j \quad \text{and} \quad y_{ij} = y_i - y_j \quad (11)$$

The j_{11}^* , j_{12}^* , j_{21}^* and j_{22}^* are the components of the inverse of the Jacobian matrix $[J]$ of the transformation between the parent and the actual element. The Jacobian matrix $[J]$ is given by,

$$[J] = \begin{bmatrix} J_{11} & J_{12} \\ J_{21} & J_{22} \end{bmatrix} = \frac{1}{4} \begin{bmatrix} x_{21} + x_{34} + \eta(x_{12} + x_{34}) & y_{21} + y_{34} + \eta(y_{12} + y_{34}) \\ x_{32} + x_{41} + \xi(x_{12} + x_{34}) & y_{32} + y_{41} + \xi(y_{12} + y_{34}) \end{bmatrix} \quad (12)$$

We then have

$$j_{11}^* = \frac{J_{22}}{|J|}; \quad j_{12}^* = \frac{-J_{12}}{|J|}; \quad j_{21}^* = \frac{-J_{21}}{|J|}; \quad j_{22}^* = \frac{J_{11}}{|J|} \quad (13)$$

The matrix $[D]$ in (6) is the plate material stiffness matrix defined by,

$$[D] = \frac{Et^3}{12(1-\nu^2)} \begin{bmatrix} 1 & \nu & 0 \\ \nu & 1 & 0 \\ 0 & 0 & (1-\nu)/2 \end{bmatrix} \quad (14)$$

The element stiffness matrix of the DKQ element in (7) can be performed by using a standard numerical integration scheme with 2x2 Gauss integration points [9] as,

$$[K] = \sum_{i=1}^2 \sum_{j=1}^2 w_i w_j [B(\xi_i, \eta_j)]^T [D] [B(\xi_i, \eta_j)] |J(\xi_i, \eta_j)| \quad (15)$$

The nodal force vector due to the applied lateral loads, $\{F_P\}$, in (4) is defined by simply considering a linear interpolation for w over the element [5] which gives,

$$\{F_P\} = \begin{bmatrix} \frac{pA}{4} & 0 & 0 & \frac{pA}{4} & 0 & 0 & \frac{pA}{4} & 0 & 0 & \frac{pA}{4} & 0 & 0 \end{bmatrix} \quad (16)$$

where A is the area of the element.



The nodal force vector due to the thermal loads, $\{F_T\}$, which has been improved in this research is defined by,

$$\{F_T\} = \frac{1}{1-\nu} \int_A [B]^T \{M\} dA \quad (17)$$

where the vector $\{M\}$ is given by,

$$\{M\}^T = [M_T \quad M_T \quad 0] \quad (18)$$

and M_T is the thermal moment as shown in (2).

Thus, the nodal force vector due to the thermal loads can be rewritten into natural coordinate as,

$$\{F_T\} = \int_{-1}^1 \int_{-1}^1 [B(\xi, \eta)]^T |J| d\xi d\eta \{M\} \quad (19)$$

which can be performed by using numerical integration in the same method to (15) as,

$$\{F_T\} = \sum_{i=1}^2 \sum_{j=1}^2 W_i W_j [B(\xi_i, \eta_j)]^T |J(\xi_i, \eta_j)| \{M\} \quad (20)$$

All of the above finite element matrices are in closed-form so that they can be implemented in the FORTRAN computer programing directly.

IV. ADAPTIVE MESHING TECHNIQUE

The basic idea of adaptive meshing [7] is to construct a completely new mesh based on the solution obtained from the previous mesh. The new mesh will have small elements in regions of large changes in solution gradients and large elements in regions where the gradient changes are small. Proper nodal spacings used for constructing a new mesh are determined by using the solid mechanics concept of finding the principal stresses, σ_1 and σ_2 , from a given state of stresses, σ_x , σ_y and τ_{xy} , i.e.,

$$\begin{bmatrix} \sigma_x & \tau_{xy} \\ \tau_{xy} & \sigma_y \end{bmatrix} \Rightarrow \begin{bmatrix} \sigma_1 & 0 \\ 0 & \sigma_2 \end{bmatrix} \quad (21)$$

At a typical node in the previous mesh, the second derivatives of the key parameter for meshing, ϕ , (analogous to the stress components in (21)) are computed and the two eigenvalues (analogous to the principal stresses) are then determined,

$$\begin{bmatrix} \frac{\partial^2 \phi}{\partial x^2} & \frac{\partial^2 \phi}{\partial x \partial y} \\ \frac{\partial^2 \phi}{\partial x \partial y} & \frac{\partial^2 \phi}{\partial y^2} \end{bmatrix} \Rightarrow \begin{bmatrix} \lambda_1 & 0 \\ 0 & \lambda_2 \end{bmatrix} \quad (22)$$

The larger eigenvalue, $\lambda = \max(\lambda_1, \lambda_2)$, is then selected for that node and the same process is repeated for all the other nodes. The selected eigenvalues are used to generate a new adaptive mesh by employing the Automesh2D software [10].

For plate bending analysis, Von Mises stress is used as a key parameter for remeshing and defined by [11],

$$\sigma_{Von \text{ Mises}} = \frac{1}{\sqrt{2}} \sqrt{(\sigma_x - \sigma_y)^2 + \sigma_x^2 + \sigma_y^2 + 6\tau_{xy}^2} \quad (23)$$

V. APPLICATIONS

Two example problems are presented in this section. The first two examples are chosen to evaluate the performance of the DKQ plate bending element. Another example demonstrates the effectiveness of the adaptive meshing technique combining with the DKQ element.

A. Simply supported and free rectangular plate

The simply supported and free rectangular plate of which the temperature varies linearly along the thickness only is considered. This plate is free along the edges $y = \pm b/2$ and simply supported along the edges $x = 0$ and $x = a$ as shown in Fig. 1. The exact solution of the deflection in z -direction (w) is given in Ref. [12] as,

$$w(x, y) = (1 + \nu) \frac{\alpha \Delta T}{t} \frac{4a^2}{\pi^3} \sum_{n=1,3,5}^{\infty} \frac{\sin \alpha_n x}{n^3} (1 + A_n \cosh \alpha_n y + B_n \alpha_n y \sinh \alpha_n y)$$

$$A_n = \frac{(1 - \nu) \frac{\beta_n}{2} \coth \frac{\beta_n}{2} (1 + \nu)}{(3 + \nu) \cosh \frac{\beta_n}{2} - \frac{(1 - \nu) \frac{\beta_n}{2}}{\sinh \frac{\beta_n}{2}}}; \quad B_n = \frac{1 - \nu}{(3 + \nu) \cosh \frac{\beta_n}{2} - \frac{(1 - \nu) \frac{\beta_n}{2}}{\sinh \frac{\beta_n}{2}}}$$

$$\alpha_n = \frac{n\pi}{a}; \quad \beta_n = \frac{n\pi b}{a} \quad (24)$$

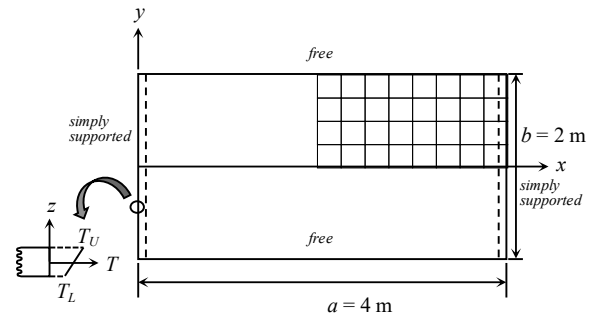


Fig. 1. Simply supported and free rectangular plate with linear temperature gradient through its thickness.

In this example, the geometric properties of plates are the width (a) of 4 m, the length (b) of 2 m, and the thickness (t) of 0.01 m. The physical properties of the plate are taken as the modulus of elasticity (E) of 190 GPa, the Poisson's ratio (ν) of 0.3, and the thermal expansion coefficient (α) of $16 \times 10^{-6} / ^\circ\text{C}$. The temperatures of the upper surface (T_U) and the lower surface (T_L) of the plate are 60°C and 0°C , respectively.



Due to its symmetry, only the top right quarter of the plate in Fig. 1 is modeled and analyzed. The model is discretized into uniform square meshes of 4×2, 8×4 and 16×8 intervals (15, 45 and 153 nodes, respectively) as shown in Fig. 2 (a)-(c). DKQ and standard four-node rectangular (REC) elements are used in the analysis. From the problem statement, the plate tends to bend with the maximum transverse deflections occurred at the center of the plate. The maximum transverse deflections at the center of the plate obtained from using both elements are shown in Fig. 3. The results from both elements converge to the exact solution as the meshes are refined. Figure 4 shows the predicted transverse deflections along the x-axis obtained from both element types (with 16×8 interval mesh). It can be seen that the results obtained from both element types closely match the exact solution. The predicted maximum transverse deflections at the center of the plate for the 16×8 mesh including their percentage errors compared with the exact solution are also shown in Table I. The table and Figure 3 show that DKQ element performs very well and provides higher solution accuracy than the standard rectangular element (REC). Moreover, DKQ element can be used in the case of the element shape is not in a uniform rectangle, but also can be used in the case of the element shape is quadrilateral or parallelogram in the next example.

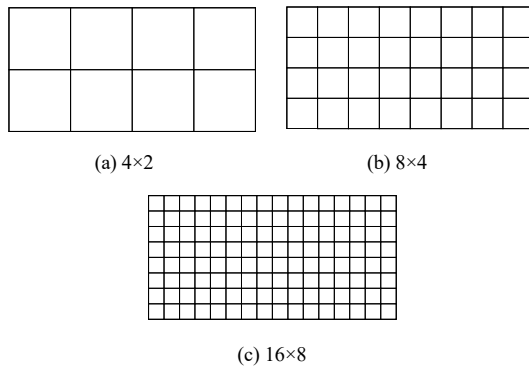


Fig. 2. Finite element meshes in the computations.

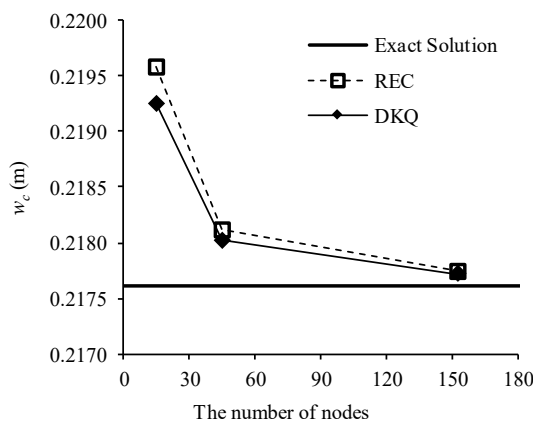


Fig. 3. Deflections at the center of the plate with mesh refinement.

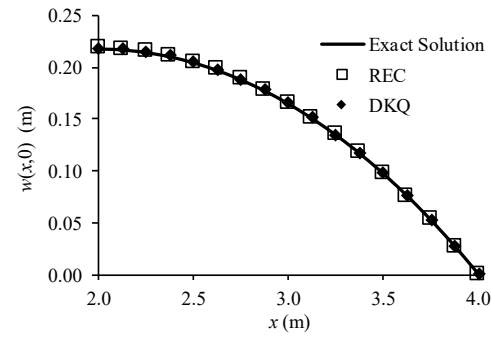


Fig. 4. Comparative transverse deflections along x-axis.

TABLE I. COMPARISON OF THE PREDICTED MAXIMUM TRANSVERSE DEFLECTIONS AND PERCENTAGE ERRORS

	w_c (m)	error (%)
Exact solution	0.217610	-
DKQ element	0.217712	0.0470
REC element	0.217738	0.0588

B. Simply supported parallelogram plate

Figure 5 shows a problem statement of the simply supported parallelogram plate with the linear temperature distribution through the thickness. The dimensions of the plate in the analysis are $a = 2$ m, $b = 1$ m and $\gamma = 30^\circ$. The plate is assumed to have the modulus of elasticity (E) of 190 GPa, the Poisson's ratio (ν) of 0.3, the thermal expansion coefficient (α) of $16 \times 10^{-6} / ^\circ\text{C}$, the thickness (t) of 0.01 m, the upper surface temperature (T_U) of 60 $^\circ\text{C}$, and the lower surface temperature (T_L) of 0 $^\circ\text{C}$. The exact central transverse deflection (w_c) of the simply supported parallelogram plate for $a/b = 2$ and $\gamma = 30^\circ$ is given by [13],

$$w_c = 0.090135 \frac{M_T b^2}{D} \quad (25)$$

where D and M_T are the same as written in (2) and (3), respectively.

The model is discretized into uniform meshes of 4×2 (15 nodes), 8×4 (45 nodes) and 16×8 (153 nodes) intervals as illustrated in Fig. 6 (a)-(c). The predicted central transverse deflections, which is the maximum deflection, compared with the exact solution are shown in Fig. 7. The results indicate that DKQ element apparently provides good solution accuracy and the computational result converges to the exact solution as the meshes are refined.

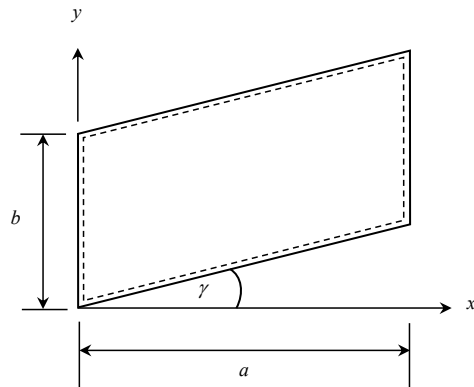


Fig. 5. Simply supported parallelogram plate with linear temperature gradient through its thickness.

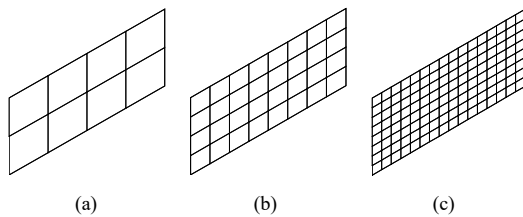


Fig. 6. Finite element meshes of parallelogram plate.

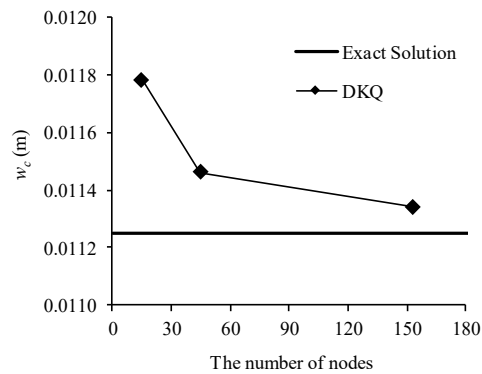


Fig. 7. Predicted central deflections of the simply supported parallelogram plate compared with the exact solution.

C. Clamped L-shaped plate

An L-shaped plate with linear temperature variation through its thickness is shown in Fig. 8. The plate has the thickness of 1 cm and is clamped along the inner sides. The plate is assumed to have the modulus of elasticity (E) of 1.9×10^{11} N/m², Poisson's ratio (ν) of 0.3, the thermal expansion coefficient (α) of 23.2×10^{-6} /°C, the upper surface temperature (T_U) of 120 °C, and the lower surface temperature (T_L) of 0 °C.

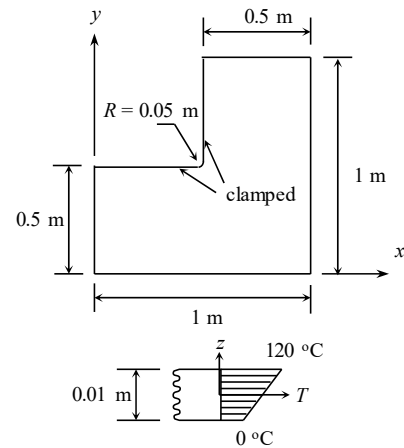


Fig. 8. An L-shaped plate with temperature gradient through its thickness.

An initial unstructured mesh consisting of 561 nodes and 508 elements is shown in Fig. 9(a). The computed Von Mises stresses obtained from this initial mesh are used as the key parameters for generating an adaptive meshing. The new adaptive mesh, with 935 nodes and 861 elements, is shown in Fig. 9(b). Small elements are clustered in the region of high stress gradients to provide a more accurate stress solution. The second adaptive meshes with 1,385 nodes and 1,289 elements are shown in Fig. 9(c). The figures show refined elements are in the high stress concentration region to capture detailed solution for increased solution accuracy.

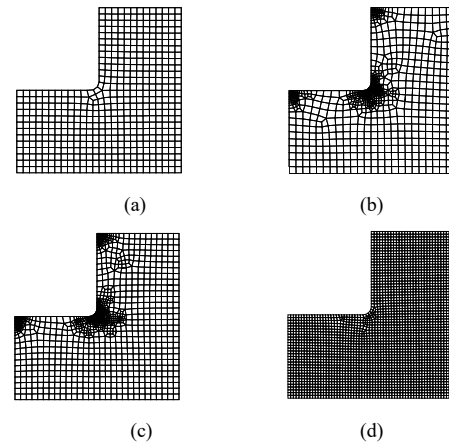


Fig. 9. Finite element meshes: (a) initial mesh, (b) 1st adaptive mesh, (c) 2nd adaptive mesh and (d) uniform mesh.

Fig. 10 shows that the predicted Von Mises stress at the center of inner curve of the plate converges to the analytical solution [14] of 0.735 GPa with the steps of adaptive remeshing. The number of the accumulated elements in the analysis (from initial mesh to 2nd adaptive mesh) are totally 2,658 elements. The uniform refined mesh in Fig. 9(d) with 2,782 elements which is close to the total number of elements in the adaptive meshing analysis is also used to compare the



computational time and the solution accuracy. The predicted Von Mises stress at the center of inner curve of the plate is about 0.615 GPa as shown in Fig. 10. Moreover, the computational time spent in the uniform mesh analysis is about 15.87 times compared to the adaptive meshing analysis. The results demonstrate the advantages of the technique as it can provide better solution accuracy, and it is unnecessary to use refined element all over the whole domain which will cost much computational time. The deformation of the plate and the Von Mises stress contours from the second adaptive finite element mesh are also shown in Fig. 11 and Fig. 12, respectively.

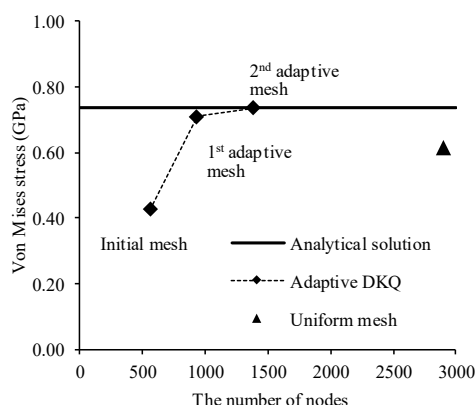


Fig. 10. Convergence of Von Mises stress at the center of inner curve of the plate by adaptive meshes.

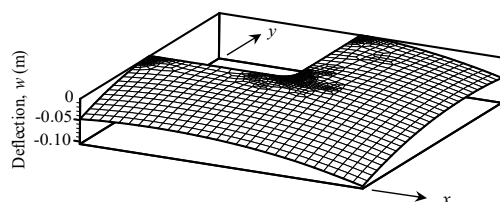


Fig. 11. Predicted deformation of the plate obtained from the 2nd adaptive mesh.

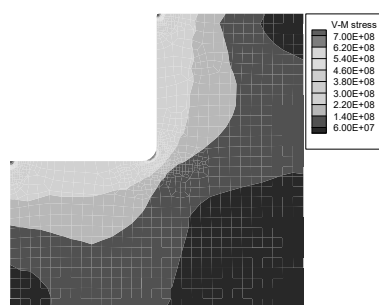


Fig. 12. Von Mises stress contours of the plate obtained from the 2nd adaptive mesh.

VI. CONCLUSION

The DKQ plate bending finite element formulation with detailed finite element matrices for thermal plate bending analysis were derived and presented. The DKQ plate bending element has been combined with the adaptive meshing technique to improve the solution accuracy and reduce the computational effort. The examples presented in this paper demonstrated that solutions obtained from DKQ element perform very well for analyzing thermal bending of thin plate problems, and the combined method can provide improved solution accuracy by adapting the mesh to the physics of the solutions and reduce the total number of unknowns used in the computation by generating proper small elements in the regions with high solution gradients and large elements in the other regions.

REFERENCES

- [1] M.M. Hrabok and T.M. Hrudey, "A review and catalogue of plate bending finite elements", *Comput. Struct.*, vol. 19(3), pp. 479-495, 1984.
- [2] J. Mackerle, "Static and dynamic analysis of plates using finite element and boundary elements - a bibliography (1992-1994)", *Finite Elem. Anal. Des.*, vol. 20(2), pp. 139-154, 1995.
- [3] J.L. Batoz, K.J. Bathe, and L.W. Ho, "A study of three-node triangular plate bending elements", *Int. J. Num. Meth. Engng.*, vol. 15(12), pp. 1771-1812, 1980.
- [4] J.L. Batoz, C.L. Zheng, and F. Hammadi, "Formulation and evaluation of new triangular, quadrilateral, pentagonal and hexagonal discrete Kirchhoff plate/shell elements", *Int. J. Num. Meth. Engng.*, vol. 52(5-6), pp. 615-630, 2001.
- [5] J.L. Batoz, and M.B. Tahar, "Evaluation of a new quadrilateral thin plate bending element", *Int. J. Num. Meth. Engng.*, vol. 18(11), pp. 1655-1677, 1982.
- [6] O.C. Zienkiewicz and R.L. Taylor, *Finite Element Method Volume 2: Solid Mechanics*, 5th ed., Oxford: Butterworth-Heinemann, 2000.
- [7] P. Dechaumphai, "Improvement of plane stress solutions using adaptive finite elements", *J. Chin. Inst. Eng.*, vol. 19(3), pp. 375-380, 1996.
- [8] P. Dechaumphai, *Finite element method: fundamentals and applications*, Oxford: Alpha Science International, 2010.
- [9] P. Dechaumphai and N. Wansophark, *Numerical methods in engineering*, Oxford: Alpha Science International, 2011.
- [10] X.W. Ma, G.Q. Zhao, and L. Sun, "Automesh-2D/3D: robust automatic mesh generator for metal forming simulation", *Mater. Res. Innov.*, vol. 15(Supp 1), pp. S482-S486, 2011.
- [11] R.D. Cook, D.S. Malkus, M.E. Plesha, and R.J. Witt, *Concepts and applications of finite element analysis*, 4th Ed., New York: John Wiley & Sons, 2002.
- [12] W. Nowacki, *Thermoelasticity*, Oxford: Pergamon Press, 1962.
- [13] V.M. Kulakov, A.A. Uspenskii, and A.N. Frolov, "Thermal deflection in a parallelogram plate", *Strength Mater.*, Vol.7(11), pp. 1362-1364, 1975.
- [14] P. Bhothikhun, P. Dechaumphai, *Adaptive DKT Finite Element for Plate Bending Analysis*, *KMUTNB: IJAST*, Vol. 6(3), pp. 83-90, 2013.



Risk Assessment for Drought in Thailand Using Hidden Markov Models

Pitsanu Tongkhaw¹ and Rachadasak Supengcum²

Department of Industrial Engineer, Faculty of Engineer, Rajamangala University of Technology, Pranakhon
Bangkok Thailand

¹pitsanu.t@rmutp.ac.th, ²rachadasak.s@rmutp.ac.th

Abstract— The objective of this research was to propose a proper model for risk assessment for drought in Thailand. A hidden Markov model was adopted. The results indicate that the amount of rainfall depends on the hidden states, drought or non-drought state. If the state changes from drought to non-drought the amount of rain will increase. The probability of changing from drought state to non-drought state is higher than from drought state to drought state. The probability of drought occurrence in February is highest, followed by in November, March, December, January, July, April, June, October, September, August and May, respectively. When the temperature increases, the probability of drought occurrence will increase.

Keywords— Hidden Markov models (HMMs), Drought in Thailand, Probability function, Bayesian estimation

I. INTRODUCTION

Experts said that the drought crisis of 2014-2015 was the biggest drought in 10 years, from October 2014 to the present. The department of disaster prevention and mitigation announced drought relief zones in 15 provinces and 58 districts. Farmers in many provinces began to release their crops and all the crops died due to inadequate agricultural water supply in the dry season. The volume of water in the main reservoirs of the country was low. In addition, the problem of sea water required more drainage from the reservoir to dilute the salinity [1]. [2] studied the hidden Markov models and concluded that the hidden Markov model was widely used in time series data and can be applied to solve many problems. [3] investigated the defect detection of machines using hidden Markov models and applied spindle-based multi-head machines to produce the product. [4] studied factors influencing drought risk. [5] analyzed drought risk areas and provided guidance for sustainable land in the central river basin, Chiangmai province, using multiple criteria and geographic information systems. The seven factors related to the average annual rainfall were land use water absorption capacity, water consumption density of streams, size of sub-basin area and slope. [6] assessed and monitored drought in Tamil Nadu, India using remote sensing and geographic information system (GIS). [7] studied on remote sensing techniques and geographic information systems (GIS) for drought risk assessment. [8] assessed and monitored drought in east Shewa, Ethiopia, using remote sensing and geographic information system (GIS) too. From the above mentioned

problems, the researcher is interested in creating a model of the Hidden Markov models for analysis of drought data in Thailand in order to predict drought in each month accurately.

II. METHOD AND APPLICATION

A. Generalized Linear Mixed Model (GLMM)

The Poisson regression model [9] is as follows.

Let Y_i , $i=1, \dots, n$ be a variable with a count value. The Poisson distribution whose mean is μ_i is assumed. That is $Y_i \sim \text{Poisson}(\mu_i)$. The probability distribution of Y_i is written as follows.

$$P(Y_i = y_i; \mu_i) = \frac{e^{-\mu_i} \mu_i^{y_i}}{y_i!}, y_i = 0, 1, 2, \dots$$

$$E(Y_i) = \text{Var}(Y_i) = \mu_i$$

Let $X_i = (X_{i0}, X_{i1}, \dots, X_{ip})^T$ when $i=1, \dots, n$ be a variable that has a linear relationship with Y_i . A widely used form of canonical link is a natural log function.

Let $\beta_i = (\beta_0, \beta_1, \dots, \beta_p)^T$ be a parameter. The relationship is as follows.

$$E(Y_i) = \mu_i = e^{x_i^T \beta}$$

We can estimate the parameters by using the method of maximum likelihood and solve the equation by using a numerical iterative method.

B. Hidden Markov model (HMM)

HMM is a kind of a statistical Markov model with a theoretical assumption stating that the Markov process is invisible. The HMM which requires mathematical principles was first proposed by [10]

The theory principle of HMM

When defining $O = O_0, O_1, \dots, O_T$ to be visible event given a parameter $\lambda = (A, B, \pi)$, we can find the value of

the posterior, then Gibbs sampling to estimate each parameter is applied. When the MCMC converges to any distribution, one distribution, it will estimate each parameter and the credible interval of each parameter.

III. RESULTS

Application

For general information, the average amount of rainfall ranking top 10 provinces were in Trat (405.08), Ranong (344.83), Phangnga (337.25), Chanthaburi (286.17), Nakhon Si Thammarat (216.58), Phuket (199.67), Yala (198.83), Krabi (194.17), Nakhon Phanom (192.33), respectively. The factors affecting drought are shown in Table I.

The HMMs has the following form.

$$Y_{it}, i=1,2,3,\dots,76 \quad t=1,2,3,\dots,12$$
$$Y_{it} \sim N(\mu_{it}, \sigma^2) \text{ by } \mu_{it} \sim \lambda_1 + \lambda_2 C_{it}, C_{it} \sim \text{Bern}(\theta_{it})$$

C_{it} is 0 or 1. If C_{it} is 0, it means that it is in drought status. If C_{it} equals 1, it means that it is in a non-drought state.

X_{it1} = forest area, X_{it2} = january, X_{it3} = february, ...,

$$X_{it13} = \text{December,}$$
$$\beta_1, \beta_2, \dots, \beta_{15} \sim \text{Norm}(0, 1000)$$

$$\lambda_1, \lambda_2 \sim \text{Norm}(0, 1000).$$

Factors	Mean	S.D	95% Credible Interval	
λ_1	47.16	7.16	33.02	61.75
λ_2	167.8	8.39	151.7	184.5
Intercept (β_1)	24.97	9.02	4.15	39
Prior state (β_2)	24.06	10.62	5.35	49.47
Forest area (β_3)	0.0006	0.0005	0.0001	0.002
January (β_4)	0.73	31.42	-59.57	62.5
February (β_5)	-37.59	18.69	-79.28	-7.86
March (β_6)	-17.82	21.84	-66.75	15.13
April (β_7)	17.19	6.23	8.51	32.48
May (β_8)	44.16	15.97	19.84	81.8
June (β_9)	22.74	21.31	-11.9	70.87
July (β_{10})	13.06	19.15	-12.77	61.21
August (β_{11})	29.98	21.9	-7.78	77.01
September (β_{12})	27.46	21.75	-8.75	75.46
October (β_{13})	23.9	21.16	-12	70.85
November (β_{14})	-33.82	18.14	-76.5	-9.18
December (Reference)	-	-	-	-
Temperature (β_{15})	-1.45	0.39	-1.97	-0.52

28/6/2561 15:38:13



situation in April, May, June, July, August, September and October is lower than in December drought. On the other hand the probability of drought in February, March and November is higher than the Drought in December. Finally, the estimates of β_{15} (-1.45) are negative, meaning that if the temperature rises, the probability of drought is higher. And some examples of drought forecasts in each province of each month are shown in Table II.

TABLE II. DROUGHT FORECAST VALUES

Province	Month	Mean	S.D.	95% Credible Interval	
Amnat Charoen	Jan.	1	0	1	1
Amnat Charoen	May	1	0	1	1
Amnat Charoen	Aug.	1	0	1	1
Amnat Charoen	Sep.	1	0	1	1
Ang Thong	Jan.	1	0	1	1
Ang Thong	May	1	0	1	1
Ang Thong	Sep.	1	0	1	1
Ang Thong	Oct.	1	0	1	1
Bangkok	Jan.	1	0	1	1
Bangkok	May	1	0	1	1
Bangkok	Sep.	1	0	1	1
Buri Ram	Jan.	1	0	1	1
Buri Ram	May	1	0	1	1
Buri Ram	Aug.	1	0	1	1
Buri Ram	Sep.	1	0	1	1
Buri Ram	Oct.	1	0	1	1
Chachoengsao	Jan.	1	0	1	1
Chachoengsao	May	1	0	1	1
Chachoengsao	Sep.	1	0	1	1
Chai Nat	Jan.	1	0	1	1
Chai Nat	May	1	0	1	1
Chai Nat	Oct.	1	0	1	1
Chaiyaphum	Jan.	1	0	1	1
Chaiyaphum	May	1	0	1	1
Chaiyaphum	Sep.	1	0	1	1
Chanthaburi	Jan.	1	0	1	1
Chanthaburi	May	1	0	1	1

Table II illustrates that the probability that Amnat Charoen province is in a non-drought state in January, because a probability of 1.00 and that it is in a non-drought state in February and March is also equal with a probability 1.00. The probability that Ang Thong will be in a dry state in January with a probability of 1.00 and a non-drought status in February

and March, has a probability of 1.00. In other provinces, similarly described.

IV. DISCUSSION

A hidden Markov model (HMM) describes the magnitude of the factorial influence of each same unit. The HMM presented by Baum and Petrie (1966) is used when weather the states are unknown (hidden state). However, there are some states related to that state. For example, if the rainfall is too high, this may not indicate drought. HMM can also be used for time series data. If the time information is derived, it results from the state of the hidden weather. Bayesian estimation is becoming more popular since it can solve problems from simple problems to complex problems in which the maximum likelihood method can not be applied. The Bayesian estimation considers that the parameters are random variables that occur under any distribution model. The prior distribution is based on the belief of the investigator. Then, a number of sample data are collected, then the information from the data is actually obtained. The probability of occurrence of the sample set is to improve the initial probability model that was originally defined. The result is a modified probability model called posterior distribution of the parameters of interest. Then, the expected values of the parameters under the modified probability model are used as Bayesian probabilities. Nowadays, more and more popular. Since it can solve problems from simple problems to complex problems.

V. CONCLUSION

The main research objective was to propose proper model for risk assessment for drought in Thailand. A Hidden Markov Model (HMM) was applied. The dependent variables were the rainfall in each province of Thailand. The results show that when no factors are involved, the average monthly rainfall are 47.16 millimeters. The average rainfall in each month depends on hidden drought state. If the status changes from drought to non-drought, the average rainfall will increase 167.80 millimeters. By nature, at the current month, the probability of drought is lower than the probability of non-drought. The probability of changing drought state to non-drought is higher than from drought to drought. If the forest area increases, the probability of drought is lower. The probability of drought state in February is lower than the drought in December. However, the probability of drought in February, March and November is higher than the drought in December. when the temperature rises, the probability of drought is higher.

ACKNOWLEDGMENT

Authors gratefully acknowledge the Rajamangala university of technology Phra Nakhon, Institute of Research and Development Rajamangala University of Technology Phra Nakhon and the faculty of Engineering for their technical and financial support.

REFERENCES



- [1] TDRI. "Drought crisis in 2014, caused by the nature or failure of flood protection policy over drought". ThaiPublica, 2014. <http://thaipublica.org/2014/03/disaster-drought-2014/>.
- [2] P. Blunsom. Hidden Markov Models, 2004. <http://digital.cs.usu.edu/~cyan/CS7960/hmm-tutorial>.
- [3] A.H.Tai, W-K Chingb, and L.Y. Chana. Detection of machine failure: Hidden Markov Model approach. Computers & Industrial Engineering, ScienceDirect, 2009, 57: 608-619.
- [4] P. Chanchaeng. "Risk analysis of drought in Kamphaeng Saen area by applying geographic information system", National Institute of Development Administration, 2010, pp. 29-37.
- [5] J. Sawadee. "Drought risk analysis in the central river basin for using sustainable land", Master of Science (sustainable land use and natural resource management), land use and sustainable natural resource management program, 2011.
- [6] D. Muthumanickama, P. Kannana, R. Kumaraperumala, S. Natarajana, R. Sivasamy and C. Poongodib. "Drought assessment and monitoring through remote sensing and GIS in western tracts of Tamil Nadu, India". International Journal of Remote Sensing, 2011. 32(18): 5157-5176.
- [7] A. Belal, A., H.R. El-Ramady, E.S. Mohamed, and A. M. Saleh. "Drought risk assessment using remote sensing and GIS techniques". Arabian Journal of Geosciences, 2014. 7(1): 35-53.
- [8] G. Legesse and K.V. Suryabhagavan. "Remote sensing and GIS based agricultural drought assessment in East Shewa Zone", Ethiopia. Tropical Ecology, 2014. 55(3): 349-363.
- [9] P. McCullagh and J. Nelder. 1989. Generalized Linear Models, 2nd ed. Boca Raton: Chapman and Hall/CRC.
- [10] Baum, L. E. and T. Petrie. 1966. Statistical inference for probabilistic functions of finite state Markov chains. Annals of Mathematical Statistics, 37: 1554-1563.
- [11] TMD, Rainfall data and temperature data. 2017. <http://www.tmd.go.th/services/services.php>, 2017.
- [12] I. Ntzoufras, Bayesian modeling using WinBUGS. Hoboken, NJ: Wiley, 2009.



Wurtzite-to-Rocksalt like Phase Transformations in Case of LiGaO₂ from First principles

Wutthigrai Sailuam¹

Lecturer, Department of Applied Physics,
Faculty of Engineering, Rajamangala University of
Technology ISAN, Khon Kaen Campus, Thailand
E-mail; wutthigraiphys33@gmail.com

Kanoknan Parcheruk²

Assistant Professor, College of Nanotechnology
King Mongkut's Institute of Technology Ladkrabang,
Bangkok, Thailand
E-mail; kanoknans@hotmail.com

Abstract— A homogeneous wurtzite-to-rocksalt like phase transformation in LiGaO₂ is studied using first principle calculations. We found that under specific conditions, LGO can show structure of a rocksalt-like structure that have not been previously reported the body-centered tetragonal (I41/amd) occurs under hydrostatic compression. We characterize the stability of the phase transformation processes by calculating enthalpy surfaces and barriers and find that the smallest barrier correspond to the (I41/amd) structure (86.25 meV/atom) at 3.7 GPa compressive strain.

Keywords— Phase Transformations, LiGaO₂, B4-B1 pathway

I. INTRODUCTION

Lithium gallate; LiGaO₂ (LGO) a typical I-II-VI₂ semiconductor can be obtained as single crystals by the conventional Czochralski melt-pulling method [1,2]. The I-II-VI₂ ternary semiconductor also crystallizes with the wurtzite-type structure [3,5]. The wurtzite structure is common crystalline form for $A^N B^{8-N}$ binary semiconductors [6]. For instance, ZnO and GaN. The pressure-induced wurtzite to rocksalt (B4-B1) structural transition in binary semiconductors are functionally important for both basic solid-state science and applied materials research [7,10]. The transformation of hexagonal wurtzite type structure (B4) to cubic rocksalt-type structure (B1) is a significant transition pathway in $A^N B^{8-N}$ binary semiconductors. Because of the need to understand the microscopic mechanism for this structural application of $A^N B^{8-N}$ binary semiconductors, the general B4-B1 pathway, which itself cannot be observed. Investigating the pressure-induced structural transitions in ternary wurtzites is also very important for our knowledge of transition mechanisms from pure and deficient wurtzite-type semiconductors in both the theoretical and experimental aspects.

In this work, we use Density Functional Theory (DFT) calculations to study phase transformations for ternary wurtzite show a pathway from the distorted-wurtzite-type of LGO

(Pna2₁) to new high-pressure rocksalt phases of LGO (I41/amd) by calculating enthalpy surface diagrams for the transformation of β -LGO from the ambient conditions structure (Pna2₁). We explore, for high hydrostatic pressure, β -LGO can undergo transformations into the body center tetragonal (BCT, I41/amd phase structure is shown in Fig. 1.

II. MATERIAL AND METHODOLOGY

We perform density functional theory (DFT) calculations using the generalized gradient approximation (GGA) exchange correlation (XC) functional [11], with the projector augmented wave method (PAW) as implemented in the VASP package [12]. Although the Local Density Approximation (LDA) XC functional [13] has been used more frequently in previous studies [4,14], it is well known that it underestimates lattice constants. On the other hand, while GGA slightly overestimates lattice parameters, it provides fairly accurate relative energies among the different structures at ambient pressure. A typical unit cell for the study of a homogeneous phase transformation consists of 16 atoms (4 Li atoms, 4 Ga atoms, and 8 O atoms), and we used plane wave expansions set up to 520 eV and at least $7 \times 7 \times 7$ Monkhorst-Pack [15] for sampling of the first Bruloin zone, obtaining fully relaxed structures when acting forces on each atom are less than 0.1 meV/Å which allow for total energies convergence of up to 0.1 meV/atom. The stability of each phase can be determined by analyzing the enthalpy as a function of cell shape defined using the ratios c/a and b/a , as described in detail by Jungthawan and Limpijumnong [2]. For different pressure loads, we use distinct equations of state from which we obtain the minimum enthalpy for each combination of c/a - b/a pairs and loading condition. Keep in mind that two minimum enthalpies becoming comparable indicate that those phases are equally favored.

The enthalpy (H) under hydrostatic pressure is defined as



$$H = E + pV, \quad (1)$$

where E is the energy per unit cell, $p = -(\partial E / \partial V)$ is the pressure, and V is the unit cell volume. For each c/a and b/a pairs, V is allowed to relax to minimize H . In principle, for a given p , the c/a and b/a ratios that give the lowest enthalpy define the most stable cell shape. In practice, we give transition path, is taken as the criterion to select the most probable path for individual transformation of β -LGO calculate the enthalpy surface as a function of two independent strain parameters, i.e., c/a and b/a in the range from 0.787 to 0.468 and 0.848 to 0.468, respectively. A total of 36 strained configurations, corresponding to increments of 0.05 in c/a and 0.05 in b/a in the c/a - b/a space (Fig. 2), are investigated. For uniaxial loading, the stability of each crystal and compound can be determined by

$$H\left(\frac{c}{a}, \frac{b}{a}\right) = E(c, b, a) \mp A_{jk} \times \sigma_i q_i, \quad (2)$$

where E is the formation energy, σ_i is the stress along the i direction, q_i is the lattice parameter in the i direction, A_{jk} is the cross section area of the unit cell perpendicular to the stress direction, and $A_{jk} \times \sigma_i q_i$, for compression stress along the c axis, $i = c$, $A_{ab} = ab$ and $q_c = c$, with $-\sigma_c$ being a compressive stress and $+\sigma_c$ a tensile stress. For each strained configuration (each c/a - b/a pair), the energies associated with at least five different unit cells are calculated. An equation of state (energy-volume relation) is obtained by a third-degree polynomial fit.

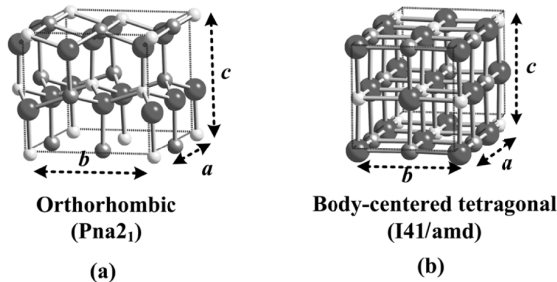


Fig. 1 Schematic illustrations of crystalline structures the ambient and the high-pressure conditions structure: (a) The Orthorhombic (Pna2₁) is the natural state at ambient condition, (b) the body-centered tetragonal (I41/amd) occurs under hydrostatic compression (P_t) and; green spheres represent group Ga cations, blue spheres represent group Li cations and red spheres represent O anions. Parameters a , b and c are indicated.

III. RESULTS AND DISCUSSIONS

We studied two-phase transitions: Pna2₁ to I41/amd and found that the equilibrium hydrostatic pressure for the phase transformations is 3.7 GPa. In order to estimate the equilibrium pressure for a given transition process under hydrostatic pressure, we calculate the common-tangent lines [18,19]. Table I. shows the calculated equilibrium lattice parameters, bulk modulus (B_0), transformation pressures (P_t), stress, and volume for all the different phases studied under pressure conditions. The lattice parameters of these structures

are in good agreement with previous theoretical and experimental data. We calculate enthalpy surfaces for different phase-pairs to further investigate transformations of LGO under high pressure (Fig. 3 and Fig. 4).

For instance, $\Delta H = H^{I41/amd} - H^{Pna21}$, indicates the relative enthalpy of I41/amd with respect to Pna2₁ as a function of lattice parameters, at 0 GPa and 3.7 GPa. At 0 GPa, the minimum occurs for the Pna2₁ structure with (c/a , b/a) = (0.787, 0.848), and at (c/a , b/a) = (0.468, 0.468) for I41/amd, with a $\Delta H = 0.76$ eV (Pna2₁ is more stable), Fig. 2(a). Interestingly, hydrostatic compression ($P_t = 3.7$ GPa) causes the Pna2₁ structure to collapse into the denser phase I41/amd, with a considerable transition energy barrier (1.3 eV) between phases in the phase transformation path, Fig. 2(b) Figures 2(c) and 2(d) show cross-section plots of the enthalpy surfaces curves along $b/a = 0.468$ (red line) and $b/a = 0.848$ (blue line) for 0 GPa and 3.7 GPa, respectively. These values represent the b/a ratio at which the minimum energy values for I41/amd and Pna2₁ structures are found, respectively. From these, we can easily observe that the equilibrium pressure is 3.7 GPa (enthalpy values of both structures become comparable) at hydrostatic pressure conditions.

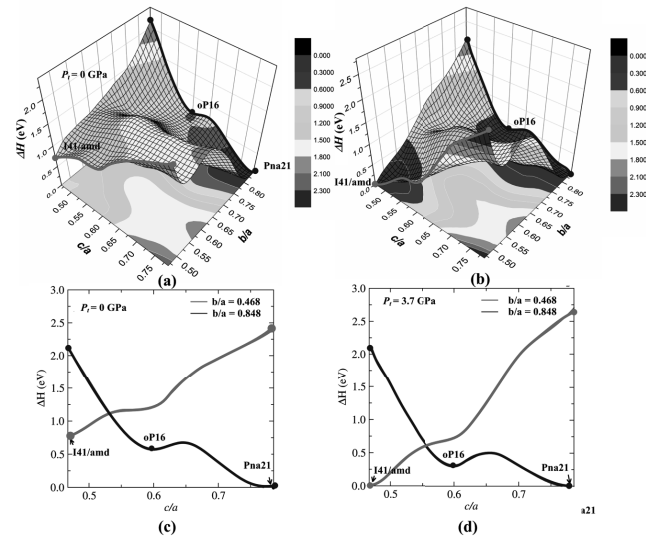


Fig. 2 Enthalpy surface map (eV), and 2-D sections of the enthalpy surface maps for a Pna2₁, oP16 and I41/amd unit cell. Each point on the surface represents the minimum energy volume (V) is allowed to relax while c/a and b/a are kept constant: (a) Enthalpy surface map (eV) at $P_t = 0$ GPa, (b) Enthalpy surface map (eV) at $P_t = 3.7$ GPa, (c) 2-D sections of the enthalpy surface maps at $P_t = 0$ GPa and (d) 2-D sections of the enthalpy surface maps at $P_t = 3.7$ GPa. For $b/a = 0.468$ (red line) and $b/a = 0.848$ (blue line).

The enthalpy surface at our calculated equilibrium transition pressure $P_t = 3.7$ GPa is shown in Fig.3 We can immediately see lowest transformation barrier of 38.8 meV. In the Fig 3(a) we illustrated three transformation paths in the multidimensional c/a - b/a space. The first path (dotted line) corresponds to the transformation induced by a c/a strain (i.e., a parallel strain). Along this path, for each c/a we find b/a with

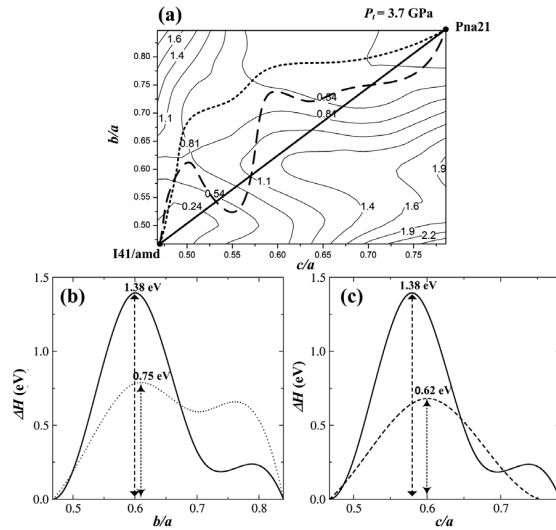


Fig. 3 (a) Contour plot of the minimized enthalpy as a function of c/a and b/a in LGO under the equilibrium transition pressure at $P_t = 3.7$ GPa. Dotted (dashed) line indicates the parallel (in-plane) strain induced transformation path. Solid line indicates the straight diagonal path. (b,c) Minimum enthalpy difference ΔH at the equilibrium transition pressure $P_t = 3.7$ GPa along different paths: dotted line (b), parallel strain induced path; (c), in-line strain induced path; solid lines, straight diagonal path.

TABLE I. SCHEMATIC ILLUSTRATIONS OF LATTICE PARAMETERS, PERCENTAGE CHANGES, BULK MODULUS B_0 , AVERAGE BOND LENGTH AND AVERAGE BOND ANGLES: PNa2₁ AND I41/amd STRUCTURES UNDER THEIR EQUILIBRIUM LOADING CONDITIONS.

Parameter	PNa2 ₁ , $p_f = 0$			I41/amd $p_f = 3.7$ GPa
	Present work	LDA ^{a,b}	Exp ^d	
a (Å)	6.457	6.255 ^a , 6.322 ^b	6.372	8.728
b (Å)	5.479	5.361 ^a , 5.375 ^b	5.402	4.082
c (Å)	5.080	4.953 ^a , 4.996 ^b	5.007	4.082
b/a	0.848			0.468
c/a	0.787			0.468
V (Å ³ /f.u.)	44.93	41.53 ^a , 42.44 ^b	43.09	29.09
ΔV (%)	-			-19.99
Δb (%)	-			-25.50
Δc (%)	-			-19.65
B_0 (GPa)	80.93	95.69 ^b		164.79
Average bond lengths (Å)				
Ga-O	1.896	1.858	1.848	2.029
Li-O	1.988	1.923	1.985	2.161
Average Bond angles (Å ³)				
O-Ga-O	110.21	112.3	109.2	92.21
O-Li-O	108.68	107.5	103.3	90.36

^a VASP code DFT- LDA calculation by A. Boonchun et al.[14]

^b CASTEP code DFT-LDA calculation by Li Lei et al.[16]

^c Piston and cylinder device by M.Mareziro [17]

^d General Electric XRD by M.Mareziro [5]

minimum enthalpy. Following similar logic, the second path (dashed line) corresponds to the transformation induced by a b/a strain (i.e., an in-plane strain). The third path is defined as $[(b/a)-1] = 1.19 [(c/a)-1]$. The cross sections of the enthalpy surface along all three paths clearly show the transformation barrier of around 1.38 eV or 86.25 meV/atom as shown in Fig.3(c). The homogeneous transformation barrier of LGO is higher than transformation barrier of ZnO which reported 37.50 meV/atom [20].

IV. CONCLUSIONS

In conclusion, a detailed study of phase transformations of LGO under high pressure conditions is carried out using first principles enthalpy calculations. We identified metastable phases of LGO (I41/amd) that had not been previously reported, we found that high hydrostatic pressure induces transformations depending the body center tetragonal (BCT, I41/amd), a previously unidentified structure. Interestingly, the LGO rocksalt-like structure (I41/amd) shows a difference behavior from that of its ZnO counterpart, with corresponding enthalpy barriers with is larger than 2 times of 86.25 meV/atom and 37.50 meV/atom, respectively. This indicates that the creation of nucleation regions may be responsible for the phase transformation in both compounds.

ACKNOWLEDGMENT

W. Sailuam wishes to thanks Faculty of Engineering, Rajamangala University of Technology ISAN, Khon Kaen Campus, Thailand for support. Computations were carried out at the Synchrotron Light Research Institute (Public Organization), Thailand.

REFERENCES

- [1] C. Chen, C.-A. Li, S.-H. Yu, and M. M. C. Chou, Journal of Crystal Growth **402**, 325 (2014).
- [2] S. Limpijumong and S. Jungthawan, Physical Review B **70**, 054104 (2004).
- [3] G. Delgado, A. J. Mora, C. Pineda, and T. Tinoco, Mater. Res. Bull. **36**, 2507 (2001).
- [4] T. Kamijoh and K. Kuriyama, J. Cryst. Growth **51**, 6 (1981).
- [5] M. Marezio, Acta Crystallographica 0365-110X **18**, 481 (1965).
- [6] A. Mujica, A. Rubio, A. Muñoz, and R. J. Needs, Rev. Mod. Phys. **75**, 863 (2003).
- [7] S. E. Boulfelfel, D. Zahn, Y. Grin, and S. Leoni, Phys. Rev. Lett. **99**, 125505 (2007).
- [8] S. Limpijumong, W. R. L. Lambrecht, B. Segall, and K. Kim, MRS Online Proceedings Library **449**, null (1996).
- [9] F. Shimojo, S. Kodiyalam, I. Ebbsjö, R. K. Kalia, A. Nakanp, and P. Vashishta, Phys. Rev. B **70**, 184111 (2004).
- [10] K. Sarasamak, A. J. Kulkarni, M. Zhou, and S. Limpijumong, Physical Review B **77**, 024104 (2008).
- [11] J. P. Perdew, K. Burke, and M. Ernzerhof, Physical Review Letters **77**, 3865 (1996).
- [12] G. Kresse and J. Furthmüller, Computational Materials Science **6**, 15 (1996).
- [13] J. P. Perdew and A. Zunger, Physical Review B **23**, 5048 (1981).
- [14] A. Boonchun and W. R. L. Lambrecht, Physical Review B **81** (2010).
- [15] H. J. Monkhorst and J. D. Pack, Physical Review B **13**, 5188 (1976).



- [16] L. Lei, H. Ohfujii, J. Qin, X. Zhang, F. Wang, and T. Irifune, Solid State Communications **164**, 6 (2013).
- [17] M. Marezio and J. P. Remeika, Journal of Physics and Chemistry of Solids **26**, 1277 (1965).
- [18] Y. G. Yu, R. M. Wentzcovitch, T. Tsuchiya, K. Umemoto, and D. J. Weidner, Geophysical Research Letters **34**, n/a (2007).
- [19] W. Sailuam, W. Sarasamak, M. A. M. Polanco and S. Limpijumnon, Ceramics International 43, 376-380 (2017).
- [20]. S. Limpijumnon and S.Jungthawan, Physical Review B 70,054104 (2004)



Performance Testing of Transformers used in Distribution Systems

S. Siriporananon , B. Suechoey , N. Pringsakul
Department of Electrical Engineering, Graduate School
Southeast Asia University, 19/1 Phetkasam Rd., Nongkhaem
Bangkok , Thailand
e-mail : somsaks@sau.ac.th

Abstract— This research is to test the efficiency of three-phase oil immersed distribution transformer system. Routine and type tests are carried out on the topic of temperature rise test of various points and the obtained results were calculated to find the properties of transformer as defined by standards. To conduct the tested with three-phase distribution transformer 50 Hz 22000-400/230 volt power rating 50 kVA , 100 kVA , and 160 kVA according to PEA standards and TIS-384 Standard. According to the testing results of the transformer, it could be known the transformer efficiency. And can be developed into software. To use it in practice for actual operation.

Keywords—distribution transformer; routine test; temperature rise test

I. INTRODUCTION

Transformer which consider such kind of electrical equipment for convert input AC voltage level to desire voltage level, is one of importance equipment in electrical transmission and distribution system [1]. As a result of this, during manufacture process an appropriate test require to perform in order to certify that transformer can be perform well in operation as well as safe. The other factor which must be taken into consideration is transformer loss. Transformer loss are consisting of copper loss and core loss. Copper loss resulting in heat increasing in transformer winding while core loss leading to hysteresis loss. These hysteresis loss generated from primary and secondary winding. Including, eddy current loss or in other word skin effect on conductor surface.

II. THEORY

A. Transformer

Testing of transformer is very importance in order to ensure that these equipment quality, design as follow relevance standard. Transmission transformer require an appropriate test of general specification which follow requirement or not as well as confirm safe operation of transformer during expected accident. Generally, two kinds of test are requiring as follow

1) *Routine Test*: According to regulation, all transformer has to perform routine test under ambient environment conditions as define 10-40 °C with conditions that test outcome has to adjust to reference value at room temperature as illustrates in Table 1. [2],[3]

TABLE I. REFERENCE TEMPERATURE

Insulation Temperature Class	Reference Temperature (°C)
Class A,E,B	75
Class F,H	115

Routine test are as follows :

a) *Measurement of winding resistance which can be classify into two methods.*

- Measurement from primary side.
- Measurement from secondary side.

b) *Measurement of voltage ratio and check of phase displacement.*

The transformer ratio can be determined as per state in Eq. (1)

$$\text{Ratio} = \frac{V_{P(\text{rated})}}{V_{S(\text{rated})}} \quad (1)$$

Where;

$V_{P(\text{rated})}$ = Primary Voltage

$V_{S(\text{rated})}$ = Secondary Voltage

c) *Measurement of short circuit impedance and load loss.*

$$\text{Load loss at } 75^{\circ}\text{C} = (P_{\text{CU}} \times k) + \left(\frac{P_{\text{SC}} - P_{\text{CU}}}{k} \right) \quad (2)$$

$$k = \frac{225 + 75}{225 + \text{Temp}} \quad (3)$$



$$\%Z = \sqrt{\%R^2 + \%X^2} \quad (4)$$

$$\%R = \frac{\text{load loss at } 75^\circ\text{C}}{S} \times 100 \quad (5)$$

$$\%X = \sqrt{\left(\frac{V_{SC(\text{ave})}}{V_{P(\text{rated})}} \times 100\right)^2 - \left(\frac{P_{SC}}{S} \times 100\right)^2} \quad (6)$$

$$\text{Voltage Regulation} = \%R + \left(\frac{\%X^2}{200}\right) \quad (7)$$

Where;

235 = Copper constant

225 = Aluminum constant

75 = Reference temperature ($^\circ\text{C}$)

Temp = Ambient Temperature ($^\circ\text{C}$)

P_{SC} = Loss during supply load (W)

$V_{SC(\text{ave})}$ = Average Voltage during supply load (V)

S = Transformer rated (VA)

$\%Z$ = Impedance

$\%R$ = Resistance

$\%X$ = Reactance

d) Measurement of no load loss.

$$\%\text{No load current} = \frac{I_{OC(\text{ave})}}{I_{P(\text{rated})}} \times 100 \quad (8)$$

$$\eta \text{ at } 75^\circ\text{C} = \frac{S}{S + \text{No load loss} + \text{load loss at } 75^\circ\text{C}} \times 100 \quad (9)$$

$$\text{Total losses at } 75^\circ\text{C} = \text{No load loss} + \text{Load loss at } 75^\circ\text{C} \quad (10)$$

Where;

$I_{OC(\text{ave})}$ = Average current during no-load condition (A)

$I_{P(\text{rated})}$ = Rated current at primary (A)

$\eta \text{ at } 75^\circ\text{C}$ = Efficiency at 75°C

2) Type Test: These type test are perform based on request. The test includes as express below:

a) Temperature rise: The purpose for temperature rise test are identify temperature rise on top oil during steady-state and temperature rise on winding as show the criteria in Table 2. [4],[5].

TABLE II. .. Limitation of temperature rise

	Temperature rise ($^\circ\text{C}$)
Top Oil	60
Winding	65

III. EXPERIMENT

A. List of equipment

- Thermometer Tesio Model:TM-4808
- Thermocouple Type K
- Digital Micro Ohm Meter (Micro Junior 2)
- Transformer Turns Ratio Meter (TR-Mark 3)
- Clam On Power Hitester (HIOKI 3169-20)
- Transformer 50 kVA 3ph 22,000-400/230 V Dyn11

B. Units Method and Result

Experiment procedure can be discussing as show in flowchart Fig 1. [6],[8].

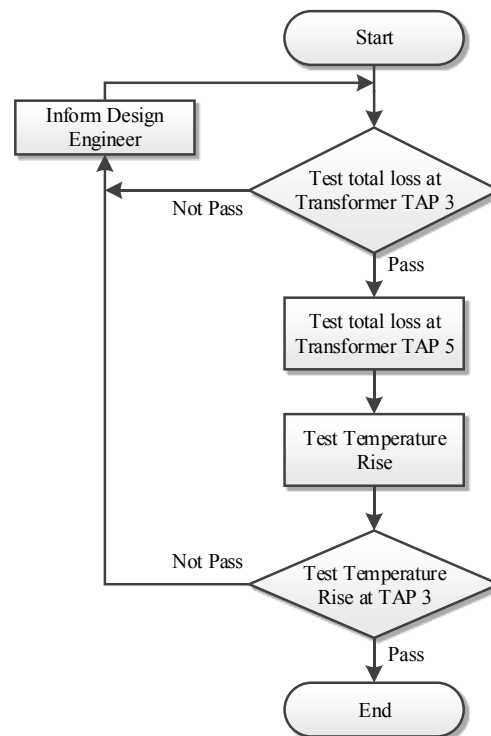


Fig 1. Flowchart of experiment

1) Procedure for Routine Test

a) Understanding detail of transformer by reading through nameplate

b) Recording ambient temperature as well as resistance as

c) Perform experiment to access total loss under both load and no-load conditions.

- By input voltage at secondary side of transformer at rated voltage, the connected circuit as per shows in Fig 2. and the result shows in Fig 3

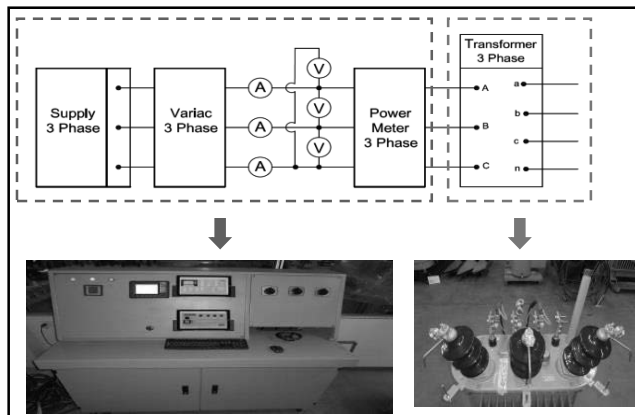


Fig 2. Test circuit for open circuit

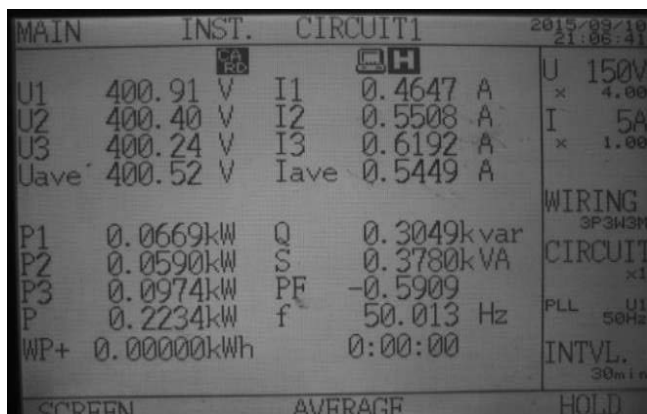


Fig 3. Open Circuit Result

- Next, perform short circuit at secondary side of transformer and input current at primary side rated by connected circuit as show in Fig 4. and test result are show in Fig 5

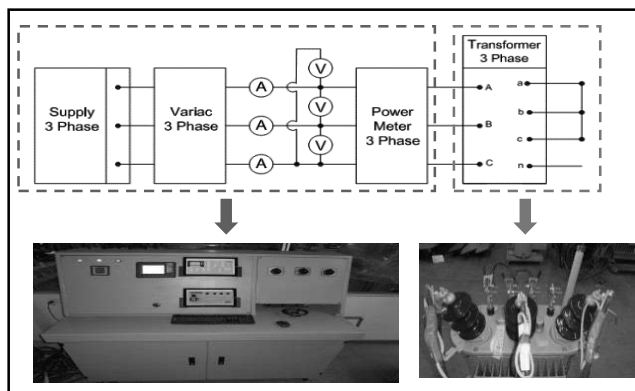


Fig 4. Test circuit for short circuit

- Perform calculation all parameter as well as transformer loss.

- Perform test to determine total loss of transformer at tap 5 which similar procedure to test on tap 3

2) Procedure for test temperature rise

- Perform short circuit at transformer secondary side and supply voltage at primary side until wattmeter reading loss as total transformer loss as

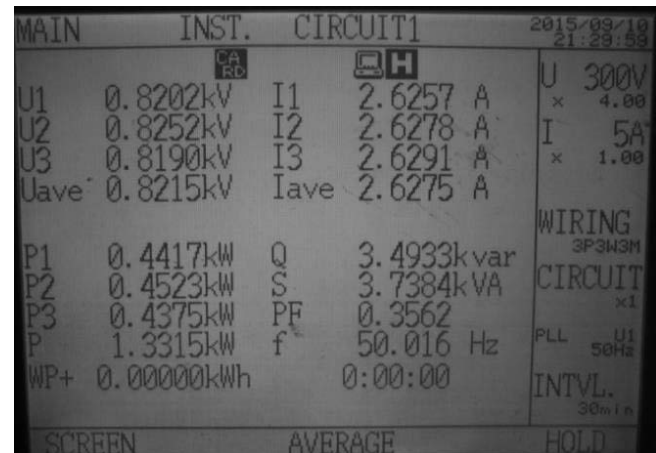


Fig 5. Short Circuit Result

- Record data by recording current, voltage and total loss of transformer by interval one hour until oil temperature reach steady state. The steady state is defined that temperature are steady three hours with deviation on range $\pm 0.5^\circ\text{C}$ as show in Fig 6. After that shutdown supply power and perform recording the resistance

TIME	VT	IT	W	1.AMB	2.AMB	3.AMB	4.AMB	AV.AMB	5. OIL	6.TOP	7.MEDIUM	8.BUNDER	TOP OIL
22:40:06	864.6	3.1829	1797.8	28.79	28.75	28.34	28.52	28.80	28.80	30.04	30.00	29.67	0.00
23:40:06	839.4	3.0459	1792.4	28.58	28.51	28.07	28.37	28.38	40.73	39.54	34.63	13.92	
0:40:06	836.2	2.9971	1792.6	28.29	28.20	27.81	28.03	28.08	51.16	49.76	47.94	39.97	23.08
1:40:06	834.2	2.9973	1790.2	28.37	28.15	27.79	28.02	28.09	57.28	55.55	52.46	43.47	29.19
2:40:06	824.2	2.9554	1790.6	28.13	28.21	27.69	27.96	28.00	61.49	59.62	56.57	46.11	33.49
3:40:06	817.6	2.9315	1789.3	28.23	28.03	27.66	27.90	27.96	64.16	62.16	58.66	47.91	36.21
4:40:06	822.4	2.946	1791.6	28.31	28.10	27.81	28.04	28.06	65.98	63.57	60.05	49.21	37.91
5:40:06	807.7	2.8888	1792.1	28.30	27.89	27.66	27.80	27.92	67.17	64.64	60.84	49.99	39.26
6:40:06	827.4	2.9541	1789.6	28.15	27.92	27.59	27.88	27.89	67.97	65.12	61.65	50.71	40.08
7:40:06	820.8	2.9283	1788.6	28.31	28.52	28.07	28.24	28.29	68.60	65.80	62.77	50.89	40.31
8:40:06	821.6	2.9348	1791.6	29.53	29.28	29.16	29.28	29.31	69.61	66.56	63.19	51.89	40.30
9:40:06	814.9	2.9112	1792.9	30.45	30.44	30.36	30.90	30.54	70.82	67.34	63.88	53.47	40.28
10:40:06	762.3	2.766	1600.1	31.22	31.24	30.88	31.50	31.21	71.54	67.88	65.06	53.84	40.33
11:40:06	774.6	2.764	1600.6	31.87	31.75	31.62	32.03	31.82	68.16	64.57	62.21	53.28	36.34
12:40:06	780.7	2.765	1636.8	31.81	31.70	31.77	31.95	31.81	69.76	66.38	64.03	54.97	37.95

Fig 6. Result of temperature rise

IV. RESULTS

A. Routine Test

From routine test result of 50 kVA , 100 kVA and 160 kVA 3 Phase 50 Hz 22 kV/400-230 V are satisfy the standard requirement [2],[7],[9].

The test results are reveal as show in Table 3,4 and 5.



TABLE III. Routine test of transformer rated 50 kVA

Parameter	Test Result	
	Tap 3 (Routine Test)	Tap 5 (Temperature Rise)
No-Load Current (%)	0.59	0.59
No-Load Loss (W)	142	142
Load Loss at 75 °C (W)	942.07	968.64
Impedance Voltage at 75 °C (%)	3.98	3.96
Efficiency at 75 °C (%)	97.88	97.83
Voltage Regulation at 75 °C (%)	1.95	2.00
Total Losses at 75 °C (W)	1084.09	1110.64

Table IV. Routine test of transformer rated 100 kVA

Parameter	Test Result	
	Tap 3 (Routine Test)	Tap 5 (Temperature Rise)
No-Load Current (%)	0.38	0.38
No-Load Loss (W)	223.4	223.4
Load Loss at 75 °C (W)	1536.76	1564.29
Impedance Voltage at 75 °C (%)	3.81	3.68
Efficiency at 75 °C (%)	98.27	98.24
Voltage Regulation at 75 °C (%)	1.60	1.62
Total Losses at 75 °C (W)	1760.16	1787.60

Table V. Routine test of transformer rated 160 kVA

Parameter	Test Result	
	Tap 3 (Routine Test)	Tap 5 (Temperature Rise)
No-Load Current (%)	0.38	0.38
No-Load Loss (W)	312.7	312.7
Load Loss at 75 °C (W)	2094.78	2214.69
Impedance Voltage at 75 °C (%)	4.09	4.39
Efficiency at 75 °C (%)	98.52	98.44
Voltage Regulation at 75 °C (%)	1.38	1.47
Total Losses at 75 °C (W)	2407.48	2527.39

B. Result for type test and transformer temperature by perform short circuit Test

From the experiment perform by transformer rated 50 kVA, 100 kVA and 160 kVA 3 Phase 50 Hz 22 kV/400-230 V at each position show that the result as follow industrial standard [2]. As show in Fig 7, 8 and 9. And Table 6. Through Table 8.

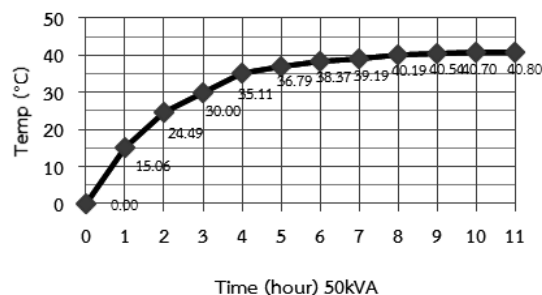


Fig 7. Transformer rated 50 kVA top oil temperature

Table VI. Specific test of transformer rated 50 kVA

Parameter	Test Result
Total losses (W)	1110.64
Hottest spot of top oil (°C)	70.22
Hottest spot of LV.wdg (°C)	76.22
Hottest spot of HV.wdg (°C)	89.24
Top oil temp. rise (°C)	40.70
LV.wdg temp. rise (°C)	46.76
HV.wdg temp. rise (°C)	58.19
Amb. Top oil (°C)	29.52
Amb. LV.wdg (°C)	29.46
Amb. HV.wdg (°C)	31.05

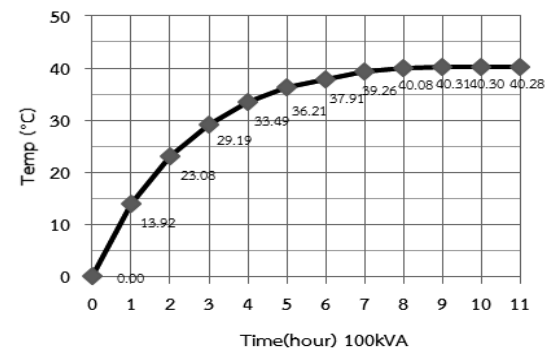


Fig 8. Transformer rated 100 kVA top oil temperature

Table VII. Specific test of transformer rated 100 kVA

Parameter	Test Result
Total losses (W)	1787.69
Hottest spot of top oil (°C)	70.82
Hottest spot of LV.wdg (°C)	76.92
Hottest spot of HV.wdg (°C)	86.41
Top oil temp. rise (°C)	40.28
LV.wdg temp. rise (°C)	45.71
HV.wdg temp. rise (°C)	54.60
Amb. Top oil (°C)	30.54
Amb. LV.wdg (°C)	31.21
Amb. HV.wdg (°C)	31.81

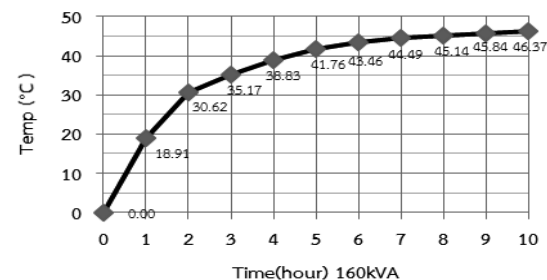


Fig 9. Transformer rated 160 kVA top oil temperature



Table VIII. Specific test of transformer rated 160 kVA

Parameter	Test Result
Total losses (W)	2527.39
Hottest spot of top oil (°C)	74.66
Hottest spot of LV.wdg (°C)	82.67
Hottest spot of HV.wdg (°C)	87.23
Top oil temp. rise (°C)	46.37
LV.wdg temp. rise (°C)	54.28
HV.wdg temp. rise (°C)	59.03
Amb. Top oil (°C)	28.29
Amb. LV.wdg (°C)	28.39
Amb. HV.wdg (°C)	28.20

C. Result by designation mathematic equation

From experiment of temperature rise. It reveals that temperature increasing on transformer oil of each transformer size can be express by polynomial equation R^2 as shows in Fig 10-12.

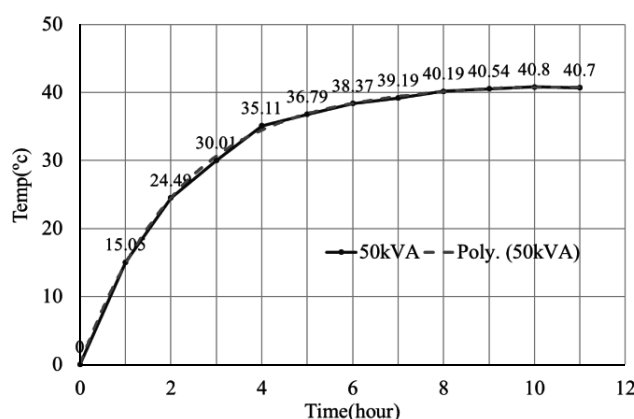


Fig 10. Temperature rise of 50 kVA transformer when compare with polynomial equation

From Fig 10. Can be determine polynomial equation and R^2 as state in Eq. 11 and 12.

$$y = 0.0004x^5 - 0.0199x^4 + 0.3693x^3 - 3.5117x^2 + 17.9x - 0.0797 \quad (11)$$

$$R^2 = 0.9995 \quad (12)$$

From Fig 11. Can be determine polynomial equation and R^2 as state in Eq. 13 and 14.

$$y = 0.0006x^5 - 0.0241x^4 + 0.377x^3 - 3.2704x^2 + 16.771x - 0.0159 \quad (13)$$

$$R^2 = 1 \quad (14)$$

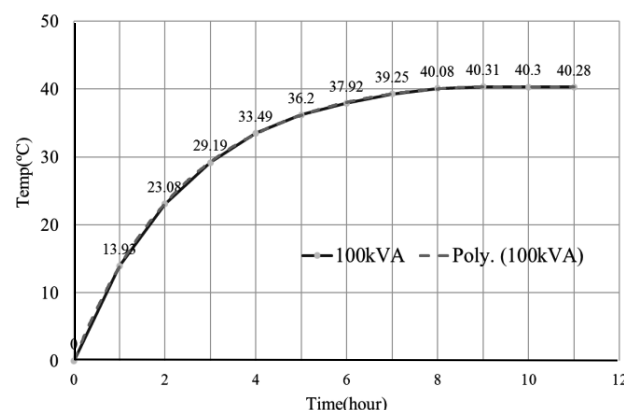


Fig 11. Temperature rise of 100 kVA transformer when compare with polynomial equation

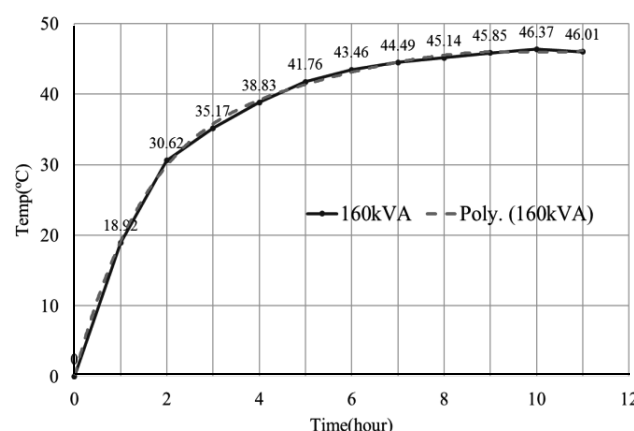


Fig 12. Temperature rise of 160 kVA transformer when compare with polynomial equation

From Fig 12. Can be determine polynomial equation and R^2 as state in Eq. 15 and 16.

$$y = 0.0019x^5 - 0.0689x^4 + 0.9518x^3 - 6.5914x^2 + 24.843x - 0.0025 \quad (15)$$

$$R^2 = 0.9992 \quad (16)$$

V. CONCLUSION

A. Routine Test

From routine test result of 50 kVA , 100 kVA and 160 kVA 3 Phase 50 Hz 22 kV/400-230 V are satisfy with industrial standard [2].

B. Type Test

From type test result of 50 kVA , 100 kVA and 160 kVA 3 Phase 50 Hz 22 kV/400-230 V are satisfy with industrial standard [2].



C. Performance Test

From performance test result of 50 kVA , 100 kVA and 160 kVA 3 Phase 50 Hz 22 kV/400-230 V

Performance testing of 50 kVA = 97.827%

Performance testing of 100 kVA = 98.243%

Performance testing of 160 kVA = 98.445%

From the above results, they show that the proposed program can work well. It is the good tool for testing transformer, and it reduces expenses, time and error that occurred from human the research in future is to add some tool in order to the proposed program is completed.

ACKNOWLEDGMENT

The authors would like to acknowledge T.D.TRANSFORMER CO., LTD., Thailand, for supporting data used in this research.

REFERENCES

- [1] B. Suechoey, "Distribution Transformer Design," Graduate School Southeast Asia University, page. 151-164, 2007.
- [2] TIS 384, Power Transformer Bangkok, Thailand, 2000.
- [3] IEC 600354, Loading Guide for Oil-Immersed Power Transformer, 2006.
- [4] IEC 60076-2, Power Transformer Part 2 : Temperature Rise, 2011.
- [5] Provincial Electricity Authority (PEA) Thailand, Three-Phase Transformer for 22 kV and 33 kV Distribution Systems with Ability to Withstand Short Circuit, Specification No. RTRN-035/2558, 2015
- [6] ANSI/IEEE C57.12.00, An American National Standard IEEE Standard General Requirements for Liquid-Immersed Distribution, Power, and Regulating Transformers, 1993
- [7] ANSI/IEEE C57.91, IEEE Guide for Loading Mineral Oil-Immersed Overhead and Pad Mounted Distribution Transformer Rated 500 kVA and Less with 65 °C or 55°C Average Winding Rise, 1981
- [8] B. Suechoey, N. Chotiwanaporn, P. Jayasak and C. Chompoo-inwai, "Proposition of Individual Guide for Distribution Transformer Design to Withstand Short Circuit Condition," in Proceedings of The 20th IEEE International Conference on Electrical Engineering, Ramada Plaza Jeju Hotel, Jeju, Korea, 15-19 June 2014.
- [9] B. Suechoey, S. Tadsuan, C. Thammarat and M. Leelajindakraierk, "An Analysis of Temperature and Pressure on Loading Oil-Immersed Distribution Transformer," in Proceedings of The 7th International Power Engineering Conference, Marina Mandarin Hotel, Singapore, 29 November – 2 December 2005.



Implementation of Load Cycle Simulation for Studies of Loss Energy and Lifetime of Oil-Immersed Transformers

B. Suechoey¹, S. Siriporananon³, N. Pringsakul⁴

^{1,3,4}Department of Electrical Engineering
Graduate School, Southeast Asia University
19/1 Phetkasam Rd. Nongkhaem, Bangkok, Thailand
e-mail : tdlert@hotmail.com

A.Thongrak²

²Dept. of Electronics and Telecommunication Engineering
Faculty of Engineering, RMUTP
1381 Pracharat Rd. Bangsue, Bangkok, Thailand
e-mail : aphichata.t@rmutp.ac.th

Abstract—This paper studies about the decrease of loss energy and the extension for the lifetime of Oil-Immersed transformers. The simulation of a load cycle when parallel connected is compared with individual connected of two transformers. Loss energy, Top oil temperature, Hottest-spot, Loss of Life and Life are calculated in the studies. The results of research applicable to the field work and useful for determining the limit load of transformer, The protection from overheat and an economic aspect of transformer.

Keywords— Loss Energy; Hottest-spot Temperature

I. INTRODUCTION

Technique, for reducing energy loss and for increasing the transformer life, must be considered to reduce the production cost and to increase the income profit. The thermal behavior in windings depend on the transformer at no load and on load. This will be indicated the transformer efficiency. For example, if the temperature in windings is low below the normal, the transformer will supply the load current more than the rated. On the other hand, if the temperature in windings is high above the normal, the transformer will supply the load current less than the rated. $P_{loss} = i^2 R$, R = resistance in the conductor, vary to the temperature. So the factor, to limit the load transformer current, is the temperature, such as the hot spot on the conductor, on top oil temperature and including the ambient temperature. For detail, about the energy losses and the transformer life, will be explained in the following paragraph.

II. METHOD OF ANALYSIS

The degrading of the insulator life depend on the function of temperature and time. While consideration the function of the insulator, will have the different effect, such as at the hottest spot will degrade more than the other parts. So the study of insulator life effect on the transformer was made by the consideration at the hottest spot.

From [1,2], we assumed that the degrading of the insulator is corresponding to Arrhenius equation, said that the function of the insulator life is like an algorithm as (1).

$$\text{Log}_{10} \text{ life (hour of life)} = A + \frac{B}{T} \quad (1)$$

Where; A , B = the constant according to table 1

TABLE I. OIL-IMMERSED TRANSFORMER PARAMETER (A , B) AT VARIABLE KVA FROM [2,3,4]

Transformer capacity	Average winding temp. rise °C	A	B
Rated 500 kVA and less	65	-11.269	6328.8
	55	-11.968	6328.8
Rated 500 kVA-100 MVA	65	-30.834	16054.0
	55	-32.543	16054.0
More than 100 MVA	65	-13.391	6972.15

So we get the hour of life as follows

$$\text{hour of life} = 10^{\left(A + \frac{B}{T}\right)} \quad (2)$$

According to the inverse of the insulator life is loss of life, we get the result as follows.

$$\text{Loss of Life} = 10^{-\left(A + \frac{B}{T}\right)} \quad (3)$$

Where; $T = \Theta_h + 273$

Observing (3), Also, while considering in interval time, t . We get as follows.

$$\text{Loss of Life} = t \times 10^{-\left(A + \frac{B}{T}\right)} \quad (4)$$

From (4), we can apply only the time at $T(\Theta_{hs} + 273)$, but in the real world, there are many the levels of all interval time at $T(\Theta_{hs} + 273)$. So the total loss of life becomes.



$$\text{Total Loss of Life} = \left(\sum_{t=1}^{l=n} 10^{-\left(A+\frac{B}{T}\right)} \right) \quad (5)$$

So the transformer life, which invert to total loss of life, is

$$\text{Life} = \frac{1}{\text{Total Loss of Life}} = \frac{1}{\left(\sum_{t=1}^{l=n} 10^{-\left(A+\frac{B}{T}\right)} \right)} \quad (6)$$

And the other corresponding equations are as follows.

A. At steady state condition

$$\Theta_{ou} = \Theta_{or} \left[\frac{1 + RK^2}{1 + R} \right]^n \quad (7)$$

$$\Theta_h = \Theta_a + \Theta_{or} \left[\frac{1 + RK^2}{1 + R} \right]^n + \Theta_{gr} \cdot K^{2n} \quad (8)$$

B. At transient condition

$$\Theta_{ot} = \Theta_{oi} + (\Theta_{ou} - \Theta_{oi}) \left(1 - e^{-\frac{t}{\tau}} \right) \quad (9)$$

$$\Theta_h = \Theta_a + \left[\Theta_{oi} + (\Theta_{ou} - \Theta_{oi}) \left(1 - e^{-\frac{t}{\tau}} \right) \right] + \Theta_{gr} \cdot K^{2n} \quad (10)$$

$$K = \frac{I}{I_{rated}} = \frac{S}{S_{rated}} \quad (11)$$

Where; τ is Oil time constant, h; R is ratio of load loss at rated load to no-load loss; Θ_{or} is top-oil rise over ambient at rated load, °C; Θ_{or} is hottest-spot conductor rise over top-oil at rated load, °C; Θ_{oi} is initial top-oil rise over ambient at start of time interval, °C; Θ_{ou} is ultimate top-oil rise over ambient for any load K, °C; Θ_{ot} is top-oil rise for any load at transient condition, °C; Θ_h is hottest-spot conductor, °C; Θ_a is ambient temperature, °C; K is load expressed in per unit of transformer nameplate rating; and n is constant

While loading the transformer, the ambient temperature must be considered significantly as in [5,6], with double sinusoidal function, as follows

$$\Theta_a = \Theta_{ay} + A_{year} \cos \left[\frac{2\pi}{365} (\text{day} - DX) \right] + B_{day} \cos \left[\frac{2\pi}{24} (\text{hour} - TX) \right] \quad (12)$$

Where; Θ_{ay} is average ambient temperature per year, °C; A_{year} is the amplitude of yearly variation of daily mean ambient temperature, °C; B_{day} is the amplitude of daily variation of ambient temperature, °C; DX is the hottest day of a year; TX is the hottest hour of the day; day is the day number; and hour is the hour of the day.

For the total power loss and all day energy loss of transformer are showed in (13) and (14) respectively, by

$$P_T = P_{(core_rated)} + (K^2 \times P_{(cu_rated)}) \quad (13)$$

$$W_T = [P_{(core_rated)} \times 24] + \sum_{m=1}^{m=24} (K_m^2 \times P_{(cu_rated)}) \quad (14)$$

Where; W_T is total energy loss of transformer in any day, Wh/day; P_T is total loss of transformer, W; $P_{(core_rated)}$ is no load loss, W; $P_{(core_rated)}$ is load loss, W; and m is number of hour 1,2,3,...,24.

III. SIMULATION AND RESULTS

Two equipped transformers, with the same parameters corresponding to [1], shown in Table 2, are assumed to be taken place in simulation method as in Fig.1, with calculation flow chart as Fig.2.

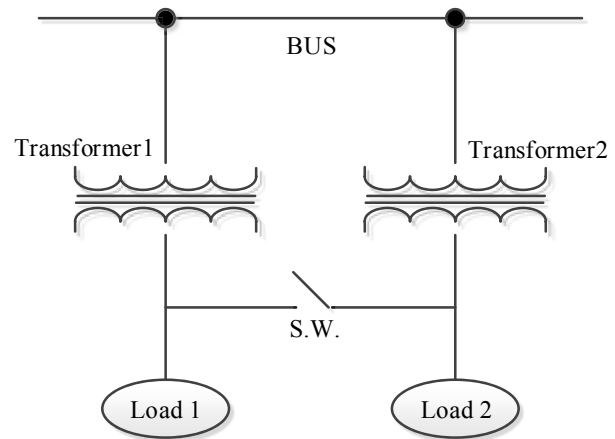


Fig. 1. Single line diagram of transformer

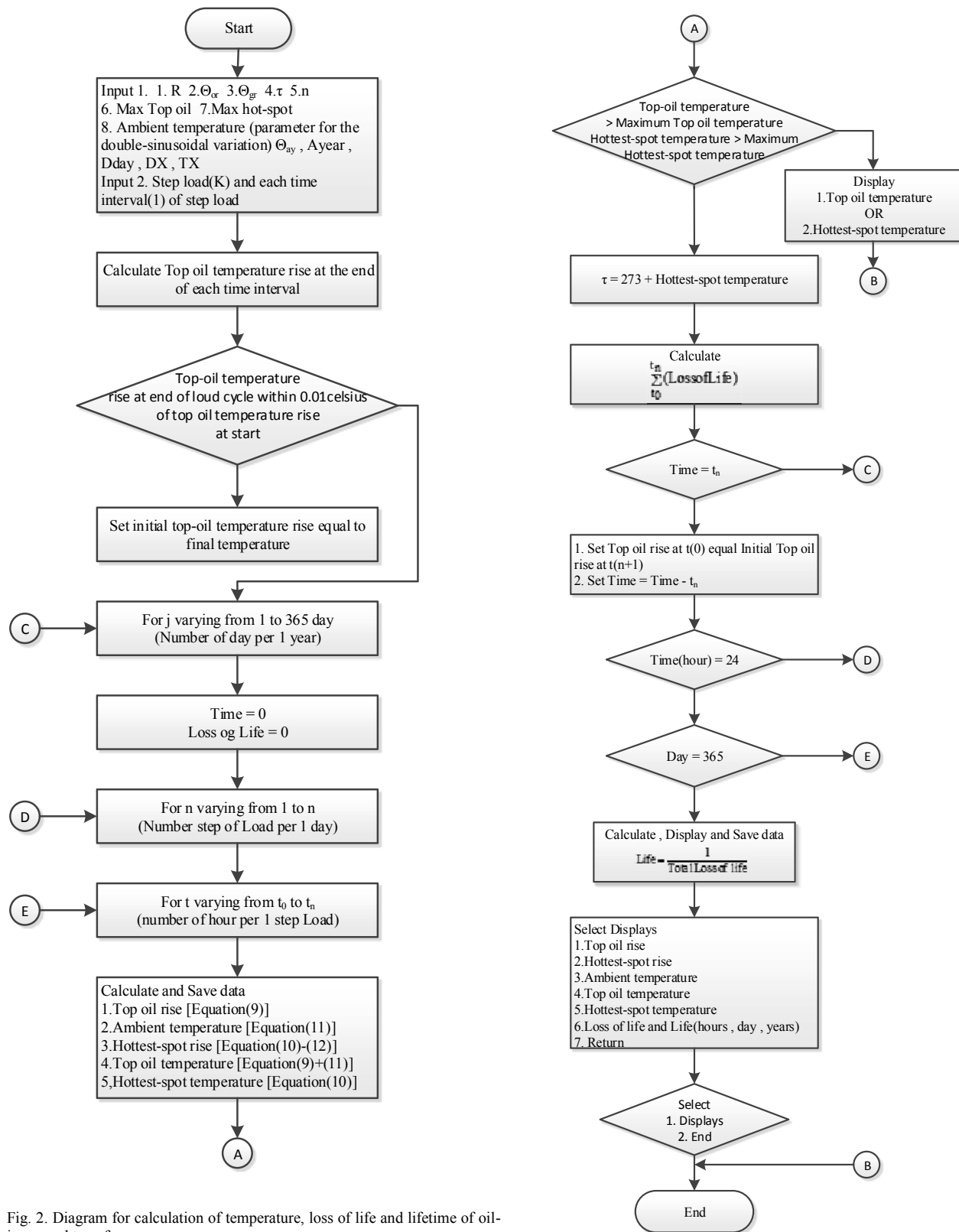


Fig. 2. Diagram for calculation of temperature, loss of life and lifetime of oil-immersed transformer

a. Max Top Oil Temp and Max Hottest-spot from [5-6]

Rated = 500 kVA	$\Theta_{or} = 55$	$\Theta_{gr} = 20$
R = 2.7	$\mathfrak{T} = 3.5$	N = 0.8
Max Top Oil Temp. rise = 60 °C ^a	Max Hottest-spot = 140 °C ^a	
Average winding Temp. rise = 65 °C		$\Theta_{ay} = 30$ °C
A _{year} = 8	B _{day} = 5	DX = 110 TX = 14

a. Max Top Oil Temp and Max Hottest-spot from [5-6]

The result of prediction, top oil temperature and hottest spot or lifetime, will be equaled with practical by using the ambient temperature for each local existing transformer in recent year [6]. From Fig. 3 is load cycle of the first transformer is equipped in parallel. And Fig. 4, the two transformer is equipped in parallel. Also the simulation results are summarized in Fig 5.6 and Table 3.

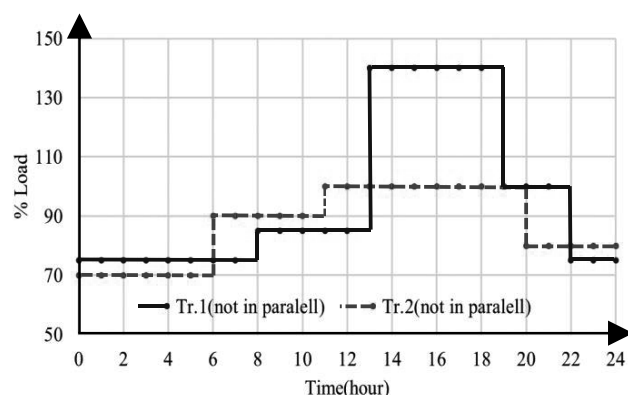


Fig. 3. Load cycle of transformer (not in parallel)

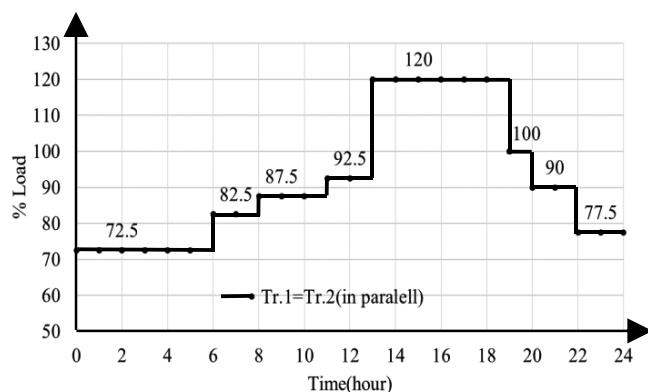


Fig. 4. Load cycle in parallel transformer

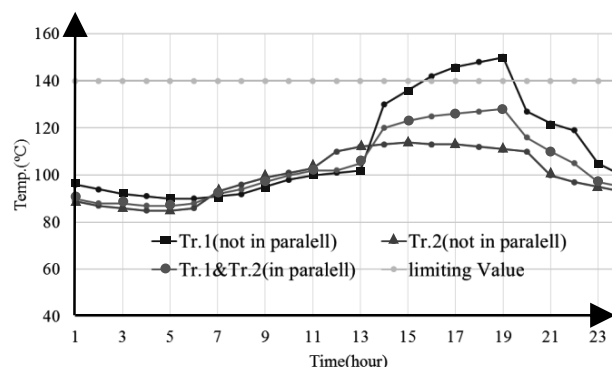


Fig. 5. Compare of hottest-spot temp. (not in parallel / in parallel)

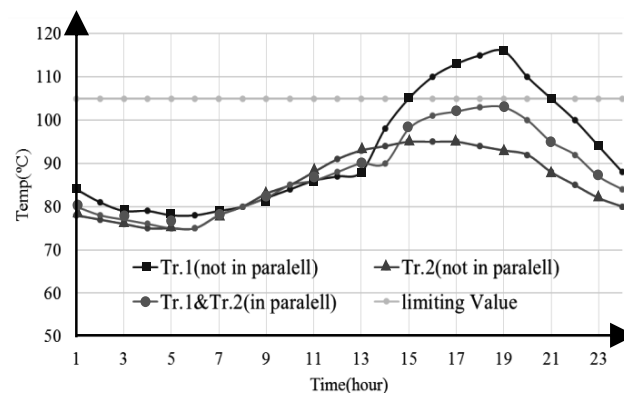


Fig. 6. Compare of top oil temp. (not in parallel / in parallel)

TABLE III. % LOSS OF LIFE AND LIFE TIME

	% Loss of life	Life time
Transformer 1 (not in parallel)	18.8397	5.307927
Transformer 2 (not in parallel)	1.7886	20
Parallel transformer	4.8746	20

During the simulation process, we assumed that the rated on load power loss is according to Provincial Electricity Authority (PEA), at 500kVA, 22kV-400/230 V = 4,950/R, where R from name plate = 2.7. And the no load power loss is 1,833.33 W. For the results from calculation are shown in fig. 7-9 and Table 4.

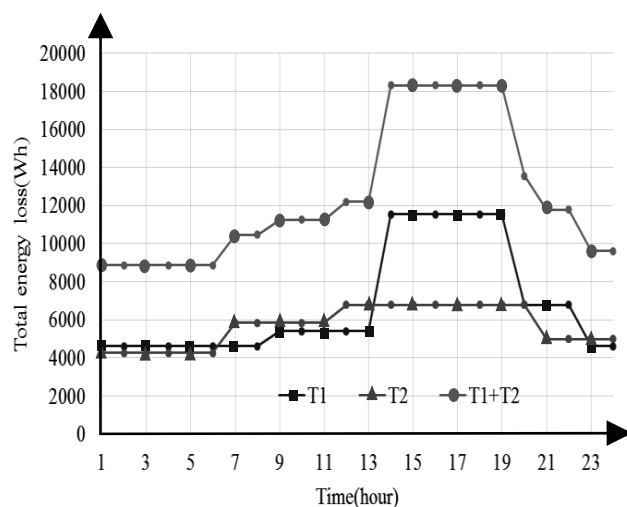


Fig. 7. Total energy loss of transformer (not in parallel)

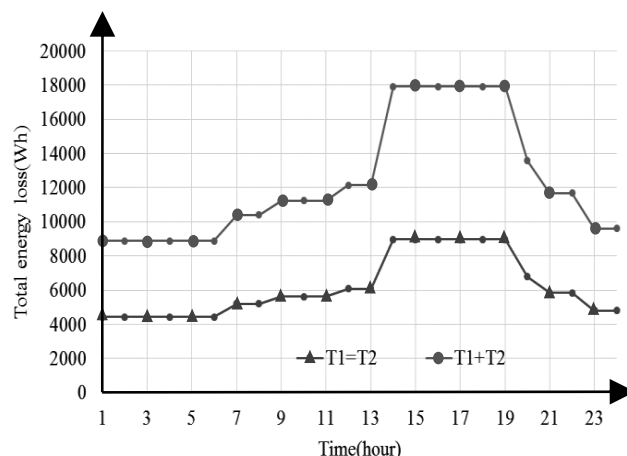


Fig. 8. Total energy loss of transformer (in parallel)

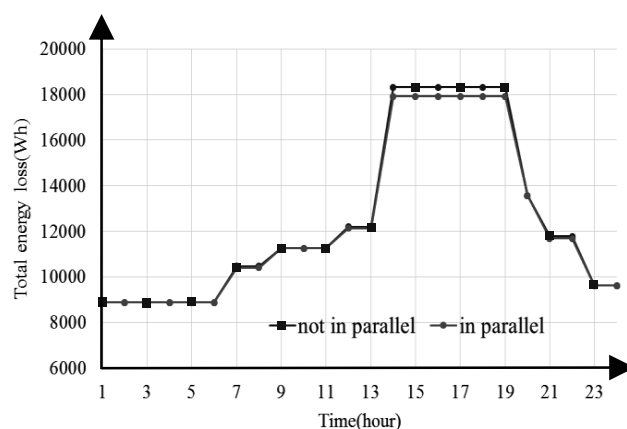


Fig. 9. Total energy loss of transformer comparison (not in parallel/in parallel)

TABLE IV. ENERGY LOSS OF TRANSFORMER COMPARISON (NOT IN PARALLEL/IN PARALLEL)

h	Not in parallel			In parallel		
	T1	T2	T1+T2	T1	T1=T2	T1+T2
1	4617.7	4258.8	8876.5	4435.2	4435.2	8870.4
2	4617.7	4258.8	8876.5	4435.2	4435.2	8870.4
3	4617.7	4258.8	8876.5	4435.2	4435.2	8870.4
4	4617.7	4258.8	8876.5	4435.2	4435.2	8870.4
5	4617.7	4258.8	8876.5	4435.2	4435.2	8870.4
6	4617.7	4258.8	8876.5	4435.2	4435.2	8870.4
7	4617.7	5842.8	10460.5	5202.4	5202.4	10404.8
8	4617.7	5842.8	10460.5	5202.4	5202.4	10404.8
9	5409.7	5842.8	11252.5	5623.2	5623.2	11246.4
10	5409.7	5842.8	11252.5	5623.2	5623.2	11246.4
11	5409.7	5842.8	11252.5	5623.2	5623.2	11246.4
12	5409.7	6783.3	12193	6068.7	6068.7	12137.4
13	5409.7	6783.3	12193	6068.7	6068.7	12137.4
14	11535.3	6783.3	18318.6	8961.33	8961.33	17922.66
15	11535.3	6783.3	18318.6	8961.33	8961.33	17922.66
16	11535.3	6783.3	18318.6	8961.33	8961.33	17922.66
17	11535.3	6783.3	18318.6	8961.33	8961.33	17922.66
18	11535.3	6783.3	18318.6	8961.33	8961.33	17922.66
19	11535.3	6783.3	18318.6	8961.33	8961.33	17922.66
20	6783.3	6783.3	13566.6	6783.3	6783.3	13566.6
21	6783.3	5001.33	11784.63	5842.83	5842.83	11685.66
22	6783.3	5001.33	11784.63	5842.83	5842.83	11685.66
23	4617.3	5001.33	9619	4806.4	4806.4	9612.8
24	4617.3	5001.33	9619	4806.4	4806.4	9612.8

IV. CONCLUSION

The life of a transformer depends significantly on the thermal behavior in windings, and the simulation results are summarized as follows:

- To reduced the power loss while loading higher power, the transformers are equipped better in parallel than not in parallel. Not in parallel, the power loss is 298.60896 kWh/day, and, in parallel, the power loss is 295.74548 kWh/day. The different is 2.86348 kWh/day, not more significantly different in a short period but more significantly different in a long period. And, while loading lower power, the single transformer may be less power loss than equipped transformers in parallel. So, before doing this, the first action is to calculate and check the result.
- The transformers, equipped in parallel, will extent the lifetime of the transformer. As the simulation results,



the average lifetime of the transformer, not equipped in parallel, is approximate $(5.31+20)/2 = 12.655$ years, and, the average lifetime of the transformer, equipped in parallel, is 20 years, 7.345-years extension for the lifetime.

ACKNOWLEDGMENT

The authors would like to acknowledge T.D.TRANSFORMER CO., LTD., and PHONGPIMARN ELECTRIC CO., LTD., Thailand, for supporting data used in this research.

REFERENCES

- [1] S.L. Cress, 1989, "Transformer Loss-of-Life Calculation Using a Computerized Probabilistic Method," CIRED Reproduced with permission of copyright owner, Further reproduction prohibited., 1989, pp. 57-61,
- [2] ANSI/IEEE C57.91-1995, IEEE Guide for Loading Mineral-Oil-Immerse Overhead and Pad-Mounted Distribution Transformers Rated 500 kVA and Less with 65°C or 55°C Average Winding Rise, 1995.
- [3] ANSI/IEEE C57.92-1995, IEEE Guide for Loading Mineral-Oil-Immerse Overhead and Pad-Mounted Power Transformers, up to and including 100 MVA with 65°C or 55°C Average Winding Rise, 1995.
- [4] ANSI/IEEE C57.115-1995, IEEE Guide for Loading Mineral-Oil-Immerse Overhead and Pad-Mounted Power Transformers rated in excess of 100 MVA 65°C Winding Rise, 1995.
- [5] IEC 600354, Loading Guide for Oil-Immersed Power Transformer, 2006.
- [6] Provincial Electricity Authority Thailand (PEA), Three Phase Transformer for 22 kV and 33 kV Distribution Systems with Ability to Withstand Short Circuit, Specification No. RTRN-035/2558, 2015.
- [7] TIS 384-2543, Power Transformer, 2000.
- [8] B. Suechoey, S. Bunjongjit and M.kando, "The Result Analysis of Economic Distribution Transformer Design in Thailand," IEEE/PES T&D Conference 2002: Asia Pacific, 6-10 October 2002, Yokohama Japan.



Low Cost Submarine for Under Water

Nattapong Phanthuna

Faculty of Engineering
Rajamangala University of Technology Phra Nakhon
Bangkok, Thailand
Nattapong.p@rmutp.ac.th

Somkieat Thongkeaw

Faculty of Engineering
Rajamangala University of Technology Phra Nakhon
Bangkok, Thailand
Somkieat.t@rmutp.ac.th

Abstract—In an agriculture, water is an important factor that affects both quality and quantity of agriculture products. Therefore, a quality of water needs to be evaluated. If the salinity is higher than the requirement, the quality of products is poor and/or the quantity may be lower than expected. In this paper, we propose a low-cost submarine to be used for collecting water samples from the farmer's garden. The collected water samples are used to evaluate the quality of the water which is contaminated by salts. To develop the low-cost submarine, firstly, we study the details of practical submarine architecture. To control the low-cost submarine, we implement several sensors, depth sensor, temperature sensor and pressure sensor, and microcontrollers. The results from sensors and microcontrollers are displayed on LCD monitor. Movements of the submarine are controlled by 3 motors and the water samples are collected by collecting kit. As a result, 5 meters from the surface, the low-cost submarine can collect water samples from several water depths and transmits the data from sensors efficiently. Therefore, the user can use the water efficiently.

Keywords— submarine; low cost; sensor

I. INTRODUCTION

Currently, the number of disaster occurrence has been increased noticeably. Once the disaster occurs, search and rescue personnel need to survey losses that occurred by those occurrences of disaster. However, in some areas, it is difficult to perform a surveying by human and it may cause a high cost of surveying. Moreover, if the surveying needs to be performed under the water, the difficulty and cost of the survey is noticeably high. In addition, the risk of danger for search and rescue personnel is much higher than a surveying on land. Therefore, a loss from disaster surveying by submarine is proposed to improve the performance of surveying. Moreover, it also reduce the cost of survey and reduce the risk of danger from the surveying to the search and rescue personnel.

In an agriculture, the quality of water is an important factor that must be concerned since the poor quality of water affect a low quality and quantity of agriculture products. The salinity of water is the critical parameter that is need to be evaluated continually. To evaluate the salinity by human, the personnel needs to collect the sample of water and then evaluate the quality of water which causes a high cost. In order to determine the salinity of water, several parameters are measured including pressure and temperature. It should be mentioned that these

parameters cannot be evaluated in real-time if the survey is done by human.

Therefore, in this paper, we develop the low-cost submarine in order to be implement in practice. The developed submarine is implemented with several sensors in order to measure the quality of water including depth sensor, temperature sensor and pressure sensor. Moreover, the microcontroller is also implemented into the submarine to control it by remote controller. At the remote controller, we implemented the display on it, then the observer can be observed the measured parameters in real-time. In our experiments, we evaluate the performance of the low-cost submarine in order to collect the water samples and also measure the temperature, pressure and depth of water. From the experimental results, the low-cost submarine can collect water samples from several water depths and transmits the data from sensors efficiently. Therefore, the user can use the water efficiently.

The remainder of this paper is organized as follows. Section II describes the principle of Archimedes. Development of low-cost submarine and its structure are described in section III. The experimental results are shown in Section IV. Finally, conclusions are presented in Section V.

II. PRINCIPLE OF ARCHIMEDES

As stated in the principle of Archimedes [1],[2], if the object is immersed in a fluid such as liquid or gas, the exerted buoyant force (FB) that is occurred in an upward direction through the center of gravity of the liquid is equal to the weight of the fluid that displaces the object. The centroid of the displaced fluid volume is called center of buoyancy (CB)

Therefore, the principle of Archimedes can be described as follows:

- If the density of the object is equal to the fluid, the object will float on the water because FB is equal to the weight of the object (W).

$$FB = W. \quad (1)$$

- If the density of the object is more than the fluid, the object will sink into the bottom of the object that filled with the water because FB is less than W.

$$FB < W. \quad (2)$$



- If the density of the object is less than the fluid, the object will float on top of the surface of water because FB is more than W.

$$FB > W. \quad (3)$$

III. LOW COST SUBMARINE

In this section, the designing of the low-cost submarine is described together with the overview of structure and equipment. The objective of the low-cost submarine are to survey the environment under the water of the agricultural area and evaluate the quality of the water in real-time. The image that is detected by camera can be observed in real-time. Moreover, the temperature and pressure under the water can be determined in real-time by utilizing microcontroller.[3]

A. Equipments

- 3 units of bilge pump 1100 gph.
- Submersible Pump DC 12V
- 1 set of 6 channels relay module.
- 3 sets of EP Propeller.
- 1 unit of LED 3 W. 12V.
- 1 unit of Arduino board.
- Switching Power Supply 12V 15A
- CCTV HD CAMERA
- 1, 2 and 3/4 inches of PVC pipes and accessories
- Steel plate

B. Structural Desing

Before we develop our low-cost submarine, we first study the details of practical submarine architecture. Then, we applied those principle the design our low-cost submarine for agriculture by utilizing the PVC pipes — 1, 2 and 3/4 inches — as shown in fig. 1.



Fig. 1. PVC pipes for assembly the low-cost submarine

The 3 units of bilge pump 1100 gph DC 12V are modified in order to implemented with EP propellers. Therefore, the bilge pumps are used to drive the propellers in order to control the submarine movement.



Fig. 2. modified bilge pump for low-cost submarine

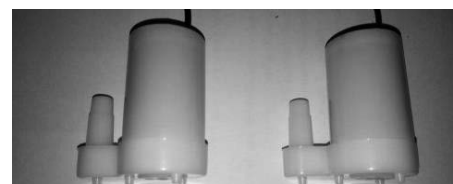


Fig. 3. A modified bilge pump for low-cost submarine



Fig. 4. Arduino board for low-cost submarine

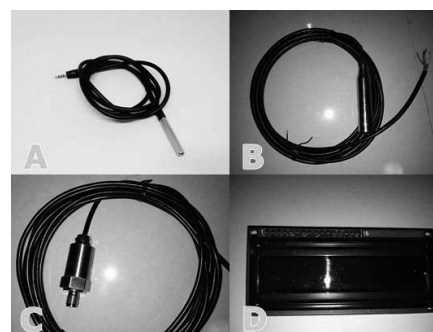


Fig. 5. Transmitter and receiver for pressure and temperature senors and display module.

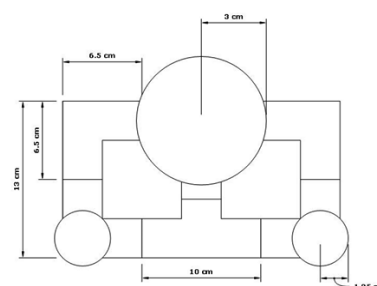


Fig. 6. Front layoutof the low-cost submarine

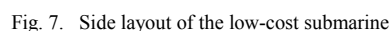


Fig. 8. Bottom view of the low-cost submarine



Fig. 9. Top view of the low-cost submarine



Fig. 10. Front view of the low-cost submarine

Moreover, we design a circuit, where the circuit diagram is shown in fig. 11, and implemented in the control box. As depicted, Arduino board receives the data from PLUG OUTPUT[4,5] which contains the data from relay module and submarine movement control switches. The information from temperature, pressure and depth sensors are displayed on the LCD monitor. The camera captures the observed area and sends the data to display the image on the LCD display in real-time.

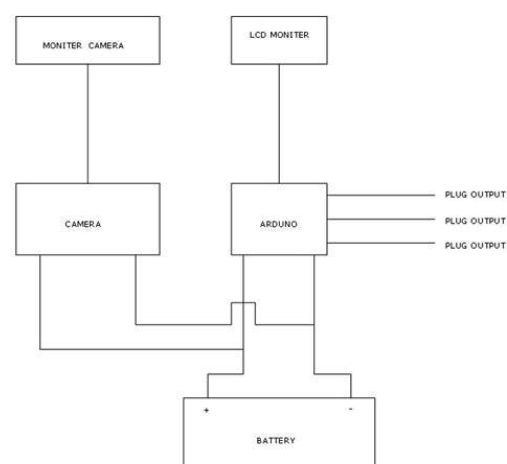


Fig. 11. Control circuit diagram

As shown in fig.12, the data from temperature and pressure sensors which are supplied by 5V of electrical are processed by Arduino board. On the other hand, level sensor is supplied by 12V. The movement of submarine is controlled by motors that are modified to be implemented with the EP propellers. The operations of motor are controlled by the Arduino command through the relay modules. The pumps are directly connected to the power switching power supply. The LEDs are utilized for improving the quality of detected image.

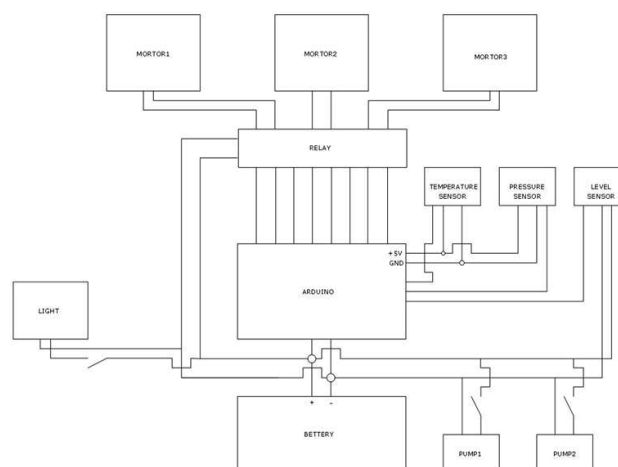


Fig. 12. Circuit diagram of the low-cost submarine



IV. EXPERIMENTS

In this section, we evaluate the performance of the developed low-cost submarine for measuring the temperature, pressure and depth of water. The characteristic of the developed low-cost submarine is shown in table I.

TABLE I. LOW-COST SUBMARINE CHARACTERISTIC

Width	30 cm
Height	60 cm
Depth	17 cm
Weight	7 cm

In the experiment, we evaluate the performance of submarine by determining maximum level of water where the submarine can transmit the detected information — data from the sensors and image from camera — to the display efficiently. The experimental results are shown in table II.

TABLE II. EXPERIMENTAL RESULTS

Day	Time of observation	Water level (cm)	Pressure (kPa)	Temperature (°C)
1	8:00	10	0.16	24.45
	12:00	10	0.16	29.33
	15:00	10	0.17	25.17
	18:00	10	0.15	22.09
2	8:00	100	4.11	23.60
	12:00	100	4.66	28.56
	15:00	100	3.89	24.23
	18:00	100	3.97	22.34
3	8:00	200	5.34	21.43
	12:00	200	5.45	22.98
	15:00	200	5.77	23.23
	18:00	200	5.12	20.12
4	8:00	500	9.89	20.34
	12:00	500	9.12	21.56
	15:00	500	9.22	21.99
	18:00	500	9.35	20.12

As shown in the table, the maximum level of water that the low-cost submarine can dive and can transmit the data to be displayed on the LCD monitor is 5m from the top surface of water. At 5 m, the error of measuring value is less than 5%. Moreover, it also collects the water samples from several water depths efficiently.



a.



b.



c.

Fig. 13. The displayed data on the LCD display at different levels of water, a) 12 cm, 49 cm and 93 cm.

From the experimental results, we can notice that the error of data measuring is less than 5% which is acceptable in practice. This error is affected by the quality of equipment and the observed environment.

V. CONCLUSION

In this paper, we develop a low-cost submarine for measuring the quality of water for an agriculture. The quality of water is determined by the pressure and temperature of the water. The low-cost submarine is implemented with pressure sensor, temperature sensor, depth sensor and camera. The measured data and detected image are transmitted and are displayed on the LCD monitor at the observer station. From the experimental results, the low-cost submarine can transmit the data to the observer station when the depth of water is less than 5m. The error from the measuring is less than 5% which is accepted in practice.

REFERENCES

- [1] Chen, C.-H., Chen, C.-H., Mertzman, S.A., Shen, J.J.-S., 1999. An unusual late Cenozoic volcanic zone in northern Taiwan-behind southern Okinawa Trough. *J. Geol. Soc. China* 42, 593–612.
- [2] Chen, C.-H., Shen, J.J.S., 2005. A refined historical record of volcanic eruptions around Taiwan: tectonic implications in the arc-continent collision area. *Terr. Atmos. Ocean. Sci.* 16 (2), 331–343.
- [3] Doo, W.-B., Hsu, S.-K., Armada, L., 2015. New magnetic anomaly map of the East Asia with some preliminary tectonic interpretations. *Terr. Atmos. Ocean. Sci.* 26, 73–81. [http://dx.doi.org/10.3319/TAO.2014.08.19.07\(GRT\)](http://dx.doi.org/10.3319/TAO.2014.08.19.07(GRT)).
- [4] Hsu, S.-K., Liu, C.-S., Shyu, C.-T., Liu, S.-Y., Sibuet, J.C., Lallemand, S., Wang, C., Reed, D., 1998b. New gravity and magnetic anomaly maps in the Taiwan-Luzon region and their preliminary interpretation. *Terr. Atmos. Ocean. Sci.* 9, 509–532.
- [5] Rau, R.-J., Ching, K.-E., Hu, J.-C., Lee, J.-C., 2008. Crustal deformation and block kinematics in transition from collision to subduction: global positioning system measurements in northern Taiwan, 1995–2005.
- [6] Wen, H.-Y., Sano, Y., Takahata, N., Tomonaga, Y., Ishida, A., Tanaka, K., Kagoshima, T., Shirai, K., Ishibashi, J., Yokose, H., Tsunogai, U., Yang, T.F., 2016. Helium and methane sources and fluxes of shallow submarine hydrothermal plumes near the Tokara Islands. *Southern Japan Scientific Reports*, 1–9



Smart Home Control Unit via Mobile Ringtone

Vitawat Sittakul

Department of Electronics Engineering Technology
College of Industrial Technology
King Mongkut's University of Technology North Bangkok
vitawat.sittakul@gmail.com

Nattapong Phanthuna

Faculty of Engineering,
Department of Electrical Engineering
Rajamangala University of Technology Phra Nakhon
Nattapong.p@rmutp.ac.th

Abstract—This paper presents a smart home control unit via mobile ringtone. The control unit comprises a switching power supply, a GSM module and a signal over DC module. The mobile ringtone with different rings (Interval time) can be used to switch on/off each lamp inside a building without the need of internet access. The rings of mobile ringtone are received and mapped with the output command by the GSM module. The output command is used to switch on/off up to 10 lamps inside the building. Finally a prototype of smart home is implemented and the experimental results show that the accuracy of the system is between 86 and 99%.

Keywords—GSM, Smart Home, Mobile Phone, Signal over DC

I. INTRODUCTION

The concept of “smart home” was firstly proposed in 1984, by the National Association of Home Builders (NAHB) [1]. As for smart home, it has to include interoperability between the devices, remote access, and ability to extend the system [2]. Today, the concept of smart home becomes more popular around the world due to a huge growth of low-cost intelligent devices such as smart plug, camera, sensor and wireless sensor for home automation. This allows them to have their own configuration interface and easy to interact among them [3]. In addition, the internet of things (IoT) plays an important role to enhance the performance of them to connect to the internet network and they can be controlled via any equipment that has the internet access e.g. smart phone.

There are three main smart home applications. Firstly, in the medical care, it is focused on monitoring and assisting elder, disabled persons or patients in the rural areas to improve quality of health and health care. Secondly, in the buildings, it automates and controls the entire devices by networking and sensor technologies to provide a standard living in urban areas. Finally, in the energy management, it can integrate with sensors to calculate or manage the energy consumption such as smart meters [4, 5].

In this work, we focus on the smart home in the buildings in which the appliances can be controlled from the remote site via a smart phone. As shown in [6-9], a wireless sensor network with ZigBee (IEEE 802.15.4 standard) in 2.4 GHz band can be used to connect and control household appliances

via the smart phone over the internet network. This allows the user to switch on/off the appliances via any application on smart phone as can be seen in Fig. 1

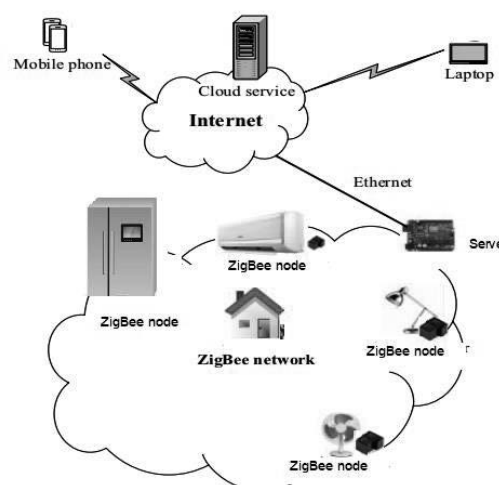


Fig. 1 Smart home network on Internet

However, there is a possibility that the users may not be able to connect to the internet due to data limit in their tariffs or the internet network failures. Therefore, it shall be another low-cost redundant network to handle this difficulty. In this work, we propose a smart home control unit via mobile ringtone. The control unit comprises a switching power supply, a GSM module and a signal over DC module. The mobile ringtone with different rings (Interval time) can be used to switch on/off each lamp inside a building without the need of internet access. The rings of mobile ringtone are received and mapped with the output command by the GSM module. The output command is modulated on DC signal of the signal over DC module. The output command is serially transmitted through all modules. Then, the output command is compared with the command stored on each module. If the command is matched with any module, the output signal from that module will be used to switch on/off the smart plug.

The block diagram of proposed smart home system architecture can be seen in Fig. 3.

Fig. 2. Proposed Smart Home System Architecture

Fig. 3 Block diagram of Proposed Smart Home System Architecture

When the GSM module received the call from the mobile phone, the time interval is analyzed and converted to be ASCII code on the module. With 1 ring of ringtone, the “All off” is transmitted to the entire signal over DC modules to switch off all smart plugs (all LEDs are off). With 2 rings of ringtone, the



“#A” data is transmitted to the entire signal over DC modules and the 1st signal over DC module is active (on the top left of the diagram). It can be seen that all data transmitted can be from “(#A to #J)” to control 10 signal over DC modules. The complete control signal can be seen in Table I. The symbols “S1 to S10” on the right hand of the diagram stand for the manual switches to manually switch on/off the smart plugs.

III. IMPLEMENTATION

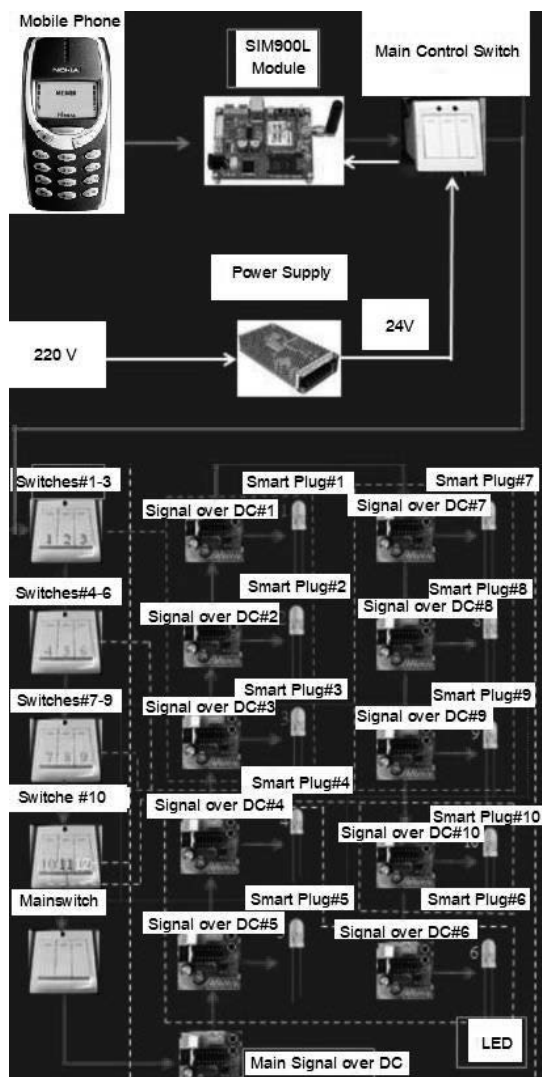


Fig.4. Implemented Smart Home Controlled Unit controlled by Ringtones

The system is now implemented using the power supply, signal over DC module, GSM module (SIM900L), LEDs (Smart plugs), switched as shown in Fig. 4

A. GSM Module

The GSM module is ET-BASE GSM SIM900 from SIMcom Company as shown in Fig.5. It is a small GSM/GPRS Module that supports GSM frequency in the range of 850/900/1800/1900 MHz. It can communicate through port RS232 by AT command. In this work, this module is used to receive a call from the remote mobile phone and the ringtone will be calculated and mapped with the output data of Table I. Then the output data will be later transmitted to the signal over DC module.

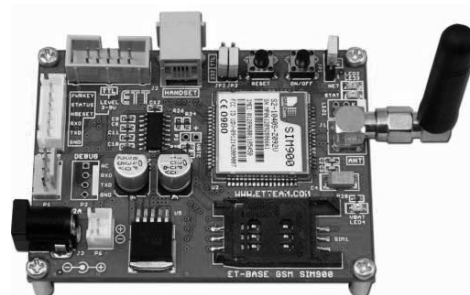


Fig. 5 GSM Module

B. Signal over DC module

To achieve the design, the signal over DC module has to be created from Low-pass Filter (LF), Microcontroller Unit (MCU) and Encoder as shown in Fig. 6.

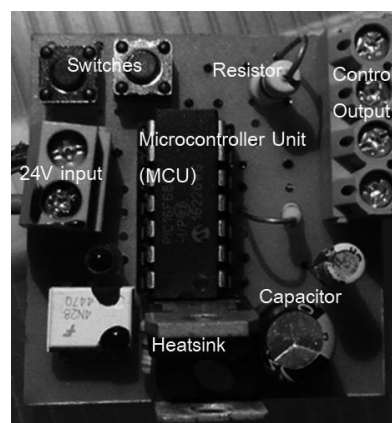


Fig. 6 Signal over DC module

Fig. 6 illustrates the signal over DC module. It can be seen that capacitors and a resistor can perform as an LF. The 24V input is used to drive the MCU. The MCU is PIC16F877 manufactured by Microship Technology Company. One of signal over DC modules is used as the main device. It receives the output data transmitted from the GSM module in ASCII code from #A to #H (Binary) and distributes the output data between them. Each module will respond only the same code



as shown in the Table I. For example, if the ASCII code “#E” is received, the signal over DC module connected to the lamp no. 5 will be turned on.

TABLE I. COMPLETE COMMAND TO SIGNAL OVER DC MODULE

#Number of Ring(s) From Mobile Phone	Output Command from GSM unit (SIM900L Module)	#Lamp (ON)
1	All off	All Off
2	#A	1
3	#B	2
4	#C	3
5	#D	4
6	#E	5
7	#F	6
8	#G	7
9	#H	8
10	#G	9
11	#H	10

IV. EXPERIMENT

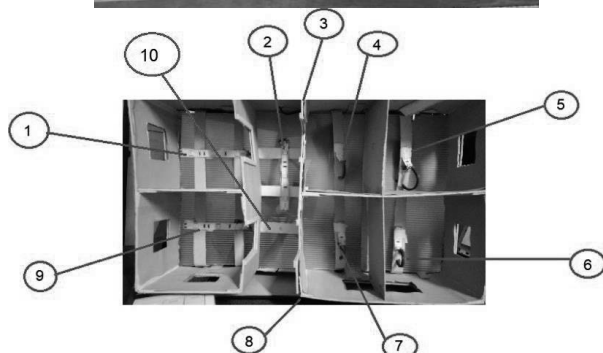


Fig.7. Smart Home – Pattern (Top) Outside View, (Bottom) Inside View

In this section, smart home pattern is created as shown in Fig. 7 with the proposed system as shown in Fig. 4. This is to make it easy to test the accuracy of the system. In this test, each lamp is remotely switched on/off for 50 calls by external mobile phone. Then, the errors will be recorded and used to calculate the accuracy of the system. The experimental results

can be seen in Table II. It can be seen that the accuracy of the system is between 86% and 99%.

TABLE II. EXPERIMENTAL RESULTS (ACCURACY TEST)

#Lamp	Command	Rounds	Error	Accuracy)%(
Lamp 1	ON	50	7	86%
	OFF	50	2	96%
Lamp 2	ON	50	1	91%
	OFF	50	1	98%
Lamp 3	ON	50	6	88%
	OFF	50	4	92%
Lamp 4	ON	50	1	98%
	OFF	50	3	94%
Lamp 5	ON	50	2	96%
	OFF	50	7	86%
Lamp 6	ON	50	2	96%
	OFF	50	4	92%
Lamp 7	ON	50	1	99%
	OFF	50	5	90%
Lamp 8	ON	50	3	94%
	OFF	50	2	96%
Lamp 9	ON	50	2	96%
	OFF	50	4	92%
Lamp 10	ON	50	3	94%
	OFF	50	3	94%

V. CONCLUSION

A smart home control unit controlled by mobile ringtones is successfully demonstrated. It is shown that it is possible to remotely switch on/off the smart plugs in a building using the mobile phone call without the need of internet access. A prototype of smart home with 10 lamps (simulate the smart plugs) is created and it is shown that the accuracy of the system is between 86 and 99%.

REFERENCES

- [1] Erec, “Home automation systems,” in Reporter, February, 2002, Vol. 19.
- [2] “M.Schneppe, ITU G.hn concept and Home Automation, 2010
- [3] I.I.Pătru, M. Carabaș, M.Bărbulescu, L.Gheorghe, “Smart home IoT system”, 15 th RoEduNet Conference, Networking in Education and Research, 9 Sept. 2016, Bucharest, Romania
- [4] S.Suresh, P.V.Sruthi, “A Review on Smart Home Technology”, 2015 Online International Conference on Green Engineering and Technologies (IC-GET 2015)
- [5] D.M. Han and J.H. Lim, “Design and implementation of smart home energy management systems based on zigbee” IEEE Transactions on Consumer Electronics 56(3):1417 - 1425 · September 2010.
- [6] D. Bordenca, H. Valean, S. Folea, A. Dobircu, “Agent Based System for Home Automation, Monitoring and Security,” in Proc. of the 34.th International Conference on Telecommunications and Signal Processing TSP 2011, Budapest, Hungary, Aug. 18–20, pp. 165–169, ISBN 978-1- 4577-1409-2, IEEE catalog number: CFP1188P-CD
- [7] S.Folea, D.Bordenca, C.Hotea and H.Valean, “Smart Home Automation System Using Wi-Fi Low Power Devices”, IEEE International Conference on Automation Quality and Testing Robotics (AQTR), 24-27 May 2012, Cluj-Napoca, Romania.
- [8] K. Gill, et al, “A zigbee-based home automation system,” IEEE Trans. on Consumer Electronics, vol. 55, pp. 422–430, 2009.
- [9] M. Varchola, “Zigbee Based Home Automation Wireless Sensor Network”, Acta Electrotechnica, 2007, Vol. 7, No. 4.



Comparison of Performance of Regenerative Power for Electric Vehicles between Single and Dual DC Motor Drive Systems

Suriyun Srisongkham, Saharat Phualek, Phurich Ngamkong, Wilaiporn Ngermbath and Chonlatee Photong*
Solar Energy and Energy Resources Research Unit, Faculty of Engineering, Mahasarakham University, Kham Rieng,
Kantarawichai, Maha Sarakham, 44150, Thailand
phurich.ng@gmail.com and chonlatee.p@msu.ac.th*

Abstract—This paper presents comparison of performance of regenerative power for electric vehicles between a single and a dual dc motor drive systems. Both drive systems under study had the same rated power of 10kW and speed of 1,750 rpm when the test conditions under the study were at full load, medium-low load, reduced speed and breaking conditions. The test results obtained from MATLAB Simulink program showed that both drive systems could not generate power at full load but the dual motor drive system had less inrush current by 11.98% in average than the single motor drive system. At medium-low load, the dual motor drive system could regenerate power of 1.5kW, while the single motor driver could not. At the reduced speed and breaking conditions, both drive systems could regenerate similar amount of power by 1.3kW, which was 13.0% of the rated power of the motors.

Keywords—Regenerative power; single motor drive; dual motor drive, efficiency, electric vehicles

I. INTRODUCTION

Electric Vehicles (EVs) are one of the modern innovations that have been interested researchers and investors due to the global trend of low CO₂ vehicles. Statistical data from [1] showed (Fig.1) that the number of EVs increased by 10-15% in production volume every year. However, one of the main problems for most EVs is short time of supplying power for the EVs from batteries; otherwise, a number of batteries must be used but would cause problems of high weight and thus higher amount of power is required. Indeed, light weight, high quality batteries could be used but with higher costs.

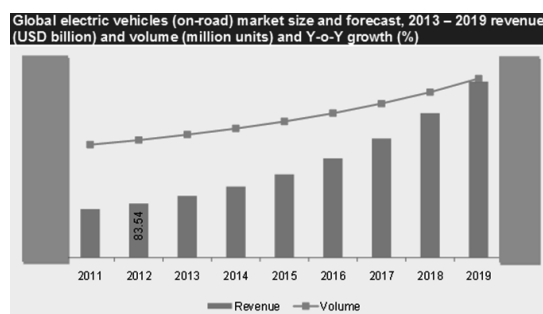


Fig. 1. world on-road EVs market size and forecast, 2011-2019 [1]

One possible technique to eliminate these problems would be by using regenerative system for the EVs. There are several techniques could be used [2]-[12]; However, most motor drive systems commonly install high efficient power electronics for control motor speed-torque, as well as provide efficient regenerative systems on the EVs. In most cases, the more the motors are used for the drive system, the more complicated and difficult in control the power electronic circuits are encountered [13] (see Fig.2). Therefore, all the motor drive systems, the single and dual drive systems seem to be the most attractive in terms of simple and robust motor control. However, a single motor drive system for the EVs, especially heavy-duty EVs, would require oversize motor in order to achieve sufficient torque under extra-high load conditions. Therefore, the two-motor or dual motor drive systems [14] would be more preferable. This is because of flexibility of managing power from/to the motors, i.e., using two motors for full-high power but using one of them for medium-low power.

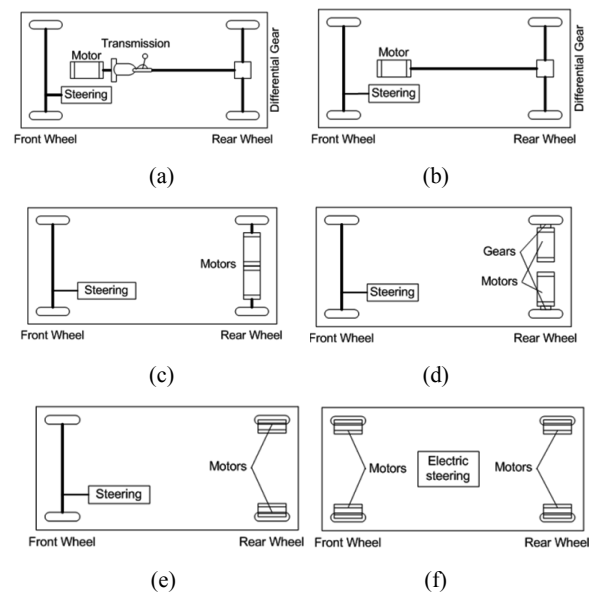


Fig. 2. Conventional motor drive systems for EVs: (a)-(b) single motor drive; (c)-(d)-(e) dual motor drive; and (f) four motor drive system [13]



This paper studied and compared efficiency of the regenerative power systems between the conventional single motor drive system and the dual motor drive system proposed in [14] with rated power level of 10kW and rated speed of 1,750 rpm (the most common power level and speed rating for most general-purpose EVs) [15]. The regenerative capability of both drive system types were tested via a MATLAB-Simulink simulation program when both motor drive systems operated at near full load (10kW), medium-low load (1-5kW), reduced speed/breaking conditions. Details of the single and dual motor drive system are explained in Section II while results obtained from the simulation tests are presented and discussed in Section III; followed by the conclusions in Section IV.

II. METHODOLOGY

A. Structures of Motor Drive Systems under Study

Fig. 3(a) and 3(b) showed the structures of the conventional single motor drive system and the dual motor drive system proposed by [14]; where the specification of the motors used for the study are listed in Table 1.

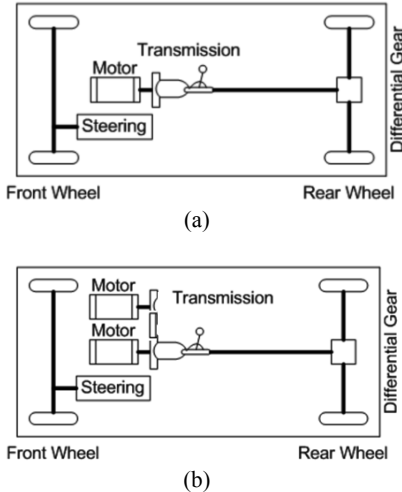


Fig. 3. Motor drive systems for EVs under study: (a) conventional single motor drive system; (b) dual motor drive system proposed by [14]

TABLE I. SPECIFICATION OF MOTOR USED IN THIS STUDY

Motor drive type	Rated Parameters	
	Power (W)	Speed (rpm)
Single	10kW	1,750
Dual	5kW x 2	1,750

B. Simulation Models of the Motor Drive Systems

Fig. 4(a)-(c) showed the MATLAB-Simulink simulation models of the conventional single motor drive system and the dual motor drive system when operated at full load, medium-low load and reduced speed/breaking conditions, respectively. The identical DC motors (except power rating) and the same motor controllers and sensors (except the control strategies);

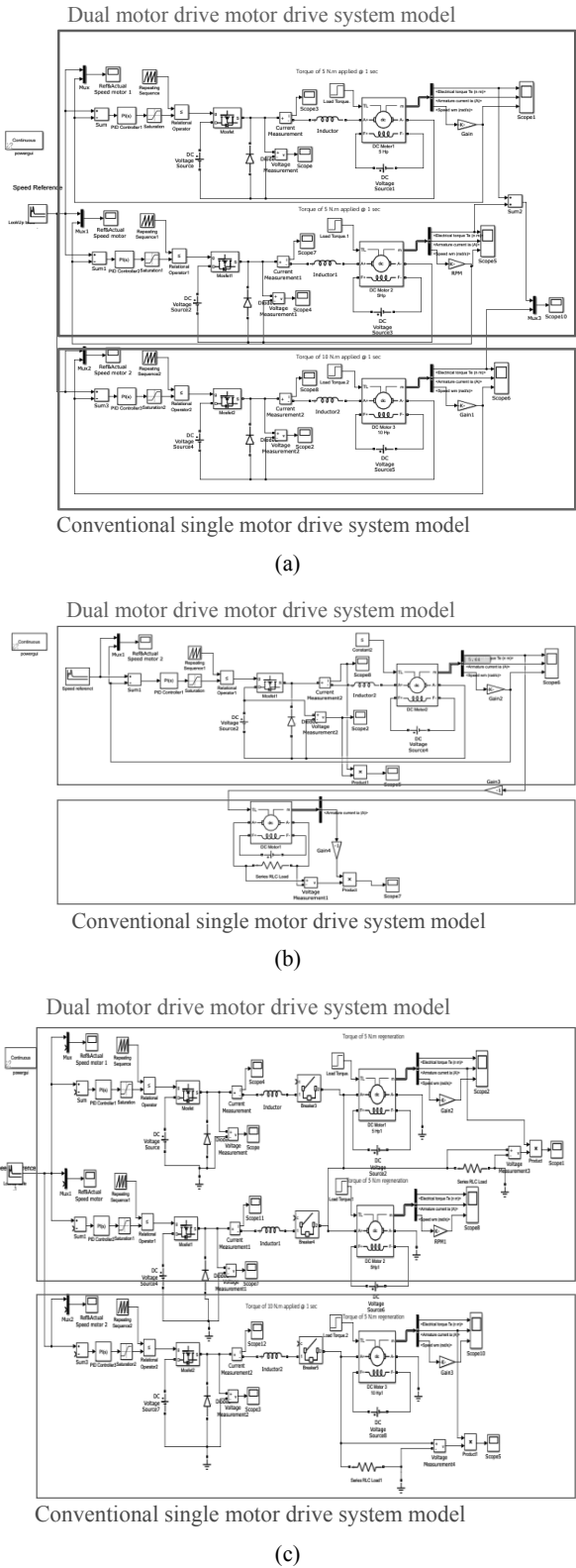


Fig. 4. The MATLAB-Simulink simulation models for the motor drive systems under study: (a) at full load, (b) at medium-low load and (c) reduced/breaking conditions



detail in [14]) were implemented for both motor drive systems in order to provide comparable conditions.

III. RESULTS AND DISCUSSIONS

Fig. 5, 6, 7 and 8 show simulated results obtained from the following test scenarios, respectively:

Test Result 1: comparison of the speed profile for both the investigated motor drive systems (Fig.5). The result showed that both the motor drive systems conducted the same profiles of speed compared to the reference speed. This result confirmed that both motor drive systems are identical in terms of the speed control and thus all the relevant results between them should be comparable.

Test Result 2: comparison of armature current for both the investigated motor drive systems when applied constant load of 10 N.m (Fig.6). The result showed that the dual drive system operated with peak current (max. peak of 76.63 at time=1.526 sec; when speed of the EVs up from 780 rpm to 1,500 rpm), which was lower peak current by 11.89% in average compared to the single drive system (max. peak of 82.4A at time=1.526 sec).

Test Result 3: comparison of regenerative power for both the investigated motor drive systems when operated at medium-low load (Fig.7). The result showed that the dual drive system could allow one motor to drive and one to regenerate power of 1.5kW at constant 1,750 rpm speed through the decoupling steering configuration. On the other hand, the single motor drive system, indeed, could not regenerate any power.

Test Result 4: comparison of regenerative power for both the investigated motor drive systems when reduced speed/breaking from 1,750 rpm to zero speed (stop) within 1.5 sec (Fig. 8). The result showed that the dual drive system and the conventional single motor drive system generated similar profile and amount of power of 1.3 kW in average.

It could be concluded that the dual motor drive system provides better efficiency and performance in terms of lower peak current, regenerative capability at medium-low load; but they generate similar amount of power under the reduced speed/breaking conditions.

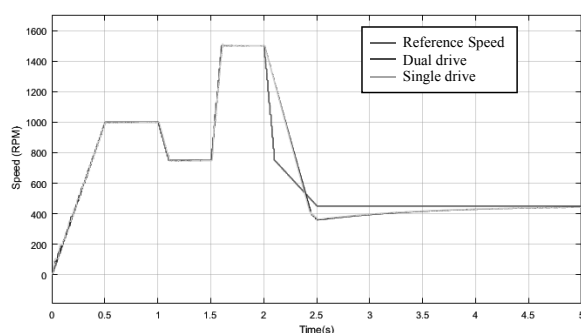


Fig. 5. Comparison of the speed profile between the conventional single motor drive system and the dual motor drive system

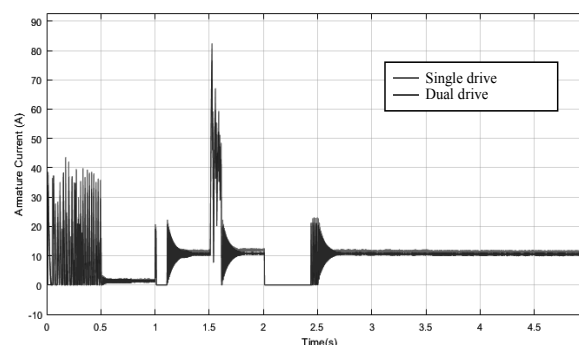


Fig. 6. Comparison of the armature current between the conventional single motor drive system and the dual motor drive system according to the speed control in Fig. 5.

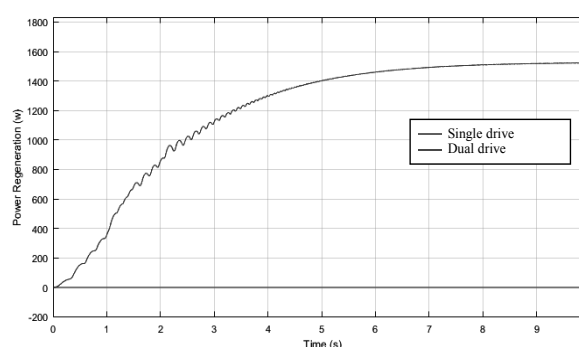


Fig. 7. Comparison of the regenerative power between the conventional single motor drive system and the dual motor drive system when operated from start to full load.

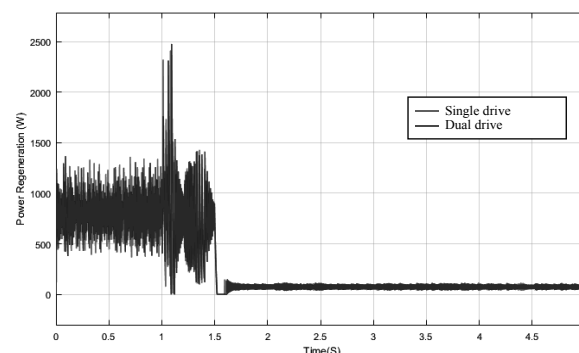


Fig. 8. Comparison of the regenerative power between the conventional single motor drive system and the dual motor drive system when reduced speed/breaking from 1,750 rpm to stop condition.

IV. CONCLUSIONS

This paper proposed comparison of efficiency and performance between the conventional single motor drive system and the dual motor drive system, which were designed for 10kW, 1,750 rpm electric vehicles. The simulation models based on MATLAB-Simulink were developed and tested. The simulated results showed that with the same speed control, the dual motor drive system could be able to regenerate power of



1.5kW at rated speed, medium-low load condition, while the single motor drive system could not generate any power. Both motor drive systems generated similar amount of power of 1.3kW when operated under reduced speed/breaking from the rated speed to zero speed. These results would confirm that the dual motor drive system provides better efficiency and performance over the conventional single motor drive system in terms of the operation in regenerative modes. In addition, the results showed that the peak current drawn by the dual motor drive system was 11.98% lower than the single motor drive system.

ACKNOWLEDGMENT

Authors would like to sincerely thank Solar Energy and Energy Resources Research Unit, Faculty of Engineering, Mahasarakham University, for supporting equipment and information.

REFERENCES

- [1] Company Annual Report, Industrial Journal, Technical Publications, KOLs and TMR analysis, <https://www.simbainformation.com/Global-Scientific-Technical-9295952/>, 2015.
- [2] Chunting Mi, Hui Lin and Yi Zhang, "Iterative Learning Control of Antilock Braking of Electric and Hybrid Vehicles", IEEE Transaction on Vehicular Technology, Vol. 54, No. 2, Sep. 2005.
- [3] Nobuyoshi Mutoh, Hiromichi Yahagi, "Electrical Braking Control Methods for Electric vehicles with Independently Driven Front and Rear Wheel Structure", Industrial Electronics, IEEE transaction on, Vol. 54, Issue 2, April 2007.
- [4] Li Yu-shan, Zeng Qing-liang, Wang Chenglong, Wang Liang, "Research on Control strategy for Regenerative Braking of a Plug in Hybrid Electric City Public Bus", IEEE Intelligent Computation Technology and Automation, Oct. 2009.
- [5] Yimin Gao, Liang Chu, Mehrdad Ehsani, "Design and Control Principles of Hybrid Braking System for EV, HEV and FCV", IEEE Vehicle Power and Propulsion Conference, Sept. 2007.
- [6] Liang Chu, Wanfeng Sun, Liang Yao, Yongsheng Zhang, Yang Ou, Wenruo Wei, Minghui Liu, Jun Li, "Integrative control strategy of regenerative and hydraulic braking for hybrid electric car", IEEE Vehicle Power and Propulsion Conference, Oct. 2009.
- [7] S. R. Clikanek, K. E. Bailey, "Regenerative Braking System for A Hybrid Electric Vehicle", Proceedings of the American Control Conference, Anchorage, AK May, 2002.
- [8] M. van der Voort, M. Dougherty, "Reducing fuel consumption by using a new fuel-efficiency support tool", IEEE Africon, Sep.1999,
- [9] A. Varhelyi, M. Hjalmdahl, C. Hyden, and M. Draskoczy, "Effects of an active accelerator pedal on driver behaviour and traffic safety after long-term use in urban areas", Accident Analysis and Prevention, vol. 36 no. 5, pp. 729-737, 2004.
- [10] T. Yabe, K. Akatsu, N. Okui, T. Niikuni, and T. Kawai, "Efficiency Improvement of Regenerative Energy for an EV," World Electric Vehicle Journal, vol. 5, no. 2, pp. 494-500, Jun. 2012.
- [11] G. Buja, M. Bertoluzzo, and C. Fontana, "Reactive Power Compensation Capabilities of V2G-Enabled Electric Vehicles," IEEE Transactions on Power Electronics, vol. 32, no. 12, pp. 9447-9459, Dec. 2017.
- [12] W. Jiang, Y. Yang, and P. Suntharalingam, "All-Electric Vehicles and Range-Extended Electric Vehicles," Energy, Power Electronics, and Machines, pp. 491-516, Oct. 2014.
- [13] X. D. Xue, K. W. E. Cheng and N. C. Cheung, "Selection of eLECTRIC mOTOR dRIVES for electric vehicles," 2008 Australasian Universities Power Engineering Conference, Sydney, NSW, 2008, pp. 1-6.
- [14] P. Panmuang, T. Thongsan, N. Suwapaet, J. Laohavanich, and C. Photong, "A novel dual motor drive system for three wheel electric vehicles," 2018.
- [15] Eckhard Karden, Servé Ploumen, Birger Fricke, Ted Miller, Kent Snyder, Energy storage devices for future hybrid electric vehicles, Journal of Power Sources, Volume 168, Issue 1, 2007, Pages 2-11.



Analysis of High Performance Savonious Wind Turbines for Low Speed Wind Applications

Kwanjai Nachaiyaphum and Chonlatee Photong*

Solar Energy and Energy Resources Research Unit, Faculty of Engineering, Mahasarakham University, Thailand
kwanjai.na@rmuti.ac.th and chonlatee.p@msu.ac.th*

Abstract— Generating high amount of electric power from wind turbines requires high speed wind. Unfortunately, most lowlands where most people live have only low speed wind (0.5-2.65 m/s). This paper presents analysis of high performance Savonious wind turbines that could operate efficiently at low speed wind. The analysed results showed that implementation of external wind tunnel(s) provided significantly high performance by more than double (103.7% and 148-171%_{max} increased for a single tunnel and double tunnels, respectively). Implementation of special design of configurations or blades provided improved performance upto 40% compared to the conventional turbines; using bach-type blades, two-blade configuration, valve-aided blades, and twisted blades could provide higher power generation approximately by 39.5%, 18.7-20.0%, 5.0-19.5% and 6.9%_{max}, respectively.

Keywords—Savonious wind turbines; low speed wind; high performance

I. INTRODUCTION

Wind is the second largest renewable energy resources in the world with the power capability of 25-75 TW/yr. compared to 23,000TW/yr. of solar power. This amount is sufficient for total world power consumption of 16 TW/yr. However, wind power would have more advantages and more cost-effective than solar power in terms of both day-night power generations and less installation space [1].

Converting wind power into the most convenient power form such electricity from the wind normally requires wind turbines that convert mechanical power into electricity. There are several types of wind turbines available but the most commonly used are ones shown by the C_p - λ curves in Fig. 1 [2]; where C_p is the power coefficient that indicates how much the power that the turbine (rotor) can extract from the wind and λ is the tip speed ratio that is the ratio between the tangential wind speed on the blade of turbine to the actual wind speed.

This research focuses on generating electricity from wind for supplying households or small factories where the wind turbines could be directly installed and could deliver electricity with shorter distant power transmission and thus lower power losses. Research studies [3]-[4] showed that households and factories mostly locate in the lowlands where the speed of wind is very low (0.5-2.65 m/s for downtown and rural areas, respectively) [3].

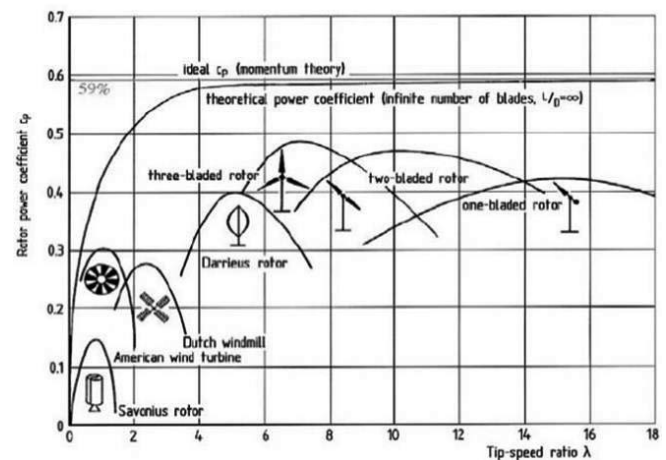


Fig. 1. Most often used wind turbines [2]

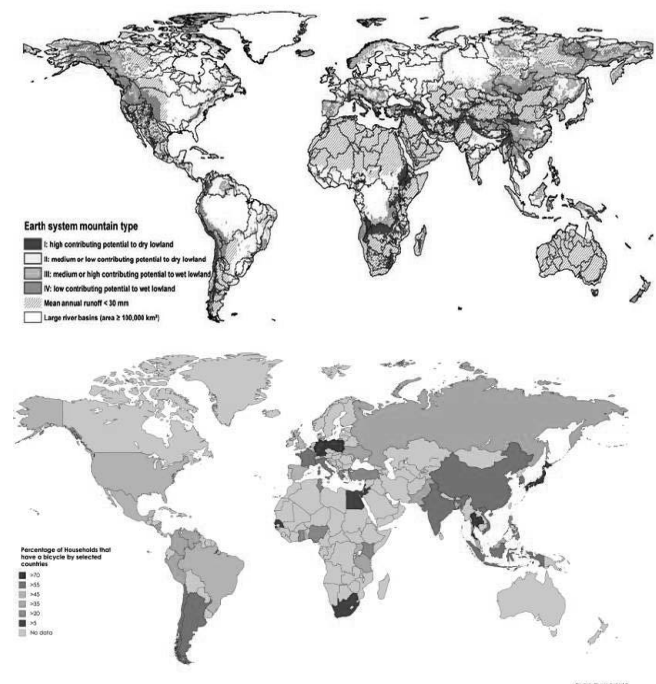
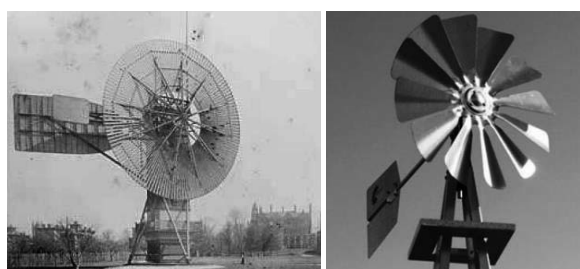


Fig. 2. World map of lowlands vs percentage of households [3]-[4]



According to the propose of the research that is to determine suitable wind turbines for low speed wind and when considering Fig.1 and Fig.2, the American wind turbines (windmills) [5] and the Savonius wind turbines [6] would be the most attractive. American wind turbines (see Fig.3(a)) would have advantages of being able to run with a damaged blade and the one opposite removed without resulting in an unbalanced mill. However, American wind blades must be designed to be large in order to extract sufficient power from low speed wind, but this gives result in larger area of installation and cost. On the other hand, the Savonius wind turbines (see Fig.3(b)) would be more sophisticated when these turbine types allow operation with low speed wind but with smaller size and lighter weight compared to American wind turbines. Analysis on these Savonius wind turbines in order to achieve high performance of electric generation under low speed wind thus is presented, which is detailed in the next following sections.



(a)



(b)

Fig. 3. Possible conventinal low speed wind turbine; (a) American wind turbine and (b) Savonius wind turbines [5]-[6]

II. ANALYTICAL METHODOLOGIES

In order to analyze and determine suitable configurations for Savonius wind turbines for low speed wind applications, two analytical methodologies were carried out: internal components and external components. Details are as follows:

A. Analytical Methodology on Internal Components

There are several internal components that could affect performance of the Savonius wind turbines. However, review on several literatures [7]-[11] pointed out that the main internal factors would be ones shown in Fig. 4(a), which are as follows:

- (a) rotor configurations: with/without ended covers
- (b) number of blades: 2 blades, 3 blades, +3 blades

(c) blade shapes and arrangements: considered in two factors: bach/non-bach blades and twisted/non-twisted blades

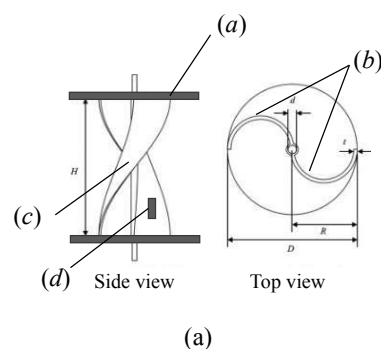
(d) valve-aided blades: when some holes are made/not made on the blades to improve dynamic of wind flow

B. Analytical Methodology on External Components

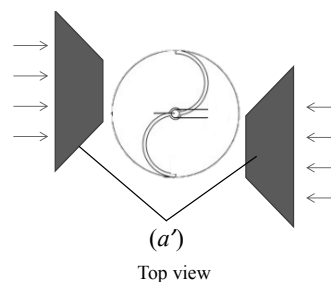
Some research work [12]-[14] utilized the principle of Bernoulli's by using the external components (Fig.4(b)) such as wind tunnels to narrow down the path of wind flow and hence provide higher speed wind at the tails of the tunnels, which could be classified as:

(a') partial wind tunnel configurations

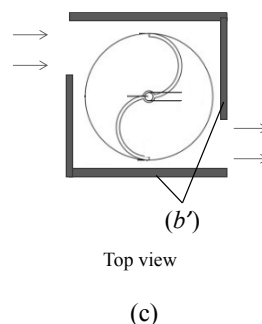
(b') full wind tunnel configuration



(a)



(b)



(c)

Fig. 4. Analytical Methodologies: (a) internal component analysis; (b) external components with partial tunnels analysis and (c) external components with full tunnel analysis.



The power coefficient (C_p) is the measure used for the analysis and assessment of both internal and external components of the Savonius wind turbines. Results of the analysis are presented in Section III.

III. RESULTS AND DISCUSSIONS

The results of analysis of high performance Savonius wind turbines for low speed wind applications are divided according to Section II into 6 parts as follows:

A. Analytical Results on Rotor Configurations

Different geometries affect performance of Savonius wind turbines. It was found that the rotors without overlap ratio (β) are better in operation than those with overlaps. The power coefficient improved with respect to the increase of the aspect ratio (α) and the rotor with end plates gives higher efficiency than those of without end plates as shown in Fig.5-7 [7].

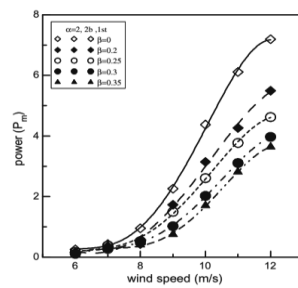


Fig. 5. The mechanical power variation with wind speed for different overlap ratios.

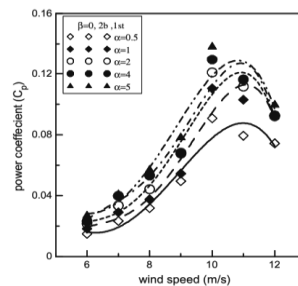


Fig. 6. The power coefficient variation with wind speed for different aspect ratios.

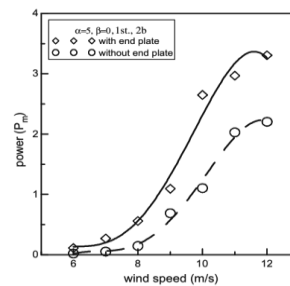


Fig. 7. Variation of mechanical power with wind speed for rotors with and without end plates.

B. Analytical Results on Number of Blades

According to Mohammed Hadi Ali', two-blade Savonius wind turbines had more efficient and high power coefficient (C_p) than that of three-blade Savonius wind turbines when operating at the same conditions as shown in Fig.8 [8].

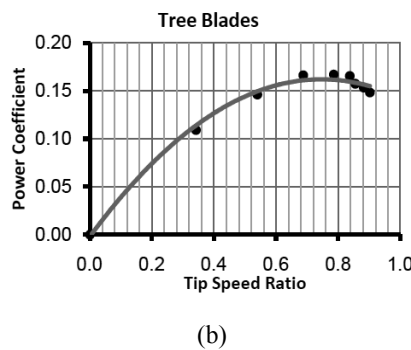
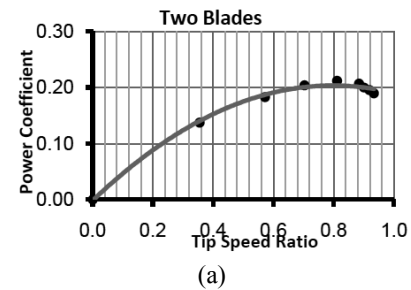


Fig. 8. The power coefficient variation with the tip speed ratio for: (a) two-blade and (b) three-blade wind turbines.

C. Analytical Results on Blade Shapes and Arrangement

The important parameter that affects the performance of the Savonius wind turbine is the blade shape. We have found that the maximum power coefficient (C_p) of the conventional blade shape (Fig.9(a)) and bach-type shape (Fig.9(b)) were 18.9% and 26.35%, respectively [9]. The twisted blade in a three-bladed types had been tested in a low speed wind tunnel, and compared with conventional semicircular blades (with twist angle of 0°). The experimental results showed that the twisted bladed rotor has higher efficiency compared to that of the conventional bladed rotor shown in Fig.10 [10].

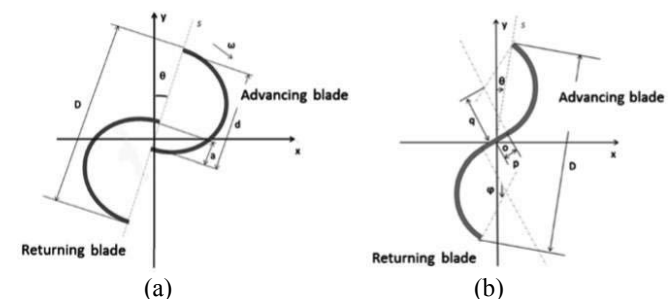


Fig. 9. Rotor configuration and geometrical parameters: (a) Conventional Savonius-type rotor (b) Bach-type rotor.

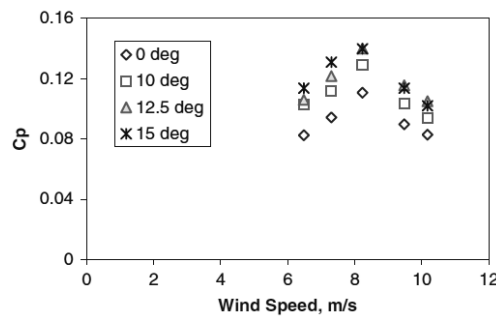


Fig. 10. The power coefficient variation with velocity for various twisted bladed rotors.

D. Analytical Results on Valve-Aided Blades

Experiment results were carried out with valve-aided Savonius wind turbine shown in Table I. It showed that valve-aided Savonius three-bladed rotor had better power coefficient (C_p) compared to the conventional one [11].

TABLE I. PERFORMANCE OF VALVE-AIDED THREE-BLADED SAVONIUS ROTOR SYSTEM

Blade shape	Blade height (m)	Blade chord (m)	Aspect ratio	Projected area (m ²)	Free stream velocity (m/s)	Max. power coefficient (C_p)
Semicircular Twisted	0.122	0.077	1.58	0.0377	7.30	0.31 0.32

E. Analytical Results on Partial Wind Tunnel Configurations

The geometrical parameters of the curtain arrangement as Fig.11 were optimized to generate more optimum performance. The effects of the four variables which are the lengths (l_1 and l_2) and angles of the curtains (α and β) on the power coefficient have been examined. The lengths of the curtains used in the experiments are given in Table II. The maximum power coefficient of the Savonius wind turbine is increased to about 38.5% (Fig.12) with the optimum curtain arrangement are curtain 1, $\alpha=45^\circ$ and $\beta=15^\circ$ [12].

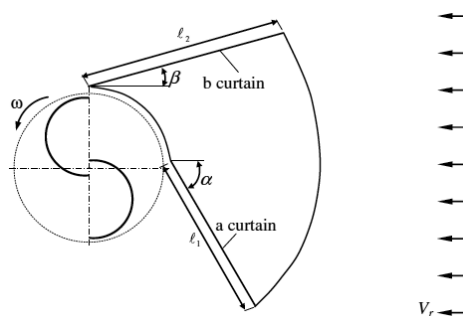


Fig. 11. Geometrical parameters of the curtain arrangement.

TABLE II. DIMENSIONS OF CURTAIN ARRANGEMENTS

Type of curtain arrangement	Distance l_1 (cm)	Distance l_2 (cm)
Curtain 1	45	52
Curtain 2	34	39
Curtain 3	22	26

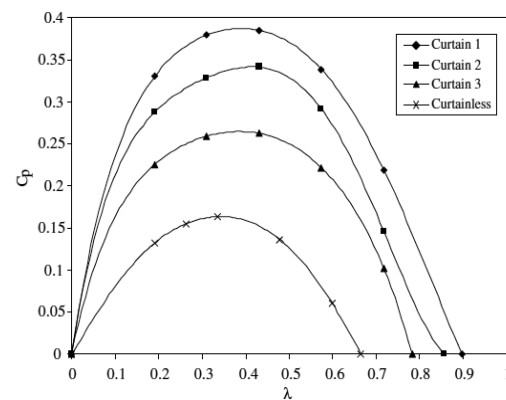


Fig. 12. The effects of curtain lengths on the power coefficient with respect to the tip speed ratio ($\alpha = 45^\circ$ and $\beta = 15^\circ$).

The double wind tunnels as a new design had been investigated to increase the efficiency of the conventional Savonius wind turbine [13]. The double wind tunnels with geometrical parameters is illustrated in Fig. 13. The results shown that the double wind tunnels could generate voltage with higher levels for all the wind angles approximately by 45-68% in average (Fig.14).

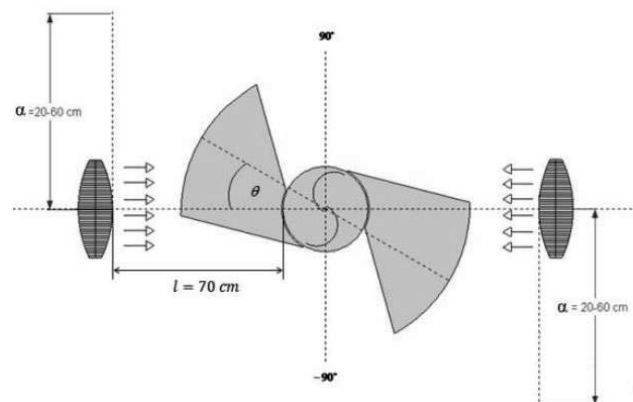


Fig. 13. Diagrams of experimental setting for double wind tunnels

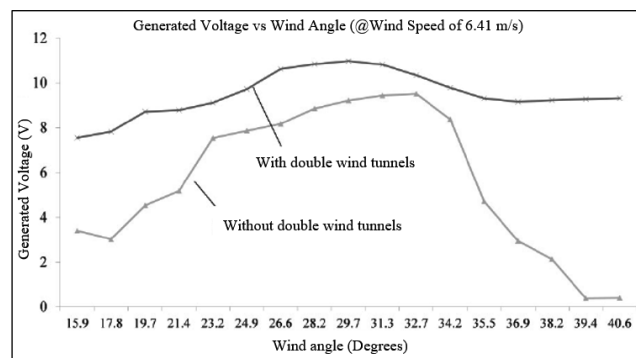


Fig. 14. Experimental results: comparison of generated voltage levels at different wind angles (when wind tunnel angle at 30°) between the proposed with double and conventional wind turbines.



F. Analytical Results on Full Wind Tunnel Configurations

Hussain designed two boundary devices similar as the rectifier. The performance of three groups of rotor are tested and compared in open condition and boundary device condition (Fig.15). Rotor 1 obtains the maximum C_p of 0.52 in the semi-boundary condition, and 0.42 in open condition [14].

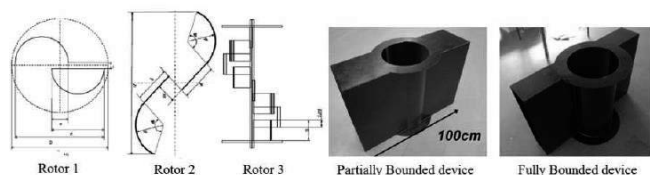


Fig. 15. Savonius turbine rotor and the boundary device structure.

IV. CONCLUSIONS

This paper presents analysis of high performance Savonius wind turbines for low speed wind applications. The results obtained from internal and external components analyses on power generation capability showed that implementation of external wind tunnels provided significantly high performance by 103.7% and 148-171% for a single tunnel and double tunnels, respectively. Using special design of rotor or blade configurations provided improved performance upto 40% compared to the conventional turbines; using bach-type blades, two-blade configuration, valve-aided blades, and twisted blades could provide higher power generation performance by 39.5%, 18.7-20.0%, 5.0-19.5% and 6.9%, respectively.

ACKNOWLEDGMENT

Authors would like to thank the Solar Energy and Energy Resources Research Unit, Faculty of Engineering, Mahasarakham University, Thailand, for all the technical and equipment supports.

REFERENCES

- [1] W. Kuckshinrichs, "Carbon Capture and Utilization as an Option for Climate Change Mitigation: Integrated Technology Assessment," Carbon Capture, Storage and Use, pp. 1-9, Oct. 2014.
- [2] E. Muljadi and C. P. Butterfield, "Pitch-controlled variable-speed wind turbine generation," IEEE Transactions on Industry Applications, vol. 37, no. 1, pp. 240-246, 2001.
- [3] F. T. B. Samodra and I. A. Indrawan, "Proposal of stack Effect technology for predicted future years," IOP Conference Series: Earth and Environmental Science, vol. 99, p. 012024, Dec. 2017.
- [4] T. Hamilton, "The Material World of a Household and Collection," Oxford Scholarship Online, May 2017.
- [5] F. J. Athearn and R. W. Righter, "Wind Energy in America: A History," The Western Historical Quarterly, vol. 27, no. 4, p. 546, 1996.
- [6] Sandra Eriksson. Evaluation of different turbine concepts for wind power[J]. Renew Sustain Energy Reviews, 12(5) (2008), p. 1419-1434.
- [7] N. H. Mahmoud, A. A. El-Haroun, E. Wahba, and M. H. Nasef, "An experimental study on improvement of Savonius rotor performance," Alexandria Engineering Journal, vol. 51, no. 1, pp. 19-25, Mar. 2012.
- [8] M. H. Ali, "Experimental comparison study for Savonius wind turbine of two and three blades at low wind speed," International Journal of Modern Engineering Research, vol. 3, issue 5, 2013.
- [9] T. Zhou and D. Rempfer, "Numerical study of detailed flow field and performance of Savonius wind turbines," Renewable Energy, vol. 51, pp. 373-381, Mar. 2013.
- [10] U. K. Saha and M. J. Rajkumar, "On the performance analysis of Savonius rotor with twisted blades," Renewable Energy, vol. 31, no. 11, pp. 1776-1788, Sep. 2006.
- [11] U. K. Saha, S. Thotla, and D. Maity, "Optimum design configuration of Savonius rotor through wind tunnel experiments," Journal of Wind Engineering and Industrial Aerodynamics, vol. 96, no. 8-9, pp. 1359-1375, Aug. 2008.
- [12] B. D. Altan, M. Atılgan, and A. Özdamar, "An experimental study on improvement of a Savonius rotor performance with curtaining," Experimental Thermal and Fluid Science, vol. 32, no. 8, pp. 1673-1678, Sep. 2008.
- [13] C. Promdee and C. Photong, "Effects of Wind Angles and Wind Speeds on Voltage Generation of Savonius Wind Turbine with Double Wind Tunnels," Procedia Computer Science, vol. 86, pp. 401-404, 2016.
- [14] Z. P. Tang, Y. X. Yao, L. Zhou, and B. W. Yu, "A Review on the New Structure of Savonius Wind Turbines," Advanced Materials Research, vol. 608-609, pp. 467-478, Dec. 2012.



Design and Construction of a Simple Dual DC Motor Drive System for Three Wheel Electric Vehicles

Kritsada Thiangphadung, Kmonchanok Adkalan, Wilaiporn Ngermbath, Phurich Ngamkong and Chonlatee Photong*
Solar Energy and Energy Resources Research Unit, Faculty of Engineering, Mahasarakham University, Kham Rieng,
Kantarawichai, Maha Sarakham, 44150, Thailand
wilaiporn.ng@gmail.com and chonlatee.p@msu.ac.th*

Abstract—This paper proposes design and construction of a simple dual DC motor drive system for a three wheel electric vehicle. The proposed system consisted of 2 separately excited DC motors, batteries, a simple speed controller with variable resistive control, magnetic contactors and protection circuits. The Global Positioning System (GPS) navigation system which could be able to control via a mobile phone was also presented. The experimental results from the system prototype showed that the designed system could drive the vehicle with passengers up to 750 kg, maximum speed of 50 km/hr, and up to 15 degree-slope climbing ability.

Keywords—three wheel vehicles; electric vehicles; design; dual drive system

I. INTRODUCTION

Three wheel vehicles are one of the most famous and well known passenger vehicles in Thailand; sometimes called “Tuk Tuk” or “Sky-lab” [1],[2]. This is because of the fact that they have unique structures (see Fig.1), possible for small and narrow roads and low cost when compared to other types of passenger vehicles with the same driving power. However, most three wheel vehicles currently used in Thailand utilize combusted power engines such as gasoline engines and thus emit high CO₂ into the air.

This paper proposes design and construction of a simple dual DC motor drive system for three wheel electric vehicles. The designed system should meet the following basic criteria for the heavy-duty three wheel vehicles [3]:

- (1) able to carry total weight of 670 kg (350 kg for the vehicle itself and 400kg for total weight of 5 passengers)
- (2) able to climb the road with slop upto 15 degrees
- (3) able to speed up whilst running at 50 km/hr
- (4) batteries supply sufficient power for the vehicle to run continuously at speed of 40 km/hr for at least 1 hr and all the auxiliary components
- (5) position of the motors and batteries must be higher than 45 cm to avoid wet ground



Fig. 1. Photographs of famous three wheel vehicles in Thailand: (a) Tuk Tuk and (b) Sky-Lab [1],[2]

Details of design and construction of the system prototype are presented in Section II. The tests results of the system prototype are shown and discussed in Section III; following by the conclusions in Section IV.

II. DESIGN AND CONSTRUCTION OF THE SYSTEM PROTOTYPE

The full explanation on the dual motor drive system has been presented in [3]. In this paper the design procedures and construction for the system when applied for three wheel vehicles.

A. Design of the System Prototype

The steps of design are power source design, control circuit design, and power circuit and protection design:

Step 1: power source design

This design step is to ensure sufficient power for the vehicles. The design starts by considering the designed load of 670kg. by using following equations [3],[4], the maximum load can be determined; where the parameter shown in Fig. 2 and Table :

$$F_{rr} = \mu_{rr} N = \mu_{rr} mg \cos(\alpha) \quad (1)$$

$$F_{ad} = \frac{1}{2} \rho c_d A v^2 \quad (2)$$

$$F_{cr} = mg \sin(\alpha) \quad (3)$$

$$F_{acc} = ma \quad (4)$$



$$F_{te} = F_{rr} + F_{ad} + F_{cr} + F_{acc} \quad (5)$$

$$P_{te} = F_{te} v \quad (6)$$

; where F_{rr} = running resistance force (N)
 F_{ad} = aerodynamic drag force (N)
 F_{cr} = climbing resistance force (N)
 F_{acc} = acceleration force (N)
 F_{te} = tractive force (N)
 u_{rr} = friction coefficient (see Table 1)
 N = normal force (N)
 m = vehicle mass (kg)
 g = gravity of earth (9.807 m/s²)
 α = climbing angle (degree)
 ρ = air density (1.225 kg/m³)
 c_d = drag coefficient (see Table 2)
 A = air density (1.225 kg/m³)
 v = vehicle velocity (m/s)
 a = vehicle acceleration (m/s²)

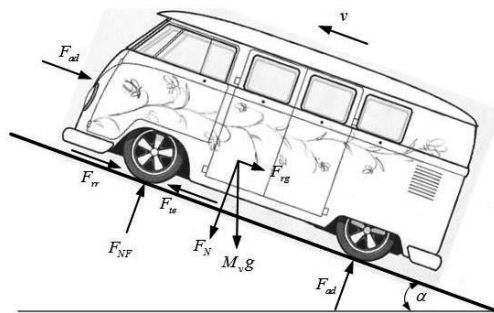


Fig. 2. Parameters for power load calculation [3],[4]

TABLE I. FRICTION COEFFICIENT FOR DIFFERENT ROAD TYPE (u_{rr}) [5]

Type/Condition	u_{rr}
Paved & Concrete	
- excellent	0.014-0.018
- Fair	0.018-0.020
flagstone	0.023-0.030
gravel	0.020-0.025
soil	
- dried	0.025-0.035
- wet	0.050-0.150
sand	0.100-0.300

TABLE II. CLIMBING COEFFICIENT (C_d) [7]

Vehicle Type	C_d
Aerodynamic design	0.15-0.20
Research design	0.22
General car	0.3
Sport car	0.43

	Adapted car	0.53
	Universal Sport car	0.57-0.63
	Motorcycle	0.56-0.63
	Convertible car	0.6-0.7
	Bus	0.6-0.7
	Truck	0.7-1.50

When considered using $u_{rr}=0.02$; $c_d=1.5$; $A= w0.7 \times h1.2= 0.84$ m², $m=750$ kg; $\rho=1.225$ kg/m³; $v=0-13.89$ m/s and $\alpha=0-15^\circ$, using (1)-(6) to determine the desired power for the issues (1)-(3) when $m=750$ kg; $\rho=1.225$ kg/m³; $c_d=1.5$; $v=0-13.89$ m/s and $\alpha=0-15^\circ$ in 2 following conditions:

Condition 1: at full load, full speed and no-slop road:

$\alpha=0^\circ$; $v=13.89$ m/s (50 km/hr)

$$F_{rr} = 0.02 \times (750) \times (9.807) \times \cos(0^\circ) = 147.11 \text{ N}$$

$$F_{ad} = (1/2) \times (1.225) \times (1.5) \times (0.84) \times (13.89^2) = 148.90 \text{ N}$$

$$F_{cr} = F_{acc} = 0 \text{ N}$$

$$F_{te} = 147.11 + 148.90 + 0 + 0 = 296.01 \text{ N}$$

$$P_{te@100\%n} = (296.01) \times (13.89) = 4,111.58 \text{ W}$$

Condition 2: at full load, speed of 10 km/hr and 15° slop:

$\alpha=15^\circ$; $v=2.78$ m/s (10km/hr)

$$F_{rr} = 0.02 \times (750) \times (9.807) \times \cos(15^\circ) = 142.09 \text{ N}$$

$$F_{ad} = 0.5 \times (1.225) \times (1.5) \times (0.84) \times (2.78^2) = 5.96 \text{ N}$$

$$F_{cr} = 750 \times 9.807 \times \sin(15^\circ) = 1,903.68 \text{ N}$$

$$F_{acc} = 0 \text{ N}$$

$$F_{te} = 142.09 + 5.96 + 1,903.68 + 0 = 2,051.73 \text{ N}$$

$$P_{te@100\%n} = (2,051.73) \times (2.78) = 5,703.81 \text{ W}$$

And for support some possible overload conditions, the safety factor of 25% and system efficiency of 0.90 were taken into account and gave total power of $5,703.81 \times 1.25 / 0.90 = 7,921.96$ W or about 8,000 W. Based on the dual motor drive system and information from above; two 4kW separately excited DC motors model ZC448 (Fig.3) [5] and the batteries system of 8kW/hr were therefore selected.

TABLE IV. SPECIFICATION OF DESIGNED DC MOTORS [5]

Model	Rated Power (kW)	Rated Voltage (V)	Rated Current (A)	Rated Speed (rpm)	Rated Torque (N.m)	Overload (Times)
ZC448	4.0	48	104	2,800	13.6	3.4



Fig. 3. Photographs of the dc motors ZC4-48 used for the prototype vehicle

Step 2: control circuit design

Fig. 4(a)-(b) show the control diagram of the proposed simple dual motor drive system. The control circuit operates when CB5A, Emergency-stop and Key switch are turned on, then K1 switch will be turned on. If the driver wants to turn both motors on for high torque conditions, the driver can turn on Switch and thus the K2 operates. The driver can be simply selected manually dependent on situation of power load demands. The speed of the motor can be simply controlled (0-50 km/hr.) by varying value of resistor through the handle of the vehicle; by meant of varying duty cycle of the controlled inverter. Fig. 5 show photograph of the controller (model 1204M-5203, 48V 275A Curtis 120xM series) used for the prototype vehicle under study.

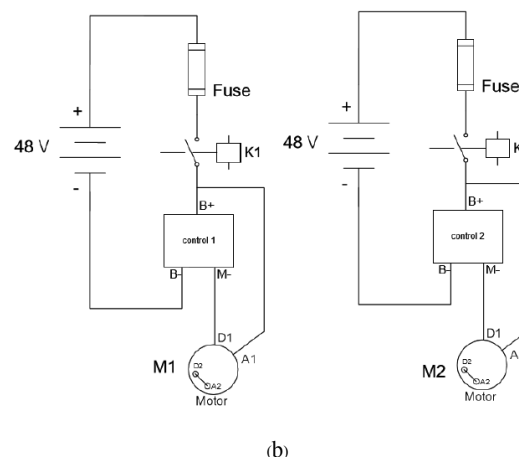
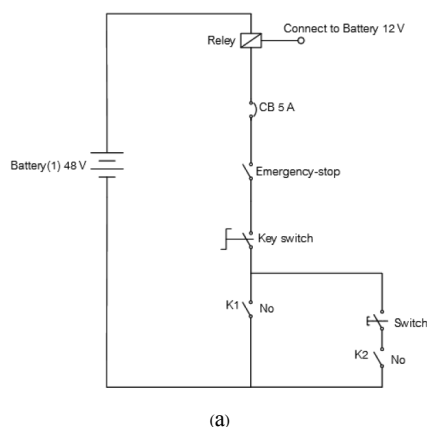


Fig. 4. Control Diagram of the proposed simple dual DC motor drive system: (a) overall control circuit and (b) dual motor control circuits



Fig. 5. Controller for the prototype vehicle

Step 3: power circuit and protection design

Fig. 6 show circuit diagram of power and control circuits for the proposed drive system. The contact relays and fuses are used to be the connecting parts and protection parts for the prototype vehicle. The rated value of the fuses was calculated using standard IEC 60269, which was by multiplying 1.5 to the rated motor current; i.e. $1.5 \times 104A$ for this case (see Table I) and thus gave 156A and thus choose the fuse's rated of 125A.

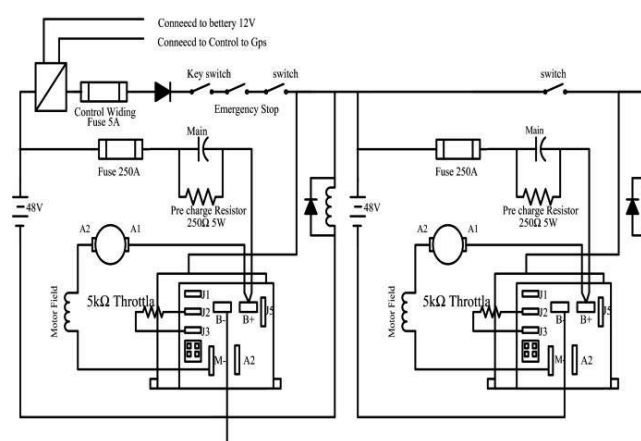


Fig. 6. Power circuit with the controllers of the proposed drive system



B. Construction of the System Prototype

Fig.7 shows the photograph of the prototype vehicle. The motors were installed at the front base of the vehicle. The controllers were placed inside the water-resisted box. Two sets of 4 batteries were placed on each side of the base of the vehicle for balancing the load weight.

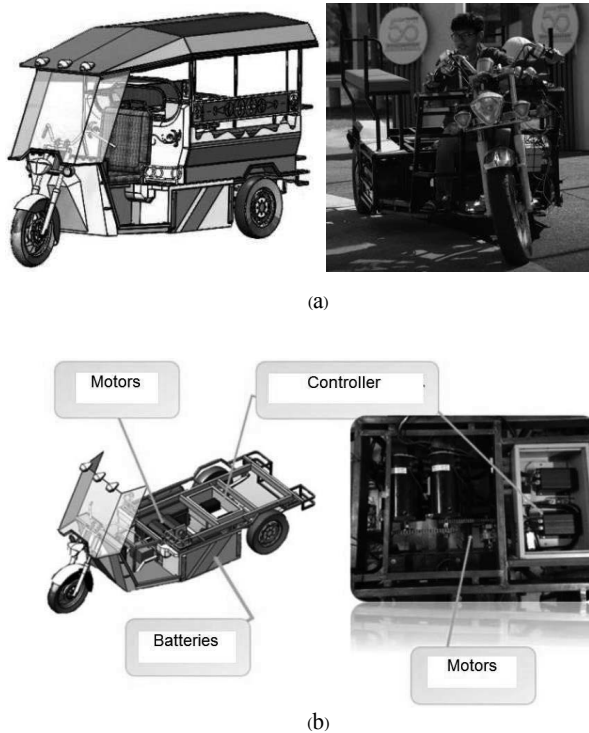


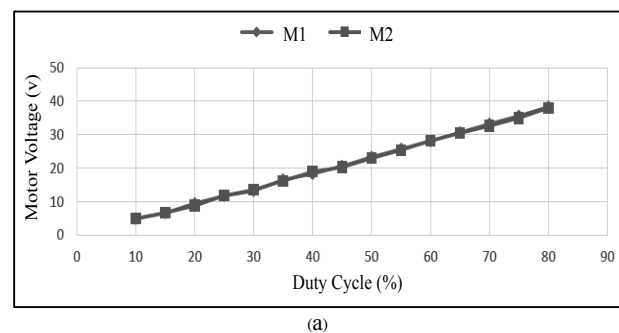
Fig. 7. Prototype of (a) the vehicle and (b) the proposed simple dual DC motor drive system under this study

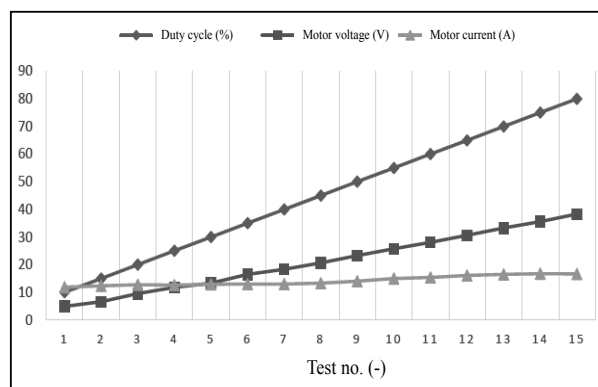
III. TEST RESULTS AND DISCUSSIONS

The system prototype was tested (see Fig. 8). The test results showed that the proposed system could operate efficiently as designed. The speed of the motor could be controlled via the handle correctly as showed in Fig. 9 (a)-(c). The test results showed that the proposed drive system provided identical control for both motors (see Fig. 9(a)), therefore, there would have no problem of speed synchronizing between the two motors. The curves of duty cycle-voltage-current shown in Fig. 9(b) and 9(c) for the motor 1 and the motor 2 were similar during the operations in different speeds; This means that these two motor could run independently. The selection of one or two motor drive is therefore simply and independently controlled. Results in Table V showed that the prototype vehicle could climb the slop of 15 degrees running successfully, however, could not operate with high speed during running on the slop for 5 meters.

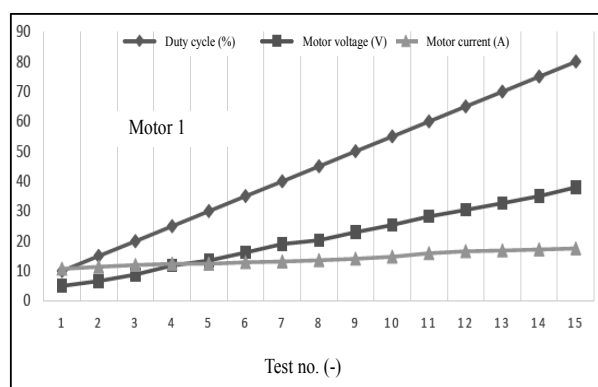


Fig. 8. Test of the proposed simple dual DC motor drive system: (a) driving tests and (b) speed-resistive control for one-two operating motor(s) control





(b)



(c)

Fig. 9. Test results: (a) curves of speed control test for both motors (voltage-%duty cycle); (b)-(c) curves of duty cycle-voltage-current of the motor 1 and motor 2 under different test scenarios.

TABLE V. TEST RESULTS AT CONDITIONS OF 15 DEGREE SLOP

Running Speed (km/hr)	Test Results	
	Without passenger	With 5 passengers
10	Yes	Yes
20	Yes	Modulate
30	Yes	No
40	No	No
50	No	No

IV. CONCLUSION

The proposed system consist 2 separately excited DC motors. The test results showed that the proposed system could operate efficiently as designed these two motor could run independently. The result at condition 15 degree slope the vehicle could climb successfully. however, could not operate with high speed running.

ACKNOWLEDGMENT

Authors would like to thank you the Solar Energy and Energy Resources Research Unit, Faculty of Engineering, Maharakham University and Atipong Motor Co., Ltd. for financial and technical support this research.

REFERENCES

- [1] Thai Tuk Tuk Association, 2015.
- [2] Athipong. (2018, May 15) Athipong Motor. Retrieved form <https://www.atipongmotor.com>
- [3] P. Panmuang, T. Thongsan, N. Suwapaet, J. Laohavanich, and C. Photong, "A novel dual motor drive system for three wheel electric vehicles," 2018.
- [4] J. Larminie and J. Lowry, "Electric Vehicle Technology Explained," Aug 2012.
- [5] Department of Land Transport. (2017 August 1) Retrieved form <https://www.dlt.go.th>
- [6] Alibaba (2017 August1) Retrieved form <https://supermotor.en.alibaba.com>



Application of Heat Pipes to cool down high power Light-Emitting Diode

Benjamin Gérard
Physics Degree, Rennes 1 University
Rennes, France
ben.gerard95@gmail.com

Thanad Katpradit
Engineo Co. Ltd.
Chiang Mai, Thailand

Abstract— This paper has for goal to compare and test the viability of heat pipes as cool down solution for Light-Emitting Diode. We will observe and measure the temperature of the LED in different conditions and try to determine the possible heat transfer to cool down LED with the use of heat pipes.

Keywords—heat pipes; LED; Cool Down system

I. INTRODUCTION

High power LED are used for public lighting by night. Their big issue is that they have a large dissipation of energy with heat liberation. They getting hot and by this way damage themselves that decrease their lifetime. This topic has for goal to find a cool down solution without use of extern energy to decrease the heat dissipation inside the LED. This issue can be in part resolved by Heat Pipe technology. In fact, Heat Pipe is a thermodynamic system that works only due of overheating and it can carry and move heat from the LED to the ambient atmosphere. Accompanied with a heatsink, for most efficient perspective, and in modeling condition, we will try to find how heat pipe can be useful for reduce the heat of the LED.

In fact, we need a cheap device with quality, good efficiency and with low energy consumption. Made of copper, using water of working fluid and no addition of more energy; heat pipe is a good answer for our problematic. For our experiments, we will use some devices each describes below:

II. DEVICES SPECIFICATIONS

A. Heat pipes

A heat pipe is a heat-transfer device that combines the principles of both thermal conductivity and phase transition to effectively transfer heat between the heat pipe and the Led. Here we will use flat Heat Pipe to enlarge contact zone between LED and Heat Pipe for more efficient value.

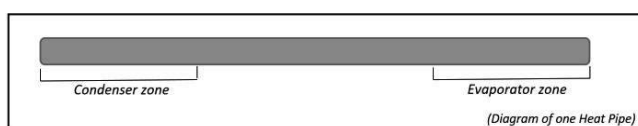


Fig. 1 Heat pipe diagram

Table 1. Heat Pipe features

Total Length	20cm
Evaporator Length	5cm
Adiabatic Length	7cm
Condenser Length	8cm
Outside Diameter	6mm
Material	Copper
Working Fluid	Water

B. Light-Emitting Diode

LEDs are electronics components using semiconductor technology that emit light when they are crossed by a current. We use a 30 Watts power COD (Chip On Board) LED composed by 30 LEDs chips. They work with a DC (Direct Current) based on 30-34 Volts.

Table 2. LED features

Power Dissipation	30W
Forward Voltage	30-34V
Forward Current	1A
Luminous Efficacy	100lm/W
Maximum Operating Temperature	85° C
Diameter	5.3 cm
Thickness	2.5mm
Number of chips	30

According with the builder, the maximum operating temperature correspond to the ideal maximum temperature where the LED don't damage itself.

III. EXPERIMENTAL

The experiment consists to measure the temperature of the LED until his maximum operating temperature as 85°C in three cases:

- Without heat pipe
- With one heat pipe
- With two heat pipes



Each experiment starts at ambient temperature: 25°C
The physical idea it's that the heat emits by the LED heats the evaporation zone of the heat pipe what launch the thermodynamic process of it. The heat sink's goal is to evacuate the heat by the condenser zone of heat pipe.

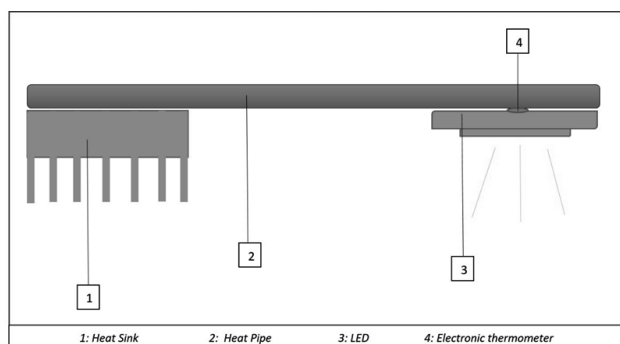


Fig. 2 Experimental set up diagram

IV. MEASURES

First, we measured the temperature of the led without heat pipe to know it behavior in real conditions and after with one and two heat pipes:

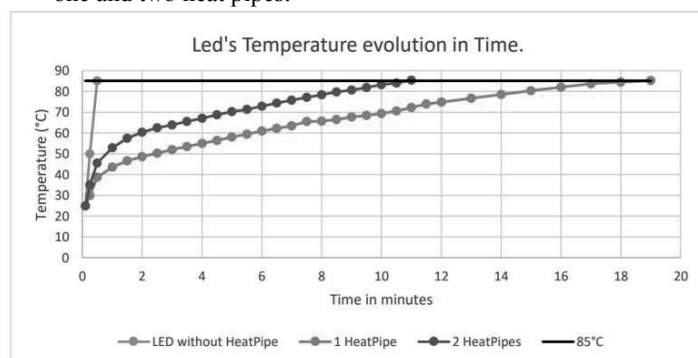


Fig. 3 LED's temperature evolution in time

According with our expectation; temperature of the LED without heat pipe increases very quickly. In fact, LED reaches his maximum operating temperature in less than one minute. This temperature is reaches at 10 minutes with one heat pipe and 15 minutes with two. There is actually a strong heat travel due to the heat pipe accentuated by one more heat pipe. We can see that adding of one heat pipe reduce the augmentation of the temperature in a no linear way.

In a second time we measure the temperature of the LED without heat pipe after it reaches his maximal temperature operating, to get an approximation of the maximum temperature reach by the LED:

We can see LED temperature increase very quickly to reach a stabilization temperature around 175°C.

Also, we put a thermometer in the condenser zone to can use the difference of the temperature in the condenser and

the evaporator zone to make an approximation of the heat transfer:

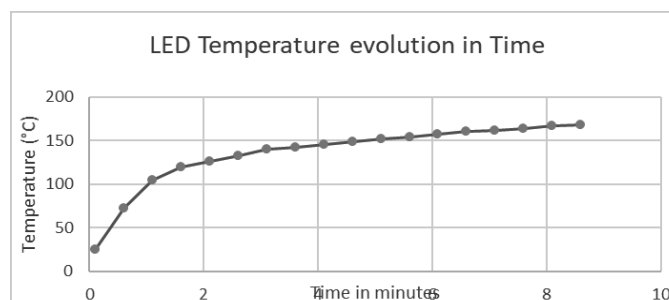


Fig. 4 LED's temperature evolution in time

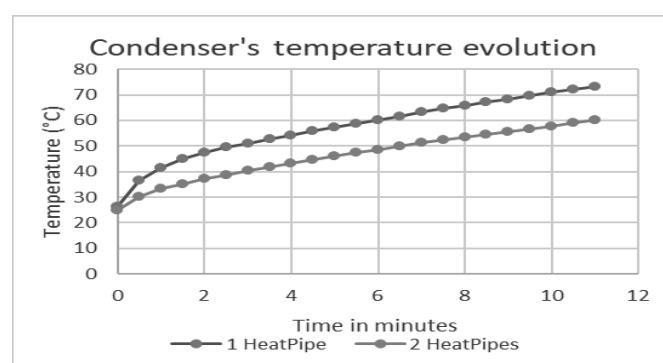


Fig. 5 Condenser's temperature evolution in time

V. DATA ANALYZE AND PROJECTION

According with our experience, we get the evolution of the LED temperature at igniting for the first 20 minutes of lighting. We can make an approximation of the trend follow by the temperature with utilization of a logarithmic trend. In fact, we think that the temperature increases less and less following a logarithmic curve. The physical signification of this can be explain by the fact of thermodynamics systems can be modeling with mathematical curve with the condition that the extrapolation can't be too longer in time. We choose to show this trend during 1 hours that is in the same order of magnitude than the real utilization of LED in our case.

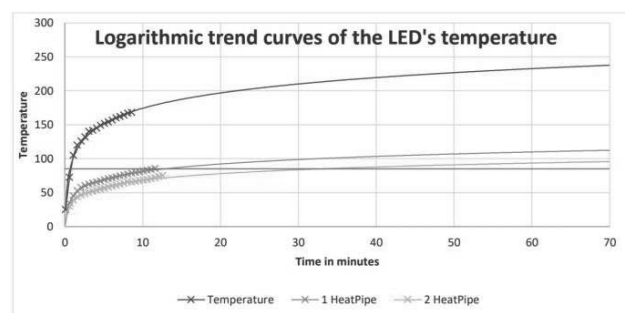


Fig. 6 Logarithmic trend curves o the LED's temperature



The slowest curve for the augmentation of the temperature corresponding well to the cool down system with two heat pipes, it seems to be the more efficient.

To make an estimation of the value of adding heat pipes to cool down LEDs, we can calculate an approximation of the heat transfer in each heat pipe with using this formula:

$$Q = \frac{\Delta T}{R} \quad (1)$$

ΔT : difference in temperature with the condenser and the evaporator zone. (°C)

R: The resistance of the heat pipe in experiment condition (°C/Joule)

Q: Heat transfer by heat pipe (Joule)

Thanks to thermometers placed on both sides of the heat pipe, we can calculate the ΔT :

By averaging ΔT in time, we obtain for each cases:

- 1) 1 heat pipe: $\Delta T_1 = 12,4^\circ\text{C}$
- 2) 2 heat pipes: $\Delta T_2 = 11,6^\circ\text{C}$

The fact of the difference of temperature with one heat pipe is superior as with 2 heat pipes could let us think, according to the equation (1), that the heat transfer is larger with only one heat pipe. In fact, it's true for each heat pipe alone because the heat transfer is spread over several heat pipes. So, for the experiment with two heat pipes; we need to add each heat transfer for each heat pipe used.

For a hypothetic R defined by the experiment and unchanged, we can estimate the heat transfer by the cool down system in each cases of our experiment:

Q_1 : Heat transfer by one heat pipe (J)

Q_2 : Heat transfer by two heat pipes (J)

$$Q_1 = \frac{\Delta T_1}{R} \quad (2)$$

$$Q_2 = \left(\frac{\Delta T_2}{R}\right) \times 2 \quad (3)$$

$$Q_2 = \left(\frac{2 \cdot \Delta T_2}{\Delta T_1}\right) \times Q_1 \quad \frac{2 \cdot \Delta T_2}{\Delta T_1} = 1,8 \quad (4)$$

$$Q_2 = 1,8 Q_1 \quad (5)$$

With the hypothesis that R stay unchanged during all experiment, we can say in our experiment conditions, the heat transfer with two heat pipes corresponding to 1,8 more than with only one heat pipe. That demonstration confirms that the adding of heat pipe for cool down LED can be more efficient in a no linear way.

VI. CONCLUSION

We tried to bring closer our model with the reality condition of using LED. For that, we used at the laboratory an average temperature of 25°C corresponding to the ambient temperature of LED's using. After collect of data about our devices (LED and Heat Pipe) we made experiment in modeling conditions to test and find the better cool down system with the using of heat pipe. We can say now that the utilization of two heat pipes reduces in a no-insignificant way the augmentation of the LED's temperature at the igniting.

Our experiments were made in a small time interval in contrary with the real using of LED for public lighting which prevents us from definitively concluding. But, we can say that Heat Pipes could be a cheap and a simple way to cool down and preserve LEDs.

ACKNOWLEDGMENT

I'd like to thank M. Thanad Katpradit who gives me the opportunity to make this research, and as well the graduate students at Chiang Mai University who helped me carry out this experiment.

REFERENCES

- [1] Raymond SONAN OCHOI*, Squad HARMAND1, Daniel LEGER1, Michel FAKES "Modélisation du comportement thermique transitoire d'un caloduc," Congrès Français de Thermique, SFT 2007, Ile des Embiez, 29 mai -1 juin 2007
- [2] "Heat Pipe Technology" Department of Mechanical Engineering, Faculty of Engineering, Chiang Mai University
- [3] "Systèmes diphasiques de contrôle thermique, thermosyphons caloducs" Jocelyne Bonjour
- [4] <https://celsiainc.com/blog-heat-pipe-design-considerations-pt-2/>



Simulation of Straight Line Trajectory Planning for a Manipulator based on Modified RMRC Method

Supachock Tuntivivat, Sarun Chattunyakit, Witcha Upaphai, Adisorn Jarunvorakunvong, and Amnat Chenjitsiri

Faculty of Industrial Education,
Rajamangala University of Technology Phra Nakhon
399 Samsen Rd., Vachira Phayaban, Dusit, Bangkok, 10300
supachock.tu@rmutp.ac.th

Abstract— This paper proposes a dynamic simulation of a straight line trajectory planning for a 6 DoFs manipulator. In this study, resolved motion rate control (RMRC) method is used to control the manipulator from point to point. However, the trajectory of an end-effector is not moved in a straight manner. To overcome this problem, we employ the unit vector technique to discover the series of point which represent the straight line and applied them with RMRC method. In the simulation, it was found that our proposed method can provide better results of trajectory planning compared to the original RMRC method. This study has shown that the proposed method can be used to control a manipulator with a straight line trajectory, which is beneficial to utilize in an industrial application that requires a straight line planning, such as grapping, welding, and cutting.

Keywords—Trajectory; Manipulator; Control; RMRC; Straight Line Planning

I. INTRODUCTION

Nowadays, robotic systems play an important role to substitute humans for several purposes. In 1970, the factory robots were much debated to change the way of employment [1]. Since then, the number of industrial robots had been increased highly around the globe. A rigid manipulator is one of the well-known electrical machine that is widely used in a number of factories – assisting humans to minimize difficulty and working hours. The mechanism of manipulator was invented and developed by imitating the basic concept of human's arm movement. Generally, manipulators consist of four standard mechanical components, i.e. base, joints, links and end-effector. Robot base is normally constructed with floor, wall or ceiling, depended on required work. Joints and links are similar to human's elbow and arm. The important part is an end-effector or end of arm tooling, which is utilized to attach some specific tools according to target applications, such as gripper, welding head, etc. As a result, the position of the end-effector is a key factor in order to control a manipulator. The position of an end-effector can be calculated from joint angles with forward kinematic equation. By contract, the end-effector can be controlled by calculating all angles of each joints with inverse kinematic process. In practical situation, a manipulator should control its effector not only the position but also the motion, to avoid hitting the surrounding objects.

In recent years, there has been an increasing interest in manipulator trajectory planning with new techniques, for example, CPG-based method and self-organizing maps based method [2][3]. Although these method can be operated with manipulators successfully; however, they cannot provide the straight line trajectory, which is required to avoid an obstacle in some situation. Straight line trajectory planning for an end-effector of manipulator had been proposed by Russell H. Taylor with the concept of interpolation between points in Cartesian space and manipulator's kinematic equation [4]. In [5], other interpolation techniques, called as "line interpolation with polynomial blending" and "cubic interpolation", was employed to discover the trajectory with the control of velocity and acceleration instead of joint angel control.

In this paper, we propose a new straight line trajectory planning with the modification of resolved motion rate controller (RMRC) which was implemented in [6][7]. Our algorithm employs the similar concept with interpolation technique used in [4]. Each joint of manipulator is controlled by the angular velocities calculated by RMRC approach. However, original RMRC method does not provide the straight line trajectory. We therefore employ unit vector computational technique to generate the straight line trajectory. Using a numerical simulation, it was possible to prove the proposed method is feasible to discover the straight line trajectory.

II. MEDTHODOLOGY

To design the model of a manipulator, we employ an ABB IRB120 model shown in Fig. 1 as a main model. The reason of selecting ABB IRB120 is that it has 6 DoFs and a common structure of manipulators used widely. We simulate motion of a manipulator using the forward kinematic approach. Resolve motion rate control is used to find the trajectory of end-effector from point-to-point. As aforementioned that it cannot provide a straight line trajectory, we calculate series of point with unit vector to make the end-effector moving in the straight direction.

A. Forward Kinematic

We employ the traditional Denavit – Hartenberg parameters (DH) to calculate the position of an end-effector, respecting to



Fig. 1. ABB IRB120 model manipulator.

a zero frame. There are 4 parameter for DH method, θ_i , d_i , a_i and α_i , which are joint angle, link offset, link length and link twist of link number i -th, respectively [8]. Table I shows the Denavit-Hartenberg Parameter of the studied manipulator.

TABLE I. DENAVIT – HARTENBERG PARAMETERS OF THE

i	a_{i-1}	α_{i-1}	d_i	θ_i
1	0	0	d_1	θ_1
2	0	-90°	d_2	θ_2
3	a_2	0	d_3	θ_3
4	a_3	-90°	d_4	θ_4
5	0	90°	0	θ_5
6	0	-90°	d_6	θ_6

The end-effector of the manipulator can be controlled with cross product of matrix as shown in (1).

$$T_i^{i-1} = \begin{bmatrix} \cos\theta_i & -\sin\theta_i & 0 & a_i \\ \sin\theta_i \cos\alpha_{i-1} & \cos\theta_i \cos\alpha_{i-1} & -\sin\alpha_{i-1} & -\sin\alpha_{i-1}d_i \\ \sin\theta_i \sin\alpha_{i-1} & \cos\theta_i \sin\alpha_{i-1} & \cos\alpha_{i-1} & \cos\alpha_{i-1}d_i \\ 0 & 0 & 0 & 1 \end{bmatrix} \quad (1)$$

The forward kinematic of ABB robot from 0-th frame to 6-th frame can be calculated as follows:

$$T_6^0 = T_1^0 T_2^1 T_3^2 T_4^3 T_5^4 T_6^5 \quad (2)$$

B. Resolved Motion Rate Control (RMRC)

In this study, the simulation of manipulator trajectory planning consists of two main parts, i.e., position-to-position control using RMRC and trajectory generation using unit vector

concept, which will be discussed in next section. Resolved motion rate controller (RMRC) is a method that is used to find inverse kinematic of a manipulator by computing angular velocities of all joints, which is written as:

$$\dot{\theta} = J^{-1}(\dot{x}_d + K(x_d - x)) \quad (3)$$

where J is the inverse Jacobian, K is a gain to control a convergence of an error, x_d is the desired end-effector position and x is the actual position of a manipulator. From the angular velocity theory, we can achieve the angel of each motor as:

$$\theta = \theta + \dot{\theta}\Delta t \quad (4)$$

where θ is an angel of joints, $\dot{\theta}$ is an angular velocity and Δt is the time difference from motion. From (3) and (4), we can get the angular velocity by using numerical calculation approach.

C. Modified RMRC

To make an end-effector of a manipulator moving in a straight line, a unit vector is employed to find a series of points for a robot to track by considering it as three vectors system. Fig. 2 shows the relationship between position vector of an end-effector and base frame. With this consideration, we can determine the relationship of vectors as:

$$\vec{r}_{d/s} = \vec{r}_d - \vec{r}_s \quad (5)$$

when \vec{r}_s is a vector of an end-effector respect to a zero frame; \vec{r}_d is a vector of desired position respect to a zero frame; and $\vec{r}_{d/s}$ is a vector of desired position respect to an end-effector. In this case, we can plan the straight line trajectory as:

$$\vec{r}_i = \vec{r}_s + \hat{u}_{r_{d/s}} \times \vec{r}_{p/s} \times i \quad (6)$$

where \vec{r}_i is a vector of moving an end-effector respect to a zero frame; $\hat{u}_{r_{d/s}}$ is a unit vector of $\vec{r}_{d/s}$; and i is a distance between each points.

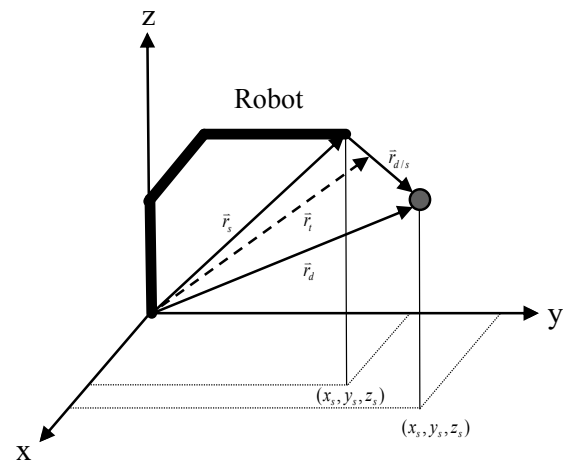


Fig. 2. ABB IRB120 model manipulator.



To ensure that the proposed method can provide the straight line trajectory, we design the control system in the simulation via MATLAB. It firstly calculates the trajectory with unit vector and then send the values back to the RMRC process step by step with considering of errors. If the current position of an end-effector get close to the desired position, the new position will be calculated and control the robot repeatedly. This process can be seen in Fig.3.

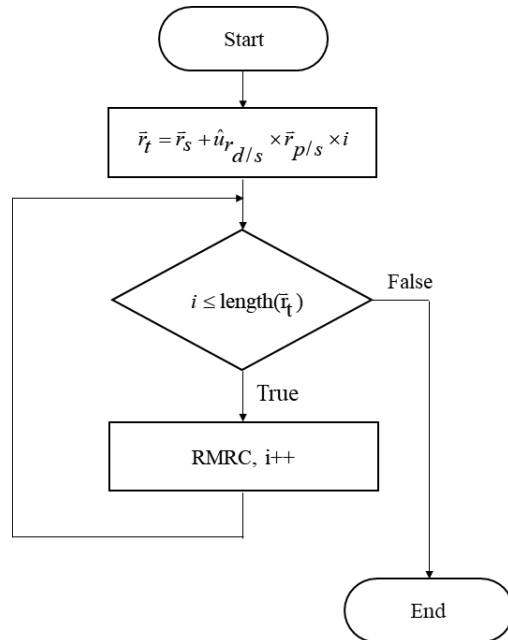


Fig. 3. Flowchart of the proposed method.

III. RESULTS AND DISCUSSION

In this study, we implemented our proposed method to control an end-effector in Matlab in 3 situations, which are:

- a) *Case I Moving along x-axis*: the end-effector was controlled to move from position (39, 0, 67) to (19, 0, 67).
- b) *Case II Moving along y-axis*: the end-effector was controlled to move from position (39, 0, 67) to (39, 20, 67).
- c) *Case III Moving along z-axis*: the end-effector was controlled to move from position (39, 0, 67) to (39, 0, 47).

Changes of trajectory in RMRC and Modified RMRC were also compared using Standard deviation (SD) value to check the robot trajectory. Normally, SD is used in statistics field to check the amount of variation in data set. If all data in data set are equal, the SD will become 0. So, we employ this concept to confirm the straight line trajectory. If the SD value is close to 0, it means that the trajectory of the end-effector is straight. The results obtained from the simulation are listed as follows:

A. Case I: Moving along x-axis

Fig. 5 presents the trajectory of an end-effector of RMRC and modified RMRC moving along x-axis, from left to right. It shows that our proposed method provide better result in term of the straight line. According to Table II, the SD values of modified RMRC are less than the SD values of original RMRC. The trajectory of robot in the simulation can be seen in Fig. 4.

B. Case II: Moving along y-axis

As shown in Fig. 6, what is interesting in this figure is that the proposed method still provide the straight line trajectory when compared to the original one. As same as shown in Table II, our method give smaller SD values, meaning that the manipulator controlled with modified RMRC can move in a straight direction.

C. Case III: Moving along z-axis

The results, as shown in Fig. 7, indicate that RMRC cannot make a robot move straight in z direction. As reported in Case I and Case II, our proposed method can still control the end-effector better than RMRC approach.

TABLE II. STANDARD DEVIATION VALUES OF MANIPULATOR'S TAJECTORY

SD		Case I	Case II	Case III
RMRC	x	-	0.0299	0.0296
	y	0.0102	-	0.0103
	z	0.0230	0.0102	-
Modified RMRC (proposed method)	x	-	0.0035	0.0040
	y	0.0035	-	0.0040
	z	0.0036	0.0035	-

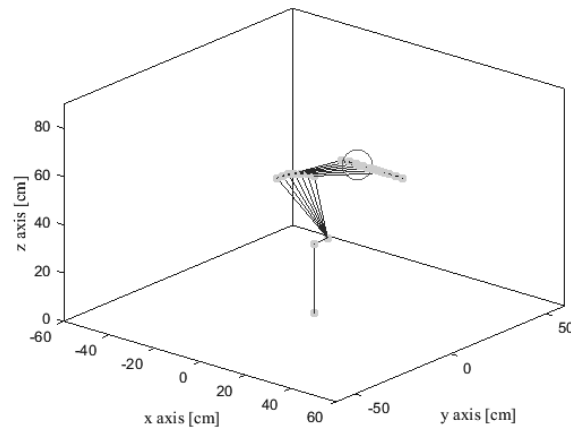


Fig. 4. Simulation of robot trajectory with modified RMRC method moving along x-axis.

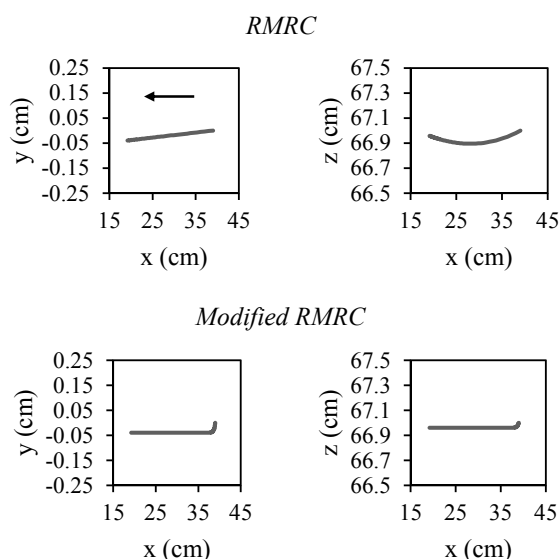


Fig. 5. Simulation of an end-effector moving along x-axis.

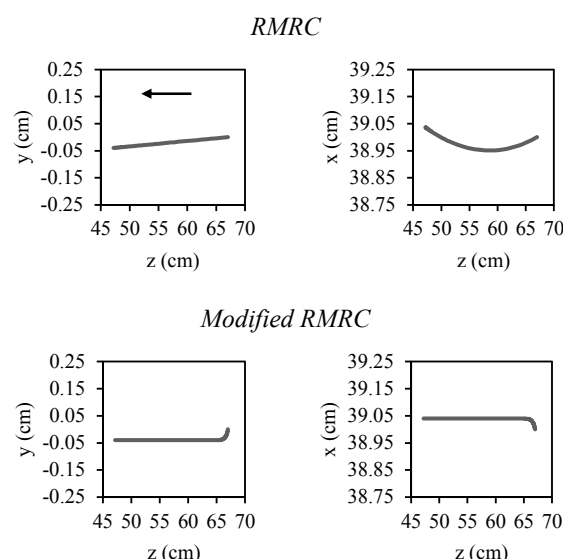


Fig. 7. Simulation of an end-effector moving along z-axis.

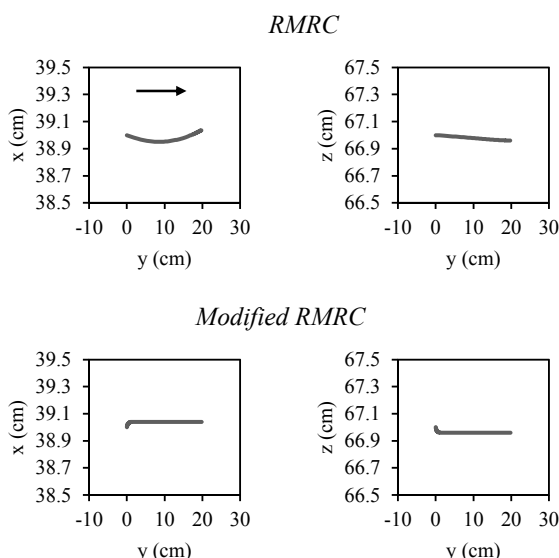


Fig. 6. Simulation of an end-effector moving along y-axis.

IV. CONCLUSION AND FUTURE WORK

According to the experiments, we can compare the simulation results between RMRC and modified RMRC (proposed method) which generates the straight line trajectory by using the series of points to control the end-effector of a manipulator with RMRC method. The results show that our proposed method provide better results when compared to the

original RMRC in terms of standard deviation values. Moreover, this method can be developed further to control the robot in plane space. In the future, we plan to implement and develop the modified RMRC with the an actual robot to improve the performance of the proposed method.

REFERENCES

- [1] L. Royakkers, and R. van Est, "A Literature Review on New Robotics: Automation from Love to War," International Journal of Social Robotics, Volume 7, Issue 5, pp. 549–570, November 2015.
- [2] Y. Fang, J. Hu, W. Liu, B. Chen, J. Qi, and X. Ye, "A CPG-Based Online Trajectory Planning Method for Industrial Manipulators," presented in the Asia-Pacific Conference on Intelligent Robot Systems, 2016.
- [3] R. C. Benante, and A. F. R. Araújo, "Self-organizing Maps to Generate State Trajectories of Manipulators", presented in the IEEE International Conference on Systems, Man and Cybernetics, Canada, 2017.
- [4] R. H. Taylor, "Planning and Execution of Straight Line Manipulator Trajectories," IBM Journal of Research and Development, 23(4), pp.424-436, July 1979.
- [5] M. Svejda, and T. Cechura, "Interpolation Method for Robot Trajectory Planning," presented in the International Conference on Process Control (PC), Slovakia, June 9–12, 2015.
- [6] D. E. Whitney, "Resolved Motion Rate Control of Manipulators and Human Prostheses," in IEEE Transactions on Man-Machine Systems, vol. 10, no. 2, pp. 47-53, June 1969.
- [7] P. Prempraneerach, "Implementation of Resolved Motion Rate Controller with 5-Axis Robot Manipulator Arm," presented in The First TSME International Conference on Mechanical Engineering, Thailand, 2010.
- [8] J. Denavit, and R. S. Hartenberg, "A Kinematic Notation for Lower-pair Mechanisms based on Matrices," Trans. of the ASME. Journal of Applied Mechanics, Vol. 22, pp. 215-221, 1955.



A Study of the Injury Mitigation of Pedestrians Based on Head Injury Criterion Using the Lifted-up Hood Technique

Supachai Lakkam^{1st*} and Kullayot Suwantaraj^{1st}

^{1st}Department of Mechanical Engineering
Faculty of Engineering, Rajamagala University of Technology Phra Nakhon,
Bangkok, Thailand
*supachai.l@rmutp.ac.th

Abstract—Nowadays, car is one of important factors for the human life whereas critical traffic dramatically affects the risk of accident between cars and pedestrians. Therefore, the road accident is the enormous loss of human resources. Regarding this problem, this research aims to find the solution to reduce the rate of death or injury of pedestrians based on head injuries situation. The lift-up hood idea was suggested to study the trend that it is selection method to reduce the pedestrian injuries. There are 8 steps of the vertical space under the hood in this study to verify the reduction of Head Injury Criterion using headform. The Pedestrian Protection Test Procedures in EURO NCAP was referred in this study. From experimental works, the increasing gap between the bottom edge of hood and the engine valve cover tends to decrease the values of HIC. The HIC15 and HIC36 in case of the 4th test decrease 59 and 29 of percentage comparing to the 1st test. The 18 cm of the vertical space is suggested for the injury reduction of pedestrians based on head injuries situation. However, this value may be variable depending on car hood materials and also the design of each car.

Keywords—Injury; Head Injury Criterion; Lifted-up hood

I. INTRODUCTION

Since the car has come to be an important factor of human life and also play a role in the transportation area. In Thailand, the number of road accidents are continuously increased. The World Health Organization (WHO) discovered in the road safety report that Thailand has road accident to the second in the world with 36.2 deaths per 100,000 populations in 2015 [1]. From accident statistics, road accidents between cars and pedestrians often occur and cause many deaths of the victims which most people walk on sidewalks or street.

From accidental injury patterns, the behavior of the accident between car and pedestrians were found that pedestrians were hit by bumpers at lower legs and knees. Then, head of pedestrians was impacted by frontal parts of car. There are classified into 4 patterns: 1) head crashed with hood 2) head hit with A-pillar beam 3) the head bumps the joint between hood and frontal windshield 4) head crashed with frontal windshield.

Regarding the hood is automotive parts which is located in the front of the secondary car from the front bumper. Therefore, car hood is main automotive parts leading to deaths up to 57.06%.

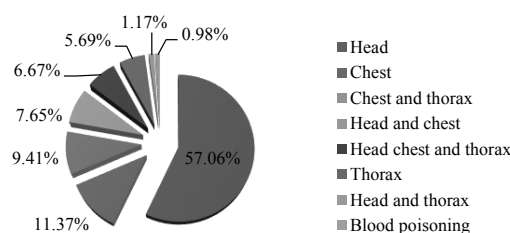


Fig. 1. Cause of deaths [2].

Regarding this problem, this research aims to find the solution to reduce the rate of death or injury of pedestrians based on head injuries situation. The lift-up hood idea was suggested to study the trend that it is selection method to reduce the pedestrian injuries. By the design, the construction of hood was increased the gap between the lower edge of the bonnet and the upper edge of the engine to reduce stiffness during the impact of car-to-pedestrian.

II. LITERATURE REVIEW

A. Injury restraint innovations for pedestrians

Generally, there is a huge amount of studies available focusing on the accident avoidance measures of Heavy Goods Vehicle (HGV). Systems like Anti-lock Brake System (ABS), Electronic Stability Control (ESC) and Brake Assistant (BA) have led to a significant gain in safety in recent years. However, publications in relation to Vulnerable Road Users (VRU) of buses are rare. Most of research focuses primarily on small trucks and Light Truck Vehicles (LTVs).

For difference of injury patterns between flat-front and bonnet-front vehicles in Japan, 101 cases of pedestrians who were struck by the front of a vehicle was investigated [3]. The



result represents that the frequency of chest injuries in flat-front vehicle collisions (30.3%) was significantly higher than that in bonnet-front vehicle collisions (11.8%). Lower leg fractures were more common in the bonnet-front vehicle collisions than in the flat-front vehicle collisions. The pedestrians who were struck by flat-front vehicles tended to sustain more severe injuries, particularly in the chest under the lower impact speeds.

In the United States of America, the influence of different vehicle front profiles on the injuries with different regions of the human body was focused [4]. Based on statistic records, there is a correlation between injury patterns of VRU-LTV and VRU-HGV accidents. From the Maryland Trauma Registry information, it was revealed that cars, Sport Utility Vehicles (SUVs) and pickups caused a higher risk of serious injuries to the thorax and abdomen. However, there was a lower risk of injury at the region below the knee. Furthermore, 59% of the fatalities had Abbreviation Injury Score (AIS) 4+ at torso based on statistical records of pedestrian injuries [5].

Furthermore, the Pedestrian Crash Data Study (PCDS) was used as database to study injury patterns of pedestrians struck by different vehicle types [6]. The injury patterns of VRU hit by either a passenger car or LTV, it implied that extremely thoracic injuries frequently occurred between LTV and VRU collisions. Besides, the impact area for the passenger car was frequently found at the windshield and bumper, whilst for the LTV it was at the hood and leading edge.

B. Injuries and injury sources

Besides, the Head Injury Criterion (HIC) was subsequently developed by Versaca [7]. It is calculated from the head's centre-of-gravity resultant linear acceleration. The integration time interval between t_1 to t_2 which equal levels of acceleration occur either side of an instant of maximum acceleration is the most injurious part of the impulse. It was stated that at a HIC of 1000, there is an 18% probability of a severe head injury, a 55% probability of a serious injury and a 90% probability of a moderate head injury to the average adult [8]. The head injury criterion, HIC15, is used for head injury assessment in both pedestrian regulations and consumer tests. NHTSA indicated that it planned to limit the maximum HIC time interval to 36 milliseconds. The agency recognized that available human volunteer tests demonstrated that the probability of injury in long duration events was low, but reasoned that the agency should take a cautious approach and not significantly change the expected pass/fail ratios that the then unlimited HIC time interval provided. Evaluation, at the time, of the proposed 17 millisecond limit against various test sets from NCAP and FMVSS 208 testing available at the time was found to reduce the failure rate from 46% to 35%. This fact contributed to the decision of agency to reject the proposal of reducing the maximum HIC time interval to either 15 or 17 milliseconds without a commensurate reduction of the maximum HIC value. However, the agency did propose limiting the maximum time interval to 36 milliseconds. This provision allowed the maximum average long duration acceleration to rise to a limit of 60 G's. It was shown that an impact of 15 ms or less was critical in skull fractures and concussions [9]. The HIC is a measure of head injury severity which includes the effect of the head's linear

acceleration and duration of acceleration. A higher acceleration can be tolerated for a short duration and vice versa for a longer duration. The duration assessed is maximized at 15 ms in pedestrian test applications.

III. MATERIALS AND METHODOLOGY

A. The Design of the Lifted-up Hood Test Kit

The lifted-up hood test kit was set up to study the trend of pedestrian violence and injury reduction. By the 8 adjusting vertical space levels between the lower edge of the bonnet and the upper edge of the engine from 12 to 23 cm, the active bonnet mechanism was installed to lift up the bonnet. The design and construction of the hood set as shown in Fig. 2.

B. Headform

The headform impactor was designed and build as engineering tools (see in Fig.3) to assess the injury level of pedestrian head according to EURO New Car Assessment Programs in terms of pedestrian protection testing [10] which defined the mass of headform 4.5 kg and the impact velocity at 40 km/h.

C. Methodology

For the experimental test, the dropped mass in vertical direction was defined to simulate the collision situation. The 40 km/hr or 11.11 m/s of the impact speed (according to EURO New Car Assessment Programs in terms of pedestrian protection testing) was converted to 6.2 meter of dropped height according with potential energy and kinetic energy balance. Besides, pedestrian protection testing was classified as child and adults case as shown in Table 1.

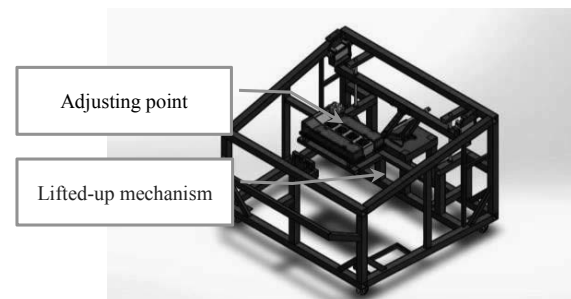


Fig. 2. The lifted-up hood test kit.

TABLE I. Testing Condition

Details	Impact simulation	
	Child	Adult
Impact velocity (km/hr)	40	40
Impact angle from horizontal (°)	50	65
Mass of headform (kg)	3.5	4.5
Distance of edge line along the car (mm)	1,000 to 1,500	1,700 to 2,100

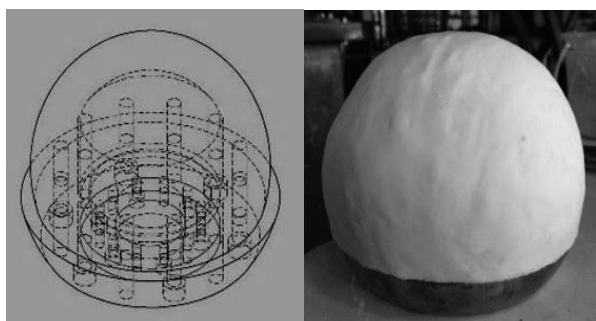


Fig. 3. Headform

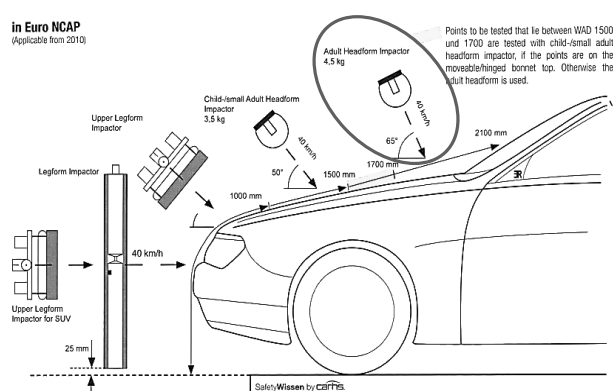


Fig. 4. Impact angle according to EURO New Car Assessment Programs in terms of pedestrian protection [10].

According to EURO New Car Assessment Programs in terms of pedestrian protection testing, the impact angle between adult headform impactor and car hood is 65° as shown in Fig. 4. In this research, vertical space levels between the lower edge of the bonnet and the upper edge of the engine was divided into 8 levels starting from the gap of 12 cm to the first level expanding to 14, 16, 18, 19.5, 21, 22, and 23 cm respectively. These vertical space are divided based on the limitations of the lifted-up hood mechanism.

D. Head injury Criterion

The Head Injury Criterion (HIC) is a measure of the likelihood of head injury arising from an impact. The HIC can be used to assess safety related to vehicles, personal protective gear, and sport equipment. The maximum time duration of HIC, $t_2 - t_1$, is limited to a specific value between 3 and 36ms[11] usually 15ms. When the impact time is over 36 ms, the acceleration will not rather change compared to the acceleration graph and the acceleration is almost zero. Therefore, the storage of data over a period of 36 ms is not acceptable. Normally the variable is derived from the measurements of an accelerometer mounted at the centre of gravity of a dummy head or headform when the dummy is exposed to crash forces. The HIC formula is defined below:

$$HIC = \max_{t_1, t_2} \left\{ (t_2 - t_1) \left[\frac{1}{t_2 - t_1} \int_{t_1}^{t_2} a(t) dt \right]^{2.5} \right\} \quad (1)$$

When

HIC	is	Head Injury Criterion
\max_{t_1, t_2}	is	maximum acceleration between t_1 and t_2
t_1	is	the initial times [sec]
t_2	is	the final times [sec]
a	is	acceleration [G]

IV. RESULTS

The experimental result in case of 12 cm of the vertical space reveals that the during time from 0 to 15 ms the maximum acceleration is recorded at 5.065 G. As the same time, the during time from 15 to 36 ms the lowest acceleration is recorded at 0.928. As a result, the HIC15 and HIC36 in case of the space level at 12 cm are 215.76 and 292.79 respectively which are high chance of death for pedestrians.

Simultaneously, the 18 cm of vertical space testing result discover that the during time from 0 to 15 ms the maximum acceleration is recorded at 5.34 G. As the same time, the during time from 15 to 36 ms the lowest acceleration is recorded at 0.71 G. As a result, the HIC15 and HIC35 in case of the space level at 18 cm are 90.17 and 208.16 respectively. Which the value is a high level of injury for pedestrians.

Regarding the experimental work, Fig. 5 illustrate that the injury level tends to decrease when the vertical space is increased because of the stiffness reduction. However, the 5th and 6th testing results were found that there are some variable tendencies. There is obit behavior around x direction and z direction of headform in the 5th and 6th testing. Therefore, the acceleration in coordinate axes were unstable during the impact. It can be explained by the hypothesis that the material which strike with the highly flexible material will take more distance and impacted time. As a result, the severity of head injury (HIC15, HIC36) was higher value.

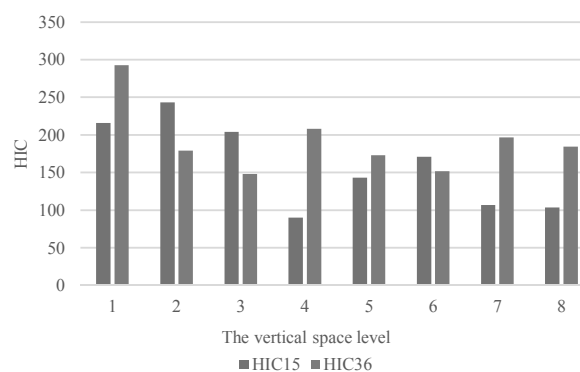


Fig. 5. The HIC15 and HIC35 in 8 vertical space level.



V. CONCLUSION

As a result, the criteria based on head injury were determined. The HIC15 and HIC36 are also downward trend when the gap between the lower edge of the bonnet and the edge of the engine were increased. Besides, it was also found that the highest HIC was obtained with the first testing at 12 cm of the vertical space while the 4th testing at 18 cm of the vertical space was found the lowest value of HIC. The results indicate that The HIC15 and HIC36 in case of the 4th test decrease 59 and 29 of percentage comparing to the 1st test. The HIC tendency of the testing behind (5th to 8th) are gradually steady. The 18 cm of the vertical space is suggested for the injury reduction of pedestrians based on head injuries situation. However, this value may be variable depending on car hood materials and also the design of each car.

ACKNOWLEDGMENT

The authors are grateful for the financial support for this research from Rajamangala University of Technology Phra Nakhon.

REFERENCES

- [1] World Health Organization, Global status report on road safety, 2015, P 270, http://www.who.int/violence_injury_prevention/road_safety_status/2015/en/
- [2] W. Sithicharoon, "Alcohol in the blood of the death victims from the road accident," Thesis, Chulalongkorn University, 2006 (in Thai)
- [3] G. Eason, B. Noble, and I.N. Sneddon, "On certain integrals of Lipschitz-Hankel type involving products of Bessel functions," Phil. Trans. Roy. Soc. London, vol. A247, pp. 529-551, April 1955. (references)
- [4] M.F. Ballesteros, P.C. Dischinger and P. Langenberg, "Pedestrian injuries and vehicle type in Maryland," Accid. Anal. Prev., 2004, Vol. 36, pp. 73-81.
- [5] B. Fildes, H.C. Gabler, D. Otte, A. Linder, "Pedestrian impact priorities using real-world crash data and harm," IRCOB conference. Graz, 2004.
- [6] D. Longhitano, B. Henary, K. Bhalla, J. Ivarsson, "Influence of Vehicle Body Type on Pedestrian Injury Distribution," SAE World Congress, Detroit, 2005.
- [7] J. Versaca, "A Review of the Severity Index," Proceedings of the 15th Stapp Car Crash Conference, New York, Society of Automotive Engineers, 1971, pp. 771-796.
- [8] M. Mackay, "The increasing importance of the biomechanics of impact trauma," Sadhana, Aug 2007, Vol. 32, pp. 397.
- [9] P. Prasad and H.J. Mertz, "The position of the United States delegation to the ISO working group 6 on the use of HIC in the automotive environment," Washington DC, USA., SAE Government Industry Meeting and Exposition, 1985, Doc. No. 851246.
- [10] EURO New Car Assessment Programs (Pedestrian protection procedures)
- [11] B.G. McHenry, "Head Injury Criteria and the ATB," McHenry Software, Inc.



Simulation on Porosity of Twisted Fiber Bundle Wick

Jetsadaporn Simsiriwong*, Niti Kammuang-lue, Phrut Sakulchangsattajai, Pradit Terdtoon
Department of Mechanical Engineering, Faculty of Engineering, Chiang Mai University,
Chiang Mai, Thailand. Tel:+66-53-944144 Fax. +66-53-226014
*Corresponding author; E-mail: jetsadaporn36@gmail.com

Abstract— Porous wick is an important component which affect to thermal performance of heat pipe. In manufacturing of fiber bundle wick that commonly used in the miniature heat pipe for cooling compact electronic devices such as smartphone, is twisted to maintain its shape. The twisting fiber affect the pore size and the flow of working fluid in fiber bundle wick. This study presents the simulation of fiber arrangement in twisted fiber bundle wick, in order to investigate twisting effect on porosity of fiber bundle wick. The open-packing method was used to simulate cross-section of twisted fiber bundle wick to determine the porosity by cross-section area. In analysis procedure, the porosity of non-twisted fiber bundle wick was compared with porosity of twisted fiber bundle wick with pitches of 0.5, 1, 5, 10 and 20 mm. According to studies, Non-twisted fiber bundle wick had more porosity than twisted fiber bundle wick. When the pitch decreased which meant tight twist, the porosity also increased. Because of the same bundle size, the twisted fiber bundle wick with more pitch can contain fewer fibers. Moreover, the porosity of mixing of fiber's diameter between 30 and 50 μm had slightly higher than use only fiber's diameter 30 μm . Because of lower number of fiber, it can save production costs.

Keywords—fiber bundle wick; twisted fiber; porosity; simulation; open-packing

I. INTRODUCTION

Heat pipe is a two-phase heat transfer device that transfers heat from the heat source to the heat sink by latent heat of vaporization of working fluid. Heat pipe has low thermal resistance that is very reliable and high performance for application in electronic cooling.

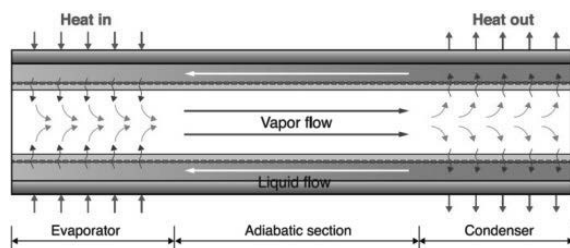


Fig. 1 Operation of heat pipe. [1]

From Fig. 1, The operation of heat pipe starts when one end of heat pipe is heated, working fluid in evaporator will evaporate. Vapor is transported towards the other side that is

called a condenser and condenses to liquid again. The condensed working fluid will flow back to a evaporator to receive heat again. This fluid moves by the support from the capillary pressure in the porous wick inside the heat pipe. [1-2]

The characteristics that have been used widely in evaluating the performance of the heat pipe are the capillary pressure and permeability, because both of these values affect the circulation of the working fluid in the heat pipe, because the evaporator requires working fluid for continuous heating.

The capillary pressure and permeability of porous wick depend on the porosity that depends on the pore radius. Each porous wick has different pore characteristics that cause different capillary pressure and permeability. Porous wicks commonly used in heat pipe consist of 4 types that are groove wick, mesh wick, sintered powder wick and fiber wick. [3-5] Comparison of capillary pressure and permeability for each wick type as show in the Fig. 2. [5]

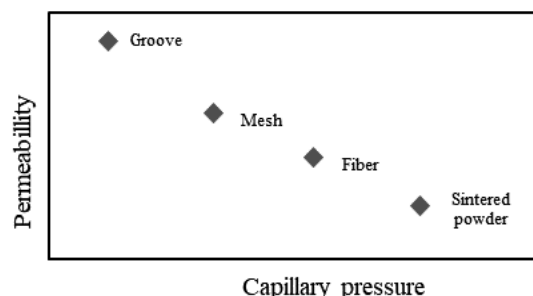


Fig.2 Comparison of capillary pressure and permeability. [6]

From Fig. 2, The sintered powder wick has highest capillary pressure and lowest permeability, because the sintered powder wick has smallest pore radius while the groove wick has lowest capillary pressure and highest permeability, because the groove wick has largest pore radius. The mesh wick and fiber wick have medium porosity and permeability.

Manufacturing of miniature heat pipe that used to cool small electronic device focuses on fiber wick because fiber wick has a high permeability and capillary pressure high enough. [3,6-7]

The study of the thermal performance of heat pipe can be done by experiments directly and used the mathematical



models. In previous research, fiber heat pipes were investigated by experiments to compare fiber wick with other wick types, without the mathematical models that need porosity and permeability is input parameter. In addition, there is no study on porosity of fiber wick by mathematical models.

In previous works, the idealized packing of circular fiber in yarns has been discussed. It was called "Open-packing". The yarn was assumed to be circular in cross-section and composed of a series of concentric cylinders of differing radius as shown in Fig. 3. [8] That has been applied to study the arrangement of twisted fiber bundle. However, this study has not been investigated the porosity of fiber bundle. [9-10]

Thus, the objective of this study is to model twisted fiber bundle arrangement in order to investigate the porosity of twisted fiber bundle wick. The open-packing method was used to simulate cross-section of twisted fiber bundle wick to determine the porosity by cross-section area. It is expected that this study will be beneficial for the modeling of thermal performance of heat pipe with twisted fiber bundle wick, the industry that produces fiber heat pipe and researchers interested in the porosity of porous fiber material.

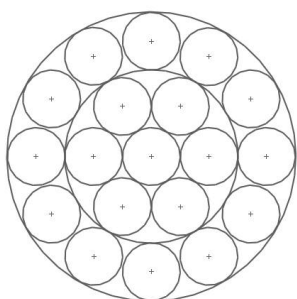


Fig.3 Open-packing of circular fiber, showing center, 2nd and 3rd layers. [8]

II. MODELING OF FIBER ARRANGEMENT

In considering the twisted fiber bundle model, the fibers were considered the twisting effect. Each fiber follows a uniform helical path around one of the concentric cylinders, so that its distance from the bundle axis remains constant. A fiber at the center will follow the straight line of the bundle axis but, going out from the center, the helix angle gradually increases, since the number of turns of twist per unit length (Pitch) remains constant in all the layers as shown in Fig. 4. [8] Where h is pitch, α and θ are helix angle, R and r are distance between bundle center and fiber center, L and l are fiber length in case of 1 pitch.

In this study, the porosity was calculated from the cross-section area of bundle wick. Thus, it was necessary to know the cross-section area of twisted fiber. Twist causes a particular example of change in fiber shape. Because the fibers in the outer layers cross the plane perpendicular to the bundle axis obliquely, they effectively have an elliptical cross section, the minor axis of the ellipse, lying along a bundle radius, equals the fiber diameter, so that radial width of a layer is unchanged. But, because of the greater major axis, the number of fibers

which can be fitted into a given layer is less than predicted for circular fibers.

In order to calculate the size of ellipse easier, twisted fiber with horizontal plane has been considered as non-twisted fiber with inclined plane as shown in Fig. 5. Major axis and area of ellipse were calculated by Equation (1) and (2) respectively.

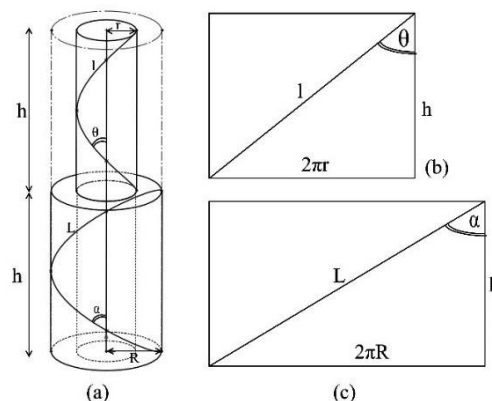


Fig.4 Idealized helical yarn geometry. (a) Idealized geometry; (b) "opened-out" diagram of cylinder at radius r ; (c) "opened-out" yarn surface. [8]

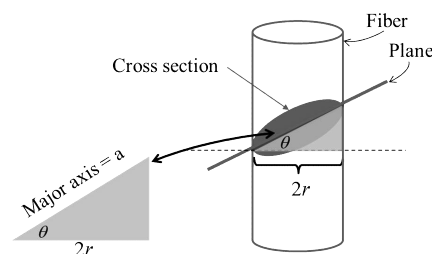


Fig.5 Cross-section of straight fiber which cut by inclined plane

$$a = \frac{2r\sqrt{(2\pi R)^2 + h^2}}{h} \quad (1)$$

$$A_{\text{ellipse}} = \frac{\pi}{4}(a \times b), b = 2r \quad (2)$$

Where a is major axis of ellipse, b is minor axis of ellipse, r is radius of fiber, R is distance between bundle center and fiber center and h is pitch.

As mention previously, the pitch was remained constant in all the layers. Therefore, the major axis of ellipse depends on the distance between bundle center and fiber center (R). The ellipses in layer that is going out from the center, the major axis gradually increases. The number of ellipse in each layer has been considered in close-packed as shown in Fig. 6 which can be written as the following Equation (3).

$$R_{\text{layer}} \cos\left(\frac{180}{m}\right) = r_{\text{major}} \quad (3)$$



Where R_{layer} is radius of circle circumscribing n^{th} layer that is distance between bundle center and ellipse center, r_{major} is major radius of ellipse n^{th} layer

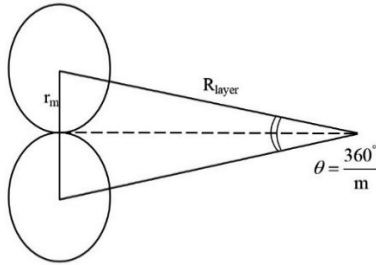


Fig.6 Showing angle subtended at center of circle by m fibers closed-packed in a circle.

Therefore, the hypothesis of the simulation of the twisted fiber bundle wick by open-packing method was follows:

1. For layer 1, The cross-section of fiber was a circle at coordinate $(x,y) = (0,0)$.
2. The boundaries of each layer were adjacent and not overlapping.
3. The center of all ellipse in same layer had equal distance from the bundle center, equal size and equal gap between each other.
4. All ellipse was not overlap.

The operation of the simulation of the twisted fiber bundle wick by open-packing method was follows:

1. Set the input information: fiber radius (r_f), number of layer (i) and pitch (P)
2. Plot: the circle in layer 1
3. Calculate: layer radius (R_{layer}), major radius and number of ellipse which can be fitted into a layer.
4. Plot: all ellipse in layer that ellipse has same gap between each other.
5. Repeat Section 3 and 4 until the number of layers is complete.
6. Cross-section of the twisted fiber bundle wick is shown, and the porosity is calculated from Equation (4)

$$\varepsilon = \frac{\pi(r_w^2) - \frac{\pi}{4} \sum_{j=1}^m a_j r_f}{\pi(r_w^2)} \quad (4)$$

Where ε is the porosity, r_w is the radius of fiber bundle wick, r_f is the radius of fiber, m is the number of fiber and a_j is the major radius of ellipse j . The flowchart of this model shows in Fig. 7

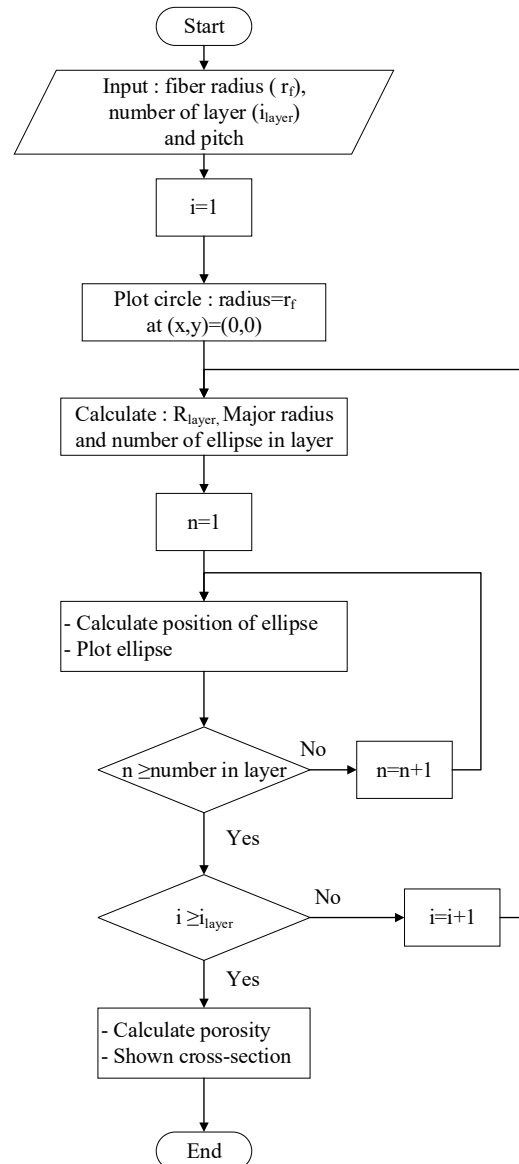


Fig.7 Flowchart of this model.

III. PROCEDURE TO EVALUATE POROSITY

In order to study the porosities of twisted fiber bundle wick, the porosity of non-twisted fiber bundle wick was compared with the porosities of twisted fiber bundle wick with pitches of 0.5, 1, 5, 10 and 20 mm by fiber's diameter was 50 μ m and bundle diameter was 0.75 mm. In addition, considering the porosities with pitch in range 0.1 to 20 mm every 0.1 mm which were show trend of porosity.

Because of the industry's production of fiber bundle wick that used in miniature heat pipe focuses on mixing of fiber's diameter between 30 and 50 μ m, because fiber's diameter 30 μ m can be applied for the very thin heat pipe better than the fiber's diameter 50 μ m, but it is very fragile and expensive. Thus, it has been improved the model for each layer with



different fiber sizes. The fiber's diameter 50 μm was placed in layer 1. After that, the fiber's diameter 30 and 50 μm was alternately packed in each layer. Investigation of the porosity, the porosity of non-twisted fiber bundle wick was compared with the porosities of twisted fiber bundle wick with pitches of 0.5, 1, 5, 10 and 20 mm by fiber's diameter was 50 μm and bundle diameter was 0.75 mm. In addition, considering the porosities with pitch in range 0.1 to 20 mm every 0.1 mm which were show trend of porosity.

IV. RESULT AND DISCUSSION

The porosity of non-twisted fiber bundle wick was higher than twisted fiber bundle wick because of the greater major axis, the number of fibers which can be fitted into a given layer is decreased as shown in Fig. 8 and 9(b).

However, Considering the twisted fiber bundle wick with pitches in range 0.1 to 20 mm every 0.1 mm, it was found that when the pitch decreased, the porosity decreased and increased periodically. The porosity decreases with the equal number of fiber because it was enough space to expand the major axis of the equal number of fiber when the pitch decreased. The porosity increases as the number of fibers decreases because there were not enough spaces to expand the major axis of the equal number of fiber when the pitch decreased as shown in Fig. 9. For very low pitches, the porosity was very high because the fiber was expanding beyond the boundary of bundle that large gap had occurred.

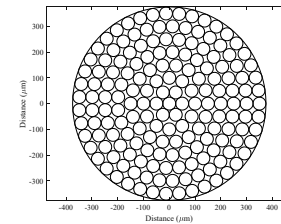
For the mixing of fiber's diameter between 30 and 50 μm which had trend of porosity as well as use of fibers single size. The porosity of non-twisted fiber bundle wick was higher than twisted fiber bundle wick because of the greater major axis, the number of fibers which can be fitted into a given layer is decreased as shown in Fig. 10

In addition, the mixing of fiber's diameter between 30 and 50 μm which had lower porosity than use of only fiber's diameter 50 μm because gap that occurred between the fiber's diameter 30 and 50 μm was smaller than the fiber's diameter 50 μm contact each other. Similarly, when compared with the packing of only fiber's diameter 30 μm , the mixing of fiber's diameter between 30 and 50 μm which had higher porosity because gap that occurred between the fiber's diameter 30 and 50 μm was bigger than the fiber's diameter 30 μm contact each other as shown in Fig. 11 and 12.

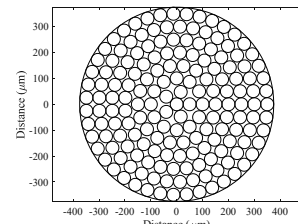
Fig. 12(b), showed the porosities with pitches of 0.5, 1, 5, 10 and 20 mm which is value for manufacturing process. It can save production costs because number of fiber decreased when pitch decreased and mixing fiber's diameter was used less fiber's diameter 30 μm which is very expensive. In addition, mixing fiber's diameter is stronger than use only fiber's diameter 30 μm .

However, for the mixing of fiber's diameter between 30 and 50 μm with very low pitches, the model was slightly accurate. If all ellipses were close-packed, fiber's diameter 30 μm may be placed in the remaining space as shown in Fig. 10(f).

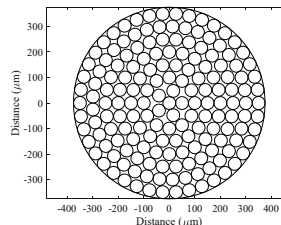
(a) Number of fiber = 173



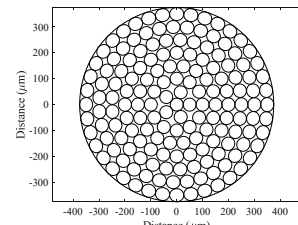
(b) Number of fiber = 172



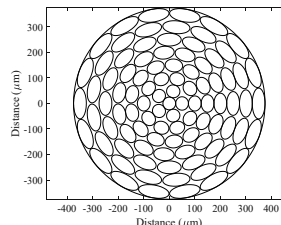
(c) Number of fiber = 169



(d) Number of fiber = 164



(e) Number of fiber = 95



(f) Number of fiber = 56

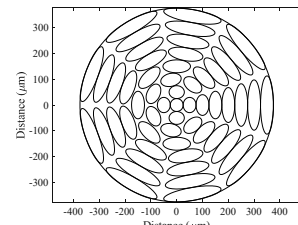


Fig.8 Cross-section of fiber bundle wick with fiber diameter 50 μm in case (a) Non-Twisted, twisted with pitch of (b) 20 mm (c) 10 mm (d) 5 mm (e) 1 mm and (f) 0.5 mm

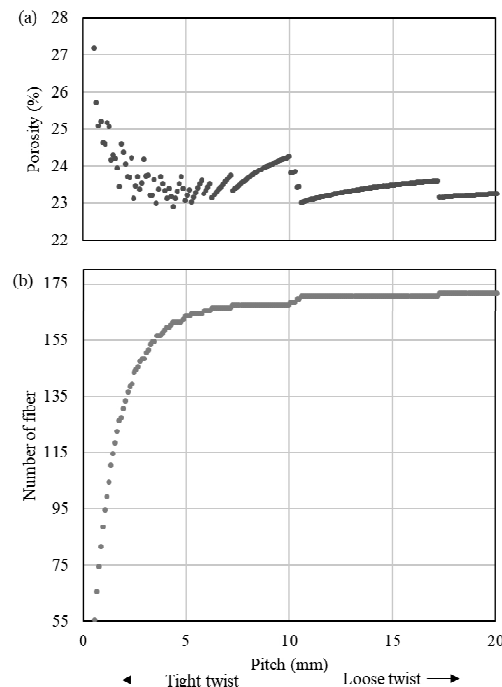


Fig. 9 The relationship between porosity and pitch of twisted fiber bundle wick with fiber diameter 50 μm

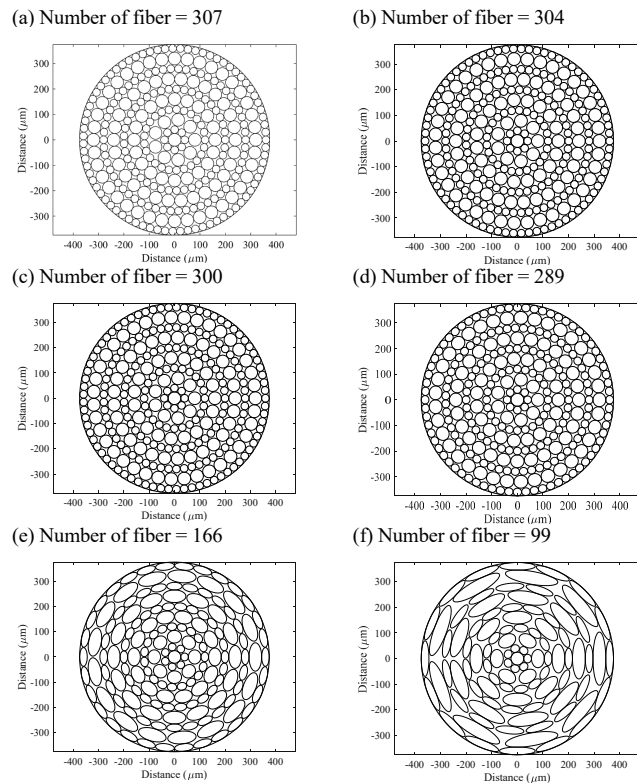


Fig.10 Cross-section of fiber bundle wick with mixing fiber diameter 30 and 50 μm in case (a) Non-Twisted, twisted with pitch of (b) 20 mm (c) 10 mm (d) 5 mm (e) 1 mm and (f) 0.5 mm

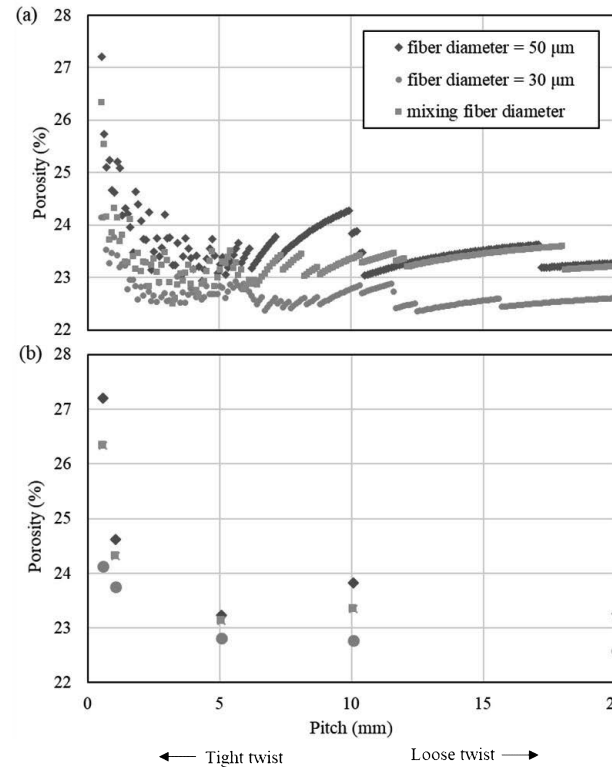


Fig. 12 The relationship between porosity and pitch of twisted fiber bundle wick with mixing fiber diameter 30 and 50 μm (a) pitch in range 0.1 to 20 mm (b) pitch of 0.5, 1, 5, 10 and 20 mm

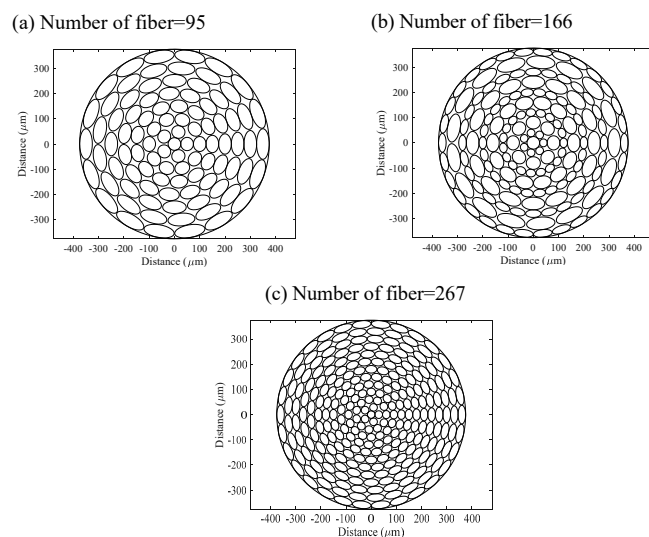


Fig.11 Cross-section of twisted fiber bundle wick with pitch of 1 mm in case (a) fiber diameter 50 μm (b) mixing fiber diameter 30 and 50 μm (c) fiber diameter 30 μm

V. CONCLUSION

The results can be summarized as follows:

1. The porosity of non-twisted was higher than twisted fiber bundle wick because of the greater major axis, the number of fibers which can be fitted into a given layer is decreased.
2. The porosity of mixing of fiber's diameter between 30 and 50 μm had slightly higher than use only fiber's diameter 30 μm , and lower number of fiber. It can save production costs.
3. it was slightly accurate to twist at very low pitches because the fiber's cross-section changed to the ellipse that was so large to fit in the boundary of the porous wick.

Suggestion: Because of twisting with very low pitches, the working fluid hardly flows through the porous material. Although, it had low porosity which was high capillary pressure. Therefore, appropriate of twisted fiber bundle wick must be considered both porosity and permeability that would study in the future.



ACKNOWLEDGMENT

The presented work was financially supported by The Thailand Research Fund (TRF) and Fujikura Electronics (Thailand) Ltd. (Contract no. PHD58I0062) Furthermore, this research was conducted in Heat Pipe and Heat System Laboratory, Department of Mechanical Engineering, Faculty of Engineering, Chiang Mai University, Thailand.

REFERENCES

- [1] B. Chan, Chapter 3: Heat Pipe and Phase Change Heat Transfer Technologies for Electronics Cooling, Electronics cooling, 3.0 license, 2016.
- [2] D.A. Reay, A.P. Kew, and J. R. McGlen, (6th edition.), Heat Pipe. Elsevier Ltd., Kidlington, Oxford OX5 1AJ. England, 2014.
- [3] Y. Kawahara, M. Mochizuki, Y. Saito, Y. Horiuchi, and S. M. Ahamed, "One-millimeter heat pipe and application to cooling module for electronic devices", Fujikura technical review, 2011, pp. 34 – 38.
- [4] J.Y. Lin, S.K. Hwang, "Effect of particle size and particle size distribution on heat dissipation of heat pipes with sintered porous wicks", Metallurgical and materials transactions A, 40(9), 2009, pp. 2071 – 2078.
- [5] M. Mochizuki, Y. Saito, T. Nguyen, K. Mashiko, V. Kumthongkittkun, H. Kuriyama, and P. Ektummakii, "The Development of composite wick heat pipe", 1st International seminar on heat pipe and heat recovery system, Malaysia, 2004.
- [6] I. Sauciuc, M. Mochizuki, K. Mashiko, Y. Saito, and T. Nguyen, "The design and testing of the super fiber heat pipes for electronics cooling applications", 6th IEEE Semi-therm symposium, 2000, pp. 27–32.
- [7] D.S. Schampheleire, D.K. Kerpel, T. Deruyter, D.P. Jaeger, and D.M. Paepe, "Experimental study of small diameter fibres as wick material for capillary-driven heat pipes", Applied thermal engineering, 78, 2015, pp. 258–267.
- [8] J. W. S. Hearle, P. Grosberg, and S. Backer, Structural mechanics of fibers yarns and fabrics, vol. 1, WileyInterscience, New York, 1969.
- [9] R.I. Bruss, and M.G. Grason, "Non-euclidean geometry of twisted filament bundle packing", Proceedings of the national academy of sciences of the united states of America, 109(27), 2012, pp. 10781–10786.
- [10] M. G. Grason, "Geometry and optimal packing of twisted columns and filaments", Reviews of modern physics, 87(2), 2015, pp. 401-419.



Effect of Flattening of Heat Pipe with Double Heat Sources on Thermal Resistance of Grooved - Fibre Heat Pipes

Wisoot Sanhan*, Phrut Sakulchangsatjatai, Niti Kammuang-lue, and Pradit Terdtoon
Heat Pipe and Heat System Laboratory, Department of Mechanical Engineering,
Faculty of Engineering, Chiang Mai University,
Chiang Mai, Thailand
*corresponding author: e-mail: wsanhan@yahoo.com

Abstract—Effect of flattening of heat pipe with double heat sources on thermal resistance of grooved - fibre heat pipes were experimentally studied. The copper tubes with an original diameter of 6.0 mm were used as sealed container and flattened into three final thicknesses of 2.5, 3.0 and 4.0 mm. The heat pipe had distilled water as a working fluid. The heat pipe was tested in horizontal orientation. The two heaters were used to supply heat pipe at two evaporator sections. Additionally, both heat evaporator sections were supplied with combination of two heat inputs at 40W from 0 to 40 W by increment of 10 W each. The operating temperature was controlled at 60 ± 1 °C. The results showed that the trends of the flattening effect depended on how evaporator section#1 and evaporator section#2 were supplied. When final thickness increased, thermal resistance of the heat pipe decreased with supplying heater#1 and heater#2 at heat source variations of 40W:0W and 30W:10W. The both cases had the least thermal resistances of 0.34 and 0.42 K/W at final thickness of 6.0 mm while flattening of heat pipe had little effects on thermal resistances at heat source variations of 20W:20W and 10W:30W with difference thermal resistance of 0.07 and 0.03 K/W respectively. For the heat source variation of 0W:40W, when heat pipe was flattened from final thickness of 6.0 mm into the critical final thickness of 4.0 mm, thermal resistances decreased from 0.34 to 0.27 K/W after that the thermal resistance increased to thermal resistance of 0.39 K/W at final thickness of 2.5 mm. Therefore, decreasing final thickness showed smaller thermal resistances until final thickness reached critical final thickness of 3 mm for heat source variations of 20W:20W and 30W:10W and of 4.0 mm for heat source variation of 30W:10W.

Keywords—Grooved – Fibre Composite Wick; Flattened Heat Pipe; Double Heat Sources; Capillary Heat pipe

I. INTRODUCTION

Heat pipe is the passive heat transfer device that can transfer a large amount of heat energy at very small temperature difference due to latent heat of working fluid inside heat pipe container. Heat energy is transfer from evaporating section to condensing section through evaporative

process, then working fluid as a condensate is drawn back to evaporative section by capillary force in porous media [1].

Recently, laptop computer becomes more compatible and lighter in weight. A miniature heat pipe is one of most efficient for thermal management and widely used as a cooling device. There are two main heat sources in laptop computer such as CPU and GPU which cause temperature to increase in several points within the computer. Accordingly, heat pipe is used in laptop computer to distribute and release the heat. The heat pipe has been necessary designed to transfer heat from those two heat sources inside the circuit board by using one heat pipe in order to reduce number of heat pipe and thus reduce cost. The grooved-sintered heat pipes with two heat sources were investigated to find effects of different heat source variations on the thermal performance [2].

There are various means to study effects of shapes of a heat pipe on thermal resistance. Experimental study on mini-Axial Groove Heat Pipe (HGHP) with fully and partially flattening forms has been reported [3]. It was found that the thermal resistance of fully flattened heat pipe was higher than that of partially flattened heat pipe. Moreover, sintered-wick heat pipe was investigated [4], the effects of flattening of heat pipe was studied. The results showed that flattening of heat pipe has significant effect on thermal resistance. Although many studies have been done to find the heat pipe that has the least thermal resistance and the most suitable for application in laptop computer. Normally the heat pipe in laptop is flattened and responsible for two heat sources simultaneously. Reference [5] studied the effect of flattening of the heat pipe that had two evaporator sections acting as CPU and GPU heat sinks. The miniature grooved-sintered heat pipe was conducted to find thermal resistance for each final thickness of heat pipe that has two heat sources. It was evident that flattening heat pipe and placing higher heat load as near to the condenser section could decreased the thermal resistance.



Although flattening miniature grooved-sintered heat pipe seem fine with transferring heat out of laptop, it has some bad sides such as crack after flattening on sintered wick [6] and higher cost of manufacture. In this study, focus on replacement of sintered wick over fibre wick in miniature heat pipe to increase performance of the heat pipe.

II. EXPERIMENTAL SETUP AND PROCEDURE

A. Heat pipe specification

The heat pipes used in this work were round and flattened heat pipes which were made from the copper tube with a 6.0 mm outer diameter and 200.0 mm length. The inner-wall tube was axially grooved for 50 grooves. The 200 fibre strands were inserted into the tube to compose a groove - fibre composite wick. To secure the fibres distributed uniformly alongside and closed with grooves, the 0.44 mm diameter spring with spiral shape was placed innermost of the tube. Both the ends of the tube were swaged and then one end was sealed leaving another for filling working fluid into the tube. The open end was evacuated and then deionized water was filled in for 100% of wick void volume. After the wick was saturated with the working fluid, the opened end was sealed to enclose the tube. The heat pipes were heated to prevent crack and leakage in flattening process. Heated heat pipes were pressed to their final thickness (*FT*) such as 2.5, 3 and 4 mm.

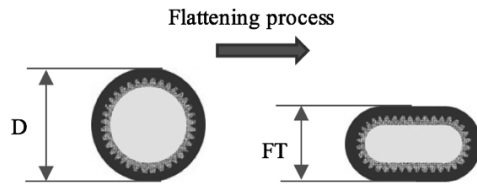


Fig. 1. Flattened heat pipe cross section

B. Experimental setup

The experimental setup was placed on a horizontal platform at ambient temperature of $25 \pm 1^\circ\text{C}$. The apparatus was composed of two heating modules, a cooling module and a data acquisition module as illustrated in Fig. 2. The heating modules were designed as the evaporator sections of the heat pipe which consisted of adjustable DC powers, copper blocks and heating rods. The heat inputs were controlled by the adjustable DC power equipment (GW Instek GPR-7550D). The heating rods were used through heat copper blocks to transfer heat flux uniformly to heat pipe. The cooling module was designed as the condensing section of heat pipe which was cooled by the aluminum heat sink attaching 12V DC fan. The data acquisition module consisted of data logger (BrainChild VR18) and type-K thermocouple. The temperature of heat pipe was monitored by the data logger that had an uncertainty of $\pm 1^\circ\text{C}$. In addition, the thermocouple 16 points were installed on the outer surface of heat pipe as displayed in Fig. 3 (Black dots are temperature measurement probes).

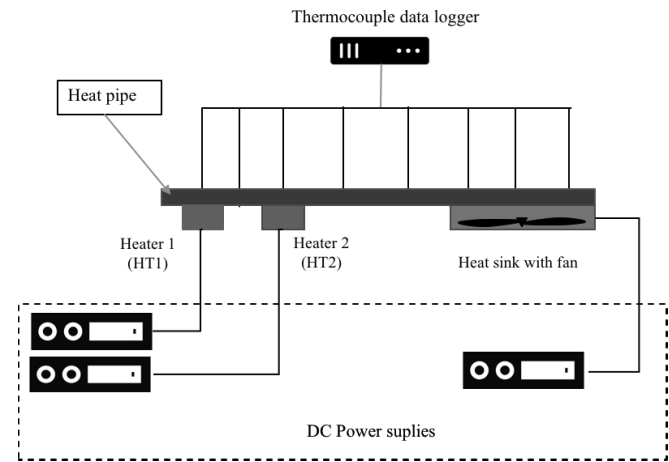


Fig. 2. Experimental setup

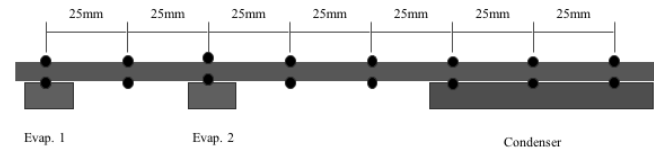


Fig. 3. Temperature measuring points

C. Procedure

The experimental test was performed to investigate the thermal performance of grooved-fibre heat pipes. Firstly, evaporation section#1 and section#2 were supplied by heater#1 (HT1) and heater#2 (HT2) as heat sources. Each heater was varied from 10 to 40 W with an increment of 10 W. Secondly, the operating temperature or adiabatic temperature was controlled at $60 \pm 1^\circ\text{C}$ by adjudging DC case fan voltage at cooling module. Finally, the temperature points (black dots in Fig. 1) were measured and recorded at steady state condition. The thermal resistance of grooved-fibre heat pipe was then calculated.

D. Thermal resistance

As heat pipe is a heat transfer device, the performance of it is presented in term of thermal resistance, R_{th} , which is calculated as follow.

$$R_{th} = (T_e - T_c) / Q_{total} \quad (1)$$

Where T_e is the average of the temperature at the bottom of both evaporator section#1 and section#2, T_c is the average of condensing section temperatures at the bottom, as shown in Fig. 3, Q_{total} is heat inputs to the heat pipe at evaporator section#1 and section#2.



The thermal resistance represents the performance of a heat pipe. It indicates that the less thermal resistance provides the more performance of a heat pipe at particular conditions.

III. RESULTS AND DISCUSSION

A. Effect of flattening of heat pipe on thermal resistance

The results shown in the Fig.1 that the trends of the flattening effect depended on how evaporator section#1 and evaporator section#2 were supplied. It was found that when final thickness (FT) increased, thermal resistance (R_{th}) of the heat pipe decreased with supplying heater#1 and heater#2 at heat source variations of 40W:0W and 30W:10W. The both cases had the least R_{th} of 0.34 and 0.42 K/W at FT of 6.0 mm (Round heat pipe) while flattening of heat pipe had very little effects (nearly no effect) on R_{th} at heat source variations of 20W:20W and 10W:30W with maximum different R_{th} of 0.07 and 0.03 K/W respectively. For the heat source variation of 0W:40W, when heat pipe was flattened (FT decreased) from 6.0 mm into the critical FT of 4 mm, R_{th} decreased from 0.34 to 0.27 K/W after that the R_{th} increased to R_{th} of 0.39 K/W at FT of 2.5 mm. Similar work, Reference [5] which had the same testing platform to this work but the major difference was this work used grooved-fibre wick while Reference [5] used grooved-sintered wick instead, was brought to compare with this work. Reference [5] has studied flattening of grooved-sintered heat pipe. It was found that decreasing of FT showed smaller R_{th} until FT reached its critical value which is 3 mm for heat source variations of 20W:20W and 30W:10W and of 4 mm for the heat source variation of 30W:10W. Similar work [5] was brought in order to compare these flattening effects. In Fig.4, the comparison also showed that R_{th} decreased as FT decreased to critical FT of 3.0 mm. For the heat source variation of 20W:20W [5] which R_{th} changes most due to flattening effect, the R_{th} decreased from 0.97 to 0.79 K/W.

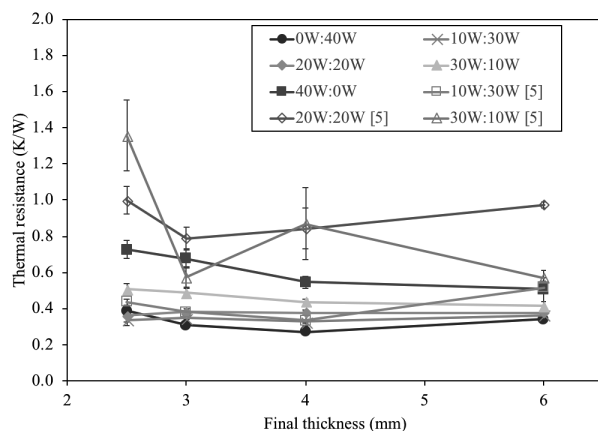


Fig. 4. Effect of flattening of heat pipe on thermal resistance

B. Results of Heat source variations on thermal resistance

The results in the Fig.5 showed that the trends of the flattening effect depended on final thickness and heat source variation. However, the trends of any FT of the heat pipes agree very well to one another that supplying HT1 less than HT2 show smaller R_{th} 's. The most different R_{th} occurred at the FT of 2.5 mm that R_{th} decreased from the R_{th} of 0.39 K/W to 0.73 K/W which was up to 87% decreasing R_{th} from heat source variation of 40W:0W to 0W:40W. More over the heat source variation cases from reference [5] were compared to this work. It also shows similar trends that supplying HT2 higher than HT1 gave smaller R_{th} . Especially at FT of 2.5 mm [5], the thermal resistance decreased from 1.36 to 0.44 K/W when heat source variations are 30W:10W and 10W:30W respectively.

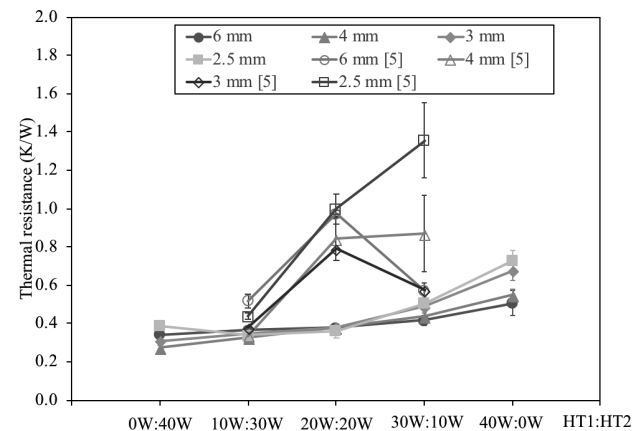


Fig. 5. Effect of flattening of heat pipe on thermal resistance

IV. CONCLUSIONS

Both flattening and heat source variations are the major influences on thermal resistance of a heat pipe. Flattening of heat pipe can benefit to heat pipe performance (reduction in R_{th}), however if the heat pipe keeps being flattened then some heat pipes are likely to perform worse at the heat pipe with the heat source variation of 40W:0W which R_{th} is 0.73 K/W. The lowest R_{th} which is 0.27 K/W occurs at FT of 4 mm at heat source variation of 0W:40W.

The heat source variation of 0W:40W show the least R_{th} when compare to other cases. It leads to conclusion that supplying higher heat load closer to condenser section transfers heat better than the other cases. The most change in R_{th} found at FT of 2.5 mm which is 0.92 K/W difference in R_{th} .

Using grooved-fibre heat pipe is likely less R_{th} as grooved-fibre wick heat pipe has less damage when flattening of the heat pipe. In contrast to grooved-sintered wick heat pipe, flattening of heat pipe can damage wick structure and prevent fluid to flow back to evaporator sections.



ACKNOWLEDGMENT

This research was granted by Research and Researchers for Industries-RRI and Fujikura Electronics (Thailand) Ltd. Furthermore, this research was conducted in Heat Pipe and Heat System Laboratory, Mechanical engineering department, faculty of Engineering, Chiang Mai University.

REFERENCES

- [1] A. Faghri, "Heat Pipes : Review, Opportunities and Challenges," *Frontiers in Heat Pipes*, pp. 1-48, 2014.
- [2] N. Tharawadee, P. Terdtoon, and N. Kammuang-lue, "An Investigation of Thermal Characteristics of a sintered-wick Heat Pipe with Double Heat Sources," *American Journal of Applied Science*, pp. 1077-1089, 2013.
- [3] T. HanZhong , Z. Hong, Z. Jun and J. W. Bowmans, "Experimental study of partially flattened axial grooved heat pipes," *Chinese Science Bulletin, Springer*, vol. 53, no. 19, pp. 3058-3072, October 2008.
- [4] W. Intagun, P. Terdtoon and P. Sakulchangsattajai "Flattening Effect on Heat Transfer Characteristics of Sintered-Wick Heat Pipe," *American Journal of Applied Sciences*, pp. 760-766, 2013.
- [5] W. Sanhan, P. Sakulchangsattajai, N. Kammuang-lue and P. Terdtoon, "Effect of Flattening of Grooved-Sintered Heat Pipes with Double Heat Sources on Thermal Resistance," *The 9th International Conference on Sciences, Technology and Innovation for Sustainable Well – Being (STISWB 2017)*, pp. 232-236, 2017.
- [6] L. Jiang, J. Ling, L. Jiang, Y. Tang, Y. Li, W. Zhou and J. Gao, "Thermal performance of a novel porous crack composite wick heat pipe," *Energy Conversion and Management*, pp. 10–18, February 2014.



Development of Remote Monitoring System of Locomotive Engine via Cloud Network for the State Railway of Thailand

Kullayot Suwantaraj^{1st}, Supachai Lakkam^{1st*} and Anan Tempiem^{1st}

^{1st} Department of Mechanical Engineering
Faculty of Engineering, Rajamagala University of Technology Phra Nakhon,
Bangkok, Thailand
*supachai.l@rmutp.ac.th

Abstract—Rail transport is a quantitativetype of transport. Therefore, a rail accident affects on great damage both human life and properties. One of the causes of the accident is the deterioration of the life span. The performance tests of the locomotive are always essential and unavoidable. This research aims to develop a system for testing and monitoring of diesel locomotive performance. Moreover, the database system for diagnosis of diesel locomotive was established. To achieve this, locomotive brand HITACHI number 4513 within Cummins KTA 50 engine was selected to install the Performance Curve Testing and Performance Tracking Systems. As a results, the maintenance officer of the State Railway of Thailand can monitor the performance of diesel engines, plan the maintenance and also unwanted situation during procession of the locomotive. These systems can reduce the risk of accidents during the procession in practical way.

Keywords—Locomotive; remote monitoring; cloud network

I. INTRODUCTION

Currently, Rail transport system is a mass transit and commercial transport system with low accident rates compared to other land transport systems. Because rail transport is a quantitative transport, it can be said that each transport has a large volume of passengers or cargo. Then, an accident of rail transport system causes great damage to both life and properties. Most accident with the rail transport are caused by many factors such as the integrity and condition of the locomotive, disrespect of traffic laws and negligence of road users on junction way between rail way and other land transport. In according with the long lift of Thai locomotive, in particle way, some locomotives are found that they are not ready-to-use and also overload in maintenance plan. From these reasons, these problems can be prevented by management method.

In preprimary study, there are about 200 locomotive of Thailand currently and also they have been used around 16 to 47 years. As the same time, it is difficult to change the locomotives under limitation budget situation. Therefore, The State Railway of Thailand has maintained to monitor most locomotive and also inspect the availability of the locomotive before take out to

service people. Following the maintenance schedule, all locomotive engines must be overhaul every 2 years or 12,000 working hours to confirm the engine performance.

In practice way, there are many problems with the measurement and instrumentation. It is rather obsolete and does not cover the multiple factors effect on the performance of a locomotive diesel engine. Moreover, there is no database for performance testing of diesel locomotive. As a result, it is not only leading to an obstacle for the maintenance plan, but also became the diagnostics of diesel engine performance problems.

From this reason, this study is aim to develop a real time performance monitoring system of diesel engine for the locomotive. There are many engine parameters are monitored such as electric power, engine status information and map position of locomotive by cloud data network. It is helpful to alarm some unwanted situation before existing.

II. LITERATURE REVIEW

Presently, there are many technologies which were applied to manage the locomotive. The pre-scheduled timetable on a single-track railway line was setup to assign locomotives to unscheduled trains with pre-planned departure times instead of trains [1]. Considering both rigorous and relaxed situations, this paper formulates two mixed-integer programming models of the integrated optimization models, to simultaneously assign locomotives to trains and schedule trains, so that train delay is minimized. In order to solve these problems within reasonable computational times, we develop an efficient optimization approach on the basis of designed locomotive assignment rules and train movement simulation methods. The extensive numerical experiments to validate the dependability and effectiveness of the proposed optimization models and approaches were implemented.

Dynamic loads in the traction drive of freight locomotive was studied by the methods of field tests [2]. The mathematical modeling of the dynamics of the traction drive with a limited set of realizations of perturbations from the railway, it is desirable to use for the study a qualitative picture of the occurrence of





dynamic loads, to determine important factors of loading and comparison of dynamic properties of different designs of under-carriage options. The results of the study showed that the statistical characteristics of the loads in the drive components significantly vary depending on the length of the area of operation. The rational areas of simulation use and field experiments when creating new designs of traction drive are suggested.

In Japan, the concept of the locomotive syndrome (LS) has become widely accepted [3] consisting of the 25-question Geriatric Locomotive Function Scale (GLFS-25), a quantitative, evidence-based diagnostic tool for LS which was developed as the same time. However, the association between the GLFS-25 score and the outcome of physical capacity tests has never been investigated. Furthermore, which physical tests are good indices for evaluating and monitoring the severity of locomotive syndrome have not been identified. In addition, the impact of knee and low back pain on locomotive syndrome is unclear. The purpose of this study is to confirm the validity of GLFS-25 by demonstrating its significant correlation with the outcome of physical function tests and to determine which tests are good indicators for monitoring the severity of LS. The secondary aim of the project is to investigate how much influence knee and low back pain may have on the LS of the middle-aged and elderly.

Moreover, there is a technique for analyzing exhaust emission plumes from unmodified locomotives under real world conditions [4]. It was applied to the task of characterizing plumes from railway trains servicing an Australian shipping port. The method utilizes the simultaneous measurement, downwind of the railway line, of the following pollutants; particle number, PM2.5 mass fraction, SO₂, NO_x and CO₂, with the last of these being used as an indicator of fuel combustion. Emission factors are then derived, in terms of number of particles and mass of pollutant emitted per unit mass of fuel consumed. Particle number size distributions are also presented.

III. MATERIALS AND METHODOLOGY

The conceptual research is creating of a performance monitoring system of the locomotive. By the integrating knowledge between the fields of mechanical engineering and software engineering, the engine situation of locomotive can be monitored during procession and measured in case of parking in test station. The data are divided into 3 groups following:

- Electrical power
- Engine parameters
- Fuel consumption

All 3 groups can be recorded on the locomotives and at the test station to monitor and record the power as shown in Table 1 and forward the information to the software engineering department.

TABLE I. MEASURED AND MONITORED DATA

No.	Data group	Measuring at test station	Monitoring during procession
1	Electrical power	Available	Available
2	Fuel consumption	Available	-
3	Engine status data	Available	Available
	· Cooling water, lubrication, air intake and exhaust temperature	Available	Available
	· Lubrication and fuel pressure	Available	Available
	· Engine revolution	Available	Available

For Software Engineering work, the monitoring system is created to connect the measured data from the mechanical engineering work. The software was established by the researchers. The monitoring system can be connected via an electronic device with a web browser as shown in Fig 1

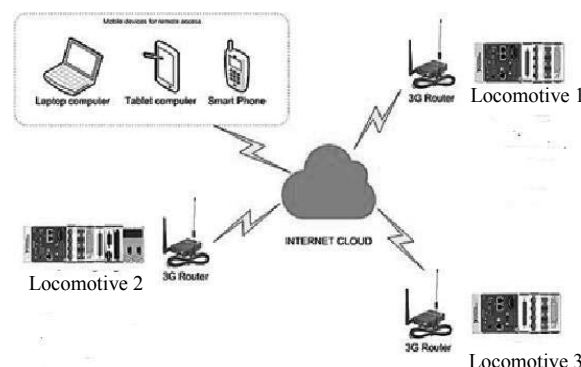


Fig. 1. Monitoring chart during procession of locomotive.

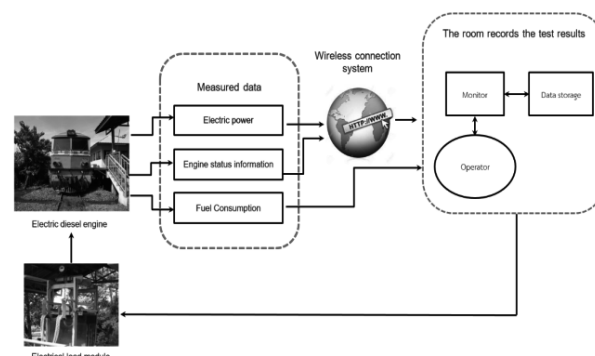


Fig. 2. Network connection with a web browser.

In addition, the alarm function was also created to alert technical staffs. The information will be send to inform the operator in case of the abnormality during the operation. Although the measured value has not been corrected by the operating department, the software can send a signal to control the engine components to prevent damage. In this study, the cummins KTA50-L engine that install on the locomotive brand Hitachi was selected to test at test station.



A. Measuring at Test Station

Performance testing of locomotive are measured at test station by the load simulation test bench. It consists of a water tank, steel plates, a 3-phase motor and electric power cable. The steel plate is raised - down by the 3-phase motor to simulate the locomotive load. The steel plate is divided into two sets, a set of positive plates and negative plate. The electric current is generated from locomotive and distributed through the electric power cable as shown in Fig 3.

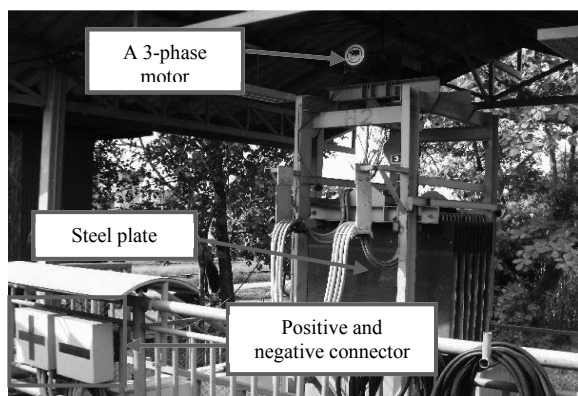


Fig. 3. The load simulation test bench.

Test conditions is referred to UIC 623-3 or the requirements of the State Railway of Thailand, such as the Regulation Characteristics Curve as shown in Table 2.

TABLE 2. TEST CONDITION

Engine revolution (rpm)	700	800	900	1,000	1,100	1,200	1,300	1,400	1,500
Electric current (Amp)	800	1,147	1,275	1,657	1,852	1,875	2,040	2,490	2,000

B. The Design of Monitoring System

For Software Engineering work, the monitoring system is created to connect the measured data from transducers. There are 3 groups of data : 1) electric power 2) engine parameters and 3) Fuel consumption using the NI cDAQ set and processing equipment as shown in Fig. 4.

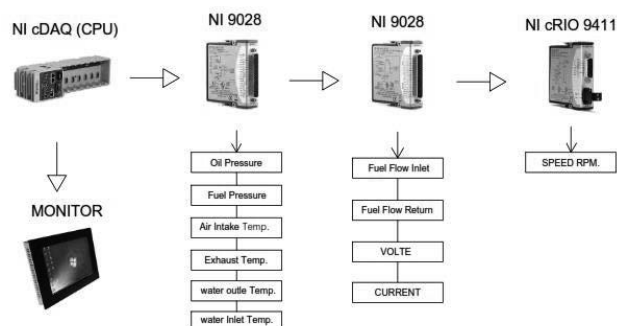


Fig. 4. The connection between NI Cdaq and transducers.

C. Human Machine Interface (HMI)

The HMI (Human Machine Interface) feature in hardware communication can communicate with other measuring devices and transducers. There are several types of signals available, and can communicate with the devices such as power meter, controller etc. via internet connection.

The measured data can be saved in Excel format, as well as easy access to information via the Web Browser, even user is not on a locomotive. The data can be monitored via smart phone or tablet. The display screen shows the value of the screen, the value recorded in the memory card or control changes as shown in Fig. 5.

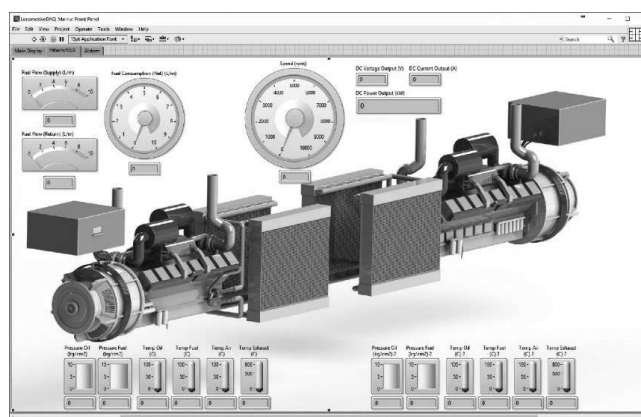


Fig. 5. Human Machine Interface (HMI).

IV. RESULTS

After the installation of the transducers and monitoring system on the locomotive, the connection of the device to the software of the diesel engine testing and tracking system has been carried out during procession of locomotives outside the test station. The 3 groups of data: 1) electric power 2) engine parameters and 3) Fuel consumption can be monitored as well via the Web Browser as shown in Fig. 6. The data access can be done easily.

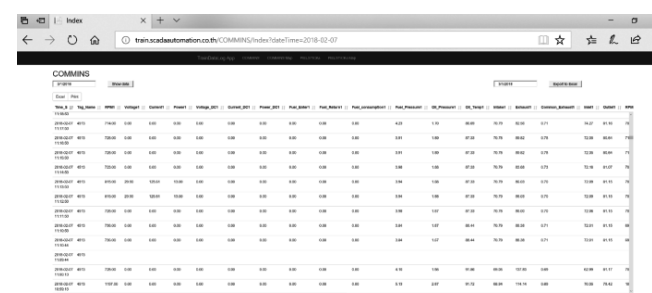


Fig. 6. The data access via Web Browser.

V. CONCLUSION

As a result, the system for testing and monitoring of diesel locomotive performance was developed for the State Railway of Thailand. The database system for diagnosis of diesel locomotive was established. The locomotive brand HITACHI number 4513 within Cummins KTA 50 L engine was selected



to install the transducers. The Performance Curve Testing and Performance Tracking Systems are referred to the testing condition. As a results, the maintenance officer of the State Railway of Thailand can monitor the performance of diesel engines. These systems can reduce the risk of accidents during the procession in practical way.

ACKNOWLEDGMENT

The authors are grateful for the financial support for this research from National Science and Technology Development Agency.

REFERENCES

- [1] X. Xuab, K. Lib, and X. Lua, "Simultaneous locomotive assignment and train scheduling on a single-track railway line: A simulation-based optimization approach," *Computers & Industrial Engineering*, Available online 6 November 2017.
- [2] D.Ya. Antipina, D.A.Bondarenkoa, and O.V. Izmerovb, "Study of Dynamic Loads in Traction Drive of Freight Locomotive under the Influence of Railway Track Irregularities," *Procedia Engineering*, vol. 206, pp. 1583-1586, 2017.
- [3] A. Muramoto, S. Imagama, Z. Ito, K. Hirano, N. Ishiguro, and Y. Hasegawa, "Physical performance tests are useful for evaluating and monitoring the severity of locomotive syndrome," *Journal of Orthopaedic Science*, vol.17, Issue 6, November 2012, pp. 782-788.
- [4] G.R. Johnsona, E.R. Jayaratnea, J. Laub, V. Thomasc, A.M. Juwonoae, B. Kitchend, and L. Morawska, "Remote measurement of diesel locomotive emission factors and particle size distributions," *Atmospheric Environment*, vol.81, December 2013, pp. 148-157.



Mathematical Model of the Optimal Closed-loop Pulsating Heat Pipe Used in an Evacuated Glass Tube Solar Water Heater

Methida Siritan*, Phrut Sakulchangsattajai, Niti Kammuang-lue, Pradit Terdtoon

Department of Mechanical Engineering, Faculty of Engineering, Chiang Mai University,
Chiang Mai, Thailand. Tel: +66-53-944144 Fax. +66-53-226014

*Corresponding author; E-mail: metida.siritan7@gmail.com

Abstract—This research aims to design the optimal closed-loop pulsating heat pipe (CLPHP) for applying into an evacuated glass tube solar water heater to obtain required heat transfer rate and save initial investment. Correlation of thermal performance of CLPHP is another useful tool in design of CLPHP because it can predict heat transfer rate of CLPHP. In this study, correlation of Khandekar *et al.* [7] was used to predict the heat transfer rate of CLPHP and the optimal CLPHP was evaluated by Net Saving Method which was referred in the thermo-economics analysis [8]. The mathematical model was simulated to determine effect of various parameters on net saving. CLPHP was designed by variation of these following parameters: inner diameters of 1.0, 1.5 and 2.0 mm, evaporator length varied from 1.0 to 1.7 m, number of turns increased from 16 to 50 turns and distilled water, R123 and ethanol as working fluids. The diabatic length of 0.05 m, condenser length of 0.3 m and 50% filling ratio of total internal tube volume were controlled. According to latitude of Chiang Mai, Thailand, the solar water heater system was tilted at 18° from horizontal with 644 W/m² of average solar radiation. The results of the mathematical model found that the optimal CLPHP consisted of evaporator length of 1 m, 16 turns, inner diameter of 0.0015 m, distilled water as working fluid and 10 evacuated glass tubes with the maximum of net saving at 48,687 baht for ten years. Thus, the evacuated glass tube solar collector with CLPHP at the optimal parameters will be constructed and tested for the prototype of the system.

Keywords—Solar water heater; evacuated glass tube; closed-loop pulsating heat pipe; correlation; thermo-economics analysis

I. INTRODUCTION

The solar water heater is interesting for heating water to replace electric power because average daily solar radiation in a year in Thailand exceeds 18.0 MJ/m² per day. The solar collector which popular using is evacuated glass tube. It consists of two borosilicate glass tubes and outside of inner tube is coated with a solar selective coating to enhance solar absorption. The evacuated glass tube solar water heater (EGTSWH) can be classified into two main types: single-phase open thermosyphon type and two-phase closed thermosyphon type as shown in Fig. 1. Comparison of both types was found that the annual heat gains through the two-phase collector design 12.9% higher than one [1]. Heat pipe is heat transfer

device into the evacuated glass tube for transferring heat from the collector to water. From previous researches of applying the heat pipe in the EGTSWH was found that maximum efficiency of system with wick heat pipe, thermosyphon and pulsating heat pipes (PHPs) were 46%, 52% and 76%, respectively [2-4]. Application PHPs into the EGTSWH showed increasing efficiency of system. Inside PHPs formed bubble-liquid slug system due to dominance of surface tension forces. When PHPs are received heat at one end and cooled at the other, bubble is going to generate and develop in evaporator section and collapse in condenser section. PHPs can be designed in at least three ways: closed-end pulsating heat pipe (CEPHP), closed-loop pulsating heat pipe (CLPHP) and closed-loop pulsating heat pipe with check valves (CLPHP/CV) [5]. Although the CLPHP/CV has shown to improve the thermal performance, miniaturization of the device makes it difficult and expensive to install such valves [6]. Thus, the CLPHP is most favorable from many practical aspects.

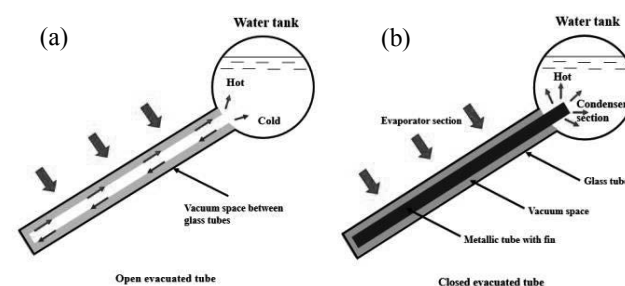


Fig. 1. Working principle of evacuated-tube solar water heaters; (a) single-phase open thermosyphon type and (b) two-phase closed thermosyphon type.

In addition, designing of the optimal CLPHP for applying into the EGTSWH to obtain required heat transfer rate, it can save initial investment of constructing CLPHP. Correlation of thermal performance of CLPHP is another useful tool to design CLPHP because it can predict heat transfer rate of CLPHP [7]. Therefore, the main objective of this work is to apply the mathematical model to design optimal size of CLPHP for



the EGTSWH system with Net Saving Method which was referred in the thermo-economics analysis presented by Soylemez *et al.* [8].

II. MATHEMATICAL MODEL

A. Heat transfer rate required for designing

Specifications of EGTSWH which was designed, it can indicate to heat transfer rate required for designing (Q_{design}). Q_{design} can be calculated by Eq. (1).

$$Q_{design} = \frac{MC_p(T_f - T_i)}{t} \quad (1)$$

where M is mass of water in water tank (kg), C_p is specific heat (kJ/kg °C), T_f is final water temperature or water temperature required of consumption, T_i is initial water temperature and t is operating period.

B. Heat generated into the evacuated glass tube

Q_{design} was used for designing the optimal number of the evacuated glass tube. The number of evacuated glass tube indicated amount of heat generated by the sun into the collector. Chiang Mai in Thailand had average solar irradiation (I_G) approximately 644 W/m² [9]. Thus, the amount of heat generated into the evacuated glass tube (Q_{EGT}) was 68.5 W per tube with loss of reflectance absorptance and emittance of the evacuated glass tube and the coating approximately 20%. Therefore, Q_{EGT} in the system was defined as Eq. (2) when surface area of inner evacuated glass tube (A_c) was shown in Eq. (3).

$$Q_{EGT} = I_G A_c n \quad (2)$$

$$A_c = \pi r L \quad (3)$$

where n is number of evacuated glass tube, r is diameter of inner evacuated glass tube and L is length of evacuated glass tube.

Therefore, the optimal number of the evacuated glass tube which designed by Q_{design} had to gain Q_{EGT} more than Q_{design} because it was amount of heat which transferred to water for providing the final water temperature required.

C. Correlation prediction of thermal performance

In this study, CLPHP was used as heat transfer device of EGTSWH for transferring the heat generated into the evacuated glass tube to water. This model focused on using earlier correlation of thermal performance of CLPHP to design CLPHP for applying into EGTSWH. Khandekar *et al.* [7] proposed correlation to predict thermal performance of CLPHP in all operating orientations (0-90°), evaporator length not over 150 mm and resulting in an overall drift in predictions within $\pm 30\%$ as shown in Eq. (4).

$$q = 0.54(\exp(\beta))^{0.48} Ka^{0.47} Pr_l^{0.27} Ja^{1.43} N^{-0.27} \quad (4)$$

where β is operating orientation (rad), N is number of turns and there are three dimensionless parameters in Eq. (4) Ka , Pr_l and Ja are defined, respectively as follows:

$$Ka = \frac{\rho_l (\Delta P)_{sat}^{e-c} D_i^3}{\mu_l^2 L_{eff}} \quad \text{where} \quad L_{eff} = 0.5(L_e + L_c) + L_a \quad (5)$$

$$Pr_l = \left(\frac{c_{p,l} \mu_l}{k_l} \right) \quad (6)$$

$$Ja = \frac{h_{fg}}{C_{p,l} \Delta T_{sat}^{e-c}} \quad (7)$$

where Ka is calculated for the liquid phase consisting of the pressure difference between vapor and liquid, Pr_l is used to show the single-phase convective effect on heat transfer and Ja highlights the relative importance of sensible and latent portions of heat transfer in a CLPHP.

Then, heat transfer rate and the evaporator area of CLPHP (A_e) can be calculated by Eq. (8) and (9), respectively.

$$Q_{CLPHP} = q A_e \quad (8)$$

$$A_e = 2\pi D_i L_e N \quad (9)$$

where D_i is inner diameter and L_e is evaporator length of CLPHP.

When Eq. (4) and (9) were substituted in Eq. (8), heat transfer rate of the CLPHP (Q_{CLPHP}) can be calculated from Eq. (10).

$$Q_{CLPHP} = (0.54(\exp(\beta))^{0.48} Ka^{0.47} Pr_l^{0.27} Ja^{1.43} N^{-0.27}) (2\pi D_i L_e) \quad (10)$$

D. Thermo-economics analysis

The optimal quantity of variable parameters for CLPHP was selected based on the heat transfer rate and the thermal economics analysis. As a result, Net Saving Method presented by Soylemez *et al.* [8] as shown in Eq. (11).

$$S = \frac{year}{1+d} C_p H Q_{CLPHP} - (1-R_v(1+d)^{-year})(C_{collector}) \quad (11)$$

where C_p is the price of electric power (Baht/Wh), H is operating lifetime of the solar water heater system (hrs/year), Q_{CLPHP} is an amount of annual total thermal energy stored by the solar water heater (Wh), $Q_{collector}$ is the first cost of the solar water heater system (Baht), d is the interest (%) and R_v is the resale value of the solar collector (%), and $year$ is lifetime of solar water heater system.



III. MODELING OF CLPHP DESIGN

From the previous equations, a flowchart of calculating heat transfer rate of CLPHP with correlation and net saving method was shown in Fig. 2. The varied and controlled parameters of calculating heat transfer rate from correlation were summarized as follows:

- Working fluid (WF): distilled water, R123 and ethanol
- L_e : 1,000 - 1,700 mm with 100 mm increments
- N : 16 - 50 turns with 1 turn increments
- D_i : 1, 1.5 and 2 mm
- n : 1 - 10 tubes with 1 tube increments
- Filling ratio (FR): 50% of total internal tube volume
- Condenser length (L_c): 300 mm
- Adiabatic length (L_a): 50 mm
- Evaporator temperature (T_e): 145 °C
- Condenser temperature (T_c): 25 °C
- β : 18° from horizontal axis
- Operating period: 9:00 a.m. to 4:00 p.m.

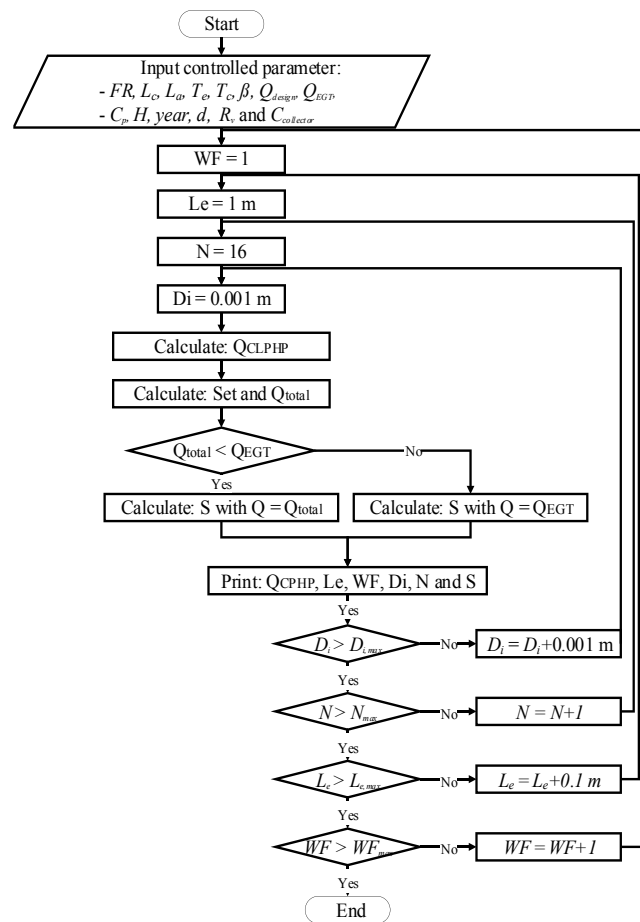


Fig. 2. Flowchart of calculating heat transfer rate of CLPHP with correlation prediction and net saving method.

Then, the controlled parameters of net saving method were presented as follows:

- Interest rate of Minimum Retail Rate (d): 7.12 % per year [10]
- A lifetime of solar water heater system: 10 years
- Resale value of EGTSWH (R_v): 15% of first cost
- Price of electric power (C_p): 0.0035 Baht/Wh
- Operating lifetime of EGTSWH (H): 2555 hrs/year

The simulation modeling was started with the controlled parameters of correlation and net saving method, Q_{design} and Q_{EGT} . In this study, the specifications of EGTSWH consisted of 100 L of capacity and operating period of 7 hrs. Moreover, T_i and T_f were 25 and 65 °C, respectively. Therefore, Q_{design} which was calculated by Eq. (1) was 664 W. Then, Q_{EGT} was input from the varied evacuated glass tubes. In this case, 10 evacuated glass tubes which generated 685 W, were more than Q_{design} . Thus, this Q_{EGT} was input to the modeling. Next, the initial conditions of WF, L_e , N and D_i were respectively input and then Q_{CLPHP} was calculated from Eq. (10). In addition, Q_{total} and the number of set of CLPHP defined as Q_{CLPHP} to Q_{design} were calculated. The Q_{total} indicated heat transfers rate all of sets of CLPHP. Next, the Q_{total} or Q_{EGT} was selected to calculate net saving from Eq. (11). Then, WF, L_e , N and D_i would be iterated until given maximum values. Finally, the optimal CLPHP was the maximum net saving for EGTSWH.

IV. RESULTS AND DISCUSSION

The results of simulation modeling can be divided by three working fluids. Fig. 3 showed that the effect of number of turns on net saving of distilled water. It can be seen that the maximum net saving was occurred at Q_{total} that was slightly over than Q_{EGT} and the number of set was not over one because the maximum Q_{EGT} was 685 W. Furthermore, as the number of turns increased, the net saving steadily decreased because the CLPHPs had a more heat transfer rate than Q_{EGT} . Hence, it was an overdesign of CLPHP. At the same number of turn, it could be shown that the net saving at D_i of 1 mm was more than D_i of 1.5 and 2 mm because bigger inner diameters provided the more heat transfer rate than Q_{EGT} in case the number of turns was 16 turns. Therefore, the maximum of net saving was 48,687 baht for ten years. CLPHP consisted of evaporator length of 1 m, 16 turns and inner diameter of 1.5 mm. In this optimal sizing, the heat transfer rate was 1,205.8 W

Fig. 4 showed the effect of number of turns on net saving of R123. The trend was similar to those in Fig. 3 but at the same number of turn, only D_i of 2 mm gave the more heat transfer rate than Q_{EGT} in case the number of turns was 16 turns. Therefore, the maximum of net saving was 48,584 baht for ten years. CLPHP consisted of evaporator length of 1.1 m, 17 turns and inner diameter of 1.5 mm. In this optimal size, heat transfer rate was 691.64 W.

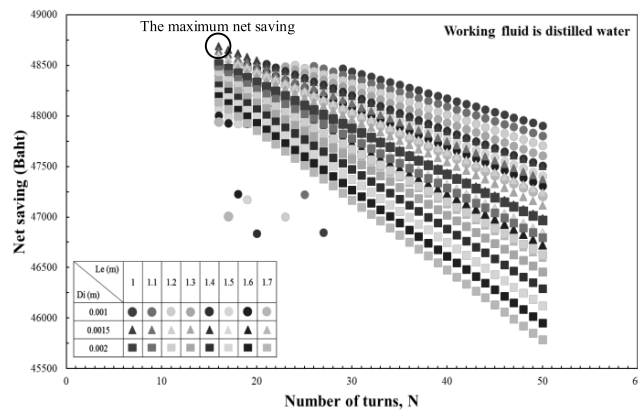


Fig. 3. Effect of number of turns on net saving of distilled water

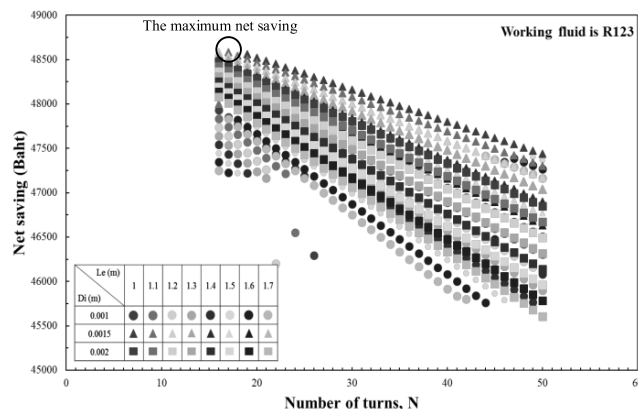


Fig. 4. Effect of number of turns on net saving of R123

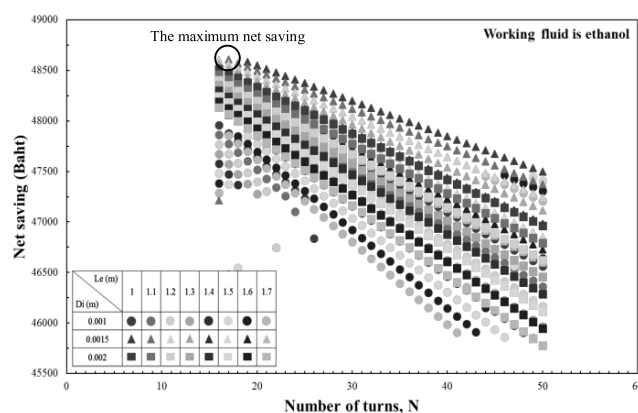


Fig. 5. Effect of number of turns on net saving of ethanol

Fig. 5 showed the effect of number of turns on net saving of ethanol. The trend was similar to those in Fig. 4. Therefore, the maximum of net saving was 48,607 baht for ten years.

CLPHP consisted of evaporator length of 1.1 m, 17 turns and inner diameter of 1.5 mm. In this optimal size, heat transfer rate was 698.08 W.

When all working fluids was compared, it could be seen the maximum of net saving could be obtained with distilled water as working fluid. Because distilled water had higher Ja more than the others. Therefore, the optimal size of CLPHP which was applied to the EGTSWH used distilled water as working fluid and there was sizing followed by the maximum of net saving.

V. CONCLUSION

The simulation modeling to determine the optimal CLPHP for applying into the EGTSWH from correlation prediction and Net Saving Method was conducted. The results of the mathematical model to obtain required heat transfer rate it was found that the optimal CLPHP consisted of evaporator length of 1 m, 16 turns and inner diameter of 1.5 mm, distilled water as working fluid and 10 evacuated glass tubes with the maximum of net saving at 48,687 baht for ten years. Therefore, the evacuated glass tube solar collector with CLPHP at optimal parameters will be constructed and tested for the prototype of the system.

ACKNOWLEDGMENT

The presented work was financially supported by The Thailand Research Fund (TRF) and Green Energy Corporation (Thailand) Co., Ltd. (Contract no. PHD5910056) Furthermore, this research was conducted in Heat Pipe and Heat System Laboratory, Department of Mechanical Engineering, Faculty of Engineering, Chiang Mai University, Thailand.

REFERENCES

- [1] T.T Chow, Z. Dong, L.S. Chan, W.F. Fong, and Y. Bai, "Performance evaluation of evacuated tube solar domestic hot water systems in Hong Kong," *Energy and buildings*, vol. 43, pp. 3467-3474, 2011.
- [2] R. Daghighi, and A. Shafieian, "Theoretical and experimental analysis of thermal performance of a solar water heating system with evacuated tube heat pipe collector," *Applied thermal engineering*, vol. 103, pp. 1219-1227, 2016.
- [3] L. Ayompe, and A. Duffy, "Thermal performance analysis of a solar water heating system with heat pipe evacuated tube collector using data from a field trial," *Solar energy*, vol. 90, pp.17-28, 2013.
- [4] S. Rittidech, A. Donmaung, and K. Kumsombut. "Experimental study of the performance of a circular tube solar collector with closed-loop oscillating heat-pipe with check valve (CLOHP/CV)," *Renewable energy*, vol. 34, pp. 2234-2238, 2009.



- [5] S. Maezawa, K.Y Gi, A. Minamisawa, and H. Akachi, "Thermal Performance of Capillary Tube Thermosyphon," Proceedings of the 9th International Heat Pipe Conference, Albuquerque, New Mexico, vol. 2, pp. 791-795, 1995.
- [6] H. Akachi, US Patent, Patent Number 5490558, 1996.
- [7] S. Khandekar, P. Chareonsawan, M. Groll, and P. Terdtoon, "Closed-Loop Pulsating Heat Pipe Part B: Visualization & semi-empirical modeling," Applied Thermal Engineering, vol. 23, pp. 2021-2033, 2003.
- [8] M. Soylemez, "the thermoeconomical optimization of heat pipe heat exchanger HPHE for waste heat recovery," Energy Conversion and Management, vol. 44, pp. 2509–2517, 2003.
- [9] Ministry of energy. Solar radiation. (2018, February 22). Retrieved from http://www.dede.go.th/ewt_news.php?nid=562&filename=index
- [10] Bank of Thailand. Interest Rates in Financial Market (2005-present). (2018, February 27). Retrieved from <http://www2.bot.or.th/statistics/BOTWEBSTAT.aspx?reportID=223&language=ENG>



Effects of Using a Solid Desiccant Dehumidifier with an Air Conditioner on Energy Consumption

Phornrak Wangnamjai, Thosapon Katejanekarn
Department of Mechanical Engineering
Faculty of Engineering and Industrial Technology
Silpakorn University Muang, Nakhon Pathom, Thailand
phornrak@hotmail.com, thosaponk@hotmail.com

Abstract—Effects of using a solid desiccant dehumidifier with an air conditioner on energy consumption and thermal comfort are presented in this paper. The energy consumption of three systems which were 1) air conditioner only 2) overcool and reheat system and 3) air conditioner with a solid desiccant dehumidifier was compared. Human thermal comfort of each system was also considered. A batch type solid desiccant dehumidifier with the dimension of 0.26 m x 0.26 m x 0.50 m comprising 10 shelves (each shelf contains 1 kg of silica gel) was placed inside an air conditioned room. All experiments were carried out in two rooms of the same dimension of 1.94 m x 2.60 m x 3.53 m. There were 21 total experiments. The first system was tested three times. The second system was tested 9 times. The third system was tested 9 times where air velocity was varied at 0.2, 0.3, and 0.4 m/s and the amount of silica gel was varied at 5, 7, and 10 kg. A set of artificial load of two persons working for 4 hours a day was placed inside each room. The setpoint of each room was 25°C, 50%RH except the first system that only temperature was controlled. The experiments were done in Nakhon Pathom province, Thailand during October and November of 2017. The results showed that the average energy consumption of the case of air conditioner only system was 0.97 kWh/4hr. The average PMV and PPD were 0.11 and 5.91%. The average energy consumption of the overcool and reheat system was 5.20 kWh/4hr which was 5.36 times that of the first system. The average PMV and PPD were 0.16 and 6.55%. The average energy consumption of the case of using an air conditioner with a solid desiccant dehumidifier was 2.73 kWh/4hr which was 1.78 times that of the first case. The average PMV and PPD were -0.07 and 5.7%. It can be concluded that all three systems could achieve the thermal comfort condition. The first system consumed least energy. However, the use of an air conditioner with a solid desiccant dehumidifier gave the best thermal comfort. When comparing between the second and third systems that both temperature and relative humidity were controlled, the use of an air conditioner with a solid desiccant dehumidifier could save energy by 66.74%.

Keywords— solid desiccant dehumidifier; comparison of energy consumption; thermal comfort

I. INTRODUCTION

The world's population grew up 1.1% every year and urban population increased 2% every 5 years all over the world [1]. Air conditioner usage was increased 4.3% every year all over the world especially the countries in Asia Pacific and America [2]. In Thailand, the use of air conditioners was increased 25% per year from 1994 to 2000 especially Bangkok and perimeter [3]. The energy consumption was increased 4.5% per year and up by 7.5% in the year of 2016. Bangkok and perimeter used energy 70% of the entire country [4]. Buildings accounted for a large part of energy consumption and environmental pollution [5, 6]. According to the U.S. Department of Energy (DOE), Singapore, and Thailand's reports, buildings consumed 31-40% of the primary energy and space air cooling accounted 50-60% of total building energy [7-9].

The building energy demand is used to provide indoor comfort condition. Air conditioning is essential for maintaining thermal comfort. The thermal comfort is recommended at the operative temperature between 21-28°C and the relative humidity between 10-80% according to the ASHRAE Standard 55-2010 while the room setpoint is recommended at 25°C, 50%RH according to Niu et al, [10, 11].

Currently, more than 90% of space cooling is provided by the vapor compression system. Other types of systems include the evaporative cooling and the desiccant based evaporative cooling system [12]. The cooling process is accomplished by a cooling coil which removes both sensible and latent load [13].

The conventional vapor compression system can provide comfort condition when sensible heat ratio (SHR) of cooling load is greater than 0.7. If the SHR is less than 0.7, the comfort condition may not be achieved since the latent part cannot be handled completely [13].

The hourly temperature and humidity from the Meteorological Department of Nakhon Pathom province in Thailand showed that 2060 hours out of 8760 hours in 2016



had SHR less than 0.7 [17]. That means the air conditioner only system may not be able to control the humidity or the condition of thermal comfort may not be achieved for 23.52% of the total time.

The latent load handling using conventional air conditioners can be achieved by cooling the air below its dew point and removing the moisture by condensation. Then the air needs to be reheated to bring the temperature back to the desired level. This overcool and reheat control scheme is energy-inefficient since it needs additional energy to overcool and reheat the air. One option is to handle the sensible and latent loads separately by using the desiccant dehumidifier with an air conditioner [5, 11]. The desiccant system takes care of the latent load while the air conditioner handles the sensible load. This option consumes less energy because dehumidification systems normally use fans which consume less energy than compressors in conventional systems. Recent researches showed that the systems that controlled sensible and latent load separately could reduce energy consumption by 15.6 to 60% [5-7, 11, 14, 15].

Desiccants can be liquid or solid. Liquid desiccants can hold moisture more than solid desiccants, for example, LiCl can hold moisture 130% of its mass but silica gel can only hold 35-40%. However, liquid desiccant systems are bigger, have more equipment, and too messy to use in air conditioned areas directly [16].

Common applications often reduced the moisture in the ventilation air before supplying to air conditioned spaces because most of the moisture comes from the ventilation air. There were only a few researches that used the dehumidifier inside the air conditioned room directly. Therefore, we were interested in studying the effects of using a solid desiccant dehumidifier with an air conditioner on energy consumption. This research was intended to compare the energy consumption among 3 systems which were 1) air conditioner only system 2) overcool and reheat system and 3) using a solid desiccant dehumidifier with an air conditioner. Also, the thermal comfort condition of all 3 systems was considered.

II. METHODOLOGY

A. Experimental Set Up

1) Experimental rooms

Two office rooms were used to compare the energy consumption of the three systems in this study. The two equal rooms were 1.94 m long, 2.60 m wide, and 3.53 m high each. The west of the two rooms had two slide opaque glass windows with an equal size. The rest three walls were brick and plaster, and the east wall of each room had one equal size door. The experimental rooms are shown in Fig.1.



(a)



(b)



(c)

Fig. 1. Experimental rooms. (a) Front view of experimental rooms. (b) Inside Room 1. (c) Inside Room 2.

Room 1 was used to test the overcool and reheat system and Room 2 was used to test the air conditioner only system and the use of a solid desiccant dehumidifier with an air conditioner system. Artificial load equivalent to two persons with an occupancy schedule from 10:00 to 14:00 pm was placed in each room. The equipment in each experimental room is shown in Tables I and II.

Table I. EQUIPMENT FOR EXPERIMENTAL ROOM 1

	Equipment	Qty.	Size	Power (kW)	Voltage (Volt)	Freq. (Hz)
1	Air conditioner	1	9000 Btu/hr	0.78	220	50
2	Heater	1	2000 W	2.00	220	50
3	Lighting	3	46 W	0.138	220	50
4	Humidifier	1	25 W	0.025	220	50



Table II. EQUIPMENT FOR EXPERIMENTAL ROOM 2

	Equipment	Qty.	Size	Power (kW)	Voltage (Volt)	Freq. (Hz)
1	Air conditioner	1	9000 Btu/hr	0.78	220	50
2	Dehumidifier	1	370 W	0.37	380	50
3	Lighting	3	46 W	0.138	220	50
4	Humidifier	1	25 W	0.025	220	50

2) Latent load for the dehumidifier

The latent load was calculated to design the size of the dehumidifier by using the real ambient climate of Nakhon Pathom province located at the latitude of 14 01' 42.5 " N and longitude of 99 58' 12.1 E. The annual average temperature was found to be 28.42°C and the average relative humidity was 74.13%RH [17]. The setpoint in the room was 25±1°C, 50±1%RH.

The cooling loads were calculated based on 2 persons. Each person generated 75 W of sensible heat and 45 W of latent heat with an occupied schedule from 10:00 to 14:00 pm. The total latent load is shown in Table III.

Table III. LATENT LOAD FOR DEHUMIDIFIER

Description	Quantity	Unit	Remark
Ambient			
Dry-bulb temperature	28.42	C	Yearly average climate of Nakhon Pathom (Meteorological Department)
Relative humidity	74.13	%	
Humidity ratio	0.0182	kg _w /kg _{da}	
Indoor			
Dry-bulb temperature	25	C	Summer comfort zone of ASHRAE [11]
Relative humidity	50	%	
Humidity ratio	0.0099	kg _w /kg _{da}	
Room's dimension			
Width	1.94	m	Experimental room T 423, 4 th floor Department of Mechanical Engineering, Silpakorn University, Nakhon Pathom, Thailand
Length	2.60	m	
Height	3.53	m	
Indoor latent load			
Type of work	Office		ASHRAE (1997)
Level of work	Sedentary		
Latent load from 2 persons	90	W	
Infiltration	0.3	ACH	
Latent load from infiltration	36.04	W	
Total latent load	126.04	W	
h _{fg}	2501	kJ/kg	
Operation time	4	hr	
Total moisture from latent load	0.73	kg _w	

According to the properties of silica gel, 7 kg of silica gel is sufficient to eliminate the moisture load of 0.73 kg_w which complies with the prediction of the mathematical model that this amount of silica gel can adsorb from 0.61 kg_w to 0.78 kg_w [18, 19].

The silica gel dehumidifier was designed and built. It could be loaded 10 kg of silica gel maximally and contained 10 shelves. Each shelf with a dimension of 0.26 m x 0.26 m x 0.02 m loaded 1 kg of silica gel. The silica gel dehumidifier is shown in Fig. 2.

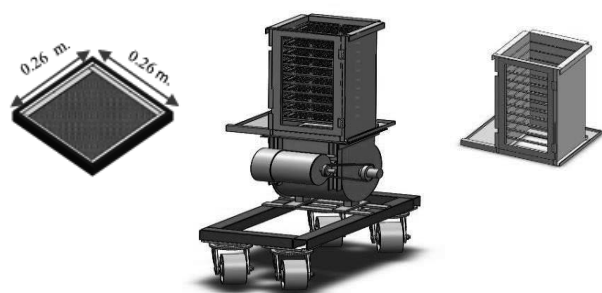


Fig. 2. The silica gel dehumidifier.

B. Cases of Experiments

There were 21 tests as below:

1) For the case of air conditioner only system, it was tested 3 times in Room 2. The setpoint in the room was 25°C and the humidity was not controlled.

2) For the case of overcool and reheat system, it was tested 9 times in Room 1. The setpoint in the room was 25°C and 50%RH.

3) For the case of using a solid desiccant dehumidifier with an air conditioner system, it was tested 9 times in Room 2. The air velocity was varied at 0.2, 0.3, and 0.4 m/s. The amount of silica gel was varied at 5, 7, and 10 kg. The setpoint in the room was 25°C and 50%RH.

All experiments were carried out during October to November, 2017.

The energy consumption of equipment such as air conditioners, heater, and dehumidifier, as well as temperature and humidity of indoor, outdoor, and outlet of the dehumidifier were recorded by data loggers every second. The adsorption rate could be calculated by using (1).

$$m_w = G_a (\omega_{a,in} - \omega_{a,out}) \quad (1)$$

where m_w = moisture removal rate, kg/s
 G_a = air flow rate, kg/s
 $\omega_{a,in}$ = humidity ratio of inlet air, (kg_w/kg_{dry air})
 $\omega_{a,out}$ = humidity ratio of outlet air, (kg_w/kg_{dry air})

This research considered not only energy consumption but also human thermal comfort. According to ASHRAE, the sensation scale can be divided into 7 scales from -3 to +3 as shown in Table IV.

Table IV. THERMAL SENSATION SCALE

PMV	Sensation
+3	Hot
+2	Warm
+1	Slightly warm
0	Neutral
-1	Slightly cool
-2	Cool
-3	Cold

The level of comfort is calculated from the predicted mean vote (PMV) by considering two groups of parameters which are personal factors and environmental factors. The personal factors are metabolism and clothing insulation level. The environmental factors are air temperature, mean radiant temperature, air velocity, and air humidity. All factors appear in terms of parameters M and L as shown in (2) [10].

$$PMV = [0.303 \exp (-0.036M) + 0.028]L \quad (2)$$

where M = metabolic rate

W = activity level

$L = \{(M-W)\}$

- $\{3.96 \times 10^{-8} f_{cl} [(t_{cl} + 273)^4 - (t_r + 273)^4]\}$

- $\{f_{cl} h_c (t_{cl} - t_a)\}$

- $\{3.05 [5.73 - 0.007(M-W) - P_a]\}$

- $\{0.42 [(M-W) - 58.2]\}$

- $\{0.0173 M (5.87 - P_a)\}$

- $\{0.0014 M (34 - t)\}$

= internal heat production in the human body

- heat loss by radiation

- heat loss by convection

- heat loss through skin

- heat loss by sweating

- latent respiration heat loss

- sensible respiration heat loss

The predicted percentage dissatisfied (PPD) that shows how many percent of people would not feel comfortable can also be estimated. The PPD relates to the PMV as shown in (3) [10].

$$PPD = 100 - 95 \exp [- (0.03353PMV^4 + 0.2179PMV^2)] \quad (3)$$



III. RESULTS AND DISCUSSION

A. Case of the Air Conditioner Only System

1) Energy consumption

The results showed that the average energy consumption of the air conditioner only system was 0.97 kWh/4hr. When the ambient temperature and humidity was higher, the energy consumption was higher too. The results of the 3 experiments are shown in Table V.

Table V. ENERGY CONSUMPTION OF THE AIR CONDITIONER ONLY SYSTEM

No.	Initial Ambient Air		Energy Consumption (kWh/4hr)
	T (°C)	RH (%)	
1	28.83	73.30	1.11
2	26.54	70.18	0.80
3	26.54	79.46	1.00
Average	27.30	74.45	0.97

2) Room temperature and relative humidity

The temperature and humidity in the room for 4 hours from the second of 3 tests are shown in Fig. 3. The setpoint in the room was 25°C while the humidity was not controlled. The ambient air was 26.54°C and 70.18%RH. The results showed that this system could control the temperature and the humidity within the range of 25.14±0.85°C and 72.17±17.28%RH. The results of the other tests were similar to the second test.

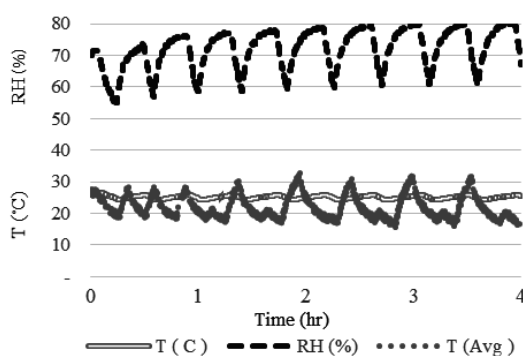


Fig. 3. Temperature and humidity inside the room from the second test of the air conditioner only system.

3) Hours of comfort

The room condition was taken into calculation using (2). It was found that the humidity level in the room was quite high (72.17%RH) since it was not controlled. The maximum PMV was found to be +0.4 while the minimum value was -0.2. The average PMV was 0.11 and PPD was 5.91% as shown in Fig.4.

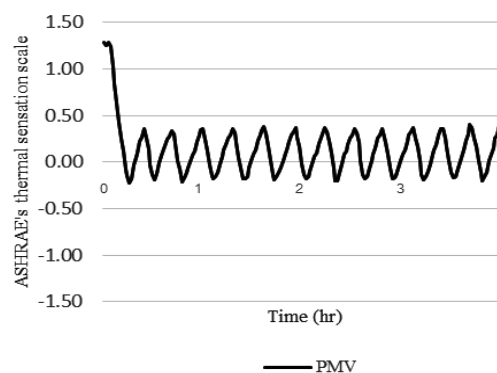


Fig. 4. PMV from the second test of the air conditioner only system.

B. Case of the Overcool and Reheat System

1) Energy consumption

The results showed that the average energy consumption of the overcool and reheat system was 5.21 kWh/4hr. The maximum energy consumption was 5.87 kWh/4hr and the minimum energy consumption was 4.66 kWh/4 hr. The results of all 9 tests were shown in Table VI.

Table VI. ENERGY CONSUMPTION OF THE OVERCOOL AND REHEAT SYSTEM

No.	Initial Ambient Air		Energy Consumption (kWh/4hr)		
	T (°C)	RH (%)	Air conditioner	Heater	Total
1	28.76	67.01	1.97	3.63	5.60
2	27.61	76.52	1.91	3.12	5.03
3	27.49	80.12	1.90	3.10	5.00
4	26.80	72.85	1.92	2.74	4.66
5	26.02	66.05	1.75	3.38	5.13
6	27.59	66.60	1.88	3.65	5.53
7	27.61	53.56	1.81	3.18	4.99
8	26.93	67.03	1.93	3.94	5.87
9	26.92	68.87	1.90	3.13	5.03
Average	27.30	68.73	1.89	3.32	5.21



2) Room temperature and relative humidity

The temperature and humidity in the room for 4 hours from the fifth test of 9 tests are shown in Fig. 5. The setpoint in the room was 25°C and 50%RH. The ambient air was 26.02°C and 66.05%RH. The results showed that the overcool process had to bring the room temperature down to 17°C to reduce the humidity ratio and the heater brought up to 25°C to get the desired temperature and relative humidity of 50%RH. The results showed that this system could control the temperature and humidity within the range of 24.8±1.75°C and 57.45±16.26%RH. The results of the other tests resembled the fifth test.

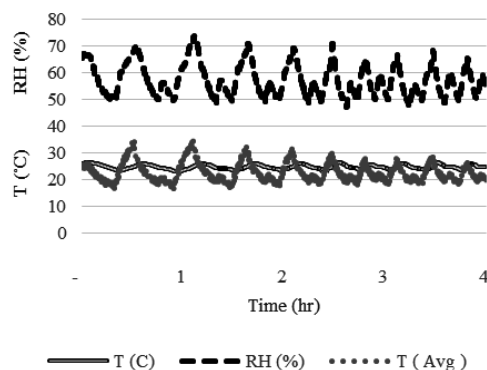


Fig. 5. Temperature and humidity inside the room from the fifth test of the overcool and reheat system.

3) Hours of comfort

The room condition was taken into calculation using (2). It was found that this system could control both temperature and humidity. The maximum PMV was +0.4 and the minimum PMV was -0.7. The average PMV was -0.16 and the average PPD was 6.55% as shown in Fig. 6.

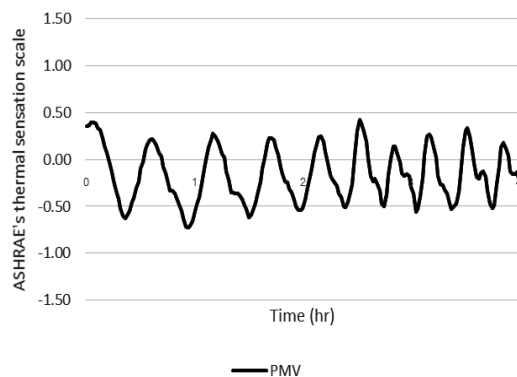


Fig. 6. PMV from the fifth test of the overcool and reheat system.

C. Case of Using a Solid Desiccant Dehumidifier with an Air Conditioner.

1) Energy consumption

The results showed that the average energy consumption of this system was 1.73 kWh/4hr. The maximum energy consumption was 1.97 kWh/4hr and the minimum energy consumption was 1.45 kWh/4hr as shown in Table VII.

Table VII. ENERGY CONSUMPTION OF THE USE OF A SOLID DESICCANT DEHUMIDIFIER WITH AN AIR CONDITIONER SYSTEM

No.	Case	Initial Ambient Air		Energy Consumption (kWh/4hr)		
		T (°C)	RH (%)	Air cond.	Dehum.	Total
1	5 kg, 0.2 m/s	28.76	67.01	1.30	0.44	1.74
2	5 kg, 0.3 m/s	27.61	76.52	1.19	0.62	1.81
3	5 kg, 0.4 m/s	27.49	80.12	1.17	0.68	1.85
4	7 kg, 0.2 m/s	26.80	72.85	1.09	0.52	1.61
5	7 kg, 0.3 m/s	26.02	66.05	0.91	0.54	1.45
6	7 kg, 0.4 m/s	27.59	66.60	1.10	0.69	1.79
7	10 kg, 0.2 m/s	27.61	53.56	1.04	0.55	1.59
8	10 kg, 0.3 m/s	26.93	67.03	1.12	0.65	1.77
9	10 kg, 0.4 m/s	26.92	68.87	1.16	0.81	1.97
	Average	27.3	68.73	1.12	0.61	1.73

2) Room temperature and relative humidity

The temperature and humidity in the room for 4 hours of the fifth test from 9 tests are shown in Fig.7. The setpoint in the room was 25°C and 50%RH. The ambient air was 26.02°C and 66.05%RH. The results showed that this system could control both temperature and humidity within the range of 25.18±0.89°C and 52.76±8.96%RH. The results of the remaining tests resembled this fifth test.

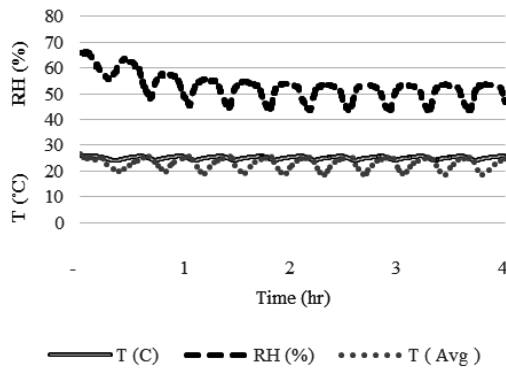


Fig. 7. Temperature and humidity inside the room from the fifth test of the use of a solid desiccant dehumidifier with an air conditioner system.

3) Hours of comfort

The room condition was taken into calculation using (2). It was found that both temperature and humidity could be controlled by this system. The maximum PMV was +0.2 and the minimum PMV was -0.3. The average PMV was -0.07 and the average PPD was 5.70% as shown in Fig. 8.

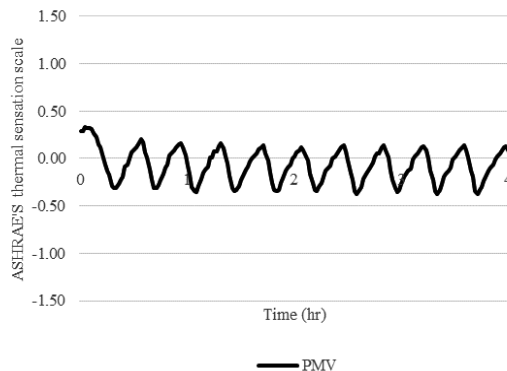


Fig. 8. PMV from the fifth test of the use of a solid desiccant dehumidifier with an air conditioner system.

IV. COMPARISON AMONG 3 SYSTEMS

The result showed that the average energy consumption of the air conditioner only system was 0.97 kWh/4hr, the average PMV was 0.11, and the average PPD was 5.91%.

The average energy consumption of the overcool and reheat system was 5.21 kWh/4hr that is 4.24 kWh/4hr or 5.36 times more than that of the first case. The average PMV was -0.16 and the average PPD was 6.55%.

The average energy consumption of the case of using a solid desiccant dehumidifier with an air conditioner system was 1.73 kWh/4hr that is 0.76 kWh/4hr or 1.78 times more than that of the first case. The average PMV was -0.07 and the average PPD was 5.70% as shown in Table VIII.

Table VIII. THE SUMMARY OF THE ALL 21 EXPERIMENTS

Case	Average Energy Consumption (kWh/4hr)	PMV	PPD (%)
Air conditioner only	0.97	0.11	5.91
Overcool and reheat	5.21	-0.16	6.55
Air conditioner with dehumidifier	1.73	-0.07	5.70

The comparison of the average energy consumption among three systems is shown in Fig. 9.

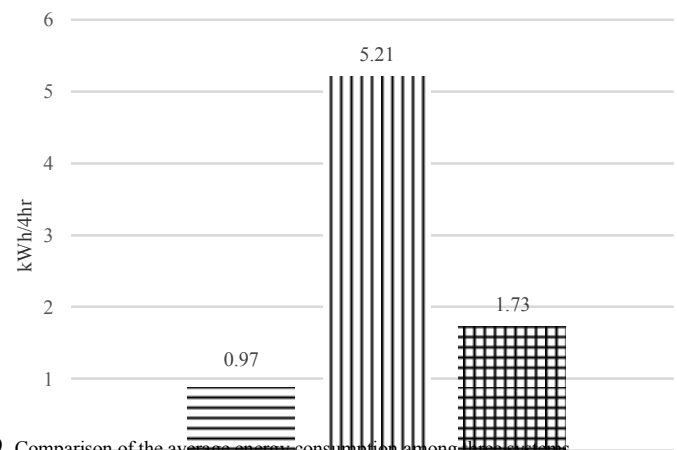


Fig. 9. Comparison of the average energy consumption among three systems.

Although the use of a solid dehumidifier with an air conditioner system consumed more energy than the air conditioner only system by 78.45%, but this system could achieve a better comfortable condition because the average PMV was -0.07 which was closer to zero or neutral condition and the average PPD was less than the air conditioner only system.

The overcool and reheat system consumed much more energy than the air conditioner only system and the average PMV was far away from the neutral condition.

When comparing between the overcool and reheat system and the case of using a solid desiccant dehumidifier with an air conditioner that both of which controlled both temperature and humidity, the latter could save energy as high as 66.74%.

V. CONCLUSION

The air conditioner only system consumed energy of 0.97 kWh/4hr. The average PMV was 0.11 and the average PPD was 5.91%. The overcool and reheat system consumed energy



of 5.21 kWh/4hr. The average PMV was -0.16 and the average PPD was 6.55%. The use of a solid desiccant dehumidifier with an air conditioner system consumed energy of 1.73 kWh/4hr. The average PMV was -0.07 and the average PPD was 5.70%.

The results of all experiments showed that all 3 systems can achieve thermal comfort. The air conditioner only system consumed the least energy while the humidity level in the room was quite high since it was not controlled. Using a solid desiccant dehumidifier with an air conditioner system achieved the best condition of thermal comfort but consumed more energy consumption than the air condition only system. When comparing between the overcool and reheat system and the case of using a solid desiccant dehumidifier with an air conditioner that both of which control both temperature and humidity, the latter could save energy as much as 66.74%.

The next phase of this study would be to run the experiments to cover all three seasons of Thailand for the whole year.

ACKNOWLEDGMENT

The authors would like to thank the Department of Mechanical Engineering, Faculty of Engineering and Industrial Technology, Silpakorn University for all supports to complete this work.

REFERENCES

- [1] World-population, 2017. World-population. Available: <http://www.worldometers.info/world-population> (accessed 7.3.17)
- [2] The weather prediction, 2017. The ultimate weather education website. Urban Weather. Available: <http://www.theweatherprediction.com/urbanwx/> (accessed 7.3.17)
- [3] EPPO 2008, Electricity consumption for the whole country. Energy Policy and Planning Office, Ministry of Energy, Thailand. Available: http://www.eppo.go.th/info/summary_stat.htm (accessed 3.2.16)
- [4] M. S. Parkpoom and G. P. Harrison, "Analyzing the Impact of Climate Change on Future Electricity Demand in Thailand," IEEE, vol. 23, no. 3, pp. 1441-1448, 3 August 2008.
- [5] Y. Jiang, T. S. Ge, R. Z. Wang, and Y. Huang, "Experimental investigation on a novel temperature and humidity independent control air conditioning system – Part I: Cooling condition," Applied Thermal Engineering, vol. 73, no. 1, pp. 784-793, 2014.
- [6] N. Enteria, K. Mizutani, Y. Monma, T. Akisaka, and N. Okazaki, "Experimental evaluation of the new solid desiccant heat pump system in Asia-Pacific climatic conditions," Applied Thermal Engineering, vol. 31, no. 2-3, pp. 243-257, 2011.
- [7] R. Xing, Y. Rao, W. TeGrotenhuis, N. Canfield, F. Zheng, D. W. Winiarski, and W. Liu "Advanced thin zeolite/metal flat sheet membrane for energy efficient air dehumidification and conditioning," Chemical Engineering Science, vol. 104, pp. 596-609, 2013.
- [8] K. J. Chua, S. K. Chou, W. M. Yang, and J. Yan, "Achieving better energy-efficient air conditioning – A review of technologies and strategies," Applied Energy, vol. 104, pp. 87-104, 2013.
- [9] Energy Policy and Planning Office, Ministry of Energy, 2003. Available: www.oic.go.th/ginfo/moreinfo (accessed 7.3.16)
- [10] ANSI/ASHRAE Standard 55-2010. Thermal Environmental Conditions for Human Occupancy, ASHRAE Standard, no. 1791 Tullie Circle NE, Atlanta, GA 30329, 2010.
- [11] J. L. Niu, L. Z. Zhang, and H. G. Zuo, "Energy savings potential of chilled-ceiling combined with desiccant cooling in hot and humid climates," Energy and Buildings vol. 34, p. 487- 495, 2002.
- [12] M. Mujahid Rafique, P. Gandhidasan, S. Rehman, and L. M. Al-Hadhrani, "A review on desiccant based evaporative cooling systems," Renewable and Sustainable Energy Reviews, vol. 45, pp. 145-159, 2015.
- [13] T. Katejanekarn and S. Kumar, "Performance of a solar-regenerated liquid desiccant ventilation pre-conditioning system," Energy and Buildings, vol. 40, no. 7, pp. 1252-1267, 2008.
- [14] X. Han, X. Zhang, L. Wang, and R. Niu, "A novel system of the isothermal dehumidification in a room air-conditioner," Energy and Buildings, vol. 57, pp. 14-19, 2013.
- [15] X. Han and X. Zhang, "Experimental study on a residential temperature-humidity separate control air-conditioner," Energy and Buildings, vol. 43, no. 12, pp. 3584-3591, 2011.
- [16] ASHRAE, 2005 ASHRAE Handbook Fundamentals, 2005. Atlanta, Georgia, USA.
- [17] Meteorological Department of Thailand, 2015. "Statistic of average relative humidity (%) around the year of Thailand," Available: <http://www.tmd.go.th/info/info.php?FileID=56> (accessed 7.3.16)
- [18] T. Katejanekarn and K. Suksub, "Performance evaluation procedure for a small batch-type solid desiccant dehumidifier," The 6th International Conference on Science, Technology and Innovation for Sustainable Well-Being (STISWB VI), Siem Reap, Kingdom of Cambodia, 28-30 August 2014, 2014.
- [19] K. Suksub, Portable Batch Type Solid Desiccant Dehumidifier for Museum. Department of Mechanical Engineering, Faculty of Engineering and Industrial Technology, Silpakorn University, Nakhon Pathom, Thailand, 2014.



Thermal Comfort of People in Textile Factories

Suthimon Kuirat, Thosapon Katejanekarn
Department of Mechanical Engineering
Faculty of Engineering and Industrial Technology
Silpakorn University
Muang, Nakhon Pathom 73000, Thailand
suthimon.kui@gmail.com, thosapon@su.ac.th

Abstract— This research aims to investigate the thermal comfort of employees who worked in seven textile and garment factories located in Bangkok and Nakhon Pathom, Samut Sakhon, and Samut Prakan provinces of Thailand. In order to get a 95% confidence interval with a $\pm 5\%$ uncertainty, 843 subjects were randomly selected from the total population of 872. This study was conducted using a questionnaire and measuring the related parameters including air temperature (T_a), relative humidity (%RH), air speed (v), mean radiant temperature (T_r), clothing insulation (I_{clo}), metabolic rate (M), and the immediate thermal sensation of the samples. In this study, the thermal comfort was assessed via two evaluation methods: the ASHRAE model using PMV (predicted mean vote) value which was computed from the related parameters and the Adaptive Comfort model using CV (comfort vote) value which reflected the employees' actual sensation. The assessment also took other factors affecting thermal comfort into consideration including gender, age, body mass index, and the work environment (air-conditioned or non-air-conditioned). Neutral (or comfort) temperature (T_n) in terms of dry-bulb temperature (T_a) and operative temperature (T_o) were calculated for the thermal comfort assessment. It was discovered that T_n from the ASHRAE evaluation in terms of T_a and T_o were 25.18°C and 25.33°C whereas those figures in the Adaptive Comfort model were 26.25°C and 26.44°C. This illustrated that T_a and T_o using the ASHRAE model were about 1.07°C and 1.11°C lower than those of the Adaptive Comfort model, and these results indicated that T_a and T_o can be used interchangeably as an indicator to assess the thermal comfort. The study also found that the factors that affected the thermal comfort were gender, age, body mass index, and air-conditioned or non-air-conditioned workplaces.

Keywords— thermal comfort; textile factory; adaptive comfort; predicted mean vote (PMV)

I. INTRODUCTION

Air conditioning is the process of controlling temperature, humidity, cleanliness, air distribution, and airflow volume to maintain a comfortable atmosphere. The energy use from air

conditioning generally accounts for 60% of total building energy use [1]. Air conditioning for residential buildings aims to create a level of residential comfort whereas the purposes of industrial air conditioning are to create workers' comfort, increase work efficiency, and improve productivity [2]. However, factors such as air temperature, humidity, and activity level can be at higher levels. The design of an effective air conditioning and control system is therefore required not only for energy saving and energy efficiency purposes, but also for increasing work efficiency and productivity.

ASHRAE [3] has defined a comfort chart based on human comfort assessments, and it illustrates that the most effective condition for human comfort is within 21-28°C and 10-80%RH. Factors that affect thermal comfort are both environmental and personal. Environmental factors include air temperature, air humidity, air velocity, and mean radiant temperature while personal factors are clothing and activities. If the conditions of these factors fall outside the boundaries of the comfort zone, employees may feel uncomfortable, frustrated, and are likely to lose focus at work [4].

Therefore, this study aims to investigate thermal comfort in industrial factories by applying two evaluation methods: the ASHRAE model and the Adaptive Comfort model. In the ASHRAE evaluation, the participants' thermal sensation scale was calculated under climate-controlled conditions. On the contrary, in the Adaptive Comfort model evaluation, the sensation scale was obtained from the participants who were working in the actual environment without any controlled variables because the Adaptive Comfort model is based on the idea that people are able to adapt themselves to the environments that they are exposed to.

Air conditioning an entire factory is a waste of energy due to energy consumption from excessive cooling for machines and manufacturing processes. In contrast, a spot cooling system is a way to save energy [5]. Providing cold airstreams to each employee and to a precise area where it is needed the most can be a good solution to reduce energy consumption by as much as 60% [6].



A large number of research studies have been conducted regarding thermal comfort assessment in buildings [7-35] whereas a few researches have been conducted regarding thermal comfort in industrial factories [36-39]. For this reason, this study investigated the thermal comfort of employees in industrial factories located in Bangkok and the provinces of Nakhon Pathom, Samut Sakhon, and Samut Prakan. In this case, textile and garment factories were the main subject of this study as they are significant in regards to Thailand's economic development. The textile and garment industry accounts for 245 billion baht or 2.2% of GDP. This ranked fourth on a proportion of value added to GDP, after the food and beverage industry, office machinery industry, and automotive industry, respectively [40]. The findings of this study, therefore, can be used as a guide on how to improve the workplace environment by designing an effective air conditioning system to save energy and increase productivity. This study analyzed thermal comfort conditions in factories based on the ASHRAE standard and the Adaptive Comfort model and compared the results to previous researches. The factors affecting the employees' comfort sensation including gender, age, body mass index, and whether the workplaces were air-conditioned or non-air-conditioned were also assessed.

II. STANDARDS OF THERMAL COMFORT

In order to study human comfort conditions, it is necessary to investigate the factors affecting thermal comfort. The study can be conducted using two evaluation methods: the ASHRAE model and Adaptive Comfort model.

A. Thermal Comfort in the ASHARE Model

According to the ASHRAE model, the factors that affect thermal comfort conditions include air temperature (T_a), relative humidity (%RH), air speed (v), and mean radiant temperature (T_r) while personal factors are metabolic rates (M) relative to activity levels and clothing insulation level (I_{clo}).

Furthermore, the operative temperature (T_o) is also calculated for thermal comfort analysis by combining the dry-bulb temperature with the mean radiant temperature of the surrounding room surfaces as shown in (1):

$$T_o = \frac{(h_c T_a + h_r T_r)}{(h_c + T_r)} \quad (1)$$

where h_c = convective heat transfer coefficient (W/m²-K)
 h_r = radiative heat transfer coefficient (W/m²-K)

The ASHRAE thermal sensation scale consists of rating scales used to indicate a certain level of thermal sensation over a period of time as shown in Table 1.

TABLE I. ASHRAE THERMAL SENSATION SCALE [41]

PMV	Sensation
+3	Hot
+2	Warm
+1	Slightly warm
0	Neutral
-1	Slightly cool
-2	Cool
-3	Cold

Predicted mean vote or PMV can be calculated by using (2), taking into account the environmental and personal factors reflected in the variable L which is defined as heat losses from different parts of the human body.

$$PMV = [0.303 \exp(-0.036M) + 0.028]L \quad (2)$$

where M = metabolic rate
 W = activity level

$$\begin{aligned} \text{and } L &= \{(M-W)\} \\ &- \{3.96 \times 10^{-8} f_{cl} [(t_{cl} + 273)^4 - (t_r + 273)^4]\} \\ &- \{f_{cl} h_c (t_{cl} - t_a)\} \\ &- \{3.05 [5.73 - 0.007(M-W) - P_a]\} \\ &- \{0.42 [(M-W) - 58.2]\} \\ &- \{0.0173 M (5.87 - P_a)\} \\ &- \{0.0014 M (34 - t)\} \\ &= \text{internal heat production in the human body} \\ &- \text{heat loss by radiation} \\ &- \text{heat loss by convection} \\ &- \text{heat loss through skin} \\ &- \text{heat loss by sweating} \\ &- \text{latent respiration heat loss} \\ &- \text{sensible respiration heat loss} \end{aligned} \quad (3)$$

B. Thermal Comfort in the Adaptive Comfort Model

The Adaptive Comfort model is based on the assumption that people can adapt to their environment, and for this reason, the model is called "adaptive comfort". Neutral temperature (T_n) is dependent on the average temperature in the environment. In recent studies, model equations in relation to different types of temperature have been used to find the value of the neutral temperature. There have been many researches studying comfort temperature in buildings which can be classified into the following types of surrounding temperatures:

Comfort temperature in terms of effective temperature:

Research study no. 1 [7]

$$T_n = 22.6 + 0.04ET^*(\text{air-conditioned})$$

$$T_n = 18.9 + 0.225ET^*(\text{non-air-conditioned})$$



Comfort temperature in terms of operative temperature:

Research study no. 2 [22]

$$T_n = 0.59T_o - 17.21$$

Research study no. 3 [33]

$$T_n = 0.12T_o - 2.78$$

Comfort temperature in terms of outdoor temperature:

Research study no. 4 [18]

$$T_n = 18.303 + 0.158T_{\text{outdoor}}$$

Comfort temperature in terms of dry-bulb temperature:

Research study no. 4 [30]

$$T_n = 0.407T_a - 9.855 \text{ (Yaounde)}$$

$$T_n = 0.355T_a - 8.843 \text{ (Ala town)}$$

Research study no. 5 [32]

$$T_n = 0.1148T_a - 4.7913 \text{ (winter)}$$

$$T_n = 0.1847T_a - 6.6027 \text{ (rainy season)}$$

In contrast, a few researches have been conducted on thermal comfort for industries. For example, Wijewardane and Jayasinghe [36] did a thermal comfort survey in factory buildings located in Sri Lanka and obtained a model equation: $T_n = 17.6 + 0.31T_o$. The survey found that the comfort temperature was 30°C and could be increased to 34°C when the air velocity was 0.6 m/s. A survey on thermal comfort in non-air-conditioned textile factories in Sri Lanka undertaken by Kosala and Vilasine [37] reported that the comfort temperature was 30°C and the relative humidity should be decreased to 70%. Another survey in textile factories in Thailand carried out by Loomyim and Tongla [38] creating neutral temperature equations in terms of dry-bulb temperature as $T_n = 0.2641T_a - 6.6863$ and operative temperature as $T_n = 0.2518T_o - 6.2845$, respectively.

III. RESEARCH METHODOLOGY

This research was conducted by surveying a sample of employees who worked in seven textile and garment factories located in Bangkok and the provinces of Nakhon Pathom, Samut Sakhon, and Samut Prakan, Thailand. The questionnaire and the measurement of related variables were designed to gather information from a sample of 843 employees who were randomly selected from a total population of 872 to get a 95% confidence interval with a $\pm 5\%$ uncertainty which required at least 399 subjects. All the employees were in similar industrial factory conditions. The survey was conducted after the subjects had spent one hour in the factories so that the subjects could acclimate themselves to the factory environment [3]. The areas surveyed contained both air-conditioned and non-air-conditioned spaces. The surveys in each area were conducted by measuring environmental factors conforming to the ASHRAE Standard 55 [41] which include air temperature, air speed (measured at 0.1, 1.1, and 1.7 m above the ground and set for an interval of 3 minutes), relative humidity (measured 1.1 m above the ground), and globe temperature (measured at the center of the surveyed room and 1.5 m above the ground). The globe thermometer was left for 15-20 minutes before the values were collected so that the heat transfer was already in a steady state condition.

Other data and personal factors including clothing, activities, gender, age, weight, height, and the comfort vote (CV) were collected using the questionnaire. The CV was measured by referring to the 7 thermal sensation scale and was considered as the samples' actual thermal sensation.

The data derived from the survey was analyzed and classified to find various factors affecting the thermal comfort which included gender, age, body mass index (BMI), and air-conditioned or non-air-conditioned workplaces. The data was then analyzed and compared using the ASHRAE model and the Adaptive Comfort model to examine the thermal comfort.

To evaluate the thermal comfort using the ASHRAE thermal sensation scale, the values were derived from the survey, and the analysis was calculated to find the predicted mean vote (PMV). A graph was created to show the relationship between PMV and two forms of temperature which included the dry-bulb temperature (T_a) and the operative temperature (T_o). Then the values were presented as a linear line from curve fitting. The intersection point of the line and the X-axis (PMV = 0) was the comfort temperature using the ASHRAE model. To evaluate the thermal comfort using the Adaptive Comfort model, the values of CV from the survey were also presented as a graph against the two types of temperature. The intersection point of the line from linear curve fitting and the X-axis (CV = 0) was the comfort temperature using the Adaptive Comfort concept.

IV. RESULTS AND DISCUSSION

The survey was carried out from March to May, 2017 which is considered as the summertime in Thailand [42]. The survey was conducted from 08:30 to 16:00. Employees who worked in all the air-conditioned or non-air-conditioned areas of 7 factories were asked to answer the questionnaire. The data from 843 out of 872 subjects was deemed usable. Data from the subjects who were sick or had a cold were not analyzed to avoid any deviation of the results. The data from the survey were summarized in Table II.

TABLE II. SUMMARY OF THE SURVEYED PARAMETERS

Parameter	Min.	Max.	Avg.	SD.
T_a (°C)	23.33	35.20	31.09	2.91
T_o (°C)	23.12	35.00	31.06	2.89
T_r (°C)	22.80	34.80	31.02	2.93
Relative humidity (%)	37.30	82.53	62.21	9.53
Air velocity (m/s)	0.01	0.67	0.24	0.14
Clothing level (clo)	0.06	1.18	0.53	0.22
Metabolic rate (met)	1.00	2.10	1.46	0.33

From Table II, the data demonstrated that the average dry-bulb temperature was 31.09°C which was slightly different from the average operative temperature (31.06°C). The average relative humidity was 62.21%, and the average air speed was 0.24 m/s. The value of clothing insulation was the sum of the



clothes the employees were wearing at work, such as 0.08 clo for collar T-shirts, 0.49 clo for jeans, 0.04 clo for underwear, and 0.02 clo for socks. Metabolic rates were set as 1.0 met, 1.2 met, 1.4 met, and 2.1 met which were equivalent to typical activities at work in an office, in production lines in a sitting position, in production lines in a standing position, and typical activities of walking or lifting something, respectively.

A. Analysis of Comfort Temperature

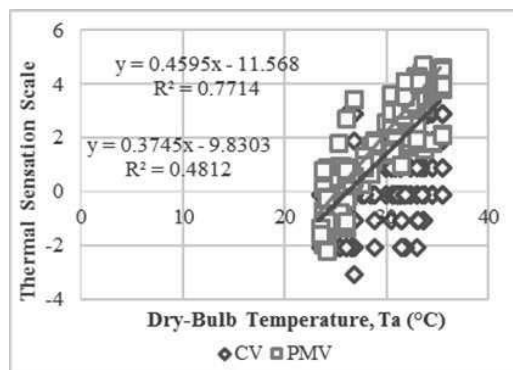


Fig. 1. Relationship between PMV, CV, and dry-bulb temperature

Figs. 1 and 2 illustrated the results from the analysis using the ASHRAE model. The comfort temperature was displayed as the intersection point of the linear line from curve fitting and the X-axis (PMV = 0). From the two figures, it can be explained that the comfort temperature in terms of T_a was 25.18°C and T_o was 25.33°C, respectively.

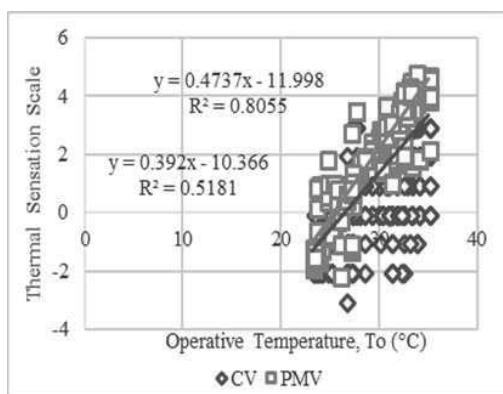


Fig. 2. Relationship between PMV, CV, and operative temperature

Figs. 1 and 2 also showed the results from the analysis using the Adaptive Comfort model based on CV (or the samples' actual thermal sensation). From the figures, the data revealed that the comfort temperature in the form of T_a was 26.25°C and T_o was 26.44°C, respectively.

From Fig. 1, it was found that the comfort temperature in the form of dry-bulb temperature in the ASHRAE model was approximately 1.07°C lower than the one in the Adaptive

Comfort model. From Fig. 2, the comfort temperature in the form of T_o in the ASHRAE model was approximately 1.11°C lower than the one in the Adaptive Comfort model. This implies that the ASHRAE model underestimates the comfort temperature by about 1°C.

When considering a $\pm 0.5^\circ\text{C}$ uncertainty, it was evident that the comfort temperatures in the form of T_a and T_o were not significantly different. Therefore, from this point on, the comfort temperature in this study would focus only in the form of dry-bulb temperature.

B. Analysis of Parameters Contributing to Thermal Comfort

Parameters contributing to the thermal comfort in this study including gender, age, body mass index, and working in air-conditioned or non-air-conditioned areas were analyzed.

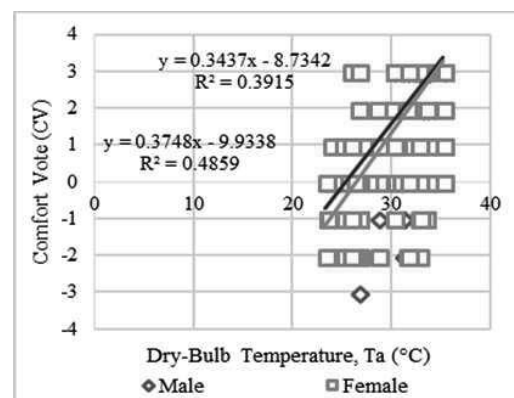


Fig. 3. Comfort temperatures of males and females

a) Gender

It was found that gender significantly affected the comfort temperature. Females' comfort temperature was 1.09°C higher than males'. As shown in Fig. 3, females' comfort temperature was 26.50°C while males' comfort temperature was 25.41°C. The reason why females' comfort temperature was higher could be explained by the type of clothing women generally wear which is considered lighter than men's clothing [43], and also the metabolic rate of women which is typically lower than men's rates [13]. The findings of this research are in line with previous researches as shown in Table III.



TABLE III.COMFORT TEMPERATURES OF MALES AND FEMALES

Researcher	Number of Samples (people)			Comfort Temperature (°C)		Difference (°C)
	Male	Female	Total	Male	Female	
Beshir and Ramsey [44]	31	15	46	23.40	24.90	1.50
Karyono [13]	345	227	569	25.20	26.30	1.10
Busch [9]	-	-	1,100	24.60	25.40	0.80
Lumyim and Tongla [38]	204	195	399	25.44	25.68	0.30
This research study	381	462	843	25.41	26.50	1.09

TABLE IV. HUMAN DEVELOPMENTAL STAGE [45]

Age Period	Age Range
Prenatal period	Fertilization - maternity
Infancy period	Birthdays - 2 years
Childhood	2 - 12 years
Puberty	12 - 14 years
Adolescence	14 - 21years
Adulthood	21 - 40 years
Middle age	40 - 60 years
Old age	60 years old up

b) Age

The results from the analysis of age according to age periods in Table IV revealed that age was a factor that significantly affected comfort temperatures. The comfort temperatures of the three groups: adolescence, adulthood, and middle age, were 26.11°C, 25.16°C, and 26.54°C, respectively. As illustrated in Fig. 4, when the comfort temperatures of adolescents and adults were compared, the difference was 0.95°C, which was significantly different. There was also a significant difference between those of adults (21-40) and middle-aged people (41-60), and the difference was 1.38°C. A closer look at the data showed that the adult factory employees in this study worked harder than the other two groups. As a result, their comfort temperature was lower than those of the other two groups. Additionally, the highest comfort temperature in the middle-aged group in this study is in line with the findings in the study conducted by Karyono indicating that the comfort temperature of people who were over the age of 40 was higher than that of the people under the age of 40 due to their lighter workload [13] as illustrated in Table V.

TABLE V. COMFORT TEMPERATURES OF PEOPLE IN DIFFERENT AGE PERIODS

Researcher	Number of Samples (people)				Comfort Temperature (°C)			Difference (°C)
	Adolescence	Adult	Middle Age	Total	Adolescence	Adult	Middle Age	
Karyono [13]				596	26.5		26.4	0.1
ASHRAE [46]								0.6
Marincic [47]				150				0.6
This research study	54	580	209	843	26.11	25.16	26.54	0.95-1.38

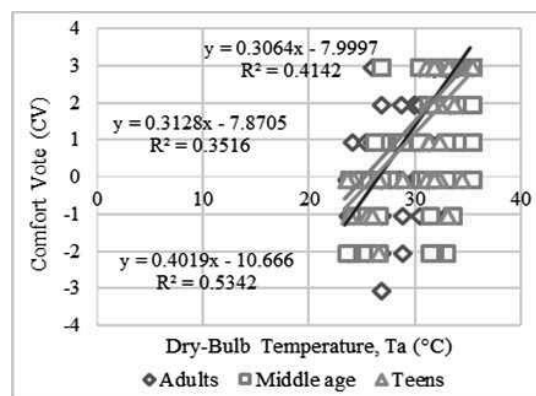


Fig. 4. Comfort temperatures of humans in different age periods

TABLE VI. BODY MASS INDEX (BMI) CRITERIA FOR ASIAN POPULATION [49]

Group	Criteria for Asian Population
Low weight	<18.5
Normal weight	18.5 - 22.99
Excess weight	≥ 23

c) Body Mass Index (BMI)

In the present study, the factor of body mass index (weight in kg divided by height in m²) was analyzed according to the body mass index group. As demonstrated in Table VI, the body mass index factor significantly affected the comfort temperatures. The comfort temperatures of the samples in the three groups: low weight, normal weight, and excess weight, were at 26.73°C, 26.05°C, and 26.26°C, respectively. The results can be explained that the employees with low weight and normal weight had significantly different comfort temperatures. The difference of the temperatures was 0.68°C. However, there was no significant difference between the



comfort temperatures of the employees with normal weight and those with excess weight. The difference was approximately 0.21°C. In sum, the employees with normal weight and with excess weight had lower comfort temperatures than the ones with low weight. It is probably because people with excess weight have excess fat as an insulator [48-50] so the employees with excess weight in this study had a lower comfort temperature than those with low weight as demonstrated in Fig. 5. This result concurs with the study by Karyono, indicating that people with excess weight had 0.7°C lower comfort temperature than people with normal weight, and 1.0°C lower comfort temperature than people with low weight [51] as illustrated in Table VII.

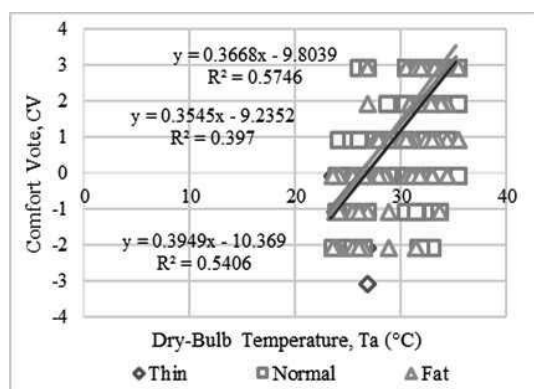


Fig. 5. Comfort temperatures of each body mass index range

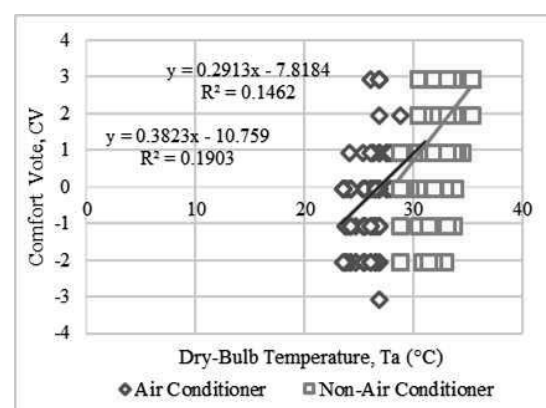


Fig. 6. Comfort temperatures of people in air-conditioned and non-air-conditioned workplaces

d) Air-conditioned and non-air-conditioned workplaces

The analysis of the factor related to air-conditioned and non-air-conditioned work environments indicated that this factor affected the comfort temperatures significantly. As illustrated in Fig. 6, the comfort temperature of the employees in the air-conditioned workplaces was 1.30°C lower than those in non- air-conditioned workplaces. To be more specific, the comfort temperature of the employees in the air-conditioned workplaces was 26.84°C whereas the comfort temperature of the employees in the non-air-conditioned workplaces was 28.14°C. These results are in line with a previous study as shown below in Table VIII.

TABLE VII. COMFORT TEMPERATURES OF EACH BODY MASS INDEX RANGE

Researcher	Number of Samples (people)				Comfort Temperature (°C)			Difference (°C)
	Low Weight	Normal weight	Excess weight	Total	Low Weight	Normal weight	Excess weight	
Karyono [13]	199	273	49	521				0.7-1.0
Marincic [47]				150	33.0		32.5	0.5
Blaza and Garrow [48]	5		5	10	23.2-26.4	23.3-26.2		0.1-3.1
Fanger [8]	128		128	256				0.17-0.26
This research study	94	415	336	845	26.73	26.05	26.26	0.21-0.68

TABLE VIII. COMFORT TEMPERATURES OF PEOPLE IN AIR-CONDITIONED AND NON-AIR-CONDITIONED WORKPLACES

Researcher	Number of Samples (people)			Comfort Temperature (°C)		Difference (°C)
	Air Con	No Air Con	Total	Air Con	No Air Con	
Lumyim and Tongla [38]	62	337	399	25.41	26.51	1.10
This research study	158	687	845	26.84	28.14	1.30



TABLE IX. COMPARISON OF THE PRESENT STUDY AND PREVIOUS STUDIES

Researcher	Comfort Temperature (°C)		Country	Location
	T_a	T_o		
Sekhar [10]	28.9	28.9	Singapore	Building
De Dear et al. [52]		28.5	Singapore	Building
Wong et al. [15]		28.9	Singapore	Building
Wong and Khoo [19]		28.8	Singapore	Building
Karyono [13]	26.4	26.7	Indonesia	Building
Feriadi and Wong [22]	29.1	29.2	Indonesia	Building
Khedari et al. [14]	29.5		Thailand	Building
Tun [24]		27.0	Thailand	Building
Sriprasert et al. [26]	28.1	28.3	Thailand	Building
Nantasiri and Rasisutti [32]	28.9 - 29.0		Thailand	Building
Memon et al. [27]		29.3	Pakistan	Building
Nguyen et al. [28]		29.8	Southeast Asia	Building
De Dear et al. [33]		25.1	Australia	Building
Zhao et al. [53]	30.0		China	University
Wijewardane and Jayasinghe [36]		31.0	Sri Lanka	Factory
Kosala et al. [37]		30.0	Sri Lanka	Factory
Lumyim and Tongla [38]	25.1	24.7	Thailand	Factory
This research study	26.2	26.4	Thailand	Factory

C. Comfort Temperature in Buildings and Factories and Suggested Controlled Temperatures for the Factories

Table IX illustrated that in previous studies the dry-bulb temperatures (T_a) were within 25.1-30.0°C and the operative temperatures (T_o) were within 24.7-30.0°C, whereas T_a in this study was 26.24°C and T_o was 26.44°C which agree well with previous studies. When the present study was compared with two previous studies in Sri Lanka, it was found that T_o in Sri Lanka were 30.0°C and 31.0°C, which were higher than the comfort temperature in this study. This can be explained by the climate in Sri Lanka being hotter than the climate in Thailand. However, T_a in a previous study in Thailand was 25.1°C and T_o was 24.7°C, which were different from the results in the present study. Hence, it is suggested that further studies should be conducted in more industrial factories in Thailand in order to attain more conclusive findings.

From the analysis in this study, it is suggested that the controlled temperatures in the air-conditioned and the non-air-conditioned spaces are 25.99°C and 26.24°C, respectively, so that people with all genders, all ages, and all BMIs would feel comfortable.

V. CONCLUSIONS

This study explored the thermal comfort of the employees in industrial factories: three factories in Samut Sakhon, two factories in Nakhon Pathom, one factory in Samut Prakan, and one factory in Bangkok. Overall, 843 subjects were randomly

selected from a total population of 872 to get a 95% confidence interval with a $\pm 5\%$ uncertainty. The results revealed that the comfort temperature assessed by the ASHARE model was 25.34°C, which was almost 1°C lower than the one assessed by the Adaptive Comfort model (26.25°C). It is seen that the comfort temperature from the Adaptive Comfort model is more reliable since it represents the actual thermal sensation. In turn, it might be said that the ASHRAE model underestimates the true comfort temperature by around 1°C. Moreover, this present study also showed that the comfort temperatures in the form of the dry-bulb temperatures and the operative temperatures had no significant difference. Therefore, either one can be used as the comfort indicator.

Regarding the analysis of parameters in the thermal comfort, it can be concluded that gender, age, body mass index, as well as air-conditioned and non-air-conditioned work environments, were influential on thermal comfort. Females had 1.09°C higher comfort temperature than males. Adults had 1.38°C higher comfort temperature than the adolescents and 0.95°C higher than the middle-aged group. People with excess weight had 0.68°C higher comfort temperature than people with low weight. Also, people working in air-conditioned workplaces had 1.30°C lower comfort temperature than those in non-air-conditioned workplaces. All of these results agree well with previous studies.

This study suggests that the controlled temperature in air-conditioned and non-air-conditioned spaces should be 25.99°C and 26.24°C so the people with all genders, all ages, and all BMIs would feel comfortable.

ACKNOWLEDGMENT

The authors would like to thank the Department of Mechanical Engineering, Faculty of Engineering and Industrial Technology, Silpakorn University for all supports to complete this work

REFERENCES

- [1] Department of Alternative Energy Development and Efficiency, Energy Conservation Technology Center Project, 2011.
- [2] G. Kats, L. Alevantis, A. Berman, E. Mills, and J. Perlman, "The costs and financial benefits of green buildings," 2003.
- [3] ASHRAE, 2005 ASHRAE Handbook Fundamentals, 2005.
- [4] H. Ohashi, H. Tsutsumi, S. Tanabe, K. Kimura, H. Murakami, and K. Kiyohara, "Subjective thermal comfort in the environment with spot cooling system," 2007.
- [5] N. Azer, "Design guidelines for spot cooling systems: Part 1. Assessing the acceptability of the environment," ASHRAE Trans. United States, 1982, (CONF-820112-).
- [6] S. Atthajariyakul, "Thermal comfort for air-conditioning in Thailand," KCU Engineering Journal, vol. 34, pp. 141-150, 2012.
- [7] R.J. De Dear and G.S. Barger, "Thermal comfort in naturally ventilated buildings," ASHRAE Trans, vol. 34, pp. 549-561, 2002.
- [8] P.O. Fanger, "Thermal comfort. Analysis and applications in environmental engineering," Book Reviews, pp.164, 1970.
- [9] J. Busch, "Thermal responses to the Thai office environment," ASHRAE Trans. United States, vol. 96, 1992.



- [10] S. Sekhar, "Higher space temperatures and better thermal comfort—a tropical analysis," *Energy and Buildings*, vol.23, pp. 169-174, 1995.
- [11] F. Nicol and S. Roaf, "Pioneering new indoor temperature standards: the Pakistan project," *Energy and Buildings*, vol.23, pp. 169-174, 1996.
- [12] A.G. Kwok, J. Reardon, and K. Brown, "Thermal comfort in tropical classrooms/Discussion," *ASHRAE Trans.*, vol. 104, p. p. 1031, 1998.
- [13] T.H. Karyono, "Report on thermal comfort and building energy studies in Jakarta—Indonesia," *Energy and Buildings*, vol. 35, pp. 77-90, 2000.
- [14] J. Khedari, N. Yamtraipat, N. Pratintong, and J. Hirunlabh, "Thailand ventilation comfort chart," *Energy and Buildings*, vol. 32, pp. 245-249, 2000.
- [15] N. Wong, H. Feriadi, P. Lim, K. Tham, C. Sekhar, and K. Cheong, "Thermal comfort evaluation of naturally ventilated public housing in Singapore," *Energy and Buildings*, vol. 37, pp. 1267-1277, 2002.
- [16] J.F. Nicol, and M.A. Humphreys, "Adaptive thermal comfort and sustainable thermal standards for buildings," *Energy and Buildings*, vol. 34, pp. 563-572, 2002.
- [17] J. Nakano, S. Tanabe, and K. Kimura, "Differences in perception of indoor environment between Japanese and non-Japanese workers," *Energy and Buildings*, vol. 34, pp. 615-621, 2002.
- [18] K.W.H. Mui, and W.T.D. Chan, "Adaptive comfort temperature model of air-conditioned building in Hong Kong," *Energy and Buildings*, vol. 38, pp. 837-852, 2003.
- [19] N.H. Wong, and S.S. Khoo, "Thermal comfort in classrooms in the tropics," *Energy and Buildings*, vol. 35, pp. 337-351, 2003.
- [20] N. Yamtraipat, J. Khedari, and J. Hirunlabh, "Effect of physical factors on thermal sensation of thai people in office environment," *Energy and Buildings*, vol. 21, pp. 42-46, 2004.
- [21] S. Chirarattananon, P. Rakwamsuk, V.D. Hien, J. Taweekun, and V. Mettanan, "Development of a building energy code for new buildings in Thailand," In proceedings of the Joint International Conf on Sustainable Energy and Environment. Thailand, 2004.
- [22] H. Feriadi, and N.H. Wong, "Thermal comfort for naturally ventilated houses in Indonesia," *Energy and Buildings*, vol. 36, pp. 614-626, 2004.
- [23] C. Bouden, and N. Ghrab, "An adaptive thermal comfort model for the Tunisian context: a field study results," *Energy and Buildings*, vol. 37, pp. 952-963, 2005.
- [24] N. N. N. M. Tun, "Field assessment of thermal comfort in common spaces in Asian Institute of Technology," *Energy and Buildings*, 2005.
- [25] S.P. Corgnati, M. Filippi, and S. Viazzo, "Perception of the thermal environment in high school and university classrooms: Subjective preferences and thermal comfort," *Energy and Buildings*, vol. 42, pp. 951-959, 2007.
- [26] M. Sriprasert, W. Sabhasuk, and S. Chaiunn "Assessment of the comfort of people in Silpakorn University Sanam Chandra Palace Campus," Department of Technical Engineering Faculty of Engineering and Industrial Technology, Silpakorn University, Nakhon Pathom, 2007.
- [27] R.A. Memon, S. Chirarattananon, and P. Vangtook, "Thermal comfort assessment and application of radiant cooling: A case study," *Energy and Buildings*, vol. 43, pp. 1185-1196, 2008.
- [28] A.T. Nguyen, M.K. Singh, and S. Reiter, "An adaptive thermal comfort model for hot humid South-East Asia," *Building and Environment*, vol. 56, pp. 291-300, 2012.
- [29] S. Rattanavijit, Thermal Discomfort of Passengers in an Airport Terminal, 2012.
- [30] M.K. Nematchoua, R. Tchinda, and J. A. Orosa, "Adaptation and comparative study of thermal comfort in naturally ventilated classrooms and buildings in the wet tropical zones," *Energy and Buildings*, vol. 85, pp. 321-328, 2014.
- [31] M.C. Katafygiotou, and D.K. Serghides, "Thermal comfort of a typical secondary school building in Cyprus," *Sustainable cities and Society*, vol. 13, pp. 303-312, 2014.
- [32] P. Nuntasiri, and S. Rasisuttha, "Thermal comfort of low income people: case study of Baan Mankong Non Nong Wat 2," *Buil Environment Inquiry*, vol. 14, pp. 127-141, 2015.
- [33] R. De Dear, J. Kim, C. Candido, and M. Deuble, "Adaptive thermal comfort in Australian school classrooms," *Building Research and Information*, vol. 43, pp. 383-398, 2015.
- [34] Y. Liu, J. Jiang, D. Wang, and J. Liu, "The indoor thermal environment of rural school classrooms in Northwestern China," *Indoor and Building Environment*, p. 1420326X16634826, 2016.
- [35] S. Manu, Y. Shukla, R. Rawal, L. E. Thomas, and R. de Dear, "Field studies of thermal comfort across multiple climate zones for the subcontinent: India Model for Adaptive Comfort (IMAC)," *Building and Environment*, vol. 98, pp. 55-70, 2016.
- [36] S. Wijewardane, and M.T.R. Jayasinghe, "Thermal comfort temperature range for factory workers in warm humid tropical climates," *Renewable Energy*, vol. 33, pp. 2057-2063, 2008.
- [37] W.V.R. Kosala, P.N. Vilasini, and J. R. Gamage, "Comfort study of work environment of apparel industry," 2011 IEEE International Conference on Industrial Engineering and Engineering Management, pp. 789-793, 2011.
- [38] P. Lumyim, and W. Tonglar, "A survey on thermal comfort of people in industrial factories," Department of Technical Engineering Faculty of Engineering and Industrial Technology, Silpakorn University. Nakhon Pathom, 2013.
- [39] N.D.M. Pinto, A.A.D.P. Xavier, and K. Hatakeyama, "Thermal comfort in industrial environment: conditions and parameters," *Procedia Manufacturing*, vol. 3, pp. 4999-5006, 2015.
- [40] Office of Small and Medium Enterprises Promotion (OSMEP), Small and Medium Enterprises Promotion Initiative in the Textile and Garment Industry, 2011.
- [41] ASHRAE, Thermal Environmental Conditions for Human Occupancy, 2003.
- [42] Meteorological Department, Season of Thailand, 2016, www.tmd.go.th (accessed 10.6.17)
- [43] J. Spagnolo, and R. de Dear, "A field study of thermal comfort in outdoor and semi-outdoor environments in subtropical Sydney Australia," *Building and Environment*, vol. 38, pp. 721-738, 2003.
- [44] M. Beshir, and J. Ramsey, "Comparison between male and female subjective estimates of thermal effects and sensations," *Applied Ergonomics*, vol. 12, pp. 29-33, 1981.
- [45] S. Chanam, "Human development," *Developmental Psychology*, pp. 50-57, 1999.
- [46] ASHRAE, Chapter 8 Physiological Principles, ASHRAE Handbook - Fundamentals, 1989.
- [47] I. Marincic, J. Ochoa, M. Alpuche, and G. Gomez-Azpeitia, "Adaptive Thermal Comfort in Warm Dry Climate," *Building and Environment*, 2009.
- [48] J.S. Garrow, and S. Blaza, "Thermogenic response to temperature, exercise and food stimuli in lean and obese women, studied by 24 h direct calorimetry," 1983.
- [49] M. Mozaffarieh, A. Schotzau, S. Orgul, J. Flammer, and K. Krauchi, "Research thermal discomfort with cold extremities in relation to age, gender, and body mass index in a random sample of a Swiss urban population," *Population Health Metrics* 2010, 2010.
- [50] R.H.P. Tuomaala, K. Piira, and M. Airaksinen, "Impact of individual characteristics-such as age, gender, BMI, and fitness-on human thermal sensation," *Building Simulation*, 2013.
- [51] T.H. Karyono, "Report on thermal comfort and building energy studies in Jakarta—Indonesia," *Building and Environment*, 2000. vol 35, pp. 77-90.
- [52] R.J. De Dear, G.S. Brager, J. Reardon, and F. Nicol, "Developing an adaptive model of thermal comfort and preference/Discussion," *ASHRAE Trans.*, vol. 104, 1998, pp. 145.
- [53] L. Zhao, X. Zhou, L. Li, S. He, and R. Chen, "Study on outdoor thermal comfort on a campus in a subtropical urban area in summer," *Sustainable Cities and Society*, vol. 22, pp. 164-170, 2016.



Effect of Drying Temperature on Colour and Anthocyanin Contents in Purple Corn Kernel

Dhetsuwan Khum-oh^{1*}, Suparek Charmongkolpradit¹, Bhuchiss Tanwanichkul² and Wichien Sang-aroon³

^{*1}Department of Mechanical Engineering, ²Department of Post-Harvest and Processing Engineering,

³Department of Chemistry, Faculty of Engineering,

Rajamangala University of Technology Isan Khon Kaen Campus, Thailand, 40000

khumohzoneudon@gmail.com, supchar2005@hotmail.com, dr.bhuchiss@gmail.com, wichien.sa@rmu.ac.th

Abstract: The objective of this research were to study the effect of drying temperature on colour and anthocyanin contents in purple corn kernel. By using tunnel dryer experimental, corn kernels were dried. The drying temperature was at 40, 60 and 80°C. The initial moisture content was 56.45%, 49.38% and 49.60% (Wet Basis) respectively, velocity of 1.5 m/s. Drying was continued until the final moisture content of approximately 13% (Wet Basis). Experimental results of drying temperatures 40, 60 and 80 °C showed that the average drying time was 480, 360 and 300 minutes, respectively. It also showed that, increasing drying temperature reduced the drying duration. The results of statistical colour value analysis showed that, previous drying of corn kernels with colour values L *, a * and b * more than dried corn kernels. The increase in temperature causes the color values L *, a * and b * to decrease. The results of total anthocyanin content analysis showed that, at temperature of 40, 60 and 80°C previous drying of corn kernels had the total anthocyanin content of 3662.46, 4335.11 and 4834.52 mg/100g, respectively. The dried corn kernels had the total anthocyanin content of 3680.31, 4431 and 3190.05 mg/100g, respectively. The results showed that the dried corn kernels at temperature of 40 and 60°C resulted in slight increases in total anthocyanin contents. At temperature of 80 °C the total anthocyanin content decreased. It was concluded that the increase in temperature had a significant effect on both color values and total anthocyanin content.

Keywords: Drying; Purple corn; Anthocyanin.

I. INTRODUCTION

Purple corn (*Zea mays* L.), there is an increasing interest in purple waxy corn due to its health promoting properties. This type of corn was compounds of anthocyanin is a natural pigment in a group of flavonoids. Which can be found in the section with the blue. Purple, red and orange colors of many fruits and vegetables. [1] Anthocyanins has the ability of antioxidants that are beneficial to the body than vitamin C and E up to double which can help enhance the function of red blood cells, help slow down the occurrence of fat in the arteries, reduces the chance of cancer, help strengthen the body against disease and wound healing and slow down the deterioration of cells. [2] The highest amount of anthocyanin that humans can consume is on average 200 milligrams per

day. [3] Purple corn is an important source of anthocyanin found in many parts of corn including whole cob, whole kernel and kernel pericarp. There were 3,752, 618 and 3,105 mg/100 g (wet basis), respectively. [4]

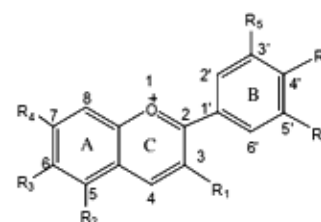


Fig. 1. Structure of total anthocyanin. [5]

Anthocyanin found in fruits and vegetables are phenolic compounds which is an unstable soluble pigment. It is easily dissolved by heat, oxygen, light, temperature, during storage and various factors. From the process of processing include temperature and duration of heating affect the anthocyanin content. In addition, the factors influence the change of anthocyanin are the chemical structure and composition of anthocyanin pH, temperature, light and combination with other substances. Anthocyanin found in fruits and vegetables are phenolic compounds unstable soluble pigment. It is easily dissolved by heat, oxygen, light, temperature, during storage and various factors. From the process of processing include temperature and duration of heating affect the anthocyanin content. [6]

As mentioned above the researchers have seen the importance of nutritious food is a healthy anthocyanin in purple corn. Therefore, the researchers were a study of effect of drying temperature on colour and anthocyanin contents in purple corn kernel. To achieve optimum drying temperature and anthocyanin content after drying the most.



II. MATERIALS AND METHODS

A. Theoretical

Drying is a process to reduce moisture generally drying will use hot air as drying medium. By heat transfer from the air to the material. The heat is used to evaporate the water out of the material. Which can be divided into the drying of 2 range. [7]

1) Constant drying rate

Heat transfer and mass transfer between materials and air occurs only around Material surface which on drying will occur at the surface of the material before. The important variables that affect the drying rate is temperature, relative humidity and air velocity.

2) Falling drying rate

During the drying rate decreases moisture content of the material is lower than the critical moisture (M_{Critical}). Heat transfer and mass transfer does not occur only on the surface of the material but will occur within the material. The movement of water from the material to the surface more slowly, than convection moisture from the surface of the material to the air, the drying rate decreases and the moisture is gradually reduced, until the equilibrium moisture content (M_{eq}).

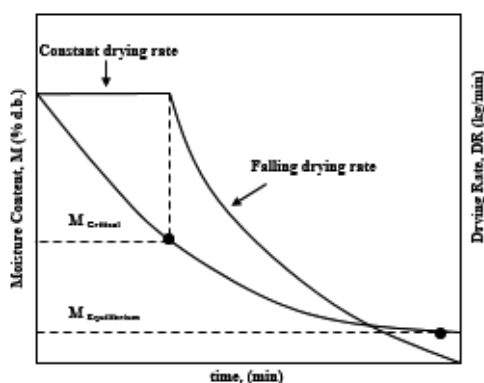


Fig. 2. Drying during the drying rate constant and the reduced. [7]

B. Moisture Content (MC)

Moisture in the grain the amount of water contained in the seeds when compared the weight of the water contained in the grain to dry weight of the grain, which will be constant throughout. The moisture content of the grain is described in the form of a percentage [8] which is divided into 2 standards.

1) Wet Basis Moisture Content

Wet Basis Moisture Content (M_w) is described by the percentage equivalent of the ratio of the mass of water to the total mass of the material. Commonly used in the trade is generally referred to as a percentage, as follows.

$$M_w = \frac{W - d}{W} \times 100 \quad (1)$$

Where M_w is wet basis moisture content (%wb). Also, W and d are initial mass of material (kg) and the dry mass of material (kg), respectively.

2) Dry Basis Moisture Content

Dry Basis Moisture Content (M_d) is described by the percentage equivalent of the ratio of the mass of water to the mass of the dry matter. Commonly used to analyze the drying of the theory because it helps to calculate the mass of dry material is easier because there will be a constant or nearly constant during drying, as follows.

$$M_d = \frac{W - d}{d} \times 100 \quad (2)$$

Where M_d is dry basis moisture content (%db). Also, W and d are initial mass of material (kg) and the dry mass of material (kg), respectively.

C. The experimental design and drying.

The experiment of drying purple waxy corn varieties Suprime harvest 70-75 days. (Fig. 3) The previous experiments measurement initial moisture content by standard method Association of Official Agricultural Chemists (AOAC, 1990) [9], measure the color value and measurement total anthocyanin. The experiments using the tunnel dryer blower power 350 Watts heater power 600 watts and the load cell recorded weight automatically, as shown in Figure 4. Experiment of drying corn kernels 100g. Drying experiments were carried out at 40, 60 and 80 °C drying air temperatures and 1.5 m/s drying air velocity. Drying was continued until the final moisture content to approximately 13% (wb). Then, bring corn kernels after drying to analyze color value and total anthocyanin content was analyzed.



Fig. 3. Purple corn kernel.

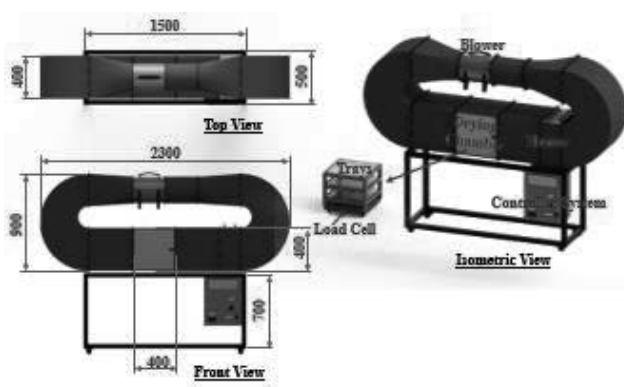


Fig. 4. Tunnel dryer.



Fig. 5. Experimental set-up.

D. The analyze color value.

Analysis of the color by color measurement (Portable Color Difference Meter TCD100). Displayed in the form of the values L^* , a^* and b^* . The color value indicates the

brightness (L^*), the color values indicates red or green (a^*), and the color indicate the yellow or blue (b^*). Furthermore, the recorded results of the experiments were analysed.

E. The analysis of total anthocyanin content.

The extraction is the first step of the analysis of anthocyanins. Adapted from the method (Rodriguez-Saona and Wrolstad, 2001 and Jing et al., 2007). [1] [10] Grind the corn kernels thoroughly. Extracted by infusion in a solvent methanol into acidic, (0.01% (v/v) hydrochloric acid in methanol), left 24 hours. After that, filter by vacuum filtration with filter paper No.1. Distillation of the methanol with evaporator vacuum rotary at 40 °C will be coarse extract. Keep away from sunlight at temperature of 4 °C, the extract to measure the absorbance value.

Measurement the absorbance of the extract anthocyanin. Adapted from the method (Giusti and Wrolstad, 2001). [11] The analysis of total anthocyanin content was by pH differential method. The coarse extract of anthocyanin to check the absorbance characteristics. The coarse extract of anthocyanin dissolved in the solvent methanol to adjustable acidity 0.01 (v/v) and adjust pH of solution with the hydrochloric acid to equals 1. Measure the absorbance in the range UV-Visible is 400-800 nm. Analysis by spectrophotometer. The absorbance value was calculated to determine of anthocyanins content.

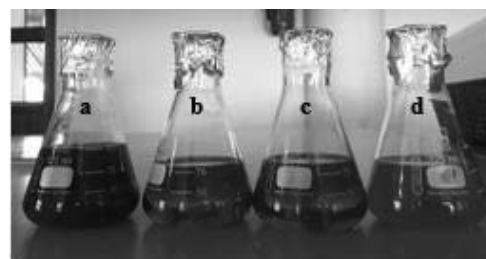


Fig. 6. Extraction anthocyanin. Example at temperature 80 °C. a) Fresh Corn. b) First, 80 °C. c) Second, 80 °C. d) Third, 80 °C.

III. RESULTS AND DISCUSSION

A. Experimental results of drying.

The results of experiment of drying purple waxy corn varieties Supreme at temperatures of 40, 60 and 80 °C, with initial moisture content of 56.45%, 49.38% and 49.60% (wb), respectively. Drying was continued until the final moisture content to approximately 13% (wb). From Fig. 7, the drying at air temperatures of 40, 60 and 80 °C found the required average time for drying process to be 2013, 372 and 160 min, respectively. Furthermore, the analysis results of corn kernels drying found that increases in temperature can reduce the drying time.

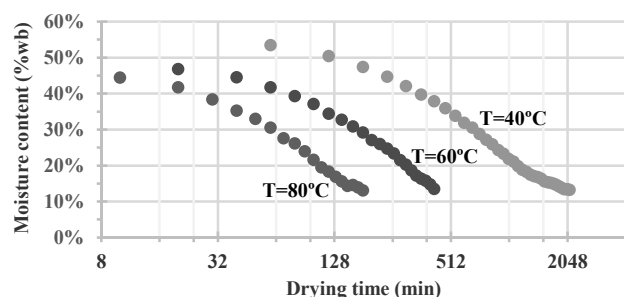


Fig. 7. Variation of moisture content of corn kernels at $v=1.5$ m/s for different levels of drying air temperature.

B. The results of analysed color value.

The results of analysed color value is displayed in the form of the values L^* , a^* and b^* . From Table I, the results of statistical color value analysis showed that, previous drying of corn kernels with color values L^* , a^* and b^* more than corn kernels dried. Because the temperature of drying affects the variation of color value of corn kernels. The increase in temperature causes the color values L^* , a^* and b^* decreased shows that the color value of the corn kernel after drying was darker.

TABLE I. Variation of color value (L^* , a^* and b^*) of corn kernels for different levels of drying air temperature.

Temperature (°C)	Drying time (min)	Color value		
		L^*	a^*	b^*
Fresh Corn	-	+31.47	+18.48	+4.14
40	2013	+29.80	+16.22	+3.92
60	372	+27.43	+14.96	+3.86
80	160	+25.19	+12.34	+3.78

C. The results of analyze total anthocyanin content.

The results of drying corn kernels temperature of 40 °C, the total anthocyanin content before drying 3662.46 mg / 100g and after drying 3680.31 mg / 100g. At temperature of 60 °C, the total anthocyanin content before drying 4335.11 mg / 100g and after drying 4431 mg / 100g. And temperature of 80 °C, the total anthocyanin content before drying 4834.52 mg / 100g and after drying 3190.05 mg / 100g. (Table II.) The results of total anthocyanin content analysis showed that the drying of corn kernel at temperatures 40 and 60 °C has total anthocyanin content increased little more. Because the corn kernel after drying with less water content in corn kernel before drying and after drying the corn kernels was darker. And may be due to experiment measurement anthocyanin content. Therefore, it effects on variation of Total anthocyanin content of corn kernels. And the drying of corn kernel at temperatures 80 °C has total anthocyanin content decreased significantly. Because

the temperature of drying increases cause effects of the total anthocyanin content decreased. This is according to the article Leong and Oey, 2012, [6] which the temperature and duration of heating influence variation anthocyanin content.

TABLE II. Variation of Total anthocyanin content of corn kernels for different levels of drying air temperature.

Temperature (°C)	Total anthocyanin content (mg/100g)	
	Fresh Corn	Dried Corn
40	3662.46	3680.31
60	4335.11	4431.00
80	4834.52	3190.05

IV. CONCLUSIONS

Drying of corn purple kernel, the final moisture content to approximately 13% (wb) it was found that the increases in temperature can reduce the drying time. And the results of statistical color value analysis showed that the increase in temperature causes the color values L^* , a^* and b^* decreased. Furthermore, the results of total anthocyanin content analysis showed that the drying of corn kernel at temperatures 40 and 60 °C has total anthocyanin content increased little more. And the drying of corn kernel at temperatures 80 °C has total anthocyanin content decreased significantly. It was concluded that the increase in temperature had a significant effect on both color values and total anthocyanin content.

ACKNOWLEDGMENT

We would like to express our thanks to the Department of Mechanical Engineering, Department of Post-Harvest and Processing Engineering, Department of Chemistry, Faculty of Engineering, and Rajamangala University of Technology Isan, Khon Kaen Campus, for their invaluable research support.

REFERENCES

- [1] Jing, P. and M. M., Giusti, "Effects of extraction conditions on improving the yield and quality of an anthocyanin-rich purple corn (*Zea mays* L.) extract". *J. Food Sci.* 72: 363-368, 2007.
- [2] Shipp, J. and E.S.M. Abdel-Aal, "Food Applications and Physiological Effects of Anthocyanins as Functional Food Ingredients", *The Open Food Science Journal*, 4, 7-22, 2010.
- [3] Department of Science Service, Anthocyanin. Science Library - Department of Science Service, Ministry of Science and Technology, Thailand, 1992.
- [4] Boliavar A. Cevallos-casals and Luis Cisneros-zevallos, "Stoichiometric and kinetic studies of phenolic antioxidants from Andean purple corn and red-fleshed sweet potato", *J Agric Food Chem* 51:3313-3319, 2003.
- [5] Araceli Castaneda-Ovando, Ma. de Lourdes Pacheco-Hernández, Ma. Elena Paez-Hernandez, Jose A. Rodriguez and Carlos Andres Galan-Vidal, "Chemical studies of anthocyanins: A review", *Food Chemistry* 113; 859-871, 2009.



- [6] Leong, S. Y., and I. Oey, "Effect of processing on anthocyanins, carotenoids and vitamin C in summer fruits and vegetables", *Food Chem.* 133:1577-1587, 2012.
- [7] Somchart sophonronnarit, "Drying Grains and Some Types of Foods", 7th edition, KMUTT, Bangkok, 338p. (in Thai), 1997.
- [8] Viboon Thepent, "Grain moisture measurement", Senior Agricultural Engineer, Agricultural Engineering Research Institute, Department of Agricultural, Thailand, 2009.
- [9] A.O.A.C., "Association of Official Analytical Chemist", Washington DC, Official Methods of Analysis. 15th Edition, 1990.
- [10] Rodriguez-Saona, L. E., and R. E. Wrolstad, "Extraction, Isolation, and Purification of Anthocyanins", P. F1.1.1-F1.1.11. In: R. E. Wrolstad. *Current Protocols in Food Analytical Chemistry*. John Wiley & Sons, NY, 2001.
- [11] Giusti, M.M. and R.E. Wrolstad, "Characterization and measurement of anthocyanins by UV-visible spectroscopy", In: *Current Protocol in Food Analytical Chemistry* (R.E. Wrolstad., ed.) Jone Willy & Sons Inc., New York, pp. F1.2.1-F1.2.13, 2001.



Performance Limit of Closed-Loop Pulsating Heat Pipe Filled with Water-Ethanol Blended Working Fluid

Adisak Janthothai*, Niti Kammuang-lue, Phrut Sakulchangsattajai, Pradit Terdtoon

Department of Mechanical Engineering, Faculty of Engineering, Chiang Mai University,
Chiang Mai, Thailand. Tel: +66-53-944144 Fax: +66-53-226014

*Corresponding author; E-mail: Janthothai_a@hotmail.com

Abstract—This research aims to experimentally investigate the thermal characteristics of a closed-loop pulsating heat pipe (CLPHP) charged with water-ethanol blended working fluids at critical state. Moreover, this research can be compared with pure working fluid. The volume mixing ratio (MR) of blended working fluid is 1:1 with volume filling ratio of 50%. This inclination of this study is 5° from horizontal axis. The CLPHP is made of a copper capillary tube with the internal diameter of 2 mm and turn of 16. The evaporator section length is 50 mm. The adiabatic and condenser lengths are equaled to the evaporator section. A low-voltage and high-current power transformer is used as the heat source which supplies from the top to bottom of copper bus bar. Furthermore, the condenser section is placed in the cooling jacket. A solution of water and ethylene glycol with 1:1 by volume is set as coolant. This coolant is circulated to transfer heat from condenser section to heat sink or cooling bath. The adiabatic temperature is controlled at 50±5 °C. It is concluded that, when the working fluid changed from ethanol to the blended working fluid of water and ethanol, the maximum heat flux increased from 10.2 to 20 kW/m² because of the ability of dry-out prevention on the evaporator surface. Moreover, the blended working fluid was high oscillating amplitude and frequency due to the thermo-physical properties of water.

Keywords— Performance Limit; Pulsating Heat Pipe; Blended Working Fluid

I. INTRODUCTION

The closed-loop pulsating heat pipe (CLPHP) was first presented by Akachi et al. [1]. It was a heat transfer device which had excellent features, such as high thermal performance, rapid response to high load, operating without an external mechanical power, simple design and low cost. Therefore, CLPHP was considered as one of the promising technologies for cooling devices. CLPHP was made of a long copper capillary tube and bent into an undulating tube. The ends of tube connected to join a closed-loop. When the CLPHP was charged with working fluid after air evacuation, the working fluid randomly forms into liquid slug and vapor plug along the entire length of the tube which was called “slug-train”. Their operation was based on the principle of a phase

change phenomena. When one end of the bundle of the heat pipe was subjected to heat or high temperature, the working fluid which formed into liquid slug and vapor plug would evaporate, expand and move to condenser section. Then, the vapor plug would condense collapse and release heat into the environment. This working fluid circulated and transferred heat in a cycle which was called “Replacement mechanism” [2]. It was clearly known that the diameter of the capillary tube used to make the pulsating heat pipe must not exceed the critical diameter [3].

$$D_{i,max} = 2 \sqrt{\frac{\sigma}{\rho_l g}} \quad (1)$$

Generally, if liquid quantity in the evaporator section was sufficient to transfer heat, CLPHP could be normally transfer the heat and an operation with this condition was defined as “normal operating state”. When heat input gradually increased until liquid quantity in the evaporator section was not sufficient to transfer heat, dry-out of liquid film occurred and heat transferred by the heat pipe was decreased. This evident was defined as “critical state”. Therefore, the maximum heat flux which the CLPHP worked properly just before its dry-out was defined as “performance limit” [4].

In a recent year, several researches conducted experimental investigations on CLPHP, and the results indicated that the thermal performance mainly depended on the working fluid, Filling ratio, internal diameter, evaporator section length, number of turns, orientation and inside phenomena. There were many studies on heat transfer characteristics of CLPHP at normal operating and critical state with pure working fluids [4-6]. investigated the heat transfer characteristics of a CLPHP with an internal diameter of 2 mm and 10 turns charged with water ethanol methanol and acetone which the latent heat ranged 520 to 2,300 kJ/kg. It was found that acetone which was the lowest latent heat showed the best thermal performance [5]. However, in critical state, an experimental investigation on horizontal CLPHP was made form 2.03 mm of internal diameter, 10 turns and 100 mm of all section lengths. It was found that when the working fluids changed from R123 to



ethanol or water, the latent heat changed from 161 kJ/kg to 1,000 kJ/kg or 2,382 kJ/kg, respectively. Furthermore, the maximum heat flux increased from 24.1 kW/m² to 24.3 kW/m² or 47.9 kW/m², respectively [4]. The mentioned results were correspondence to the previous work [6].

According to their advantages of different working fluids, the blended working fluids had also various heat transfer characteristics which depended on the thermo-physical properties of mixtures, volume mixing ratio of each mixture and inside phenomena which was different from phase transition of pure working fluid [7]. There were a few of studies on heat transfer characteristics of closed-loop pulsating heat pipe at normal operating state with blended working fluid. Han *et al.* [7] investigated the effect of water-based binary mixtures (volume mixing ratios of 13:1, 4:1, 2:1, 1:1, 1:4 and 1:13) at various filling ratios from 35% to 70%. It was shown that at 35% 45% and 55% of filling ratios, most of binary mixture exhibited better performance against the onset of dry-out compared with using pure working fluid. It could possibly be attributed to the Phase-Change-Inhibition Effect (PCIE), i.e. the vapor slugs abundant with lower boiling point component of higher saturation pressure suppress the evaporation of water. In contrast, the thermal performance of the CLPHP charged with the binary mixtures generally had no superiority to the pure fluids especially to the pure water at 60% and 70% of filling ratios. In the same way, the experiment investigated the heat transfer characteristics of a CLPHP with water-acetone mixture (volume mixing ratios of 13:1, 4:1, 2:1, 1:1, 1:4 and 1:13) at filling ratios from 35% to 70% [8]. It was presented that at low filling ratios (45% and 55%), water-acetone mixture at 4:1, 1:1, 1:4 and 1:13 of volume mixing ratios presented improved performance against the onset of dry-out compared with using pure water or acetone. Under a heat input of 50 W, thermal resistances of the CLPHP with water-acetone mixture (at volume mixing ratios of 4:1, 1:1, 1:4 and 1:13) decreased from 33.6% to 68.9% compared with pure working fluids. Especially, at the volume mixing ratio of 1:1 water-acetone mixture kept low thermal resistance throughout the heat supply.

As mention above, the study of a CLPHP with blended working fluid at critical state has not been investigated. The objective of study was to experimentally investigate the effect of blended working fluids on the maximum heat flux of CLPHP.

II. EXPERIMENTAL SETUP AND PROCEDURE

Fig. 1 showed the CLPHP which were made of long capillary tubes with internal diameter of 2.03 mm and bent into 16 turns. Two copper busbars were welded on the top and bottom of evaporator section which were 50 mm of section length. The adiabatic and condenser section length were equal to the evaporator length to eliminate the effect of heat flux transformation. The working fluid was pure water and ethanol and blended working fluid of water-ethanol at 1:1 volume mixing ratio. The filling ratio was 50% by total volume. The CLPHP was set into 5° from horizontal axis.

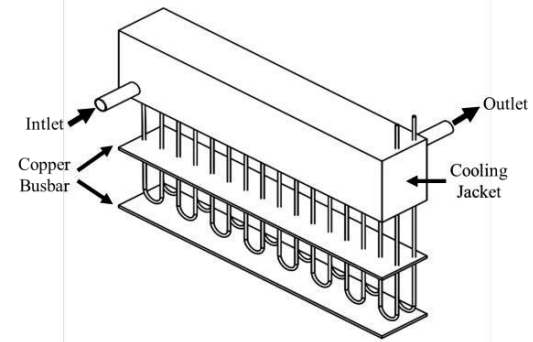


Fig. 1. Sample of Closed-loop pulsating heat pipe

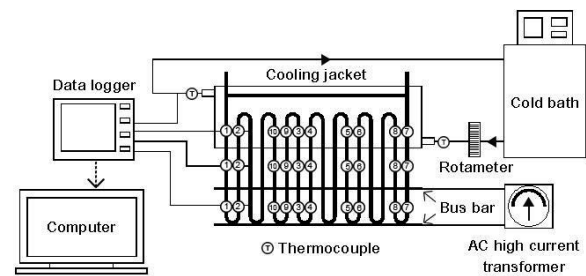


Fig. 2. The experimental setup

Fig. 2 showed schematic diagram of the experiment setup in this study. A low-voltage, high-current power transformer was used as the heat source by supplying the electrical current from upper to lower bus bar. The copper tube was a resistance equivalent to the resistance in the electrical circuit, so the evaporator section heated. The quantity of heat was controlled by voltage adjustment. The condenser section was placed in a cooling jacket. The cooling medium which was a solution of water and ethylene glycol with 1:1 by volume circulated to transfer heat from condenser section to heat sink. The flow rate was measured by a rotameter (Platon, PGB411, accuracy of ± 0.1 L/min). All sections were insulated by a thermal insulation (Aeroflex, 3/8 in. thickness). Thirty-four Chromel-Alumel thermocouples (Omega, Type K, accuracy of ± 0.5 °C) were attached on the outer surface to measure the specific temperature of CLPHP. The specific temperature was monitored by a data logger (Brainchild, VR18, accuracy ± 0.1 °C). Ten thermocouples were fixed on the outer wall of each section (Number 1-6 fixed on the front row and Number 7-10 fixed on the back row). Moreover, two thermocouples were fixed on each inlet and outlet of cooling jacket in order to measure the variations of cooling medium temperature and calculate the heat flux at specified times by means of the calorific as Eq. (2).

$$\dot{q}_c = \frac{\dot{m}_c c_{pc} (T_{\text{cond,out}} - T_{\text{cond,in}})}{A_{\text{cond}}} \quad (2)$$



Where \dot{m}_c is the mass flow rate of the cooling medium, c_{pc} is the specific heat of the cooling medium, $T_{cond,out} - T_{cond,in}$ is the different temperatures of the cooling medium in cooling jacket and A_{cond} is the outer surface area of the tube in condenser section.

The experimental procedure was as follows: Heat was supplied in a small step into evaporator section. In each step, the adiabatic temperature was controlled at 50 ± 5 °C because this was a suitable working fluid temperature which did not exceed the critical point of all working fluids. Both the temperature and mass flow rate of coolant were adjusted to control the adiabatic temperature. When system reached the steady state, the temperature of each point in evaporator section was recorded. If all temperatures gradually changed, it showed that the heat pipe could transfer heat. After that, the heat was further increased. When the heat was higher than a certain level, one or more points at evaporator section suddenly rose in temperature. It was showed that the heat pipe has reached critical state. The data just before critical state, such as the mass flow and the both temperatures on inlet and outlet of coolant, can be used to determine the maximum heat flux from Eq. (2).

The error of maximum heat flux could be calculated from Eq. (3). Where dq is the error of the critical heat flux, $d\dot{m}_c$ was the accuracy from measuring the mass flow rate of coolant, $dT_{cond,in}$ and $dT_{cond,out}$ were the accuracy from measuring the inlet and outlet temperature, respectively.

$$dq = \left[\left(\frac{\partial q}{\partial \dot{m}_c} d\dot{m}_c \right)^2 + \left(\frac{\partial q}{\partial c_{pc}} dc_{pc} \right)^2 + \left(\frac{\partial q}{\partial T_{cond,out}} dT_{cond,out} \right)^2 + \left(\frac{\partial q}{\partial T_{cond,in}} dT_{cond,in} \right)^2 \right]^{1/2} \quad (3)$$

III. RESULT AND DISCUSSION

A. Critical state of each working fluid

It was known that the critical state of the CLPHP occurred because there was not sufficient liquid to transfer heat from the evaporator section to the condenser section. Then, the heat cannot be removed from the evaporator section and dry-out of liquid film occurred. After that, the CLPHP changed from “normal operating state” to “critical state”. The maximum heat flux which the CLPHP worked properly just before its dry-out was defined as “Performance limit”. The most suitable method to identify the critical state of the CLPHP was the dramatically increase of evaporator temperature and the decrease of the heat transfer rate and the condenser temperature respectively. The criteria of this study controlled the adiabatic temperature at 50 ± 5 °C.

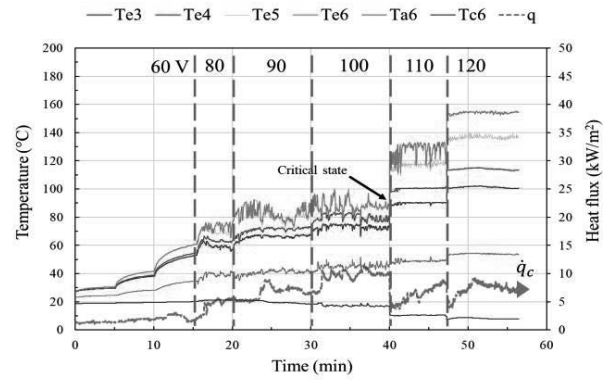


Fig. 3. The variation of each section temperature of ethanol

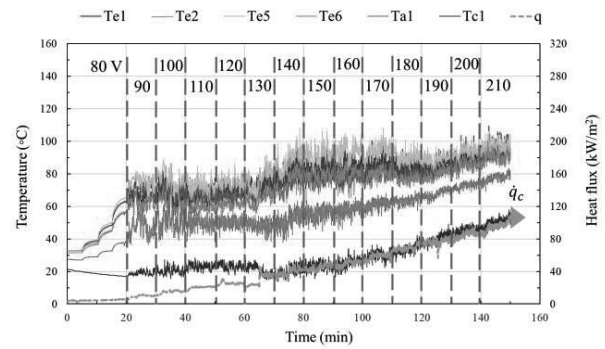


Fig. 4. The variation of each section temperature of water

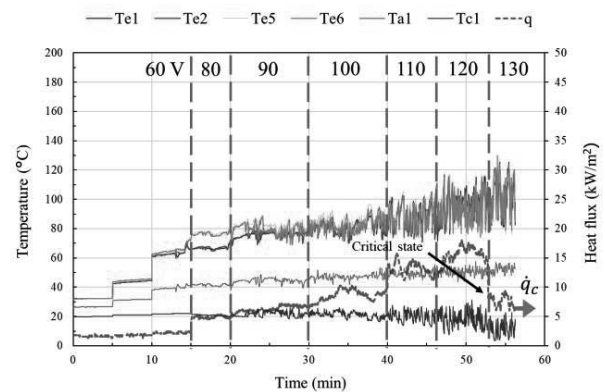


Fig. 5. The variation of each section temperature of blended working fluid

Fig 3 showed each section temperature and heat supply which represented by Variac level (V) of the CLPHP with the internal diameter of 2.03 mm, evaporator section length of 50 mm, 16 turns and ethanol as the working fluid. It was found that, when heat was supplied into the evaporator section, the evaporator temperature gradually increased. At 80 V, the working fluid started up and circulated to transfer heat. When



heat was supplied up to 110V, the evaporator temperature dramatically increased and heat transferred rate and the condenser temperature will decrease respectively. It can be identified that dry-out occurred inside the evaporator surface. Therefore, the maximum heat flux which the CLPHP can properly work just before its dry-out was 10.2 kW/m². In contrast, Fig. 4, the CLPHP charged with water started up and circulated working fluid at 90V. After that, CLPHP continuously transferred heat. The CLPHP can transfer heat up to the maximum heat supply (210 V) and cannot identify the dry-out of all ranges. It can explain that, the high latent heat of water (2,383 kJ/kg) showed the better ability to carry and transfer energy under the same condition, so the CLPHP can transfer heat in a longer range of heat supply. The maximum heat flux was more than 106 kW/m². Fig. 5. showed the variation of temperature of the CLPHP with the blended working fluid of water and ethanol at 1:1 of volume mixing ratio. It was found that the CLPHP transferred heat at 80V as same as the CLPHP charged with ethanol. Because the evaporator extremely oscillated, the critical state can be identified by the decrease of heat transfer rate and condenser temperature. When heat supplied up to 130 V, there was not sufficient liquid at evaporator section to transfer heat to condenser section. Then, dry-out occurred and heat transfer rate and condenser temperature decreased. The maximum heat flux of blended working fluid was 20 kW/m². It concluded that, when the working fluid was changed from ethanol to blended working fluid of water and ethanol, the normal operating state of the CLPHP can extend to 130V. Moreover, the maximum heat flux increased from 10.2 to 20 kW/m² because of the phase-change-inhibition effect (PCIE) [7]. It can explain that the low boiling point component (ethanol) evaporated and suppressed the evaporation of the high boiling point component (water) by the higher pressure of vapor slug, water was still a liquid phase in the evaporator section and prevented dry-out on surface.

B. Variational adiabatic temperature of each working fluid

Fig 6 showed the adiabatic temperatures of adjacent tubes (T_{a3} and T_{a4}) in case of heat supply of 100V. Fig 6(a) showed that the CLPHP charged with ethanol circulated in one direction from left to right. It can be observed that the T_{a4} was higher than the T_{a3} . Because the vapor flowed to the condenser section in the right tube, after that the vapor condensed to liquid and returned to evaporator section. In the same way, Fig. 6(b) showed that the CLPHP charged with water had a same direction to CLPHP charged with ethanol; however, the working fluid flowed with fluctuating direction in period of 31-33 minutes. In contrast, Fig. 6(c) showed that the CLPHP charged with blended working fluid of water and ethanol circulated from right to left. Moreover, the working fluid flowed with fluctuating direction after 38 minutes.

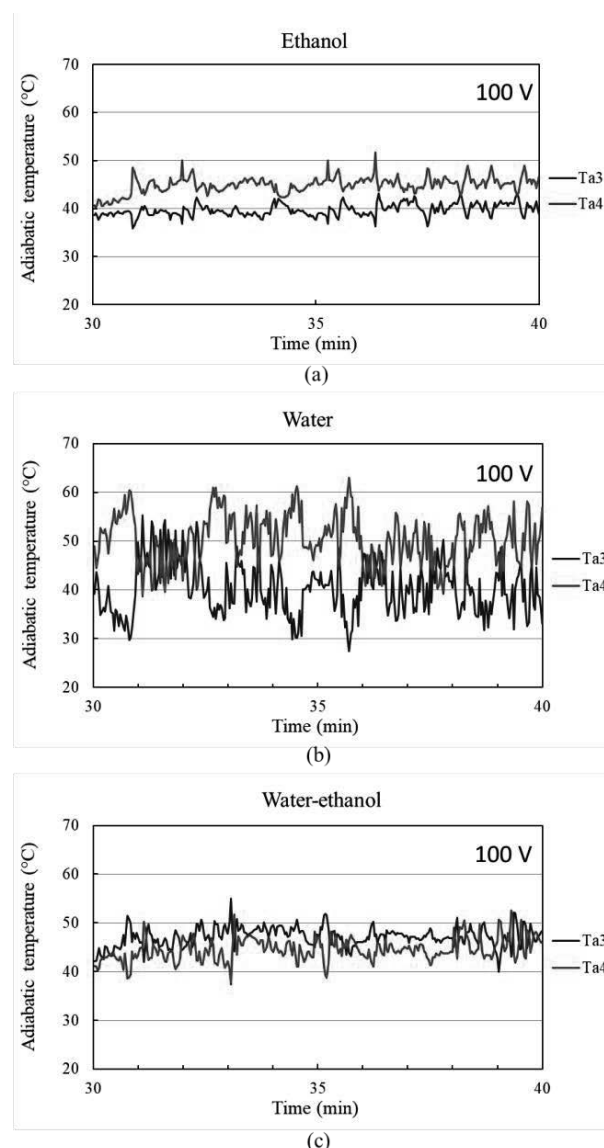


Fig.6. Adiabatic temperature of all working fluids

Fig. 7 showed the evaporator temperatures of adjacent tubes (T_{a3} and T_{a4}) in case of heat supply at 100V, the CLPHP charged with ethanol had low amplitude and frequency of evaporator temperature. On the other hand, the CLPHP changed working fluid from ethanol to water had higher amplitude and frequency as shown in Fig. 7(b) because the velocity of vapor slug was fast. Fig 7(c) showed that the CLPHP charged with blended working fluid of water and ethanol was higher amplitude and frequency than pure ethanol due to the thermo-physical properties of water.

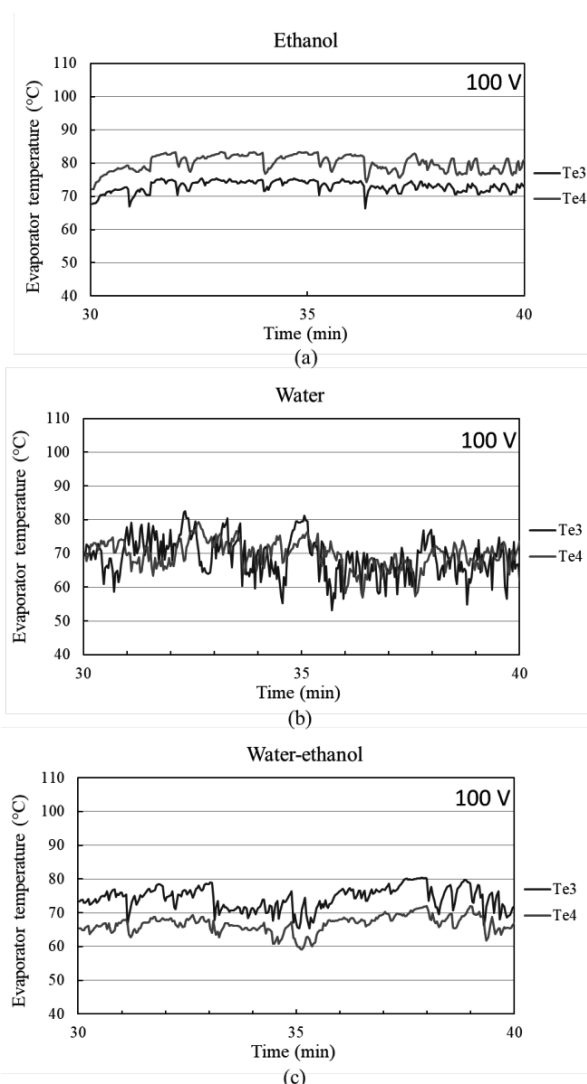


Fig.7. Evaporator temperature of all working fluids

IV. CONCLUSIONS

The effect of working fluids on Thermal characteristic of the CLPHP has been experimentally investigated in this paper. When the working fluid changed from ethanol to the blended working fluid of water and ethanol, the maximum heat flux increased from 10.2 to 20 kW/m² because of the ability of

dry-out prevention on the evaporator surface. Moreover, the blended working fluid was high oscillating amplitude due to the thermo-physical properties of water. For the CLPHP charged with water, the performance limit cannot be identified in the experimental condition. Therefore, the CLPHP charged with water was neglected to compare with the others.

ACKNOWLEDGMENT

The presented work was financially supported by The Thailand Research Fund (TRF) and Engineo (Thailand) Co., Ltd. (Contract no. MSD59I0005) Furthermore, this research was conducted in Heat Pipe and Heat System Laboratory, Department of Mechanical Engineering, Faculty of Engineering, Chiang Mai University, Thailand.

REFERENCES

- [1] Akachi, H., Polasek, F. and Stulc, P., "Pulsating Heat Pipe", Proc. of the 5th International Heat Pipe Symposium, Melbourne Australia, pp. 208-217, 1995.
- [2] Soponpongpipat, N., Sakulchangsattajai, P., and Kammuang-lue, N., "Investigation of the Startup Condition of a Closed-Loop Oscillating Heat Pipe", Heat Transfer Engineering. Vol. 30, pp. 626-642, 2009.
- [3] Maezawa, S., Gi, K.Y., Minamisawa, A. and Akachi, H., "Thermal Performance of Capillary Tube Thermosyphon", Proc. of the IX International Heat Pipe Conference. Albuquerque USA. Vol. II, pp. 791-795, 1995.
- [4] Kammuang-lue, N., Charoensawan, P., Ritthidech, S., Budhajan, K., and Terdtoon, P., "Effect of Working Fluids on Heat Transfer Characteristics of Closed-Loop Pulsating Heat Pipe at Critical State", Procs. of the 1st International Seminar on Heat Pipe and Heat Recovery System. Kuala Lumpur Malaysia., pp. 96-102, 2004.
- [5] Pachghare, P. and Mahalle, A., "Effect of pure and binary fluids on closed loop pulsating heat pipe thermal performance", Procedia Engineering, Vol. 5, pp. 624-629, 2013.
- [6] Kammuang-Lue, N., Hudakorn, T. and Terdtoon, P., "Establishment, Verification and Application of a Correlation to Predict the Maximum Heat Flux of a Horizontal Closed - Loop Pulsating Heat Pipe", Energy Research Journal 1, Vol. 2, pp. 96-103, 2010.
- [7] Han, H., Cui, X., Xu, T., Sui, Y. and Sun, S., "Experimental Study on a Closed - Loop Pulsating Heat Pipe (CLPHP) Charged with Water-based Binary Zeotropes and the Corresponding pure Fluids", Energy. Vol. 109, pp. 724-736, 2016.
- [8] Zhu, Y., Cui, X., Han, H. and Sun, S., "The Study on the Difference of the Start-up and Heat Transfer Performance of the Pulsating Heat Pipe with Water-acetone Mixtures", International Journal of Heat and Mass Transfer. Vol. 77, pp. 834-842, 2014.



A Study of Geo-polymer Concrete by Using Waste Powder Coating

Pawin Kantawong*, Parkpoom Jarupoom and
Pracha Yeunyongkul
Faculty of Engineering, Rajamangala University of
Technology Lanna
Chiang Mai, 50300, Thailand

*Corresponding author: 577200@egat.com

Pasinee Siriprapa¹ and Watcharee Funfuenha²
¹Faculty of Arts and Architecture
²Faculty of Science and Agricultural Technology
Rajamangala University of Technology Lanna
Chiang Mai, 50300, Thailand

Abstract— This research was conducted to study a possibility of producing geo-polymer concrete by using waste powder coating. This study tested and investigated a mixing ratio in order to compare among various factors, such as physical characteristics, mechanical properties, economic value, and actual availability. In particular, the research tested different ratios between waste powder coating and metakaolin, as well as concentration of dissolved substances influencing strength of the concrete geo-polymer. Three sets of metakaolin and waste powder coating were tested with the ratio of 90:10, 80:20, 70:30 and 60:40, respectively. Results showed that maximum strength occurred at the metakaolin and waste powder coating ratio of 60:40 and mixture with NaOH :Na₂SiO₃ of 1:2.5. When NaOH of 10 molar was concentrated, the maximum strength reached 87.28 kg/cm². Results of this study confirmed that waste powder coating can be used and mixed to produce cement replacement materials like geo-polymer concrete.

Keywords—geo-polymer concrete; compressive strength; waste powder coating; kaolin

I. INTRODUCTION

The market size of powder coating has continuously increased every year. This is because powder coating is an extremely popular choice for customers. Consequently, there are a lot of industrial wastes after producing powder coating. In Thailand, industrial waste was produced more than 250 tons each year, which affect the environment like air pollution. Moreover, the industries have to deal with waste elimination, including quantity and approaches to get rid of the waste which can hardly be managed in the future. Geo-polymer concrete is generated from geo-polymerization of alkaline solution, silicon oxide and aluminum. Geo-polymer concrete is as strong as Portland cement, which can be used as an alternate of cement. The material used to make geo-polymer is Pozzolanic material containing silica and alumina, of which are metakaolin, calcite kaolin, and ashes derived from industrial and agricultural waste, like fly ash dust-bagasse and rice-husk ash [5]. The researcher needs to increase value of waste powder. Therefore, the study aims to explore chemical characteristics of waste powder, then adapt and use it by mixing with geo-polymer materials in order to: 1) reduce the cost of eliminating waste powder, and 2) replace the Portland

cement to reduce the emission of CO₂ that leads to greenhouse effect [1,2]. The significance of this research is to increase the value of waste powder by using geo-polymer technology which focuses on the experiment. The experiment will examine and seek for appropriate ratio of geo-polymer concrete comprising of metakaolin and waste powder coating, in which dispersion, compression, drying shrinkage, water absorption, porosity, density, and thermal conductivity are measured.

II. RESEARCH METHODOLOGY

A. Literature reviews

In 1950, geo-polymer was found by a Russian, Dr. Victor Glukhovskiy. Then, Prof. Joseph Davidovits, a French chemist, gave the definition of geo-polymer. Geo-polymer is generated from geo-polymerization of high-concentrated alkaline solution, silicon oxide and aluminum. Geo-polymer structure is amorphous. Geo-polymer concrete is as strong as Portland cement, which is an alternative of cement. The material used to make geo-polymer is Pozzolanic materials containing silica and alumina, such as metakaolin, calcite kaolin, and industrial and agricultural waste, such as fly ash dust-bagasse and rice-husk ash [9]. Internationally, many industries, such as electronic industry, use geo-polymer for many purposes by mixing with fly ash to make footpaths in Australia. In contrast, geo-polymer is a new technology in Thailand, where the industries did not start to use it [5].

Geopolymer production process

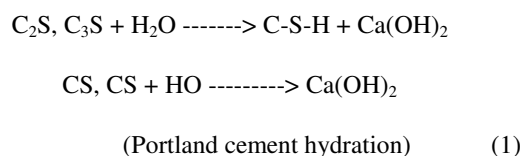
Geo-polymer is created by geosynthetic of silica and alumina materials. The first process occurs when an aluminosilicate material was dissolved and transformed into sodium silicate by using alkaline hydroxide. This process produces alumina and silicate, which can dissolve solid particles, freeing alumina and silicate and transforming them into monomeric solution, making speciation equilibrium which is a mixture of silicate aluminate and aluminosilicate. Therefore, appropriate production of geo-polymer must be 2:1 [3]. Then, gelation of saturated aluminosilicate solution occurs and will be condensed and restructured. Reorganization, polymerization, and hardening will turn into 3-dimensional



aluminosilicate called geo-polymer. Water then occurs and is released during this process until geo-polymer changes to hard form [5]. When a ratio of silica and alumina is 1:1, the mixing of tetrahedron is called Poly (sialate). Meanwhile, when the ratio of silica and alumina is 2:1, the structure is called Poly (sialate-siloxo); therefore, producing appropriate geo-polymer should be 2:1 [3].

B. Theoretical framework

The hydration reaction of Portland cement and geo-polymer is totally different. The structure of Portland cement comprises of Calcium Silicate Hydrate (C-S-H) which is created by hydration reaction, as shown in equation (1).



When a cement plate or solid mortar is compacted and mixed with Portland cement, Pozzolanic reaction will occur. This reaction produces a lot of mixture that affects strength and durability of the concrete or cement plate. Geo-polymer has a different structure from Portland cement's hydration because of its elements of materials and reaction. For example, the structure of polymer comprises of silicon (Si) alumina (Al) and oxygen (O₂). These elements react with alkaline solution, creating a polymer chain which is accelerated by heat at the same time, as shown in the Fig. 1. [8].

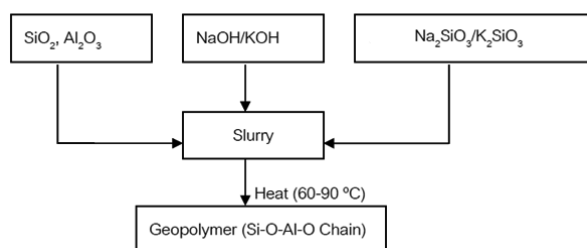
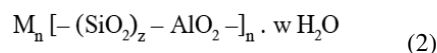


Fig. 1 Geo-polymer chain (Sakkarin, 2008)

Geo-polymer has various different molecule structures of geo-polymer chain, depending on the ratio of Si : Al. The equation of geo-polymer's molecule is as follows:



Where:

M = alkaline element or cation such as potassium, sodium or calcium; the symbol
- = presence of a bond
z = Polymerisation

n = degree of polycondensation
w = number of water molecules

The materials comprising SiO₂ and Al₂O₃ are used as monomer. They can be found in fly ash, rice-husk ash, and kaolin. These materials create geo-polymerization. Therefore, applying these materials with geo-polymer synthesis can create a new anaplasmosis, which can be used to replace cement making concrete [10].

C. Methodology

This research studied the processes, approaches and possibility of transforming waste powder coating into geo-polymer materials, which will be used for cement replacement materials. Metakaolin was used by mixing with waste powder coating and monomericin solution, and then molded. Subsequently, the objects were tested based on ASTM standard.

1) Materials

The materials used in this study are as follows;

- metakaolin with elemental SiO₂ and Al₂O₃ between 36% - 49% and 33% - 39%
- waste powder coating as shown in Fig.2
- sodium silicate (Na₂SiO₃) with (SiO₂ 34.27%, Na₂O 16.53% and H₂O 49.2%
- sodium hydroxide (NaOH)

2) Equipment and Devices

The equipment and devices used for the experiment are as follows;

- mixing machinery
- geo-polymer mould of 5x5x5 cm.
- beaker of 1 litter
- digital weight scale
- vernier calliper
- compression test-universal testing machine
- sequential x-ray fluorescence spectrometer



Fig. 2. Waste powder coating

3) Mixing ratio

The ratios of geo-polymer concrete used for the study are as follows;



- metakaolin and waste powder coating ratio 90 : 10, 80 : 20, 70 : 30 and 60 : 40
- sodium silicate and sodium hydroxide ratio 1 : 1.5, 1 : 2.0 and 1 : 2.5 using sodium hydroxide solution 10 and 12 M.
- water ratio 0.60

4) Test procedure

A geo-polymer's compressive strength test was conducted using different ratios of metakaolin and waste powder coating. Three sets of metakaolin and waste powder coating were tested with the ratio of 90:10, 80:20, 70:30 and 60:40, respectively. Then, kaolin was burnt at 700 °C for 6 hours. Sodiumhydroxide solution of 10 and 12 M were tested with sodium silicate at the ratio of 1:1.5, 1:2.0 and 1:2.5, respectively. Baking temperature was 80 °C for 4 hours. Then, the specimens were left in the oven for 24 hours, then taken off and wrapped for 7 days.

III. RESULTS AND DISCUSSIONS

Chemical results of waste powder coating deriving from x-ray fluorescence spectrometer are shown in Table 1.

TABLE I. Waste powder coating elemental composition

number	element	test result	unit	LOQ	LOD	Test methods
1	Al	2.14	% W/W	-	-	EDXRF
2	Si	1.1	% W/W	-	-	EDXRF
3	S	6.3	% W/W	-	-	EDXRF
4	Ti	31.4	% W/W	-	-	EDXRF
5	Fe	1.23	% W/W	-	-	EDXRF
6	Zn	0.14	% W/W	-	-	EDXRF
7	Sr	1.45	% W/W	-	-	EDXRF
8	Ba	56.3	% W/W	-	-	EDXRF

Table I shows chemical composition of waste powder coating. It can be seen that proportion by weight of Al, Si, Ti and Ba was 2.14, 1.1, 31.4 and 56.3%, respectively. Therefore, it could be concluded that waste powder coating can be a composition of geo-polymer materials.

In all ratios, metakaolin and waste powder coating ratio and sodium silicate and sodium hydroxide ratio with sodium hydroxide solution of 10 and 12 M were tested. It was found that all cases can be formed as shown in Fig. 3. Then, strength of specimens was tested by using a compression test-universal testing machine. The specimen as shown in Fig. 4 shows a damage of sample after the test with compressive testing machine.



Fig. 3. Geo-polymer concrete forming



Fig. 4 Compressive strength testing

The effect of metakaolin and waste powder coating ratio, sodium silicate ratio on compressive strength with sodium hydroxide solution of 10 M are as shown in Fig. 5. In all of sodium silicate and sodium hydroxide ratios, compressive strength increased when composition of waste powder coating increased. Referring to Table 1, 31.4 % of Ti was contained in waste powder coating composition. Therefore, when waste powder coating composition increased, it caused compressive strength to increase as well. Trends at each ratio of sodium silicate and sodium hydroxide are similar. Moreover, the compressive strength was tested as having a maximum of 87.28 kg/cm² with the metakaolin: waste powder coating of 60:40 and sodium silicate: sodium hydroxide of 1: 2.5. The effect of metakaolin and waste powder coating ratio, sodium silicate ratio on compressive strength with sodium hydroxide solution of 12 M were as shown in Fig.6. All trends are similar to the sodium hydroxide solution of 10 M (Fig. 5). The maximum compressive strength was 80.35 kg/cm² with the metakaolin: waste powder coating of 60:40 and sodium silicate: sodium hydroxide of 1: 2.5. However, when the compressive strength with 10 M and 12 M were compared with the same metakaolin and waste powder coating ratio and sodium silicate and sodium hydroxide ratio, it was found that the compressive strength with 10 M was increased to about 8.6 %.

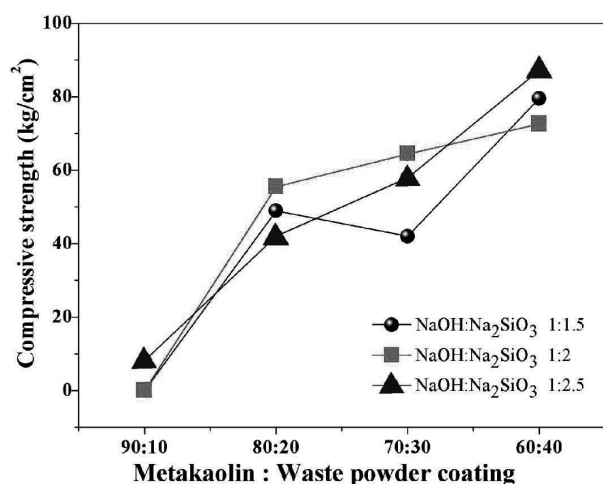


Fig.5. Effect of metakaolin and waste powder coating ratio, sodium silicate ratio on compressive strength with sodium hydroxide solution of 10 M.

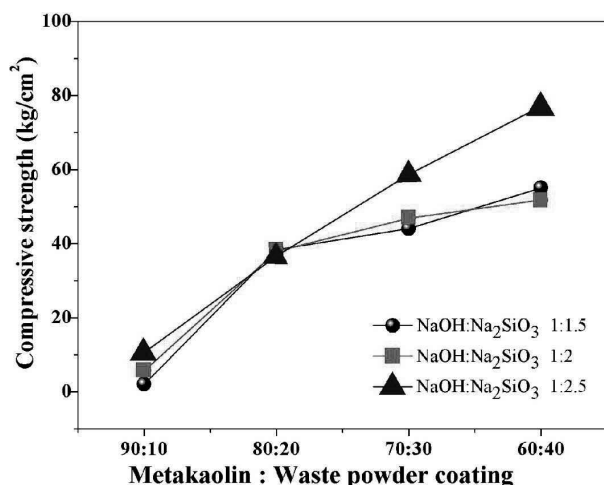


Fig.6. Effect of metakaolin and waste powder coating ratio, sodium silicate ratio on compressive strength with sodium hydroxide solution of 12 M.

IV. CONCLUSION

From this study the following can be concluded:

- All ratios of the metakaolin: waste powder coating and the sodium silicate : sodium hydroxide with 10 M and 12 M can be formed.
- The compressive strength increased when the composition of waste powder coating increased.
- The compressive strength with 10 M was higher than the compressive strength with 12 M by about 8.6 %.

To improve the compressive strength, our future work will change the sodium hydroxide solution from 10 M and 12 M to other concentrations.

Acknowledgment

This research was conducted under the support of the National Science and Technology Development Agency (NSTDA), Jotun Thailand Limited and Rajamangala University of Technology Lanna (RMUTL).

References

- [1] A. M. Rashad & S. R. Zeedan, "The effect of activator concentration on the residual strength of alkali-activated fly ash pastes subjected to thermal load", *Construction and Building Materials*, vol 25, no 7, pp. 3098-3107, July 2011.
- [2] E. Gartner, "Industrially interesting approaches to "low-CO₂" cements". *Cement & Concrete Research*, vol. 34, no. 9, pp. 1489-1498, September 2004.
- [3] J. Davidovits, "Chemistry of Geopolymeric Systems Terminology. *Proceedings of Geopolymer*", International Conference, France, 1999.
- [4] J. Sorathiya, S. Shah and S. Kacha, "Effect on Addition of Nano "Titanium Dioxide" (TiO₂) on Compressive Strength of Cementitious Concrete", *Kalpa Publications in Civil Engineering*, vol 1, 2017, pp. 219-225.
- [5] Kasetsart University Research and Development Institute, "Suwan Vajokkasikij Building", October 14, 2015. [Online]. Available: <http://www3.rdi.ku.ac.th/?p=21510>
- [6] L. A. Guzmán-Aponte, R. Mejía de Gutiérrez and A. Maury-Ramírez, "Metakaolin-Based Geopolymer with Added TiO₂ Particles: Physicomechanical Characteristics", *Coatings*, vol 7, no. 233, December 2017, pp. 1-12, doi:10.3390/coatings7120233
- [7] P. Duxson, A. Fernandez-Jimenez, J. L. Provis, et al, "Geopolymer technology: the current state of the art", *Journal of Materials Science*, vol 42, no 9, pp. 2917-2933, May 2007.
- [8] P. Jindaprasit and C. Jaturaphitakul, "Portland Cement and concrete", *Thailand Concrete Association*, 2004.
- [9] Rmutphysics, "Geo-polymer production replace cement to decrease global warming", 2012. [Online]. Available: http://www.neutron.rmutphysics.com/teaching/glossary/index.php?option=com_contenttask=view&id=8105&Itemid=35
- [10] S. Luangkarnjorn, "Geopolymer material", *Journal of Concrete*, vol 3, April 2008.
- [11] S. Naskar and A. K. Chakraborty, Effect of nano materials in geopolymer concrete, *Perspective in Sciences*, vol 8, April 2016, pp. 273-275.



Simulation of Molasses Cooling Using Carbon Steel Thermosyphon Heat Pipe Heat Exchanger

Thanasit Wongsiriamnuay, Tipapon Khamdaeng,
Pisuthi klinkajorn, Nyanakorn Sutassanamarlee and
Numpon Panyoyai*

Faculty of Engineering and Agro-Industry
Maejo University San Sai, Chiang Mai, Thailand 50290

*Corresponding author: n.panyoyai@gmail.com

Passawat Watcharadumrongsak and Taweekuk
Taweewitayakarn

Department of Mechanical Engineering, Faculty of
Engineering, Rajamangala University of Technology Lanna,
Chiang Mai, Thailand 50300

Abstract— The objectives of this research were to study the heat transfer characteristic and fabricate, carbon steel thermosyphon heat pipe heat exchanger (HPHE) to reduce the temperature of molasses in a storage tank with natural convection under steady-state condition. Our computational program was applied to simulate the optimum HPHE for transfer heat amount 224.24 kW including consideration of the net savings and limitations of installation. The simulation results show that the maximum net saving of approximately 43.375 million-baht was obtained in the case of the HPHE with outside diameter of 0.0488 m, area of heat transfer approximately 18,397 m² and using R-123 as working fluid. The molasses storage tank was constructed to compare the simulation with the experimental results, using a scale of 1:40. The simulation results show that the maximum net saving of approximately 875 baht was obtained in the case of the HPHE with outside diameter of 0.0488 m, the area of transfer heat of 4.596 m² and R-134a was used as working fluid. It was found that at the molasses temperatures of 40, 45, 50, 55 and 60°C, the heat transfer rate was equal to 32.6, 56.2, 92.1, 120.1 and 144.9 watt, respectively. The standard deviation between the experimental and simulation results was equal to 15.69 %.

Keywords— simulation, molasses, carbon steel thermosyphon, heat pipe, heat exchanger

I. INTRODUCTION

Molasses can be divided into two types of molasses from sugar cane, corn, citrus fruit and molasses from beet. The unique properties of molasses are a viscous liquid brown and black. The molasses trade commonly use the term Brix as an indicator of specific gravity [1]. Molasses derived from the last process of sugar production by nature molasses. In sugar fabrication, various cooking and cleaning processes for producing crystal sugar ends up with providing brown syrup containing about 50% sugar, and another substance which is called molasses [2]. However, blackstrap molasses have many different organic components with varying functional groups [3]. Current molasses have important in the industrial sector. It can be used as raw material in a variety of industries. Whether the energy industry for the production of ethanol. Food and beverage industry, such as the fertilizer used to feed animals. In

the storage industry molasses be stored in a tank with a large spherical high have strength withstands high heat. The main problem of the molasses is overflow out of the stored tanks. The temperature inside the stored tank of molasses is a significant variable, which has an impact on the overflow behavior from the tank of molasses. It suggests that the cooling can solve this problem. This problem could be achieved by the heat exchanger for reduce temperature of molasses. In this this research we study about the thermosyphon heat exchanger used to solve previous problem. Thermosyphon heat exchanger is a type of the heat pipe which has been widely used in waste heat recovery sector. The container of thermosyphon heat exchanger can be produced from various materials (e.g., copper tube, stainless steel tube, carbon steel tube). The metal was generally selected because of its excellent thermal conductivity, compatibility with working fluid and ease of fabrication and welding. Since the most of thermosyphon was made of metal and was installed at different conditions and applications, the corrosion can easily occur [4-7]. The scope of this simulation study are to: Design and fabricated the carbon steel thermosyphon heat pipe heat exchanger for use to reduce temperature of molasses in storage tank and comparison the simulation with experimental result of thermosyphon heat pipe heat exchanger.

II. MATERIALS AND METHODS

A. Simulation program

In order to calculate for sizing, the appropriate heat pipe heat exchanger for cooling molasses, there is a complex calculated procedure. Thus, it is necessary to use computer program in calculation. The flow chart of program is shown in figure 1. The procedure starts with receive the input data, i.e. container material, working fluid, the evaporator and condenser section length, the inside and outside diameter of thermosyphon, molasses temperature at the initial state and the ambient temperature at initial state. The number of tube of HPHE is also input. From the fact that there is amount of heat that makes the molasses temperature higher. This term is called generated heat. We should input the generated heat to the simulation program. The estimated value from the operation tank site is 224.24 kW. After that, the iteration technique is



used to predict the heat transfer rate of heat exchanger. This can be done by trial the cooling rate and heat transfer rate of heat exchanger. Then the molasses temperature at the specific time after the initial state and heat resistant are calculated. The new value of heat transfer rate of heat exchanger can be calculated from the relation of temperature different of evaporator and condenser section of heat pipe. If the trial cooling rate and trial heat transfer rate are equal to the last calculated result, the calculation complete. The calculated result is the heat transfer rate and cooling rate of heat exchanger. Moreover, the economic aspect is also considered. The Soylemez method is used to determine the optimize size of heat exchanger [8]. The input values to calculate are as follow; the molasses temperature is 60 °C, the ambient temperature at the initial state is 30 °C, the outside diameter are 0.0217, 0.0342 and 0.0488 m respectively, the evaporator section length is 3600 mm. The number of pipes is 69,984 and the mass of molasses is 8,186,329 kg. The calculation is done by very the condenser section length of 10,000, 15,000 and 18,000 mm. After that, the calculation also be done with the increasing 500 mm of condenser section length per step of calculation until the condenser length up to 20,000 mm.

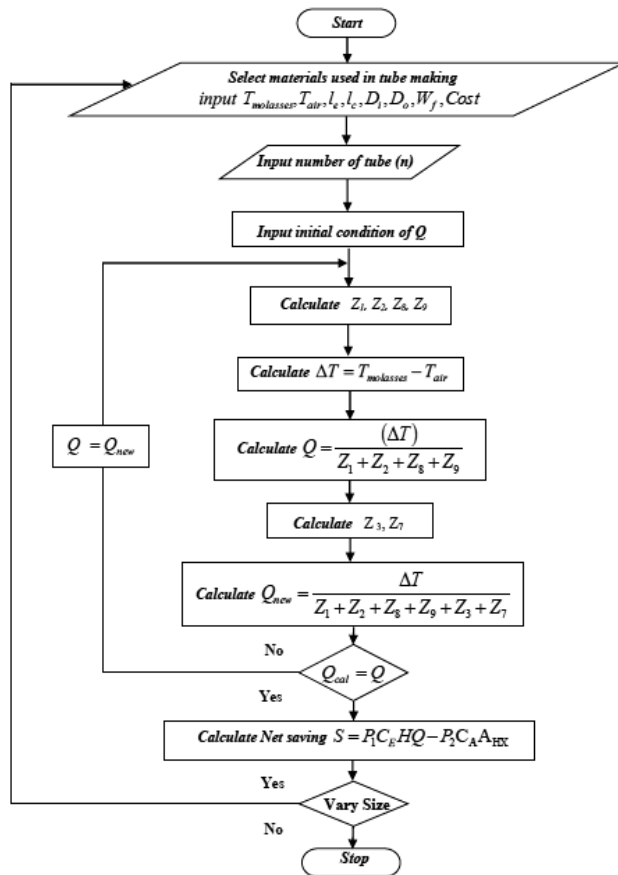


Fig. 1 Show flowchart of molasses heat exchanger

B. Experimental set up

From flowchart of the molasses HPHE, the simulation results show that the maximum net saving of approximately 62.863 million-baht was obtained in the case of the HPHE with using R123 as working fluid. However, cannot use this data to construct the experimental set up even though it is the optimize size. It is because the condenser length is too long and not suitable to install in the operating system. Thus to compare the simulation with the experimental results, the molasses storage tank model was constructed using a scale of 1:40. The test set is established with the same condition. The HPHE made with carbon steel tube, outside diameter of 0.0342 m, evaporator section length of 0.3 m and condenser section length of 0.7 m was used. Pipe number was 30 and R134a was used as working fluid. The experimental set up of the heat exchanger as shown in figure 2.



Fig. 2 Experimental setup of the heat exchanger

C. Experimental Procedure

The performance of molasses HPHE is done by considering the molasses temperature in storage tank model. The molasses temperature at evaporator section and condenser section of HPHE and ambient temperature are recorded by a data logger (Wisco AI 210, accuracy ± 0.2%). After that the heat transfer rate is calculated as following equation:

$$Q = \left((mc_p)_{molasses} + (mc_p)_{copper} \right) \frac{(T_{h\beta} - T_{hy})}{\Delta t} \quad (1)$$

Where $T_{h\beta}$ and T_{hy} are the initial and specific time molasses temperature. The experimental procedure is separated into 2 parts as follow. First, the system heat loss evaluation, it can be obtained by balance energy method around the experimental setup. This method gives the heat loss at various temperature differences between molasses tank and the



surrounding. For this experiment can be written the energy balance equation as follow:

$$Q_{input} = Q_{loss} + U_{system} \quad (2)$$

where Q_{input} , Q_{loss} and U_{system} in this equation are the supplied heat using plate heater, system heat loss, and energy of molasses respectively to the evaluation of heat transfer rate of HPHE. This experiment can be done by install HPHE into the experimental setup. In this case, it can be written the energy balance equation as follow:

$$Q_{input} = Q_{loss} + Q_{heatpipe} + U_{system} \quad (3)$$

where $Q_{heatpipe}$ denote the heat transfer rate of thermosyphon heat pipe heat exchanger. If the temperature difference between molasses and surrounding was obtained, the heat loss could be determined from the first part of the experiment. For $Q_{heatpipe}$ can be obtained when measuring the molasses temperature at various time and control heat input of plate heater at a specific value.

III. RESULTS AND DISCUSSION

This study aims to comparisons between the simulation and experimental results of molasses heat pipe heat exchange.

A. The result of simulation program of molasses HPHE

The result of the simulation in figure 3 which illustrates the relationship of net saving to the area of heat transfer on heat pipe heat exchanger.

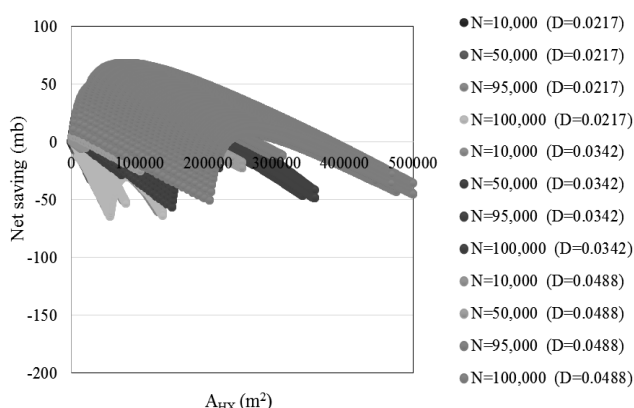


Fig. 3 Simulation of HPHE used R123 as working fluid

Figure 3 shows that the relation of maximum net saving and heat transfer area of HPHE which used R123 as working

fluid and outside diameter of 0.0217, 0.0342 and 0.0488 m. It was found that the maximum net saving approximately of 62.863 million-baht was obtained in this case. The optimize size of heat pipe heat exchanger consist of outside diameter is 0.0488 m, area of heat transfer of 99,651 m². For transfer heat amount 224,240 watts including, the simulation results show that the maximum net saving of approximately 43.375 million-baht was obtained in the case of the HPHE with outside diameter of 0.0488 m too, the area of heat transfer approximately 18,397 m² respectively. However, cannot use this data to construct the experimental set up even though it is the optimize size. It is because the condenser section length is too long and not suitable to install in the molasses storage tank system. Thus to compare the simulation result with the experimental results, the molasses storage tank model was constructed using a scale of 1:40 that shows in fig 2.

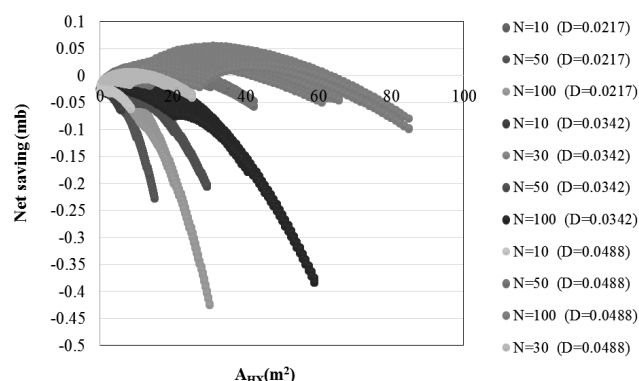


Fig. 4 The simulation of heat pipe heat exchange with the scale of molasses storage tank of 1:40

Figure 4 shows that result of simulation of heat pipe heat exchanger used R134a as working fluid with carbon steel tube with outside diameter of 0.0217 0.0342 and 0.0448 m, evaporator section length of 0.3 m, condenser section length of 0.7 m and pipe number was 30. It was found that the maximum net saving approximately of 52,124 baths. The optimize size of heat pipe heat exchanger consisting of outside diameter of 0.0488 m, the area of heat transfer of 29.908 m². For transfer heat amount 55.5 watts the maximum net saving approximately of 875 baths. The optimize size of heat pipe heat exchanger consisting of outside diameter of 0.0488 m, the area of heat transfer of 4.596 m² respectively.

B. The comparison result of heat transfer between simulation and experimental result

Figure 5 shows a comparison result between heat transfer rate from experimental and simulation. From the experimental result at the molasses temperatures of 40, 45, 50, 55 and 60°C, the heat transfer rate was equal to 32.6, 56.2, 92.1, 120.1 and 144.9 watt, respectively

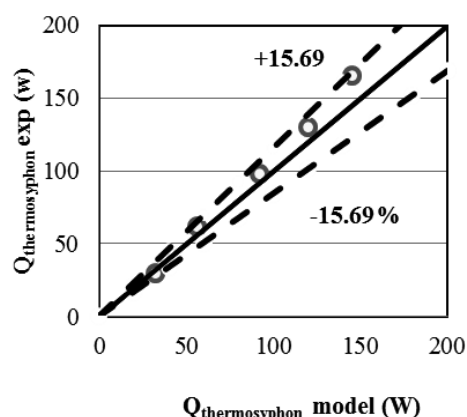


Fig. 5 Comparison of heat transfer between the simulation and experimental result

It was found that the simulation values have a standard deviation from the experimental data of $\pm 15.69\%$. It can be concluded that simulation is established to predict the heat transfer rate which in this study can predict values have a standard deviation from the experimental data of $\pm 15.69\%$

IV. CONCLUSIONS

The result indicates that the principles and fabricate of HPHE can draw heat from the molasses storage tank with natural convection under steady-state condition. It can be concluded that the computational program was applied to simulate the optimum HPHE for transfer heat including consideration of the net savings and limitations of installation. The simulation results show that the maximum net saving of approximately 43.375 million-baht was obtained in HPHE with using R123 as working fluid was obtained with outside diameter of 0.0488 m, the area of heat transfer approximately 18,397 m². To compare the simulation with the experimental results show that the maximum net saving of approximately 875 baht was obtained with outside diameter of 0.0488 m, the area of transfer heat of 4.596 m² and R134a was used as working fluid too. The standard deviation between the experimental and simulation results was equal to 15.69 %.

ACKNOWLEDGMENT

This study was supported by Faculty of Engineering and Agro-Industry, Maejo University and Department of Mechanical Engineering, Faculty of Engineering, Rajamangala University of Technology Lanna, Chiang Mai, Thailand. We would like to express their appreciation of this support.

REFERENCES

- [1] Leo V. Curtin. (1983). Molasses – general consideration. Molasses in animal nutrition. National Feed Ingredients Association West Des Moines, Iowa USA.
- [2] Akar, C., & Canbaz, M. (2016). Effect of molasses as an admixture on concrete durability. *Journal of Cleaner Production*. 112, 2374-2380.
- [3] Brian P. Quinn., Ulrich R. Bernier., Christopher J. Geden., Jerome A. Hogsette., & David A. Carlson. (2007). Analysis of extracted and volatile components in blackstrap molasses feed as candidate house fly attractants. *Journal of Chromatography*. 1139, 279–284.
- [4] Panyoyai, N., Pathike, P., Wongsiriamnuay, T., Khamdaeng, T., & Tanongkankit, Y. (2016). Drying characteristics of paddy dried by thermosyphon heat pipe heat exchanger. *Journal of Science and Technology*, 35(6), 658-664.
- [5] Tundee, S., Terdtoon, P., Sakulchangsatjatai, P., Singh, R., & Akbarzadeh, A. (2010). Heat extraction from salinity-gradient solar ponds using heat pipe heat exchangers. *Solar Energy*, 84(9), 1706-1716.
- [6] Kamonpet, P., Booddachan, K., Terdtoon, P., Preechawuttipong, I., & Kobayashi, Y. (2003). Creep behavior of HDPE thermosyphon under long-term operation. *The 7th International Heat Pipe Symposium* (pp. 137-140). Korea: Korean Society of Mechanical Engineers.
- [7] Booddachan, K., Kamonpet, P., Terdtoon, P., Sutjaritakul, T., & Kobayashi, Y. (2003). Tensile strength of HDPE thermosyphon. In *The 7th International Heat Pipe Symposium* (pp. 147-150). Korea: Korean Society of Mechanical Engineers.
- [8] Soylemez, MS. (2003). On the thermoeconomical optimization of heat pipe heat exchanger HPHE for waste heat recovery. *Energy Conversion and Management*, 44 (2003), 2509–2517.



Review on Heat Transfer and Pressure Drop in Circular Tube with Twisted Tape

Kittisak Khuwaranyu* and Pongsiri Jaruyanon

Mechanical Engineering Department,
Faculty of Engineering and Industrial Technology, Silpakorn University,
Nakhon Pathom, 73000, Thailand.

*corresponding author; e-mail: kittisak_mesu@yahoo.com

Abstract—The objective of this article is to review the previous research on the flow and heat transfer in circular tube with twisted tape. The parameters used in the experiment include the designing and constructing wind tunnel, testing and measurement, flow analysis and heat transfer, and the types of twisted tape. The conclusion of previous research could lead to further studying on the appropriate designing and constructing wind tunnel, the most efficient type of twisted tape for heat transfer, and then the improvement of heat exchanger.

Keywords—twisted tape; heat transfer; pressure drop; heat exchanger

I. INTRODUCTION

To date, the heat exchanger is widely used in both factory as key mechanism for heating, cooling, refrigerating, and building as cooling and air-conditioning, water heating etc. This relatively leads to the research and development, designing, and improvement of heat transfer which help reduce the nonrenewable energy with less manufacturing cost. It can also make heat transfer smaller or more compact [1]. As a result, it is essential to design the heat transfer for usage.

Referring to power and refrigeration cycle, it can be stated that the heat exchanger is one of critical machine as it transfers heat from one fluid medium to another under the different temperatures. Within the industry, the manufacturer uses the heat exchanger as to exchange or transfer heat energy from one fluid medium to another under various temperatures [2,3]. The technology which are typically used consists of making fluid medium cooler (reducing temperature) or taking heat to make fluid medium hot such as those in food, petrochemical, energy, electronics, air-conditioning, and cooling industries, etc.[4-6]. In addition, the setting and internal tube layout within the heat exchanger is important to heating and cooling as well as other equipment i.e. fans, condenser, coolant, and tubes. All of these functions collaboratively to the efficient heating and cooling.

For this reason, the development of heat exchange equipment is also vital for manufacturing industry where the heat exchanger have widely been applied such as drying machine, industrial oven, heat exchanger, heat sink, cooler and air-conditioner, distillery, condenser, engine or machine cooling in manufacturing, etc. (as Fig. 1 and 2). Consequently, it can be concluded that due to the philosophy in designing the

more effective heat exchanging equipment and system, it is necessary to consider the ability to serve customer's needs such as usability, reasonable price, high heating performance, simple structure, compact size, durability, easy maintenance and fixing, high reliability and safety.

Performance of the heat transfer system or increasing coefficient of heat transfer can be done by enhancing heat transfer capability. Also, the augmentation is another way of maximizing performance which makes the heat exchanger becomes smaller, reduces production cost, and even increases coefficient of heat transfer which eventually causes temperature drive force, increase efficiency (as rule No. 2 of thermodynamics) and lessens the entropy generation. The techniques which are normally used in improving the performance of heat transfer can be categorized into three main groups. The first one is the passive methods which includes twisting tape, inserting helical screw tape, making rough surface, extending surface, and filling additives for liquid and gases. The next one is called active methods which strengthens external pressure e.g. increasing mechanical treatment, increasing surface fluid vibration, and applying electrostatic fields, etc. The last one is called the compound method which combines between the first two. The passive method requires the lowest costs among all. As a result, the twisted tape is important and predominant in flow and heat transfer [7].

Currently, the efficiency improvement of heat transfer in heat exchanging system in engineering and manufacturing works is necessarily required for energy saving and cost reduction. The heat transfer is always used in heat exchanging in order to increase heat transfer ratio and heating performance. In this process, the turbulence promoter such as turbulator is always set up into the flow tubes which impedes the development of heat transfer boundary layer, enlarges the heat transfer surface, and increases heat transfer rate. By adding turbulence or the immediate mixture of fluid.

II. THEORY

A. Study of flow and heat transfer by experiment

Heat transfer and flow in circular tubes by increasing heating performance can be divided into three main groups as follows:



1) Active techniques: pulling external energy (mechanical/electrical equipment) to increase heat transfer which causes to surface vibration.

2) Passive techniques: designing the special tube surface (different the plain one) and improving fluid and working fluid in order to increase the heat transfer rate without external energy.

3) Compound techniques: designing by mixing passive techniques and the passive one.

The most popular technique is the passive method which sets up turbulence promoter which helps increase the speed of fluid and mixture of fluid. This really brings about the more effective heat transfer and the better heating performance. Actually, increasing heat transfer rate in circular tube is one of driving methods to the efficient heat transfer. In this article, it is proposed to the passive method – setting the twisted tape within circular tube. By doing so, the fluid becomes more turbulent and then increase coefficient of heat transfer and heat transfer rate. In contrast, since the twisted tape hinders the fluid flow, this increases the friction and eventually affects the pressure drop.

B. Wind tunnel

The research on aerodynamics, the wind tunnel is always applied to study the phenomenon of air moving past solid object. The design of wind tunnel is significantly important for testing and validating the result. In the research, it is to set the object in the middle of tube so that the air moves past the object by the wind or any other methods.

The wind tunnel can be classified into two types -- Open Circuit wind tunnel and Closed Circuit wind tunnel. The first one (as shown in Fig.1) requires the high force to drive air flow through the tunnel since it loses energy for the outflow air but it is easily invented and requires less cost. In addition, the Open Circuit wind tunnel is safe for the fluctuated temperature and the back flow. The Open Circuit wind tunnel can be categorized into two sub-types -- induced draft and forced draft. The forced draft has more flexibility since the fan is set at the entrance of tunnel whereas the induced draft is sensitive for any changes or disturbance.

The Closed Circuit wind tunnel has the circle-rounded pattern (the closed circuit flow which the ending point meets to the starting one) which the fluid at the end flows directly back to the starting point. The Closed Circuit wind tunnel is always gigantic and difficult to construct. Moreover, it is carefully designed to ensure the frequency of the back flow. This type of tunnel is run by the axial fan which the wind is definitely circulated and reduces energy (low speed). Furthermore, it is feasible to set up the condition of controlling the low speed in the experiment. The wind tunnel can also be classified into many types such as ultrasonic wind tunnel which has maximum 0.4 m/s, transonic wind tunnel which has maximum 1.3 m/s, supersonic wind tunnel which has maximum 4.0-5.0 m/s, and hypersonic wind tunnel which has more than 5.0 m/s.

C. Enhancing heat transfer performance by twisted tape

To analyze the flow and heat transfer in circular tube with twisted tape, the heat factors which are normally used in measuring the heat transfer includes twisted tape, coil, etc. The high-performing equipment for heat transfer necessarily holds the significantly high coefficient of heat transfer yet least increasing value of friction factor.

The thermal performance factor can be calculated by the rate of heat transfer divided by the rate of friction as equation below:

$$\eta = \frac{h}{h_p} \bigg|_{pp} = \frac{Nu}{Nu_p} \bigg|_{pp} \quad (1)$$

Nu , h , Nu_p and h_p refer to Nusselt number and Convective coefficient for calculating the variables of turbulator-setting tube and the plain tube or smooth wall, respectively.

III. TWISTED TAPE INSERTS DEVICES

Typically, twisted tape is made from twisting metal sheet or aluminum sheet in proper method to get the appropriate size and shape. The application of twisted tape becomes more renown because it really makes the main flow circulated and eliminates boundary layer accordingly. Even though this phenomena causes the higher coefficient, it also loses pressure since the twisted tape obstructs the flow. Consequently, most research have further been conducted by quantitative method in order to verify the best design and the most efficient heat transfer with less pressure drop. In addition, it is mentioned that increasing the heat transfer can be done by the ratio of pitch and twist. The rate of twist (γ) is calculated by the ratio between the length of twist field and diameter within the tube ($\gamma = H/d$) – while H stands for the length of twist field and d refers to the diameter within the tube. The space refers to the distance between two spots in the same plane and can be measured in parallel with the twisted tape rod.

As the table 1, it can be found that the previous research on setting the twisted tape in the flow channel in 8 types of tape. Each tape is designed and produced by mitigating the weakness of the previous one as follows: 1) Typical twisted tape which the length of twisted tape is equal to the length of tube. 2) Varying length, alternative-axes and pitches twisted tape which the length of twisted tape differs to the length of tube, alternated between two lengths of twisted tape, different pitch, or even different twists with switching the rod. 3) Multiple twisted tapes 4) Twisted tape with rod and varying spacer 5) Twisted tape with attached fins and baffles 6) Twisted tapes with slots, holes cuts 7) left-right twisted tape with screw and 8) Tape with different surface modifications.

IV. EQUIPMENT DESIGN FOR TESTING FLOW AND HEAT TRANSFER WITHIN CIRCULAR TUBE

A. Equipment and experiment steps

The equipment shown in Fig. 5 consists of (1) Blower–pushing air at high speed into the testing field (2) Inverter –



controlling the motor speed in blower (3) Orifice flow meter – measuring the rate of air flow (4) Inclined/U manometer – measuring pressure (5) Electrical heater – adding the heat and air within the testing field (controlling the air temperature or heat to the fluid tube) (6) RTD Thermometer - measuring temperature at the entrance and temperature of hot air at the heat exchanging tube (7) Twisted tapes (8) Thermocouples (Type-T)– being installed at the tube surface in copper area in order to measure temperature in the duct wall (9) Variac transformer – controlling the heat set and (10) Volt meter and power meter – measuring potential difference and electric power at the power supply to the testing field.

The Fig. 6 illustrated the testing field of heat transfer by the flow within circular tube. The testing part is made from copper tube which is elastic and insulator can control the even heating by controlling the electricity inserting to the testing field. To measure the air temperature in the tube, it can be done by measuring the space of the same rod of thermocouple which is installed at the niche outside the duct. To install the thermocouple, the silicone heat-resist insulator is also attached above the thermocouple in order to prevent the direct bumping to RTD thermometer which is set up at the inflow rod to measure the inflow temperature and at the outflow rod to measure the outflow temperature.

B. Data processing [37]

1) The measurement of heat transfer

To identify the value of the heat transfer by the ambient air (Q_{air}) can be done by the difference in temperature as formula below:

$$Q_{air} = mC_p(T_o - T_i) \quad (2)$$

Under condition of heat balance, it was found that the volume of heat transfer in the air is equal to that of heat transfer in the testing tube.

$$Q_{air} = Q_{conv} \quad (3)$$

Where

$$Q_{conv} = hA(\bar{T}_w - T_b) \quad (4)$$

Where

Q_{conv} = convective heat transfer in test section (kJ)

h = heating surface area (m²)

\bar{T}_w = the wall temperature (K)

T_b = the bulk temperature (K)

by

$$\bar{T}_w = \sum T_w / 36 \quad (5)$$

$$T_b = (T_o - T_i) / 2 \quad (6)$$

From equation (2) and (6), the value of Average Convective Coefficient (h) can be calculated as below:

$$h = mC_p(T_o - T_i) / A(\bar{T}_w - T_b) \quad (7)$$

Calculating convection heat transfer coefficient depends on the surface temperature at specific area. Nusselt number can be defined as equation (8)

$$Nu = hD/k \quad (8)$$

Where

D = diameter of testing tube

k = air thermal conductivity

2) Measuring flow friction

The pressure drop (Δp) along the length of testing tube (L) is defined by friction factor calculation below:

$$f = (D/L) / (2\Delta p / \rho U^2) \quad (9)$$

U = average speed calculated by the air flow rate (Q) divided by sectional area at the entrance (A).

And Reynolds number (Re) is defined by the diameter within the tube which is calculated by equation (10) below:

$$Re = \rho U D / \mu \quad (10)$$

The thermo-physics properties k , ρ and C_p which is used for calculating Nusselt number (Nu), Reynolds number (Re), and Prandtl number (Pr) and fluid temperature can be calculated by equation (5)

3) Measuring heat performance

In this study, it is also calculated the equal power of water pumping to measure heat performance. Consequently, when the energy value is static, it equals to power supply as following equation:

$$(\dot{V}\Delta P)_p = (\dot{V}\Delta P)_t \quad (11)$$

From equation (11), this can be referred to the relationship between friction factor and Reynolds number under the static power use as below:

$$(fRe^3)_p = (fRe^3)_t \quad (12)$$

The thermal performance factor (η) refers to the ratio of convection heat transfer coefficient by enhancement device (h_t) divided by the ratio of convection heat transfer without enhancement device (h_p) as below:

$$\eta = \left(\frac{h_t}{h_p} \right)_{pp} \quad (13)$$

$$\eta = \frac{h}{h_p} \bigg|_{pp} = \frac{Nu}{Nu_p} \bigg|_{pp} = (Nu/Nu_p) / (f/f_p)^{1/3} \quad (14)$$

From equation (14), it can be found that when the value of thermal performance factor is more than 1, it can be indicated that the system with enhancement device benefits to the energy saving.



V. CONCLUSION

From all previous research in this article, it can infer to the importance of the approach to increase efficiency of heat transfer by passive method which can be done by setting up the twisted tape at flow channel. In addition, it indicates that the different twisted tapes significantly affect the heat transfer performance. However, it is also necessary to consider the pressure drop due to twisted tape. Hence, in order to study the impact of twisted tape to the flow and heat transfer, it is recommended that the wind tunnel should be designed and construct properly and ensure the accurate and reliable testing result. To sum up, the recommendation for further study can be as follows:

1) Designing and constructing the appropriate wind tunnel for flow and heat transfer for tube with twisted tape.

2) Exploring the form of twisted tape which leads to efficiency of heat transfer and lessens pressure drop.

3) Applying the result of flow and heat transfer to improve or develop the heat exchanger for heating and cooling.

ACKNOWLEDGMENT

This research was supported by Department of Mechanical Engineering, Faculty of Engineering and Industrial Technology, Silpakorn University, Thailand.

REFERENCES

- [1] Liu, S. and Sak, M. 2013. A comprehensive review on passive heat transfer enhancements in pipe exchangers. *Renewable and Sustainable Energy Reviews*, 19, 64-81.
- [2] Alamgholilou, A. and Esmailzadeh, E. 2012. Experimental investigation on hydrodynamics and heat transfer of fluid flow into channel for cooling of rectangular ribs by passive and EHD active enhancement methods. *Experimental Thermal and Fluid Science*, 38, 61-73.
- [3] Dewan, A. Mahanta, P. Sumithra, K. and Suresh, P. Review of passive heat transfer augmentation techniques. Part A. 2004. *Journal of Power and Energy*, 509-27.
- [4] Kumar, A. and Prasad, B.N. 2000. Investigation of twisted tape inserted solar water heaters – heat transfer, friction factor and thermal performance results. *Renewable Energy*, 19, 379-398.
- [5] Noothong, W. Eiamsa-ard, S. and Promvong, P. 2006. Effect of twisted-tape inserts on heat transfer in a tube. The 2nd international conference on "Sustainable Energy and Environmental (SEE 2006). 21-23 November 2006, Bangkok, Thailand. 1-5.
- [6] Sarada, N. Raju, S. Kalyani Radha, A.V. and Shyam, K. 2010. Enhancement of heat transfer using varying width twisted tape inserts. *International Journal of Engineering, Science and Technology*. 2, 107-118.
- [7] Suhas V.P. and P.V. Vijay Babu. 2011. Heat Transfer Augmentation in a Circular tube and Square duct Fitted with Swirl Flow Generators: A Review. *International Journal of Chemical Engineering and Applications*, 2, 326-331.
- [8] Bapu, J. and Rana M.M. Design, 2014. Construction and Testing open circuit low speed wind tunnel. *International Journal of Engineering Research and Reviews*. 2, 1-9.
- [9] Hasanpour, A., Farhadi, M. and Sedighi, K. 2014. A Review study on Twisted tape inserts on Turbulent Flow Heat Exchanger: The Overall Enhancement Ratio Criterion. *International Communications in Heat and Mass Transfer*, 55, 53-62.
- [10] <http://media2.enerquip.com/media/8fe1ce8e-c60f-4493-bed9-fada15b848ec/img/4700/14136490.jpg>
- [11] Kumar, A. and Prasad, B.N. 2000. Investigation of twisted tape inserted solar water heaters heat transfer, friction factor and thermal performance results. *Renewable Energy*, 19:379-98.
- [12] Eiamsa-ard, S., Thianpong, C., Eiamsa-ard, P. and Promvong, P. 2009. Convective heat transfer in a circular tube with short-length twisted tape insert. *International Communications in Heat and Mass Transfer*, 36: 365-71.
- [13] Jaisankar, S., Radhakrishnan T.K., Sheeba K.N. and Suresh, S. 2009. Experimental investigation of heat transfer and friction factor characteristics of thermosyphon solar water heater system fitted with spacer at the trailing edge of left-right twisted tapes. *Energy Conversion and Management*. 50: 2638-2649.
- [14] Eiamsa-ard, S. and Promvong, P. 2010. Performance assessment in a heat exchanger tube with alternate clockwise and counterclockwise twisted-tape inserts. *International Journal of Heat and Mass Transfer*, 53: 1364- 1372.
- [15] Eiamsa-ard, S., Somkleang, P., Nuntadusit, C. and Thianpong C. 2013. Heat transfer enhancement in tube by inserting uniform/nonuniform twisted-tapes with alternate axes: Effect of rotated-axis length. *Applied Thermal Engineering*, 54(1): 289-309.
- [16] Eiamsa-ard, S., Thianpong, C., Eiamsa-ard, P. and Promvong, P. 2010. Thermal characteristics in a heat exchanger tube fitted with dual twisted tape elements in tandem. *International Communications in Heat and Mass Transfer*, 37: 39-46.
- [17] Eiamsa-ard, S. and Promvong, P. 2005. Enhancement of heat transfer in a tube with regularly-spaced helical tape swirl generators. *Solar Energy*, 78: 483-494.
- [18] Krishna, S.R., Pathipaka, G. and Sivashanmugam, P. 2009. Heat transfer and pressure drop studies in a circular tube fitted with straight full twist. *Experimental Thermal and Fluid Science*, 33: 431-438.
- [19] Bas, H. and Ozceyhan, V. 2012. Heat transfer enhancement in a tube with twisted tape inserts placed separately from the tube wall. *Experimental Thermal and Fluid Science*, 41: 51-58.
- [20] Eiamsa-ard, S., Wongcharee, K., Eiamsa-ard, P. and Thianpong, C. 2010. Thermohydraulic investigation of turbulent flow through around tube equipped with twisted tapes consisting of centre wings and alternate-axes. *Experimental Thermal and Fluid Science*, 34: 1151-1161.
- [21] Eiamsa-ard, P., Thianpong, C. and Eiamsa-ard, S. 2011. Influences of Twisted-Tape with Parallel Rectangular-Wing on Thermal Performance of a Heat Exchanger. 2011 International Conference and Utility Exhibition on Power and Energy Systems: Issues & Prospects for Asia (ICUE), Pattaya, Thailand, Sept. 28-30, 2011.
- [22] Eiamsa-ard, S., Wongcharee, K., Eiamsa-ard, P. and Thianpong, C. 2010. Heat transfer enhancement in a tube using delta-winglet twisted tape inserts. *Applied Thermal Engineering*, 30: 310-8.
- [23] Wongcharee, K. and Eiamsa-ard, S. 2011. Heat transfer enhancement by twisted tapes with alternate-axes and triangular, rectangular and trapezoidal wings. *Chemical Engineering and Processing: Process Intensification*, 50: 211-219.
- [24] Seemawute, P. and Eiamsa-ard, S. 2010. Thermohydraulics of turbulent flow through a round tube by a peripherally-cut twisted tape with an alternate axis. *International Communications in Heat and Mass Transfer*, 37: 652-659.
- [25] Eiamsa-ard, S., Seemawute, P. and Wongcharee, K. 2010. Influences of peripherally-cut twisted tape insert on heat transfer and thermal performance characteristics in laminar and turbulent tube flows. *Experimental Thermal and Fluid Science*, 34: 711-719.
- [26] Murugesan, P., Mayilsamy, K. and Suresh, S. 2010. Turbulent Heat Transfer and Pressure Drop in Tube Fitted with Square-cut Twisted Tape. *Chinese Journal of Chemical Engineering*, 18(4): 609-617.
- [27] Murugesan, P., Mayilsamy, K., Suresh, S. and Srinivasan, P.S.S. 2011. Heat transfer and pressure drop characteristics in a circular tube fitted with and without V-cut twisted tape insert. *International Communications in Heat and Mass Transfer*, 38: 329-234.



- [28] Thianpong, C., Eiamsa-ard, P., Promvong, P. and Eiamsa-ard, S. 2012. Effect of perforated twisted-tapes with parallel wings on heat transfer enhancement in a heat exchanger tube. *Energy Procedia*, 14: 1117-1123.
- [29] Bhuiya, M.M.K., Chowdhury, M.S.U., Saha, M. and Islam, M.T. 2013. Heat transfer and friction factor characteristics in turbulent flow through a tube fitted with perforated twisted tape inserts. *International Communications Heat and Mass Transfer*, 46: 49-57.
- [30] Jaisankar, S., Radhakrishnan, T.K. and Sheeba, K.N. 2011. Experimental studies on heat transfer and thermal performance characteristics of thermosyphon solar water heating system with helical and left-right twisted tapes. *Energy Conversion and Management*, 52: 2048-2055.
- [31] Eiamsa-ard, S., Yongsiri, K., Nanan, K. and Thianpong, C. 2012. Heat transfer augmentation by helically twisted tapes as swirl and turbulence promoters. *Chemical Engineering and Processing: Process Intensification*, 60: 42-48.
- [32] Thianpong, C., Eiamsa-ard, P., Wongcharee, K and Eiamsa-ard, S. 2009. Compound heat transfer enhancement of a dimpled tube with a twisted tape swirl generator. *International Communications in Heat and Mass Transfer*, 36: 698-704.
- [33] Eiamsa-ard, S. and Promvong, P. 2010. Thermal characteristics in round tube fitted with serrated twisted tape. *Applied Thermal Engineering*, 30: 1673-1682.
- [34] Murugesan, P., Mayilsamy, K. and Suresh, S. 2010. Heat transfer and friction factor studies in a circular tube fitted with twisted tape consisting of wire-nails. *Chinese Journal of Chemical Engineering*, 18: 1038-1042.
- [35] Nanan, K., Thianpong, C., Pimsan, M., Chawattanakul, S. and Eiamsa-ard, S. (2017) Flow and thermal mechanisms in a heat exchanger tube inserted with twisted cross-baffle turbulators. *Applied Thermal Engineering*, 114, 130-147.
- [36] Tamna, S., Kaewkohkhat, Y., Skullong, S. and Promvong, P. (2016) Heat transfer enhancement in tubular heat transfer with double V-ribbed twisted-tapes. *Case Studies in Thermal Engineering*, 7, 14-24.
- [37] Nanan, K., Yongsiri, K., Wongcharee, K., Thianpong, C. and Eiamsa-ard, S. (2013) Heat transfer enhancement by helically twisted tapes inducing co- and counter-swirl flows. *International Communications in Heat and Mass Transfer*, 46, 67-73.
- [38] G. Eason, B. Noble, and I.N. Sneddon, "On certain integrals of Lipschitz-Hankel type involving products of Bessel functions," *Phil. Trans. Roy. Soc. London*, vol. A247, pp. 529-551, April 1955.
- [39] J. Clerk Maxwell, *A Treatise on Electricity and Magnetism*, 3rd ed., vol. 2. Oxford: Clarendon, 1892, pp.68-73.
- [40] I.S. Jacobs and C.P. Bean, "Fine particles, thin films and exchange anisotropy," in *Magnetism*, vol. III, G.T. Rado and H. Suhl, Eds. New York: Academic, 1963, pp. 271-350.
- [41] K. Elissa, "Title of paper if known," unpublished.
- [42] R. Nicole, "Title of paper with only first word capitalized," *J. Name Stand. Abbrev.*, in press.
- [43] Y. Yorozu, M. Hirano, K. Oka, and Y. Tagawa, "Electron spectroscopy studies on magneto-optical media and plastic substrate interface," *IEEE Transl. J. Magn. Japan*, vol. 2, pp. 740-741, August 1987 [Digests 9th Annual Conf. Magnetics Japan, p. 301, 1982].
- [44] M. Young, *The Technical Writer's Handbook*. Mill Valley, CA: University Science, 1989.

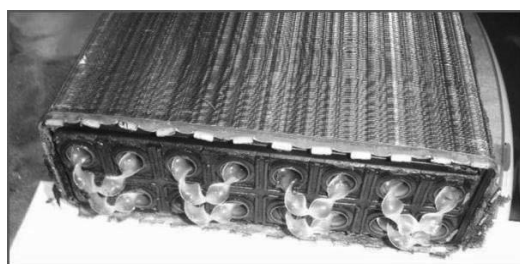


Fig. 1. A circular tube automobile radiator with aluminum twisted tape [9]

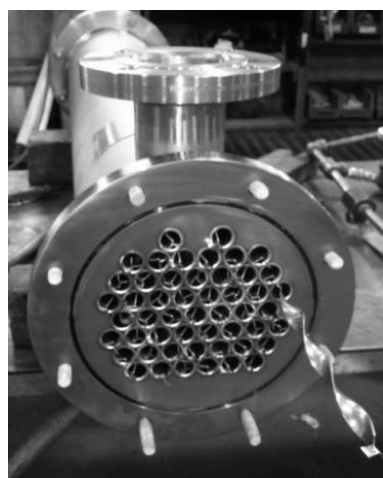


Fig. 2. Twisted tape turbulators [10]

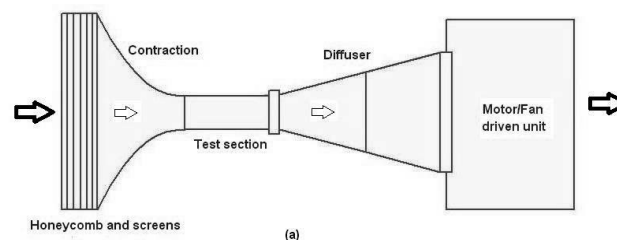


Fig. 3. Open Circuit Wind Tunnel [8]

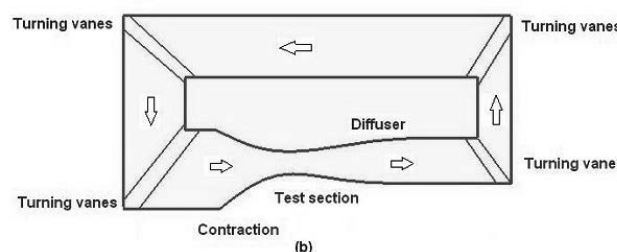


Fig. 4. Closed Circuit Wind Tunnel [8]

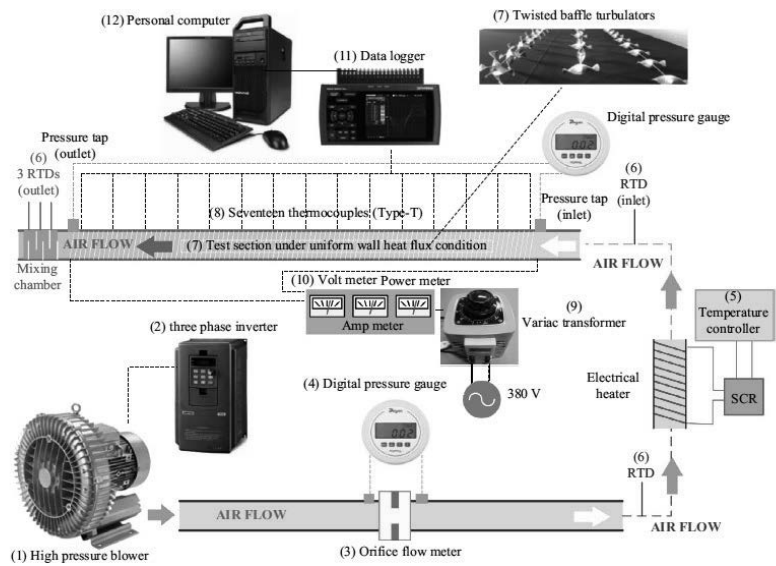


Fig. 5. Schematic diagram of the experimental set-up Nanan et al. [35].

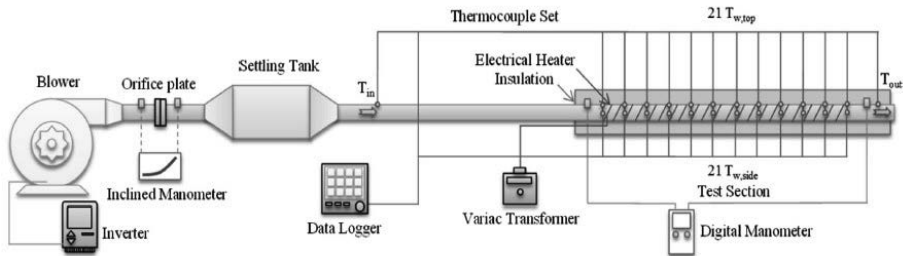





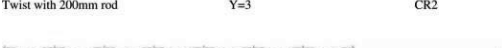
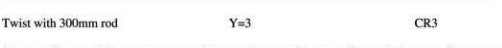
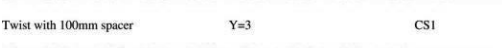
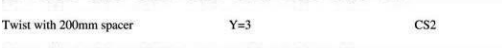
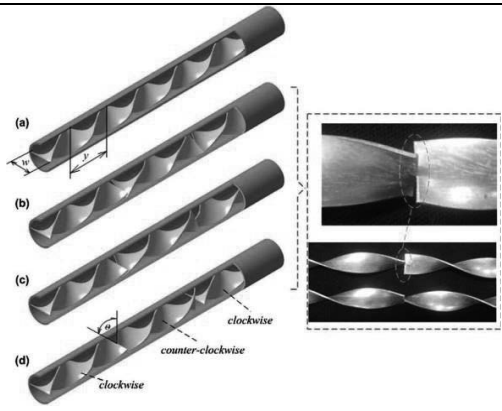
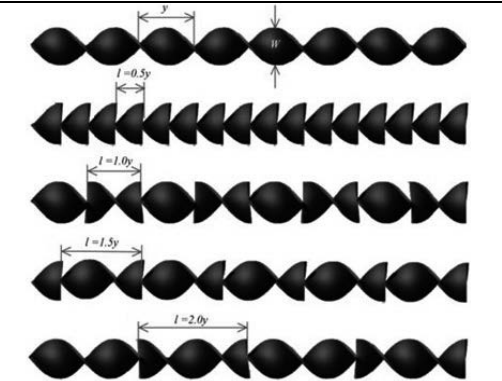
Fig. 6. Heat transfer test section area of the experimental set-up [36].

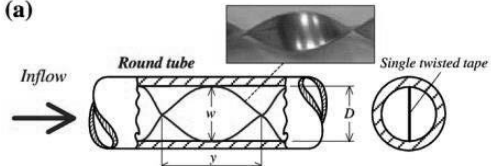
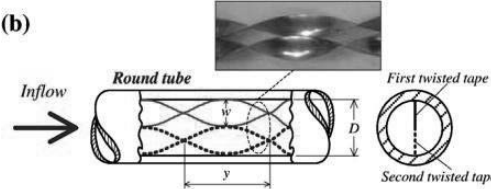
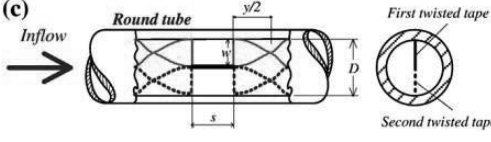
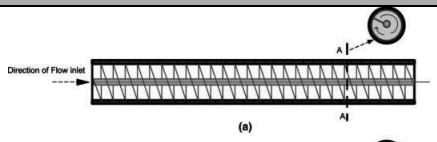
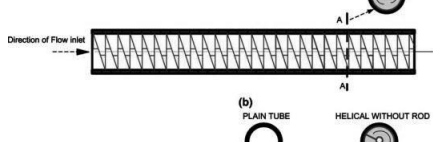
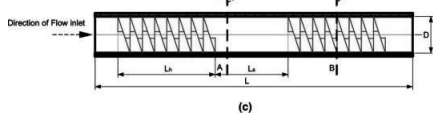

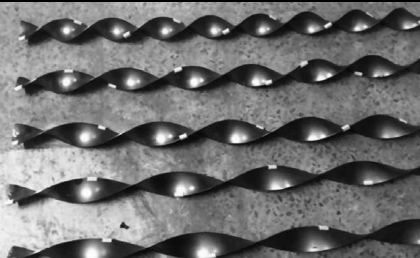
TABLE I. TWISTED TAPE TYPE TURBULENCE PROMOTER IN A TUBULAR HEAT EXCHANGER

Type (No.) [Ref.]	Twisted tape type
	Picture of Twisted tape
	1. Typical twisted tape
1 (1) [11]	

Type (No.) [Ref.]	Twisted tape type
	Picture of Twisted tape
	2. Varying length, alternative-axes and pitches twisted tape
2 (1) [12]	



Type (No.) [Ref.]	Twisted tape type Picture of Twisted tape
2 (2) [13]	 Y=3 C  Y=3 CR1  Y=3 CR2  Y=3 CR3  Y=3 CS1  Y=3 CS2  Y=3 CS3
2 (3) [14]	
2 (4) [15]	

Type (No.) [Ref.]	Twisted tape type Picture of Twisted tape
3. Multiple twisted tapes	
3 (1) [16]	  
4. Twisted tape with rod and varying spacer	
4 (1) [17]	  
4 (2) [18]	 <p>1.00 inch ID, Twist ratio 4, Spacer distance 2 inches</p>
4 (3) [19]	



Type (No.) [Ref.]	Twisted tape type Picture of Twisted tape
5. Twisted tape with attached fins and baffles	
5 (1) [20]	<p>Typical twisted tape, TT</p> <p>Twisted tape with centre wing, WT ($\beta = 74^\circ$)</p> <p>Twisted tape with centre wing, WT ($\beta = 53^\circ$)</p> <p>Twisted tape with centre wing, WT ($\beta = 43^\circ$)</p> <p>Twisted tape with alternate-axis, T-A</p> <p>Twisted tape with centre wing and alternate-axis, WT-A ($\beta = 73^\circ$)</p> <p>Twisted tape with centre wing and alternate-axis, WT-A ($\beta = 53^\circ$)</p> <p>Twisted tape with centre wing and alternate-axis, WT-A ($\beta = 43^\circ$)</p>
5 (2) [21]	
5 (3) [22]	

Type (No.) [Ref.]	Twisted tape type Picture of Twisted tape
5 (4) [23]	<p>Front view Top view</p> <p>T-Tra</p> <p>Front view Top view</p> <p>T-Rec</p> <p>Front view Top view</p> <p>T-Tri</p>
6. Twisted tapes with slots, holes cuts	
6 (1) [24]	<p>(a)</p> <p>PT-A</p> <p>PT</p> <p>TT</p> <p>(b)</p> <p>Alternate axis</p>
6 (2) [25]	<p>PT, $d/W = 0.11$, $w/W = 0.33$</p> <p>PT, $d/W = 0.11$, $w/W = 0.22$</p> <p>PT, $d/W = 0.11$, $w/W = 0.11$</p> <p>TT, $y/W = 3.0$</p>



Type (No.) [Ref.]	Twisted tape type Picture of Twisted tape
6 (3) [26]	
6 (4) [27]	
6 (5) [28]	
6 (6) [29]	
7. Left-right twisted tape with screw	
7 (1) [30]	
7 (2) [31]	

Type (No.) [Ref.]	Twisted tape type Picture of Twisted tape
8. Tape with different surface modifications	
8 (1) [32]	
8 (2) [33]	
8 (3) [34]	





Experimental Determination of Discharge Coefficient of Through Rectangle Trapezoid Shape and Triangle Weir

Nasru Tuenga¹, Rotjapun Nirunsin¹, Churat Thararux¹, and Tanate Chaichana^{1*}

¹College of Alternative Energy Maejo University 63 Moo 4, Nongbua Sub-District, San Sai District, Chiang Mai 50290

* Contact: E-mail; tanatecha@hotmail.com, telephone number 0815406768

Abstract—This research objective to study the effect of weir model on the flow characteristics of water and discharge coefficient of flowing through rectangular trapezoidal and triangular weir. The study was conducted three format in to open-water tunnels. During the experiment, this will measured the discharge of water Q , the height of the water overflow weir h , the point of water fall after weir x , compression angle of water θ , the Calculate discharge of water Q from experiment and theoretical to induct calculate the discharge coefficient. The study indicated that through rectangular trapezoidal and triangles. At the through rectangular weir $b_L = 0.17$ 0.19 and 0.21 m trapezoidal weir $A = 5$ 10 15 and 20 degree and the triangular weir $W_H = 0.05$ 0.075 and 0.105 m. The weir ratio with water level above weir h/p increased. Effect on discharge coefficient C_d decreases. this is rectangular and triangular weir, and then it will increased, this is trapezoidal weir. The weir ratio with water level above weir h/p increased. Effect on discharge of water Q increased, this is rectangular and trapezoidal weir. Then it will decreases, this is triangular weir..Effect to discharge coefficient of each weir pattern that open water of flow at 100% as 0.7714 0.7635 and 0.5052 , respectively. at the had a high slit width $W_H = 0.105$ m. the discharge coefficient the flowing of triangular weir with an average 0.5052 and at the width of the weir $b_L = 0.21$ m, the discharge coefficients the flowing of through rectangular weir with an average 0.7714 . Experimental determination of discharge coefficient of through rectangular weir is the best. But it must be developing formulae for the better of thick-crested weir to discharge coefficient.

Keywords— discharge coefficient Rectangular dam Trapezoid Triangle Cross-sectional area thick-crested

I. INTRODUCTION

Weirs is an engineering structure that matches the flow of water and usually results in a change in the height of the river level. Therefore, the important role of the structure is to ensure the safety. Weir have been used for centuries by hydraulic engineers for flow measurements, regulation of flow depth, energy dissipation, flow, and flow diversion [1,2]. Weirs have many types (i.e., water overflow weir, sharp-crested weir, narrow-crested weir, fayoum weir, submerged weir, broad-crested weir, ogee weir, ordinary weir, and rectangular weir). Weirs are overflow structures

for flow measurements discharge coefficient and controlling flow in open channels [3]

Weirs are the variety of different structures that are used to control the flow of water. Insufficient capacity of weirs has been the cause of one-third of weir failures[4]. For a specific head width and thickness, Therefore, the important role experimental for flow measurements theory of discharge coefficient with different structures. Weirs are overflow have many types of determination (i.e., Through Rectangle Weir, Trapezoid Shape Weir and Triangle Weir). flow measurements of discharge coefficient might be increased and depreciate the discharge capacity of the determination.

Nikou et al. (2016) derived an analytical method for estimating the discharge coefficient of a pivot weir for both free and submerged flow conditions using only the Bernoulli equation. The validation of this relation with experimental data showed $\pm 20\%$ error, which indicates, Insufficient accuracy in estimating the discharge coefficient [5]. Di Stefano et al. (2016) conducted research using previous experimental results to estimate the weir discharge coefficient in order to provide a general discursive equation for estimating the discharge coefficient for complex types of weir. The validation of this equation with the experimental results shows a $\pm 10\%$ relative error [6]. Seyyed Mojtaba Azimfar et al (2018) A review of previous studies shows that most researchers used experimental equations to estimate the pivot weir discharge coefficient with a focus on vertical sharp-edge weirs. These investigations impose numerous experimental coefficients in a hypothetical regression form for estimating the discharge coefficient. The downside of such assumption is that assuming a regression form is not always realistic and may not provide acceptable accuracy.[7]

All the aforementioned researchers studied the using previous experimental results to estimate the weir discharge coefficient in order to provide a general discursive equation for estimating the discharge coefficient for complex types of characteristics determination weir. In order to study Experimental determination of discharge coefficient of through rectangle trapezoid shape and triangle weir.



II. RESEARCH METHODOLOGY

Conducted water tunnel and determination of weirs design. that are been used solid work program because be a model to manufacture. After that Install weirs are overflow design for measuring flow measurements with data collection . Bring information to Calculations from equation to find the flow rate of water from experimental results to provide for each types of weir. The validation and analyze with theory and experimental determination of discharge coefficient of weirs.

A. Weir design

1) Design and construct are the through rectangular trapezoidal and triangular weir. As shown in Fig.1 Acrylic clear 0.5 cm thick high of weir $H=0.40$ m and width of weir $W_L=0.39$ m

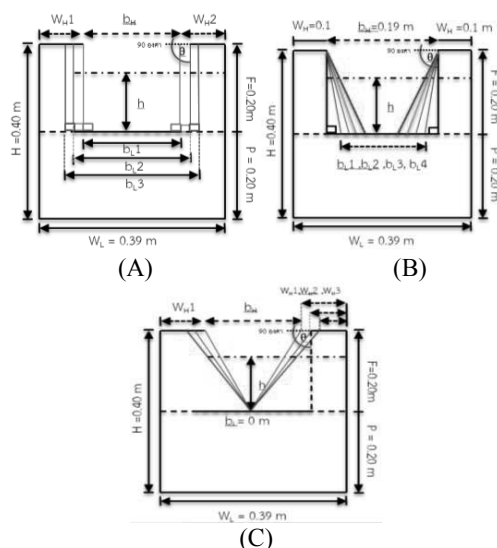


Fig. 1. shows the pattern of the weir (A) the through rectangular weir (B) the trapezoid weir and (C) the triangular weir.

TABLE I. EXPLANATION OF SYMBOLS THAT SIZE OF OVERFLOW WEIR AT DESIGN AND ANOTHER TYPES OF WEIR.

Explanation and symbols	Size and unit
low width that weir (W_L)	0.39 m
height weir (H)	0.40 m
height overflow of weir (p)	0.20 m
height overflow above of weir (F)	0.20 m
Rectangular weir The width of overflow weir at low. (b_L) there are 3 values	0.17 0.19 0.21 m
Trapezoidal weir Gross sectional area (A) there are 4 values	5 10 15 20 degree
Triangular weir The width of overflow weir at high (W_H) there are 3 values	0.05 0.075 0.105 m

2) Install an overflow weir with different of weir types on front of open water tunnel.



Fig. 2. Open water tunnel at width 0.39 m, high 0.40 m, and long 4.80 m

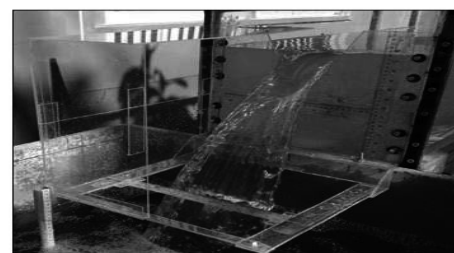


Fig. 3. shows the actual to water overflow of weir

B. Data collection

1) Test and collect water flow data through water overflow weir. There is a measuring set of weir testers, which is shown in Fig.4.

- height of the water above the weir (h)
- distance Fall point of water overflow weir (x)
- Compression ratio the water overflow weir (A)
- Width of water overflow river mouth (N)

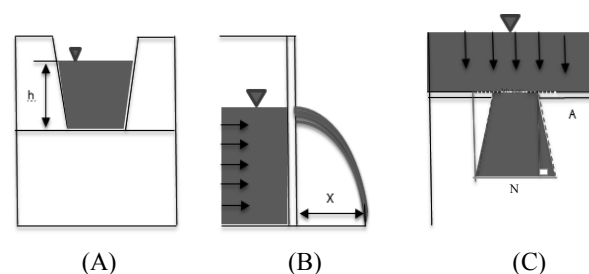


Fig. 4. Flow Characteristics of Water Through Overflow weir (A) Front (B) Side (C) Top



C. Calculations from equation

analytical method for estimating the discharge coefficient of water overflow weir for experimental results to measuring discharge and controlling flow in open water tunnel. The data is analyzed for the discharge of water From the experiment (Q_{measure}) and the discharge of water From theoretical ($Q_{\text{theoretical}}$) Take this two values for find the discharge coefficient.

1) Analyze the discharge coefficient with discharge of data from experimental. As shown in equations (1).

2) Calculate the discharge coefficient C_d based on equations 1-4. [9]

$$Q_{\text{measure}} = C_d Q_{\text{theoretical}} \quad (1)$$

by

$$Q_{\text{theoretical}} = \frac{2}{3} C_d b \sqrt{2g} \left(h^{\frac{3}{2}} \right) \quad (2)$$

Equation for Overflow weir of through rectangular.

$$Q_{\text{theoretical}} = \frac{2}{3} C_d b \sqrt{2g} \left(h^{\frac{3}{2}} \right) + \frac{8}{15} C_d \left(h^{\frac{5}{2}} \right) \sqrt{2g \tan^2 \frac{\theta}{2}} \quad (3)$$

Equation for overflow weir of trapezoidal.

$$Q_{\text{theoretical}} = C_d \frac{8}{15} \sqrt{2g \tan \frac{\theta}{2}} \cdot h^{\frac{5}{2}} \quad (4)$$

Equation for overflow weir of triangular.

Where

b is the width of the weir face (m)

h is the height of the water above the weir (m)

θ is Gross- sectional area of weir (degrees)

III. RESEARCH RESULTS AND DISCUSSION OF RESEARCH FINDINGS.

Weir have many types, model configurations through rectangle weir trapezoid shape weir and triangle weir. Analytical method for estimating the discharge coefficient by measuring discharge and controlling overflow open water tunnel channels. Weir overflow are also considered distance Fall point of water overflow weir and Compression of drop point and discharge coefficient C_d of the weir as measuring and controlling flow devices of water overflow weir.

1. discharge of water

1.1 Through Rectangle Weir discharge of water Q

The ratio during the height of the water above the weir and the height water overflow of weir h/p increased. Effect on discharge coefficient C_d decreases. Meanwhile, the ratio h/p increasing with the discharge coefficient C_d was increased, the influence discharge of water Q increased. As shown in Fig. 5.

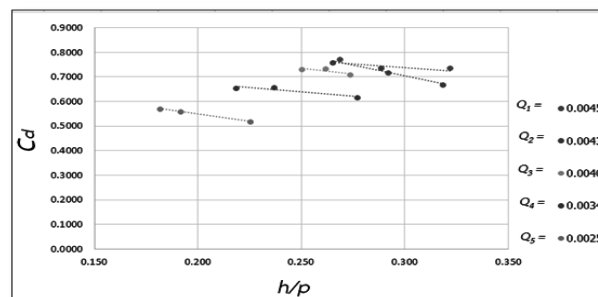


Fig. 5. The relationship between discharge coefficient C_d and h/p at discharge of water Q1-Q5. Through Rectangle Weir

1.2 Trapezoid Shape weir

The ratio during the height of the water above the weir and the height water overflow of weir h/p increased. Effect on discharge coefficient C_d increased. Meanwhile, the ratio h/p increasing with the discharge coefficient C_d increased. the influence discharge of water Q was increased, As shown in Fig. 6.

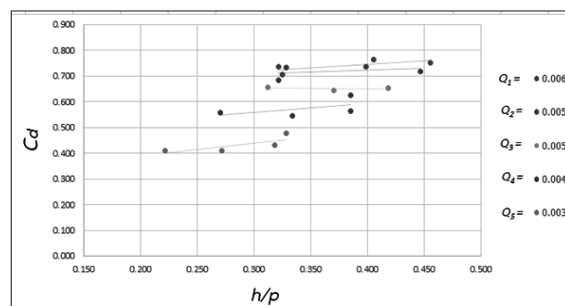


Fig. 6. The relationship between discharge coefficient C_d and h/p at flow Q1-Q5. Trapezoid Shape weir

1.3 Triangle Weir

The ratio during the height of the water above the weir and the height water overflow of weir h/p increased. Effect on discharge coefficient C_d decreases. Meanwhile, the ratio h/p increasing with the was discharge coefficient C_d . decreases, influence, discharge of water Q decreases. As shown in Fig. 7.

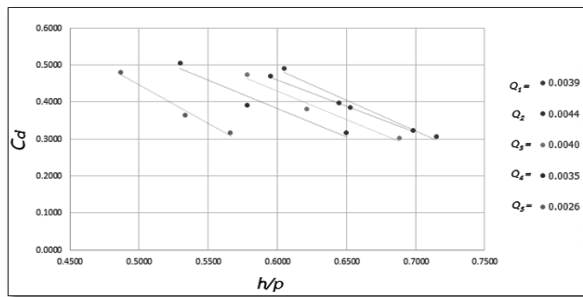


Fig. 7. The relationship between discharge coefficient C_d and h/p at flow rate Q1-Q5. Triangle Weir.

TABLE II. THE SHOWS DATA OF THE DISCHARGE COEFFICIENT C_d DISCHARGE OF WATER Q AND THE RATIO h/p .

t	Rectangle			Trapezium			Triangle		
	h/p	Q m^3/s	C_d	h/p	Q m^3/s	C_d	h/p	Q m^3/s	C_d
1	0.322	0.0048	0.7361	0.325	0.0044	0.707	0.7150	0.0044	0.3053
2	0.292	0.0043	0.7166	0.405	0.0047	0.764	0.6533	0.0026	0.3835
3	0.268	0.0044	0.7714	0.322	0.0044	0.737	0.6050	0.0047	0.4888
4	0.318	0.0043	0.6676	0.322	0.0042	0.684	0.6983	0.0044	0.3211
5	0.288	0.0044	0.7361	0.398	0.0046	0.738	0.6450	0.0044	0.3973
6	0.265	0.0043	0.7598	0.328	0.0044	0.735	0.5950	0.0043	0.4678
7	0.262	0.0041	0.7328	0.312	0.0041	0.657	0.6883	0.0039	0.2998
8	0.273	0.0041	0.7106	0.370	0.0039	0.645	0.6217	0.0039	0.3814
9	0.250	0.0039	0.7318	0.418	0.0040	0.653	0.5783	0.0040	0.4727
10	0.277	0.0036	0.6177	0.270	0.0034	0.558	0.6500	0.0036	0.3148
11	0.237	0.0034	0.6571	0.333	0.0033	0.547	0.5783	0.0033	0.3910
12	0.218	0.0032	0.6546	0.385	0.0038	0.625	0.5300	0.0035	0.5052
13	0.225	0.0026	0.5193	0.222	0.0025	0.412	0.5667	0.0026	0.3149
14	0.192	0.0025	0.5585	0.272	0.0024	0.409	0.5333	0.0025	0.3651
15	0.182	0.0024	0.5714	0.328	0.0028	0.477	0.4867	0.0026	0.4782

2. distance Fall point of water overflow weir

When the lap area height of the water above the weir with the decrease width of the h/p . discharge of water Q increased and decreases (the discharge of water 100% - 25%), Effect on distance Fall point of water overflow weir x increased and decrease by model configurations through rectangle weir, having the maximum $x=0.188$ m and the smallest $x=0.119$ m, trapezoidal weir The maximum $x=0.219$ m and the smallest $x=0.064$ m, and the triangular weir with the maximum $x=0.266$ m and the smallest $x=0.210$ m, can be seen at discharge of water Q increased. As the cutting area decreases, the x value increases. The maximum all of weir. This is triangular weir at $x = 0.266$ m.

3. Compression of drop point

Compression of drop point for through rectangle weir. The difference in width of The width of overflow weir ($b_L = 0.17, 0.19$ and 0.21 m) was in the range of $96.24 - 144.33$ degrees. respecting of trapezoid shape weir At different angles ($A = 5, 10, 15$, and 20 degrees), the values were in the range of $97.79-117.94$ degrees. The respecting of triangle weir width of the width of overflow weir at high with different values ($W_H = 0.05, 0.075$ and 0.105 m) were in the range of $96.07 - 124.27$ degrees, consequently, Compression degrees of water fall were higher when the discharge of water Q increased. But only slightly increase.

4. discharge coefficient C_d of the weir

The data collected from the experiments were analyzed for the discharge of water Q in two methods. Computational analysis of the experimental weir (measuring the water in the tank Set the height of the water up to 0.1 m, then make a timer) and analyze the theory. Both methods were used to estimate the discharge coefficients with three weir. Discover the discharge coefficients through by the rectangular weir. this have Average 0.7714 discharge coefficient through trapezoid shape weir. this have Average 0.7640 and the discharge coefficient of through the triangular weir as shown in Table 2, the discharge coefficients of the three weir types show that the calculated discharge of water Q differs from the measurement.

The discharge of water Q equation was analyzed. Is the equation for the sharp-crested weir. In this research, the weir is thick, the value of which has been Erroneously. At present, there is no equation for calculating the discharge of water Q with equation thick-crested weirs. The next step is to develop the equation.

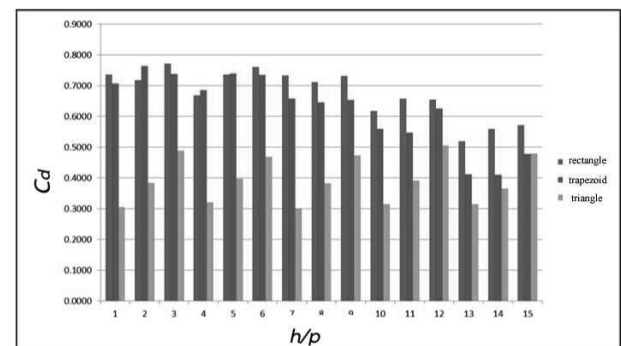


Fig. 8. The relationship between discharge coefficient C_d and h/p at through rectangle weir trapezoid shape weir and triangle weir

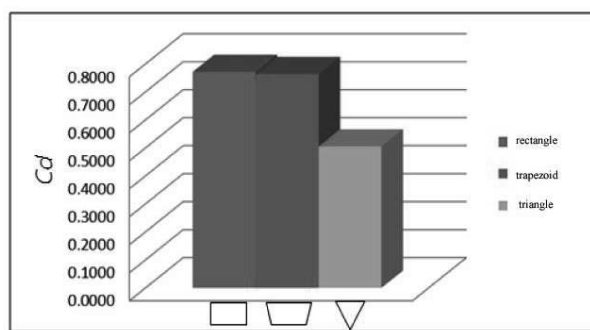


Fig. 9. The relation between the discharge coefficient C_d and the weir model.

RESEARCH RESULT

The study have aimed to effect of h/p as Affect characteristics discharge of water Q and the discharge coefficients through the rectangular weir Trapezoid weir and trapezoid weir the thick-crested weirs. Can be summarized as follows.

1.The proportion of h/p increases. the discharge coefficients decrease. At the same time, the discharge of water Q increases. This case is specifically a rectangular weir

2.The proportion of h/p increases. the discharge coefficients increase. At the same time, the discharge of water Q increases. This case is specifically a triangular weir.

3. The proportion of h/p increases. the discharge coefficients decrease. At the same time, the discharge of water Q decreases. The case is specifically to trapezoidal weir.

4. At all forms of weir The distance Fall point of water overflow weir x will be increases when the discharge of water Q increases and the area of the weir decreases. The rectangular weir will have a minimum fall of $x=0.119$ m and the triangular weir will have a maximum fall of $x=0.266$ m.

5. Compression of drop point for rectangular weir values in the range of 96-144 degrees. triangular weir values range at 97-117 degrees, and trapezoidal weir. values are in the range of 96-124 degrees.

6. The discharge coefficient through the rectangular weir. this have Average $C_d=0.7714$, the triangular weir this have Average $C_d=0.7640$ and trapezoidal weir this have Average $C_d=0.5052$, Appear, the discharge coefficient through the triangular weir. The best value at average 0.7714.

ACKNOWLEDGMENTS

- Open water tunnel project for hydraulics, water power and measuring discharge of water. The water tunnel support for the experiment.
- School of Renewable Energy, the support for student the proceed research

REFERENCE

- [1] G. Abouzeid, Improvement of the hydraulic performance of sharp-crested side weirs in circular channels. In: English International Water Technology Conference, IWTC8 2004, Egypt, 2004, pp. 499–509
- [2] W. Boiten, Flow measuring structures, Delft Hydraulics, Publications number 478, August 1993.
- [3] R.S. Khurmi, A Text Book of Hydraulics, Fluid Mechanics and Hydraulic Machines, 12 ed., 1982
- [4] A. Schleiss, From Labyrinth to Piano Key Weirs—A Historical Review. Labyrinth and Piano Key Weirs, CRC Press, London, 2011, pp. 3–15.
- [5] N.S.R. Nikou, M.J. Monem, K. Safavi, Extraction of the flow rate equation under free and submerged flow conditions in pivot weirs with different side contractions, *Irrig. Drain. Eng.* (2016), [http://dx.doi.org/10.1061/\(ASCE\)IR.1943-4774.0001027\(04016025\)](http://dx.doi.org/10.1061/(ASCE)IR.1943-4774.0001027(04016025)).
- [6] C. Di Stefano, V. Ferro, M. Bijankhan, New theoretical solution of the out flow process for a Weir with complex shape, *J. Irrig. Drain. Eng.* (2016) doi: 10.1061 (ASCE) IR.1943-9774.0001045.
- [7] Seyyed Abbas Hosseini, Seyyed Mojtaba Azimfar "Derivation of discharge coefficient of a pivot weir under free and submergence flow conditions, Department of Civil Engineering, Science and Research, Islamic Azad University, Tehran, Iran, Volume 59, March 2018, Pages 45-51, <https://doi.org/10.1016/j.flowmeasinst.2017.11.010>
- [8] Department of Alternative Energy Development and Efficiency, "Alternative Energy Development Plan (AEDP2015) 28 July 2016 2560)
- [9] Pramote et al., "The Principles for Calculating Irrigation Water through Irrigation", Knowledge Management in Knowledge Management Plan to Support Strategic Issues, Royal Irrigation Department, Fiscal Year 2011
- [10] Asst.Prof.Dr.Peeraporn Kosa, "Surge Engineering", Hydraulics
- [11] Ferrari A, (2010), SPH simulation of free surface flow over a sharp-crested weir, *Advances in Water Resources* 33, pp 270-276
- [12] Rahimpour, Keshavarz M, Zohreh, Ahmadi, M-M. (2011), Flow over trapezoidal side weir, *Flow measurement and Instrumentation* 22, pp 507-510
- [13] Zahiri A, Azamathulla H.Md, Bagheri S. Discharge coefficient for compound sharp crested side weirs in subcritical flow conditions (2013), *Journal of Hydrology* 480, pp 162–166
- [14] Gharahjeh S, Aydin, Altan-Sakarya A.B. Weir velocity formulation for sharp-crested rectangular weirs (2015), *Flow Measurement and Instrumentation* 41, pp 50–56
- [15] Burcu Altan-Sakarya A, Ismail Aydina, Cigdem Sismanb. Discharge formula for rectangular sharp-crested weirs (2011), *Flow Measurement and Instrumentation* 22, pp 144–151
- [16] Farzaneh N, Davood F, Mohammad A. Discharge coefficient for trapezoidal side weir (2015), *Alexandria Engineering Journal* 54, pp 595–605
- [17] Yousef Sangse fidia, Mojtaba Mehraeinb, Masoud Ghodsian, "Experimental study on flow over in-reservoir arced labyrinth weirs", Faculty of Civil and Environmental Engineering, Tarbiat Modares University, 14115-397 Tehran, Iran, 59(2018) 215-224. <https://doi.org/10.1016/j.flowmeasinst.2017.12.002>
- [18] Ahmed M. El-Belasy, "Developing Formulae for combined weir and orifice" (case study: EL-Fayoum weirs), Hydraulics Research Institute, National Water Research Centre, Egypt,. Available online 15 September 2013, www.elsevier.com/locate/aej.



Effect of Blade Radius to Characteristics of Undershot Water Wheel

Muhammadkhoiri Hayibaka¹, Rotjapun Nirunsin¹, Churat Tararuk¹, and Tanate Chaichana^{1*}

¹School of Renewable Energy, Maejo University, Chiang Mai, 50290, Thailand

*Corresponding author: Tel.: 081-5306768. E-mail address: Tanatecha@hotmail.com

Abstract— Undershot water wheel is a hydro turbine that has been the current interest. Because it has the advantage of being cheaper and simpler to build. The objective this research was to study effect of blade radius to characteristics of undershot water. The water wheel was test in the open flow water tunnel at water-submerge level of 100% with blade high and 5 water flow rate of 0.0048, 0.0044, 0.0039, 0.0034, and 0.0028 sq-m/s. The water wheel with the blade radius of 50%, 75%, 100%, 125% and 150% with blade length. Each blade had the area length of 30 cm, height of 6 cm, thickness of 3 mm and blade numbers of 12 blades. From the results of the study at each blade radius and each water flow rate, it was found that the decreased rotation speed and torque occurred when the higher blade radius, but in the case of torque decreases trend at blade radius of 50% with blade length. The maximum rotation speed about 11.98 rpm at blade radius of 50% with blade length and the maximum torque about 0.0108 N-m at blade radius of 75% with blade length. The maximum power coefficient and torque coefficient at blade radius of 50% with blade length about 47.9% and 41.97% respectively.

Keywords—blade radius; characteristics; undershot water wheel

I. INTRODUCTION

Hydro energy is a clean fuel that doesn't pollute the air. Hydro Energy is the technology that converts the energy of moving water into mechanical or electrical energy, and one of the earliest devices used to convert the energy of moving water into usable work was the Waterwheel. Water wheel design has evolved over time with some water wheels oriented vertically, some horizontally and some with elaborate pulleys and gears attached [1].

Undershot water wheel is a hydro turbine that has been the current interest. Because it has the advantage of being cheaper and simpler to build, but is less powerful and can only be used where the flow rate is sufficient to provide torque [2]. A lot of researches that try to design and produce water wheel for higher efficiency.

A. Tevataa, and C. Inprasita (2011) studied effect of blade numbers and water-submerge level, it was found that the highest performance occurred when the paddle number was 6 and the immersed radius ratio was 0.5. The torque load at the maximum power depended on the immersed radius ratio. And, at the same immersed radius ratio, the 6, 8 and 12 paddle

numbers water wheel models had the same torque load at the maximum power [3]. T. Chaichana, et.al., (2011) has conducted a research on a water wheel. In his report, a water wheel was of tested using varying rates of water-submerge level, it was found that the maximum shaft power about 6.4 W occurred when the water-submerge level 100% [4].

Therefore, this is the source of this research to study effect of blade radius to characteristics of undershot water wheel for information will design and construction undershot water wheel.

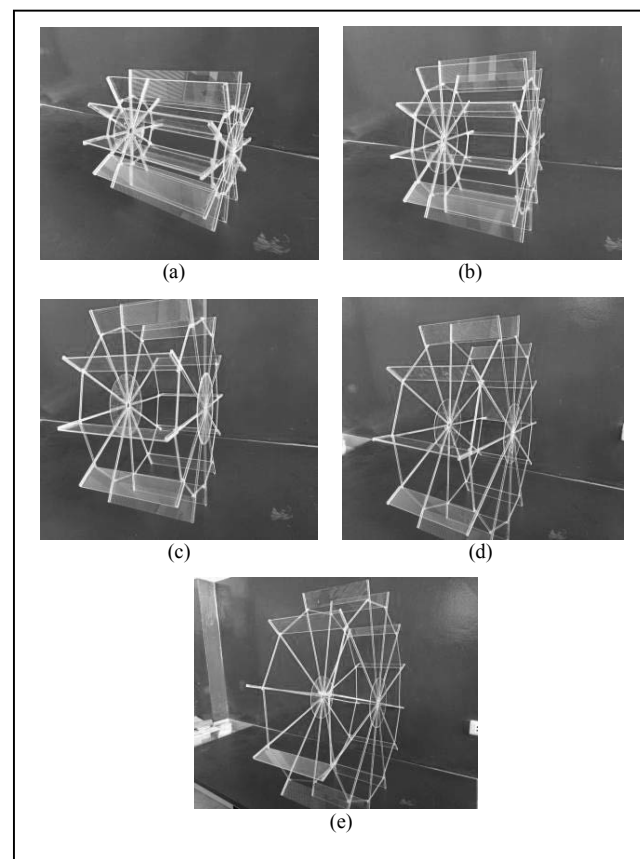


Fig. 1. Undershot water wheel at various blade radius (a) 50%, (b) 75%, (c) 100%, (d) 125%, and (e) 150% with blade length.



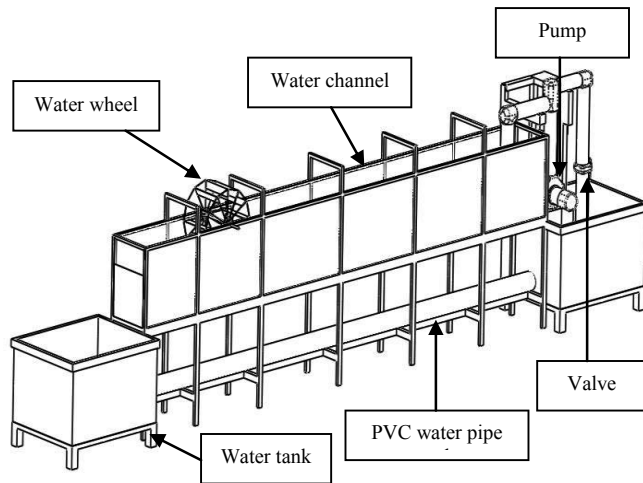


Fig. 2. Water wheel was installed in an open flow water tunnel.

II. EQUIPMENT AND METHOD

To study effected of blade radius to characteristics of undershot water, the water wheel model was test in the open flow water tunnel that the water channel had a width of 40 cm, height of 40 cm, and length 480 cm. The water wheel models with the blade radius of 50%, 75%, 100%, 125% and 150% with blade length as shown in Fig. 1. Each blade had the area length of 30 cm, height of 6 cm, thickness of 3 mm and blade numbers of 12 blades. Then the water wheel was installed in an open flow water tunnel as shown in Fig. 2 and it was measured from the force applied by the brake horsepower.

To test water wheel at water-submerge level of 100% with blade high, 5 water flow rate of 0.0048, 0.0044, 0.0039, 0.0034, and 0.0028 sq-m/s. and were tested of each blade radius. Then the data was analyzed rotation speed, torque as shown in equation 1, power coefficient this is the ratio between the power of hydro turbine with the kinetic energy of water as shown in equation 2. and torque coefficient as shown in equation 3 this is the ratio between power coefficient with tip speed ratio as shown in equation 4.

$$\tau = Fr \quad (1)$$

Where τ = Torque (N-m)
 F = Force at the blade (N)
 r = Radius of pulley (m)

$$C_P = \frac{2\pi N \tau}{1/2 \rho A v^3} \times 100 \quad (2)$$

Where C_P = Power coefficient (%)
 N = Rotation speed (rps)
 ρ = Density of water (kg/m³)

A = Cross sectional area considered (m²)

v = Speed of water (m/s)

$$C_T = \frac{C_P}{\lambda} \times 100 \quad (3)$$

Where

C_T = Torque coefficient (%)

λ = Tip speed ratio

$$\lambda = \frac{R 2 \pi N}{v} \quad (4)$$

Where

R = Radius of water wheel (m)



Fig. 3. Water wheel model was test in the open flow water tunnel.

III. RESULTS AND DISCUSSIONS

A. Rotation speed

The rotation speed at each blade radius and each water flow rate as shown in Fig. 4. It was found that the decreased rotation speed occurred when the higher blade radius. This may because the distance between blades is tight at small radius. Therefore, the speed of the water flowing to the next blade is faster. The maximum rotation speed about 11.98 rpm at blade radius of 50% with blade length.

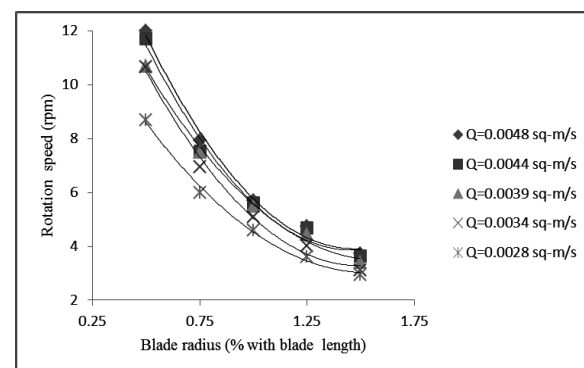


Fig. 4. Relationship between blade radius with rotation speed.



B. Torque

The torque as shown in Fig. 5. It was found that the decreased torque occurred when the higher blade radius. The same with that rotation speed. But decreases trend at blade radius of 50% with blade length. This may because the lowest drag force at the blade back [3]. The maximum torque about 0.0108 N-m at blade radius of 75% with blade length.

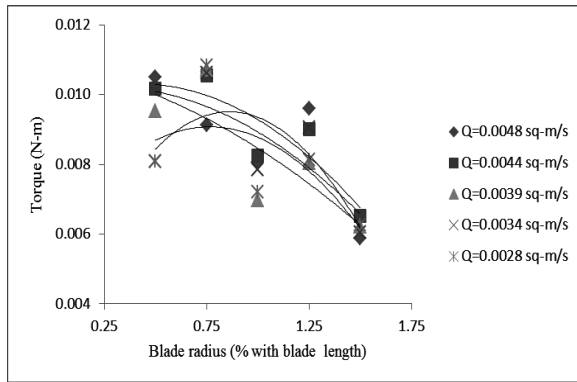


Fig. 5. Relationship between blade radius with torque.

C. Power coefficient and torque coefficient

Coefficient of water wheel studies 2 parts is power coefficient and torque coefficient. The power coefficient at each blade radius and each water flow rate as shown in Fig. 6. It was found that the decreased trend power coefficient occurred when the higher blade radius. The average power coefficient about 20%. The maximum power coefficient about 47.9% at blade radius of 50% with blade length.

The torque coefficient at each blade radius and each water flow rate. It was found that the decreased trend torque coefficient occurred when the higher blade radius. The same with that power coefficient. The average torque coefficient about 17.66%. The maximum torque coefficient about 41.97% at blade radius of 50% with blade length as shown in Fig. 7.

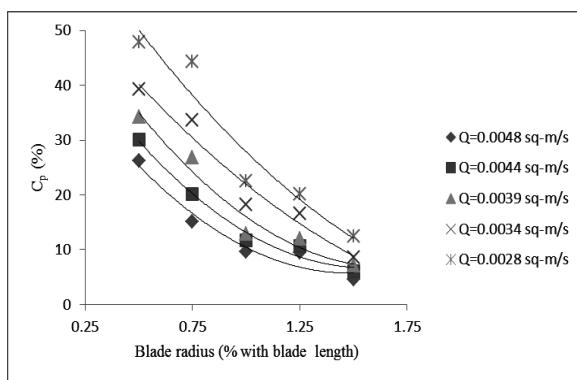


Fig. 6. Relationship between blade radius with power coefficient.

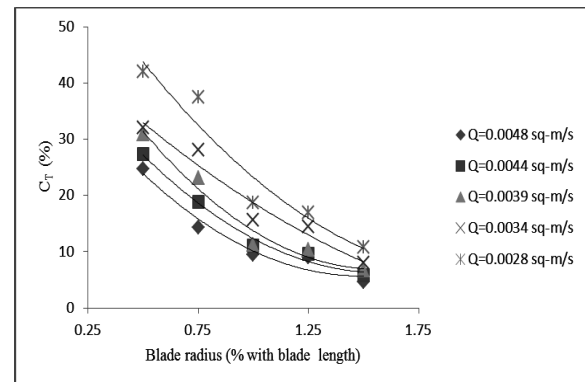


Fig. 7. Relationship between blade radius with torque coefficient.

TABLE I. THE INFORMATION OBTAINED FROM THE EXPERIMENT.

Q (sq-m/s)	Blade radius (% with blade length)	Rpm	Torque (N-m)	C _p (%)	C _t (%)
0.0048	0.5	11.98	0.0105	26.20	24.74
0.0048	0.75	7.93	0.0091	15.07	14.34
0.0048	1	5.71	0.0081	9.58	9.50
0.0048	1.25	4.74	0.0096	9.46	9.04
0.0048	1.5	3.72	0.0059	4.56	4.62
0.0044	0.5	11.69	0.0102	30.12	27.30
0.0044	0.75	7.53	0.0106	20.12	18.89
0.0044	1	5.61	0.0082	11.70	11.06
0.0044	1.25	4.70	0.0090	10.72	9.68
0.0044	1.5	3.63	0.0065	6.00	5.84
0.0039	0.5	10.70	0.0095	34.19	30.87
0.0039	0.75	7.48	0.0107	26.82	23.08
0.0039	1	5.50	0.0070	12.84	11.27
0.0039	1.25	4.45	0.0080	11.97	10.39
0.0039	1.5	3.41	0.0062	7.10	6.70
0.0034	0.5	10.65	0.0081	39.21	32.11
0.0034	0.75	6.95	0.0106	33.60	28.09
0.0034	1	5.09	0.0079	18.16	15.57
0.0034	1.25	4.02	0.0091	16.59	14.38
0.0034	1.5	3.12	0.0060	8.59	8.01
0.0028	0.5	8.69	0.0081	47.90	41.97
0.0028	0.75	5.99	0.0108	44.29	37.55
0.0028	1	4.59	0.0072	22.58	18.73
0.0028	1.25	3.62	0.0081	20.08	16.91
0.0028	1.5	2.93	0.0063	12.51	10.83



The information obtained from the experiment as shown in table 1. Analyze the equation for to find the relationship between power coefficient with flow rate, blade radius and rotation speed as shown in equation 5 ($R^2=0.9037$).

$$C_p = 0.70 - 89.11 Q - 0.21 B + 0.0009 \text{ RPM} \quad (5)$$

IV. CONCLUSION

The results of the experiment effected of blade radius to characteristics of undershot water wheel in an open flow water tunnel were as follows.

- The decreased rotation speed occurred when the higher blade radius. The maximum rotation speed about 11.98 rpm at blade radius of 50% with blade length.
- The decreased torque occurred when the higher blade radius. But decreases trend at blade radius of 50% with blade length. The maximum torque about 0.0108 N-m at blade radius of 75% with blade length.
- The maximum power coefficient and torque coefficient at blade radius of 50% with blade length. Power coefficient about 47.9% and torque coefficient about 41.97%.

ACKNOWLEDGMENT

This research was supported by Project to produce and develop graduate capacity in renewable energy in ASEAN countries for graduate students of the College of Alternative Energy. Maejo University For the academic year 2016. And project open water tunnels for hydraulic and power testing and water flow coefficients through overflow dams that support water tunnels.

REFERENCES

- [1] Alternative energy tutorials, "Hydro energy," Available at: <http://www.alternative-energy-tutorials.com/hydro-energy/waterwheel-design.html>
- [2] Top Alternative Energy Sources.com, "Water wheel design," Available at: <http://www.top-alternative-energy-sources.com/water-wheel-design.html>
- [3] A. Tevataa, and C. Inprasita, "The Effect of Paddle Number and Immersed Radius Ratio on Water Wheel Performance," Department of Mechanical Engineering, Faculty of Engineering, Rajamangala University of Technology Lanna Tak, 2011.
- [4] T. Chaichana, A. Priklake, and Kraisorndaidate, "Local Wisdom Innovation in Alternative Energy of Small Flow Type Hydro-Power System for Open Channel of Water Flow," Full research reports, Office of the Higher Education, Commission Under the Research Promotion Program in Higher Education, Thaksin University, 2011.
- [5] S. Chaitep and T. Chaichana, "Alternative Energy Systems To produce electricity in the project area due to the Royal Initiative (wind and water)," Institute of Science and Technology, Chiang Mai University, 2008.
- [6] A. date, A. date, and A. akbarzadeh, "Investigating the potential for using a simple water reaction turbine for power production from low

head hydro resources," Energy Conversion and Management 66, 2013, 257-270, 2013.

- [7] A. date, A. date, and A. akbarzadeh, "Performance investigation of a simple reaction water turbine for power generation from low head micro hydro resources," Smart Grid and Renewable Energy, (3): p. 239-245, 2012.
- [8] Department of Alternative Energy Development and Energy Conservation, "Alternative Energy and Alternative Energy Development Plan 2015-2016 (AEDP2015)," Ministry of Energy, 2015.
- [9] Luther Sule, I.N.G. Wardana, Rudy Soenoko, and Slamet Wahyudi, "Angled and Curved Blades of Deep-Water Wheel Efficiency," Australian Journal of Basic and Applied Sciences, P. 186-192, 2014.
- [10] Snidvongs Suravut, Jongjit Hirunlabh, Joseph Khedari, and Kunagone Kiddee, "Stand Alone Water Wheel Low Speed Surface Aerator Chaipattana RX-2-3 Controller System," International Conference on Alternative Energy in Developing Countries and Emerging Economies 2017 AEDCEE, Bangkok, Thailand, 2017.



Computational Simulation on Hydrodynamics Behaviour of Air-Sand Bed in Twin Cyclonic Fluidized-bed Combustor

Poramet Arromdee*, Kasama Sirisomboon, and Chatthanon Bhothikhun

Laboratory of Advance Combustion Technology and Energy Systems (LACTES),
Department of Mechanical Engineering,
Faculty of Engineering and Industrial Technology,
Silpakorn University Nakhon Pathom 73000, Thailand

*Corresponding Author: poramet@gmail.com, (+6634) 259 025 Fax: (+6634) 219 367

Abstract—This research aimed to study on the hydrodynamics behavior of air-sand bed in a Twin Cyclonic Fluidized-bed Combustor (TFBC). The experiments were conducted by using silica sand bed particle size range of 300–500 μm , while ranging excess air from 20 to 80%, and the proportion of secondary air to primary air from 0 to 0.5 at the height of 0.45 m above the air distributor. The experimental results were used for computer simulation to predict the radial solid holdup profiles in TFBC. The results from computational simulation are agreed well with the experimental results. From the analysis of both experimental and computational simulation results, excess air has higher impact on the bed expansion of the fluidized bed compared to secondary air to primary air ratio.

Keywords—component; Swirling Fluidized Bed; Secondary Air; Computational Fluid Dynamics (CFD)

I. INTRODUCTION

Fluidized bed technology is proven to be one of the best technologies for energy conversion from biomass fuels. In a fluidized bed, two substances are distinguished: particles of a single solid bed material or mixture consisting of different solids, and a gas causing and sustaining bed fluidization and thus ensuring high-intensive heat and mass transfer in the bed volume. Much research studies have been addressed on firing biomass fuels with various types and sizes of bed materials depend on the designed geometry of the reactors and operating conditions [1–3]. To understand the behavior of the fluidization, computational fluid dynamics (CFD) plays an important role in modelling and design of fluidization systems, e.g., particle dispersion, fluidization behavior.

Typically, accurate results can be attained when the model has been validated against the experimental results. Abundant research have been recently conducted with different aims in different design circumstances [4–10]. Rajeswari et al. [4] proves that the CFD is an effective tool to simulate and examine their fluidized bed air jet mill. The numerical results are found to be coincide with the experimental results, with the acceptable error of 9–21% depends on the input variables and simulation conditions. Peng et al. [5] used DEM model to

simulate the experiment of Müller et al. [6]. The simulation results are found in good agreement with the experimental results and can be used for prediction of velocity and granular temperatures in the bubbling fluidized bed. Parker et al. [7] studied on flow behavior of pharmaceutical fluidized bed processors (bubbling and spouting modes) at three scales by comparing experimental results with CFD simulation results. The numerical method and simulation approach were found to successfully predict the flow behavior of several different sizes of fluidized beds based solely on material properties, processor loading, inlet air flow rate and fluidized bed process geometry. Wang et al. [8] simulated flow behavior of particles in an inverse liquid–solid fluidized bed compared with the experimental results of Renganathan and Krishnaiah [9]. Simulations indicate that axial velocities of particles and the bed expansion height are increased with an increase of liquid velocity. The effects of liquid viscosity and temperature on flow behavior of particles are generally scarce using CFD. The comparison shows that the Huilin–Gidaspow drag model can be used to capture flow behavior of liquid and solids phases in an inverse fluidized bed. Zhanga et al. [10] presented simulation results of Eulerian granular multiphase model on a three-dimensional (3D) hydrodynamics of a 150 MWe circulating fluidized bed (CFB) boiler for predicting the two-phase flow behavior. The solids vertical velocity is mainly positive in the center and negative near the wall. The study also state that the measurement of solid flux is difficult for experiments especially on a commercial CFB boiler, however it can be easily investigate by computer simulations.

Therefore this work was aimed to study on the hydrodynamics behavior of air-sand bed in a Twin Cyclonic Fluidized-bed Combustor (TFBC). The simulation model was validated with the experimental results. Effects from different excess air and the proportion of secondary air to primary air on the solid hold up of the bed material at the height of 0.45 m above the air distributor was the main focus of this study.



II. EXPERIMENTAL AND MODELING APPROACH

2.1. Experimental

2.1.1. Experimental set up

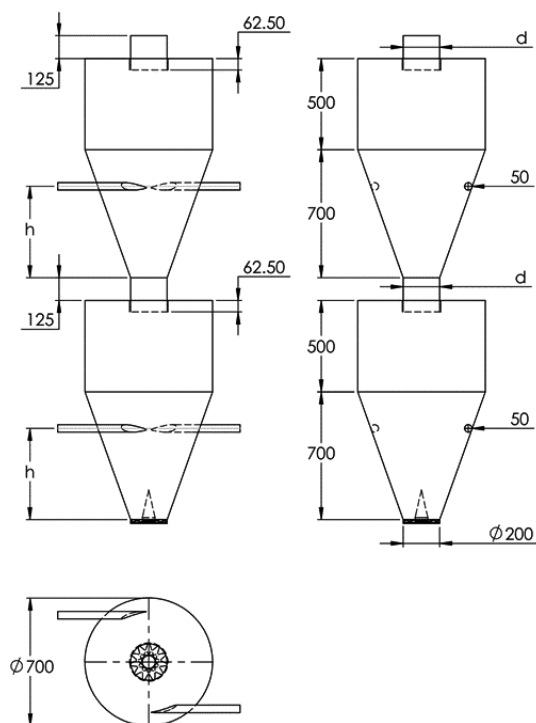


Fig.1 Layout of the Twin Cyclonic Fluidized-bed Combustor.

The cold-state experiment test was done in the twin cyclonic fluidized-bed combustor to verify the accuracy of the modeling predictions. Fig. 1 depicts the layout of the combustor with its equipment. The combustor consists of 2 main sections, lower section connected with upper section through the 0.25 m inner diameter pipe. Note that the lower

and the upper section have the same geometry, thus can be defined as “twin”, each section composes of 2 main parts: 1) conical module with inner diameter of 0.25 m at the bottom and 0.7 m inner diameter at the top of 1 m height and 40° cone angle and 2) cylindrical module of 0.7 m inner diameter of 0.5 m height. A 10 hp blower was used for supplying the air flow through the 0.1 m pipe at the bottom of lower conical module of the combustor before generated the fluidized bed by using an annular spiral air distributor. A 7.5 hp blower was used to provide tangential secondary air injection at the level of 0.5 m above the air distributor, via two pipes of 0.06 inner diameters that installed in the opposite side of the combustor (see Fig. 1). The air was controlled by globe valves installed at the discharge of each blower. The bed material that used in this experiment was silica sand of size ranges 300–500 μm with the solid density of 1700 kg/m^3 . The static bed height used in this study was fixed at 30 cm above the air distributor for all tests. Note that the density of silica sand used in this experiment was measured with ASTM E-873 standard.

2.1.2. Solid hold up

Fig. 2 illustrates the probe used for sampling the solid hold up of the bed material in the experiment and the selected radial sampling points of the combustor like in the modeling approach. As seen in Fig. 2a the apparatus has a box like shape made from acrylic, applied from the study of Chen et al., 2008. The solid hold up measurement probe has a total length of 100 cm separated eventually into 7 slots with the length of 7.14 cm, 2.2 cm height, 1.8 cm width, and the volume of each proportion of 28,280 mm^3 . The probe was designed into two parts, which the first part was composed of 7 rectangular frames as mentioned previously and the second part was the rectangular box designed to cover the rectangular frames. To measure the solid hold up for each condition in the experimental tests, the rectangular frame was inserted into the combustor in the radial direction, which the radial measuring points (r/R) were fixed at -1, -0.67, -0.33, 0, 0.33, 0.67, and 1 as shown in Fig. 2b.

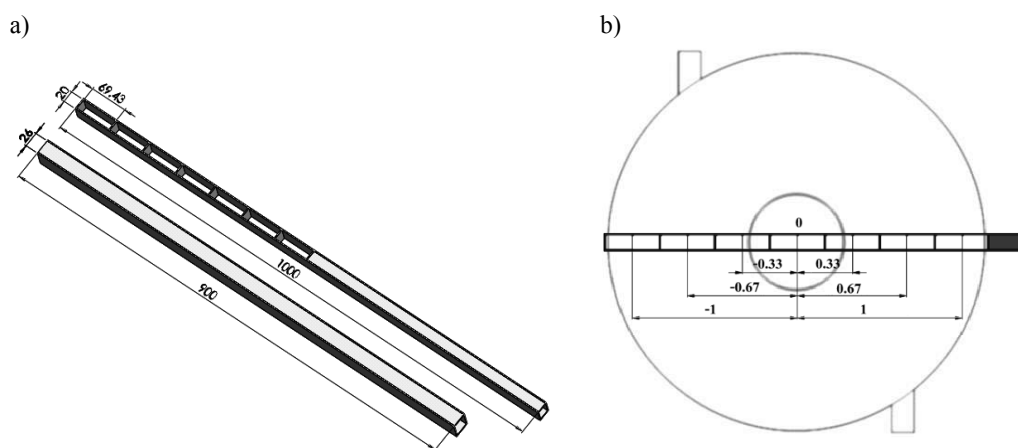


Fig.2 Probe used for sampling the solid hold up of the bed material a) and the radial sampling points selected in the experiment b).



Table 1. Properties of peanut shells used in experimental and simulation studies

Biomass Fuel	Ultimate analysis basis (wt% ., as-received basis)					Proximate analysis basis (wt% ., as-received basis)				LHV
	C	H	O	N	S	W	A	VM	FC	kJ/kg
Peanut shells	56.59	6.45	35.34	1.53	0.09	9.3	5.7	65.4	19.6	16,400

To compare between the experimental tests and computational simulation, the solid hold up experiments were conducted at excess air of 20, 40, 60, and 80% and at the proportion of secondary air to primary air at 0.1, 0.3, and 0.5 during the combustion test of TFBC. The solid hold up was calculated from the equation (1), during the test the solid hold up measurement probe was inserted into the combustor at the level 0.45 m above the air distributor. The measurement was done at least ten times for each operating conditions to ensure the repeatability of test results, which the average value was used as the presented data for analysis.

$$\varepsilon_i = \frac{m_i}{\rho_s V_i} \quad (1)$$

where m_i is the mass of sand in each slot of the probe (kg)

V_i is the volume of each slot (m³)

ρ_s is the density of silica sand (kg/m³)

2.2. MODELING

2.2.1. COMPUTATIONAL GEOMETRY

For computational simulation of an air–sand bed in a twin cyclonic fluidized bed that has a conical section of 0.7 m height with 40° cone angle. Computer programing “ANSYS version 15.0” was run by a computer, “Intel Core I7”, four cores, twelve threads, 2.5 GHz frequency, and 16 GB RAM. The grid was created in Tetrahedron shape with 53,397 nodes and 265,735 elements as shown in Fig.3.

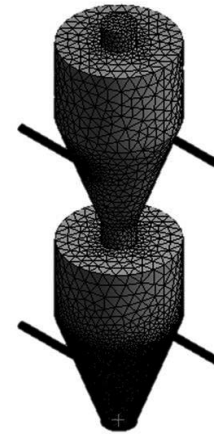


Fig.3 The computational model mesh used for simulation.

2.2.2. Calculated input parameters

In the computer programming the input parameters such as solid density of bed material, particle size of bed material, and density of air were used the same value as in the experimental conditions. However, the primary and secondary air inlet velocities were calculated by equation (2) and (3) as follows:

$$v_{inlet,primary} = \frac{Q_a}{A_p} \times (1 - S/T) \quad (2)$$

$$v_{inlet,secondary} = \frac{Q_a}{A_s} \times (S/T) \quad (3)$$

Table 2. The input variables of solid bed particle and gas/air for each simulation conditions

Variable	Value	
Particle diameter D_p , (m.)	0.004, 0.006, 0.0085	
Particle density ρ_s , (kg/m ³)	1700, 1660.66, 1640.26	
Gas density ρ_g , (kg/m ³)	1.225	
Gas viscosity μ_g , (kg/m-s)	1.789×10^{-5}	
Gas velocity v_g , (m/s)	Inlet primary	Inlet secondary
EA =20% (S/T =0, 0.1, 0.3, 0.5)	3.89, 3.50, 2.72, 1.94	0, 0.36, 1.08, 1.80
EA =40% (S/T =0, 0.1, 0.3, 0.5)	4.54, 4.08, 3.18, 2.27	0, 0.42, 1.26, 2.10
EA =60% (S/T =0, 0.1, 0.3, 0.5)	5.18, 4.67, 3.63, 2.59	0, 0.48, 1.44, 2.40
EA =80% (S/T =0, 0.1, 0.3, 0.5)	5.83, 5.25, 4.08, 2.92	0, 0.54, 1.62, 2.70



Table 3. Simulation conditions used in this study

Descriptions	Values
Granular viscosity	Gidspow [2,11]
Granular Bulk viscosity	Lun et al. [2,12]
Frictional viscosity	Schaeffer [2,13]
Angle of internal friction	20
Granular temperature	Algebraic
Drag law	Gidspow [2,11]
Coefficient of restitution for particle collisions	0.9
Inlet boundary condition	Velocity inlet
Outlet boundary condition	Pressure outlet
Wall boundary condition	No slip for air, specularity coefficient 0 for solid phase
Initial bed height	0.3 m
Initial volume fraction of solid phase	0.55
Convergence criteria	1×10^{-5}
Time step	1×10^{-3} s.

Where Q_a is the air volume flowrate (m^3/h), A_p is the crosssectional area of the air distributor (m^2) that equals 0.0096 m^2 , A_s is the crosssectional area of the secondary air injection pipe that equals 0.0026 m^2 and S/T is the proportional of secondary air to primary air injection. Q_a can be calculated by equation (4) as follows;

$$Q_a = \alpha V^0 FR \quad (4)$$

Where V^0 is theory required volume of air (m^3/kg fuel), FR is fuel feedrate (kg/h) that for this study is fixed at $20 \text{ kg}/\text{h}$, and α is excess air ratio ranged at $1.2, 1.4, 1.6$, and 1.8 , respectively. V^0 can be calculated by equation (5) as follows;

$$V^0 = 0.0889(C + 0.375S) + 0.265H - 0.033O \quad (5)$$

Where C, S, H, O are the carbon, sulphur, moisture content, and oxygen (wt. %, on as-received basis), respectively, as shown in Table 1.

Table 2 shows the input variables of solid bed particle and gas/air for each simulation conditions (various excess airs and secondary air to primary air proportions). The solid particle diameter and density were set for different three size ranges of the bed, however, the gas density and gas viscosity were set to be corresponded to the experimental tests at the fixed value of $1.225 \text{ kg}/\text{m}^3$ and $1.789 \times 10^{-5} \text{ kg}/\text{m}\cdot\text{s}$. The primary gas and secondary gas velocity for each case were also shown in Table 2. Table 3 depicts the simulation conditions settings for fluidized bed in this study. For the bed expansion, the data was collected every 5 minutes at the height of 0.35 m , 0.40 m , and 0.45 m above the air distributor with 7 radial positions at each height of $-1, -0.67, -0.33, 0, 0.33, 0.67, 1$, which the set of data were then average and used as the axial simulation results.

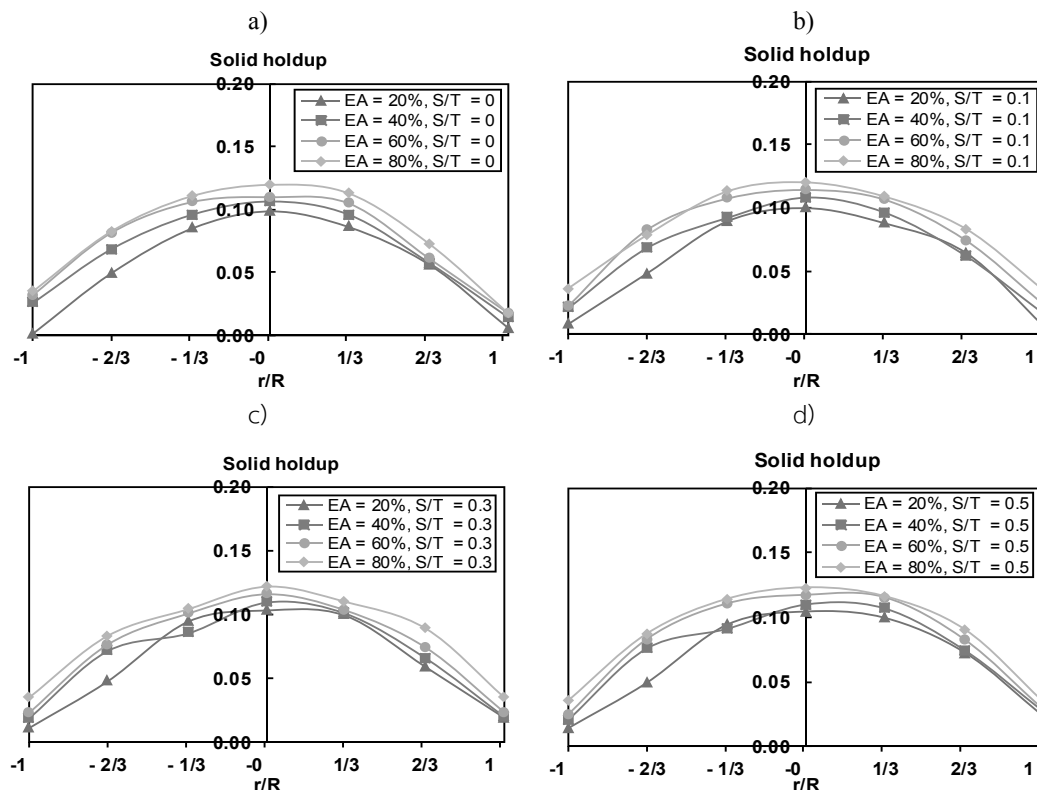


Fig. 4 The radial solid holdup profiles in TFBC at the height of 0.45 m above the air distributor used silica sand bed particle-size range $300\text{--}500 \mu\text{m}$ for various excess air (20–80%) and secondary to primary air ratio 0 a), 0.1 b), 0.3 c) and 0.5 d).

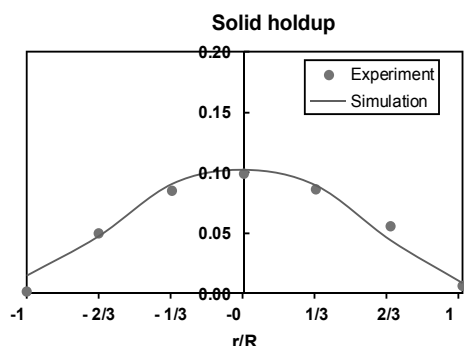


Fig. 5 Comparison between the experimental and simulation results in the radial direction of the combustor for excess air 20% at the height of 0.45 m above the air distributor.

III. Experimental and Simulation Results

3.1. Experimental results

Fig. 4 shows radial solid hold up profiles in TFBC at the height of 0.45 m above the air distributor used silica sand bed particle-size range 300–500 μm for various excess air (20–80%) and secondary to primary air ratio (0–0.5). At first glance, the maximum solid hold-up was found at the center of the combustor and decline along the direction away from the center for all operating conditions. With the increasing in excess air, the bed expansion increase as resulted to the higher solid hold-up of this measuring surface. There was no substantial effect on the solid hold-up when increasing secondary to primary air ratio as can be seen from the experimental results.

3.2. Simulation Model Validation

The simulation model validation was done by comparing solid hold up results from CFD (line) with the experimental results (dots) at excess air 20% without the injection of secondary air ($S/T = 0$) in the radial direction of the combustor at the height 0.45 m above the air distributor as shown in Fig. 5. As seen, both CFD and experimental results have the same trend with the maximum solid hold up at the center of the combustor and decrease consecutively from the center to the peripheral area. The simulation results are found in good agreement with the experimental results and therefore will be used for solid hold up prediction for future studies.

Fig.6 illustrates the comparison graph of solid hold up results from simulation and from the experiment at the center of the combustor used silica sand bed particle-size range 300–500 μm for various excess airs from 20 to 80%. It can be seen

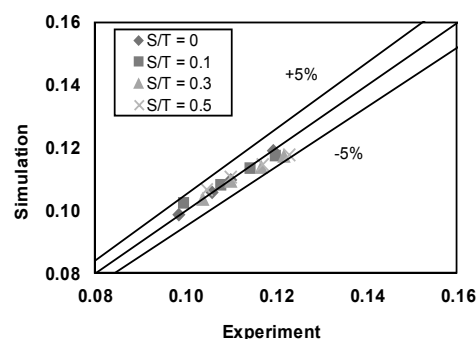


Fig. 6 Comparison of solid hold up between experimental and simulation results at the center of the combustor used silica sand bed particle-size range 300–500 μm for various excess airs from 20 to 80%.

that the simulation results has been confirmed to agree well with the experimental results with in the error band of $\pm 5\%$, the comparison result from this study is corresponded with the study of Rajeswari et al. [4] that the solid hold up result from simulation has slightly higher value than from the experimental, however, in the acceptable error band.

IV. CONCLUSIONS

The hydrodynamics behavior of air-sand bed has been successfully done in a Twin Cyclonic Fluidized-bed Combustor. From the analysis of both experimental and computational simulation results, excess air has higher impact on the bed expansion of the fluidized bed compared to secondary air to primary air ratio. With the increasing in excess air, the bed expansion increase as resulted to the higher solid hold-up of this measuring surface. The results from computational simulation are agreed well with the experimental results.

ACKNOWLEDGMENTS

The authors wish to acknowledge financial supports from Department of Mechanical Engineering, Faculty of Engineering and Industrial Technology, Silpakorn University.

REFERENCES

- [1] R. Kaewklum, V. I. Kuprianov, P. L. Douglas, "Hydrodynamics of air-sand flow in a conical swirling fluidized bed: A comparative study between tangential and axial air entries," *Energy Conversion and Management*, Vol. 50, Issue 12, pp. 2999-3006, 2009.
- [2] V.I. Kuprianov, and P. Arromdee, "Combustion of peanut and tamarind shells in a conical fluidized-bed combustor: a comparative study," *Bioresource Technology*, Vol. 140, pp. 199–210, 2013.
- [3] V.I. Kouprianov, and W. Permchart, "Emission from a conical FBC fired with a biomass fuel," *Applied Energy*, Vol. 74, pp. 383–392, 2003.
- [4] M. S. R. Rajeswari, K. A. M. Azizli, S. F. S. Hashim, M. K. Abdullah, M. A. Mujeebu, M. Z. Abdullah, "CFD simulation and experimental analysis of flow dynamics and grinding performance of opposed fluidized bed air jet mill," *Int. J. Miner. Process.* 98, pp. 94–105, 2011.
- [5] W. Peng, Y. He and T. Wang, "Granular temperature with discrete element method simulation in a bubbling fluidized bed," *Powder Technol.* 25, pp. 896–903, 2014.
- [6] C. R. Müller, D. J. Holland, A. J. Sederman, S. A. Scott, J. S. Dennis and L. F. Gladden, "Granular temperature: comparison of magnetic resonance measurements with discrete element model simulations," *Powder Technol.* 184, pp. 241–253, 2008.
- [7] J. Parker, K. LaMarche, W. Chen, K. Williams, H. Stamato, and S. Thibault, "CFD simulations for prediction of scaling effects in pharmaceutical fluidized bed processors at three scales," *Powder Technol.* 235, pp. 115–120, 2013.
- [8] B. Wang, and A. B. Yu, "Numerical study of particle–fluid flow in hydrocyclones with different body dimensions," *Minerals Engineering* 19, pp. 1022–1033, 2006.
- [9] T. Renganathan, and K. Krishnaiah, "Voidage characteristics and prediction of bed expansion in liquid–solid inverse fluidized bed," *Chem. Eng. Sci.* 60, pp. 2545–2555, 2005.
- [10] N. Zhang, B. Lu, W. Wang, and J. Li, "3D CFD simulation of hydrodynamics of a 150 MWe circulating fluidized bed boiler," *Chem. Eng. J.* 162, pp. 821–828, 2010.
- [11] M. Syamlal, W. Rogers, T.J. O’Brain, *MFIX Documentation: Volume 1, Theory Guide*, National Technical Information Services, Springfield. 1993.
- [12] L. C. Gómez and F. E. Milioli, "Numerical study on the influence of various physical parameters over the gas-solid two-phase flow in the 2D riser of a circulating fluidized bed," *Powder Technol.* Vol. 132, pp. 216–225, 2003.
- [13] D. G. Schaeffer, "Instability in the evolution equations describing incompressible granular flow," *J Differ.* Vol. 66, pp. 19–50, 1987.



Energy Consumption Evaluated of Compact Solar Drying Chamber

Sivapong Phetsong*, Vichuda Mettanant
Department of Mechanical Engineering
Silpakorn University
Nakhon Pathom, Thailand
E-mail: phetsong_s@su.ac.th

Asst.Prof.Dr.-Ing. Nantawatana Weerayuth
Department of Mechanical Engineering
Ubon Ratchathani University
Ubonratchathani, Thailand
Email: weerayuth_gm@hotmail.com

Abstract— This research study about solar drying chamber design. In this design, it contains flat plate solar collector which used to heat air temperature, and use DC fan with damper to control air temperature by using microcontroller. Microcontroller consist with software to control fan speed and damper angle to control ratio of mixing air lead to target temperature. In the experiment with target temperature at 42 °Celsius. The first experiment with fix mixing ratio and vary air flow rate. We founded that the system required average power 1.39 W at control temperature 50 °Celsius, average power 1.95 W at 45 °Celsius and average power 8.46 W at 42 °Celsius. The second experiment with varying mixing ratio and fix air flow rate. We founded that in every control temperature, required average power 1.89 W. And the last experiment with varying both of mixing ratio and air flow rate. We founded that the system required average power 1.81 W at 50 °Celsius, required average power 2.01 W at 45 °Celsius and average power 3.20 W at 42 °Celsius.

Keywords— Solar Drying Chamber; Temperature Control; Microcontroller

I. INTRODUCTION

Fruit is a major export product of Thailand every year. Every year, Thailand has exported several fruits and vegetables in various forms, such as fresh product, chilled and frozen product or even processed products. Even, Thailand can sell or export them in every season all year but several fruits have to be preserved to make them available in the whole year because of the high demand and supply in some season and the uncertainty of the market price. In this research, we focus on the banana, which is the favorite fruit in every household in Thailand. Because of the countryside Thai lifestyle. The people can use almost of all parts of banana tree in the household and it is also easy to grow up. People can use it as the direct product or use it as indirect product. For example, banana leaf can use to directly packed food or prepare cooked food. And we can use parts of banana tree as a rope. Banana can be plant around Thailand and the farmer can get the fruit product throughout the year. The problem of the fresh banana is the shelf life. It has a very short shelf life. After a couple day, it become soft and black, then it cannot be on the shelf anymore. To make longer shelf life, the banana product need to be process before sent it out from farm. The drying process is the easiest way to preserve product and

also the cheapest way to investment. The longer drying time, the longer storage time.

In the past, people placed the product on the container and place it direct the sunlight. Heat from sunlight will cause the water evaporate from the product. With this traditional method, there are several problems, such as problem from dust, insects and animals, problem from temperature. Farmer cannot control the target temperature that is suitable for products. The temperature depended on the sunlight. On the sunny day in summer, the temperature may be too high and damage all drying product. In The rainy season, it may be more time to dry. To solve these problems, we change to the solar oven system with the temperature control unit. [1][2] Microcontroller has been used to control temperature inside the oven. This system contains two system modules; the first module is the solar collector to preheat the air into the oven. The second module is the oven with air mixing chamber to control temperature at the inlet port with the controllable ventilation fan. [3][4]

This work is the successive work from the prior controllable drying chamber. In the past, drying chamber is a very long and hard to move to the different location, especially in farm without electric power. In this models, the drying chamber has been modified to become more compact and easy to move. [5]

II. SYSTEM DESIGN

The designing of drying chamber has been split into three main parts as shown in figure 1, the first part is the solar collector, the second part is the oven and the third part is the control module. These all modules must be fit in the compact size and easy to move. Flow direction has been shown in figure 2.

The drying chamber has been designed with the flat plate solar collector on the top. Solar collector has the 0.80x 1.20 sq. meter dimensions and cover with the 3mm clear glass on top. It contains guide to make the air flow in the designed direction. The chamber has 0.60x0.60x0.55 cubic meter dimensions and cover with 5 mm thick insulation shield. The chamber is place under the solar collector and it has three inlet port on the top with small damper. These damper is controlled by servo motor to set opening angle of inlet-port, figure 3. At the bottom of chamber, Small DC fan has been installed to make the flow pass through





the chamber from the top to bottom. In this design, we used 3 small DC fan to make energy efficient and reduce side flow effect. [6]

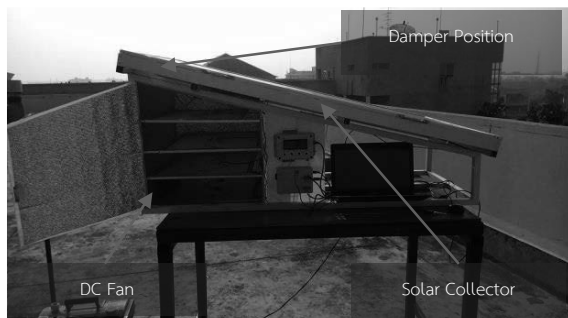


Fig. 1. Solar drying chamber structure

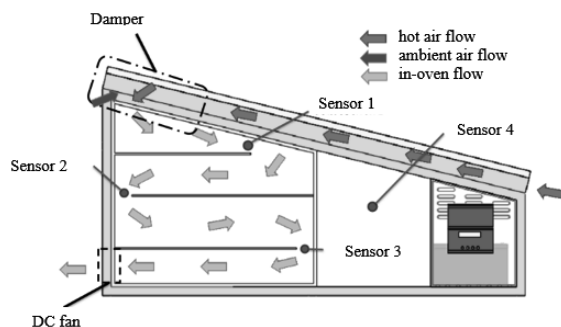


Fig. 2. Flow direction in solar collector and chamber

The last part is the microcontroller unit which we used Arduino Nano to handle all task of the modules control in figure 4. And we also installed the power measurement module to calculate real-time energy consumption by all components in drying chamber. [7]



Fig. 3. Damper install position

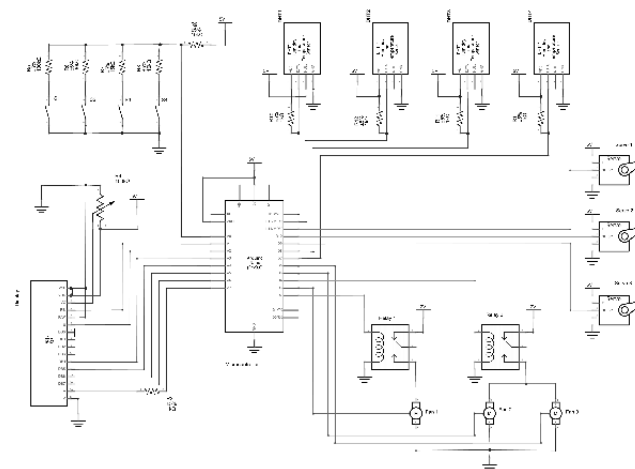


Fig. 4. Schematic of controller module

III. EXPERIMENTS AND SETUP

From our design, we have some experiment to test the drying result and energy consumption. We setup an experiments to control drying chamber temperature to 42 °Celsius along the daytime. In the first experiments, we founded that the energy from sunlight is vary in the morning and afternoon. Then we decide to split the experiments period from 08.00 - 16.00 to be 3 periods. The first period is between 08.00-11.30. in this period, sunlight is enough to preheat air temperature in some sunny day. The second period is between 11.30-13.30. In this period, sunlight is different from the first period. Solar collector can heat air to higher temperature. And the third period is between 13.30-16.00. normally, in this period. Sunlight has more energy than the earlier but in our experiments time, it is always rain in this period of time, even it was a sunny day in the morning.

The first experiment, System has been set up by fix mixing ratio rate between hot and cold air and vary air flow rate by controlling the ventilation fan. In this experiment, we set the mixing ratio for the period one to 100 percent hot air. The second period, air mixing ratio will be 50% hot air and 50% ambient air. The third period at 13.30-16.00, mixing ratio will be 70% hot air and 30% ambient air.

The second experiment, System has been setup by varying the damper position to vary mixing ratio and fix air flow rate to desired speed. In the first period, flow rate has been set to 0.021m³/s (43.7 CFM). The second period, flow rate has been set to 0.030 m³/s (64.1 CFM) and the third period, flow rate has been set to 0.053 m³/s (111.4 CFM)

The third experiment, System has been setup by vary both of damper angle and air flow rate.

In all experiments, Microcontroller read temperature by using DHT22 Sensor and also monitor the temperature in various position in chamber by using DS18B20 sensor. DC Power required by the system is also recorded and calculated to energy consumption in every 15 minutes' interval. [8][9]

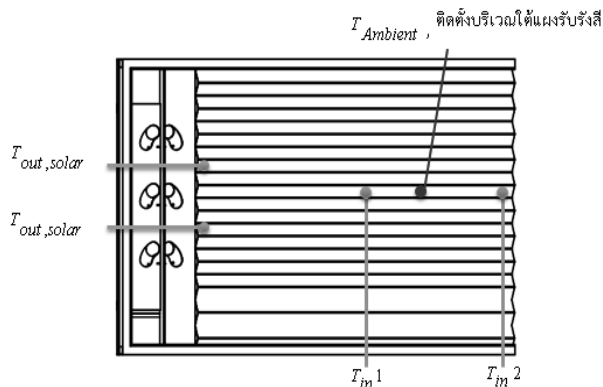


Fig. 5. Temperature sensor position at solar collector surface

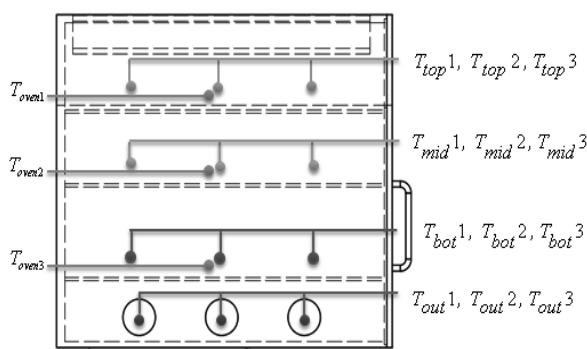


Fig. 6. DS18B20 Sensor position in the drying chamber

Microcontroller has been program to read temperature from various position as shown in figure 5 and figure 6, then average temperature to estimate the overall temperature. Microcontroller use temperature data to decide what to do with fan speed and damper position. In the same time, all data has been recorded to SD Card for future use. [10]

IV. RESULT

The result from experiment can separate into three cases by the experiment setup, constant mixing ratio vary flow rate, vary mixing ratio constant flow rate and vary both of mixing ratio and flow rate

A. Constant mixing ratio and vary flow rate

From the first setup at 42 °Celsius set point. The result of average temperature inside chamber and time can be describe from figure 7 and figure 8. It shown that the temperature inside the chamber is almost constant all the time. When air temperature from solar collector increase, fan speed has been raised and consume more power. When air temperature decrease, fan speed is also slow down and consume less energy. The average power consumption in the system is approx. 8.46 W. In the other experiment shown that the system required 1.95 W at 45 °Celsius set point and 1.39 W at 50 °Celsius set point.

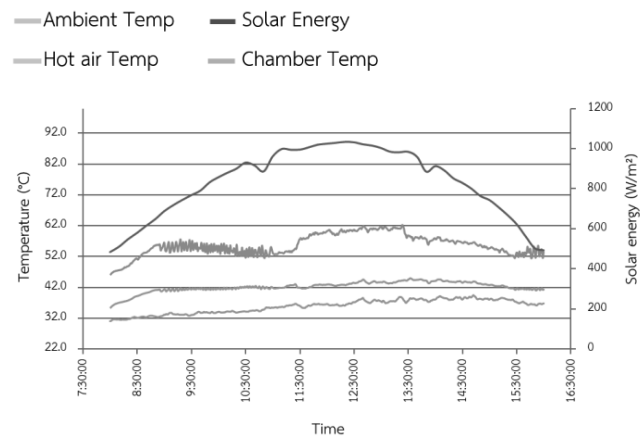


Fig. 7 Relation of temperature at various position, constant mixing ratio vary flow rate (42 °Celsius)

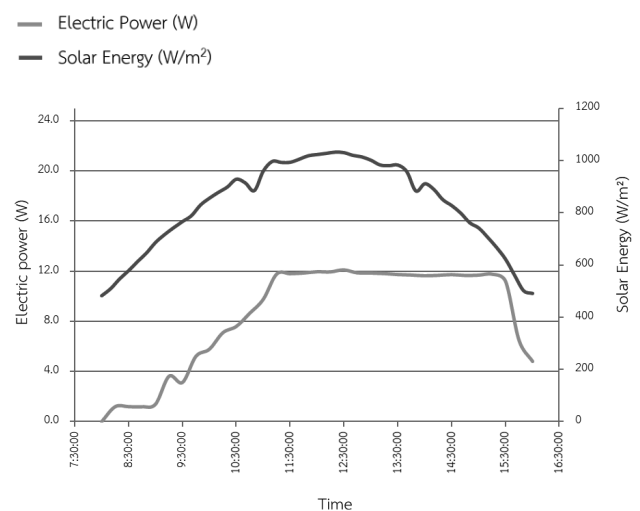


Fig. 8. Relation of electric power and solar energy for constant mixing ratio vary flow rate (42 °Celsius)

B. Vary mixing ratio and constant flow rate

From the second setup at 42 °Celsius set point. The result has shown in figure 9 and figure 10. Temperature in the chamber for the whole process is constant at 42 °Celsius. Even the hot air temperature increase by sun light but damper can control volume of hot air. The inlet air temperature has been control to set point temperature all the time. The average electric power consumption is constant at 1.94 W for 42 °Celsius set point. For other set point temperature, the result is shown only a few power different.

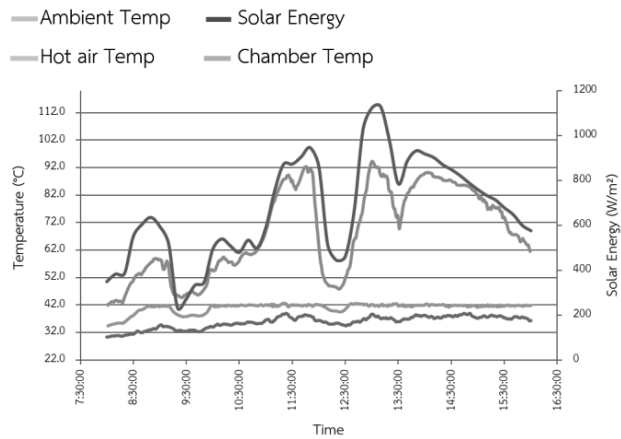


Fig. 9. Relation of temperature at various position, vary mixing ratio constant flow rate (42 °Celsius)

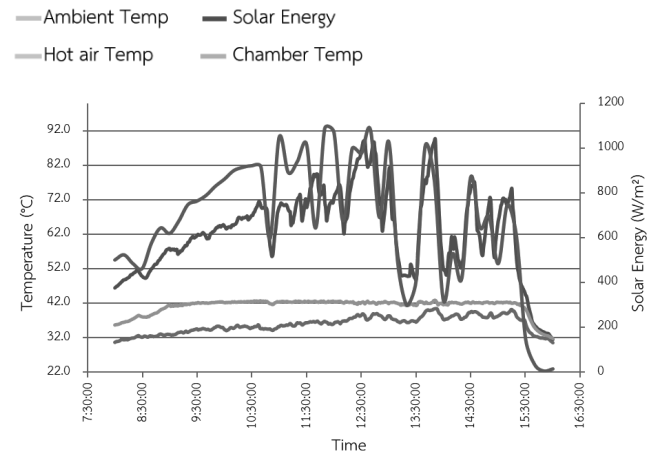


Fig. 11. Relation of temperature at various position, vary mixing ratio and flow rate (42 °Celsius)

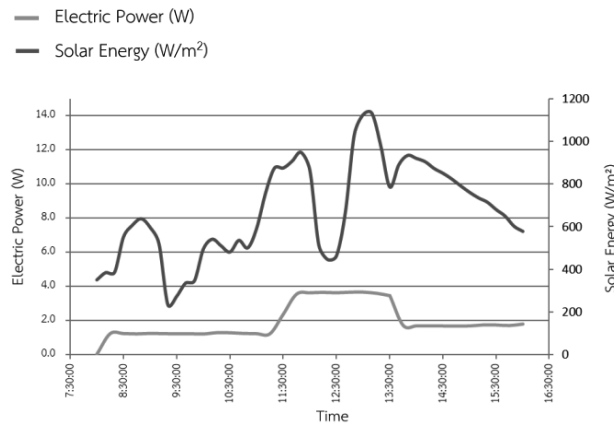


Fig. 10. Relation of electric power and solar energy for vary mixing ratio constant flow rate (42 °Celsius)

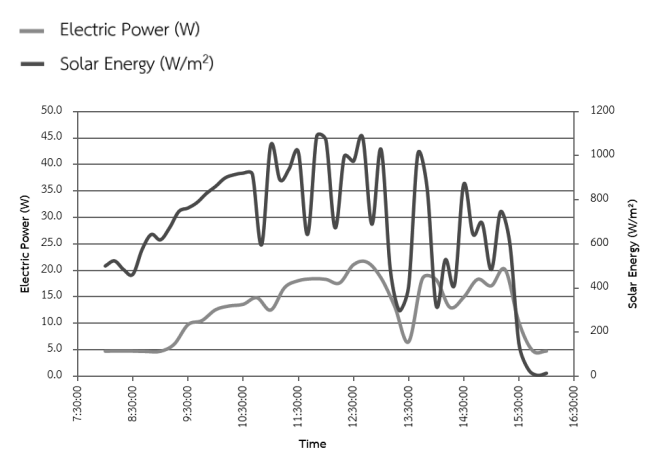


Fig. 12. Relation of electric power and solar energy, vary mixing ratio and flow rate (42 °Celsius)

C. Vary both of mixing ratio and constant flow rate

In last setup at 42 °Celsius set point, both of mixing ratio and flow rate can be vary. The result in figure 11 and figure 12 has shown that the temperature in the chamber is constant. When the system detects the different temperature in chamber and set point, it will first try to vary damper angle then flow rate. In this software algorithm, it tries to vary both parameter in every calculation step. The average power consumption is 3.20 W. For the 45 °Celsius set point, power consumption is 2.01 W and it became 1.81 W at 50 °Celsius set point.

V. DISCUSSION AND CONCLUSION

From the experiment results, both of varying mixing ratio or varying air flow rate affected to the chamber temperature. The temperature is in range with some error because of the software offset setting. Most of the electric power require for driving DC fan. It reflects to the most energy consume component. In the first and last experiments, System have to drive DC fan to full power to blow hot air out of chamber. These consume more energy. Especially in the low temperature set point, system has to drive fan to full speed all the time. Compare with 50 °Celsius set point, system required slower fan speed. Then it need less power. In the second experiment, damper which required a few electric power, control air temperature from input by mixing hot and cold air together. The input temperature is at the set point in the first stage or a little bit different (in the last experiment).



System don't need to run DC fan to full speed. It just keeps low fan speed that enough for ventilated.

In the conclusion, it is very important to keep DC fan running at low speed. And the last experiment show that the system still required optimization to make it consume lowest power as possible. Then, it required smallest solar panel to product electricity for the whole system.

VI. REFERENCE

- [1] S. VijayaVenkataRaman, S. Iniyan, and Ranko Goic, "A review of Solar drying technologies", *Renewable and sustainable energy reviews*, vol. 16, pp. 2652-2670, 2012.
- [2] K.S. Jairaj, S.P. Singh, and K. Srikant, "A review of solar dryers developed for grape drying", *Solar Energy*, vol. 83, pp. 1698-1712, 2009.
- [3] Andre Guimaraes Ferreira, et al, "Solar drying of a solid waste from steel wire industry", *Applied thermal engineering*, vol. 73, pp. 102-108, 2014.
- [4] Pei-Wen Li, Peter Kane, and Matthew Mokler, "Modeling of solar tracking for giant Fresnel lens solar stoves", *Solar Energy*, vol. 96, pp. 263-273, 2013.
- [5] Sivapong Phetsong, "Development of Temperature Controlling system in drying chamber by mixing air inlet", *The Mahasarakham University Journal of Science and Technology*, Vol 32, No 1, pp. 101-105, Jan-Feb 2013.
- [6] Jacek Smolka, Zbigniew Bulinki, and Andrzej J. Nowak, "The experimental validation of a CFD model for a heating oven with natural air circulation", *Applied Thermal Engineering*, vol. 54, pp. 387-398, 2013.
- [7] Pieter Verboven et al., "Computational fluid dynamics modelling and validation of the isothermal airflow in a forced convection oven", *Journal of food engineering*, vol. 43, pp. 41-53, 2000.
- [8] Herliyani Suhartta, K. Abdullah, and A. Sayigh, "The Solar Oven: Development and field-testing of user-made designs in Indonesia", *Solar energy*, vol. 64, No4-6, pp. 121-132, 1998.
- [9] Seyfi Sevik, "Design, experimental investigation and analysis of a solar drying system", *Energy Conversion and Management*, vol. 68, pp. 227-234, 2013.
- [10] S.Prakash, S.K. Jha and N. Datta, "Performance evaluation of blanched carrots dried by three different driers", *Journal of Food Engineering*, vol. 62, pp. 305-313, 2004.



Study of Cooling of Compressors in Underground Wells

Boonrueang Ponil*, Taweesak Taweewithyakarn and
Pracha Yeunyongkul
Faculty of Engineering, Rajamangala University of
Technology Lanna
Chiang Mai 50300, Thailand

*Corresponding author: rueng_opj@hotmail.com

Ronnachart Munsin¹
College of Integrated Science and Technology
Rajamangala University of Technology Lanna
Chiang Mai, 50220, Thailand

Abstract— The aim of this study is to investigate the cooling of oil compressor of the wellhead drilling rig. The Simulation model was established by using Computational Fluid Dynamics (CFD) and compared with the experimental results by collecting actual data from actual testing while drilling underground wells. Parameters, oil and air temperatures, oil and air flow rates were collected from actual testing and then the parameters were inputted into the simulation model. Flow behavior, heat transfer rate and effectiveness of cooling unit were determined by the simulation model and compared with the experimental results. The experiment was divided to three depth range: 40, 80 and 120 m, respectively. Each depth range was obtained air mass flow rate of 1.41, 1.59 and 1.77 kg/s, respectively. The experimental result showed that heat transfer rate with the depth range of 40, 80 and 120 m were 49.1, 60.4 and 65.2 kW, respectively. While the effectiveness of the cooling unit with the depth range of 40, 80 and 120 m were 0.53, 0.55 and 0.57, respectively. Moreover, it was found that maximum of heat transfer rate and effective ness occurred with the depth range of 120 m.

I. INTRODUCTION

The world population is increasing every year. Water resources are limited, resulting in a shortage of water for everyday consumption. Now, this is a matter that many countries deem very important. Water is an important factor in human life and is one of the economic drivers of water use, whether in agriculture sector or industrial sector. Groundwater is therefore a vital water source for living, especially when other water sources are not adequate. It is also an alternative water source for industrial and agricultural development in the country. Drilling wells is an option for water use as to address the shortage of water during the drought. Therefore, groundwater drilling is a specialized profession that requires many fields of study. It consists of academic, engineering, geological and scientific fields [1]. There are many ways to use groundwater wells, but there are three popular approaches: impact drilling, pneumatic drilling and rotary drilling. There are two types of rotary drilling: straight drilling and reverse drilling. For the drilling machine of the Chiangmai Provincial Administrative Organization, a rotary drilling machine is used and mixed with pneumatic drill. This type of drilling machine

can be drilled well in hard rock and drilling is quick and when penetrated to the water layer, it will be known immediately, because the wind will come out blowing. Drilling capacity of underground drilling machine of Chiangmai Provincial Administrative Organization Can drill up to 300 meters deep [2]. For the drilling of underground wells of the Chiangmai Provincial Administrative Organization, compressor type double screw compressor will be used. This is a very important tool for hard rock drilling and the aerator can also be used to develop a well. Inside the compressor is oil for lubrication and cooling of the screw sets. In the conditions where the compressor is drilling for groundwater of oil temperature, screw set it is very high for the oil to flow for cooling off. But sometimes in deep wells, the compressor must work continuously for several hours, causing the oil to heat up and becomes defective. The important thing is that it shortens service life, resulting in the leakage of high-temperature and high-pressure oil until the combustion in the compressor room occurs, causing damage to the system several times. As a result, the cost of maintenance is high as well. So to solve such problems that might happen again, especially in the summer, where the outside air temperature is about 40 °C. It is necessary to study the cooling of the compressor in the pit well as to reduce the temperature of the oil so it is not too high when the compressor is continuously hard working while using compressed air to drill hard rock. For the reasons mentioned above, this study investigates the cooling of the compressor in the wellhead drilling rig. But the main problem of the research in the experimental part was that it required a relatively high budget to design and build an oil-immersed simulator for real-world measurement. So to reduce the cost of the experiment, researchers are interested in studying, Computational Fluid Dynamics (CFD) to simulate the heat transfer characteristics of air which will help us know the effectiveness of the actual cooling unit. Then, this model is used to improve the heat dissipation for the compressor oil heat pipe.



II. MODELING THEORETICAL FRAMEWORK AND METHODOLOGY

Modeling of cooling equipment for compressors used with compressors is the calculation of algebraic fluid dynamics. Computational fluid dynamics (CFD) uses computer to analyze fluid behavior in workpieces by numerical method to solve the equation. Other equations are used to solve problems simultaneously under initial conditions and boundary conditions. The analysis of the results and the display of the solution are in various forms as needed.[3]

A. Research Theory

1) Governing equations

Considering the surface, surface, speed, and heat-sensitive layers. The assumptions are as follows:[4]

- 1) Fluid flow and heat transfer under steady state 3D
- 2) The fluid flow is turbulent.
- 3) Unstable fluid and stable physics.
- 4) Do not consider cooling due to viscosity.
- 5) Do not consider heat radiation and heat conduction due to thin pipes.
- 6) Do not consider heat loss.
- 7) No surface slip

B. Theoretical framework

From the above assumptions, the flow equation with the fins is given which are Mass Conservation Equation or Continuum Equation, Navier-Stok equation and energy equations. The three equations can be written as follows:[4]

1) Mass conservation equation or Continuity equation

The equation derived from the mass balance equation of the control volume according to the mass preservation rule. Conservation of mass, which describes the rate of mass change within the control volume. It must be equal to the difference in the flow of the incoming mass and the volume control can be written in the equation as follows:[5]

$$\frac{\partial \rho}{\partial t} + \left[\frac{\partial(\rho u)}{\partial x} + \frac{\partial(\rho v)}{\partial y} + \frac{\partial(\rho w)}{\partial z} \right] = 0 \quad (1)$$

or write in the vector as.

$$\frac{\partial \rho}{\partial t} = \nabla \cdot (\rho \vec{V}) = 0 \quad (2)$$

$$\text{or} \quad \frac{\partial \rho}{\partial t} = \rho \cdot (\nabla \cdot \vec{V}) = 0 \quad (3)$$

Where ρ is the density of the fluid (kg/m³)

t is the time (s)

u is the speed in the axis x (m/s)

v is the speed in the axis y (m/s)

w is the speed in the axis z (m/s)

\vec{V} is the flow velocity vector (m/s)

2) Momentum equation

It is the equation that describes the sum of all forces acting on the surface. The control volume must be equal to the sum of the rate of change of momentum within the control volume. (Net outflow of momentum). This can be written in the equation as follows:[5]

$$\frac{\partial(\rho u)}{\partial t} + \nabla \cdot (\rho \vec{V} u) = -\frac{\partial p}{\partial x} + \frac{\partial \tau_{xx}}{\partial x} + \frac{\partial \tau_{xy}}{\partial y} + \frac{\partial \tau_{xz}}{\partial z} + \rho f_x \quad (4)$$

$$\frac{\partial(\rho v)}{\partial t} + \nabla \cdot (\rho \vec{V} v) = -\frac{\partial p}{\partial y} + \frac{\partial \tau_{xy}}{\partial x} + \frac{\partial \tau_{yy}}{\partial y} + \frac{\partial \tau_{yz}}{\partial z} + \rho f_y \quad (5)$$

$$\frac{\partial(\rho w)}{\partial t} + \nabla \cdot (\rho \vec{V} w) = -\frac{\partial p}{\partial z} + \frac{\partial \tau_{xz}}{\partial x} + \frac{\partial \tau_{yz}}{\partial y} + \frac{\partial \tau_{zz}}{\partial z} + \rho f_z \quad (6)$$

Where τ is the shear stress (N/m²)

f is the force caused by the weight of the fluid (N)

p is the pressure of the fluid (N/m²)

3) Energy equation

The rate of change of energy within a mass is equal to the amount of heat given to the total mass and the rate of work due to various forces acting on the mass. This can be written in the equation as follows:[5]

$$\begin{aligned} & \frac{\partial}{\partial t} \left[\rho \left(e + \frac{V^2}{2} \right) \right] + \nabla \cdot \left[\rho \left(e + \frac{V^2}{2} \right) \vec{V} \right] \\ &= \rho q^* + \frac{\partial}{\partial x} \left(k \frac{\partial T}{\partial x} \right) + \frac{\partial}{\partial y} \left(k \frac{\partial T}{\partial y} \right) + \frac{\partial}{\partial z} \left(k \frac{\partial T}{\partial z} \right) \\ &+ \frac{\partial(u\tau_{yx})}{\partial y} + \frac{\partial(u\tau_{zx})}{\partial z} + \frac{\partial(v\tau_{xy})}{\partial x} + \frac{\partial(v\tau_{zy})}{\partial y} \\ &+ \frac{\partial(w\tau_{xz})}{\partial x} + \frac{\partial(w\tau_{yz})}{\partial y} + \frac{\partial(w\tau_{zx})}{\partial z} + \rho fV \quad (7) \end{aligned}$$

Where e is the internal energy (J)

q^* is the heat transfer rate per unit area (W/m²)

k is the thermal conductivity coefficient (W/m²K)

T is the temperature (°K)



4) Heat transfer equation of heat exchanger

The heat transfer rate equation is based on the difference between the temperature of the fluid and the surface of the material flowing through it and the convection coefficient of fluid flowing through the surface of the material according to the Newton's law of cooling:[6,7]

$$Q_{conv}^{\bullet} = hA_s(T - T_s) \quad (8)$$

Where Q_{conv}^{\bullet} is the heat transfer rate using convection (W)

h is the convection coefficient (W/m².°K)

A_s is the surface area of the material in contact with the fluid (m²)

T_{∞} is the surface temperature of the material (°K)

T_{∞} is the temperature of the fluid is far from the surface (°K)

$(T_s - T_{\infty})$ is the difference in temperature between the fluid and the material surface where the fluid flows (°K)

The efficiency of the heat exchanger is the ratio between the actual heat transfer rate (Q_{actual}) and the maximum heat transfer rate (Q_{max})

$$\varepsilon = \frac{Q_{actual}}{Q_{max}} \quad (16)$$

Where $Q_{max} = C_{min}(T_{o,in} - T_{a,in})$ (17)

$$Q_{actual} = C(T_{o,in} - T_{o,out}) \quad (18)$$

C. Research Methodology

The research was carried out by experimental method of modelling and by determining the relationship of the convection heat exchanger set of compressor screw sets of drilling wells such as air inlet and outlet, oil temperature in and out the flow of oil and air, as shown in Fig. 1. Diagram of the test kit consists compressed air and heat meters of 5 sets of heat meters and 5 sets of air velocity sensors which are installed as shown in Fig. 2. The heat and air velocity measuring tool consist of two main components: part 1) the hardware has Encoder, Thermocouple, Arduino and 7 Segment display monitor. The end of the Encoder is attached to the rotor as to get the wind from the rotor and thermocouple attached to the position is used to measure: part 2) is the software used in the program Microcontroller. This instrument uses the Arduino software to program the readings from the encoder and the thermocouple while the Microcontroller reads

from the encoder and the thermocouple sends the display to the 7 segment display monitor and sends the data to the Internet using 3G.

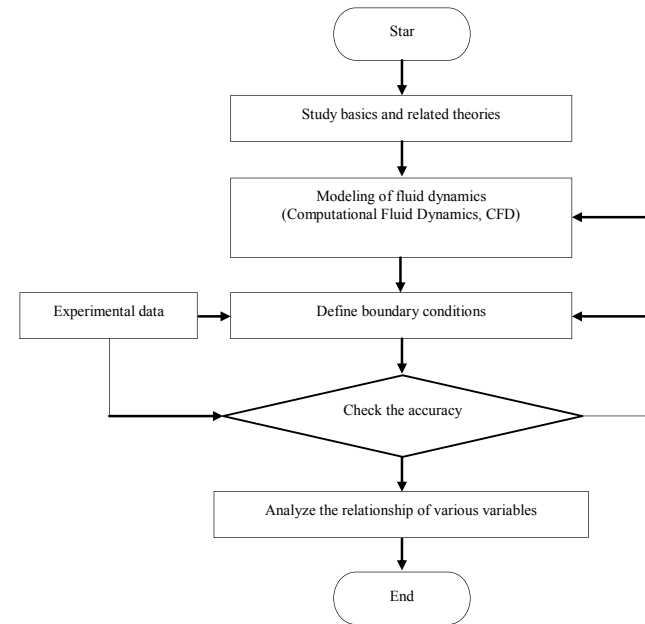


Fig. 1. Principles of modeling of ventilation equipment used with compressors.[5]

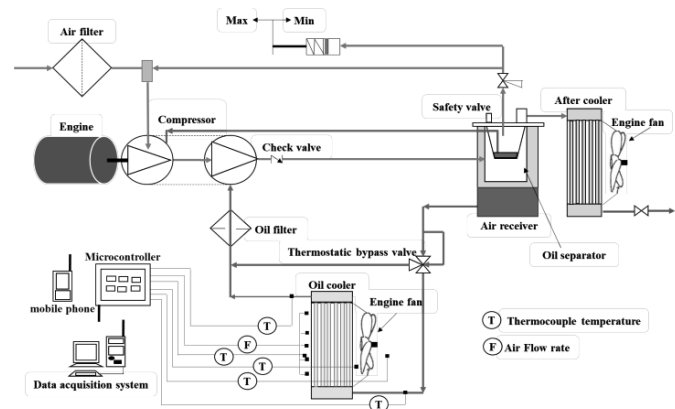
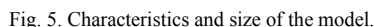
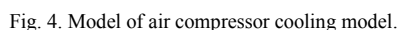


Fig. 2. shows the Schematic diagram of the screw compressor of the wellhead drilling rig.

CFD is a simulation of liquid-based systems engineering using modelling and numerical methods to solve this fluid flow problem, Solid Works Program for modelling. The procedure is shown in Fig. 3. In the heat transfer simulation modelling of the screw assembly, the compressor will use the Solid works program in the simulated design. The size and shape are similar to the compressed air cooling unit that were actually used. The size of the model is as shown in Fig. 4-6.



in Fig. 5. Part 2) Tube and fin are made of aluminum. Inside the tube is an oil for lubrication screw compressor assembly for cooling heat to the flowing air.

For simulating the cooling system, the screw compressor unit of the compressor for drilling wells in this rock layer used the results of the actual test of the values of the variables as shown in Table I. in order to determine boundary condition in the solid works flow simulation program for analysis of the correlation coefficient. We are interested in studying to solve the problem of fluid flow of the system.

TABLE I. Variables derived from the real test

For the flow direction of the air and the oil flowing to the exchanger heat of the cooling system, the lubricant of the screw compressor assembly of the compressor for the drilling of the well is shown in Fig. 6. In simulating the fluid flow, the air velocity is between 1.41-1.77 kg/s at 30-35 °C and the oil flow rate is between of 0.81-1.00 kg/s at 85-89 °C. The depth of drilling wells is between 40-120 m.



III. RESEARCH AND DISCUSSION

The results of the flow model and the heat transfer of the cooling system, of the screw compressor set of the compressor for drilling the wells in the hard rock layer are as shown in Fig. 7-10.

Fig.7 Show the modeling grid with a solid wok program. While Fig.8 shows the flow characteristics of the air through the cooling unit at a temperature of about 30-35 °C. Then the air was heated by exchanging heat with high temperature of oil therefore the temperature of air was increased when flowing through cooling unit. While Fig. 9 shows heat distribution in the cooling unit, it can be seen that the distribution of the temperature was difference depend on air velocity. Referring to Fig.10, air and oil flow through the



cooling unit. It was found that the temperature of oil was decreased while the temperature of air was increased.

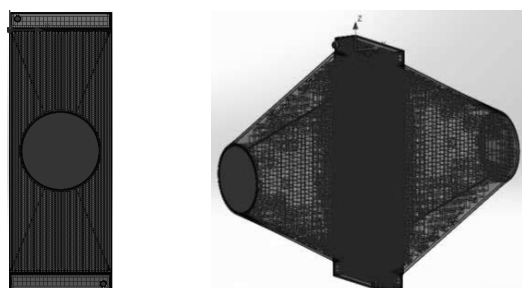


Fig. 7. Creating a grid in a model of a heat sink.

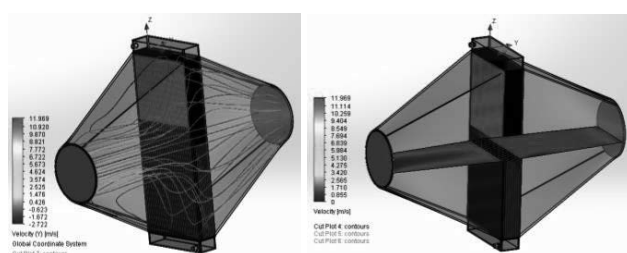


Fig. 8. Flow characteristics of the air through cooling unit.

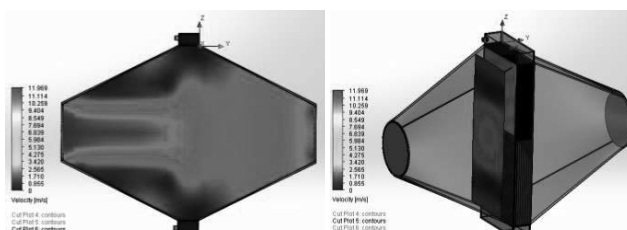


Fig. 9. Cooling characteristics of the flowing of air through the cooling unit.

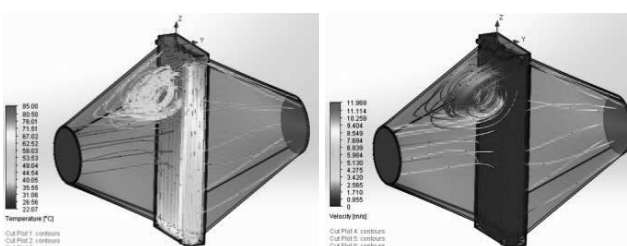


Fig. 10. Flow characteristics of oil and air flowing through the heat sink.

The air mass flow rate that flow through the cooling unit were calculated by the simulation model were shown in Table II. while the experimental results were shown in Table III. Then the values in the tables can be used to calculate the oil and air convection coefficients, the Reynolds number and the effectiveness of the heat exchanger or cooling unit.

TABLE II. Simulation results

Depth range (m)	rpm	\dot{m}_o (kg/s)	\dot{m}_a (kg/s)	$T_{o,i}$ (°C)	$T_{a,i}$ (°C)	$T_{o,o}$ (°C)	$T_{a,o}$ (°C)
40 to 60	1750 to 1800	0.81	1.41	85	30	58.51	34.26
60 to 90	1800 to 1850	0.96	1.59	87	32	58.69	36.03
90 to 120	1850 to 1900	1.00	1.77	89	35	59.86	38.75

TABLE III. Experimental result

Depth range (m)	rpm	\dot{m}_o (kg/s)	\dot{m}_a (kg/s)	$T_{o,i}$ (°C)	$T_{a,i}$ (°C)	$T_{o,o}$ (°C)	$T_{a,o}$ (°C)
40 to 60	1750 to 1800	0.81	1.41	85	30	56	33
60 to 90	1800 to 1850	0.96	1.59	87	32	57	35
90 to 120	1850 to 1900	1.00	1.77	89	35	58	39

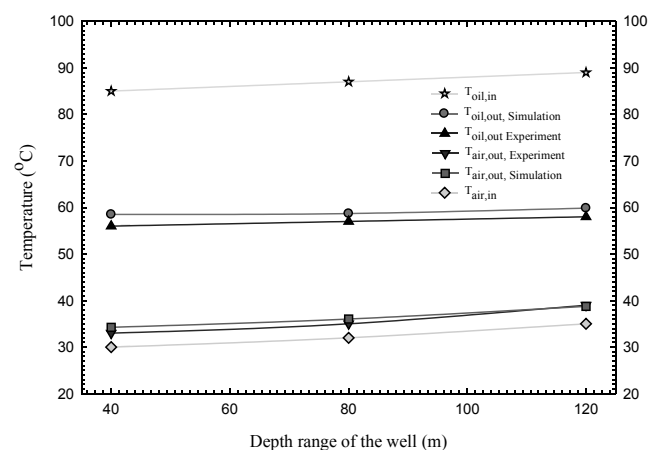


Fig. 11. Effect of the depth range on air and oil temperature.

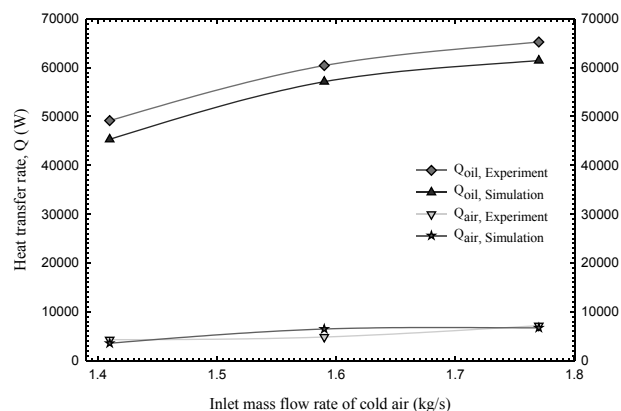


Fig. 12. Effect of mass flow rate of cold air in each depth range on heat transfer rate.

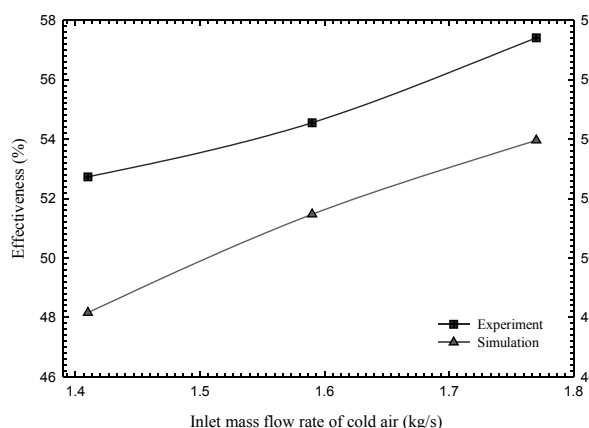


Fig. 13. Effect of mass flow rate of cold air in each depth range on effectiveness.

Under all depth ranges of the well, when the depth ranges was increased, the oil and air temperature were increased due to the speed of engine was increased when the depth ranges was increased. Moreover, it can be seen that all trends were similar as shown in Fig. 11. The mass flow rate of air flow through the cooling unit with 40, 80 and 120 m were 1.41, 1.59 and 1.77 kg/s, respectively and it was found that when the mass flow rate of air were increased, the heat transfer rate of oil and air in the cooling unit were increased as shown in Fig. 12. The trends of the simulation and experimental results were similar. Fig. 13 shows the effect of the mass flow rate of air on the effectiveness. It was found that the maximum of effectiveness of the simulation and experimental results were 0.54 and 0.57, respectively

IV. CONCLUSION

From this study the following can be concluded:

- The comparison of simulation model and experimental results, it is consistent.

- The maximum of heat transfer rate of oil was 65.2 kW with the mass flow rate of air 1.77 kg/s.
- The simulation model can be used to solve the problem of heat generated by air compressors used in underground drilling and industrial applications with compressed air of the same type.

ACKNOWLEDGMNT

This research was conducted under the support of Chiangmai Provincial Administrative Organization and Rajamangala University of Technology Lanna (RMUTL).

REFERENCES

- [1] Department of Groundwater Resources, "Standard for underground wells drilling," Retrieved from <http://www.dgr.go.th>, February 2017.
- [2] F. Singharajwarapan, "Groundwater, Birth and Sustainable Development," Groundwater Technology Service Center Department of Geology, Faculty of Science, October 2005.
- [3] W. Chanyuak, "Solidworks flow simulation CFD analysis," December 2016.
- [4] J. Khanthong, Seney Sirichai and Uthai Phongrasamee, "Numerical Study of Heat Transfer Rate in a shell and Tube Economizer," Chulalongkorn University, Faculty of Engineering, Chulalongkorn University, Ubon Ratchathani Rajabhat University, Journal of the 6th year, No. 1, 2016.
- [5] R. Munsin, "Simulation and validation of the interior of a passenger compartment using fluid dynamics," Department of Mechanical Engineering Chiang Mai University, 2008.
- [6] C. Lhasomsriand and Pawun Ruangareeratch, "Design and Assmby a Radiator for Student Formula," Mechanical Engineering Faculty of Engineering Rajamangala University of Technology Lanna, 2012.
- [7] Y. A. Cengel, "Heat and Mass Transfer," 3 ed., Singapore, McGraw-Hill Companies, 2006.
- [8] W. Zuo, "Introduction of Computational Fluid Dynamics," FAU Erlangen-Nürnberg JASS 05, St. Petersburg, 2005. Retrieved from http://erivera-2001.com/MEC-2249/NAVIER_STOCKS_Zuo_paper, February 2017.
- [9] G. Eason, B. Noble, and I.N. Sneddon, "On certain integrals of Lipschitz-Hankel type involving products of Bessel functions," Phil. Trans. Roy. Soc. London, vol. A247, pp. 529-551, April 1955. (references)
- [10] I.S. Jacobs and C.P. Bean, "Fine particles, thin films and exchange anisotropy," in Magnetism, vol. III, G.T. Rado and H. Suhl, Eds. New York: Academic, 1963, pp. 271-350.
- [11] J. Clerk Maxwell, A Treatise on Electricity and Magnetism, 3rd ed., vol. 2. Oxford: Clarendon, 1892, pp.68-73.
- [12] K. Elissa, "Title of paper if known," unpublished.
- [13] M. Young, The Technical Writer's Handbook. Mill Valley, CA: University
- [14] R. Nicole, "Title of paper with only first word capitalized," J. Name Stand. Abbrev., in press.
- [15] W. Chanyuak, "Solidworks flow simulation CFD analysis," December 2016.
- [16] Y. Yorozu, M. Hirano, K. Oka, and Y. Tagawa, "Electron spectroscopy studies on magneto-optical media and plastic substrate interface," IEEE Transl. J. Magn. Japan, vol. 2, pp. 740-741, August 1987 [Digests 9th Annual Conf. Magnetics Japan, p. 301, 1982].



Numerical Study of High-Moisture Parboiled Paddy Drying in an Impinging Stream Dryer

Patiwat Khomwachirakul and Wirote Ritthong

Department of Mechanical Engineering, Faculty of Engineering,
Rajamangala University of Technology Phra Nakhon,
1381 Pracharat 1 Road, Wongsawang, Bang Sue, Bangkok 10800

*Corresponding author: patiwat.k@rmutp.ac.th

Abstract—In this study, a numerical method for high-moisture parboiled paddy drying in an impinging stream dryer was proposed. Computational fluid dynamics (CFD) was used to predict the effects of operating parameters of the dryer, i.e., parboiled paddy mass flow rate, inlet air temperature and inlet air velocity on the overall performance, in term of the volumetric water evaporation rate. The results showed that the model gave predictions that were in good agreement with the experimental mean parboiled paddy moisture content data. In addition, an increase in the particle feed flow rate, inlet air temperature and inlet air velocity led to an increase in the volumetric water evaporation rate.

Keywords—CFD; drying; impinging stream dryer; moisture content; paddy

I. INTRODUCTION

Impinging stream dryer (ISD) has proven to be an energy efficient alternative for removing surface moisture from a particulate material. The principle of ISD is based on collision of opposite streams of gas; either one or more streams carry a wet material to be dried. Collision of opposite streams promotes excellent conditions for heat, mass and momentum transfer between the drying medium and particles [1].

Due to the extremely complicated of gas flow behavior, particle behavior and interactions in the drying chamber, it is difficult to obtain detailed information on the drying characteristics within ISD. Numerical simulation has therefore become an important tool to support the design and study of ISD.

Computational fluid dynamics (CFD) method has been proved to get the accurate solutions for transport phenomena in the system, such as the complex flow, particle tacking and heat and mass transfers. To get the detail information from CFD was easier than the experiment. CFD has been used increasingly to improve process design capabilities in many process applications, including drying processes. A number of investigators have therefore resorted to CFD to study the multiphase transport phenomena within an ISD. Grasemi et al. [2], for example, numerically investigated the flow behavior of a two-impinging stream cyclone reactor via CFD modeling. The effects of solid and liquid flow rates on the performance

behavior of dryer were investigated in lab-scale dryer. However, heat and mass transfer process were not considered. The results showed that the CFD model could be successfully used to predict the particles holdup and particle mean residence time. The particle holdup was dependent on the value of the particle flow rate at each liquid flow rate, while the particle mean residence time was found to decrease with an increase in the liquid flow rate at each particle flow rate. Choicharoen et al. [3] later simulated the flow and drying characteristics of high-moisture particles (soy residue) in an impinging stream dryer by CFD model. The effects of inlet air temperature, inlet air velocity, particle flow rate and impinging distance on the transport and performance behavior of dryer were investigated. The results showed that the CFD model could be successfully used to predict the mean particle moisture content, air humidity ratio and particle mean residence time. However, the effects of various parameters on the overall performance, in term of the volumetric water evaporation rate were not considered.

In this study, CFD was applied to investigate the effects of operating parameters of the dryer, i.e., parboiled paddy mass flow rate, inlet air temperature and inlet air velocity on the overall performance, in term of the volumetric water evaporation rate. Simulated mean moisture content of parboiled paddy was compared with the corresponding experimental data.

II. MATHEMATICAL MODEL

Gas-phase equations

Continuity equation [4]:

$$\frac{\partial}{\partial t}(\rho) + \frac{\partial}{\partial x_i}(\rho u_i) = M_m \quad (1)$$

Momentum equation [4]:

$$\frac{\partial}{\partial t}(\rho u_j) + \frac{\partial}{\partial x_i}(\rho u_i u_j) = -\frac{\partial P}{\partial x_j} + \frac{\partial}{\partial x_i} \left[(\mu + \mu_t) \left(\frac{\partial u_i}{\partial x_j} + \frac{\partial u_j}{\partial x_i} \right) \right] + \rho g + M_F \quad (2)$$



Energy equation [4]:

$$\frac{\partial}{\partial t}(\rho c_p T) + \frac{\partial}{\partial x_i}(\rho c_p u_i T) = \frac{\partial}{\partial x_i} \left(k \frac{\partial T}{\partial x_i} \right) + M_h \quad (3)$$

Species (water) equation [4]:

$$\frac{\partial(\rho C)}{\partial t} + \frac{\partial(\rho u_i C)}{\partial x_i} = \frac{\partial}{\partial x_i} \left(\left(\rho D + \frac{\mu_t}{Sc_t} \right) \frac{\partial C}{\partial x_i} \right) + M_m \quad (4)$$

where M_m , M_F and M_h are mass, momentum and energy source terms, respectively.

Turbulence model:

The realizable k - ϵ equations can be expressed as [3]:

$$\frac{\partial(\rho k)}{\partial t} + \frac{\partial(\rho k u_i)}{\partial x_i} = \frac{\partial}{\partial x_j} \left[\left(\mu + \frac{\mu_t}{\sigma_k} \right) \frac{\partial k}{\partial x_j} \right] + G_k + G_b - \rho \epsilon \quad (5)$$

$$\begin{aligned} \frac{\partial(\rho \epsilon)}{\partial t} + \frac{\partial(\rho \epsilon u_i)}{\partial x_i} &= \frac{\partial}{\partial x_j} \left[\left(\mu + \frac{\mu_t}{\sigma_\epsilon} \right) \frac{\partial \epsilon}{\partial x_j} \right] \\ &- \rho C_2 \frac{\epsilon^2}{k + \sqrt{\nu \epsilon}} + C_{1\epsilon} \frac{\epsilon}{k} C_{3\epsilon} G_b \end{aligned} \quad (6)$$

Particle-phase equations

The motion of individual particles was calculated by Newton's second law of motion, which is written as [3]:

$$\frac{du_p}{dt} = \frac{18\mu}{\rho_p d_p^2} \frac{C_D \text{Re}}{24} (u_g - u_p) + g_i \frac{\rho_p - \rho_g}{\rho_p} \quad (7)$$

The relative Reynolds number (Re) and drag coefficient (C_D) are described in detail by Choicharoen et al. [3].

Heat and mass transfer between phases

The particle temperature can be calculated by [3]:

$$m_p c_p \frac{dT_p}{dt} = h A_p (T_g - T_p) + \frac{dm_p}{dt} h_{fg} \quad (8)$$

The gas-particle convective heat transfer coefficient (h) was calculated using the following correlation [3]:

$$\text{Nu} = 2 + 0.6 \text{Re}^{1/2} \text{Pr}^{1/3} \quad (9)$$

where

$$\text{Nu} = \frac{h d_p}{k_g} \quad (10)$$

$$\text{Pr} = \frac{c_{p,g} \mu}{k_g} \quad (11)$$

The moisture transfer rate between the paddy and gas was calculated by Eq. (12):

$$\frac{dm_p}{dt} = -N_i A_p M_{w,i} \quad (12)$$

where N_i is the moisture transport flux, which is given by [3]:

$$N_i = k_c (C_{i,s} - C_{i,g}) \quad (13)$$

where $C_{i,s}$ and $C_{i,g}$ are the water vapor concentration at the particle surface and the water vapor concentration in the gas phase, respectively.

The gas-particle convective mass transfer coefficient (k_c) was calculated using the following correlation [3]:

$$\text{Sh} = 2.0 + 0.6 \text{Re}^{1/2} \text{Sc}^{1/3} \quad (14)$$

where

$$\text{Sh} = \frac{k_c d_p}{D} \quad (15)$$

$$\text{Sc} = \frac{\mu}{\rho D} \quad (16)$$

where D is the diffusion coefficient of water vapor in air, which is given by [5]:

$$D = 4.56 \times 10^{-9} T_g^{1.5} \quad (17)$$

The paddy properties for simulation are shown in Table I [6].

TABLE I. PADDY PROPERTIES

Property	Expression
c_p	$1110 + 44.8 M_w$
k_p	$0.0863 + 0.00134 M_w$
ρ_p	$(552 + 282 M_p) / (1 - (0.623 - 0.25 M_p))$

Calculate of volumetric water evaporation rate

The performance of the dryers was evaluated in term of the volumetric water evaporation rate, which was calculated by [1]:

$$N_v = \frac{W_p (X_i - X_o)}{V_r} \quad (18)$$

III. MODEL ASSUMPTION AND SIMULATION CONDITIONS

The following assumptions were adopted in the present study: properties of air, including viscosity, thermal conductivity and heat capacity, were specified as a polynomial function of temperature [7]; heat loss through the drying chamber wall was neglected; parboiled paddy had monodisperse dimension and was in spherical shape; particle-



wall interaction was considered; but particle-particle interaction was neglected, paddy did not change in shape during/after collision with the wall, the shrinkage of the paddy kernels was neglected during drying process. The impinging stream dryer of Choicharoen et al. [3] was used for the simulation (see Fig. 1). For the gas phase, the PISO algorithm was used for coupling between the pressure and velocity terms. The spatial discretization was performed using the power-law scheme for the conservation equations. For the particle phase, the particle equations were solved using Runge-Kutta scheme. A grid number of 22714 was used in this study; the selection was based on the grid independence test. The simulation conditions are listed in Table II.

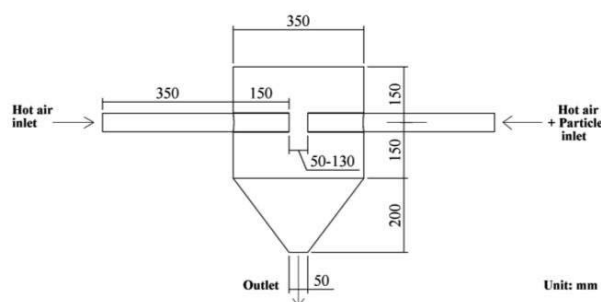


Fig. 1 Schematic diagram of the simulated dryer [3].

TABLE II. SIMULATION CONDITIONS

Parameter	Value
Paddy diameter (m)	0.0039
Initial moisture content of paddy (% d.b.)	46
Inlet air temperature (°C)	130,150,170
Inlet air velocity (m/s)	20, 30, 40
Parboiled paddy mass flow rate (kg/h)	40, 120
Impinging distance (m)	0.05

IV. BOUNDARY CONDITIONS

At the inlets, the flow of gas was assumed to be uniform. The turbulence intensity was assumed to be 5% [3]. At the wall no-slip boundary condition was assumed for the gas phase. The outlet was assumed to be at an atmospheric pressure.

V. RESULTS AND DISCUSSION

Model validation

Fig. 2 compares the simulated and experimental mean moisture content of parboiled paddy at outlet of dryer; the experimental data are those of Pruengam et al. [8]. It is seen that the mean moisture of the simulation differed from the experimental data approximately 6%.

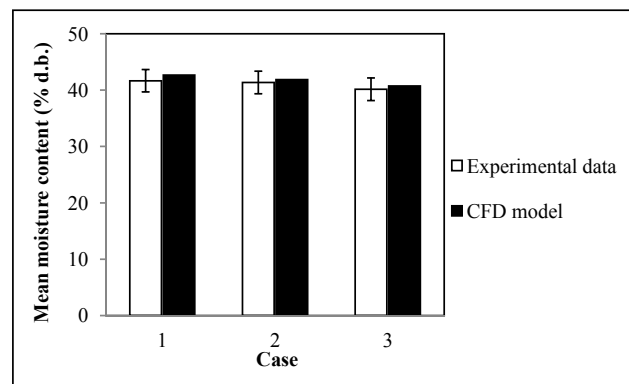


Fig. 2 Comparison between simulated and experimental mean moisture content of parboiled paddy at inlet air velocity of 20 m/s, impinging distance of 0.05 m and particle mass flow rate of 40 kg_{dry solid}/h. Case 1= Inlet air temperature of 130 °C. Case 2= Inlet air temperature of 150 °C. Case 3= Inlet air temperature of 170 °C. Experimental data are those of Pruengam et al. [8].

Parboiled paddy mean residence time

Because the parboiled paddy mean residence time in a drying system is generally not affected by the inlet air temperature [9], in this study, the simulated effects of inlet air velocity and parboiled paddy mass flow rate on parboiled paddy mean residence time were investigated. The simulated effect of inlet air velocity on the mean residence time of parboiled paddy is shown in Fig. 3. It is seen that the parboiled paddy mean residence time increased with an increase in the inlet air velocity. This is because higher inlet air velocity implies higher momentum of the parboiled paddy to penetrate into the opposite stream and perform oscillatory motion within the impingement zone. This led to the longer time the parboiled paddy stayed in the system. For the effect of parboiled paddy mass flow rate on the mean residence time was not significantly different at different conditions (see also Fig. 3).

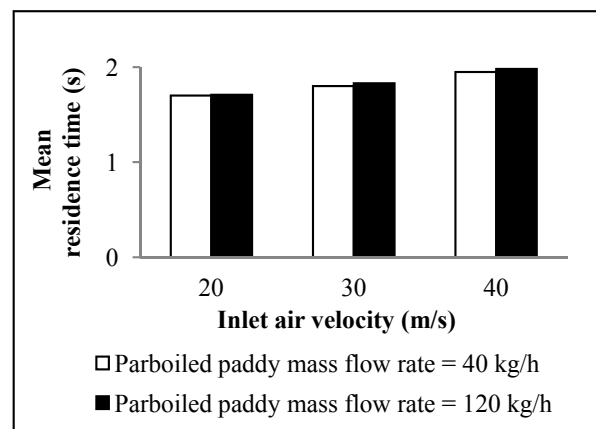


Fig. 3 Simulated effects of inlet air velocity and parboiled paddy mass flow rate on mean residence time of parboiled paddy at impinging distance of 0.05 m.



Parboiled paddy mean outlet moisture content

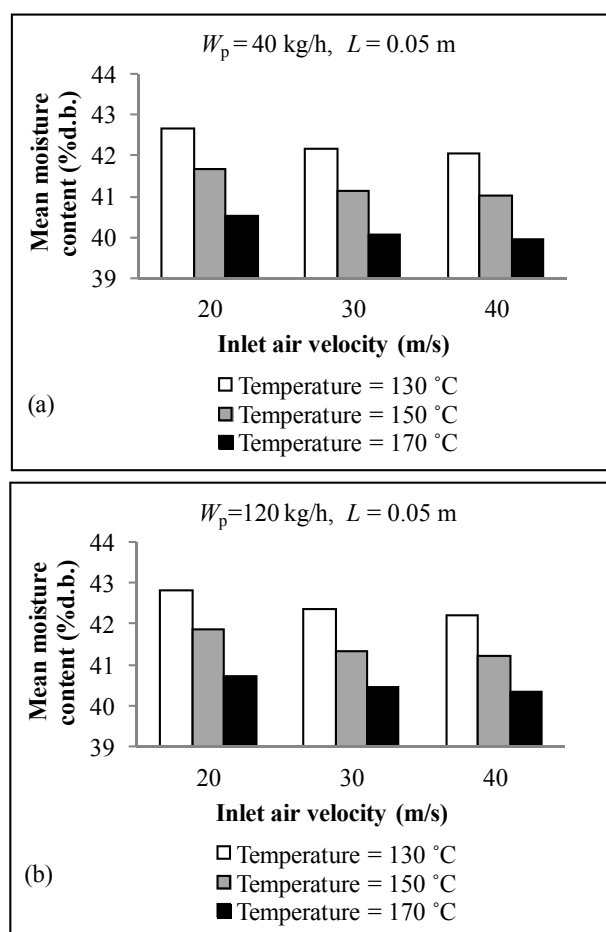


Fig. 4. Simulated parboiled paddy mean outlet moisture content at difference drying conditions.

Fig. 4 shows simulated the effects of different drying conditions on the parboiled paddy mean outlet moisture content. The simulated results found that the final moisture content of parboiled paddy at the dryer outlet was in the range of 39.94 - 42.81% (d.b.). This implied that the impinging stream dryer could reduce the moisture content of parboiled paddy by 3.19 - 6.06% (d.b.) within 2 s (see Fig. 3 for parboiled paddy mean residence time).

The effect of the inlet air temperature on the parboiled paddy mean outlet moisture content is also shown in Fig. 4. It is seen that an increase in the inlet air temperature led to a decrease in the parboiled paddy mean outlet moisture content at a fixed inlet air velocity and a fixed parboiled paddy mass flow rate. This is because the temperature difference between the drying air and paddy surface at a higher temperature is larger than that at a lower temperature, therefore a larger driving force for heat (and mass) transfer. An increase in the inlet air velocity also led to a decrease in the parboiled paddy mean outlet moisture content at a fixed inlet air temperature

and a fixed parboiled paddy mass flow rate. This is because a higher inlet air velocity led to the increased parboiled paddy mean residence time (see Fig. 3). This in turn led to an increase in the rates of heat and mass transfer to and from paddy.

For the effect of the parboiled paddy mass flow rate on the parboiled paddy mean outlet moisture content, it is seen in Fig. 4 that there were no differences in the parboiled paddy mean outlet moisture content in all cases at a fixed inlet air temperature and a fixed inlet air velocity. This is because the parboiled paddy mean residence time was not significantly different at different conditions (see Fig. 3).

Volumetric water evaporation rate of the dryer

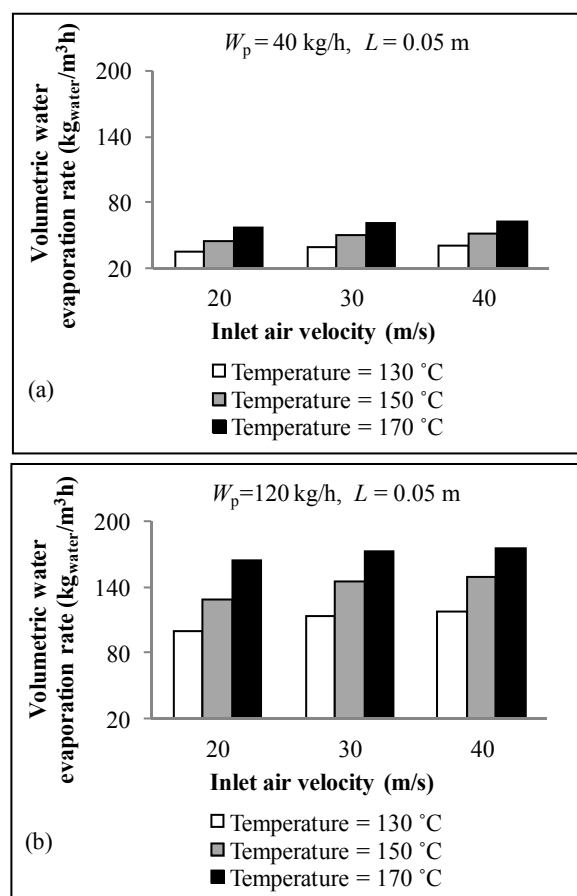


Fig. 5. Simulated effects of operating parameters on the volumetric water evaporation rate at different drying conditions.

Fig. 5 shows simulated the effects of different drying conditions on the volumetric water evaporation rate of the dryer. In this study, the simulated results found that the volumetric water evaporation rate was in the range of 35 - 176 kgwater/m³h. The highest value of the volumetric water evaporation rate from the simulation was occurred at inlet air temperature of 170 °C, inlet air velocity of 40 m/s and parboiled paddy mass flow rate of 120 kg/h.



The effects of the inlet air temperature, inlet air velocity and parboiled paddy mass flow rate on the volumetric water evaporation rate are shown in Fig. 5. It was found that the volumetric water evaporation rate, which is strongly related to the difference between initial and final moisture content of the parboiled paddy, an increase in the inlet air temperature led to an increase in the volumetric water evaporation rate at a fixed inlet air velocity and a fixed parboiled paddy mass flow rate, as expected.

The effect of inlet air velocity on the volumetric water evaporation rate is again shown in Fig. 5. It was found that an increase inlet air velocity led to an increase in the volumetric water evaporation rate at a fixed inlet temperature and a fixed parboiled paddy mass flow rate. This is because at a higher inlet air velocity led to a longer parboiled paddy mean residence time in the system (see Fig. 3) and hence higher rate of water removal (see Fig. 4).

The effect of parboiled paddy mass flow rate on the volumetric water evaporation rate is also shown in Fig. 5. Although the amount of moisture reduction changed insignificantly with the parboiled paddy mass flow rate (see Fig. 4), however, an increase parboiled paddy mass flow rate led to an increase in the volumetric water evaporation rate at a fixed inlet temperature and a fixed and inlet air velocity. This is because the capacity of the dryer exceeded the loaded required to evaporate water from the parboiled paddy entering the system; the more entering the system, the higher volumetric water evaporation rate [10].

VI. CONCLUSIONS

CFD model was used to predict the heat transfer and drying characteristics of parboiled paddy in an ISD at different conditions. Simulated parboiled paddy mean residence time, parboiled paddy mean moisture content and volumetric water evaporation rate were analyzed. The simulated results show that the CFD model gave predictions that are in good agreement with the experimental data. An increase in the inlet air velocity led to an increase in the mean residence time. On the other hand, the mean residence time changed insignificantly with the parboiled paddy mass flow rate. An increase in the inlet air temperature and inlet air velocity led to a decrease in mean outlet moisture content of parboiled paddy. However, the effect of the parboiled paddy mass flow rate on the mean outlet moisture content was found to be insignificant. The volumetric water evaporation rate increased with an increase in the inlet air temperature, inlet air velocity and parboiled paddy mass flow rate. The simulated results found that the volumetric water evaporation rate was in the range of 35 – 176 kg_{water}/m³h. The highest value of the volumetric water evaporation rate from the simulation was occurred at inlet air temperature of 170 °C, inlet air velocity of 40 m/s and parboiled paddy mass flow rate of 120 kg/h.

NOMENCLATURE

A_p	= Area of particle (m ²)
c_p	= Heat capacity of particle (J/kg · K)
$c_{p,g}$	= Heat capacity of drying air (J/kg · K)
C_D	= Drag coefficient
$C_{i,g}$	= Vapor concentration in drying air (kg mol/m ³)
$C_{i,s}$	= Vapor concentration at particle surface (kg mol/m ³)
d_p	= Diameter of particle (m)
$\frac{dm_p}{dt}$	= Moisture evaporation rate (kg/s)
F_D	= Drag force (N)
F_g	= Gravitational force (N)
g	= Gravitational acceleration (m/s ²)
h	= Heat transfer coefficient (W/m ² · K)
h_{fg}	= Latent heat of vaporization (J/kg)
k	= Turbulence kinetic energy (m ² /s ²)
k_c	= Mass transfer coefficient (m/s)
k_g	= Thermal conductivity of drying air (W/m · K)
L	= Impinging distance (mm)
m_p	= Mass of particle (kg)
M_F	= Source term in momentum equation
M_h	= Source term in energy equation
M_m	= Source term in mass equation
$M_{w,i}$	= Molecular weight of water vapor (kg/kg mol)
N_i	= Molar flux of water vapor (kgmol/m ² · s)
T_p	= Temperature of particle (K)
u_g	= Velocity of drying air (m/s)
u_p	= Velocity of particle (m/s)
u_i, u_j	= Velocity component of drying air (m/s)
W_p	= Particle mass flow rate (kg/h)
X_i	= Local bulk mole fraction of water vapor
x_i, x_j	= Coordinates (m)

Greek Letters

ε	= Energy dissipation rate (m ² /s ³)
μ	= Dynamic viscosity of drying air (kg/m · s)
μ_t	= Turbulent viscosity (kg/m · s)



ν	= Kinematic viscosity (m^2/s)
ρ	= Density of drying air (kg/m^3)
ρ_p	= Density of particle (kg/m^3)
σ_k	= Turbulent Prandtl number for k
σ_ε	= Turbulent Prandtl number for ε
σ_T	= Turbulent Prandtl number

- [9] C. Nimmol, K. Sathapornprasath, S. Devahastin, "Drying of high-moisture paddy using a combined impinging stream and pneumatic drying system", *Drying Technology*, vol. 30, 2012, pp. 1854-1862
- [10] K. Choicharoen, S. Devahastin, S. Soponronnarit, "Performance and energy consumption of an impinging stream dryer for high-moisture particulate materials", *Drying Technology*, vol. 28, 2010, pp. 20-29.

Dimensionless Numbers

Nu	= Nusselt number
Pr	= Prandtl number
Re	= Reynolds number
Sc	= Schmidt number
Sc_t	= Turbulent Schmidt number
Sh	= Sherwood number

REFERENCES

- [1] A. Tamir, *Impinging-stream reactors: Fundamentals and applications*, Elsevier, Amsterdam, 1994.
- [2] N. Ghasemi, M. Sohrabi, M. Khosravi, A.S. Mujumdar, M. Goodarzi, "CFD simulation of solid-liquid flow in a two impinging streams cyclone reactor: Prediction of mean residence time and holdup of solid particles", *Chemical Engineering and Processing: Process Intensification*, 2010, pp. 1277-1283.
- [3] K. Choicharoen, S. Devahastin, S. Soponronnarit, "Numerical simulation of multiphase transport phenomena during impinging stream drying of a particulate material", *Drying Technology*, 2012, pp. 1227-1237.
- [4] R.B. Bird, W.E. Stewart, E.N. Lightfoot. *Transport phenomena*, 2nd ed., John Wiley, New York, 2002.
- [5] A. Rahimi, A. Niksiar, "Mathematical modeling and simulation of drying of a single wet particle in a coaxial impinging stream dryer", *Chemical Engineering Communications*, vol. 197, 2010, pp. 692-708.
- [6] N. Meeso, A. Nathakaranakule, T. Madhiyanon, S. Soponronnarit, "Modelling of far-infrared irradiation in paddy drying process", *Journal of Food Engineering*, vol. 78, 2007, pp. 1248-1258.
- [7] A. Frydman, J. Vasseur, J. Moureh, M. Sionneau, P. Tharrault, "Comparison of superheated steam and air operated spray dryers using computational fluid dynamics", *Drying Technology*, vol. 16, 1998, pp. 1305-1338.
- [8] P. Pruengam, S. Soponronnarit, S. Prachayawarakorn, S. Devahastin, "Rapid drying of parboiled paddy using hot air impinging stream dryer", *Drying Technology*, vol. 32, 2014, pp. 1949-1955.



Braking Performance Comparison between Hole Profiles on Brake Rotors under Various Operating Temperatures

Siripol Tongorn * and Songwut Mongkonlerdmanee

Department of Mechanical Engineering, Faculty of Engineering, Rajamangala University of Technology Phra Nakhon, Bangkok, 10800, Thailand

*Corresponding author: siripol.t@rmutp.ac.th

Chaiyot Damrongkijkosol

Department of power engineering technology, College of Industrial Technology, King Mongkut's University of Technology North Bangkok, Bangkok, 10800, Thailand

Abstract—The main objective of this research is to find appropriate criteria of drilling pattern for both of quantity and direction of hole under the various operating temperatures of brake. By using the brake under specified below in accordance with JASO C406 standard. The drilling patterns was selected as the normal brake disc, two-hole brake drilling, three-hole brake drilling in both of straight and radial holes. This paper presents the starting speed before braking of 50 km/hr and 80 km/hr under the pressure 4 MPa by comparing the working temperature range 50 °C to 250 °C. The results revealed that the normal brake disc was reasonable for low temperature working in both of temperature range. In case of speed before braking of 50 km/hr, the straight hole that was the reasonable in high temperature whether the three-hole brake drilling in radial is more effective. For speed before braking of 80 km/hr, drilling patterns were reasonable for low temperature working.

Keywords— *braking performance; hole profiles and operating temperatures*

I. INTRODUCTION

Thailand is not only the motorcycle and car manufacturer country but also Thailand is a leading auto part manufacturer country. In 2012, Thailand had the export value for auto parts around 3 hundred thousand million baht which made Thailand the number one for Ventilated Disc Brake this export [6]. For the safety equipment in the vehicle, disc brake is considered one of the most important auto part. The disc brake must have the proper properties for using in different vehicles. Nowadays the disc brake must be qualified the test before assembled in the vehicle. There are 2 types of the disc brake tests which are the lab test using brake chassis dynamometer and the field test. (FMCSA, 2002) The tested parameters for the disc brake are temperature pressure strain and heat transfer. Lakkam, et al. [11] studied about the heat transfer of the front-and back – vented brake discs at 100 °C, 200 °C and 300 °C which the

result found that at 300 °C had the best heat transfer. Kullayot Suwantaraj et al. [1] studied the physical appearance of the disc brake that affected to the braking performance of the motorcycle using the brake test bench for 3 types of disc brake which the result showed that holed disc brake has the best braking performance. Phupoom Puangcharoenchai et al. [5] studied about the behavior of the nonlinear heat conduction of disc brake at 50 °C to 400 °C at 1, 5 and 8MPa which the result showed that the different disc brake types had the different heat conduction value. Songwut Mongkonlerdmanee et al. [2] studied about the ratio of the mixture of material used to produce the disc brake and found that low carbon fiber mixture gave the high internal energy per volume while on the other hand, high fiber mixture had a high flexibility because of low collapse value.

The heat transfer of the disc brake is the important property that related to the braking performance. Thoatsanope Kamnerdtong et al. [3] found that the temperature at the surface of disc brake can be changed deepened on the cycle of usage and the dispersion of the temperature was not stable. Saiprasit Koetnityom et al. [7] found that the format of the disc brake determined the direction of the temperature and the braking performance. Qi and Day (2007) found that pressure or load, rotation speed, material and the hole for the heat transfer affected to the braking performance. Boonthum Wonchai et al. [4] drilled the disc brake for the different 27 patterns to studied the strain in the spiral pattern at 1.5, 8.842 and 10 rps which the result showed that the strain is not stable deepened on the number of spiral and the hole on the disc brake. However there is no study about the braking performance that can be measured using the braking distance and the deceleration. Therefore this research had the objective to evaluate the braking performance of the two hole disc brake and three hole disc brake drilled at straight and radial direction at temperature 50 °C to 250 °C.



II. BASIC OF THE BRAKING PERFORMANCE

A. Disc Brake

Disc brake is the important part in the safety system of the vehicle which builds up the friction to decelerate or stop the motion of the wheel using the force and energy from the surface between the brake liner and disc brake. When the driver activated the brake, the disc brake contacted with brake liner is always slipped because the properties of the brake liner material and disc brake such as the heat transfer and strain made the temperature between the contact surface around 80 - 300 °C. This phenomenon affects to the coefficient of friction of brake and the wear. Moreover if the discontinuity occurred, the braking performance is reduced [2].

Pattern of the disc brake Nowadays there are three patterns of the disc brake (1) Solid Disc brake (2) Ventilated Disc Brake (3) Ventilated and drilled Disc Brake. The use condition for this three pattern disc brake is different. The solid disc brake as shown in figure 1(a) mostly uses with the small vehicle which the braking performance is reduced when extreme usage applied continuously such as the downhill braking. The Ventilated disc brake as shown in figure 1(b) mostly uses with passenger car and small truck because of the better heat transfer. Finally the ventilated and drilled disc brake as shown in figure 1(c) mostly uses with the high performance vehicle that needs the good heat transfer therefore in this case the hole drilled at the disc brake gives more heat transfer surface.



Fig. 1. Patterns of the disc brake

B. Braking Performance

Braking performance depended on various parameters such as the driving behavior, road condition, weather condition and brake force. For the brake force, it also depended on the deceleration and brake distance shown in equation 1 and 2 respectively

$$d_{avg} = \frac{V_1 - V_2}{t_2 - t_1} \quad (1)$$

$$S_1 - S_0 = \int_{t_1}^{t_2} V(t) dt \quad (2)$$

Where

d_{avg} - average deceleration rate (m/s²)

V_1 - initial velocity (m/s)

V_2 - final velocity (m/s)

t_1 - time at the start of the shaft rotate (s)

t_2 - time at the shaft stop rotate (s)

S_2 - distance at the shaft stop (m)

S_1 - distance before stop rotating the shaft (m)

$V(t)$ - linear velocity at radius of operating point (m/s)

III. RESEARCH METHODOLOGY

A. Disc brake testing preparation

The research objective is to evaluate the braking performance of the two hole disc brake and three hole disc brake drilled at straight and radial direction at temperature 50 °C to 250 °C. The braking performance can be measured using the brake distance and deceleration. This study was compared 5 disc brake patterns (1) solid disc brake (2) 2 straight hole disc brake (3) 2 radial hole disc brake (4) 3 straight hole disc brake (5) 3 radial hole disc brake. For the testing condition, the velocity before braking was determined at 50 km/hr and 80 km/hr, pressure at 4 MPa compared at temperature 50, 100, 150, 200, 250 °C, 6 mm hole size for both straight and radial drill while the distance between each hole is 17.5 cm for the straight drill and 10 cm for the radial drill which the position of the first hole and the next hole is 72° for both straight and radial drill as shown in figure 2.



Fig. 2. Hole patterns of the disc brake

B. Testing Equipment

This research used the brake chassis dynamometer as shown in figure 3 to test the brake performance. This brake chassis dynamometer can simulate the vehicle mass up to 1500 kg using the inertia of the flywheel theory and produced pressure using the pressure using the weight acting to the brake cylinder closed to the disc brake that has the heat convection at speed 11 m/s.

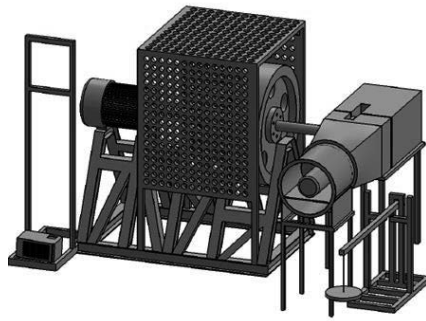


Fig. 3. Brake dynamometer

IV. RESULTS

Figure 4 is shown the results of the braking performance by using the braking distance measurement at the different temperature and initial speed. At 50 km/hr (figure 4a) shown that 2 radial hole disc brake at 200 °C had the best braking performance around 10.55 m however comparing with the 2 straight hole disc brake found that the 2 straight hole disc brake has more braking performance. When the temperature increasing 150 °C, the braking performance of 2 hole straight disc brake less than 2 hole radial disc brake. For the 2 hole drilling, both straight hole and radial hole had the best braking performance at 200 °C while the 3 hole drilling, the 3 straight hole disc brake had higher braking performance than 3 radial hole disc brake. The 3 straight hole disc brake had the best braking performance at 250 °C while 3 radial hole disc brake had the best braking performance at 200 °C. At the initial speed 80 km/hr (figure 4b), the 3 straight hole disc brake at 100 °C had the best braking performance around 18.36 m. The 2 straight hole and 3 straight hole drilling at 50 °C to 150 °C had the braking performance than 2 radial hole and 3 radial hole drilling. However when the temperature increasing, the radial hole drilling had higher braking performance.

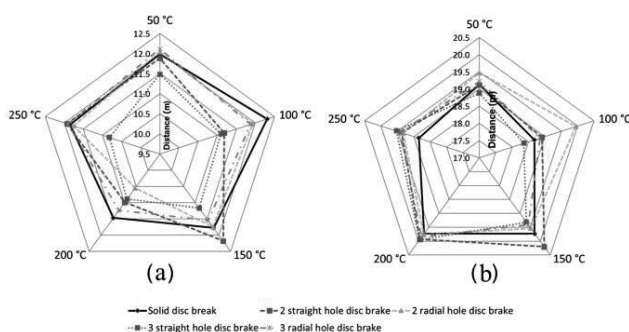
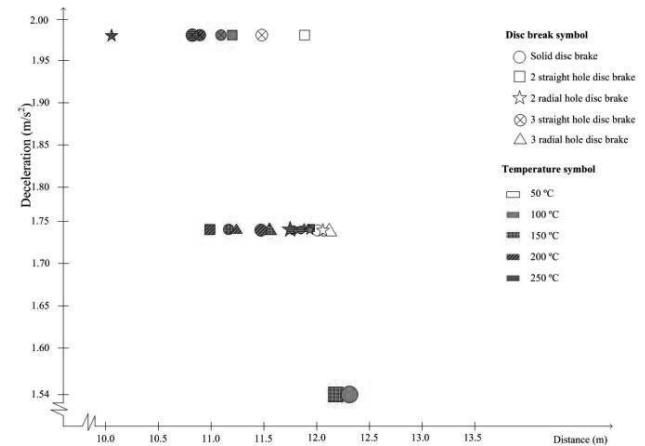
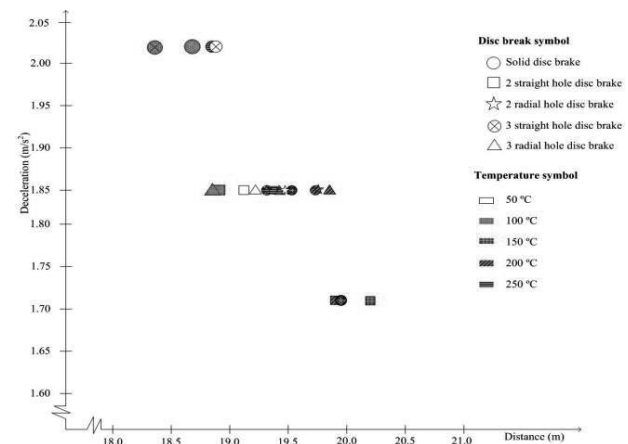


Fig. 4. Braking performance between different temperatures and speed
(a) 50 km/hr (b) 80 km/hr



(a) The speed before braking of 50 km/hr



(b) The speed before braking of 80 km/hr

Fig. 5. Braking performance between deceleration and distance at speed before braking 50 and 80 km/hr

The relation between braking performance and deceleration at initial velocity 50 km/hr and 80 km/hr is shown in figure 5. At 50 km/hr, the 2 radial hole disc brake had the shortest braking distance at 200 °C therefore at this point it also had the maximum deceleration. The average brake distance at initial velocity 50 km/hr was 11.5-12.3 m while the average deceleration was 1.74 m/s². At 80 km/hr, the 3 straight hole disc brake had the shortest braking distance and maximum deceleration at 100 °C. The average brake distance at initial velocity 80 km/hr was 19.0-19.3 m while the average deceleration was 1.85 m/s².

V. CONCLUSION AND RECOMMENDATION

The testing is based on JASO C406 Standard using the initial velocity at 50 km/hr and 80 km/hr under pressure 4 MPa at working temperature 50, 100, 150, 200 and 250 °C using the Brake Dynamometer to simulate the 1500 kg of



vehicle mass and the heat convection at speed 11m/s for testing 2-3 straight and radial hole disc brake.

The result showed that at the initial speed 50 km/hr had the better breaking performance than 80 km/hr. At 50 km/hr, the 2 radial hole disc brake had the shortest braking distance at 200 °C while at 80 km/hr, the 3 straight hole disc brake had the shortest braking distance and maximum deceleration at 100 °C. Kullayot Suwantaroj et al.[1] was studied about the deceleration of the disc brake using in motorcycle at normal temperature and high temperature found that the average deceleration decreased around 2%. From this study at both 50 and 80 km/hr, it found that most of the deceleration was decreased or unchanged following the increasing temperature. Hence the temperature was not the main factor that can affect the deceleration. Moreover the hole drilling was considered to be the important factor that can affect to the braking performance however using different initial velocity gave the different braking performance for different hole drilling pattern. Therefore the relationship between the braking performance and time at the same temperature under the same pressure should be researched.

ACKNOWLEDGMENT

We would like to express our profound gratitude to Rajamangala University of Technology Phra Nakhon for the financial support.

REFERENCES

- [1] K., Suwantaroj, S., Mongkonlerdmanee and S., Lakkam, (2013). "A Study of the Physical Shapes of Brake Disc and their Effects on Braking Performance", The Journal of KMUTN, Vol. 23, No. 2, 323-331.
- [2] S., Mongkonlerdmanee, P., Boonmee and S., Lakkam, (2013). "Influence of Volume Fraction from Brake Linings to the Flexibility Behavior and Internal Energy", KKU Res. J., 18(2): 297-310.
- [3] S., Chutima, T., Kamnerdtong and A., Siri Wattanapolkul, (2015). "Temperature Distribution Analysis in Automotive Brake Disc", The 32nd conference of Mechanical Engineering Network of Thailand, 19-21 October 2005.
- [4] B., Wonchai, (2018). Stress Analysis in Disc Brake by Finite Element Method. The 22nd Conference on Mechanical Engineering Network of Thailand, 15-17 October 2008
- [5] P., Puangcharoenchai, S., Lakkam and S., Mongkonlerdmanee. "An Investigation on Non-linear Thermal Conductivity Behavior of Brake Pads", KMUTT Research and Development Journal, Vol. 38, No. 1, 243-253.
- [6] The Federation of Thai Industries, (2016). "Car manufacturing export record in April 2016"
- [7] S., Koetnuyom, (2013). "Temperature Analysis of Automotive Brake Discs", The Journal of KMUTNB, Vol. 13, No. 1, 323-331.
- [8] S., Koetnuyom, (2006). "Study of Heat Convection Coefficient in Automotive Brake Disc", The 20th Conference on Mechanical Engineering Network of Thailand, 18-20 October 2006.
- [9] Federal Motor Carrier Safety Administration (FMCSA), (2002). "Rules and Regulations for brake performance", U.S. Department of Land Transport, United State of America, Part 393.52.
- [10] Japanese Automotive Standard, (2000). "JASO C406: 2000, Passenger car-Braking device-Dynamometer test Procedures"
- [11] S., Lakkam, K., Suwantaroj, P., Puangcharoenchai, S., Mongkonlerdmanee, and S., Koetnuyom, (2013). "Study of heat transfer on front- and back-vented brake discs", Songklanakarin Journal of Science and Technology, Vol 35 No.6, 671-681
- [12] H.S., Qi and A.J., Day, (2007). "Investigation of disc/pad interface temperatures in friction braking", Wear 262, 505-513



A Study Performance of Split Type Air-Condition System using 5 Plus Technology

Wirote Ritthong, Watcharin Pachittyen, Patiwat Khomwachirakul, and Nutthawut Singthuean

Mechanical Engineering, Faculty of Engineering
Rajamangala University of Technology Phra Nakhon
Bangkok, Thailand

wirote.r@rmutp.ac.th, wpachitt@gmail.com, patiwat.k@rmutp.ac.th, nutthawut-si@rmutp.ac.th

Abstract— This project was to aims study split type air-condition system by using 5 Plus technology. The original systems air-condition system modular size of 12,000 BTU/h and inside refrigerant was R-407c. This project used 5 Plus technology used pressure control mechanic devices for balance system to refrigeration pressure system in a time start and stop to compressor and compare the Energy Efficiency Ratio (EER) and Electrical power per Ton of Refrigeration (kW/TR). In study we have 2 cases were Case (1) Split Type air-condition system and Case (2) Split type air-condition system with 5 Plus technology. The testing with the result that the test temperature of the room in split-type air-condition system at steady state were 23°C, 25°C and 27°C with the result of EER and kW/TR to the best condition at 27°C in two cases with conclusions was follow. In decrease of used energy of EER and kW/TR with the best condition at Part Load of steady state of split-type air-condition system. So that we see case (2) EER = 23.34 more than case (1) approximately 25.01% and in case (2) kW/TR = 0.51 less than case (1) approximately 20.31%

Keywords—5 Plus technology (5 Plus), Energy Efficiency Ratio (EER), kW/TR

I. INTRODUCTION

In recent years, global warming has caused the change of temperature in many places of the world. The world's temperature increases approximately 0.7 °F in every 10 year, and from the data 2016, it indicated that the temperature on the earth was 0.07°C higher than that in 2015 or has increased 32.12 °F for up to 3 consecutive years [1]. Moreover, since Thailand is located in the humid tropical zone where the weather is quite hot, air conditioners are needed for more comfort. In 2016, the air-conditioners were exported from Thailand up to 57.7 percent and/or the average growth rate is 22.1 percent per year [2]. An air-conditioner is a relatively high electric power appliance that is approximately 70% of electrical usage within office buildings or department stores, although the air

conditioners in residence which are cooled with condensers would be standardized with the standard of energy saving (Number5).

An air conditioning system consists of a compressor that compresses low-temperature, low-pressure gas substance in order to increase pressure and temperature, and then flows through to the condenser to reduce the temperature to the condensation point and change the state from gas to liquid. Afterwards, the liquid refrigerant flows through the pressure control equipment (Expansion valve) to reduce the pressure. This pressure reduction process causes refrigerant change the state from low-temperature, high-pressure liquid into low-temperature, low-pressure gas. And then the gas flows into the evaporation machine in order to exchange the heat inside the room, then flows back into the compressor again throughout the work of air conditioners [3].

At present, there is a trial by using the thermosyphon with closed-loop oscillating heat pipe (CLOHP) to reduce the heat of refrigerant and also using wasted water from evaporation machine to aid in lowering the temperature of the refrigerant inside the CLOHP hose [4] for releasing the heat of the refrigerant before entering into the pressure reduction equipment of air-conditioners for better cooling. This makes the refrigerant less temperature than the saturated liquid until it becomes subcooling, which increases the efficiency of the air-conditioners [5]. However, it is also a concern to the installation cost. The production team has a concept of bringing the 5 Plus Energy saving technology to balance the compressor's pressure while the compressor is stopping which balances the pressure of suction and the extruded side to reduce the compressor load during the next starting period to be in a low current [6]. As a result, the installation of the 5 Plus energy saving system can reduce power consumption by the measurement of KW/TR, prolong the cooling period of air-conditioner, control moisture to be stable inside the room throughout the work of air-conditioner, reduce wear and prolong the operating life of the equipment in the air-conditioning system [5], etc.



II. RESEARCH METHODS

This research is used to do experiment with separate air-conditioning-system in size of 12,000 BTU/h using R407c refrigerant in case (1) and case (2) to apply measurement results to calculates the EER and KW/TR values to compare the performance and power of the air-conditioning system, which is equipped with the operating temperature and pressure detector systems in 5 positions:

- position 1st The refrigerant is removed from compressor
- 2nd The refrigerant is out of the condenser
- 3rd The refrigerant before accessing the pressure reduction device
- 4th The refrigerant is removed from the pressure reduction device
- 5th The refrigerant is out of the evaporation machine

A. Measuring Tools Equipment

Preparing Equipment

- 1) *Anemometer* - Used for measuring the average wind velocity to be calculated for value Volume flow rate (CFM)
- 2) *Thermometer* - Used for measuring temperature and humidity within air-conditioned rooms by checking the supply air inlet and return air inlet from the evaporation machine to find the value of enthalpy.
- 3) *The Memory Hilogger sensor and the Thermo copper type K cables* - Used to detect the temperature of refrigerant in each position of a modular air-conditioning system
- 4) *High pressure gauge/low pressure gauge* - Used to measure the pressure of refrigerant within a split-type air-conditioning system.
- 5) *The electronic tools* are used for measuring electrical values such as electric meter clamp, for measuring voltage and electrical current of air-conditioning circuit.

B. Experimental Procedure

will be conducted in the case of (1), the normal split-type air-conditioning system and the case (2) Integrated split-type air-conditioning system with 5 Plus energy saving technology.

C. Measurement Procedures

- 1) In the trial there are various values that define variables and are measured at various positions, with the following steps:
 - a) The air-conditioned room temperatures tested are 23 °C, 25 °C and 27 °C.
 - b) record total pressure and temperature at 5 positions.
 - c) The area of air-conditioned room tested equals to 13.50 m².
- 2) Air-conditioner experiments in each case with the following steps:
 - a) Check the air-conditioner and control cabinet.

b) Set the Memory Hilogger to collect the temperature values.

c) Turn the control-cabinet switch on to start the device.

d) Turn on the Power switch at the remote control of the air-conditioner to control the fan speed at high, medium and low speed.

e) Turn the valve on and off at different positions to test in case (1) and case (2) respectively.

f) Record the pressure and temperature of the refrigerant at all 5 positions.

g) Record electricity and voltage values.

D. Project Design

1) *The design of the setting thermosyphon with closed-loop oscillating heat pipe along with wasted water from evaporation and 5-Plus energy-saving technology.*

To install a split-type air-conditioning system with 5 Plus energy saving technology, it can be shown as Fig.1.

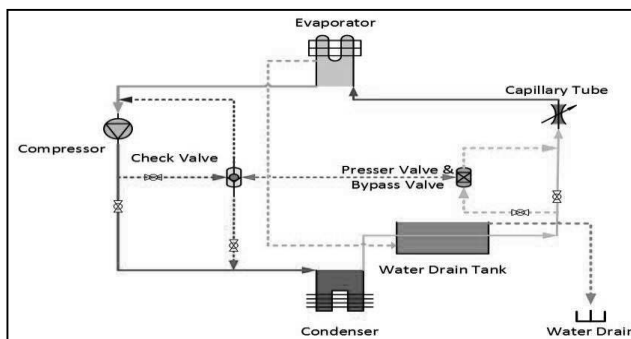


Fig.1. Split-type air-conditioning system circuit with 5 Plus Energy saving Technology [5]

2) The Theory Associated For Calculation

The enthalpy can be found in two ways: (1) from the table of Refrigerant and (2) using the Mollier's Diagram (p-h diagram) of refrigerant, as shown in Fig. 2.

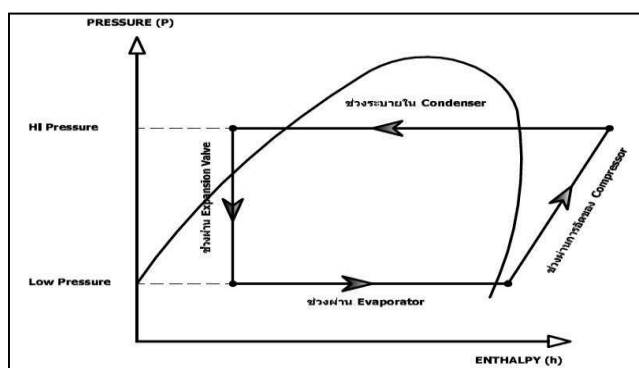


Figure.2. Mollier's Diagram [7]



To calculate the coefficient of cooling and electrical energy per ton of refrigeration, it can be found in the equation (1) and the equation (2) respectively as follows:

$$EER = \frac{Q_{Evap}}{P_{Input}} \quad (1)$$

When EER is Cooling performance (BTU/h/W)

Q_{Evap} is All the coolness received (BTU/h)

P_{Input} is Total power supplied to air conditioning system (W)

$$\frac{kW}{TR} = \frac{P_{input}}{TR} \quad (2)$$

When KW is Power ton of refrigeration

P_{Input} is Total power supplied to air conditioning system
TR is ton of refrigeration (TR)

III. RESULT

In the experiment, the fixed temperatures are controlled in the air-conditioned room at 23 °c, 25 °c and 27 °c. The researchers began to experiment by measuring the pressure and temperature of all five positions, shown in table 1 and table 2 as well as electricity energy as shown in table 3 to receive various values; for example, pressure and temperature can calculated to find enthalpy as shown in table 4, and then take the data to calculate the EER and KW/TR respectively.

Table I. Average Pressure Value of Case (1) And Case (2) At Air Conditioned Room Temperature 27 °c

Case	P ₁ (bar)	P ₂ (bar)	P ₃ (bar)	P ₄ (bar)	P ₅ (bar)
(1)	17.59	17.50	17.16	5.54	5.37
(2)	17.91	17.27	17.22	4.90	4.76

Table II. Average Temperature of Case (1) And Case (2) At Air-conditioned Room Temperature 27 °c

Case	T ₁ (°C)	T ₂ (°C)	T ₃ (°C)	T ₄ (°C)	T ₅ (°C)
(1)	61.79	32.65	30.33	11.52	13.43
(2)	74.20	36.96	36.45	10.13	14.31

Table III. Average Electric Power of Case (1) And Case (2) At Air-conditioned Room Temperature 27 °c

Case	Voltage (V)	Current (A)	PF (-)
(1)	223	5.03	0.567
(2)	222.3	4.71	0.55

Table IV. Average Enthalpy of Case (1) and Case (2) At Air-conditioned Room Temperature 27 °c

Case	h ₁ (kJ/kg)	h ₂ (kJ/kg)	h ₃ (kJ/kg)	h ₄ (kJ/kg)	h ₅ (kJ/kg)
(1)	451.25	251.24	246.76	246.76	423.36
(2)	463.83	258.66	257.56	257.56	425.39

A. Result from calculation to find the efficiency and electricity power per ton refrigerant

From graph in Figure 5 we will see that in the case (2) the EER value is higher than the case (1) in all temperatures which shows us that the installation of 5 Plus energy saving technology can increase cooling efficiency and reduce power consumption And the maximum EER value is at 27 °c in air-conditioned room.

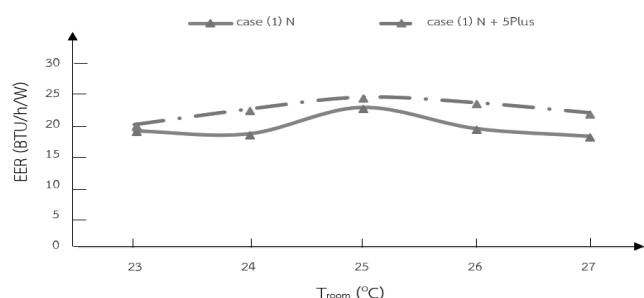


Fig.3. Cooling performance at room temperature 23 °c, 25 °c and 27 °c

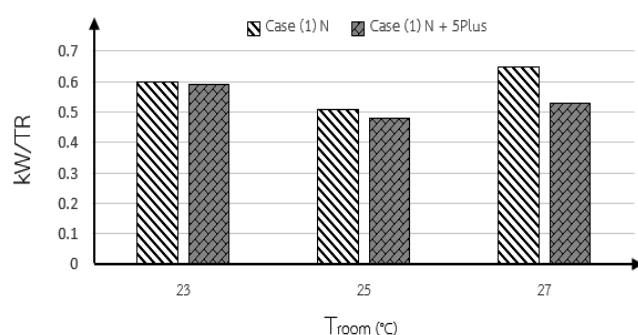


Fig.4. Electricity power per ton of refrigerant at room temperature 23 °c, 25 °c, and 27 °c in case (1) and case (2)

B. Research Result

From the test results, it indicates that the case (2) split-type air-conditioning system with the thermosyphon with closed-loop oscillating heat pipe along with wasted water from a evaporator with a 5 Plus power saving system reduces more power consumption than the case (1) because the 5-Plus Energy saving system balances the refrigerant pressure which makes the start of the compressor enable to run under low current conditions and maintain the state of the refrigerant. It helps to reduce compressor load and can control temperature and humidity in the air-conditioned room which makes us feel comfortable and don't feel sticky while in the air-conditioned room.

C. Summary of Research Result

As a result, the team has tried and compared between a split-type air-conditioning system with using thermosyphon with closed-loop oscillating heat pipe along with wasted water from the evaporator of the system with and without installation the 5 Plus power saving technology The main purpose is to compare usage of the power of electricity per refrigerant, cooling performance of air-conditioning system and reduce wear of internal equipment. From the experiment, it can be summarized that the installation of the 5 Plus Energy

saving Technology in case (2) can reduce power consumption better than case (1) in the range of 19.44%-20.31% and the EER value of (2) is higher than the case (1) in the range of 20.10%-25.01%, and it can be seen that at air-conditioned room 27 °c there will be the most effective value.

Acknowledgment

The study of this project has been helped by **Asst. Prof. Dr. Wirote Ritthong**, and all faculty members. With their advising, conveying their knowledge, as well as controlling the term of study of research, the research projects can be fully successful. Thanks to ECI International Co., Ltd to provide 5 Plus energy saving technology to be used for research. Thank you for the faculty of Engineering, Rajamangala University of Technology to support all work for the project.

REFERENCES

- [1] Thai BBC News, "The average temperature of the world in 2016 is unprecedented hot," unpublished.
- [2] Kasikorn Research Center, "Intelligent air-Conditioner...technology to the future," Kasikornthai Econ Analysis, vol. 2846, pp. 1, May 2017.
- [3] S. Panyasompak, "Evaporator and condenser," unpublished.
- [4] S. Wannapakhe, "Heat pipe and thermosyphon applications in Thailand," The Journal of Kmutnb, vol. 22, No. 3, pp. 689-692, July 2012.
- [5] ECI International Co., Ltd, "Split type air-condition system using closed loop oscillation thermo syphon heat pipe and 5 plus technology," unpublished.
- [6] ECI International Co., Ltd, "Advantage to save energy and create comfort in air-conditioning and refrigeration system," unpublished.
- [7] Department of Alternative Energy Development and Efficiency, "Principle of refrigeration and a/c systems, and guidelines for energy conservation," Training textbook of heat energy, pp. 2-9.



A Study on the Mechanical Properties of Polypropylene at Different Mixing Ratios by Molding Test Pieces According to ASTM D638-10 and D256-10

Thawachchai Chattamnan^{1st}, Prasong Kankaew^{2nd}, Prasit Phangphet^{3rd} and Jack Chum-in^{4th}
Tool and Die Engineering Department
Engineering Faculty RMUTP
Bangkok, Thailand
thawachchai.ch@rmutp.ac.th, prasong.k@rmutp.ac.th, prasit.p@rmutp.ac.th, jack.c@rmutp.ac.th

Abstract— The mechanical properties of polypropylene changed from different composite ratios by plastic Injection forming test specimens in accordance with ASTM D638-10 and D256-10. Measurement of the properties of materials with force acting in different methods such as Tensile strength testing Impact Strength testing Because it is applied to any product. Those products will have to be done more or less. Designers know the mechanical properties. It helps to design the product properly and appropriately. All types of materials will decrease mechanical property. It is not popular to forming again. It will be mixed with new materials to reduce production costs or to improve mechanical properties to proper the application. From the 4 test pieces of new PP and used PP 100:0, 80:20, 70:30 and 60:40 meet the results of Tensile Strength 37.5, 40.3, 40.9, 41.5 MPa and Impact Strength 30.4, 29.5, 29.5 and 27.6 J / m respectively. The rate of change in the material changes. The lowest value ingredients are 70:30.

Keywords— plastic injection; mechanical properties

I. INTRODUCTION

Approach to Thailand 4.0 Science and engineering advances rapidly. New types of materials have been developed. And the requirement for products that are suitable for function use in many industries makes the manufacturer cannot choose from the experience to select materials and production methods to suit the function and design of the product anymore. So, the properties of the materials testing have been gradually introduced into the production process. The concept of this paper is to find the mechanical properties of polypropylene from different composite ratios by forming test specimens in accordance with ASTM D638-10 and D256-10 [1]. Test results for design workpieces appropriate and economical.

II. RESEARCH METHODOLOGY

Tensile strength testing is the most popular and well-known test for basic mechanical properties testing of

materials. The test will be take force linear of workpiece testing in the opposite direction to create tension in the workpiece. This type of test is used to test materials such as metals and polymers the tensile test specimen has a cross sectional area in which the strain gauge is to be measured. It is in the center of the workpiece and is smaller in size than the clamp area. Dumbbell is the center of the workpiece because it is the area with the highest stress due to the lowest cross-sectional area. The broad-waisted dumbbell type is suitable for soft plastic testing.

Impact Strength Test The impact strength test is based on the Charpy test, where the polymer is characterized by high impact velocity [2].

A. Research Processes

The material used for testing polypropylene plastic is POLIMAXX 1100NK [3] as shown in Figure 1.



Fig. 1. polypropylene plastic material

The properties of the polypropylene plastic used in the design of the test piece are shown in Table 1.



TABLE I. polypropylene properties [4]

polypropylene properties	
Type of plastics	Polypropylene
PP Hardness	0.91 g / cm ³
PP liquid density	0.76 g / cm ³
Shrinkage rate	1.5%
Mold closed pressure	30.9 MN / mm ²
Melting temperature	200°C
Mold temperature	50°C
Discharge temperature	70°C
Closing time	2 sec
Heat Transfer	0.067 watt/m ²

Designing for Standard testing ASTM D638-10 and D256-10 are drawn with UGNX6 (UNIGRAPHICSNX6) as shown Figure 2.

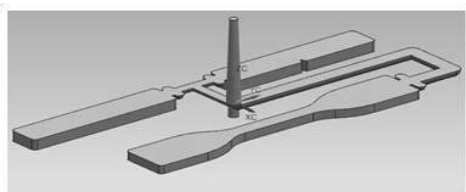


Fig. 2 Test piece design

B. Materials and Methods

The process of mixing plastic ratio between New polymer homopolymer with polypropylene used the ratio is determined by the scale as shown in Figure 3.



Fig. 3 mixing plastic ratio

Using a pellet plastic recycle crushed PP plastic, the specimen was removed from the test specimen to be mixed with the new granules as shown in Figure 4.



Fig. 4 pellet plastic recycles crushed PP plastic

Then, Use the Jet master c series JM168-C ES injection molding machine for inject test pieces as shown in Figure 5.



Fig. 5 injection molding machine

The value used to inject for Injection process is shown in Table 2.

TABLE II. Injection parameter [5]

Injection parameter	
Injection volume	12 g
Liquid volume (V)	16.57 cm ³
Screw Lead (L)	18 mm
Mold close force (T)	370 kN
Cooling Time (Tk)	32.41 sec
Injection time (Tfill)	3 sec
Tack Time	1 sec
Cycle Time	25 sec
Heat required to drain	207.682 J / g

The test specimens were injected with the injection molding machine as shown in Figure 6.



Fig. 6 PP specimens



Prepare tensile and impact strength test pieces according to ASTM D638-10 AS shown in Figure 7 and 8

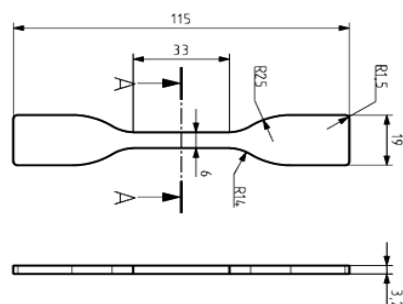


Fig. 7 tensile test specimens

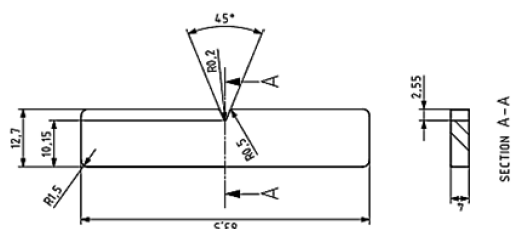


Fig. 8 Impact test specimens

The Zwick Z020 Universal Testing Machine is shown in Figure 9 and INSTRON MACHINE CALE 9050 Impact Resistance Tester, as shown in Figure 10.



Fig. 9 Tensile testing machine



Fig. 10 Impact testing machine

III. RESULTS

The average tensile strength and impact strength according to ASTM D 638-10 and D 256-10 are shown in Table 3.

TABLE III. The average tensile strength and impact strength

Testing type	PP 100	PP 80	PP 70	PP 60
Tensile (MPa)	37.5	40.3	40.9	41.5
Impact (J/m)	30.4	29.5	29.5	27.6

The tensile strength test according to ASTM D638-10 has a higher tensile strength ratio, as shown in Figure 11.

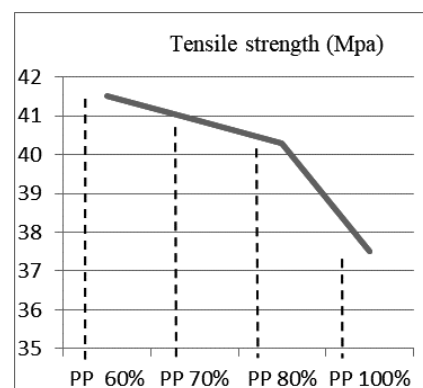


Fig. 11 Tensile strength trend

From Figure 11, The tensile strength of the New PP and PP used samples were proportionally prepared. The hardness of the samples was increased, resulting in higher tensile strength up respectively.

ASTM D256-10 Impact Resistance Test results in a reduction in the composition of the debris, as shown in Figure 12.

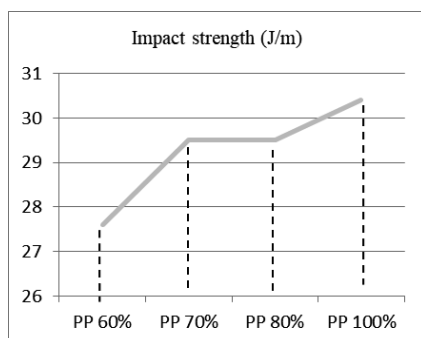


Fig. 12 Impact strength trend

From Figure 12, The impact strength of the New PP and PP used samples were proportionally prepared. The toughness of the samples was decreased, resulting in lower impact strength down respectively.

IV. CONCLUSIONS

The mechanical properties of polypropylene were changed from the different composite ratios by forming test specimens

in accordance with ASTM D638-10 and D256-10 from 4 test specimens. The results of Tensile Strength 37.5, 40.3, 40.9, 41.5 MPa and Impact Strength 30.4, 29.5, 29.5, 27.6 J / m. The rate of change in the material changes. The suitable value ingredients are 70:30.

ACKNOWLEDGMENT

The authors are grateful for the Participants in the study and research. Faculty of Engineering Production Engineering Thank you for this. From Rajamangala University of Technology Phra Nakhon.

REFERENCES

- [1] ASTM/. "Standard Test Methods for Determining the Izod Pendulum Impact Resistance of Plastics." Interationnal, 2010
- [2] Crawford, R. J. Plastic Engineering. 3rd ed. Oxford : Linacre Houes, Jordan Hill. 1998
- [3] IRPC, "Polypropylene Homopolymer Grade 1100NK ."Public Company Limited, 2018
- [4] Germany. Bayer Engineering Thermoplastic. Processing DaTa for the Injection Moulder. 8th ed Germany. 1998.
- [5] Glanvill, A.B.The plastic Engineering's DataBook. American Edition. 3rd printing. Brighton: Machinery Puplicshing Co. 1974.



GEE and LMM with Spatial Effects for Cassava and Rubber Yields in Thailand

Krisada Lekdee

Department of Mathematics and Statistics, Faculty of
Science and Technology, Rajamangala University of
Technology Phra Nakhon, Bangkok, Thailand
Krisadal.l@rmutp.ac.th

Pornpit Sirima

Department of Industrial Engineering, Faculty of Engineering,
Rajamangala University of Technology Phra Nakhon
Bangkok, Thailand
Pornpit.s@rmutp.ac.th

Abstract—The objectives of this research were to propose an efficient and proper model for cassava and rubber yields in Thailand. A generalized estimating equation (GEE) and a linear mixed model (LMM) with spatial effects assumed to be the conditional autoregressive model (CAR) were applied. The dependent variables were the cassava and rubber yields collected from each month in every province of Thailand and the factors were rainfall, averaged temperatures, and regions. The results from GEE and LMM revealed that the factors influencing on the cassava and rubber yields were rainfall, averaged temperature, and region. Both GEE and LMM fitted the correlated data very well. The GEE is used to explain the factor influence for all provinces while the LMM is used to explain the factor influence for each province.

Keywords—Linear Mixed Model (LMM); Cassava and rubber yields; Conditional autoregressive model (CAR) spatial effects; spatial analysis

I. INTRODUCTION

Cassava is an important commercial crop in Thailand. In 2016 the harvested area was 9,315,012 rai and the yield was 31,161,103 tons. Thailand is a cassava exporter, and the product is in the top of the world continuously. Rubber is another important economic crop in Thailand. The harvest area was 18,223,833 rai and the production was 4,566,260 tons. The South region of Thailand has the highest potential for rubber plantation [1]. From the above information, researchers were interested in the analysis of cassava and rubber production to be used for production planning for the related persons. The production of cassava and rubber is collected continuously every year. It was published on the website of the Office of Agricultural Economics, Department of Agriculture, Ministry of Agriculture and Cooperatives [1]. The report is based on descriptive statistics, presenting in tables, graphs, values, and percentages. The data will be more useful if they are analyzed in depth with mathematical and statistical models.

For an analysis of repeated measures data, the most commonly used model is a generalized estimating equation (GEE) presented by [2]. It is a model that expresses the relationship between the independent variables and the dependent variables without the assumption of independence. The related data occur when the same data are collected in the same unit. The dependent variables can be both continuous and discrete. The GEE describes the magnitude of the influence of factors in the overall population. This is called a population-averaged model. Reference [3] used GEE model to analyze the risk of malaria. Another model that analyzes this type of data is a linear mixed model (LMM). A LMM is a flexible model. We can add some types of variables into the model easily, for example, a variable that represent a spatial relationship. The spatial relationship is due to the fact that things that are closer together are more closely related than those that are far away. There are several ways to estimate LMM parameters, but the method is widely used when the model is complex is a Bayesian method [4]. Reference [5] analyzed the disease incidence using a generalized LMM model with a spatial relationship, and their model was widely used by other authors, for examples, [6-8].

As mentioned above, the GEE and LMM have not been applied to the cassava yield data that are collected continuously. The researchers were interested in studying and developing a model for cassava and rubber yields to be used for production planning in Thailand, using the GEE and LMM models. The basic factors to consider were rainfall, averaged temperature and region (Central, North, Northeast, South, East and West)

II. METHOD AND APPLICATION

Data were collected from all provinces in Thailand from 2002-2016. The cassava and rubber yields came from the Office of Agricultural Economics [1] and the rainfall,



and temperature came from the Meteorological Department of Thailand, Ministry of Digital Economy and Society [9].

The GEE has the following form.

Let Y_{ij} be the yield in province i year j where $i = 1, \dots, 76$ and $j = 1, \dots, 15$.

$$y_{ij} \sim N(\mu_{ij}, \sigma^2), i = 1, \dots, 76 \quad j = 1, \dots, 15$$

The relationship of the dependent variable to the factors is in the following form.

$$\mu_{ij} = \beta_1 + \beta_2 * rain_{ij} + \beta_3 * temp_{ij} + \beta_4 * north + \beta_5 * northeast + \beta_6 * south + \beta_7 * east + \beta_8 * west \quad (1)$$

$rain_{ij}$ is the amount of rainfall (mm) in province i year j . $temp_{ij}$ is the average temperature (Celsius) in province i year j . $north$ is the province i in the north region. $northeast$ is the province i in the northeast region. $south$ is the province i in the south region. $east$ is the province i in the east region. $west$ is the province i in the west region. β_1 is an intercept and β_2, \dots, β_8 are regression coefficients. The pattern of data relationships in the same unit is first-order autoregressive model since the data are collected as time series data.

The linear mixed model (LMM) [10] with spatial effects and Bayesian parameter estimation has the following form.

Let Y_{ij} be the yield in province i year j where $i = 1, \dots, 76$ and $j = 1, \dots, 15$.

$$y_{ij} | \mathbf{b} \sim N(\mu_{ij}, \sigma^2) \quad i = 1, \dots, 45 \quad j = 1, \dots, 15$$

$$\mu_{ij} = \beta_1 + \beta_2 * rain_{ij} + \beta_3 * temp_{ij} + \beta_4 * north + \beta_5 * northeast + \beta_6 * south + \beta_7 * east + \beta_8 * west + \beta_9 * j + b_{li} + b_{2ij} + v_i \quad (2)$$

β_9 is the coefficient of the linear trend, b_{li} is a variation between province i and b_{2ij} is a variation between province i and within year j . v_i is a spatial effects which follows the CAR model [11] defined in this form.

$$v_i | \mathbf{v}_{(-i)} \sim N\left(\sum_{k=1}^m \frac{w_{ik} v_k}{w_{i+}}, \frac{\tau_v^2}{w_{i+}}\right)$$

$$\text{and } \mathbf{v} \sim N(\mathbf{0}, \tau_v^2 (\mathbf{D}_w - \mathbf{W})^{-1})$$

$$\text{or } p(\mathbf{v}) \propto \exp\left\{-\frac{1}{2\tau_v^2} \mathbf{v}^T (\mathbf{D}_w - \mathbf{W}) \mathbf{v}\right\},$$

$\mathbf{W} = (w_{ik})$ is the weight matrix of each area where $w_{ij} = 1$ if area i and k are neighbors where $i \neq k$, $w_{ij} = 0$ if area i and k are apart.

$\mathbf{D}_w = \text{diag}(w_{i+})$ is a diagonal matrix whose element in the main diagonal (i, i) is equal to $w_{i+} = \sum_k w_{ik}$.

Under Bayesian estimation, non-informative priors are assigned as follows.

$$\beta_1, \beta_2, \beta_3, \dots, \beta_9 \sim N(0, 10000), \quad b_{li} \sim N(0, \tau_{b1}^2), \\ b_{2ij} \sim N(0, \tau_{b2}^2), \\ \tau_{b1}^2, \tau_{b2}^2, \tau_v^2 \sim \text{InvGamma}(0.01, 0.01).$$

The R program was used to find the estimate of each parameter.

III. RESULTS

By GEE model, factors influencing rubber yield were rainfall, averaged temperature, North, Northeast, South, West and Central was a reference group as shown in Table I. If the rainfall increases 1 mm, the yields will be decreased by 4.21 tons. If the average temperature rises by 1 °C, the rubber yield will be decreased by 317.80 tons. Northern region rubber yield is 8,680.58 tons more than Central region. Northeastern region is 12,355.25 tons less than Central region. Southern region is 208,546.17 tons higher than Central region. Eastern region is 52,691.44 tons higher than the Central region. The western region is 7,599.88 tons higher than the Central region.

Similarly, by LMM model, factors influencing rubber yield were rainfall, averaged temperature, North, Northeast, South and West as shown in Table II. By GEE model, factors influencing cassava yields were rainfall, averaged temperature, North, Northeast, South and West as shown in Table III. By LMM model, factors influencing cassava yield were rainfall, averaged temperature, North, Northeast, South and West as shown in Table IV.



TABLE I. FACTORS AFFECTING RUBBER YIELD BY GEE MODEL

Parameter	B	Std. Error	95% Wald Confidence Interval		Hypothesis Test	
			Lower	Upper	Wald Chi-Square	Sig.
(Intercept)	16,234.28	7,913.80	723.51	31,745.05	4.21	0.04
rain	-4.21	3.54	-11.15	2.73	1.42	0.23
temp	-317.8	315.27	-935.72	300.12	1.02	0.31
North	8,680.58	5,358.85	-1,822.57	19,183.73	2.62	0.11
Northeast	12,355.25	2,893.92	6,683.28	18,027.22	18.23	0
South	208,546.17	41,160.02	127,874.01	289,218.32	25.67	0
East	52,691.44	18,856.50	15,733.37	89,649.51	7.81	0.01
West	7,599.88	4,041.84	-321.98	15,521.75	3.54	0.06
Central (Reference)

IV. DISCUSSION

A linear mixed-mode model (LMM) describes the magnitude of the factorial influence of each unit. This model is so-called a subject-specific model. The GEE model presented by Liang and Zeger (1986) differs from the non-randomized LMM model. A model that describes the magnitude of the influence factors in the overall population. This is so-called a population-averaged model. Bayesian estimation is becoming more popular since it can solve problems from simple problems to complex problems in which the maximum likelihood method cannot be applied. In overall, rubber yield in each province is highest in the South, followed by the Eastern, the Northeast, the Northeast, the Central and the West, respectively. Southern Thailand is located in the tropical zone whose environment is more suitable for rubber planting than other regions in Thailand, such as soil, rainfall, relative humidity, temperature, and wind speed [12].

The cassava has the highest yield in each province in the East, followed by the Northeast, the Central, the Western, the North and the South. The ideal environment for growing cassava is that the sea level is not over 200 meters, no flood, loamy soil, sandy soil, good drainage and the pH value is less than 7 [13]. The Eastern region has those qualifications. Therefore, it is suitable for cassava cultivation.

TABLE II. FACTORS AFFECTING RUBBER YIELD BY LMM MODEL

Factors	Mean	Stadard Diviation	95% Credible Interval	
Intercept	8.2	33.84	-75.22	73.69
rain	1.63	0.05	1.55	1.71
temp	0.92	6.03	-7.27	5.73
North	65.91	72.68	-133.2	156.6
Northeast	-70.44	48.23	-124.4	62.88
South	29.09	55.62	-150.5	125.5
East	48.5	62.55	-94.1	115.3
West	16.75	53.43	-111.9	125.2
Central (Reference)
Trend	201.3	19.58	155.7	227.7

TABLE III. FACTORS AFFECTING CASSAVA YIELD BY GEE MODEL

Parameter	B	Std. Error	95% Wald Confidence Interval		Hypothesis Test	
			Lower	Upper	Wald Chi-Square	Sig.
(Intercept)	954,097.76	257,685.47	449,043.53	1,459,152.00	13.71	0
rain	-115.32	36.36	-186.58	-44.07	10.06	0
temp	-9,993.35	3,886.38	-17,610.52	-2,376.19	6.61	0.01
North	-510,025.91	177,511.15	-857,941.37	-162,110.45	8.26	0
Northeast	279,458.41	359,046.43	-424,259.66	983,176.47	0.61	0.44
East	432,167.26	207,240.00	25,984.32	838,350.20	4.35	0.04
West	-78,096.29	307,652.76	-681,084.62	524,892.04	0.06	0.8

TABLE IV. FACTORS AFFECTING CASSAVA YIELD BY LMM MODEL

Factors	Mean	Stadard Diviation	95% Credible Interval	
Intercept	0.14	100.2	-195.1	195.4
rain	-80.48	35.85	-151.9	-10.35
temp	5.45	99.5	-186.2	202.4
North	-0.63	99.73	-195.9	193.9
Northeast	-0.48	100.4	-198	198.4
South	0.91	99.39	-194.6	195
East	-1.32	100.1	-197.3	193.7
West	0.56	99.51	-194.4	194.7
Central (Refe)
Trend	10.1	99.75	-184.3	206.5

V. CONCLUSION

The main research objectives were to propose an efficient and proper model for cassava and rubber yields in Thailand. A generalized estimating equation (GEE) and a linear mixed model (LMM) with spatial correlation were applied. The dependent variables were the monthly cassava and rubber yields in each province of Thailand. The results from GEE and LMM revealed that the factors influencing on the cassava and rubber yields were rainfall, averaged temperature and region. The GEE is the population-averaged model while the LMM is the subject-specific model.

ACKNOWLEDGMENT

Authors gratefully acknowledge the Rajamangala University of Technology Phra Nakhon, Institute of Research and Development and the faculty of Engineering for their technical and financial support.



REFERENCES

- [1] OAE, Agricultural production data <http://www.oae.go.th/production.html>, 2017.
- [2] K.Y. Liang and S.L. Zeger, 1986. "Longitudinal data analysis using generalized linear models," *Biometrika*, 1986, vol. 73, pp. 13-22.
- [3] K. Lekdee and L. Insrisawang, "Generalized Linear Mixed Model (GLMM)," *Journal of Health Science*, 2010, vol. 19(3), pp. 364-373.
- [4] P. Congdon, *Bayesian Statistical Modelling*. 2nd ed. John Wiley & Sons, NY, 2006.
- [5] D. Clayton and J. Kaldor, "Empirical Bayes estimates of age-standardized relative risks for use in disease mapping," *Biometrics*, 1987, vol. 43, pp. 671-681.
- [6] R.K. Tsutakawa, "Mixed model for analysing geographic variability in mortality rates," *J. Amer. Statist. Assoc.*, 1988, vol. 83, pp. 37-42.
- [7] N. Cressie and N.H. Chan, "Spatial modeling of regional variables," *J. Amer. Statist. Assoc.*, 1989, vol. 84, pp. 393-401.
- [8] N. Cressie, "Smoothing regional maps using empirical Bayes predictors," *Geograph. Anal.*, 1992, vol. 24, pp. 75-95.
- [9] TMD, Rainfall data and temperature data. <http://www.tmd.go.th/services/services.php>, 2017.
- [10] B.T. West, K.B. Welch, and A.T. Galecki, *Linear mixed models: A practical guide to using statistical software*. Chapman & Hall/CRC, NY, 2007.
- [11] S. Banerjee, B.P. Carlin, and A.E. Gelfand, *Hierarchical Modeling and Analysis for Spatial Data*. Chapman and Hall/CRC Press, FL, 2004.
- [12] Wikipedia, Rubber in Thailand. <https://th.wikipedia.org>, 2016.
- [13] AGROW, How to get better yield of cassava? Thailand case study. http://www.agrowproduct.com/index.php?option=com_k2&view=item&id=85:5&Itemid=124&lang=en, 2017.



Comparative Eco-efficiency of Ferrous and Non-Ferrous Parts Manufacturer : a Case Study of Part Manufacturing Industry in Thailand

Suwat Paengteerasukkamai¹, Natworapol Rachsiriratcharabul¹

¹ Department of Sustainable Industrial Management Engineering, Faculty of Engineering
Rajamangala University of Technology Phra Nakhon
1381 pracharat 1 road wongsawang district, bangsue, Bangkok 10800 Thailand
E-mail: suwat.pa@rmutp.ac.th

Abstract— Various organizations have responded to the policy by encouraging their own organization to become more environmentally friendly. The calculation of corporate greenhouse gas (GHG) emissions, so called carbon footprint for organization, and eco-efficiency are common tools that businesses in Thailand pay very much attention. This paper conducts a study to calculate eco-efficiency base on amount of greenhouse gas emissions analysis of ferrous and non-ferrous parts using data from part manufacturing industry in Thailand. The study have started by calculating carbon footprint for organization in order to determine direct and indirect greenhouse gas emissions. The result indicate that greenhouse gas emissions from ferrous parts manufacturer is equal to 212,011.72 TonCO₂e. Considering each source of the greenhouse gas emissions, the most significant contribution come from electricity consumption in the organization, and stationary combustion GHG emissions by a percentage equal to 71.13 and 21.63 respectively. While Non-ferrous parts manufacturer have greenhouse gas emissions of 79,703.72 TonCO₂e. The major emissions are process emission and electricity consumption in the organization with a ratio of 89.72 and 7.20 percentage respectively. The study provides environmental impact of greenhouse gas emissions assessed with the volume of products in the year of collection. The results also show that the non-ferrous industry case had an eco-efficiency of 2.51 units / TonCO₂e compared to the ferrous industry case of 1.08 units / TonCO₂e. The benefits of Eco-efficiency in the commercial business, marketing can bring the results of the evaluation to improve their own products for better performance. Can reduce the cost of production. In terms of energy use and resource use. Can improve productivity.

Keywords— *Eco-efficiency, Carbon footprint for organization, Emission, Ferrous, Non-Ferrous*

I. INTRODUCTION

Thailand's economic trend is in constant growth. Based on information provided by information division, the office of Industrial Economics, in the Industrial Economic Status Report on January 2008, Industrial Production Index (January 2008) +75.66% Production of motor vehicles +6.59% Production of air conditioners +30.67% Electronics and circuit boards +4.68% and iron and steel production +10.70%, respectively. [1] Especially the industrial sector is constantly developing. Impact on the use of natural resources reduced. Industrial waste and pollutants that are responsible for the global warming are

increasingly intensified. The effects are all from human activities. Currently, Ministry of Industry (MOI) of Thai royal government has developed strategic plan 2017 – 2021 (Revised Edition) which show missions to improve and develop the industrial ecosystem to facilitate the transformation towards Industry 4.0 and promote environmentally friendly production in all industrial sector [2]. It has expanded with the development of environmentally-friendly management systems or the green industry. One way to increase environmental friendliness of the industry is to focus on reduction of greenhouse gases, which is the cause of global warming that affects global climate change. Carbon Footprint Assessment This will allow their organizations to know the amount of greenhouse gases released into the atmosphere. This leads to an assessment of the eco-efficiency of the product. This can help in the planning of corporate governance, both in reducing greenhouse gas emissions and in economics, which can reduce the cost of energy and other unnecessary resources. In other words, it enhances the competitiveness of the industry and can be used as a marketing strategy and to promote the image of the company. It is a leader in the development and production of sustainable products. [3]

II. MATERIAL AND METHOD

Data Collection

Collect data on the source of the greenhouse gas emissions of the organization for a 12-month case study. Collect the collected data to determine the extent of the greenhouse gas emissions, which are directly and indirectly emitted (Indirect emission)

Calculate the amount of greenhouse gas emissions.

Bring the information that has divided the source of greenhouse gas emissions into carbon footprint calculations. According to the guidelines of the Greenhouse Gas Management Organization (Public Organization), the formula can be calculated as follows.



Greenhouse Gas Emission

$$= \text{Activity Data} \times \text{Emission Factor} \quad (1)$$

Analysis of greenhouse gas emissions

Analysis of significant greenhouse gas emissions from a factory. The type of direct greenhouse gas emission source is divided into 4 categories

- Greenhouse gas emissions from stationary combustion, such as those used in alternative power generators Fire Extinguishers Or the use of natural gas in non-mobile machinery.
- Emissions from mobile combustion (mobile combustion), such as the use of various types of fuel in vehicles that the organization is able to control operations such as Diesel Gasoline, Natural gas (NG), Liquefied Petroleum Gas (LPG) etc.
- Greenhouse gas emissions from the use of product or raw material improves. Processes emission, such as methane emissions from wastewater treatment systems. The use of reagents or chemicals in the process of improving the product when oxidation affects greenhouse gas emissions.
- Leakage of any substance that results in a greenhouse gas (Fugitive emission) such as methane leakage from the use of toilets, employees in the organization space. Various types of refrigerant leakage (except R22), leakage of CO2 extinguishers or various dry chemicals.

Evaluate eco-efficiency

Take the greenhouse gas emissions of the case study. It is considered to be an environmental impact factor considering the capacity of the industrial product. To assess economic eco-efficiency.

Compare the results of the eco-efficiency assessment.

Apply the results of the eco-efficiency assessment to compare the most eco-efficient case studies.

III. RESULT AND DISCUSSION

Based on data collected from the greenhouse gas emission sources of organizations in the ferrous parts industry, two case studies and the non-ferrous parts industry, two case studies in Thailand. Can display direct and indirect greenhouse gas emissions. The amount of raw materials, resources and fuel used by the organization is as follows: TABLE I. and TABLE II.

TABLE I. Types of Greenhouse Gas Emissions from a case study of ferrous parts manufacturing industry in Thailand

Scope emission	Types of Greenhouse Gas Emissions	Total (TonCO ₂ e)	Percentage (%)
Direct	Stationary Combustion	45,865.52	21.63
	Mobile Combustion	76.47	0.04
	Process emission	15,239.08	7.19
	Fugitive	16.59	0.01
Indirect	Electricity	150,814.05	71.13
Total		212,011.72	100.00

In Table 1, direct and indirect emissions of greenhouse gases were found to have a significant effect on the ferrous component industry, i.e., the amount of electricity consumed by the organization. The second highest was the greenhouse gas emissions of 21.63 percent and the least significant greenhouse gas emissions were greenhouse gas emissions. At 0.01 percent.

TABLE II. Types of Greenhouse Gas Emissions from a case study of two non-ferrous parts manufacturing industry in Thailand

Scope emission	Types of Greenhouse Gas Emissions	Total (TonCO ₂ e)	Percentage (%)
Direct	Stationary Combustion	1,788.15	2.24
	Mobile Combustion	118.11	0.15
	Process emission	71,508.15	89.72
	Fugitive	552.54	0.69
Indirect	Electricity	5,736.77	7.20
Total		79,703.72	100.00

Table 2 shows the direct and indirect greenhouse gas emissions. It is found that the amount of greenhouse gases affecting the non-essential component industry is the greenhouse gas emissions from the product. Or raw materials for various types of production. The second highest was the use of electricity in the manufacturing and office buildings. The lowest level of greenhouse gas emissions was observed. Fuel combustion comes from the use of corporate vehicles. At 0.15 percent

From Table 1 and Table 2, the data were analyzed. By comparing the percentage of greenhouse gas emission sources can be displayed as Figure 1.

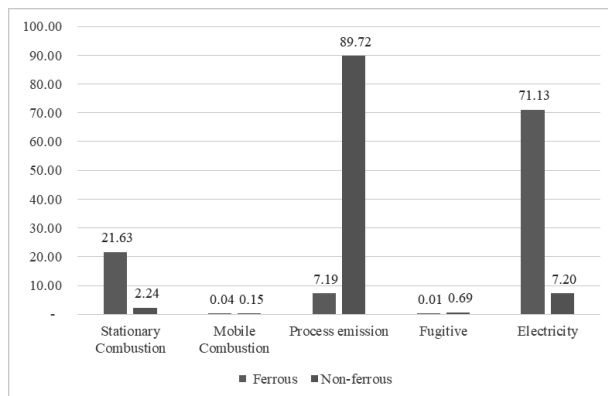


Fig. 1. The graph comparative percentages of greenhouse gas emissions, Case Study of ferrous and Non-ferrous parts manufacturing industry.

From Figure 1. Showing the graph of comparative percentages of greenhouse gas emissions, case study of ferrous and non-ferrous parts manufacturing industry. Process emissions and electricity. Considering the reasons for stationary combustion emissions, the emissions of greenhouse gases produced by the ferrous working industry GHG emissions from the production process are used in large quantities of NG, LPG, LCB, Anthracite and Diesel. In contrast, the non-manufacturing industry. Only use LPG and diesel fuel as TABLE III.

TABLE III. Source of Greenhouse gas emissions, Case studies that affect the difference in stationary combustion.

Source of Greenhouse Gas Emissions	Emission Factor (EF)	Unit	Ferrous	Non-ferrous
Natural gas (NG)	0.0573	kgCO ₂ e	✓	-
Liquefied Petroleum Gas (LPG)	3.1133	kgCO ₂ e	✓	✓
Light Cracker Bottom (LCB)	0.0427	TJ/Ton	✓	-
Anthracite	3.1014	kgCO ₂ e	✓	-
Diesel (Generator and fire pump)	2.7079	kgCO ₂ e	✓	✓

Difference of greenhouse gas emission in process emission case study. The non-ferrous parts industry has a clearer amount of greenhouse gases than ferrous parts. As a result of the manufacturing process of the non-ferrous parts industry, the injection molding agent is used in the melting process to prevent the non-ferrous material adhering to the mold. The mixture of the solution is a substance that is made of fuel oil and crushed. When spraying into molds at very high temperatures for melting, the combustion and emission of greenhouse gases, especially carbon dioxide when considering the calculation, it will be considered. Cannot calculate directly from the emission factor. It must be calculated from the net heating value of the fuel oil. The researcher selected the residual fuel oil of 0.04040 TJ / Ton [4] to calculate the default emission factors as shown in Fig.2.

TABLE 2.2 DEFAULT EMISSION FACTORS FOR STATIONARY COMBUSTION IN THE ENERGY INDUSTRIES (kg of greenhouse gas per TJ on a Net Calorific Basis)								
Fuel	CO ₂			CH ₄			N ₂ O	
	Default Emission Factor	Lower	Upper	Default Emission Factor	Lower	Upper	Default Emission Factor	Lower Upper
Crude Oil	73 300	71 000	75 500	r 3	1	10	0.6	0.2 2
Orimulsion	r 77 000	69 300	85 400	r 3	1	10	0.6	0.2 2
Natural Gas Liquids	r 64 200	58 300	70 400	r 3	1	10	0.6	0.2 2
Motor Gasoline	r 69 300	67 500	73 000	r 3	1	10	0.6	0.2 2
Aviation Gasoline	r 69 300	67 500	73 000	r 3	1	10	0.6	0.2 2
Jet Gasoline	r 69 300	67 500	73 000	r 3	1	10	0.6	0.2 2
Jet Kerosene	r 71 600	69 800	74 400	r 3	1	10	0.6	0.2 2
Other Kerosene	71 900	70 800	73 600	r 3	1	10	0.6	0.2 2
Shale Oil	73 300	67 800	79 200	r 3	1	10	0.6	0.2 2
Gas/Diesel Oil	74 100	72 600	74 800	r 3	1	10	0.6	0.2 2
Residual Fuel Oil	77 400	75 500	78 800	r 3	1	10	0.6	0.2 2
Liquefied Petroleum Gases	63 100	61 600	65 600	r 1	0.3	3	0.1	0.03 0.3
Ethane	61 600	56 500	68 600	r 1	0.3	3	0.1	0.03 0.3
Naphtha	73 300	69 300	76 300	r 3	1	10	0.6	0.2 2
Bitumen	80 700	73 000	89 900	r 3	1	10	0.6	0.2 2
Lubricants	73 300	71 900	75 200	r 3	1	10	0.6	0.2 2
Petroleum Coke	r 97 500	82 900	115 000	r 3	1	10	0.6	0.2 2
Refinery Feedstocks	73 300	68 900	76 600	r 3	1	10	0.6	0.2 2

Fig. 2. Default emission factors for stationary combustion in the energy industries (Residual Fuel oil)

Fig. 2. When considering the default emission factors used to calculate the greenhouse gas emissions of these fuels, Co₂ is 77,400 CH₄ equal to 3 and N₂O is 0.6, all of which are variable in the calculation. The use of injection molding fuels has a significant effect on the amount of greenhouse gas emissions at 89.72%, while the ferrous parts industry does not use injection molding.

The difference between indirect greenhouse gas emissions considering the usage of electricity in the organization, it was found that the manufacturing of ferrous parts has a greenhouse gas emission rate of 71.13. Office building Number of people working hours all the electricity consumption in the organization. From the data collection of the ferrous parts industry, case study. Is a large industry The 80,000 square meter area of the non-ferrous industry is a medium-sized industry that works 8 hours a day, making it clear that the larger size of the industry is so large. Small and medium power industry use

Carbon footprint for organization is calculated for corporate greenhouse gas emissions. Leads to the assessment of the eco-efficiency of the information industry case study. The equation for evaluating the eco-efficiency. Can be displayed as follows.

$$\text{Eco-efficiency} = \frac{\text{Value of a product or service}}{\text{Environmental impact of a product or service}} \quad (2)$$

When calculating the ecological efficiency, the values can be expressed as TABLE IV.



TABLE IV. Calculate the eco-efficiency of the case study industry.

A case study	Value of a product (Per unit)	Environmental impact of a product (Ton CO ₂ e)	Eco-efficiency (Unit/ton CO ₂ e)
Ferrous	229,375.12	212,011.72	1.08
Non-ferrous	200,456.00	79,703.72	2.51

TABLE IV. Calculate the eco-efficiency of the case study industry. From the data collected on the production of units of the ferrous and non-ferrous components industry when computed with the environmental impact of a product or service. This is due to the calculation of greenhouse gas emissions. The eco-efficiency values were 1.08 and 2.51, respectively.

IV. CONCLUSION

From calculation of carbon footprint for organization, according to the assessment of the Greenhouse Gas Management Organization the public sector is considering direct and indirect greenhouse gas emissions from the ferrous and non-ferrous industries. The case studies show that there are three types of emission reductions: Stationary Combustion, Process Emission and Electricity the results of the calculation of greenhouse gas emissions were compared. The ferrous parts industry has more greenhouse gas emissions than the non-ferrous parts industry. The factors in the use of natural resources. Materials help fuel the energy, the number of employees in the organization, the more chemical the size of the industry. As a result, the amount of greenhouse gases increased. With the production of industrial products for eco-efficiency evaluation, the non-ferrous component industry has higher eco-efficiency than the ferrous parts industry. This is due to the fact that the amount of greenhouse gas emissions is significantly lower and that the production of products is slightly different from the industry. The assessment of eco-efficiency is another way for the industry to consider its own eco-friendly business. This leads to improved planning, which will be beneficial in many areas, such as when improving production processes to reduce electricity consumption. As a result, the industry will continue to grow in line with the global economic trends. The coexistence of this world society.

ACKNOWLEDGMENT

The author would like to acknowledge industrial Ferrous and non-ferrous parts manufacturing case study. For information to support research and Rajamangala University of Technology Phra Nakhon for this place of study.

REFERENCES

- [1] Office of industrial Economics. Thailand Industrial Index in January 2018. Retrieved from http://indexes.oie.go.th/industrial_status.
- [2] Policy and Strategy Bureau, Office of the Permanent Secretary, Ministry of Industry. Ministry of Industry's Strategic Plan 2017-2021 (Revised Edition). Retrieved from <http://www.industry.go.th/>
- [3] Nuangruthai panitchawalit. And puttipong pathanakittipong. (2009), Ecological efficiency (Eco-efficiency; EE) for development. Retrieved from <http://www.mtec.or.th/>
- [4] Intergovernmental Panel on climate change. Draft 2006 IPCC Guidelines for National Greenhouse Gas Inventories, Chapter 2: Stationary sources. pp. 2.15.



An Ergonomic Risk Improvement in a Hard Disk Drive Production Process

Thanapon Jilao, Wanchai Leelakaweewong,
Kedsarin Phoosup and Phuwisa Phetchuay
Department of Industrial Engineering and Management,
Faculty of Engineering and Industrial Technology,
Silpakorn University, Nakornpathom, Thailand
thanapon.jilao@gmail.com, leelakaweewong_w@su.ac.th

Nutthipong Vilaiyawong
HGST (Thailand) Co., Ltd.
Prachinburi, Thailand

Abstract— This research aims to reduce an ergonomic risk in a Hard Disk Drive production process by developing a new innovative pallet to help operators work easier and more comfortable and to increase an efficiency of the process. A NIOSH lifting index is used to assess risk levels. The present situation has a NIOSH lifting index more than 3, that means this work situation is not safe with a high ergonomic risk. At this score, the NIOSH lifting theory recommends that this working method must be improved immediately. The new automatic pallet can help operators to work at the best position by using spring power to adjust a height of working position. Working without bending down is easier and more comfortable, thus the NIOSH lifting index is reduced to 2.87 in every height levels, which is in a range of acceptable score for safe work. The unpacking time is reduced from 425 seconds to 393 seconds per pallet and most operators are satisfied to use the new pallet.

Keywords— ergonomic risk; NIOSH lifting index; fatigue

I. INTRODUCTION

The case study company is a hard disk drive manufacturer. Many types of hard disk drive's parts are purchased from suppliers and these parts are unpacked by operators at a company's 'Semi Store' department. In the unpack process, firstly, operators have to unpack lots of boxes, then lift all parts from boxes to shelves, and then transfer shelves to a preparing station for a next process. In the unpack process, if a height of box stack is placed at the same level with operator's hands, they will can work easily and comfortably, however, if the box stack is placed in lower levels, operators will have to bend down to unpack and lift parts out of boxes as shown in Figure 1.

Due to a high volume of production, in each day, operators who work in the unpack process have to bend down in a high frequency and a long duration. An analysis of collected data shows that a high frequency and long durations of the unpacking with bending down posture is 15.3 % higher than

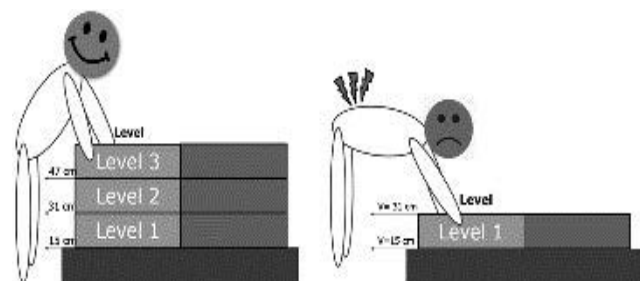


Fig. 1 Posture of working in the unpack process

the unpacking at a normal level (75 cm) (without bending down posture). Moreover, the operators have to lift quite heavy parts and bend down at the same time. Thus, this work method leads to a high level of operators' health problems, fatigue, and this will affect to an operators' work performance as well.

A medical statistic report in 2014 shows that operators have lots of muscle pain problems which about 8,251 times from a total of 8,640 companies' operators and the 'Semi Store' department has a highest statistic result. From the interviews of the 'Semi Store' operators, they complained that they always have muscle pain problems at lower back, arms, legs and shoulders from bending down their back to lift quite heavy parts with a high frequency and long durations.

For a safety management, this is a critical problem that must be eliminated. Thus, this research aims to reduce an ergonomic risk in the unpack process by developing a new innovative pallet to help operators work easier and more comfortable to increase efficiency of the unpack process.

II. LITERATURE REVIEW

A. Participatory Ergonomics (PE)

A participatory ergonomics is a method that is used to improve operator performance and well-being. Within this stated problem, PE is used to promote workers' design or



redesign of their own work, which can take place at an organizational level, process level and as small as the task level [1]. Thus, a 'participatory ergonomics' concept is used as a basis for the unpack process improvement.

B. NIOSH Lifting Index

NIOSH lifting index is an easy ergonomic tool for work's risk assessment that indicate a risk level of lifting. Before calculating the NIOSH lifting index, firstly, to calculate a recommended weight limit (RWL) for that task which is a series of multipliers that representing several aspects of a lifting task [2]. The NIOSH lifting equation and the parameters' meanings are shown below and in Figure 2.

$$RWL = LC \times HM \times VM \times DM \times AM \times FM \times CM \quad (1)$$

H = Horizontal location of the object relative to the body

V = Vertical location of the object relative to the floor

D = Distance the object is moved vertically

A = Asymmetry angle or twisting requirement

F = Frequency and duration of lifting activity

C = Coupling or quality of the workers grip on the object

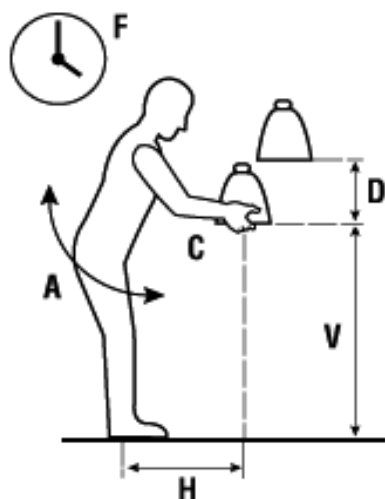


Fig. 2 NIOSH lifting equation and the multipliers' meaning [2]

After the calculation of the recommended weight limit (RWL), the lifting index can be calculated as the equation below.

$$\text{Lifting Index (LI)} = \text{Weight} / \text{RWL} \quad (2)$$

NIOSH lifting index score will be divided into 3 levels as shown in Figure 3.



Fig. 3 NIOSH lifting index meanings [2]

The NIOSH lifting index (LI) is used to help the user redesign the task. If the LI is high, that means the work parameters are poorly designed. Thus, these parameters should be the focus of a redesign attempt. Many researches use the NIOSH lifting index for risk assessment and work improvement. For examples, it is used as an empirical evaluation of training and a work analysis tool for participatory ergonomics [1], it is used for an ergonomic risk improvement for hard disk drive's box manual lifting [3], it is used for evaluating of lifting tasks frequently performed during fire brick manufacturing processes [4], it is applied to prevent musculoskeletal disorder risks [5].

III. METHODOLOGY

Figure 4 shows the research methodology which consists of: 1) data collection, 2) design and simulation, 3) prototype making, 4) prototype testing, and 5) prototype improving.

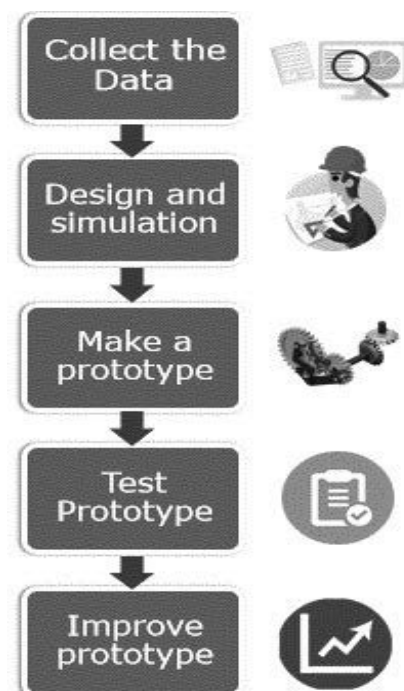


Fig. 4 Research Methodology



3.1 Collecting the data:

To collect the data from the work station, including unpacking process, unpacking activities, activities' cycle time, activities' motion, moving distance, frequency of lifting and limitations in the unpacking process. Then use the data to calculate the NIOSH Lifting Index.

3.2 Designing and Simulation

A Solid Work program is used to design a pallet and to simulate the work situation for evaluating how it work, for identifying what and how many materials that need to be prepared and for identifying problems that may occur after use.

3.3 Making a prototype

To finalize the design of pallet, preparing all materials, and then making a prototype.

3.4 Testing the prototype

To test the prototype by using at the unpack process in normal working conditions and then, recording results.

3.5 Improving the prototype

From the testing results, analyze the results for improving the prototype.

shown in Figure 5, that means this work situation is not safe with a high ergonomic risk. At this score, the NIOSH lifting theory recommends that this working method must be improved immediately.

4.2 Unpacking time before an improvement.

A time study of the unpacking process shows that at a lower box level, operator will use more time to finish the task. For example, at a top level (level 3), that operators can work easily without bending down, take about 131 seconds, whereas it takes 20 seconds more for a lowest level (level 1) that operators have to bend down their bodies as shown in Figure 6. It can be said that an improvement of the work method can lead to an increase of process efficiency.

Time to unboxes	
Level	LI
Level 3	131
Level 2	143
Level 1	151
(VCM 9.6 kg 42 boxes/pallet)	



Fig. 6 Unpacking time before an improvement

IV. RESULTS

4.1 NIOSH Lifting Index score before an improvement

NIOSH Lifting Index is calculated from working posture of operators in the unpacking process. The heaviest part, VCM, is used as a sample part. The VCM part's weight is 9.6 kilograms per box and there are 42 boxes per pallet. The calculation result shows in Figure 5.

Level	LI	RWL
Level 3	3.07	3.13
Level 2	3.24	2.96
Level 1	3.44	2.79

Height of box	LI	RWL	Risk level
box level 3 (47 cm)	3.07	3.13	not safe
box level 2 (31 cm)	3.24	2.96	not safe
box level 1 (15 cm)	3.44	2.79	not safe

Fig. 5 NIOSH lifting index scores before an improvement

From the NIOSH lifting index score before improvement, it is found that the most comfortable height of the box level is about 75 cm from ground. If the box level is lower, it will affect to an increase of NIOSH lifting index score, which means that there is a higher ergonomic risk as well. The present situation has a NIOSH lifting index more than 3 as

4.3 Prototype design result

Because NIOSH Lifting score change follow by the 'V' parameter (Distance in y axis from ground to hand that hold the object) and 'V' parameter is a factor that can be controlled. Then, researcher will pay attention in 'V' parameter and improve by creating new pallet that can fix a height of working position at about 75 cm from ground.

A 'karakuri' concept is used as a principle of the pallet design. Because this design aims to develop an equipment which is useable at a lower cost. Firstly, the new innovative pallet should be made from reused material that can be found in the factory. Secondly, it is a non-electric automatic re-leveling pallet. Thus, the researchers design the new pallet by using spring power. The new pallet drawing is shown in Figure 7.

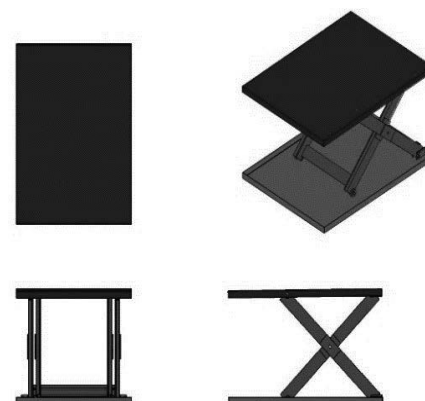


Fig. 7 Drawing of a new pallet



The concept of the new pallet design is to make the pallet that can change a height of working position automatically. By using a spring power (extension spring), if weight that is put on the pallet is lower, it will move up back to the best position (75 cm high from ground) automatically.

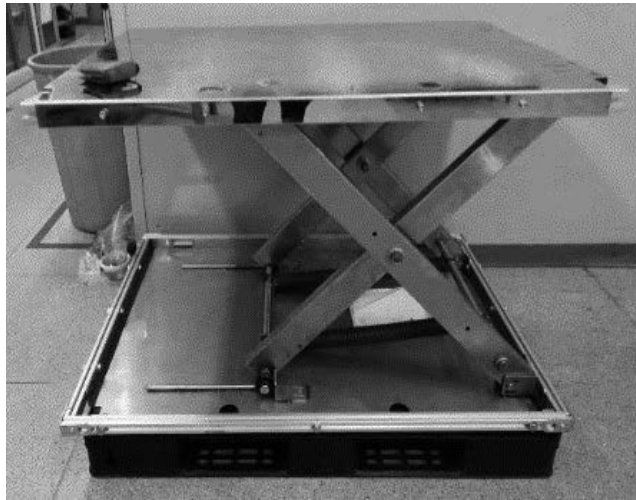


Fig. 8 A prototype of the new pallet



Fig. 9 Working posture before and after an improvement

4.4 NIOSH Lifting Index score after an improvement

As can be seen in Figure 9, before an improvement, operators have to bend down their body that is cause of the back pain and fatigue problems. After an improvement, height of the boxes is adjusted automatically by weight of load, thus, operators can always work at the best position (around 75 cm high from ground) without bending down the body.

The NIOSH lifting index scores after improvement is decreased to 2.87 in every levels as shown in Figure 10, which is in a range of acceptable score for safe work.

Before

Level

LI

Level 3

3.07

Level 2

3.24

Level 1

3.44

(VCM 9.6 kg 42 boxes/pallet)

>3

After

Level

LI

Level 3

2.87

Level 2

Level 1

(VCM 9.6 kg 42 boxes/pallet)

Fig. 10 NIOSH lifting index scores before and after an improvement

4.5 Unpacking time after an improvement

The unpacking time after an improvement is reduced from 425 seconds per pallet to 393 seconds per pallet or the unpacking time is reduced about 7.53 %. Moreover, a satisfaction survey result shows that 14 of 19 operators (73.68%) are very satisfied to use the new pallet.

V. CONCLUSION AND RECOMMENDATIONS

5.1 Conclusion

The new automatic pallet can help operators to work at the best position by using spring power to adjust a height of working position. Working without bending down is easier and more comfortable, thus the NIOSH lifting index (risk of lifting) is reduced from more than 3 in every height levels to 2.87 in every height levels, which is in a range of acceptable score for safe work. The unpacking time is reduced from 425 seconds per pallet to 393 seconds per pallet (7.53 %) and most operators are satisfied to use this new pallet.

5.2 Recommendations

Except from the 'V' parameter, a distance in y axis from ground to hand, in this situation, a 'H' parameter, which is a distance in x axis from middle of body to hand, can be improved as well. For example, the 'H' parameter can be improved by applying rotatable table concept for designing the pallet. The operator can rotate a table for adjusting boxes position to reduce reach distance (x axis) that leads to a better NIOSH lifting index score.

REFERENCES

- [1] J. S. Jason, M.K. Brian and A.N. Maury, "Empirical evaluation of training and a work analysis tool for participatory ergonomics", International Journal of Industrial Ergonomics, vol. 31, pp. 387-396, 2003.
- [2] National Institute for Occupational Safety and Health (NIOSH). "Ergonomic Guideline for Manual Material Handling". Published 2007 by the California Department of Industrial searching from <http://www.cdc.gov>. 2007, pp. 2-75, 2007.



- [3] B. Songwit, S. Sarisak and L. Sudaw, "An Ergonomic risk improvement for hard disk drive's box manual lifting", School of Health Science, Sukhothai Thammathirat Open University.
- [4] K. M. Chung and D. Kee, "Evaluation of lifting tasks frequently performed during fire brick manufacturing processes using NIOSH lifting equations", International Journal of Industrial Ergonomics, South Korea. Keimyung University, Taegu 704-701, page 249, 2000.
- [5] M. Parvena, S. Nipopom, C. Ruephuwan, "The Application of NIOSH Lifting Equation to Prevent Musculoskeletal Disorder Risks", Journal of Biosciences and Medicines, vol. 3, pp. 39-44, 2005.



Designing Fixture to Reduce Loss During Stopper Ring Assembly: A Case Study of Automotive Parts Factory

Sukanya Cherdchoongam

Department of Mechatronics Engineering
Rajamangala University of Technology Phra Nakhon
Bangkok, Thailand
sukanya.che@rmutp.ac.th

Kullanan Lakul

Department of Mechatronics Engineering
Rajamangala University of Technology Phra Nakhon
Bangkok, Thailand
La.kullanan@gmail.com

Abstract— This research studies the designing of fixture for assembling stopper ring with stabilizer bar of a car, in accordance with given standard from the customer, in order to reduce loss and customer's complaint. Studying of the current problem reveals that 89 percents of loss from stopper ring assembly comes from skewness of stopper ring outside of the given standard from the customer. This research hence intends to design fixture that prevents stopper ring from skewing during the assembly. The developed fixture was tested in a trial assembly with 3 products, 120 pieces each. The result reveals that the developed fixture can reduce the loss from stopper ring assembly at 100 percents.

Keywords— stopper ring; stabilizer bar; fixture

I. INTRODUCTION

Fixture is a support equipment for the production. It is used to define the position or support the workpiece. At the same time, it holds the workpiece in the assigned position when the workpiece is done by machine. Assembly fixture is an equipment which can reduce the manhour, increase the work precision, and increase the safety in the production process of assembly system. Assembly fixture is widely applied in the assembly system for the constant correction. The assembly times are shortened. Therefore, the installation of fixture significantly affects the quality, efficiency, and production cost [1,2].

From the above, fixture relates to the cost and quality of the production. There are researches identify that the cost of fixture design is 10%-20% of the total production cost [3]. Moreover, the development and design of fixture affect the production quality. Around 40% of the produced workpieces are rejected because of the defect of size which not conformed to the standard because of the lacking of appropriate development and design of fixture with the production process [4].

The case study of this research is of an automotive parts factory, which manufactures pickup truck's suspension, truck's suspension, coil spring, and stabilizer bar (Fig. 1). The department that is responsible for manufacturing and forming the stabilizer bar receives many complaints from the customer, as a result of non-standardized products that fail to comply with the customer's requirement. Studying of the manufacturing and forming process of the stabilizer bar reveals that there are 4 manufacturing processes involve, namely, 1. Eye forging, 2. Heat treatment, 3. Shot peening & painting, and 4. Assembly; as depict in Fig. 2.

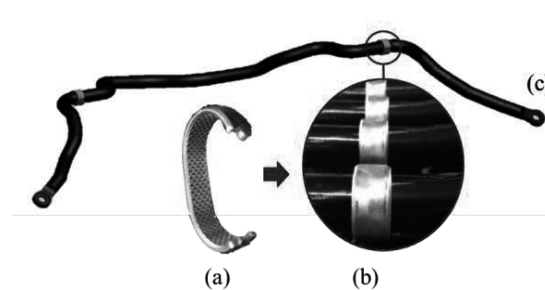


Fig. 1. Samples of stopper spring before the assembly (a) after the assembly (b) and the stabilizer bar (c) of the factory in this case study

Studying of the manufacturing and forming process of a car's stabilizer bar reveals that non-standardized products come from the 4th process, assembly. The author gathered manufacturing data of July – September, 2017 (Table 1) and found that, from total average production of 1,777 pieces, there were 18 non-standardized pieces on average, which were accounted for 1.03 percents of overall production. Further investigation revealed that there were 3 types of non-standardized products, namely, stopper ring's skewness was outside of the given standard, 2. Stopper ring cogs weren't completely aligned, and 3. Deformed stopper ring as a result of pressure. (Fig. 3)

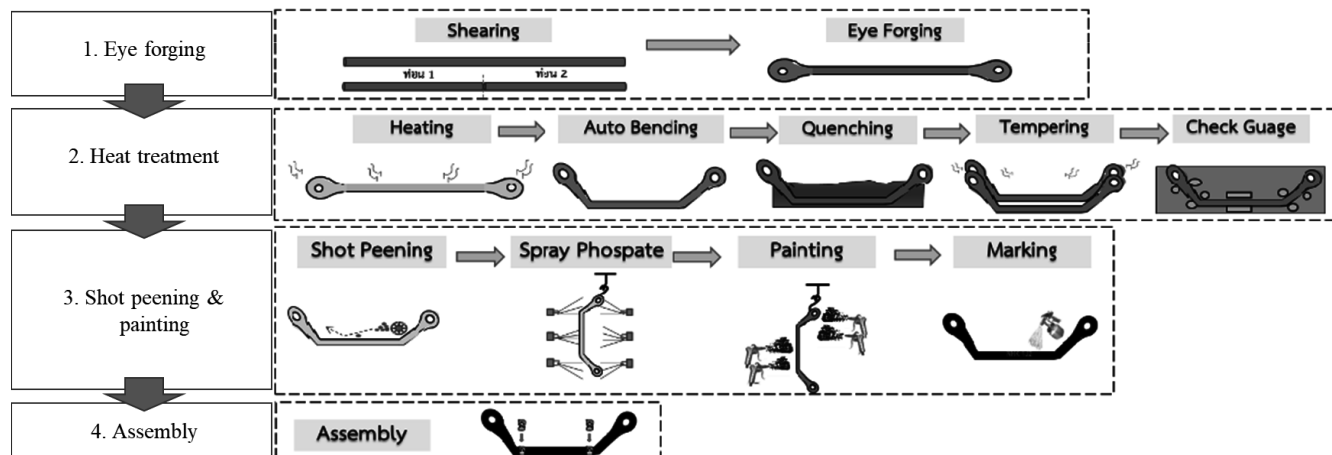


Fig. 2. Manufacturing and forming process of a car's stabilizer bar



Fig. 3. Characteristics of standardized products (a) and non-standardized products, (b) stopper ring's skewness, (c) misalignment of the stopper ring's cogs, and (d) deformed stopper ring from the pressure.

TABLE I. Numbers of non-standardized products, July – September, 2017.

Month – Year	Numbers of production (pieces/month)	Numbers of loss (pieces/month)	Numbers of loss by defect (pieces/month)		
			Stopper ring's skewness that is outside of the given standard	Misalignment of the stopper ring's cogs	Deformed stopper ring from the pressure
July 2017	42,303	620	558	31	31
August 2017	37,316	527	465	31	31
September 2017	37,616	540	480	30	30
Average	39,078	562	501	31	31

II. PROBLEM ANALYSIS

From the data of non-standardized product (Table 1), we now know that 89 percents of the non-standardized products come from stopper ring's skewness that is outside of the given standard from the customer. Therefore, the author analyzes the cause of stopper ring's skewness that is outside of the given standard, using the cause and effect chart in Fig. 4.

From the cause and effect chart (Fig. 4) that the author analyzed the problem with factory's engineer, the author found that the main reason for the problem of stopper ring's skewness that is outside of the given standard was caused by the lack of fixture equipment and tool that hold the stopper ring in place. As a result, stopper ring was swayed during the assembly.

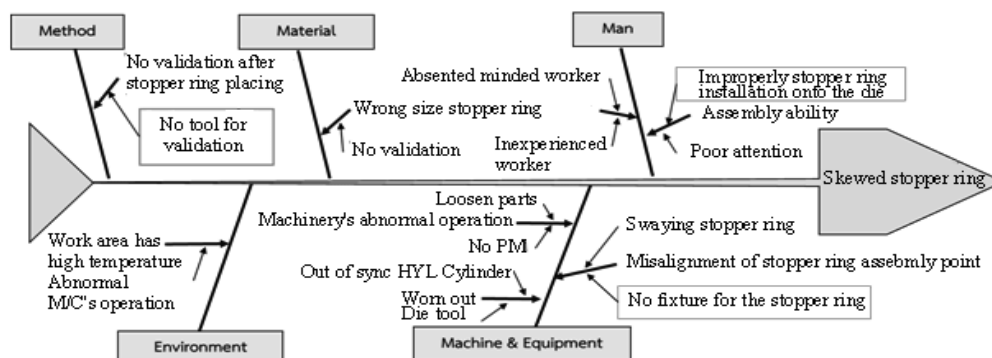


Fig. 4. The cause and effect chart of the problem of stopper ring's skewness that is outside of the given standard

Studying of the assembling of stopper ring to the car's stabilizer bar reveals that, during the process of placing stopper ring on the die set, there was no fixture that hold stopper ring to the stabilizer bar. As a result, the stopper ring was skewed outside of the given standard. (Fig. 5)



Fig. 5. Placing stopper ring in the die set

III. DESIGNING THE FIXTURE FOR STOPPER RING ASSEMBLY

In order to solve the problem of stopper ring's swaying and out of alignment during the assembly process, the author designs a fixture that operates in semi-automatic mode. This fixture utilizes PLC-controlled pneumatic system to control the double acting cylinder and gripper which will hold both sides of stopper ring while it is being placed onto other workpiece, during installation. Once the stopper ring is attached to the workpiece, the gripper will let go and remove itself from the workpiece.

The structure of stopper ring clamp can be demonstrated as follows; the width is 140 mm, the length is 430 mm, the height is 283 mm., the weight is 12 kg approximately, the power is 200 V, double acting cylinder with the range of 60 mm., and air gripper with the range of 15-30 mm., reed switch is used to detect the position of the air cylinder. The production rate is 24 second/workpiece and the clamping range can be

adjusted according to the size of stopper ring. From Fig.6, the structure of stopper ring clamp is shown. Each number is;

1. Air gripper
2. Double acting cylinder
3. Clamp base
4. Guide rail
5. Swivel bases
6. Double acting cylinder base
7. Air gripper base
8. Turning over lock base
9. Turning over lock
10. Rear base
11. Bearing for axle rotation
12. Clamping distance adjusting driven clamp
13. Spiral for clamping distance adjusting driven clamp
14. Axle lock for clamping distance adjustment
15. Distance adjustment axle handle
16. Stopper ring clamp
17. SPEED CONTROLLER of double acting cylinder
18. SPEED CONTROLLER of air gripper
19. Reed switch for cylinder position detector
20. Air cylinder controller

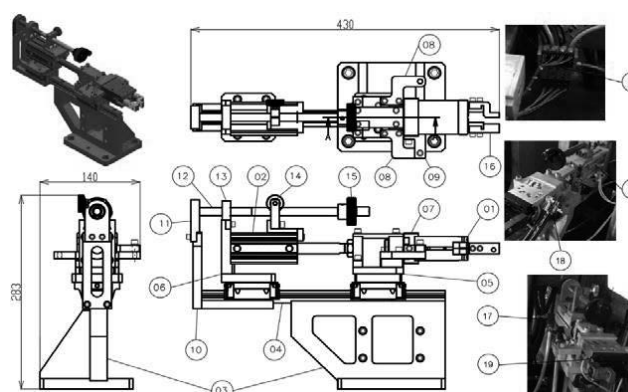


Fig. 6. Designing the fixture for stopper ring assembly



Designing of the pneumatic circuit which is controlled by PLC application; air pressure from the compressor will be delivered to the filter regulator lubricator unit (FRL Unit) and then to the 4 solenoid valves. The 1st solenoid valve controls the double acting cylinder of the equipment on the right. The 2nd solenoid valve controls the pneumatic gripper on the right. The 3rd solenoid valve controls the double acting cylinder of the equipment on the left. The 4th solenoid valve controls the pneumatic gripper on the left, as depict in Fig. 7.

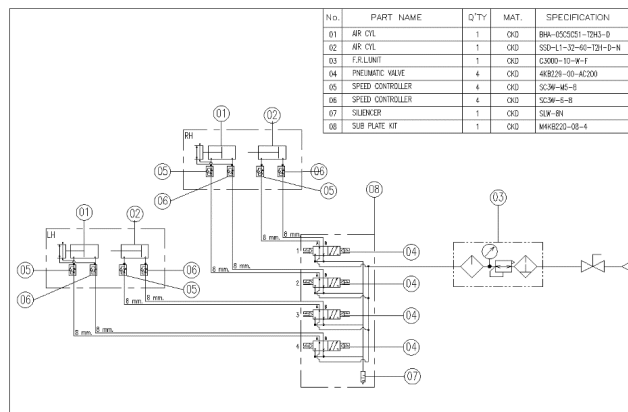


Fig. 7. Pneumatic circuit that controls the fixture

IV. OPERATION TEST RESULT

After the fixture was installed, it was tested with a trial run against 3 products, 120 pieces each, in order to determine the fixture's efficiency. Standard requirements of the 3 products are represented in Table 2. The author gathers the data with the aim to determine 25 percents of overall efficiency of the trial run, that is, sampling 30 pieces of each product and testing them for the stopper ring assembly's span; as depict in Fig. 8.

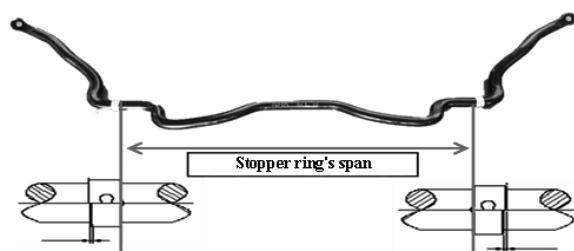


Fig. 8. Measuring stopper ring's span

TABLE II. Stopper ring's span under given assembly standard from the customer

Product Type	Span STD (mm.)	Span min (mm.)	Span max (mm.)
1	431 ± 1	430	432
2	497 ± 1	496	498
3	678 ± 1	677	679

TABLE III. Stopper ring's span from the 30 samples of each product

No.	Stopper ring's span (mm.)		
	Product Type 1	Product Type 2	Product Type 3
1	430.86	496.98	678.1
2	430.72	496.91	678.00
3	430.95	496.94	678.22
4	430.76	496.90	678.2
5	430.69	497.00	678.12
6	430.96	496.95	678.14
7	430.88	497.03	678.05
8	430.84	496.87	678.00
9	430.93	496.92	678.24
10	431.02	497.00	678.13
11	431.10	497.12	677.95
12	431.12	497.15	677.89
13	431.05	497.23	677.85
14	431.00	497.00	677.92
15	430.98	497.08	677.98
16	431.15	497.12	677.92
17	430.95	497.00	677.9
18	431.11	496.98	677.83
19	431.18	496.95	677.97
20	430.92	496.90	678.00
21	430.86	497.05	678.12
22	430.88	497.11	678.11
23	431.12	497.18	678.04
24	431.20	497.13	678.15
25	430.97	497.04	678.06
26	430.95	497.00	678.02
27	431.06	497.16	678.24
28	430.91	496.95	678.00
29	431.08	497.14	678.06
30	431.12	497.19	678.2

From the 30 samples of each product that the author had gathered, the author found none product that wasn't conformed to the customer's given standard. The gathered data is then analyzed, in order to determine the process's efficiency and capability, using Capability Sixpack function of the Minitab Application. The result is depicted in Fig. 9.

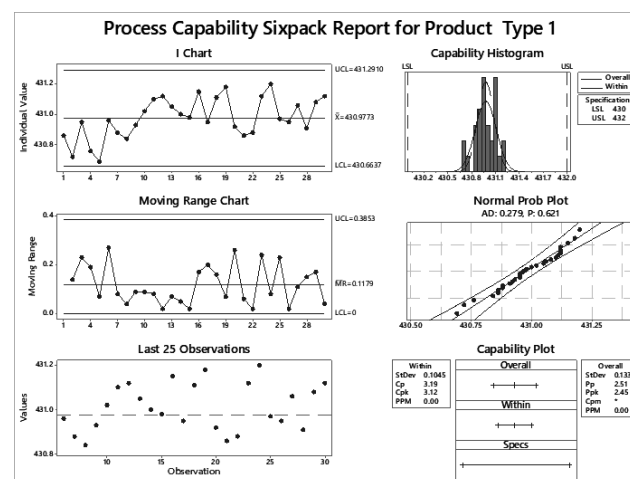


Fig. 9. Analysis using Capability Sixpack function, in order to determine the capability of type 1 process



Figure 8 shows analysis result using Capability Sixpack function, in order to determine the capability of type 1 process; whereas Lower Spec is set at 430 mm. and Upper Spec is 432 mm. Consideration of MR Chart and X Chart reveals that the data is randomly distributed under controlled range. This mean the data has normal distribution and hence can be used for determining the process's capability. Data's distribution was then analyzed via histogram, where the author found that the data was inside the scope of given LSL and US. From the Normal Prob Plot chart, P value is over 0.05 ($p > 0.05$) which confirms that the data has normal distribution. P_p is 2.45, or more than 1.33, which means the process's capability is at the same level as world class quality, or Six Sigma Quality. P_{pk} is 2.51, which is more than 1.67 and it means the process's capability is surprisingly excellent. PPM is 0 and it means from every 1 million units produced there will be no loss from the process.

TABLE IV. Summarized analysis result of the Capability Sixpack function, in order to determine the capability of type 1, 2, and 3 processes

Product	Average of stopper ring's span	P_p	P_{pk}	PPM
type 1	430.98	2.51	2.54	0
type 2	497.03	3.34	3.23	0
type 3	678.05	2.88	2.74	0

V. SUMMARY

This research designed a fixture that prevents stopper ring from swaying during the assembly. The fixture was tested under a trial run with 3 products, 120 pieces each; where 30 samples were taken and tested, in order to validate the stopper

ring's span, in comparison with standard value of each product. The stopper ring's spans of the 3 products were 431 ± 1 , 497 ± 1 , and 678 ± 1 , respectively. And the means of the workpieces of the 3 products were 430.98, 497.03, and 678.05 millimeters, respectively; which were under the scope of given standard from the customer. The author then test the process capability, using Minitab Software Application, and found that the P_{pk} of the 3 products were 2.45, 3.23, and 2.74, respectively. This means the process's capability is at the same level as world class quality, or Six Sigma Quality. P_p are 2.51, 3.34, and 2.88, respectively; and that mean the process's capability is surprisingly excellent. PPM of the 3 lots were 0 and it means from every 1 million units produced there will be no loss from the process.

ACKNOWLEDGMENT

The author would like to thank Faculty of Engineering, Rajamangala University of Technology Phra Nakhon, for all the necessary support; and to thank the factory of the case study herein, for providing data for the research.

REFERENCES

- [1] H. Hashemi, "Fixture designers guidance : A Review of recent advanced approaches," Jordan Journal of Mechanical and Industrial Engineering, 2014, pp.377-384.
- [2] R.D. Makwana and N. D. Gosvami, "A Study on Fixture Design for Complex Part," International Journal of Futuristic Trends in Engineering and Technology, 2014, Vol. 1, pp.12-15.
- [3] Z.M.Bi and W.J. Zhang, "Flexible fixture design and sutomation review, issues and future directions, " International Journal of Production Reseach, 2001, vol.39, pp.2867-2894.
- [4] N. Wan, Z. Wang and R. Mo, "An intelligent fixture design method based on smart modular fixture unit," The International journal of Advanced Manufactureing Technology, 2013, vol.74, pp.1-21



Postal Alert And Security System Via Line Application

Mr.Sunthorn Wiriya.
Faculty of Industrial Education
name of RMUTP
Bangkok, Thailand
sunthorn.w@rmutp.ac.th.

Mr.Chayakorn Sripichetkul.
Faculty of Industrial Education
RMUTP
Bangkok, Thailand
Chayakorn_64@ Hotmail.com.

Abstract—This paper aims to develop an automatic mailbox that can send a notification through a mobile phone via a Line™ application. The proposed system will alert automatically when a letter is dropped into the mailbox or when the human enter the mailbox security zone. Two photoelectric sensors which are interface to the main controller are used to detect both a letter and humans. The ESP 8266 board is connected to android mobile phone, and UNO R3 board is also connected to the main controller to control and auto-lock system using Bluetooth HC-05 module. Humans can control their mailboxes to be open and close for fetching documents or letters by Bluetooth linked to their mobile phone.

Keywords— Arduino Uno23;home's mailbox; MCU ESP8266; module Bluetooth HC-05

I. INTRODUCTION

We have a lot of activities of a day. Receiving and sending the letters are importance activity of every peoples. Today's mailboxes need to be installed in every home. Building Shelter or even along the side of the road. Check Mailing Number of mails or letters that drop into the mailbox also require humans to open it and take a lot of time for checking Number of mails or letters. To solve the problem of checking mail and alerting in areas where security is required.

Internet of Things (IoT) is "Internet in all things" means that devices, things, things, are connected to the Internet. Man can control the use of devices. Through the Internet such as the opening - closing equipment. Ordering home electricity by connecting the control device.

LINE Notify is a service and the right channel. You can send Various alerts to your own account are made through the use of an API that is executed via HTTP POST. ESP8266 / ESP8285 comes with a WiFi connection and sends the data to the user's line via the LINE API.

Add LINE Notify to Friends

Before applying the API and send notifications. You must first add LINE Notify to your friend by scanning the QR Code that show you at <https://notify-bot.line.me/th/>.

<https://notify-bot.line.me/my/> Then the system will login to us with the LINE by email. And the password has been set.

Send data through the API(Application Programming Interface) to LINE Server and be able to tie the basics to LINE Bot to help control things in the home through the application Line.

Send data through the API to LINE and be able to tie the basics to LINE Bot to help control things in the home through the application Line.

Three reasons to use postal alert and security system via line application

: (1) ease of use when checking Number of mails or letters, (2) To solve the problem of checking mail and alerting in areas where security is required. automatic compliance to electronic requirements that facilitate the concurrent or later production of electronic products, and (3) conformity of increasing mobile phone3 are built-in application ; examples of the type incorporating the applicable criteria that follow.

II. EASE OF USE

A. Three parts of hardware consists of This application.

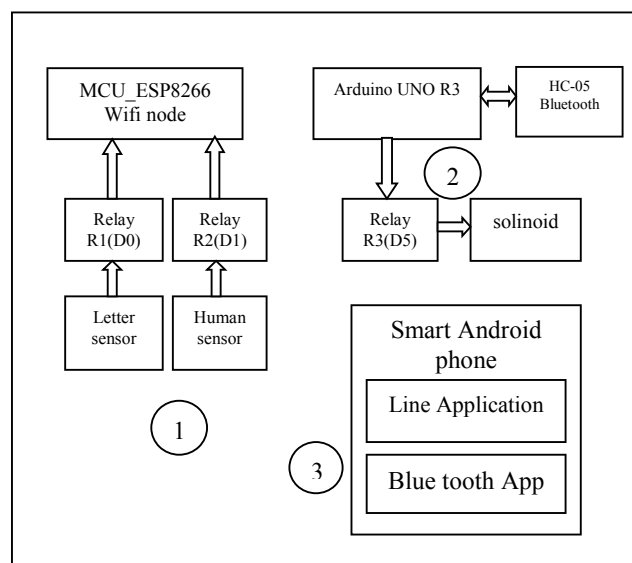


Figure 1 Block diagram of hardware module connection

Block diagram of hardware module connection consist of 3 parts are as follow:

Part 1: This part is processing of 2 photoelectric sensors interface to the main controlling unit controller ESP8266 board by relay R1 connected to D0 address and relay R2 connected to D1 address of ESP8266 to detect the letter which dropped into the mail box and human detected respectively, which is Wifi node that process by executing via HTTP POST. It is connecting and sending to the user's line via the line Application Programming Interface(API).

Part 2 :This part is processing of arduino URO R3 controller unit which interface with HC-05 Bluetooth board. Which can operate by human to open and close data to Relay 3 by send "1" to port D1 for control the solenoid to open mailbox's door for fetching documents or letters with bluetooth linked to application on mobile phone.

Part 3: This part is constructed into Android mobile phone that are line application and bluetooth application inside. To make the Android mobile phone to have more ability. first; to receive alert message from ESP8266 wifi module which register to be the member of line application whit I.D. Line member; 8266 and QR code also.

The operation of this programming part ;config connect WiFi; define ID, password, output port, input switch active low, define press LOW, and define code from Line sever LINE_TAKEN"2VD1Wnm1HmT6uKhUW7NLtoF7S1g5AeHthtjxfgko"

String message="8266:You receive a new letter.:Human detected".

It will send to Line server by Line ID:8266 to User ID which register to Line server before.

B. Flow chart of the ESP8266 and Arduino URO R3 microcontrollers programming.

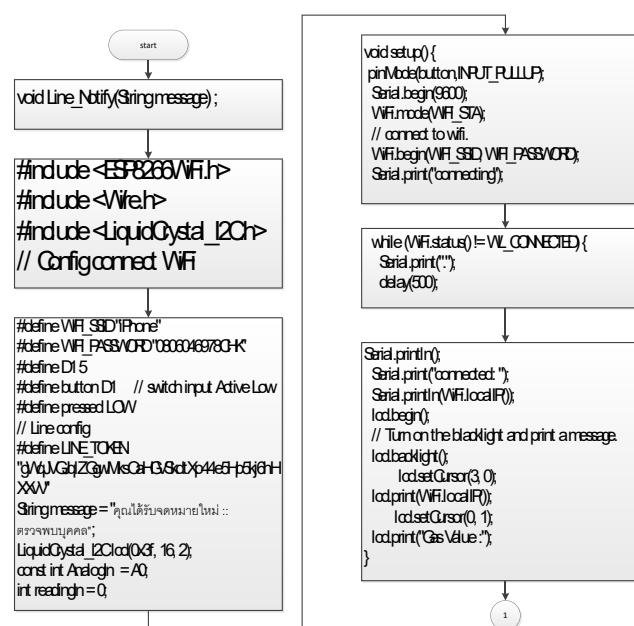
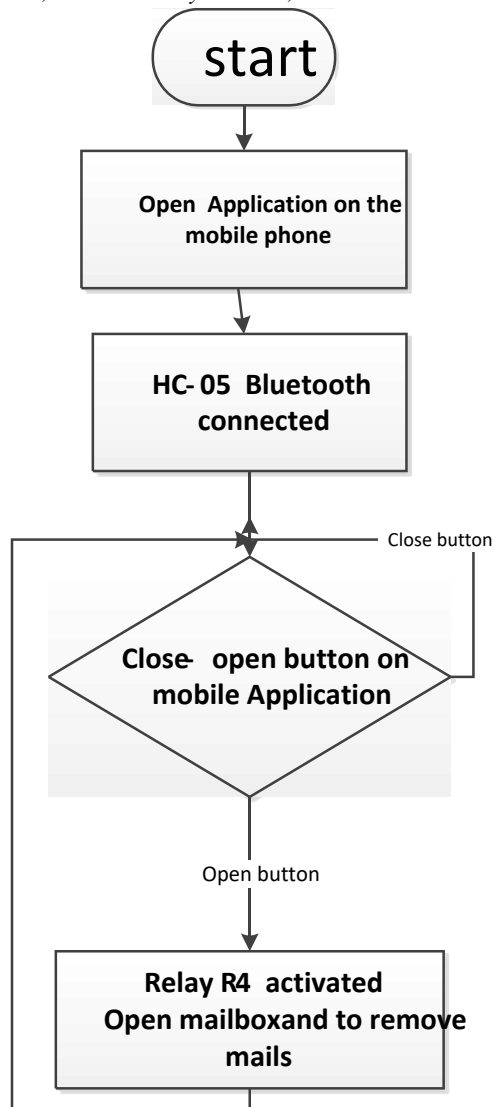


Fig 2 operation flow chart of postal alert and security system via line application; ESP8266 WIFI Node.



B: Flow chart for Arduino B programming

Fig 3 operation flow chart of postal alert and security system via line application; Arduino URO R3 interface with HC-05.

The operation flow chart of postal alert and security system via line application consist of 2 part that are

A. Flow chart of the ESP8266 programming

Line_Notify(String message) is line service function that is use for this application. To include all library of hardware and config connect WiFi then define the variables which consist of WIFI_SSID, WIFI_PASSWORD and

input signal channel which connected to ESP8266.

To setup boardrate at 9600 b/s for serial data with WIFI connecting to Line server. Then read data from sensors and if switch active by detecting of sensors then send message to Line server for toward to Line Application with Line_notify ID: esp8266: you receive new letter: Human detected.

B. Flow chart of the arduino URO R3 programming

This process begin with open Bluetooth application on the mobile phone to prepare operation to connection mobile phone to arduino R3 by HC-05 Bluetooth board which interface to the controller. The program will check close and open button on mobile application to activated for open the mailbox door. Human can fetching letters or document from mailbox. Then loop to check the button to close again until the application is closed.

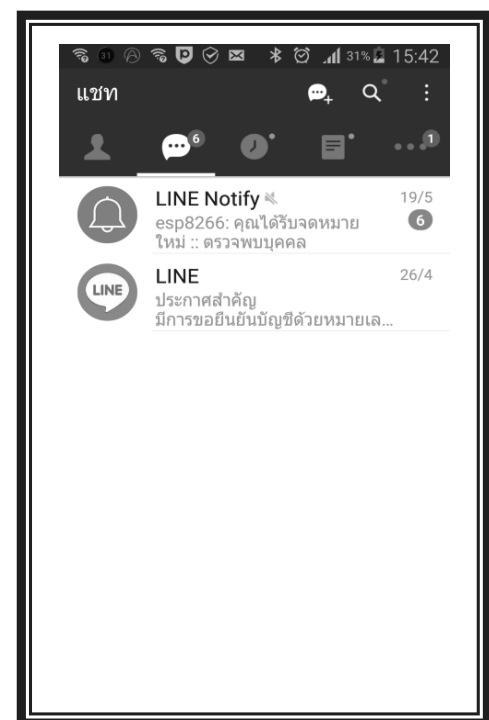


Fig 4 Output of Line Application on Mobile phone of postal alert and security system via line application



Fig 5 Application on Mobile phone of postal alert and security system via line application; Arduino URO R3 interface with HC-05

C. postal alert and security system via line application

Picture of postal alert and security system via line application; consist of a Clear box

Which contain of Arduino URO R3 interface with HC-05 and ESP8266 and The red box is Mail Box



Fig 6 Picture of postal alert and security system via line application.

D. Summary and Recommendations

The importance step when we already programming into ESP8266. We must add it to Notify function which is free service of Line system which it will send registration 'Notify' ID and password which are used for register to Line server. This step ESP8266 get QR code which use it to setting up by Add friend to USER Line ID by telephone Number which is Line ID to receive alert from ESP8266.

TABLE I. TESTING PROCESS OF POSTAL ALERT AND SECURITY SYSTEM VIA LINE APPLICATION

Test times	Table of Testing		
	Sensors	Alert	Control system
1	Activated	ok	ok
2	Activated	ok	ok
3	Activated	ok	ok

a.

The result from send the message "you receive the new letter::Human detected" to API Line sever to send to Line application into mobile phone. The Node MCU ESP8266 is process data to receive signal from Photo sensors and send alert wifi signal to Line application which was designed

This application of microcontroller's technology can develop to be a communication network connection which can send and receive the data to control electric remote devices.

ACKNOWLEDGMENT (Heading 5)

REFERENCES

- [1] <https://www.ioxhop.com/article/47/esp8266-alert>. (references)
- [2] Venus supply Co,LTD"basic of using ESP8266 node MCU"and Application.2017.
- [3] <https://www.Thaeasyelec.com/article-wiki/review-product-article>.
- [4] <http://www.vdolearning.com/vdotutor/android-application/134-talk-to-me-application>



A Talking Device of Weight and Height for the Visually Impaired Students

Upady Hatthasin

Department of Computer Engineering
Faculty of Engineering, Rajamangala University of Technology Lanna (RMUTL Chiang Mai)
Chiang Mai, Thailand
Email: UHT@rmutl.ac.th

Abstract— This research is intended to facilitate the measurement of weight and height with the body mass index detail for the visually impaired students by creating a digital measuring instrument that supports digital voice. We focused on reducing the cost and the material required in prototyping while maintaining the quality and accuracy of the device. To achieve this, we used Arduino microprocessors and ultrasonic sensors to measure the height and load cells to measure weight, and used digital screen to display measurement results. The users can press buttons, labelled in Braille, to listen to the measured values of height, weight, and BMI in Thai language. There are buttons, labelled in Braille, for listening to the measurement result. The proposed device has been evaluated by 30 sighted and 15 visually impaired volunteers who extensively used the device and provided scores in six aspects: ease of use, speed to work, ease of move, easy installation, reasonable weight of device, and introduction sound. The device received overall satisfactory scores, and due to its relatively low cost, is well-suited for individuals with low income.

Keywords— weight; height; strain gauges; ultrasonic

I. INTRODUCTION

In the present, there are two types of blindness in Thailand: 1) the eyes do not to see, and 2) The eyes are dim. The visually impaired are said in other words. The visually impaired individuals are many in Thailand. The visually impaired have come from birth, from getting an accident, and from the numbers increasing for many reasons. Especially, the most affected group of the visually impaired is childhood from the birth to age up into 15 years olds. From the teacher, Siriporn Wongrugeepirog, at the Northern School for the Blind under the Patronage of the Queen Chiang Mai, gave us know that most of the problems in the school are the shortage of personnel to monitor the physical growth, check the weight, and check the height of visually impaired students.

Because in the process of measuring these students. One teacher is required to measure a student's height, and another teacher has to measure a student's weight. The results of these measurements are then brought to calculate the body mass index to determine the physical growth of visually impaired students. The problem is that there are few staff (teacher) to

students. It is difficult for students with visual impairment to monitor their own weight and body mass index. So the resulting, the measurement process get delayed and take a long time. So the solution to such problems, it is necessary to have a prototype system as the device that encourages students to measure themselves. This proposed support device is not available for purchase in the general market as of students with normal vision.

The research team then applied a prototype system to weigh and measure height and alerted the body through the BMI. The cost of creating this system is reasonable. In the proposed system, the Ultrasonic Sensor [1] is used for high-level measurement. Load Cell Sensor [2] is used for weighing. The use of digital [3] for a display in case of the eyes are dim. The measured body mass index (BMI) was used to calculate the body mass index (BMI), which was calculated from weight and height [4]. Measurement is $BMI = \text{Weight} / (\text{Height} * \text{Height})$. Usually use body weight is in kilograms. The height is in meters. The unit is Kg / m^2 , which often abandon the BMI when calculating body mass index, then compare it with the following criteria:

- Too slim: less than 18.5 (<18.5)
- Appropriate: More than or equal to 18.5, but less than 25 (≥ 18.5 but <25).
- Overweight: More than or equal to 25 but less than 30 (≥ 25 but <30)
- Fat: more than or equal to 30 but less than 40 (≥ 30 but <40)
- Very fat: More than or equal to 40 (≥ 40)

II. DESIGN AND IMPLEMENTATION

A. Conceptual design

The conceptual design of the system consists of two parts, the Controller and the Manual part, which can be seen in Figure 1. Each of these sections has the following functions:

- Block A: Send / Receive Sensor by Ultrasonic detecting the height of the user. The Load Cell receives the signal from standing above the user's load base.



- Block B: Processed by a microprocessor that received data from the sensor. The calculated values are compared for the BMI.
- Block C: Displays the results by displaying the measurement results on the LCD monitor for the visually impaired person and displaying the measured speech output to the speaker.
- Block D: On-off acts as a switch for power on / off.
- Block E: Press the sound button to hear the voice of the measured value.

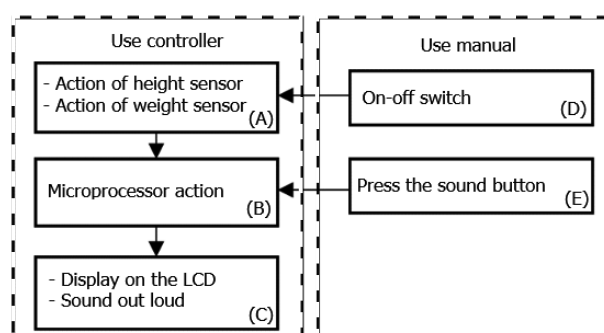


Fig. 1. The conceptual design diagram of the proposed device

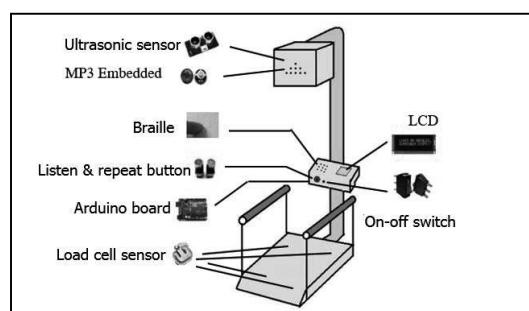


Fig. 2. The model of measuring the weight and height from 45 degree view

B. The design of the hardware components

The prototype model of our proposed measurement in height and weight is illustrated in Figure 2. The hardware components have a rough operation when the switch is turned on. Then the power supply flows to the system. Ultrasonic Sensor acts as an input. If there are objects in the radius of the sensor, it will get the same value as the Load Cell Sensor acts as input. If there is an object on the weighing platform, the sensor will get out. The LCD will act as the output of the message or information. At the same time, it voices out the speaker, which is the output, to display the results of the value or data acquired. Then when the values or data are displayed, users can also return to listen to the same information by pressing the button to listen to the sound with a Braille stick next to it to tell the point or function of the button. There are another button to hear repeatedly to have the same data again

one round. Once, if the machine does not receive any input, the program will clear the value, and wait for new information. If you do not want to use this model, turn off switch.

C. The circuit Diagram of the proposed device

A circuit diagram is shown in Figure 3. Connect the Ultrasonic Sensor to the Arduino Mega or Mega 2560 board by pin trig Pin7 pin echo Pin8 of 5V to the ground and the ground normally connect the load cell to the amplifier HX711. Load Cell 1 to the E pin. Arduino Mega or Mega 2560 Arduino connectors are connected to the AUX pin.

The Auxiliary pin is connected to the A pin of the SCK pin to the A0 of the Arduino Mega or Mega 2560 board. LCD to i2c Module with SDA pin and SCL pin connected to Arduino Mega or Mega 2560 board with 5V power Ground Speaker, Switch, Sound Button and Switch Button Repeat 1 pin to 5V power pin 2 to R10K and ground down to connect to pin 2 and pin 3 of Arduino Mega or Mega 2560 board by pin 2 as audio switch. Pin 3 is a repeat button switch and connect the Adapter 12V to the Arduino Mega or Mega 2560 board to plug the power.

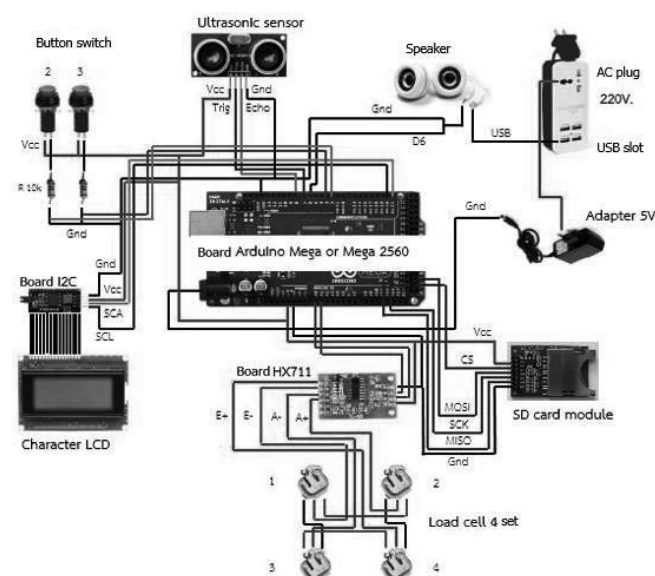


Fig. 3. The circuit diagram of the proposed device

D. The assembling equipment of the proposed device

Assembling equipment and building it into a system start by wiring each device from the diagram of Figure 3. Connect the power cable to the Arduino Mega board, including the 4-point load cell which shows the position shown in Figure 4. Next, connect the device to the board. Then, insert the circuit board into the system control cabinet. The speaker jack is connected to the Arduino board, then the speaker box is positioned for the control box, then discharge electricity into the system to test the system as device.

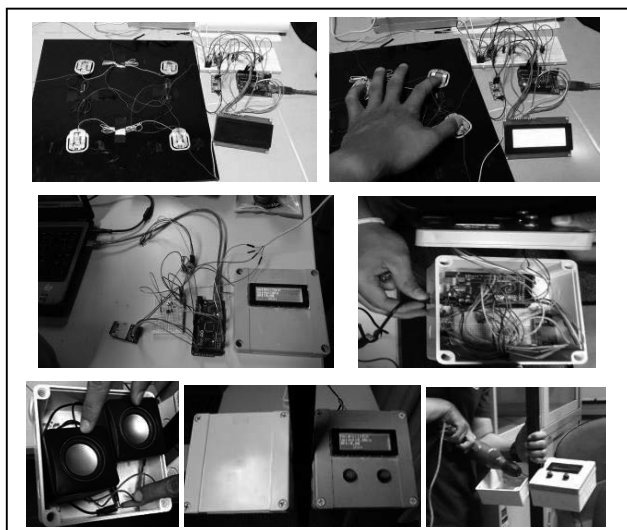


Fig. 4 Assembly of control circuits into a package

Once the device has been installed and the components are assembled properly. It is a prototype system as shown in Figure 5. Initially, the device will enable the function and location of each device that will be used, such as positioning ultrasonic sensor for measuring height, speaker box, LCD monitor, voice button with Braille, repeat button with Braille, and pedal stand for weight, respectively.

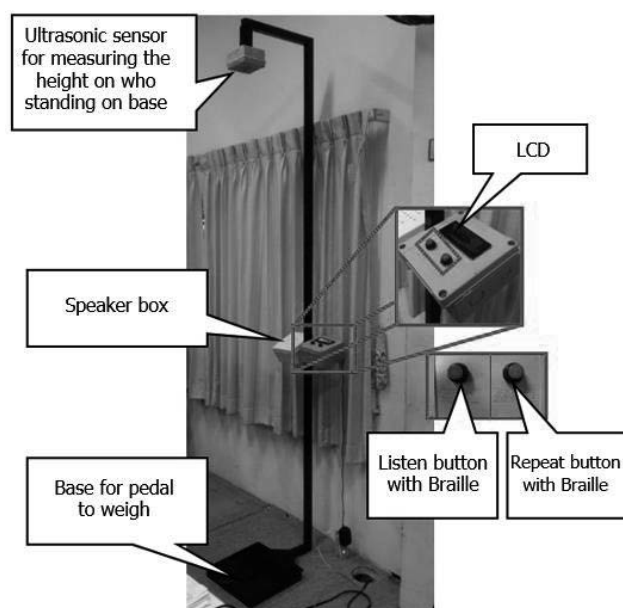


Fig. 5 The completed package of the control box

E. The design of software components

Figure 6 shows the flowchart of the control software on the play button. Its works when you press the play button. The ultrasonic sensor is used to calculate the value of the height. The value of the load cell sensor is used to calculate the value of the weight. Both the values of weight and height, then, are brought to calculate for the value of the BMI. After that, the function of the sound files is sorted to match and to play as the output.

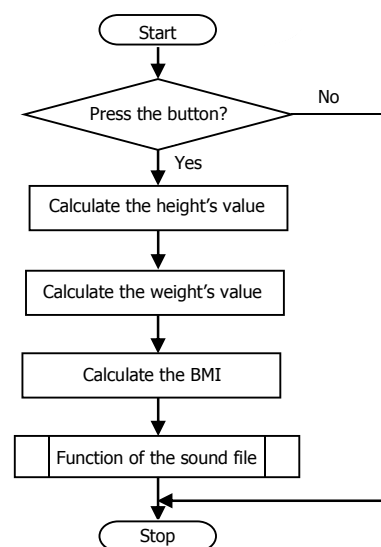


Fig. 6 The flowchart of the control software

III. EXPERIMENTAL RESULTS

The system test is divided into two parts: the part of the system's function and the part of testing with the user.

In section of the functional testing, we asked volunteers who have a normal vision of 10 people as a variable of information. There are 3 tests per person: 1) Weight, 2) Height, and 3) BMI. In the experimental term of LCD display and sound, the average and maximum of testing are described as following. The maximum weight is 80%. The lowest is 30%. The highest is 90%. The lowest is 40%. Finally, the BMI is 100%. The body mass index (BMI) of the volunteers [4] was compared the body weight balance. Meanwhile in accuracy, the percentage of precision measured is formulated in the equation (1):

$$Accuracy (\%) = 100 - \left(\left| \frac{x_{mea} - x_t}{x_t} \right| \times 100\% \right) \quad (1)$$

when x_{mea} is a measured distance, and x_t is the real distance.

In general, we usually use the body weight in kilograms and the height is in meters. The unit is Kg / m^2 . When BMI is calculated, it is compared to the BMI standard, which is expressed as a weighted index using the symbol " kg / m^2 ".



"Less than 18.50 || in slim or thin", "between 18.50 to 22.90 || in normal or slender", "between 23 - 24.90 || in abdominal or plump", "between 25 - 29.90 || in fat or fat", "more than 30 "Very fat or too very fat". In general of the height of man, the BMI formula is used in the equation (2):

$$BMI = Weight / (Height * Height) \quad (2)$$

In section of the testing with users, we asked the bachelor students as 30 volunteers from the field of computer engineering, Rajamangala University of Technology Lanna, Chiang Mai, and the high school students as 15 visually impaired volunteers from the Northern School for the Blind under the Patronage of the Queen Chiang Mai. The testing atmosphere is shown in Figure 7.



Fig. 7 The atmosphere during the assessment of the device

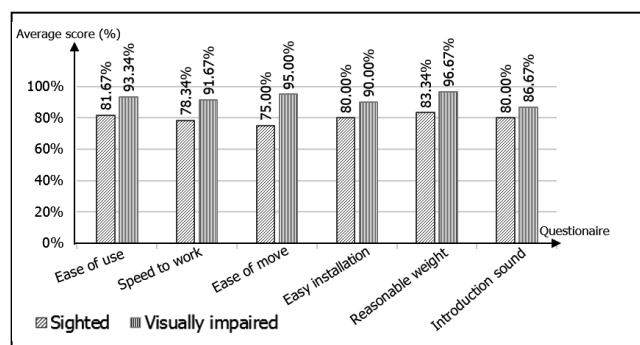


Fig. 8 The comparison of questionnaire scores from the sighted and the visually impaired participants

Apart from the simulated test, our proposed device was tested by the forty five mentioned volunteers as participants. Then those participants fill out the questionnaire forms. Through actual usage and satisfaction questionnaires, the device was assessed in six aspects: ease of use, speed to work, ease of move, easy installation, reasonable weight of device, and introduction sound. The score is set to four levels is very good, good, fair, and should improve. The questionnaire scores

were then calculated based on percentage using the equation (3), and the results are plotted in the bar graph as shown in Figure 8.

$$Percentage\ of\ score = (total\ score / full\ score) \times 100 \quad (3)$$

The graph in Figure 8 shows the comparison between the two participant groups. It is evident that the design result is a percentage of the visual impairment. It is higher than the visual assessment of the individual. The environment and experience including the vision of the sighted person is higher than that of the visually impaired. But the results are still higher than 75% which is a good result and it is acceptable. This is because the cost of composing this device is lower compared to the price of the weighing and measuring instruments sold in the commercial market. The machine sold in the market is priced at 30,000. - 4,000 baht while our proposed device of weight and height measurement offered is below 3,000 baht, and also the braille is attached to the important position supporting self-service for the visually impaired.

IV. CONCLUSION

This research developed an affordable talking device of weight and height for visually impaired students that support self-service and learn the BMI for healthy. We have designed and constructed a system as a device using microprocessors with ultrasonic sensor for height and load cell sensor for weight. The proposed device has been tested by average sighted people as well as satisfactory feedback regarding six aspects. In addition, due to its low cost, the device is affordable among individuals with low income.

ACKNOWLEDGMENT

We would like to thank Siriporn Wongrugeepirog and teaching staffs at the Northern School for the Blind under the Patronage of the Queen Chiang Mai for providing valuable information about visually impaired students, as well as accommodating for the experiment. Thanks to RMUTL for the research fund.

REFERENCES

- [1] Venus Supply Company Limited, Thailand. "Ultrasonic Ranger" [Online], Search from: <http://www.thaieasyelec.com/products/sensors/infrared-ultrasonic/grove-ultrasonic-ranger-Detail.html> [February 8, 18]
- [2] Venus Supply Company Limited, Thailand. "Load Sensor - 50kgs" [Online], Search from: <http://www.thaieasyelec.com/products/sensors/flex-force-Weight/Load-sensor-50kgs-detail.html> [February 8, 18]
- [3] Thomas L Floyd, "Digital Fundamentals", 10th Edition, ISBN: 0132359235.
- [4] Wikipedia, the free encyclopedia "Body mass index." 2017, August; [Online], Search from: <https://th.wikipedia.org/wiki/ดัชนีมวลกาย> [February 8, 18].



The Realization of Four-mode First-order Allpass Filter Based-on CCCCTAs

Thitiporn Janda

Dept. Electronics and Telecommunication Engineering
Faculty of Technical Education, Rajamangala University of
Technology Isan, Khonkaen Campus, Khonkaen, Thailand
E-mail: Thitiporn_koy@hotmail.com

Wichcha Onsa-ard, Adirek Jantakun¹

Dept. of Electronics and Telecommunication Engineering
Faculty of Engineering, Rajamangala University of
Technology Isan, Khonkaen Campus, Khonkaen, Thailand
E-mail: ¹adirek.ja@rmu.ac.th

Abstract— The realization of four-mode first-order allpass filter is presented in this paper. The proposed four-mode first-order allpass filter provides two current controlled current conveyor transconductance amplifiers and single grounded capacitor. It can be operated in voltage-mode, current-mode, trans-impedance-mode and trans-admittance-mode without changing the circuit configurations. The gain and phase response of proposed circuit can be adjusted electronically/independently by DC bias current. The Pspice simulation results are agreed with the theoretical analysis.

Keywords— Allpass filter; Four-mode; CCCCTA.

I. INTRODUCTION

First-order allpass filter (APF) or a well-known as phase shifter is serves the phase shift of the signal [1-5]. It is widely-adapted in many communication systems and analog signal processing, such as quadrature oscillator (QO), multiphase sinusoidal oscillator (MSO), high Q bandpass filter and etc [6-15]. From the reasons mentioned above, the APF circuit has been regularly researched and investigated. Many works of APF had been used high performance active building blocks such as CDTA, CCTA, CFTA, DBTA and etc. In addition, all of them focus on controlling by electronics method because it may easily be controlled by microcontroller, microprocessor and automatic system [16-20]. The benefits and weaknesses of APF circuits can be summarized as follow: the circuits presented in [1, 6, 8-9, 12, 16-18] uses single active element and single grounded capacitor which are compacted as well as expediently minimized for monolithic architecture. Furthermore, the grounded capacitor is connected at high-impedance ports that is compensated the stray capacity at port or node. Although, these circuits cannot adjust the gain at oneself, when applied APF in QO [6, 14] or MSO [13] with independently adjustment of the condition and frequency of oscillation, but it must be added the amplifier. Similarly, the amplifier is required in high Q bandpass filter based-on APF [6-7, 10, 21-22] while desire freely the Q. Some circuits, such as in [2, 8-12, 20, 23-25], have benefit from electronics controlling. Nevertheless, they are used external resistor where it is difficult to implementation [6] and maybe increases the power consumption. Moreover, in [5, 10-11, 13, 19-21, 23-

29], prefer to adjust the pole frequency and phase response with electronics method but they are suffered from using floating capacitor because the floating capacitor requires a large area when fabricated the circuit [30]. The MSO and QO in [4, 8, 31], use APF to adjusts the condition of oscillation without effects to the frequency of oscillation. Since, the APF can be adjusted the gain by oneself. However, all mentions above of APF, it can be operated in either only current-mode [1-4, 6-7, 13, 17-19, 21-23, 26] or only voltage-mode [5, 9-12, 14-16, 20, 24-25, 27-29].

The purposed of this paper introduces the first-order allpass filter based-on CCCCTAs. The circuit can be operated on four-mode including voltage-mode, current-mode, trans-impedance-mode and trans-admittance-mode without changing the configuration of the circuit. The circuit consists of two CCCCTAs and single grounded capacitor which is advantage for IC implementation. The gain and phase response can be controlled by electrically method. The Pspice simulation results exhibits that the curves and theoretical are well matched to theoretical analysis results.

II. THE DESCRIPTION OF PROPOSED CIRCUIT

A. CCCCTA

Current controlled current conveyor transconductance amplifier or CCCCTA has been presented by Montree and Winai [32] on 2008. It is very interesting device because it can be applied to both voltage-mode and current-mode circuit. Especially, the input port x has the parasitic resistance that can be adjusted electronically by the DC bias current. The electrical symbol and ideal equivalent circuit of CCCCTA have been shown in Fig. 1 (a) and (b), respectively. The electrical characteristics of CCCCTA describes by the hybrid matrix below:

$$\begin{bmatrix} I_y \\ V_x \\ I_{z,zc} \\ I_o \end{bmatrix} = \begin{bmatrix} 0 & 0 & 0 & 0 \\ 1 & R_x & 0 & 0 \\ 0 & 1 & 0 & 0 \\ 0 & 0 & 0 & \pm g_m \end{bmatrix} \begin{bmatrix} V_y \\ I_x \\ V_o \\ V_z \end{bmatrix} \quad (1)$$

If CCCCTA is implemented by a bipolar technology, the parasitic resistance R_x at port x is given as



$$R_x = \frac{V_T}{2I_A}, \quad (2)$$

and transconductance gain g_m is expressed by

$$g_m = \frac{I_B}{2V_T}, \quad (3)$$

It can be seen that the parasitic resistance, R_x , can be adjusted electronically by DC bias current I_A . Simultaneously, the transconductance gain, g_m , can be adjusted by I_B .

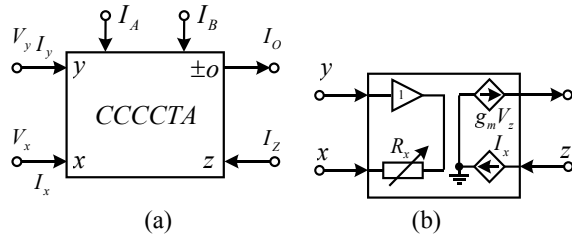


Fig. 1. CCCCTA (a) electrical symbol (b) ideal equivalent circuit

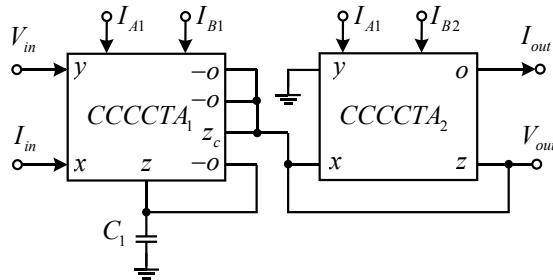


Fig. 2 Proposed four-mode first-order allpass filter

B. Proposed first-order allpass filter

The novel circuit configuration of four-mode first-order allpass filter is exhibited in Fig. 2. The circuit provides 2 CCCCTAs and single grounded capacitor which is suitable for integrated circuit implementation. In addition, the grounded capacitor will be compensated the latent capacity at the node or the port. It can be explained as follows:

• Voltage-mode and trans-admittance-mode operation

The proposed circuit can be operated in voltage-mode and trans-admittance-mode by the I_{in} is connected to ground. This can be clearly seen that the input voltage V_{in} is connected to the first CCCCTA and it has high input-impedance. The output current I_{out} is high-impedance that is easy to drive load. Fig. 2 can be explained by using electrical characteristic in (1). Therefore, the voltage transfer function of the Fig. 2 can be written as

$$\frac{V_{out}(s)}{V_{in}(s)} = \frac{R_{x2}}{2R_{x1}} \left(\frac{C_1 s - g_{m1}}{C_1 s + g_{m1}} \right). \quad (4)$$

The voltage gain can be expressed as follows:

$$G(\omega) = \frac{V_{out}}{V_{in}} = \frac{R_{x2}}{2R_{x1}}, \quad (5)$$

Again, the electrical characteristic in (1) is used to realize the transfer function of trans-admittance-mode. The detail of admittance transfer function can be described as

$$\frac{I_{out}(s)}{V_{in}(s)} = \frac{R_{x2}g_{m2}}{2R_{x1}} \left(\frac{C_1 s - g_{m1}}{C_1 s + g_{m1}} \right). \quad (6)$$

From (6) the admittance gain can be analyzed as

$$G(\omega) = \frac{R_{x2}g_{m2}}{2R_{x1}}. \quad (7)$$

However, the pole frequency and phase response of voltage-mode and trans-admittance-mode are the same that can be expressed as follows:

$$\omega_0 = \frac{g_{m1}}{C_1}, \quad (8)$$

and

$$\phi(\omega) = 180 - 2 \tan^{-1} \left(\frac{\omega C_1}{g_{m1}} \right). \quad (9)$$

It is evidenced that, the gains in (5) and (7) can be adjusted electronically by R_{x1} or R_{x2} or g_{m2} without affect of pole frequency and phase response. The pole frequency and phase response can be adjusted electronically by g_{m1} .

• Current-mode and trans-impedance-mode operation

Likewise, the proposed circuit can be operated in current-mode and trans-impedance-mode which also can be connected V_{in} to the ground. If setting the value of the DC bias current I_{A1} as high, the input-impedance of circuit is low as possible. Then, the output-impedance is high that is easy for connecting to next stages or driving to load. The current transfer function of circuit can be obtained as

$$\frac{I_{out}(s)}{I_{in}(s)} = \frac{R_{x2}g_{m2}}{2} \left(\frac{C_1 s - g_{m1}}{C_1 s + g_{m1}} \right). \quad (10)$$

From (10) the current gain is given as

$$G(\omega) = \frac{I_{out}}{I_{in}} = \frac{R_{x2}g_{m2}}{2}. \quad (11)$$

The impedance transfer function and impedance gain of trans-impedance-mode can be analyzed in equation (12) and (13), respectively.

$$\frac{V_{out}(s)}{I_{in}(s)} = \frac{R_{x2}}{2} \left(\frac{C_1 s - g_{m1}}{C_1 s + g_{m1}} \right), \quad (12)$$

and

$$G(\omega) = \frac{R_{x2}}{2}. \quad (13)$$

The pole frequency and phase response are the same as (8) and (9), respectively. In addition, the gains of (11) and (13) can be easy/electronically adjusted by R_{x2} or g_{m2} or R_{x1} which is non-interactive of pole frequency and phase response.

III. NON-IDEAL ANALYSIS

The non-ideal analysis is necessary. Let's start with the voltage and current tracking errors with the characteristic of CCCCTA where it can be given as



$$\begin{bmatrix} I_y \\ V_x \\ I_z \\ I_o \end{bmatrix} = \begin{bmatrix} 0 & 0 & 0 & 0 \\ \gamma & R_x & 0 & 0 \\ 0 & \alpha & 0 & 0 \\ 0 & 0 & 0 & \pm \beta g_m \end{bmatrix} \begin{bmatrix} V_y \\ I_x \\ V_o \\ V_z \end{bmatrix}, \quad (14)$$

where γ is voltage tracking error of the voltage at port y transfers to port x. α is current tracking error of the current at port x transfers to port z. β is the voltage tracking error at port z transfers to transconductance at port o. These parameters may be caused by the misfit of BJT of internal construction and parasitic elements of CCCCTA and, those are depended on frequency of operation and temperature.

In this case, the transfer function of proposed APF in voltage-mode operation and the voltage gain can be rewritten as

$$\frac{V_{out}(s)}{V_{in}(s)} = \frac{\alpha_1 R_{x2}}{R_{x1}(1+\alpha_2)} \left(\frac{C_1 s - \gamma_1 \beta_1 g_{m1}}{C_1 s + \gamma_1 \beta_1 g_{m1}} \right), \quad (15)$$

and

$$G(\omega) = \frac{V_{out}}{V_{in}} = \frac{\alpha_1 R_{x2}}{R_{x1}(1+\alpha_2)}. \quad (16)$$

Then, the transfer function of trans-admittance-mode and the admittance gain are became as

$$\frac{I_{out}(s)}{V_{in}(s)} = \frac{\alpha_1 \beta_2 R_{x2} g_{m2}}{R_{x1}(1+\alpha_2)} \left(\frac{C_1 s - \gamma_1 \beta_1 g_{m1}}{C_1 s + \gamma_1 \beta_1 g_{m1}} \right), \quad (17)$$

and

$$G(\omega) = \frac{I_{out}}{V_{in}} = \frac{\alpha_1 \beta_2 R_{x2} g_{m2}}{R_{x1}(1+\alpha_2)}. \quad (18)$$

Accordingly, the transfer function of current-mode operation and the current gain become

$$\frac{I_{out}(s)}{I_{in}(s)} = \frac{\beta_2 \alpha_1 R_{x2} g_{m2}}{(1+\alpha_2)} \left(\frac{C_1 s - \beta_1 g_{m1}}{C_1 s + \beta_1 g_{m1}} \right), \quad (19)$$

and

$$G(\omega) = \frac{I_{out}}{I_{in}} = \frac{\alpha_1 \beta_2 R_{x2} g_{m2}}{(1+\alpha_2)}. \quad (20)$$

An non-ideal analysis of the transfer function of trans-impedance-mode and the impedance gain are changed to

$$\frac{V_{out}(s)}{I_{in}(s)} = \frac{\alpha_1 R_{x2}}{(1+\alpha_1)} \left(\frac{C_1 s - g_{m1}}{C_1 s + g_{m1}} \right), \quad (21)$$

and

$$G(\omega) = \frac{V_{out}}{I_{in}} = \frac{\alpha_1 R_{x2}}{(1+\alpha_2)}. \quad (22)$$

Moreover, the pole frequency and phase response are same and modified to equation (23) and (24), respectively.

$$\omega_0 = \frac{\gamma_1 \beta_1 g_{m1}}{C_1}, \quad (23)$$

$$\phi(\omega) = 180 - 2 \tan^{-1} \left(\frac{\omega C_1}{\gamma_1 \beta_1 g_{m1}} \right). \quad (24)$$

IV. THE SIMULATION RESULTS

To demonstrate the performance of the proposed APF, the PSPICE program is used. The internal construction of CCCCTA based-on bipolar technology is used in [4]. The simulated parameters of The NPN and PNP transistors are NR200 and PR200 bipolar transistor of ALA400 transistor array. The proposed APF biases with $\pm 1.5V$ supply voltage.

The proposed APF working as current-mode operation is investigated. The simulation parameters are $C_1 = 500pF$, $I_{A1} = 100\mu A$, $I_{A2} = 25\mu A$, $I_{B1} = 50\mu A$ and $I_{B2} = 200\mu A$ therefore, pole frequency is 306.06kHz, $\phi(\omega) = 90^\circ$ and $G(\omega) = 1$. The theoretical and simulated results of gain and phase response of current-mode operation can be plotted in Fig. 3. It is evident that the gain and phase response of simulation is agreed well. Fig. 4 shows theoretical and simulated results of the phase response while adjusting $I_{B1} = 25\mu A, 50\mu A, 100\mu A$ and $200\mu A$. Therefore, the pole frequency is changed to 153.03k Hz, 306.06kHz, 612.12 kHz and 1.22 MHz, respectively. The results confirm that the pole frequency can be controlled electronically by adjusting bias current I_{B1} . The time-domain response can be demonstrated by applying a sinusoidal signal with 306.06 kHz frequency and $80\mu A$ p-amplitude to the APF input. The result of time-domain response is shown in Fig. 5.

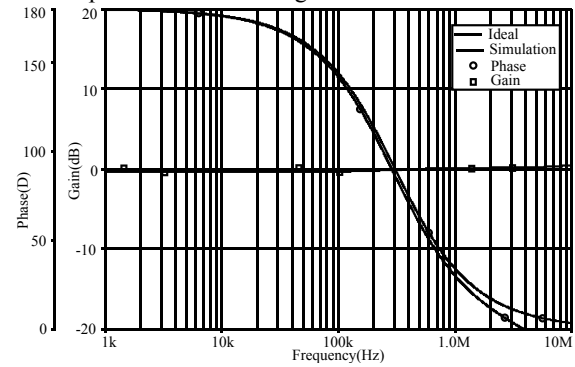


Fig. 3 Gain and phase response of current-mode operation

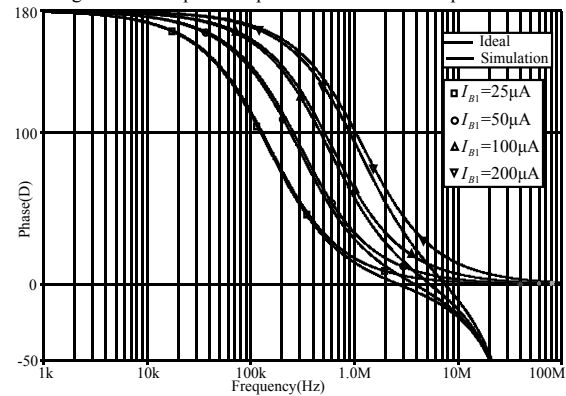


Fig. 4 Electronically adjustment of phase responses

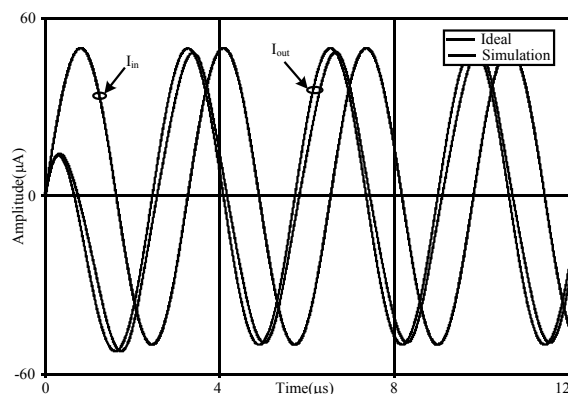


Fig. 5 Time-domain responses with 306.06 kHz frequency

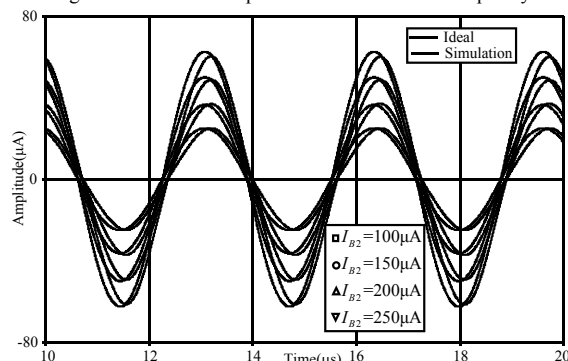


Fig. 6 Current gain of proposed APF when I_{B2} is varied

In addition, to verify the current gain of the proposed APF which can be adjusted electronically without affects to pole and phase response. The example of this is done by varying the current gain from 0.5, 0.75, 1 to 1.25, and tune the DC bias currents I_{B2} as $25\mu A$, $75\mu A$, $100\mu A$ and $125\mu A$, respectively. The result is displayed in Fig. 6. However, the results of computer simulation have been errors because the voltage and current tracking errors of characteristic of CCCCTAs as explained in topic III. These errors can be compensated/improved by adjusting the DC bias current of CCCCTAs.

V. CONCLUSION

The proposed APF which operates voltage-mode, current-mode, trans-impedance-mode and trans-admittance-mode without changing the circuit configuration has been proposed. It consists of two CCCCTAs and one grounded capacitor. The pole frequency and phase response are the same in forth mode and can be electronically adjusted by DC bias currents. The gain of APF can be freely adjusted by the DC bias current without affects to the pole frequency and phase response. Moreover, the output signals provide a simple voltage-mode and current-mode which is very flexible to apply and use. The performance of proposed APF circuit base-on BJT technology has been simulated by Pspice. The simulation results are well matched with the theoretical.

ACKNOWLEDGMENT

This work is supported and fund by the faculty of engineering, Rajamangala University of Technology Isan, Khonkaen Campus, Khonkaen, Thailand.

REFERENCES

- [1] D. Birolek and V. Biolkova "Allpass filter employing one grounded capacitor and one active element," *Electronics Letters*, vol. 45 no. 16, 2009, pp. 807-808.
- [2] A. Iamarejin, S. Maneewan, P. Suwanjan, and W. Jaikla, "Current-mode variable gain first-order allpass filter employing CFTAs," *PRZEGLĄD ELEKTROTECHNICZNY*, no. R. 89(Nr 2a/2013), 2013, pp. 238-241.
- [3] W. Tangsrirat, "Cascadable current-mode first-order allpass filter using current controlled conveyor," *PRZEGLĄD ELEKTROTECHNICZNY*, R. 89(Nr 1a/2013), 2013, pp.187-190.
- [4] W. Jaikla, A. Noppakarn and S. Lawanwisut, "New gain controllable resistor-less current-mode first order allpass filter and its application," *Radioengineering*, vol. 21, no. 1, 2012, pp. 312-316.
- [5] S. Maneewan, N. Udorn, D. Duangmala, P. Silapan and W. Jaikla "A voltage-mode first order allpass filter based on VDTA," *Adv. Electric. & Electro. Eng.*, vol. 12, no. 1, 2014, pp. 40-46.
- [6] W. Tangsrirat, P. Mongkolwai, and T. Pukkanun "Current-mode high-Q bandpass filter and mixed-mode quadrature oscillator using ZC-CFTAs and grounded capacitors," *Indian J. of Pure & Applied Physics*, vol. 50, 2012, pp.600-607.
- [7] A. Toker, S. Ozoguz, O. Cicekoglu, and C. Acar "Current-mode all-pass filters using current differencing buffered amplifier and new high-Q bandpass filter configuration," *IEEE Transactions on Circuits and Systems II*, vol. 47, no. 9, 2000, pp. 949-954.
- [8] K. Pitaksuttayaprot, and W. Jaikla "Electronically tunable current-mode multiphase sinusoidal oscillator employing CDCTA-based allpass filters," *The 2014 International Conference on Circuits, Systems and Control*, Interlaken, 22-24 February 2014, pp. 69-73.
- [9] Vavra, J., Bajer, J., & Birolek, D. (3-4 July 2012). Differential-input buffered and transconductance amplifier-based all-pass filter and its application in quadrature oscillator. *35th International Conference on Telecommunications and Signal Processing*, pp. 411-415.
- [10] A. Toker, E. O. Gunes and S. Ozoguz "New high-Q band-pass configuration using current controlled current conveyor based all-pass filters," *The 8th IEEE International Conference on Electronics, Circuits and Systems*, 2-5 September 2001, pp. 165-168,
- [11] M. Kumngern "Realization of electronically tunable first-order allpass filter using single-ended OTAs," *2012 IEEE Symposium of Industrial Electronics and Applications (ISIEA2012)*, Bandung, 23-26 Sept. 2012, pp. 100-103.
- [12] N. Pandey, R. Pandey and S. K. Paul "A first order all pass filter and its application in a quadrature oscillator," *Journal of Electron Devices*, vol. 12, 2012, pp.772-777.
- [13] W. Tangsrirat, W. Tanjaroen and T. Pukkalanun "Current-mode multiphase sinusoidal oscillator using CDCTA-based allpass sections," *Int. J Electron. Commun. (AEU)*, vol. 63, 2009, pp. 616-622.
- [14] B. Chaturvedi, S. Maheshwari "An ideal voltage-mode all-pass filter and its application," *Journal of Communication and Computer*, vol. 9, 2012, pp. 613-623.
- [15] J. Bajer D. Birolek "Voltage-mode electronically tunable all-pass filter employing CCCII+, one capacitor and differential-input voltage buffer," *2010 IEEE 26-th Convention of Electrical and Electronics Engineers in Israel*, 17-20 Nov. 2010, pp. 934-937.
- [16] N. Pandey, P. Arora, S. Kapur and S. Malhotra "First order voltage mode MO-CCCCTA based all pass filter," *2011 International Conference on Communications and Signal Processing (ICCCSP)*, Calicut, 10-12 Feb. 2011, pp. 535-537.
- [17] A. Lahiri and A. Chowdhury "A novel first-order current-mode all-pass filter using CDCTA," *Radioengineering*, vol. 18, no. 3, 2009, pp. 300-305.



- [18] N. Pandey and S. K. Paul "Single CDTA-based current mode all-pass filter and its application," *Journal of Electrical and Computer Engineering*, 2011, ID 897631, doi:10.1155/2011/897631.
- [19] W. Tangsrirat and W. Tanjaroen "Current-mode second-order notch filter using CDTA-based allpass section," *SICE Annual Conference 2008*, Japan, 20-22 August 2008, pp.1143-1146.
- [20] S. Maheshwari "Voltage-mode all-pass filters including minimum component count circuits," *Active and Passive Electronic Components*, 2007, ID 79159, doi:10.1155/2007/79159.
- [21] S. Tangkulboriboon, W. Pechetakit and W. Kiranon "Electronically tunable current mode high Q bandpass filter," *2005 International Conference on Control, Automation and Systems*, Gyeonggi-Do, Korea, 2-5 June 2005, pp. -.
- [22] M. Kumngern "Electronically tunable current-mode all-pass filter-based high-Q bandpass filter using minimum elements," *2009 IEEE Region 10 Conference*, Singapore, 23-26 Jan. 2009, pp. 1-4,
- [23] U. Torteanchai and M. Kumngern "First-order allpass network using CFTA," *The 4th Joint International Conference on Information and Communication Technology, Electronic and Electrical Engineering*, Chiang Rai, 5-8 March 2014, pp. 1-4.
- [24] N. Herencsar, J. Koton, K. Vrba and B. Metin "Fully cascable dual-mode all-pass filter based on single DBTA," *2012 35th International Conference on Telecommunications and Signal Processing (TSP)*, Prague, 3-4 July 2012, pp. 374-377,.
- [25] N. Herencsar, J. Koton and K. Vrba "Differential-input buffered and transconductance amplifier (DBTA)-based new trans-admittance- and voltage-mode first-order all-pass filters," *International Conference on Electrical and Electronics Engineering*, Bursa, 5-8 Nov. 2009, pp. II-256-II259.
- [26] M. Kumngern and J. Chanwutitum "An electronically tunable current-mode first-order allpass filter using a CCCCTA," *The 2013 International Conference on Advanced Technologies for Communications*, Hochiminh City, Vietnam, 16-18 October 2013, pp. 733-736.
- [27] N. Herencsar, J. Koton, S. Minaei, E. Yuce and K. Vrba "Novel resistorless dual-output VM all-pass filter employing VDIBA," *7th International Conference on Electrical and Electronics Engineering (ELECO)*, Bursa, (1-4 Dec. 2011), pp. II-82-II-84,
- [28] N. Herencsar, J. Koton, K. Vrba and B. Metin "Novel voltage conveyor with electronic tuning and its application to resistorless all-pass filter," *2011 34th International Conference on Telecommunications and Signal Processing (TSP)*, Budapest, 18-20 Aug. 2011, pp. 265-268.
- [29] N. Herencsar, S. Minaei, J. Koton, E. Yuce and K. Vrba "New resistorless and electronically tunable realization of dual-output VM all-pass filter using VDIBA," *Analog Integr Circ Sig Process*, vol. 74, no. 1, 2012, pp. 141-154.
- [30] M. Bhushan and R. Newcomb "Grounding of capacitors in integrated circuits," *Electronics Letters*, vol. 3, no. 4, 1967, pp. 148-149.
- [31] W. Jaikla and P. Prommee "Electronically Tunable Current-mode Multiphase Sinusoidal Oscillator Employing CCCDTA-based Allpass Filters with Only Grounded Passive Elements," *Radioengineering*, vol. 20, no. 3, 2011, pp. 594-599.
- [32] M. Siriprachayanun and W. Jaikla "Current controlled current conveyor transconductance amplifier (CCCCTA): a building block for analog signal processing," *Electrical Engineering*, vol. 90, 2008, pp.443-453..



Electrochromic Properties of WO₃ Thin Film

Sanya Khunkhao, Aphichata Thongrak, Korn Puangnak
Dept. of Elelectronics and Telecommunication Engineering
Rajamangala University of Technology Phra Nakhon. Bangkok, Thailand.
Sanya.k@rmutp.ac.th, aphichata.t@rmutp.ac.th

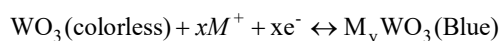
Wanchai Chankaipol
Dept. of Electrical and Electronics Application Engineering
Sripatum University Bangkok, Thailand.
wanchai.ch@spu.ac.th

Abstract— This research investigated the behavior of electrochromic thin films of tungsten oxide (WO₃) by vaporization with electrolyte. As a result of applied bias, the change in color intensity increases and decreases as well as the color retention when no bias voltage is applied. By measuring the electrical properties of the direct current and pulse signal, there are factors that affect the exchange of electrons and ions on thin films with tungsten oxide and the concentration of the electrolyte solution. This is the result of the oxidation and reduction effects of the switching time on the sensitivity.

Keywords—electrochromic; switching time; thin film; WO₃

I. INTRODUCTION

An electrochromic invention is an innovation that adjusts color intensity from oxidation-reduction reactions that have the ability to respond to light under an electric field. Also, it can be reverse to the initial state by giving the electric field a polarization. The glass is coated with an oxide compound that reacts electrically with the electrolyte. Once the voltage has been paid, there is a change in the electric field. It will be change the color intensity with the redox reaction. Furthermore, the speed and time interval, it is the change in the state of the change in color intensity. By adjusting the status, time and speed of the switch from colorless to color. Also, electrochromic device occurs in inorganic metal oxides by cathodic(injection) or anodic(ejection) of ions and electrons(e⁻). Also, the charged ions of the lithium ion (Li⁺), hydrogen ions (H⁺) and silver ions (Ag⁺) go back inside the layer. For in organic electrochromic materials WO₃ film are represented cathodic coloration states under negative bias and bleaching states under positive bias. The part of electrode and the layer of the chemical causing the redox reaction to replace the ionic charge can be shown as follows.



It is consists of $M^+ : H^+, Li^+, Na^+ \text{ or } K^+$ and the ions replace the electrons in each element of the electrochromic substance with the electrolyte solution. At present, the ionic charge of the element used in the electrochemical reaction for color change is charged to the ions of lithium ion (Li⁺), hydrogen ions (H⁺) and silver ions (Ag⁺). The oxide compounds as used in the creation of electrochromic materials are as follows. Tungsten Oxide(WO₃), Nickel Oxide(NiO), Iridium Oxide(IrO₃), Vanadium oxide(V₂O₅) and Molybdenum oxide(MoO₃)[1].

The electrochemical reactions of tungsten oxide are compounds to change the color, which requires the use of electrolyte solution in contact with the layer of tungsten oxide deposited on the transmittance polarized glass. It is a color that is able to control the transmission of light according to the distribution of the electric field in the electrochromic material substrate. Therefore, the stability of the chemical reaction can be increased by the chemical layer in the coloration of the electrochemical reaction for ion exchange [2]. The design for ionizing charge ejects back into the layers of the coating on the glass to give color when the voltage is dispensed and fades away with reverse voltage.

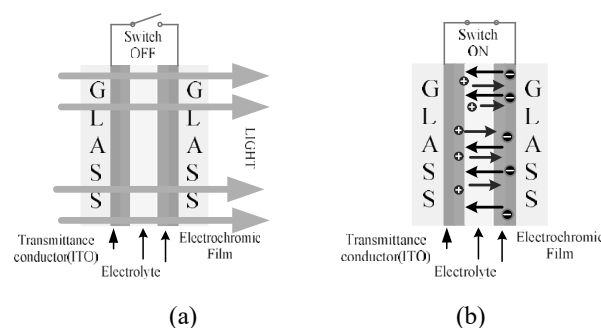


Fig.1. Shown the electrochromic structure device where the chemical layer is coated on a translucent glass substrate (a) off state and (b) on state.



Tungsten oxide coatings are deposited on a layer of translucent metal oxide, which is the conductor layer, with a layer of electrolyte or ionic conductors between the tungsten oxide compounds. The electrodes and layers of chemicals that give rise to the color of the chemical reaction can be shown in Fig.1.

This study are investigated the change of the electrochemical state of the electrolyte concentration on thin-film tungsten oxide from H_2SO_4 and HCl . Considering the difference in thin film thickness that induces are change of absorption and activation of color through the electrolyte solution [3]. This is due to the loss of electrons, a positive charge, and free radicals called polaron or radical cation. In order to prepare the coated glass of tungsten oxide, the glass is coated with translucent metal oxide made of tin oxide compound, called ITO Glass, by cutting the ITO glass plate to the size of $3.3 \times 2.5 \text{ cm}^2$, then clean the glass with acetone and rinse with deionization water as shown in Fig. 2.

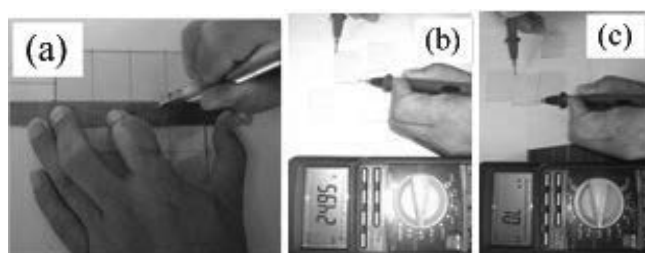


Fig.2. (a) Glass cutting show ITO and laminated glass test ITO with a measurement of the resistance of about 22-25 ohm (b), the glass side has a very high resistance(c).

II. PREPARATION AND DEPOSITED TUNGSTEN OXIDE.

1. Tungsten oxide film has been prepared by evaporation technique. By weighing scale 0.1 g of WO_3 into the tungsten boat and place it's on an evaporator chamber. After that the pressure in the vacuum chamber was removed the contaminant inside.
2. The internal pressure has been reduced to a minimum of 0.4 Pascal to start adjusting the voltage at the control current to the tungsten heat filament. In this step, heat up the tungsten filament by adjusting the voltage to 100 volts from the auto-transformer. The current are flows through the tungsten filaments upon 100 amps which it's gradually increase until a current up to 150 amps.
3. The tungsten oxide is evaporated at the current of 150 amps which it vapors to evaporate in the first stage as wait 30 seconds. After that open the shutter between the glass plate and the tungsten filament, the tungsten oxide will be vapors evaporated deposit on substrate transmittance conductor glass. At this stage, the current must be maintained at 150 amps until it is evaporated completely.

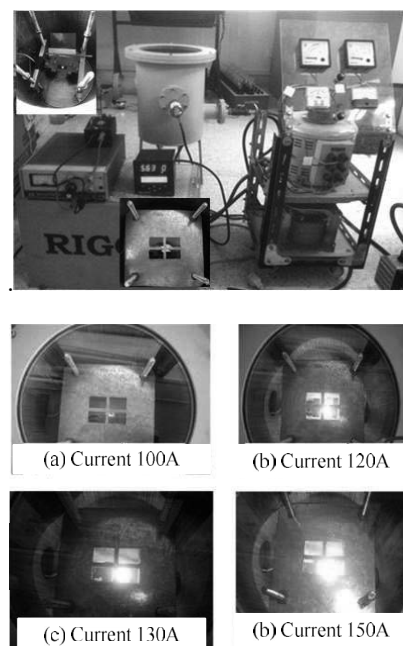


Fig.3. Shown the vacuum system to established vaporize oxide depositing on ITO glass.

4. Once the tungsten oxide are evaporated complete, which the pressure also reduced until the current flow through the filament is lowered to zero. The internal pressures are adjusted to the normal pressure. The glass covers are removed from the vacuum chamber as shown in Figure 3.

5. The tungsten oxide is deposited on ITO glass. An electrochromic device is took to sintering and mixed with the nitrogen gas. This condition of flow rates at 0.5 liters per minute also sintering the temperature up to $200^{\circ}C$. Finally the temperature reduced 1 hour until it reaches to the room temperature

III. TEST AND MEASURMENT OF ELECTRICAL PROPERTIES

Electrochromic materials have significant of a new generation of technologies called switchable glazing. A layers of tungsten oxide have been deposited on conductive transparent electrode; ITO [4]. An electrolyte solution has been inserted of into the layer of WO_3 and counter electrode. The characteristic of the electrochromic device is determined the current and voltage in the measurement system as present in Fig.4. For applied bias across the electrochromic device an ion storage thin film is separated by an electrolyte under processed responsible for coloration from transparent to blue in WO_3 films and single metal electrode [5-6]. An electrochromic device is elementary a rechargeable battery in which the electrochromic electrode is separated by a liquid electrolyte from a charge balancing counter electrode. The color changes are occurred by charging and discharging the oxidation-reduction with applied potential of a few volts [7].



The electrochromic glass and dip electrode plates were dissolved in 0.1 mol hydrochloric acid (HCl) solutions as shown in Figure 4. Adjust the applied voltage increase in 0 to 1.5 volts and decrease from 1.5 to 0 volts without changing the electrode. Record current and observe data information. After that electrochromic device has been given the applied bias to start a physical change is effect to change the color to blue. Figure 5 (a) and (b). The resulting pulse of current has decayed and the color change has been effected, the new redox state persists, with little or no input of power, is called “memory effect or Hysteresis”.

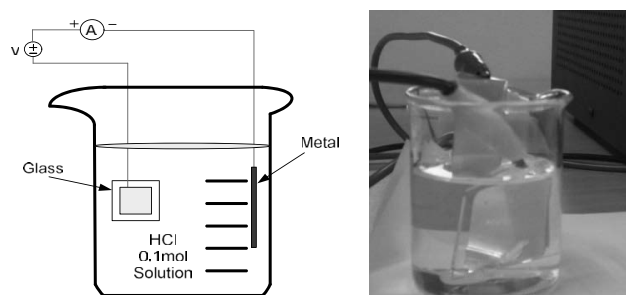


Fig.4. Scheme of measuring for electrochromic device characteristics.

Figure 4 illustrates an electrochromic device configuration. Since the charge stored at the capacitor is pushed into the electrolyte and transported to the reactant. The electron exchange of the redox reaction to the electrochromic layer results in light absorption or reflection, which makes the film to blue color. By reducing the applied bias, the color of the device under test remains the same, with increasing pressure due to the electrochromic, which is capable of color recognition or may be due to the crystalline state of the tungsten oxide.

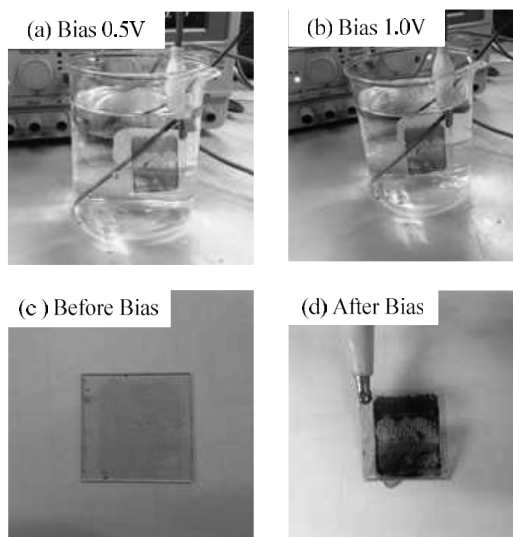


Fig.5. Shown the coloring of electrochromic device:(a)-(b) at bias voltage 0.5V and 1.0 V (c) before bias and (d) color persist after bias.

With the electrolyte solution or between the transmittance coatings, compare with the device before bias voltage Fig. 5(c). The color of the glass remains dark as shown in Fig.5 (d). Furthermore; the experiments Hysteresis curve is provided direct current bias with reference electrode to tungsten oxide deposited into glass plate. An applying DC biased as a positive potential for the metal as negative potential is connecting to the electrochromic layer shown in Fig. 6.

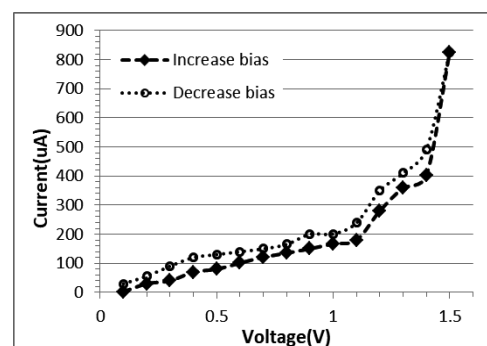


Fig.6. The Hysteresis curve of current and negative bias voltage of WO₃ films. HCl solution dissolved 0.1 mol was used as an electrolyte with and metal terminal.

IV. PROPERTIES OF CHANGING THE POLARITY DC BIAS

This experiment uses the experiment shown in Fig. 4. This case will be increased to change the polarity of the DC power supply to the positive electrode at the glass and the cathode at the electrode in Fig. 7.

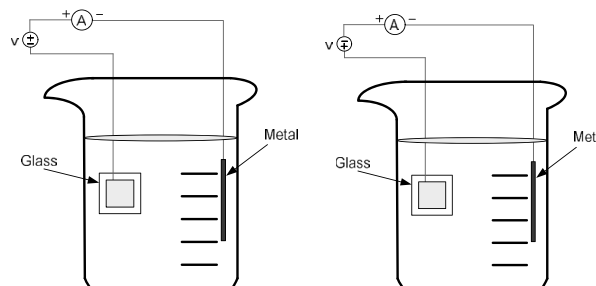


Fig.7. Schematics of DC biased circuit of forward bias and reverse bias

For the experiment to measure current and change of color by increasing the voltage from 0-1.5 volts and changing the polarity of the power supply to 0-1.5 volts. Record the results and observe the results. Control of the concentration of the solution used in testing that affects the change of electrochromic device. Also, polarity switching the DC power supply will affect the glass. The experiments were carried out using HCl solution concentration of 0.1, 0.01 and 0.001 mol. The experiment was carried out representing in Figure 4, which the voltage increase was from 0-1.5 volts. Then switch the power supply to 0-1.5 volts. The results of experimental shown that the concentration of HCl solution was 0.1, 0.01 and 0.001 moles respectively.

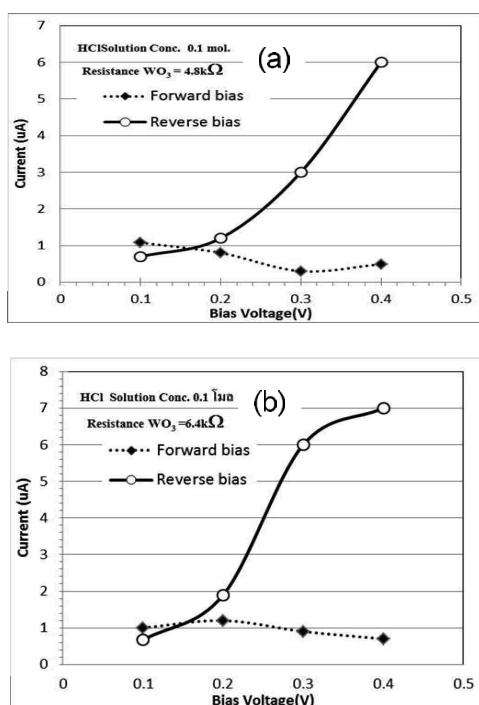


Fig.8. Typical current and voltage at forward biased and reverse biased in 0.1 mol of HCl solution at resistance 4.8kΩ (a) 6.4kΩ (b).

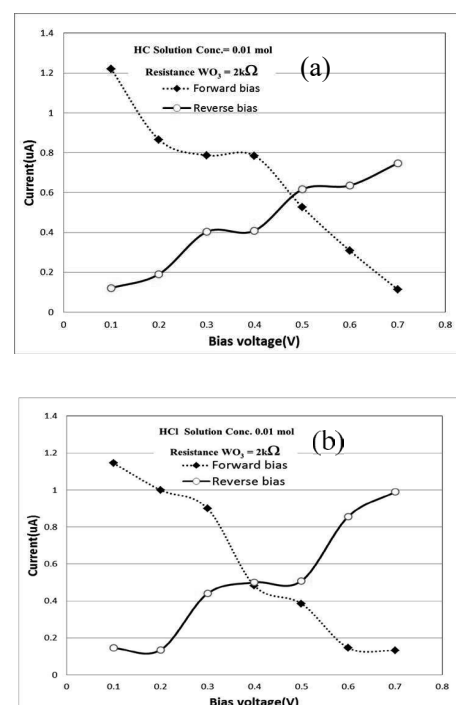


Fig.10. Typical current and voltage at forward biased and reverse biased in 0.001 mol of HCl solution at resistance 2kΩ (a) 2kΩ (b).

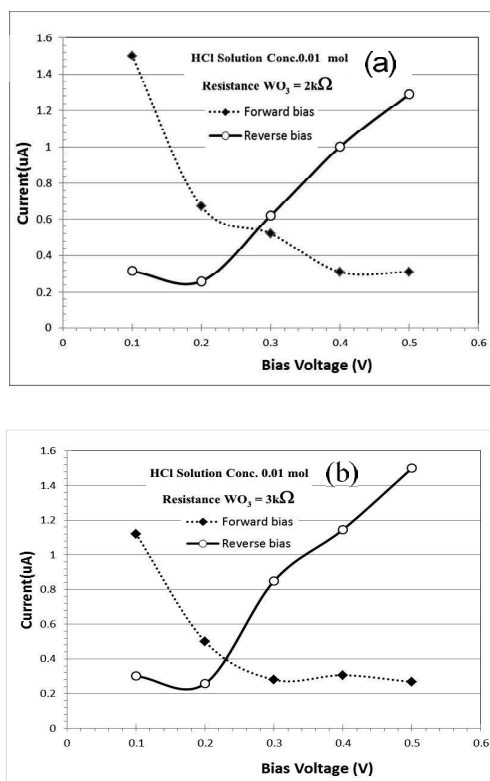


Fig.9. Typical current and voltage at forward biased and reverse biased in 0.01 mol of HCl solution at resistance 2kΩ (a) 3kΩ (b).

The result is changed the concentration of HCl solution 0.1, 0.01 and 0.001 moles. It was found that at the concentration of the solution to the highest concentration on the lowest concentration while the coloration of the WO₃ film can be variate by changing the applied bias to control the amount of the intercalated H⁺ ions in to WO₃ film as, shown in Fig.8-10. Also, when switching the power supply terminals, the dark colored glass will return to its original color. Since the charge in this film is pushed back to the same layer of film, it reduces the intensity of the color of the tungsten oxide film. The electrochromic reaction depends on the electrode of the source, where the layers of the electrochromic thin film connected to the negative terminal cause color change by reverse bias state.

IV. SWITCHING TIMES RESPONSE PROPERTIES

The synthesized WO₃ thin film was assembled on the surface of the ITO glass, showing tunable coloration of blue colors at different voltages, high stability both in HCl and H₂SO₄ electrolytes, comparable contrast and switching coloration/bleaching responses. The alternating current test is a direct and reverse bias voltage at low frequencies. The alternating current signal is the reaction against a change in reaction or ion exchange with the use of 0.25 mol and 0.1 mol HCl solutions. An electrochromic device is connected with the measuring resistance series have been supplied with a function generator. The pulse signals input on 3Vp-p at frequencies of 10Hz, 100Hz and 200Hz as shown in Fig. 11, respectively.

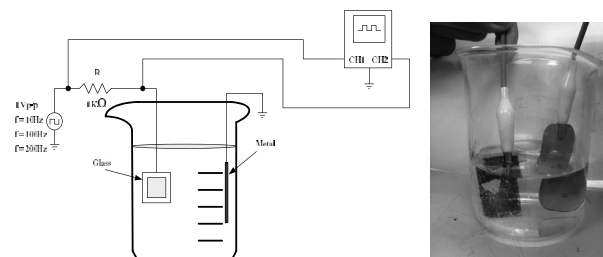


Fig.11. Schematics of experimental circuit of the AC signal response. Shown the response of the alternating current between EC versus metal electrode.

At HCl solution conc. 0.25 mol

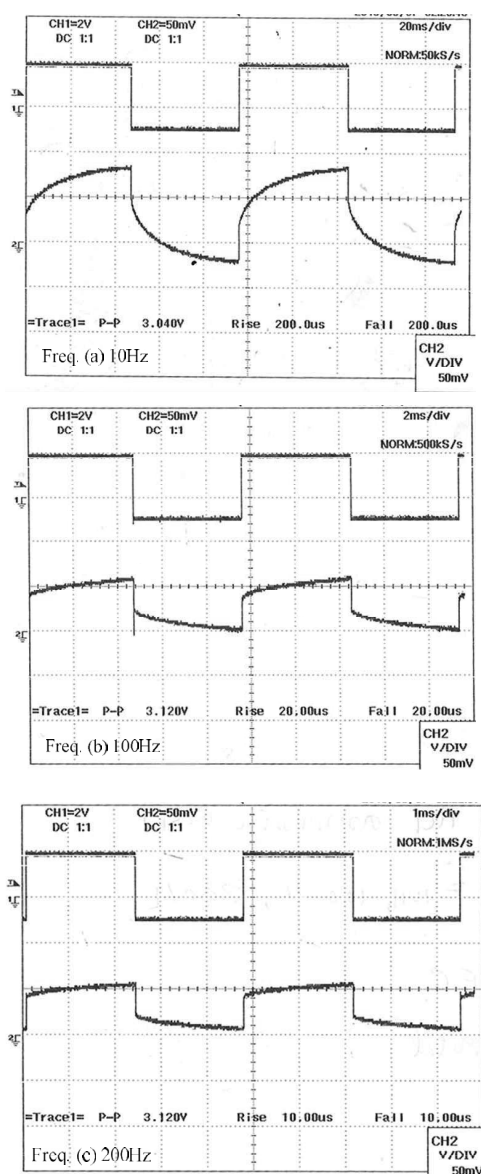


Fig.12. Typical of Signal response at frequency 10 Hz,100 Hz and 200 Hz with HCl concentration at 0.25 mol.

Result of experimental HCl solution concentration 0.25 and 1.0 mol are response switching signal output between electrochromic thin films on ITO glass of metal electrode as shown in Fig. 12 and 13. This signal input voltage is equal to the voltage drops in the electrochromic device, in the first channel. The signal output is measured on the output resistance of the generator. The signal current flowing in the loop circuit represented a signal output drop on the resistor "R" which it's recorded in the second channel by storage oscilloscope.

At HCl solution conc. 1.0 mol

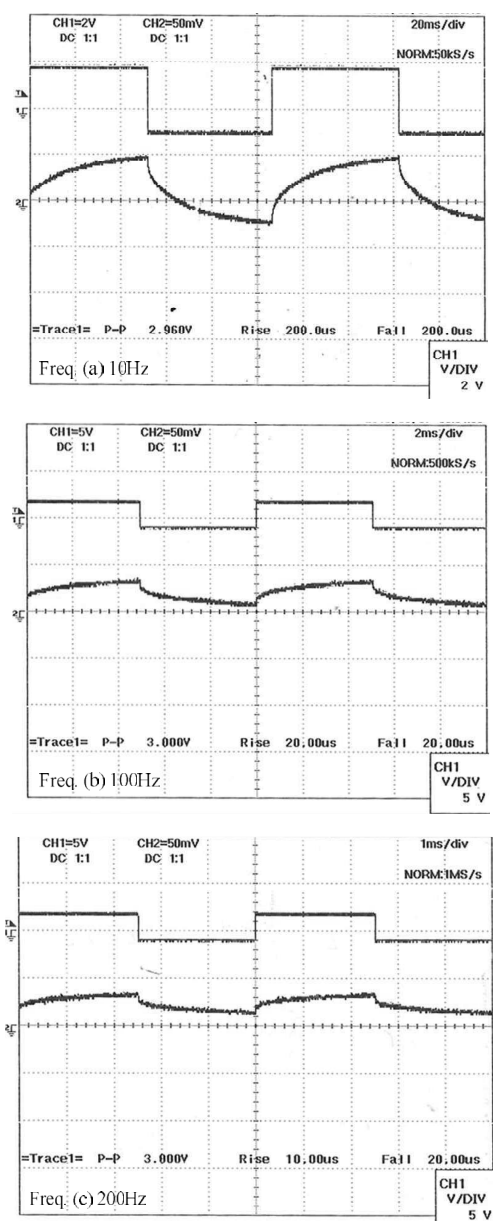


Fig.13. Typical of Signal response at frequency 10 Hz ,100 Hz and 200 Hz with HCl concentration 1.0 mol.



Test results of alternating current input with electrochromic device to confirm the voltage applied to the test sample of a metal conductor electrode in the exchange of electrons. The positive sign is the reverse bias, which turns blue, while the negative sign changes the color of the light. A solution to HCl concentrated 0.25 and 1.0 mol between the electrochemical sample and the metal plate. The output signals to represent the change in the redox reaction against the electrolyte solution. This change will indicate that there is a switch to 90% of the input signal level shows in Fig14.

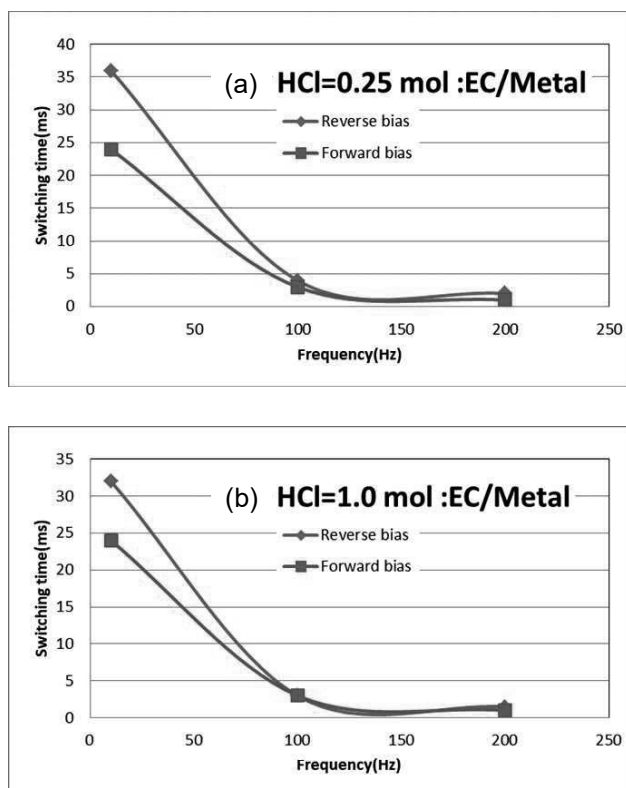


Fig.14.The results showed that color change in frequency of 10,100 and 200 Hz between EC and metal electrode in HCl 0.25mol(a) and 1.0 mol(b).

The typical results of a test sample are shown in Fig.13.,corresponding to the concentration of the 0.25 and 1.0 mol HCl solution, coloration and color reduction were at 6ms and 20ms at 10Hz. At higher frequencies, color changes occur very rapidly, and at a concentration of 1.0 mol HCl, there is a rapid change in color. It is expected that the color shading will take a shorter time of coloration, which is expected to be due to a decrease in transit time.

CONCLUSION

The worked out electrochromic device made up four layer glass/ITO/WO₃/electrolyte/counter electrode. The electrolyte

of HCl solution has been applied the enhancement of optical response measurements. Under applied bias drives the ions from the ion storage layer, through the ion-conducting layer and into the electrochromic layer. The reverse process of voltage is reversed, driving the ions in the opposite direction, out of the electrochromic layer, through the ion-conducting layer, and into the ion storage layer.

ACKNOWLEDGMENT

The authors thank the Prof.Dr.Kazunori Sato for advice and recommend gratefully acknowledged.

REFERENCES

- [1] Prakash R. Somani a, S. Radhakrishnan, "Electrochromic materials and devices: present and future," Elsevier Science B.V.,Materials Chemistry and Physics vol. 77, pp. 117-133, 2002.
- [2] E. Avendan, L. Berggren, G.A. Niklasson, C.G. Granqvist , A. Azens, "Electrochromic materials and devices," Elsevier B.V., Thin Solid Films vol.496, pp.30 – 36,2006.
- [3] M. Kucharski, T. Łukaszewicz, and P. Mrozek, "New electrolyte for electrochromic device," OPTO-ELECTRONICS REVIEW Rew.12, no.2,pp.175–180,2004.
- [4] Jinmin Wang,Xiao Wei Sun, and Zhihui Jiao, "Application of Nanostructures in Electrochromic Materials and Devices": Recent Progress,Materials,vol.3,pp.5029-5053;2010.
- [5] A. D. Tenner,L. Zonneveldt .: "Switchable Facades and Visual Comfort" Proceedings Right Light Vol.5, May 29-31:279-283. 2002.
- [6] A. L. Holt, J. M. Leger, and S. A. Carter.: "Solid-state electrochromic devices based on poly phenylene vinylene polymers" Applied physics letter.Vol. 86 :86-88. 2005.
- [7] Y. Domori, T. Nanba, Y. Miura.. "Coloration and Bleaching phenomena of amorphous WO₃ flims due to the electrochromical insertion of divalent cations" 6th Pacific Rim Conference on Ceramic & Glass Technology, September 13.1-6. 2005.



Load Sharing and Fault Tolerant Systems over Multiple Inter-Domain Paths

Khanista Namee^{1st}, Jirawat Paiboon

Faculty of Industrial Technology and Management
King Mongkut's University of Technology North Bangkok, Prachinburi, Thailand
Khanista.N@Fitm.Kmutnb.ac.th, 5606021622036@Fitm.Kmutnb.ac.th

Abstract—This research is purposed to understand the efficiency of load sharing to solve the problem of large networks having high traffic load to network sharing. How much will it solve the traffic on the network in wide area network? This trial uses the Border Gateway Protocol (BGP), a popular routing protocol used in wide area networks, and examines the functionality of BGP protocols such as Route map, Prefix-list. Moreover, the error detection system has been implemented to analyze the data exchanged within the network. The results showed that this method resulted in improved efficiency of 70 percent. Bandwidth is 20 Mbps. The maximum upload rate is 5.08 Mb / s and the maximum download rate is 12.05 Mb / s. The average upload rate is 578.99 kb / s and download at 1.42 Mb / s, which is not a problem that occurs because the graph value is still active without the system down or the graph is stagnant.

Keywords—Load Sharing; Fault Tolerant; Load Balancing; Multiple Inter-Domain Paths; MPLS

I. INTRODUCTION

Communication, including the use of the Internet, is essential for organizations. Because most of them are used to communicate with each other through the internet within the organization. Therefore, to create a new organization and to develop the organization, it must take into account the network structure and network design. To suit their organization and most effective.

When deploying a large enterprise network, organizations need to be able to receive and send data at any time without interruption or problems that will result in the transmission of those data delayed. There are a number of ways to solve the problem, such as increasing the bandwidth, the route to use the network to a larger size to send more packets. However, load balance is to use two or more lines together. And traffic management to work on two pairs of cables effectively. Load sharing is the same as Load balance, but it can be used to determine the traffic to which the packet is sent. Load sharing is very useful for organizations that need to send information quickly and efficiently, and reduce the problem that they are experiencing. Influence the transmission of information within the system. And can be online at any time, reducing the problems that cause the network is not working.

For this reason, there must be a network design that can work with routing load sharing to solve the problem of delayed

data transmission. The traffic of the data in the network as well as the efficiency of the network within the organization is more efficient. It also gives the organization more credibility.

The meaning of load sharing is the work of spreading the data out to other paths to share the load of the path. By transmitting data to a single path, which is similar to load balancing, which works just to distribute the information that is sent to the equality or to balance the load sharing will be different and different. Straightforward control over flexible data transmission. It can control the service to choose to force to send data to the specified path. For example, there are two routes are the main route and alternate routes. E-mail and general information in the main route. The backup route can only send data that is video call, voice, etc. So, it is seen that load sharing can control data transmission better than load balancing.

Fault Tolerant is checks for errors or system failures. To be able to solve the problem promptly before the long-term consequences. It can be used in a variety of ways. Configuration in the device to be able to check the network device to enable the Simple Network Management Protocol (SNMP) network management and management, allowing access to device names and device status flags. It can also remove the error detection program. It helps to monitor the usage and status of network devices. In order to be able to analyses the data and prevent any problems with the network that will cause damage to the network in the future or that will affect the long-term.

This research is designed to understand the efficiency of load sharing to solve the problem of large networks having high traffic load to network sharing. How much will it solve the traffic on the network in wide area network? This trial uses the Border Gateway Protocol (BGP), a popular routing protocol used in wide area networks, and examines the functionality of BGP protocols such as Route map, Prefix-list [1]. Moreover, the error detection system has been implemented to analyze the data exchanged within the network. In addition, this project we have installing a detection failure system into the network for detecting errors. Also, the benefit of this system is to analyze the data traffic within the network.

The rest of this paper is organized as follows. Section II provides a brief overview of some theory, related works and



software which had to be implemented within this research. Then, in Section III, the system designs of hardware and software components are presented in detail. The experimental deployment is presented in Section IV to demonstrate the design. The measurement results and performance are presented in Section V. Finally, conclusions are drawn in Section VI and following with acknowledgement section.

II. BACKGROUND

A. Implementation programs

- 1) *Microsoft Office Visio* is a program that was created to help you create a Flow Chart or Diagram.
- 2) *Graphic Network Simulator 3 (GNS3)* is a program that simulates the software (IOS) in the real device of the network.
- 3) *Xshell5* program is used to simulate the use of command line applications (Terminal Line) or terminal type program.

B. Load sharing with load balancing

The meaning of load sharing is the work of spreading the data out to other paths to share the load of the path. By transmitting data to a single path, which is similar to load balancing, which works just to distribute the information that is sent to the equality or to balance the load sharing will be different and different. Straightforward control over flexible data transmission. It can control the service to choose to force the data to be sent to the path where it is [2].

C. Detection failure [3]

It checks for errors or system failures. To be able to solve the problem promptly before the results. We can use a variety of ways configuration. In the device to be able to inspect the network device to enable the use of the Simple Network Management Protocol (SNMP) management and management.

D. The multi-constrained inter-domain path [4]

The multi-constrained inter-domain path computation over multiple domain routes problem can be defined as finding paths that obey to the constraints vector $C[j]$ (where $C[0]$ is the bandwidth constraint and the other weight components are the QoS additive metrics) and respect the non-dominance rule, from the source node s to the destination node t over a set of inter-domain routes S .

$$\forall p \in P_{s,t}^*, W_{p,j} = \sum_{e \in p, j=1}^m w_{e,j} \leq C_j \quad (1)$$

$$\min_{e \in p} w_{e,0} \geq C_0 \quad (2)$$

Equation (1) expresses the selection of the optimal path from the set of non- dominated paths computed over the S inter-domain routes. Equation (2) expresses the additive resource constraints on selected path segments within the different inter-domain routes.

III. SYSTEM DESIGN AND NETWORK DIAGRAM

Network design requires systematic work. To get the network that meets the needs of users, high network throughput and low cost. The procedure is as follows. Start by exploring the former network diagram and component. Then, get the results of the survey and user requirements. Finally, the system design to meet the needs of users and improve performance efficiency.

The network devices that we chose in this system consists of Cisco router 2851 model, Cisco switch Catalyst 3750x and Cisco Switch Catalyst 2960x.

A. Traffic Policy

The purpose of traffic engineering is to improve network performance through the optimization of network resources. We used the Quality of Service (QoS) parameters to manage the traffic in the network bandwidth which is divided into two groups.

- The important data group: Real-time applications such as voice or video conferencing are required to be sent through the network at the correct time. Include the type of information that the organization is most important or top priority such as ERP (Enterprise Resource Planning) system, and that type of information must be most stable without any problems that may affect the organization later.
- General Data Group: It is not necessary to use Real-time communication, such as accessing web pages, searching for information or sending an E-mail that is not needed to receive and interact immediately. The services that can leave time to wait. This includes all information that is not included in the sensitive data.

B. Network Diagram

The study of the structure of the former network diagram as shown in Figure 1, to identify any issues. This diagram shows the network and all four branches of the user company. This research had improved performance only 3 branches which are HQ, IPP and BKK branches. We are designed to enhance the performance of today's networks by configuration the current network devices to support load sharing as we designed in traffic policy. The devices have to be configure as follows in Figure 1.

1) Cisco Router

- a) *Border Gateway Protocol (BGP)* so that the router can communicate with each other on the Internet or Intranet.
- b) *Hot Standby Router Protocol (HSRP)* so that the device can back up the route and select the appropriate route by detect at device and cable.
- c) *IP Prefix List* to filter packets to enter or exit the router according to the conditions set. This is more efficient than ACL.

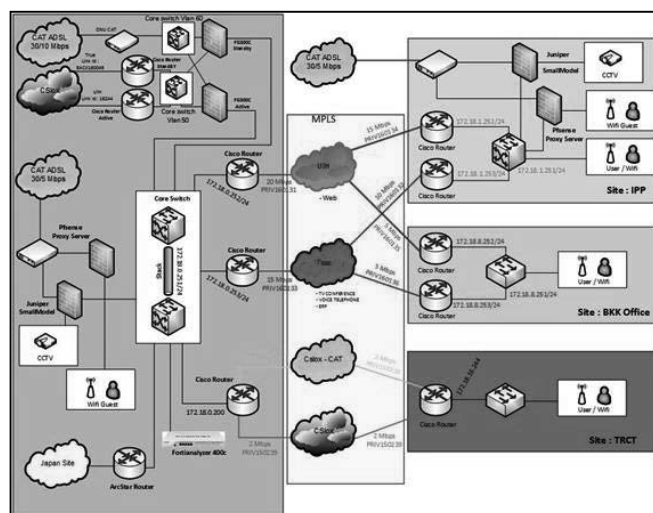


Fig. 1 Former Network Diagram

2) Cisco switch

a) *Virtual Lan (VLAN)* to group the port of a group of switches for the purpose of limiting or controlling the communication between the shared port. Also known as the limited broadcast domain.

b) Port security to protect the MAC address of a particular port, as well as limit the number of users per port.

C. Load Sharing Configuration

The load sharing in this research uses BGP routing. Due to the customer site, fiber optic cabling between the various branches within the organization and the media provider with up to 2 providers, or it is to do Multi-home and routing to make multi-home is BGP routing, and BGP can also control the traffic more easily, with the introduction of BGP extended attributes to control the traffic by IP filter method to cause load sharing. Also, it will configure path with path value. The value of the service line that can be versatile and flexible than with filter IP, destination IP source including the Port, which is a set of instructions that must be shared as follows [5].

1) *IP Prefix-list command*

This command is available for selecting route declaration or IP filtering. Also, it does not allowed to pass IP Prefix-list is a command similar to ACL, but IP Prefix-list is characterized by more flexibility in the work, by assigning IP and network as well as writing the word. The order is shorter. However, the disadvantage is to understand the syntax and options, and to do Load Sharing, it is necessary to use this command to help to force the data to run through. The BGP routing and route map for better performance. Command structure as follows.

```
# ip prefix-list list-name [seq seq-value] deny | to permit
mang / len [ge ge-value] [le le-value]
```

Procedures:

Use the **ip prefix-list** command followed by the name to define what this prefix-list does and to make it easier to

remember. Then enter the **seq** or sequence in the work, then configure to deny or permit the IP set.

Sample:

```
# ip prefix-list BKK seq 5 permit 172.18.8.21/32
```

Meaning:

Prefix-list name BKK No. 5 Allows IP 172.18.8.21 to pass.

2) *The Route-map command* is like creating a new route map. The policy is to force the address to be able to go somewhere, and the path to the back of the address.

3) *BGP Routing* is a command to select routes. Also, to choose which one is the best. When the best route is selected, this route is added in the Routing Table.

```

!
router bgp 65003
  bgp log-neighbor-changes
  neighbor 10.20.0.1 remote-as 65001
  neighbor 10.20.0.1 description Local BGP to Tokai_HQ_UIH
  neighbor 10.20.0.1 password 7 06051C20435600170318
  neighbor 10.20.0.1 update-source GigabitEthernet0/0
  neighbor 10.20.0.1 version 4
  neighbor 10.20.0.2 remote-as 65002
  neighbor 10.20.0.2 description Local BGP to Tokai_IPP_UIH
  neighbor 10.20.0.2 password 7 094F5D08516D1E1C0D03
  neighbor 10.20.0.2 update-source GigabitEthernet0/0
  neighbor 10.20.0.2 version 4
  neighbor 172.18.8.253 remote-as 65003
  neighbor 172.18.8.253 description Local BGP to Tokai_BKK_True
!
!
address-family ipv4
  neighbor 10.20.0.1 activate
  neighbor 10.20.0.1 soft-reconfiguration inbound
  neighbor 10.20.0.1 prefix-list BKK out
  neighbor 10.20.0.1 route-map BKK_TO_ESIE out
  neighbor 10.20.0.2 activate
  neighbor 10.20.0.2 soft-reconfiguration inbound
  neighbor 10.20.0.2 prefix-list BKK out
  neighbor 10.20.0.2 route-map BKK_TO_IPP out
  neighbor 172.18.8.253 activate
  neighbor 172.18.8.253 next-hop-self
  neighbor 172.18.8.253 soft-reconfiguration inbound
  no auto-summary
  no synchronization
  network 172.18.8.0 mask 255.255.255.0
  network 172.18.8.21 mask 255.255.255.255
  network 172.18.8.221 mask 255.255.255.255
  network 172.18.8.222 mask 255.255.255.255
!
!

```

Fig. 2 Preview the BGP Configuration results

D. Alternate Routes Configuration

1) *HSRP command* is a command that allows the device to back up the route and select the right path. It will check the device. Can I still work?

2) *Tunnel command* is a command to create. Virtual network Work with the structure of the public network. Or may be running on the IP network can maintain the specific network of the organization. Encrypt the packet before sending.

3) *The Track Tunnel command* is a command that checks the true and false values of the tunnel command that is up or down. If the tunnel in the track is down, it will result in the track being false and when the track value is false. To remove the priority attached to that track [6].



```
track 1 interface Tunnel1 line-protocol
!
track 2 interface Tunnel2 line-protocol
!
!
interface Tunnel1
description Check Link status for customer Tokai Eastern Rubber Co.,Ltd
ip unnumbered GigabitEthernet0/0
keepalive 10 3
tunnel source 10.20.0.3
tunnel destination 10.20.0.1
!
interface Tunnel2
ip unnumbered GigabitEthernet0/0
keepalive 10 3
tunnel source 10.20.0.3
tunnel destination 10.20.0.2
!
!
interface GigabitEthernet0/1
ip address 172.18.8.252 255.255.255.0
no ip redirects
no ip proxy-arp
load-interval 30
duplex auto
speed auto
standby 10 ip 172.18.8.251
standby 10 priority 105
standby 10 preempt
standby 10 track 1 decrement 10
standby 10 track 2 decrement 10
!
router bgp 65003
bgp log-neighbor-changes
neighbor 10.20.0.1 remote-as 65001
neighbor 10.20.0.1 description Local BGP to Tokai_HQ_UIH
neighbor 10.20.0.1 password 7 06051C2D435600170318
neighbor 10.20.0.1 update-source GigabitEthernet0/0
neighbor 10.20.0.1 version 4
neighbor 10.20.0.2 remote-as 65002
```

Fig. 3 Preview the HSRP Configuration results

E. Error Detection Configuration

1) *SNMP command* is a command used to help manage the network to make it easier to manage, may be used together with various monitoring programs.

2) Configuration of HSRP

The HSRP will be used to redundant the device. In this section have been applied to combine the redundant of the fiber cable connected to the device. When one of the lines loses connection, it will switch to the other router immediately without waiting for the main device to lose or not work and then change the device.

3) SNMP Configuration Value

Enable the SNMP Protocol allow program to detect errors. Also, it can access the value of the Router device to monitor the operation of the device. To analyze the system protection and to solve the problem of the network before the network all affected by the program used. Error checking is a PRTG program.

IV. IMPLEMENTATION

After finalizing the device and its functions, the job started testing the device and configuration it. To test the functionality of the router, the switch can use the functions designed and defined as appropriate as required.

A. Explore the Optic Fiber

Explore the optic fiber cable of the media provider for inspection. By checking all three branches of the user. After the Fiber optic cable survey of the Media provider, the results were as accurately defined.

B. Communication Path

Internal and external communications will be communicated through the UIH and TRUE service providers as intermediaries for linking the three branches together. The path of the UIH provider is the primary route to send information that is not in the specification, separated by IP lines. The TRUE carrier path is defined as a backup route.

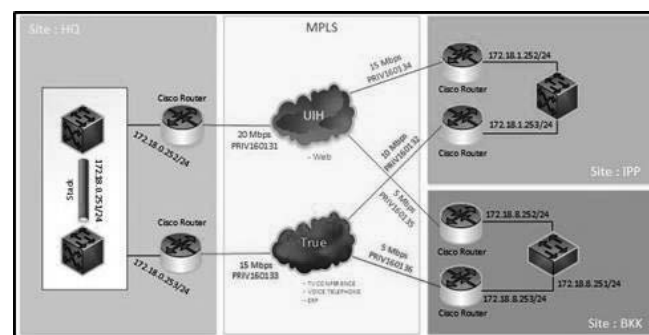


Fig. 4 Shows the Diagram in the three data communication interfaces

1) *BKK IPP and HQ routers connected to the UIH.* The routers that are connected to the UIH are located one per branch. They are defined as Active from the Configurations and the UIH Routing is the primary route to send the data and less important.

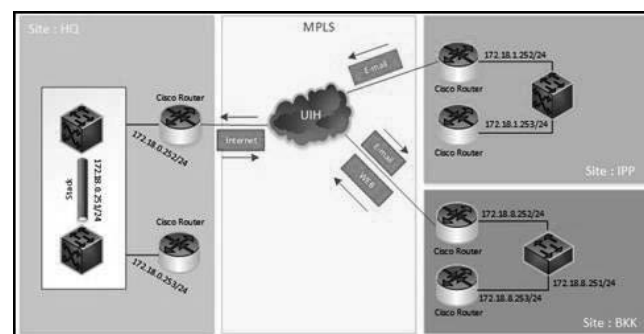


Fig. 5 Diagram shown in main communication section

2) *BKK IPP and HQ routers connected to TRUE.* Each branch will have a status of the standby. Configurations set the TRUE path as a backup path for sending data, and is also the primary route used to send data that is classified as sensitive data.

3) *Main route or backup route is disconnected.* If the line UIH mainstream lack of connectivity. This will change to the TRUE backup path and give the TRUE path a primary path. If the main UIH is connected again, it will change the main path that is TRUE to the same UIH path. However, if the TRUE backup route is disconnected, all data will change to the main UIH path.

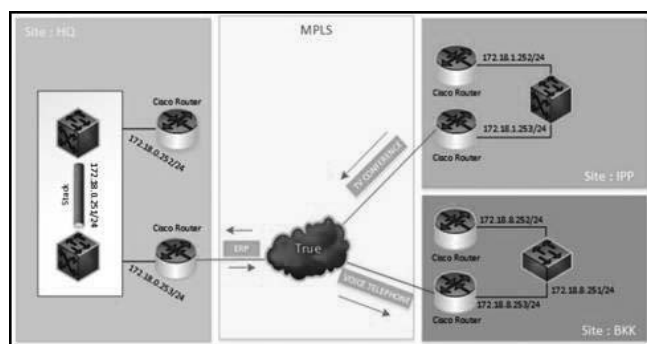


Fig. 6 Diagram showing the alternate route communication

V. RESULTS AND PERFORMANCE EVALUATION

A. Error detection program

Use a program called PRRG Network Monitor to see the operation of the machine and the amount of data used. It can be reported through E-mail or text information can help protect. Improve and develop network in the organization effectively.



Fig. 7 Preview the PRTG error detection program.

B. Result of Traceroute

By testing with traceroute simulation, the result is as set out in the agreed policy by separating the IPs that have been defined for the application, such as Conference Voice and ERP, with IP. Simulated from BKK branch to IPP branch as shown in Figure 8.

1) Result of Traceroute IP for Conference

The Traceroute will be Traceroute from the conference IP machine that has set IP, which will have an IP address of 172.18.8.21 as the IP address in the Conference mode will cause the route to use TRUE instead of the main route. UIH to avoid overloading Traffic with general information not defined in policy. The result is shown in Figure 9.

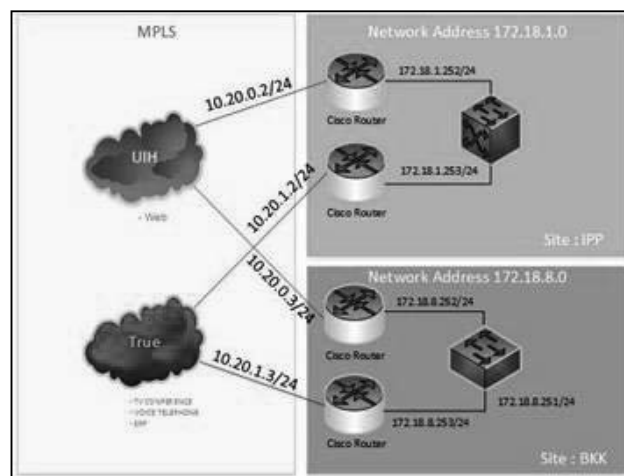


Fig. 8 Shows IP and route to Traceroute

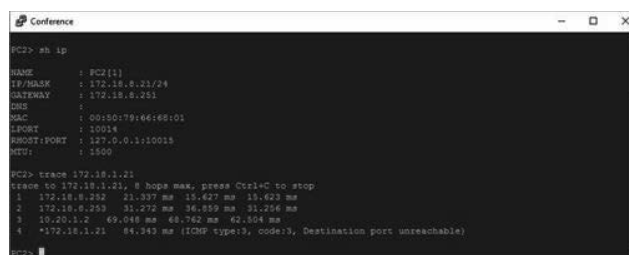


Fig. 9 Shows the path to IP Conference Traceroute

C. Result of path error detection

As a result of the graph, monitor the path of each branch of the customer for inspection. An error that could have a negative impact on the network in the future. The result of the graph shows the Bandwidth of the route, including Outbound or Inbound, or Download and summarize the average. The minimum value for downloading a unit is bit / s, as well as a percentage of usage.

1) UIH branch line graph values

Bandwidth is 20 Mbps. The maximum upload rate is 5.08 Mb / s and the maximum download rate is 12.05 Mb / s. The average upload rate is 578.99 kb / s and Download. At 1.42 Mb / s, which is not a problem that occurs because the graph value is still active without the system down or the graph is stagnant. No Bandwidth or UIH traffic in the HQ branch as shown in Figure 10.

2) UIH branch network graph values

The graph shows Bandwidth information is 15 Mbps, with the highest upload rate is 9.18 Mb / s and Download is 6.49 Mb / s. The average upload is 1.35 Mb / s and Download. At 590.30 kb / s, there are no problems with the graph. Still, there is no down time. No Bandwidth or UIH in the IPP. The result is shown in Figure 11.

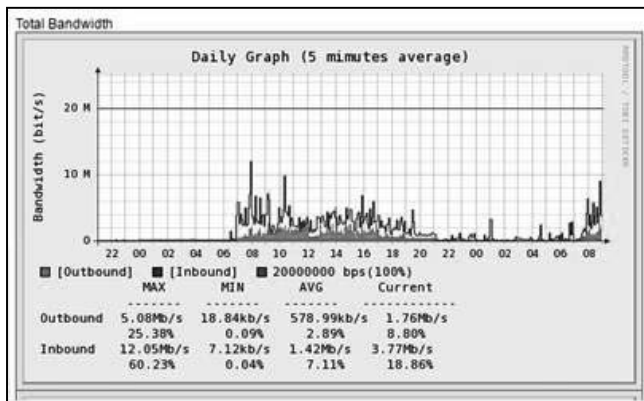


Fig. 10 Shows a graph of the HQ branch of the UIH route

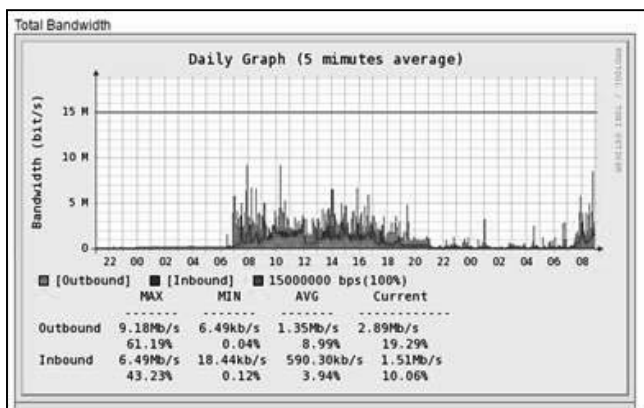


Fig. 11 Shows the graph of the IPI of the UIH

3) UIH branch line graph of BKK branch

The bandwidth information is 5 Mbps, with the highest upload rate is 1.14 Mb / s, and the most downloaded is 1.18 Mb / s. The average upload is 86.03 kb / s and Download. At 11.45 Kb / s, which has not encountered any problems due to the value of the graph is still active, there is no down system or graph is stagnant. No bandwidth or UIH traffic in the BKK branch.

VI. CONCLUSIONS

This research is designed to understand the efficiency of load sharing to solve the problem of large networks having high traffic load to network sharing. How much will it solve the traffic on the network in wide area network? This trial uses the Border Gateway Protocol (BGP), a popular routing

protocol used in wide area networks, and examines the functionality of BGP protocols such as Route map, Prefix-list. Send information include appropriate network resources management. Moreover, the error detection system has been implemented to analyze the data exchanged within the network. In addition, this project we have installing a detection failure system into the network for detecting errors. Also, the benefit of this system is to analyze the data traffic within the network. The detection failure system monitors the traffic in the network such as bandwidth usages, the inbound and outbound of the network by displays them graphically for understanding easily. Also, check for network malfunction, such as flat panel details. The value of the data sent and sent from the network by the graph. To make it easier to check. The results showed that this method resulted in improved efficiency of 70 percent. Bandwidth is 20 Mbps. The maximum upload rate is 5.08 Mb / s and the maximum download rate is 12.05 Mb / s. The average upload rate is 578.99 kb / s and download at 1.42 Mb / s, which is not a problem that occurs because the graph value is still active without the system down or the graph is stagnant.

ACKNOWLEDGMENT

This research could not have been completed successfully without supporting from Department of Information Technology, Faculty of Industrial and Technology Management at King Mongkut's University of Technology North Bangkok. We would like to deliver our greatest appreciation for their support.

REFERENCES

- [1] K. Liu, B. Jabbari, and S. Secci, "Generalized Multipath Load Sharing Using Vectorized Routing Model," Globecom 2013 – Communications QoS, Reliability and Modelling Symposium, p.1507-1512, 2013.
- [2] G. Bertrand, S. Lahoud, G. Texier, and M. Molnar, "A Distributed Exact Solution to Compute Inter-domain Multi-constrained Paths," EUNICE, p. 21-30, 2009.
- [3] R. Casellas, J. L. Rougier, and D. Kofman, "Packet Based Load Sharing Schemes in MPLS Networks," pp.18-28, 2002.
- [4] N. Djarallah and H. Pouyllau, "Multi-constrained path computation for inter-domain QoS-capable services," Int.J. of Communication Networks and Distributed Systems, Vol. 10, 2011.
- [5] Z. Zhao, Y. Shu, L. Zhang, and H. Wang, "Flow-level multipath load balancing in MPLS network," IEEE Communication Society, 2004.
- [6] N. B. Djarallah, N. L. Sauze, H. Pouyllau, S. Lahoud, and B. Cousin., "Distributed E2E QoS-Based Path Computation Algorithm Over Multiple Inter-Domain Routes," 2011 International Conference on P2P, Parallel, Grid, Cloud and Internet Computing, pp.169-176, 2011.



Voltage Controlled Sinusoidal Oscillator Based-on Commercially Available VDGA's

Songyos Rungsa, Adirek Jantakun¹

Dept. of Electronics and Telecommunication Engineering
Faculty of Engineering, Rajamangala University of
Technology Isan, Khonkaen Campus, Khonkaen, Thailand
E-mail: ¹adirek.ja@rmu.ac.th

Thitiporn Janda

Dept. Electronics and Telecommunication Engineering
Faculty of Technical Education, Rajamangala University of
Technology Isan, Khonkaen Campus, Khonkaen, Thailand
E-mail: Thitiporn_koy@hotmail.com

Abstract— The sinusoidal oscillator based on voltage differencing gain amplifiers (VDGA) has been used for this research. The proposed oscillator is easily constructed with only two VDGA's without external passive capacitors. The condition and frequency of oscillation are adjusted to give simultaneous and equal transconductance gains. Furthermore, the external voltage signals can easily be adjusted according to the frequency and amplitude of the sinusoidal signal that can be conveniently used in communication systems or for training in education. The output-impedance is low which is directed to connect or drive load. The simulation results obtained by the use of commercially available active devices are satisfactory a theoretical analysis.

Keywords— Sinusoidal oscillator; voltage differencing gain amplifier; external passive capacitor.

I. INTRODUCTION

The sinusoidal oscillator is extremely useful in communication systems, electronic power systems, instrumentation and/or measurement systems etc [1-3]. Furthermore, a sinusoidal signal is a key part of training students in electrical and electronic engineering in the laboratory [3-5]. Such laboratories include basic communication systems, for example, amplitude modulation (AM), amplitude shift keying (ASK), binary phase shift keying (BPSK), frequency modulation (FM) and frequency shift keying (FSK). Furthermore, AM/FM communication systems are also commercially available because this they can be used to communicate easily at considerable distances [4]. Today, sinusoidal oscillators are frequently used in research and the results have been published [1-22]. They employ different high performance active building blocks and exhibit several advantages such as: their condition and frequency of oscillation can be orthogonally or independently adjusted with transconductance gains [3-9, 12, 15-17, 20-22] or parasitic resistances [2-4, 13, 16, 18] or voltage gains [1, 10, 14]. The sinusoidal signal provides only voltage-mode [1-2, 7, 10-14, 19-20] or current-mode [3, 6, 8-9, 15, 18, 22]. Also, some circuits provide voltage and current-mode simultaneously [4-5, 16-17]. However, there are some drawbacks as it has been found that (i) there are many passive or active devices [6, 10-11, 13, 18-19] (ii) there is a requirement for an extension or

copy terminal of active devices [3-4, 9, 15, 17] (iii) the use of floating capacitors may cause parasitic effects [8, 19, 21] (iv) output-impedance of the voltage signal does not have low-impedance which is required for a voltage buffer [2, 5, 7, 10-13, 17, 19-20] (v) the amplitude of the sinusoidal signal cannot be tuned [1-2, 6-22] which makes it inconvenient for used in laboratory demonstrations or applications in communication systems.

This paper proposes a synthesis of the voltage-mode sinusoidal oscillator. The proposed sinusoidal circuit enjoys several advantages such as (i) construction of a circuit is very simple employing two VDGA's (ii) active devices are not required to extend terminals (iii) without external passive capacitors (iv) low-impedances of output voltage signals (v) availability of adjustment of amplitude/frequency of sinusoidal signals and (vi) low sensitivity of active and passive devices..

II. THE DESCRIPTION OF PROPOSED CIRCUIT

The proposed sinusoidal oscillator can be explained in terms of the concept of VDGA, the details of the proposed circuit, a sensitivity analysis and the non-ideal analysis

A. The concept of VDGA

VDGA or a voltage differencing gain amplifier was researched by Satansup and Tangsrirat [23] in 2013. They were able to use a CMOS VDGA for analog signal processing. It was implemented using only tunable transconductance cells and presented a voltage-mode biquadratic filter as an example which provided satisfactory results. The electrical symbol of VDGA has been depicted in Fig. 1. It has four terminals that are p, n, z and w. The p and n terminals have a different input voltage which has high-impedances. The z terminal is the output current that also has high-impedances. In addition, the w terminal is the output voltage which a low-impedances and can be directed to drive load or to connect with the next stage. The ideal characteristics of voltage and current of VDGA are expressed by the equation (1) which are

$$i_p = i_n = 0, i_z = g_m(v_p - v_n) \text{ and } v_w = \beta v_z. \quad (1)$$

Where β is voltage gain that can be controlled by external bias currents [23]. Nowadays, commercially available integrated circuits (IC) for implementing VDGA can be



essentially cascaded with OPA860 [24] at the front-end and AD835 [25] at the rear-end as shown in Fig. 2. This construction is appropriate for use as a replacement for the fabrication of an integrated circuit which is very expensive. OPA860 is a single-output diamond transistor which is simply implemented as OTA (Operational Transconductance Amplifier) and the transconductance gain g_m can be easily adjusted by changing the values of passive the resistor R_m [24]. AD835 is a very fast multiplication of application for voltage gain amplifier [1], where the gain B is easy to adjust by changing the external voltage V_{SET} . The positive and negative gain B can be smoothly configured with polarity by the external voltage V_{SET} . It can also be expressed as $B = \pm V_{SET}(R_{f1} + R_{f2}) / R_{f2}$.

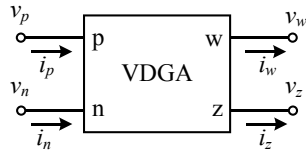


Fig.1 Electrical symbol of VDGA

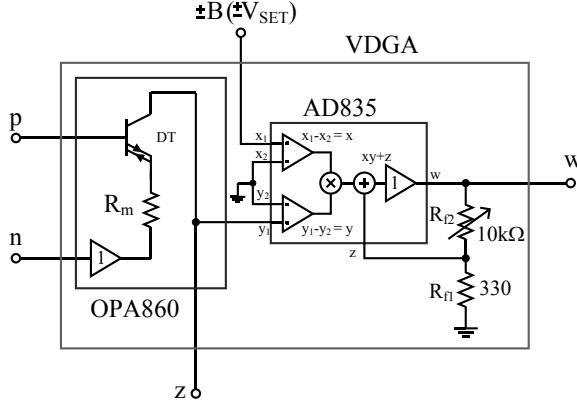


Fig.2 Implementation of VDGA

B. The details of the proposed sinusoidal oscillator

The proposed sinusoidal oscillator is implemented by using commercially available VDGAAs as shown in Fig. 3 which are simple and low cost. It can smoothly provide two VDGAAs. Neither of the VDGAAs are at all suitable for the extension of terminals. No external passive capacitors are necessary. The capacitance at node C_1 and C_2 should be approximately combined with the parasitic capacitance of active devices (OPA860, AD835). It is clear, therefore, that the proposed circuit can be fitted without external passive capacitors. The characteristic equation for a sinusoidal oscillator can be analyzed as

$$s^2 + \frac{C_1 g_{m2} - C_2 g_{m1}}{C_1 C_2} s + \frac{g_{m1} g_{m2} (B_1 - 1)}{C_1 C_2} = 0. \quad (2)$$

Where the sinusoidal circuit is ready to generate the sinusoidal signal when it is set

$$C_2 g_{m1} \approx C_1 g_{m2}, \quad (3)$$

This is also known as the condition of oscillation (CO). The frequency of the oscillation (FO) can be expressed as

$$\omega_{osc} = \sqrt{\frac{g_{m1} g_{m2} (B_1 - 1)}{C_1 C_2}}. \quad (4)$$

The FO can be linearly controlled by adjusting the voltage gain B_1 that may be applied to the FM/FSK system. However, it is also limited by the input limitation/saturation of active devices. Furthermore, the FO can be set by simultaneously adjusting and equalizing the transconductance gains (g_{m1} and g_{m2}) of VDGAAs.

The output of the oscillator is low-impedance which is simply used for connecting to the load without a voltage buffer. The amplitude of the sinusoidal signal can be expressed as

$$V_O = B_2 v_{z2}. \quad (5)$$

It is evident from (5) that the sinusoidal signal can be modified/changed as required by the amplitude with voltage gains B_2 that are AM, ASK and BPSK signals which will be generated by the information signal of V_{SET2} . Therefore, this oscillator circuit can be appropriately applied in communication systems and used for demonstrations in the electronic/electrical engineering laboratory.

C. The sensitivity analysis

The sensitivity analysis is used for explaining the performance criteria of the oscillator circuit. The active and passive values can be used to show the relation between the sensitivities of the FO and the deviation that is

$$S_{g_{m1}, g_{m2}, B_1}^{\omega_{osc}} = \frac{1}{2}. \quad (6)$$

From (9), it is clear that, the sensitivities are low since the absolute values of the sensitivities are less than unity.

D. Non-ideal analysis

The non-ideal characteristic of VDGA is explained in [12]. They are transfer gain errors of VDGA. These errors are changed the ideal characteristic of VDGA to

$$i_p = i_n = 0, \quad i_z = g_m (\alpha v_p - \alpha v_n) \quad \text{and} \quad v_w = \gamma B v_z, \quad (7)$$

where α is transconductance inaccuracy factor [12] from terminal p and n to z. γ is voltage gain error. The characteristic of VDGA in (7) can be used to reanalysis of CO and FO of proposed oscillator that can be expressed as:

$$\alpha_2 C_2 g_{m1} \approx \alpha_1 C_1 g_{m2}, \quad (8)$$

and

$$\omega_{osc} = \sqrt{\frac{\alpha_1 \alpha_2 g_{m1} g_{m2} (\gamma_1 B_1 - 1)}{C_1 C_2}}. \quad (9)$$

It can be seen that, the transfer gain errors of VDGA has been slightly affected of CO and FO. However, these errors can be easily compensated/accomplished by tuning the transconductance gain g_m and voltage gain B of VDGAAs.

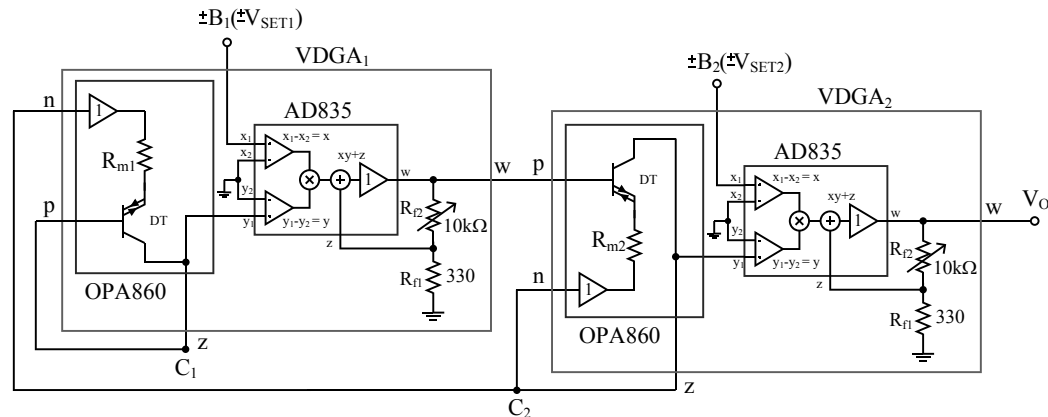


Fig. 3 Implementation of proposed oscillator with commercially available VDGA's

III. COMPUTER SIMULATION RESULTS

The implementation of proposed sinusoidal oscillator by using commercially available VDGA's as depicted in Fig. 3 which has a nominal and unobtrusive structure.

The capacitance at node C_1 should be approximately combined with the parasitic capacitance of active devices at about 6.1pF [24-25]. At the same time the total capacitance at node C_2 is about 8.2pF [24-25]. In this case, we have chosen the values of the transconductance gains with $g_{m1} = g_{m2} = 0.30\text{mS}$ by setting $R_{m1} = R_{m2} = 3.3\text{k}\Omega$. The supply voltage of the active elements was $\pm 5V$. The bias voltages were set as $V_{SET1} = V_{SET2} = 1V$. The verification of the performance of the proposed circuit used the Pspice program. The first results of the experiment are shown in Fig. 4 which consist of the transient and steady state response of the sinusoidal output waveform. The spectrum analysis of the sinusoidal signal is displayed in Fig. 5 with 4.90MHz frequency of oscillation and about 4.24% percent of THD. The demonstration of FSK of sinusoidal signal by stepping-up V_{SET1} from 1V to 1.5V are depicted in Fig. 6, which shows that the FO is explicitly changed from 4.90MHz to 7.0MHz, respectively, as well as their spectra as displayed in Fig. 7.

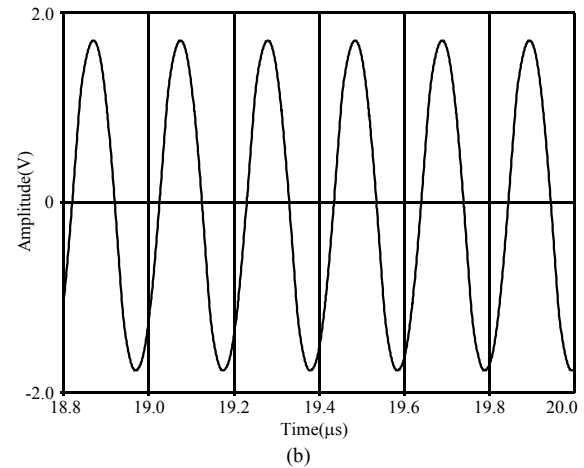
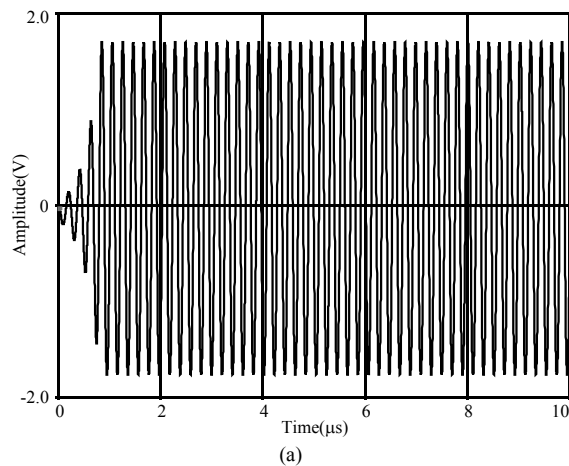


Fig. 4 Sinusoidal output waveform (a) transient response (b) steady state response

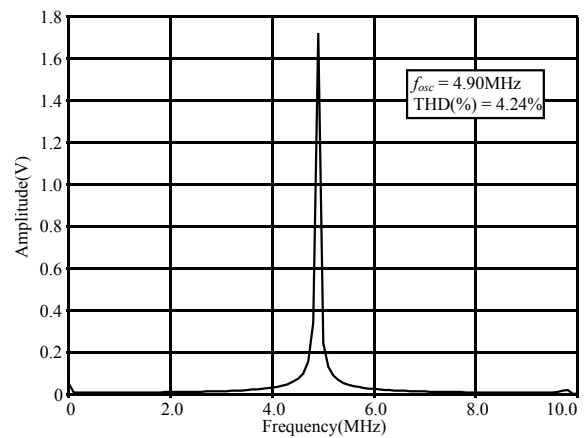


Fig. 5 Spectrum and THD of sinusoidal signal

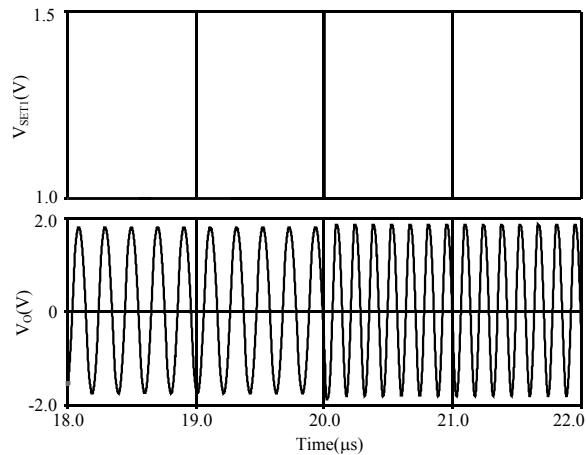


Fig. 6 FSK signal

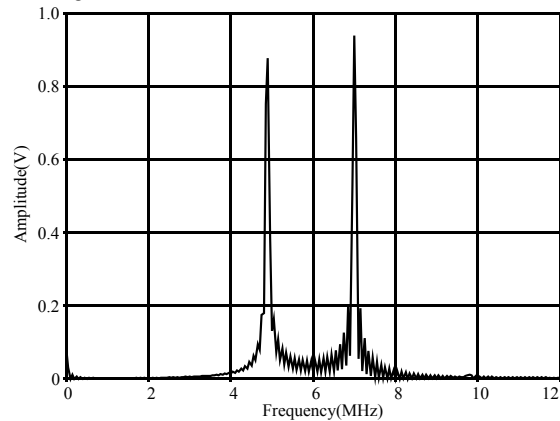


Fig. 7 Spectra of FSK signal

Fig. 8 illustrates the waveform of the sinusoidal signal when V_{SET2} is rapidly varied from 0.1V to 1V in 40 μ s. It can be seen that the amplitude of the sinusoidal signal is increased according to V_{SET2} . An examination of the AM generation can be demonstrated by feeding the sinusoidal signal at 50kHz frequency and 2Vp-p amplitude to V_{SET2} . The waveform in Fig. 9 shows a desirable outcome because the output signal can be generated by the AM signal. The ASK signal in Fig. 10 is generated by feeding a square wave/unipolar signal to V_{SET2} . The amplitude of the sinusoidal output is changed to zero for the V_{SET2} signal which has the value 0V and else is kept fixed. The next simulation result is applied to the proposed circuit to modulate the BPSK signal. We fed the bipolar signal to V_{SET2} which had swings between 1V and -1V. The phase of the sinusoidal signal is changed to 180° when the V_{SET2} signal is stepped-up from -1V to 1V as presented in Fig. 11. All of the above results for the simulations are in accord and are satisfactory in terms of the theoretical analysis which shows that the proposed sinusoidal oscillator is suitable for practical use in basic communication systems and for education training in the electronic/electrical engineering laboratory. The voltage control of FO can be demonstrated by adjusting the voltage signal V_{SET1} with various transconductance gains. The results are plotted in Fig. 12 that is proportional to the voltage signal

V_{SET1} . It can be clearly seen that V_{SET1} is directly controlled by the FO which confirms the theoretical analysis as in (4). The statistical results of Monte-Carlo analysis with 5% tolerance of g_m are test in Fig. 13. The Gaussian distribution and 100 times random were used. The maximum and minimum of the FO are 5.15MHz and 4.35MHz, respectively. The standard deviation of FO is 160kHz.

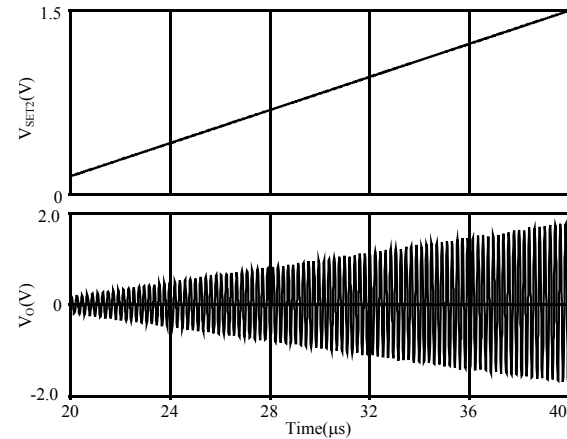


Fig. 8 Amplitude of sinusoidal signal versus voltage control V_{SET2}

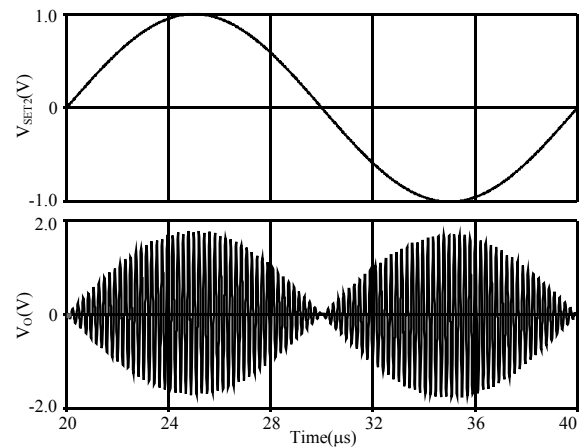


Fig.9 AM signal

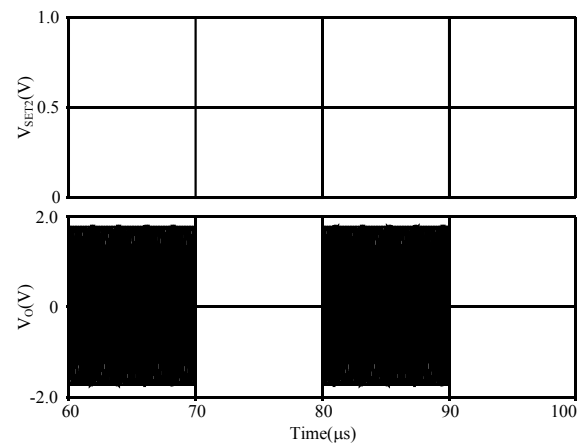


Fig. 10 ASK signal

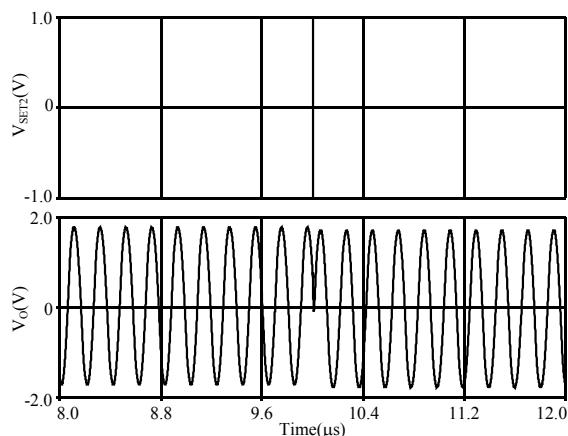


Fig. 11 BPSK signal

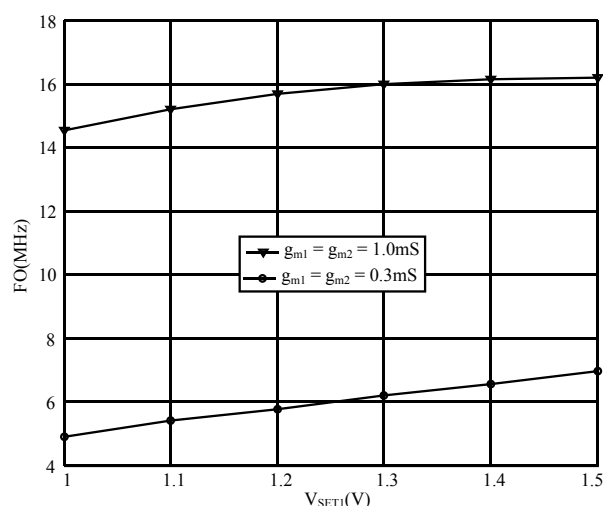


Fig. 12 The FO versus V_{SET1}

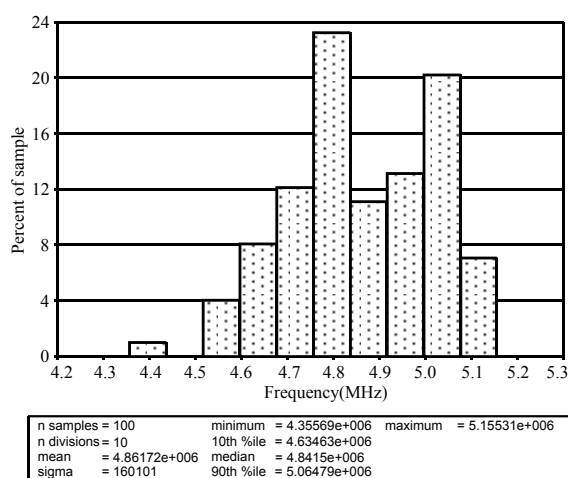


Fig.13 Monte Carlo analysis with 5% tolerance g_m

IV. CONCLUSION

The VDGAs based on the sinusoidal oscillator are presented in this paper. The proposed sinusoidal oscillator is constructed with a minimum number of active, and only two VDGAs are used. The frequency and amplitude can be independently controlled by external voltage signals. The voltage sinusoidal output has a low output impedance terminal and can be connected to a suitable load without a voltage buffer or impedance matching. The implementation of the proposed circuit uses commercially available ICs which are simple and low cost. Furthermore, the implemented circuit is without external passive capacitors so it is suitable for off-the-shelf design. The output signal can generate AM, ASK, FSK and BPSK signals which are convenient for applications in basic communication systems and demonstrations in the electronic/electrical engineering laboratory. The performance of the proposed oscillator is demonstrated by the Pspice program that shows an agreement with the theoretical analysis.

ACKNOWLEDGMENT

This work is supported and fund by the faculty of engineering, rajamangala university of technology Isan, khonkaen campus, khonkaen, Thailand.

REFERENCES

- [1] R. Sotner, J. Jenrabek, L. Langhammer, J. Polak, N. Herencsar, R. Prokop, J. Petrzela and W. Jaikla "Comparison of two solution of quadrature oscillator with linear control of frequency of oscillator employing modern commercially available devices," *Circuits Syst Signal Process.*, vol. 34, 2015, pp. 3449-3469.
- [2] F. Khateb, W. Jaikla, D. Kubanek and N. Khatib "Electronically tunable voltage-mode quadrature oscillator based on high performance CCCDBA," *Analog Integr Circ Sig Process.*, vol. 74, 2013, pp.499-505.
- [3] A. Jantakun "Current-mode quadrature oscillator using CCCCTAs with non-interactive current control for CO, FO and amplitude," *Journal of Microelectronics, Electronic Components and Materials*, vol. 45: 2015, pp. 47-56.
- [4] H. P. Chen, Y. S. Hwang and Y. T. Ku "Voltage-mode and current-mode resistorless third-order quadrature oscillator," *Applied Sciences*, vol. 179, 2017, pp. 3-18.
- [5] A. Jantakun "Voltage differencing transconductance amplifiers based mixed-mode quadrature oscillator," *Rev. Roum. Sci. Techn. Electrotechn. Et Energ.*, vol. 61, 2016, pp. 68-72.
- [6] Y. Li, C. Wang and S. Chen "Current-mode four-phase quadrature oscillator," *Rev. Roum. Sci. Techn. Electrotechn. Et Energ.*, vol. 60; 2015, pp. 293-301.
- [7] R. Sotner, J. Jenrabek, W. Jaikla, N. Herencsar, K. Vrba and T. Dostal "Novel oscillator based on voltage and current-gain adjusting used for control of oscillation frequency and oscillation condition," *Elektronika ir Elektrotechnika*, vol. 19, 2013, pp. 1392 – 1215.
- [8] J. Jin and C Wang "Current-mode universal filter and quadrature oscillator using CDTAs," *Turkish Journal of Electrical Engineering & Computer Sciences*, vol. 22, 2015, pp. 276-286.
- [9] S. Summart, C. Thongsopa and W. Jaikla "New current-controlled current-mode sinusoidal quadrature oscillator using CDTAs," *Int. J. Electron. Commun. (AEU)*, vol. 69, 2015, pp. 62-68.
- [10] R. Sotner, A. Lahiri, A. Kartci, N. Herencsar, J. Jenrabek and K. Vrba "Design of novel precise quadrature oscillator employing ECCIs with electronic control," *Advances in Electrical and Computer Engineering*, vol. 13, 2013, pp. 65-72.



- [11] S. Maheshwari "Voltage-mode four-phase sinusoidal generator and its useful extensions," *Active and Passive Electronic Components*, 2013, <http://dx.doi.org/10.1155/2013/685939>.
- [12] O. Channumsin and W. Tangsrirat "Sinusoidal quadrature oscillator using voltage differencing gain amplifiers (VDGAs)," *7th International Conference on Information Technology and Electrical Engineering (ICITEE)*, Chaingmai, Thailand, 2015, pp. 118-121.
- [13] S. Maheshwari and Verma R "Electronically Tunable sinusoidal oscillator circuit," *Active and Passive Electronic Components*, 2012. doi:10.1155/2012/719376
- [14] R. Sotner, J. Jenrabek, N. Herencsar, Z. Hrubos, T. Dostal and K. Vrba "Study of adjustable gain for control oscillation frequency and oscillation condition in 3R-2C oscillator," *Radioengineering*, vol. 21, 2012, pp. 392-402.
- [15] J. Jin "Current-mode resistorless SIMO universal filter and four-phase quadrature oscillator," *International Journal of Electrical, Electronic Science and Engineering*, vol. 7, 2013, pp. 96-101.
- [16] W. Tangsrirat "Dual-mode sinusoidal quadrature oscillator with single CCCTA and grounded capacitors," *Journal of Microelectronics, Electronic Components and Materials*, vol. 46, 2016, pp. 130-135.
- [17] N. Pandey and R. Pandey "Approach for third order quadrature oscillator realization," *IET Circuit, Devices & Systems*, vol. 9, 2015, pp. 161-171.
- [18] S. Summart, C. Thongsopa and W. Jaikla "CCCII-based sinusoidal quadrature oscillator with non-interactive control of condition and frequency," *Indian Journal of Pure & Applied Physics*, vol. 52, 2014, pp. 277-283.
- [19] R. Pandey, N. Pandey, G. Komanapalli and R. Anurag "OTRA based voltage mode third order quadrature oscillator," *ISRN Electronics*, 2014, <http://dx.doi.org/10.1155/2014/126471>
- [20] N. Herencsar, J. Konton, K. Vrba, A. Lahiri "New voltage-mode quadrature oscillator employing single DBTA and only grounded passive elements," *IEICE Electronics Express*, vol. 6, 2009, pp. 1708-1714.
- [21] J. Jin and C. Wang "Single CDTA-based current-mode quadrature oscillator," *Int. J. Electron. Commun. (AEU)*, vol. 66, 2012, pp. 933-936.
- [22] W. Tangsrirat and W. Tanjaroen "Current-mode sinusoidal quadrature oscillator with independent control of oscillation frequency and condition using CDTAs," *Indian J. Pure App. Phys.*, vol. 48, 2010; pp. 363-366.
- [23] J. Satansup and W. Tangsrirat "CMOS realization of voltage differencing gain amplifier (VDGA) and its application to biquad filter," *Indian J Eng Mater Sci.*, vol. 20, 2013. pp. 457- 464.
- [24] OPA860: Wide Bandwidth operational transconductance Amplifier (OTA) and buffer, Texas Instruments. www.ti.com/lit/ds/symlink/opa860.pdf
- [25] AD835: 250 MHz, voltage output 4-quadrant, analog devices http://www.analog.com/static/imported-files/data_sheets/AD835.pdf



Electrical Power Consumption Monitoring and Control of Appliances with IoT

Wanapun Waiyawut
Computer Engineering, Faculty of Engineering
Rajamangala University of Technology Phra Nakhon
Bangkok, Thailand
Wanapun.w@rmutp.ac.th

Abstract—Nowadays, we use the Internet widely, in our office, home and others. Also, we use with wireless via wifi system. Internet of things is developed to connect everything to the internet. With the cloud technology, we can share information with smart devices, desktop computers, smartphones anywhere, by connecting to the Internet. This paper is to design a smart system with the internet of things technology and embedded systems technology, small and cheap, which employ the integration of wifi. This system is embedded with the outlet. We monitor and control the use of electric devices through the Internet. With cloud technology, we can monitor and check the status of devices, on or off, power consumption. We can control the devices to turn on or off and control demand of power consumption by the limit value of current. If it is greater than the set value, it will be turned off. Overload power consumption may be due to defective of devices or short circuit problem. So we can control the devices turn on or off, power consumption monitoring and overload or short circuit protection.

Keywords—internet of things (IoT); ESP8266.

I. INTRODUCTION

Internet technology is a part of daily life, if we can control the appliances, in autonomous via an internet network, that we can control and monitor devices' status turn them on or off, anytime and anywhere. In this project was designed to take the technology, Internet of Thing, IoT, apply it with appliances in the home, to autonomous home. In everyday life, users can control appliances, check working status (power on-off status) and prevent them from the overload of the electrical appliances equipment, cause of a short circuit, which may cause the fire to ensure the safety of lives and property. The device has been implemented in real life, cooperative with program [1] work with a web browser in the smart devices, used in everyday life or can be applied to develop a mobile application that is used by another work. This project is divided into two parts:

A. Hardware

By using NodeMCU ESP8266 [6], be connected with internet, WIFI and Arduino UNO R3 board [7], and control relays' contact, which connects AC power lines with the outlets and read power load current via the current sensors,

which relative to the power consumption of the electrical devices connected from outlets.

B. Software

The second part of this project is software, which is used to develop applications such as programming on ESP8266, used by hardware modules and software that be used in order to connect with cloud database [5], and web development applications.

II. PROCEDURES

A. Working with nodeMCU ESP8266

NodeMCU ESP8266 is an open source IoT platform contains firmware that runs with the ESP8266, with WIFI module, SoC, from Espressif Systems [15] and hardware modules based on the ESP-12. [12] There is a module used to connect to the WIFI network, small size, 32 bits processor run with 80 MHz signal clock (default), memory 32 KiB for instructions, and 80 KiB for user data, 16 GPIO pins are available. 4 MiB external flash memory [13]. This module can run by itself (SoC), do not require other microcontroller board. Development software is used with Arduino board software, Arduino IDE, with package esp8266 added.

B. Working with Google Firebase

Google Firebases a service of Google [15], which provides both Web Database, Web Hosting, Web Authentication and Web Storage section. The used services are:

- 1) Firebase Real-time Database is NoSQL database, with Cloud computing service, to store information in the form of JSON and sync the data in real-time with all devices that connect automatically. It is supported with offline mode (stored data in the local will automatically sync). The database works with security rules, are designed to make the conditions of access to both read and write.
- 2) Firebase Hosting is a web hosting is available for free. But the caveat is that there is a file placed on



Firebase Hosting requires static files, used with the static web, cannot work with the web language such as PHP, Javascript or server-side script, but you can use the database with the Firebase service, Firebase real-time database.

- 3) Firebase Authentication. It is a service to manage the backend to register, sign-in, reset the password, be developed with an SDK from Android, IOS or Web Application. It supports the sign-in of a variety of forms, from a popular social network, from the Email and Password of the user or anonymous user.

C. LINE Notify

LINE Notify is a service of LINE [10]. This service channel can send a notification to various registered accounts through the API, which is called via HTTP POST. The limitations of LINE Notify, it is able to send notifications to those who request only, or the applicant users.

D. Web application

Web application [2], [3] is developed to allow the users use with simple application via Web Browser, which is used with smart devices (mobile phones or laptop computers) with the different screen size, (with responsive design), it can be adjusted its display size according to the condition of the device. And by using the ESP8266 module, it can work in the form of a Web Server by itself.

From block diagram, use data store in the real-time database, running on Firebase via the Internet and control appliances. This section is divided into two parts, the first part is used ESP8255 receive data Analog signal from Current sensors 4 and sending data over the Internet to keep on Firebase real-time database and displayed through a Web application. the second part is the control appliances via the 4 outlets with the command "on" or "off" in Firebase real-time database data. The commands' "on" or "off", a user can control through the Web application in order to control ESP8266, turn on or off with relay that connects to the outlet, and the electrical device.

2) Web Application Design

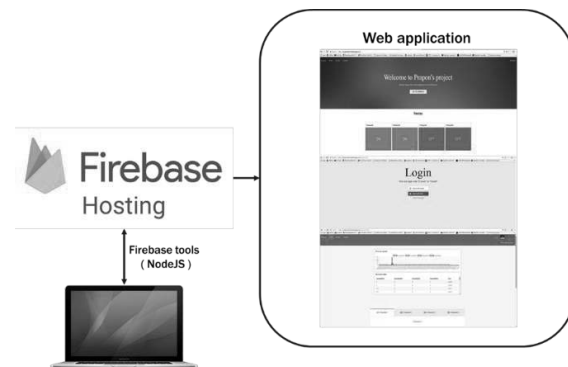


Fig. 2. Design, Web application

III. DESIGN AND TESTING

This section provides an overview of the system. Designed to collect data on FireBase circuit design and test control systems with electric bulb :

E. System Overview

1) System Overview

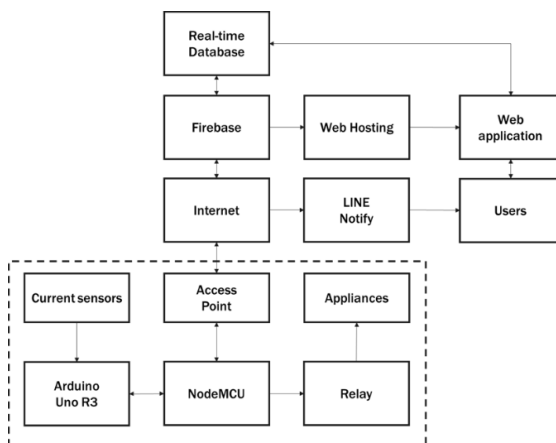


Fig. 1. Block Diagram of the system

Design Web application is divided into three parts: one is the front Homepage on this page, users can view the status of the socket and Channel 4 is the second part of the Login page to a page using, you can log in via Google account or Login Account provider E-mail the other part is the third Control page on the page, users can set the maximum allowable wattage power supplies available. View graphs and tables of statistics of electrical power connected. You can plug all 4 channels open or close immediately.

3) Circuit Design

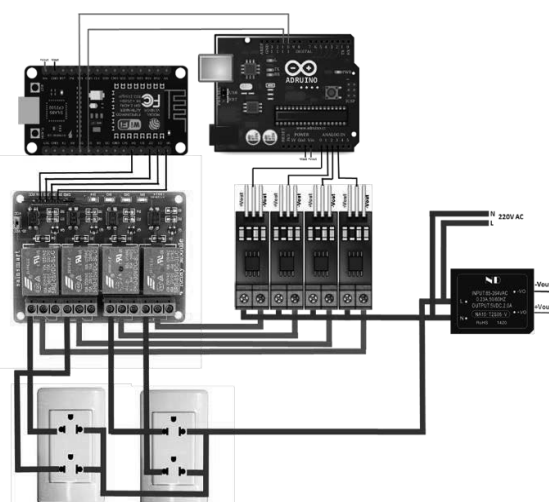


Fig. 3. Circuit design

NodeMCU will receive the consumed current data from the current sensors on Arduino board, input port channel A0-A3 (Analog), respectively, then sends out the data to the Digital port of the Arduino board via ESP8266 pin D10 and D11 by serial, next ESP8266 will read out the power and status of that channel from Firebase real-time database, to state of Relay will read all four values, which is the value of the Channel of the Relay. If the channel's status is on, the relay of that channel will turn on. In the other way, if it is off status, the relay turns the device off. But this status, turn on or off must depend on the condition, the value of the electric power or current does not exceed the value is set. If the excess will not be able to turn on power to that channel. In the same way, if it recovers that the power of the device is plugged into consuming more power than the set value, ESP8266 will turn the power of that channel's device to turn the power off.

4) Realtime Database



Fig. 4. Firebase data storage

Realtime Database is used for a convenience, use the cloud-hosted database with Google Firebase Realtime Database. System data is stored as JSON format, NoSQL cloud database, every time connected from the client, real-time data is synchronized. It can use cross-platform apps. Database instance will receive the update automatically. If the system offline, data still be in system disk or storage.

5) Results

Figure 5 is an experiment in open lamp Channel 1 can be seen that the tubes. the light But there is a delay in the order of 2-3 seconds.



Fig. 5. Turn on the lamp on channel 1

IV. CONCLUSION

The Electrical Power Consumption Monitoring and Control of Appliances with IoT system start the procedures with the concept, how to control and monitor power consumption of appliances, design the circuits, design the database format with a cloud framework, develop code to control and read appliance status, interface power circuit and control circuit. Design the system connect to the internet, design user interfaces with the Web application, to control and gather data to the real-time database, and then take action as designed. The final step is a tried and tested system. By using the Web application to turn on or off the appliances read power consumption from the data stored in a database, test limited of the set value. There are the problems with the delay time and quality of the internet.

ACKNOWLEDGMENTS

Thank Mr. Prapol Khong-Ausaha, assembles hardware circuit and software coding, thanks to the department of



computer engineering members, Faculty of Engineering and
Rajamangala University of Technology Phra Nakhon.

REFERENCES

- [1] Jerawat Warint, "Website development with modern HTML5 CSS3 + jQuery Unlimited Edition" Simplify Publishing House. Bangkok 2017.
- [2] Jerawat Warint, "CSS3 Web Design Unlimited Edition" Simplify Publishing House. Bangkok 2012.
- [3] Pracha Prukprasert, "Create web and add features with Java Script DHTML" Simplify Publishing House. Bangkok 2010.
- [4] Pracha Prukprasert, "Basic C Language for ARDUINO" AppSoftTech Co., Ltd. Bangkok 2017.
- [5] Firebase. To query information materials (online). Access from. <https://firebase.google.com/official/site> (December 14, 2558).
- [6] ESP8266 Serial-to-WiFi module For IoT Jobs. <http://cpre.kmutnb.ac.th/esl/learning/index.php?article=esp8266-modules>. (January 2, 2016).
- [7] Example of Arduino-Relay-Module. <https://www.thaieasyelec.com/article-wiki/review-product-article>. (January 9, 2016).
- [8] AC Power Meter with current sensor IC, ACS712 / ACS714. <http://cpre.kmutnb.ac.th/esl/learning/index.php?article=acs71x-current-sensor>. (January 9, 2016).
- [9] Arduino UNO R3 Microcontroller sheet lab 9. <http://www.ce.kmitl.ac.th>. (January 17, 2016).
- [10] Line Notify. <https://notify-bot.line.me/en/> (February 8, 2016).
- [11] Development of tracking and notification systems for intelligent homes using Internet of thing technology. <http://iotsmarthome.azurewebsites.net/pdf/chapter1.pdf> (February 8, 2016).
- [12] NodeMCU Wiki. <https://en.wikipedia.org/wiki/NodeMCU>. (May 1, 2018).
- [13] ESP2086 Wiki. <https://en.wikipedia.org/wiki/ESP8266>. (May 1, 2018).
- [14] Arduino ide. <https://www.arduino.cc/en/Main/Software>. (May 1, 2018).
- [15] Espressif Systems (Shanghai) Pte., Ltd. <https://www.espressif.com/> (May 1, 2018).



A Circularly Polarized Loop Antenna with Reflector for RFID Handheld Reader

Kittima Lertsakwimarn

Faculty of Industrial Technology and Management,
King Mongkut's University of Technology North Bangkok,
Prachinburi Campus, Prachinburi 25230, Thailand
e-mail: kittima.l@fitm.kmutnb.ac.th

Chuwong Phongcharoenpanich

Faculty of Engineering, King Mongkut's Institute of
Technology Ladkrabang, Bangkok 10520, Thailand
e-mail: pchuwong@gmail.com

Abstract— This paper presents a circularly polarized loop antenna with reflector for UHF RFID handheld reader. A circularly polarized loop antenna with reflector is achieved by using a phase difference excitation of two port probe feeds. It is found that the return loss at port 1 and 2 of antenna design are less than -10 dB and the axial ratio is less than 3 dB along operating frequency. It can be operated in UHF RFID system for Thailand from 920-925 MHz. The radiation gain along operating frequency is better than 6 dBic. The axial ratio at center frequency (922.5 MHz) is about 1.2 dB. The overall size of the proposed antenna is 90×100×25 mm³. Therefore, the proposed circularly polarized loop antenna with reflector can be used for a handheld UHF RFID readers.

Keywords—Circular polarization(CP);UHF RFID; Loop antenna

I. INTRODUCTION

Radio frequency identification (RFID) systems in the ultra-high frequency (UHF) band have gained much interest in several service industries, purchasing and distribution logistics, manufacturing companies and goods flow systems [1]. The UHF band has been authorized for RFID applications depending on countries and regions such as 865-868 MHz in Europe, 902-928 MHz in North and South Americas, 950-956 MHz in Japan and some Asian countries whereas 920-925 MHz band is used in Thailand. RFID system consists of the reader and the tag. The reader can be a read device that uses an antenna which sends a radio frequency signal to a tag.

For the applications involving item-level management, a RFID handheld reader plays an important role owing to its advantages of compactness, flexibility, and maneuverability. Circularly polarized (CP) operation is one of the requirement for RFID handheld reader. Because it can reduce the loss caused by the multipath effects between the reader and the tag antenna. A CP antenna with a low profile, small size, and light weight is required in a handheld RFID reader. Most of antennas have circular polarization, but its size is big for handheld reader.

A typical technique for producing circular polarization is to excite two orthogonal linearly polarized modes (horizontally and vertically polarized radiation pattern) with a 90° phase difference. In recent years, there are many types of designed antenna produced for handheld RFID reader such as helical antenna [2], loop antenna [3], PIFA antenna [4] and monopole antenna [5]. In order to achieve the CP radiation pattern, a loop antenna is a suitable choice. The small loop antenna has a uniform current distribution and can act as a magnetic dipole to achieve the horizontally polarized radiation pattern. Several kinds of modified Alford loop-structure antennas [6]–[7] have been studied and introduced as a useful design for generating magnetic dipole radiation patterns. However, the most these designs are linearly polarization.

This paper proposed circularly polarized loop antenna with reflector for UHF RFID handheld reader which is feeding by phase difference technique. The antenna configuration is given in Section 2. Section 3 presents the simulated and measured of the proposed antenna results. Finally, conclusion is discussed in Section 5.

II. ANTENNA DESIGN AND PARAMETER ANALYSIS

A. Antenna structure

The configuration of the proposed antenna is shown in Fig.1. The proposed antenna comprises of dual copper rectangular loops and a reflector. The three elements are arranged in the form of stacked each other. The proposed antenna has dual fed by a perpendicular feeding portion. The feeding points are installing at middle of each loops with balance feeding like a folded dipole antenna. The signals at the feeding points between port 1 and port 2 are equal magnitude and 135-degree phase difference. The air interval between loop 1 (inter loop) to loop 2 (outer loop) and reflector are 20 mm and 10 mm respectively. The length of width of two loops are designed to operate at a center frequency of UHF band of 922.5 MHz (corresponding to a free-space wavelength of $\lambda_0=320$ mm). The size of reflector is chosen as the same size with the outer loop of size 90 x 100 mm². The dimensions of the proposed antenna are shown in Table 1.

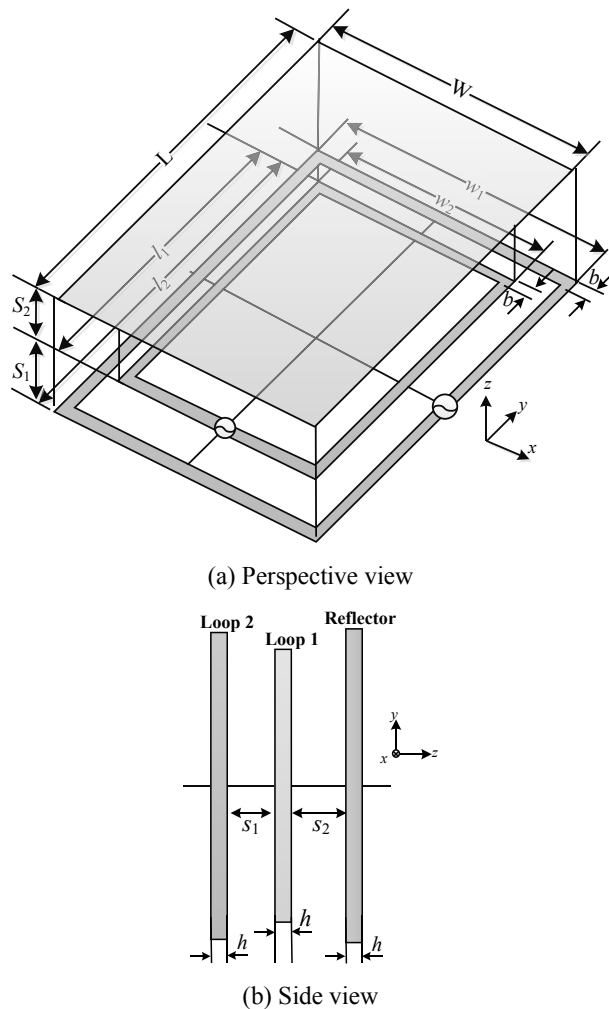
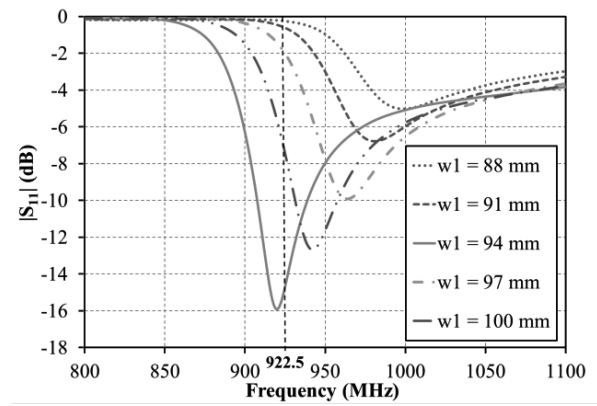


Fig.1 Geometry of the proposed antenna.

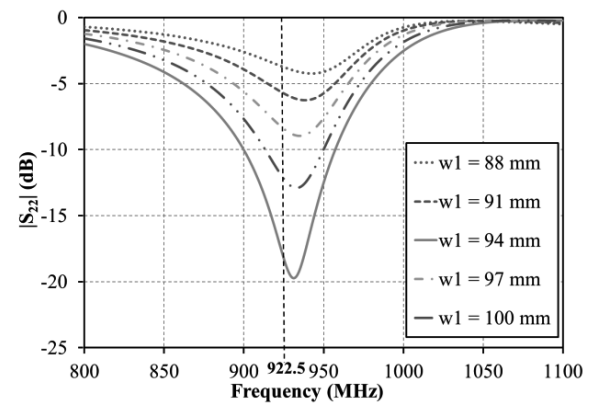
B. Parameters analysis

To verify the properties of the design, several vital parameters of the proposed antenna are analyzed in details. The proposed antenna is stated with single loop that can be obtain linearly polarization. To generated circularly polarized, another loop has been adding by stacked form.

First, the length of loop perimeter in x-and y-axis have been studies. Figure 2 shows the simulated S-parameter of the proposed antenna with different w_1 (length of the loop in x-axis). With reference to the figure, the resonant frequency are shifts to lower frequency with an increase in w_1 from 88 to 100 mm as shown in Figure 2(a). The simulated gain and AR in the boresight direction ($\phi=90^\circ$, $\theta=0^\circ$) with different w_1 at 922.5 MHz are shown in Fig.3. It can see that the length of loop perimeter in x-axis is effect to Gain and AR.



(a) port 1



(b) port 2

Fig.2 Simulated S-parameters against frequency with various parameter w_1 .

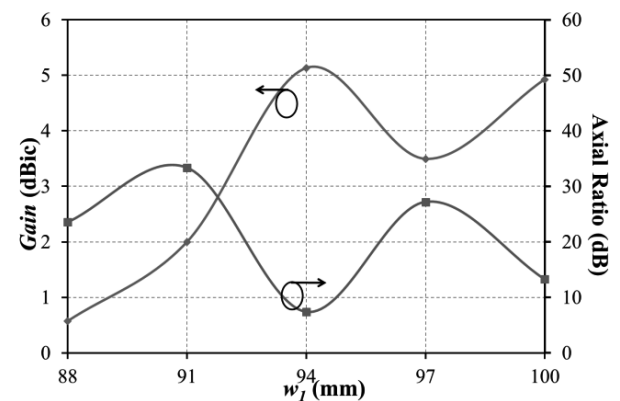


Fig.3 Simulated Gain and AR against parameter w_1 at 922.5 MHz in the boresight direction ($\phi=90^\circ$, $\theta=0^\circ$).

Next, the effect of l_1 (length of the loop in y-axis) on gain and AR at 922.5 MHz are illustrated in Fig.4. With the increase of l_1 , Gain is slightly change and AR is gradually increased. the parameter l_1 should be chosen as 87 mm for this design. Finally, the other parameters are optimized. The dimensions of the proposed antenna are shown in Table 1.

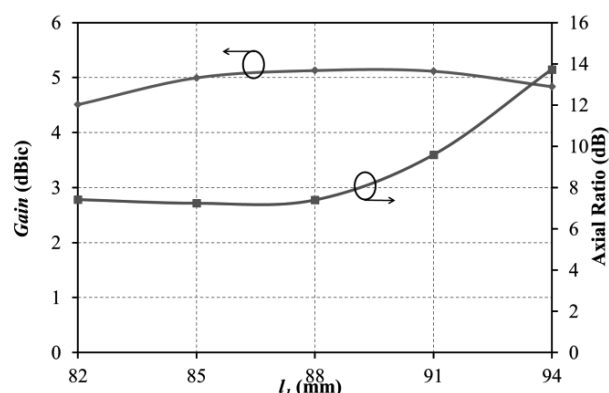


Fig.4 Simulated Gain and AR against parameter l_1 at 922.5 MHz in the boresight direction ($\phi=90^\circ$, $\theta=0^\circ$).

TABLE I. The Structural parameter of the proposed antenna

Parameter	W	L	l_1	l_2	w_1	w_2	b	s_1	s_2	h
Size in mm	90	100	87	79	98	78.5	5	20	10	0.5

III. ANTENNA RESULTS

In this section the simulated results are compared with the experimental ones. The experimental results were carried out based-on the prototype antenna with the optimization parameters in Table 1 as shown in Fig. 5. Figure 6 shown the anechoic chamber setup for measurement the antenna characteristics. The S-parameter characteristics are depicted in Fig. 7. It is seen that the simulated and measured $|S_{11}|$ and $|S_{22}|$ results are in good agreement. The simulated and measured -10-dB $|S_{11}|$ and $|S_{22}|$ bands can cover the UHF RFID band (920-925 MHz).

The simulated radiation patterns at 922.5 MHz are shown in Fig. 8 in the xz-and yz- planes. The radiation patterns of LHCP has been normalized by the simulated peak gain of RHCP (Co-polarization). The simulated gains are more than 6 dBic along UHF RFID band.

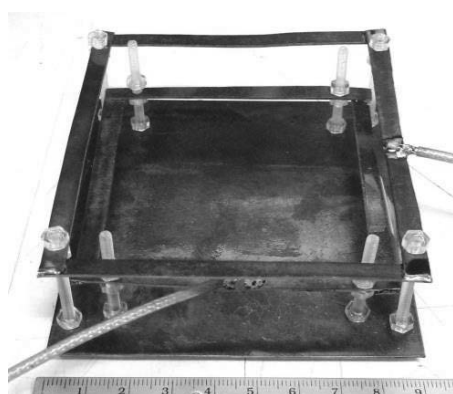


Fig. 5 Photo of the antenna prototype.

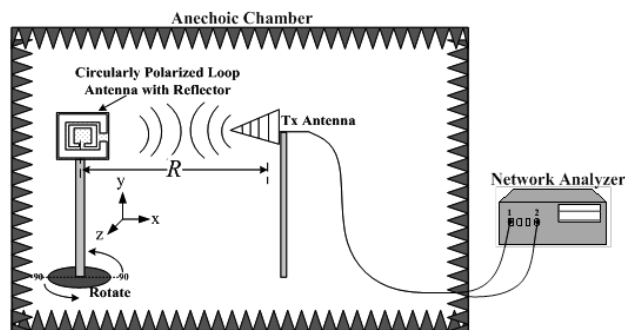
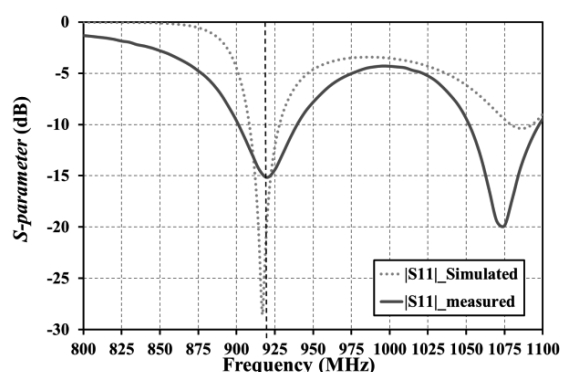
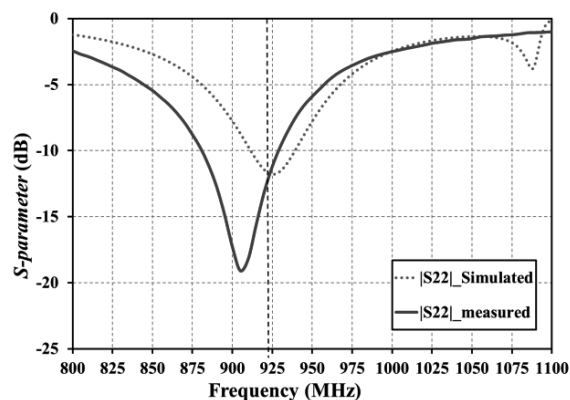


Fig.6 Anechoic chamber setup

The simulated 3-dB axial ratio bandwidth can cover the interesting frequency band (920-925 MHz). The simulated and measured axial ratio pattern of the proposed antenna in xz-and yz-planes at 922.5 MHz are shown in Fig.9.



(a) at port 1



(b) at port 2

Fig. 7 The simulated and measured S-parameter characteristics.



It can see that AR is less than 3 dB at the boresight direction for the simulation result. The angle range (3-dB AR angle) in the radiation patterns where the XPD (cross-polarization discrimination) is more than 15 dB are approximately 60-degree and 100-degree in yz-and xz-planes, respectively. However, there is a lot of difference between simulated and measured results. The difference may be caused by the fabrication error and the feed coaxial cable.

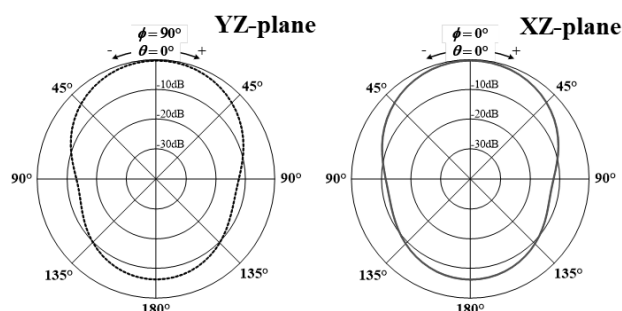
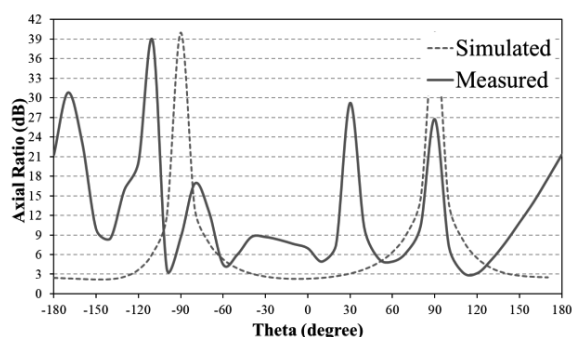
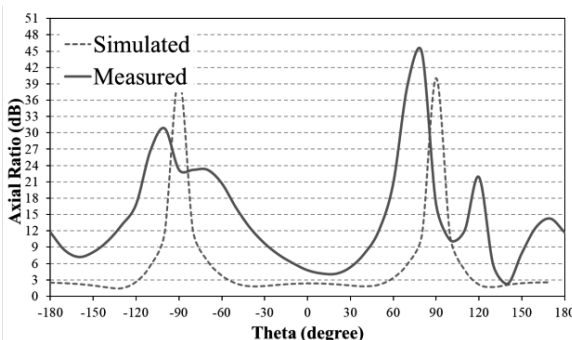


Fig. 8 The simulated normalized radiation patterns of the proposed antenna at 922.5 MHz in xz-and yz-planes.



(a) yz-planes



(b) xz-planes

Fig. 9 The simulated and measured Axial Ratio of the proposed antenna at 922.5 MHz.

IV. CONCLUSIONS

This paper presents a UHF RFID circularly-polarized reader antenna with dual loop structure and reflector. Dual feeds on dual loops with equal magnitude and 135-degree phase difference signal are used to achieve the circularly polarized characteristic. The impedance and AR bandwidth of proposed antenna are covers the frequency range of UHF RFID band in Thailand (920-925 MHz). The proposed antenna has a good radiation performance with gain more than 6 dBic. The axial ratio at center frequency (922.5 MHz) is about 1.2 dB. The overall size of the proposed antenna is 90×100×25 mm³. Therefore, the proposed antenna is suitable for use in handheld/portable UHF RFID readers.

REFERENCES

- [1] L. Ukkonen, L. Sydanheimo and M. Kivikoski, "Reader range performance comparison of compact reader antennas for handheld UHF RFID reader," IEEE International conference on RFID, pp. 63-70, 2007.
- [2] S. H. Zauind-Deen, H. A. Malhar, and K. H. Awadalla "Octafilar helical antenna for handheld UHF RFID reader," National radio science conference (NRSC), 2011 28th National , pp.1,8, 26- 28 April 2011.
- [3] M.-J. Chang and H.-M. Chen, "Compact near-field folded-loop antenna for UHF RFID handheld reader," Proceedings of ISAP 2014, Number WE3A_08, December 2014.
- [4] M.-G. Huang, Z.M. Xie, and X.-Z. Lai, "A compact multiband PIFA for handheld RFID applications," Microwave and optical technology letters, vol.58, no.8, August 2016.
- [5] S.-Y. Lin, Y.C. Lin, and M.-H. Chen, "Monopole antenna with circular polarization for handheld RFID," Proceedings of APMC 2012, Number 4C5-01, December 2012.
- [6] H. R. Chuang, "Omni-directional horizontally polarized alford loop strip antenna," U.S. Patent 5,767,809, Jun. 16, 1998.
- [7] C. C. Lin, L. C. Kuo, and H. R. Chuang, "A horizontally polarized omnidirectional printed antenna for WLAN applications," IEEE Transaction antennas propagations, vol. 54, no. 11, pt. 2, pp. 3551–3556, Nov. 20



MISO Current-mode Universal Biquadratic Filter Using VDCC

Pukanit Thuibuengchim

Department of Electrical Engineering, Faculty of
Engineering, Rajamangala University of
Technology Isan Khon Kaen Campus,
Khonkaen, Thailand.
e-mail pukanit15@gmail.com

Saweth Hongprasit

Department of Computer Engineering,
Faculty of Engineering, Rajamangala University of
Technology Isan Khon Kaen Campus,
Khonkaen, Thailand.
e-mail saweth12@gmail.com

Abstract— This paper presents a Multiple Input Single Output (MISO) Current-mode Universal Biquadratic Filter, based on Voltage Differencing Current Conveyor (VDCC). The proposed circuit consists of VDCCs, two grounded capacitors and one grounded resistor which can be controlled to operate as a low-pass (LP), high-pass (HP), band-pass (BP), band-reject (BR) and all-pass (AP) filters, the output signal is controlled by defining input signals. Theoretical analysis of the proposed circuit is verified by PSPICE simulation results.

Keywords—VDCC; current-mode; universal biquadratic filters;

I. INTRODUCTION

An analog filter is an important in electronic engineering and widely used in various parts of electronic control systems such as communications, measurement and control systems [1]. A current mode active building blocks have several advantages such as dynamic range, wide bandwidth and low power consumption [2]. The design of current-mode active filters using current-mode active building blocks have become quite popular for a wide variety of applications.

Voltage differencing current conveyor (VDCC) is one of active building blocks which have been recently introduced in [3]. VDCC is very suitable for the electronic circuit design such as active filters, oscillators and amplifier, the transconductance gain of VDCC is electronically tunable while simultaneously transferring both voltage and current in its respective terminals[4].

Universal biquadratic filter is one of most popular analog filter circuit which provides several functions (low-pass filter, high-pass filter, band-pass filter, band- reject filter and all-pass filter). Because of the several advantages of VDCC properties such as low input impedance and high output impedance [5]. From literature survey, it is found that several implementations of current-mode universal biquadratic filters using CCCII [1], CCTA [2], VDCC [4, 6], CCCTA [7, 8], CCDDCCTA [9], CCII [10], CCIII [11], CDBA [12], CDTA [13], CFDA [14, 15], DVCC [16], FDCCII [17], VDTA [18]. Unfortunately, these reported circuits suffer the following disadvantages such as a circuits cannot be electronically controlled, the quality factor and pole frequency cannot be independently adjusted,

employed various active elements, used the floating passive elements and provided completely standard functions.

Therefore, this paper is to propose a current-mode universal biquadratic filter. Features of the proposed circuit are that, the quality factor and pole frequency can be independently adjusted with electronic method, the circuit using two VDCC and grounded passive elements, the proposed of circuit can be configured to work as a low-pass, high-pass, band-pass, band-reject and all-pass filter.

II. CIRCUIT DESCRIPTION

A. Voltage Differencing Current Conveyor (VDCC)

The symbol and internal structure of the active element VDCC is shown in Fig. 1, where P and N are input terminals and Z, X, WP and WN are output terminals. All the terminals exhibit high impedance, except the X terminal [4].

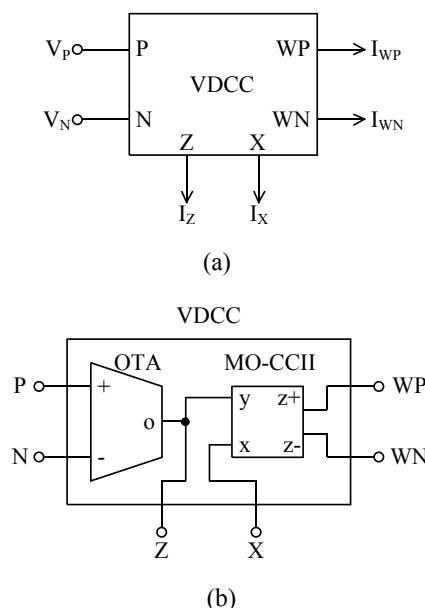


Fig. 1. (a) Symbol and (b) internal structure of the VDCC.



The current voltage relationship of different terminals of VDCC can be described by following hybrid matrix:

$$\begin{bmatrix} I_P \\ I_N \\ I_{Z,ZC} \\ V_X \\ I_{WP} \\ I_{WN} \end{bmatrix} = \begin{bmatrix} 0 & 0 & 0 & 0 \\ 0 & 0 & 0 & 0 \\ g_m & -g_m & 0 & 0 \\ 0 & 0 & 1 & 0 \\ 0 & 0 & 0 & 1 \\ 0 & 0 & 0 & -1 \end{bmatrix} \begin{bmatrix} V_P \\ V_N \\ V_Z \\ I_X \end{bmatrix} \quad (1)$$

The g_m is transconductance gain of VDCC which can be defined by:

$$g_m = \frac{I_B}{2V_T} \quad (2)$$

Where V_T is the thermal voltage.

I_B is bias current.

B. Proposed Circuit

The proposed current-mode universal biquadratic filter circuit is shown in Fig. 2, consists of two VDCCs, two grounded capacitors and two resistors. The characteristic equation of the proposed circuit can be written as in Eq. (3).

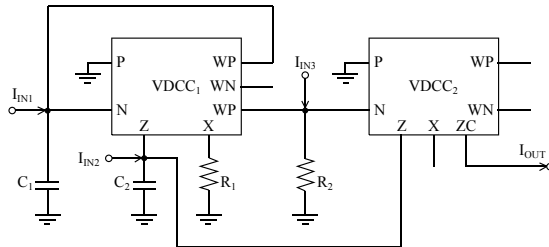


Fig. 2. The proposed current-mode universal biquadratic filter.

$$I_{OUT} = \frac{-R_2 g_{m2} \left[\left(s^2 + \frac{g_{m1}}{C_1 C_2 R_1} \right) I_{IN3} + s \frac{1}{C_2 R_1} I_{IN2} - \frac{g_{m1}}{C_1 C_2 R_1} I_{IN1} \right]}{s^2 + s R_2 g_{m2} \frac{1}{C_2 R_1} + \frac{g_{m1}}{C_1 C_2 R_1}} \quad (3)$$

From Eq. (3), the input currents I_{IN1} , I_{IN2} and I_{IN3} can be chosen to define five standard filtering responses as follows:

- The low-pass response: $I_{IN1} = I_{IN}, I_{IN2} = I_{IN3} = 0$
- The high-pass response: $I_{IN1} = I_{IN3} = I_{IN}, I_{IN2} = 0$
- The band-pass response: $I_{IN2} = I_{IN}, I_{IN1} = I_{IN3} = 0$

- The band-reject response: $I_{IN3} = I_{IN}, I_{IN1} = I_{IN2} = 0$

- The all-pass response: $I_{IN2} = -I_{IN}, I_{IN3} = I_{IN}, I_{IN1} = 0$

The pole frequency (ω_o) and quality factor (Q) can be expressed to be

$$\omega_o = \sqrt{\frac{g_{m1}}{C_1 C_2 R_1}} = \sqrt{\frac{I_{B1}}{2V_T C_1 C_2 R_1}} \quad (4)$$

and

$$Q = \frac{1}{R_2 g_{m2}} \sqrt{\frac{C_2 R_1 g_{m1}}{C_1}} = \frac{2V_T}{R_2 I_{B2}} \sqrt{\frac{C_2 R_1 I_{B1}}{2C_1 V_T}} \quad (5)$$

C. Non-Ideal Analysis

In the non-ideal case, the VDCC can be characterized by the following hybrid matrix [19]:

$$\begin{bmatrix} I_P \\ I_N \\ I_{Z,ZC} \\ V_X \\ I_{WP} \\ I_{WN} \end{bmatrix} = \begin{bmatrix} 0 & 0 & 0 & 0 \\ 0 & 0 & 0 & 0 \\ \gamma g_m & -\gamma g_m & 0 & 0 \\ 0 & 0 & \beta & 0 \\ 0 & 0 & 0 & \alpha \\ 0 & 0 & 0 & -\alpha \end{bmatrix} \begin{bmatrix} V_P \\ V_N \\ V_Z \\ I_X \end{bmatrix} \quad (6)$$

The parameters α , β and γ are the voltage/current transfer which is deviating from one, depending on the value of intrinsic impedances and temperatures. Considering this fact and make it possible in practice, these deviations are very small and can be ignored in theory. In non-ideal case the current transferring functions from Eq. (3) become

$$I_{OUT} = \frac{-\gamma_2 R_2 g_{m2} \left[\left(s^2 + \frac{\alpha_1 \beta_1 \gamma_1 g_{m1}}{C_1 C_2 R_1} \right) I_{IN3} + s \frac{\alpha_1 \beta_1}{C_2 R_1} I_{IN2} - \frac{\alpha_1 \beta_1 \gamma_1 g_{m1}}{C_1 C_2 R_1} I_{IN1} \right]}{s^2 + s \gamma_2 R_2 g_{m2} \frac{\alpha_1 \beta_1}{C_2 R_1} + \frac{\alpha_1 \beta_1 \gamma_1 g_{m1}}{C_1 C_2 R_1}} \quad (7)$$

In this case, the ω_o and Q are changed to

$$\omega_o = \sqrt{\frac{\alpha_1 \beta_1 \gamma_1 g_{m1}}{C_1 C_2 R_1}} = \sqrt{\frac{\alpha_1 \beta_1 \gamma_1 I_{B1}}{2C_1 C_2 R_1 V_T}} \quad (8)$$

$$Q = \frac{1}{\gamma_2 R_2 g_{m2}} \sqrt{\frac{\gamma_1 C_2 R_1 g_{m1}}{\alpha_1 \beta_1 C_1}} = \frac{2V_T}{\gamma_2 R_2 I_{B2}} \sqrt{\frac{\gamma_1 C_2 R_1 I_{B1}}{2\alpha_1 \beta_1 C_1 V_T}} \quad (9)$$



D. Sensitivity Analysis

The active and passive sensitivities of the proposed circuit are as

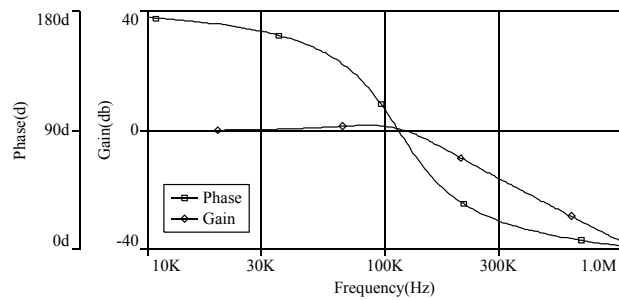
$$S_{\alpha_1, \beta_1, \gamma_1, g_{m1}}^{a_o} = \frac{1}{2}, S_{C_1, C_2, R_1}^{a_o} = -\frac{1}{2} \quad (10)$$

and

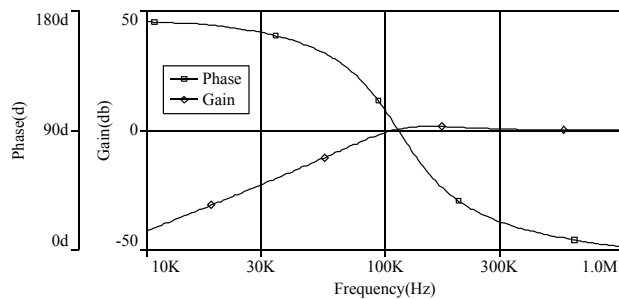
$$S_{\gamma_1, C_2, R_1, g_{m1}}^Q = \frac{1}{2}, S_{\alpha_1, \beta_1, C_1}^Q = -\frac{1}{2}, S_{\gamma_2, R_2, g_{m2}}^Q = -1 \quad (11)$$

III. SIMULATION RESULTS

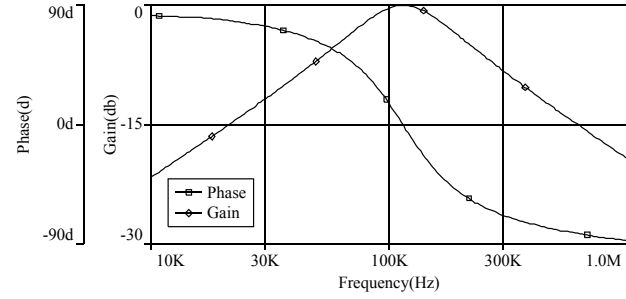
To verify the qualifications and performance of the proposed current-mode universal biquadratic filter in Fig. 2, the VDCC is implemented by using commercially available AD844 and LM13600N [20]. The circuit was designed for $Q=1$ and $f_o = \omega_o/2\pi = 120.57$ KHz, the supply voltages of circuit are $V_{DD} = -V_{SS} = 5V$, $I_{B1} = I_{B2} = 130\mu A$, $C_1 = C_2 = 3.3nF$, and $R_1 = R_2 = 400\Omega$. Fig. 3. shows the simulated phase and gain responses of the low-pass, high-pass, band-pass, band-reject and all-pass at pole frequency 114.82 KHz which consistent with the theoretical analysis. Fig. 4. shows the magnitude responses of BP function for different values of I_{B2} , by keeping $I_{B1} = 130\mu A$, $C_1 = C_2 = 3.3nF$, and $R_1 = R_2 = 400\Omega$. The quality factor can be adjusted to vary from 2.0, 1.0 and 0.5, by keeping constant pole frequency as 114.82 KHz for three values of I_{B2} as $65\mu A$, $130\mu A$ and $260\mu A$, respectively, which is shown the quality factor in the BP response.



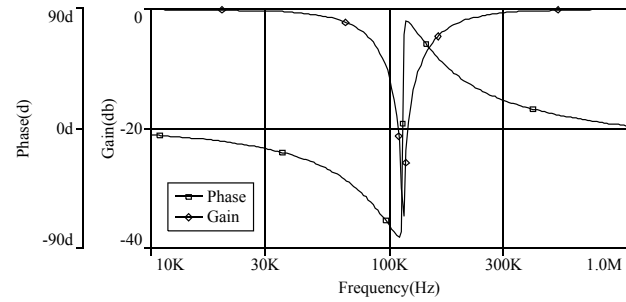
(a)



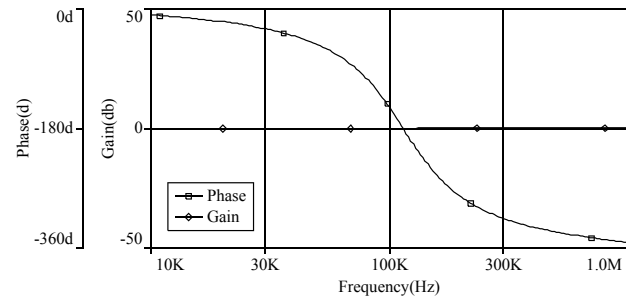
(b)



(c)



(d)



(e)

Fig. 3. Gain responses of the proposed circuit (a) low-pass, (b) high-pass, (c) band-pass, (d) band-reject and (e) all-pass.

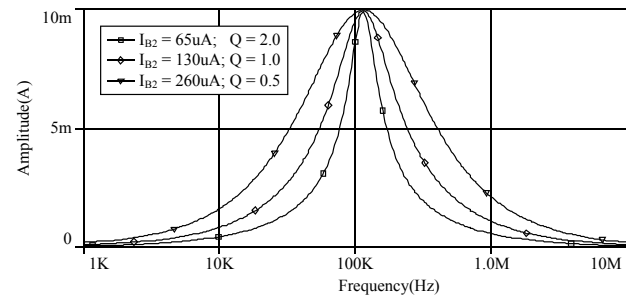


Fig. 4. Band Pass responses for different value of I_{B2} .



IV. CONCLUSION

The current-mode universal biquadratic filter employing two VDCCs, two grounded capacitors and two grounded resistors is presented. The advantages of the proposed circuit are: the pole frequency and quality factor of circuit can be independently and electronically adjustable, the proposed filter circuit can be performed by multiple functions: low-pass, high-pass, band-pass, band-reject and all-pass filter. The results of PSPICE simulation are consistent with the theory analysis.

ACKNOWLEDGMENT

This work was supported by the Faculty of Engineering Rajamangala University of Technology Isan, Khonkaen Campus.

REFERENCES

- [1] T. Tsukutani, Y. Sumi and N. Yabuki, "Electrically tunable CCCII-based current-mode biquadratic circuit," Industrial Electronics & Applications (ISIEA), Malaysia, 2014, pp. 97-100.
- [2] S. V. Singh, R. S. Tomar, and D. S. Chauhan, "Single MCCTA based single input three output electronically tunable current-mode Active-C biquad filter," Signal Processing and Communication (ICSC), India, 2015, pp. 267-272.
- [3] D. Biolek, R. Senani, V. Biolkova and Z. Kolka, "Active Elements for Analog Signal Processing: Classification, Review and New Proposals," Radioengineering, vol. 17, no. 4, 2008, pp. 15-32.
- [4] D. Prasad, A. Ahmad and A. Shukla, "Novel VDCC based low-pass and high-pass Ladder filters," India Conference (INDICON), India, 2015.
- [5] S. V. Singh, G. Gupta, R. Chhabra, K. Nagpal, Devansh, "Universal Current-Controlled Current-Mode Biquad Filter Employing MOCCCTAs and Grounded Capacitors," Circuits and Systems, vol. 1, pp. 35-40, 2010.
- [6] P. Lamun, P. Phatsomsiri and U. Torteanchai, "Single VDCC-based Current-mode Universal Biquadratic Filter," Information Technology and Electrical Engineering (ICITEE), Thailand, 2015, pp. 122-125.
- [7] J. Budboonchu and W. Tangsrirat, "Single-Input Three-Output Current-Mode Multifunction Filter Using Single CCCTA," Electrical Engineering/Electronics, Computer, Telecommunications and Information Technology (ECTI-CON), Thailand, 2017, pp. 242-245.
- [8] J. Budboonchu and W. Tangsrirat, "Three-input single-output current-mode universal filter using single CCCTA," Information Technology and Electrical Engineering (ICITEE), Thailand, 2017.
- [9] A. K. Kushwaha and S. K. Paul, "Current Mode Biquadratic Universal Filter," Microelectronics and Electronics (PrimeAsia), India, 2015, pp. 42-46.
- [10] T. Ettaghzouti, N. Hassen, K. Besbes, "SIMO type mixed mode biquadratic filter using second generation current conveyor circuits," Sciences of Electronics, Technologies of Information and Telecommunications (SETIT), 2016, pp. 539-543.
- [11] T. S. Arora and R. K. Sharma, "Realization of current mode KHN-equivalent biquad employing third generation current conveyor," Computational Techniques in Information and Communication Technologies (ICCTICT), India, 2016, pp. 558-562.
- [12] U. Rana, S. Suyal and T. S. Arora, "Single Input Multiple Output multifunction filter employing current differencing buffered amplifier," Computational Techniques in Information and Communication Technologies (ICCTICT), India, 2016, pp. 586-590.
- [13] M. Kumngern and A. Chaichana, "MIMO-type current-mode multifunction biquadratic filter using a MCDTA," Communications (APCC), Indonesia, 2013, pp. 54-57.
- [14] S. V. Singh, R. S. Tomar and D. S. Chauhan, "Current tunable current-mode TISO biquad filter consisting of two MCFTAs and minimum number of grounded capacitors," Signal Processing and Integrated Networks (SPIN), India, 2014, pp. 555-560.
- [15] A. Malcher, "Resistorless universal biquad filter based on digitally programmable current follower transconductance amplifier," Mixed Design of Integrated Circuits and Systems, Poland, 2017, pp. 416-421.
- [16] T. Tsukutani and N. Yabuki, "A multiple-mode biquadratic circuit employing only plus type DVCCs," International Conference on Electronics, Information, and Communication (ICEIC), 2018, pp. 215-218.
- [17] U. Torteanchai and M. Kumngern, "Three-input single-output current-mode universal filter using a single FDCCII and grounded passive components," Intelligent Signal Processing and Communication Systems (ISPACS), Malaysia, 2014, pp. 275-278.
- [18] C. Shankar, S. V. Singh, A. K. Verma and R. Sharma, "Three input single output current mode biquad filter using single VDTA," India, 2016, pp. 386-391.
- [19] S. Summart, C. Saetiauw, C. Thongsopa and W. Jaikla, "CCTA Based Current-mode First Order Filter and Its Application in Quadrature Oscillator," Przegląd Elektrotechniczny, 2013, pp. 104-108.
- [20] M. Srivastava and D. Prasad, "VDCC Based Dual-Mode Quadrature Sinusoidal Oscillator with Outputs at Appropriate Impedance Levels," Advances in Electrical and Electronic Engineering, 2016, pp. 168-177.



Development of School Bus Passenger Notification System Using RFID and Arduino Module

Therdpong Daengsi
Dept. of Sustainable Industrial Management Engineer
Faculty of Engineering
Rajamangala University of Technology Phra Nakhon
Bangkok, Thailand
therdpong1@gmail.com

Praveen Maiget
Office of Student Loan Fund
Siam Technology College
Bangkok, Thailand
maiget02@hotmail.com

Pongpisit Wuttidittachotti
Dept. of Data Communication and Networking
Faculty of Information Technology
King Mongkut's University of Technology North Bangkok
Bangkok, Thailand
Pongpisit.w@it.kmutnb.ac.th

Abstract—This paper presents the system and application to notify about taking a school bus of primary school students. This system aims to prevent the students from being left on the bus as well as increasing the trust from their parents. The system uses Arduino module and Radio Frequency Identification (RFID) tag to record data. The students will have student cards that identify themselves when getting on and off the bus, while the school bus will have card reader to record the data from student cards. Then, the recorded data will be sent to the server via Internet as well as through the application in almost real-time. The updated status about students will show on mobile phones of teachers and parents via the Android based application. For the performance of this system, the accuracy of the part of card reader is about 93 %, while the accuracy of the mobile application is 100 %.

Keywords—*Arduino; Android; RFID; IoT; school bus*

I. INTRODUCTION

Almost every year, there was at least one case about leaving children (without intention) in vehicles (e.g., cars, vans or school bus) [1-3]. In every case, children eventually die. For example, the case of a girl in Samut Prakan Province that was left in a van and then she died. Solutions for such case are required, therefore, the development of school bus passenger notification system has been proposed. This project has been conducted based on the Internet of Things (IoT) concept, using RFID tag and the Arduino UNO WiFi board.

For the structure of this paper, it has been organized into five sections. After this section, Introduction, previous studies and background information are presented in Section II, including previous systems from other developers/researchers, and RFID, the Arduino module. Section III covers system and application development. Section IV is about performance

evaluation. Lastly, discussion, conclusion and future work are presented in Section V.

II. RELATED PREVIOUS WORK AND BACKGROUND

A. Related previous work

For related previous work, there are several systems. However, focusing on systems or projects related with the case of forgetting or leaving children in vehicles. It has been found few projects as follows:

1) The sensor system that can detect children or pets in vehicles was proposed by Lampang Technical College [4]. After detecting a sign of kid or a pet the alarm will be activated, the door will be opened and then the Short Message Service (SMS) will be sent to 5 mobile phone numbers that have been provided previously.

2) The controller that can detect the quantity of carbon dioxide in vehicles if it is higher than 1,000 ppm was proposed by Nakhon Pathom Technical College [4]. After detecting the high quantity of carbon dioxide, the alarm and the siren light will be activated. Then the fan will be turned on. Finally, the door glasses will be opened.

3) One interesting work that studied about the monitoring alarm and prevents children from being left on parked vehicle was presented last year (2017) [5]. The comparative study to compare among RFID, photo sensor, and passive infrared (PIR) sensor was conducted. After studying and evaluating, it has been found that RFID and PIR sensor provide better performance than photo sensor, while PIR sensor is better than RFID when considered about usage. Arduino board has been



applied to this work as well. Besides, this system can make calls to alert on a specific mobile phone number.

After surveying on similar systems above, only the last research work [5] that is similar to this work. However, there is a gap to propose an advanced solution beyond that work still. For example, proposing notification application that can be used on mobile phones.

B. RFID overview [6-9]

It can be stated that RFID is a part of IoT in this era [6]. In general, RFID systems mainly consist of tags and readers (see Fig. 1) [7-9]. RFID tags are attached to the item being tracked and have data (e.g. a student ID) stored in their memory. Tags are divided into two categories, active tags and passive tags. Active RFID tags contain their own small power supply, usually an on-board battery. Passive tags obtain power from the signal of an external reader. For RFID readers, they are the devices that read data from, and depending on the RFID system write data to tags and are connected to a network (e.g., wireless network) to transport the data to the RFID server to process the data. Similar to RFID tags, RFID readers also come in active and passive varieties, depending on the type of tags they read.

RFID yields great productivity gains because it can be used for a wide variety of applications ranging from the familiar building access control proximity cards to supply chain tracking, toll collection, vehicle parking access control, retail stock management, tracking library books, theft prevention, vehicle immobilizer systems and railway rolling stock identification and movement tracking, for example [10].

C. Arduino module overview

Arduino is an electronics prototyping platform that is used, by many users (e.g., students), as a way to learn about digital electronics because it offers easy access to a whole body of knowledge [11]. Arduino is an open source programmable circuit board that can be integrated into a wide variety of projects both simple and complex [12]. It consists of both a physical programmable circuit board (often referred to as a microcontroller) and a piece of software, or IDE (Integrated Development Environment) that runs on a computer (using a simplified version of C++, making it easier to learn to program) used to write and upload computer code to the physical board [13]. The IDE, it is able to be programmed to sense and control objects physically. Arduino module is able to interact with a large array of outputs such as LEDs, motors and displays. Arduino modules have been used widely for creating interactive hardware projects because their costs are not expensive [12].

D. Android operating system and Android Studio

Android operating system is an open source and Linux-based operating system for mobile devices (e.g., smartphones and tablet computers). Android was developed by the Open Handset Alliance, led by Google, and other companies [14]. It offers a unified approach to application development for mobile devices which means developers need only to develop for Android, and their applications should be able to run on

different devices that use Android operating system. For the Android architecture, it can be presented as in Fig. 3 [15]

For Android studio, it is the official Integrated Development Environment (IDE) for Android app development, based on IntelliJ IDEA, which is a Java integrated development environment (IDE) for developing computer software [16]. On top of IntelliJ's powerful code editor and developer tools, Android Studio offers features that can enhance productivity of developers when building Android apps, for example:

- A flexible Gradle-based build system
- A fast and feature-rich emulator
- A unified environment where you can develop for all Android devices
- Instant Run to push changes to your running app without building a new APK
- Code templates and GitHub integration to help you build common app features and import sample code
- Extensive testing tools and frameworks
- Lint tools to catch performance, usability, version compatibility, and other problems
- C++ and NDK support
- Built-in support for Google Cloud Platform

III. DESIGN AND DEVELOPMENT

A. System design

Before designing the system, system requirement, obtaining from teachers, school bus drivers and parents, and system analysis were conducted. Then, the proposed system has been created as shown in Fig. 4. This system consists of RFID tags and reader, Arduino module with Wifi, called Arduino Uno Wifi, for Internet access, mobile application and server with database. For the concept of this system, when each student with his or her RFID tag gets on the school bus the RFID reader will detect and then record the student ID and time stamp. When the bus arrives at the school, the Arduino module with Wifi will connect Internet via wireless network and the transmitted data to the server, including number of students, student ID and time stamp. Also, when each student gets off, the system will work in the same way. However, the teacher on the school bus has to confirm via mobile application when all students get off the bus, otherwise, the system will send notification to the teacher and the parent of the child who has been left on the bus via the mobile application (see the process as show in Fig. 5).

B. System and application development

After designing the system, the system implementation and development were conducted. One of important parts in the phase is about the Arduino Uno Wifi setting that it connects to RFID reader and acts as the middleware that connects to the main server via Internet. For the application development, Android Studio has been used to build the mobile application that is required to install on smart phones. Then, the mobile application will be deployed to parents and teachers' mobile phones (see the main menu of the mobile application in Fig. 6, status of the student in Fig. 7 and daily report in Fig. 8).

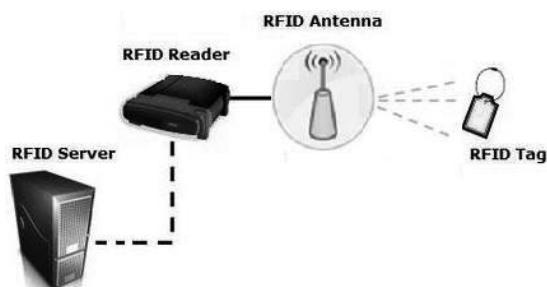


Fig. 1. RFID system overview, adopted from [8]



Fig. 2. Arduino UNO Wifi board

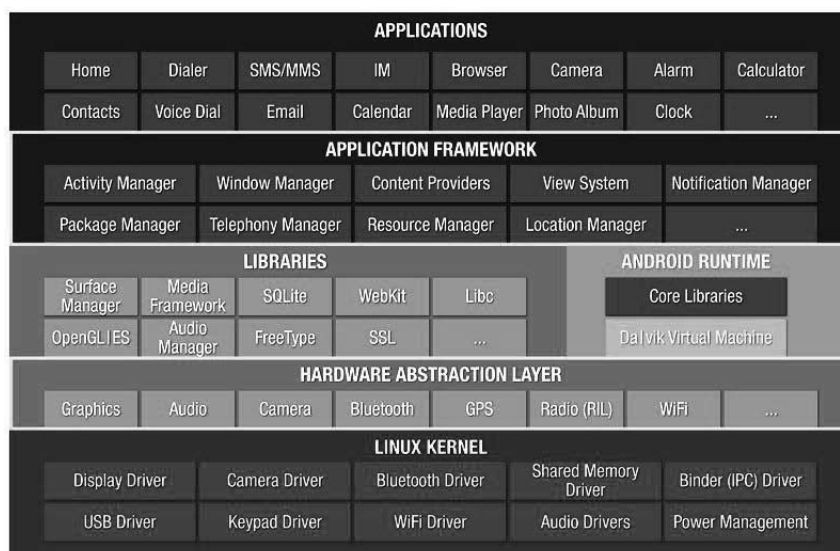


Fig. 3. Android architecture

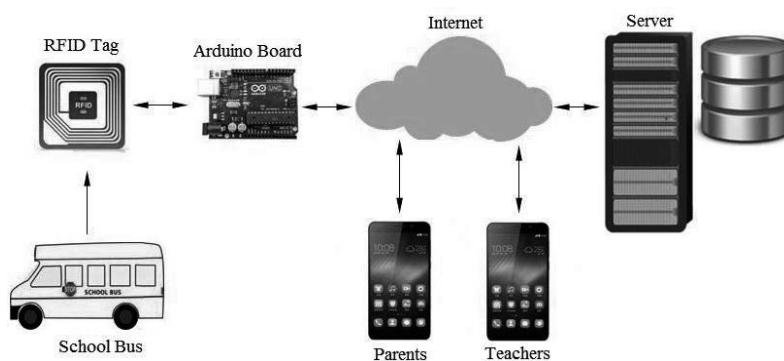


Fig. 4. The proposed system overview



IV. PERFORMANCE EVALUATION

After finishing system development, the performance of the system has been evaluated by simulating as students taking a school bus. After testing 30 times totally, the system can detect 28 times. That means the performance of the card reader module is $28/30 \times 100 = 93.33\%$. However, for the part of notification, the system can notify correctly for 30 times. That means the part of notification can work 100%.

Besides, the mobile application has been evaluated by 5 teachers and 10 parents based on 5-point scale as well (5 is excellent and 1 is bad). It has been scored as 3.9 ± 0.13 by teachers, while it has been scored as 4.1 ± 0.13 by 10 parents.

V. DISCUSSION, CONCLUSION AND FUTURE WORK

This study has presented the proposed solution to save children from being left on school bus. While implementing the system using Arduino module, it has been found issue about the hardware performance such as memory issue. That means the other hardware with higher performance might be considered to implement instead of the module used in this study. Besides, the higher performance of antenna for RFID reader has to be considered as well.

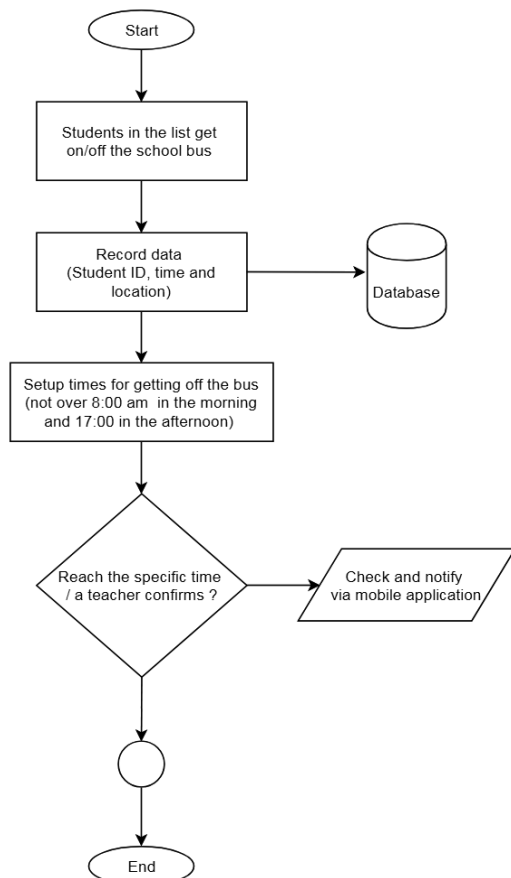


Fig. 5. The proposed system process

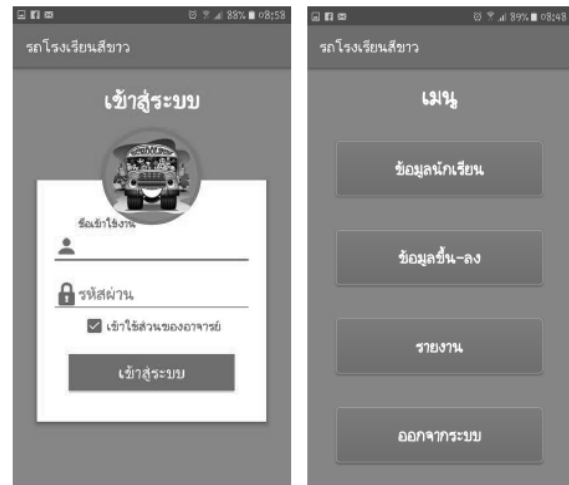


Fig. 6. Login page and main menu page

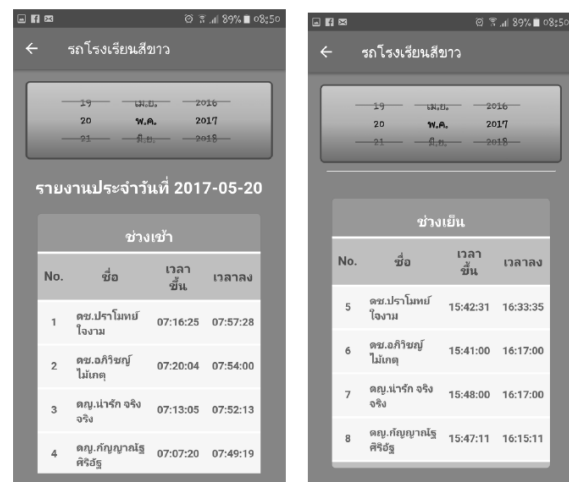


Fig. 7. Status of the student



Fig. 8. Daily report



For conclusion, after implementing, the system has been tested and evaluated. It has been found that this system has very good system performance, while it has been also evaluated by users, teachers and parents. They are satisfied with score of 3.9-4.1. However, there are several issues that should be extended from this work. For example, a comparative study with other hardware (e.g., Raspberry Pi) is very interesting to study in future. Besides, the mobile application should be extended to support other operation system as well (e.g., iOS).

ACKNOWLEDGMENT

Thank you to all (e.g., teachers and student's parents) who are involved with this study.

REFERENCES

- [1] Komchadluek News, "How many sacrifices child's are forgotten in a van?" 13th May 2016, <http://www.komchadluek.net/news/crime/227541>, Available on 31th May 2018 (in Thai)
- [2] Thairath News, "Forget the kid in the car, shocked, the driver surrendered carelessly" 2nd August 2017, <https://www.thairath.co.th/content/1024126>, Available on 31th May 2018 (in Thai)
- [3] ThaiPBS News, "Uthumporn Pittaya Teacher Prepares to Acknowledge the Allegations, Forget about 3 years old in a pickup truck" 15th May 2013, <http://news.thaipbs.or.th/content/169606>, Available on 31 May 2018 (in Thai).
- [4] Khaosod News, "Ministry of Education Shows - Help kids stick in a Car, Using the siren sensor as the door open" 15th May 2016, https://www.khaosod.co.th/view_newsonline.php?newsid=1463455822, Available on 31th May 2018 (in Thai)
- [5] G. Srikote, W. Nuakumuang, "The monitoring alarm and prevent children from being left on parked vehicle" UTK journal Vol 11, No 1 (2017), <http://journal.rmutk.ac.th/index.php/rmutk/article/view/230>, Available on 31th May 2018 (in Thai)
- [6] E.W.T.NgaiaKaren, K.L.MoonbFrederick, J.RigginscCandace and Y.Yib, "RFID research: An academic literature review (1995–2005) and future research directions", International Journal of Production Economics. Volume 112 Issue 2, April 2008, Pages 510-520, Elsevier, <https://doi.org/10.1016/j.ijpe.2007.05.004>, Available on 31th May 2018.
- [7] R. der TogtaPiet, J.M.BakkerbMonique and W.M.Jaspersa, "A framework for performance and data quality assessment of Radio Frequency Identification (RFID) systems in health care settings" Journal of Biomedical Informatics. Volume 44, Issue 2, April 2011, Pages 372-383, Elsevier, <https://doi.org/10.1016/j.jbi.2010.12.004>
- [8] www.divilabs.com, ivilabs, "How RFID Works-Everything That You Need To Know!", <https://www.divilabs.com/2013/03/how-rfid-works-everything-that-you-need.html>, Available on 31th May 2018.
- [9] R. Weinstein, "RFID: a technical overview and its application to the enterprise" IT Professional (Volume: 7, Issue: 3, May-June 2005), 01 August 2005. <http://dx.doi.org/10.1109/MITP.2005.69>
- [10] Otago university, "Radio Frequency Identification (RFID)", https://ourarchive.otago.ac.nz/bitstream/handle/10523/1247/RFID_Pre_Publication.pdf?sequence=5, Available on 31th May 2018.
- [11] Medea, "Arduino FAQ – With David Cuartielles", 5th April 2013, <http://medea.mah.se/2013/04/arduino-faq/>, Available on 31th May 2018.
- [12] www.makerspaces.com, "Arduino For Beginners" <https://www.makerspaces.com/arduino-uno-tutorial-beginners/>, Available on 31th May 2018.
- [13] learn.sparkfun.com, "What is an Arduino?" <https://learn.sparkfun.com/tutorials/what-is-an-arduino>, Available on 31th May 2018.
- [14] www.tutorialspoint.com, "What is Android?" https://www.tutorialspoint.com/android/android_overview.htm, Available on 31th May 2018.
- [15] A. Agrawal, Android "Application Security Part 2-Understanding Android Operating System" <https://manifestsecurity.com/android-application-security-part-2/>, 10th Jan 2015, Available on 31th May 2018.
- [16] developer.android.com, "Meet Android Studio", <https://developer.android.com/studio/intro/>, Available on 31th May 2018.



SCIENCES AND TECHNOLOGY

- Environmental Management
- Energy Technology and Management
- Manufacturing and Process Management
- Food Science and Biotechnology
- Advanced Materials and Nanotechnology
- Related Topics.





Study of Greenhouse Gases Emission and Storage of Suranaree University of Technology, Thailand

Wichayanee Puttipiriyangkul^{1st} and Sudjit Karuchit

School of Environmental Engineering,
Institute of Engineering
Suranaree University of Technology
Nakhonratchasima, Thailand
view74713@gmail.com, sudjit@sut.ac.th,

Abstract—This paper presented a study of the greenhouse gas emission and storage of Suranaree University of Technology for academic year 2016, using the guidelines of the Thailand Greenhouse Gas Management Organization (Public Organization). The study classified sources of emissions and storages into 4 scopes as follow: 1) direct emission 2) indirect emission 3) other indirect emission and 4) storage from green area. The results show that the total greenhouse gas emission of Suranaree University of Technology for academic year 2016 was 13,251 tCO₂eq, and 0.73 tCO₂eq per person. Scope 2, indirect emission, was the major source that generated 8,809 tCO₂eq or 66% of the overall emission. Emission from scope 1 and 3 were 2,864 tCO₂eq or 21%, and 1,634 tCO₂eq or 12%, respectively. On the other hand, carbon dioxide storage of trees in the university area was 53,905 tCO₂eq.

Keywords—Greenhouse gas; University; Emission; Carbon footprint; Climate change

I. INTRODUCTION

Greenhouse gas (GHGs) emission from human activities has caused the climate change problem, which is becoming more intense. Many countries are aware of how to manage and reduce GHGs emission, including Thailand. The Carbon Footprint Assessment of Thailand by the Thailand Greenhouse Gas Management Organization (Public Organization) has been launched in 2011 for the government and private organization. It raised awareness of the greenhouse gases emission and storage from their operations and provided a set of management guidelines to effectively reduce greenhouse gas emissions [2]. There were GHGs emission studies of universities in Thailand, including Thammasat University [3], Kasetsart University [4], Huachiew Chalermprakiet University [5], and King Mongkut's University of Technology Thonburi [6]. Suranaree University of Technology showed a clear determination to be a green university by announcing the Green and Clean University policy. It obtained a good position in the UI Green Metric World University Ranking in 2013-2017. Furthermore, the university has been supportive for activities, projects, research studies, and invention concerning the environmental issues. However, there have been no study of GHGs emission and storage at the whole university level.

This paper studied the emission and storage of GHGs of Suranaree University of Technology based on data from academic year 2016. The approach followed the Carbon Footprint Assessment of Thailand by the Thailand Greenhouse Gas Management Organization (Public Organization) [7]. The GHGs were calculated in units of carbon dioxide equivalent (CO₂eq) and 6 types of GHGs were studied as defined in the Kyoto Protocol.

II. METHODOLOGY

A. Organizational Boundary

The first step was the identification of the university's boundary – the sources of GHGs emission and storage to be included in the analysis.

B. Operational Boundary

Operational Boundary of the university can be classified into 4 scopes as follow: 1) direct emission such as power generation, cooking fuels and fuel consumption of vehicles. 2) indirect emission from electricity 3) other indirect emission such as water supply, waste and office equipment, and 4) carbon dioxide storage from trees within the university's 7,000 rai area.

C. Data collection and GHGs inventory

This study collected information from the university's activities in academic year 2016. They included both primary data (e.g. disbursement record) and secondary data (e.g. equipment and supplies record, receipt) related to emissions of scope 1, 2 and 3. For scope 4, primary data regarding plant types, height and diameter at breath height (DBH) at 1.3 meter of trees were collected.

D. Calculation

The amount of GHGs emission was calculated from the activity data and corresponding emission factors using the following 2 equations:

$$\begin{aligned} &\text{CO}_2\text{eq emission from activity} \\ &= \text{Activity data} \times \text{Emission factor} \end{aligned} \quad (1)$$



CO₂eq emission from trip

$$= (\text{Distance/Fuel consumption rate}) \times \text{Emission factor} \quad (2)$$

Estimation of carbon storage from trees can be calculated from the total above-ground biomass (W_T) using the Allometric Equation [1], [8]. W_T can be estimated from the sum of stem wood biomass (W_S), branch biomass (W_B) and leaf biomass (W_L), Equation (3). The heights and diameters at breast height (DBH) at 1.3 meter of the trees were obtained from field survey of trees in the university area for computing W_S and W_B . W_T values are in kilograms unit.

The total above-ground biomass (W_T)

$$= W_S + W_B + W_L \quad (3)$$

The calculation of carbon sequestration of green area can be calculated using W_T from equation (3) multiplied by 0.47, the conversion factor [1]. Carbon dioxide storage calculation of green area can be computed from carbon sequestration multiply by the molecular weight of carbon dioxide per carbon (44/12) to change unit to the mass of carbon dioxide equivalent.

III. RESULT AND DISCUSSIONS

The university boundary for this study were the internal units under the operation control of university that is university council, office of the president, institution, center/institution, enterprise unit and other units. There were also units based on area, including residential area, recreational area, waste disposal systems, and Center of Excellence in Biomass. The GHGs emission factor used in the calculation of each activity is based on recommendations by the Thailand Greenhouse Gas Management Organization (Public Organization) as shown in Table I.

Table II shows the results of greenhouse gas emission estimation from scope 1, 2 and 3 which were found to be 2,807.92, 8,808.63 and 1,634.21 tCO₂eq or 21%, 66% and 12%, respectively. The CO₂ storage in green area was estimated to be 53,904.90 tCO₂eq. Details of each scope are discussed further below.

A. GHGs emission from scope 1 activities

The GHGs emissions from scope 1: Direct emissions were 2,807.92 tCO₂eq. Contributions from each source are displayed in Fig.1. The source was refrigerant usage in air conditioners, 2,095.18 tCO₂eq or 74.62%, followed by manure from SUT's farm, 319.98 tCO₂eq or 11.39%, vehicle's fuel combustion, 305.97 tCO₂eq or 10.90%, and other activities, 86.80 tCO₂eq or 3.09%. The university's air conditioning systems were equipped with 7 centralized air conditioners and 2,500 split-type air conditioners. Regarding the usage of refrigerant which was the highest GHGs emissions, it was found that the refrigerant used in air conditioners were R-22 and R-407, which have the global warming potential (GWP) about 1,810 and 2,107 times higher than carbon dioxide, respectively [9]. So it caused of high level of GHGs emissions even with the use of 1,129 liters of refrigerant usage.

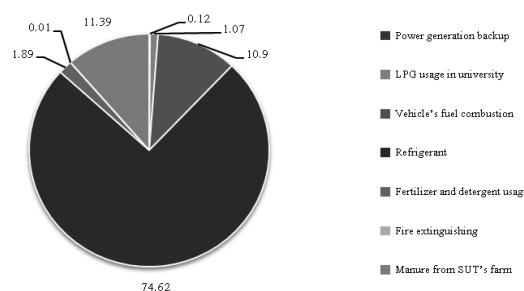


Fig. 1. Greenhouse gas emission from scope 1 activities.

B. GHGs emission from scope 2 activity

The GHGs emissions from scope 2: Indirect emissions were 8,808.63 tCO₂eq or 66% of the total emissions. Most contributions were due to the use of electricity by internal units under the operation control of the university, e.g. university council, president office, institution, and enterprise units (Fig.2). Others included residential area, recreational area, waste disposal systems, and Center of Excellence in Biomass. Although the corresponding emission factor is less than other activities, electricity consumption was the highest source of GHGs emission. The main source was academic zone that is the school buildings, laboratory buildings, and research buildings for learning and teaching activities. It was found the highest electricity consumption was from study building 1 as it was a building for lecture, seminar and computer-based learning courses for students throughout the semester.

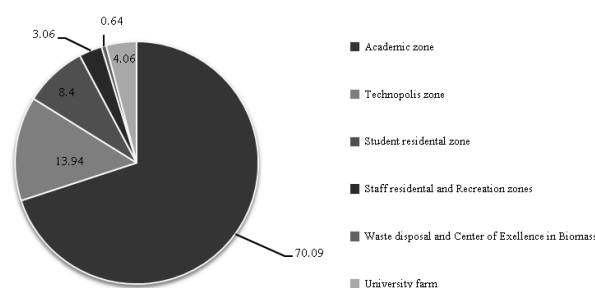


Fig. 2. Greenhouse gas emissions from scope 2 activity of each building zone.

C. GHGs emission from scope 3 activities

The GHGs emissions from scope 3: Other indirect emissions were 1,634.21 tCO₂eq. The highest emission came from waste disposal, 716.60 tCO₂eq or 43.85%, followed by water supply used of university, 484.63 tCO₂eq or 29.66%, electricity used by tenants, 263.46 tCO₂eq or 16.12 %, and other activities, 169.52 tCO₂eq or 10.37 % (Fig.3). The amount of waste generated was high, 850,959 kilograms,



resulting in high level of GHGs emission. It was followed by the emission from the use of 688,103 m³ of water supply. The source of usage are student dormitory buildings because of the daily use of water supply by students throughout the semester, which includes washing, cleaning and watering trees in the dormitory by the cleaning staff.

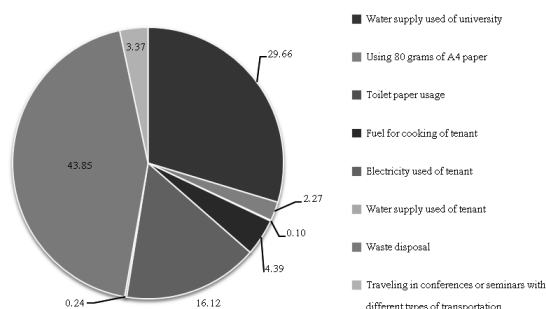


Fig. 3. Greenhouse gas emissions from scope 2 activity of each building zone.

D. Comparison of GHGs emission study

The GHGs emissions of Suranaree University of Technology for academic year was 0.73 tCO₂eq per person. Table III shows the emission of GHGs of other educational institutions. It shows that GHGs emissions from scope 2 activities have the highest emission of GHGs for most educational institutions. In addition, Suranaree University of Technology has lower GHGs emissions per person than most institutes. The results, however, depend on the scope of the data collection in each study. Especially for scope 3, which concerns activities other than scope 1 and 2, different activities included in the calculation can lead to significant different in GHG emission. Other factors include the size, type of institution, number of faculty, staff, and students. These factors affect the amount of corporate GHGs emissions.

E. Carbon dioxide storage by tree (green area)

The university's green area of about 2,056 rai yielded the total of carbon storage of 53,904. tCO₂eq. The amount of carbon dioxide storage per rai was 26.22 tCO₂eq. This was less than the amount of carbon dioxide storage per rai in Ban Wung-Kwauy Forest, Ngo District, Lampang province and

TABLE I. THE GHGS EMISSION FACTOR OF EACH ACTIVITY

Scope	Activities	Activities/Consumption data		Emission factor (tCO ₂ eq/unit)	Reference
		type	Unit		
Scope 1	Power generation backup	Diesel	liter	2.70797	[9]
	LPG usage in university	LPG	kg	3.1133	[9]
	Vehicle's fuel combustion	Diesel	liter	2.7446	[9]
		Gasohol 91	liter	2.1896	[9]
	Refrigerant	R-22	liter	1.810	[9]
		R-407	liter	2.804	[9]
	Fire extinguishing	Sodium Bicarbonate	kg	0.8921	[9]
	Fertilizer and detergent usage	Soap	kg	1.6685	[10]
		Composed fertilizer	kg	0.2458	[11]
		Manure fertilizer	kg	0.1100	[11]
Scope 2	Manure from SUT's farm	Fertilizer formula 15-15-15	kg	1.5083	[9]
		Cow	kg	0.2528	[11]
		Chicken	kg	0.3157	[11]
		Goat	kg	0.3473	[11]
	Electricity usage	Pig	kg	0.2621	[11]
		-	kWh	0.5821	[9]
		Medium-sized car (1600cc) Gasoline engine	km/L	15.238	[9]
		Domestic flight	pkm	0.1733	[9]
		International flight	pkm	0.1143	[9]
		-	m ³	0.7043	[10]
Scope 3	Water supply used of university	-	m ³	0.7043	[10]
	Using 80 grams of A4 paper	-	kg	0.7350	[11]
	Toilet paper usage	-	kg	1.4755	[11]
	Fuel for cooking of tenant	LPG	kg	3.1133	[9]
	Waste disposal	General waste	kg	0.8421	[11]
	Electricity used of tenant	-	kWh	0.5821	[9]
	Water supply used of tenant	-	m ³	0.7043	[10]
	CO ₂ storage in green area	Type/spices of tree	-	-	[1]



TABLE II. ESTIMATED GHGS EMISSION AND STORAGE OF SURANAREE UNIVERSITY OF TECHNOLOGY, ACADEMIC YEAR 2016

Scope	Activities	Amount	GHGs emission/storage value (tCO ₂ eq)	%
Scope 1	Power generation backup	1,255 liter	3.39	0.12
	LPG usage in university	11,268 kg	30.05	1.07
	Vehicle's fuel combustion	113,842 liter	305.97	10.90
	Refrigerant	1,129 liter	2,095.18	74.62
	Fire extinguishing	151 kg	0.13	0.01
	Fertilizer and detergent usage	127,666 kg	53.23	1.89
	Manure from SUT's farm	127,677 kg	319.98	11.39
	Total		2,807.92	100
Scope 2	Electricity usage	15,132,506 kWh	8,808.63	100
	Total		8,808.63	100
Scope 3	Traveling in conferences or seminars with different types of transportation	43,6211 km	55.15	3.37
	Water supply used of university	688,103 m ³	484.63	29.66
	Using 80 grams of A4 paper	50,415 kg	37.06	2.27
	Toilet paper usage	1,138 kg	1.68	0.10
	Fuel for cooking of tenant	23,034 kg	71.71	4.39
	Waste disposal	850,959 kg	716.60	43.85
	Electricity used of tenant	452,597 kWh	263.46	16.12
	Water supply used of tenant	5,587 m ³	3.93	0.24
	Total		1,634.21	100
Scope 4	CO ₂ storage in green area	2,056 rai	53,904.90	-
	Total		53,904.90	-

TABLE III. GHGS EMISSIONS FROM SURANAREE UNIVERSITY OF TECHNOLOGY AND OTHER INSTITUTES

Educational Institution	Amount of student/staff (person)	Amount of GHGs emission (tCO ₂ eq/yr)					year
		Scope of activity			Total	tCO ₂ eq/yr-person	
		1	2	3			
Suranaree University of Technology	18,341	2,828	8,809	1,634	13,251	0.73	2559 ^a
Thammasat University	21,240 (student only)	1,693	31,271	1,391	34,355	1.617	2553 ^b
Department of Chemical Engineering, Kasetsart University	464	921	3,033	686	4,640	1.85	2553 ^a
Huachiew Chalermprakiet University	11,030	35	548	244	826	0.358	2553 ^a
Graduate School of Energy and Environment, King Mongkut's University of Technology Thonburi	132	9	70	79	166	1.25	2556 ^b

^a. Academic year.

^b. Study year.

TABLE IV. CARBON DIOXIDE STORAGE CAPACITY OF SURANAREE UNIVERSITY OF TECHNOLOGY AND OTHER ORGANIZATIONS

Project area	Area size (rai)	The total above-ground biomass (tC/rai)	Carbon sequestration (tC/rai)	Carbon dioxide storage (tCO ₂ eq)						Ref.
				Baseline		Year 2		MAF		
				per rai	per all area	per rai	per all area	per rai	per all area	
Suranaree University of Technology	2,056	15.2	7.1	26.22	53,904.90	37.65	77,401.73	5.72	11,748.42	-
Ban Wung-Kwuay Community Forest, Ngo District, Lampang Province	1,450	8.7	11.0	40.20	58,295.00	50.0	72,531.50	4.90	7,118.25	[12]
Forest Park Area, Forestry Industry Organization	1,151,731	-	14.85	54.52	62,789,589	-	-	-	-	[13]

^c. Mean Annual Increment.



Forest Park Area of Forestry Industry Organization, which were 40.20 and 54.52 tCO₂eq, respectively, as shown in Table IV. Furthermore, the amount of carbon storage in the total project area of Ban Wung-Kwuay is more than Suranaree University of Technology, even with less project area. The difference in estimated values might be due to environmental conditions, e.g. suitability factors for tree growth (topography, soil characteristics and climate), the ability to absorb carbon dioxide of plants (type and genetic characteristics, age, and spacing density) [6]. In case of Ban Wung-Kwuay, most of the trees in project area were suitable. Forest Park Area, Forestry Industry Organization also found that the amount of carbon dioxide storage of the project areas was high, which may be a result of suitable project areas for plantation and maintenance of the tree species.

Most of the tree species found at Suranaree University of Technology was *Laucaena* (*Laucaena leucocephala*). It had higher carbon sequestration of the total biomass than the teak (*Tectona grandis*) tree species found in Ban Wung-Kwuay.

IV. CONCLUSION

The GHGs emission of Suranaree University of Technology for academic year 2016 has a total of 13,250.76 tCO₂eq. The greatest source of GHGs emissions was from the electricity usage of the university, which was approximately 66% of the total emissions. On the other hand, the GHGs storage from green area of the university was 53,904.90 tCO₂eq. These findings, along with the database and inventory of GHGs emissions from campus activities are beneficial to the university. This study is the first comprehensive GHGs emission estimation of the university and it supports further analyses for effective ways to reduce GHGs emissions from the operation of the university.

ACKNOWLEDGEMENT

This study was financially supported by The Environment Fund, Suranaree University of Technology.

REFERENCES

- [1] Intergovernmental Panel on Climate Change (IPCC), IPCC Guidelines for National Greenhouse Gas Inventories: Chapter 4 Forestland. National Greenhouse Gas Inventories Programme, IGES, Japan, 2006.
- [2] Thailand Greenhouse Gas Management Organization (Public Organization). (2016). [Online]. Available: <http://thaicarbonlabel.tgo.or.th/admin/uploadfiles/download/ts7be0b6757c.pdf>.
- [3] Phairat Usubharatana and Hampon Phungrussami, "Carbon Footprint of Organization: Case Study for Thammasat University," Thai Journal of Science and Technology, Vol. 22, no. 1, 2014.
- [4] Thanat Poonpratin, Carbon Footprint of the Department of Chemical Engineering at Kasetsart University, Master of Engineering (Chemical Engineering) Department of Chemical Engineering, Kasetsart University, 2012.
- [5] Isaree Rodtusana, Assessment of Greenhouse Gas Emissions of Huachiew Chalermprakiet University, Huachiew Chalermprakiet University, p. 84, 2013.
- [6] Chayani Sangsue, Carbon Footprint of Academic Organization: Case Study of the Joint Graduate School of Energy and Environmental, Master of Engineering, Department of Environmental Engineering, King Mongkut's University of Technology Thonburi, 2014.
- [7] Thailand Greenhouse Gas Management Organization (Public Organization), Thailand Voluntary Emission Reduction Program Reference Manual: Forestry and Agriculture Sector, Vol. 1, 2015.
- [8] Faculty of Forest, Kasetsart University. (2011). [Online]. Available: http://www.conference.tgo.or.th/download/tgo_main/publication/ARFR_Guideline/ARFR.pdf
- [9] Emission Factor CFO, (2016). [Online]. Available: http://thaicarbonlabel.tgo.or.th/admin/uploadfiles/emission/ts_822ebb1ee5.pdf.
- [10] Emission Factor CFP, (2017) [Online]. Available: http://thaicarbonlabel.tgo.or.th/admin/uploadfiles/emission/ts_11335ee08a.pdf.
- [11] Emission Factor. [Online]. Available: <http://cfologov.com/search/searchData>.
- [12] Warakom Wongchai, Adisorn Thomya and Ekkarat Inthavongsa, "Voluntary Emission Reduction for Sustainable Forestation: Case Study in Wung-Kwuay's Community Forest Ngo District Lamphang," The 7th Thailand Renewable Energy for Community Conference (TREC-7), p. 429, 2014.
- [13] The office of Economic Wood Innovation, Forest Industry Organization, Ministry of Natural Resources and Environment. (2010). [Online]. Available: <http://www.fio.co.th/p/km/document/km-530108.pdf>.



Investigating the Role of Factors Determining Drainage System Performance for Water-Efficient Toilet

Anurak Kusolchoo

Faculty of Environment and resource studies
Mahasarakham University
Kantharawichai District, Mahasarakham 44150, Thailand
e-mail: a_nurak_1991@hotmail.com

Wichitra Singhirunnusorn

Multidisciplinary Research Center for Environmental
Sustainability (MRCES), Mahasarakham University
Kantharawichai District, Mahasarakham 44150, Thailand
e-mail: swichitra@gmail.com

Abstract— This research focused on the saving of flush volume through drainage system design. Factors influencing drainage system performance (water-flow velocity) and flush volume were investigated including drain-pipe diameter, draining slope, draining distance, and vertical drop height. The research conducted its experiment under setting conditions to examine the ability of water-efficient toilet. The transport waste through the draining line and the drainage efficiency of the toilet were investigated. Results reveal that for the no-slope setting, installing with 150 mm. vertical drop height and the distance of 8 meters shows the best efficiency in water saving in both 2 and 3 inch-diameter pipes. The draining efficiency of all pipe sizes for the longer distance can be improved by increasing drop height. For the sloping setting, the higher the slopes, the more the draining efficiencies. The draining slope 1:50 shows the best performance in terms of water-flow velocity with the condition of 150-mm drop height and 2-3 inch-pipe sizes. For the longer draining distance, slope shows the significant impact on water efficiency and draining performance.

Keywords—Drainage System; Flush Volume; Water-Efficient Toilet

I. INTRODUCTION

Water use for households and commercial buildings is on the rise due to the increase in population. A huge amount of water is daily used for flushing toilet. This has led to a great concern on the possibility of reducing the amount of water used. Choosing a toilet to save water is another option for saving water. The use of water for the cleaning of waste or sewage for the toilet in the conventional way. The amount of water to cleanse is about 13 liters/person. People normally flush a toilet 3-4 times/person/day. If one flushes toilet 4 times a day, there is approximately 52 liters of water used per person [1]. Water used for toilet becomes the main household water consumption. In order to reduce the consumption of water, some current researches attempt to find a solution to reduce water consumption for toilet. Parameters affecting the amount of flush volumes in toilet were examined. Such parameters include a drainline slope, vertical drop height, drain distance and drain diameter. Previous study found that the slope of draining can affect the optimization of solid transport in pipes

and also reduce the flush volume [5]. Vertical drop height was found that can increase the solid transport in drain pipe. However, it was only shows a slightly impact on the draining performance [3]. Draining distance is another important parameter influencing the flush volume. Longer distance will need more flush volume to increase the ability of solid movement [3]. The size of pipe diameter could increase the water flow velocity and improve the movement of solid in the pipe line [5]. This study, therefore, aims to investigate the feasibility of designing and developing the water saving system for the toilet. The design of drain system will be studied. Factors affecting water velocity, solid movement, and flush volume were examined. The findings will be recommended for the appropriate drainage design for water-efficient toilet.

II. MATERIALS AND METHODS

In the study, effects of factors were investigated through the design of the drainage system as follows:

A. Design and experimental set up

This study analyzed the influence of appropriate factors that include drain slope, vertical drop height, drain distance, and drain diameter to set up the drainage system for reducing water usage. The experimental setup was described below.

I.) Installation of equipment under the following conditions.

I.I) The slope of drainage used here comprise no slope, 1:200, 1:100 and 1:50, respectively. When the slopes were increased at different pipe lengths, the height at the end of pipe were decreased as shown in Table 1.

TABLE I. DESIGN SLOPE OF DRAIN USED IN THE TEST

Slope	Drain distance (meter)			
	4 m.	8 m.	12 m.	16 m.
Non slope	0 cm.	0 cm.	0 cm.	0 cm.
1:200	2 cm.	4 cm.	6 cm.	8 cm.
1:100	4 cm.	8 cm.	12 cm.	16 cm.
1:50	8 cm.	16 cm.	24 cm.	32 cm.



I.II) Vertical drop height ducts were set to 150, 500, and 800 mm.

I.III) The drain distance paths were set to 4, 8, 12 and 16 m.

I.IV) Drain diameter were set to 50, 75, and 100 mm. or 2-, 3- and 4-inch pipes.

I.V) Quantities of water in the test were set to 2, 3, 4, 5, and 6 liters.

II.) Each test was treated in the same way. Devices with a 50-mm drain diameter and no slope were installed. A vertical drop height of 150 mm. and 4-m drain distance were utilized in the test. Appropriate factors were determined by checking the flow velocity of the water in the drainage with varieties of flush volume at 2, 3, 4, 5, and 6 liters and drain diameter at 75 and 100 mm. The slopes (i.e., 1: 200, 1: 100, and 1:50), the vertical drop height (i.e., 500 and 800 mm) and

the drain distance (8, 12, 16 m.) were investigated. The flow velocity of the water in the drain was then adjusted to meet the condition set. An example of experimental design was shown in Fig. 1.

B. Experimental procedure

I.) Test slope, vertical drop height, drain distance and drain diameter for the amount of flush volume at 2, 3, 4, 5 and 6 liters according to the conditions of the design and installation process mentioned above.

II.) Consider the appropriate factors by checking the flow velocity of water in the drainage pipe by measuring the distance per time (in unit of seconds) where the water flows from the source to the end of the drain as well as the amount of water used to wash less and flow velocity of the water in the drain with possibly to induce water savings. The flow velocity of the water in the drain no less than 0.6 m/s [2].

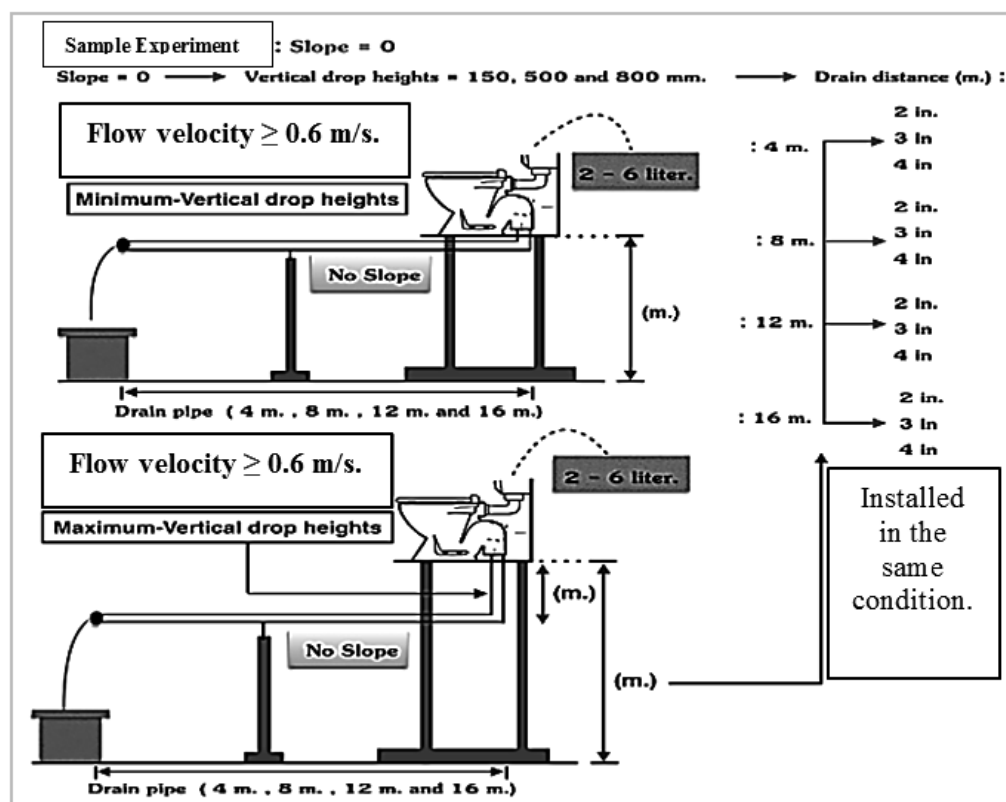


Fig. 1. Experimental design

III. RESULTS

III.I) Influence of factors on the installation of drains in non-sloping conditions.

Considering the flow velocity of the water in the drainage at the vertical drop height installation of 150 mm. and the pipe length of 4 m., at the decreases, flush volume. In this situation, it is not possible to design a drainage

system that contributes to water saving efficiency because the flow velocity in the drain is less than 0.6 m/s. The results of such studies will be shown in Fig. 2. To improve the drainage system in non-slope conditions to gain more effectiveness in saving water, we investigated more in-depth details on the influence of the factors i.e., drain distance and vertical drop height to seek for a more efficient drainage system. The results are shown in Fig. 3.

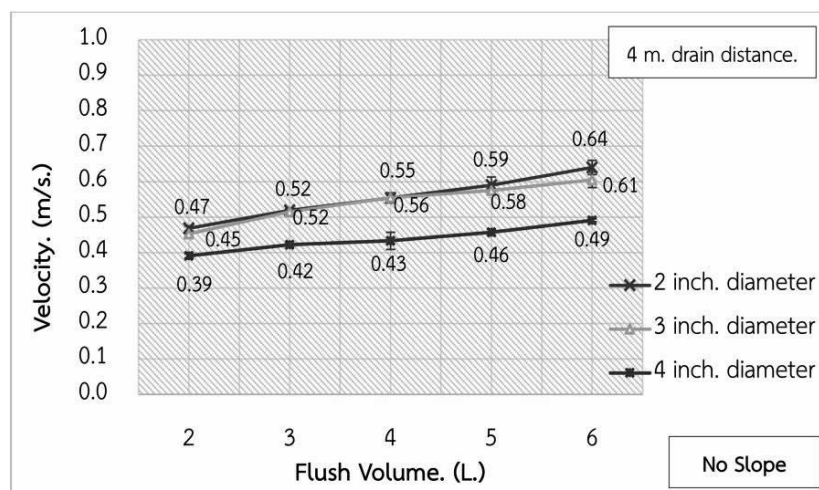


Fig. 2. The influence of factor in each pipe size at 0 slopes.

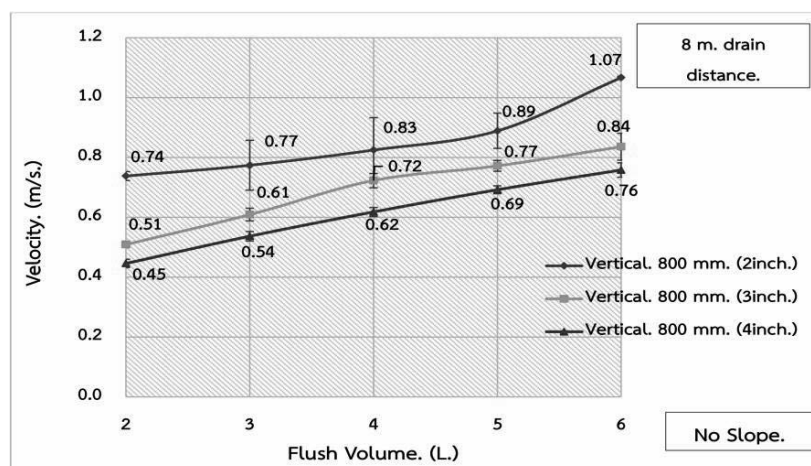


Fig. 3. The influence of Drain distance and Vertical drop height in each pipe size at 0 slope.

From the relationship shown in Fig. 3, it was found that the flow velocity of the water in the pipe meet the criteria defined and resulted in effective water saving. As seen from the results, when considering at the drain pipe diameter of 2 inches and drain distance increased to 8 m., the amount of water is used to flush at least 2 liters at the velocity of the water flow in the drain of 0.74 (SD = 0.02) m/s. But for the 3-inche drain diameter with the pipe length was increased to 8 m., the amount of water is used to flush at least 3 liters. At the velocity of the water flow in the drain of 0.61 (SD = 0.02) m/s. While for 4-inche drain diameter, the amount of water was used to flush at least 4 liters with a minimum

velocity of the water flow of 0.62 (SD = 0.01) m/s. As results, the smaller drainage hose led to more efficient in water saving than the larger one and increases in the vertical drop height and drain distance can elevate the efficiency of water saving.

III.II) Influence of factors when the drain pipe is installed in slope conditions.

The results showed that the three sizes of drainage were installed in slope conditions. The drain with a vertical drop height of 150 mm and a drain distance, 4 meters. The results are shown in Fig. 4.

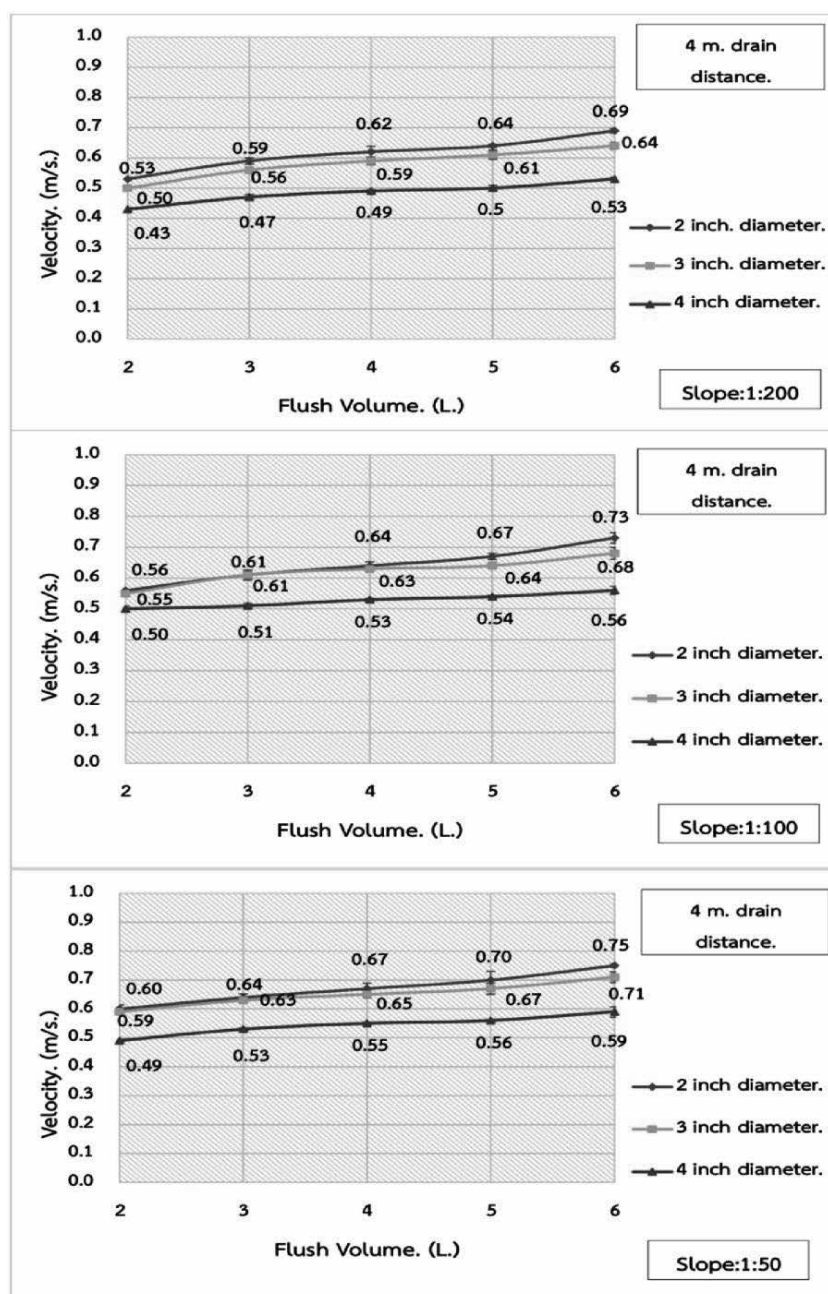


Fig. 4. The influence of Drain distance and Vertical drop height in each pipe size at 1/200, 1/100 and 1/50 slope.

From the relationship shown in Fig. 4, an increase in slope has resulted in elevation of the velocity of water flow. It can be seen that the pipe diameters at 2 and 3 inches with slope of 1:50 affected the flow velocity of the water in the drain. According to this, it can meet the criteria with the minimum flush water was only 2 and 3 liters with the velocities of the water flow in the drain of 0.60 (SD = 0.01) and 0.63 (SD = 0.004) m/s, respectively. When the slope was decreased to 1:100 and 1:200, for the 2-inch drainage

pipe had the lowest water content of only 3 and 4 liters with the velocities of the water flow at 0.61. (SD = 0.02) and 0.62 (SD = 0.02) m/s, respectively. But for 3-inch drain hose, it would use a minimum of 3 liters of water at a slope of 1:100 with the velocity of the water flow in the drain of 0.61 (SD = 0.01) m/s. and the 4-inch drain diameter found that the drainage system could not be designed to save water in the distance and slope.



III.III) Influence of drain distance and vertical drop height on slope conditions.

As a result, at the highest slope used, the most water saving efficiency was found and the installation with the

vertical drop height of only 150 mm. was considered to be sufficient for improvement of efficiency of water saving. The results were shown in Fig. 5.

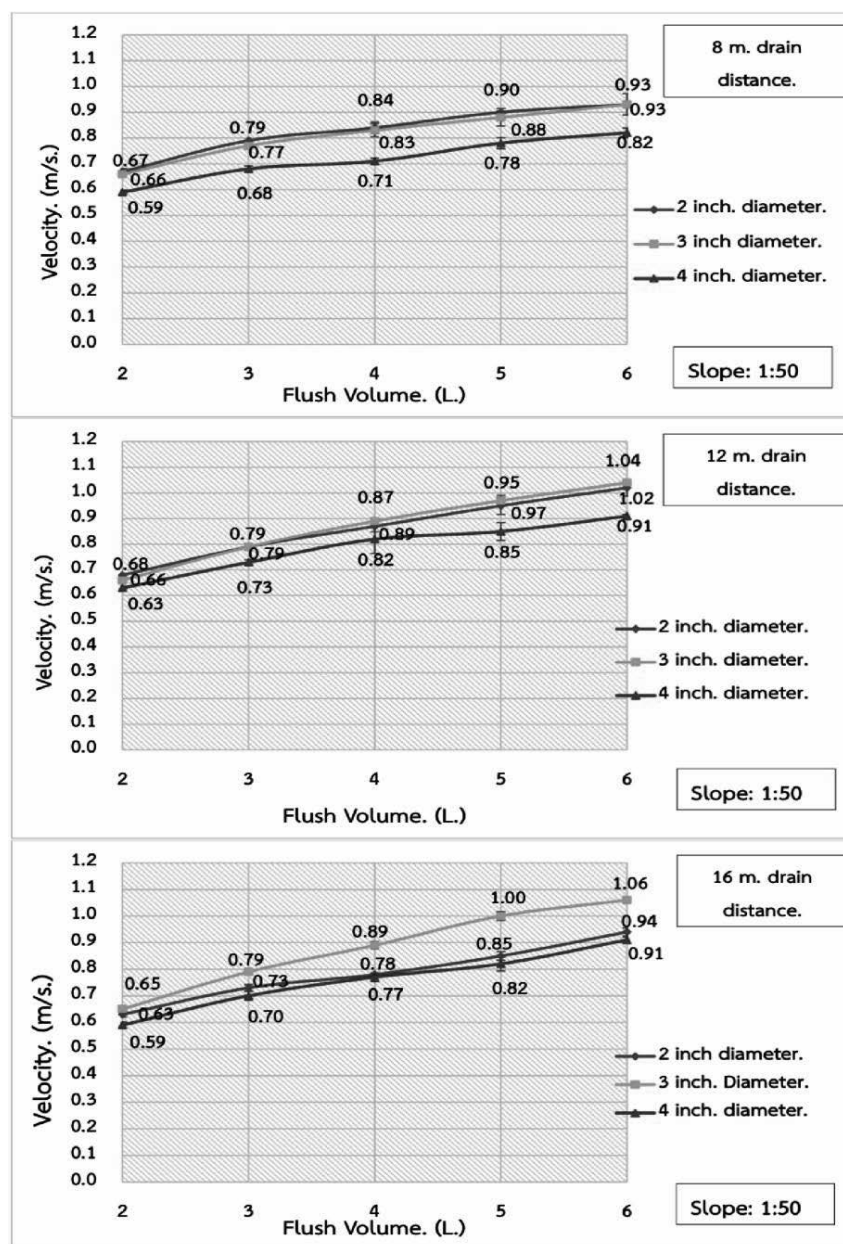


Fig. 5. The influence of drain distance and vertical drop height in each pipe size at 1/50 slope.

From the relationship shown in Fig. 5, it was found that when installed at a maximum slope of 1:50, the ducts with 2- and 3-inch diameters can be used in the design of drainage system at all drain distances i.e., 8, 12 and 16 meters, with the minimum water consumption of 2 liters. While for the 2-inch diameter, the velocities of the water

flow were 0.67 (SD = 0.01), 0.63 (SD = 0.01), and 0.67 (SD = 0.01) m/s, respectively. For the rest, the velocities were 0.66 (SD = 0.004), 0.66 (SD = 0.01) and 0.65 (SD = 0.01) m/s., respectively. For the 4-inch drain diameter, it can be designed to drainage system at drain distances of 8, 12 and 16 meters, with the minimum water consumption of 3 liters



and the velocity of the water in the drain of 0.68 (SD = 0.01), 0.73 (SD = 0.01) and 0.70 (SD = 0.02) m/s, respectively.

The results mentioned above, this has led to multiple regression analysis to study the influence of the factors that influence the speed of the flow of water in drains causing water saving efficiency. The results showed that the five independent variables explained the factors influencing the velocity of water flow in the drainage pipes of all three sizes to 75% by the factors that influence the velocity of the water flow in the drain i.e. flush volume, drain line slope, drain diameter, drain distance and vertical drop height. To forecast influence of the speed of the water flow in the sewer, flush volume, drain line slope, drain diameter, drain distance and vertical drop height are the most important variables with a statistically significance at .05. The relationship can be written as a multiple regression equation for prediction of flush water and is shown in Equation (1).

$$Y = 0.342 + 0.071X_1 + 0.094X_2 - 0.002X_3 + 0.009X_4 + 0.00093X_5 \quad (1)$$

Notes: X_1 = flush volume (liter),
 X_2 = drainline slope,
 X_3 = drain diameter (millimeter),
 X_4 = drain distance (meter),
 X_5 = vertical drop height (millimeter),
 Y = flow velocity in drain (meter per second).

IV. CONCLUSION

Installation of drainage system in non-slope condition does not affect water saving. However, when improvements were made by installing the drainage system in the conditions as previously mentioned through increases in the drain distance and vertical height. Consequently, the drainage system has improved efficiency in water saving. The most effective diameters are 2, 3 and 4 inches, respectively. In this condition, the drain distance, vertical drop height, and drain diameter are factors influencing water saving efficiency. While for slopes conditions, when drain line slope and drain distance were increased, it was found that water saving in sewer systems are more effective than that in non-slope condition. Moreover, it can be installed at a low vertical height and still remains effectiveness in water saving. Among all the studied variables, flush volume, drain line slope, drain diameter, drain distance and vertical drop height are key influencing factors on water saving efficiency.

V. RECOMMENDATION

I. Drainage system in non-slopes condition must be installed in drain distances ranging from 8-16 m. and vertical drop height of 800 mm. with 2- and 3-inch drains were used.

II. For slope condition with the distance of drain pipe not over 4 m, it must be installed at 1:50 and 1: 100 slopes and at vertical drop height of 150 mm. with 2- and 3-inch drains were used.

III. For slope condition with drain distance ranging from 8 to 16 m, it must be installed at vertical drop height of 800 mm. a 1:50 slope with 2-, 3- and 4-inch drains were used.

ACKNOWLEDGMENT

I would like to thank staffs at the Faculty of Environment and Resource Studies for providing useful guidance. This research was financially supported by Mahasarakham University (MSU) and the National Research Council of Thailand (NRCT).

REFERENCES

- [1] Green Label Project Secretariat Office Thai Environmental Institute and the Office of Industrial Product Standards. Green label requirements for ceramic sanitaryware products:toilet. July: 2011 Retrieved from [http:// www. tei .or.th/greenlabel/download/TGL-5-R3-11.pdf](http://www.tei.or.th/greenlabel/download/TGL-5-R3-11.pdf).
- [2] Kriengsak Udomsirirotj. Design Building Pipe and Building Environment. (pp.121-161). Nonthaburi: Mitthara Printing; 2549 Volume 2: 121- 161.
- [3] Bill Gauley, John Koeller. Evaluation of Water-Efficient Toilet Technologies to Carry Waste in Drainlines. Canada Mortgage and Housing Corporation Project. 2005; (1) :1-32.
- [4] J A McDougall, J A Swaffield. The influence of water conservation on drain sizing for building drainage systems. Building Services Engineering Research and Technology. 2003; 24(4) : 229-243.
- [5] J A McDougall, R H M Wakelin. The influence of flush volume and branch drain cross-section on deformable solid transport in attenuating flows. Building Services Engineering Research and Technology. 2007; 28(1) : 7-22.



Health risks due to radon in groundwater at Amphoe Muang Maha Sarakham

Vitsanusat Atyotha 1st
Rajamangala University of Technology Isan
Khon Kaen campus
e-mail: v_atyotha@hotmail.com

Junthara Somtua 2nd
Group Strategy Management and Research
Regional Health Promotion Center 7, KhonKaen.
e-mail: junthara_2526@hotmail.com

Abstract— Research aims to identify a possible cause of cancer in 59 ground water samples at Amphoe Muang Mahasarakham. This was determined by measuring Radon concentration in Ground water using RAD H₂O. The Radon concentrations of all samples were in the range of 0 to 2.21 Bq/l with the average of 0.69 Bq/l. The risks of Annual Equivalent Dose were found to be in the range of 0 to 0.016 mSv/y with the average of 0.005 mSv/y. The results were then compared to the standard value of the US Environmental Protection Agency (Radon concentration should be less than 11 Bq/l for drinking water and less than 150 Bq/l for using water and Annual Equivalent Dose should be less than 0.1 mSv/y). It was found that both radon concentrations and annual equivalent doses of all ground water samples were lower than the standard values. Therefore, ground water at Amphoe Muang Mahasarakham is safe for consumption without the worry of carcinogens in Ground water (Radon)

Keywords— Radon, Cancer, Ground Water, Maha Sarakham

I. INTRODUCTION

Radon is a radioactive that can accumulate in the environment, such as rocks, soil, water, plants and food [1]. However, if radioactive is accumulated in the human body in high level, it will affect your health. When people drink water containing radium dissolved in a high volume, this can be a cause of cancer in various organs such as the lungs, liver, kidneys and endocrine organs [2, 3]. When ground water evaporate, Radon can release Alpha decay into the air. When we are breath, the alpha radiation from the decay of radon can damage lung tissue and cause a lung cancer. Radon is the second leading cause of lung cancer, where the first one is cigarette. The study reported that each increase of 1 Bq / m³ (Radon in water every 0.001 Bq /l) in radon concentration in the air will increase the chance of lung cancer more than 1.6 x 10⁻⁴ times [4]. Radon can accumulate in the body by breathing and consumption of water and food. This will all affect health in future. The researchers are aware of the problems in this regard, so we have measured the amount of Radon in Ground water that people use on a regular basis. We choose to study water samples from villages in research areas in order to measure the safety and the risks that affect the health of people in the study area.

II. RESEARCH OBJECT

- Measuring Radon concentration in groundwater at Amphoe Muang Mahasarakham.
 - Estimating the risk of cancer caused by a use of groundwater at Amphoe Muang Mahasarakham
- Maintaining the Integrity of the Specifications

III. MATERAIL AND METHOD

A. Groundwater sampling

The 111 sampling ground waters of village in Amphoe Muang Mahasarakham were packaged in 500 milliliter bottles (Before packing, the water must be opened 5 - 10 minutes). In or der to prevent radon in the water to leak out a lot, Radon in water samples were measured as soon as possible (less than 1 week) by RAD H₂O at Radon laboratory of Thailand Institute of Nuclear Technology (Public Organization).



Fig. 1 Ground water Sampling



Fig. 2 Ground water



B. RAD H₂O (RAD 7: Radon electronic detector)

A 250 mL of Ground water sample was pumped into the sampling device connected to the RAD7 electronic radon detector (shown in Figure 3). RAD 7 will measure average Radon concentration with the measurement time of 20 hr/sample. Unit of the result will in Bq/l.

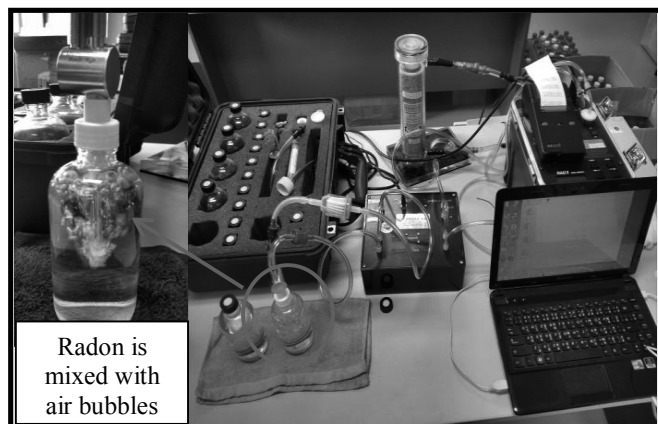


Fig. 3. Set-up for radon concentration measurement by RAD H₂O

C. Annual Equivalent Dose Analysis

The amount of Radon concentration received per year from drinking contaminated water supply caused by the Radon (Annual Equivalent Dose, AED) was calculated. To assess the radiation from Equation 1 [4]

$$AED = A \times W \times \text{Dose factor} \quad (1)$$

AED = Annual Equivalent Dose (mSv/y)

A = activity of Radon in Groundwater (Bq/L)

W = Water consumption per year, which is based on a minimum of 2 L of drinking water per day and minimum of 200 L of using water per day.

Dose factor = Radiation factor used in the assessment of the body radiation per year is 10⁻⁸ SV/Bq.

IV. RESULTS AND DISCUSSION

From 59 water samples, the variance value (S²) and the Standard Deviation (S) of Radon were found to be 0.31 and 0.56, respectively. Since there are many sampling area, 14 interesting regions with high average of Radon have presented in the Table 1. It can be seen that both Radon concentration and Annual Equivalent Dose) are lower than the standard values of US Environmental Protection Agency [6, 7]. From Table 1 and Figure 4, the radon in some area is quite high. Therefore, the radon concentration in these areas should be regularly monitored because in the long-term, the contamination of Radon in ground water may continuously increase and can be the cause of cancer in people who use the water in the future. Therefore, the behavior of radon in Ground water in these areas should be regularly monitored to create security for the people.

TABLE I. RADON AND ANNUAL EQUIVALENT DOSE IN GROUND WATER

Research areas	Radon)Bq/L(AED (mSv/y)
1. Ban Gudcan Tambom Nongno	2.21	0.0161
2. Ban Nonsomboon Tambon Nongpling	2.21	0.0161
3. Ban Nongno Tambom Nongno1	2.04	0.0148
4. Ban Bhoi Tambon Thasongkhon	1.87	0.0136
5. Ban Nongjuanoi Tambon Thasongkhon	1.70	0.0124
6. Ban Nongjig Tambon Kaewa	1.70	0.0124
7. Ban Nongyai Tambon Ganglengjan	1.19	0.0087
8. Ban Nongpling Tambon Nongpling	1.19	0.0087
9. Ban Saunmhom Tambom Nongno	1.19	0.0087
10. Ban Donwhan Tambom Donwhan	1.19	0.0087
11. Ban Na Phaeng Don Tambon Huai Ang	1.02	0.0074
12. Ban Nong I Dam Tambom Nongno	1.02	0.0074
13. Ban Nongno Tambom Nongno2	1.02	0.0074
14. Ban Channak Tambon Nongpling	1.02	0.0074

From table 1, radon concentrations in 59 groundwater samples of Amphoe Maha Sarakham were determined by techniques RAD H₂O using RAD 7: Radon electronic detector. The results found that Radon concentrations of all samples were range of 0 to 2.21 Bq/l with the average of 0.69 Bq/l. The risks of Annual Equivalent Dose were found to be in the range of 0 to 0.016 mSv/y with the average of 0.005 mSv/y. The results were compared to standard value of US Environmental Protection Agency (a standard value of radon concentration in drinking water should not exceed 11 Bq/l, in consumptive water should not exceed 150 Bq/l and Annual effective dose should be less than 0.1 mSv/y). It was found that Radon concentrations in consumptive groundwater use from all areas were lower than the standard value. Radon concentration in Table 1 were then used to create graph for comparison of Radon concentration in Ground water

Radon concentration in Ground water)Bq/l(

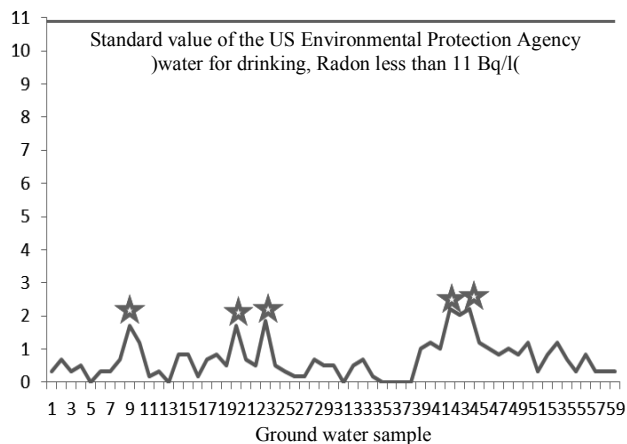


Fig. 4. Radon concentration in ground water

Remark ☆ = Radon concentration in this area is higher than other therefore it should be regularly monitoring in these areas that

The results (radon concentration and GPS coordinates of sampling) were then use to create contour map for distribution of radon concentration in Amphoe Kantharawichai, as shown in Fig.5

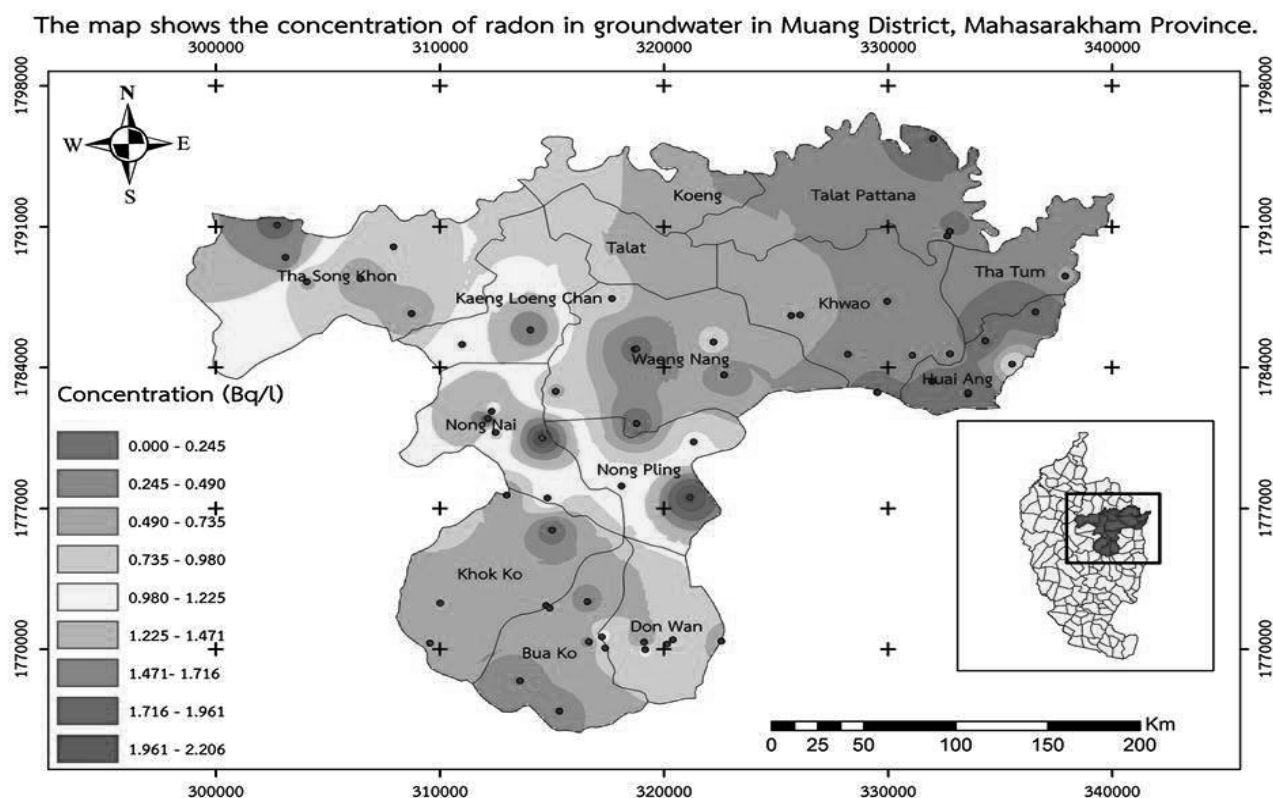


Fig.5 contour map for distribution of radon concentration in Amphoe Maha Sarakham

From figure 5. Radon concentration is higher in the west northern part of Tambon Tha Song Khon, eastern part of Tambon Nong Nai and eastern part of Tambon Nong Pling which are in the range of 1.716 – 2.206 Bq/l. The western part of Tambon Tha Song Khon, center of Tambon Kaeng Loeng Chan and western part of Tambon Nong Nai, radon concentration is in the range of 1.225 – 1.716 Bq/l. Part of Tambon Tha Song Khon, Tambon Nong Nai, Tambon Kaeng Loeng Chan and Tambon Nong Pling, radon concentration are in the range of 0.98 – 1.225 Bq/l. Radon concentration has the lowest value at Tambon Khok Ko, Tambon Bua Ko, Tambon Don Wan, Tambon Waeng Nang, Tambon Huai Ang, Tambon Talat, Tambon Koeng, Tambon Khwao, Tambon Talat Pattana and Tambon Tha Tum, radon concentration is in the range of 0 – 0.98 Bq/l. This contour map will give us the radon distribution in the research area for radon projection in areas that have not yet been measured.

V. CONCLUSION

The radon concentrations, which is factors that cause cancer in people, in 59 groundwater samples at Amphoe Mahasarakham was studied. Radon concentration was measured in Ground water by using RAD H₂O. The Radon concentration of all sampling water was found to be in the range 0 to 2.21 Bq/l with the average value of 0.69 Bq/l. The Annual Equivalent Dose of all sampling water was found to be in the range of 0 to 0.016 mSv/y with the average value of 0.005 mSv/y. These results

are lower than the standards value of US Environmental Protection Agency. However, in some areas the radon concentration is high so it should be regularly monitored. People are unsure whether water is safe or not therefore a way to prevent the risk of radon-contaminated groundwater affecting public health you should discussed. Using a water filter with a filter aeration (Aeration System) or a filter with the filter scale carbon (Granular activated carbon) is a promising way to protect ground water from contamination of radon. Carbon filters tend to cost less than Aeration System, but radioactivity collected on the filter may require special disposal methods for platelet carbon filter [8, 9]. People should always check the condition and lifespan of this filter. If filter expires, it should be replaced immediately.

ACKNOWLEDGMENT

This study was supported by research grants of Rajabhat Maha Sarakham University in 2015. Thank you to Mrs. Phachirarat Sola for giving us the advice and thanks to the Thailand Institute of Nuclear Technology (Public Organization) for supporting this research tool.

REFERENCES

- [1] Javier Avalos. Public Health Goal for Radium-226 and -228 in Drinking Water, California: USA, 2006. p.5 - 8.



- [2] World Health Organization. Guidelines for Drinking-water Quality. 4th ed, Geneva, Switzerland, 2011.
- [3] Egbe Egiebor, Vinay Allagadda. Evaluation of Uranium and Radium in a Private Well. Letter Health Consultation, Pittsylvania, Virginia, USA. 2014.
- [4] World Health Organization. Guidelines for Drinking-water Quality fourth edition incorporating the first and second addenda, WHO, Geneva. 2014.
- [5] IAEA. Radiation Protection and Safety of Radiation Sources: International Basic Safety Standards. Interim Edition, Vienna, Austria, 2011.
- [6] Office of Water, U.S. Environmental Protection Agency. Edition of the Drinking Water Standards and Health Advisories, Washington DC, USA. 2012.
- [7] B.C. Shivakumara, M.S. Chandrashekar*, E. Kavitha, L. Paramesh. Studies on ²²⁶Ra and ²²²Rn concentration in drinking water of Mandya region, Karnataka State, India. Journal of Radiation Research and Applied Sciences 7, 2014, p. 491 – 498.
- [8] USEPA. (2015, October). Basic Information about Radon in Drinking Water. Retrieved from <https://archive.epa.gov/water/archive/web/html/basicinformation-2.html>.
- [9] Connecticut Department of Public Health Environmental Health Section Radon Program. (2015, October). Radon in Your Well Water. Retrieved from http://www.ct.gov/dph/lib/dph/environmental_health/radon/pdf/Radon_in_Your_Water.pdf



Estimation of Attenuation Coefficient of Solar Radiation in the Atmosphere of Thailand

Sayan Phokate

Applied Physics, Faculty of Engineering, Khon Kaen Campus, Rajamangala University of Technology Isan,
Khon Kaen, 40000, Thailand
e-mail : syphokate@hotmail.com

Abstract— The estimation of the attenuation coefficient of solar radiation in the atmosphere were used solar radiation data on a cloudless day. The data were collected from four measuring stations located in Chiang Mai, Ubon Ratchathani, Bangkok, and Songkhla during the years 2011-2015. Then, the relationship between the attenuation coefficient from solar radiation data and the surface data (air temperature, relative humidity and visibility data) in a mathematical model was investigated in this paper. The result showed that the relationship had a relatively high level of reliability. The attenuation coefficient was nearly equal to the value from the model. The attenuation coefficient from 85 meteorological stations across the country was calculated from the model. The result showed that seasonal change of the attenuation coefficient was high in the dry season and low in the rainy season.

Keywords— attenuation coefficient; visibility data; cloudless sky; solar radiation

I. INTRODUCTION

The attenuation is the reduction of the intensity of the solar radiation as it passes through the atmosphere to the Earth due to the composition of the atmosphere. The atmosphere of the Earth composes air molecules, water vapor, aerosols and clouds. Generally, the amount properties and distribution of atmospheric composition also depends on the area and time of year [1]. When extraterrestrial radiation propagates through the atmosphere, it is absorbed and scattered by the atmospheric constituents. Solar radiation reaching the surface is energy sources both directly and indirectly of creatures of all kinds in the world. It also influences the environment of the world [2,3]. The composition of the atmosphere play an important role both directly and indirectly by absorption and scattering which is the key in making the solar radiation that reaches the Earth's surface decreases [4,5]. For cloudless sky, the attenuation depends mainly on a relative air mass of the atmosphere. It is defined as the actual air mass through which the radiation propagates and the air mass in the direction perpendicular to the earth surface. In addition, the data of

solar radiation attenuation due to absorption and scattering in the atmosphere also need to use in the field of remote sensing using satellite. For example, finding the distribution of the solar radiation at the Earth's surface from satellite images [6]. That is, the satellite will receive solar radiation reflected from the Earth's surface and atmosphere including various elements of the atmosphere with aerosols. We need to know the amount of solar radiation that is absorbed and scattered by the composition of the atmosphere, it can calculate the radiation to enter the Earth's surface [7,8].

Generally, global solar radiation is of economic importance as renewable energy alternatives. It has being studied due to its importance in providing energy for Earth's climatic system. The successful design and effective utilization of solar energy systems and devices for application in various facets of human needs depend on the availability of information on solar radiation characteristic of the location in which the system and are to be situated. The data of solar radiation is the basis of the solar energy. This is because the need to design and evaluate the performance of the solar system. Such as electricity with solar cells, solar water heating system and solar drying, etc.[9]. Furthermore, such information also is critical to the conservation of energy such as calculating the heat transfer from the exterior to the building and computation load of the air conditioning [10]. In Thailand, despite the solar radiation data for more than 40 years but there is also a limited number of stations. Including the high cost of measurement and data collection. Solar radiation monitoring stations are mostly located in the capital. Therefore, to reduce costs and meet the policies of the government, which wants to increase the proportion of renewable energy in the country. By accelerating the development and application of renewable energy, especially solar energy. Order to obtain statistically reliable data for illustrative finding renewable energy in the future. Including, study the performance of solar radiation devices at a particular location before their installation and used in climate modeling and pollution studies [11]. Therefore requires techniques to calculate the solar radiation to provide a complete and up to date use in research development and application of solar energy efficiently anyway. In this research, the objective is to find a mathematical model in order to estimation of attenuation coefficient of solar radiation from



surface data. Which would be useful to study and analyze the solar system next.

II. MATERIALS AND METHODS

This study, the data at four meteorological monitoring stations, namely Chiang Mai, Ubonratchathani, Bangkok and Songkla during the years 2011-2015 were used. Finding a attenuation coefficient of solar radiation required solar radiation on a cloudless sky. A selection of the data that corresponds to clear sky conditions is applied for that reason. This criterion consists to choose data where the cloud data on the same day were used which must contain at less than 1 part of the sky 10 parts [12]. The attenuation of light through a medium is proportional to the distance traversed in the medium and to the local flux of radiation. This simple law applies in most instances, whether the energy is absorbed or scattered. The transmittance is given by the following [13].

$$\tau = \frac{H}{H_0} = \exp(-\delta_{att} m_r) \quad (1)$$

where H is the daily global solar radiation on the surface of the earth at a given location (W/m^2), H_0 is the extraterrestrial daily radiation (W/m^2), δ_{att} is the attenuation coefficient, m_r is the relative optical air mass, and τ is the daily total atmospheric transmittance to solar radiation. It is often assumed that the transmittances are multiplicative for a cloudless day, such that we can write.

$$\tau = \tau_r \tau_g \tau_o \tau_w \tau_a \quad (2)$$

The transmittances by Rayleigh scattering (τ_r), ozone (τ_o), uniformly mixed gases (τ_g), water vapor (τ_w) and aerosols (τ_a) are given by the parametric model C by Iqbal [13]. The transmittances τ_r and τ_g depend on air mass only. The transmittance τ_o needs information on ozone content, which may be calculated from location and time. The transmittance by water vapor τ_w uses air mass and precipitable water vapor content as inputs [14].

The attenuation coefficient calculated from the measurements of solar radiation only, which are limited for Thailand. Therefore, the values of δ_{att} correlated with relative humidity, air temperature, and visibility data from the same station. Which will have a relationship in empirical equation for the calculation δ_{att} of the stations without measuring the solar radiation.

III. RESULTS AND DISCUSSION

Use the data in a clear day were calculated the attenuation coefficient. Because finding the δ_{att} by the above methods do only for points the measured solar radiation. When such measurements are not available, the δ_{att} may be determined from surface data. The empirical model that shows the

correlation between the attenuation coefficient with the air temperature, relative humidity and visibility data. A best-fitted equation representing this relation was established as follow.

$$\delta_{att} = 0.21879 + 0.008171T + 0.002205RH - 0.02249V_{vis} \quad (3)$$

where δ_{att} is the attenuation coefficient (dimensionless), T is air temperature ($^{\circ}C$), RH is relative humidity (%) and V_{vis} is the visibility data (km).

The attenuation coefficient was found to be strongly correlated with air temperature, relative humidity and visibility data. The correlation coefficient (R^2) was 0.83. The results obtained from the solar radiation were compared with the model. It uses data on cloudless days. Found that, the difference in the root mean square error (RMSE) was equal to 0.0177, and the mean bias error (MBE) was 0.0024. The findings were presented shown in Figure 1.

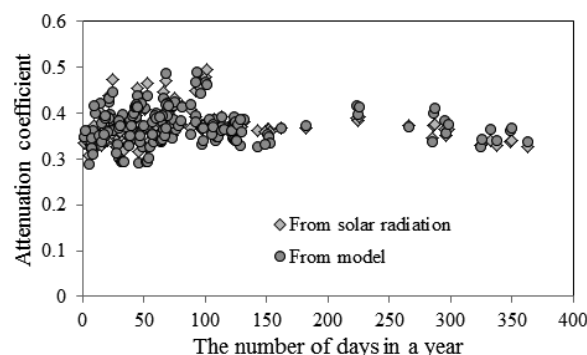


Fig. 1. The value of attenuation coefficient form the solar radiation compared with the model using a cloudless day during 2011-2015 of the four stations.

The average data between 2011-2015 of 85 stations nationwide were used to calculate the attenuation coefficient from the model. Found that, the maximum was equal to 0.522 in March and minimum was equal to 0.307 in December. That is, the attenuation coefficient of solar radiation during February to April and during September to November are very valuable, which the most average in March equal to 0.432 ± 0.034 . Because of, the atmosphere has a storm blew through. There are a lot of dust in the atmosphere. In mid-October, 1-2 weeks is a seasonal change from the rainy season to the winter weather is unpredictable. During the rainy season (May to September) is less by the lowest average in June equal to 0.395 ± 0.033 . The rain will help remove dust in the air, the δ_{att} value has decreased. The annual average was 0.410 ± 0.034 . Consistent with Esposito et al. [1] and Utrillas et al. [15] found that the attenuation of solar radiation is less in the rainy season and very valuable in the dry season, with an average during the 0.02 to 0.6. Which is constantly changing



according to season and geography. The relationship of the δ_{att} with time of the year is shown in Figure 2.

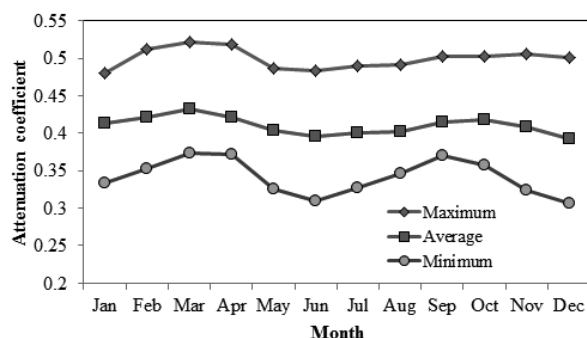


Fig. 2. Variation of the attenuation coefficient by the time of the year using average monthly of 85 stations nationwide during the years 2011-2015.

IV. CONCLUSIONS

Estimation of the attenuation coefficient of solar radiation in the atmosphere is based on the radiation intensity data on a clear day. Because radiation intensity data is limited. Therefore, the relationship between attenuation coefficient and surface data is used in mathematical models for use in areas where radiation is not available. The research found that, the attenuation coefficient is correlated with air temperature, relative humidity, and visibility data. The correlation coefficient (R^2) is 0.83. The attenuation coefficient of solar radiation has changed the time of year. There is high value in March and October. It is low in June. The attenuation coefficient is less in the rainy season and high value in the dry season with the average annual equal to 0.410 ± 0.034 .

ACKNOWLEDGMENT

The researchers would like to thank Rajamangala University of Technology Isan for supporting the research. The Meteorological Department for providing valuable information on the research was also acknowledged.

REFERENCES

- [1] Esposito, F., Leone, L., Pavese, G., Resteiri, R., and Serio, C. Seasonal variation of aerosols properties in South Italy: a study on aerosol optical depths, Angstrom turbidity parameters and aerosol size distributions. *Atmospheric Environment*. Vol.38, pp1605-1614, 2004.
- [2] Boland, J., McArthur, L.C., and Luther, M. Modeling the diffuse fraction of global solar radiation on a horizontal surface. *Environmetrics*. Vol.12, pp.103-116, 2001.
- [3] Wan Nik, W.B., Ibrahim, M.Z., Samo, K.B., and Muzathik, A.M. Monthly mean hourly global solar radiation estimation. *Solar Energy*. Vol.86, pp. 379-387, 2012.
- [4] Nunez, M. The development of a satellite-based insulation model for the Tropical Pacific Ocean. *Journal of Climatology*. Vol.13, pp. 607- 627, 1993.

- [5] Belcher, B.N., and DeGaetano, A.T. A revised empirical model to estimate solar radiation using automated surface water observations. *Solar Energy*. Vol.81, pp. 329-345, 2007.
- [6] Janjai, S., Laksanaboonsong, J., and Thongsathiy, A. Development of a method for generating operational solar radiation maps from satellite data for a tropical environment. *Solar energy*. Vol.78, pp. 739-751, 2005.
- [7] Brineand, D.T., and Iqbal, M., Diffuse and Global solar spectral irradiance under cloudless skies. *Solar Energy*. Vol.30, 447-456, 1983.
- [8] Martinez-Lozano, J.A., Utrillas, M.P., Tena, F., and Cachorro, V.E. The parameterization of the atmospheric aerosol optical depth using the angstrom power law. *Solar Energy*. Vol.63, pp. 303-311, 1998.
- [9] Janjai, S., and Keawprasert, T. Design and performance of a solar tunnel dryer with a polycarbonate cover. *International Energy Journal*. Vol.7, pp.187-194, 2006.
- [10] Wiginton, L.K., Nguyen, H.T., and Pearce, J. M. Quantifying rooftop solar photovoltaic potential for regional renewable energy policy, *Computers. Journal Environment and Urban Systems*. Vol.34, 345-357, 2010.
- [11] Trabelsi, A., and Masmoudi, M. An Investigation of Atmospheric Turbidity over Kerkennah Island in Tunisia. *Atmospheric Research*. Vol.101, pp. 22 – 30, 2011.
- [12] Ineichen, P. Comparison of eight clear sky broadband models against 16 independent data banks. *Solar Energy*. Vol.80, pp. 468–478, 2006.
- [13] Iqbal, M. *An Introduction to Solar Radiation*. New York: Academic Press, 1983.
- [14] Phokate, S. Calculation of solar radiation absorption from precipitable water vapor in the atmosphere of Thailand. *Burapha science Journal*. Vol.16, pp. 77-83, 2011. (in Thai)
- [15] Utrillas, M.P., Martinaz-Lozano, J.A., Cachorro, V.E., and Tena, F. Comparison of aerosol optical thickness retrieval from spectroradiometer measurement and from two radiative transfer model. *Solar Energy*. Vol.68, pp. 197-205, 2000.



Feasibility on the Utilization of Agricultural Unused Banana Trees as the Feedstock for the Ethanol Fermentation

Natthanicha Sukasem¹ and Pawinee Phetnok²

^{1,2} School of Renewable energy, Maejo University, Chiang Mai, 50290, Thailand

¹ Corresponding author: E-mail; jewy.ja@gmail.com

Abstract— Unused banana trees are the agricultural wastes that have a potential feedstock for the bioethanol production. Because of the ethanol is friendly energy which does not release the toxic pollutants to the environment, thus, the ethanol is used in various applications especially in the car transportation or even in the electricity generation by fuel cell technology. The research was to improve the efficiency of ethanol production by using unused banana trees as material. The unused banana trees were physically treated by chopping and grinding, then followed by the 2 steps of acid/base chemical pretreatment at 100°C for 3 hours and finally hydrolyzed by cellulase from *Trichoderma reesei* at pH 4.8 and 42°C. The HCl and H₂SO₄ were added into the pretreatment mixture reach the concentration of 2-4%(v/v) as final concentration. The HCl treatment produces the highest total sugar at 16.89 g/ g plant including with amounts of xylose and glucose at 2.37g/g plant and 2.29 g/g plant. Remarkably, the HCl is strong acid same property as the NaOH is strong base consequently release the highest amount of total sugar at 6.01 g/g plant. The 2 steps of chemical pretreatment dramatically increase the proportion of cellulose from original content at 26.96% to 66.9%. In the other hand, the hemicellulose contents were reduced from 24.69% to 0.5%. The ethanol fermentation using the separated hydrolysis and fermentation (SHF) technology was done after the cellulase digestion by the ethanol yeast *Saccharomyces cerevisiae* at 37°C under anaerobic condition. The maximum of ethanol concentration in only glucose control condition was at 9.33% (v/v) whereas in the hydrolyzed sugar with the addition of glucose showed the highest ethanol concentration at 8% (v/v). In finally, the results establish the pretreatment technology for unused banana trees that can be applied for other lignocellulosic materials in the future.

Keywords—Unused banana trees; Lignocellulosic materials; Chemical pretreatment; Cellulase digestion; Bioethanol

I. INTRODUCTION

Nowadays, the populations around the global world have been increasing in every day. The development of technology requires making our daily life comfortable and convenient. Since the energy is significantly important for the life quality, the demand of energy excesses but, on another hand, the energy sources and the production have been limited [1]. Therefore, the looking for new sources especially the renewable energy should be considering priority. The bioethanol is the renewable energy that it possible uses instead

of fossil oil. The ethanol is not only a renewable energy but it also is a green energy which does not produce the pollutants to make environmental pollution [2].

The bioethanol can produce from the 3 mainly material groups which are sugar, starch, and lignocellulosic material. The yeast *Saccharomyces cerevisiae* is the ethanol yeast that produces the high ethanol concentration and directly uses sugars such as glucose and sucrose, without the pretreatment technology. On another way, the starch and lignocellulose require the pretreatment technology to release the high glucose concentration for fermentation by the ethanol yeast [3]. Therefore, the banana trees which are the low cost lignocellulosic material widely found in almost area of Thailand, the banana tree requires the physical, chemical and enzymatic pretreatment for breaking down the large polymer such as lignocellulose into mainly the small monomeric sugars such as glucose and xylose [4].

The two steps of acid/alkaline pretreatment are critical step to destroy the chemical bonding among the cellulose, hemicellulose, and lignin [5]. Under the acid condition, the pretreatment removes the lignin and the some part of hemicellulose. The breakdown of hemicellulose releases the xylose, arabinose, rhamnose, for examples [6]. The HCl and H₂SO₄ acid are general widely used because they have the high strength of acid that exhibits the high degrees of saccharification. In this step, the most of lignin and hemicellulose removes from their structure which the proportion of cellulose increases [7]. The alkaline solution, NaOH and other bases, decreases the degrees of cellulose crystallization making their structures swollen. The enzymatic digestion of cellulose need one or more enzyme to cleave the beta- 1,4 glycosidic bond in cellulose to short polymers or glucose [8]. The efficiency of the binding among cellulase enzyme and its cellulose substrates due to the potential of integration of cellulase get through inside the cellulose structure. If the degree of crystallization is decreased. It is meant that the cellulose dramatically changes to swollen structure [9].



The goal of this study was to improve the unused banana trees which are the low cost and high yield agricultural wastes to be the potential feedstock for the bioethanol production.

II. MATERIALS AND METHODS

The overall steps of ethanol production from unused banana trees were shown in figure 1. All processes consisted of plant physically preparation, the 2 steps of chemical pretreatments, cellulase enzymatic digestion and finally the ethanol fermentation.

A. Raw material collection and preparation

The fresh unused banana tree wastes were collected in Chiang Mai province, Thailand, at longitude and latitude cc. The fresh banana trees were cut and grinded as the physical treated into small pieces in range between 0.5 to 1 cm long and 1 cm wide. Then, the grinded plants were heated until them dried to remove the moisture inside the plants. To know the lignocellulosic composition, the analysis of cellulose and hemicellulose necessary required by following the analytical methods of Ververis et al. [10]

B. The two steps of acid/alkaline pretreatments

There were 2 steps in these pretreatments. The acid pretreatments using 2-4%(v/v) of HCl and H₂SO₄ were the first step and then, continuing with 2-4%(w/v) of NaOH and Ca(OH)₂ as alkaline pretreatments were the second step. Both 2 steps were achieved at the 1:10 ratio of banana (g): treated solution (ml), heating up to 100°C by the hot air oven for 3 hr. To separate the solid treated bananas from the suspension, the Watman no.1 filter paper was used for this separation. The treated bananas were dried again and let them to analyze the cellulose and hemicellulose whereas the liquid samples were measured the total sugar by using total phenol sulfuric method [11], the reducing sugar by Somogi-Nelson method [12], and the glucose and xylose by simultaneous direct estimation of glucose and xylose in serum method [13].

C. The cellulase enzymatic digestion

The enzymatic digestion was the final step of banana pretreatment before into the step of bioethanol fermentation. The 6 g of acid/alkaline treated bananas were soaked in 100 ml of 0.05 M sodium citrate buffer (pH 4.8). The hydrolysis by using cellulase required the enzyme activity at 24 FPU/g dried plant. The cellulase solution was incubated at 42°C, 200 rpm until the hydrolysis absolutely completed. During the hydrolysis, the samples were taken at every 4 hr to determine the total sugar concentration [14].

D. Scanning electron microscope (SEM) analysis

The surface area analysis of the original and all solid treated samples were observed by using the SEM technique to identify the effects of pretreated against banana lignocellulosic structure.

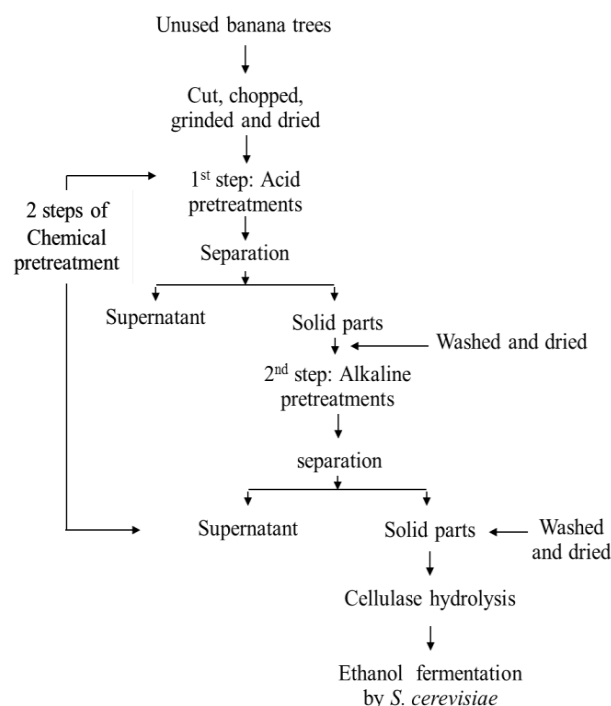


Fig 1. Overall steps of ethanol production from unused banana trees

E. Bioethanol fermentation

1. Inoculum preparation of ethanol yeast *S. cerevisiae*

The 0.1 g of the powder ethanol yeast was cultivated in 100 ml of the YM broth at 200 rpm, 37°C for overnight. Then, 1 ml of inoculum was grown again in 100 ml of YM broth at same condition until the absorbance of culture reached to 0.5. These yeast culture were used for the starter of bioethanol fermentation.

2. Bioethanol fermentation by *S. cerevisiae*

The sugar solutions from the pretreatment steps were used as carbon source for the bioethanol fermentation. These were (1) the sugar solution from enzymatic digestion, (2) the sugar solution from enzymatic digestion with the pure glucose addition to 200g/L, (3) the pure glucose at its concentration same as the enzymatic sugar solution, (4) the concentration of pure glucose at 200 g/l in final concentration.

The ethanol fermentation broth was prepared including with 6 g/l of yeast extract, 5 g/l of peptone, 2 g/l of (NH₄)₂SO₄, 2 g/l of KH₂PO₄, and 1 g/l of MgSO₄·7H₂O in final concentration. The pH value at 5.5 was adjusted by using diluted the NaOH and HCl acid solution. The stabilization at 121°C, 1.5 psi for 20 min required to eliminate the contamination of the unwanted microorganism. In the fermentation step, the 5 ml of yeast *S. cerevisiae* starter grown in the ethanol fermentation at 37°C under anaerobic condition. Moreover, the efficiency of fermentation was observed and analyzed in terms of (1) the reduction of sugar concentration,



(2) the increment of ethanol fermentation, (3) the ethanol yield, and (4) the percentage of theoretical ethanol yield

III. RESULTS AND DISCUSSION

A. Identification the optimum acid solution for unused banana tree pretreatment.

The improvement of potential banana feedstock is not only require the physical pretreatment but the 2 steps of chemical pretreatment and enzymatic digestion are also necessary steps to produce the high concentration of glucose in the finally (Fig. 2). Firstly, the HCl and H₂SO₄ pretreatment directly remove the lignin and hemicellulose out of the lignocellulosic banana structure to produce the short polymer of polysaccharide and monomeric sugar such as xylose from the hemicellulose [15]. Moreover, the both acid solution also degrade the cellulose into glucose. Thus, in the treated solution, the xylose and glucose are found. The results in this study are similar to previous research. The corn stoves were treated with the dilute HCl solution recover the high yield of xylose and glucose at 81.0% and 64.0%, respectively. [16] Moreover, on the other pretreatment, the corn stoves were also treated by using HCl solution, the amounts of xylose and glucose were found at 97.0% and 78.0%, respectively [17]. According the removal of hemicellulose and lignin, the proportion of cellulose in their structures dramatically increases higher than the untreated original banana tree. So, to compare with the untreated banana, the higher cellulose contents at 2.5 folds from the both acid pretreatments are obtained.

However, on the acid pretreatment of elephant grass, the treatment reduces the hemicellulose and lignin components from the original, hemicellulose and lignin at 20.9%, 19.4% to 13.5%, 13.4% whereas the amount of cellulose increase from 22.6% to 24.0% [18]. Regard to the identify the suitable reagent type and concentration between the HCl and H₂SO₄ solution, because of the HCl is the stronger acid than H₂SO₄ consequence to the HCl pretreatment releases the high concentration of total sugar, xylose and glucose [19]. The increment of sugar concentration relates to the reduction of hemicellulose.

Due to the effect of different acid concentration, the increment of H₂SO₄ and HCl from 2-4% (v/v) lead to the total sugar concentration, glucose and xylose also increase, especially in the HCl pretreatment release the 1.2 folds of higher total sugar concentration when compare to the H₂SO₄ pretreatment. The other researches shows that the HCl concentration at 0.5 – 5.0% (v/v) release the highest yields of xylose and glucose at 63.38 g/L and 14.57 g/L [20] when compare to the pretreatment by using H₂SO₄ and HNO₃ solution [20]. The acid pretreatment does not only generate the high concentration of xylose and glucose but the treatment also releases the high concentration of reducing sugar (0.611 g/g). The advantages of acid pretreatment are that the acid pretreatment removes the hemicelluloses out of the fraction of

the lignocellulosic biomass which increasing the xylose concentration in liquid fraction and the treatment also accelerates the swollen structure of cellulose that makes the cellulose structure is better accessible by the enzymes [21]. In addition, the glucan also is recovered at 66.28% [22] or at 64.58% glucan. These results depend on the types and concentrations of acid solution [23]. In finally, in this condition, at 4% (v/v) of HCl solution is the compromised pretreatment for the unused banana trees

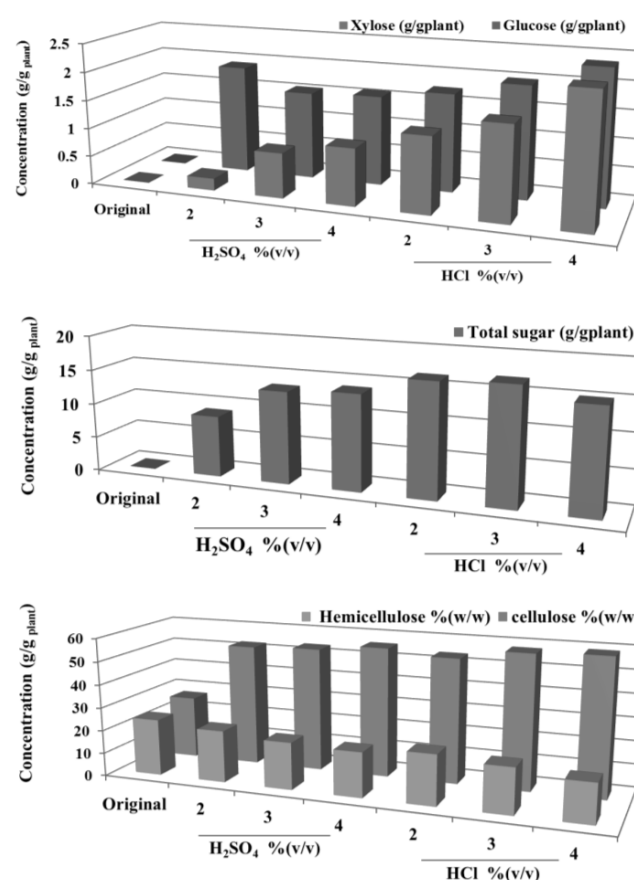


Fig 2. The effect of H₂SO₄ and HCL pretreatment against the alteration of sugars concentration and lignocellulosic components

B. Identification the optimum alkaline solution for unused banana trees pretreatment.

The second step of chemical pretreatment was the alkaline pretreatment using the NaOH and Ca(OH)₂ concentration of 2 to 4% (w/v). Because of NaOH is stronger base than Ca(OH)₂ [24], the experiment results show the same relationship as the acid pretreatment (Fig. 3)



Therefore, the NaOH breakdown the hemicellulose and release the total sugar at higher concentration than $\text{Ca}(\text{OH})_2$. Thus, the amount of hemicellulose dramatically down to nearly low concentration estimates about 0.4% by pretreating with both alkaline solutions at 4% (w/v). The NaOH pretreatment gives the high efficiency on plant pretreatment. This results is similar to the Napier grass hydrolysis using NaOH, $\text{Ca}(\text{OH})_2$, NH_3 and H_2O . These alkaline solutions alter in the crystallization of cellulose and lead to release the sugar at high concentration. Thus, after the enzymatic hydrolysis, the treated Napier grass by NaOH produces 94% of glucan whereas $\text{Ca}(\text{OH})_2$, NH_3 and H_2O treatment release the glucan concentration at 60%, 51% and 42%, respectively [25]. Because of NaOH is stronger base than $\text{Ca}(\text{OH})_2$, the pH condition during the pretreatment by NaOH is higher than $\text{Ca}(\text{OH})_2$. This lead to indicate that NaOH solution has a high effective on the lignin removal in pretreatment by using autoclave at 121°C. The lignin was removed estimate about 29.6% [26].

In general, the important rule of NaOH pretreatment is the reduction of crystallization degree of cellulose and alters the cellulose structure into the high swollen structure [27]. The swollen structure permits the cellulase pass through their inner structure easily to digest the cellulose into high concentration of glucose in finally [28].

C. The efficiency of sugar production from the cellulase enzymatic digestion

Figure 6 Illustrates the determination of glucose production by using the cellulase digestion. The highest concentration of glucose is estimated at 48.14 g/l or 8.024 g/g_{plant}. This glucose concentration does not high enough for the bioethanol fermentation therefore in the fermentation; the extra sugar is added to 200 g/l in final concentration. However, the hydrolyzed sugar concentration (48.14 g/l, 8.024 g/g_{plant}) shows the higher concentration when compare to previous study which the concentration of hydrolyzed sugar from rice straw is 0.718 g/g_{plant} by using *T.reesei* cellulose [29].

D. The efficiency of the bioethanol fermentaion by using the separate hydrolysis and fermentation (SHF) technology

The SHF bioethanol fermentation using the different hydrolyzed glucose concentration from banana was done by using the *S.cerevisiae* (Figure 7). The yeast *S.cerevisiae* uses the hydrolyzed glucose from unused banana trees as well as the pure added glucose. The figure 7 shows that the high sugar consumption by yeast lead to the high concentration of ethanol approximately at 8.2 % (v/v). So, the experiment confirms that the unused banana trees have the potential feedstock material for the ethanol fermentation

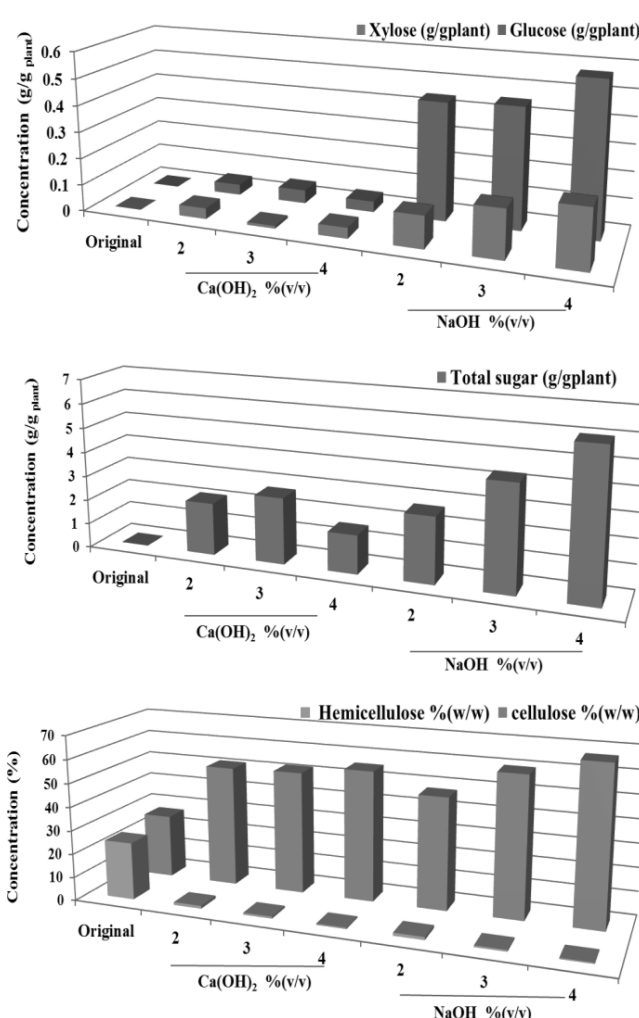


Fig 3. The effect of NaOH and $\text{Ca}(\text{OH})_2$ pretreatment against the alteration of sugars concentration and lignocellulosic components.

E. The economic pay back

The cost of ethanol production was analyzed by calculating from the chemical price and the electricity. During the ethanol production, the cost of the pretreatment was at 558.21 Bath/L_{ethanol} and the fermentation was 51.18 Bath/L_{ethanol}.

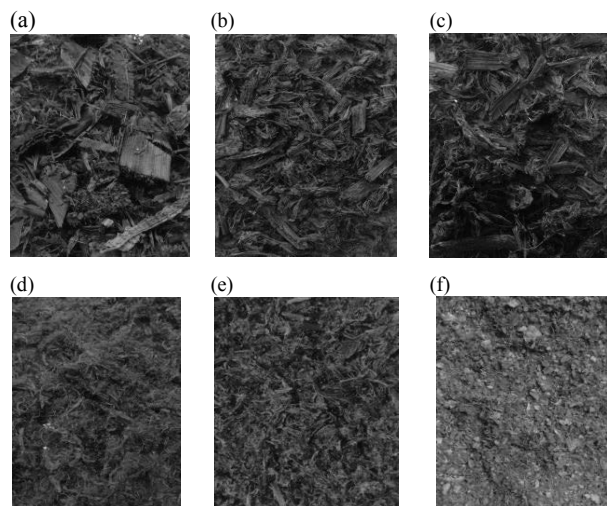


Fig 4. The morphology of unused banana trees after the 2 steps of chemical pretreatment and cellulase hydrolysis.: a) Original, b) 4% (v/v) HCl, c) 4% (v/v) H₂SO₄, d) 4% (v/v) NaOH, e) 4% (v/v) Ca(OH)₂, and f) Cellulase digestion

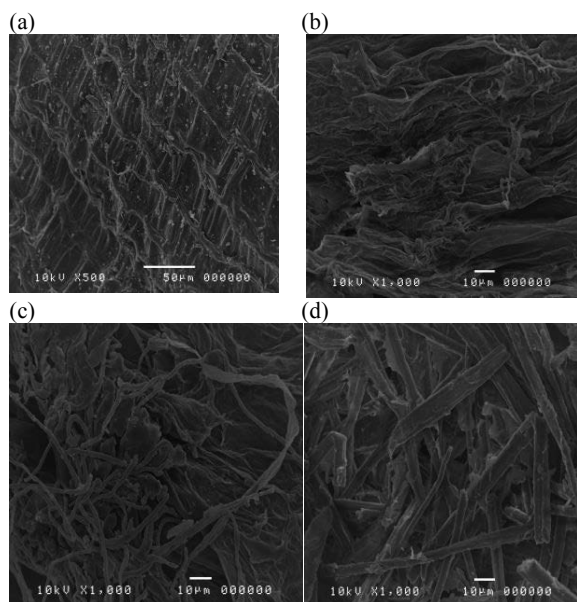


Fig 5. The SEM analysis of pretreated unused banana trees at selected condition: a) Original unused banana trees, b) 4% (v/v) of HCl, c) 4% (w/v) of NaOH, and d) Cellulase digestion.

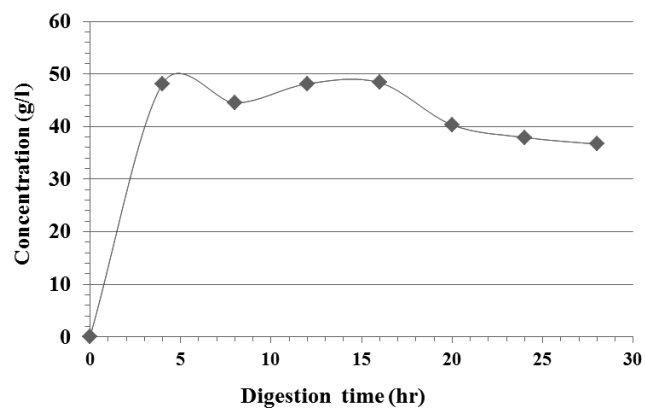


Fig 6. Cellulase digestion of 2 steps treated unused banana trees

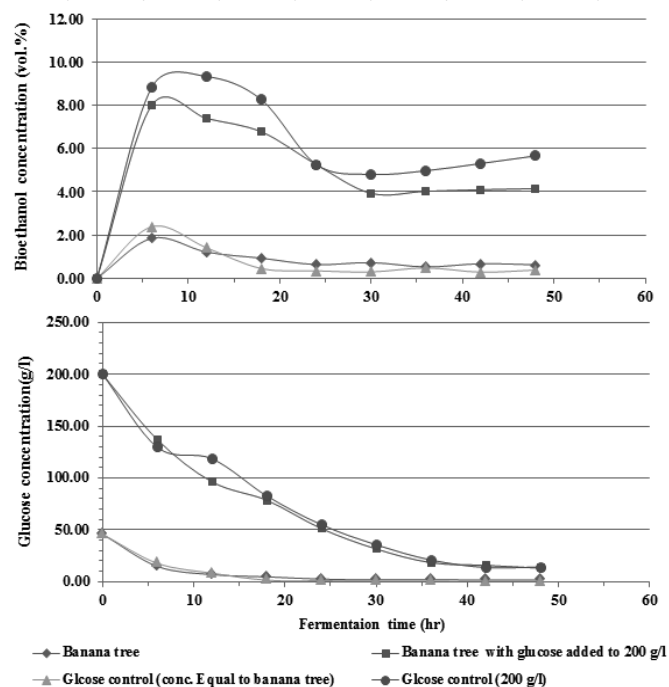


Fig 7. Ethanol and glucose concentration during the bioethanol fermentation using the hydrolyzed glucose with/without the addition of glucose

IV. CONCLUSION

The unused banana trees which are the agricultural wastes that have the potential feedstock for bioethanol production. The 2 steps of chemical pretreatment and cellulase hydrolysis of banana tree removes lignin and hemicellulose out of their structures and also produces the high glucose concentration. However, in the fermentation needs the addition of glucose up to 200 g/l as working concentration. The hydrolyzed glucose



can be used instead of extraordinary added glucose approximate at ¼ of total concentration. Since the efficiency of ethanol fermentation also depends on the original sugar concentration, the pretreatment technology including both of the chemical pretreatment and cellulase digestion have to be developed to remove the large amounts of lignin and hemicellulose and also produce the high glucose concentration under the low cost of the ethanol production. Thus, the pretreatments both chemical and enzyme techniques suitable for each agricultural plant should be the first priority considered sequence to the high efficiency of ethanol fermentation in the future.

ACKNOWLEDGMENT

I would like to thank you the National Research Council of Thailand for Look Kai funding research for all supports. Moreover, I also thank you to my School of Renewable Energy and Maejo University, Thailand for supporting all facilities. I would like to thank you my colleagues to help me everything until the research successes.

REFERENTS

- [1] L.A. Tiago, M.C. Antonio and J.A. Fuinhas, "Strategies to make renewable energy sources compatible with economic growth," *Energy Strategy*, vol 18, 2017, pp. 121-126.
- [2] K. Santosh, S. Neetu and P. Ram, "Anhydrous ethanol: A renewable source of energy," *Renewable and Sustainable Energy Reviews*, vol 14, 2010, pp. 1830-1844.
- [3] C. Hongyan, L. Jinbao, C. Xing, C. Daming, X. Yuan, Ping, L. Hualin Lin and H. Sheng, "A review on the pretreatment of lignocellulose for high-value chemicals," *Fuel Processing Technology*, vol 160, 2017, pp. 196-206.
- [4] B.G. Ana., B. Ignacio and B. Mercedes, "The potential of agricultural banana waste for bioethanol production," *Fuel*, vol. 213, pp. 176-185.
- [5] C. Laura, B.R. Maria, G. Mairan, D.F. Mario and L. Claudia. "Evaluation of dilute acid and alkaline pretreatments, enzymatic hydrolysis and fermentation of napiergrass for fuel ethanol production," *biomass and bioenergy*, vol. 74, 2015, pp. 193-201.
- [6] Y. Suryanarayana and S. Yogendra, "Optimal control of dilute acid pretreatment and enzymatic hydrolysis for processing lignocellulosic feedstock," *Journal of Process Control*, vol. 56, 2017, pp. 100-111.
- [7] S. Nipat, N. Sunee and K. Suttipun, "Evaluation of dilute acid pretreatment for bioethanol fermentation from sugarcane bagasse pith," *Agriculture and Natural Resources*, 2018, pp. 1-8.
- [8] M.C. Danila., H.Q. José and L.C. Jorge, "Assessment of alkaline pretreatment for the production of bioethanol from eucalyptus, sugarcane bagasse and sugarcane straw," *Industrial Crops and Products*, vol 94, 2016, 932-941.
- [9] R.M. Javier, M.B. Claudio, P.C. Yolanda, M.R.S. Francisco and D.G. Bruno, "Additives enhancing enzymatic hydrolysis of lignocellulosic biomass," *Bioresource Technology*, vol. 244, 2017, pp. 48-56.
- [10] C. Ververis, K. Georgiou, D. Danielidis, D.G. Hatzinikolaou, R. Santas and V. Corleti, "Cellulose hemicelluloses, lignin and ash content of some organic materials and their suitability for use as paper pulp supplements," *Bioresource Technology*, vol. 98, 2007, pp. 296-30.
- [11] M. Dubois et al, "Colorimetric method for determination of sugars and related substances," *Anal. Chem.*, vol 28 (3), pp. 350-356.
- [12] N. Nelson, "A photometric adaptation of the somogyi method for the determination of glucose," *Journal of Biological Chemistry*, vol. 153, pp. 375-380.
- [13] F. Jesse and Goodwin, "Method for simultaneous direct estimation of glucose and xylose in serum," *Clinical Chemistry*, vol. 6(2). 1968.
- [14] P. Pawinee and S. Natthanicha, "Effect of chemical pre-treatments and enzymatic hydrolysis against sugar production and ethanol fermentation from maize straws" 13th International Conference on Ecomaterial, November 19-23, 2017.
- [15] L. Huiling, D. Qingqing, R. Junli, J. Longfei, P. Feng, S. Runcang and L. Guoliang, "Effect of structural characteristics of corn cob hemicelluloses fractionated by graded ethanol precipitation on furfural production," *Carbohydrate Polymers*, vol. 136, 2016, 203-209.
- [16] L. Qiyu, L. Wenzhi, M. Qiaozhi, A. Shengxin, L. Minghao, J. Hasan, H. Chang, "Pretreatment of corn stover for sugar production using a two-stage dilute acid followed by wet-milling pretreatment process," *Bioresource Technology*, vol. 211, 2016, pp. 435-442.
- [17] Z. Shuai, Z.L. Wen, Z. Mingjian, L. Zihong, Z. Wang, J. Hasan, C. Hou-min, "Pretreatment of corn stover for sugar production using dilute hydrochloric acid followed by lime," *Bioresource Technology*, vol. 152, 2014, pp. 364-370.
- [18] E. Cardona, J. Rios, J. Penna and L. Rios, "Effects of the pretreatment method on enzymatic hydrolysis and ethanol fermentability of the cellulosic fraction from elephant grass," *Fuel*, vol. 118, 2014, pp. 41-47.
- [19] N.D. Narendra, V.V. Dasu, V.V. Goud and P. S. Rao "Development of dilute sulfuric acid pretreatment method for the enhancement of xylose fermentability," *Biocatalysis and Agricultural Biotechnology*, vol. 11, 2017, pp. 224-230.
- [20] M. Presanthan, E.B. Gueguim, "Comparative study of three optimized acid-based pretreatments for sugar recovery from sugarcane leaf waste: A sustainable feedstock for biohydrogen production," *Engineering Science and Technology, an International journal*, vol. 21, 2018, pp. 107-116.
- [21] P. Binod, K.U. Janu, R. Sindhu and A. Pandey. "Hydrolysis of lignocellulosic biomass for bioethanol production," *Biofuels: Alternative Feedstocks and Conversion Processes*, 2010, pp. 229-250.
- [22] L.S. Felipe, Q. M. Patricial, H.C.G. Pedro, B. M. Ranieri, C.P. Fernando, S. Wanderley, S.A. Celso, B. Michel, "Acid, alkali and peroxide pretreatments increase the cellulose accessibility and glucose yield of banana pseudostem," *Industrial Crop and Products*, vol 115, 2018, 62-68.
- [23] Li, K. Li, S. Fu, H. Zhan, Y. Zhan and L. Lucia, "Analysis of the chemical composition and morphological structure of banana pseudostem," *Bio Resources*, vol. 5, 2010, pp. 576-585.
- [24] Y. Zhipei, L. Jihong, C. Sandra, C. Ting, J. Yan, Y. Menghui, Z. Lei, Z. Gang, Q. Panlun and L. Shizhong, "Lignin relocation contributed to the alkaline pretreatment efficiency of sweet sorghum bagasse," *Fuel*, vol 158, 2015, pp. 152-158.
- [25] P. Paripok, S. Kazuo and R. Khanok, "Structural changes and enzymatic response of Napier grass (*Pennisetum purpureum*) stem induced by alkaline pretreatment," *Bioresource Technology*, vol. 218, 2018, pp. 247-256.
- [26] J. Xu and J.J. Cheng, "Pretreatment of switchgrass for sugar production with the combination of sodium hydroxide and lime," *Bioresour. Technol*, vol. 102 (4), 2011, pp. 3861-3868.
- [27] A. Safaria, K. Keikhosro and S. Marzieh, "Dilute alkali pretreatment of softwood pine: A biorefinery approach," *Bioresource Technology*, vol. 234, pp. 67-76.
- [28] Leena P. K.K. Devendra and P. Ashok, "Evaluation of hydrotropic pretreatment on lignocellulosic biomass," *Bioresource Technology*, vol. 213, 2016, pp. 350-358.
- [29] C. Arisara and S. Natthanicha, "Pretreatment of rice straw with acid and alkaline for ethanol production by *Saccharomyces cerevisiae*," 13th Conference On Energy Network of Thailand (E-NETT), pp. 1191-1198,



Enhancement of Hydrogen Production under Alkaline Condition using Various Electrode Materials and Shape Types

Pattarachai Noppakun¹, Jirawat Leaksantad², and Natthanicha Sukasem³
^{1,2,3} School of Renewable Energy, Maejo University, Chiang Mai, 50290, Thailand

E-mail; ¹nonnoppkun@outlook.co.th, ²Oksantad@gmail.com

Corresponding author: E-mail; ³jewy.ja@gmail.com

Abstract—Hydrogen is source of green energy that can be generated by the electrolysis of water. Hydrogen can be used in various applications because it is friendly to the environment. In this study, the hydrogen system was connected with the hydrogen fuel cell to obtain the performance of hydrogen production system. The efficiency of hydrogen production under the 0.5 molar solution of sodium hydroxide as alkaline electrolyte was developed by using the different electrode materials and shapes. Both stainless steel and aluminium in whole sheet type with/without small holes were applied in hydrogen production. The highest of efficiency of hydrogen production was found by using the stainless steel 304 code 2.3S as electrode. The system generated the voltage output at 40.22 milliVolts, the current density at 0.396 microampere per square centimetre, and the power density at 15.96 microwatt per square centimetre. These results indicated that the performances of electrode are important for the development of hydrogen production in the future.

Keywords—Aluminium; Stainless steel; Alkaline electrolyte; Hydrogen gas;

I. INTRODUCTION

In the present, the peoples around the world relies on the environment pollution which possible occurred by the energy production. Moreover, the utilization of fossil oil in various applications such as the electricity [1] lead to the air pollution [2]. The renewable energy is developed as the sources of energies especially the Nuclear energy [3], water power [4], wind power [5], Solar energy [6], and Hydrogen Energy [7]

Hydrogen energy is a renewable energy which releases the high energy. Normally, the water electrolysis generates the hydrogen gas under alkaline or acid condition [8] by addition of DC electricity. This hydrogen can be used in vehicle industrial and electricity production. The water electrolysis system consists of anode and cathode. Normally, the hydrogen gas occurs at cathode and anode is used for the oxygen gas.

The equations bellow show the chemical reaction at the both anode and cathode, they are [7]

The reaction at anode:



The reaction at cathode:



The reaction at Overall:



The goal was to improve the performance of hydrogen production system by variation in the critical parameters especially the electrode materials and shape types. Both of these characteristics mainly affects to the efficiency of hydrogen production. Thus, the stainless steel and aluminium were used as electrode materials in various shape types to identify the suitable condition for high performance of hydrogen production.

II. METHODOLOGY

A. Instruction of the hydrogen production system

The hydrogen production was operation under close condition. The system consisted of 2 chambers; cathode and anode chamber. The 2 electrodes, cathode and anode, were put and soaked in the 1.5 L of NaOH solution in the cathode and anode chamber. This NaOH solution was used for the alkaline electrolyte for the hydrogen production. During the operation of hydrogen system, an each electrode connected to the QJE-PS3005 DC power supply for injecting the DC voltage into the system. The hydrogen concentration was detected by MQ8 sensor collecting data in every 10 second. The system shown in the figure 1.

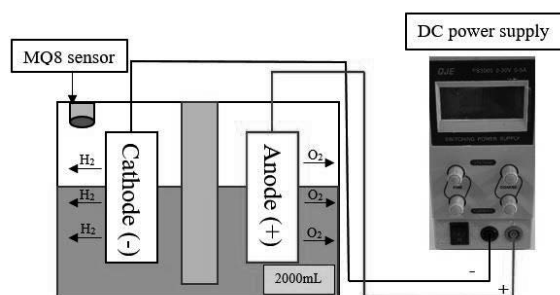


Fig 1 Hydrogen separation system

B. The PEM fuel cell for electricity production

The hydrogen production system was conjugated with the PEM fuel cell for the electric production. In the two chambers PEM fuel cell, the Nafion no. 117 and aluminium were used as the PEM membrane and electrodes, respectively. The anode and cathode connected together with the 2k Ω of external loading resistance. During the operation of fuel cell for 3 hr, the digital multimeter WENS 510 detected and collected the system voltage in every 10 second.

C. Study on the variouys material types and their shapes on the hydrogen production

The stainless steel 304 and aluminium materials in shaping of whole sheet, whole sheet with 6 mm of diameter of hole and the 2 mm of diameter of hole (table 1 and figure 2).

Before the operation of system, the stainless steel 304 electrodes were activated by using the 65% (v/v) of H₂SO₄ and HNO₃ in the ratio of H₂SO₄ to HNO₃ at 3:1 [9]

Table 1 The electrode material types and their shape in study

Test no.	Material	Shapes	
		Anode	Cathode
1	Stainless steel 304	Whole sheet(SW)	Whole sheet(SW)
2		Whole sheet with the hole at dia. 5.9 mm (5.9S)	Whole sheet with the hole at dia. 5.9 mm (5.9S)
3		Whole sheet with the hole at dia. 2.3 mm (2.3S)	Whole sheet with the hole at dia. 2.3 mm (2.3S)
4	Aluminium	Whole sheet(AW)	Whole sheet(AW)
5		whole sheet with the hole at dia. 5.9 mm (5.9A)	whole sheet with the hole at dia. 5.9 mm (5.9A)
6		whole sheet with the hole at dia. 2.3 mm (2.3A)	whole sheet with the hole at dia. 2.3 mm (2.3A)

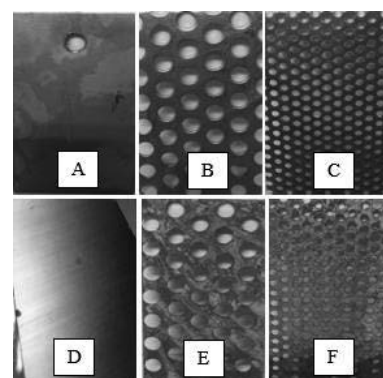


Fig 2 The electrode material types and shapes.
The details referred as their code number (A) SW, (B) 5.9S, (C) 2.3S, (D) AW, (E) 5.9A and (F) 2.3A

D. Study the voltages in various voltage that affect the residual hydrogen concentration in the system

To improve the efficiency of hydrogen production, the effect of voltage loading was analyzed to select the optimum voltage loading. In this study, the loading voltages were varied from 0.5V to 15V. At each the voltage condition, the hydrogen production was operated until the system stable.

E. Analytical method

To analyze the system values, the Ohm's law was used for calculation. The equation was bellowed [10]

$$V = IR \quad (1)$$

$$P = IV \quad (2)$$

$$\text{Current density} = I/A \quad (3)$$

$$\text{Power density} = P/A \quad (4)$$

Where; V (V) is the cell voltage
I (A) is the current
R (Ω) is the resistance value
A (cm²) is the area of electrode
P (W) is the power.

III. RESULTS AND DISCUSSION

A. The effect of different electrodes on the production of hydrogen

In the experiments, the hydrogen production system was conjugated with the PEM fuel cell. The both hydrogen and oxygen were sent through the PEM fuel cell for the electricity production. Therefore, the hydrogen concentration in their production system was the remained hydrogen during the hydrogen was used in PEM fuel cell. The characteristic of hydrogen production system and PEM fuel cell were shown in table 2 and figure 3.1 – 3.2



Table 2 The characteristic of hydrogen production system connected with the electricity production at 2kΩ of external loading

Test No.	Remained H ₂ conc. (ppm)	Electric production			
		voltag es (mV)	Curren ts (μA)	Curr ents/ area (μA/c m ²)	Power /area (μW/c m ²)
SW	20.4	5.40	2.70	0.038	0.208
5.9S	21.3	21.72	10.86	0.220	4.782
2.3S	21.7	40.22	20.11	0.396	15.96
AW	41.5	23.56	11.78	0.168	3.971
5.9A	53.5	0.550	0.27	0.005	0.003
2.3A	43.6	6.482	3.24	0.063	0.4145

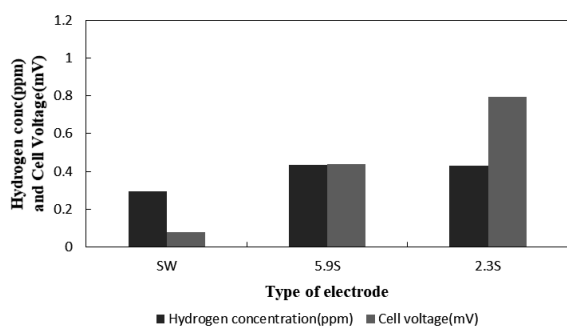


Fig 3.1 Effects of various shapes of stainless steel 304 electrode on the Hydrogen concentration and cell voltage in PEM fuel cell

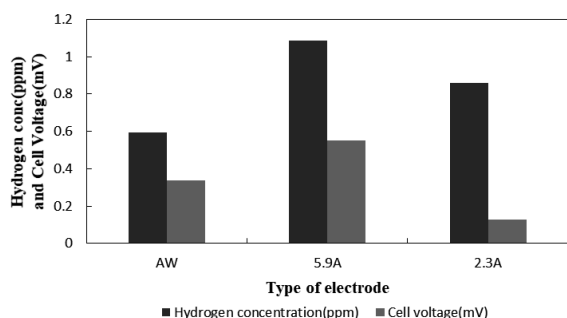


Fig 3.2 Effects of various shapes of aluminium electrode on the hydrogen concentration and cell voltage in PEM fuel cell

From the comparison of electrode material types and shape, the hydrogen gas generated by the stainless steel (2.3S) was used for the electricity higher than aluminium (5.9A). The result possible indicates that stainless steel generates the higher hydrogen concentration and this gas is easily to use for the electricity than aluminium types. This lead to increase the highest electricity at 40.2 mV.

The one phenomenon is observed during the hydrogen production, when the voltage loading increase lead to the increase the water electrolysis generates the high amount of hydrogen in finally. At this state, there are a lot of hydrogen bubbles inside the alkaline electrolyte and remove out of solution in finally. However, if the hydrogen gases are not quickly used in the electric production consequence to the high pressure in the hydrogen production chamber. This make the hydrogen bubbles cannot release and then it accumulate into the NaOH solution.

Moreover, the stainless steel has more resistant to acid or alkaline solution. The stainless steel 304 soaking in acid alkaline under pH solution at, the corrosion on stainless steel does not occur especially in the case of operation under alkaline condition, this corrosion on stainless steel is difficultly occurs [11]. However, the aluminum shows higher the corrosion than the stainless steel even in both acid and alkaline solution. This corrosion also increases a huge amount of bubbles lead to increase the high concentration of hydrogen (Figure 4 and figure 5). If the corrosion is too high, the bubble does not suddenly remove out from water and then lead to generate the low voltage output of their system [12]. This phenomena is observed when the production using the alminium electrodes (Figure 4). Therefore, the optimum material types and shapes of anode and cathode in this research are the stainless steel in type of Whole sheet with the hole at dia. 2 mm (2.3S)

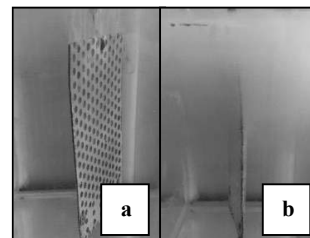


Fig 4 (a) Aluminum soaked in sodium hydroxide without voltage and (b) Aluminum soaked in sodium hydroxide by voltage

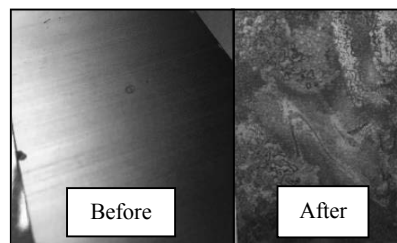


Fig 5 Aluminium before and after reaction

B. The difference in the input voltages that affect the output current

The effects of different voltage loading were determined using the optimum cathode and anode which was the electrode 2.3S as shown in table 3 and figure 6



Table 3 The variation of voltage loading into hydrogen production against the electric generation

Voltage Input in H2 productions System	In the hydrogen PEMFC system			
	Cell Voltage (mV)	Current (mA)	Current density (mA/cm ²)	Power density (mW/cm ²)
0.5V	35.29	0.018	0.348	0.013
1V	40.23	0.020	0.397	0.017
3V	16.48	0.008	0.163	0.003
5V	45.99	0.023	0.454	0.022
7V	64.69	0.032	0.638	0.042
9V	63.51	0.032	0.627	0.040
15V	117.17	0.059	1.156	0.139

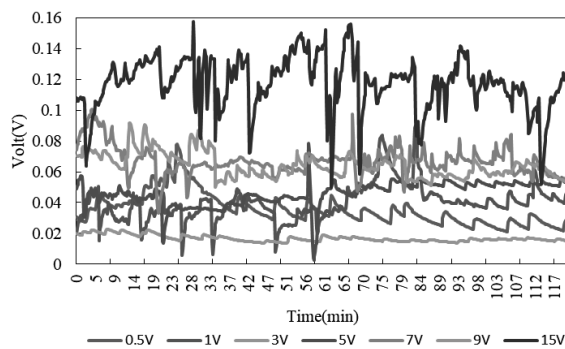


Fig 6 The characteristics of PEM fuel cell at different voltage loading into the hydrogen production system

Table 3 and figure 5 illustrate that the increment of voltage loading into hydrogen production system also dramatically increase the voltage of electricity generation especially at 15V of voltage loading. However, the electricity line at voltage loading 1-15V, the voltage outputs of PEM fuel cell were not stable especially in 15V. It may be the flow of electricity is in the opposite direction lead to the current swing [6].

However, at 0.5 voltage loading shows quiet more stable in electric line which indicates that the hydrogen production system is in steady state which producing the hydrogen concentration stable. Moreover, it also indicates that in this condition, the pressure level in hydrogen production does not too high to press the hydrogen bubble in NaOH electrolyte. Since the removal of hydrogen bubbles from the NaOH solution at high voltage loading is fluctuates that may influent to the electric line also fluctuate.

So, the voltage loading at 0.5V is the optimum loading for hydrogen production. Nevertheless, this result is not similar to previous researches explain that the reaction of water electrolysis should be done at least 1.28V loading to completely the hydrogen production [6]. On the other hand, at voltage loading at 0.5V can breakdown the bonding in water molecules to hydrogen gas for the PEM fuel cell which the electricity can be noticed in finally.

IV. CONCLUSION

The alkaline hydrogen production combine with the PEM fuel cell for the generation of electricity are established. These systems still do not show the high efficiency of electricity production but the electricity can be noticed. Moreover, the fluctuation of electricity line is the critical factor to develop the system more highly stable even in the high voltage loading into the hydrogen production system. The optimum both 2 electrodes are the stainless steel in type of whole sheet with the hole at dia. 2.3 mm (2.3S) and at 0.5 voltages loading. The other should be considered that the fluctuation of electricity dramatically highly increase or decrease in very short time. Therefore, the development of hydrogen production to generate the highly hydrogen concentration under the low voltage loading is the first priority done in the future.

ACKNOWLEDGMENT

Thank you for the School of Renewable Energy, Maejo University to support all facilities in this research. Moreover, I would like to thank my advisor, Dr.Nathanicha Sukasem who gives me the opportunity to participate in this research and also advise me on this research.

REFERENCES

- [1] E. Ulrich, M. Bernd, and V.H Rittmar, "Fuel cell electric vehicles and hydrogen infrastructure," *Energy environ*, 2012, pp. 8780-8798.
- [2] L. Fangyi, X. Xilin, X. Wu, M. Dawei, S. Zhuo and L. Kunpeng, "Estimating air pollution transfer by interprovincial electricity transmissions," *Journal of Cleaner Production*, vol. 183, May 2018 pp. 56-66.
- [3] S. Suman, "Hybrid nuclear-renewable energy system:A review," *Journal of cleaner Production* 181, 2018, pp. 166-177.
- [4] S.J. Pereira-Cardenal, B. Mo, A. Gjelsvik, N.D. Riegel, K. Arnbjerg-Nielsen, P. Bauer-Gottwein, "Joint optimization of regional water-power system," *Advances in water Resources* 92, 2016, pp. 200-207.
- [5] A. Zerrahr, "Wind Power and Externalities," *Ecological Economics* 141, 2017, pp. 245-260.
- [6] E. Kabir, P. Kumar, S. Kumar, A.A. Adelodun, K.H. kim, "Solar energy: Potential and future prospects," *Renewable and Sustainable Energy Reviews* 82, 2018, pp. 894-900.
- [7] C. Jun, Y. Hongmei, "Water electrolysis based on renewable energy for hydrogen production," *Chinese Journal of Catalysis* 39, 2018, pp. 390-394.
- [8] R. Ogawa, R. Tanii, R. Dawson, H. Matsushima, M. Ueda, "Deuterium isotope separation by combined electrolysis fuel cell," *Energy* 149, 2018, pp. 98-104.
- [9] A.A. Adelodun, "Effect of basicity on amination of activated carbon pellets modified for CO₂ adsorption," *Journal of Purity, Utility Reaction and Environment* Vol. 3, February 2014, pp. 1-17.
- [10] J. Labato, G.C. Araceli, J.F Francisco, C. Pablo, A.R. Manuel, "Lagooning miccroial fuel cell:A first approach by coupling electricity-producing microorganisms and algae," *Applied Energy*, 2013, pp. 220-226.
- [11] N. Kumraksa, and B. Plangklang, "Hydrogen Electrolizer by Using Separated Electrolyzed cell Process," *Thailand Energy Network Conference* 7th, 2011, pp. 745-749.
- [12] M. Kavch, B.S Nasri, M. Hossein, "Electrical Efficiency of Electrolytic Hydrogen Production," *Int.J.Electrochem Sci*, Vol. 7, 2012, pp. 3314-3326



Evaluation of Acid and Alkaline Pretreatments, to Enhance Enzymatic Hydrolysis and Fermentation Ethanol by Agricultural Corn Cob.

Pawinee Phetnok¹, Natthanicha Sukasem²

^{1, 2} School of Renewable energy, Maejo University, Chiang Mai, 50290, Thailand.

E-mail; ¹pawinee-29@hotmail.com

Corresponding author: E-mail: ²jewy.ja@gmail.com

Abstract— Corn cob is a promising as feedstock because of high yields and low costs, which does not compete with food prices. Dilute acid pretreatment for hydrolysis hemicellulose under different type of acid (HCl and H₂SO₄) and level dilute acid concentration 1-4% (v/v), effective to obtain high concentration xylose and glucose of 10.53 and 16.58 g/l under condition 4% (v/v) HCl at 100 °C for 3 hr. An ethanol concentration of 11.28 g/l after 12 hr. by using the yeast *S. cerevisiae*. An additional alkaline pretreatment applied to the solid fraction remaining from the diluted acid pretreatment (APSD), improved the lignin and hemicellulose removal and increase cellulose under level dilute NaOH concentration 1-4% (v/v). The highest increase 20.69% to 42.49% (w/w) of cellulose and decreased 39.20% to 4.35% (w/w) of hemicellulose under condition 4% (w/w) NaOH at 100 °C for 3 hr. The enzymatic hydrolysis obtained the sugar concentration at 32.2 g/l of addition Tween 80 from solid residual the diluted acid and alkaline pretreatment (AAPSD). The fermentation of the sugar solution from cellulosic fraction with *S. cerevisiae*, showed the highest ethanol concentration 22.25 g/l. Thus, corn cob is an interesting as feedstock conversion to produce ethanol as good as the fermentation. Show than fig. 1 the strategy of ethanol production from Corn cob

Keywords— Corn cob, Acid pretreatment, Alkaline pretreatment, Enzymatic hydrolysis, Fermentation ethanol.

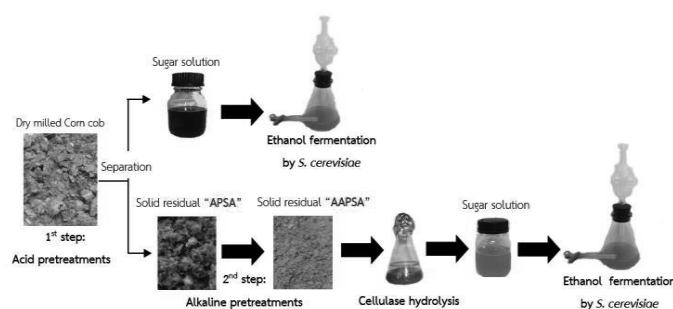


Fig. 1. Strategy of ethanol production from Corn cob

I. INTRODUCTION

Biofuel ethanol is a renewable energy sources to reduce the consumptions of fossil fuels which are the mainly causes

of environmental pollutions. The bioethanol is an appropriate liquid energy by mixing with the gasoline because of the ethanol has the high octane [1]. Lignocellulosic materials can be converted into the small sugars for ethanol production which the wastes are the agricultural wastes, woods and energy crops for examples [2]. Corn cobs are the lignocellulosic materials from the agricultural wastes; they are promising as feedstock because of high yields and low costs. Moreover, the managements of technologies should be considered to impact of environmental from corn cobs [3].

Lignocellulosic materials are mainly composed of cellulose, hemicellulose and lignin. Both the cellulose and hemicellulose fractions are the polymer of 5 and 6 carbon sugars for a potential source of ethanol production [4]. Principally, the conversions of lignocellulose to be the bioethanol involve the 3 main steps: chemical and physical pretreatments for plant cell wall destruction, enzymatic hydrolysis of the cellulose conversion into glucose and finally the yeast ferments sugars into the ethanol production [5]. Pretreatment techniques are the first step of the most important processes which has been developed to improve the digestibility of the lingocellulosic structure.

The pretreatment can be done by using the dilute or strong acid such as H₂SO₄ or HCl which have been widely used and the most studied [6]. Regard to hydrolysis efficiency of hemicellulose, the process releases the monomeric sugar such as, glucose xylose and arabinose as the potential sources of ethanol production [7]. However, the soluble by-products (furfural, 5-hydroxymethyl furfural, acetate) formed during the dilute acid hydrolysis inhibit the microbial growth and retard the fermentation rates [8]. The elimination of by products in treated acid sugar solution has to consider before applying the sugar solution into the ethanol fermentation. Moreover, the utilization of treated acid sugar solution instead of enzymatic digestion can reduce overall the production costs [9].

However, the solid fraction obtained after the diluted acid pretreatment is low effective in the lignin removal. In the two steps of acid couples with alkaline pretreatment, the acid



pretreatment is one of two techniques to higher increase the efficiency of lignin removal in the solid fraction [10]. The diluted NaOH is usually used for the alkali pretreatment causing alter the lignocellulosic biomass into swell structures, leading to an increase in the internal surface areas include the decreasing in the degree of crystallinity and disrupting the lignin structure [11].

The enzymatic hydrolysis converts the large amounts of cellulose into the high yields of glucose but the enzyme digestion dramatically significantly increases the cost of ethanol process [12]. The addition of non-ionic surfactants (tween 20 and 80) to the enzymatic hydrolysis stage is suggested to reduce the enzyme requirements and increase the cellulose conversion yields [13]. Because the surfactant is the capable of modification of the cellulose surface property and also minimization of the irreversible binding of cellulase enzyme on cellulose to hydrolysis sugar [14]. *Saccharomyces cerevisiae* is the most widely used in the ethanol fermentation because the yeast *S.cerevisiae* is the fermenting hexose yeast in the industrial process owing to their high efficiency of glucose conversion into the ethanol and it's easily to adaptable itself under the various fermentation conditions [15].

The goal of this study was to improve the corn cobs which were the lignocellulosic of agricultural wastes, to be the potential feedstock for ethanol fermentation by using the yeast *S. cerevisiae* fermenting xylose and glucose. Moreover, the 2 steps of acid/alkaline pretreatment and commercial cellulase enzymatic hydrolysis with the addition of tween 80 as surfactant were necessary require for the development of the ethanol efficiency.

II. MATERIALS AND METHODS

A. Raw material

Corn cobs were collected from a field local in Loei, Thailand. The biomass was physically pretreated by cutting of small size 0.5-1 cm and dried at 70 °C in an oven for 48 hr. The dried solid samples were analyzed the components of both cellulose and hemicellulose before the chemical pretreatment process.

B. Pretreatments

Dried biomass was mixed with diluted H₂SO₄ and HCl acid solution. The treatment condition was done at acid concentration 1, 2, 3 and 4% (v/v) to reach a solid/liquid ratio of 1:10 (w/v) and then the samples were treated by hot air oven at 100 °C for 3 hr. The suspension was separated by using filter Paper (No.1). The filtrated solid was washed with tap water till achieving pH close to neutrality. After that sample was dried at 70 °C for 48 hr. This solid residue referred as a dry acid pretreated solid (DAPS).

Two steps of alkali pretreatment were carried out on the DAPS samples by using the diluted NaOH at concentration 1, 2, 3 and 4% (w/v) to reach a solid/liquid ratio of 1:10 (w/v). Then the samples were treated by hot air oven at 100 °C for

3 hr. The suspensions were filtrated by using the filter Paper (No. 1). The filtrated solid was washed with tap water till achieving pH close to neutrality. After that sample was dried at 70 °C for 48 hr. This solid residues referred as a dry acid and alkali pretreated solid (DAAPS).

Assays were carried out on the samples after the 2 steps of acid/alkali pretreatment. The liquid fractions were determined on the amounts of total sugar, reducing sugar, glucose and xylose whereas the solid (DAPS and DAAPS) residues were analysed on the proportions of cellulose and hemicellulose

C. Enzymatic hydrolysis

The enzymatic hydrolysis was performed by using the industrial cellulase grade (Activity 75 FPU/g). The enzymatic reaction contained the cellulase loading at 140 FPU/ 100 ml of 0.05 M sodium citrate buffer (pH 4.8), the DAAPS samples at 6% (w/v) and the tween 80 concentration as surfactant at 0.5 ml/g of plant. The reactions were incubated at 42 °C by rotary shaking at 200 rpm for 28 hr. The samples (1.5 ml) were taken in every 4 hr. then the supernatants were used for total sugar analysis and kept at -20 °C.

D. Ethanol fermentation

The yeast *S. cerevisiae* was cultured in a yeast malt extract agar (YMA) with consisted of several (concentrations in g/l): glucose 10; peptone 5; malt extract 3; yeast extract 3; agar 20 and pH 5.5. Stock cultures were stored at 4 °C. The yeast inoculum, therefrom, was subculture from the agar plate into a yeast fermentation medium (YM) following the compositions of (concentrations in g/l): glucose 10; peptone 5; malt extract 3; yeast extract 3; and pH 5.5, 200 rpm and 37 °C for 24 hr. Therefore, after the optical density at wavelength 600 nm reached to (~1.5) at 0.5, the culture broth was used as the starter for the ethanol fermentation.

The sugar solutions were from treated 4 % (v/v) HCl sugar solutions and from the cellulase digestion. In fermentation, the extra glucose was added into the fermentation broth until the final concentration reached to 200 g/l. The yeast fermentation medium (YFM) consisted (g/L) of yeast extract 6; peptone 5; (NH₄)SO₄ 2; KH₂PO₄ 4; MgSO₄·7H₂O 1 at pH 5.5. The *S.cerevisiae* inoculum at 1% (v/v) of total volume was transferred into the fermentation broth and incubated at 37±2 °C for 48 hr under anaerobic condition. Samples were collected at every 6 hr intervals time throughout the fermentation process. The samples were analyzed for the ethanol and remained sugar concentration.

E. Analytical methods

The proportion of cellulose and hemicellulose were determined by following the method of Ververis et al. using 72% (w/w) of H₂SO₄ solution for 4.5 hr. [16]. Total sugar and reducing sugar concentration were analyzed by following the method of total phenol sulfuric method [17] and the Somogyi-Nelson method [18] by UV spectroscopy at 490 nm and 660 nm, respectively. Moreover, the glucose and xylose were also



measured by spectroscopy (630 nm of glucose, 480 Xylose [19]. The treated solid corn cobs from the steps of chemical pretreatment and cellulase digestion were observed for the surface area analysis by scanning electron microscope (SEM). The ethanol concentration was detected by using the dichromate method by UV spectroscopy (600 nm) [20].

F. Statistical analysis

The data was analyzed by one-way analysis of variance (ANOVA). T-Test was used to compare the difference of means among treatment groups. Differences of $p < 0.05$ were considered significant.

III. RESULTS AND DISCUSSION

A. Components of corn cob.

Corn cobs are the lignocellulosic agricultural waste. The material was characterized to determine, major cell wall components it consisted 20.69% (w/w) of cellulose and 39.20% (w/w) of hemicellulose. This research was interested the potential of corn cobs for ethanol production.

B. saccharification under acid pretreatment.

Acid pretreatment of corn cob was performed under different at various type of inorganic acid (H_2SO_4 and HCl) and diluted acid concentrations (1-4% (v/v)). This study is the hydrolysis of hemicellulose fraction to monomeric sugar (glucose and xylose) is essential for bioethanol production. Fig. 2. Showed that the total sugars, glucose and xylose concentration obtain in the liquid fraction under acid pretreatment. The results diluted acid concentration was gradually increasing of both H_2SO_4 and HCl were significant ($p < 0.05$) for increasing sugar product. High yields of sugar product to increasing were performed under diluted acid concentration of 4% as both H_2SO_4 and HCl were found 7.54 and 10.22 g/l of glucose concentration, 10.53 and 16.58 g/l of concentration xylose, respectively

Comparing with at level concentrations on the same of H_2SO_4 and HCl (such as 1% H_2SO_4 : 1% HCl) were found difference of total sugar, glucose and xylose concentration were significant ($p < 0.05$) of every level of sugar concentration. The effect of HCl for hydrolysis hemicellulose obtain as high yields sugar more that H_2SO_4 pronounced at level on the same and every level dilute 1-4% v/v concentration. Because HCl is highly corrosive and considered a strong acid [21, 22]. This is study be similar to report other to compare type of acid to break hemicellulose bonds. A high yield of xylose can usually be obtained with the addition concentration of HCl, such as report amount 30.82 and 3.99 g/l [23], 22.59 and 1.50 g/l [24], 21.50 and 5.84 g/l [25], of xylose and glucose concentration, respectively. However, I have been applied to pretreat high acid concentration is less attractive for ethanol production due to the formation of inhibiting compounds and affect the microorganism metabolism in the fermentation step [26]. Principally, acid pretreatment is also

highlights about the cost price of interest for applying at commercial scale [9].

Thus, acid pretreatment under concentration with HCl 4% (v/v) into hydrolysis hemicellulose decrease from original 39.20% to 6.54% (w/w) of residue under solid fraction. And increase of cellulose 20.69% to 28.06 (w/w) show than in Table 1. Which was similar to that reported the addition of HCl had a positive influence on hemicellulose removal, decreased by 28.38% to 16.53% (w/w) of hemicellulose [27]. However, acid pretreatment is not conducive to the removal of lignin residue solid fraction. The effect removal lignin and hemicellulose and increate cellulose in a two-step pretreatment [28].

C. Digestibility upon acid-alkali pretreatment.

The main objective was to two-step with alkali pretreatment of APDS, to remove residue the hemicellulose and/or lignin of the solid fraction. Thus improving the reactivity of the remaining polysaccharides than it is could hinder the efficiency of enzymatic saccharification [29]. In this study, alkali pretreatment with NaOH under diluted alkali concentration of 1-4% (w/w) were performed Fig. 3. The results show that, the high total sugar concentrations 7 g/l of 1% (w/v) NaOH when increate concentration of NaOH up to 2-4% (w/v) into decreases sugar production, releasing monomeric sugar consist as amount slight glucose and xylose concentration.

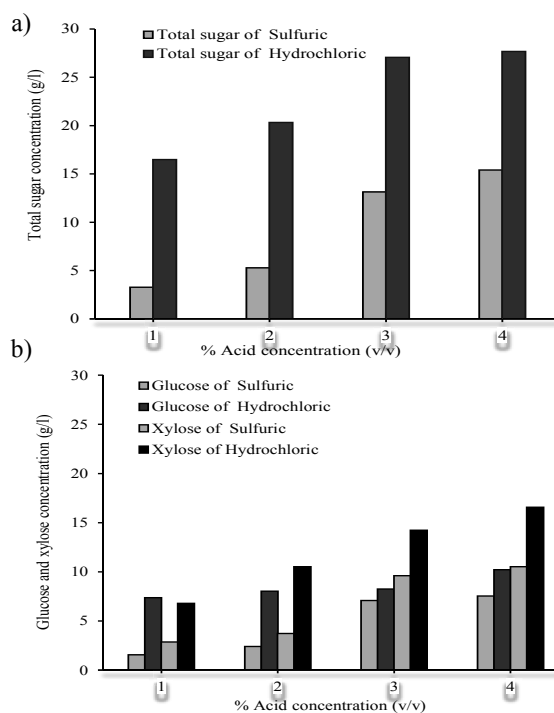


Fig. 2. Sugar production of a) total sugar b) glucose, xylose in the liquid fraction obtained after diluted acid pretreatment under condition by using 1-4 % (v/v) of H_2SO_4 and HCl at 100 °C for 3 hr.



Table 1. Show than the chemical composition of DAAPS sample. As the results of the effect of NaOH concentration pretreated increase the swollen structures in cellulose, the increase of NaOH concentration was significant $p > 0.05$ in high cellulose content from 28.06% to 42.79% (w/w) and it can decrease hemicellulose content from 6.17% to 4.17% (w/w) of 4% (w/v) NaOH. However, this is study was low effect alkali pretreatment for increase the surface area of cellulose due to corn cob was been higher lignin percentage which provides a compact structure difficult to transform [30]. However, higher alkali concentration resulted in higher release of carbohydrates, what reduce polysaccharide availability for the enzymatic hydrolysis [31].

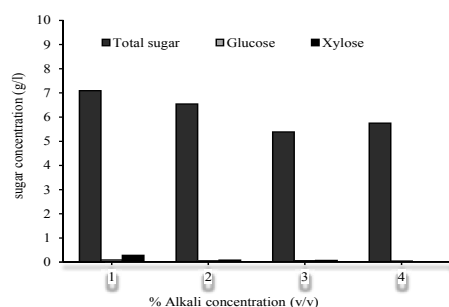


Fig. 3. The sugar production after the alkaline pretreatment at different the concentrations by using 1-4 % (v/v) of NaOH at 100 °C for 3 hr.

Table 1. The chemical composition of residue solid fraction of corn cob after the pretreatment.

Pretreatment and Emzymactic hydrolysis		Cellulose (% (w/w))	Hemicellulose (% (w/w))
Acid (v/v)	Untreat	20.69	39.20
	H ₂ SO ₄ 1%	22.66	18.76
	H ₂ SO ₄ 2%	24.10	12.67
	H ₂ SO ₄ 3%	27.19	12.17
	H ₂ SO ₄ 4%	29.84	10.65
	HCl 1%	23.95	15.04
	HCl 2%	24.12	11.15
	HCl 3%	25.69	9.29
	HCl 4%	28.06	6.59
Acid-Alkali (w/v)	NaOH 1%	29.09	6.17
	NaOH 2%	35.99	4.56
	NaOH 3%	39.44	4.27
	NaOH 4%	42.79	4.35

D. Enzymatic hydrolysis of DAAPS.

The effect of surfactant on the absorption of cellulases onto substrate as show in Fig. 4. To evaluate the adsorption of enzyme to substrate with and without addition of Tween 80. The enzymatic hydrolysis was obtained the highest total sugar concentration at 32.2 g/l of addition Tween 80 and 30.2 g/l of without Tween 80 within 28 hr. in incubation time. Addition of Tween 80 showed is a slight increased rate approximately of 7.8% d different with without Tween 80 on time at 28 hr. However, the initial hydrolysis rate was also addition Tween

80 increased more than without surfactant approximately 39.44%, 22.31%, 17.30% on time at 4, 8, 12 hr, respectively. Therefore, the addition of non-ionic surfactants could help save enzyme loading without decreasing the hydrolysis yield [13]. This is study similarly by Z. Yan, et al. addition Tween 80 was significantly higher than that of control (24.7%) on filter paper [14]. Castanon and wike, show study the rate of enzymatic hydrolysis was improved by 33% using Tween 80 as a surfactant in the hydrolysis of newspaper [32].

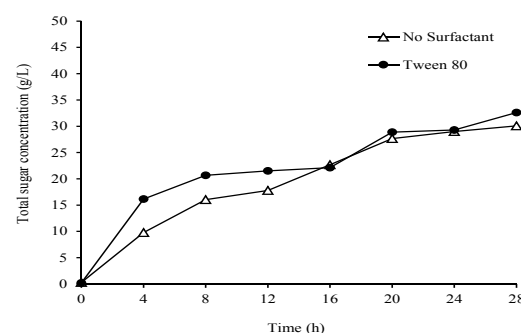


Fig. 4. Total sugar production under no surfactant and addition Tween 80 during enzymatic hydrolysis of DAAPS at 42 °C for 28 hr.

E. Scanning electron microscope (SEM) of solid residues

The scanning electron microscopy (SEM) used solid sample for surfaces analysis magnified at 500 folds. To study the effect after pretreatment of HCl (only step) and HCl/NaOH (two step) under condition concentration of 2% (v/v) HCl and 4% (w/w) NaOH and enzymatic hydrolysis of solid residues fraction. The result is show morphological features and surface characteric of corn cob in fig. 5. The original crystallinity of corn cob is highly fibrous structures of cellulose relatively smooth and regular (Fig. 5 a)). After was obtain HCl pretreated, protective surface layer included hemicellulose and lignin was degraded (fig. 5 b)). The cellulose was obviously exposed after NaOH pretreatment (fig. 5 c)). Which increase surface area so that cellulose becomes more accessible to enzymes [33]. Increase in surface area can access into increase glucose yield during enzymatic hydrolysis [34], and break the cellulose structure into the small particles of solid residue (fig. 5 d))

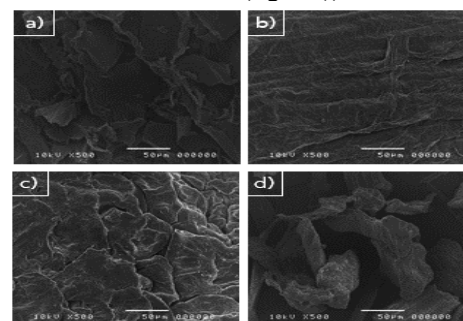


Fig. 5. SEM of the solid residue corn cob analysis magnified at 500 folds: a) untreated, b) HCl acid pretreated, c) HCl/NaOH pretreated, d) enzymatic hydrolysis.



F. Separate hydrolysis and fermentation (SHF)

Ethanol fermentation by separated hydrolysis fermentation (SHF) technology by yeast *S.cerevisiae*, they are sugars as carbon source obtain at both the liquid fraction after the diluted acid pretreatment and cellulase hydrolysis show in fig. 5-6 and Table 2. The results were showed (Fig. 6 a)) the reduction of sugar concentration obtain the liquid fraction of 4% (v/v) HCl pretreatment, the initial sugars production were obtain at 28.18 g/l of total sugar, 11.60 g/l of glucose and 16.25 g/l of xylose, respectively. The produces the maximum concentration of ethanol at 1.43% (v/v) or ethanol yield 0.40 g/g after 12 hr. of fermentation time (fig. 6 b)). The glucose concentration was trend to decrease continues, final glucose concentration remainder 1.51 g/l (86.98% consumption). While xylose was consumed after 12 hr. and final xylose concentration remainder to 5.25 g/l (67.69% consumption). Moreover, the pure glucose and xylose were used as the control experiments at the same concentration from the acid pretreatment. The result account that yeast can use both pure glucose and xylose as carbon sources even in the sugars from acid hydrolysis hemicellulose. However, the yeast *S.cerevisiae* slightly use the acid treated sugar including the xylose sugar [35].

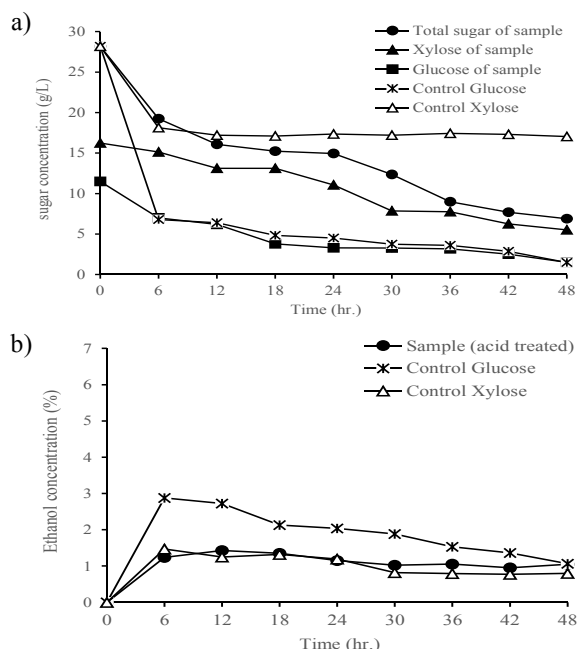


Fig. 6. Ethanol production in SHF of sugar production from hydrolysis hemicellulose by *S.cervisiae*. (a) Sugar production, (b) Ethanol production at 37 °C for 48 hr.

An after the enzymatic hydrolysis conversion into sugar yield. The results were showed in Fig. 7 a), the initial sugar concentration was obtain at 31.86 g/l, addition of sugar up to 200 g/l for the liquid fraction after the enzymatic hydrolysis, and it's control (pure glucose 200 g/l) are used to identify the ethanol efficiency. The yeast uses sugars to produce the

ethanol concentration at 2.82% (v/v) or ethanol yield 0.60 g/g and 12.26% (v/v) or ethanol yield 0.48 g/g with the sugar consumption at 91.68 % and 95.59% by using enzymatic sugars and add glucose 200 g/l, respectively (fig. 7 b) and Table 2). The results explain that the pure glucose can be replaced with the hydrolysate sugars at the proportion of total sugar concentration. Thus, the results indicate that the yeast *S.cerevisiae* ferment by acid pretreatment and hydrolysate sugar solutions from corn cob to produce ethanol as good as the fermentation by using the glucose solution as in the control experiment.

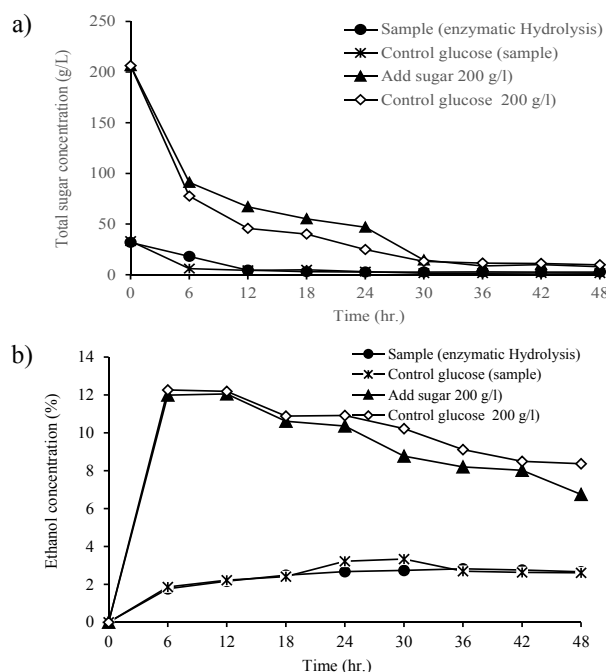


Fig.7 Ethanol production in SHF of sugar production from enzymatic hydrolysis by *S.cervisiae*. (a) sugar production, (b) Ethanol production at 37 °C for 48 hr.

Table 2. The initial and final sugars production for ethanol fermentation

Condition	Hemicellulose	Enzymatic	Add sugar
Total sugar fermentation (g/l)			
Initial	28.18	31.86	200
Final	6.90	2.65	8.01
Ethanol fermentation			
Ethanol concentration (%)	1.43	2.82	12.26
Ethanol concentration (g/l)	11.28	22.25	96.73
Ethanol yield (g/g)	0.40	0.69	0.48

IV. CONCLUSION

Corn cob is a promising as feedstock .Dilute sulfuric acid pretreatment was obtain of 4% (v/v) HCl was effective to high yields of sugars from hydrolysis hemicellulose. The use alkaline pretreatment improved increase the swollen structures in cellulose amount 42.79% (w/w) of cellulose. To evaluate the adsorption of enzyme to substrate with addition of Tween 80



was less effective conversion into sugar yields. The strategy was high ethanol produced 11.28, 22.22 and 96.83 g/l from the hemicellulose, cellulose and add sugar, respectively. Thus, corn cob is an interesting as feedstock conversion to produce ethanol as good as the fermentation.

ACKNOWLEDGMENT

This research was supported by funding from the school of renewable energy. Maejo University

REFERENCES

- [1] R. Yatri. Shaha and J.S. Dhruvo, "Bioalcohol as green energy - A review," Int J Cur Sci Res, vol 1(2), 2011, pp. 57 – 62.
- [2] M. Knauf and M. Moniruzzaman, "Lignocellulosic biomass processing: a perspective," Int. Sugar J. vol. 106, 2004, 147–150.
- [3] M.D. Jose, C. Ningjun, C.S. Gongh and G. T. Tsaoh, "Dilute acid hemicellulose hydrolysates from corn cobs for xylitol production by yeast," Bioresource technology, vol. 61, 1997, pp. 85-90.
- [4] A. Kumar, L.K. Singh, and Ghosh, S, "Bioconversion of lignocellulosic fraction of water-hyacinth (*Eichhornia crassipes*) hemicellulose acid hydrolysate to ethanol by *Pichia stipitis*," Bioresour Technol, vol. 100, pp. 4374 – 4380.
- [5] H. Rabemanantsoa and S. Saka, "Various pretreatments of lignocellulosics," Bioresource technology, vol. 199, 2016, pp. 83-91.
- [6] P. Kumar, M. Diane, Michael, J. Delwiche, and P. Stroeve, "Methods for pretreatment of lignocellulosic biomass for efficient hydrolysis and biofuel production," Chem, vol. 49, 2009, pp. 3713–3729.
- [7] N.K. Sharma, S. Behera, R. Arora, S. Kumar and K. Rajesh, "Xylose transport in yeast for lignocellulosic ethanol production: Current status," Journal of Bioscience and Bioengineering, Vol. 125, 2018, pp. 259-267,
- [8] B.C. Saha, L.B. Iten, M.A. Cotta, Y.V. Wu, "Dilute acid pretreatment, enzymatic saccharification and fermentation of wheat straw to ethanol," Process Biochem, vol. 40, 2005, 3693–3700.
- [9] JM. Urbanchuk, "Economic impacts on the farm community of cooperative ownership of ethanol production, LEGG, LLC, Wayne, PA, February, 2007,.
- [10] R. Ravindrana, S. Jaiswal, A.G. Nissreen, and K. Amit, "Two-step sequential pretreatment for the enhanced enzymatic hydrolysis of coffee spent waste", Bioresource Technology, vol. 236, 2017, pp. 276-284.
- [11] S. Binzhe, P. Gege, D. Lian, X. Aihua and L. Xiaoxia, "retreatment by NaOH swelling and then HCl regeneration to enhance the acid hydrolysis of cellulose to glucose," Bioresource Technology, vol 196, 2015, pp. 454–458.
- [12] R. Vitalijs, J.R. Karina, G. Pawel, and S. Dalija, "Non-waste technology through the enzymatic hydrolysis of agro-industrial by-products," Trends in Food Science & Technology, vol. 77, 2018, pp. 64–76.
- [13] Z. Yan, C. Hongmei, Q. Feng, Z. Xuebing, and L. Dehua, "Non-ionic surfactants do not consistently improve the enzymatic hydrolysis of pure cellulose," Bioresource Technology, vol. 182, 2015, 136–143.
- [14] M. Yang, A. Zhang, B. Liu, W. Li, and J. Xing, "Improvement of cellulose conversion caused by the protection of Tween-80 on the adsorbed cellulase," Biochem. Eng. J. 56, 2011; 125–129.
- [15] J.W. Kyong, U. Youngsoon, M.W. Han, H.K. Kyoung, and M.L. Sun, "Ethanol production from lignocellulosic hydrolysates using engineered *Saccharomyces cerevisiae* harboring xylose isomerase-based pathway," Bioresource Technology, vol. 209, 2016, pp. 290–296.
- [16] C. Ververis, K. Georghiou, D. Danielidis, D.G. Hatzinikolaou, R. Santas and V. Corleti, "Cellulose, hemicelluloses, lignin and ash content of some organic materials and their suitability for use as paper pulp supplements," Bioresource Technology, vol. 98, 2007, pp. 296-301.
- [17] M. Dubois, "Colorimetric method for determination of sugars and related substances," Chem., vol 28 (3), 1956. pp 350–356.
- [18] N.Nelson, "A photometric adaptation of the somogyi method for the determination of glucose", Journal of Biological Chemistry, vol. 153, 1994, pp. 375-380.
- [19] F. Jesse and Goodwin, "Method for simultaneous direct estimation of glucose and xylose in serum," Clinical Chemistry, vol. 6(2), 1968.
- [20] H. B. Seo, "Measurement of ethanol concentration using solvent extraction and dichromate oxidation and its application to bioethanol production process," J Ind Microbiol Biotechnol, vol. 36(2), 2009, pp. 285–292.
- [21] L. Qiyu, L. Wenzhi, M. Qiaozhi, A. Shengxin, L. Minghao, J. Hasan, H. Chang, "Pretreatment of corn stover for sugar production using a two-stage dilute acid followed by wet-milling pretreatment process," Bioresource Technology, vol. 211, 2016, pp. 435–442.
- [22] N.D. Narendra, V.V. Dasu, V.V. Goud and P. S. Rao "Development of dilute sulfuric acid pretreatment method for the enhancement of xylose fermentability," Biocatalysis and Agricultural Biotechnology, vol. 11, 2017, pp. 224-230.
- [23] M. Preshanthan and Gueguim, "Comparative study of three optimized acid-based pretreatments for sugar recovery from sugarcane leaf waste: A sustainable feedstock for biohydrogen production," Engineering Science and Technology, vol. 21, 2018, pp. 107-116.
- [24] L. Pattana, , Arthit, T., Vichean, L. and Lakkana, L. "Acid hydrolysis of sugarcane bagasse for lactic acid production," Bioresource Technology, 2009.
- [25] A.K. Chandel, P.K. Kapoor and R.C. Kuhad, "Detoxification of sugarcane bagasse hydrolysate improves ethanol production by *Candida shehatae* NCIM 3501," Bioresour Technol, vol. 98, pp. 1947-1950.
- [26] Ke, Z., Zhijian, P. and Donghai, W. "Organic solvent pretreatment of lignocellulose biomass for biofuels and biochemicals: A review," Bioresource Technology 199, 2016, 21-33.
- [27] T. Xue, L. Juan, Z. Panyue, N. Mohammad, J. Shuguang, L. Fan, W, Siqi and Y. Junpei, "Reinforced acid-pretreatment of *Triarrhena lutarioriparia* to accelerate its enzymatic hydrolysis," International journal of hydrogen energy, vol. 42, 2017, pp. 18301-18308.
- [28] C. Laura, R.R. Maria, G. Guigou, D.F. Mario and L. Claudia, "Evaluation of dilute acid and alkaline pretreatments, enzymatic hydrolysis and fermentation of napiergrass for fuel ethanol production," Biomass and bioenergy, vol. 74, 2015, pp. 193-201.
- [29] G. Hongliang, C. Yingju and J.L. J.I. Duu, Enzymatic saccharification of lignocellulosic biorefinery: Research focuses, Bioresource Technology, vol. 252, 2018. 198-215..
- [30] R.L. Ruan, Y. Chen, PL. Liu, Z. Pan, X., "Enzymatic hydrolysis of corn Stover pretreated by combined dilute alkaline treatment and homogenization," Trans ASAE, vol. 2004, pp. 5-821.
- [31] P.F.H. Harmsen, W.J.J. Huijgen, L.M. Bermudez, and R.R.C. Bakker, "Literature Review of Physical and Chemical Pretreatment Process for Lignocellulosic Biomass," Energy Research Centre of the Netherlands, 2010, pp. 1-48.
- [32] M. Castanon and C.R. Wilke, "Effect of the surfactant Tween 80 on enzymatic hydrolysis of newpaper," Biotechnol Bioeng, vol. 23, 1981, 1365-1372.
- [33] B. Shuaizhu, P. Lincai, C. Keli and Z. Zhengliang, "Enhanced enzymatic saccharification of sugarcane bagasse pretreated by combining O₂ and NaOH," Bioresource Technology, vol. 214, 2016, pp. 692–699.
- [34] Z. Teng and J.Z. Ming, "Enhancing enzymolysis and fermentation efficiency of sugarcane bagasse by synergistic pretreatment of Fenton reaction and sodium hydroxide extraction," Bioresource Technology, vol. 214, 2016. pp. 769–777.



Simple PV-Slat Window Control Method for Net-Zero Buildings

Vichuda Mettanant, Sivapong Phetsong

Department of mechanical engineering, Faculty of engineering and industrial technology, Silpakorn University
Nakorn Pathom, Thailand
vichuda.mettanant@gmail.com

Abstract—To meet the target of net-zero buildings and plus energy buildings, lighting and cooling power savings as well as power generation by Photovoltaic panels become critical. Across variable sun angles, dynamic PV integrated shading devices have the possibility to achieve maximum diffuse daylight and electricity production when direct solar radiation is no longer present. This research investigates slat angles for horizontal PV-slat windows on north and south facades of buildings in Bangkok, Thailand. The calculations were performed for hourly sun positions over a year by using the location of Bangkok, Thailand. The simple control schemes for horizontal PV-slat windows are presented. For south facades, the slats should be tilted downward during 7:00-9:00 and 16:00-18:00 in 1st January-9th March and 13th October-31st December. For north facades, the slats should be tilted downward from 6:00-7:00 and 18:00 from 11th April to 2nd September. For the rest of the time, the slats should be set at fully open.

Keywords—PV-slat window; daylighting; critical angle

I. INTRODUCTION

A Photovoltaic (PV) slat window can produce power and control daylight and glare which is suitable for net-zero and plus energy buildings. A PV-slat window requires less space because it can be placed on existing structures. When using with dimmable lighting system, a PV-slat window helps reduce electricity in lighting, and air-conditioning systems by introducing daylight and blocking direct solar radiation. Electricity produced from a PV slat window is supplied to meet energy consumption of buildings. Khedari et al. investigated performance of a PV-slat window by experiments in 1x1x1.5 m³ small models under the climate of Thailand. The results show that the PV-slat window produced power up to 15 W, provided indoor illuminance about 750 lx, and decreased indoor temperature by 2-3°C [1]. Hong et al. proposed two control methods for a PV blind used for a school building in Seoul, Korea. The first control method is applied when both daylight and artificial lights were used to meet the required interior illuminance (400-600 lx) and maximize electricity production from the PV-slat. The second control method is for using daylight to meet the required interior illuminance and maximize electricity production from the PV-slat [2]. Stamatakis et al. performed an analysis of PV panels mounted on south-facing shading devices of office buildings in the Chania, Greece, for Mediterranean climate. The results show

that horizontal PV louvers provide power generation of 146.29 Wh/m². Comparing to a room with simple window without shading device, the cooling energy is reduced from 45,459.05 Wh/m² to 573.83 Wh/m² and the lighting energy is dropped from 259,622.40 Wh/m² to 181,171.20 Wh/m² in order to achieve light levels of at least 500 lx in the desk level during office hours (9:00–17:00) for 5 days per week [3]. Chantawong conducted experiments on a PV blinds glazed solar chimney wall assisted with DC fan for a small house in Bangkok, Thailand. The results showed that the electrical current can be generate sufficiently and the DC fan can produce high ventilation rate around 1.20-3.25 m/s. The PV blinds glazed solar chimney wall produced hot water around 34-40°C and reduced heat from sunlight by 42.5 percent comparing to a single glass widow installed at the south facade [4].

As benefits of using PV-slat window and high daylight availability for a whole year in Thailand [5], a simple enough control method is required to operate it. Appropriate slat angles might be different depending on locations and weather conditions. Therefore, this research aims to examine angles of PV integrated horizontal shading devices that completely shade direct solar radiation and maximize daylight in buildings. Finally, simple control methods are developed for buildings installing PV-slat windows on north and south facades.

II. THEORY OF SLAT ANGLE

The slats are at their critical angle when they completely block direct solar radiation and provide maximum opening in order to maximize daylight and view as shown in Fig. 1.

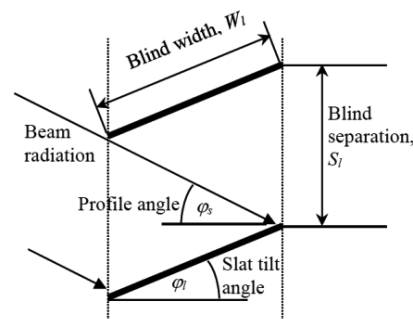


Fig. 1. Incidence of beam radiation on the slat window



The critical blind angle (ϕ) can be determined from (1)

$$\phi_s = \tan^{-1} \left(\frac{1 - \frac{W_l}{S_l} \sin \phi_l}{\frac{W_l}{S_l} \cos \phi_l} \right) \quad (1)$$

Where W_l is the slat width, S_l is the slat separation, and ϕ_s is the solar profile angle, which is the angle between the outward normal of the window and the projection of the vector from the window to the sun on the vertical plane containing the outward normal. The solar profile angle can be determined from (2) [6]

$$\phi_s = \tan^{-1} \left(\frac{\tan \alpha_s}{\cos(\gamma_s - \gamma_w)} \right) \quad (2)$$

Where α_s is the altitude angle of the sun, γ_s is the azimuth angle of the sun, and γ_w is the azimuth angle of the window.

III. METHODOLOGY

The critical blind angles were determined from sunrise to sunset with 1 hour time step by using (1) and (2). A whole year weather data of Bangkok, Thailand (13.4° N, 100.3° E) were used in this study. The analysis were performed for two window orientations, south and north, which are suitable for horizontal slats. Slat width of a PV-slat window should be designed to be equal to its slat separation for obtaining highest solar radiation. From (1), the critical angle depends on the ratio of slat width to slat separation. Consequently, the ratio of 1 was selected in this study. The slat window is set at fully open position (0° slat angle) when there is no beam solar radiation incident on the window.

IV. RESULTS AND DISCUSSION

The critical angles for the south slat window and those for the north slat window are reported and discussed. Results from the analysis are used to determine schemes for altering the slat windows.

A. The south slat window

Fig. 2 shows hourly critical angles for a whole year of the south slat window. The slats tilt downward during 7:00-9:00 and 16:00-18:00 to block beam solar radiation when the solar altitude angles are low. During 10:00-15:00, the sun rises with higher altitude angles so the blind angle at 0° (fully open) can completely block direct solar radiation.

In a year, the sun rises before 6:00 during 1st May-8th July which is the time when the sun travels into the northern sky. Therefore at 6:00, beam solar radiation does not incident on the south window so the critical angle is 0°. In the morning, the critical blind angle is maximum at 74°, 29°, and 5°, at 7:00,

8:00, and 9:00, respectively. In the afternoon, the critical blind angle is maximum at 13, 46, and 90, at 16:00, 17:00, and 18:00, respectively.

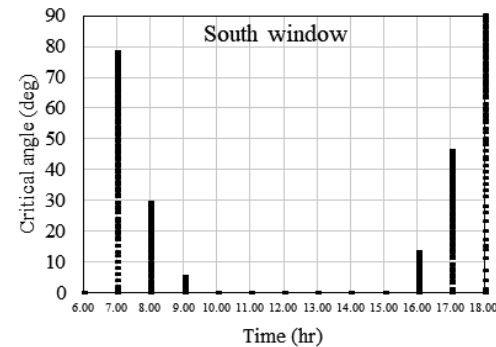


Fig. 2. Hourly variation of critical angles for the south slat window

Fig. 3 shows the critical angle at different julian dates (the number of elapsed days since the beginning of a year) during 7:00-9:00 and 16:00-18:00 for the south slat window. The critical slat angles are high during the beginning and end of a year when the sun travels into the southern sky. During 10th March-12th October (day 70-286), the sun travels into the northern sky so the blind angles are at 0° (fully open) to optimize daylight and view.

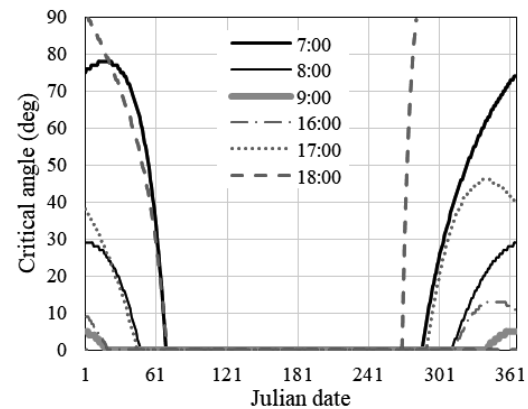


Fig. 3. Daily variation of critical angles for the south slat window

B. The north slat window

Hourly critical angles for the north slat window are shown in Fig. 4. When the solar altitude angles are low at 6:00, 7:00 and 18:00, the slats tilt downward to block beam solar radiation. The maximum critical angles in a year at 6:00, 7:00 and 18:00 are 90°, 22°, and 44°, respectively. From 8:00 to 17:00, the sun rises with higher altitude angles so the blind angle at 0° (fully open) can completely block direct solar radiation.

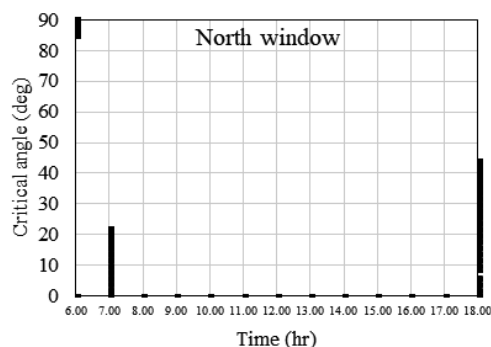


Fig. 4. Hourly variation of critical angles for the north slat window

Fig. 5 shows the critical angle on various days in a year at 6:00, 7:00 and 18:00. For the north slat window, the slats tilt downward with high critical slat angles in the middle of a year (11th April-2nd September) when the sun travels into the northern sky. For the rest of a year, the slat angles should be fully open for the whole days.

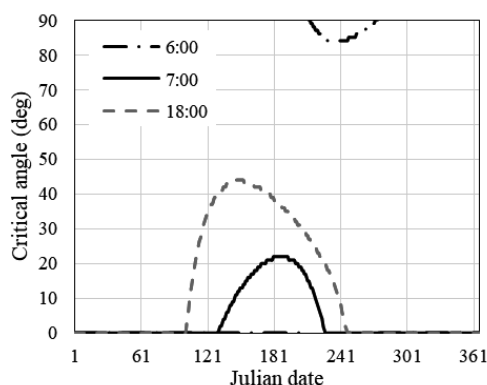


Fig. 5. Daily variation of critical angles for the north slat window

C. Schemes for the slat angle control

The results in section A and B are used to identify schemes to control a slat window when it is installed on north and south facades as shown in Table I. The critical blind angles are rounded into 5 degree interval for ease of operation. For the south slat window, the slats can be tilted in 3 patterns. In the beginning and end of a year, the slats should tilt downward at the angles described in Table I during 7:00-9:00 and 16:00-18:00. For the rest of the day, the slats should be fully opened (0°) for maximum daylight and view. In the middle of a year (10th March-12th October) the slats should be fully opened. In contrary, the slats of the north window should tilt downward during 6:00-7:00 and 18:00 in the middle of a year and fully

open the whole day during the rest of a year. During night time slats can be fully opened (0°) for view or fully closed (90°) for privacy depending on user preference.

The proposed schemes can be used with an automated PV-slat window which can be controlled by using a motor driver to amplify motor control signals from the microcontroller and supplies electricity to the step motor to adjust the PV slats.

TABLE I. CONTROL SCHEMES

Window orientation	Application Duration	Slat Angle (degree)															
		Time (hr)															
		6:00	7:00	8:00	9:00	10:00	11:00	12:00	13:00	14:00	15:00	16:00	17:00	18:00			
South	1Jan-9Mar	0	80	30	5	0	0	0	0	0	0	0	10	40	90		
	10Mar-12Oct	0	0	0	0	0	0	0	0	0	0	0	0	0	0		
	13Oct-31Dec	0	75	30	5	0	0	0	0	0	0	0	15	45	0		
North	11Apr-2Sep	90	25	0	0	0	0	0	0	0	0	0	0	0	45		
	1Jan-10Apr	0	0	0	0	0	0	0	0	0	0	0	0	0	0		
	3Sep-31Dec	0	0	0	0	0	0	0	0	0	0	0	0	0	0		

V. CONCLUSIONS

The schemes for controlling PV integrated slat windows have been proposed in this study for Bangkok, Thailand and nearby locations. These schemes can be applied for any horizontal slats that their slat widths are equal to their slat separations. The shading devices can be internal or external horizontal shades. These schemes are also valid for in between glass blinds. The schemes are simple so slats can be controlled by using less effort from a controller in order to facilitate use of daylight and production of clean energy from a PV-slat window. Further research is needed to determine amount of solar radiation absorbed by a PV-slat and its energy production. The study for vertical PV-slat windows is interesting also.

REFERENCES

- [1] J. Khedari, J. Waewsak, W. Supheng, J. Hirunlabh, "Experimental investigation of performance of a multi-purpose PV-slat window," *Sol. Energy Mater. Sol. Cells*, vol. 82, 2004, pp. 431-445.
- [2] T. Hong, J. Oh, K. Jeong, J. Kim, and M. Lee, "Establishment of Optimal Control Strategy of Building-Integrated Photovoltaic Blind Slat Angle by Considering Interior Illuminance and Electricity Generation," in *Machine Learning, Optimization, and Big Data: Second International Workshop, MOD 2016, Volterra, Italy, August 26-29, 2016, Revised Selected Papers*, vol. 10122, Springer, pp. 451-453.
- [3] A. Stamatakis, M. Mandalaki, and T. Tsoutsos, "Multi-criteria analysis for PV integrated in shading devices for Mediterranean region," *Energy Buildings*, vol. 117, 2016, pp. 128-137.
- [4] P. Chantawong, "Experimental study of a PV blinds glazed solar chimney assisted with DC fan for hot water production," *Energy Procedia*, vol. 138, 2017, pp. 20-25.
- [5] S. Chirattananon and P. Chaiwattworakul, "Distributions of sky luminance and radiance of North Bangkok under standard distributions," *Renew. Energ.*, vol. 32, 2007, pp. 1328-1345.
- [6] P. Chaiwattworakul, S. Chirattananon, P. Rakkwamsuk, "Application of automated blind for daylighting in tropical region," *Energy. Convers. Manage.*, vol. 50, 2009, pp. 2927-2943.



The Study of Knowledge, Understanding, and Behavior on Electric Power in Household in Muang District, Nakhon Pathom Province

Kittisak Khuwaranyu*

Mechanical Engineering Department, Faculty of
Engineering and Industrial Technology, Silpakorn
University, Nakhon Pathom 73000, Thailand

*corresponding author; e-mail: kittisak_mesu@yahoo.com

Duangkamol Ruen-ngam Rattanakosin

College of Sustainable Energy and Environment,
Rajamangala

University of Technology Rattanakosin,
Nakhon Pathom 73170, Thailand

Abstract— The objectives of this research was to identify the difference between personal data and information perception on electric power at individual level which affects behavior on electric power saving in household as well as to study the relationship between knowledge and understanding and frequency of information perception on electric power saving in household. The sample of this study was the people who live in Muang district, Nakhon Pathom province. The research findings indicated that most respondents held Bachelor Degree, had monthly income at medium level (quite low), lived in single family (3-4 family members), lived in single house, and paid the medium to low amount of electricity price. As for the knowledge and understanding on electric power saving, it was found that most respondents were at the medium level and received information 1-2 times per month. Referring to the hypothesis testing, it could be found that the personal information, knowledge and understanding, and frequency of information perception on electric power had statistically significant relationship to the behavior in selecting and maintaining home appliances.

Keywords— energy saving; knowledge, understanding, and behavior; household

I. INTRODUCTION

The research and development and innovation in science and technology has contributed to the humankind. This really brings the convenience and better well-being to life. In addition, the energy is essential and fundamental element as it can serve all basic needs to human-being and successfully drives industry and business sectors through most of major activities. Consequently, it is necessary to ensure the energy supply in reasonable price, and great quality to serve the user's needs. According to the electric power usage in 2016, it was seen that it increases at 3.84% from the previous year as the electric power was increasing in almost all sectors excluding agricultural sector. In addition, it was found that among all, the industry sector holds the biggest ratio (42%), followed by household (24%). According to the electric usage during 2013 – 2016, it was indicated that the household holds the most increasing portion among all as the volume was at 43,932 GWh (increasing at 6.41 % from previous years) [1].

Anuwongnawatana [2] concluded the result of research on behavior in electric power saving in 300 high school students in a high school in Nakhon Pathom province. The research findings revealed as follows: 1) Individual factor in occupation of family head from all occupations and household monthly income in all student levels significantly affected the electric power saving at medium level. 2) Supporting factors in attitude towards electric power saving were at high level while the information perception on electric power and knowledge on electric power saving were at medium level. 3) High school students had different level of attitudes towards electric power saving but had no different behavior in saving electric power at statistical level of significance. Tilai [3] studied the behavior in saving electric power of 175 operations workers who work more than one year in electric power generating function in Ratchaburi province and found as follows: 1) Individual factor including different ages had different behavior in saving electric power at statistical level of significance. 2) Supporting factors i.e. the different knowledge on electric power saving and valuing on electric power saving significantly affected the different behavior in saving electric power at statistical level of significance. Laicane [4] examined the measurement on electric power saving in household and analysis on the user's needs on electric power in household by calculating the volume of usage in four people in one family. The volume of power usage were from investigating the characteristics and behavior in daily life in household in Smart Meter campaign and the findings was that the efficiency in using electric power in household can save energy at 13% which mostly came from adjusting some behaviors in using home appliances which could be regarded as critical factor in electric power saving. Ohler [5] investigated factors which influenced behavior in saving electric power and eco-friendly electric power usage by observing behavior in saving electric from the targeted group and others in terms of motives in using electric power in each individual and others, behavior in saving electric power, volume of electric power used. The controlled variable in this research was the average income. The findings were that the sample group demonstrated some behavior in saving electric power.



As for the electric power for household, it is assumed that all people could contribute to the study and be one of important parameters. As a result, the researcher recognized on the importance of investigating knowledge, understanding, and behavior in saving electric power in household in Muang district, Nakhon Pathom province in order to understand the level of knowledge and understanding on electric power saving, the needs of information perception on electric power saving and source of information, and even the behavior in saving electric power in household.

II. RELATED THEORY

A. Definition of knowledge and understanding

Knowledge refers to the basic behavior which learner could only remember by recalling, seeing, or hearing something to recall. The knowledge in this level includes definition, meaning, fact, theory, rule and regulation, structure, solution, standard, etc. It can be inferred that the remembrance or cognition does not require any complicated process, meaning that it does not require brain ability either. Therefore, the meaning of knowledge and understanding in this level can refer to curiosity and something from studying, searching, remembering, and experience in expressing the meaning. This can really occur after perceiving information by a variety of listening, seeing, reading, or writing methods to interpret or guess the meaning to achieve the mission.

B. Information perception Theory

The information perception can be divided into two main types as follows:

1) Information perception by mass communication – the mass media is expected by the message receivers that the information consumption can serve their needs. This can also changes attitude, knowledge, or even characteristics and behavior. Upon their different and specific objectives and intention, the message receivers select the information consumption.

2) Information perception by personal media – the person who takes the information from someone to another by the interaction between them. In order that the receiver is expected to perceive information or the message is communicated more effectively, it is advisable that the person should be the channel to deliver information.

III. RESEARCH METHODOLOGY

A. Sample Group

The sample group in this research was the people who live in Muang district, Nakhon Pathom province where the 109,778 household resides, according to the Civil Registration Database (as of October, 2017). Referring to Yamane's sample calculation, the researcher finalized the 400 numbers of sample group at 95% of confidence and 5% margin of error [6].

B. Research Hypothesis

Hypothesis 1: The different personal information including sex, age, occupation, educational background, average income, number of family member, residential type, monthly electricity and price, significantly affected behavior in saving electric power in household.

Hypothesis 2: The different level of knowledge and understanding had relationship to behavior in saving electric power in household.

Hypothesis 3: The different information perception had relationship to behavior in saving electric power in household.

Hypothesis 4: The different frequency in information perception had relationship to behavior in saving electric power in household.

As Fig. 1, it illustrated the research framework which identify statistical tools used in this research – means, Independent t-test, and One-Way ANOVA method. If the result of analysis was different, the researcher would apply

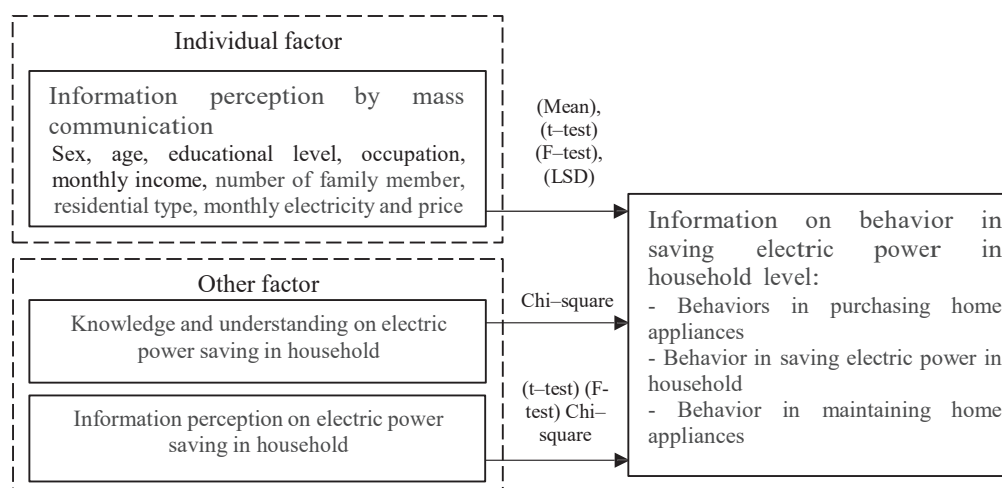


Fig. 1. Research framework



Least – Significant (LSD) for further validation. In terms of knowledge and understanding on electric power saving, the Chi-Square test was applied to test the two independent variables. As for information perception on electric power saving, the Independent t-test and One-Way ANOVA were applied. In case that the result of analysis was different, the Least – Significant (LSD) was applied accordingly and followed by Chi-Square test for testing the two independent variables.

C. Research Tool

In this study, the research tools were the questionnaire on knowledge, understanding, and behavior in saving electric power in household which can be categorized into 4 main sections.

Part 1: Personal information of sample group which consists of the check-list format in sex, age, educational background, occupation, monthly income, number of family members, residential type, and monthly electricity price.

Part 2: Information on knowledge and understanding of sample group on electric power saving in household in closed-ended set of questions. The format includes both Yes/No and the mixed positive and negative questions.

Part 3: Information on information perception on electric power saving in check-list format and five-rating Likert-scale and closed-ended set of questions which was divided into 5 levels (more than 4 times per week, 3-4 times per week, 3-4 times per month, 1-2 times per week, 1-2 times per month, and never)

Part 4: Information on behavior in saving electric power in household in five-rating scale (always, frequently, occasionally, seldom and never).

D. Validity and reliability assessment of questionnaire

The researcher examined the Item Objective Congruence (IOC) Questionnaire by asking professionals in electric power saving to complete questionnaire in order to identify the validity. Referring to the criteria which IOC is more than 0.5, the question item can be used in questionnaire. Whereas IOC in less than 0.5 would be adjusted or taken out. Since the IOC for this questionnaire was 0.910, the researcher validate the reliability by try-out to 30 questionnaire set sand analyzed the α - coefficient. If α is in between $0 \leq \alpha \leq 1$ and close to 1, it indicated that the questionnaire has high reliability and can be applied to the sample group. For this research, α of this questionnaire was 0.817.

IV. RESULT OF DATA ANALYSIS

A. Personal information of sample group

The result of analysis to personal information which affect the behavior in saving electric power in household. It was found that most respondents were female (56.75%), were between 30-39 years old, held Bachelor Degree, were employee, had monthly income between 10,001-20,000 THB,

had 3-4 members in their family, resided in single house, and paid electricity price between 1-1,000 THB.

B. Knowledge and understanding on electric power saving in household

The result of analysis to knowledge and understanding on electric power saving in household. It could be seen that the respondents had the knowledge and understanding on electric power saving at medium level (76.25%).

C. Information perception on electric power saving in household

1) In this part, the researcher investigated the information perception, information application, and the information source on electric power saving in household.

It could be found that almost all respondents (98%) have ever received information on electric power saving and applied the information in practice. It was also found that 60% of them have applied frequently and some times. The main information channel was television (47.50%) while Facebook is following (29.50%).

2) Frequency in information perception on electric power saving in household

From table I which presented the means, S.D., and frequency on electric power saving in household, it indicated that most respondents received information on television, followed by Facebook and newspaper respectively. Also, it was found that they received information 1-2 times per month.

D. Knowledge and understanding on electric power saving in household

According to table II, it was seen that the respondents demonstrated behavior in using electric power with cost-efficiency and frequently did maintenance properly. It also shows the frequency in demonstrating all aspects of behavior in saving electric power both positively and negatively.

E. Result of analysis on difference between personal information and behavior in saving electric power in household

1) Hypothesis 1: The different personal information including sex, age, occupation, educational background, average income, number of family member, residential type, monthly electricity and price, significantly affected behavior in saving electric power in household. The statistical tools used for testing this hypothesis included Independent t-test, One-Way ANOVA and Least – Significant (LSD).

Referring to table III, it was found that the different residential style and monthly electricity and price did not affect the behavior in saving electric power whereas the different sex, age, occupation, educational background, average income, number of family member affected the behavior in saving electric power in household at statistical level of significance.



2) Hypothesis 2: The different level of knowledge and understanding had relationship to behavior in saving electric power in household. The statistical tool used for testing this hypothesis was Chi-Square test.

Referring to table IV, it could be found that the P-value was 0.000 in all aspects of behaviors in purchasing home appliances and maintaining home appliances, this implies that the respondents had knowledge and understanding on electric power saving both in positively and negatively at statistical level of significance.

3) Hypothesis 3: The different information perception had relationship to behavior in saving electric power in household. The statistical tools used for testing this hypothesis were firstly the One-Way ANOVA and followed by Least – Significant (LSD) if there was any difference found in the findings.

Referring to table V, it was found that the difference in information perception and needs for information on electric power saving did not affect the behavior in saving electric power. Also, the application from different information sources significantly affected the electric power saving at level of statistical significance.

4) Hypothesis 4: The different frequency in information perception had relationship to behavior in saving electric power in household. The statistical used for testing this hypothesis was Chi-Square test.

Referring to table VI, it could be seen that all aspects of behavior, (purchasing, using, and maintaining) had P-value less than 0.5, this significantly implies that the frequency of information perception on electric power saving in household did not affect the behavior in purchasing and maintaining home appliances at level of statistical significance.

V. CONCLUSION

Referring to the analysis on the relationship between knowledge and understanding and behavior in electric power saving in household in Muang district, Nakhon Pathom province, it could be concluded that the respondents held

Bachelor Degree, had monthly income at medium (to low) level, lived in single family which had 3-4 family members, lived in single house, and paid electricity price at medium to low rate. As for knowledge and understanding on electric power saving, it was found that the respondents had the medium level of knowledge and understanding on electric power saving and received information on electric power saving for 1-2 times per month. Referring to hypothesis testing, it was also found that the different personal information of the respondents significantly affected the different behavior in purchasing, using, and maintaining home appliances. As for the different information perception on electric power saving in household did not have behavior in purchasing, using, and maintaining home appliances. Finally, the knowledge and understanding and frequency on information perception on electric power saving in household significantly affected the behavior in purchasing, using, and maintaining home appliances.

ACKNOWLEDGMENT

This research was supported by Department of Mechanical Engineering, Faculty of Engineering and Industrial Technology, Silpakorn University, Thailand.

REFERENCES

- [1] Ministry of Energy, Thailand (2016). Energy Annual Report 2016.
- [2] P. Anuwongnawaratana (2008). Electrical energy saving behavior of the primary school students under the Department of Formal Education, Nakhon Pathom Province, Master of Business thesis, Nakhon Pathom Rajabhat University.
- [3] J. Tilai (2009) Saving electric energy behaviors in the office of the Electricity Generating Authority of Thailand Officers Ratchaburi Power Plant, Master of Art thesis (Program of Public and Private management), Silpakorn University.
- [4] I. Laicane (2015). "Evaluation of household electricity savings. Analysis of household electricity demand profile and user activities", Energy Procedia, Vol.72, pp.285 – 292.
- [5] A.M. Ohler, (2014). "Does environmental concern change the tragedy of the commons? Factors affecting energy saving behaviors and electricity usage", Ecological Economics, Vol.107, pp.1–12.
- [6] Y. Taro. Statistics: An Introductory Analysis (2ed.). NewYork: Harper and Row, 1967.

TABLE I. MEAN, STANDARD VARIATION AND LEVEL OF FREQUENCY OF INFORMATION PERCEPTION ON ELECTRIC POWER SAVING IN HOUSEHOLD

Electric power saving in household information Sources	Frequency on electric power saving in household		
	Mean	S.D.	Demonstrated behavior
1. Newspaper	1.77	1.399	1-2 times per week
2. Television	2.70	1.255	3-4 times per week
3. Radio	1.73	1.417	1-2 times per week
4. Social media : Facebook	2.24	1.545	1-2 times per week
5. Social media : Line app.	1.65	1.618	1-2 times per week
6. Social media : Instagram app.	1.04	1.435	1-2 times per month
7. Social media : Twitter	0.80	1.330	Never
8. Website	1.26	1.445	1-2 times per month
9. Brochure	1.17	1.208	1-2 times per month
10. Poster media	1.28	1.213	1-2 times per week
11. Journal/Magazine	1.06	1.196	1-2 times per month
12. Other media	1.58	1.356	1-2 times per month
Average	1.52	1.468	1-2 times per month



TABLE II. BEHAVIOR IN ELECTRIC POWER SAVING IN HOUSEHOLD

Behavior in electric power saving in household	Behavioral value in electric power saving in household		
	Mean	S.D.	Interpretation from mean
Behavior in purchasing home appliances (Positively)	3.99	1.141	Frequently
Behavior in purchasing home appliances (Negatively)	3.30	1.539	Occasionally
Behavior in saving electric power in household (Positively)	3.87	1.271	Frequently
Behavior in saving electric power in household (Negatively)	3.08	1.496	Occasionally
Behavior in maintaining home appliances (Positively)	3.53	1.308	Frequently
Behavior in maintaining home appliances (Negatively)	3.79	1.441	Almost never

TABLE III. INDIVIDUAL FACTOR INFLUENCE A BEHAVIOR IN SAVING ELECTRIC POWER IN HOUSEHOLD

Information perception by mass communication	Level of Behavior in electric power saving in household		
	Purchasing (P-Value)	Saving (P-Value)	Maintaining (P-Value)
1. Sex	0.021*	0.257	0.518
2. Age	0.000*	0.055	0.001*
3. educational level	0.001*	0.018*	0.017*
4. occupation	0.001*	0.027*	0.027*
5. monthly income	0.000*	0.179	0.001*
6. number of family member	0.041*	0.361	0.889
7. residential type	0.748	0.222	0.539
8. monthly electricity and price	0.415	0.527	0.669

*at the statistical significance level of 0.05

TABLE IV. THE RELATIONSHIP BETWEEN LEVEL OF KNOWLEDGE AND UNDERSTANDING HAD RELATIONSHIP TO BEHAVIOR IN SAVING ELECTRIC POWER IN HOUSEHOLD

Information on behavior in saving electric power in household level	Knowledge and understanding on electric power saving
	P-value
Behaviors in purchasing home appliances	0.000*
Behavior in saving electric power in household	0.000*
Behavior in maintaining home appliances	0.000*

*at the statistical significance level of 0.05

TABLE V. DATA ANALYSIS OF HYPOTHESIS 3

Information perception	Level of Behavior in electric power saving in household		
	Purchasing (P-Value)	Saving (P-Value)	Maintaining (P-Value)
1. Information Received	0.408	0.193	0.184
2. Information sources	0.000*	0.001*	0.000*
3. Needs of information perception	0.325	0.279	0.516

*at the statistical significance level of 0.05



TABLE VI. DATA ANALYSIS OF HYPOTHESIS 4

Information on behavior in saving electric power in household level	Frequency in information
	P-value
Behaviors in purchasing home appliances	0.220
Behavior in saving electric power in household	0.779
Behavior in maintaining home appliances	0.081

*at the statistical significance level of 0.05



Fuzzy Logic Concepts for Investment Decision Making: A review

P. Samartkit, P. Tongard and S. Pullteap*
Department of Mechanical Engineering, Silpakorn University
Nakhon Prathom, Thailand
*E-mail: saroj@su.ac.th

Abstract – As fuzzy logic is widely accepted and implemented in several fields to compensate for the lack of precision in our daily life, therefore this work presents the applications of fuzzy logic concepts, particularly, for the investment decision making through the reviewing of recently articles that were published in the past five years. As a result, the essential contents of each work have been reviewed, along with our opinions for the utilizations of fuzzy logic, namely, as the single and multiple fuzzy approaches. In conclusion, we have suggested that fuzzy logic concepts are suitable for the investment decision making by clarifying the previously obscure criteria to provide objective and decisive results.

Keywords—Fuzzy logic concepts; investment decision making; multi-criteria decision making model; business planning

I. INTRODUCTION

In 1965, Fuzzy logic has been introduced by Zadeh as a useful branch of logic which is specially designed to compensate for the imprecision, fuzziness, and uncertainty seen in our daily routine [1]. In addition, since it describes the human reasoning processes in mathematical terms, computers are able to “think” much more like humans. Therefore, fuzzy logic is widely accepted and implemented in the field of engineering, control system, management, medicine, etc. [2], [3]. Interestingly, the traditional decision making, which is carried out by humans through subjective opinions, has been, inevitably, formalized by incorporating the fuzzy logic technique in the process; thereby reducing the imprecision of the decisive result.

This review has been conducted to study the utilization of fuzzy logic for the investment decision making. Primarily, the applications have been explained to clarify the methodology of each research topic. Nevertheless, we have analyzed the contents and synthesized our opinions for the proposed fuzzy logic model. In a broader perspective, nine research articles recently published on the International Scientific Indexing (ISI) based journals in the past five years, have been selected and reviewed for this presentation.

II. CONCEPTS OF FUZZY LOGIC

A. Fuzzy logic

This branch of logic is introduced as a mathematical computation method to compensate for the imprecision, fuzziness, and uncertainty which are presented in our everyday life. Consequently, it allows computers to process akin to the human thinking and reasoning. Therefore, the fuzzy logic is widely used as an artificial intelligence (AI) to assist in operations where obscure component is presented.

Unlike the “Boolean logic” which expresses a sharp limitation of “0” or “1” only, fuzzy logic demonstrates a fuzzy boundary between “0” to “1” and indicates a degree of membership to its corresponding members, i.e. when classifying “a tall man”, Boolean logic would only state if an individual is “tall” or “not tall”, while fuzzy logic would be able to express the “degree of tallness” of said person, such as “slightly tall” or “considerably tall”, etc. [4], [5].

B. Fuzzy set theory

A fuzzy set is a set which utilizes the fuzzy logic to assign its members with their respective degree of membership. Therefore, these members are not necessary the absolute population of the set and may exist between any given groups, as seen on Fig. 1.

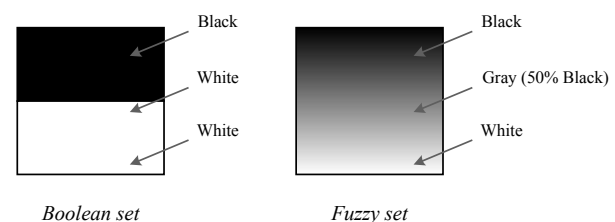


Fig. 1 Comparison between Boolean and fuzzy sets

In mathematical terms, a fuzzy set A in the universe of discourse X is defined by [6]:





$$A = \{x, \mu_A(x) : x \in X\} \quad (1)$$

Where: A is the fuzzy set
 x is the member of fuzzy set A
 $\mu_A(x)$ is the degree of membership of x
 X is the universe of discourse

C. Fuzzy inference mechanism

Commonly, once fuzzy logic is applied as an inference mechanism, three steps of operation would occur; the fuzzification, the fuzzy inference system, and the defuzzification. Moreover, a knowledge database is conducted to administer these steps to provide a desirable output, as shown in Fig. 2.

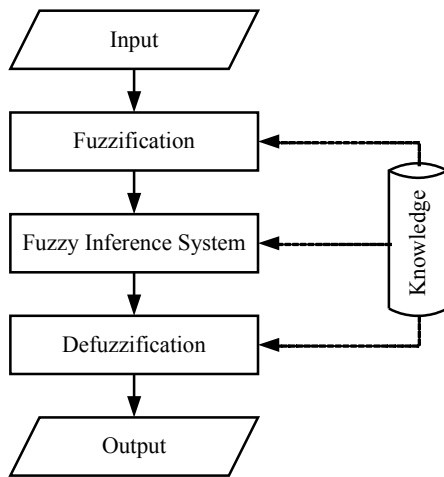


Fig. 2 Fuzzy inference mechanism

D. Fuzzification

This step enables the conversion of numerical data into linguistic fuzzy members of the fuzzy set. The triangular and trapezoidal fuzzy sets are generally utilized as they provide less intensive geometric functions, as their expressions are given by (2) and (3), respectively [7]:

$$\mu_{\Delta}(x) = \begin{cases} (x-a)/(b-a) & , \text{ if } a \leq x \leq b \\ (c-x)/(c-b) & , \text{ if } b \leq x \leq c \\ 0 & , \text{ if otherwise} \end{cases} \quad (2)$$

$$\mu_{\square}(x) = \begin{cases} (x-a)/(b-a) & , \text{ if } a \leq x \leq b \\ 1 & , \text{ if } b \leq x \leq c \\ (d-x)/(d-c) & , \text{ if } c \leq x \leq d \\ 0 & , \text{ if otherwise} \end{cases} \quad (3)$$

Furthermore, the variables given above may be described through Fig. 3.

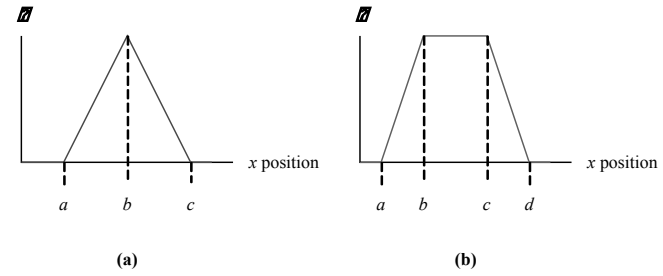


Fig. 3 Concepts of fuzzy sets; (a) Triangular sets, and (b) Trapezoidal sets

As mentioned above, it has been implied that the possibility of any inputs obtaining a maximum degree of membership in the trapezoidal fuzzy sets is higher than that in the triangular sets, due to the former having a wider determination range, spanning between the variables b and c , while the latter only indicates any members with the same value as the variable b a full degree of membership.

E. Fuzzy inference system

Due to the linguistic descriptions of the fuzzy sets, the fuzzy inference system is employed to compute these fuzzy parameters through a set of “If-then” rules. Additionally, a logic operator, such as “And”, “Or”, and “Compliment”, is usually applied to these rules for the formation of a more complex system [8]. Therefore, each fuzzy rule is generally described as:

If x is $\mu_i(x)$ And y is $\mu_i(y)$, then z is $\mu_i(z)$

Where: $\mu_i(x)$ is the membership degree of the input x
 $\mu_i(y)$ is the membership degree of the input y
 $\mu_i(z)$ is the membership degree of the output z
 i is the sequence number of a fuzzy rule

Consequently, the logic operators determine the output membership degree of each rule, as their expressions are given according to the rule formation in the following [2]:

a) Fuzzy rule “If-And-Then”

$$\mu_i(z) = \mu_i(x) \cap \mu_i(y) = \min(\mu_i(x), \mu_i(y)) \quad (4)$$

b) Fuzzy rule “If-Or-Then”

$$\mu_i(z) = \mu_i(x) \cup \mu_i(y) = \max(\mu_i(x), \mu_i(y)) \quad (5)$$



F. Defuzzification

The fuzzy inference system allows the fuzzy parameters to be compute and generate appropriate outputs. However, these results are not suitable for further mathematical operations. As such, defuzzification is introduced as a step for converting the fuzzy parameters into numerical data. Several methods of defuzzification have been proposed, and each solution is utilized to achieve a desirable output depending on the user. Nevertheless, the most widely accepted method is known as the “Centroid of Area (COA)” or the “Center of Gravity (COG)”, which is described according to the following [9]:

$$D = \frac{\int_{i=1}^I (\mu_i(z) \times z)}{\int_{i=1}^I \mu_i(z)} \quad (6)$$

Where: D is the output from the defuzzification
 z is the centroid of the fuzzy output set
 I is the total sequence of the fuzzy rule

The distinctive point of this method is the acceptable accuracy of its output, due to the calculation employs each and every fuzzy rule accordingly. However, this method can only be applied to a fuzzy mechanism with a fuzzy output set, as the centroids of its subsets are required.

III. FUZZY LOGIC FOR APPLYING IN INVESTMENT DECISION MAKING

Nine selected research articles, published on the ISI based journals between the year 2014-2018, has been reviewed. Additionally, the utilization of fuzzy logic concepts in each research has been given, along with any presented case study, as mentioned in the following:

Omwando *et al.* incorporated a bi-level fuzzy logic as an analytic decision support tool for assessing the remanufacturing possibility of a product. Several parameters, such as manufacturing time, overhead costs, energy savings, and equipment utilizations, had been fuzzified into the technological, economic, environmental, and resource utilization indices, respectively. Consequently, these indices had been converted through another fuzzy inference mechanism to assess the re-manufacturability index, which would be considered as the decision-making criterion. Furthermore, a case study of two different families of control drivers had been conducted, of which result stated that the larger and more aging product had the re-manufacturability index of 0.662. Conclusively, these drivers were deemed more appropriated for the remanufacturing than the ones with the index of 0.448. Therefore, this research had summarized that the proposed tool was versatile for comparing families of products to determine their remanufacturing possibility, and could support the decision making in this field [10].

The substantial increase of solar energy investment in recent years had caused a problem in selecting a convenient location for a new project. Thus, Tavana *et al.* demonstrated the use of fuzzy logic as a multi-criteria decision support system for the solar farm location planning. Initially, the considered inputs, namely the environmental and economic criteria, were defined and evaluated through opinions of experts and from the literature reviews. The obtained data were, then, analyzed to adjust the weight which would later impact the inference mechanism. Consequently, the fuzzy inference system, comprised of thirty-seven “If-then” rules, was employed for the analysis to determine the setup priority within a designated area. As such, the best possible location was, ultimately, chosen by selecting an area with the highest setup priority. Furthermore, the researchers had conducted a study to select the best location for a solar farm project in the Iranian regions of Kerman and Yazd, which the proposed method had, conclusively, determine the best setup location in an area north-west of the Kerman region; thereby proven the efficacy of this research [11].

To prospect the suitable area for the wood panel industries installation, Santos, *et al.* proposed the application of fuzzy logic as an analysis tool in the case study supervised in Brazil. Agriculmatological zoning of different species and eucalyptus hybrids was, firstly, conducted to select the desirable vector variables. Euclidian distance was, next, applied to these specimens for the definition of the matrix variables, which were later employed by the fuzzy logic for simulating the planting area. To finalize this research, the overlapping fuzzy outputs were utilized to locate the best suitable area for the installation. The researchers, in addition, stated that the proposed work afforded flexibility for the wood panel industries installation. Additionally, this could bring great economic and social benefits to the local population. Therefore, it was encouraged for further developments and implementations in other agricultural fields [12].

Macedo *et al.* presented a methodology to indicate the priority order of the smart grid implementation criteria, namely the technical, economic, and environmental factors, through the application of fuzzy logic. By indicating the said criteria first, the fuzzy inference system would analyze these components and generate the priority factor which would ultimately assist in the decision making for the deployment of smart grid systems. For the verification, six random electrical systems in Brazil had been evaluated. Regarding this study, the system with the greatest return of investment had presented the highest priority factor, thereby concluding that this evaluated system was chosen for a smart grid implementation [13].

The criteria considered for any investment were stated to be subjective and extremely difficult to express as numbers. However, Kiliç and Kaya introduced a solution by utilizing fuzzy logic to assess these vague criteria into computable mathematic indices. As such, the selection of investment model criteria was initially identified. Then, the fuzzy operations were carried out to display the numerical indices.



Finally, another mechanism, namely, the fuzzy Technique for Order of Preference by Similarity to Ideal Solution (TOPSIS) was employed to evaluate the ranking of the investment projects. Moreover, the result from a case study performed in the Middle Black Sea Development Agency (OKA) in Turkey had suggested that the presented model was effective in the evaluation of multi-criteria group decision making problems with broader perspective and flexibility [14].

As facility layout is crucial to the improvement of plant productivity, Liu *et al.* demonstrated the layout design for the thin film transistor-liquid crystal display module manufacturing plant. Firstly, the systematic layout planning had been conducted to generate several layout alternatives, of which performances had, then, been evaluate into both the quantitative and qualitative indices. In addition, the fuzzy logic had been applied to assess the effectiveness of each layout. Hence, a layout with the highest rank had been decided based on its total move distance. Moreover, a practical case study had been performed to illustrate the application, of which analysis shown the results of four designs before selecting the layout with the least moving distance. Therefore, this study summarized that the demonstration was suitable for the practical application in the evaluation of the facility layout design selection [15].

Oh *et al.* proposed a method for deciding the discontinuation of the declining product, as further manufacturing would cause more expense than profit. Initially, numerical data, such as the market demands, inventories, and post logistics productions, had been extracted. The end-of-life analyses had, next, been applied before the outputs were utilized for the fuzzy inference mechanism to decide if the product would be discontinued. Furthermore, a case study of three washing machines had been studied to verify the performance of the proposed method. Ultimately, the declining model had an inferred score of 25.27, the lowest among the three. As such, this model had been considered the first priority for the discontinuation. Thus, the research had concluded that this method provided a review of the products, as well as their sales percentages, which could potentially support the decision making of the user [16].

To predict the decision making of the air conditioner consumers, the fuzzy model for the residential energy assessment was presented by Spandagos and Ng. The inputs utilized for this model, namely, the monthly income, planning horizon, electricity price, ambient temperature, relative humidity, and environmental responsibility, had been synthesized with three fuzzy inference mechanisms, of which results would assess the cooling capacity, energy efficiency ratio, and usage possibility. As such, these outputs had suggested the residential energy usage of the consumers. Moreover, the model had been verified using the previous studies of energy consumption, which, conclusively, shown that the presented work was suitable for the assessment. In addition, it could be inferred that this model would assist in the air conditioner selection for the consumer based on its

outputs, and may provide the industrial sector with optimal investment for the development of this technology [17].

Salaken *et al.* developed a fuzzy decision support system to evaluate the output uncertainty in terms of percentage score, which would improve the information quality of the analyzed results. Firstly, the considered parameters had been included into the system, which had, then, been inferred using the interval type-2 fuzzy logic technique. Finally, the uncertainty score had been shown for further interpretation of confidence. Furthermore, a sales price forecasting experiment had been demonstrated to verify the practicality of the developed system. By using the sales price occurred between the year 2007-2016 as the input, the predicted output was 11.9575 with the uncertainty score of 0.618%. This ultimately provided valuable information which could be applied as a risk metric in further decision making. Therefore, the research had concluded that this system could be utilized to enhance the confidence of information for the decision making process [18].

IV. DISCUSSIONS ON FUZZY LOGIC APPLICATIONS

Since the reviews of the selected researches have been conducted, we have analyzed and synthesized the proposed fuzzy logic utilizations for the investment decision making. Consequently, the applications have been divided into two types according to the amount of fuzzy inference mechanism incorporated into each stage; the single and multiple fuzzy approaches.

The single fuzzy approach is a method which incorporate the fuzzy inference mechanism in only a stage of the system, as seen by [11]–[13], [15]–[18], where the fuzzy logic technique had been applied in a step only once (in case of [17], three fuzzy mechanisms had been utilized simultaneously in one stage). This has been seen to be implemented when the calculation of linguistic values are essential. Therefore, the advantage of the single fuzzy approach is its simplicity to be performed and validated. However, this method would, ultimately, limit the complexity of the decision making system, which may reduce the accuracy of the whole model.

Another type of the implementation is the multiple fuzzy approaches, where the output of one inference mechanism is utilized as the input for another mechanism, creating a more complex decision making model. For example, [10], [14] had applied a fuzzy logic system to synthesize the fundamental parameters before inferring them with the other fuzzy mechanism which conclusively provide the final result. As such, this implementation technique is complex and may cause difficulties when validating the model for any possible errors. Nevertheless, its output would have more accuracy, which would improve the quality of the result for further applications.



To consolidate this discussion, Table I has displayed the advantages and drawbacks of the single and multiple fuzzy

approach, as well as the reviewed works which adopted these fuzzy logic concepts.

TABLE I FUZZY LOGIC CONCEPTS IN EACH REVIEWED WORK

Fuzzy approach	Definition	Advantages	Drawbacks	Adopted researches
Single	Only one process step applies the fuzzy logic concept	Simple to implement and validate for error estimation	Limited complexity may significantly alter the targeted accuracy	<ul style="list-style-type: none"> – Tavana <i>et al.</i> [11] – Santos <i>et al.</i> [12] – Macedo <i>et al.</i> [13] – Liu <i>et al.</i> [15] – Oh <i>et al.</i> [16] – Spandagos & Ng [17] – Salaken <i>et al.</i> [18]
Multiple	More than one process steps implements the fuzzy logic technique	Allow more complex inference system for better result accuracy	Possible difficulty in error detection due to model complexity	<ul style="list-style-type: none"> – Omwando <i>et al.</i> [10] – Kiliç & Kaya [14]

V. CONCLUSION

In this work, a review of fuzzy logic concepts for the investment decision making has been presented. Nine researches related to the topic have been cited. As such, we have analyzed the contents and stated our opinions in the proposed fuzzy logic applications of each work. By classifying the utilizations of fuzzy logic in each decision making model, the single and multiple fuzzy approaches have been presented, each with its own advantages and drawbacks. The single fuzzy approach is suitable for less complex decision making process as its setup are simple to be perform and validated, but the accuracy of the output is limited. On the contrary, any elaborated decision making models would apply the multiple fuzzy approaches for their complex judgement system, yet their complicated setup procedures may be undesirable. As a result, this review has concluded that fuzzy logic concepts can be applied in the field of investment decision making by various means, which would support the optimizations of any proposed project through the clarification of imprecise, vague, and uncertain criteria into assessable indices.

VI. REFERENCES

- [1] L. A. Zadeh, "Fuzzy logic—a personal perspective," *Fuzzy Sets and Systems*, vol. 281, pp. 4–20, 2015.
- [2] P. Gupta, "Applications of Fuzzy Logic in Daily life," *International Journal of Advanced Research in Computer Science*, pp. 1796–1800, 2017.
- [3] P. Kadam and A. M. Patki, "Fuzzy logic controller: an overview and applications," *Imperial Journal of Interdisciplinary Research*, vol. 2, no. 6, pp. 795–797, 2016.
- [4] O. Ozdemir and A. Tekin, "Evaluation of the presentation skills of the pre-service teachers via fuzzy logic," *Computers in Human Behavior*, vol. 61, pp. 288–299, 2016.
- [5] S. Rajak, P. Parthiban, and R. Dhanalakshmi, "Sustainable transportation systems performance evaluation using fuzzy logic," *Ecological Indicators*, vol. 71, pp. 503–513, 2016.
- [6] S. Chaudhari and M. Patil, "Study and Review of Fuzzy Inference Systems for Decision Making and Control," pp. 88–92, 2014.
- [7] S. Petropoulos, C. S. Karavas, A. T. Balafoutis, I. Paraskevopoulos, S. Kallithraka, and Y. Kotseridis, "Fuzzy logic tool for wine quality classification," *Computers and Electronics in Agriculture*, vol. 142, pp. 552–562, 2017.
- [8] P. Nayak and A. Devulapalli, "A Fuzzy Logic-Based Clustering Algorithm for WSN to Extend the Network Lifetime," *IEEE Sensors Journal*, vol. 16, no. 1, pp. 137–144, 2016.
- [9] S. Shams, M. Monjezi, V. J. Majd, and D. J. Armaghani, "Application of fuzzy inference system for prediction of rock fragmentation induced by blasting," *Arabian Journal of Geosciences*, vol. 8, no. 12, pp. 10819–10832, 2015.



- [10] T. A. Omwando, W. A. Otieno, S. Farahani, and A. D. Ross, "A Bi-Level fuzzy analytical decision support tool for assessing product remanufacturability," *Journal of Cleaner Production*, vol. 174, pp. 1534–1549, 2018.
- [11] M. Tavana, F. J. Santos Arteaga, S. Mohammadi, and M. Alimohammadi, "A fuzzy multi-criteria spatial decision support system for solar farm location planning," *Energy Strategy Reviews*, vol. 18, pp. 93–105, 2017.
- [12] A. R. D. Santos *et al.*, "Fuzzy logic applied to prospecting for areas for installation of wood panel industries," *Journal of Environmental Management*, vol. 193, pp. 345–359, 2017.
- [13] M. N. Q. Macedo, J. J. M. Galo, L. A. L. Almeida, and A. C. C. Lima, "Methodology for the calculation of the factor of priority for smart grid implantation using fuzzy logic," *International Journal of Electrical Power & Energy Systems*, vol. 78, pp. 563–568, 2016.
- [14] M. Kiliç and İ. Kaya, "Investment project evaluation by a decision making methodology based on type-2 fuzzy sets," *Applied Soft Computing*, vol. 27, pp. 399–410, 2015.
- [15] Y.-S. Liu, L.-N. Tang, Y.-Z. Ma, and T. Yang, "TFT-LCD module cell layout design using simulation and fuzzy multiple attribute group decision-making approach," *Applied Soft Computing*, vol. 68, pp. 873–888, 2018.
- [16] J. Oh, J. Han, and J. Yang, "A fuzzy-based decision-making method for evaluating product discontinuity at the product transition point," *Computers in Industry*, vol. 65, no. 4, pp. 746–760, 2014.
- [17] C. Spandagos and T. L. Ng, "Fuzzy model of residential energy decision-making considering behavioral economic concepts," *Applied Energy*, vol. 213, pp. 611–625, 2018.
- [18] S. M. Salaken, A. Khosravi, T. Nguyen, and S. Nahavandi, "Output uncertainty score for decision making processes using interval type-2 fuzzy systems," *Engineering Applications of Artificial Intelligence*, vol. 65, pp. 159–167, 2017.



Development of a Capital Investment Decision Function via a Spreadsheet Program: A Case Study of LED T8 Production in Thailand Industry

T. Tanongtanachai, G. Smithisup and S. Pullteap*

Department of Mechanical Engineering, Faculty of Engineering and Industrial Technology
Silpakorn University, Nakhon Pathom, 73000, Thailand

*E-mail: saroj@su.ac.th

Abstract— This paper presents the development of a capital investment decision function via a spreadsheet program for a case study of LED T8 production in Thailand industry. The financial data such as revenue, labor costs, raw material costs, packaging and freight costs were used as input variables for investigating the results of Net Present Value (*NPV*), Internal Rate of Return (*IRR*), Benefit-Cost Ratio (*BCR*), and also Payback period (*PB*) for investment analysis. The calculation was done by using a financial calculator, and also the developed function via spreadsheet program. The results of *NPV*, *IRR*, *BCR* and *PB* value were reported of 620,067.30, 17.57%, 1.02 and 3.16, respectively. Consequently, the analyzed results from the program were similar to the calculations and without any errors. Moreover, we found that using the developed function is more compatible and simpler than the calculator in several ways such as data entering, data editing, and data analyzing, etc. This implies that proposed function is especially suitable in the utility of entrepreneurs for making a decision on investment.

Keywords—investment; feasibility analysis; financial calculator; economic tools; spreadsheet program

I. INTRODUCTION

In the present, LED lighting has been developed to use substitute almost any lightings whether in household light, decorative building light, vehicle light, illuminated light, advertising signs, even the light of telephone or computer screen. Kasikorn research center (KReserch) reported the competition of LED lighting price occurred on increasing in amount of manufacturer. Due to the LED lighting is, now a popular component, also the demand of consumer is growing up. In addition, the LED specifications are energy-saving and also longer lifespan than typical lighting such as incandescent, fluorescent, and neon lamp. Therefore, the replacement of LED light makes long-term value. As advantages of LED that mentioned previously, the demand for LED light in Thailand is 33% growth. Furthermore, the KReserch estimated that if household and business sectors replacing to LED light in 50 percent of the exist lighting, Thailand would be able to save costs of using electricity for lighting up to 40,949.9 million baht per year or 29.4% of using the electricity costs for lighting [1]. Therefore, the investment decision-making tool is an activity to conclusion on selecting which project should

investment and thus can be turned up the profit higher. Using of a fundamental of economic tools is the population method [2]-[3] for finding the values of the Net Present Value (*NPV*), Internal Rate of Return (*IRR*), Benefit-Cost Ratio (*BCR*) and Payback period (*PB*). To calculate these parameters, the financial data such as revenue, labor costs, raw material costs, packaging and freight costs [4]-[5] would be used as the input for finding out the analytical results.

This paper first presents the comparison of *NPV*, *IRR*, *BCR* and *PB* value from the developed function via a spreadsheet program with computing from a financial calculator. The concluding the contrast of features between both applications would then be presented in the last section.

II. RELATED THEORIES

A. Fundamental of economic tool

Economic tools that usually are used in analysis of financial data that will lead to conclusion in deciding the project should invest or not by calculating *NPV*, *IRR*, *BCR*, and *PB*, which show the detail as following.

- **Net Present Value:** (*NPV*) is the difference between the present value of benefit and present value of costs. However this parameter is used to consider the capital investment decision. Consequently, when *NPV* value is greater than “0” or positive, it means that project can be profitable, which calculated by:

$$NPV = \sum_{t=0}^n \frac{(B_t - C_t)}{(1+r)^t} \quad (1)$$

Where:

- B_t = the benefit during the period t
- C_t = the costs during the period t
- r = the discount or interest rate
- t = a number of year (1, 2, 3, ... n)
- n = the time period of the project



- **Internal Rate of Return: (IRR)** is the discount rate that achieves the set of *NPV* value equal to zero. This parameter can calculate by trial and error method, representing difference discount rate until *NPV* is “0”. To find the value of *IRR*, it can be expressed by:

$$0 = \sum_{t=0}^n \frac{(B_t - C_t)}{(1 + IRR)^t} \quad (2)$$

- **Benefit-Cost Ratio: (BCR)** is the total present value of benefit divided by the total present value of costs. The project should investment when *BCR* is greater than “1”. In general, the *BCR* value is calculated as follows:

$$BCR = \frac{\sum_{t=0}^n \frac{B_t}{(1+r)^t}}{\sum_{t=0}^n \frac{C_t}{(1+r)^t}} \quad (3)$$

- **Payback Period: (PB)** is the calculation to find out the time period of returning project benefit is equal to the invested money as calculated by:

$$PB = T + \frac{|CCF_T|}{NCF_{(T+1)}} \quad (4)$$

Where:

T = parameter of last year that indicated negative cumulative cash flow

CCF_T = Cumulative cash flow at period T

$NCF_{(T+1)}$ = Net cash flow at the period $T+1$

B. Decision Making

Decision making on investment is a tools for considering when project is acceptable by deciding through the criteria as following: [6]

- *NPV* is greater than “0” or positive value
- *IRR* is greater than discount rate or interest rate
- *BCR* is greater than “1”
- *PB* is less than the time period of the project

III. EXPERIMENTAL SETUP

A. Collecting data

To collect data is the first step for investment decision-making. In this paper we classified data into two categories; financial data, and secondary data respectively. The details of each data are shown in Figure 1.

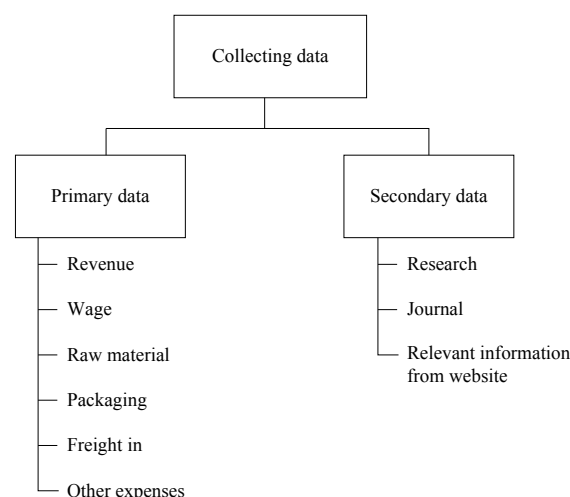


Fig. 1. Collecting data process

According to Fig. 1, the data were collected to be used in feasibility analysis of our case study project. First, the financial data, the numeral of benefit and costs that were assumed such as revenue, costs of labor, raw material, packaging and freight. Furthermore, the secondary data which were relevant information we have collected from available sources like research, journals and websites. The data would be used in next process that is shown in Fig. 2.

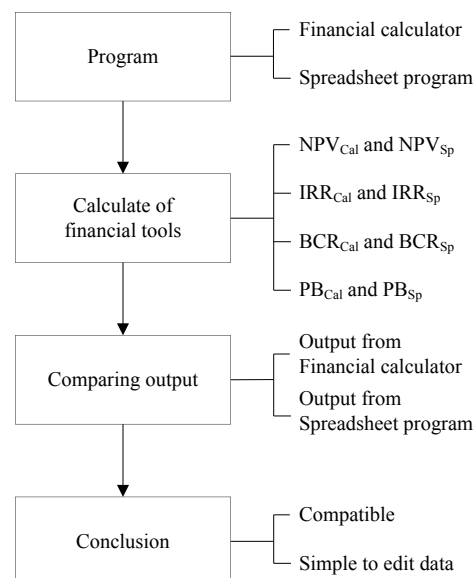


Fig. 2. Process flowchart of developed program

As shown in Fig. 2, when data is completely collected, it would be inserted to a financial calculator a program with developed function for comparing of *NPV*, *IRR*, *BCR* and *PB* value to measure its accuracy. Finally, the conclusion of the contrast features of both applications has been summarized.



B. Calculation by using a financial calculator

The calculator model: *BA II Plus professional* is used to calculate the outputs of *NPV*, *IRR*, and *PB* in this work. The analyzer must, initially, read the calculator guidebook that can download from the owner website [7] to learn how to use it. For calculating the *BCR* value, the analyzer have to compute total benefit and total costs of the project, then bring the number of each results for calculating as (3). An example of the display result is illustrated in Fig. 3.

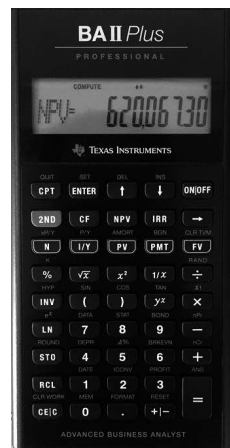


Fig. 3. Example of displaying result from financial calculator

C. Calculation by using development function via spreadsheet program

The developed function is operated on spreadsheet program in Microsoft Excel 2013. We have built-in the formulas on the program and designing the user interface (UI) for data entering or data editing in only one windows display. The user interface and result display of the program is shown in Figure 4.

According to Figure 4 (a), shows the main function that using for data inserting or data editing in section *A*, *B*, *C*, *D* and *E* respectively. The details of each section are presented by:

Section: A Add project name, duration, and interest rates respectively.

Section: B Add initial cost of project

Section: C Add revenue

Section: D Add cost of goods sold

Section: E Add operating expenses

After completely adding data in section *A* to *E*, the results of decision-making will automatically show the values on the result display as can be seen in Figure 4 (b), the outputs would display in section *F* and *G*. The details of format are indicated below:

	AB	C	D	E	F	G	H	I	J	K	L	M	N	O	P
2															
3			Project												
4			Age	A											
5			Interest rate												
6															
7			Estimated revenue & expenses												
8				0	1	2	3	4	5	6	7	8	9	10	
9			Initial cost												
10			Revenue:												
11			Sales												
12			Cost of goods sold:												
13			Raw materials												
14			Packaging												
15			Labor												
16			Freight												
17			Depreciation												
18			Total COGS	0.00	0.00	0.00	0.00	0.00	0.00	0.00	0.00	0.00	0.00	0.00	
19			Operating expenses:												
20			Selling expenses												
21			Administrative expenses												
22			R&D cost												
23			Utilities												
24			Total expenses	0.00	0.00	0.00	0.00	0.00	0.00	0.00	0.00	0.00	0.00	0.00	
25															
26															

	A	B	C (a)	D	E	F
1			Criteria			Decision result
2	NPV	> 0	620,067.30	>	0	ACCEPTED
3	IRR	> Interest rate	17.57%	>	1.450%	ACCEPTED
4	BCR	> 1	1.02	>	1	ACCEPTED
5	PB	< Age	3.16	<	5	ACCEPTED
6						
7						

Fig. 4. Example the proposed spreadsheet program: (a) User interface (b) Format of display result



Section: F Present values of *NPV*, *IRR*, *BCR* and *PB*, respectively.

Section: G Indicate results of investment decision-making; “*Accepted*” would appears when the values match the criteria, “*Ignore*” would appear when the values do not match.

IV. EXPERIMENTAL RESULTS AND DISCUSSION

As computing the data with the calculator and the program, the outputs of *NPV*, *IRR*, *BCR* and *PB* are shown in Table I.

TABLE I. COMPARISON OF OUTPUTS FROM CALCULATION BY USING FINANCIAL CALCULATOR AND SPREADSHEET PROGRAM

Parameters	Output from Financial calculator	Output from Spreadsheet program
<i>NPV</i>	620,067.30 THB	620,067.30 THB
<i>IRR</i>	17.57%	17.57%
<i>BCR</i>	1.02	1.02
<i>PB</i>	3.16	3.16

According to the Table I, we can summarize that all results that obtained from both instruments are similar without any errors. The *NPV* is exploited of 620,067.30 THB, while *IRR*, *BCR*, and also *PB* are indicated of 17.57%, 1.02, and 3.16 respectively. These imply that the developed function is high performance compared with the commercial instrument. Moreover, the comparison of the feature usages from both instruments has been summarized in Table II.

TABLE II. COMPARISON OF OUTPUTS FROM CALCULATION BY USING FINANCIAL CALCULATOR AND SPREADSHEET PROGRAM

Features	Financial calculator	Spreadsheet program
a) User interface	Show individual viewing	Show overview
b) Insert data	Add ready-made form of net cash flow	Add financial data directly
c) Edit data	Complex to find some wrong data	Simple to edit
d) Calculating	Operate by built-in function	Automatically calculation from developed function (can adjust or update more function)
e) Result showing	Show one by one	Show all results on one display

As you have seen in the Table II, operating the data with spreadsheet function is more convenient than the calculator in any feature. Besides, the function could adjust to be appropriate for other investment cases.

V. CONCLUSION

To develop function of a capital investment decision via a spreadsheet program, we have seen the *NPV*, *IRR*, *BCR* and *PB* values from the program are equivalent to the financial calculator. Furthermore, in considering of application usage, we found the developed function program’s features are more compatible, and simple to edit data. The estimated time saving of the calculations and data input by utilizing the spreadsheet program is approximately 5 minutes when compared with the financial calculator. This program is easy to understand and operate also suitable employs to analyze project feasibility for investor, even so business owner. In the future, the developed functions would, however, be operated on the mobile applications.

REFERENCES

- [1] KResearch, “LED Bulbs, 2016: Growing 33 Percent Due to Falling Prices”, *K-Econ Analysis*, no. 2751, 10 June 2016.
- [2] Thailand Securities Institute, “*CISA level 1: Corporate Finance*”, Amarin Printing & Publishing Public Company Limited, 2012.
- [3] Sasinan Jirachapatt, “*The Study of the Feasibility for Investment in the Business of Air Conditioner Distribution in Minburi, Bangkok*”, Srinakharinwirot University, 2011.
- [4] Faculty of Management Science, “A Study of Cost and Return on the Elderly Care Center Business in Thailand”, *Veridian E-Journal, Silpakorn University*, ISSN 1906 - 3431, 2016.
- [5] K Varalakshmi, “Feasibility Analysis of Meat processing plant – Case of medium scale plant for Restructured chicken products”, *International Journal of Advanced Research*, vol. 3, issue 8, pp. 750-763, 2015
- [6] Wuttikorn Jantaphan, “An Economic Worthiness Study of Residential Building Construction Project for Civil Servants and Employees of Nakhon Ratchasima Rajabhat University”, *Suranaree University of Technology*, 2014
- [7] Texas Instruments Incorporated, “*BA II Plus Professional Guidebook*”, <https://education.ti.com/>



Biogas Production from Wastewater of Yeast Fermentation with Microorganism under Mesophilic Condition

Thanatcha Santhadkha, Teerasak Hudakorn and Noppong Sritrakul

Department of Mechanical Engineering, Faculty of Engineering and Industrial Technology,
Silpakorn University (Sanam Chandra Palace Campus)
6, Rajamankha Nai Rd., Amphoe Muang Nakhon Pathom, Nakhon Pathom Province, Thailand
e-mail: baitoeytnc@hotmail.com

Abstract—This paper was to investigate the biogas production from the wastewater of yeast fermentation. The main raw material was wastewater of yeast fermentation co-digestion with microorganisms in ratio of 1:1 (8 liters of wastewater of yeast fermentation and 8 liters of microorganism). The digester was made from the 20 liters PVC tank for hydraulic retention time (HRT) 45 days. We measured the volume of biogas produced by water displacement method once per day. The composition of biogas such as methane (CH₄), carbon dioxide (CO₂) and oxygen (O₂) was used to analyze the specific methane yield (SMY). The results showed that the wastewater of yeast fermentation with microorganisms gave highest biogas production with 73% CH₄, 19.7% CO₂ and 1% O₂ and 6.3% of other gases. The specific methane yield was 0.028 m³CH₄/kgCOD_{removed} and the biochemical methane potential was 7.89%.

Keywords—biogas; wastewater of yeast fermentation; potential methane production.

I. INTRODUCTION

Currently, energy consumption tends to increase continuously that result in insufficient of energy. Promoting the use of renewable energy (such as solar energy, water power, wind power, geothermal energy, biomass energy, biogas energy, etc.) is used to replace the energy of oil and coal, which are non-renewable energy. There are many factories in Thailand. Characteristic of factory is the large amount of wastewater generated by the production process to be treated, while most wastewater treatment in factory use open-pond wastewater treatment system. The area is not only taken to wastewater treatment, but also surrounding foul smell. Therefore, promoting the use of wastewater and waste from factory to biogas production can be used as a renewable energy, solve the pollution problem, and reduce the production cost. [1]

Wastewater and waste from factory are used produce biogas. In the research, biogas is produced from wastewater and waste from factory is studied, which is depending group of anaerobic microorganism. Whether it is using wastewater from factory as raw materials for fermentation [2-10], using wastewater from factory with household waste [11-13], using

wastewater from factory with cow dung [11, 14-15], using wastewater from factory with manure [16], using wastewater from factory with other wastes [1, 17-19]. It is found that the use to fermented of wastewater from factory with raw materials can produce biogas. The potential of biogas production depends on the ratio of wastewater from factory and raw materials to fermentation, including the type of raw materials to be fermented.

The amount of biogas produced depends on the amount of organic matter in wastewater to feed and technology used. Furthermore, level of amount of biogas is high whenever level of COD is high; or whenever there is wastewater treatment in the tank heated or continuous spinning of wastewater. [20]

Therefore, wastewater from factory was choice to produce renewable energy that can be used to produce biogas. Researchers had idea to bring wastewater from industrial to produce biogas to reduce the import of energy from abroad and to effectively manage waste.

II. MATERIALS AND METHODS

A. Raw materials

This research used wastewater of yeast fermentation as a raw material. The wastewater of yeast fermentation was collected from industrial plant in Nakhon Pathom, Thailand. Microorganism was collected from overflow of CSTR in Hin Mun, Nakhon Pathom, Thailand.

B. Installations

In this experiment, the biogas digester made of polyethylene (PVC) tanks had a capacity of 20 liters. The digester was connected to the displacement tank and the gas collector. The digester was connected with gas tube and tube for measuring solution inside the digester. At the end of both tubes was installed valves. Then, silicone was used to seal at joints. And lastly, checking leakage of gas tubes, valves and lid of digester. The schematic diagram of installation is shown in Fig. 1

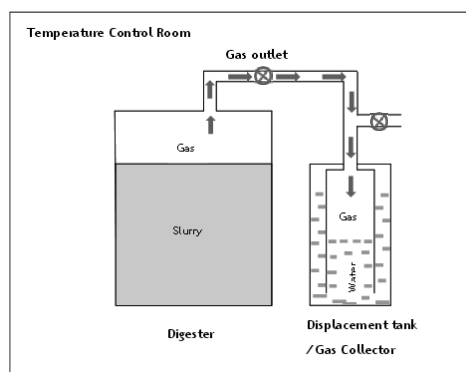


Fig. 1 Schematic diagram of installation

C. Experimental setup

In this experiment, the wastewater of yeast fermentation was mixed with microorganism at ratio 1:1 (The wastewater of yeast fermentation 8 liters and microorganism 8 liters) in digester. Before closing the lid of the digester raw materials must be mixed together, then the lid was closed and sealed with silicone to prevent leakage at the lid. In this experiment, the pH value was controlled of 6.5-7.5. If acid or alkaline content is too high, it will affect the bacteria in the digester. The digestion was done in a temperature control room, in the anaerobic condition at a temperature of $35 \pm 2^\circ\text{C}$ (Mesophilic condition) was used. For measuring, the volume of gas produced was measured by the water displacement method that the volume of biogas produced is equals to the rising water in the water tank. The experimental setup is shown in Fig. 2



Fig. 2 Experimental setup

D. Analysis method

The following parameters of wastewater of yeast fermentation and inculum were analyzed. For biogas components analysis, a portable biogas monitor (Geotech 350/biogas-check) was connected to the experiment set in

order to measure and record the data. For pH analysis, a pH meter (Lutron/pH-220) was used. For chemical oxygen demand (COD), biochemical oxygen demand (BOD), total solids (TS), total volatile solids (VS), and total kjeldahl nitrogen (TKN) analysis, the sample of raw material in ratio 1:1 was collected and sent to analyze at laboratory of Department of Environmental science, Faculty of Science, Silpakorn University, Sanam Chan Palace. The result of properties of raw materials is shown in Table 1.

TABLE I. SHOW THE RESULT OF PROPERTIES OF RAW MATERIAL

Parameters	Analysis methods	Result	
		Before	After
COD (mg/L)	Potassium dichromate digestion	26,100	16,325
BOD ₅ (mg/L)	5-day BOD test	10,000	3,150
TS (mg/L)	Total solid dried at $103-105^\circ\text{C}$	54,710	20,912
VS (mg/L)	Volatile solids ignited at 550°C	15,870	10,982
TKN (mg/L)	Macro-kjeldahl method	1,500	1,828

E. Calculation of specific biogas yield

The experimental results were analyzed to specific methane yield (SMY) and the biochemical methane potential (BMP) by the following equation:

a) Equation of specific methane yield (SMY)

$$\text{SMY} = \frac{\text{Cumulative biogas volume (ml)}}{\text{Volatile solid volume (mg)}} \quad (1)$$

b) Equation of biochemical methane potential (BMP)

$$\text{BMP} = \frac{\text{Cumulative biogas volume (l)}}{\text{Theoretical methane production (l)}} \quad (2)$$

Assumed that: 1 kgCOD_{removed} equal 350 LCH₄ (0.35m³CH₄) produced. [21]

III. RESULT AND DISCUSSIONS

The measured data were collected for hydraulic retention time (HRT) 45 days from the anaerobic digestion of wastewater of yeast fermentation with microorganisms in each experiment to compare the results by the following.

A. Daily biogas volume from the wastewater of yeast fermentation

From the collection of data on the volume of biogas from the wastewater of yeast fermentation with microorganisms. Using wastewater of yeast fermentation as the main raw material, it was co-digested with microorganisms in ratio of 1:1. Fig. 3 shown that the daily biogas volume from the



wastewater of yeast fermentation with microorganisms of 1:1 has the highest daily biogas volume of 340 ml on day 22.

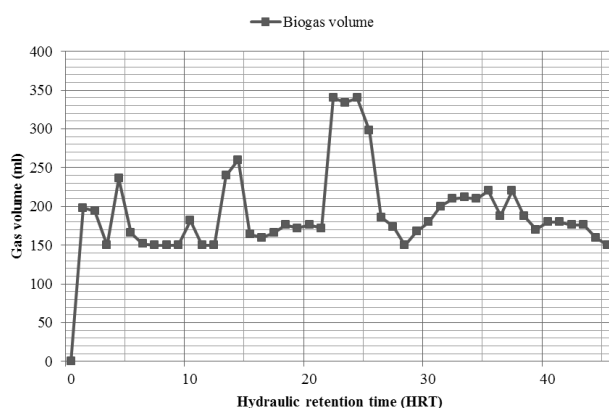


Fig. 3 Daily biogas volume and hydraulic retention time

B. Composition analysis of produced biogas (CH_4 , CO_2 , and O_2)

The production of biogas from wastewater of yeast fermentation co-digestion with microorganism in the 1:1 ratio in hydraulic retention time for 45 days, there are variables such as methane (CH_4), carbon dioxide (CO_2) and oxygen (O_2) percentage to compare the experimental results. The comparison results for each variable are as follows.

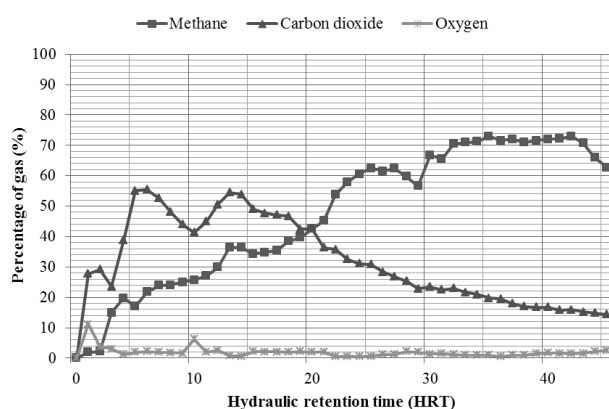


Fig. 4 Relationship between average gas percentage in ratio of 1:1 and hydraulic retention time.

Fig.4 shown that the methane content of wastewater of yeast fermentation with microorganisms in the 1:1 ratio increases gradually and reaches a peak. Then, the methane volume decline steadily. The highest methane volume was 73% on day 35 in the process.

Including, the carbon dioxide content in the same direction that the carbon dioxide percentage as highly and gradually decreases follow the hydraulic retention time. At the beginning of the co-digestion process, the highest carbon

dioxide percentage was 55.5% on day 6 and gradually decreases on day 7-10 was 41.4%, after that the carbon dioxide percentage gradually increases again on day 11-13 was 54.5% then gradually decreases, obviously. We could be surmised that the wastewater of yeast fermentation content direct variation with the amount of carbon dioxide that was higher and reduced because it was changed into methane.

C. Comparison of cumulative methane volume to cumulative biogas volume

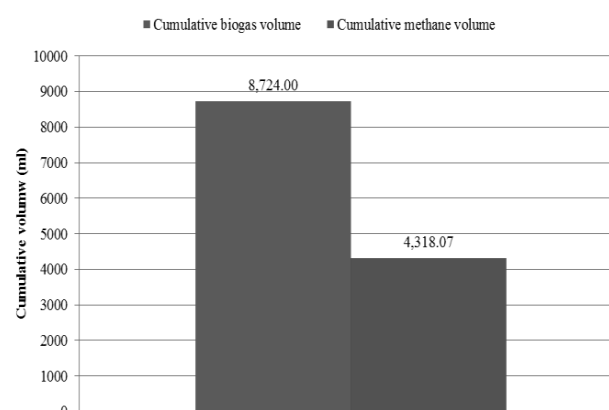


Fig. 5 Relationship between the accumulated biogas volume and methane volume

Fig. 5 shown that the relationship between the accumulated biogas volume and the methane volume. If the volume of biogas was lower resulting in the volume of methane was also low. But if the volume of biogas was higher, methane volume was also high. The highest accumulated biogas volume and methane volume were 8,724 ml and 4,318.07 ml, respectively.

D. Specific Methane Yield

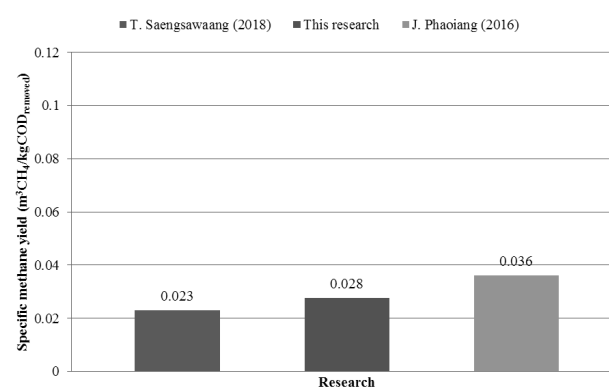


Fig. 6 Specific methane yield

Fig. 6 shown that the specific methane yield can be derived from equations (1). The specific methane yield in ratio of 1:1



can be gave the highest methane yield was 0.028 $\text{m}^3\text{CH}_4/\text{kgCOD}_{\text{removed}}$ that was similar to the biogas production from wastewater of yeast extract plant [21] and wastewater of sweet corn cob milling process [22]. It can be giving maximum biogas was 0.023 and 0.036 $\text{m}^3\text{CH}_4/\text{kgCOD}_{\text{removed}}$, respectively. Which the research that used wastewater of sweet corn cob milling process as raw material was made at ratio 3:1 (The wastewater 0.6 liters and microorganism 0.2 liters), while this research was made at ratio 1:1.

E. Biochemical methane potential

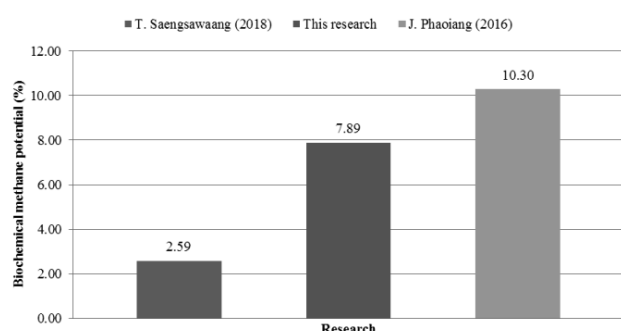


Fig. 7 Biochemical methane potential

Fig. 7 shown that the biochemical methane potential (BMP) can be derived from equations (2). The biochemical methane potential in ratio of 1:1 was 7.89% that was higher to the biogas production from wastewater of yeast extract plant [21] was 2.59%. But there was lower to the biogas production from wastewater of sweet corn cob milling process [22] was 10.30%, because the research that used wastewater of sweet corn cob milling process as raw material was made at ratio 3:1 (The wastewater 0.6 liters and microorganism 0.2 liters), while this research was made at ratio 1:1.

IV. CONCLUSIONS

The batch anaerobic digestion of waste water of yeast fermentation and microorganism for the mixing ratio 1:1 reported that it had the highest biogas volume of 340 ml on day 22 of the fermentation process. The highest accumulated biogas volume and methane volume were 8,724 ml and 4,318.07 ml, respectively. The highest methane volume was 73% on day 35 in the process. The specific methane yield was 0.028 $\text{m}^3\text{CH}_4/\text{kgCOD}_{\text{removed}}$. The biochemical methane potential was 7.89%.

ACKNOWLEDGMENT

The author would like to thank Research and Development Center for Sustainable Engineering (RDSE-SU), Department of Mechanical Engineering, Faculty of Engineering and Industrial Technology, Silpakorn University, and my work companion for all support to this work.

REFERENCES

- [1] S. Netsongkram, A. Kaewrawang, and R. Suntivarakorn, "Effect of Wastewater to Cassava Pulp Ratio on Biogas Production," Graduate Research Conference 2014, pp. 562-569, 2014.
- [2] G.N. Demirer, M. Duran, E. Güven, Ö. Ugurlu, U. Tezel, and T.H. Ergüder, "Anaerobic treatability and biogas production potential studies of different agro-industrial wastewaters in Turkey," Biodegradation, vol. 11, No. 6, pp. 401-405, August 2000.
- [3] J.R. Banu, S. Kaliappan, and D. Beck, "Treatment of sago wastewater using hybrid anaerobic reactor," Water quality research journal of Canada, vol. 41, No.1, pp. 56-62, 2006.
- [4] P. Melidis, E. Vaiopoulou, E. Athanasoulia, and A. Aivasis, "Anaerobic treatment of domestic wastewater using an anaerobic fixed-bed loop reactor," Desalination, vol. 248, No. 1-3, pp. 716-722, January 2009.
- [5] U.S. Hampannavar, and C.B. Shivayogimath, "Anaerobic treatment of sugar industry wastewater by upflow anaerobic sludge blanket reactor at ambient temperature," International journal of environmental sciences, vol. 1, No. 4, pp. 631, 2010.
- [6] J. Chotwattanasak, and U. Puetpaiboon, "Full scale anaerobic digester for treating palm oil mill wastewater," Journal of Sustainable Energy & Environment, vol. 2, No. 3, pp. 133-136, 2011.
- [7] A.S. Tanksali, "Treatment of sugar industry wastewater by upflow anaerobic sludge blanket reactor," International Journal of ChemTech Research, vol. 5, No. 3, pp. 1246-1253, April 2013.
- [8] T. Senanikhom, W. Kampeerawat, and A. Kaewrawang, "A Study on Producing Biogas from the Leachate," Graduate Research Conference 2014, pp. 499-507, 2004.
- [9] T. Phonphunthin, W. Uttamaprakrom, and Prasert Reubroycharoen, "A Study of Biogas Production Potential from Industrial Wastewater," Journal of Energy Research, Vol. 11, No. 1, pp. 50-62, 2016.
- [10] L. Artsupho, P. Jutakradsada, A. Laungphairojana, J.F. Rodriguez, and K. Kamwilaisak, "Effect of Temperature on Increasing Biogas Production from Sugar Industrial Wastewater Treatment by UASB Process in Pilot Scale," Energy Procedia, Vol. 100, pp. 30-33, 2016.
- [11] I. Angelidaki, and B.K. Ahring, "Codigestion of olive oil mill wastewaters with manure, household waste or sewage sludge," Biodegradation, Vol. 8, No. 4, pp. 221-226, July 1997.
- [12] R. Cheerawit, T.S. Thunwadee, K. Duangporn, R. Tanawat, K. Wichuda, A. Niyl, and H.C. Pearline Ng, "Biogas production from co-digestion of domestic wastewater and food waste," Health and the Environmental Journal, Vol. 3, pp. 1-9, July 2012.
- [13] M. Minale, and T. Worku, "Anaerobic co-digestion of sanitary wastewater and kitchen solid waste for biogas and fertilizer production under ambient temperature: waste generated from condominium house," International Journal of Environmental Science and Technology, Vol. 11, No. 2, pp. 509-516, March 2014.
- [14] M.A. Dareioti, S.N. Dokianakis, K. Stamatelatu, C. Zafiri, and M. Kornaros, "Biogas production from anaerobic co-digestion of agroindustrial wastewaters under mesophilic conditions in a two-stage process," Desalination, Vol. 248, No. 1-3, pp. 891-906, November 2009.
- [15] M.A. Dareioti, S.N. Dokianakis, K. Stamatelatu, C. Zafiri, and M. Kornaros, "Exploitation of olive mill wastewater and liquid cow manure for biogas production," Waste Management, Vol. 30, No. 10, pp. 1841-1848, October 2010.
- [16] M. Monou, N. Pafitis, N. Kythreotou, S.R. Smith, D. Mantzavinos, and D. Kassinos, "Anaerobic co-digestion of potato processing wastewater with pig slurry and abattoir wastewater," Journal of chemical technology and biotechnology, Vol. 83, No. 12, pp. 1658-1663, May 2008.
- [17] R.T. Romano, and R. Zhang, R, "Co-digestion of onion juice and wastewater sludge using an anaerobic mixed biofilm reactor," Bioresource technology, Vol. 99, No. 3, pp. 631-637, February 2008.
- [18] S. Luostarinen, S. Luste, and M. Sillanpää, "Increased biogas production at wastewater treatment plants through co-digestion of sewage sludge



- with grease trap sludge from a meat processing plant,” *Bioresource technology*, Vol. 100, No. 1, pp. 79-85, January 2009.
- [19] W. Khamjanla, and R. Suntivarakorn, “Biogas production by using sludge cake from cassava starch process,” *Proceedings of 50th Kasetsart University Annual Conference: Architecture and Engineering*, pp. 182-189, 2012.
- [20] K. Panpong, N. Amage, and T. Ophithakorn, “Enhanced Efficiency for Biogas Production from Distillery Wastewater of Community Refined Liquors Plant by Using the Co-Digestion Strategy,” 2015.
- [21] T. Saengsawaang, H. Peunerasamee, T. Hudakorn, and P. Usuparat, “A study on the effect of methane degradation potential on water hyacinth and yeast extraction effluent,” *Walailak Procedia* 2018, Vol. 2018, No. 2, March 2018.
- [22] J. Phaoiang, J. Chanathaworn, Ch. Thararak, and N. Dutsadee, “Study of biochemical methane potential by co-digestion of wastewater from sweet corn cob milling process and wastewater from production process under anaerobic digestion,” *The 2nd national conference on industrial technology and engineering (NCITE 2016)*, pp.459-470, 2016.



Using closed loop oscillating heat pipe for cooling battery in charging process

Poomin Krisangsri, Teerasak Hudakorn and Noppong Srirakul
Department of Mechanical Engineering,
Faculty of Engineering and Industrial Technology,
Silpakorn University, (Sanam Chan Palace)
e-mail: Pookado-4@hotmail.com

Abstract—This research is the application of closed-loop oscillating heat pipe (CLOHP) for cooling the battery while charging. The CLOHP made of copper tube with diameter of 0.055 inch (1.397 mm) and fill R-134a at filling ratio of 50% by volume. The evaporator section of CLOHP was attached to outer side of battery and condenser section was cooled by air. Rechargeable Lead-acid Battery size of 12 V 24 Ah with dimensions of 75 x 180 x 170 mm was used in the experiment. The experiment for cooling of battery while charging were 2 cases as follow: 1 without heat pipe with natural convection and 2 heat pipe with natural convection. The results of battery charging efficiency were 55.44% and 69.69%, respectively. The results of battery temperature were 36.42 °C and 33.44 °C. The conclusion of this research was using closed-loop oscillating heat pipe for cooling the battery while charging can reduce the temperature and increase the charging efficiency of the battery.

Keywords—closed loop oscillating heat pipe, CLOHP, battery, cooling, charging

I. INTRODUCTION

The battery will heat up while charging. Without appropriate cooling system, the accumulating heat may cause higher battery temperature. It is vulnerable to the danger and degradation of the battery. If the battery is well cooled, the charging will be faster and also result in increasing of charging efficiency. Thus, there are various researches on reducing the battery temperature by using heat pipe. Heat pipe is divided into 2 types, consisting of thermo-syphon and oscillating heat pipe. In addition to the oscillating heat pipe is divided into 3 types, consisting of closed end oscillating heat pipe (CLOHP), closed-loop oscillating heat pipe (CLOHP), closed-loop oscillating heat pipe with check value (CLOHP/CV)[1-4]. This research uses a closed-loop oscillating heat pipe (CLOHP) to cool the battery. Considering the efficiency of the heat pipe such as internal diameter of pipe, diameter of coil, temperature of evaporator, number of turns, and filling ratio working fluid[5]. Heat pipe is a type of heat exchanger that does not require external energy to operate. It uses the principle of heat transfer from the latent heat of the substance inside the pipe to evaporate that is the heat pipe is heated from the heat source. Heat transfer to the working fluid (water or air) in the heat pipe and condensed into liquid in order to revert to the evaporator section again by gravity force. Therefore, the researcher is interested in making a cooling unit

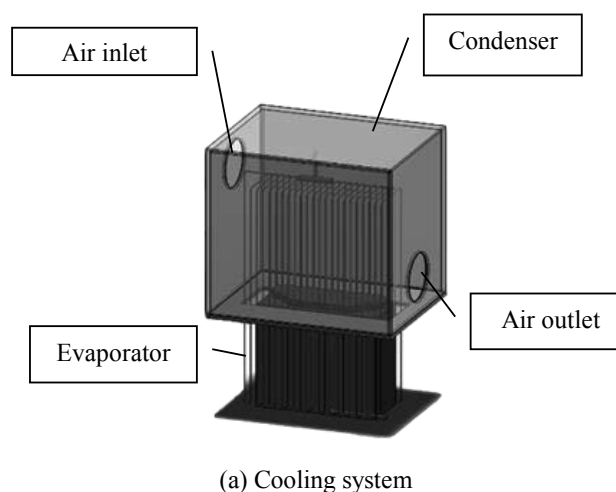
of battery by closed-loop oscillating heat pipe (CLOHP) in order to extend the life of the battery due to the high temperature of the battery while charging.[6-7].

II. Research Methodology

A. Design of experiments

- Thermal design in thermal battery 1 pack.

The main components of thermal battery consisted of copper pipe capillary tube boned to cycle the size of pipe is the diameter of 1.397 mm, length of 87 cm, and 34 turns. It was bended to fit with the battery, and a size of copper plate is wide of 18 cm length of 17 cm and thick of 1.2 mm, as shown in Fig. 1 (a). In experiment is used to insulate sheet (Aeroflex) wrapped the copper sheet to prevent heat loss. The cooling of the battery, we were used to the box is punched in diameter of 75 cm at the top and bottom of the box as shown in fig.1a. The box is intended for a boundary of experiments to control the temperature and wind speed, as shown in Fig. 1 (b)



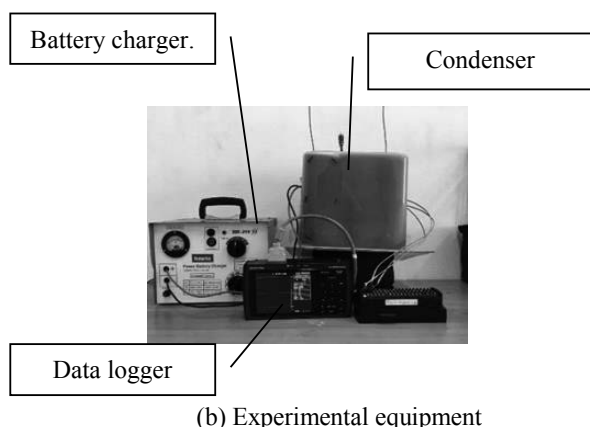


Fig. 1 The cooling of the battery pack, 2 cubes

(a) Cooling system (b) Experimental equipment

B. Details of the equipment in the experiment.

a) It is a device the battery. The device is newta 38A-24V, which can charge up to 24 V and up to 30 A, as Shown in Fig.2



Fig. 2 Battery charger

b) Battery electric motorcycle it is used to charge the motorcycle battery used to be Toyotron 12V, 24 Ah/20HR that is a battery of 12 V can charge as high as 24 Ah, as Shown in Fig. 3.



Fig. 3 Battery electric motorcycle

c) Heat pipe: Copper pipe diameter of 1.397 mm (0.055 in) as Shown in Fig.4



Fig. 4 Heat pipe (copper tube)

d) The working fluid R-134a: As a working fluid can be changed by phase When the heat pipe is heated, cause charge state to vapor and charge state to liquid when point of R-134a is 26.1 °C, as Shown in Fig. 5



Fig. 5 Working fluid R-134a

e) Copper plate: For use as the heat from the battery while charging. Act as an evaporator (Evaporator).It is used a heat receiver from battery while charging, called evaporator as shown in Fig.6

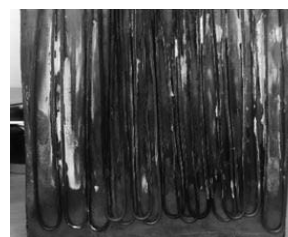


Fig. 6 Copper plate

f) Vacuum pump: Serve all the air out of copper pipes as Shown in Fig. 7



Fig. 7 Vacuum pump

g) It is used to record temperature in different spots automatically via thermos coupling. The data logger is araptec which can be measured more than 20 point and measure moisture, and pressure in direct current (DC) as Shown in Fig. 8



Fig. 8 Data logger

h) A cable that is used with the auto data recorder (Data logger) It receives the temperatures from various points then sends the data to a data recorder and display it on the display screen. K-type temperature from -40 to 1200 degrees Celsius. As Shown in Fig. 9



Fig. 9 Thermocouple

C. The working principle of thermal battery by using heat pipe.

When assembling the device completed, it was turned on the battery charger then adjust the voltage and current as required. It caused the battery heat up and passed through the copper plates until the temperature rises and passed to the heat pipe. The heat pipes in this section is evaporator, it is contained working fluid R-134a within pipe. When then working fluid was boiled cause it is evaporate became to vapor and float to the top of the heat pipe, it is called condenser. In this section, there was heat transfer from the heat pipe by the natural convection force convection, and charged state to liquid in order to flow into the evaporator. It works as a cycle. The heat is generated cause the air outlet temperature in each point is recorded by data logger then brought the air inlet and the cooling of the battery.

D. Equations for optimal heat pipe diameter.

The diameter of the heat pipe in the test, which should not exceed the calculated value due to the condensation inside the heat pipe resulting in a heat pipe is not performing well enough. The equation for a pipe diameter was heated.

$$D_{\max} \leq 2\sqrt{(\sigma/\rho g)} \quad (1)$$

By D_{\max} is the diameter of the heat pipe at most (m), σ is the surface tension (N / m), ρ is the density (Kg / m³), g is the gravity force (m / s²)

E. The equation for heat pipe design circular, round.

Heat Pipe design is the equation used to calculate the length of the condenser, which can be calculated from the equation.

$$\frac{\dot{Q}}{(\pi D_o \times N \times 2L_c)} = [0.54(\text{Exp}^{(B)})^{0.48} K_a^{0.47} \text{Pr}^{0.27} \text{Ja}^{1.43} N^{-0.27}] \quad (2)$$

B = the angle of the heat pipe from the horizontal plane K_a = Carman number Pr = Prandtl number Ja = number of tubes N = number of tubes D_o = Inside diameter (m) L_c = Condenser section length

F. Calculation of the volume of the working fluid in the heat pipe.

Calculation of the volume of the working fluid in the heat pipe is can be calculated from the equation.

$$V = \pi r_{\text{heat pipe}}^2 \times h_{\text{heat pipe}} \quad (3)$$

G. Calculation of weight of the substance to work in heat pipe (Heat pipe).

Calculation of the volume of the working fluid in the heat pipe is ρ density volume of working fluid, which can be calculated from the equation.

$$m = \rho v \quad (4)$$

By ρ is density (kg/m³) and v is volume of working fluid (m³)

H. Calculation of the heating value of the battery.

Calculating the heat of the battery and can be calculated from the equation.

$$Q = mC_p(\Delta T) \quad (5)$$

By m is the flow rate, C_p is specific heat capacity of air, and ΔT Is air outlet temperature-the air inlet temperature (°C)

I. From the above theory, the conclusion is the size of the test set as follows.

TABLE I. THE CONCLUSION IS THE SIZE OF THE TEST SET

Materials laboratory	Size
Diameter of copper pipe	1.397 mm.
Condenser length (L_c)	20.5 mm.
Evaporator length (L_e)	17 cm.
Number of turns (turn)	30 turn



III. RESULTS AND DISCUSSION

A. The test results, the ability to reduce the temperature of the battery 1 pack.

From Fig. 10, it was seen that the test for the cooling of the battery pack has a heat pipe. It caused to reduce the temperature of the battery while charging. When the air came into the

cooling to the battery was reduce the temperature of the battery obviously. The average temperature of the electric without heat pipe It can be conclude that the use of the heat pipe for battery cooling while charging was able to reduce the temperature better than without heat pipe.

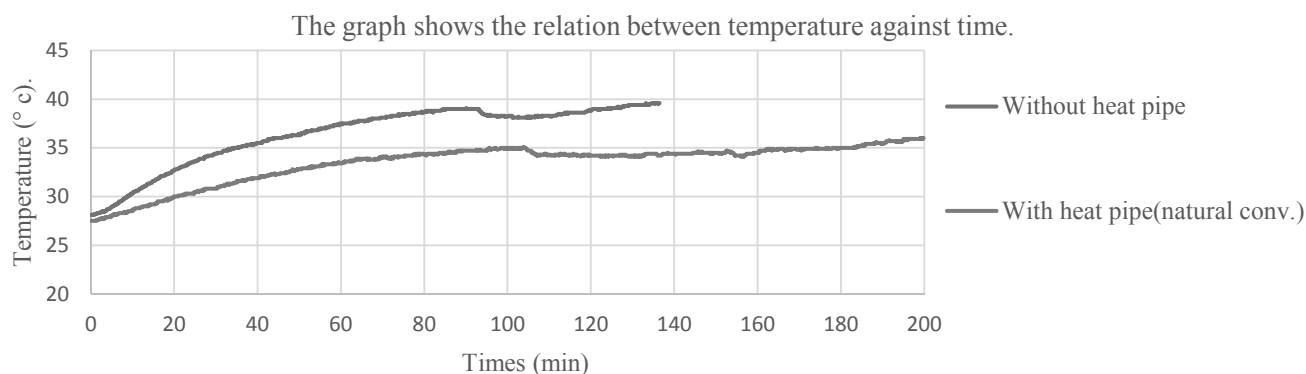


Fig. 10 Relationship between temperature against time of battery 1 pack.

B. The results of charging efficient of the battery 1 pack.

Fig. 11 The power of the battery charging without heat pipe was less than the battery with a heat pipe. It can be concluded that cooling of 1 pack battery with a heat pipe was more

efficient than without heat pipe. There also can be described in table II.

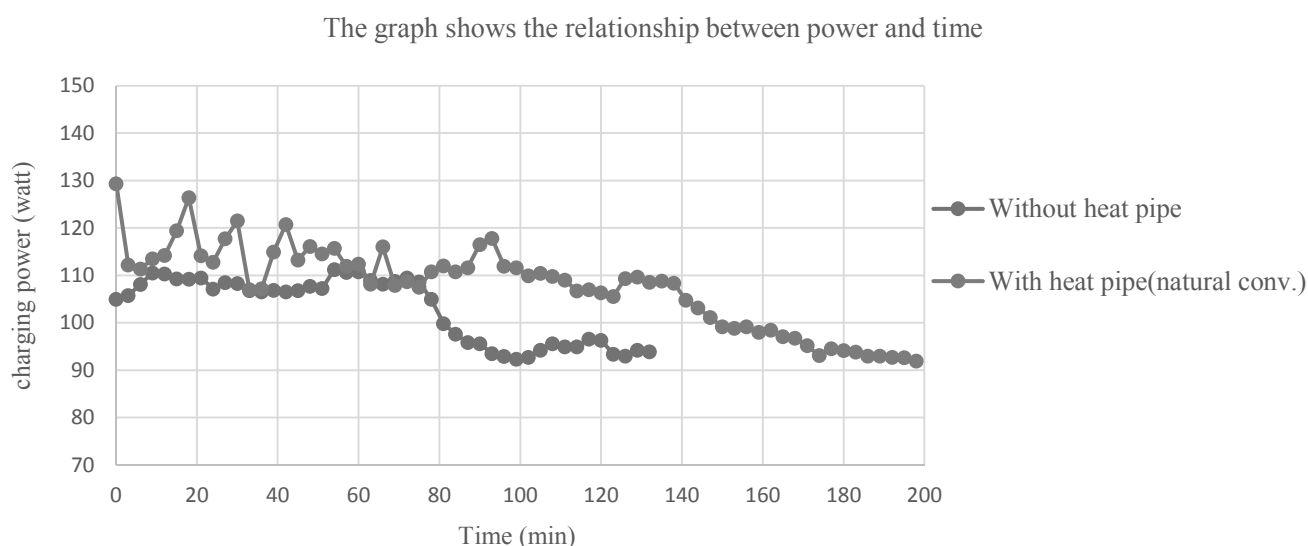


Fig.11.Relationship between the capacity of the battery 1 pack.



TABLE II.SHOWS THE RESULTS OF CHARGING EFFICIENT OF THE BATTERY
1 PACK

Battery	Case	Charge (KJ)	Discharge (KJ)	Efficiency (%)
1 Pack	Without heat pipes	814.65	451.68	55.44
	With heat pipe (natural conv.)	1279.72	891.87	69.69

From table II, the result show that using heat pipe for cooling of battery. It has higher performance than without heat pipe. Considering the table II it could be seen that in experiment of battery 1 pack (without heat pipe) to cooling of 55.44 %, while the battery with heat pipe have efficiency of cooling was increased by 69.69 %.This research also tested the effect of the force convection cooling from Table 1 that when the wind speed has increased the performance of charging battery would decreased. Which concluded that using natural heat and winds are the most powerful.

IV. CONCLUSION

The conclusion of this research was using closed-loop oscillating heat pipe for cooling the battery while charging can reduce the temperature and increase the charging efficiency. It can be considered the electric power in charging, electric power discharge of the battery, battery temperature and charging efficiency of battery. The results of cooling battery without heat pipe were 814.65 KJ, 451.68 KJ, 36.42 °C and 55.44%.respectively. The results of cooling battery with heat pipe (natural convection) were 1,279.72 KJ, 891.87 KJ, 33.44 °C and 69.69% respectively.

ACKNOWLEDGMENTS

The authors would like to thank the Department of Mechanical Engineering, Faculty of Engineering and Industrial Technology, Silpakorn University for all supports to complete this work.

REFERENCES

- [1] N. Putra, B. Ariantara, and R. A. Pamungkas, "Experimental investigation on performance of lithium-ion battery thermal management system using flat plate loop heat pipe for electric vehicle application," *Applied Thermal Engineering*, vol. 99, pp. 784-789, April 2016.
- [2] N. N. Babu, and H. Kamath, "Materials used in heat pipe," *Materials Today: Proceedings*, vol. 2, No. 4-5, pp. 1469-1478, 2015.
- [3] F. F. Li, Y. H. Diao, Y. H. Zhao T. T. Zhu, and J. Liu, "Experimental study on the thermal performance of a new type of thermal energy storage based on flat micro-heat pipe array," *Energy Conversion and Management*, vol.112, pp. 395-403, March 2016.
- [4] Y. Deng, Y. Zhao, W. Wang, Z. Quan, L. Wang, and D. Yu, "Experimental investigation of performance for the novel flat plate solar collector with micro-channel heat pipe array (MHPA-FPC)," *Applied Thermal Engineering*, vol. 54, No. 2, pp. 440-449, May 2013.
- [5] T. T. Zhu, Y. H. Diao, Y. H. Zhao, and F. F. Li, "Thermal performance of a new CPC solar air collector with flat micro-heat pipe arrays," *Applied Thermal Engineering*, vol. 98, pp. 1201-1213, April 2016.
- [6] L. Ling, Q. Zhang, Y. Yu, S. Liao, and Z, "Sha Experimental study on the thermal characteristics of micro channel separate heat pipe respect to different filling ratio," *Applied Thermal Engineering*, vol. 102, pp. 375-382, June 2016.
- [7] Y. Deng, Y. Zhao, Z. Quan, and T Zhu, "Experimental study of the thermal performance for the novel flat plate solar water heater with micro heat pipe array absorber," *Energy Procedia*, vol. 70, pp. 41-48, May 2015.



Biogas Production from Water Hyacinth Leaf and Petiole co-digestion with Microorganism under Mesophilic Condition

Chessadabhorn Kitjettanee and Teerasak Hudakorn

Department of Mechanical Engineering, Faculty of Engineering and Industrial Technology,
Silpakorn University (Sanam Chandra Palace Campus)
6, Rajamankha Nai Rd., Amphoe Muang Nakhon Pathom, Nakhon Pathom Province, Thailand
e-mail: Chessadabhorn@gmail.com

Abstract— This paper was to investigate the biogas production from the water of water hyacinth leaf and petiole (WWH) by using the Biochemical Methane Potential Test (BMP). The main raw material used was WWH co-digestion with microorganism in ratio of 1: 1 (8 liters of WWH / 8 liters of microorganism), 1:0 (only WWH) and also 0:1 (only microorganism), respectively. The digester was made from the 20 liters of the PVC tank for hydraulic retention time (HRT) 60 days. We measured the volume of biogas produced by water displacement method once per day. The composition of biogas such as Methane (CH₄), Carbon dioxide (CO₂) and Oxygen (O₂) was used to analyze the specific methane yield (SMY) and the potential for biodegradation into methane. The results showed that the WWH with microorganisms gave highest biogas production with 74.5% CH₄, 17.85% CO₂ and 7.65% of other gases. The specific methane yield and the potential to biodegrade methane were 0.13233 m³ CH₄ / kg VS_{added} and 50.51%, respectively.

Keywords— Biogas; water of water hyacinth; potential methane production.

I. INTRODUCTION

Water hyacinth is a water plant that is quickly breeding. It is a free-floating weed known for its production abilities and pollutant removal. It can be withstanding hot and cold weather. The seeds of water hyacinth can live up to 30 years and can breed by way of breaking up and become a trunk [1]. When the strong tides cause water hyacinth stem to disjoint, as a result, the water hyacinth will be easily distributed into subsets and in spread out in various places.

The Tha Chin River is experiencing a serious problem regarding water hyacinth which affects the environment directly such as water quality, mental health of people that they, cannot uses water, difficulties in doing fish farm, obstruction of water transport as well as tourism. An indirect economic damage assessment has been made from the outbreak of water hyacinth in the Tha Chin River. The damage is several million baht/year. It does not include the cost of each agency involved in the removal of water hyacinth each

year. The budget for water hyacinth removal more than 10 million baht/year.

In addition to the damage caused by water hyacinth as mentioned above. It can also be used as a variety of materials such as mushroom cultivation, used as a great bio-fertilizer. Moreover, it can also be used to produce biogas as well. From the previous researches, the water hyacinth was used as a raw material to produce the biogas in the anaerobic digestion process. It was found that the water hyacinth with household sludge [2-4], water hyacinth with microorganisms [5-9], water hyacinth with pig manure [10], water hyacinth with cow dung [10-16] and water hyacinth with sheep manure as a raw material could produce the biogas. The potential of biogas production depended on the ratio of water hyacinth and digested raw materials. Consequently, this method includes of the type of raw materials to be digested. However, bio-degradable of water hyacinth can also be used as a bio-fertilizer which does not cause any chemical residues in the environment.

To increase the production of biogas, the pre-treatment raw materials (before fermentation) were used such as using the heat [18] or the ionic liquids [19]. Moreover, the biogas fermentation under high temperature conditions [18, 20] to be increased the potential of biogas production.

Furthermore, found that the use of water hyacinth as raw materials to digest. It must be used the Continuous Stirred Tank Reactors (CSTR) large size. Due to the use of water hyacinth, it has high suspended solids cause by the cost of construction of biogas systems more expensive. To solve the problem above, the water from water hyacinth leaf and petiole as a raw material is used to reduce the amount of suspended solids and a construction of biogas systems. In addition, the crude fiber from the squeeze of water hyacinth leaf and petioles can also be used as a biomass pellet.

The objective of this research is to investigate the potential biogas production which uses water from leafs and petioles of water hyacinth under the Biochemical Methane Potential Test (BMP)



II. MATERIALS AND METHODS

A. Raw materials

This research uses a WWH as a raw material shown in Fig. 1b. The water hyacinth was collected from Tha Chin River (see in Fig. 1a) . It was chopped before feeding into the squeezer. It brought the water derivable squeeze to mix with microorganisms in a ratio of 1: 1 (WWH 8 liters per microorganism 8 liters) in a PVC tank capacity of 20 liters and was kept in the room temperature controlled at $35 \pm 2^{\circ}\text{C}$ (Mesophilic) for Hydraulic Retention Time (HRT) 60 days.

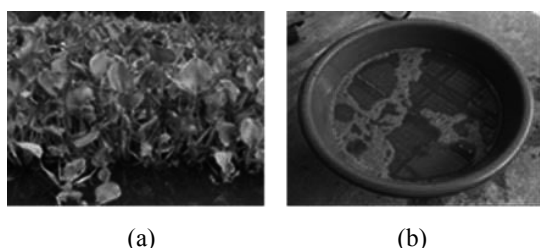
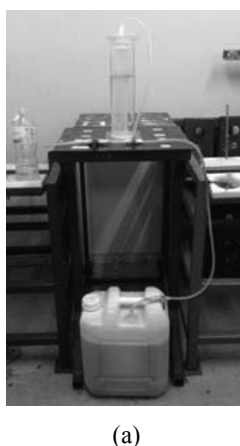


Fig. 1 Raw materials (a) Water hyacinth; (b) water of water hyacinth leaf and petiole (WWH)

B. Experimental setup and Installation

The experiments set for digestion in the anaerobic conditions at a temperature of $35 \pm 2^{\circ}\text{C}$ (Mesophilic) was used. The biogas digester made of PVC tank had a capacity of 20 liters (see in Fig. 2a). The digester connected to the gas collector and the displacement tank. Plastic pipe set were used to connect digester and gas collector. The gas produced in the digester through the pipeline to the gas collector. Another plastic pipe was used for in connection with a portable biogas monitor. The digestion was done in a temperature controlled room. For measuring, the volume of gas produced was measured by the water displacement method that the volume of biogas produced is equals to the rising water in the water tank. The schematic diagram of the experimental setup is shown in Fig. 2b



(a)

Temperature Control Room

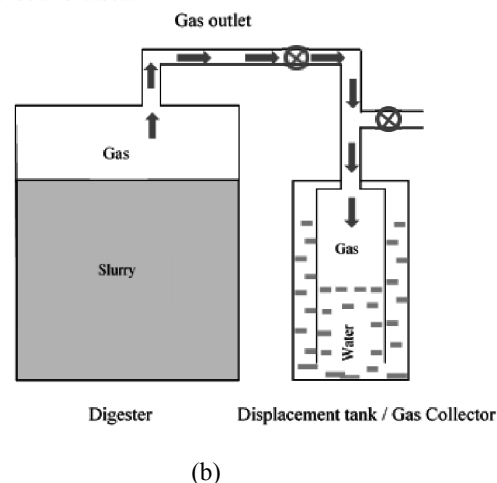


Fig. 2 Experimental setup and installations (a) experiments setup; (b) Schematic diagram of experimental setup.

C. Analysis method

The following parameters in the experiment of WWH and microorganism were analyzed. For biogas analysis, a portable biogas monitor) Geotech350/biogas-check(was connected to the experiment set in order to measure and record the data. For pH analysis, a pH meter) Lutron/ PH-220(was used. For Chemical Oxygen Demand) COD(, total Solids) TS(, total volatile solids) VS(and Total Kjeldahl Nitrogen) TKN(analysis, the sample of raw material in ratio of 1: 1 was collected about 1 liter and sent to analyze at laboratory of the Department of Environmental science, Faculty of Science, Silpakorn University) Sanam Chandra Palace Campus(. The result of properties of raw materials is shown in Table I in order to use these values to analyze the specific methane yield)SMY(and the biochemical methane potential)BMP(.

TABLE I. SHOW THE RESULT OF PROPERTIES OF RAW MATERIAL

Parameters	Analysis Methods	Analytical results	
		Pre-test	Post-test
COD(mg/L)	Potassium Dicromate Digestion	5,960	1,420
TS(mg/L)	Total Solids Dried at 103-105°C	10,760	12,788
VS(mg/L)	Volatile Solid Lgnited at 550°C	3,455	2,150
TKN(mg/L)	Macro-kjedahl Method	408	431

D. Equation

The experimental results were analyzed to specific methane yield (SMY) and biochemical methane potential (BMP) by the following equations



a) Equation of specific methane yield (SYM)

$$SMY = \frac{\text{Cumulative biogas volume (ml)}}{VS_{\text{added}} \text{ (kg)}} \quad (1)$$

b) Equation of biochemical methane potential (BMP)

$$\%BPM = \frac{\text{Cumulative biogas volume (l)}}{\text{Theoretical methane production (l)}} \times 100 \quad (2)$$

Assumed that; 1 kg COD removed equal 0.35 m³ CH₄ produced (Euiso Choi, 2007)

III. RESULT AND DISCUSSIONS

The measured data were collected for HRT 60 days from the anaerobic digestion of WWH co-digestion with microorganisms in each experiment to compare the results by the following.

A. Daily biogas volume from the WWH

The collection of data on the volume of biogas from the WWH. The main raw material used to produce biogas is water hyacinth, it was co-digested with microorganisms in ratio of 1: 1. The result shown that the daily biogas volume from the WWH with microorganisms of 1: 1 (see in Fig. 3) has the highest daily biogas volume of 1,119 ml on day 13. While in ratio of 0: 1 (only Microorganism) and 1: 0 (only WWH) it have the highest daily biogas volume of 40 and 350 ml on day 3 and 5, respectively.

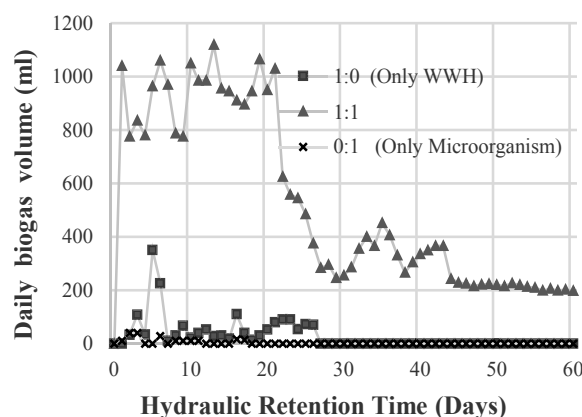


Fig. 3 Daily biogas volume and hydraulic retention time

B. Composition analysis of produced gas (CH₄, CO₂, and O₂)

The production of biogas from WWH co-digestion with microorganisms in ratio of 1: 1 for HRT 60 days. There are

variables such as Methane (CH₄), Carbon dioxide (CO₂), and Oxygen (O₂) percentage to compare the experimental results. The comparison results for each variable are as follows.

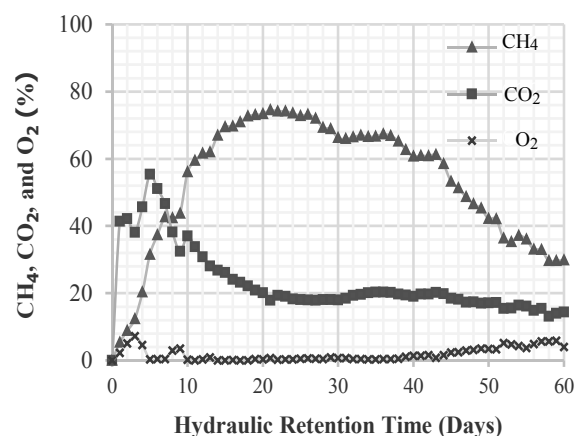


Fig. 4 Relationship between average gas percentage in ratio of 1: 1 and hydraulic retention time.

From Fig. 4 shows the methane content of WWH co-digestion with microorganisms in the ratio of 1: 1 gradually increases to maximum and then gradually decreases, obviously. The highest methane of 74.5% on day 21 of the process. While in the ratio of 0: 1 (only Microorganism) and 1: 0 (only WWH) has lower a gas percentage which can be considered from Fig. 3 because it can cause a lower gas percentage.

However, the model of the digester only allowed one feed at a time. No feed of waste materials into the digester after the initial feed resulted in the reduction of biogas production depending on the capacity of digester [21]

The carbon dioxide content in the same direction that the carbon dioxide percentage as highly and gradually decreases follow the hydraulic retention time. At the beginning of the co-digestion process, the highest carbon dioxide content was 55.4% on day 5 and sharply decreases on day 6-9 was 32.5% then gradually decreases until nearly stable. We could be surmised that the WWH content direct variation with the amount of carbon dioxide that was higher and reduced because it was changed into methane.

C. Comparison of cumulative methane volume to cumulative biogas volume

The relationship between the accumulated biogas volume and the methane volume is shown in Fig. 5. If the volume of biogas was lower, it resulting in the volume of methane was lower. But if the volume of biogas was higher, the methane volume was higher. The highest of biogas and methane volume was ratio of 1: 1 was 31,713 and 17,265.12 ml, followed by the ratio of 1: 0 (only WWH) and 0: 1 (only Microorganism) which had accumulation biogas volume of 1,748 and 188 ml and methane volume of 0.61 and 0.51 ml, respectively. The use of WWH co-digestion with microorganisms in ratio of 1: 1 was the mixing that suitably because the mixing ratio of 1: 0 (only WWH) and 0: 1 (only



Microorganism) had lower an accumulated biogas volume and methane volume which can be considered from Fig. 3 because it can cause a lower gas percentage.

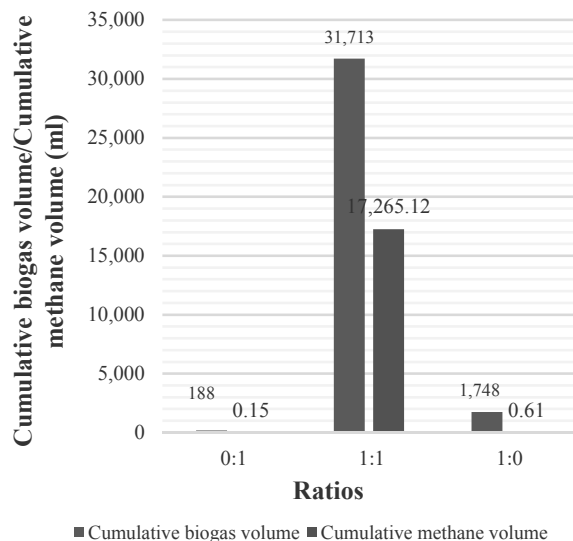


Fig. 5 Relationship between the accumulated biogas volume and methane volume.

D. Specific Methane Yield

The specific methane yield can be derived from (1). The Specific Methane Yield in ratio of 1: 1 can be gave the highest methane yield was 0.13230 m³ CH₄ / kg VS_{added} (see in Fig. 6) that was similar to the research by Gao (2012) a study on the effect of water hyacinth with ionic liquid on structural elements. It can be given maximum biogas of 0.1434 m³ CH₄ / kg VS_{added}. The research by Booddachan and Wannapakhe (2013) they are studies of household biogas production from water hyacinth. The water hyacinth used to ferment with batch test at 35°C.

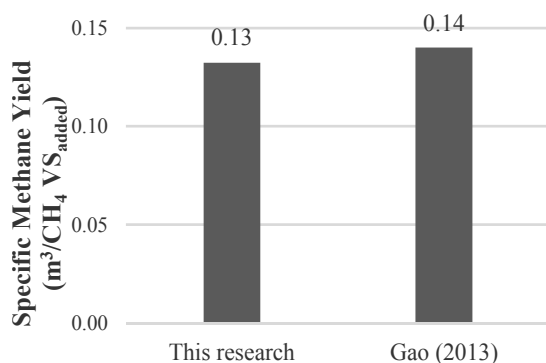


Fig. 6 Specific methane yield.

E. Potential for methane production

When calculating the biochemical methane potential (BMP), it was found that the WWH co-digestion with microorganisms in the ratio of 1: 1 had the highest BMP of 50.51% (see in Fig. 7). That was similar to the research by Singhal and Rai (2003) studied the production of biogas from water hyacinth and channel grass used for phytoremediation of industrial effluents shown that the highest %BMP was 53.18% and Asikong (2012) studied the potential of biogas production from water hyacinth and cassava peels. The highest %BMP was 52.43%.

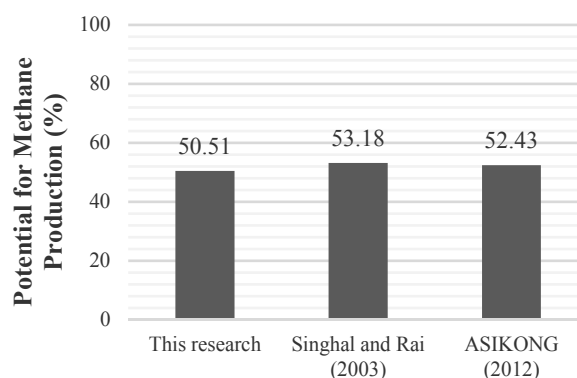


Fig. 7 Relationship between the potential for organic degradation to methane with hydraulic retention time

IV. CONCLUSIONS

The batch anaerobic digestion of WWH and microorganisms for the mixing ratio 1: 1 were reported that it had the highest biogas volume of 1,119 ml on day 13 of the fermentation process. The accumulated biogas volume and methane volume of 31,713 and 17,265.12 ml, which given methane yield up to 0.13230 m³ CH₄ / kg VS_{added}. It had potential for biodegradation of methane (BMP) was 50.51%. This has including to the biodegradation potential of methane (%BMP) average up to was 50.51% BMP.

The overall results show the WWH co-digestion with microorganisms for the mixing ratio 1: 1 had the potential for biogas production.

ACKNOWLEDGMENT

The authors would like to thank the Department of Mechanical Engineering, Faculty of Engineering and Industrial Technology, Silpakorn University (Sanam Chandra Palace Campus) for supports. And my work companion for all supports to this work.

REFERENCES

- [1]. N. Boonchai, C. Somsong, K. Teeradech, S. Pongpat., Water hyacinth management in watershed. Department of Water Resources., 2012.



- [2]. D.P. Chynoweth, S. Gosh, M.P. Herny, D.E. Jerger, V.J. Srivastava, "Biogasification of blends of water hyacinth and domestic sludge," In Proceedings of the International Gas Research Conferences, Los Angeles, pp.742–755, 1981.
- [3]. D.P. Chynoweth, D.A. Dolec, S. Gosh, M.P. Herny, D.E. Jerger, V.J. Srivastava, "Kinetics and advanced digester design for anaerobic digestion of water hyacinth and primary sludge," Biotechnology and Bioengineering Symposium, Vol. 12, pp. 381–398, 1982.
- [4]. M. Delgado, E. Guariola, and M. Bigeriego, "Methane generation from water hyacinth biomass," Journal of Environmental Science and Health, Part A: Environmental Science and Engineering and Toxicology, Vol. 27, Issue 2, pp. 347-367, 1992.
- [5]. D.L. Klass, and S. Ghosh, "Methane production by anaerobic digestion of water hyacinth (*Eichhornia crassipes*)," Technical Report, American Chemical Society meeting/2. Chemical congress of the North American Continent, Las Vegas, NV, USA, Vol. 24 Aug 1980.
- [6]. K.K. Moorhead, R.A. Nordstedt, "Batch anaerobic digestion of water hyacinth – effects of particle size, plant nitrogen content and inoculum volume," Bioresource Technology, Vol. 44, No. 1, pp. 71–76, 1993.
- [7]. R.C. Srivastava, "Kinetics of fresh water hyacinth digestion in semi-continuous operation," Chemical Engineering Journal, Vol. 56, pp. 109–113, 1995.
- [8]. V.Singhal, and J.P.N Rai, "Biogas production from water hyacinth and channel grass used for phytoremediation of industrial effluents," Bioresource Technology. Vol. 86, pp. 221–225, 2003.
- [9]. B. E. Asikong, J. Epoke, and E.E. Antai, "Potentials of Biogas Generation by Water Hyacinth (*EICHORNIA CRASSIPES*) and Cassava (*MANIHOT ESCULENTUM*) Peels in Cross River State Nigeria," Global Journal of Environment Sciences. Vol. 11, No.1 & 2, pp. 9-20, 2012.
- [10]. S.Thananachai, T. Chatchanin, U. Prachak, and P. Boonma, "Study on the potential of bio-gas production of plants as alternative energy for the community," Conference Kasetsart University No.6, 8-9 Dec 2009, pp 608-615, 2009.
- [11]. D. Madamwar, A. Patel, V. Patel, N.V. Shastri, "Effect of a mixture of surfactants and adsorbents on anaerobic digestion of water hyacinth cattle dung," Applied Biochemistry and Biotechnology, Vol. 36 (3), pp. 163–169, 1992.
- [12].M. Jayaweera, J. Dilhani, R.Kularatne, and S. Wijeyekoon, "Biogas production from water hyacinth (*Eichhornia crassipes* (Mart.) Solms) grown under different nitrogen concentrations," Journal of Environmental Science and Health, Part A: Environmental Science and Engineering and Toxicology Vol. 42, Issue 7, pp. 925-932, 2007.
- [13]. T. Chaisri, and S. Kovit, "Production of renewable energy from agricultural residues and weeds in Amphawa district, Samut Songkhram province," Completed research, Environmental Science, Suan Sunandha Rajabhat University, 2011.
- [14]. M.Yusuf, and N. Ify, "The effect of waste paper on the kinetics of biogas yield from the co-digestion of cow dung and water hyacinth," Biomass and bioenergy, Vol. 35, pp. 1345-1351, 2011.
- [15]. K. Booddachan, and S. Wannapakhea, "Household Biogas from Water Hyacinth," Technology and Innovation for Sustainable Well-Being (STISWB V), Luang Prabang, Lao PDR. 4-6 Sep 2013. [The Fifth International Conference on Science].
- [16]. K. Sudhakar, R. Ananthakrishnan, and A. Goyal, "Biogas Production from a mixture of Water Hyacinth, Water Chestnut and Cow Dung, International Journal of Science," Engineering and Technology Research (IJSETR), Vol. 2, Issue 1, pp. 35-37, 2013.
- [17]. J.H. Patila, L. AntonyRaja, B. Shankar, M.K. Shetty, P. Kumard, "Anaerobic Co-Digestion of Water Hyacinth and Sheep Waste," Energy Procedia, Vol. 52, pp. 572 – 578, 2014.
- [18]. I. Ferrer, J. Palatsi, E. Campos, X. Flotats, "Mesophilic and thermophilic anaerobic biodegradability of water hyacinth pre-treated at 80 °C," Waste Management, Vol. 30, pp. 1763–1767, 2010.
- [19]. J. Gao, L. Chen, Z. Yan, L.Wang, "Effect of ionic liquid pretreatment on the composition, structure and biogas production of water hyacinth (*Eichhornia crassipes*)," Bioresource Technology. Vol. 132, pp. 361-36. 2013.
- [20]. A. Díaz, C. del Toro, E.L. Delgado, E. Giraldo, "Anaerobic digestion of *Eichhornia crassipes* (water hyacinth) in a vertical downflow thermophilic reactor with leachate recirculation." In: Proceedings of the 9th Anaerobic Digestion World Congress, Antwerpen (Belgium), Part 1, pp. 555–559, 2001.
- [21]. K. Karim, R. Hoffmann, K. T Klasson, and A. M. H. Dahhan, "Anaerobic digestion of animal waste: effect of mode of mixing," Water Research, Vol. 39, pp. 3397-3606, 2005.
- [22]. C. Euiso, Piggery Waste Management, BE - Science, Aug 31, 2007, pp. 50-51.



A review of thermochemical heat storage

Aumarit Panthai, Teerasak Hudakorn and Pongsiri Jaruyanon.

Department of Mechanical Engineering, Faculty of Engineering and Industrial Technology,
Silpakorn University, (Sanam Chan Palace)
6, Rajamankha Nai Rd., Amphoe Muang Nakhon Pathom, Nakhon Pathom Province, Thailand
e-mail: Aum444Aum444@hotmail.com

Abstract— Heat storage technologies are used to improve energy efficiency of power plants and recovery of process heat. Chemical heat storage has been proved to be a feasible and promising method to store thermal energy. As compared to other thermal energy storage methods, chemical heat storage exhibits high energy storage density as well as feasibility for long-duration energy storage. In this paper, the basic principle of the chemical heat storage is firstly elaborated. Then the selection criteria of the chemical reaction are given. The aim of this review is to provide an insight into the promising candidate reactions for chemical heat storage application. The associated reversible chemical reactions available for thermal energy storage systems are summarized. Ongoing research and development studies illustrate that chemical heat storage is a very favorable option for the different application when diverse promising candidate reactions are selected. As working temperature is one of the key parameters for thermal energy storage systems, emphasis is given to the judgment of application temperature range for chemical heat storage. The determination of applicative temperature range of reversible chemical reactions is discussed. Besides, the challenge and prospect of the chemical heat storage technology are analyzed in the paper.

Keywords—Thermal energy storage; Chemical heat storage; Chemical reaction heat storage; Chemical sorption heat storage

I. INTRODUCTION

Energy is an important element for the economic growth, social and environmental sustainable development. With the incremental depletion of conventional primary energy, the new alternative energy source becomes more and more important for the energy conservation. However, on the one hand, the renewable energy source, such as solar energy and wind energy, is intermittent and time dependent and thus restricts the large-scale utilization. On the other hand, more rational and efficient utilization of the energy is confronted with many technical difficulties. Energy storage provides a feasible solution due to improving the efficiency of the energy system and storing the surplus energy.[1] Thermal energy storage (TES) has shown potential in improving the overall performance in concentrating solar power plants [1], shifting of thermal load demand, and matching of uneven energy availability in time and in space. TES includes sensible, latent, and thermal-chemical heat storage units. Latent TES system demonstrates advantages over sensible TES system for their high storage density and small

temperature swing. These characteristics result in a greater flexibility and more compactness of PCTES unit [2]. PCTES unit can be classified in two main purposes: thermal protection and heat storage. One main difference between these two purposes is related to the thermal conductivity of PCM. For thermal protection purposes a low thermal conductivity is desirable. On the other hand, in the TES systems low thermal conductivity of PCM is a disadvantage for heat charging or discharging. For example, in the TES process, more than enough energy may be available, but the TES system can not store as much energy at a limited period, which reduces the efficiency of the TES system. Therefore, PCTES has been a main research topic for the last 20 years.[2]

Chemical heat storage has attracted considerable interest in recent years. Chemical heat storage has the capacity of high energy density and long-term storage duration at near ambient temperature among different thermal energy storage methods. The reactant undergoes the decomposition reaction with the aid of heat input, and therefore the thermal energy is converted into internal energy and simultaneously stored. The stored heat can be kept for a long time as long as the reaction products are separately stored. This makes this energy storage method a viable and effective technology for long-duration thermal energy storage and transport. This paper focused on the reversible chemical reactions available for chemical heat storage. A large number of promising candidate reactions for chemical heat storage are categorically summarized. In addition, the selection criteria of chemical reactions and the determination of applicative temperature range for chemical heat storage are addressed. Moreover, a more holistic view of the current state and the further direction and challenge of chemical heat storage are also presented and discussed. [1]

II. EXPERIMENTAL

A. Chemical reaction heat storage

For chemical reaction heat storage, the heat storage and heat release process can typically be described as:



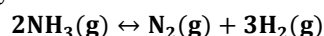
The compound A is split into chemical substances B and C through an endothermic dissociation reaction. The produced chemical substances, B and C, stores thermal energy in the form of the chemical potential energy. The reaction products B and C are stored separately to achieve



long period heat storage with little heat loss. When the reversible reaction occurs for the later heat utilization, compound A is regenerated resulting from the synthesis reaction between substances B and C as a result, the stored thermal energy is retrieved [2]

1) Chemical reaction heat storage using gas–gas reaction

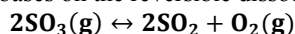
a) The $\text{NH}_3/\text{N}_2/\text{H}_2$ chemical reaction heat storage system. Ammonia-based chemical reaction heat storage system uses reversible dissociation of ammonia to store thermal energy. The chemical reaction is:



The reaction enthalpy is 66.8 kJ/mol ammonia at 20 MPa and 300 K. This reaction can be faster by introduction of an appropriate catalyst. The application of ruthenium-on-carbon catalyst in place of the iron-based catalyst helps to lower the dissociation temperatures to 673 K and below. [3,4]

b) The $\text{SO}_3/\text{O}_2/\text{SO}_2$ chemical reaction heat storage system.

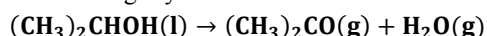
The sulphur trioxide (SO_3) chemical reaction heat storage system based on the reversible dissociation of SO_3 :



In this storage system, the resultant gases of dissociation reaction, SO_2/O_2 can be delivered via the pipes, and used for the heating purposes. SO_3 can be generated by recombination of the SO_2/O_2 gas mixture in the presence of catalytic at 773–873 K and release the chemical reaction heat [5–7]

2) Chemical reaction heat storage using liquid–gas reaction

a) The isopropanol/acetone/hydrogen chemical reaction heat storage system.



This liquid–gas endothermic reaction occurs at 353–363 K in presence of an appropriate catalyst. The exothermic reaction is the hydrogenation of acetone. This reaction occurs at 423–483 K with suitable catalyst [8]. The reaction equation is shown as follows:

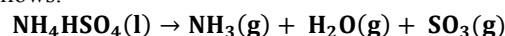


The overall system mainly consists of two reactors: an endothermic reactor and exothermic reactor. In the dehydrogenation process of isopropanol, it needs to separate isopropanol from the reaction products. The fractional condensation can easily be achieved at ambient temperature by equipping a distillation column in the system [9,10]. Kitikatsophon and Piumsomboon [11] investigated the dynamic behavior of isopropanol/acetone/hydrogen system by the steady-state simulation. They found the system stability hinged on the working pressure in distillation column and at the outlet of the compressor. The simulation results showed the corresponding thermal efficiency was 0.06 when the reaction conversions of dehydrogenation and hydrogenation reactions were 7.9% and 17.9%, respectively. KlinSoda and Piumsomboon developed an

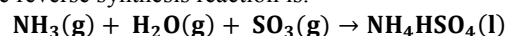
isopropanol/acetone/hydrogen chemical heat pump system. The conversions in the endothermic and exothermic reactors were about 8.5% and 11.6%, respectively. As a result, the fluid temperature in the exothermic reactor rose from 368 to 409 K. Theoretically, the exit fluid temperature in the exothermic reactor could be as high as 473 K. Improving the performance of the exothermic reactor could lift the level of thermal energy upgrading. The thermal efficiency of the system was around 38% and the exergy efficiency was 27%

b) The ammonium hydrogen sulfate chemical reaction heat storage system.

The decomposition of ammonium hydrogen sulfate (NH_4HSO_4) into ammonia (NH_3), water (H_2O), and sulfur trioxide (SO_3) for the thermal energy storage stage is shown as follows:



The reverse synthesis reaction is:



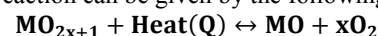
The actual temperature required for energy storage stage (T_1) and energy release (T_2) depends on the reaction conditions. The thermal energy storage density provided by this process (storage of H_2O , NH_3 , and SO_3 as liquids at ambient temperature) is between 3.098 GJ/m³ (740 kcal/l) and 4.102 GJ/m³ (980 kcal/l) [12]

3) Chemical reaction heat storage using solid–gas reaction

a) Thermal dissociation reaction of metal oxides for chemical reaction heat storage system.

The reduction reaction of multivalent metal oxides and reverse oxidation reaction can be used for storing thermal energy. Using air as reactant in the reverse exothermic reactions can avoid storing product gases. Furthermore, metal oxides have good stability and thus are considered as the candidate materials for chemical reaction heat storage

The redox reaction can be given by the following equation:



Fahim and Ford [13] illuminated the selection criteria of reversible chemical reaction used for the thermal energy storage reaction system of BaO_2/BaO

The activation energy of forward dissociation reaction of BaO_2 and backward oxidation reaction of BaO are 140.6 kJ/mol and 51.9 kJ/mol, respectively. Compared with the other oxides system, they concluded BaO_2/BaO system is a promising candidate reaction for the thermal energy storage. This system has the energy storage density of 3.01 GJ/m³ based on the solid product. The corresponding chemical equation is shown as:



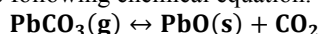
b) Decarbonation reaction of carbonate for chemical reaction heat storage system.

Kato et al. [14] surveyed the utility of several chemical reactions available for heat pump system. They mainly focused on inorganic oxide/carbon dioxide reaction

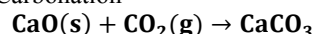


systems owing to their high chemical reaction heat. They found that the following inorganic oxides such as PbO, MgO, CuO, MnO, ZnO, NiO and CoO can be selected as candidates. As for the chemical reaction heat storage, the lead oxide/carbon dioxide (PbO/CO₂) reaction displays the most outstanding features.

The working principle of PbO/CO₂ reaction system is based on the following chemical equation:



The principle of chemical reaction heat storage system using PbO/CO₂ [14]. Kyaw et al. [15,16] investigated calcium oxide/carbon dioxide reaction for chemical reaction heat storage, the corresponding reversible chemical reaction can be written as: Carbonation



Decarbonation:



The CaO/CO₂ reaction system is very attractive for storing high temperature thermal energy. The characteristics of this system are as follows [15,17]: (1) CaCO₃ decomposes at 1100 K under 101 kPa of CO₂ pressure; (2) the substances involved in this reversible reaction are non-toxic and non-corrosive; (3) there are no undesirable side reactions during this reversible reaction; (4) CaCO₃ is an abundant and relatively cheap raw material; (5) this reaction system has a relatively high energy storage density (about 3.26 GJ/m³).

c) Dehydration reaction of hydroxide for chemical reaction heat storage system

Darkwa and O'Callaghan [18] evaluated the potential of inorganic oxides/hydroxides reaction system for chemical reaction heat storage. Thermal energy storage utilizing inorganic oxides/hydroxides reaction system can produce high heat energy and possess much higher thermal energy storage capacities (about 1-3 GJ/m³). CaO/Ca(OH)₂ system, as well as CaO/CaCO₃ system, has been claimed to be among the best candidates for thermal energy storage of high temperature heat [19].

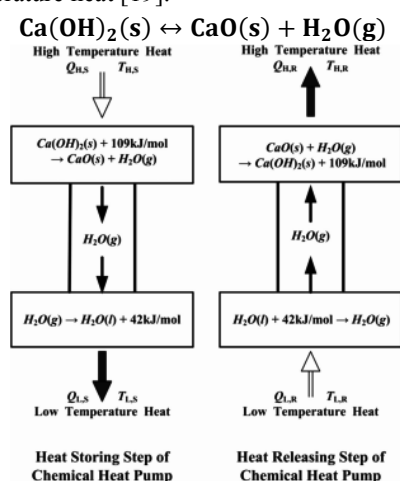


Fig. 1. Schematic diagram of CaO/Ca(OH)₂ chemical reaction heat storage system.

Fig. 1 shows the schematic diagram of the chemical reaction heat storage system using the CaO/Ca(OH)₂ [20]. The CaO/Ca(OH)₂ system stores thermal energy through dehydration of calcium hydroxide, and releases the stored energy on demand by means of the hydration of calcium oxide. Ogura et al. [21] investigate the performance of CaO/Ca(OH)₂ chemical heat pump. The obtained thermal energy storage/release density is 1.86 MJ/kg CaO or 1640 MJ/m³. Fujimoto et al. [22] conducted a dynamic simulation of CaO/Ca(OH)₂ chemical heat pump using energy and exergy analyses. They stated that CaO/Ca(OH)₂ chemical heat pump systems can meet the demands of the heating and cooling. The energy and exergy efficiencies are 58.7% and 61.6% for heating and 12.7% and 4.5% for cooling, respectively

MAGNESIUM OXIDE/WATER REACTION
Many researches investigate the thermal energy storage using a reversible magnesium oxide/water reaction. To test the possibility of a developing magnesium oxide/water system, Kato et al. [23] performed the kinetic study of the hydration of magnesium oxide. The MgO/Mg(OH)₂ chemical reaction heat storage system is based on the following equation:

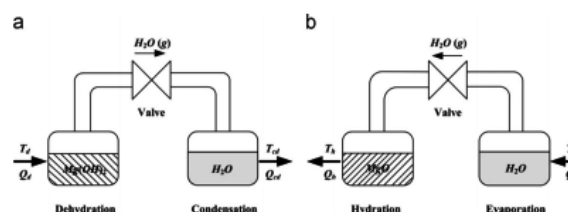
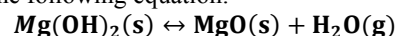


Fig. 2. Schematic diagram of MgO/Mg(OH)₂ chemical reaction heat storage: (a) heat storage mode; (b) heat output mode

Fig. 2 shows the working principle of the chemical reaction heat storage system using MgO/Mg(OH)₂. This system can be used for the storage of middle temperature heat. The dehydration temperature is about 523 K. The dehydration time highly depends on the temperature. Moreover, the reaction process highly relies on the heat and mass transfer. A relatively low dehydration temperature is more favorable for practical utilization. The enhancement of heat conductivity in the reactor can reduce the dehydration temperature. The dehydration could occur at below 583 K by enhancing the heat conductivity of the reactor. The more rapidly the hydration proceeds, the higher is the vapor pressure. In addition, a higher-pressure hydration reaction is favorable for improving the heat output performance of the heat pump. The output heat at a temperature of around 473 K was produced under the vapor pressure of 203 kPa [24].

B. Chemical sorption heat storage

Sorption is such a phenomenon that the certain gas or vapor (sorbate) is captured or dissolved onto surface of some solid or inner of liquid (sorbent). The working principle of chemical sorption heat storage is also relied upon a reversible



chemical reaction, endothermic in one direction and exothermic in the inverse direction. The process is either exothermic reaction (adsorption) or endothermic reaction (desorption) according to the thermodynamic conditions as shown in the following typical reaction:



Here, MX is the solid chemical reactant or liquid absorbent. The representative reaction salts are metallic halides (such as CaCl_2 , MnCl_2 , CoCl_2 , BaCl_2 , NiCl_2 , NaBr , etc.). G is the gas reactant, (such as NH_3 , H_2O , H_2 , etc.), and ΔH is the reaction enthalpy. The common sorption systems mainly include ammoniated salt pairs, hydrated salts and concentration-dilution. All of these systems are specified below. Both the gas–solid equilibrium and the vapor–liquid equilibrium are mono variant [25]. The equilibrium pressure in association with the constraint temperature is determined by the following equation [26,27]:

$$\ln(p) = -\frac{\Delta\text{H}}{\text{RT}} + \frac{\Delta\text{S}}{\text{R}}$$

where p is the equilibrium pressure of the solid–gas pair, ΔH and ΔS are the enthalpy and entropy changes during the reaction, respectively. R is the universal gas constant and T is the absolute temperature

1) Ammoniated salt pairs

As a kind of reversible solid–gas reaction, chemisorption can be used for chemical heat storage. A simple thermal energy storage using chemical sorption comprises of four main processes: desorption, condensation, evaporation and adsorption. The fundamental of chemisorption is the mono variant reversible gas–solid chemical reaction which occurs in a reactor coupled with a condenser and an evaporator

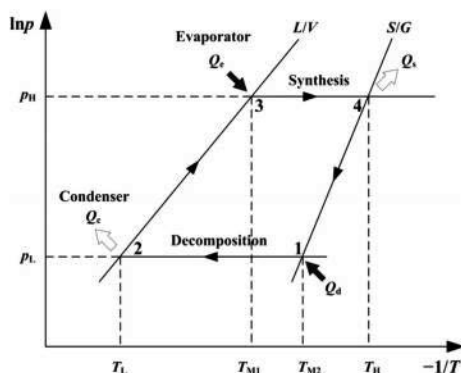


Fig. 3. Diagram of Clausius–Clapeyron showing operation principle.

Fig. 3 shows the operating principle of chemical sorption heat storage system [25,28]. The whole cycle is illustrated by a liquid/vapor equilibrium line (L/V line) and a solid/gas reaction equilibrium line (S/G line)

a) manganese chloride/ammonia

Thermal energy storage plays a key role in the application of renewable energy and low-grade thermal energy. A laboratory test unit of thermochemical heat storage with

manganese chloride (MnCl_2) as the reactive salt and ammonia (NH_3) as the working gas was constructed, in which expanded graphite was used to improve the heat and mass transfer performance of composite materials. The experimental campaigns show some promising conclusions on the heat storage performances of such a storage unit. With 3.78 kg of composite materials, the highest thermochemical heat storage density is about 1391 kJ/kg when the charging and discharging temperature is 174 C and 50 C, respectively. The corresponding volume density of thermochemical heat storage is 179 kWh/m³. The maximum of thermochemical heat storage efficiency obtained is 48%. The maximum of instantaneous thermochemical heat output power is more than 50 kW. The maximum for the average thermochemical heat output power reaches to 9.9 kW under the experimental conditions. The application prospects of such an thermochemical heat storage system are presented. The promising results have been gained, but some problems must be envisaged. The improvement measures to overcome these problems are also brought forward in order to make the thermochemical heat storage technology realize a successful application in practical systems [29]

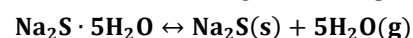
2) Hydrated salt pairs

Hydrated salt working pair is another potential candidate for chemical sorption heat storage. Hydrated salts become into anhydrous salts by releasing water during the energy storage phase when they are heated. These hydrophilic anhydrous salts can easily react with water to release the stored heat during energy release phase. Moreover, it is feasible to realize the long term storage of the thermal energy by separating the anhydrous salt and water at ambient temperature. Different from the most chemical heat storage systems, the charging and discharging processes of hydrated salt pairs usually have almost same temperatures, which are similar to the characteristics of latent heat storage using PCM. Therefore, many researchers regard the hydrated salt as one of kinds of inorganic PCM. Strictly speaking, the hydrated salt should be considered as one type of chemical storage material. The hydrated salt can be used to store thermal energy according to the following general chemical reaction:



During the charging phase, thermal energy is stored by performing the dehydration reaction of a hydrated salt. During the discharging phase, the stored heat is released by undergoing the hydration reaction of the salt. The process is achieved by addition of water vapor to anhydrous salt. This hydration effect is exothermic, hence results in the generation of heat. Among different hydrated salts, sodium sulphide and magnesium sulphate have been widely discussed and studied.

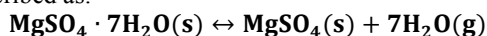
The chemical heat storage system using sodium sulphide is based on the following chemical equation:





Sodium sulphide (Na₂S) has high thermal energy storedensity due to the large sorption capacity and the high heat of sorption. Furthermore, the Na₂S/H₂O pair (pentahydrate Na₂S·5H₂O) has the high thermal power density as well as the large energy storage density (1980 kW h/m³ for heating and 1300 kW h/m³ for cooling) [30,31].

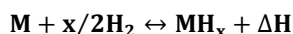
Magnesium sulphate (MgSO₄) is considered as another potential storage material, and its reversible reaction is described as:



This material is very tempting for the seasonal storage of solar heat. Posern and Kaps [32] demonstrated the working performance of MgSO₄/H₂O system. The hydration and dehydration of the chemical material proceed in the reactor. The system can employ either a separate reactor or an integrated reactor[33].

3) Metal hydrides

The metal hydrides are widely used for many industrial purposes, such as hydrogen storage, thermal energy storage, etc. Many metals, alloys or intermetallic compounds can react reversibly with hydrogen under the certain conditions. This reaction is exothermic during the adsorption phase, whereas an endothermic reaction occurs when hydrogen is desorbed from the metal hydrides during the desorption phase. The universal reaction can be described as follows:[34]



The hydrogen storage capacity increases from 1.88 to 2.5 wt% when the pressure varies from 1.5 to 2.0 MPa. The thermal energy storage efficiency increases from 0.5 at 1 MPa to 0.74 at the pressure of 3 MPa when the temperature was 423 K. For the given operating conditions under the pressure of 2 MPa and temperature of 423 K, the maximum amount of stored thermal energy is about 0.714 MJ/kg and the corresponding thermal energy storage coefficient is 0.74.[35]

4) Concentration-dilution

Concentration-dilution heat storage employs the concentration change of acid and alkali or salt solution to store or release the thermal energy. Stephan et al. [36] investigated the dynamic behavior of a heat transformer with NaOH–H₂O as working substances employing numerical and experimental methods. The maximum temperature lift is 45 K when absorber temperatures range from 403 to 428 K and evaporator temperatures are between 373 and 383 K. The coefficient of performance for this heat transformer can be as high as 0.49. Weber and Dorer [37] analyzed sodium hydroxide (NaOH)–water-based process for longterm solar heat storage. The required solar heat input temperature is more than 393 K during the energy storage process. In comparison with the traditional hot water storage, system-volume heat capacity is about six times higher for low-temperature space heating with the supply temperature of 313

K. Meanwhile, it is about three times higher for domestic hot water supply with the temperature of 338–343 K.[38]

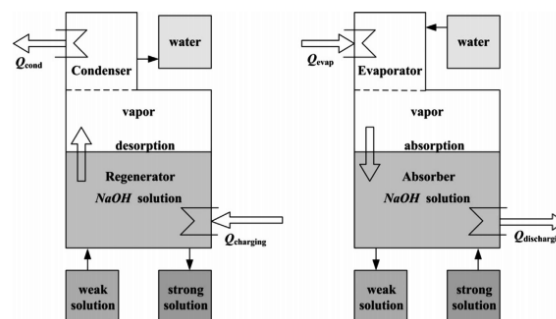
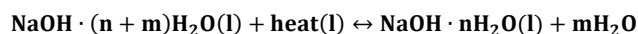


Fig. 4 shows the charging and discharging process of thermal energy storage with sodium hydroxide–water as the working pair [113]. The NaOH–water reaction system can be described as follows:



The system operates in charging mode when solar heat is available and discharging mode during the heating demand periods. In the charging mode, solar heat is introduced to the dilute NaOH solution in the regenerator. The solution is desorbed and releases some water vapor. This leads to the increase in the concentration of NaOH lye. The generated water vapor flows into the condenser where it condenses. The liquid water is stored in the water tank. In the discharging mode, the high concentrated NaOH lye in the absorber absorbs the water steam from the evaporator heated by a low-temperature heat source. The absorption enthalpy of this exothermic process can be supplied to the heat utilization device. To further improve the thermal energy storage density, EMPA (Swiss Federal Laboratories for Materials Testing and Research in Switzerland) proposed a double-stage closed absorption storage system. (Fig. 4) [39,40]

III. CONCLUSION

In this paper, previous research works on the chemical heat storage are reviewed. The selection criteria of chemical reactants and the reversible chemical reactions available for thermal energy storage systems are discussed and summarized. The performance of a chemical heat storage system is strongly dependent on the kinetics and thermodynamic properties of the chemical reactions utilized. Based on the current situation of chemical heat storage technology, it appears that chemical heat storage might be suitable for different application by selecting diverse promising candidate reactions. However, it is necessary to resolve numerous problems in the research and development stage before extensive application, such as the complexity of reaction process, appropriate catalyst, special consideration of safety, the large initial investment and the low efficiency. Thus, further works should be conducted to implement chemical heat storage in practice, such as the development of new composite reactants, chemical reaction kinetics, optimization designs, control strategy, and so on



ACKNOWLEDGMENT

The author would like to thank Research and Development Center for Sustainable Engineering (RDSE-SU), Department of Mechanical Engineering, Faculty of and Industrial Technology, Silpakorn University, and my work companion for all support to this work

IV. REFERENCES

- [1] T. Yan, R. Z. Wan, T. X. Li, L. W. Wang, and I. T. Fred, "A review of promising candidate reactions for chemical heat storage," *Renewable and Sustainable Energy Reviews*, vol. 43, pp. 13-31, March 2015.
- [2] T. Nagel, H. Shao, C. Robkopf, M. Linder, A. Wörner, and O. Kolditz, "The influence of gas-solid reaction kinetics in models of thermochemical heat storage under monotonic and cyclic loading," *Applied Energy*, vol. 136, pp. 289-302, 2014.
- [3] K. Lovegrove and A. Luzzi, "Endothermic reactors for an ammonia based thermochemical solar energy storage and transport system," *Sol Energy*, vol. 56, pp. 361-371, 1996.
- [4] H. Kreetz and K. Lovegrove, "Exergy analysis of an ammonia synthesis reactor in a solar thermochemical power system," *Sol Energy*, vol. 73, pp. 87-941, 2002.
- [5] JH. Mccrory, GE. Mccrory, TA. Chubb and YS. Won, "An experimental study of SO₂ dissociation as a mechanism for converting and transporting solar energy," *Sol Energy*, vol. 27, pp. 40-433, 1998
- [8] I. KlinSoda and P. Piumsomboon, "Isopropanol-acetone-hydrogen chemical heat pump: a demonstration unit," *Energy Convers Manage*, vol. 48, pp. 7-1200, 2007.
- [9] N. Meng and S. Shinoda, Y. Saito "Improvements on thermal efficiency of chemical heat pump involving the reaction couple of 2-propanol dehydrogenation and acetone hydrogenation," *Int J Hydrogen Energy*, vol. 22, pp. 7-361, 1997.
- [10] W. Mooksuwan and S. Kumar, "Study on 2 - propanol/acetone/hydrogen chemical heat pump: endothermic dehydrogenation of 2-propanol," *Int J Energy Res*, vol. 24, pp. 22-1109, 2000.
- [11] W. Kitikiatsofphon and P. Piumsomboon, "Dynamic simulation and control of an isopropanol-acetone-hydrogen chemical heat pump," *Sci Asia*, vol. 30, pp. 47-135, 2004.
- [12] WE. Wentworth and E. Chen, "Simple thermal decomposition reactions for storage of solar thermal energy," *Sol Energy*, vol. 18, pp. 14-205, 1976.
- [13] MA. Fahim and JD. Ford, "Energy storage using the BaO₂-BaO reaction cycle," *Chem Eng J*, vol. 27, pp. 8-21, 1983
- [14] Y. Kato, Y. Watanabe and Y. Yoshizawa, "Application of inorganic oxide/carbon dioxide reaction system to a chemical heat pump," In: *Proceedings of the 31st intersociety energy conversion engineering conference*, vol.2, pp.8-763, 1996.
- [15] K. Kyaw, H. Matsuda and M. Hasatani, "Applicability of carbonation/decarbonation reactions to high-temperature thermal energy storage and temperature upgrading," *J Chem Eng Jpn*, vol. 29, pp. 25-119, 1996.
- [16] K. Kyaw, M. Kubota, F. Watanabe, H. Matsuda and M. Hasatani "Study of carbonation of CaO for high temperature thermal energy storage," *J Chem Eng Jpn*, vol.31, pp.4-281, 1998.
- [17] K. Kyaw, T. Shibata, F. Watanabe, H. Matsuda and M. Hasatani "Applicability of zeolite for CO₂ storage in a CaO-CO₂ high temperature energy storage system," *Energy Convers Manage*, vol. 38, pp. 33-1025, 1997.
- [18] K. Darkwa and PWO. Callaghan, "Green transport technology(GTT): analytical studies of a thermochemical store for minimising energy consumption and air pollution from automobile engines," *Appl Therm Eng*, vol. 17, pp. 14-603, 1997.
- [19] JM. Criado, M. Macias and AM. Machin, "Analysis of the system CaO-CO₂-H₂O for storage of solar thermal energy," *Sol Energy*, vol. 49, pp. 6-83, 1992.
- [20] JM. Criado, M. Macias and AM. Machin, "Analysis of the system CaO-CO₂-H₂O for storage of solar thermal energy," *Sol Energy*, vol. 49, pp. 6-83, 1992.
- [21] H. Ogura, T. Yamamoto and H. Kage, "Efficiencies of CaO/H₂O/Ca(OH)₂ chemical heat pump for heat storing and heating/cooling," *Energy*, vol. 28, pp. 93-1479, 2003.
- [22] S. Fujimoto, E. Bilgena and H. Ogura, "Dynamic simulation of CaO/Ca(OH)₂ chemical heat pump systems," *Exergy Int J*, vol. 2, pp. 6-14, 2002.
- [23] Y. Kato, N. Yamashita, K. Kobayashi and Y. Yoshizawa, "Kinetic study of the hydration of magnesium oxide for a chemical heat pump," *Appl Therm Eng*, vol.6, pp. 62-853, 1996.
- [24] T. Yan, R. Z. Wang, and T. X. Li, "Experimental investigation on thermochemical heat storage using manganese chloride/ammonia," *Energy* vol. 143, pp. 562-574, 2018
- [25] HJ. Huang, GB. Wu, J. Yang, YC. Dai, WK. Yuan and HB. Lu, "Modeling of gas-solid chemisorption in chemical heat pumps," *Sep Purif Technol*, vol. 34, pp. 191-200, 2004
- [26] Y. Zhong, RE. Critoph, RN. Thorpe, Z. Tamainot-Telto and YI. Aristov, "Isothermal sorption characteristics of the BaCl₂-NH₃ pair in a vermiculite host matrix," *Appl Therm Eng*, vol. 27, pp. 26-245, 2007.
- [27] M. Sorin, B. Spinner, D. Stitou, "Thermodynamic techniques for the conceptual design of thermochemical refrigerators using two salt materials," *Chem Eng Sci*, vol. 57, pp.51-423, 2002.
- [28] YQ. Yu, P. Zhang, JY. Wu, RZ. Wang, "Energy upgrading by solid-gas reaction heat transformer: a critical review," *Renewable Sustainable Energy*, vol. 12, pp. 24-1302, 2008.
- [29] T. Yan, R. Z. Wang, and T. X. Li. "Experimental investigation on thermochemical heat storage using manganese chloride/ammonia," *Energy*, vol. 143, pp. 562-574, 2018.
- [30] KE. N'Tsoukpoe, H. Liu, N. Le Pierrès, L. Luo, "A review on long-term sorption solar energy storage," *Renewable Sustainable Energy Rev*, vol. 13, pp. 96-2385, 2009.
- [31] M. Ucar, B. Pounder, "Heat-of-adsorption solar thermal energy storage," *J Therm Insul*, vol. 6, pp. 48-58, 1982.
- [32] K. Posern, C. Kaps, "Humidity controlled calorimetric investigation of the hydration of MgSO₄ hydrates," *J Therm Anal Calorim*, vol. 92, pp. 9-905, 2008.
- [33] HA. Zondag, A. Kalbasenka, M. van Essen, L. Bleijendaal, R. Schuitema, W. van Helden, et al, "First studies in reactor concepts for thermochemical storage," Available from <http://ftp.ecn.nl/pub/www/library/report/2009/m09008.pdf> 2009.
- [34] FS. Yang, GX. Wang, ZX. Zhang, XY. Meng and V. Rudolph "Design of the metal hydride reactors-A review on the key technical issues," *Int J Hydrogen Energy*, vol. 35, pp. 40-3832, 2010.
- [35] BS. Sekhar, P. Muthukumar and R. Saikia, "Tests on a metal hydride based thermal energy storage system," *Int J Hydrogen Energy*, vol. 37, pp. 24-3818, 2012.
- [36] K. Stephan M. Schmitt, D. Hebecker and T. Bergmann, "Dynamics of a heat transformer working with the mixture NaOH-H₂O," *Int J Refrig*, vol. 20, pp. 95-483, 1997.
- [37] R. Weber, and V. Dorer "Long-term heat storage with NaOH," *Vacuum*, vol. 82, pp. 16-708, 2008.
- [38] T. Tanaka, K. Sakuta, M. Kamimoto, T. Tani, S. Sawata and T. Horigome, "Solar thermal energy storage using heat of dilution: analysis of heat generation in multistage mixing column," *Energy Convers*, vol. 18, pp. 57-65, 1978.
- [39] C. Wyman, J. Castle and F. A. Kreith, "Review of collector and energy storage technology for intermediate temperature applications," *Sol Energy*, vol. 24, pp. 40-517, 1980.
- [40] G. Cacciola and N. Giordano, "Chemical processes for energy storage and transmission," *Appl Energy*, vol. 25, pp. 37-315, 1986.



Microbial Production of Syrup from Broken Organic Jasmine Rice Grain

Kanokwan Tandee*, Chananya Ramananus, Pattayamon Mekyapisit, and Junjira Wunchana

Faculty of Engineering and Agro-Industry, Maejo University, Chiang Mai, Thailand

*Corresponding author: ktandee@gmail.com

Abstract—Organic jasmine rice generally has a high production cost but milling could partially break a full-length grain, resulting in a low market price. This research was thus aimed to increase a price of broken organic jasmine rice grain via syrup production. Five molds and two yeasts were selected for starch hydrolysis aerobically or anaerobically for a week. Microbial count, starch, reducing sugar, dextrose equivalent (DE), total sugar, and total acid were daily analyzed. Results indicated that *Rhizopus oryzae* was suitable for syrup production from broken organic jasmine rice grain aerobically as reducing sugar, DE, and total sugar were present at a higher content than other six fungi, which were *Aspergillus awamori*, *Aspergillus niger*, *Aspergillus oryzae*, *Rhizopus oligosporus*, *Candida tropicalis*, and *Saccharomycopsis fibuligera*. Using 1% *Rhizopus oryzae* spore, instead of 10%, was enough for hydrolysis of starch into syrup within six days. Syrup production from broken organic jasmine rice grain by microbial activity was economically feasible and could raise a market price of broken organic jasmine rice grain.

Keywords—organic jasmine rice; *Rhizopus oryzae*; starch hydrolysis; syrup production

I. INTRODUCTION

Organic jasmine rice generally has a high production cost but milling could partially break a full-length grain and result in a low market price due to the consumer unacceptance. Processing of broken organic jasmine rice grain into more valuable food could hence support the organic farming. Raw material with high starch content could be transformed into various products [1] including a syrup which is widely used as sweetener, thickening and anti-caking agent in sweet, preserved fruit and vegetables, jam, jelly, beverage, candy, ice cream, sauce, etc. Industrial production of syrup is involved with the enzymatic reaction by alpha-amylase, glucoamylase, amylo-glucosidase to hydrolyze starch into sugar [2]. Such process is considered unsustainable because enzyme can be degraded and needs to be added over time.

Application of amylase-producing fungi, i.e. mold and yeast, in starch hydrolysis might be able to reduce a production cost of syrup from broken organic jasmine rice grain. Fungi have several advantages over enzyme such as high adaptability to the process condition via spore formation and self-proliferation in suitable nutrients, e.g. rice starch. As the result, fungi could be transferred from old to new batch of production without starter addition.

Glucoamylase from *Aspergillus awamori* and *Aspergillus niger* was able to hydrolyze starch from corn, wheat, and sorghum into 90-95% glucose and <10% maltose and isomaltose. This enzyme could further produce 20-25% glucose syrup within 24-48 h [3]. In addition, amyloglucosidase from *Rhizopus* was able to hydrolyze starch from maize, millet, and sorghum into 11.32-17.15 mg/L reducing sugar with dextrose equivalent (DE) 65.66-78.28 at >59.25°C for 10 min [4]. Furthermore, glucoamylase from *Aureobasidium pullulans* was able to hydrolyze both α -1,4 and α -1,6 glycosidic bonds in potato starch, resulting in 68.5% glucose at 60°C within 6 h [5]. Extracellular amylolytic enzymes were also produced from *Arxula adeninivorans*, *Candida japonica*, *Filobasidium capsuligenum*, *Lipomyces*, *Saccharomycopsis*, and *Schwanniomyces* [6].

The objective of current study was to select for a microorganism with high amylase activity to rapidly hydrolyze starch into syrup but producing a low level of by-products such as acid or ethanol. Moreover, syrup production was improved by optimizing a level of starter microorganism.

II. MATERIALS AND METHODS

A. Starter Cultures, Raw Materials, and Chemicals

Seven fungal species, which were *Aspergillus awamori* TISTR 3193, *Aspergillus niger* TISTR 3063, *Aspergillus oryzae* TISTR 3019, *Rhizopus oryzae* TISTR 3052, *Rhizopus oligosporus* TISTR 3001, *Candida tropicalis* TISTR 5087, and *Saccharomycopsis fibuligera* TISTR 5097, were obtained from the culture collection of Thailand Institute of Scientific and Technological Research (TISTR). Broken organic jasmine rice was purchased from a local market in Chiang Mai while Tapioca flour was bought from Bangkok. All chemicals were purchased from Ajax Finechem and microbiological media were obtained from HiMedia Laboratories.

B. Preparation of Starter Cultures

Five molds were plated on potato dextrose agar (PDA) until sporulation. 10 g of broken organic jasmine rice was soaked in 10 ml of distilled water for 30 min before sterilized in Petri dish at 121°C for 15 min. Spores from PDA were inoculated in sterile broken organic jasmine rice and incubated at 25°C until sporulation. Spores in rice were dried at 45°C until humidity



was 6%. After ground into powder, 1 g of spores in rice was mixed with 100 g of tapioca flour and stored at 4°C until used.

Two yeasts were grown in nutrient broth (NB) for 16 h. 10 ml of cultures was collected at 3000×g for 10 min and supernatant was discarded. After washed twice in 0.9% NaCl, cultures were resuspended in 10 ml of 0.9% NaCl.

C. Selection of Starter Cultures

500 g of broken organic jasmine rice and 500 ml of distilled water were cooked in a rice cooker. After cooled down, cooked rice was mixed with 10 g of mold spores or 10 ml of yeast cultures. Aerobic syrup production was conducted in a muslin cloth within a basket while anaerobic syrup production was carried out in a plastic bag for a week. Samples were daily removed to analyze microbial count, starch, reducing sugar, dextrose equivalent (DE), total sugar, and total acid. Experiment was repeated in triplicate for each species.

D. Optimization of Syrup Production

500 g of broken organic jasmine rice and 500 ml of distilled water were cooked in a rice cooker. After cooled down, cooked rice was mixed with 10 g or 100 g of mold spores and placed in a muslin cloth within a basket for a week. Samples were daily removed to analyze microbial count, starch, reducing sugar, dextrose equivalent (DE), total sugar, and total acid. Experiment was repeated in triplicate for each level of spores.

E. Sample Analysis

For microbial count, 25 g of samples was diluted in 225 ml of distilled water before spread on PDA and incubated at 25°C for five days. For starch analysis, 0.1 ml of diluted samples was mixed with 2.4 ml of 5% iodine solution before absorbance at 620 nm was read. For analysis of reducing sugar 0.5 ml of diluted samples was mixed with 0.5 ml of 1% DNS solution before boiled for 10 min and placed on ice. 5 ml of distilled water was added before absorbance at 520 nm was read. Dextrose equivalent (DE) was calculated by dividing reducing sugar content by dry weight, which was analyzed by drying 2 g of samples at 105°C for 4 h. For analysis of total sugar, 1 ml of diluted samples was mixed with 1 ml of 5% phenol solution. After 5 ml of 98% sulfuric acid was added, solution was left for 10 min, mixed, and waited for 30 min. Absorbance was read at 480 nm. For analysis of total acid, diluted samples were titrated with 0.1N NaOH until pH 8.7 was reached. Total acid was calculated by multiplying 0.06 with an amount of NaOH used. Microbial count was repeated in duplicate while chemical analysis was conducted in triplicate for each sample.

F. Statistical Analysis

Microbial count, starch, reducing sugar, dextrose equivalent (DE), total sugar, and total acid were tested for statistical difference at 95% confidence by Analysis of Variance in General Linear Model (GLM) followed by Tukey's-b test (SPSS Statistics 17.0)

III. RESULTS

A. Selection of Starter Cultures

Microbial counts in broken organic jasmine rice syrup were between 4.19-6.46 log CFU/g. Numbers of *Aspergillus awamori* and *Aspergillus oryzae*, which evidently grew in broken organic jasmine rice syrup, were significantly higher than other five species during days 4-7 of syrup production. *Rhizopus oligosporus* was present at the statistically lowest level (Fig. 1). Additionally, numbers of *Aspergillus awamori*, *Aspergillus niger*, *Aspergillus oryzae*, *Rhizopus oryzae*, *Rhizopus oligosporus* and *Saccharomyces fibuligera* were significantly higher in aerobic than anaerobic condition (data not shown).

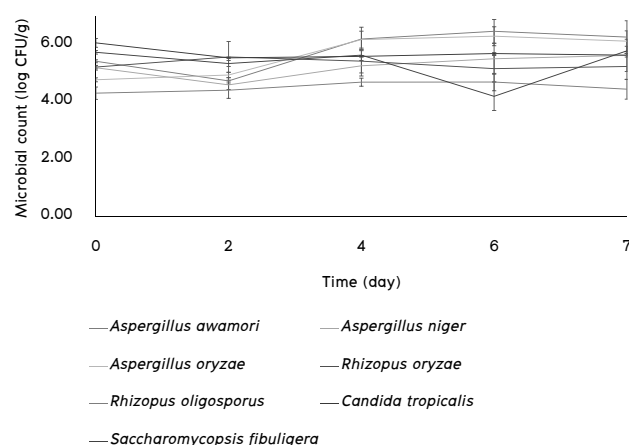


Fig. 1. Microbial counts in broken organic jasmine rice syrup produced by seven fungal species for a week. Each value was calculated from six replicates and presented as mean±SE.

Starch contents in broken organic jasmine rice syrup were between 325.06-1972.40 g/L. *Aspergillus oryzae* and *Rhizopus oryzae* significantly increased starch contents during days 1-3 of syrup production (Fig. 2). Moreover, starch contents resulted from *Aspergillus awamori*, *Aspergillus niger*, *Aspergillus oryzae*, *Rhizopus oryzae*, *Rhizopus oligosporus* and *Saccharomyces fibuligera* were statistically higher in aerobic than anaerobic condition (data not shown).

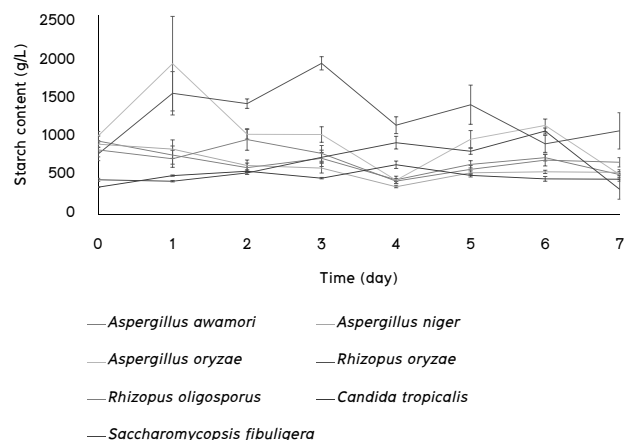


Fig. 2. Starch contents in broken organic jasmine rice syrup produced by seven fungal species for a week. Each value was calculated from nine replicates and presented as mean±SE.

Reducing sugar contents in broken organic jasmine rice syrup were between 2.69-361.09 g/L. *Rhizopus oryzae* and *Candida tropicalis* significantly produced the highest and lowest contents of reducing sugar on day 5 of syrup production. In general, *Aspergillus oryzae* and *Rhizopus oryzae* increased reducing sugar contents approximately 55-60 times during syrup production (Fig. 3). Furthermore, reducing sugar contents resulted from *Aspergillus awamori*, *Aspergillus niger*, *Aspergillus oryzae*, *Rhizopus oryzae*, and *Rhizopus oligosporus* were statistically higher in aerobic than anaerobic condition (data not shown).

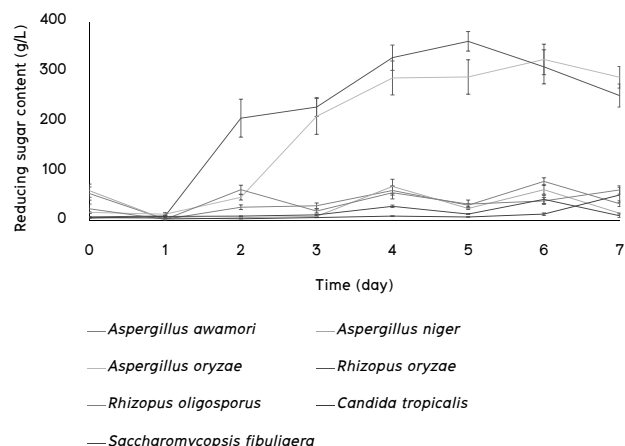


Fig. 3. Reducing sugar contents in broken organic jasmine rice syrup produced by seven fungal species for a week. Each value was calculated from nine replicates and presented as mean±SE.

Dextrose equivalent (DE) in broken organic jasmine rice syrup were between 0.07-7.22. *Rhizopus oryzae* and *Saccharomyces fibuligera* significantly resulted in the highest and lowest dextrose equivalent (DE) on day 5 of syrup production. Generally, *Aspergillus oryzae* and *Rhizopus oryzae* increased dextrose equivalent (DE) approximately 65-70 times

during syrup production (Fig. 4). In addition, dextrose equivalent (DE) resulted from *Aspergillus awamori*, *Aspergillus niger*, *Aspergillus oryzae*, *Rhizopus oryzae*, and *Rhizopus oligosporus* were statistically higher in aerobic than anaerobic condition (data not shown).

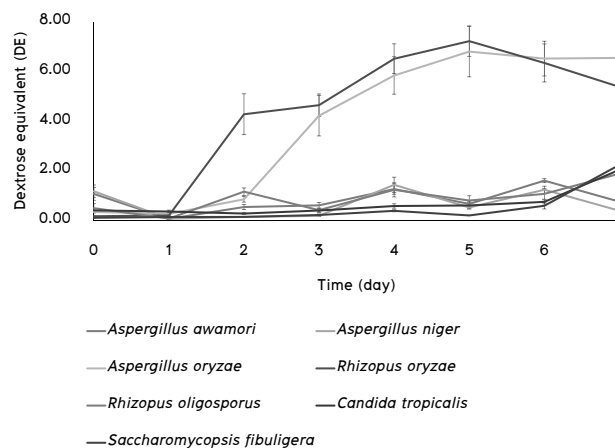


Fig. 4. Dextrose equivalent (DE) in broken organic jasmine rice syrup produced by seven fungal species for a week. Each value was calculated from nine replicates and presented as mean±SE.

Total sugar contents in broken organic jasmine rice syrup were between 16.24-9248.80 g/L. *Rhizopus oryzae* significantly produced the highest total sugar content, which was increased approximately 4600 times during syrup production, on day 5 of syrup production (Fig. 5). Besides, total sugar contents resulted from *Aspergillus oryzae*, *Rhizopus oryzae*, and *Rhizopus oligosporus* were statistically higher in aerobic than anaerobic condition (data not shown).

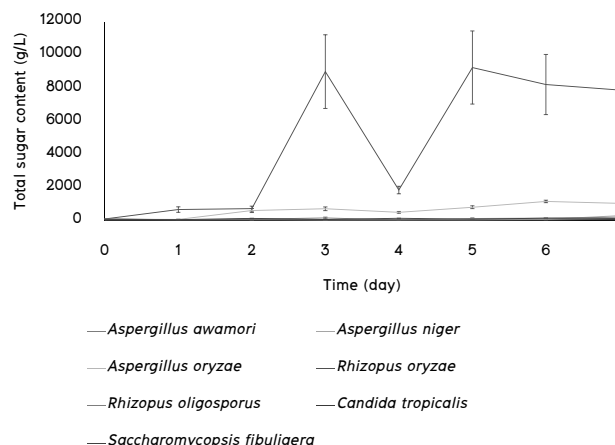


Fig. 5. Total sugar contents in broken organic jasmine rice syrup produced by seven fungal species for a week. Each value was calculated from nine replicates and presented as mean±SE.

Total acids in broken organic jasmine rice syrup were between 0.03-1.22%. *Rhizopus oryzae* and *Candida tropicalis* significantly produced the highest and lowest total acids on day



3 of syrup production. *Rhizopus oryzae* increased total acids approximately 40 times during syrup production (Fig. 6). Additionally, total acids resulted from *Aspergillus awamori*, *Aspergillus niger*, *Aspergillus oryzae*, *Rhizopus oryzae*, *Rhizopus oligosporus*, and *Saccharomyces fibuligera* were statistically higher in aerobic than anaerobic condition (data not shown).

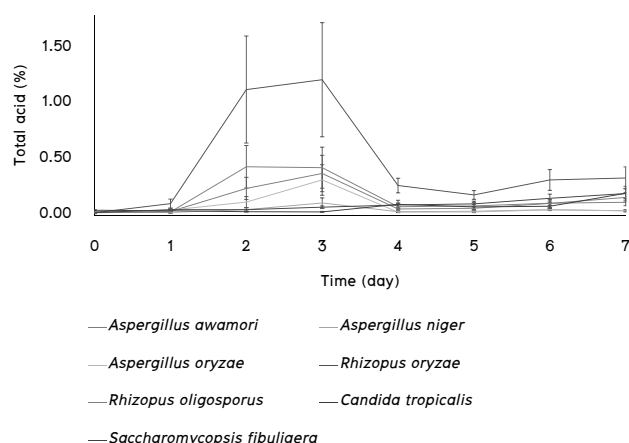


Fig. 6. Total acids in broken organic jasmine rice syrup produced by seven fungal species for a week. Each value was calculated from three replicates and presented as mean±SE.

B. Optimization of Syrup Production

Microbial counts in broken organic jasmine rice syrup were between 4.15-5.46 log CFU/g. 1% of *Rhizopus oryzae* spores significantly resulted in higher microbial counts than 10% of spores on days 4-6 of syrup production (Fig. 7).

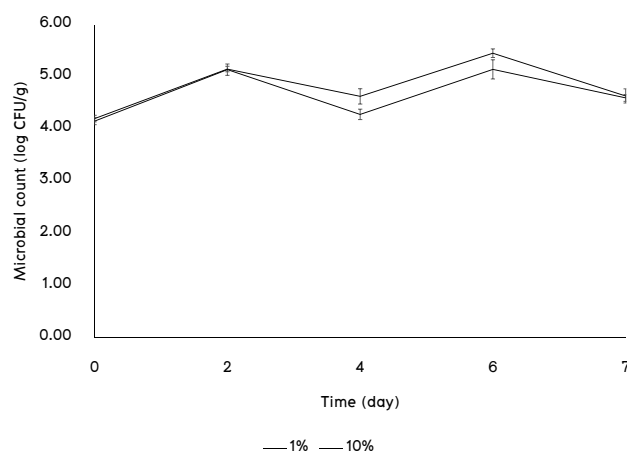


Fig. 7. Microbial counts in broken organic jasmine rice syrup produced by 1% and 10% *Rhizopus oryzae* spores for a week. Each value was calculated from six replicates and presented as mean±SE.

Starch contents in broken organic jasmine rice syrup were between 511.38-1379.74 g/L. 1% of *Rhizopus oryzae* spores

significantly resulted in higher starch contents than 10% of spores on days 2-7 of syrup production (Fig. 8).

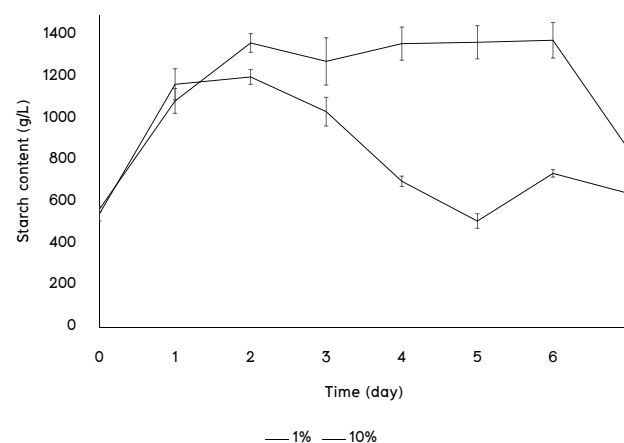


Fig. 8. Starch contents in broken organic jasmine rice syrup produced by 1% and 10% *Rhizopus oryzae* spores for a week. Each value was calculated from nine replicates and presented as mean±SE.

Reducing sugar contents in broken organic jasmine rice syrup were between 8.03-467.72 g/L. 1% of *Rhizopus oryzae* spores significantly resulted in higher reducing sugar contents than 10% of spores on days 2-7 of syrup production (Fig. 9).

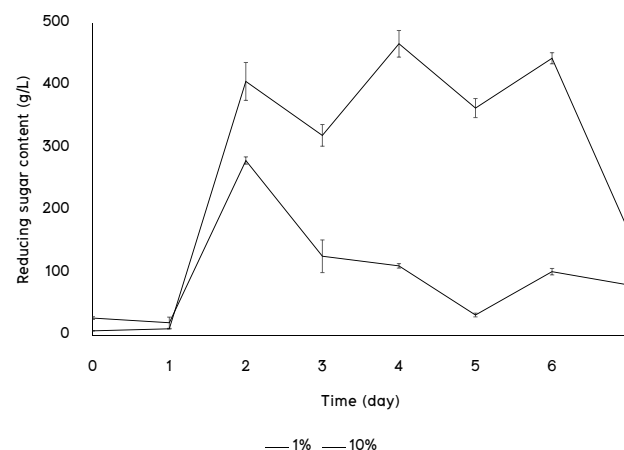


Fig. 9. Reducing sugar contents in broken organic jasmine rice syrup produced by 1% and 10% *Rhizopus oryzae* spores for a week. Each value was calculated from nine replicates and presented as mean±SE.

Dextrose equivalent (DE) in broken organic jasmine rice syrup were between 0.16-13.35. 1% of *Rhizopus oryzae* spores significantly resulted in higher dextrose equivalent (DE) than 10% of spores on days 2-7 of syrup production (Fig. 10).

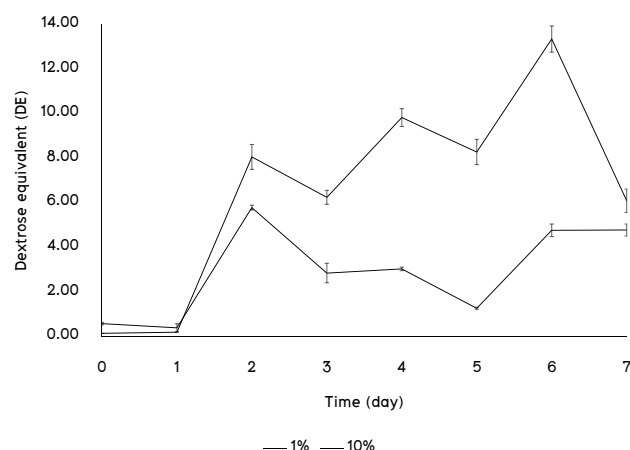


Fig. 10. Dextrose equivalent (DE) in broken organic jasmine rice syrup produced by 1% and 10% *Rhizopus oryzae* spores for a week. Each value was calculated from nine replicates and presented as mean±SE.

Total sugar contents in broken organic jasmine rice syrup were between 20.50-942.86 g/L. 1% of *Rhizopus oryzae* spores significantly resulted in higher total sugar contents than 10% of spores on days 2-6 of syrup production (Fig. 11).

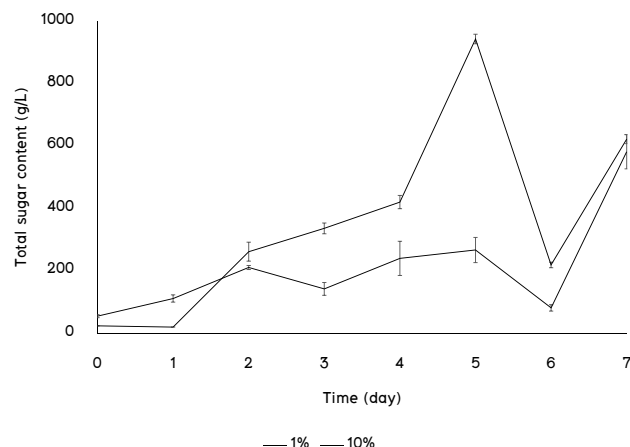


Fig. 11. Total sugar contents in broken organic jasmine rice syrup produced by 1% and 10% *Rhizopus oryzae* spores for a week. Each value was calculated from nine replicates and presented as mean±SE.

Total acids in broken organic jasmine rice syrup were between 0.01-0.21%. 1% of *Rhizopus oryzae* spores resulted in higher total acids than 10% of spores on days 5-7 of syrup production (Fig. 12).

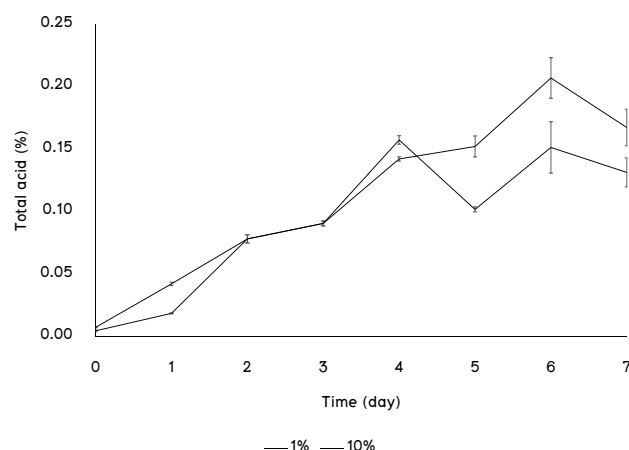


Fig. 12. Total acids in broken organic jasmine rice syrup produced by 1% and 10% *Rhizopus oryzae* spores for a week. Each value was calculated from three replicates and presented as mean±SE.

IV. DISCUSSION

Aspergillus, e.g. *Aspergillus awamori*, *Aspergillus niger*, *Aspergillus oryzae*, is a growth-limited mold and able to proliferate or sporulate at a faster rate than *Rhizopus*, e.g. *Rhizopus oryzae*, *Rhizopus oligosporus*, which is not a growth-limited mold. Since *Candida tropicalis* and *Saccharomyces fibuligera* are yeasts that require a higher water activity for growth, they grew more poorly than mold in broken organic jasmine rice. Moreover, mold is an aerobe, thus grew faster in a muslin cloth than a basket, but yeast is a facultative anaerobe, thus showed a comparable growth in both conditions [7].

Rice-hydrolyzing microorganism must be able to degrade a pericarp, which comprises proteins and fat, to release starch from an endosperm [8]. Since *Aspergillus oryzae* and *Rhizopus oryzae* are commonly found on a rice grain, hence could produce protease and lipase to degrade a pericarp [9-10], especially under an aerobic condition. However, *Candida tropicalis* might be able to produce protease under an anaerobic condition, thus more starch was released in that condition. Pichova et al. also reported a protease produced by *Candida* [11].

Once starch was released from a rice grain during an early phase of syrup production, yeast and mold would produce amylase to hydrolyze starch into sugar for growth. As the result, reducing sugar, total sugar, and dextrose equivalent (DE) were increased during a middle phase of syrup production as the highest activity of amylase was found on day 5 of syrup production. Furthermore, *Aspergillus oryzae* and *Rhizopus oryzae* could produce more amylase than other molds, especially under an aerobic condition. Whereas *Candida tropicalis* and *Saccharomyces fibuligera* showed a slower growth than molds, amylase was produced at a lower level in both conditions. Yalcin and Corbaci also reported the amylase produced by *Saccharomyces fibuligera* under an aerobic condition [6].



Alpha-amylase was expected to be produced by molds because the highest activity was found on day 5 of syrup production that was similar to the hydrolysis of corn starch by *Aspergillus niger* into dextrans with dextrose equivalent (DE) 8-15. Moreover, *Aspergillus awamori* and *Aspergillus niger* could produce glucoamylase to hydrolyze starch into glucose and other sugars, e.g. maltose, isomaltose [3]. Glucoamylase was widely used to produce glucose syrup and generally isolated from *Aspergillus niger*, *Aspergillus awamori*, and *Rhizopus oryzae* [12].

Organic acids, e.g. lactic acid, fumaric acid, acetic acid, were by-products from sugar metabolism by microorganisms [13-15]. Therefore, acid content was consistent with levels of reducing sugar, total sugar, and dextrose equivalent (DE) as all increased in the middle of syrup production, especially under an aerobic condition. Suitable microorganism should, however, produce organic acids at a basal level and result in a high sugar content.

Rhizopus oryzae was able to effectively release and hydrolyze starch from broken organic jasmine rice in an aerobic condition. Although its level was 1 log CFU/g lower than *Aspergillus oryzae*, contents of reducing sugar, total sugar, and dextrose equivalent (DE) were higher. Therefore, *Rhizopus oryzae* was selected for optimizing the syrup production from broken organic jasmine rice.

When two levels of *Rhizopus oryzae* spores were used, contents of microorganism, starch, reducing sugar, total sugar, dextrose equivalent (DE), and total acid were higher at 1% than 10%. Additionally, 1% of spores could increase the contents of starch, reducing sugar, total sugar, dextrose equivalent (DE), and total acid until day 6 of syrup production, which was longer than 10% of spores that syrup production was highest on day 3. It was possible that 1% of *Rhizopus oryzae* spores could produce higher levels of protease and amylase and was more suitable for syrup production from broken organic rice. Mixing tapioca flour with *Rhizopus oryzae* spores not only prevented sporulation during storage, but also decreased a moisture content of broken organic jasmine rice when used at 10%, creating an inappropriate condition for *Rhizopus oryzae* that requires the lowest water activity of 0.6 for growth [7].

Syrup produced from broken organic jasmine rice by *Rhizopus oryzae* contained dextrose equivalent (DE) 13.35, which was lower than dextrose equivalent (DE) 65.66-78.28 of syrup produced from maize, millet, and sorghum by amyloglucosidase from *Rhizopus* [4]. Moreover, it was lower than dextrose equivalent (DE) at least 20 of commercial syrup [16]. The main reason would be a low moisture content, which was inappropriate for microbial growth and activity, of broken organic jasmine rice during syrup production. Therefore, further research should control a moisture content of raw materials to decrease a production time or should evaporate water from a final product to increase dextrose equivalent (DE).

V. CONCLUSION

Syrup production from broken organic jasmine rice grain present in this research was simple, efficient, and sustainable; therefore, a product with higher profit was expected.

ACKNOWLEDGMENT

This research was financially supported by Faculty of Engineering and Agro-Industry, Maejo University, Chiang Mai, Thailand.

REFERENCES

- [1] S. Hizukuri, Y. Takeda, N. Maruta, and B.O. Juliano, "Molecular structures of rice starch," *Carbohydr. Res.*, vol. 189, pp. 227-235, 1989.
- [2] R. Sindhu, M. Kuttiraja, P. Binod, K.U. Janu, R.K. Sukumaran, and A. Pandey, "Dilute acid pretreatment and enzymatic saccharification of sugarcane tops for bioethanol production," *Bioresour. Technol.*, vol. 102, pp. 10915-10921, 2011.
- [3] M.C. Cadmus, L.G. Jayko, D.E. Hensley, H. Gasdorf, and K.L. Smiley, "Enzymatic production of glucose syrup from grains and its use in fermentations," *Cereal Chem.*, vol. 43, pp. 658-668, 1966.
- [4] A. Zainab, S. Modu, A.S. Falmata, and Maisaratu, "Laboratory scale production of glucose syrup by the enzymatic hydrolysis of starch made from maize, millet and sorghum," *Biokemistri*, vol. 23, pp. 1-8, 2011.
- [5] H. Li, Z. Chi, X. Duan, L. Wang, J. Sheng, and L. Wu, "Glucoamylase production by the marine yeast *Aureobasidium pullulans* N13d and hydrolysis of potato starch granules by the enzyme," *Process Biochem.*, vol. 42, pp. 462-465, 2007.
- [6] H.T. Yalcin and C. Corbaci, "Isolation and characterization of amylase producing yeasts and improvement of amylase production," *Turk. J. Biochem.*, vol. 38, pp. 101-108, 2013.
- [7] T. Chitov, *Food Microbiology*, Thai Trans. Bangkok: Chulalongkorn University, 2015.
- [8] Food and Agriculture Organization (FAO) of the United Nations, "Rice in human nutrition," online.
- [9] M. Machida, O. Yamada, and K. Gomi, "Genomics of *Aspergillus oryzae*: learning from the history of koji mold and exploration of its future," *DNA Res.*, vol. 15, pp. 173-183, 2008.
- [10] H. Shin, X. Guo, and R.R. Chen, "Chapter 13-Biocatalysis for chiral synthesis," in *Bioprocessing for value-added products from renewable resources*, S. Yang, Ed. New York: Elsevier, 2007.
- [11] L. Pichova, L. Pavlickova, J. Dostal, E. Dolejsi, O. Hruskova-Heidingsfeldova, J. Weber, T. Ruml, and M. Soucek, "Secreted aspartic proteases of *Candida albicans*, *Candida tropicalis*, *Candida parapsilosis* and *Candida lusitanae*," *Eur. J. Biochem.*, vol. 268, pp. 2669-2677, 2001.
- [12] F. Carina-Pavezzi, E. Gomes, and R. da Silva, "Production and characterization of glucoamylase from fungus *Aspergillus awamori* expressed in yeast *Saccharomyces cerevisiae* using different carbon sources," *Braz. J. Microbiol.*, vol. 39, pp. 108-114, 2008.
- [13] K. Amprayn, M.T. Rose, M. Kecskes, L. Pereg, H.T. Nguyen, and I.R. Kennedy, "Plant growth promoting characteristics of soil yeast (*Candida tropicalis* HY) and its effectiveness for promoting rice growth," *Appl. Soil Ecol.*, vol. 61, pp. 295-299, 2012.
- [14] J. Dijksterhuis and R.A. Samson, "Zygomycetes," in *Food spoilage microorganisms*, C. Blackbum, Ed. Cambridge: Woodhead Publishing, 2006.
- [15] S. Yang, H. Huang, A. Tay, W. Qin, L. de Guzman, and E.C. San Nicolas, "Chapter 16-Extractive fermentation for the production of carboxylic acids," in *Bioprocessing for value-added products from renewable resources*, S. Yang, Ed. New York: Elsevier, 2007.
- [16] H.M. Pancoast and W.R. Junk, *Handbook of sugars*, Westport: AVI Publishing, 1980.



Production of Yanang Leaves (*Tiliacora triandra*) Powder by Drying Techniques

Jittimon Wongsu*

Department of Agricultural Engineering for Industry,
Faculty of Industrial Technology and Management,
King Mongkut's University of Technology North Bangkok
Prachinburi Campus,
Prachinburi, Thailand
Jittimon.w@fitm.kmutnb.ac.th

Suchada Sadang

Office of the Dean,
Faculty of Industrial Technology and Management,
King Mongkut's University of Technology North Bangkok
Prachinburi Campus,
Prachinburi, Thailand
Suchada.s@fitm.kmutnb.ac.th

Abstract— Yanang (*Tiliacora triandra*) a type of native climbing plant, is used as traditional medicine and as an ingredient in many recipes of northeast Thailand and Lao PDR. Due to its nutritional value and antioxidant properties, Yanang leaves are commonly used to make herbal tea and cooking ingredient powder. Three drying methods; shade drying, hot air drying and vacuum drying were comparatively studied in order to evaluate physicochemical and antioxidant properties of Yanang powder including moisture content, color, pH, TSS and DPPH assay. Shade drying method resulted in higher moisture content (6.81 ± 0.10) compared with the other two methods ($p \leq 0.05$). The vacuum drying technique showed better color characteristics. There was no significant difference in pH and TSS between samples treated with shade and hot air drying techniques. The maximal DPPH antioxidant activity was recorded from leaves that were dried by the vacuum drying technique. The Yanang leaves powder provided 50% inhibition (IC_{50}) of 2,2-diphenyl-1-picrylhydrazyl which varies within the range between 120.23 ± 2.11 and 130.36 ± 3.08 $\mu\text{g/mL}$.

Keywords—Yanang powder; shade drying; hot air drying; vacuum drying; antioxidant

I. INTRODUCTION

Leave extract from Yanang or Bamboo grass (*Tiliacora triandra*) used in the cooking of northeastern Thailand and Lao PDR such as bamboo shoot soup [1]. In traditional Southeast Asian medicine, Yanang has been used as herbal medicine to relieve fever, alcohol intoxication, anti-inflammation, anti-oxidation, anti-cancer and anti-bacterial infection. Yanang leaves contain polyphenols, flavonoids, alkaloids, B-carotene, and minerals such as calcium and iron [2]. Recently, Yanang drinks (e.g. juices extracted from fresh leaves and dried leaves herbal tea) have become popular as herbal health drink consumed among health-conscious consumers [3].

Drying is one of the traditional and household food preservation techniques which dehydrates leaves in order to minimize microbial spoilage and deterioration reactions [4]. The technique helps to prolong shelf-life and reduce the costs

of transportation by minimizing packing space and lighter weight. The drying process can be carried out at different temperatures and under relative humidity conditions. The dried product's quality is greatly influenced by drying conditions as well as the method of drying.

The commonly used technique of drying food is natural drying or shade drying, which requires little capital, basic equipment and low energy input [5]. Shade drying is a preferred method that helps to maintain or minimize the loss of leaves and flowers' colors. On the other hand, lower temperatures should be employed in the preservation of medicinal plant materials containing volatile substances. However, shade drying has many disadvantages such as an inability to maintain quantity of large scale production and to achieve consistent quality standard. Conventional hot air drying is one of the most frequently used operations for food dehydration but the technique resulted in low porosity, high apparent density and significant color changes which occur during the hot air drying process [6]. Vacuum drying is a novel technology for Small and Micro Community Enterprise (SMCEs) which helps to achieve a high quality final product while retaining its original nutritive values. Vacuum drying is performed under low pressure conditions. The heat transfer effect is produced by the convection or radiation method.

Adverse drying techniques and drying condition such as higher temperature of the material during the drying process leads to irreversible chemical and biological reactions coupled with structural, physical and mechanical modifications. These include degradation of color, crust formation, change of shape and texture, inhibit the growth of bacteria and deactivate enzymes, decrease of sensory quality, loss of nutrient values, aroma, flavor and antioxidant compounds [7].

Natural antioxidant compounds which are abundant in foods and medicinal plants play an important role in reducing the risk of chronic diseases, such as cancer and heart disease. Plant-originated antioxidants include vitamins C and E and



beta-carotene. A rapid, simple and inexpensive method of antioxidant's activity measurement is based on the reduction of a free radical 2,2-diphenyl-1-picrylhydrazyl (DPPH) [8].

Many studies concerning chemical composition, functional properties [1, 9, 10], pharmaceutical properties [11], and production methods of canned Yanang leaves extract have been conducted. The studies revealed that benefits of dried powder of Yanang extract outweighed that of the liquid one including volume and weight reduction, smaller packaging, easier handling and transportation, and longer shelf life. Therefore, the aims of this study are; 1) to explore the most effective drying technique, whether this be shade drying, hot air drying, or vacuum drying for which Small and Micro Community Enterprise (SMCEs) may adopt and apply to their productions, 2) to produce Yanang leave extract powder that can be used as a cooking ingredient or herbal tea, 3) to determine the effect of drying technique on physicochemical properties and antioxidant of Yanang leaves powder.

II. MATERIALS AND METHODS

A. Raw Materials

Yanang fresh leaves, which can be grown throughout the year, were obtained from local farmer's markets in Prachinburi province. Leaves with the width of 3-5 cm and the length of 5-7 cm were selected for the studies.



Fig. 1. Yanang leaves

B. Preparation of Yanang Leaves Powder

In order to evaluate the effect of drying techniques on the physicochemical and antioxidant properties of Yanang leaves, the leaves were soaked and washed with tap water for 5 min before being dried by these three different drying methods:

- shade drying in which leaves were dried on trays at room temperature (25-32°C) for 30 days.
- hot air drying at 80°C for 60 min in a convective drier.
- vacuum drying at 50°C under vacuum pressure of 90 kPa (675 mmHg) and drying time of 6 hours.

All of the above mentioned samples were dried until the leaves reached moisture content of below 10%. The moisture of 10% and below is a recommended content for the dried leaves and the powder productions [12]. The dried leaves were grinded and the powder was then sieved manually by using a 850µm sieve. The obtained samples were stored at room temperature in a vacuum-packed container before use.

C. Physicochemical analyses

1) Moisture content

The moisture content was determined by using hot air oven drying method [13]. In brief, 3.0 g of ground Yanang leaves sample was weighted and dried at 105°C until a constant weight was obtained. The analysis was triplicated.

2) Color Characteristics

The color characteristics of Yanang samples were analyzed by using Hunter Lab Spectrophotometer (Mini Scan EZ 4500L, USA) which was calibrated with black and white tiles. Obtained results were expressed as Hunter color values of L^* , a^* and b^* . The L^* , a^* and b^* . Subsequently, values from the three readings were determined and averaged. The color brightness, L^* was measured against the whiteness value of a color and ranges from black (0) to white (100). The chromaticity coordinate a^* was measured red as positive and green as negative, whilst the chromaticity coordinate b^* was measured yellow as positive and blue as negative [14]. The samples were analyzed in triplicates.

3) pH

pH is a measurement of hydrogen ion concentration of samples which resulted in readable values between 1.0 to 14.0. The pH of extracted Yanang leaves powder solution was measured by using a pH meter (Eutech ECPH110001S, Singapore).

4) Total soluble solids content

The total soluble solid (TSS) was measured by using a digital hand-held refractometer (ATAGO PAL-3, Japan) and expressed in °Brix. Solution samples of Yanang leaves extracted powder were prepared for these measurements. Between each measurement, the refractometer was washed with distilled water and dried.

D. Determination of DPPH radical scavenging activity

To assess DPPH radical scavenging's activity, samples were treated with 2,2-diphenyl-1-picrylhydrazyl at 0.1 mM concentration and kept at room temperature (35±1°C), in the absence of light for 30 min. Spectrophotometer was used to measure level of absorbance at 517 nm [15] and percentage of the above said activities were measured and calculated by using the following formula;



$$\text{Scavenging activity (\%)} = [(A_0 - A_1) / A_0] \times 100 \quad (1)$$

A_0 = the absorbance of control reaction

A_1 = the absorbance of test compound

Interpolation of linear regression analysis was used to attain a concentration that inhibit half of the activity (IC₅₀).

E. Statistical analysis

The experiments were carried out in 3 replications and the mean values obtained from IBM SPSS® statistics desktop version 21 were analyzed by using variance analysis (ANOVA). The differences between treatments at $p \leq 0.05$ were considered significant. The graphs of mean value and error bars were created by using the 2016 version of Microsoft Excel.

III. RESULTS AND DISCUSSION

A. Characteristic and Physicochemical of Yanang Powder

As shown in Table I, the moisture contents of Yanang leaves powders were between 4 to 7%. Although the moisture contents among different drying techniques were significantly different, the range was relatively narrow. The moisture contents for shade-dried, hot air-dried and vacuum-dried leaves were $4.06 \pm 0.08\%$, $5.74 \pm 0.12\%$ and $6.81 \pm 0.10\%$, respectively. Slightly higher moisture content was found in shade dried powder due to low drying rates which leads to undesirable thermal degradation of the finished products [16].

Appearance and color of Yanang leaves processed by different drying techniques are presented in Fig. 2. The color attributes in terms of the Hunter L^* , a^* and b^* values of Yanang leaves samples are illustrated in Table I. The L^* value of vacuum drying techniques was the highest among all dried leaves samples (40.20 ± 0.65), while shade drying revealed the lowest L^* (30.20 ± 0.60) value among these drying techniques ($p \leq 0.05$).

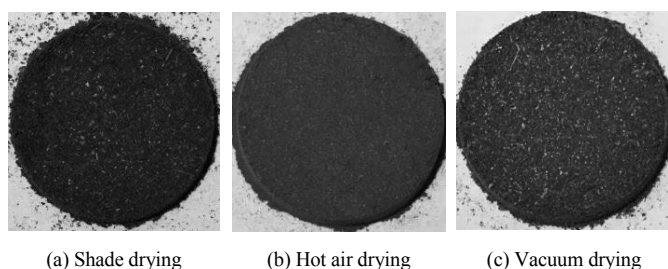


Fig. 2. Yanang powder

High temperature and long drying time is the most important factors that resulted in color damage during the drying process [14]. Vacuum drying technique showed the highest b^* values in comparison with others techniques which due largely to lower drying temperature and shorter drying

times. As a result, vacuum drying and shade drying possessed the highest and the lowest yellow color which shown as b^* value, respectively. For a^* value (greenness) vacuum drying had the highest value (more negative a^*), while hot air drying at 80°C showed the lowest green color (positive a^*). Overall, upon considering the final colors of Yanang leaves powder, hot air drying technique is considered the least desirable drying methods while and vacuum drying is perceived as the most desirable one.

Reduction in L^* and b^* values and increase in a^* values indicated that shade drying and hot air drying produced dark green or brownish products. The results revealed that changes of Yanang leaves' color depended on drying temperature and drying time. The high drying temperature could cause of the magnesium in chlorophyll to be substituted by hydrogen, thereby, converted chlorophylls to pheophytins [17]. In addition, slower drying rate at temperature below 60°C caused less browning as the color changes are the result of chlorophyll deterioration [18].

TABLE I. MOISTURE CONTENT AND COLOR OF YANANG LEAVE POWDER

Drying Techniques	Moisture Content (%)	Color		
		L^*	a^*	b^*
Shade drying	6.81 ± 0.10^c	30.20 ± 0.60^a	-2.20 ± 0.25^a	16.80 ± 0.40^a
Hot air drying	5.74 ± 0.12^b	37.43 ± 0.57^b	0.57 ± 0.32^a	23.31 ± 0.21^b
Vacuum drying	4.06 ± 0.08^a	40.20 ± 0.65^b	-13.08 ± 0.48^b	30.84 ± 0.32^c

^{a,b,c} Different letters within the same column indicate significant difference ($p \leq 0.05$)

The effects of drying techniques on pH, TSS and color attributes of Yanang leaves tea under three different drying techniques are shown in Table II. Appearance of Yanang leaves tea samples are presented in Fig. 3. The pH values of all dried Yanang leaves varied between 5.39 ± 0.09 to 5.42 ± 0.12 , respectively and TSS were 0.2°Brix . TSS and pH were not significantly affected by different drying techniques but color attributes and anti-oxidation activity were more effective in samples prepared by using vacuum drying methods.

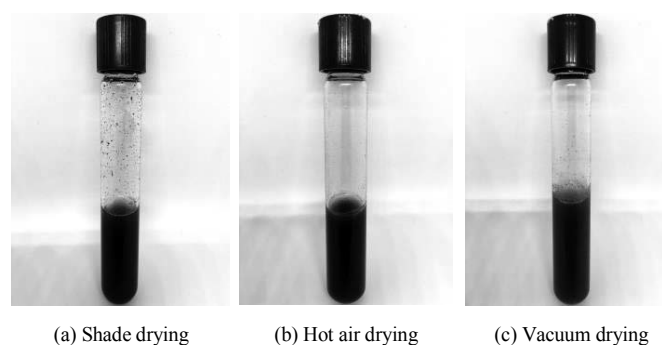


Fig. 3. Yanang leave tea



TABLE II. pH, TSS AND COLOR OF YANANG LEAVE TEA

Drying Techniques	pH ^{ns}	TSS	Color		
		Brix ^{ns}	L*	a*	b*
Shade drying	5.42±0.12	0.2±0.0	24.92±0.65 ^a	-0.58±0.12 ^a	3.58±0.52 ^a
Hot air drying	5.41±0.10	0.2±0.0	26.51±0.48 ^a	1.06±0.06 ^a	4.09±0.15 ^a
Vacuum drying	5.39±0.09	0.2±0.0	34.41±0.38 ^b	-3.16±0.10 ^b	5.36±0.50 ^b

^{a,b} Different letters within the same column indicate significant difference (p≤0.05)

Anti-oxidation activity was evaluated by DPPH radical scavenging assay. The radical scavenging activity of Yanang leaves tea was expressed in terms of the effective concentration at 50% (Table III). The strongest antioxidant scavenger was the Yanang leaves powder prepared by vacuum drying technique. Vacuum drying requires low process temperatures and faster water evaporation, which resulted in shorter drying times and higher quality of dried product compared with hot air and shade drying techniques. Although shade drying technique does not require high temperature but a longer exposure to the heat caused antioxidants to deteriorate. The IC₅₀ values were 148.60±3.50, 130.36±3.08 and 148.60±3.50 µg/mL for shade drying, hot air drying and vacuum drying, respectively.

TABLE III. DPPH RADICAL SCAVENGING ASSAY OF YANANG LEAVE POWDER

Drying Techniques	Antioxidant activity DPPH (IC ₅₀ , µg/mL)
Shade drying	148.60± 3.50 ^c
Hot air drying	130.36± 3.08 ^b
Vacuum drying	120.23± 2.11 ^a

^{a,b,c} Different letters within the same column indicate significant difference (p≤0.05)

IV. CONCLUSION

Overall analysis of the drying techniques; shade drying, hot air drying, and vacuum drying on quality of Yanang leaves powder indicated that the vacuum drying technique was the most effective technique that can preserve maximum antioxidant activities and appearance quality. Hot air drying was the second most effective technique. As the Yanang leaves powder lost most of their physicochemical and antioxidant properties as a result of shade drying technique, the possibility of using shade drying for the production of Yanang leaves powder was proven inappropriate.

ACKNOWLEDGMENT

This research was supported by the Faculty of Industrial Technology and Management, King Mongkut's University of Technology North Bangkok, Prachinburi Campus under the FITM Research gap funds (FITM-6114004-21). I would like to express sincere appreciation towards Ms. Nisaluck Panla and Ms. Supaporn Sritapanya for their assistance in preparations of laboratory facilities and collecting experimental data.

REFERENCES

- [1] J. Singthong, S. Ningsanond and S.W. Cui, "Extraction and physicochemical characterisation of polysaccharide gum from Yanang (*Tiliacora triandra*) leaves," Food Chem., vol. 114(4), pp. 1301-1307, 2009.
- [2] W. Thong-asa, P. Tumkiratiwong, V. Bullangpoti, K. Kongnirundonsuk, and K. Tilokskulchai, "Tiliacora triandra (Colebr.) Diels leaf extract enhances spatial learning and learning flexibility, and prevents dentate gyrus neuronal damage induced by cerebral ischemia/reperfusion injury in mice," Avicenna J Phytomed., vol. 7(5), pp. 389-400, 2017.
- [3] M. Weerawatanakorn, K. Rojsuntornkitti, M. Pan and D. Wongwaiwech, "Some phytochemicals and anti-inflammation effect of juice from Tiliacora triandra Leaves. J Food Nutr Res., vol. 6(1), pp. 32-38, 2018.
- [4] C. Kumar, M.A. Karim and U.H. Mohammad Joardder, "Intermittent drying of food products: A critical review," J Food Eng., vol. 121, pp. 48-57, 2014.
- [5] S. Roshanak, M. Rahimmalek and S.A.H. Goli, "Evaluation of seven different drying treatments in respect to total flavonoid, phenolic, vitamin C content, chlorophyll, antioxidant activity and color of green tea (*Camellia sinensis* or *C. assamica*) leaves," J. Food Sci. Technol., vol. 53(1), pp. 721-729, 2016.
- [6] I. Hamrouni-Sallami, F.Z. Rahali, I.B. Rebey, S. Bourgo, F. Lomam and B. Marzouk, "Total phenolics, flavonoids, and antioxidant activity of sage (*Salvia officinalis* L.) plants as affected by different drying method," Food Bioprocess Technol., vol. 6, pp. 806-817, 2013.
- [7] M. Abid, R. Gibert and C. Laguerie, "An experimental and theoretical analysis of the mechanisms of heat and mass transfer during the drying of corn grains in a fluidized bed," Int. Chem Eng., vol. 30, pp. 632-642, 1990.
- [8] V. Lobo, A. Patil, A. Phatak and N. Chandra, "Free radicals, antioxidants and functional foods: Impact on human health," Pharmacogn. Rev., vol. 4(8), pp. 118-126, 2010.
- [9] C. Mahidol, P. Sahakitpichan and S. Ruchirawat, "Bioactive natural products from Thai plants," J. Pure Appl. Chem., vol. 66, pp. 2353-2356, 1994.
- [10] P. Wiriyachitra, and B. Phuriyakorn, "Alkaloids of Tiliacora triandra," Aust. J. Chem., vol. 34, pp. 2001-2004, 1981.
- [11] T. Katisart and S. Rattana, "Hypoglycemic activity of leaf extracts from Tiliacora triandra in normal and streptozotocin-induced diabetic rats," Pharmacog J., vol. 9(5), pp. 621-625, 2017.
- [12] W. Saohin, P. Boonchoong, S. Iamlikitkuakoon, I. Jamnoiprom and W. Mungdee, "Effects of drying temperature and residual moisture content of Fa-Tha-Li (*Andrographis paniculata* (Burm.f.) Nees) crude powder for capsule preparation," Thai. J. Pharm. Sci., vol. 31, pp. 28-35, 2007.
- [13] AOAC, "Official Methods of Analysis (12th ed.)," Association of Official Analytical Chemists, Washington, D.C. USA, 2005.
- [14] D. Arslan and M.M. Ozcan, "Evaluation of drying methods with respect to drying kinetics, mineral content and color characteristics of rosemary leaves," Energy Convers Manag., vol. 49, pp. 1258-1264, 2008.
- [15] T. Parametthanuwat, S. Aichayawanich and J. Wongs, "Development of herbal gummy jelly with brown sugar and angel grass extract," The 9th International Conference on Sciences, Technology and Innovation for Sustainable Well-Being (STISWB 2017), Kunming University of Sciences and Technology, China, June 2017.
- [16] S. Dwivedy, K. Rayaguru and G.R. Sahoo, "Effect of drying methods on quality characteristics of medicinal indian borage (*Coleus aromaticus*) leaves," J Food Process Technol., vol. 3(188), pp.1-6, 2012.
- [17] S.G. Rudra, H. Singh, S. Bsau and U.S. Shivhare, "Enthalpy, entropy compensation during thermal degradation of chlorophyll in mint and coriander puree," J Food Eng., vol. 86, pp. 379-387, 2008.
- [18] D. Argyropoulos, J. Müller, "Kinetics of change in colour and rosmarinic acid equivalents during convective drying of lemon balm (*Melissa officinalis* L.)," J. Appl. Res. Medic., Aromatic Plants, vol. 1 (1), pp. 15-22, 2014.



Development of local Thai traditional cough drop

Kanokwan Sathonghon, Kewalin Poonoppakhun and Wiwat Wangcharoen*

Food science and Technology Program

Faculty of Engineering and Argo-industry, Maejo University, Chiang Mai, Thailand 50290

e-mail address* : wiwat@mju.ac.th

Abstract—A cough drop was developed from a selected local Thai traditional cough remedy in Chiang Mai. Firstly, sucrose and glucose syrup ratio was varied to make candy and it was found that the ratio at 70:30 gave the highest yield. Secondly, the quantity of local Thai traditional cough remedy was varied at 10 – 40 g per 100 g of candy mixture. It was found that the ratio of sucrose had to be increased for increasing the quantity of cough remedy in the candy mixture and the best result was at 90:10 of sucrose and glucose syrup ratio and 30 g of cough remedy per 100 g of candy mixture. This developed cough drop could prolong its herbal flavor to 10 min compared to 3 min of the powder form and it had lower microbial loads. There was no visible change and still low in moisture content and water activity when keeping in sealed polypropylene bag for 10 weeks.

Keywords—cough drop; Thai traditional cough remedy; local Thai cough powder

I. INTRODUCTION

Cough is a reflex action of the respiratory tract that is used to clear the large breathing passages from fluids, irritants, foreign particles and microbes. The cough reflex consists of three phases: an inhalation, a forced exhalation against a closed glottis and a violent release of air from the lungs following opening of the glottis, usually accompanied by a distinctive sound [1]. It is commonly caused by colds and the flu. While annoying, coughs that are productive get germy mucus, inhaled dirt or food out of your lungs and windpipe. After a cold, though, some "dry" coughs last weeks or months. That could be because coughing irritates your lungs and windpipe. Allergies, asthma, acid reflux, sleep apnea could be other causes of coughing [2].

Cough treatment should target on its cause, it could be medicine, home remedies, avoid triggers or treatment for other causes. For home remedies, it could be done by drinking warm fluids, inhaling warm and moist air, and using cough remedies [2]. Cough drop is a form of cough remedies made as a small, typically medicated tablet intended to be dissolved slowly in the mouth to temporarily stop coughs and lubricate and soothe irritated tissues of the throat [3].

In Thailand, local traditional cough remedies are in the form of mixed herbal powder which it is not convenient to consume and looked old style. This work was aimed to make it in the form of cough drops for convenience, modern style and efficiency improvement.

II. METHODOLOGY

A. Candy preparation

Sucrose and glucose syrup were boiled at 127-130 °C by varying ratio of sucrose and glucose syrup at 10:90 to 90:10 and 10% drinking water was added to solute sucrose. The boiling was done until weak brown was firstly appeared. Boiled mixture was poured into silicone mold (55 pieces of 1.5x1.1x1 cm) for shaping candy. Yield, melting and solubility of candy were recorded. Randomized complete block design and Tukey's HSD test were used for sucrose and glucose syrup ratio selection.

$$\text{Yield (\%)} = (\text{WC} / \text{WI}) \times 100$$

where: WC = Weight of all candy
WI = Weight of all ingredients

$$\text{Melting (\%)} = ((\text{W1} - \text{W2}) / \text{W1}) \times 100$$

where: W1 = Initial weight of candy
W2 = Weight after stored 12 hr in high relative humidity container

$$\text{Solubility} = \text{Time required (min) to complete solute candy (2.30} \pm 0.05 \text{ g) in 250 distilled water by magnetic stirrer (level 6)}$$

B. Development of local Thai traditional cough drop

Sucrose and glucose syrup ratio selected from (A) was used to develop local Thai traditional cough drop. A selected local Thai traditional cough remedy in Chiang Mai was used. It was varying at 4 levels; 10, 20, 30 and 40 g per 100 g of candy mixture. The problem of shaping cough drop was found when the quantity of local Thai traditional cough remedy was increased. Therefore, the study on sucrose and glucose syrup ratio at 80:20 and 90:10 were added in this step.

C. Sensory property of local Thai traditional cough drop

A Selected local Thai traditional cough drop from (B) was sensory studied by Time-intensity profiling [4] compared to the same amount in its powder form. Ten semi-trained panelists were asked to evaluate samples by 15 line scale every 20 second. Only one evaluation was done in each day and each sample was evaluated three times.



D. Microbial property of local Thai traditional cough drop

Conventional plate count [5] was used to indicate the level of microorganism in a selected local Thai traditional cough drop from (B) compared to the same amount in its powder form.

E. Storage study of local Thai traditional cough drop

A Selected local Thai traditional cough drop from (B) was kept for 10 weeks in sealed polypropylene bag at room temperature. Moisture content, water activity and appearance of them were recorded every week.

III. RESULTS AND DISCUSSION

A. Candy preparation

By varying sucrose and glucose syrup ratio, it was found that at ratio of 10:90 and 20:80 the boiled mixture was hardened too fast and it could be not poured into silicon mold, while at ratio of 80:20 and 90:10 there still was sucrose crystal found in the mixture. These results could be reasoned by the quantity of glucose syrup since it affects on hardening of candy and inhibiting sucrose crystallization [6]. Therefore, only at the ratio of 30:70 to 70:30 would be studied for yield, melting and solubility as shown in Table 1. And the ratio at 70:30 was selected because of the highest yield, while there was no significant difference from other ratio in case of melting and solubility.

Table 1. Yield, melting and solubility of candy prepared from various sucrose and glucose syrup ratio.

Sucrose and glucose syrup ratio	Yield (%)	Melting ^{ns} (%)	Solubility ^{ns} (min)
30:70	47.16±0.13 ^a	28.81±7.00	13.67±0.43
40:60	46.43±15.10 ^a	26.45±3.90	14.34±0.86
50:50	58.14±1.75 ^{ab}	24.22±9.98	13.39±0.23
60:40	67.26±4.01 ^{bc}	22.68±6.77	13.57±0.37
70:30	73.42±3.66 ^c	21.40±4.63	13.74±0.41

^{a, b, c} Means with different letter superscripts are significantly different ($p < 0.05$).

^{ns} Means are not significantly different ($p > 0.05$).

B. Development of local Thai traditional cough drop

There was no problem when adding the powder of selected local Thai traditional cough remedy in candy mixture at 10 and 20 g but at 30 and 40 g the mixture would be hardened too fast and it could not be poured into silicon mold. Therefore, sucrose and glucose syrup ratio at 80:20 and 90:10 were added in this step to reduce the quantity of glucose syrup which affects on hardening of candy [6]. The results are shown in Table 2. The sucrose and glucose syrup ratio at 90:10 and 30 g

of cough powder was selected to develop cough drop because the boiled mixture was not hardened too quickly and its herbal flavor was properly.

Table 2. Results of developing local Thai traditional cough drop

Local Thai traditional cough remedy (g)	Sucrose and glucose syrup ratio	Results
10 - 20	70:30	Boiled mixture could be shaped and it was too weak in herbal flavor and sweetness.
	80:20	Boiled mixture could be shaped and it was too weak in herbal flavor.
	90:10	Boiled mixture could be shaped and it was too weak in herbal flavor but too much sweet.
30	70:30	Boiled mixture could not be poured into silicon mold because it was hardened too fast.
	80:20	Boiled mixture could be poured into silicon mold but pouring should be done quickly before it was hardened. Its herbal flavor was properly.
	90:10	Boiled mixture could be poured into silicon mold and its herbal flavor was properly.
40	70:30	Similar to 30 g.
	80:20	Similar to 30 g, but its herbal flavor was too strong because it could cause tasteless.
	90:10	Similar to 30 g, but its herbal flavor was too strong because it could cause tasteless.

C. Sensory property of local Thai traditional cough drop

Time-intensity profiling (Fig. 1) shows that the highest flavor intensity of the developed local Thai traditional cough drop was 9.2 at 120 sec, while the one of powder form was 12.5 at 60 sec, but the flavor of cough drop was long last until 10 min, while the flavor of powder form was found until 3 min. These results could be reasoned by the slow dissolving of cough drop in the mouth [3] which it make products more effective because it helps to lubricate and soothe irritated tissues of the throat for longer time.

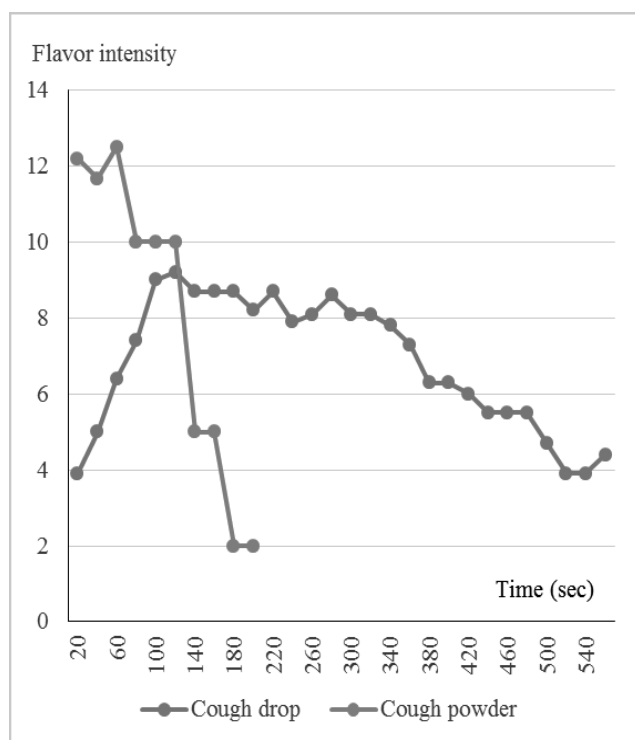


Fig. 1 Time-intensity profiling of the developed local Thai traditional cough drop and powder

D. Microbial property of local Thai traditional cough drop

Conventional plate count of the developed local Thai traditional cough drop was 5.5×10^4 CFU/g of candy and the one of powder in the same amount of 1 g of candy was 1.06×10^5 CFU. This result could be reasoned by the effect of heat treatment or boiling in candy preparation process on microbials. However, these microbial loads were higher than the standard value of candy at 1×10^3 CFU/g [7], which might show the inappropriate process and storage of local Thai traditional cough powder. However, there is no standard value for total plate count in Thai Herbal Pharmacopoeia 2000 but *Staphylococcus aureus*, *Clostridium* spp. and *Salmonella* spp. must be not found [8]. Therefore, the process of local Thai traditional powder should be improved or the powder should be treated to reduce the microbial load before using as an ingredient of cough drop.

E. Storage study of local Thai traditional cough drop

Moisture content, water activity and appearance of the developed local Thai traditional cough drop kept for 10 weeks in sealed polypropylene bag at room temperature are shown in Table 3. Their moisture content and water activity were increased because of moisture absorption from environment but there is no visible change. The highest moisture content was 7.09 (w/w) which it is higher than standard value for candy (3 % (w/w)) but still lower than the one for toffee (8 % (w/w))

[7]. The highest water activity was 0.670 which it is still safe from microbial growth (<0.700) [9].

Table 3. Relative humidity of environment, moisture content, water activity and appearance of the developed local Thai traditional cough drop

Time (week)	% RH	% MC	a_w	Appearance
0	70.0	0.00	0.475	No change
1	75.6	0.71	0.484	No change
2	71.6	1.08	0.574	No change
3	77.7	1.72	0.580	No change
4	79.2	2.77	0.562	No change
5	61.7	2.20	0.582	No change
6	58.1	2.93	0.594	No change
7	80.0	4.00	0.620	No change
8	76.0	7.09	0.670	No change
9	67.2	3.81	0.586	No change
10	66.0	4.22	0.630	No change

%RH = %Relative humidity of environment

% MC = % Moisture content of cough drop

IV. CONCLUSION

A local Thai traditional cough drop was developed by boiling sucrose and glucose syrup at the ratio of 90:10, 10% drinking water and 30 % local Thai traditional cough remedy (powder) at 127-130 °C for 10 min before it was shaped by silicon mold. The flavor of this cough drop was not strong as the powder form but it remained longer in the mouth to lubricate and soothe irritated tissues of the throat. Microbial loads of cough drop depended on the one of used local Thai traditional cough remedy. And this product could be kept in sealed polypropylene bag at least 10 weeks at room temperature without the visible change.

REFERENCES

- [1] K.F. Chung and I.D.Pavord, "Prevalence, pathogenesis, and causes of chronic cough" *Lancet*, vol **371** (Issue 9621), pp. 1364–1374. April 2008.
- [2] Anonymous, "Why you cough" Available from: <https://www.webmd.com/cold-and-flu/overview#1>.
- [3] Anonymous, "Throat lozenge" Available from: https://en.wikipedia.org/wiki/Throat_lozenge.
- [4] M. Meilgaard, C.V. Civille and B.T. Carr, *Sensory evaluation technique*, 3rd ed., Boca Raton: CRC Press, 1999, pp.168-169.
- [5] L. Maturin and J.T. Peeler, "BAM: Aerobic plate count" Available from: <https://www.fda.gov/Food/FoodScienceResearch/LaboratoryMethods/ucm063346.htm#conventional>.
- [6] S. Subhimaros, *Technology for candy and chocolate production*, Bangkok: Chulalongkorn University Press, 2000, pp. 34-140.
- [7] Food and Drug Administration (FDA.), *Candy and Toffee, The Commodity Standard No. 265/2004*.



Proceedings of the 10th International Conference on Sciences, Technology and Innovation for Sustainable Well-Being (STISWB 2018)
Vientiane, Lao PDR. July 11th-13th, 2018



- [8] Food and Drug Administration (FDA), Hand book / principle of Thai herbal medicine registration, Bangkok: War Veterans Organization Printing Mill, 2000, pp. 7.
- [9] K. Todar, "Nutrition and growth of bacteria", Available from: http://textbookofbacteriology.net/nutgro_6.html.



Surface Modification of Perlite by Using Silane for the Enhancement of Heat Aging Resistance of Natural Rubber Vulcanisates

Tithinun Rattanaplome

Worawan Pechurai and Philaiwan Pornprasit
Rubber and Polymer Technology Unit, Faculty of
Engineering and Agro-Industry, Maejo University
Chiangmai, Thailand
tithinun@mju.ac.th

Napat Chantaramee

Materials Science Unit, Faculty of Science,
Maejo University
Chiangmai, Thailand
napat@mju.ac.th

Abstract—Our previous work reported that surface modifications of perlite with optimum silane content (2–4 wt%) gave optimal properties of natural rubber vulcanisates. The objective of the present study is to investigate the heat aging resistance properties in terms of stress at 100% elongation, tensile strength, and percentage elongation at break after surface modification. Furthermore, the rebound resilience and abrasion resistance of perlite treated with silane filled in NR vulcanisates will be investigated. In a comparison, the properties of clay-filled NR vulcanisates will be determined. From the experiments, it was found that surface modifications using silane gave better perlite-NR interactions before and after aging. The better heat resistance properties of perlite-filled NR vulcanisates than those of clay-filled vulcanisates can be detected from relative property data. Nevertheless, a lower percentage of rebound resilience and abrasion resistance of perlite-filled vulcanisates before and after surface modification than those of clay-filled vulcanisates can be observed. This is owing to the large particle size, low surface area, poor dispersion, and agglomeration of perlite in NR vulcanisates. Perlite particles with high silica content are potentially used as odor-adsorbing filler in natural rubber (NR) vulcanisates but not as reinforcement filler.

Keywords—perlite; surface modification; heat resistance; mechanical properties; natural rubber vulcanisates

I. INTRODUCTION

Natural rubber (NR) has been known as a renewable natural polymer with numerous advantageous properties such as superior elasticity and resilience, low heat buildup, and high tensile and tear strength resulting from strain-induced crystallization. [1] Nevertheless, one of the major disadvantage of NR is an offensive odor or unbearable smell caused by incomplete degradation during storage, and thermal degradation during the processing of non-rubber components such as carbohydrates, proteins, and lipids.

Using the gas chromatograph-mass spectrometer (GC-MS) technique, V. P. Hoven et. al. [2] reported that the offensive odor was mainly caused by low-molecular-weight volatile fatty acids. To reduce the offensive odor, expensive odor-reducing

substances such as chitosan, zeolite13x, and activated carbon black (to adsorb physically and/or chemically) were mixed in NR vulcanisates.

Our previous work [3–5] first incorporated low-cost and porous materials such as perlite as odor-reducing fillers with a high content of SiO₂. Although NR vulcanisate with 30 phr perlite showed the potential of efficient odor reduction, it gave low tensile strength, rebound resilience, and heat resistance because of the low surface area of perlite and high in silica-silica interaction, which caused a decrease in filler-rubber interaction. It has been known that a high degree of reinforcement effect can be governed by low particle size, high surface area, good filler dispersion, and high filler-rubber interaction.

Surface modification by using silane coupling agent has long been recognized as an effective approach to increase filler-rubber interaction [6–10]. P. Sae-oui et. al. [6] explained that silane coupling agent usually possesses two functionally active end groups: an alkoxy group that is able to react with the silanol group on the silica surface, and an organosilane group that usually has sulfur atoms in its molecule and is compatible with rubber. Thus, the modified fillers provide chemically active surfaces that can be involved in vulcanization, resulting in coupling bonds between the coupling agent and both the filler and the rubber phases. In other words, silane coupling agent can act as a bridge between silica and rubber, and promote the rubber-silica interaction.

T. Rattanaplome et. al. [11] reported that a silane content of 2–4 wt% is optimum to yield the reinforcement effect of perlite-filled natural rubber vulcanisates. However, aging resistance data required for long-term application that is subjected to a heat cycle was not studied. Therefore, in this research, further investigations will be conducted on heat aging resistance tests in terms of stress at 100% elongation (M100), tensile strength, and percentage of elongation at the break after being heated at 100°C for 22 h. In addition, the rebound resilience and abrasion resistance of perlite treated with silane filled in NR vulcanisates will be studied. These properties of



vulcanisates filled with perlite treated with silane were also compared with those filled with perlite and clay.

II. METHODOLOGY

A. Materials

All materials used in the present study were used as received and were purchased from Lucky Four Co. Ltd. (Thailand), except for the expanded perlite, which was obtained from Thai Perlite Technology Co. Ltd. (Thailand). The control compound ingredients are listed in Table I. Filler loading was added and fixed at 30 parts per hundred of rubber (phr). Fillers included perlite, perlite treated with 2–8 wt% silane, and clay. Therefore, the filled-NR vulcanisates were denoted as perlite, psi2, psi4, psi6, psi8, and clay. Psi2 means NR vulcanisates filled with perlite modified with 2wt% silane. Thus, psi4, psi6, psi8, mean NR vulcanisates filled with perlite modified with 2-8wt% silane, respectively. The physical properties were determined and mentioned in our previous work [1]. The mean particle size and surface area of perlite are 38.02 μm and 3.49 m^2/g , respectively. The mean particle size and surface area of clay are 6.08 μm and 5.35 m^2/g , respectively [5, 11].

B. Surface Modification

The surface of perlite powder was modified with triethoxyvinylsilane purchased from Lucky Four Co. Ltd. In this study, the silane loading was varied from 0.0–8.0 wt% of the perlite content. For example, for a silane content of 4.0 wt%, 4.0 g of silane was mixed with 100 ml of ethanol and stirred for 30 min. To obtain a uniform distribution of silane on the perlite surface, 100 g of perlite was then added to the solution and stirred for 15 min. Then, the modified perlite was dried in an oven at 100°C for 12 h. Similarly, 2.0, 6.0, and 8.0 wt% of silane on the perlite surface were prepared by varying the initial silane content for 100 g of perlite using the same process as mentioned earlier [7].

C. Mixing and Vulcanisation Procedure.

The compound ingredients as explained earlier were mixed in a laboratory-scale two-roll mill (model YFTR-8, Yong Fong Machinery Co. Ltd., Thailand). Notably, the mixing conditions were mentioned by T. Rattanaplome et. al. [5], and D. Moonchai et. al. [12]. The NR vulcanisate or cured NR preparation involves mastication, compounding, and molding processes. To vulcanise the compounds, the compounds were compression molded using a hydraulic hot press (model HPC 100D, OOMN semiautomatic moulding press, Shanghai Zimmerli Weili Rubber and Plastic Machinery Co. Ltd., China) at 150°C. The vulcanisation times were obtained from our previous work [5, 11].

D. Heat Aging Resistance Test

The specimens were placed in an oven equipped with an air circulating system at a test temperature of 100°C for 22 h. [1]. The aged specimens were then measured for their tensile properties. According to our previous research [5, 11], the

dumbbell-shape specimens were tested at a crosshead speed at 500 mm/min and with a 500-N load cell using an Instron universal testing machine (model 5565, USA) according to ISO 37. The tensile strength was assessed from the stress at the break. In addition, the elongation at break was examined. In this study, the relative tensile properties, i.e., M100, tensile strength, and percent of elongation at break, calculated from equation (1), were used to represent the aging resistance properties.

$$\text{Relative tensile properties} = (P_{\text{aged}}/P_{\text{unaged}}) \quad (1)$$

where P_{unaged} and P_{aged} are the tensile properties of the samples before and after heat aging, respectively.

E. Mechanical Properties Test

To determine the rebound resilience, the samples were tested using a rebound tester (model Rebound Check-Pendolo Shob, Gibitre Instruments S.r.l., Italy) according to DIN53512. The abrasion resistance was evaluated according to ISO 4649 using an abrasion tester (Model AB 6252, Bareiss, Germany).

F. Morphological Study

A morphological study was carried out on the cryogenic fracture surfaces of NR vulcanisates using the JSM-5800LV scanning electron microscope (SEM). To remove the electrostatic charge buildup during the investigation, the surfaces of the samples were sputter coated with gold.

TABLE I. COMPOUND FORMULATION USED

Control ingredient	Amount (phr)
NR (STR20)	100
Sulphur	2.5
Stearic acid	2.0
Zinc Oxide	4.0
Tetramethylthiuramdisulphide (TMTD)	0.5
Dibenzothiozylidysulphide (MBTS)	1.0
Lowinox® (CPL)	1.0

III. RESULTS AND DISCUSSION

A. Heat Aging Resistance Properties

The stress at 100% elongation or modulus at 100% elongation (M100) before and after aging, including their relative properties, are shown in Fig. 1. The M100 of different NR vulcanisates could reveal that the addition of filler with and without surface treatment into the rubber causes an increase in rubber stiffness. Previous work already explained that surface modifications gave a reinforcement effect at a silane loading of 2–4 wt% [11]. Meanwhile, at high content, an excess of silane coupling agent could act as a plasticizer, resulting in a decrease



in M100 [6]. After heat aging, the M100 of perlite-filled and modified perlite-filled vulcanisates tends to increase. This could be the result of a post-curing effect or the formation of additional networks for optimum cure samples [1, 13]. For clay-filled vulcanisates, a slight decrease in M100 after aging was observed [1, 11].

Nevertheless, the M100 of clay-filled vulcanisates is slightly higher than that of perlite-filled (both treated- and untreated-surface) vulcanisates. This could be a result of the relatively small surface areas and large particle sizes of perlite. Fig. 2 shows the tensile strength of NR vulcanisates and their relative properties. As expected, surface modifications enhance the tensile strength of the perlite-filled vulcanisation before and after aging owing to strong filler-NR interaction. However, a decrease in tensile strength after aging can be clearly observed.

N. Rattanasom and S. Prasertsri [1] explained that the degree of crosslinking after aging might exceed an optimum value and cause a dense network. It is also seen that the tensile properties of perlite-filled vulcanisates (both treated and untreated surface) are lower than those of clay-filled vulcanisates. This could be the result of the smaller surface areas and larger particle sizes of perlite compared to those of clay [4]. Fig. 3 depicts the percentage of elongation at the break of NR vulcanisates, and their relative properties.

Again, surface modifications increase the elongation at the break of perlite-filled vulcanisation before and after aging. This could confirm good interfacial adhesion between perlite particles and NR matrices by using silane as a coupling agent [11]. It is also expected that the percentage of elongation at break tends to decrease after aging because the post-curing effect decreases the chain mobility of rubber molecule. When considering the relative properties from Fig. 1–3, the higher relative tensile properties of perlite treated with silane filled in NR vulcanisates could be caused by stronger perlite-NR adhesion after aging. This confirms that surface modifications enhance the degree of reinforcement, causing better heat resistance properties than clay-filled vulcanisates.

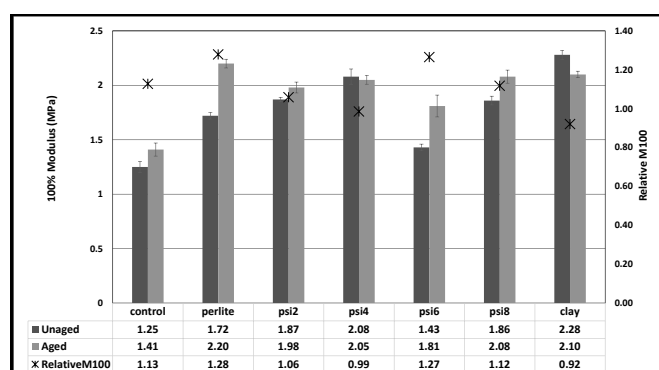


Fig. 1. 100% modulus (M100) of various NR vulcanisates

B. Mechanical Properties

Fig. 4 illustrates the percentage of rebound resilience before aging. Obviously, the addition of filler causes an increase in stiffness and modulus, but low resilience resulting from the dilution effect [4,5,12]. Again, surface modifications to perlite give rise to more stiffness but cause a higher percentage of rebound resilience. Meanwhile, NR vulcanisates filled with perlite treated with 4 wt% silane exhibit the highest percentage of rebound resilience among perlite-filled NR vulcanisates. This could explain why optimum silane content might give better filler-NR adhesion, causing better filler incorporation in the NR matrix and leading to a high percentage of rebound resilience.

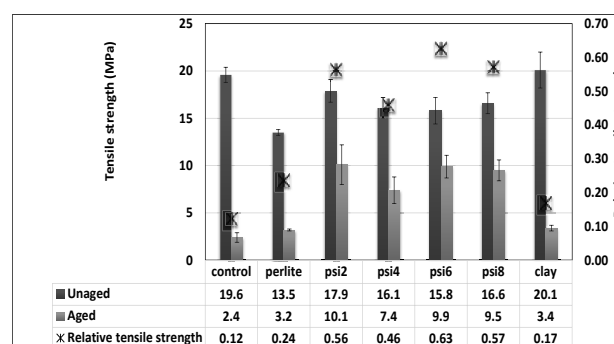


Fig. 2. Tensile strength of NR vulcanisates

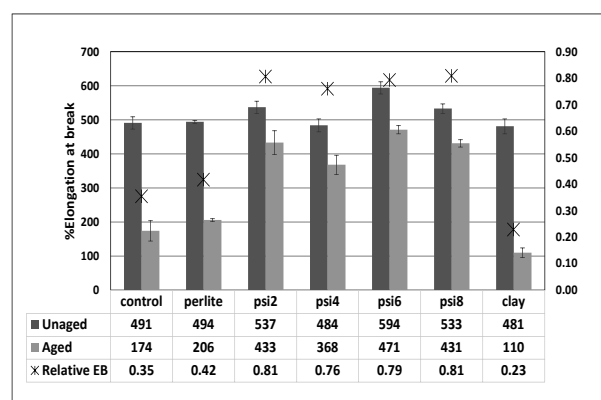


Fig. 3. The percentage of elongation at break of NR vulcanisates

Moreover, the plasticizing effect at high silane loading (6–8 wt%) might be responsible for the high percentage of rebound resilience. However, clay-filled vulcanisates gave a higher rebound resilience even possess higher M100 than perlite-filled vulcanisates. This might be responsible by difference in filler bulk hardness. Volume loss, which is proportional to the abrasion resistance of various vulcanisates, is shown in Fig. 5. It has been explained that a greater crosslinking density hardness and modulus leads to an enhancement of the abrasion resistance [14]. By contrast, it is



clearly noticed that modified perlite with a high modulus gives a higher volume loss, meaning a lower abrasion resistance.

In particular, NR vulcanisates filled with perlite treated with 4 wt% and 8 wt% silane give the highest volume loss. A possible explanation is weak physical crosslinks. As explained by T. Rattanaplome et. al. [11], the total crosslink density could arise from both the sulphide crosslinks and physical crosslinks. These researchers found that NR vulcanisates filled with perlite treated with 4 wt% silane had the highest crosslinking density but not the highest swelling resistance. As can also be seen in Fig. 5, the volume loss of perlite treated with silane filled in NR vulcanisates is lower than that of clay-filled vulcanisates. This could be the result of weak physical crosslinks in perlite treated with silane filled in NR vulcanisates and poor filler dispersion.

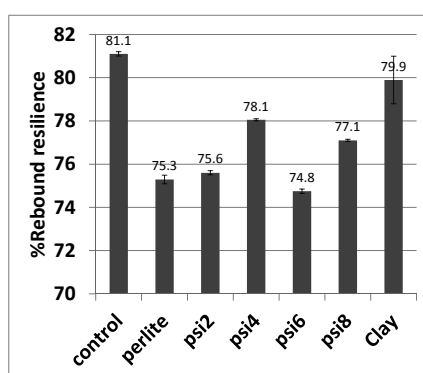


Fig. 4. The percentage of rebound resilience of NR vulcanisates before aging

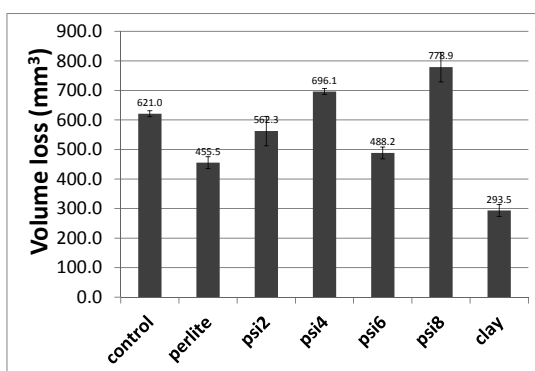


Fig. 5. Volume loss of NR vulcanisates before aging

B. Morphological Studies

SEM micrographs of various NR vulcanisates are presented in Fig. 6. From the micrographs, the agglomeration of perlite particles is greater than that of perlite treated with 2 wt% silane. This could imply that surface modification using silane enhances the better perlite-rubber interactions but is not strong enough to exhibit excellent filler dispersion. The SEM micrographs of clay-filled vulcanisates exhibit better filler

dispersion resulting from smaller particle sizes and larger surface areas, leading to a greater area to react with the NR matrix. These observations are more in accordance with a higher M100, tensile strength, percentage of rebound resilience, and abrasion resistance of clay-filled NR vulcanisates before aging than those of perlite-filled vulcanisates (both treated and untreated surfaces).

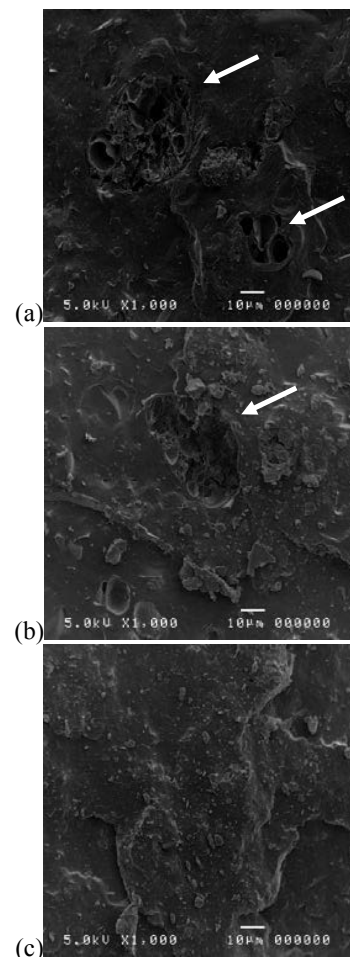


Fig. 6. SEM micrographs with magnification of 1000 of (a) perlite-filled NR vulcanisates (b) perlite treated with 2wt% silane filled in NR vulcanisates and (c) clay-filled NR vulcanisates.

IV. CONCLUSION

The key factors of the reinforcement effect in filled-NR vulcanisate include small particle size, high surface area, strong filler-NR interaction, and good filler dispersion. From the results of the tensile strength properties, it was confirmed that surface modifications using silane gave better perlite-NR interactions before and after aging. In addition, better heat resistance properties of perlite-filled NR vulcanisates than those of clay-filled NR vulcanisates was noticed from the relative property data. However, it can be seen that a large



particle size, low surface area, poor dispersion, and agglomeration of perlite treated with 2 wt% silane in NR vulcanisates leads to a lower percentage of rebound resilience and abrasion resistance than those of clay-filled vulcanisates.

REFERENCES

- [1] N. Rattanasom and S. Prasertsri, "Relationship among mechanical properties, heat aging resistance, cut growth behavior and morphology in natural rubber: Partial replacement of clay with various types of carbon black at similar hardness level" *Polymer Testing*, vol. 28, pp. 270-276, 2009
- [2] V.P Hoven, K. Rattanakarun, and Y. Tanaka, "Reduction of offensive odor from natural rubber by odor-reducing substances" *Journal of Applied Polymer Science*. Vol. 92, pp. 2253-2260, 2004
- [3] T. Rattanaplome, S. Kajitpeatjarat, S. Ariya, and N. Chantaramee, "The effect of odor-adsorbing fillers on mechanical properties of natural rubber vulcanizates" *Journal of interdisciplinary network*, vol. 2 (special issue), pp. 203-210, July-December 2013
- [4] T. Rattanaplome, N. Chantaramee, and P. Pornprasit, "The potential of perlite as an odour-adsorbing fillers in natural vulcanizates" *Macromolecular Symposium*, vol. 354, pp. 197-206, 2015
- [5] T. Rattanaplome, P. Pornprasit, and N. Chantaramee, "Utilization of perlite as an odor-reducing filler in natural rubber vulcanizates", *Proceeding of the second Asia Pacific Rubber Conference* pp. 195-205, 2015
- [6] P. Sae-oui, C. Sirisinha, U. Thepsuwan, and K. Hattthapanit, "Comparison of reinforcing efficiency between Si-69 and Si-624 in a conventional vulcanization system" *Polymer Testing*, vol. 23, pp. 871-879, 2004
- [7] S. Thongsang, and N. Sombatsompop, N., "Effect of NaOH and Si69 treatments on the properties of fly ash/natural rubber composites", *Polymer Composites*, Vol. 27/1, pp. 30-39, 2006
- [8] I. Surya, H. Ismail, and A. R. Azura, "Alkanolamide as an accelerator, filler-dispersant and a plasticizer in silica-filled natural rubber compounds", *Polymer Testing*, Vol. 32, pp. 1313-1321, 2013
- [9] Y. Li, B. Han, S. Wen, Y. Lu, H. Yang, L. Zhang, and L. Liua, "Effect of the temperature on surface modification of silica and properties of modified silica filled rubber composites". *Composites Part A: Applied Science and Manufacturing* , Vol. 62, pp. 52-69, July 2014)
- [10] F.R. Lamastra, S. Mori, V. Cherubini, M. Scarselli, F. Nanni, "A new green methodology for surface modification of diatomite filler in elastomers", *Materials Chemistry and Physics*, vol. 194, pp. 253-260, 2017
- [11] T. Rattanaplome, P. Pornprasit, and W. Pechurai, "Effect of surface modification of perlite on the properties of rubber vulcanizates", *RMUTSB Academic Journal (Science and Technology)*, in press, 2018
- [12] D. Moonchai, N. Moryadee, and N. Poosodsang, "Comparative properties of natural rubber vulcanisates filled with defatted rice bran, clay and calcium carbonate", *Maejo International Journal of Science and Technology*, Vol. 6/02 , pp. 249-258, 2012
- [13] S. Moonchai, and D. Moonchai, "Modelling and optimization of rebound resilience and hardness of defatted rice bran/calcium carbonate-filled NR vulcanisates", *Polymer Testing*, Vol. 32, pp. 1472-1478, 2013
- [14] N. Rattanasom, T. Saowapark, and C. Deeprasertkul, C., "Reinforcement of natural rubber with silica/carbon black hybrid filler", *Polymer Testing*, vol. 26, pp. 369-377, 2007



Green Natural Rubber Foam filled with Spent Coffee Grounds

Worawan Pechurai,
Sitthinan Saengdian and Wanichaya Chairuen

Program in Rubber and Polymer technology, Faculty of Engineering and Agro-Industry,
Maejo University, Chiangmai, Thailand
koy_288@hotmail.com

Abstract— The present study is focused on developing green natural rubber (NR) foam from spent coffee grounds (SCG). The SCG particles were initially characterized by various techniques prior to being added into the rubber compound. Results revealed that SCG particles had irregular shape and highly porous structure with relatively low specific surface area. It is composed of inorganic substances such as oxides of potassium, silicon, magnesium, calcium, and phosphorous. The presence of these metal oxides in SCG particles increased the rate of crosslinking (i.e. lower cure time) of the compound. The incorporation of SCG particles into NR foam gave relatively low reinforcement in terms of hardness and tensile strength, and also reduced the elastic behavior. The water absorption and relative density of the rubber foams tended to increase with SCG loading. However, SCG particles encouraged the cell formation by producing larger cell porosity and a narrower distribution in the matrix.

Keywords— natural rubber; foam; spent coffee grounds

I. INTRODUCTION

The rising concern about environmental impact is focused by many researchers [1-5]. As a consequence, they are interest in use of environmentally friendly fillers as in the case of polymer composites reinforced with natural fibers. Using natural fiber as reinforcing filler has high potential to replace traditional fillers, i.e., lower cost, lower density, no toxicity, balanced mechanical properties, and a considerably lower environmental impact fiber [4-5]. Coffee is one of the most consumed beverages in the world, thus the coffee industry generates a lot of waste. A major waste is spent coffee ground (SCG) which obtained during the brewing process [6]. Spent coffee grounds contain large amounts of organic compounds (i.e. fatty acids, lignin, cellulose, hemicellulose, and other polysaccharides) that can be exploited as a source of value-added products [7]. However, only a few research papers have considered the properties of polymer containing spent coffee grounds (SCG) as natural filler. Siri Wong et al. [8] studied the properties of spent coffee grounds (SCG) filled natural rubber (NR). Results revealed that SCG had relatively large particle size with very low specific surface area. Incorporation of SCG in NR gave relatively low reinforcement and tended to retard vulcanization due to the presence of hydroxyl groups on the SCG surface. Lee et al. [9] evaluated physical properties of polyvinyl alcohol (PVA) reinforced by used coffee grounds. It

was found that the tensile strength and young's modulus of PVA/coffee grounds nanocomposites were significantly enhanced compared with those of the PVA/CB nanocomposites. Chin-San Wu [10] studied the mechanical properties and biodegradability of composites containing polylactide (PLA) and spent coffee grounds (SCG). Maleic-anhydride-grafted polylactide (PLA-g-MA) and treated spent coffee grounds (TSCG) were used to improve the desired properties of these composites. The results showed that PLA-g-MA/TSCG materials exhibited desirable mechanical properties and water resistance relative to those of PLA/SCG. This effect was attributed to greater compatibility between the grafted polymer and TSCG. In addition, high levels of SCG substitution in composites were more biodegradable than neat PLA. García-García et al. [11] prepared green composites based on polypropylene and spent coffee ground (SCG) powder. The comparative effect of the different surface treatments and or compatibilizers on mechanical and thermal properties was studied. The results show a slight increase in flexural modulus for composites with both untreated and treated/compatibilized SCG powder (20 wt.%). Moreover, the thermal stability is improved by an increase of more than 8% in the onset degradation temperature compared to unfilled polypropylene.

Elastomeric foams or cellular rubber have been widely used in various applications involve cushioning performance, impact damping, packaging, as well as thermal and acoustic insulation [12]. To achieve improved properties in polymer foam, the use of several fillers has been widely studied. Some notable ones include inorganic materials such as calcium carbonate, silica, titanium dioxide, and talc [13-14] while some of the organic materials used as filler are carbon black and natural fibers. Bashir et al. [15] and Kim et al. [16] found that tensile strength and modulus of NR foams were gradually increased with increasing carbon black content whereas strain at break decreased. Vahidifar et al. [17] revealed that carbon black improved hardness, compression modulus and strength of the foam, while the resilience decreased. An increase in CB content also produced more cells with a smaller size and a narrower distribution. However, only a few research papers have studied the effect of natural fibers in elastomeric foam [18]. Therefore, the main objective of this study is to prepare a new type of NR foam filled with spent coffee grounds (SCG).



The effects of SCG content on properties of NR foam in terms of mechanical and morphological properties as well as water absorption were examined.

II. METHODOLOGY

A. Materials and Formulations

The NR used in this work was STR 5L, supplied by Lucky Four Company (Nontaburi, Thailand). The chemical blowing agent was oxybis (benzene sulfonyl) hydrazide (OBSH) which can generate blowing gas of 123-133 ml/g at decomposition temperature of app. 154-160°C, supplied by Thai Poly Chemical Co., Ltd. (Bangkok, Thailand). All other rubber ingredients used were commercial grade, supplied by Lucky Four Company (Nontaburi, Thailand). Spent coffee grounds (SCG) were collected from local cafes in Chiangmai, Thailand. The SCG was first dried in a hot air oven at 70°C for 24 h and then pass through 100 mesh sieve (particle sizes < 150 microns) before adding the filler into rubber compound. The obtained SCG particles were later characterized.

B. Compounding and Vulcanization

The compound formulation is shown in Table 1. All ingredients were mixed on a laboratory two roll mill (Yong Fong Machinery Co., Ltd, Thailand) at room temperature and the mixing was maintained for 30 min. The SCG was varied within a range of 0-20 phr. The obtained compounds were then foamed and vulcanized via a compression molding technique in a hot hydraulic press machine (Oomn Semi-Automatic Moulding Press, China) at temperature of 160°C with a pressure of 20 MPa according to their respective cure times.

TABLE I. COMPOUND FORMULATIONS

Ingredients	Quantity (phr)
NR STR 5L	100
Stearic acid	2.0
ZnO	5.0
OBSH	9.0
CBS	1.0
TMTD	0.5
Lowinix®CPL	1.0
SCG particles	0 - 20.0
Sulfur	1.2

C. Sample Characterizaion

SCG characterizations: The characteristics (dimensions and shape) of the SCG particles were examined using a scanning electron microscope (SEM) (JSM-5410LV, JEOL Co. Ltd., Japan). An X-ray Fluorescence spectrometer (XRF Model MESA-500W, Horiba, Japan) was used for analyzing the chemical compositions of the SCG. Their specific surface area

and average pore diameter were also characterized by a Surface Area Analyzer (Quantachrome, Autosorb-1).

TABLE II. CHEMICAL COMPOSITIONS OF SCG PARTICLES

Components	Content (%)
SiO ₂	3.20
P ₂ O ₅	7.06
SO ₃	13.40
K ₂ O	46.66
CaO	28.19
Fe ₂ O ₃	1.49

Cure characterizations: Torques, scorch time and cure time of the rubber compounds were measured in accordance to ASTM D 5289-95 by using a Moving Die Rheometer, MDR (UR-2010, U-Can Dynatex INC., Taiwan) at a temperature of 160°C.

Physical and Morphological properties: The relative foam density was measured and calculated according to ASTM D792-08, using equation (1) as given below:

$$\text{Relative density} = \frac{\text{Foam density}}{\text{Solid density}} \quad (1)$$

where foam density is the density of NR foam sample, and solid density is the total density of solid raw material used in making natural rubber foam.

Water uptake was determined with samples sizing 20 x 20 x 4 mm³. The samples were then immersed in distilled water at room temperature for 72 h. After that, the samples were removed, blotted dry with tissue paper, and then weighted. The percentage water uptake was calculated by using the following expression:

$$\text{Water uptake (\%)} = \frac{M_f - M_i}{M_i} \times 100 \quad (2)$$

where M_f is the final weight after immersion and M_i is the initial weight of the sample before immersion.

The foam morphology was characterized by utilizing a scanning electron microscope (SEM) (JSM-5410LV, JEOL Co. Ltd., Japan). The foamed samples were cooled in liquid nitrogen and fractured to produce a clean and intact surface with minimum plastic deformation. They were then gold coated by using a sputter coater for enhanced conductivity.

Mechanical properties: Hardness of the rubber foam vulcanizates was measured in accordance to ASTM D2240 by using a Shore A durometer hardness tester (Model HPE-A, Bareiss, Germany) at room temperature. NR foam samples were also submitted to accelerated aging according to ASTM



D573 in an air-circulating oven at 70 °C for 72 h. The change in hardness before and after aging was determined. Tensile properties in terms of tensile strength (TS) and elongation at break (EB) were determined according to ASTM D412 using a tensile testing machine (Model H 10KS, Hounsfield Test Equipment Co., Ltd., England) at a testing speed of 500 mm/min.

The compression set testing was conducted followed ASTM D395-03. The foam sample was in a cylindrical disk form, having a diameter of 29 mm and a thickness of 13 mm. A spacer bar of 9.5 mm thick (t_n) was used to maintain the compression deflection. The original thickness (t_0) of test sample was measured by vernier. The sample was compressed in a mold to 25% of its initial thickness for 72 h at a temperature of 70°C. The specimen was then removed from the mold and recovered under the natural state for 30 min. The final thickness (t_i) was measured immediately. The compression set was calculated from the following equation:

$$\text{Compression set (\%)} = \frac{T_0 - T_i}{T_0 - T_n} \times 100 \quad (3)$$

III. RESULTS AND DISCUSSION

A. General Characteristic of SCG

The SEM image of SCG particles has shown in Fig. 1. It revealed that the SCG particles showed an irregular shape with a highly porous structure, and individual particle size of SCG is lower than 50 μm (Fig. 1a). From the BET surface area results showed that the SCG particles has relatively low specific surface area of 2.48 m^2g^{-1} with an average pore diameter of 48.79 \AA . Table 2 shows the chemical compositions of the SCG particles. It was found that the SCG contains large amounts of potassium oxide (K_2O), calcium oxide (CaO), and other components in the minority.

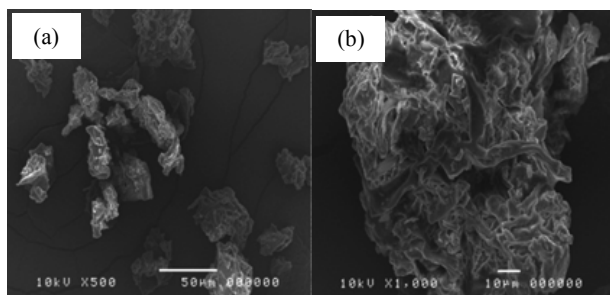


Fig. 1. SEM images of SCG particles at 500x (a) and 1000x (b) magnifications.

B. Cure characteristics

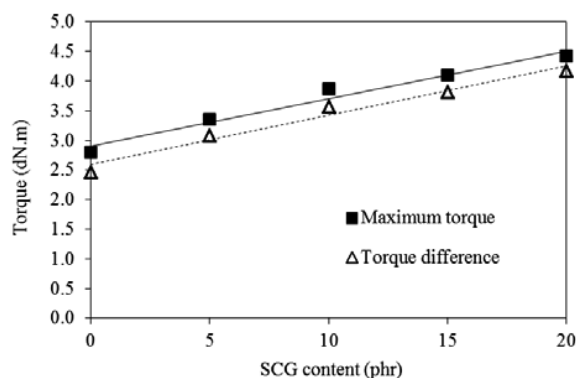


Fig. 2. Effect of SCG content on torque and torque difference of NR compounds.

Cure characteristics of the compounds were investigated and the results are given in Fig. 2. As can be seen, the addition of SCG particles increased the maximum torque of rubber compound. This is due to the presence of more filler which impart more restriction to the deformation and consequently increase the foam stiffness. Moreover, the torque difference between the maximum and minimum torques define the degree of reinforcement from the filler incorporation which is increasing as increasing amount of SCG particles. It was verified that the strong interaction between rubber molecules and the surface of the SCG particles was occurred. Scorch time and cure time of the compounds are shown in Fig. 3. It can clearly be seen that the presence of SCG particles reduced the scorch time and cure time significantly. Moreover, both properties of the NR compounds were further decreased with increasing SCG loadings. Geethamma et al. [19] reported that the mixing time of the filler in to rubber matrix will be increased as the filler loading increased and consequently generated more heat due to the additional friction. The decrease in scorch time indicated that the compounds took less time to reach the onset time of vulcanization as the SCG loading increased. In addition, the parameters such as low surface area, high moisture content and high metal oxide content can decrease the cure time of the compounds [20]. As reported by Ismail et al. [21], the curing rate of rubber compounds depends on presence metal oxide. Thus, the low surface area and high metal oxide content in SCG which filled in rubber compounds had supported the activation of the cure reaction consequently decrease the cure time.

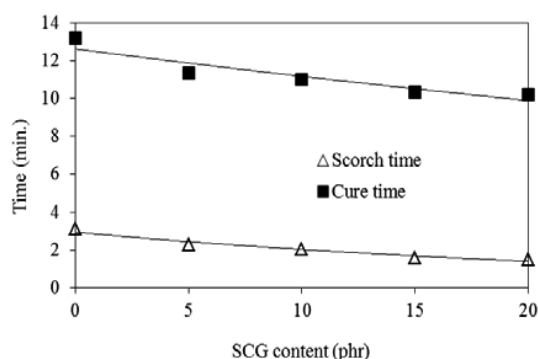


Fig. 3. Effect of SCG content on scorch time and cure time of NR compounds.

C. Mechanical Properties

Fig. 4 exhibited the effect of SCG content on hardness of rubber foam before and after accelerated aging. It is clearly seen that hardness of both samples decreased continuously with the addition of SCG content. This is due to greater cell porosity in the matrix led to lower matrix stiffness. The lack of compatibility between the SCG particles and rubber matrix is may be another reason. Furthermore, the thermal aging significantly increased the hardness of all samples due to the post cure during the aging test.

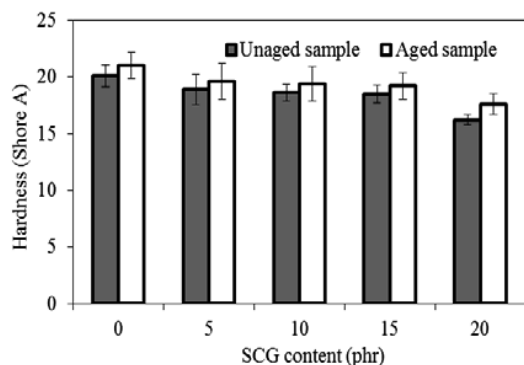


Fig. 4. Effect of SCG content on hardness of unaged and aged NR foams.

The effect of SCG loading on tensile strength in rubber foam is shown in Fig. 5. It can be seen that strength of rubber foam decreased steadily with increasing SCG content. This may be attributed to the irregular shape and low specific surface area of SCG particles which had inability to support stresses transferred from the rubber matrix. Also, the incompatibility of the hydrophilic natural fiber and hydrophobic rubber matrix yields composites with poor properties. A reduction of strain at break of rubber foam was also observed in Fig. 6. It was found that the elongation at break slightly decreased with the addition of SCG content into NR foam. The increment in filler content and larger cell size will eventual resulted in the reduction of the deformability of a rigid interface between the fill and the rubber matrix. At higher filler content, the degree of filler-filler interactions also became

more prominent. Consequently, a reduction in EB was observed.

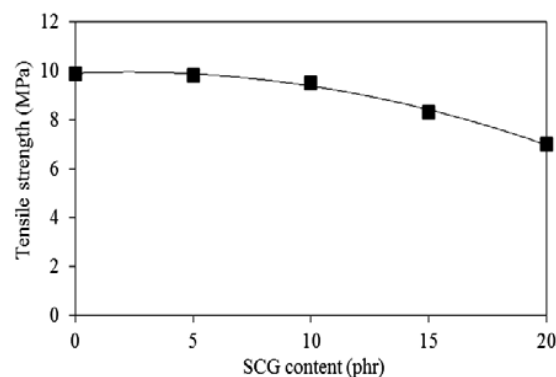


Fig. 5. Effect of SCG content on tensile strength of NR foams.

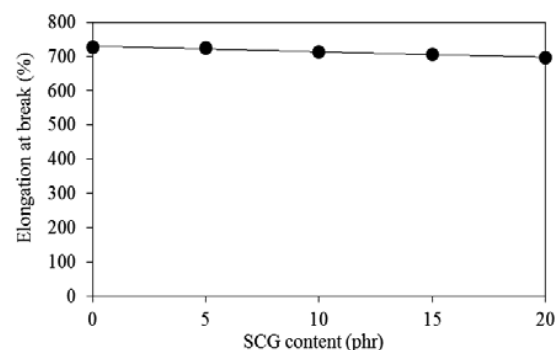


Fig. 6. Effect of SCG content on elongation at break of NR foams.

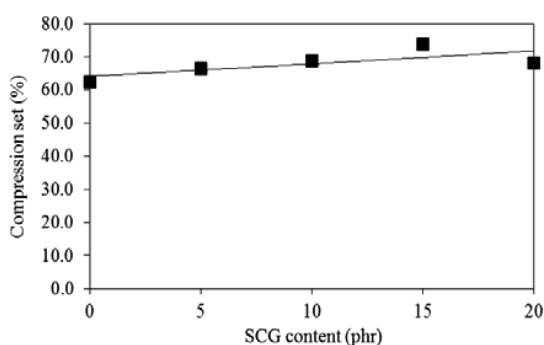


Fig. 7. Effect of SCG content on compression set of NR foams.

The compression set is the measure of the elastic behavior of the materials. From Fig. 7, it is seen that the compression set tended to increase with higher SCG loading, which indicates the poor recoverability of the SCG-filled rubber foam after unloading. This could be attributed to a deformation of the



larger cell structure after the compression. This would results in losses of the elastic recovery properties of the gas phase.

D. Physical and Morphological Properties

Fig. 8 depicts the increase of water absorption of NR foam with the increase of SCG content. Higher SCG content allowed the foam to expand and consequently producing NR foam with large unfilled space. Thus, more water is absorbed into the foam. In addition, higher amount of cellulose and hemicelluloses with hydroxyl groups in SCG particles are responsible for higher water absorption capacity in rubber foams. However, all NR foams had very low percentage of water uptake below 5%.

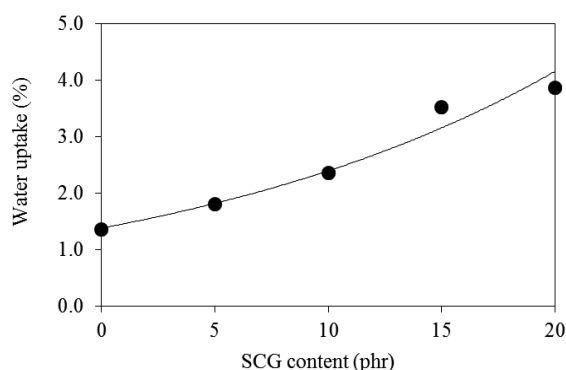


Fig. 8. Effect of SCG content on water uptake of NR foams.

One important objective in foaming composite is density reduction, which is related to the void content achieved in the polymer matrix. Interesting point is observed in Fig.9, the relative density of the foam slightly increased with increasing SCG content. The foam relative density is highly influenced by the chemical crosslinking generated among the polymer chain. The crosslinking will form a network consisting of higher packing polymer chain and results in increasing foam relative density [22]. In addition, it may be attributed to the density of SCG particles itself was higher than that of the foams, which have been reported in the literature by several authors [14, 17]. Fig. 10 shows the loading effect of the SCG particles on foam porosity of the NR foam. The experimental results showed that SCG particles had encouraged the cell foam formation by producing cell porosity with a narrower distribution in the matrix. Also, higher SCG content allowed the foam to expand and consequently producing NR foam with larger cell size.

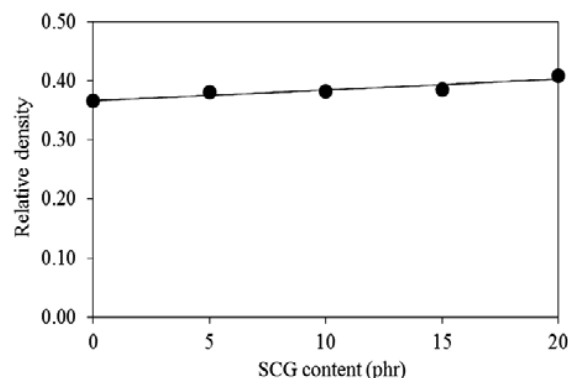


Fig. 9. Effect of SCG content on relative density of NR foams.

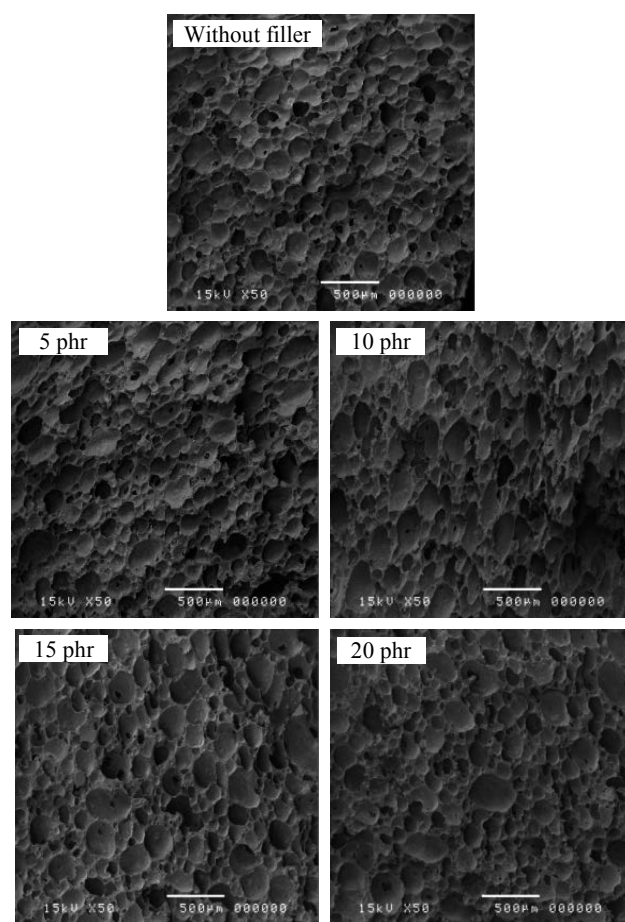


Fig. 10. SEM micrographs of NR foams with different levels of SCG particles.



IV. CONCLUSIONS

The curing characteristics, physical and mechanical properties of SCG particles filled NR foam were examined as function of filler loading. The results revealed that the scorch time and cure time decrease with increasing filler loading, while maximum torque and torque difference increased. However, the incorporation of SCG particles into NR foam gave relatively low reinforcement in terms of hardness and tensile strength and also reduced the elastic behavior (i.e. compression set and elongation at break) of the foams. From the SEM results, the SCG particles had encouraged the cell foam formation by producing cell porosity in the matrix. Hence, SCG particles can be advantageously used as natural fiber in order to produce the rubber foam.

ACKNOWLEDGMENT

The authors gratefully acknowledge the financial support from Faculty of Engineering and Agro-Industry, Maejo University, Thailand, and would like to thank the Rubber and Polymer Technology Program for supporting laboratories and facilities.

REFERENCES

- [1] L. Sobczak, R.W. Lang, and A. Haider, "Polypropylene composites with natural fibers and wood – General mechanical property profiles," *Compos. Sci. Technol.*, vol. 72, pp. 550–557, March 2012.
- [2] L. Mohammed, M. N. M. Ansari, G. Pua, M. Jawaid, and M. Saiful Islam, "A review on natural fiber reinforced polymer composite and its applications," *Int. J. Polymer. Sci.*, vol. 2015, pp. 1–15, August 2015.
- [3] K.L. Pickering, M.G. AruanEfendy, and T.M.Leac, "A review of recent developments in natural fibre composites and their mechanical performance," *Composites Part A: Applied Science and Manufacturing* Vol. 83, pp. 98–112, April 2016.
- [4] R. José dos Santos, D. Lincon da Silva Agostini, Flávio Camargo Cabrera, Elton Aparecido Prado dos Reis, Marcos Roberto Ruiz, Eduardo Roque Budemberg, Silvio Rainho Teixeira, and Aldo Eloizo Job "Sugarcane bagasse ash: new filler to natural rubber composite," *Polimeros*, vol. 24, no.6, pp.646-653, December 2014.
- [5] H. Ismail, M.R. Edyham, B. Wirjosentono, "Bamboo fibre filled natural rubber composites: the effects of filler loading and bonding agent," *Polym. Test.*, vol. 21, pp. 139–144, 2002.
- [6] S.I. Mussatto, E.M.S. Machado, S. Martins, J.A. Teixeira. "Production, composition, and application of coffee and its industrial residues," *Food Bioprocess Technol.*, vol. 4, pp. 661–672, March 2011.
- [7] R. Campos-Vega, G. Loarca-Piña, H.A. Vergara-Castañeda, and B.D. Oomah, "Spent coffee grounds: A review on current research and future prospects," *Trends Food Sci. Technol.*, vol. 45, issue 1, pp. 24–36, September 2015.
- [8] C. Siri Wong, S. Boopasiri, V. Jantarapibun, B. Kongsook, S. Pattanawanidchai, and P. Sae-Oui, "Properties of natural rubber filled with untreated and treated spent coffee grounds," *J. Appl. Polym. Sci.*, vol. 135(13), November 2017, 46060.
- [9] H. Kyung Lee, Y. Gi Park, T. Jeong, and Y.Seok Song, "Green nanocomposites filled with spent coffee grounds," *J. Appl. Polym. Sci.*, vol. 132, February 2015, 42043.
- [10] Chin-San Wu, "Renewable resource-based green composites of surface-treated spent coffee grounds and polylactide: Characterisation and biodegradability," *Polym. Degrad. Stab.*, vol. 121, pp. 51–59, November 2015.
- [11] D.García-García, A.Carbonell, M.D. Samper, D.García-Sanoguera, and R.Balart, "Green composites based on polypropylene matrix and hydrophobized spend coffee ground (SCG) powder," *Composites Part B: Engineering*, vol. 78, pp. 256–26, September 2015.
- [12] N.N. Najib, Z.M. Ariff, N.A. Manan, A.A. Bakar, and C.S. Sipaut, "Effect of blowing agent concentration on cell morphology and impact properties of natural rubber foam," *J. Polym. Sci.*, vol. 20(1), 13–25, 2009.
- [13] R.C.R. Nunes, J.L.C. Fonseca, and M.R. Pereira. "Polymer-filler interactions and mechanical properties of a polyurethane elastomer," *Polym. Test.*, vol. 19(1), pp. 93–103, February 2000.
- [14] M. A. Usman, S. O. Adeosun, and G. O. Osifeso, "Optimum calcium carbonate filler concentration for flexible polyurethane foam composite," *J. Miner. Mater. Char. Eng.*, Vol. 11, No.3, pp.311–320, 2012.
- [15] M.A. Bashir, Muhammad Shahid, Muhammad Shahid, R.A. Alvi, and A.G. Yahya, "Effect of carbon black on curing behavior, mechanical properties and viscoelastic behavior of natural sponge rubber-based nano-composites," *Key Eng. Mater.*, vol. 510–511(1), pp.532–539, May 2012.
- [16] J.H. Kim, J.S. Koh, K.C. Choi, J.M. Yoon, and S.Y. Kim, "Effects of foaming temperature and carbon black content on the cure characteristics and mechanical properties of natural rubber foams," *J. Ind. Eng. Chem.*, 13(2), pp. 198–205, 2007.
- [17] A.Vahidifar, S.N. Khorasani, C.B. Park, H.E. Naguib, and H.A. Khonakdar, "Fabrication and characterization of closed-cell rubber foams based on natural rubber/carbon black by one-step foam processing," *Ind. Eng. Chem. Res.*, Vol. 55, pp.2407–2416, 2016.
- [18] S. Shinoj, R. Visvanathan, S. Panigrahi, and M. Kochubabu, "Oil plam fiber (OPF) and its composites: a review," *Ind. Crops. Prod.*, vol. 33, no. 1, pp. 7–22, January 2011.
- [19] V.G. Geethamma, R. Joseph, S. Thomas, "Short coir fiber-reinforced natural rubber composites: effects of fiber length, orientation, and alkali treatment," *J. Appl. Polym. Sci.*, vol. 55, no.4, pp. 583–594, January 1995.
- [20] M. P. Wagner (1976) "Reinforcing silicas and silicates," *Rubber Chem. Technol.*, vol. 49, No. 3, pp. 703–774, July 1976.
- [21] H. Ismail, A. Rusli, and A.A. Rashid, "Maleated natural rubber as a coupling agent for paper sludge filled natural rubber composites," *Polym. Test.*, vol. 24(7), pp. 856–862, October 2015.
- [22] Z. M. Ariff, and N. A. A. Rahim. "Effect of compound formulation on the production and properties of epoxidised natural rubber (Enr-25) foams," in *Proceedings of the Polymer Processing Society 24th Annual Meeting ~ PPS-24 ~ June 15-19, 2008 Salerno (Italy)*, 2008.



A Spacecraft Trajectory Optimization and Modified Local Search Algorithm

Jukkrit Kluabwang

Department of Electrical Engineering
Rajamangala University of Technology Lanna Tak
Phaholyothin Road, Tak, Thailand 63000
Email: jukkrit_k@rmutl.ac.th

Sawat Yukalang

Department of Electrical Engineering
Rajamangala University of Technology Lanna Tak
Phaholyothin Road, Tak, Thailand 63000

Amorn Onkrong

Department of Electrical Engineering
Rajamangala University of Technology Lanna Tak
Phaholyothin Road, Tak, Thailand 63000

Santipab Kotthale

Department of Electrical Engineering
Rajamangala University of Technology Lanna Tak
Phaholyothin Road, Tak, Thailand 63000

Abstract—An optimization problem formulated from a trajectory design of a spacecraft named Cassini2, is introduced with some solutions by a modified local search algorithm. The optimization problem and the proposed solver are coded and also executable in MATLAB platform. Experiments has been conducted under CEC2011's evaluation criteria limited at maximum 150,000 function evaluations and due to each iteration of the modified local search evaluates five objective function values, thus the maximum iteration is set at 30,000 for each trial. There are 20 independent trials elaborated in this study. Computational results showed that the proposed local search can handle the spacecraft trajectory optimization problem and satisfy convergence property for all trials.

Keywords—spacecraft trajectory; gravity assist; local search; cassini2

I. INTRODUCTION

Space and planets still have been interested to learn for many years ago. Our solar system consists of eight planets, Mercury, Venus, Earth, Mars, Jupiter, Saturn, Uranus and Neptune in the order of closet of the sun. More than two decades, Cassini-Huygens project has been originated by the collaboration between three leading organizations: firstly, National Aeronautics Space Administration (NASA), secondly, the European Space Agency (ESA) and lastly, the Italian space agency (ISA). Its mission is to studying Saturn and its moons by sending a spacecraft, namely Cassini2, to realize these purposes [1]-[2]. Cassini2 spacecraft spent about seven years for a single trip from Earth (15th October 1997) to Saturn (1st July 2004). Distance from Earth to Saturn is about 1.2 billion kilometers or 8 times of from Earth to Sun. It is very interesting to know how to move a spacecraft from one point to another far point in the space with keeping in touch all time throughout a space telecommunication system. Cassini2 spacecraft has been designed to use gravity assist as a power propelled in the space [3]. Trajectory of Cassini2 was passed through Venus,

Jupiter and then Saturn as the destination [4]. Trajectory optimization problem for Cassini2 spacecraft had arisen with 22 parameters, such as speed and durations while it was passing among planets [5]. To solve the spacecraft trajectory optimization problem, many heuristic algorithms have been applied, for example genetic algorithm (GA), particle swarm optimization (PSO), differential evolution (DE), simulated annealing algorithm (SA). According to a technical report [6] concluded that DE significantly outperformed PSO and GA in optimizing difficult trajectories. Spacecraft trajectory optimization was also elected to be real world benchmark in a optimization contest named CEC2011 [7]. This research article would like to presented an application of an alternative heuristic technique, namely modified local search to solve the spacecraft trajectory problem.

In this article, there are five topics, introduction, methodology, computational results and conclusion. Particular aim of this study is to devoted to Cassini-Huygens project, especially to Cassini2 spacecraft which came to the grand finale by plunging through Saturn's upper atmosphere on 15th September 2017 [8].



Fig. 1. Cassini spacecraft [2]



II. METHODOLOGY

A. Problem Description

Trajectory of a spacecraft, namely Cassini2, taking a trip from the Earth to the Saturn can be formulated into an optimization problem. Gravity-assist concept is very important idea in space engineering and also has been applied to the Cassini2 project. In the objective function, duration and sequence of spacecraft movement among planets from the beginning to the end are all taken into account.

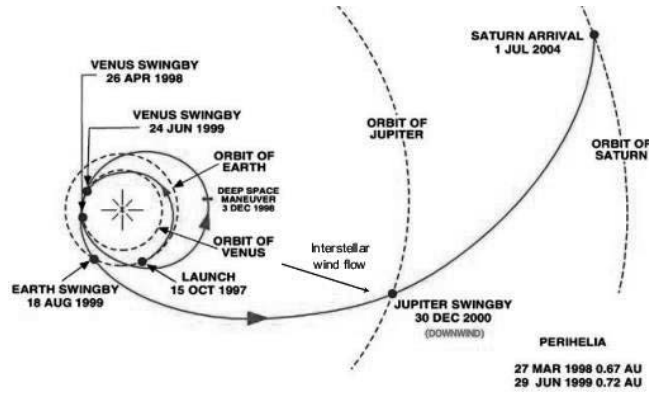


Fig. 2. CASSINI's interplanetary trajectory from earth to saturn. [4]

Fig.2 shows a journey of cassini2 spacecraft from the Earth to the Saturn for nearly seven-year-trip. The journey started on 15th October 1997 from cape Canaveral in USA and then went to the Venus orbit. It stayed over there until 26th April 1998, then swing by Venus gravity into deep space. After travelling in deep space for about a year, Cassini2 came back to the Venus orbit on 24th June 1999 and then passed through the Earth orbit again. On 18th August 1999, the spacecraft went out the Earth orbit toward the Jupiter. There is a big asteroid belt floating in the middle way between and the Mars and the Jupiter. Fortunately, it had passed through the belt and reached safely the Jupiter orbit. The craft continued moving forward to the near destination by departing the Jupiter orbit on 30th December 2000. The cassini2 spacecraft arrived the Saturn orbit on 1st July 2004. We can summarize the overall sequence of this journey as follows, Earth-Venus-Venus-Earth-Jupiter-Saturn.

The trajectory of Cassini2 can be formulated as an optimization problem [6] as follows,

$$\text{Minimization } J(\mathbf{x}) \quad (1)$$

$$\text{subject to } L < \mathbf{x} < U$$

where J , \mathbf{x} , L and U are an objective function, input argument vector or variable vector, lower boundary and upper boundary, respectively. Input vector or vector \mathbf{x} consists of 22 variables described in Table I [7].

TABLE I. INPUT ARGUMENTS DEFINITION

Item	Variables details			
	State	L	U	units
1	$x(1)$	-3000	0	MJD2000 ^a
2	$x(2)$	3	5	kilometer per second
3	$x(3)$	0	1	n/a ^b
4	$x(4)$	0	1	n/a
5	$x(5)$	100	400	days
6	$x(6)$	100	500	days
7	$x(7)$	30	300	days
8	$x(8)$	400	1,600	days
9	$x(9)$	800	2,200	days
10	$x(10)$	0.01	0.9	n/a
11	$x(11)$	0.01	0.9	n/a
12	$x(12)$	0.01	0.9	n/a
13	$x(13)$	0.01	0.9	n/a
14	$x(14)$	0.01	0.9	n/a
15	$x(15)$	1.05	6	n/a
16	$x(16)$	1.05	6	n/a
17	$x(17)$	1.15	6.5	n/a
18	$x(18)$	1.7	2.91	n/a
19	$x(19)$	-pi	+pi	radians
20	$x(20)$	-pi	+pi	radians
21	$x(21)$	-pi	+pi	radians
22	$x(22)$	-pi	+pi	radians

^a Modified Julian Dates

^b Not Applicable

B. Review of Modified Local Search Algorithm

Solver for the Cassini2 spacecraft trajectory optimization problem was a modified local search algorithm [9]. Local search is a basic search algorithm and has plays an important role as an heuristic search in computer science field for long time ago. Back-bone concept of the local search is to find the best solution in a certain location and its near surrounding and then update the center of searching to the obtained best solution. The searching cycle of local search is rotating in order to improve the global solution until one of terminal criterions (TCs), solution quality or searching time limit, is met. Normally, naïve local search is facing a bad performance problem due to becoming stuck in a local trap. To escape this unwanted situation, the proposed local search algorithm [10] has employed backtracking mechanism (BT) to bring them toward to a visited best solution and let the naïve local search continues going search successfully. To invoke the BT mechanism may come from the number of unimproved solution is met. Parameter settings are shown in appendix.



III. COMPUTATIONAL RESULTS

Problem or objective function and a solver, namely modified local search, were all coded in MATLAB platform. Experiment is designed to execute these files for 20 trials where each trial is covered randomly generating initial solution and then iteratively searching along local search concept until maximum iteration (30,000) is met. A Laptop including a CPU: AMD Dual-Core processor 1.0 GHz, RAM: 4GB DDR3 and Hard Disk Drive 500 GB, was used to run the programs. Computational results are tabulated in Table II with two main data, final objective function and searching time. The obtained data were returned from statistic analyzing of 20 trials and were also illustrated in 5 categories, minimum, median, mean, maximum and standard deviation, as well.

TABLE II. COMPUTATIONAL RESULTS FROM 20 TRIALS

Data	Items	
	Types	values
Objective Functions	Minimum	21.0889
	Median	23.7878
	Mean	24.6072
	Maximum	28.1352
	Standard Deviation	2.5987
Searching Time ^c	Minimum	1,224.5
	Median	1,251.3
	Mean	1,269.7
	Maximum	1,461.9
	Standard Deviation	65.2

^c Unit of time in seconds

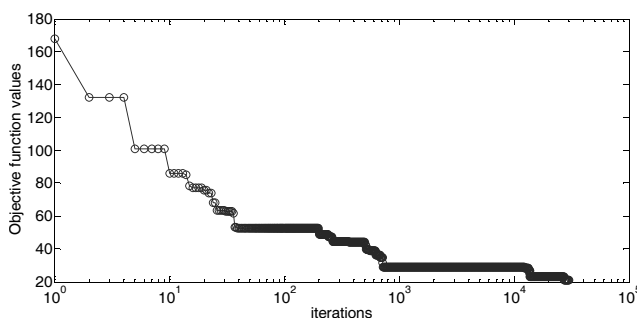


Fig. 3. A convergent curve of the best trial with the lowest objective value.

Fig. 3 shows a convergent property with a curve plotted from the obtained objective function value with respect to its each iteration. The convergence curve is of the 6th trial. It randomly began with the objective function value $J=167.8402$ and efficiently went down to $J=53.3301$ at the 36th iteration. All 20 trials stopped their searching processes with a termination criterion specifying maximum iteration at 30,000 which is equivalent to 150,000 function evaluations in [6]. The 6th trial

spent 1,252.5 seconds or about 21 minutes to reach the end at $J=21.0889$ which is the minimum value among of all trials. The obtained solution \mathbf{x} are $x(1)=-731.92$, $x(2)=3.41$ km/s, $x(3)=0.35$, $x(4)=0.28$, $x(5)=179.45$ days, $x(6)=432.20$ days, $x(7)=293.44$ days, $x(8)=567.93$ days, $x(9)=1,680.48$ days, $x(10)=0.30$, $x(11)=0.08$, $x(12)=0.09$, $x(13)=0.05$, $x(14)=0.04$, $x(15)=1.46$, $x(16)=2.58$, $x(17)=2.21$, $x(18)=267.30$, $x(19)=-1.35$ rad, $x(20)=0.99$ rad, $x(21)=-1.94$ rad, $x(22)=-1.55$ rad, respectively.

IV. CONCLUSION

This paper proposed an application of the modified local search algorithm to an optimization benchmark in orbital and spacecraft area. Cassini2 spacecraft trajectory optimization was chosen to study here. There are 22 parameters to be optimized in order to reach the minimum objective function. Experimental results show that the modified local search algorithm can properly solve the problem. Future work will be focusing on the unexplored minimum objective function of the Cassini2 spacecraft trajectory problem.

ACKNOWLEDGMENT

Authors would like to thank Rajamangala University of Technology Lanna for financial supports and also thank to Cassini-Huygens projects for providing valuable knowledges and instructional materials for us.

REFERENCES

- [1] R.T. Mitchell, "Cassini/Huygens at Saturn and Titan," Acta Astronautica, vol. 59, pp. 335-343, April 2006.
- [2] T. Greicius (2017, August 4). Cassini Overview. Retrieved from https://www.nasa.gov/mission_pages/cassini/whycassini/index.html
- [3] C.J. Hansen, S.J. Bolton, D.L. Matson, L.J. Spiker and J.P. Lebreton "The Cassini-Huygens flyby of Jupiter," Icarus, vol. 172, pp. 1-8, September 2008.
- [4] Getting to Saturn (2013, March 27). Retrieved from <http://sci.esa.int/cassini-huygens/31240-getting-to-saturn/>
- [5] T. Vinko and D. Izzo, "Global optimization heuristics and test problems for preliminary spacecraft trajectory design," in ACT TECHNICAL REPORT, ACT-TNT-MAD-GOHTPPSTD, September 2008.
- [6] P. Musegaas (2012, December 20). Optimization of space trajectories including multiple gravity assists and deep space maneuvers. Retrieved from <https://repository.tudelft.nl/islandora/object/uuid:02468c77-5c64-4df8-9a24-1ed7ad9d1408/datastream/OBJ/download>
- [7] S. Das and P.N. Suganthan (2011, February 20). Problem definitions and evaluation criteria for CEC2011 competition on testing evolutionary algorithms on real world optimization problems. Retrieved from http://www3.ntu.edu.sg/home/epnsugan/index_files/CEC11-RWP/CEC11-RWP.htm
- [8] The grand finale (2017). Retrieved from https://saturn.jpl.nasa.gov/legacy/files/Cassini_Grand_Finale_Fact_Sheet_508.pdf
- [9] A. Dholvitayakhun and J. Kluabwang, "Application of local search for optimal assignment of food exchange lists problem," International Journal of Computer Theory and Engineering, vol. 6, pp.189-191, April 2014.
- [10] A. Dholvitayakhun and J. Kluabwang, "Design of food exchangelist for obesity using modified local search," The 13th International Conference on Electrical/Electronics, Computer, Telecommunications and Information Technology (ECTI-CON 2016), Chiang Mai, June 28 – July 1, 2016.



APPENDIX

As CEC2011 criteria [7], the parameter settings of the proposed modified local search were shown in Table III.

TABLE III. PARAMETERS FOR THE MODIFIED LOCAL SEARCH ALGORITHM.

Parameters	Values
Initial solution	random
Termination criterions	Time limit through max iteration and Solution quality in objection function value
Max iteration	30,000
Objection function value target	8
Number of Neighborhood	5
Search Radius ratio (%)	20
Back-track point	5



Natural Rubber Latex Foam for Seedling

Philaiwan Pornprasit*, Aroonsri Aiemrum

Program in Rubber and Polymer Technology, Faculty of Engineering and Agricultural Industry, Maejo University, Chiangmai, Thailand, 50290

E-mail address: dphilaiwan@yahoo.com

Abstract— Latex foam from natural rubber latex with various types of fillers such as defatted rice bran (DRB), longan shell (LS)/DRB (1/1 by weight) and organic fertilizer (OF) were prepared for seedling. The properties of latex foam from natural rubber latex and polyurethane foam were compared. The results indicated that latex foam filled with LS/DRB showed the highest density and lowest compression set value. Latex foam from natural rubber latex and polyurethane foam gave an opened cell. The latex foam filled with organic fertilizer showed the highest pore size. The morning glory seed was selected for seed germination test. The results showed that latex foam filled with LS/DRB was the highest germination. Polyurethane foam gave the highest height of seedlings. However, the latex foam filled with organic fertilizer gave the second height of seedlings. Therefore, the properties of foam for seedling were low compression set, low density and high porous.

Keywords— rubber foam; longan shell; defatted rice bran; organic fertilizer

I. INTRODUCTION

Polyurethane (PU) foam plugs commonly are used as collars or supports to grow plants in solution culture [1]. The PU foam, a viscoelastic material is produced by the interaction of active hydrogen compounds, water and isocyanates [2] where is used extensively as foam cushioning material in home furnishings. Despite their utility, these foam plugs can be quite toxic to plants, particularly to small seedlings [1]. Then, the natural rubber latex foam (NRLF) is interesting material for seedlings.

The production of latex foam-moulded began in 1930 following the discovery of combined whipping and controlled gelling process by the Dunlop Rubber Company [3]. The process involves the whipping of a latex compound which has been de-ammoniated and matured, followed by the addition of a gelling agent. The delayed action gelling agent, sodium silicofluoride, is able to set the foam in a few minutes at room temperature [4]. The foamed latex is then transferred to the mould, then vulcanised in a steam oven. In this research, the biomass fillers such as defatted rice bran, longan shell, and organic fertilizer were added into the NRLF. Defatted rice bran (DRB) is a by-product of the rice bran oil extraction process. DRB is normally used to reduce the final cost of animal feed or is discarded as agricultural waste [5]. DRB has

also been used as filler in cellular NR. D. Moonchai, P. Juntamui, and R. Ruankum (2015) studied the properties of cellular NR vulcanizate filled with DRB. It was found that the cell size of cellular NR vulcanizate filled with DRB was larger than that of non-filled cellular NR vulcanizate [6]. Longan, a plant of *Sapindaceae*, has been commercially cultivated in many warm regions of the world including China, Thailand, Vietnam, Australia, and Hawaii and Florida in the USA [7]. The fresh pulp of longan is juicy and sweet, with various nutritional components, and considered to have important edible and medical value. Although its flesh is widely used, the longan shell is often discarded as a by-product of the food industry without any reasonable utilization annually [8]. Plenty of cellulose, lignin, and a few flavonoids, the main components of longan shell, enable the longan shell to give excellent ability to remove the heavy metal ions from aqueous solutions, which is confirmed by the experiments of M.R. Huang et al. [9]. Organic fertilizer (OF) is the compost from agricultural waste. OF consists of organic matter such as boron, molybdenum, iron, copper, manganese, zinc, chlorine, calcium, magnesium, and sulfur [10].

This research is focused on the properties of the filler filled- natural rubber latex foam (NRLF) and germination testing compared with polyurethane (PU) foam.

II. METHODOLOGY

A. Materials and Formulation

Table 1 shows the formulation and materials used in this research study. NRL (high ammonia (HA) type) and latex chemicals (sulphur, LOWINOX® CPL, potassium oleate, zinc-N-diethyl dithiocarbamate (ZDEC), zinc-2-mercaptobenzothiazole (ZMBT), zinc oxide (ZnO), diphenyl guanidine (DPG) and sodium silicofluoride (SSF) supplied by Lucky Four Co. Ltd. (Thailand) were used in this research. Solid materials, such as sulphur, ZDEC, ZMBT, ZnO, DPG, SSF, and CPL were prepared in dispersion form by ball-milling for 72 h. Liquid materials, specifically, potassium oleate were prepared in emulsion form by continuously stirring in room temperature until completely dissolved. Three fillers used were defatted rice bran (DRB), longan shell (LS)/DRB (1/1 by weight) and organic fertilizer (OF). DRB was purchased from Thai Edible Oil Co. Ltd. (Thailand).



Longan shell and organic fertilizer were received from farmers (Lampoon, Thailand) and Windrow Composting without Turning Learning Center (Maejo University, Thailand). DRB, LS, and OF were sieved through a 40-mesh screen before dispersing. DRB, LS, and OF fillers dispersion was prepared by grinding the mixture of filler and dispersing ingredients in a ball mill for 3 h. The dispersing ingredients were vultamol (1% wt/wt), bentonite clay (1% wt/wt), and distilled water (92% wt/wt).

TABLE I. FORMULATION OF NATURAL RUBBER FOAM FILLED FILLER

Ingredients	Total Solid Content (%)	Formulation (phr)
HA Latex	60	100
Potassium Oleate	10	1.5
Sulphur	50	2
ZDEC	50	1
ZMBT	50	1
CPL	50	1
DPG	33	0.8
ZnO	50	5
SSF	25	1
DRB	25	20
LS/DRB	25	20
OF	25	5

B. Sample Preparation

NRL was sieved, measured, mixed with filler ((DRB, LS/DRB, OF) and stirred using a stand mixer (CHAMP, CKI Family Co., Ltd.) for 3 min with high speed (No.3). Next, potassium oleate soap was added and stirred for 1 min with low speed (No.1). After that, a vulcanizing agent (sulfur), accelerators (ZMBT and ZDEC), and antioxidant (CPL), were slowly added to the mixture, stirred for 4 min with low speed (No.1) and stirred for 4 min with high speed (No.3) until the volume was increased up to three times the initial volume. Once the desired volume was obtained, the foaming speed was lowered to obtain a fine and even foam. Next, DPG together with zinc oxide (ZnO) was added to the foam as the primary gelling agent, and even beating was continued for another 90 sec. Immediately following that, sodium silicofluoride (SSF), the secondary gelling agent, was added and the foam was beaten for another 90 sec. Finally, the un-gelled foam was quickly poured into an aluminum mould and allowed to gel for 3 min at ambient temperature. The gelled foam was then cured in a hot air oven at 70 °C for 30 min. Once the foam was cured, it was stripped from the mould, then washed thoroughly with de-ionized water to remove potassium oleate soap and excessive non-reacted elements After washing,

the cured NR foam was dried in a hot air oven at 70°C for 8h. The well-dried foam appears to be brownish color.

Polyurethane foam sized 2.54×2.54×2.54 cm³ was purchased from Maejo Agriculture (Chiangmai, Thailand).

C. Measurement of Foam Density

Density of the filler-incorporated NRLF was determined by calculation from the mass and volume of a specimen as shown in Equation 1. Samples used in this test method were in regular shape not less than 16 cm³ (1 in³) in volume (according to ASTM D1056). Five samples of each filler were measured and an average of three results was reported

$$\text{Density, kg/m}^3 = M/V \quad (1)$$

where: M = mass of specimen, kg and V = volume of specimen, m³.

D. Measurement of Compression Properties

Compression behavior of fillers (DRB, LS/DRB, OF) incorporated NRLF samples were tested according to ASTM D3574-03. Samples used in this test method was in regular shape of 50 by 50 by 25 mm with parallel top and bottom surfaces and essentially perpendicular sides. Three specimens per samples were tested. Specimens were placed in test apparatus and deflected to 50% of its original thickness. Within 15 min, deflected specimens and the apparatus were placed in mechanically convected air oven for a period of 22 h with test temperature of 70±2°C. Specimens were immediately removed from apparatus and measured after 30 min recovery. The constant deflection compression set was obtained from this testing.

$$C_t (\%) = (t_0 - t_f) \times 100 / t_0 \quad (2)$$

where:

C_t = compression set expressed as a percentage of the original thickness,

t₀ = original thickness of test specimen, cm and

t_f = final thickness of test specimen, cm

E. Surface Morphology

Studies on the surface morphology of the fillers incorporated NRLF samples were carried out using Digital Microscope (Leica DVM6).

F. Seed Germination Test

The activation of the seed's metabolic machinery leading to the emergence of a new seedling plant is known as germination. The foam samples were cut in 2.54 cm by 2.54 cm cubes. After that, the foams were cut with a sharp knife at one face of the foam cube (this is where the seed will be inserted) and these foams were soaked in water. The morning glory seeds were inserted on the foam samples. Re-wetting the



foams for 7 days was requested. The actual percentage of germination was determined.

$$\text{Percentage germinations} = \frac{\text{Number of germination seeds} \times 100}{\text{Total numbers of seeds tested}} \quad (3)$$

III. RESULTS AND DISCUSSION

A. Foam Density

Fig. 1 represents the effect of filler type on the foam density of natural rubber latex foam (NRLF). Filler filled NRLF has a higher density than that of PU foam. OF filled NRLF gives, a lowest density that means it has a lowest weight. This could be due to the lower dosage of OF in NRLF. The density decreases with decreasing filler loading [11]. However, the suitable density of seedling foam should be low.

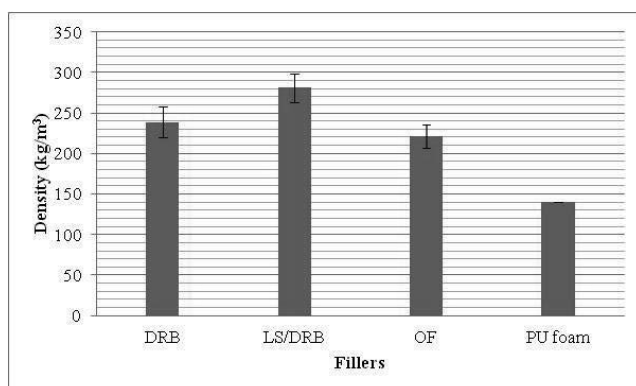


Fig.1. Density of natural rubber latex foam filled fillers and PU foam

B. Compression Set Property

The compression set is the measure of the elastic behavior of the materials. The compression set results corresponded to ability to recover after being compression loading of the samples at the specified conditions. Low compression set value indicates good recoverability of the cellular NR vulcanizates. Fig. 2 shows the constant deflection compression, C_t of natural rubber latex foam filled fillers. Recovery percentage of filler incorporated NRLF decreases with increasing filler loading. Non-elastic deformation is mainly due to deformation of the hard phase (filler) [12]. This is probably due to more deformation of the hard phase, of which more filler is present. The LS/DRB filled NRLF exhibits the lowest compression set, which indicates the higher elasticity of NRLF. However, the filler filled NRLF has a higher C_t than that of PU foam. Therefore, the suitable the constant deflection compression of seedling foam should be low.

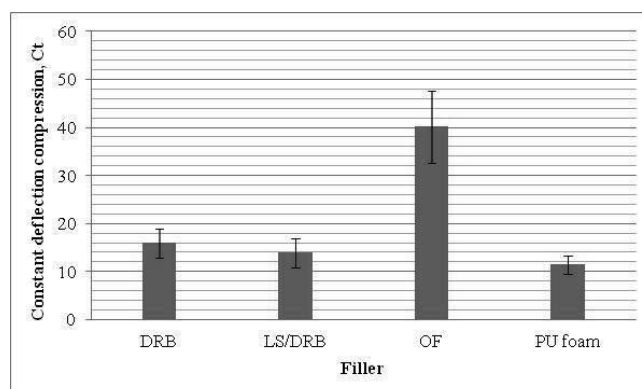


Fig.2 Constant deflection compression, C_t of natural rubber foam filled fillers and PU foam

C. Morphology

Digital Microscope (Leica DVM6) is a common method used to analyze the level of matrix-filler adhesion [13, 14]. Fig. 3 (a-c) presents the micrograph of filler filled NRLF, which clearly reveals the open cell structure of the foam. PU foam (Fig.3 (d)) also demonstrates the open cell structure of the foam. DRB filled NRLF shows the smallest pore size of foam and a piece of DRB dispersed in NRLF. The layer structure of LS/DRB filled NRLF and a piece of LS and DRB is clearly observed in Fig.3 (b). The biggest pore size of foam is observed in OF filled NRLF Fig.3(c). It may be described that the amount of OF in NRLF is only 5 phr but the other fillers is added in 20 phr. The density increases with increasing filler loading [11]

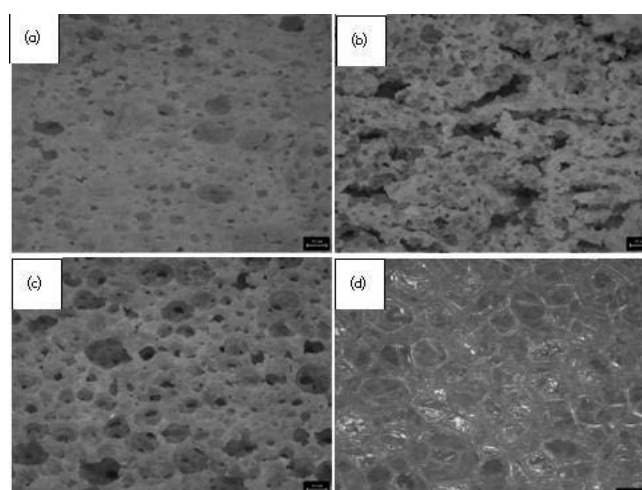


Fig.3 (a) Micrograph of surface of 20 phr DRB- filled NRLF at magnification of 50×, (b) Micrograph of surface of 20 phr LS/ DRB- filled NRLF at magnification of 50×, (c) Micrograph of surface of 5 phr OF- filled NRLF at magnification of 50×, (d) Micrograph of surface of PU foam at magnification of 50×.



D. Seed germination test

The selected morning glory seeds were used to the seed germination testing which shown in Fig. 4. Normally, early seed germination begins with imbibition of water by the seed and follows a three-stage increase in seed fresh weight due to increasing water uptake. The three phases are (1) imbibition, which is characterized by an initial rapid increase in water uptake, (2) the lag phase follows imbibition and is a period of time where there is active metabolic activity but little water uptake, and (3) radical protrusion, which results from a second period of flesh weight gain driven by additional water uptake[15]. For this research, the percentage of germinations and the height of sprout were focused. From Fig.5, the highest percentage of germinations of morning glory seed came from LS/DRB filled NRLF. This could explain that this foam can absorb the water for the imbibition stage. However, PU foam gives the highest height of morning glory sprout. It can be explained that the seed need water to germinate but after that the sprout need oxygen to respire. Then, the airy foam should be suitable for seedling. The NRLF from Dunlop method has a disadvantage. During curing, gravity pulls the foam cells downward in the mould, collapsing the cell structure and densifying the bottom of the samples. Then, the air and water are unable to flow easily.

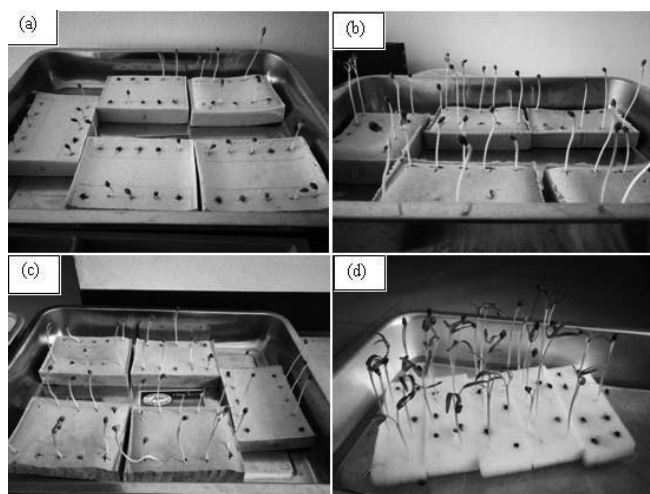


Fig.4 Seed germination test of (a) 20 phr DRB- filled NRLF, (b) 20 phr LS/DRB- filled NRLF, (c) 5 phr OF- filled NRLF, (d) PU foam

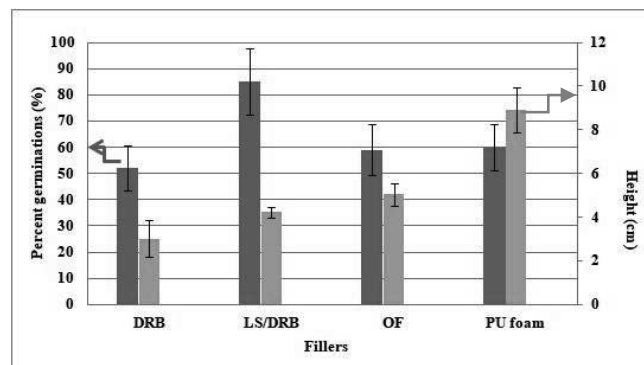


Fig.5 Percentage of germinations and height of morning glory sprout in natural rubber latex foam filled fillers and PU foam

IV. CONCLUSION

Natural rubber latex foam filled with defatted rice bran (DRB), longan shell (LS)/DRB (1/1 by weight) and organic fertilizer (OF) can be used for seedling. Especially, the LS/DRB filled NRLF gave the lowest compression set, high porosity, and highest percentage of germinations of morning glory seed, even though LS/DRB gave a highest density. In conclusion, the properties of foam for seedling were low compression set, low density and high porous.

ACKNOWLEDGMENT

This study was supported by the Faculty of Engineering and Agro-Industry, Maejo University. The authors would like to thank the Rubber and Polymer Technology Program, Faculty of Engineering and Agro-Industry, Maejo University, Thailand, for supporting laboratories and facilities.

REFERENCES

- [1] R.M. Wheeler, S.H. Schwartzkopf, T.W. Tibbitts, and R.W. Langhans, "Elimination of toxicity from polyurethane foam plugs used for plant culture", *HortScience.*, vol.20(3), pp. 448-449, June 1985.
- [2] Flexible Polyurethane Foam. Dow Chemical Pacific Ltd., 1-28.
- [3] E.W. Madge, *Latex Foam Rubber*. London: MacLaren & Sons Ltd. 1962, pp. 4-15.
- [4] W.H. Chapman, D.W.Pounder, and E.A.Murphy, British Pat. 332,525. Improvements in or relating to the manufacture of goods of rubber or similar material. 1929.
- [5] D. Moonchai, N. Moryadee, and N. Poosodsang, "Comparative properties of natural rubber vulcanisates filled with defatted rice bran, clay and calcium carbonate", *Maejo Int. J. Sci. Technol.*, vol. 6(2), pp.249-258, July 2012.
- [6] D. Moonchai, P. Juntamui, and R. Ruankum, "Utilization of defatted rice bran as a filler for cellular natural rubber", *RMUTI Journal Special Issue*. vol. 1, pp. 451-457, August 2015.
- [7] Y. Lin, Y. Lin, H. Lin, S. Zhang, Y. Chen, J. Shi, "Inhibitory effects of propyl gallate on browning and its relationship to active oxygen



- metabolism in pericarp of harvested longan fruit", LWT-Food. Sci. Technol. vol.60, pp. 1122–1128, October 2015.
- [8] L. Li, J. Xu, Y. Mu, L. Han, R. Liu, Y. Cai, X. Huang, "Chemical characterization and antihyperglycaemic effects of polyphenol enriched longan (*Dimocarpus longan* Lour.) pericarp extracts", J. Funct. Foods, vol. 13, pp. 314–322, January 2015.
- [9] M.R. Huang, S. Li, X.G. Li, "Longan shell as novel biomacromolecular sorbent for highly selective removal of lead and mercury ions", J. Phys. Chem. B., vol.114, pp. 3534–3542, January 2010.
- [10] T. Sawangpanyangkura, S. Tantikul, and C. Nitawichit, "Composting by local community in commercial scale using aerated static pile system", Proc. 30th Congress on Science and Technology of Thailand. 19-21 October 2004. Bangkok
- [11] S. Ramasamy, H. Ismail, and Y. Munusamy "Tensile and morphological properties of rice husk powder filled natural rubber latex foam" Polym. Plast. Technol. Eng., vol.51, pp. 1524–1529, November 2012.
- [12] M. Schuur, E.v.d.H., J. Feijena, and R. J. Gaymans, "Elastic behavior of flexible polyether(urethane–urea) foam materials". Polymer, vol. 45, pp. 2721–2727, March 2004.
- [13] T. Ohchi, Y. Naohiro, C. Fujikawa, and T. Hara, "Formation of microbeam using tabletop soft X-ray laser", J. Electron Spectrosc. Rel. Phenom., vol. 101–103, pp. 943–947, September 1999.
- [14] K. Wilkinson, J. Lundkvist, G.A. Seisenbaeva, and V.G. Kessler, "New tabletop SEM-EDS-based approach for cost-efficient monitoring of airborne particulate matter", Environ. Poll., vol. 159(1), pp. 311–318, January 2011.
- [15] H. T. Hartmann, D. E. Kester, F. T. Davies Jr., and R. L. Geneve, "Hartmann&Kester's plant propagation: Principles and practices", 8th edition, Pearson, London, 2010.



A Solution of Tsunami Wave by Using the Modified Adomian Decomposition Method

Jeerawan Saelao
Division of Mathematics, Faculty of Science,
Maejo University
Chiang Mai, Thailand
E-mail: jeerawan_s@mju.ac.th

Nopporn Patcharaprakiti
Department of Electrical Engineering,
Rajamangala University of Technology Lanna,
Chiangrai, Thailand
E-mail: npnopporn@rmutl.ac.th

Abstract— In this paper, the shallow Water model of tsunami wave is proposed. The nonlinear derivative equation system is derived and used for explain the velocity and wave height of tsunami. The model Adomian decomposition method is applied to find the solution as local analytical solutions which use to explain the phenomena of tsunami in short duration and distance. In short duration and distance, the slope of coastal is essential factor which make high velocity and wave height and affect to the damage of tsunami attack.

Keywords—tsunami modeling; nonlinear partial differential equation; modified Adomian decomposition method

I. INTRODUCTION

Tsunami wave or tidal wave, also known as a seismic sea wave, is a series of waves which have wavelength about 80-200 km., generally occur in an ocean or a large lake. The Earthquakes, volcanic eruptions and other underwater explosions is the main caused which affect to displacement of a large volume of water, suddenly diminish of water level and high amount of water rapidly erupt under the Crust far from the coast with small wave only 30 cm height and velocity about 600-1000 km/hr. But the wave move to the shallow water area the wave become giant wave 15-30 m. with rapidly high and enormous force to destroy human and buildings on the beach. In Thailand, the tsunami crisis has occurred at southern part on 2004 which damage to high amount human life, building and asset. In order to prevent the damage the tsunami mathematical model is one of the essential tools for prediction the phenomena. The tsunami forecast from model is use to warning, planning and evacuate the people to the safe area. Mathematicians have tried to generate model and simulate the tsunami behavior and phenomena [1-4] by using several technique follow as Artificial Artificial neural network [5], finite element method [6-7], finite different method [8]. However, these methods have cumbersome and complicate for calculate to find approximate solution and form in term of numeric solution. At present, symbolic solution can be calculated to find exacted solution for solve the mathematical model in term of non-linear derivative equation with novel method follow as modified Adomian Decomposition method [9]. Consequently, is this paper, the modified Adomian decomposition method is proposed for tsunami behavior model and simulate the velocity and height of tsunami which travel to coast from mathematical process. The principle of tsunami modeling and theory of modified Adomian decomposition

method is illustrated. The application of this method to model tsunami is performed and result as well as conclusion is proposed respectively.

II. TSUNAMI MODELING

Tsunami modeling is necessary tool for make understanding behavior of tsunami and prediction tsunami phenomena. A. G. Marchuk and A. A. Anisimov [1] has studied about the shallow water model which is the nonlinear homogenous system of the partial differential equation in one dimension to explain behavior about velocity and height of tsunami wave traveling to coast and S. Boonyapibanwong [10] has applied the system equation to transform in simplicity equation follow as

$$\begin{aligned} \frac{\partial u}{\partial t} + u \frac{\partial u}{\partial x} + \frac{\partial \eta}{\partial x} &= 0 \\ \frac{\partial \eta}{\partial t} + u \frac{\partial \eta}{\partial x} + u \frac{\partial H}{\partial x} + \eta \frac{\partial u}{\partial x} + H \frac{\partial u}{\partial x} &= 0 \end{aligned} \quad (1)$$

Subject to the initial conditions

$$\begin{aligned} u(x, 0) &= \frac{h}{\sqrt{d}} \sec h^2 \sqrt{\frac{3h}{4d^3}} x \\ \eta(x, 0) &= h \sec h^2 \sqrt{\frac{3h}{4d^3}} x \end{aligned} \quad (2)$$

where

$$\begin{aligned} u &= \frac{u^*}{\sqrt{gA}}, \quad \eta = \frac{\eta^*}{A}, \quad H = \frac{H^*}{A}, \quad h = \frac{h^*}{A}, \\ d &= \frac{d^*}{A}, \quad x = \frac{x^*}{A}, \quad t = \sqrt{\frac{g}{A}} t^* \end{aligned}$$

where u^* is the velocity, η^* is the surface elevation, H^* is the value of depth, g is gravity acceleration, x^* is the distance in horizontal, t^* is the time, h^* is the surface elevation in initial time, d^* is the depth constant of sea, and A is the surface elevation constant of maximum wave from sea level.

III. MODIFIED ADOMIAN DECOMPOSITION METHOD

The modified Adomian decomposition method is developed by J. Biazar and K. Hosseini [9] which use to find the solution of non-linear derivative system equation. The basically of this application use conventional Adomian



decomposition and consider the first term of polynomial Adomian only. This method has high efficiency and also simplify for calculate. The process of tsunami model calculation by using modified Adomian decomposition method is shown in Fig. 1.

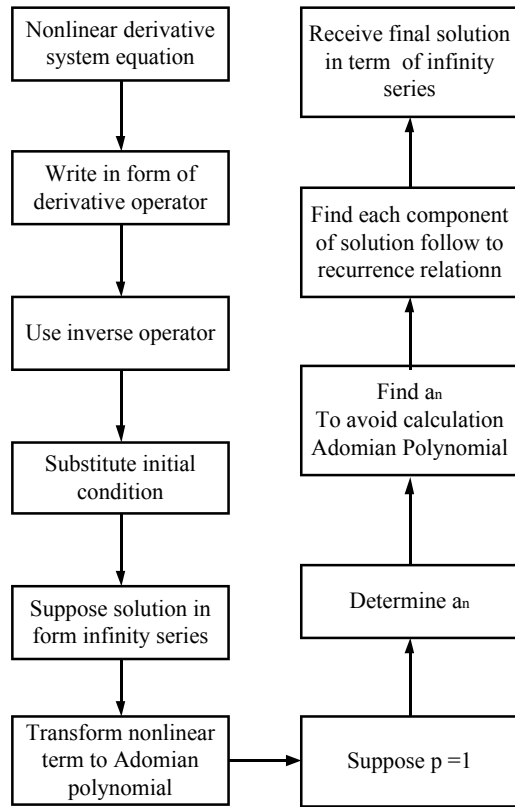


Fig. 1 Principle of Mathematical tsunami model using modified Adomian decomposition method

IV. APPLICATION

In this section, we apply the modified Adomian decomposition to tsunami modeling which have process as follow. Consider the one-dimensional homogeneous of tsunami modeling of the form:

$$\begin{aligned} \frac{\partial u}{\partial t} + u \frac{\partial u}{\partial x} + \frac{\partial \eta}{\partial x} &= 0 \\ \frac{\partial \eta}{\partial t} + u \frac{\partial \eta}{\partial x} + u \frac{\partial H}{\partial x} + \eta \frac{\partial u}{\partial x} + H \frac{\partial u}{\partial x} &= 0 \end{aligned} \quad (3)$$

Subject to the initial condition

$$\begin{aligned} u(x, 0) &= \frac{h}{\sqrt{d}} \sec h^2 \sqrt{\frac{3h}{4d^3}} x \\ \eta(x, 0) &= h \sec h^2 \sqrt{\frac{3h}{4d^3}} x \end{aligned} \quad (4)$$

and written (1) in form of derivative equation follow as

$$\begin{aligned} L_t u &= -uu_x - \eta_x \\ L_t \eta &= -u\eta_x - H_x u - \eta u_x - H u_x \end{aligned} \quad (5)$$

By the operator of sub-derivative L_t which have inverse operator $L_t^{-1}(\bullet)$ define by

$$L_t^{-1}(\bullet) = \int_0^t (\bullet) dw \quad (6)$$

Taking the inverse operator of (6) we obtain:

$$\begin{aligned} L_t^{-1} L_t(u) &= -L_t^{-1}(uu_x) - L_t^{-1}(\eta_x) \\ L_t^{-1} L_t(\eta) &= -L_t^{-1}(u\eta_x) - H_x L_t^{-1}(u) - L_t^{-1}(\eta u_x) - H L_t^{-1}(u_x) \end{aligned} \quad (7)$$

Or

$$\begin{aligned} u(x, t) &= u(x, 0) - L_t^{-1}(uu_x) - L_t^{-1}(\eta_x) \\ \eta(x, t) &= \eta(x, 0) - L_t^{-1}(u\eta_x) - H_x L_t^{-1}(u) - L_t^{-1}(\eta u_x) - H L_t^{-1}(u_x) \end{aligned} \quad (8)$$

Suppose the solution of $u(x, t)$ and $\eta(x, t)$ locate in form of infinity series form as follow

$$\begin{aligned} u(x, t) &= \sum_{n=0}^{\infty} u_n(x, t) \\ \eta(x, t) &= \sum_{n=0}^{\infty} \eta_n(x, t) \end{aligned} \quad (9)$$

and suppose term in non-linear form follow as

$$uu_x = \sum_{n=0}^{\infty} A_n, u\eta_x = \sum_{n=0}^{\infty} B_n, \eta u_x = \sum_{n=0}^{\infty} C_n \quad (10)$$

where the A_n , B_n and C_n are the Adomian polynomials [11].

By substituting (9) and (10) into (8) we obtain:

$$\begin{aligned} \sum_{n=0}^{\infty} u_n &= u(x, 0) - L_t^{-1} \left(\sum_{n=0}^{\infty} A_n \right) - L_t^{-1} \left(\sum_{n=0}^{\infty} (\eta_n)_x \right) \\ \sum_{n=0}^{\infty} \eta_n &= \eta(x, 0) - L_t^{-1} \left(\sum_{n=0}^{\infty} B_n \right) - H_x L_t^{-1} \left(\sum_{n=0}^{\infty} u_n \right) - L_t^{-1} \left(\sum_{n=0}^{\infty} C_n \right) - H L_t^{-1} \left(\sum_{n=0}^{\infty} (u_n)_x \right) \end{aligned} \quad (11)$$

By the modified Adomian decomposition method, suppose that $p = 1$ in (11) is rewritten as follow

$$\begin{aligned} \sum_{n=0}^{\infty} u_n &= u(x, 0) + L_t^{-1} \left(\sum_{n=0}^{\infty} a_n t^n \right) - p L_t^{-1} \left(\sum_{n=0}^{\infty} a_n t^n \right) - L_t^{-1} \left(\sum_{n=0}^{\infty} A_n \right) - L_t^{-1} \left(\sum_{n=0}^{\infty} (\eta_n)_x \right) \\ \sum_{n=0}^{\infty} \eta_n &= \eta(x, 0) + L_t^{-1} \left(\sum_{n=0}^{\infty} a_n t^n \right) - p L_t^{-1} \left(\sum_{n=0}^{\infty} a_n t^n \right) - L_t^{-1} \left(\sum_{n=0}^{\infty} B_n \right) - H_x L_t^{-1} \left(\sum_{n=0}^{\infty} u_n \right) \\ &\quad - L_t^{-1} \left(\sum_{n=0}^{\infty} C_n \right) - H L_t^{-1} \left(\sum_{n=0}^{\infty} (u_n)_x \right) \end{aligned} \quad (12)$$

When p is parameter which defines and determines as $a_n, n = 0, 1, 2, \dots$ to be unknown coefficient.



$$\begin{aligned} u_0(x, t) &= u(x, 0) + L_t^{-1} \left(\sum_{n=0}^{\infty} a_n t^n \right) \\ u_1(x, t) &= -p L_t^{-1} \left(\sum_{n=0}^{\infty} a_n t^n \right) - L_t^{-1} (A_0 + (\eta_0)_x) \\ u_2(x, t) &= -L_t^{-1} (A_1 + (\eta_1)_x) \\ u_3(x, t) &= -L_t^{-1} (A_2 + (\eta_2)_x) \\ &\vdots \end{aligned} \quad (13)$$

and

$$\begin{aligned} \eta_0(x, t) &= \eta(x, 0) + L_t^{-1} \left(\sum_{n=0}^{\infty} a_n t^n \right) \\ \eta_1(x, t) &= -p L_t^{-1} \left(\sum_{n=0}^{\infty} a_n t^n \right) - L_t^{-1} (B_0 + H_x u_0 + C_0 + H(u_0)_x) \\ \eta_2(x, t) &= -L_t^{-1} (B_1 + H_x u_1 + C_1 + H(u_1)_x) \\ \eta_3(x, t) &= -L_t^{-1} (B_2 + H_x u_2 + C_2 + H(u_2)_x) \\ &\vdots \end{aligned} \quad (14)$$

To avoid calculation of A_n , B_n and C_n By determine a_n , $n = 0, 1, 2, \dots$ which $u_1 = 0$ and $\eta_1 = 0$ show that $u_2 = u_3 = \dots = 0$ and $\eta_2 = \eta_3 = \dots = 0$

Determine $p = 1$ and solution of (3) written in term of infinity series follow as

$$\begin{aligned} u(x, t) &= \sum_{n=0}^{\infty} u_n(x, t) \\ &= u(x, 0) + L_t^{-1} \left(\sum_{n=0}^{\infty} a_n t^n \right) \end{aligned} \quad (15)$$

$$\begin{aligned} \eta(x, t) &= \sum_{n=0}^{\infty} \eta_n(x, t) \\ &= \eta(x, 0) + L_t^{-1} \left(\sum_{n=0}^{\infty} a_n t^n \right) \end{aligned} \quad (16)$$

From recurrence relation, the exact solution is derived as follow

$$\begin{aligned} u(x, t) &= u(x, 0) + L_t^{-1} \left(\sum_{n=0}^{\infty} a_n t^n \right) \\ &= \frac{h}{\sqrt{d}} \operatorname{sech}^2 \sqrt{\frac{3h}{4d^3}} x + \int_0^t (a_0 + a_1 t + a_2 t^2 + a_3 t^3 + \dots) dt \\ &= \frac{h}{\sqrt{d}} \operatorname{sech}^2 \sqrt{\frac{3h}{4d^3}} x + a_0 t + \frac{1}{2} a_1 t^2 + \frac{1}{3} a_2 t^3 + \frac{1}{4} a_3 t^4 + \dots \\ &= \frac{h}{\sqrt{d}} \operatorname{sech}^2 \sqrt{\frac{3h}{4d^3}} x + \frac{2h^2}{d} \sqrt{\frac{3h}{4d^3}} \operatorname{sech}^4 \sqrt{\frac{3h}{4d^3}} x \tanh \sqrt{\frac{3h}{4d^3}} x \\ &\quad + 2h \sqrt{\frac{3h}{4d^3}} \operatorname{sech}^2 \sqrt{\frac{3h}{4d^3}} x \tanh \sqrt{\frac{3h}{4d^3}} x t + \dots \end{aligned} \quad (17)$$

$$\begin{aligned} \eta(x, t) &= \eta(x, 0) + L_t^{-1} \left(\sum_{n=0}^{\infty} a_n t^n \right) \\ &= h \operatorname{sech}^2 \sqrt{\frac{3h}{4d^3}} x + \int_0^t (a_0 + a_1 t + a_2 t^2 + a_3 t^3 + \dots) dt \\ &= h \operatorname{sech}^2 \sqrt{\frac{3h}{4d^3}} x + a_0 t + \frac{1}{2} a_1 t^2 + \frac{1}{3} a_2 t^3 + \frac{1}{4} a_3 t^4 + \dots \\ &= h \operatorname{sech}^2 \sqrt{\frac{3h}{4d^3}} x + t \left(\frac{4h^2}{\sqrt{d}} \sqrt{\frac{3h}{4d^3}} \operatorname{sech}^4 \sqrt{\frac{3h}{4d^3}} x \tanh \sqrt{\frac{3h}{4d^3}} x \right. \\ &\quad \left. - \frac{mh}{2\sqrt{d}} \operatorname{sech}^2 \sqrt{\frac{3h}{4d^3}} x \right. \\ &\quad \left. + 2H(x) \frac{h}{\sqrt{d}} \sqrt{\frac{3h}{4d^3}} \operatorname{sech}^2 \sqrt{\frac{3h}{4d^3}} x \tanh \sqrt{\frac{3h}{4d^3}} x \right) \end{aligned} \quad (18)$$

By $H(x) = m(x - 100)$ is the depth from mean sea level and m is the slope level of coast.

V. RESULTS

The result of solution calculation is expressed by using tsunami equation in (17) as shown in Fig.2 which x-axis is distance in horizontal, y-axis is velocity of tsunami wave which shown in different time from $t = 0, 2, 4, 6, 8, 10$. It is implied that when the velocity of tsunami wave rip off the coast, the velocity of wave is decrease. If consider the time and velocity, it is found that when time is increase, velocity is also increase in the same way.

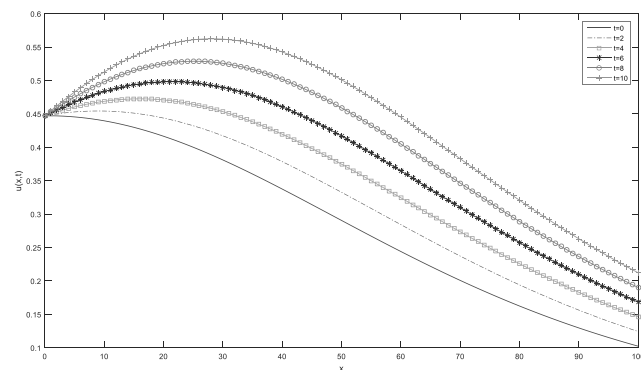


Fig. 2. The graph of the velocity of tsunami wave $u(x, t)$ at $0 \leq x \leq 100$ and $t = 0, 2, 4, 6, 8, 10$.

The next result is illustrated the relationship between distance in horizontal and surface elevation of tsunami wave from (18) at $H(x)$ in 3 level of slope level of coast $m = 0.2, 1, 5$ as shown in Fig. 3-5 respectively. With the graph, the x-axis is distance in horizontal, y-axis is surface elevation of tsunami and each graph line in figure show the different time from $t = 0, 2, 4, 6, 8, 10$ respectively.

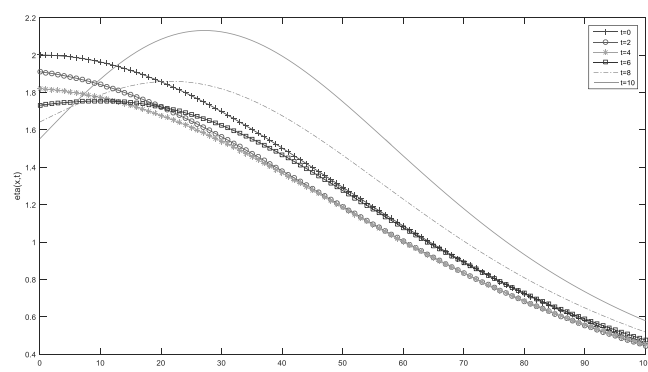


Fig. 3. The graph of the surface elevation of tsunami wave $\eta(x,t)$ at $m = 0.2$, $0 \leq x \leq 100$ and $t = 0, 2, 4, 6, 8, 10$.

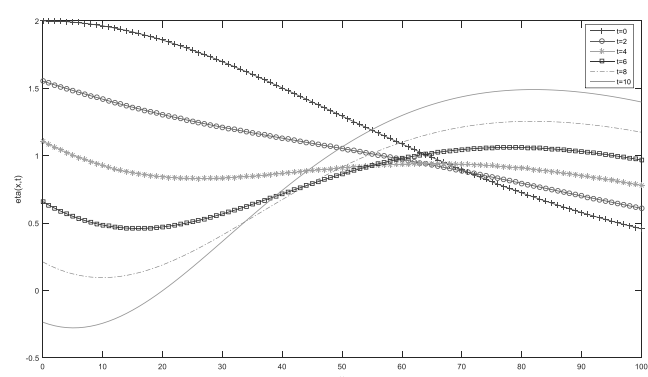


Fig. 4. The graph of the surface elevation of tsunami wave $\eta(x,t)$ at $m = 1$, $0 \leq x \leq 100$ and $t = 0, 2, 4, 6, 8, 10$.

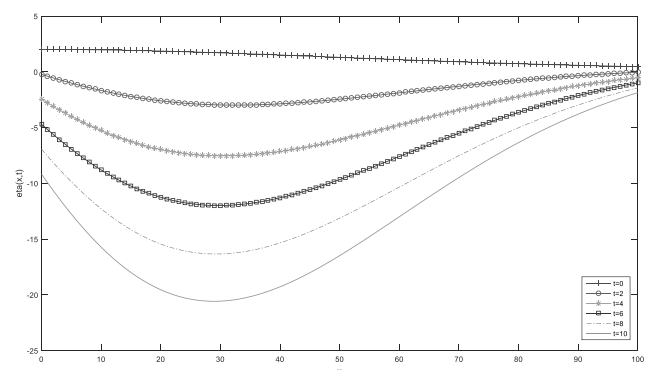


Fig. 5. The graph of the surface elevation of tsunami wave $\eta(x,t)$ at $m = 5$, $0 \leq x \leq 100$ and $t = 0, 2, 4, 6, 8, 10$.

When consider the height of tsunami as shown in Fig. 3-5, it is implied that when tsunami wave rip off to the coastal, the wave height has increase because mass of water bumps to coast lift up to on shore. The tsunami wave height is vary to

slope of coastal. The slope higher, the of tsunami is rapidly increase and when over-time pass the wave heigh is decrease to the normal level.

VI. CONCLUSION

In this research, the mathematical model of tsunami wave one dimension is proposed. The behavior of velocity and wave height of traveling tsunami wave is studied. The model Adomian decomposition method is applied to find the solution as local analytical solutions which use to explain the phenomena of tsunami in short duration and distance. In short duration and distance, the slope of coastal is essential factor which make high velocity and wave height and affect to the damage of tsunami attack.

ACKNOWLEDGEMENT

The author gratefully acknowledges the financial support from the Division of Mathematics, Faculty of Science, Maejo University, Chiangmai, Thailand.

REFERENCES

- [1] A. G. Marchuk and A. A. Anisimov, "A method for numerical modeling of tsunami run-up on the coast of an arbitrary profile," ITS 2001 Proceedings. session 7, 2001, pp. 7-27.
- [2] D.H. Peregrine and S.M. Williams, "Swash overtopping a truncated plane beach. Journal Fluid Mechanics," Vol. 440, 2001, pp. 391-399.
- [3] P. L-F. Liu, "Tsunami modeling," Class of 1912 Professor School of Civil and Environmental Engineering Cornell University Ithaca, NY USA, 2013, pp. 1-40.
- [4] A. G. Samaras, Th. V. Karambas, and R. Archetti, "Simulation of tsunami generation, propagation and coastal inundation in the Eastern Mediterranean," Ocean Sci., vol.11, pp. 643-655, 2015.
- [5] M. Romano, S. Liong, M. T. Vu, P. Zemskyy, C. D. Doan, M. H. Dao, and P. Tkalic, "Artificial neural network for tsunami forecasting", Journal of Asian Earth Sciences, vol. 36, pp. 29-37, 2009.
- [6] S. Tinti, I. Gavagni, and A. Piatanesi, "A finite -element numerical approach for modeling tsunamis", Annali Di Geofisica, vol. XXXVII, no. 5, pp. 1009-1026, September 1994.
- [7] U. Drähne, N. Goseberg, S. Vater, N. Beisiegel and J. Behrens, "An experimental and numerical study of long wave run-up on a plane beach" Journal of Marine Science and Engineering, vol. 4, no. 1, pp. 1-23, 2016.
- [8] P. L-F. Liu, Tsunami Modeling, Cornell University, USA, 2013, pp.1-40
- [9] J. Biazar and K. Hosseini, "A modified Adomian decomposition method for singular initial value Emden-Fowler type equations", International Journal of Applied Mathematical Research, vol. 5, no. 1, pp. 69-72, 2016.
- [10] S. Boonyapibanwong, "Analytical solutions of a model of tsunami run-up on the coast using Adomian decomposition method" (Master's Thesis, King Mongkut's Institute of Technology North Bangkok, Bangkok, 2007.
- [11] V.SengK.Abboui and Y.Cherruault, "Adomian's polynomials for nonlinear operators", Mathematical and Computer Modelling, vol. 24, no. 1, pp. 59-65, 1996.



Dynamic Capability Assessment

Jarut Kunanoppadol* and Supachai Wasananon
Department of Mechanical Engineering,
Faculty of Engineering and Industrial Technology
Silpakorn University, Thailand
kunanoppadol_j@su.ac.th

Abstract—This paper developed items for assessing dynamic capability based on House of Dynamic Capability model. Dynamic capability consists of four components including sensing, seizing, reconfiguring, and integrating capabilities. We collected empirical data from 506 manufacturing firms in high and medium-high technological industries by quantitative survey. Data was analyzed with partial least square structural equation modelling technique. The results indicated acceptable reliability and validity of items in our questionnaire. Items significantly loaded to their latent variables, and all latent variables respectively loaded to dynamic capability.

Keywords—dynamic capability; assessment; house of dynamic capability; structural equation modelling

I. INTRODUCTION

Under the rapid change of business environment, firms need to continuously detect the change and adapt themselves for survive and maintain their sustainable growth. Over the last two decade, Dynamic capability (DC) perspective arose to explain the source of enterprise-level advantage, and provide guidance to manage for avoiding the zero profit condition when homogenous firms compete in perfectly competitive market [1]. DC is appropriate for a dynamic environment, while resource-based view perspective is appropriate for static environment. Teece et al. (1997) originally defined DC as “the firm’s ability to integrate, build, and reconfiguration internal and external competence to address rapidly changing environments” [2]. Eisenhardt and Martin (2000) also defined DC as “the firm’s process that use resources to match and even create market change” [3]. Helfat et al. (2007) defined DC as “the capability of an organization to purposefully create, extend, and modify its resource” [4]. Resources include both tangible, intangible, human, and capabilities which firms own, control, or can access to.

Meta-analysis results from our previous study found that DC positively associate with firm performance ($R=0.356$, $Z=12.965$, $P<0.001$). We therefore designed research projects to study not only the effects of DC on other capabilities, but also investigate the impact of DC on firm performance. We developed ‘Dynamic Capability Assessment’ from literature, and tested it by quantitative data.

This paper aimed presented the method to assess dynamic capability. We provide set of questions developed from

literature. We tested them with quantitative survey with manufacturers in high and medium-high technology industries in Thailand. The results showed all items loading on all components of DC. The set of questions can be used for assess DC in further study.

This paper was organized as follows: We explained the house of DC concept and literature review in part II. Part III described research methodology including population, sample, and data collection. Part IV presented our finding. Discussion and conclusion were in the last part. Moreover, in appendix, we provided list of questions for assess DC in our work.

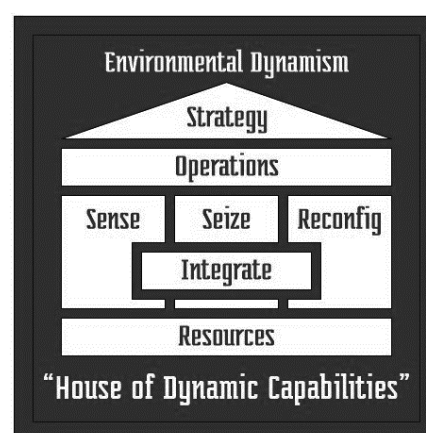


FIGURE I. House of DC

II. LITERATURE REVIEW

A. House of Dynamic Capability

The components in DC were various until Wilden et al. (2016) systematically review DC articles published in leading journals, then present the architectural model entitle “House of DC” [5]. That model defined firm as a house. Neighboring houses are competitor and other firms in same industry, and firms in other industries. All house are under the same business environment. Three main pillars of DC are sensing, seizing, and reconfiguring capability. DC is the linkage between firm’s resources and their operational capability. This concept mentioned that stair and door are the links rooms and floors



within the firms, and window is the linkage to external firms. Many articles defined integrating capability as one component of DC [6]–[9], we therefore add it to our model (see Figure I).

In our model, DC consists of four capabilities. (1) Sensing capability (SNC) is abilities to detect and understand the rapid change of environment, opportunities, and threat. Some authors called it as recognizing capability [10], [11] or sense making capability [12]. (2) Seizing capability (SNZ) is abilities to take benefit or quickly respond to the change of opportunity. Some authors called it as decision-making capability [12], [13]. (3) Reconfiguring capability (RCC) is abilities to change the structure and arrangement the processes. Some authors called it as adaptive capability [14], capitalizing capability [11], or change implementation capability [12], [13]. and (4) Integrating capability is abilities to collaborate within functions and levels in the firm, and collaboration between external firms. Some authors called it as aligning capability [15].

B. Literature review

Most of DC studies the effects of DC on firm performance by adding other variables in their model. Literature studied the effect many variables on firm performance through DC as mediator; for example, resource stoke [10], willingness for external partner's cooperation [16], process alignment [17], learning culture [18], structural and rational embeddedness [19], responsible downsizing strategy [20], market orientation [21], international diversification [11] and firm performance. Wilden and Gudergan (2015) found that DC positively affect operational capability in high competitive turbulence, but it negatively affect operational capability in low competitive turbulence [22]. They also found that marketing capability significantly affect firm performance in high competitive turbulence, while technological significantly affect firm performance in low competitive turbulence. Our meta-analysis result found the relationship between DC and operational capability is the highest value ($R=0.546$, $Z=14.936$, $P<0.001$). In our research project, we studied the effect of DC, operational capability, market orientation, and environmental dynamism on new product success.

III. METHODOLOGY

A. Questionnaire design

We selected questions for assess four components of DC from two groups of literature. Questions for assess sensing, seizing, and reconfiguring capabilities were from first group [12], [13], [23], while questions to assess integrating capability were from second group [7]–[9]. We selected only questions which had loading excess the threshold of 0.4 [24]. We used three highest loading for each capabilities. Hence, we had twelve questions for assessing DC in four components. The questions were translated into Thai, and then we confirmed the validity of translation with back translation technique. There was no translation problem. We arranged Thai question into questionnaire for data collection phase.

B. Population and Sample

Population of this work was manufacturers in high and medium-high technology [25] including pharmaceutical (C21), electronic (C26), aircraft (C303), chemical (C20), weapon (C252), electrical equipment (C27), machinery (C28), automotive (C29), transportation equipment (C30), and medical instrument (C325).

Figure II showed the process to deal with research population and sample. First, we searched the list of factories in the Department of Industrial Work (www.diw.go.th) by using Thai standard industrial classification (TSIC) for search. In this process, we discovered 15,852 factories. Second, we manually checked those lists on the Department of Business Development (www.dbd.go.th) to confirm these following criteria: (1) They are company limited or public company limited. (2) They still operate. (3) TSIC is correct. This process reduced population to 4,185 firms. After removing duplication, we had 3,776 firms in the list. Third, we manually checked financial data to classified firm size by fix-asset value. After removing firms with out-of-date financial data, we had 3,690 firms. In pilot study, we found a problem to collect data from micro firms. For example, some firms have few staff and they do not have a managerial structure. Some are very new firm. Some have financial problem. We therefore removed micro firm from the list. Hence, the research population was 2,197 manufacturing firms in high and medium-high technological industries of Thailand.

Sample size was calculated with three method [26]–[28] with 95% confidence level, 50% proportion of an attribution, and 5% level of precision, and used the highest value of 86 firms. We used stratified sampling based on industry and firm size. Within each groups, we used randomized sampling.

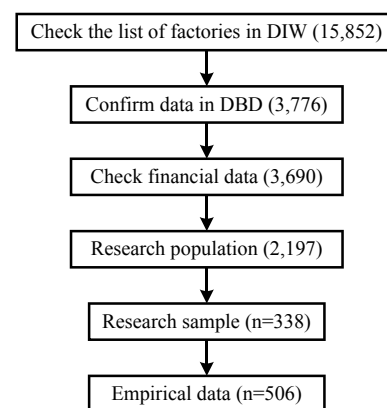


FIGURE II. Population and Sample

C. Data collection

We invited firm to participate research by phone, and then sent the survey package by postal or email. We follow up by phone after one week later. We sent out 1,240 package, and received usable 506 questionnaire. The respond rate was 40.81%.



IV. RESULTS

A. Reliability and Validity analysis

Indicator reliability was checked by considering factor loading of items. One item in sensing capability (SNC2) had loading lower than threshold 0.40 [24]. We therefore removed this item from the calculation. The remaining items had loading range between 0.727 to 0.879, indicated that items significantly load to latent variables [29].

Internal consistency reliability was checked with Cronbach's alpha. Overall alpha was 0.846. The alpha of sensing capability was 0.527 because we removed SNC2 from calculation (The alpha before removing SNC2 was 0.622). The remaining variables had alpha range between 0.675 to 0.781 exceeding the threshold 0.60 [30] indicating internal consistency of items.

Composite reliability (CR) indicated the level of measurement of item on latent variables. The items had CR range between 0.806 to 0.872 the threshold 0.60 [23]. CR is the most common to measure construct internal consistency because it focus on items reliability to estimate the model [31].

Convergent validity indicating consistency of items was considered with average variance extracted (AVE). Items had AVE range between 0.608 to 0.695 exceeding the threshold 0.40 [32], and AVE of each variables were higher than their CR [12]. High AVE indicate that the items variance is higher than error indicating acceptable convergent validity.

Discriminant validity was considered by square root of AVE higher than correlation. Table I showed correlation between latent variables, and square root of AVE in parenthesis. The results indicate good discriminant validity.

Common method bias was checked with Harman's single factor test [33]. The maximum percentage of variance was 44.384% lower than the threshold 50% [12] indicating no common method bias problem.

Non-response bias was checked by comparing data of early and late respondents [34]. The P-value range between 0.127 to 0.432 indicated no significant difference between two groups.

TABLE I. Correlation analysis

Capability	SNC	SZC	RCC	INC
SNC: Sensing	(0.822)			
SZC: Seizing	0.565**	(0.834)		
RCC: Reconfiguring	0.487**	0.515**	(0.821)	
INC: Integrating	0.498**	0.635**	0.623**	(0.780)

Value in parentheses are square root of AVE. ** is 0.01 significant level.

B. Findings

Data was analyzed with Partial Least Square Structural Equation Modelling (PLS-SEM) technique. We used SmartPLS software. We generated a factor analysis path model. In the model, all items measured by questionnaire were observed variable. Four components of dynamic capability were first order latent variables. Dynamic capability was second-order latent variable. We ran PLS algorithm to evaluate

loading of items on their latent variables, and then ran Bootstrapping to investigate significance of item loadings.

Table I showed correlations between latent variables. All variables significantly associated with others. Integrating capability highly correlate with seizing and reconfiguring capability. Correlation between sensing capability and reconfiguring capability found to be the lowest. Table II showed the cross loading of items of latent variables. The results indicated no cross loading problems.

Figure III illustrated the result model. All items significantly loaded to their latent variables, and all latent variables respectively loaded to DC.

TABLE II. Cross loading results

	SNC	SZC	RCC	INC
SNC1	0.769	0.388	0.365	0.351
SNC3	0.873	0.613	0.472	0.443
SZC1	0.510	0.810	0.410	0.331
SZC2	0.536	0.879	0.54	0.436
SZC3	0.512	0.810	0.621	0.468
RCC1	0.486	0.624	0.868	0.458
RCC2	0.381	0.519	0.859	0.476
RCC3	0.396	0.402	0.728	0.461
INC1	0.409	0.405	0.566	0.727
INC2	0.342	0.363	0.395	0.839
INC3	0.381	0.392	0.339	0.769

SNC2 was removed.

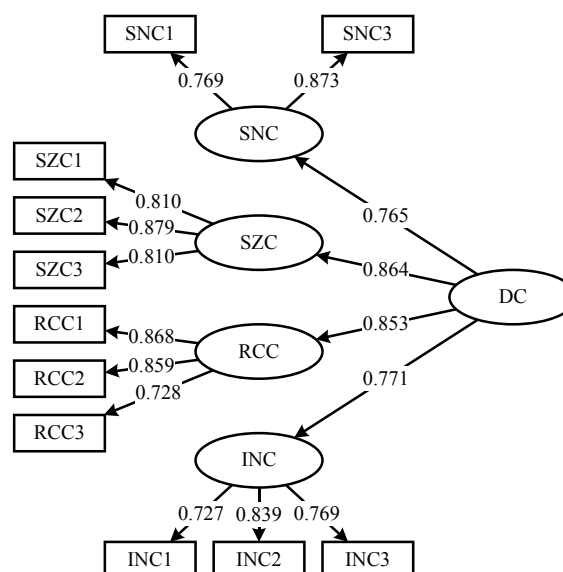


FIGURE III. Result model

V. DISCUSSION AND CONCLUSION

A. Discussion

This paper presented dynamic capability assessment. We developed items from literature and tested them with empirical data from quantitative survey. We found only one problem on the item to measure sensing capability. It had low factor



loading; hence, we had to remove it from our analysis. We checked other questions to measure sensing capability from literature [12], [13] as follow:

- We often have meetings to discuss the market demand.
- We can fully understand the impact of internal and external environment.
- We have perfect information management system.

However, Lee and Rha (2016) removed these three items from their analysis [23].

We will keep SNC2 in our further work to collect data for other industry and try other analysis method to figure out why it show low factor loading.

The remaining items were good for assess dynamic capability under the House of DC model. To control the length of questionnaire, and avoid the non-response problem, measuring each components with three items was enough because we had to collect other capabilities and new product success.

B. Limitation of this work

Our work had three limitations. First, we collected data from only manufacturers. Service and trading firms were not included in our research. Moreover, the data was collect from high and medium-high technological industries. We still needed data from medium-low and low technological industries to fulfill the gap of data. Second, since we collect other variables in our project including operational capability, market orientation, environmental dynamism, and new product success. To control the length of questionnaire, we had to collect only three items for sub-variables. We therefore had limitation to play with items.

C. Future study

Since collecting data from manufacturers in other industries is in our pipeline, we therefore suggest some ideas for further study. First, author can modify our items to assess dynamic capability on service or trading firms. Logically, all firms are in the same eco system. The business environment changes very fast. All firms (manufacturing, service, and trading) need to detect and adapt themselves to serve on the rapid change of this business environment. Second, although quantitative evidence indicated positive relationship between dynamic capability and firm performance, the research in this area still need qualitative evidence to confirm and answer the 'why and how' questions. Authors can do qualitative study in this area with small sample, or do case study research.

D. Conclusion

We developed a set of questions to assess dynamic capability. The twelve questions were classified into four capabilities: sensing, seizing, reconfiguring, and integrating capability. Empirical date was collect form 506 manufacturing firms in high and medium-high technological industries. Data was analyzed with PLS-SEM technique. The result highlight a

problem of one item in sensing capability that need further work to find a solution. The remaining items had good reliability and validity. They all loaded to their latent variables significantly. Four capabilities also loaded to dynamic capability. This set of questions can be used for dynamic capability assessment for our further works.

ACKNOWLEDGMENT

We thanks for the Department of Mechanical Engineering, Faculty of Engineering and Industrial Technology, Silpakorn University for supporting this project. We also thanks for reviewer and editors of this conference.

REFERENCES

- [1] D. J. Teece, "Explicating dynamic capabilities: The nature and microfoundations of (sustainable) enterprise performance," *Strateg. Manag. J.*, vol. 28, no. 13, pp. 1319–1350, 2007.
- [2] D. J. Teece, G. Pisano, and A. Shuen, "Dynamic capabilities and strategic management," *Strateg. Manag. J.*, vol. 18, no. 7, pp. 509–533, Aug. 1997.
- [3] K. M. Eisenhardt and J. A. Martin, "Dynamic capabilities: What are they?," *Strateg. Manag. J.*, vol. 21, no. 10/11, pp. 1105–1121, 2000.
- [4] C. E. Helfat et al., *Dynamic capabilities: Understanding strategic change in organizations*, 1 edition. Malden, MA: Wiley-Blackwell, 2007.
- [5] R. Wilden, T. M. Devinney, and G. Dowling, "The Architecture of Dynamic Capability Research: Identifying the Building Blocks of a Configurational Approach," Social Science Research Network, Rochester, NY, SSRN Scholarly Paper ID 2723201, Jan. 2016.
- [6] H. Jiao, I. Alon, and Y. Cui, "Environmental dynamism, innovation, and dynamic capabilities: The case of China," *J. Enterprising Communities People Places Glob. Econ.*, vol. 5, no. 2, pp. 131–144, May 2011.
- [7] Y. Lin and L.-Y. Wu, "Exploring the role of dynamic capabilities in firm performance under the resource-based view framework," *J. Bus. Res.*, vol. 67, no. 3, pp. 407–413, Mar. 2014.
- [8] H. Makkonen, M. Pohjola, R. Olkkonen, and A. Koponen, "Dynamic capabilities and firm performance in a financial crisis," *J. Bus. Res.*, vol. 67, no. 1, pp. 2707–2719, Jan. 2014.
- [9] W. Jiang, F. tinoziva Mavondo, and M. J. Matanda, "Integrative capability for successful partnering: A critical dynamic capability," *Manag. Decis.*, vol. 53, no. 6, pp. 1184–1202, Jul. 2015.
- [10] J. (Jon) Liao, J. R. Kickul, and H. Ma, "Organizational dynamic capability and innovation: An empirical examination of internet firms," *J. Small Bus. Manag.*, vol. 47, no. 3, pp. 263–286, Jul. 2009.
- [11] H. Wu, J. Chen, and H. Jiao, "Dynamic capabilities as a mediator linking international diversification and innovation performance of firms in an emerging economy," *J. Bus. Res.*, vol. 69, no. 8, pp. 2678–2686, Aug. 2016.
- [12] V. Wohlgemuth and M. Wenzel, "Dynamic capabilities and routinization," *J. Bus. Res.*, vol. 69, no. 5, pp. 1944–1948, May 2016.
- [13] D. Li and J. Liu, "Dynamic capabilities, environmental dynamism, and competitive advantage: Evidence from China," *J. Bus. Res.*, vol. 67, no. 1, pp. 2793–2799, Jan. 2014.
- [14] K. Z. Zhou and C. B. Li, "How strategic orientations influence the building of dynamic capability in emerging economies," *J. Bus. Res.*, vol. 63, no. 3, pp. 224–231, Mar. 2010.
- [15] O. J. Borch and E. L. Madsen, "Dynamic capabilities facilitating innovative strategies in SMEs," *Int. J. Technoentrepreneurship*, vol. 1, no. 1, pp. 109–125, Jan. 2007.
- [16] L.-Y. Wu, "Entrepreneurial resources, dynamic capabilities and start-up performance of Taiwan's high-tech firms," *J. Bus. Res.*, vol. 60, no. 5, pp. 549–555, May 2007.
- [17] R. Y. Y. Hung, B. Yang, B. Y.-H. Lien, G. N. McLean, and Y.-M. Kuo, "Dynamic capability: Impact of process alignment and organizational



- learning culture on performance,” *J. World Bus.*, vol. 45, no. 3, pp. 285–294, Jul. 2010.
- [18] S. Chien and C. Tsai, “Dynamic capability, knowledge, learning, and firm performance,” *J. Organ. Change Manag.*, vol. 25, no. 3, pp. 434–444, May 2012.
- [19] S. Zheng, W. Zhang, and J. Du, “Knowledge-based dynamic capabilities and innovation in networked environments,” *J. Knowl. Manag.*, vol. 15, no. 6, pp. 1035–1051, Oct. 2011.
- [20] P. C.-F. Tsai and C.-T. Shih, “Responsible downsizing strategy as a panacea to firm performance: The role of dynamic capabilities,” *Int. J. Manpow.*, vol. 34, no. 8, pp. 1015–1028, Nov. 2013.
- [21] D. Monferrer, A. Blesa, and M. Ripollés, “Born globals trough knowledge-based dynamic capabilities and network market orientation,” *Bus. Res. Q.*, vol. 18, no. 1, pp. 18–36, Jan. 2015.
- [22] R. Wilden and S. P. Gudergan, “The impact of dynamic capabilities on operational marketing and technological capabilities: investigating the role of environmental turbulence,” *J. Acad. Mark. Sci.*, vol. 43, no. 2, pp. 181–199, Mar. 2015.
- [23] S. M. Lee and J. S. Rha, “Ambidextrous supply chain as a dynamic capability: Building a resilient supply chain,” *Manag. Decis.*, vol. 54, no. 1, pp. 2–23, Jan. 2016.
- [24] J. F. Hair, C. M. Ringle, and M. Sarstedt, “PLS-SEM: Indeed a silver bullet,” *J. Mark. Theory Pract.*, vol. 19, no. 2, pp. 139–152, Apr. 2011.
- [25] J. Thoma, L. Carmen, and A. Digna, “High-technology and medium-high technology industries main drivers of EU-27’s industrial growth,” Eurostat: Statistics in focus, 2013.
- [26] T. Yamane, *Statistics: An Introductory Analysis*, International 3 Revised ed edition. Joanna Cotler Books, 1973.
- [27] R. V. Krejcie and D. W. Morgan, “Determining Sample Size for Research Activities,” *Educ Psychol Meas*, 1970.
- [28] W. G. Cochran, *Sampling Techniques, 2nd Edition*, 2nd edition. New York: John Wiley & Sons Ltd, 1963.
- [29] J. C. Anderson and D. W. Gerbing, “Structural equation modeling in practice: A review and recommended two-step approach,” *Psychol. Bull.*, vol. 103, no. 3, p. 411, 1988.
- [30] J. C. Nunnally and I. H. Bernstein, *Psychometric Theory*, 3rd edition. New York: McGraw-Hill, 1994.
- [31] J. F. Hair, M. Sarstedt, C. M. Ringle, and J. A. Mena, “An assessment of the use of partial least squares structural equation modeling in marketing research,” *J. Acad. Mark. Sci.*, vol. 40, no. 3, pp. 414–433, May 2012.
- [32] A. Diamantopoulos, “Incorporating formative measures into covariance-based structural equation models,” *MIS Q*, vol. 35, no. 2, pp. 335–358, Jun. 2011.
- [33] P. M. Podsakoff and D. W. Organ, “Self-reports in organizational research: Problems and prospects,” *J. Manag.*, vol. 12, no. 4, pp. 531–544, Dec. 1986.
- [34] M. Falasca, J. Zhang, M. Conchar, and L. Li, “The impact of customer knowledge and marketing dynamic capability on innovation performance: an empirical analysis,” *J. Bus. Ind. Mark.*, vol. 32, no. 7, pp. 901–912, Jul. 2017.

APPENDIX

TABLE A-I. Lists of questions and descriptive statistics

Construct / Questions		SFL	T	Mean	SD
Dynamic capability (Alpha=0.846, CR=0.880, AVE=0.407)					
<i>Sensing capability (Alpha=0.527, CR=0.806, AVE=0.676)</i>		0.765	34.772**		
SNC1	We perceive environmental change before competitors.	0.769	26.611**	3.628	0.695
SNC2	We feel the major potential opportunities and threats. (Removed)	(-0.110)	(0.259)	3.828	0.546
SNC3	We have a good observation and judgment ability.	0.873	71.073**	3.773	0.702
<i>Seizing capability (Alpha=0.781, CR=0.872, AVE=0.695)</i>		0.864	35.623**		
SZC1	We quickly deal with conflicts in the strategic decision-making process.	0.810	33.478**	3.625	0.777
SZC2	We make timely decisions to deal with strategic problems under many circumstances.	0.879	68.637**	3.589	0.721
SZC3	We reconfigure resources in time to address environmental change.	0.810	41.888**	3.824	0.688
<i>Reconfiguring capability (Alpha=0.755, CR=0.860, AVE=0.674)</i>		0.854	32.942**		
RCC1	We successfully realign or reinvent resources in response to market change.	0.868	73.290**	3.828	0.723
RCC2	We successfully reconfigure resources to come up with new productive assets.	0.859	50.182**	3.802	0.766
RCC3	We engage in resource re-combinations to better match the product-market areas.	0.728	22.767**	3.874	0.698
<i>Integrating capability (Alpha=0.675, CR=0.822, AVE=0.608)</i>		0.771	16.251**		
INC1	We integrate industry related technologies to develop new product.	0.727	24.495**	3.791	0.692
INC2	We use networks as knowledge resources.	0.839	43.764**	3.798	0.689
INC3	We share information frequently with networks.	0.769	28.927**	3.686	0.782

Alpha is Cronbach’s alpha. CR is composite reliability, AVE is average variance extracted. SFL is standard factor loading. ** is 0.01 significant level



Building a Crack Processing Toolkit

Software tools for measuring building cracks

Wangwon Khorchaiyaphum, John Morris, Krit
Chaimoon, Sahalaph Homwuttiwong
Faculty of Engineering
Mahasarakham University,
Mahasarakham 44150, Thailand
john.m@msu.ac.th

Preetham Kumar Konda
Indian Institute of Technology
Karaghpur, India

Abstract—The geometry and propagation of cracks in concrete or brick walls can give us advance warning of a potential building collapse. This is particularly important after earthquakes, when many building need to be assessed rapidly under difficult situations, so the ability to take and process images of problems is a key to saving lives from collapse of unsafe buildings. Cameras allow remote and safe access to possible dangers. However, cracks take many forms and have many different environments, so, in this project we built a library of tools for handling different environments allowing the full geometry and time evolution of a crack to be determined rapidly. Most of our test images were obtained in our civil testing laboratory, where a variety of beams were marked up in many different ways by successive groups of students. We also show how to collect and register sequences of images collected from a drone, possibly over long periods of time.

Keywords—Crack; Detection; Geometry; Processing; Software library

I. INTRODUCTION

After an earthquake, emergency response teams face the need to urgently recognize buildings which potential hazards because of structural damage. If the building is not actually moving, then teams will try to monitor visible cracks in the walls as indicators of structural faults, but these cracks may develop slowly – as a result of inherent internal damage, aftershocks or slow subsidence. Many cracks may be inaccessible, either on higher floors or blocked by rubble. Thus capturing images with cameras for subsequent processing is a key safety aid, when traditional techniques, eg placing a ruler against the crack, are infeasible. Simple techniques are also error-prone and slow and laborious, especially when the full extent of a crack needs to be determined. In principle, following cracks in flat walls would appear to be a simple, easily solved problem, but real (and therefore interesting) scenes show a host of difficulties.

A. Previous work

Several reviews have discussed aspects of this problem [1]. However, many of these focus on single types of cracks or walls, eg Hoang's 2018 review, which has a uniform

background [1]. Mohan and Poobal's more extensive review covers many approaches reported up until 2016 [2]. A large number of approaches rely on various applications of common algorithms – thresholding, Sobel, Canny edge detection, Otsu segmentation [6], etc. Nguyen et al detect cracks by applying their Phase Symmetry-Based Crack Enhancement Filter which responds to the common properties of cracks and, importantly, rejects simple edges [5].

The measurement of faults in road surfaces is an important area and has some overlap with our problem. A study by Oliveira and Correia discusses this and extensively reviews work on detecting and characterizing cracks in road surfaces [4]. Other applications requiring crack detection include cracked particles in wrought aluminum alloys [7]. German et al describe a framework for automating collection of earthquake damage data but use only basic image processing tools in simple scenarios [8].

Here we did not search for a 'universal' solution: instead, we aimed to build a collection of processing steps that can be applied to the problem at hand. We assume that we can observe the task and its characteristics and put together a data flow that will handle the observed cracks. This is reasonable for the problems that we want to tackle. With the laboratory research problems, we captured videos first and have time to select the tools appropriate for the structures to be studied. For earthquakes, we assume that, after capturing one image, we can choose the tools to be used for images captured the next day. If we are checking for slow subsidence, we use the same procedure with longer time intervals.

B. Observed Problems

We might expect that tracking a dark crack in a lighter surface would be easy and an exercise that we might ask a new image processing student to complete in a day. However, in real cracks, a host of problems arise, so that simple choosing a threshold in gray-scale image would suffice. These include

- Very narrow cracks are illuminated to some depth by ambient light.



- Concrete edges collapse as the crack forms, making their apparent width larger.
- Rubble accumulates and appears lighter.
- Paint is lost and can cause the underlying concrete to be considered part of a crack.
- Reinforcing fibre (*eg* steel wires) remains in the crack and can reflect ambient light strongly.
- Cracks sometime propagate in the depth of the material (or under paint) and do not appear at the surface for some time, causing a single crack to appear as multiple disjointed cracks.
- Additional dark marks: some enthusiastic students carefully added fiducial marks to some beams for metrology. So simplistic software finds many straight (and parallel and totally unrealistic) 'cracks'.

Fig 1 shows a sample of the cracks that we have collected and studied. Note that they range from bare concrete to newly painted surface and include additional fiducial marks added in a variety of styles by students studying the beams for understanding strength and fracture patterns. There is also a challenging weathered wall, where the paint has been partially lost, causing software to find many 'false' cracks at paint edges. A partial view of the press used to crack beams in also shown (left, centre). Fig 2 shows a pair of drone images which are matched (registered) so that crack geometry can be calculated in a common reference.

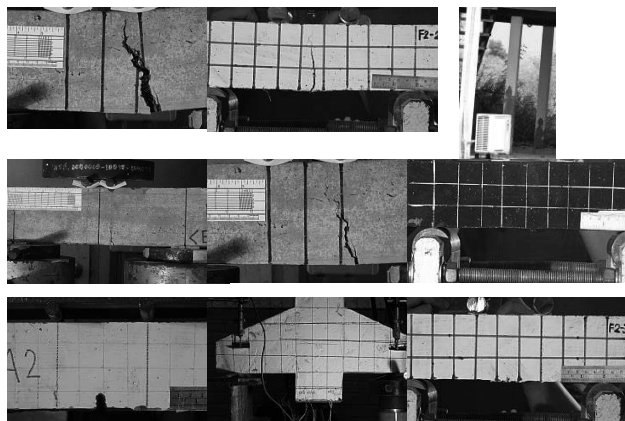


Fig 1: Variety of beam and building cracks that we have collected as test cases and processed. For the beams cracked in the laboratory, advanced cracks are shown: in the early stages they are not visible until they are a few pixels wide.

II. OPERATION

Here, we describe the data structures and methods needed to handle a variety of cracks.

A. Data Structure

A model, a C++ class, **BCrack**, is created for each separate crack found. Attributes include

Name	Data type	
BCrack	class	
Start	Point	
Original image	Mat	
Bounding box	Rect	
Mark mask	Mat	
Mark threshold	double	
Grey image	Mat	
Mark colour[]	RGB	
Crack area	double	
Crack Left, Right	CrackPoint[]	
Visited	Mat	
Predecessors	Mat<Point>	
Crack end	Vector<Point>	

B. Class methods

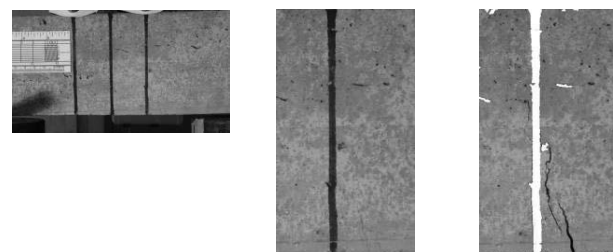
A list of the key functions built for our toolbox and brief descriptions of their operations follows.

1) Registration



Fig 2. Drone Images: Image on the right, taken from a different view at a later time, is registered to the image on the left, captured at an earlier time

When images are captured from moving platforms (*eg* a drone) or collected from 'close' locations over time (*eg* when daily records are captured for a building suspected of becoming a hazard), we need to register cracks to some arbitrary 'reference' crack - typically the first one captured for a given crack. We used OpenCV registration functions to generate a homography which allows subsequent images to be registered with the first one. Note that drone images are currently acquired without supporting calibration scales (visible in many of the beams, *eg* those in Fig 1). As this stage, subject to further analysis and discussion with experts in, *eg* earthquake studies, we believe that accurate calibration is not necessary. The key metric will be the growth of a crack relative to some initial observation: hazard assessment teams will be satisfied with a ranking that allows them to focus, for further assessment, on buildings showing the largest relative change in crack width and length.



Original image

Selected area

Mark masked

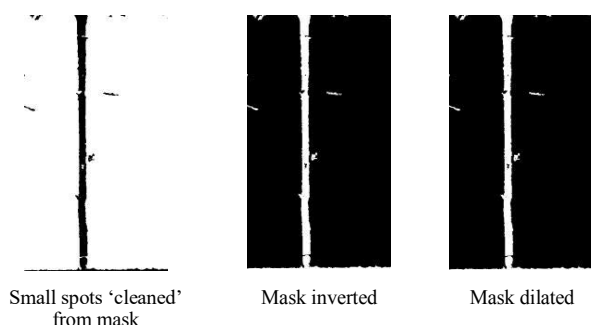


Fig 3. Steps in processing a beam: In this experiment, a concrete beam (top left) was deliberately cracked in a press in our laboratory as part of a another research project, for which fiducial marks were added to the beam. Top right shows the detected crack (contoured in red).

2) Removing marks

This step masks out the marks added to the images – either naturally occurring marks or ones added as fiducial marks. Since, in real situations, we have little control over the colour and size of such marks, we ask the operator to click on a representative mark of each colour in the image. The OpenCV `floodFill` function is then used to identify the full mark. Usually, a number of small spots remain, contours were drawn around them. Large contours were added to the mark mask and small ones treated as noise and left in place. Later, some cracks may pass through these points, so all must be retained. Cracks passing through added marks are treated in a separate pass. Finally, to allow for flooding of the mark image into surrounding pixels, which have intensities between those of the mark and the base wall, the marks were dilated by one pixel to cover these regions of uncertain colour: the steps are shown in Fig. 3.

3) Detecting cracks

Typical walls have many marks and imperfections, as well as changes in colours and other small marks (either accidental damage or 'spot' marks not detected as marks in the previous section – which removes large region marks). These marks are often 'blacker' than the black of a shallow crack in ambient light: in sunlight, strong light may penetrate the crack. Thus we opted for operator selection of relevant cracks – this is one case where our brains have no problem making the choice despite very confusing and misleading backgrounds.

4) Following cracks

Wide dark cracks are readily followed from the start point by a variety of well-known methods. This is the 'trivial' problem that any image processing student can solve. We tested distance transform [3] and contour following techniques and found both work well as the 'primary algorithm'. However, the leading edges of a crack are invariably small, narrow and difficult to see. Thus our primary algorithm tracks the wide parts of a crack until it 'disappears' in the image noise. Then we switch to a dynamic algorithm (formally one belonging to the class of greedy algorithms) which builds a least cost path from the current tip of the crack until no more candidates can be found in the region.

5) Measuring cracks

In the wide regions, we capture contours from the left and right edges of the track. Again, real cracks present some challenges because the edges are not well defined in the image and they are also fragile and collapse often. In the worst case, edges collapse into the crack and make it appear much lighter because the newly deposited material makes the crack appear shallower and fills the shadow that would normally make the crack appear very dark. We added three methods for computing the crack width: distances between

- contour edges
- chosen thresholds and
- point of maximum slope in the intensity profile through the crack.

We expected that method (c), based on the points of maximum intensity gradient on each edge of the crack, would be the most robust and reliable. However, in practice, all methods produced similar results, with (a) and (b) producing, as expected, larger widths, but all three methods tracked widths in a regular way. This is a subject for further assessment, but, given our hypothesis that measuring the increase in width is the critical factor, the differences may not be significant: a growing crack will show up whichever width is chosen.

Most of these methods were implemented as methods of a C++ **BCrack** (Building Crack) class.

C. Final system

Since we want to be able to process different styles of input (both sequences of single images and videos) and a wide variety of backgrounds, we realized that one program with a single algorithm would be inadequate. Our final system will be driven by a configuration file created to process each set of images. This file will be a 'mini program' with directions for invoking various methods in our system. For example, it might look like this

Command	Purpose
File name	Choose file and still or video
Master image	All following images should be registered to this one
Register	Register images to master image
Bounding box	Select a region of interest
Remove marks	Mask out fiducial marks and irrelevant areas
Clean	Remove small spots
Single	Follow primary (widest) crack only
Multiple	Follow branches from the main mark
Join	Join cracks which have hidden regions
Follow marks	Attempt to follow cracks in regions initially masked out by 'Remove marks'

Each command will be followed by optional parameters, eg for **Remove marks**, it will list colours of regions to be masked out; **Clean** will indicate maximum size of spots considered to be image noise only; **Join** will specify the

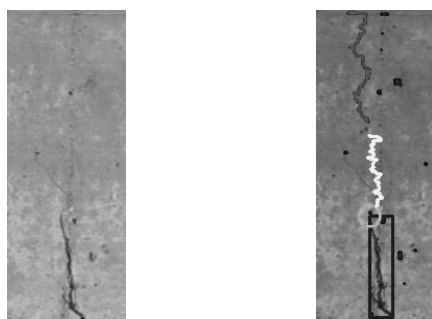


maximum length of ‘hidden’ cracks – those which become invisible, eg under paint, for a distance.

III. EXAMPLE PROCESSED CRACKS

Some samples of the range of cracks handled by the methods developed to handle the various situations encountered in captured videos. Samples include cracks forced into beams in research laboratory tests as well as some captured with telephoto lens (see Fig 1, top right – deliberately imaged with a long lens 30m away) and from a drone (Fig 2).

A. Beam A



Original Grey Scale Image

Detected cracks

Fig 4. On the right: dark red: contours of the ‘easily’ detected wide crack. Green circle: tip of the ‘easy’ crack and start of DP algorithm tracking. Yellow, purple and red: barely visible cracks detected by DP – gaps between the different colours were ‘jumped’ to follow hidden or extremely narrow cracks

Fig 4 shows a generated crack in a concrete beam showing how two algorithms are used: (a) contour following to track the wide region of the crack and (b) dynamic programming (DP) to follow the weak section of the crack. The green circle shows where we switched to the DP algorithm when the crack became barely visible.

Fig 5 shows an example of the time evolution of one crack in a beam. In this case, figure shows the width along the crack at an initial time at which the crack was clearly visible by its contour with a width of roughly 3 pixels (~0.3mm) along a length of ~600 pixels (~100mm). After 12s, it had grown uniformly along its length from about 1 mm at the start. Note: noise in the plots is due to pixelization errors: the widths are small in pixel counts, ranging from 2 to 8 pixels. The camera field of view in this image was necessarily wide, because we could not be certain where the beam would start cracking: using a narrower field of view produced better precision in other measurements. Signal averaging over neighbouring pixels as shown in the moving average plots led to smoother curves also.

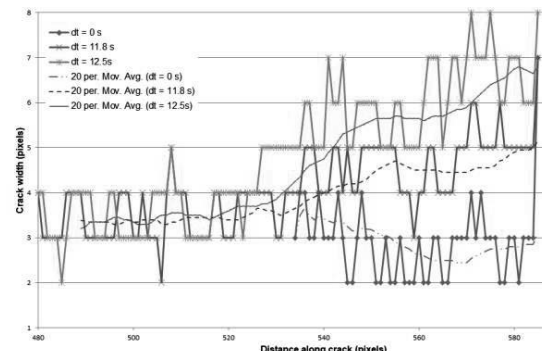


Fig 5. Evolution of a crack with time: crack width (y-axis, pixels, 5.7pix/mm) vs length along the crack (x-axis, pixels, 5.7pix/mm). The crack starts on the right (widest part) and grows (and narrows) towards the left.

B. Beam B

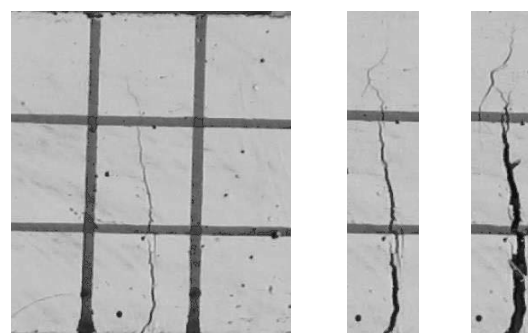


Fig 6. Images of evolving crack: left: some seconds after it appeared; middle: crack developing; right almost completely cracked

Another beam under test is shown in Figs. 6 and 7. This concrete beam was painted white and marked up in blue. The width profile for this crack at various time is shown in Fig. 7. Profiles are labeled by frame numbers: 601 to 900. Frames are separated by approximately 15 ms. The size of the growing crack is shown along the entire length of the crack, ie we have a complete 2D map of its shape over time. As expected, at early times, frame numbers 601 to 660, the profiles are short and end about midway along the profile. As the crack develops, we capture longer and longer profiles.

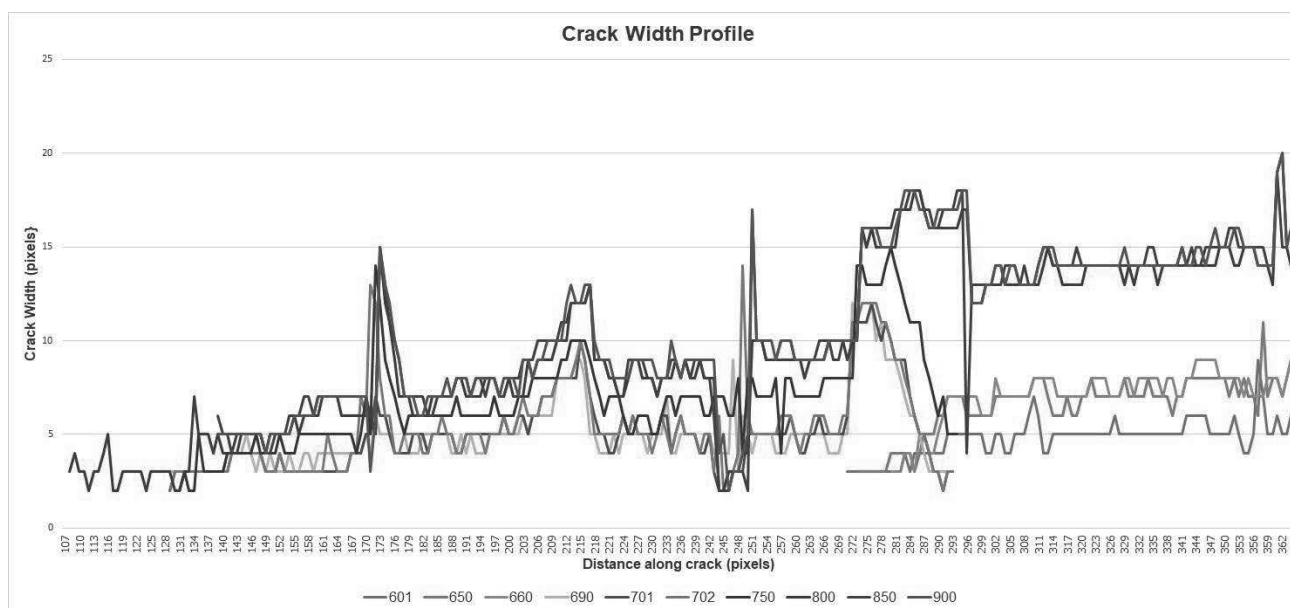


Fig 7. Evolution of a crack with time for beam shown in Fig 6: crack width (y-axis, pixels, 5.1 pix/mm) vs length along the crack (x-axis, pixels, 5.1 pix/mm). The crack starts on the right (widest part) and grows (and narrows) towards the left.

IV. CONCLUSION

We present here initial work on building a library of tools for processing building cracks to determine complete surface geometry changes over time. These geometries have two applications: (a) the early detection of buildings at risk of collapse after earthquakes or as a consequence of long term subsidence of the underlying soils and (b) understanding of the effects of various structural changes for forming building components, *eg* beams and columns, and reinforcements added to the basic material.

We collected a variety of examples of surface ‘defects’ – some added deliberately and randomly, in terms of colours and geometries, by students adding fiducial marks to test structures, and others added, equally randomly, by Mother Nature, as natural degradation of surface coatings and erosions of the underlying surface materials. Some are partially filled with rubble from degeneration of the fragile edges. We are working through our test images to improve further techniques. However, we have already successfully followed very fine cracks, by dynamic programming techniques. These fine cracks are important as the first signs of a growing and potentially dangerous defect.

A. Future Work

Our first task will be to correlate the crack opening widths with data on the beam structures.

Some drone images capture a crack on MSU engineering’s top floor, so it will be regularly monitored and

become our first benchmark for verifying the long-term usefulness of our system! We will choose a variety of atmospheric conditions (solar intensity, cloud cover, solar azimuth and elevation) to verify precision of our tools.

Thailand lies in a (mostly) earthquake-free zone so that finding growing cracks to further one aim of this study is not so easy. Readers, who can contribute existing building cracks to our study, are welcome to join us – particularly if the cracks are not easy to access, *eg* second floor and higher, and would require a drone or long lens camera to capture images. Please contact the authors.

ACKNOWLEDGMENTS

We are grateful to the MSU civil engineering students who fabricated the test beams and, incidentally, used their imaginations to add a variety of fiducial marks that provided several challenges for this study.

REFERENCES

- [1] N.-D. Hoang, “Detection of Surface Crack in Building Structures Using Image Processing Technique with an Improved Otsu Method for Image Thresholding”, *Advances in Civil Engineering*, Article ID 3924120, 2018.
- [2] A. Mohan, S. Poobal, “Crack detection using image processing: A critical review and analysis”, *Alexandria Engineering J*, Elsevier, <http://www.sciencedirect.com/science/article/pii/S1110016817300236>, 2017.
- [3] R. Kimmel, N. Kiryati, A. M. Bruckstein, “Distance maps and weighted distance transforms”, *Journal of Mathematical Imaging and Vision*, Special Issue on Topology and Geometry in Computer Vision, 6:223-233, 1996.
- [4] H. Oliveira, P.L. Correia, “Automatic Road Crack Detection and Characterization”, *IEEE Transactions on Intelligent Transportation Systems*, 14(1), 155-168(2013).
- [5] H. N. Nguyen and T. Y. Kam and P. Y. Cheng, “A novel automatic concrete surface crack identification using isotropic undecimated wavelet



Proceedings of the 10th International Conference on Sciences, Technology and Innovation for Sustainable Well-Being (STISWB 2018)
Vientiane, Lao PDR. July 11th -13th, 2018



transform", Int Symp on Intelligent Signal Processing and Communications Systems, 766-771, 2012.

[6] Nobuyuki Otsu, "A threshold selection method from gray-level histograms". IEEE Trans. Sys., Man., Cyber. **9** (1): 62-66, doi:10.1109/TSMC.1979.4310076, 1979.

[7] S. G. Lee, Y. Mao, A.M. Gokhale, J. Harris, M.F. Horstemeyer, "Application of digital image processing for automatic detection and characterization of cracked constituent particles/inclusions in wrought aluminum alloys", Materials Characterization, 60(9), 964-970, 2009.

[8] S. German, J-S Jeon, Z-H. Zhu, C. Bearman, Ioannis Brilakis, R. DesRoches, L. Lowes, "Machine Vision-Enhanced Postearthquake Inspection", J. Comput. Civ. Eng., 27(6), 622-634, 2013.



Index of Author's Names			
A		G	
	Page		Page
A.Thongrak	202	G. Smithisup	461
Adirek Jantakun	372,389	Guoqing Guan	102
Adisak Janthothai	281	H	
Adisorn Jarunvorakunvong	233		Page
Amnat Chenjitsiri	233	Hansa Khetbunphot	21,34
Amorn Onkrong	511	I	
Anan Tempiem	251		Page
Anchalee Panitjaroen	17,21,34	Ittipol Thinnoiwong	29
Anongrit Kangrang	146,152,163	J	
Anukun Arngbunta	173		Page
Anurak Kusolchoo	417	Jack Chum-in	342
Aphichata Thongrak	377	Janjira Yatom	135
Apichit Kampala	173	Jarut Kunanoppadol	26,524
Aroonsri Aiernrum	515	Jaturapatr Varith	47
Aumarit Panthai	480	Jeerawan Saelao	520
B		Jetsadaporn Simsiriwong	241
	Page	Jirawat Leaksantad	141,436
B. Suechoey	196,202	Jirawat Paiboon	383
Beesuda Daoruang	38	Jirutthitikalpongsri Hirunyagird	116
Benjamin Gérard	230	Jittimon Wongs	492
Bhuchiss Tanwanichkul	276	John Morris	529
Boonrueang Ponil	322	Jukkrit Kluabwang	511
Boonruk Vanborsel	130	Jumreans Srikamta	42
C		Junjira Wunchana	486
	Page	Junthara Sontua	423
C. Pariwatnanont	8	K	
C. Sangvornyotin	1,8		Page
Chaiyot Damrongkijkosol	334	Kanjana Narkprasom	47
Chalakorn Udomraksasakul	12	Kanoknan Parcheruk	192
Chananya Raramanus	486	Kanokwan Sathonghon	496
Chanatip Samart	102	Kanokwan Tandee	486
Chantana Sangvornyotin	4	Kasama Sirisomboon	90,312
Chantima Rewlay-ngoen	85	Kedsara Rattawan	80
Chatthanon Bhothikhun	182,312	Kedsarin Phoosup	354
Chayakorn Sripichetkul	364	Kewalin Poonoppakhun	496
Chessadabhorn Kitjettanee	475	Khanista Namee	383
Chongrug Pariwatnanont	4	Khidsadakhon Booddachan	51
Chonlatee Photong	216,220,225	Kittima Lertsakwimarn	399
Churat Tararuk	308	Kittisak Khuwaranyu	294,449
Churat Thararux	303	Kmonchanok Adkalan	225
Chuwong Phongcharoenpanich	399	Kompan Chomsamutr	12
D		Korn Puangnak	377
	Page	Krisada Lekdee	346
D. Ratsanasasart	1,8	Krit Chaimoon	529
Dhetsuwan Khum-oh	276	Kritsada Thiangphadung	225
Duangkamol Ruen-ngam	449	Kullanan Lakul	359



Index of Author's Names

K	Page	P	Page
Kullayot Suwantaroj	237,251	Paramust Juntarakod	106
Kumpon Subsomboon	130	Parkpoom Jarupoom	286
Kwanjai Nachaiyaphum	220	Pasinee Siriprapa	286
L	Page	Passawat atcharadumrongsak	290
Lamul Wiset	61	Patcharapol Posi	169
Luan Suerpadgorn	173	Pathomphong Jumnonphan	65
M	Page	Patiwat Khomwachirakul	328,338
Methida Siritan	255	Pattarachai Noppakun	141,436
Montri Kawsuk	120	Pattayamon Mekyapisit	486
Muhammakhoiri Hayibaka	308	Pawin Kantawong	286
N	Page	Pawinee Phetnok	430,440
N. Pringsakul	196,202	Phairoach Chunkaew	70
Nantawatana Weerayuth	317	Philaiwan Pornprasit	515
Nantiya Jantralux	42	Phornrak Wangnamjai	260
Napat Chantaramee	500	Phrut Sakulchangsattajai	241,247,255,281
Narin Srithikarn	74	Phurich Ngamkong	216,225
Nasru Tuenga	303	Phuwisa Phetchuay	354
Nattapol Poomsa-ad	61	Pisuthi klinkajorn	290
Nattapong Phanthuna	208	Pitsanu Tongkhaw	188
Nattapong Phanthuna	212	Pongpisit Wuttidittachotti	407
Nattaporn Chaiyat	74	Pongsiri Jaruyanong	294,480
Nattarat Chutwiboonkun	96	Poomin Krisangsri	470
Nattawut Tharawadee	96	Poramet Arromdee	182,312
Natthanicha Sukasem	135,141,430,436,440	Pornpit Sirima	346
Natthawut Panitjaroen	17,21,34	Pracha Yeunyongkul	286,322
Natworapol Rachsiriwatcharabul	350	Pradit Jiagulprasert	125
Nawee Nuntapap	74	Pradit Terdtoon	241,247,255,281
Nimit Ratsamee	74	Prasit Phangphet	342
Nimit Srikamta	178	Prasong Kankaew	342
Niti Kammuang-lue	241,247,255,281	Praveen Maiget	407
Nitigan Nakjuatong	38	Preetham Kumar Konda	529
Nitipong Soponpongpiat	29	Prin Nachaisit	116
Noppong Srirakul	465,470	Prinya Chindaprasirtat	169
Nopporn Patcharaprakiti	520	Pukanit Thuibuengchim	403
Numpon Panyoyai	56,113,290	R	Page
Nutthawut Singthuean	338	Rachadasak Supengcum	188
Nutthipong Vilaiyawong	354	Rapeepat Techarungruengsakul	146
Nyanakorn Sutassanamarlee	290	Rarisara Impaprasert	65
P	Page	Ratsuda Ngamsert	152
P. Samartkit	455	Ronnachart Munsin	74,322
P. Tongard	455	Rotjapun Nirunsin	303,308
Panya Maneechakr	102	S	Pag
		S. Pullteap	455,461
		S. Siriporananon	196,202



Index of Author's Names

S	Page	T	Page
Sahalaph Homwuttiwong	529	Thanad Katpradit	230
Saharat Phuakle	216	Thanapon Jilao	354
Sakultala Wannapakhe	51	Thanasit Wongsiriamnuay	56,113,290
Samerkhan Tantikul	113	Thanatcha Santhadkha	465
Santipab Koththale	511	Thawachchai Chattamnan	342
Sanya Khunkhao	377	Therdpong Daengsi	407
Sarun Chattunyakit	233	Thibordin Sangsawang	158
Sawat Yukalang	511	Thitibhorn Phantachang	125
Saweth Hongprasit	403	Thitiporn Janda	372,389
Sayan Phokate	427	Thosapon Katejanekarn	260,268
Seksan Papong	85	Tipapon Khamdaeng	56,113,290
Singkaew Poktern	12	Tithinun Rattanaplome	500
Sirichai Torsakul	120		
Siripol Tongom	85,334	U	Page
Sitthinan Saengdian	505	Upady Hatthasin	368
Sivapong Phetsong	317,446		
Somkieat Thongkeaw	208	V	Page
Somporn Leekongbub	169	Vichuda Mettanant	317,446
Songwut Mongkonlerdmanee	334	Vitawat Sittakul	212
Songyos Rungsa	389	Vitsanusat Atyotha	423
Suchada Sadang	492		
Sudjit Karuchit	412	W	Page
Sukanya Cherdchoongam	359	Wanapun Waiyawut	395
Sunthorn Wiriy	364	Wanchai Leelakaweewong	354
Supachai Lakkam	237,251	Wangwon Khorchaiyphurn	529
Supachai Wasananon	26,524	Wanichaya Chairuen	505
Supachock Tuntivivat	233	Wasin Wongkum	74
Suparerk Charmongkolpradit	276	Watchara Songserm	12
Suphitchaya Kalantakasuwan	47	Watcharee Funfuenha	286
Surachai Karnjanakom	102	Watcharin Pachittien	338
Suriyun Srisongkham	216	Weeranut Intagun	80
Suthimon Kuirat	268	Wichayanee Puttipiriyangkul	412
Suwat Paengteerasukkamai	350	Wichcha Onsa-ard	372
Suwit Paengkanya	65	Wichien Sang-aroon	276
		Wichitra Singhirunnusorn	417
T	Page	Wilaporn Ngernbath	216
T. Tanongtanachai	461	Wilaporn Ngernbath	225
Tananon Srisamran	90	Wirojne Kanoksilapatham	80
Tanate Chaichana	303,308	Wirote Ritthong	328,338
Tarapong Karnjanaparichat	74	Wisoot Sanhan	247
Taweesak Taweewithyakarn	322	Witcha Upaphai	233
Taweesuk Taweewitayakarn	290	Wiwat Wangcharoen	496
Teerachai Surachotivet	26,158	Worawan Pechurai	505
Teerasak Hudakorn	465,470,475,480	Wutthigrai Sailuam	192
Teerawat thongwan	163		



Proceedings of the 10th International Conference on Sciences, Technology and Innovation for Sustainable Well-Being (STISWB 2018)
Vientiane, Lao PDR. July 11th-13th, 2018



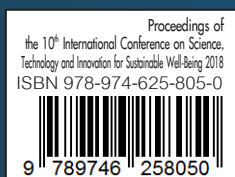
Index of Author's Names

Y	Page
Yardfon Tanongkankit	47
Yuttana Srilamai	116



STISWB 2018

Moving Towards Smart and Sustainable Technologies



Proceedings of
the 10th International Conference on Science,
Technology and Innovation for Sustainable Well-Being 2018
ISBN 978-974-625-805-0

9 789746 258050



WWW.STISWB2018.ORG

WWW.STISWB2018.ORG

Contact Organizer:

Faculty of Engineering,
Rajamangala University of Technology Phra Nakhon

Tel. (+66) 2836-3000 Ext. 4118
E-mail : STISWB2018@gmail.com

1381 Pracharat Sai 1 Road, Bangsue,
Bangkok 10800, Thailand

